WOODHEAD PUBLISHING SERIES IN CIVIL AND STRUCTURAL ENGINEERING

Advanced fibre-reinforced polymer (FRP) composites for structural applications

Edited by Jiping Bai

WP
WOODHEAD PUBLISHING

Advanced fibre-reinforced polymer (FRP) composites for structural applications

Related titles:

Eco-efficient concrete
(ISBN 978-0-85709-424-7)

Handbook of seismic risk analysis and management of civil infrastructure systems
(ISBN 978-0-85709-268-7)

Developments in fiber-reinforced polymer (FRP) composites for civil engineering
(ISBN 978-0-85709-234-2)

Details of these books and a complete list of titles from Woodhead Publishing can be obtained by:

- visiting our web site at www.woodheadpublishing.com
- contacting Customer Services (e-mail: sales@woodheadpublishing.com; fax: +44 (0) 1223 832819; tel.: +44 (0) 1223 499140 ext. 130; address: Woodhead Publishing Limited, 80, High Street, Sawston, Cambridge CB22 3HJ, UK)
- in North America, contacting our US office (e-mail: usmarketing@woodheadpublishing.com; tel.: (215) 928 9112; address: Woodhead Publishing, 1518 Walnut Street, Suite 1100, Philadelphia, PA 19102-3406, USA)

If you would like e-versions of our content, please visit our online platform: www.woodheadpublishingonline.com. Please recommend it to your librarian so that everyone in your institution can benefit from the wealth of content on the site.

We are always happy to receive suggestions for new books from potential editors. To enquire about contributing to our Civil and Structural Engineering series, please send your name, contact address and details of the topic/s you are interested in to francis.dodds@woodheadpublishing.com. We look forward to hearing from you.

The team responsible for publishing this book:

Commissioning Editor: Jess Rowley
Publications Coordinator: Emily Cole
Project Editor: Anneka Hess
Editorial and Production Manager: Mary Campbell
Production Editor: Adam Hooper
Cover Designer: Terry Callanan

Woodhead Publishing Series in Civil and Structural Engineering:
Number 46

Advanced fibre-reinforced polymer (FRP) composites for structural applications

Edited by

Jiping Bai

Oxford Cambridge Philadelphia New Delhi

Published by Woodhead Publishing Limited,
80 High Street, Sawston, Cambridge CB22 3HJ, UK
www.woodheadpublishing.com
www.woodheadpublishingonline.com

Woodhead Publishing, 1518 Walnut Street, Suite 1100, Philadelphia, PA 19102-3406, USA

Woodhead Publishing India Private Limited, 303, Vardaan House, 7/28 Ansari Road,
Daryaganj, New Delhi – 110002, India
www.woodheadpublishingindia.com

First published 2013, Woodhead Publishing Limited

British Library Cataloguing in Publication Data
A catalogue record for this book is available from the British Library.

Library of Congress Control Number: 2013943194

ISBN 978-0-85709-418-6 (print)
ISBN 978-0-85709-864-1 (online)
ISSN 2052-4714 Woodhead Publishing Series in Civil and Structural Engineering (print)
ISSN 2052-4722 Woodhead Publishing Series in Civil and Structural Engineering (online)

The publisher's policy is to use permanent paper from mills that operate a sustainable forestry policy, and which has been manufactured from pulp which is processed using acid-free and elemental chlorine-free practices. Furthermore, the publisher ensures that the text paper and cover board used have met acceptable environmental accreditation standards.

Typeset by Replika Press Pvt Ltd, India
Printed by Lightning Source

Contents

Contributor contact details

(* = main contact)

Editor and Chapter 1

J. Bai
Department of Engineering
Faculty of Computing, Engineering and Science
University of South Wales
Pontypridd CF37 1DL
UK

E-mail: jiping.bai@southwales.ac.uk

Chapter 2

E. Frollini*, C. G. Silva and E. C. Ramires
Macromolecular Materials and Lignocellulosic Fibers Group
Institute of Chemistry of São Carlos
University of São Paulo IQSC-USP
Av. Trabalhador Sãocarlense, 400
CP 780 - CEP 13560 970
São Carlos
São Paulo
Brazil

E-mail: elisabete@iqsc.usp.br

Chapter 3

N. Miskolczi
Chemical Engineering and Process Engineering Institute
MOL Department of Hydrocarbon and Coal Processing
University of Pannonia
Egyetem u 10
Veszprém
H-8200
Hungary

E-mail: mnorbert@almos.uni-pannon.hu

Chapter 4

F. Sarasini* and C. Santulli
Department of Chemical Engineering Materials Environment
University of Rome 'La Sapienza'
Via Eudossiana 18
00184 Rome
Italy

E-mail: fabrizio.sarasini@uniroma1.it; carlosantulli141@gmail.com

Chapter 5

V. Fiore* and A. Valenza,
Department of 'Ingegneria Civile, Ambientale, Aerospaziale, dei Materiali'
University of Palermo
Viale delle Scienze, Edificio 6
90128 Palermo
Italy

E-mail: vincenzo.fiore@unipa.it

Chapter 6

S. Pansart
Germanischer Lloyd Industrial Services GmbH
Renewables Certification
Brooktorkai 18
20457 Hamburg
Germany

E-mail: simon.pansart@gmx.de

Chapter 7

S. Bickerton*, Q. Govignon and P. Kelly
Centre for Advanced Composite Materials
Department of Mechanical Engineering
The University of Auckland
Private Bag 92019
Auckland 1020
New Zealand

E-mail: s.bickerton@auckland.ac.nz

Chapter 8

A. Khennane
School of Engineering and Information Technology
University of New South Wales at the Australian Defence Force Academy
Northcott Drive
Canberra
ACT 2600
Australia

E-mail: a.khennane@adfa.edu.au

Chapter 9

J. Ramôa Correia
Department of Civil Engineering, Architecture and Georesources
Instituto Superior Técnico / ICIST
Technical University of Lisbon
Av. Rovisco Pais 1
1049-001 Lisboa
Portugal

E-mail: jcorreia@civil.ist.utl.pt

Chapter 10

A. Al-Shawaf
Department of Civil Engineering
Monash University
Clayton Campus
Building 60
Wellington Road
Melbourne
Victoria 3800
Australia

E-mail: ahmed.al-shawaf@monash.edu;
ahmed.al-shawaf@bigpond.com

Chapter 11

R. M. Guedes*
Department of Mechanical Engineering (DEMec)
Faculty of Engineering of the University of Porto (FEUP)
Rua Dr. Roberto Frias s/n
4200-465 Porto
Portugal

E-mail: rmguedes@fe.up.pt

J. Xavier
CITAB/UTAD
Apartado 1013
5001-801 Vila Real
Portugal

E-mail: jxavier3@gmail.com

Chapter 12

K. Benzarti*
Université Paris-Est
IFSTTAR
MAT
F-75732 Paris
France

E-mail: karim.benzarti@ifsttar.fr

X. Colin
Arts et Métiers ParisTech
PIMM
F-75013 Paris
France

E-mail: xavier.colin@ensam.eu

Chapter 13

G. J. Turvey
Engineering Department
Lancaster University
Bailrigg
Lancaster LA1 4YR
UK

E-mail: g.turvey@lancaster.ac.uk

Chapter 14

M. F. M. Fahmy
Civil Engineering Department
Assiut University
University Road
Assiut 71516
Egypt

E-mail: mfmf1976@yahoo.com

Chapter 15

T. H. Panzera* and A. L. Christoforo
Federal University of São João del Rei (UFSJ)
Department of Mechanical Engineering
São João del Rei
36.307-352 Minas Gerais
Brazil

E-mail: panzera@ufsj.edu.br

P. H. Ribeiro Borges
Federal Centre for Technology Education of Minas Gerais (CEFET/MG)
Department of Civil Engineering
Belo Horizonte
30.421-169 Minas Gerais
Brazil

E-mail: pborges@civil.cefetmg.br

Chapters 16, 17, 19 and 20

L. C. Hollaway
Department of Civil Engineering
Faculty of Engineering and Physical Science
University of Surrey
Guildford GU2 7XH
UK

E-mail: l.hollaway@surrey.ac.uk

Chapter 18

F. Taheri
Department of Civil and Resource Engineering
Dalhousie University
1360 Barrington Street
PO Box 15000
Halifax
Nova Scotia B3H 4R2
Canada

E-mail: farid.taheri@dal.ca

Chapter 21

S. Zainuddin*, M. V. Hosur and S. Jeelani
Department of Materials Science and Engineering
Tuskegee University
Tuskegee, AL 36088
USA

E-mail: szainuddin@mytu.tuskegee.edu

A. Kumar and J. Trovillion
Construction Engineering Research Laboratory
US Army Engineer Research and Development Center
Champaign, IL 61821-9005
USA

E-mail: ashok.kumar@usace.army.mil

Chapter 22

J. Custódio* and S. Cabral-Fonseca
Laboratório Nacional de Engenharia Civil I.P. (LNEC)
Materials Department
Av. do Brasil 101
1700-066 Lisboa
Portugal

E-mail: jcustodio@lnec.pt; sbravo@lnec.pt

Woodhead Publishing Series in Civil and Structural Engineering

1 **Finite element techniques in structural mechanics**
C. T. F. Ross

2 **Finite element programs in structural engineering and continuum mechanics**
C. T. F. Ross

3 **Macro-engineering**
F. P. Davidson, E. G. Frankl and C. L. Meador

4 **Macro-engineering and the earth**
U. W. Kitzinger and E. G. Frankel

5 **Strengthening of reinforced concrete structures**
Edited by L. C. Hollaway and M. Leeming

6 **Analysis of engineering structures**
B. Bedenik and C. B. Besant

7 **Mechanics of solids**
C. T. F. Ross

8 **Plasticity for engineers**
C. R. Calladine

9 **Elastic beams and frames**
J. D. Renton

10 **Introduction to structures**
W. R. Spillers

11 **Applied elasticity**
J. D. Renton

12 **Durability of engineering structures**
J. Bijen

13 **Advanced polymer composites for structural applications in construction**
Edited by L. C. Hollaway

14 **Corrosion in reinforced concrete structures**
Edited by H. Böhni

15 **The deformation and processing of structural materials**
Edited by Z. X. Guo

16 **Inspection and monitoring techniques for bridges and civil structures**
Edited by G. Fu

17 **Advanced civil infrastructure materials**
Edited by H. Wu

18 **Analysis and design of plated structures Volume 1: Stability**
Edited by E. Shanmugam and C. M. Wang

19 **Analysis and design of plated structures Volume 2: Dynamics**
Edited by E. Shanmugam and C. M. Wang

20 **Multiscale materials modelling**
Edited by Z. X. Guo

21 **Durability of concrete and cement composites**
Edited by C. L. Page and M. M. Page

22 **Durability of composites for civil structural applications**
Edited by V. M. Karbhari

23 **Design and optimization of metal structures**
J. Farkas and K. Jarmai

24 **Developments in the formulation and reinforcement of concrete**
Edited by S. Mindess

25 **Strengthening and rehabilitation of civil infrastructures using fibre-reinforced polymer (FRP) composites**
Edited by L. C. Hollaway and J. C. Teng

26 **Condition assessment of aged structures**
Edited by J. K. Paik and R. M. Melchers

27 **Sustainability of construction materials**
J. Khatib

28 **Structural dynamics of earthquake engineering**
S. Rajasekaran

29 **Geopolymers: Structures, processing, properties and industrial applications**
Edited by J. L. Provis and J. S. J. van Deventer

30 **Structural health monitoring of civil infrastructure systems**
Edited by V. M. Karbhari and F. Ansari

31 **Architectural glass to resist seismic and extreme climatic events**
Edited by R. A. Behr

32 **Failure, distress and repair of concrete structures**
Edited by N. Delatte

33 **Blast protection of civil infrastructures and vehicles using composites**
Edited by N. Uddin

34 **Non-destructive evaluation of reinforced concrete structures Volume 1: Deterioration processes**
Edited by C. Maierhofer, H.-W. Reinhardt and G. Dobmann

35 **Non-destructive evaluation of reinforced concrete structures Volume 2: Non-destructive testing methods**
Edited by C. Maierhofer, H.-W. Reinhardt and G. Dobmann

36 **Service life estimation and extension of civil engineering structures**
Edited by V. M. Karbhari and L. S. Lee

37 **Building decorative materials**
Edited by Y. Li and S. Ren

38 **Building materials in civil engineering**
Edited by H. Zhang

39 **Polymer modified bitumen**
Edited by T. McNally

40 **Understanding the rheology of concrete**
Edited by N. Roussel

41 **Toxicity of building materials**
Edited by F. Pacheco-Torgal and A. Fucic

42 **Eco-efficient concrete**
F. Pacheco-Torgal, S. Jalali, J. Labrincha and V. M. John

43 **Nanotechnology in eco-efficient construction**
Edited by F. Pacheco-Torgal, M. V. Diamanti, A. Nazari and C. Goran-Granqvist

44 **Handbook of seismic risk analysis and management of civil infrastructure systems**
Edited by F. Tesfamariam and K. Goda

45 **Advanced fiber-reinforced polymer (FRP) composites for civil engineering**
Edited by N. Uddin

46 **Advanced fibre-reinforced polymer (FRP) composites for structural applications**
Edited by J. Bai

47 **Handbook of recycled concrete and demolition waste**
Edited by F. Pacheco-Torgal, V. W. Y. Tam, A. Labrincha, Y. Ding and J. J. de Bito

48 **Understanding the tensile properties of concrete**
Edited by J. Weerheijm

49 **Eco-efficient construction and building materials: Life cycle assessment (LCA), eco-labelling and case studies**
Edited by F. Pacheco-Torgal, L. F. Cabeza, J. Labrincha and A. de Magalhães

1
Introduction

J. BAI, University of, South Wales, UK

DOI: 10.1533/9780857098641.1

Abstract: Fibre-reinforced polymer (FRP) composites have become essential materials for maintaining and strengthening existing infrastructure. Many new innovative types of hybrid material and structural systems have been developed using FRP composite materials. Increased utilisation of FRP requires that structural engineers and practitioners be able to understand the behaviour of FRP materials and design composite structures. This book provides an overview of different advanced FRP composites and the use of these materials in a variety of application areas. This chapter specifically covers a brief review on FRP applications and gives an outline of the book.

Key words: fibre-reinforced polymer (FRP), composites, structural engineering, strengthening, concrete, civil engineering.

Over the past few decades advanced composites have increasingly become smart materials for new structures and the renewal of existing civil engineering infrastructures. This book focuses on various aspects of advanced fibre-reinforced polymer (FRP) composites in civil engineering: materials; processing and fabrication; properties, performance and testing. It also provides an overview of the applications of advanced FRP composites in civil and structural engineering. The book is a useful text for graduate students in the area of composites in general, and civil engineering and construction in particular. It is also a comprehensive and practical resource for practising engineers, researchers, manufacturers and suppliers.

Advanced composite materials were primarily developed for aerospace to enhance the performance of commercial and military aircraft [1]. They still play a significant role in current and future aerospace components. However, in recent years composite materials have become particularly attractive for civil engineering infrastructure applications due to their exceptional strength and stiffness-to-density ratios and superior physical properties [2]. Considerable advances have been made in the use of composite materials in the construction and building industries, and this trend will continue. Fibre-reinforced polymer (FRP) composites are now widely used in civil engineering applications [3–9]. The repair and maintenance of deteriorated, damaged and substandard civil infrastructures has become one of the most important issues for the civil engineer worldwide [10–12]. The use of externally bonded fibre-reinforced polymer (FRP) composites to strengthen, rehabilitate and

retrofit civil engineering structures is fully discussed throughout this book. The book is organised into four parts. Each chapter within a part is written by a leading expert (or team of experts) and deals with a specific topic with detailed referencing to primary sources for further research.

Fibre-reinforced polymer (FRP) composites are composed of fibres and matrices, which are bonded through the interface to ensure that the composite system as a whole gives satisfactory performance. Part I deals with FRP composite matrix materials which provide the foundation for composite materials. Chapter 2 reviews the chemistry of phenolic resins together with their mechanical and thermal properties. Chapter 3 discusses polyester thermoset resins as matrix materials. An overview of the chemistry of vinylester resins, together with their mechanical and chemical properties, as well as their use as a matrix material in the construction industry, is provided in Chapter 4. The final chapter in Part I begins with a review of the epoxy resins commonly available on the market, and then focuses on the principal characteristics of epoxy resin composite systems and their practical applications.

The mechanical properties of FRP composites are dependent upon the ratio of fibre and matrix material, the mechanical properties of the constituent materials, the fibre orientation in the matrix, and ultimately the processing and methods of fabrication, which are the subject of Part II. Chapters discuss prepreg processing, liquid composite moulding (LCM), filament winding processes and pultrusion of advanced fibre-reinforced polymer (FRP) composites.

FRP composite structural analysis and design require a good knowledge of material properties. Part III is primarily devoted to the properties, performance and testing of FRP composites. Chapters examine the stress-related aspects of composites in civil engineering applications – particularly the critical interfacial adhesive stresses. Part III also deals with the elastic property analysis of laminated advanced composites, gives a general overview of composite stiffness and assesses unidirectional reinforced composites. This part also looks into the basic mechanisms involved in the environmental degradation of FRP composites and the impact of the ageing mechanisms of the polymer matrix on the mechanical properties of composites. Practical tests on FRP composite substructures and full-scale structures are also discussed.

The use of FRP composites in various structural applications is reviewed in Part IV. It covers a wide range of applications of FRP in civil engineering infrastructures, including advanced FRP composites to strengthen structures vulnerable to seismic damage, FRP composite materials for bridge construction and rehabilitation, the manufacture and rehabilitation of pipes and tanks in the oil and gas industry, and for the rehabilitation of timber and concrete structures. The key material requirements for sustainable energy production are reviewed and the use of composites in renewable energy such as wind power, tidal and wave power and solar power are discussed, including the

manufacture, maintenance and recycling of advanced FRP composite wind turbine blades.

FRP composite materials are durable [13, 14] and have reasonable fatigue life [15–17]. They have high strength-to-weight ratios and are easily adapted almost into any shape and size of structure. FRP are corrosion-resistant and largely weather-resistant. They have excellent chemical resistance. Moreover, FRP composites are lightweight and relatively cheap to manufacture. The composites industry is still evolving in the area of high-performance materials for ageing civil engineering infrastructure. FRP composites will potentially play a major role in extending the service life of the world's infrastructure in this century. With its distinguished international team of authors, this book offers a valuable reference for university students, researchers and scientists, as well as a practical guide for engineers, contractors and practitioners working on the new, rehabilitation and strengthening of the civil infrastructure.

1.1 References

1. Soutis C. Fibre reinforced composites in aircraft construction. *Progress in Aerospace Sciences*, **41**(2), 2005, pp. 143–151.
2. Cripps A. *Fibre-reinforced Polymer Composites in Construction*. 2002, London: ClRlA.
3. Hollaway L C. A review of the present and future utilisation of FRP composites in the civil infrastructure with reference to their important in-service properties. *Construction and Building Materials*, **24**(12), 2010, pp. 2419–2445.
4. Bakis C, *et al*. Fiber-reinforced polymer composites for construction – state-of-the-art review. *Journal of Composites for Construction*, **6**(2), 2002, pp. 73–87.
5. Kendall D. Building the future with FRP composites. *Reinforced Plastics*, **51**(5), 2007, pp. 26–33.
6. Kim G B, Pilakoutas K, and Waldron P. Thin FRP/GFRC structural elements. *Cement and Concrete Composites*, **30**(2), 2008, pp. 122–137.
7. Cheng J, *et al*. Design and analysis of a smart composite pipe joint system integrated with piezoelectric layers under bending. *International Journal of Solids and Structures*, **44**(1), 2007, pp. 298–319.
8. Shouman A and Taheri F. Compressive strain limits of composite repaired pipelines under combined loading states. *Composite Structures*, **93**(6), 2011, pp. 1538–1548.
9. Zou G P and Taheri F. Stress analysis of adhesively bonded sandwich pipe joints subjected to torsional loading. *International Journal of Solids and Structures*, **43**(20), 2006, pp. 5953–5968.
10. Hollaway L and Teng J G. *Strengthening and Rehabilitation of Civil Infrastructures using Fibre-reinforced Polymer (FRP) Composites*. 2008, Cambridge: Woodhead Publishing.
11. Leeming M B and Hollaway L. *Strengthening of Reinforced Concrete Structures: Using Externally-bonded FRP Composites in Structural and Civil Engineering*. 1999, Cambridge: CRC Press.
12. Taheri F, Shahin K, and Widiarsa I. On the parameters influencing the performance

of reinforced concrete beams strengthened with FRP plates. *Composite Structures*, **58**(2), 2002, pp. 217–226.
13. Custódio J, Broughton J, and Cruz H. A review of factors influencing the durability of structural bonded timber joints. *International Journal of Adhesion and Adhesives*, **29**(2), 2009, pp. 173–185.
14. Guedes R M, *et al*. Prediction of long-term behaviour of composite materials. *Computers & Structures*, **76**(1–3), 2000, pp. 183–194.
15. Guedes R M. Creep and fatigue lifetime prediction of polymer matrix composites based on simple cumulative damage laws. *Composites Part A: Applied Science and Manufacturing*, **39**(11), 2008, pp. 1716–1725.
16. Guedes R M, De Moura M F S F, and Ferreira F J. Failure analysis of quasi-isotropic CFRP laminates under high strain rate compression loading. *Composite Structures*, **84**(4), 2008, pp. 362–368.
17. Shokrieh M M and Taheri-Behrooz F. A unified fatigue life model based on energy method. *Composite Structures*, **75**(1–4), 2006, pp. 444–450.

2

Phenolic resins as a matrix material in advanced fiber-reinforced polymer (FRP) composites

E. FROLLINI, C. G. SILVA and E. C. RAMIRES,
University of São Paulo, Brazil

DOI: 10.1533/9780857098641.1.7

Abstract: Thermosets such as phenolic thermosets are brittle at room temperature. Thus, in applications where good mechanical properties are required thermosets must be combined with reinforcements to improve these properties. Composites based on thermoset matrices can substitute for steel and concrete in some applications of civil construction structures because of their higher resistance to oxidation than steel and better freeze–thaw resistance than concrete. Furthermore, phenolic composites can be produced with complex shapes, and with careful design, materials can be obtained with high strength and stiffness and excellent impact strength, making these materials alternatives to metals. Construction materials require fire- and high-temperature-resistant components, and moldings and laminates based on phenolics can be utilized due to their resistance to burning and minimal smoke and toxic fumes production. Phenolic composites can positively impact the building and construction industry by improving safety and reducing cost.

Key words: phenolic-type resins, bio-based resins, synthesis, phenolic-type composites, reinforcements, properties.

2.1 Introduction to phenolic resins

Phenolic-type resins were first reported as products of the reaction between phenols and aldehydes by Baeyer in the early 1870s (Economy and Parkar, 2011; Baeyer, 1872), and ter Meer introduced the first concepts concerning the nature of the reaction (Economy and Parkar, 2011; ter Meer, 1874). One of the drawbacks found in this early period was the foaming caused by the release of formaldehyde during the reaction. In the beginning of the twentieth century, Leo Hendrik Baekeland reported the preparation of materials from the synthesis between resorcinol and formaldehyde (Baekeland, 1907). Baekeland introduced the use of pressure and fillers to address the foaming problem (Economy and Parkar, 2011; Baekeland, 1909), and he formed Bakelite GmbH by 1910 and began manufacturing phenolic resins (Pilato, 2010a).

In 1920, Hermann Staudinger first postulated the existence of high

molecular weight molecules that could be synthesized from reactions of small molecules (which he named 'polymerization'). These high molecular weight molecules were referred to as 'macromolecules' by Staudinger in 1922, but this concept only became accepted within the scientific community at the end of the 1920s and during the 1930s.[1] Although Baekeland began his work on phenolic resins without knowing their macromolecular nature, he certainly provided a very important contribution to the establishment of the plastics industry.

The stories of both modern composites and phenolic resins are interconnected. In 1500 BC, composites were already being used by Egyptians and Israelites, with mud bricks reinforced with straw used in construction. However, the beginning of the modern age of composites can be linked to the commercialization of glass fibers, which began in the 1930s. At that time, the aircraft industry had a production problem: new materials were required to actualize the innovative concepts and designs that these companies were creating. Furthermore, each change in a particular design required new molds, making it difficult to test new designs quickly. Metal molds were expensive and required long lead times, and the early plastic molds could not withstand the forces they were subjected to during the forging process. This issue led to the idea that reinforcing these plastics with glass fibers, which were already on the market, could increase their resistance to the stresses of the molding process. Molds were then made from phenolic resins and glass fibers, which proved to be adequate for the intended goal (Brent, 2002). Phenolic resins were also combined with natural reinforcements, such as wood flour filler, and used in radios, telephones and other products (Lewark, 2007; Frollini and Castellan, 2012).

World War II (WWII, 1939–1945) accelerated the development of composites, with examples of composites of phenolic resins including phenolic-reinforced paper in the construction of a structural wing box beam (PT-19 aircraft) (Brent, 2002) and the use of 'Gordon-Aerolite', prepared from unidirectional, unbleached flax yarn impregnated with phenolic resin, in aircraft fuselages (Suddell and Evans, 2005). During this time, phenolic composites reinforced with natural fibers were also used for non-aircraft applications, such as ship bearings (phenolic–cotton), switchgears (phenolic–asbestos), and brake linings (cotton/asbestos–phenolic) (Brent, 2002). In the period that followed WWII, the abundance and cheapness of oil, coupled with the development of petrochemicals, decreased the use of renewable raw materials. Interest in these renewable reinforcements has reappeared in recent decades due to the search for raw materials to replace those of fossil origin and the environmental issues associated with fossil sources.

[1]Hermann Staudinger: Father of macromolecular chemistry, http://acswebcontent.acs.org/landmarks/polymer/staudinger.htm

New fibers, known as advanced fibers, were introduced in the 1960s, including boron filaments, aramid and carbon fibers. Composites reinforced with these fibers were called advanced composite materials (ACMs) (Pilato and Michno, 1994; Herakovich, 1998). ACMs experienced a boom beginning in 1970 when the aircraft industry began to face increasing fuel costs. The resulting need to make aircraft lighter led to the replacement of metallic parts with polymeric composites. Approximately 6000 years passed from the first applications of composites by the Egyptians to the introduction of ACMs. However, the progress achieved since the last half of the twentieth century has far surpassed that of the previous 6000 years (Pilato and Michno, 1994; Herakovich, 1998) (Fig. 2.1).

2.2 Synthesis of phenolic-type matrices

Phenolic resins are highly versatile, which has led to a broad range of applications in the aircraft, aerospace, automotive, electrical and electronic industries (Pilato *et al*., 2008) as well as in the interiors of mass-transit cars and architectural and marine components (Lewark, 2007). Phenolic resins with diverse structures and properties can be obtained from different phenols, aldehydes and catalysts. In addition, resins with different properties can be prepared from a given set of parental or substituted phenol/aldehyde/catalysts by diversifying parameters such as the phenol/formaldehyde ratio and the reaction temperature and duration.

Phenolic resins are thermosetting resins produced by the condensation of aldehydes with phenols. Generally, the phenol is phenol itself and the aldehyde is formaldehyde; however, substituted phenols and higher aldehydes are used to produce phenolic resins with specific properties, including specific reactivities and functionalities (Ku *et al*., 2008; Fink, 2005). Three reaction sequences should be considered in the preparation of traditional phenolic resins: the addition of formaldehyde to phenol, chain growth or formation of the pre-polymer (resin) and the cross-linking or curing reaction. There are basically three types of phenolic resins: traditional resoles, novolacs and the more recent polybenzoxazines (Ghosh *et al*., 2007).

The novolac phenolic resins can be obtained in a moderately acidic medium (pH 4–6) in the presence of divalent metal acetate catalysts (Ca, Mg, Zn, Cd, Pb, Cu, Co and Ni) or in a strongly acidic medium (pH 1–4). Novolac resins obtained in a moderately acidic medium have many *ortho–ortho* linkages and are known as 'high–*ortho* novolacs'. The accessibility of free *para* positions leads to a high curing rate in this resin (Knop and Pilato, 1985; Pilato, 2010a).

Novolac obtained in a strongly acidic medium is synthesized by reacting formaldehyde with a molar excess of phenol (1 mol of phenol to 0.75–0.85 mol of formaldehyde) (Fig. 2.2(a)). The most frequently used catalysts are

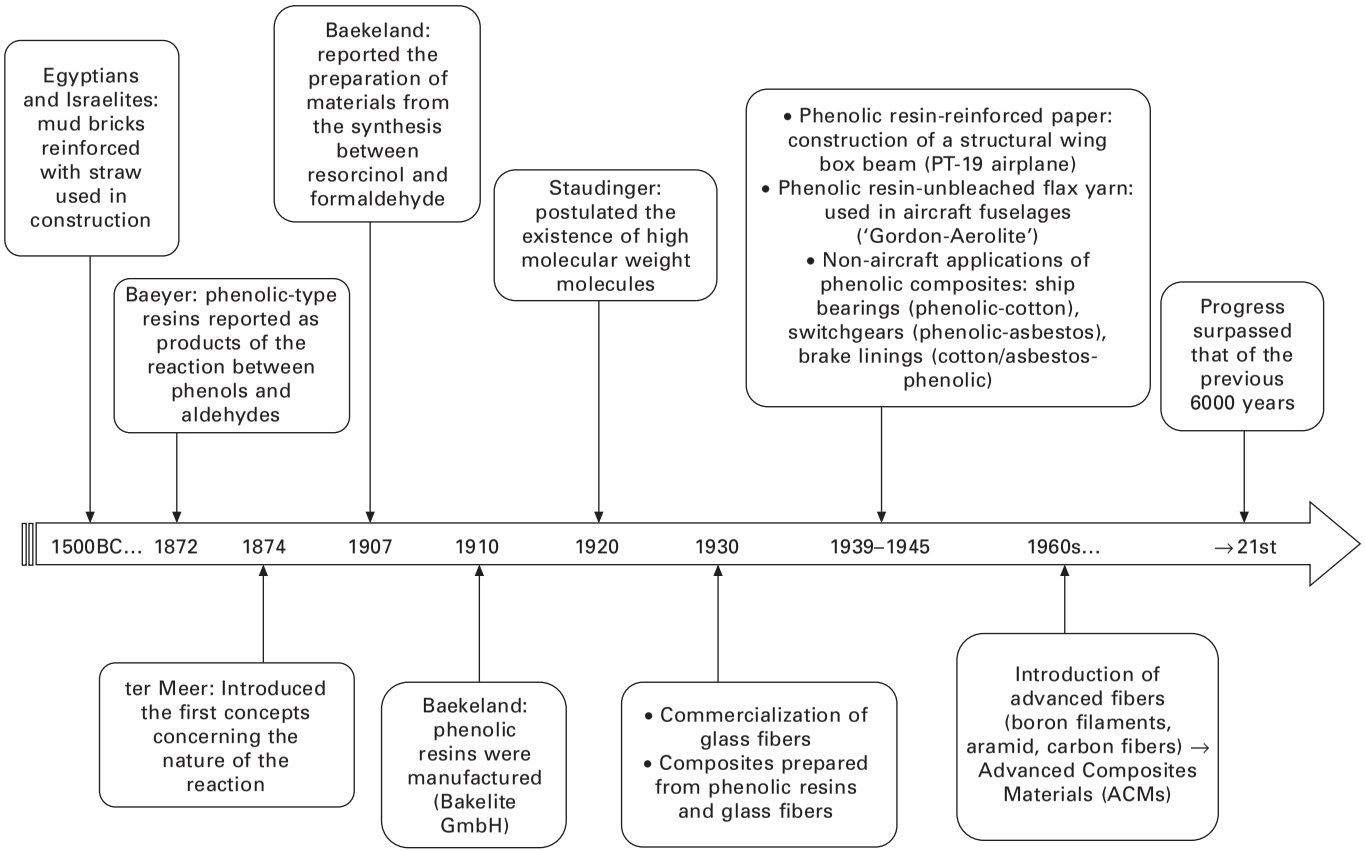

2.1 Phenolic resins and composites: Timeline of some key events.

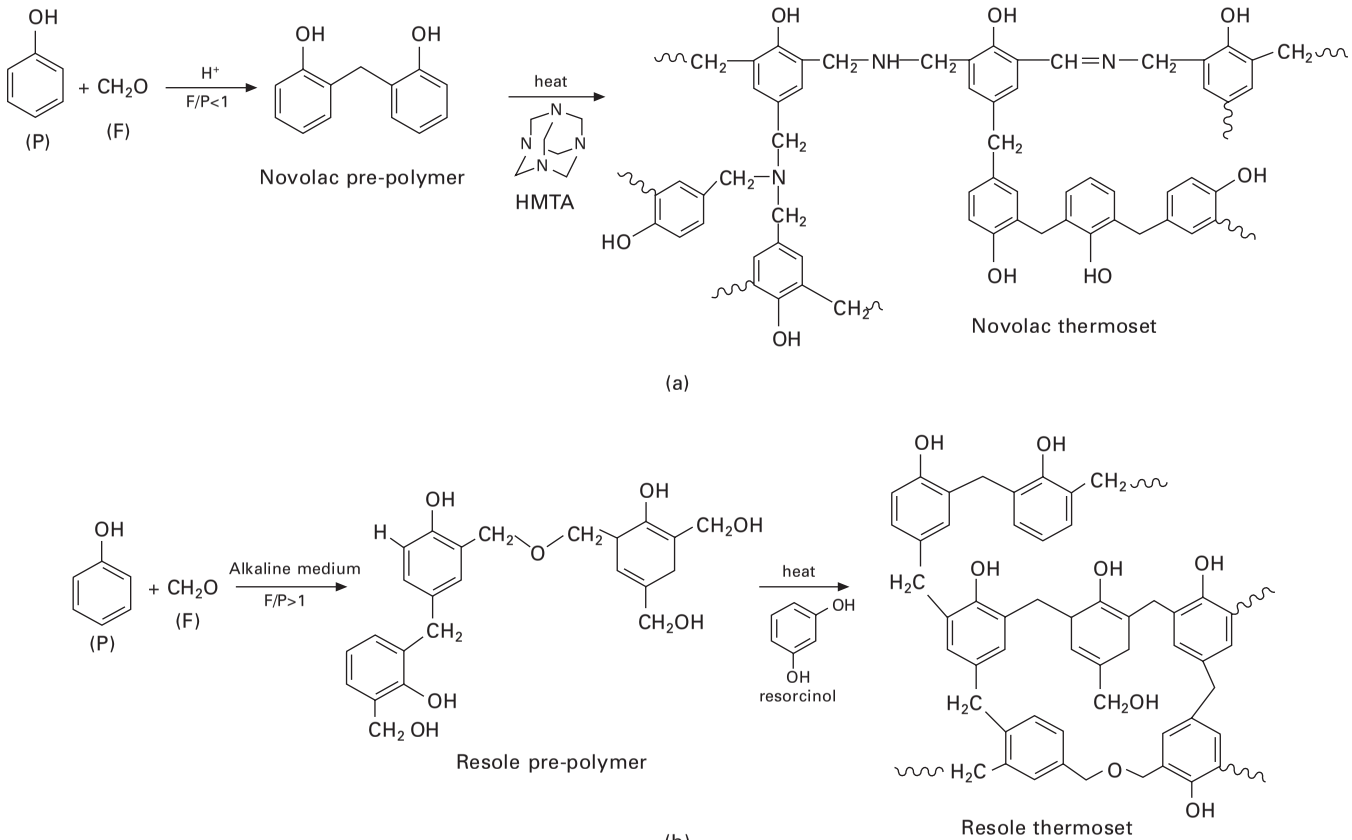

2.2 Schematic formation of (a) novolac thermoset and (b) resole thermoset (Pilato, 2010a).

oxalic acid, sulfuric acid and *p*-toluene sulfonic acid. The condensation products are linear or slightly branched, connected via methylene bridges. At room temperature, these products are brittle solids, fusible and soluble, i.e., thermoplastic. The curing reaction only occurs after the addition of a cross-linking agent that supplies formaldehyde, such as hexamethylene tetramine (HMTA) (Knop and Pilato, 1985; Peña *et al.*, 2006; Iyim, 2007; Ku *et al.*, 2008). Novolac is called a two-step resin because the HMTA must be added to cross-link the resin. Novolac cross-linking occurs between 120 and 180°C (Ku *et al.*, 2008).

The resole phenolic resin is obtained by reacting phenol with an excess of formaldehyde in an alkaline medium (Fig. 2.2(b)). The phenol:formaldehyde molar ratio in this reaction is generally between 1:1.2 and 1:3.0, generating oligomers in water with average molar masses between 600 and 1000 g mol^{-1}. Resole resin has a large number of reactive hydroxymethyl groups and is stable at room temperature, but upon heating it can be transformed into an insoluble and infusible three-dimensional cross-linked polymer. As the resole thermoset can be obtained by simple heating, resole is called a single-step resin (Knop and Pilato, 1985; Iyim, 2007; Ku *et al.*, 2008). Resole cross-linking can be accelerated using a cure accelerator such as resorcinol (10% based on phenol). Alternatively, the resole phenolic resin can be cured at room temperature by adding an acid catalyst, usually sulfonic acid (Ku *et al.*, 2008).

Benzoxazines are synthesized using phenol, formaldehyde and amine (aliphatic or aromatic) by employing solution or solventless methods (Ghosh *et al.*, 2007). The difference between benzoxazines and traditional phenolic resins is the connections between the phenolic moieties. Traditional phenolics are connected through methylene bridges, while benzoxazines are connected first through the formation of a cyclic structure from the phenolic hydroxyl to the *ortho* position (Fig. 2.3(i)), which rearranges to [–CH_2–NR–CH_2–] (Fig. 2.3(ii)) (Pilato, 2010a). The curing reaction of these materials does not require a strong acid catalyst or produce by-products (Frollini and Castellan, 2012).

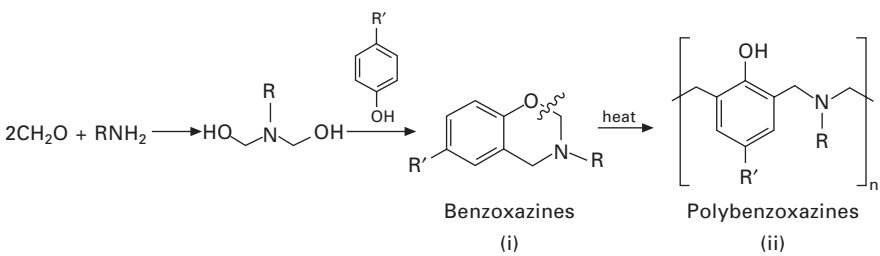

2.3 Schematic formation of polybenzoxazines (Ghosh *et al.,* 2007).

2.3 Phenols, aldehydes and other reagents

2.3.1 Phenols

Phenol is the monomer used in higher quantity in the production of phenolic resins. Phenol was initially derived from coal tar, but with the increased commercialization of phenolic resins, the demand for phenol grew significantly. Currently, the peroxidation of cumene is the predominant synthetic route for the production of phenol, accounting for over 90% of world production. In this process, cumene is oxidized with oxygen to produce cumene hydroperoxide. Subsequently, the peroxide is decomposed to phenol and acetone using a strong mineral acid as a catalyst (Fink, 2005; Weber and Weber, 2010). Cumene is in turn produced from the alkylation of benzene with propylene (Weber and Weber, 2010).

Phenol has unique chemical properties due to the presence of a hydroxyl group and an aromatic ring, which are complementary in that they facilitate both electrophilic and nucleophilic reactions. The aromatic ring of phenol is highly reactive towards electrophilic substitution, which assists its acid-catalyzed reaction with formaldehyde. Phenol is a weak acid and easily forms sodium phenoxide (NaPh) in a base-catalyzed medium. In the presence of sodium phenoxide, the nucleophilic addition of the phenolic aromatic ring to the carbonyl group of formaldehyde occurs. Thus, phenol can react with formaldehyde under acidic or basic conditions, leading to either novolac or resole resins (Weber and Weber, 2010).

The use of alkyl phenols such as cresol in phenolic resin production reduces reactivity, hardness, cross-linking density and color formation but increases solubility in non-polar solvents, flexibility, and compatibility with natural oils. At room temperature, *o*- and *p*-cresol are crystalline solids, while *m*-cresol is a viscous oil. Cresols are less soluble in water than phenol is (Weber and Weber, 2010). Approximately 60% of cresol is obtained from coal tar and crude oil using classical techniques such as distillation and liquid–liquid extraction. The remaining 40% is obtained synthetically by the alkylation of phenol with methanol (Fink, 2005). In addition to phenolic resins, cresols are also used in the production of herbicides, fungicides, disinfectants, plasticizers, epoxy resins and pharmaceuticals (Fink, 2005; Weber and Weber, 2010).

Xylenols are available in six isomeric forms, all of which are crystalline at room temperature. Xylenols can be obtained from the same natural sources as cresols and phenol. In addition to phenolic resins, xylenols are used in solvents and disinfectants (Weber and Weber, 2010).

Bisphenol-A (BPA) or 2,2-*bis*(4-hydroxyphenyl) propane is used to produce special phenolic resins for coating applications, but the main use of bisphenol-A is in the production of polycarbonates and epoxide resins (Knop and Pilato, 1985).

2.3.2 Aldehydes

Formaldehyde is the most frequently used aldehyde in the production of phenolic resins. At room temperature, it is a pungent, colorless, highly flammable gas. Formaldehyde is highly reactive and commonly commercialized in aqueous solution stabilized with methanol, where it predominantly forms adducts with the solvent, that is, equilibrium mixtures of methylene glycol, polyoxymethylene glycols and hemiformals of these glycols with methanol (Kowatsch, 2010; Fink, 2005).

Higher aldehydes react with phenol in the same manner but significantly more slowly than formaldehyde. The reaction is generally performed under strong acidic conditions to minimize aldol formation and in a water-free system by continuous aldehyde addition to the phenol melt.

Paraformaldehyde is a white, solid, low molecular weight polycondensation product of methylene glycol. Paraformaldehyde is used to prepare special resins with high solids content or to avoid distillation of wastewater (Knop and Pilato, 1985; Kowatsch, 2010).

2.4 Bio-based resins

The raw materials used in the production of phenolic resins (phenol and formaldehyde) are obtained on a large scale from non-renewable sources. Therefore, the substitution of these reagents by equivalent chemicals obtained from non-fossil sources is an interesting alternative from both economic and environmental perspectives (Razera and Frollini, 2004; Hoareau *et al*., 2006; Paiva and Frollini, 2006). Moreover, substituting formaldehyde with other aldehydes obtained from renewable sources could eliminate the potential emission of formaldehyde during the use of phenolic resins (Ramires *et al*., 2010a).

2.4.1 Lignophenolic and lignin–formaldehyde resins

Lignin is a biomacromolecule present in wood and non-wood plants that is highly branched and has a wide variety of functional groups that can act as active centers for chemical and biological interactions (El Mansouri and Salvadó, 2007). The great potential of lignin has not yet been well explored. Lignin is mainly burned as a fuel in pulping boilers (Stewart, 2008). Only a small amount of lignin sulfonates, by-products of the sulfite pulping process, are used as dispersants, oilfield drilling muds, concrete additives and adhesive extenders (Frollini and Castellan, 2012).

The saccharification and fermentation of sugarcane bagasse or other lignocellulosic fibers in biorefineries is a promising process for the production of bioethanol (Lacerda *et al*., 2012; Hernández-Salas *et al*., 2009), which

is used as both a pure fuel and a gasoline enhancer (Ewanick *et al*., 2007; Sánchez and Cardona, 2008). Lignin is a by-product of this process. Therefore, studies on new applications for this lignin are increasingly important (Ramires *et al*., 2010b; Cerrutti *et al*., 2012).

Lignin contains aliphatic and aromatic groups, with several substituted phenylpropane rings linked by different bonds such as carbon–carbon or ether bonds (Fengel and Wegener, 1989; Rowell and Han, 2000). The main units, guaiacyl (G), syringyl (S) and *p*-hydroxyphenyl (H), differ in the presence or absence of *ortho*-methoxyl groups in the aromatic rings (Ramires *et al*., 2010b) (Fig. 2.4). These phenolic aromatic rings can replace phenol in phenolic resins, making them environmentally and economically interesting alternatives to phenol–formaldehyde resins (Paiva and Frollini, 2006). The synthesis of lignin–formaldehyde resins primarily consists of hydroxymethylation. Lignin extracted from non-wood plants has more active centers towards formaldehyde than lignin extracted from wood due to the greater proportion of *p*-hydroxyphenyl units in aromatic rings (Hoareau *et al*., 2006). Electrophilic attacks can easily occur on the free *ortho* positions of these rings (related to the hydroxyl group) (Campana Filho *et al*., 1997; Hoareau *et al*., 2006), which increases their reactivity (Ramires *et al*., 2010b) (Fig. 2.4). Moreover, the lignin extracted by organosolv processes has superior thermal properties when compared to lignin obtained through kraft or sulfite processes (Doherty *et al*., 2007). Lignophenolic matrices (lignin–phenol–formaldehyde) reinforced with sugarcane bagasse (a biorefinery byproduct) have already been used to prepare fiberboards (Hoareau *et al*., 2006). A large amount of research is currently underway on composites reinforced with lignocellulosic fibers obtained from renewable sources (Ramires *et al*., 2010a, 2010b). These fibers can replace synthetic and/or poorly biodegradable fibers such as glass, aramid and carbon.

2.4.2 Tannin–phenolic resins

Tannins are considered polyphenols due to the large number of phenolic rings in their structures (Mosiewicki *et al*., 2007; Moubarik *et al*., 2009). These natural products can be found in certain plant tissues, such as bark, fruit and wood, and can be removed from these sources by extraction with water. Tannins are classified in two groups: hydrolyzable tannins and condensed tannins (Mueller-Harvey, 2001). The condensed tannins are flavonoids with complex structures (Fig. 2.5). The phenolic groups present in tannin enable this macromolecule to participate in the same reactions as phenol (Tondi and Pizzi, 2009). Condensed tannins are more suitable than the hydrolyzable type for use in the manufacture of a phenolic-type polymeric matrix due to the presence of phenolic rings with a greater number of free positions where the electrophilic attack can occur (Barbosa *et al*., 2010). The high reactivity of

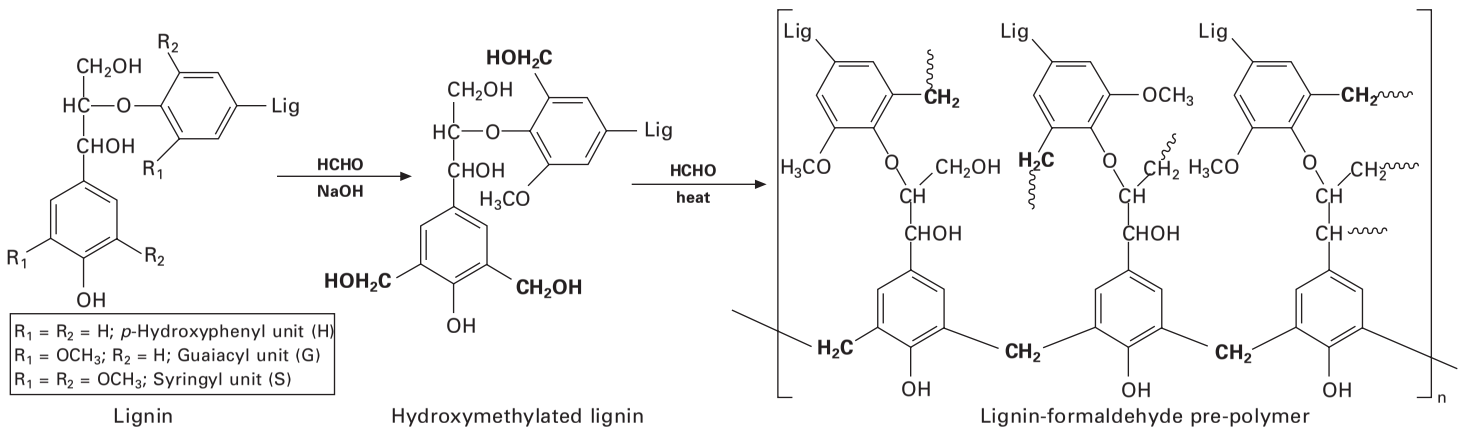

Lignin | Hydroxymethylated lignin | Lignin-formaldehyde pre-polymer

2.4 Main units in non-wood plant lignin and schematic representation of lignin–formaldehyde pre-polymers (Ramires *et al.*, 2010b; Malutan *et al.*, 2008).

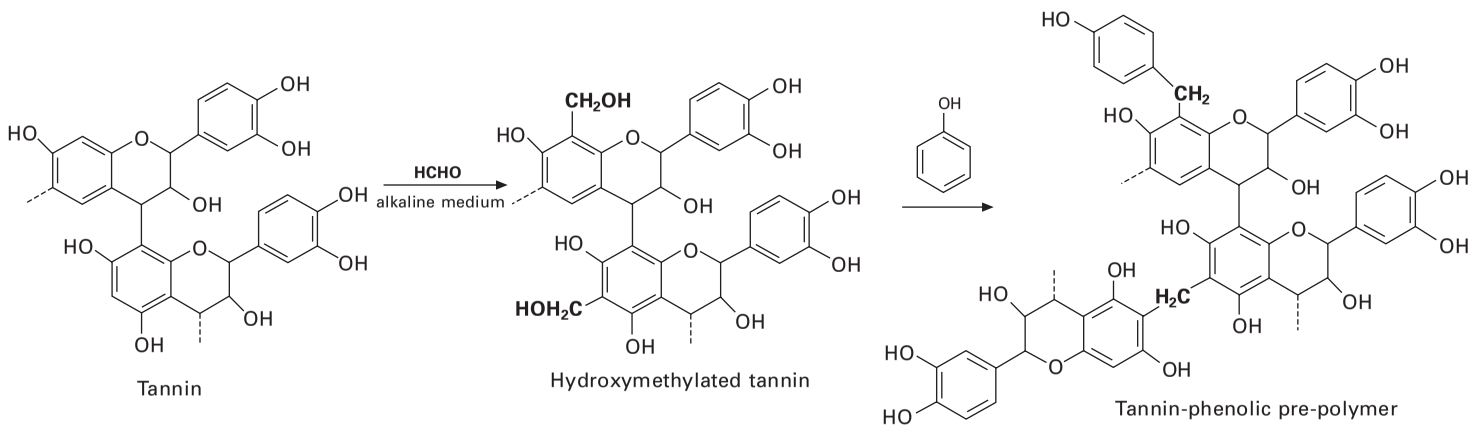

2.5 Schematic representation of condensed tannins and tannin–phenolic pre-polymers (Barbosa *et al.*, 2010; Ramires and Frollini, 2012).

most polyflavonoids towards the aldehydes, similar to that of resorcinol, is due to the presence of hydroxyl groups linked to the ring in both compounds and represents an advantage of condensed tannins over phenol. Therefore, condensed tannins show potential for use in the reaction with formaldehyde (Vázquez *et al*., 2006) (Fig. 2.5). Barbosa *et al*. (2010) reported the preparation of bio-based composites using tannin–phenol–formaldehyde resins reinforced by coir fibers. These composites showed intense fiber–matrix adhesion and high storage moduli, demonstrating improved properties when compared with the phenolic thermoset (without fibers). Ramires and Frollini (2012) prepared bio-based composites using tannin–phenol–formaldehyde matrices reinforced with sisal fibers. Inverse gas chromatography results showed that a tannin–phenolic thermoset had a dispersive component (γ_s^d) closer to sisal fibers than a phenolic (phenol–formaldehyde) thermoset, which suggests a better interfacial interaction between sisal fibers and the tannin–phenolic matrix. The impact strengths of tannin–phenolic composites reinforced with sisal fibers were higher than those of the composites reinforced with coir fibers due to the better tensile strength of sisal fibers compared to coir fibers. Lei *et al*. (2008) described tannin–lignin–glyoxal resins as adhesives for wood particulate boards. This substitution resulted in an adhesive with a total content of natural material up to 80 wt%. This resin demonstrated good adhesive properties with sufficiently strong internal bonds to meet international standard specifications for interior-grade panels.

2.4.3 Cardanol-based resins

Cardanol, a component of the agricultural by-product cashew nut shell liquid, also has a phenolic nature and can react with aldehydes under several conditions (Raqueza *et al*., 2010). Phenolic-type resins based on cardanol have been investigated for such applications as civil engineering structures (Cardona *et al*., 2010).

Cardanol has also been used in benzoxazine-type resins prepared from cardanol-based monobenzoxazine monomer, which in turn was produced by the reaction of cardanol with ammonia and formaldehyde (Calo *et al*., 2007), or from a monofunctional benzoxazine monomer synthesized by the condensation of aniline and formaldehyde with cardanol (Rao and Palanisamy, 2011).

2.4.4 Glyoxal–phenolic resins

Glyoxal (OHC–CHO) is a dialdehyde that can be obtained from several natural sources, such as from the oxidation of lipids or as a by-product of biological processes (Hirayama *et al*., 1984). The low vapor tension of the glyoxal solution and its low toxicity are some of the advantages of using

glyoxal instead of formaldehyde (Mattioda *et al.*, 1982). The two adjacent carbonyl groups make glyoxal highly reactive. Glyoxal is already used as a formaldehyde substitute in wood adhesive applications (Ballerini *et al.*, 2005; El Mansouri *et al.*, 2007a, 2007b). Glyoxal was also used to prepare glyoxal–phenolic pre-polymers in alkaline conditions to make composites reinforced with sisal fibers (Ramires *et al.*, 2010a). Some molecular structures of the resins have been proposed based on NMR analyses (Fig. 2.6). Regardless of the cure cycle used, the reinforcement of thermosets by 30% (w/w) sisal fibers improved the impact strength by one order of magnitude. Limiting the curing temperature to 150°C, the composites displayed good adhesion between the resin and the sisal fibers in addition to excellent dynamic–mechanical properties (Ramires *et al.*, 2010a).

2.5 Composites from phenolic-type matrices

Thermosets such as phenolic thermosets are brittle at room temperature and usually have poor mechanical properties. However, due to the presence of cross-links, thermosets can be used at higher temperatures, as they have higher softening temperatures and better creep properties than thermoplastics. Thermosets are also usually more resistant to chemical attack than most thermoplastics, among other characteristics (Paiva and Frollini, 2000). In applications where good mechanical properties are required in addition to these intrinsic properties of thermosets, the thermosets can be combined with reinforcements to improve these properties.

Composites based on thermoset matrices can substitute for steel and concrete in some applications of civil construction structures because they usually exhibit a higher resistance to oxidation than steel and better freeze–thaw resistance than concrete, potentially leading to structural components with improved weathering. One of the drawbacks to the application of organic materials in construction is their high combustibility. This disadvantage can be bypassed using phenolic-type resins to fabricate the composite, for

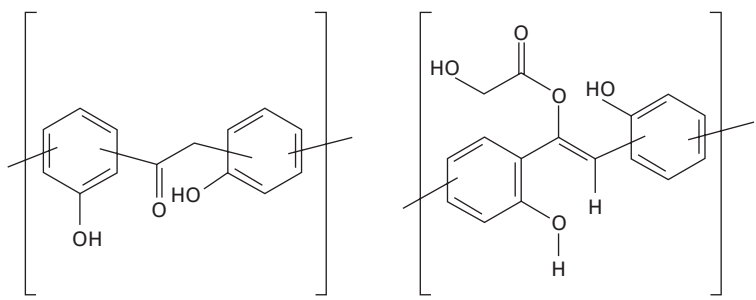

2.6 Structure of glyoxal–phenol oligomers supported by NMR data (Ramires *et al.,* 2010a).

example, which are widely used commercially due to their excellent flame-retardant properties as well as their low cost (Tyberg *et al.*, 1999; Frollini *et al.*, 2004).

Phenolic resins have been chosen for use in the production of thermoset composites for several reasons besides cost. Phenolics meet the specifications for fiber-reinforced composites used in applications that require fire, smoke and toxicity (FST) characteristics, such as in aircraft, interior panels, materials used in tunnels, and fire safety components (Pilato *et al.*, 2008). Mass transit, marine, offshore and construction materials all require fire-resistant and high-temperature-resistant components. Moldings and laminates based on phenolics have been used in these areas due to their considerable resistance to burning and because they produce minimal smoke and toxic fumes in a fire. Phenolic composites can be produced with complex shapes, and with careful design, materials can be obtained with high strength and stiffness and excellent impact strength, making these materials alternatives to metals in the rail, offshore and construction industries (Willson, 2003).

Fillers and reinforcements are usually combined in the preparation of phenolic composites. For example, the organic filler fibrous wood flour can be combined with powdered mineral fillers to modify the hardness and surface characteristics of the composite. When the molding is exposed to continuous thermal stress, in addition to an organic filler, siliceous, carbonaceous, or similar inorganic fillers are used, and mica fillers are usually the materials of choice when the insulating power is critical (Gardziella *et al.*, 2000). These examples show that the fillers are commonly used to address a specific characteristic required for a given application. Reinforcements, in turn, are usually chosen to improve the mechanical properties of the phenolic thermoset, particularly the impact strength.

2.5.1 Fabrication processes

Composites based on phenolic resins present flexibility as regards processing, and most of the conventional processes can be used to prepare such composites.

At first, the fabrication processes can be divided into three broad categories, based on considerations on both cost and performance criteria for a given application. However, certain restrictions should be considered in this categorization, since limitations may arise due to availability of both fibers and resins that are compatible with each other, as well as with the processing itself. In this context, commodity-based composites are usually processed via hand lay-up; pultrusion and filament winding have been applied in the manufacture of high-performance composites, where properties and specific shapes are required. Fibers continuous and oriented along a specific direction are usually required for manufacturing advanced composites, where typically

the molding prepreg is the process of choice (Taylor, 2010). Complex parts have been manufactured through resin transfer molding (RTM), using low-viscosity phenolic resins. These processes have been described in texts addressed to phenolic resins, such as in Taylor (2010) and Gardziella *et al.* (2000, Chapter 6).

2.6 Reinforcements

When a composite experiences a certain force, the matrix transfers the load to the reinforcement through the interface. The main function of the reinforcing agent is to carry the load along its length. The properties of short fiber composites are strongly influenced by the aspect ratio (length/diameter) of the fiber and their orientation and fraction. The criteria used to select the type, amount, length, orientation and other properties of the reinforcement depend on the matrix characteristics and the intended application.

2.6.1 Macroscale reinforcements

Macroscale reinforcements and composites have thus far received the most investigation and application. The remarkable advances in the development of these polymeric matrices composites in the twentieth century have made these materials prominent, which is expected to continue despite advances in smaller-scale, mainly nanometric, reinforcements.

Glass fibers are widely used to reinforce phenolic composites, can be produced as continuous strands or filaments with different diameters, and are available in different compositions such as E-, C- and S-glass, which are characterized by different specific properties (Frollini and Castellan, 2012). Compared to other glass composites, phenolic-glass composites have low flammability and good fire resistance, produce much less smoke, and less carbon monoxide when they are thermally degraded. These characteristics have led phenolic-glass fibers to become the composites of choice for use in the cabin interiors of wide-bodied passenger aircraft, as well as in ceiling panels, structural flooring and overhead stowage bins (Mouritz, 2006).

Glass fibers with tailored properties have been developed to meet specific applications, with some designed to be compatible with military specifications for ballistic performance (Taylor, 2010).

Phenolic composites can positively impact the building and construction industry by improving safety and reducing cost. Phenolic/glass laminates are important alternatives for construction applications due to properties such as the availability of several processing techniques, allowing a significant degree of design freedom; the inherent fire resistance of the material, eliminating the need for mineral additives and thus reducing the total weight; and the reduced risk of the spread of fire due to fire-resistant properties and the

lower thermal conductivity of phenolic-glass compared to metals (Forsdyke, 2002).

Carbon fibers (CF) can be produced in different forms, for instance as mats, continuous filament tows, and chopped fibers. CF can be prepared from organic precursors (cellulose, pitch, polyacrylonitrile (PAN), some phenolic fibers) by controlling their pyrolysis. The properties of CF such as low weight, high strength and high modulus, fatigue resistance and vibration damping, corrosion resistance, good friction and wear qualities, low thermal expansion, and thermal and electrical conductivity are highly attractive for the aerospace industry; in fact, the requirements of this sector played a major role in stimulating the development of these fibers (Choi *et al.*, 2000; Frollini and Castellan, 2012). However, the unique properties of these fibers have led to their applications in other segments, and since the 1970s and 1980s CF have been used in sporting and leisure goods such as fishing rods, golf club shafts and tennis rackets (Ogawa, 2000).

Concerns that have emerged from the last decades of the twentieth century relating to safety and environmental issues have led to further expansion of the applications of CF, including the production of natural gas tanks for vehicles due to their low carbon dioxide emissions and clean exhaust gas, and blades for wind-power generators (Ogawa, 2000).

Safety concerns have led to the use of CF-reinforced plastics (CFRP) and CF-reinforced concrete (CFR-concrete) as earthquake-resistant materials. In this area of application, CF-reinforced wood (CFRWood) may be useful in architecture because of its effectiveness in reducing carbon dioxide emissions and promoting environmental conservation. Investigations on CFRWood and PAN-based CF occurred almost simultaneously. One example is the development of CF-reinforced glued laminated timber (CFR-glulam) composed of wood, a phenolic-type resin and a CF composite sheet. Aside from good wettability for CF, the phenolic-type resin developed for this application exhibited reactivity towards the functional groups present at the CF surface. In addition, as both the CF-phenolic composite sheet and wood are rich in OH groups, the adhesion between the two is favored, and conventional resins can be used to glue them together. This type of material can be used as a board reinforcement material and for repairing house and bridge components (Ogawa, 2000).

Structural profiles based on FRP composites are produced for use in the construction industry for building and bridge superstructure applications (Bakis *et al.*, 2002). Pultrusion process is the manufacturing method of choice for this application due to product consistency and economic considerations. Pultrusion produces continuous sections of unidirectionally reinforced composites and supplies thick-walled structural components for marine, civil engineering and high-rise construction applications (Gardziella *et al.*, 2000). Phenolics are used as thermosetting resins in the pultrusion process,

along with polyesters and epoxy materials. CF fiber bundles (tows), glass fiber bundles (rovings), continuous strand mats, and nonwoven surfacing veils are used as reinforcements (Bakis *et al.*, 2002).

Phenolic composites reinforced with CF are also used for load-bearing materials. Phenolics have good resistance to seizure and work well with steel or bronze journals when lubricants such as oil or water are used. In these applications, the low thermal conductivity of phenolics is overcome by the presence of CF because the phenolic thermoset usually has a thermal conductivity of approximately 0.35 W/m K, i.e., approximately 1/150 that of steel, which may lead to bearing failure by charring (Kim *et al.*, 2009).

Aramid fibers are highly oriented fibers derived from aromatic polyamides, with Kevlar and Nomex as two prominent examples. The woven fabric of aramids combined with phenolic resins produces high-performance composites for ballistic applications, where the projectile energy is mainly absorbed by the fiber with a high strength and modulus (Gardziella *et al.*, 2000).

Fiber-reinforced composites have high stiffness-to-weight ratios, but this ratio may be increased if, instead of a monolithic structure, two thin composite facesheets of the same weight (for example, plastics reinforced with phenolic glass or carbon fibers), separated by a cellular core, are used. A phenolic resin-impregnated aramid paper honeycomb (Nomex honeycomb) is commonly used in the core structure. These structures are appropriate for applications in which weight reduction and fire safety are critical, such as in ground and air transportation.

Thermosetting phenolic resins are used in combination with other components as friction materials for brake systems. The design of such systems should account for the need to maintain a stable and reliable friction force under a variety of conditions, such as wide ranges of pedal pressure, vehicle speed, temperature and humidity. Fibers correspond to one of the ingredients and are used as reinforcement. Aramid pulp performs well as a reinforcement fiber in such systems because of its good filler retention, leading to enhanced wear resistance and friction stability (Kim and Jang, 2000).

The search for alternatives to raw materials derived from fossil fuels has accelerated in recent decades and has reached the area of polymer matrix composites. In the case of phenolic matrices, several alternatives have been considered, particularly for the phenolic component.

Regarding reinforcements, interest has re-emerged in recent decades around cellulosic and lignocellulosic fibers, which were used in early phenolic applications. Phenolic resins are used as adhesives for binding wood in different composites, such as panels, molded products and engineering lumber materials (Gardziella *et al.*, 2000). Phenolics are also stabilized binders for cotton or other cellulosic fibers for the production of interior automotive parts as well as insulating or damping materials (Schuh and Gayer, 1997).

Fibers such as sisal (Megiatto Jr. *et al*., 2009; Ramires *et al*., 2010a, 2010b), sugarcane bagasse (Hoareau *et al*., 2006; Trindade *et al*., 2004), coconut (Barbosa *et al*., 2010) and curaua (Trindade *et al*., 2005) have been used as reinforcements of phenolic-type matrices.

2.6.2 Micro- and nanoscale reinforcements

The application of microscale reinforcements in phenolic matrices has not yet been well explored. Cellulosic-type reinforcements in varied processes have proven to be suitable for this purpose. The separation of bundles of filaments during processing can lead to reinforcements with microscale diameters as was observed for phenolic matrices reinforced with cellulosic textile fibers. Reinforcement with microscale diameter resulted from the excellent impregnation of the yarn by the liquid phenolic resin, in the first stage of preparation of the composite, that split the yarn (Silva *et al*., 2012). Composites prepared from phenolic-type matrices reinforced with microcrystalline cellulose (MCC, 30–70 wt%) have exhibited excellent water-barrier properties. Despite the high hydrophilicity of cellulose, the high crystallinity of MCC hinders the entry of water into the material, which has led to a water absorption similar to that of neat thermoset (Ramires *et al*., 2010c). Surface microfibrillation of cellulose fiber improved cellulose fiber/phenolic resin interfacial adhesion in hybrid composites based on sisal and aramid fibers (Zhong *et al*., 2011).

The boom that has occurred in investigations on nano-reinforced composites is still focused on thermoplastic rather than thermoset matrices.

Nanoscale reinforcements have inherent properties that lead to different properties than other reinforcements, such as high aspect ratios. However, for the potential of these nanomaterials as reinforcements to be realized, particular challenges must be met. For example, these nanomaterials must be homogeneously dispersed in the matrix and the adhesion at the interface must allow an efficient transfer of stress from the matrix to the reinforcement. If these and other drawbacks are not overcome, disappointing results can be observed, mainly when compared to advanced composites reinforced with high-performance continuous fibers (Dzenis, 2008) .

The polar groups present in phenolics favor interactions with nanoclays, meaning that this material can be used as a reinforcement of phenolic-type matrices without any modification (Zhou *et al*., 2008; Frollini and Castellan, 2012). These polymer-layered silicate nanocomposites can exhibit improved properties including light weight, dimensional stability, heat resistance, high stiffness, barrier properties, and toughness and strength, due to the nanoscale dispersion and the high aspect ratios of the inorganic clays (Zhou *et al*., 2008).

Carbon nanotubes (CNTs), discovered in 1991 by Iijima, are unique

nanostructured materials with outstanding properties. The chemical composition of CNTs is similar to that of graphite, but they have a unique topology because they are highly isotropic. CNTs can be composed of individual cylinders of 1–2 nm diameter (single-walled nanotubes, SWNTs) or a collection of several concentric graphene cylinders (multi-walled nanotubes, MWNTs) (Breuer and Sundararaj, 2004).

Despite the exceptional intrinsic properties of CNTs, CNT-reinforced composites may exhibit worse properties than expected. The surface properties of CNTs may affect their dispersion within the matrix, and the van der Waals interactions between the nanotubes may lead to bundles that may fail at stresses below the intrinsic capabilities of a single nanotube, necessitating the tailoring of CNTs to each particular application (Breuer and Sundararaj, 2004). Studies have been developed in which CNTs grow on different substrates, such as carbon fibers, carbon felt/mat, carbon cloth and graphite foil. However, these studies have mainly focused on achieving aligned growth of CNTs for applications such as high-performance capacitors and field-emitting electron sources rather than structural materials. Mathur *et al*. (2008) have grown CNTs using substrates with unidirectional (UD), bidirectional (2D) and three-dimensional (3D) carbon fiber (CF) networks. A profuse growth of MWNTs on these substrates was observed, and the obtained hybrid preforms were used as reinforcements of a phenolic resin matrix to form CF–CNT hybrid composites, with mechanical properties increasing along with the number of deposited carbon nanotubes (Mathur *et al*., 2008).

MWNTs have been used as dispersed CNTs and network CNTs as reinforcements of phenolic matrices. Composite phenolic-dispersed CNTs were fabricated through the melt mixing method, which may lead to the agglomeration of CNTs in the matrix and introduce defects in composites. The infiltration of the resin into the network CNT generated composites with better mechanical properties when compared to the dispersed CNTs because the CNTs in the network are longer and contain fewer agglomerates and defects (Tai *et al*., 2004).

Ablation resistance is an important property of composites, with thinner ablative structures desired to reduce the overall weight of aerospace systems. Phenolic resins easily char during endothermic pyrolysis, leading to the application of phenolic composites as ablative materials for rocket nozzles (Srikanth *et al*., 2010). A phenolic matrix with a high content of carbon nanofibers (CNFs) was demonstrated to be highly appropriate for rocket nozzle applications (Yoonessi *et al*., 2008).

The formation of aggregates from CNFs affects their dispersion in resins, potentially leading to poor mechanical properties. Thus, it is mandatory to at least minimize the formation of these aggregates, which can be achieved by modifying the CNF surface. Functional groups such as esters, anhydrides

and phenolic hydroxyls can be introduced on the surface of CNFs through oxidation reactions. The presence of such polar groups on the CNF surface strengthens the interactions between the nanofibers and phenolic resins, which in turn favors the disaggregation and dispersion of fibers in the resin (Yoonessi *et al.*, 2008).

Cellulose nanowhiskers (CNWs) are bio-based reinforcements with the intrinsic properties of reinforcements at the nanoscale (including large aspect ratios and high specific surface areas). However, for these highly desirable reinforcement characteristics to be translated into good composite properties, good dispersion of the CNWs in the polymer is necessary to allow the formation of a stiff percolating network by hydrogen bonds, in turn increasing the stiffness. As observed for other nano-reinforcements, the development of composites based on CNWs has mainly focused on thermoplastic matrices. Phenolic composites reinforced by CNWs have been fabricated as films through *in situ* polycondensation and curing of phenolic resins with CNWs. Good dispersion of CNWs in phenolic resins has been achieved following the exchange of water by DMF, with a rapid development of turbidity observed after storage of the aqueous phenolic resin/CNW dispersions at 0°C; good dispersion was also observed in the cured material. CNWs have shown moderate reinforcement of the phenolic matrix (Liu and Laborie, 2011).

2.7 Interfaces and voids

2.7.1 Interfaces

When a polymer and a reinforcement are mixed, interactions between these two distinct chemical components require the existence of contact areas (*interfaces*) between the two components. The larger the area, the greater the probability of physical, chemical or physical–chemical interactions occurring between the two components (Yosomiya, 1990). In addition to the dependence on the extension of the contact area, interactions between the dispersed phase and the matrix phase at the interface also depend on the affinity between the components. A load can only be carried by a reinforcement if it is transferred to the reinforcement through the interface. The mechanical properties of composites thus depend on the chemical and physical properties of their constituents as well as their configuration (Frollini *et al.*, 2004).

The chemical structures of phenolic resins consist of low-polarity groups, such as aromatic rings, and highly polar groups, such as hydroxyls (Figs 2.2 and 2.3), allowing for favorable interactions with a range of reinforcements. This structural feature, coupled with the low viscosity in the temperature range in which composites are usually prepared, allow phenolic resins to wet the reinforcements, which in turn allows for cross-linking through the

reinforcement. These important characteristics contribute to the achievement of good adhesion at the matrix–reinforcement interface.

Lignocellulosic fibers are mainly composed of cellulose, hemicellulose (or polioses) and lignin, which correspond to macromolecules with chemical structures rich in hydroxyl groups; lignin also has phenolic-type aromatic rings in its structure. The similarities between the structural characteristics of phenolic resins and lignocellulosic fibers lead to a high affinity between them, favoring strong interactions at the fiber–matrix interface. Most of the polymeric matrices used in both thermoplastic and thermoset composites have a lower structural compatibility with lignocellulosic fibers than phenolics. Moreover, the processing of phenolic thermosetting resins takes place at temperatures below 200°C, and the thermal decomposition of lignocellulosic fibers occurs above 200°C, which means that the fiber is thermally preserved during processing, which is not always observed in processing involving other polymers and lignocellulosic fibers (Frollini *et al.*, 2004; Frollini and Castellan, 2012).

Despite the compatibility among phenolic resins and some reinforcements, it is sometimes necessary to introduce modifications to improve adhesion at the interface.

The adhesion between aramid fibers and resins is usually poor, mainly due to their high crystallinity. Treatment with cold plasma improved the interfacial adhesion between Kevlar fabric and phenolic resin (Guo *et al.*, 2009; Frollini and Castellan, 2012).

The oxidation of CFs introduces hydroxyl groups at their surfaces, improving the interactions at the fiber–matrix interface. Other groups can also be introduced depending on the reagents used. The hydroxylated surface of CF has been treated with glutaraldehyde, a dialdehyde, producing hemiacetal-type groups. The bifunctionality of the aldehyde used as a reagent allows for a reaction between the group on the surface of the CF and sites present in the structure of phenolic resins. In this case, the reinforcement and matrix have been chemically linked, and glutaraldehyde has acted as a coupling agent, resulting in better mechanical properties (Choi *et al.*, 2000).

2.7.2 Voids

In addition to the search for conditions that produce a good interface for phenolic composites, other issues must be addressed to ensure that the end material has the desired properties. One critical factor is the identification of conditions that minimize or, preferably, eliminate the presence of voids.

Phenolic resins such as resol-type resins generate water and formaldehyde during curing as by-products of condensation reactions. Hexamethylenetetramine (HMTA) can be used as a source of formaldehyde for curing novolac-type resins, producing formaldehyde and ammonia as by-products. During curing,

these small molecules can be released as volatiles, resulting in networks with a substantial content of voids that negatively affect the mechanical properties of the end material. In addition, the presence of voids usually increases the moisture/water uptake of composites. In this context, volatile control is critical in the production of fiber-reinforced phenolic resin matrix composites to ensure end materials with good properties. The control of voids can be achieved by introducing changes in processing or using new formulations, among other approaches.

Volatile control is crucial for the production of void-free phenolic-type laminates. A commercial vacuum-bag moldable phenolic prepreg system was used to test two types of vacuum-bag (VB) processes, namely single- (SVB) and double- (DVB) vacuum-bag processes. The DVB process enabled better control of volatiles, with the point of application of vacuum pressure selected to avoid excessive extravasation of resin to achieve the target resin content in the final consolidated laminate parts. Void-free quality parts have been produced using the DVB process, which exhibited improved mechanical properties compared to the parts produced by the SVB process (Hou *et al.*, 2006).

In some applications of phenolics such as in the inner lining of multilayered composites in fire-critical applications, besides the water produced as a by-product during the curing reaction, the starting material may contain water as a diluent to control the viscosity and thus facilitate injection and mold filling. The use of water as a diluent leads to the volatilization of a large number of water molecules. This problem has been addressed by substituting water with ethylene glycol, which confers low viscosity to the resin and can also act as both a plasticizer and a reagent. In the latter case, ethylene glycol is introduced to the thermoset network through the curing. This substitution has led to a decrease in void content and to an increase in density, thus leading to a final product with improved mechanical properties (Singh and Palmese, 2004).

For some applications, it is crucial to identify conditions that minimize moisture uptake, as moisture can degrade both the matrix and the fibers. An E-glass–phenolic FRP system has been used as a reinforcement of glulam (glued-laminated timber) beams, which can be applied for building and bridge construction. The reinforcement was designed and fabricated to be compatible with wood adhesives such as phenol-resorcinol-formaldehyde, leading to features such as a layered formulation and a graded void content. The moisture uptake in this case has been controlled by applying a primer to the FRP surface, filling the large voids and reducing the moisture uptake of the material compared to the unprimed material (Battles *et al.*, 2000).

The substitution of HMTA, normally used to cure novolac-type resins, with epoxies has reduced void content. To retain the fire-retardant properties of phenolics, a network was formed with a higher phenol than epoxy content,

leading to a void-free system. Composites prepared from the phenolic/epoxy resins and reinforced with unidirectional CF exhibited superior mechanical properties compared to the epoxy control (Tyberg *et al*., 2000).

Application of higher molding pressures at the gel point of a resol-type phenolic resin led to a reduction of voids in the matrix, improving the impact strength, as observed by Megiatto Jr. *et al*. (2009) in phenolic composites reinforced with sisal fiber.

The use of matrices based on benzoxazine (BZ) type resins should grow significantly because the curing of BZs occurs without the release of volatiles, potentially leading to the production of void-free composites. BZ thermosets exhibit low water absorption, low flammability (high char yield), high stiffness, and excellent dimensional stability. Composites based on BZs are promising matrix materials for composites in future aerospace applications due to their unique properties (Pilato, 2010b; Grishchuk *et al*., 2011).

2.8 Mechanical properties

Mechanical properties are critical for many composite applications. The properties of the composites depend on the combination of the properties of the matrix and the reinforcing agent or fiber. The properties of polymer composites reinforced with short fibers depend on such factors as the fiber/matrix interaction, the orientation and volume fraction of the fiber, the fiber aspect ratio (defined as L/d where L and d correspond to the fiber length and diameter, respectively) (Chawla, 1998) and processing conditions (Thomas and Pothan, 2008). Different tests can be used to evaluate the mechanical properties of the composites, such as tensile, flexural or impact resistance tests (Izod or Charpy tests).

The impact test evaluates the improvement of the thermoset properties (classified as fragile) compared to composites reinforced with fibers (synthetic or natural fibers) or thermoplastic materials (Chawla, 1998).

Thermoset materials are brittle, and most of the time it is impossible to perform mechanical tests such as strength, flexural or traction tests. The phenolic thermoset exhibits impact strength values of approximately 12 J m^{-1} (Trindade *et al*., 2004). Other thermosets based on lignin–formaldehyde, lignin–phenol–formaldehyde (Ramires *et al*., 2010b) and tannin-phenol-formaldehyde resins (Ramires and Frollini, 2012; Barbosa *et al*., 2010) were found to be as brittle as the phenolic thermoset. The reinforcement of phenolic thermoset matrices using natural or synthetic fibers improves the impact strength of the obtained composites, with the improvement depending on the type of fiber used (Ma *et al*., 1998; Kumar *et al*., 2009).

Kumar *et al*. (2009) investigated the tensile and flexural properties of phenolic composites reinforced with coir and glass fibers. The best tensile

and flexural strength results were obtained for composites prepared with fibers 20 mm in length and with 1:2 coir:glass fiber volume ratios.

Mathur *et al*. (2010) used multi-walled carbon nanotubes (MWCNTs) to reinforce phenolic resins using both the wet and dry dispersion techniques before molding. The phenolic composites reinforced with 5% MWCNTs exhibited a flexural strength 158% higher than those of neat phenolic thermosets.

Da-Peng and Hong (2008) prepared phenolic composites reinforced with glass fibers using four different matrices: a pure resol resin, a pure novolac resin, a blend with 50% resol and 50% novolac resins, and a blend with 47.5% resol, 47.5% novolac and 5% HMTA. The impact strength, flexural strength and flexural moduli of both blends were higher than those of novolac and resol composites, and the blends exhibited better adhesion and wetting properties with glass fibers. These authors also found that the cross-linking density and the interfacial bonds between glass fibers and the matrices could be increased by postcuring, leading to an increase in the mechanical properties of the composites.

Ma *et al*. (1998) prepared composites of phenolic matrices reinforced with pultruded glass fibers (fibers prepared by continuous extrusion). Poly(ethyleneoxide) (PEO) was also added to improve the mechanical properties of phenolic composites. The soft segment of PEO absorbs the loads in the network of the brittle phenolic matrix, improving the mechanical properties of the composites up to 6 wt% PEO.

Wang *et al*. (1999) prepared glass fiber-reinforced novolac-type phenolic composites modified with polyamide (PA-6 and PA-6.6). The results showed that the interface between the matrix and glass fibers was improved due to the hydrogen-bonding ability of the polyamide chain. The loads applied during mechanical tests could be absorbed by the soft segment of polyamide, which led to an increase in impact strength (approximately 50%) and flexural modulus (approximately 10%), with a maximum polyamide content of 7 wt%.

The same fiber in different phenol-type matrices can lead to different impact strengths, with the lignin–formaldehyde composite–sisal fiber exhibiting an impact strength approximately 17% higher (Ramires *et al*., 2010b) than that of the phenolic composite–sisal fiber prepared using the same conditions (Megiatto *et al*., 2008). The presence of lignin moieties in both the fiber and matrix favors interactions at the fiber/matrix interface, improving the mechanical properties of the composites.

Chemical or physical treatments can be applied to natural fibers to modify their surface (polar groups) and/or their composition (lignin, cellulose and hemicellulose content). Several treatments may enhance the interaction between the phenolic matrix and natural fibers, such as mercerization, succinic anhydride, ionized air, and others (Leão, 1997; Mu *et al*., 2009; Trindade *et al*., 2008). Barreto *et al*. (2010) prepared composites of a phenolic matrix,

formaldehyde-CNSL (cashew nut shell liquid), reinforced with jute fiber blanket with and without NaOH treatment (5% and 10%). The composites prepared with jute fibers treated with 5% NaOH had better mechanical properties because the NaOH treatment removed components of the surface fibers, leading to greater stabilization of the matrix–fiber bonding. Treatment with NaOH solutions up to 5% led to the dissolution of hemicellulose, lignin and pectin components, which made the fibers more brittle and consequently decreased the mechanical resistance of the composites.

Cardona *et al*. (2012) proposed modifications with cardanol to prepare a phenolic resin (cardanol–phenol–formaldehyde resin) for possible application in laminates and composites in civil engineering structures, resulting in more flexible and tougher materials. Increased proportions of cardanol led to materials that were less brittle and more flexible. Besides, the fracture toughness increased with increasing cardanol content in the resin, which is attributed to a greater level of flexibility in the thermoset and greater spatial rearrangement due to the aliphatic side chain of the cardanol. The authors also used polypropylene glycol (20% w/w) as a plasticizer, improving the flexural strain, stress and fracture toughness values.

Polybenzoxazines are a new class of thermosetting phenolic resin. These materials have received attention due to their highly desirable properties, such as low cost, good thermal stability, good flame retardance and low water absorption (Ghosh *et al*., 2007). Xu (2012) prepared composites based on polybenzoxazine resin (*bis*-benzoxazine: B-BOZ) reinforced with glass fiber. B-BOZ shows a high thermal stability and excellent mechanical properties. Modification of B-BOZ with hyperbranched polyborate (HBPB) improved the flexural strength and interlaminar shear strength of the composites. The flexural strength and flexural modulus of the glass/B-BOZ increased up to 21.6% with the addition of HBPB (10 wt%). This modification did not changed the glass transition temperature (T_g) and the viscosity of the resin, because of the good compatibility between HBPB and B-BOZ.

2.9 Thermal properties

2.9.1 Thermal analyses

The more common techniques used to analyze thermosets and composites are thermogravimetric analysis (TGA) and differential scanning calorimetry (DSC), which can determine the thermal properties and also the best conditions for application of the materials. These techniques can be applied to polymers to determine their specific heat, degree of polymerization, flammability, degradation, cure, glass transition temperature (T_g), and other characteristics. Analysis of composites should consider the behavior of each component, including the matrix, reinforcement, plasticizers and fire retardants.

Thermal analyses are frequently combined to interpret the results. TGA and DSC are generally comparative and complementary. The thermal transitions do not involve mass loss and are therefore not detected by TGA but are detected by DSC or DMTA (Hatakeyama and Quinn, 1994).

TGA and DSC indicate that the residual cure stage of the phenolic thermoset lies between 100 and 200°C and releases water and other volatile by-products. The cure stage is observed as an exothermic peak in the DSC curves (Siegmann and Narkis, 1977). The condensation stage involving two phenolic hydroxyls may occur around 300°C and form diphenyl-ether type bonds with consequent mass loss (Pilato, 2010a; Vázquez *et al.*, 2002; El Mansouri *et al.*, 2011). This event corresponds to an endothermic peak in DSC curves (Siegmann and Narkis, 1977).

Rajaei *et al.* (2011) analyzed glass fiber/phenolic prepregs (containing approximately 50 wt% of resol-type phenolic resin) using DSC analysis at three heating rates (2.5, 5 and 10°C min^{-1}). The authors observed that at lower heating rates, the start and end of the exothermic curing process (characterized by an exothermic peak) occurred at lower temperatures because the lower heating rates enabled more chemical groups to react. They also observed that the reaction enthalpy increased with the heating rate.

Yoonessi *et al.* (2008) observed that carbon nanofiber (CNF)/resole phenolic composites had higher glass transition temperatures (T_g) with increasing CNF weight percentage up to 4 wt% CNF. The CNF surfaces restrict the movement of adjacent segments of the polymer chain if physical or chemical interactions take place between the CNF surface and the polymer. Resin species with hydroxyl functionalities such as phenolic resins can be absorbed on CNF surfaces with oxygenated functional groups, forming hydrogen bonds. These hydrogen bonds and the chemical bonds between resin and fiber after curing restrict the mobility of the polymer segments, increasing the T_g values of the CNF/phenolic composites compared to neat phenolic thermosets.

Yang and Gu (2012) propose to improve the thermal stability of thermoset benzoxazine by introducing benzoxazole structures. The rigid benzoxazole structure could restrict the chain mobility and reduce the T_g. DMA and TGA demonstrated that the cross-linking density increased upon the incorporation of amine segments (amine groups linked with different groups attached) into the benzoxazine resin network, thus decreasing the chain mobility and improving the thermal and dimensional stability.

2.9.2 Thermal decomposition

Phenolic thermosets are known to be resistant to high temperatures and generate high amounts of char during pyrolysis (Knop and Pilato, 1985). The thermal decomposition of phenolic thermosets can be divided into three

stages characterized by weight loss and volume changes. In the first stage up to 300°C, the mass loss is small (1–2%) and occurs due to the release of water and unreacted monomers, phenol and formaldehyde entrapped during the cure. During this stage, the polymeric matrix remains virtually intact (Mouritz and Gibson, 2006). At 300°C, the second stage begins in which the phenolic matrix is decomposed, with the release of water, carbon monoxide, carbon dioxide, methane, phenol, cresols and xylenols. During this stage, the random scission of chains occurs but not depolymerization. The internal porosity of the matrix increases; consequently, the density decreases. The third stage starts above 600°C with the release of carbon dioxide, methane, water, benzene, toluene, phenol, cresols and xylenols. This stage features high shrinkage and leads to a considerable increase in density and a decrease in permeability (Knop and Pilato, 1985).

When lignin was used as a partial substitute for phenol, the lignophenolic (lignin–phenol–formaldehyde) thermoset exhibited a larger mass loss at 400°C than phenolic thermosets because the decomposition or condensation of the aromatic rings probably occurred between 400 and 500°C (Hoareau *et al*., 2006; Paiva and Frollini, 2006). The thermoset prepared with tannin (tannin–phenol–formaldehyde) exhibited a peak around 335°C corresponding to the decomposition of the moieties typical of tannin and peaks between 500 and 580°C corresponding to the decomposition of phenolic rings present in the matrix (Barbosa *et al*., 2010).

'Fiberglass-resin powder (FR powder)' consists of glass fiber and resin powder from waste printed circuit boards (PCBs). FR powder can be reused as a reinforcing filler in phenolic molding compounds (PMCs). Guo *et al*. (2010) used FR powder as a partial substitute (20%) for wood flour in the production of modified phenolic molding compound (MPMC) and studied the thermal stability and mechanical properties. The authors observed that the thermal decomposition of the MPMC occurred in three steps. The first step was due to the decomposition of wood flour (200–370°C), the second step was the main weight loss (55%) and resulted from the degradation of the polymer (370–575°C), and the third step was mainly due to the decomposition of the $CaCO_3$ additive.

Phenolic composites reinforced with lignocellulosic fibers exhibit lower thermal stability compared to phenolic thermosets because lignocellulosic fibers decompose at lower temperatures than phenolic thermosets (Paiva and Frollini, 2006). At approximately 300°C, a significant mass loss occurs in the lignocellulosic fibers due to the thermal decomposition of the cellulose and hemicellulose (Ramires *et al*., 2010a). When the lignocellulosic fibers are covered by the phenolic matrix, the thermal stability of the fibers can increase because the fibers are protected by the matrix (Ramires *et al*., 2010a). Therefore, the change in the thermal stability of the composites compared to the thermoset depends on the fiber type, its composition (content of

lignin, cellulose and hemicellulose) and its interfacial interaction with the phenolic matrix (Hoareau *et al.*, 2006; Paiva and Frollini, 2006; Barbosa *et al.*, 2010).

Guzman *et al.* (2012) prepared syntactic foams based on phenolic and epoxy resins reinforced with carbon nanotubes (CNTs) and microballoon grades. The composites were prepared with single- and multi-walled functionalized nanotubes (FCNTs). TG analysis indicated the percentage of water absorption and decomposition temperature. Only one transition step was observed in the TG curve for the phenolic–epoxy matrix (300–500°C), whereas two transition steps were observed for the FCNT-reinforced composite. The first transition for the FCNT-reinforced composite involved the evaporation of water absorbed by the composite (101–310°C), and the final transition occurred after 310°C, indicating the degradation of the polymer foam. According to Guzman *et al.* (2012), the composites are expected to contain higher moisture and exhibit a lower decomposition temperature due to the presence of the various components, carbon nanotubes and microballoon grades.

2.9.3 Thermal conductivity

Cooling, heating and air-conditioning systems for buildings are major impediments to sustainable development because traditional refrigeration cycles consume high levels of electricity and fossil energy. Thus, a good insulating material is a fundamental tool for the design and construction of energy-efficient buildings (Agoudjil *et al.*, 2011).

To prepare thermal insulating materials, Carvalho *et al.* (2003) prepared phenolic and lignophenolic (lignin–phenol–formaldehyde) foams and determined their thermal conductivities: 0.057 W m^{-1} K^{-1} (density of 0.12 g cm^{-3}) for phenolic foam and 0.072 W m^{-1} K^{-1} (density of 0.45 g cm^{-3}) for lignophenolic foam. Tondi *et al.* (2009) prepared tannin-based rigid foams with thermal conductivity values between 0.024 and 0.030 W m^{-1} K^{-1} for densities between 0.08 and 0.12 g cm^{-3}, respectively.

Thermal characteristics are also important in numerous industrial processes, and thus the development of composites with high thermal conductivity and a low coefficient of thermal expansion is important to achieve effective heat conduction (Kim *et al.*, 2007). The use of some reinforcements such as carbon nanotubes, carbon fibers, nano silica powders, metal particles, boron nitrite and glass fibers can improve the thermal conductivity of phenolic composites (Kim *et al.*, 2007; Simitzis *et al.*, 2011; Srikanth *et al.*, 2010). Kim *et al.* (2007) demonstrated that the homogeneous dispersion of 7 wt% carbon nanotubes in a phenolic resin acted as an effective thermal bridge between adjacent carbon fibers and enhanced the thermal conductivity (393 W m^{-1} K^{-1}).

2.10 Other properties: electrical conductivity, fire safety and recycling

2.10.1 Electrical conductivity

Simitzis *et al*. (2011) studied increased electrical conductivity combined with mechanical properties. Multifunctional polymer matrices were prepared using continuous or short carbon fibers at low volume percentages (15% and 5% v/v, respectively) to improve the mechanical properties of the matrix, and zinc particles were used to improve the conductivity of the novolac phenolic resin. The authors prepared a non-reinforced novolac matrix, i.e., the thermoset, and observed that the material was very brittle and exhibited a low electrical conductivity because novolac is a typical thermosetting polymer (i.e., an insulating material). The mechanical strength of the cured novolac matrix decreased with increasing Zn content. Thus, the materials (cured novolac matrix containing Zn particles) were reinforced with short (5% v/v) and continuous (15% v/v) carbon fibers, resulting in the maximal values of flexural and shear strength among all the composites. Therefore, the insertion of metal particles between adjacent carbon fibers (carbon fibers–metal particles) forms conductive paths in an insulating matrix leading to typical composite conductor behavior. Other metals are often used instead of Zn as the main conductor, e.g., Ni, Cu, Al, Ag and Au (Gul', 1996).

2.10.2 Fire safety

Phenolic resins have demonstrated superior fire, smoke and toxicity (FST) properties compared to other polymeric matrices for fire-resistance applications. The FST properties of phenolic resins are decisive for the selection of these products in many applications. No other matrix material provides the same FST performance at a comparable price level (Taylor, 2010). The self-ignition temperature of the phenolic resin is approximately 600°C and the limiting oxygen index (LOI) is in the range of 40–49%. Phenolic composites are largely used in the aircraft (interior) and mass transit industries (buses, railways), with interest increasing in marine applications. These composites are also used frequently in civil infrastructure, sporting goods and consumer products (Mouritz and Gibson, 2006).

Phenolic composites have been the material of choice when fire safety is the main criterion for the selection of building materials. Due to the intrinsic properties of the matrix, phenolic composites do not support a flame, and when exposed to fire they produce little or no smoke, which is less toxic than the smoke produced by other composites, particularly those containing certain halogenated flame retardants (Johanson, 2005).

2.10.3 Recycling

Thermosets such as phenolic thermosets cannot be melted or solubilized because they form a cross-linked structure after curing, unlike thermoplastics that can be melted several times (Goto and Santorelli, 2010).

Phenolic thermosets can be recycled using a mechanical recycling system such as milling or crushing, and the obtained powder material can be used as a filler or additive for new thermosets (Goto and Santorelli, 2010).

Recycling of composites is not easy because recycling involves the matrix and the fiber, which are chemically different (Goto and Santorelli, 2010; Gardziella *et al.*, 2000; Cardona *et al.*, 2012).

Thermoset composite materials can be recycled through mechanical comminution techniques, to reduce the size of the scrap to produce recyclates, using thermal processes to break the scrap down into materials and energy (Pickering, 2006).

Phenolic thermosets and phenolic composites are solid, combustible materials with caloric values similar to that of coal. Therefore, products based on phenolic resins can be used as an alternative solid fuel to coal (Goto and Santorelli, 2010). Depending on the fiber thermal stability, thermal processes can be used to recover fibers. The composites are heated to high temperatures, causing the separation of the fibers from the polymers (Conroy *et al.*, 2006).

2.11 Conclusion and future trends

The interest in the use of raw materials derived from renewable sources, combined with the good properties that have been observed for these materials, have led to the perspective that composites based on bio-resins and lignocellulosic and/or cellulosic fibers will experience an impressive development in a near future. Furthermore, the coming years should see an increased number of investigations on nano-reinforced thermoset composites, including phenolic composites.

The phenolic-type resins should remain an excellent option for thermoset-matrix composites, with these materials maintaining a prominent position in the area of composites based on their favorable cost/performance characteristics.

2.12 Acknowledgements

The authors gratefully acknowledge FAPESP (The State of São Paulo Research Foundation, Brazil) and CNPq (National Research Council, Brazil) for financial support.

2.13 References

Agoudjil B, Benchabane A, Boudenne A, Ibos L and Fois M (2011), 'Renewable materials to reduce building heat loss: Characterization of date palm wood', *Energy Build*, 43, 491–497.

Baekeland L H (1907), US Patent 9, 42, 699.

Baekeland L H ((1909), 'The synthesis, constitution, and uses of bakelite', *Ind J Eng Chem,* 1, 149–161.

Baeyer A (1872), 'Ueber die Verbindungen der Aldehyde mit den Phenolen und aromatischen Kohlenwasserstoffen', *Ber,* 5, 1094–1100.

Bakis C E, Bank L C, Asce F, Brown V L, Asce M, Cosenza E, Davalos J F, Asce A M, Lesko J J, Machida A, Rizkalla S H, Asce F, Triantafillou T C and Asce M (2002), 'Fiber-reinforced polymer composites for construction – State-of-the-art review', *J Compos Constr*, 6, 73–87.

Ballerini A, Despres A and Pizzi A (2005), 'Non-toxic, zero emission tannin–glyoxal adhesives for wood panels', *Holz Roh Werkst*, 63, 477–478.

Barbosa Jr V, Ramires E C, Razera I A T and Frollini E (2010), 'Biobased composites from tannin-phenolic polymers reinforced with coir fibers', *Ind Crops Prod*, 32, 305–312.

Barreto A C H, Esmeraldo M A, Rosa D S, Fechine P B A and Mazzetto S E (2010), 'Cardanol biocomposites reinforced with jute fiber: microstructure, biodegradability, and mechanical properties', *Polym Comp*, 31, 1928–1937.

Battles E P, Dagher H J and Abdel-Magid B (2000), 'Durability of composite reinforcement for timber bridges', *Transportation Research Record*, 1696, 131–135.

Brent S A (2002), 'History of composite materials – Opportunities and necessities', *Composites Manufacturing*, 1–8.

Breuer O and Sundararaj U (2004), 'Big returns from small fibers: A review of polymer/carbon nanotube composites', *Polym Compos*, 25, 630–645.

Calo E, Maffezzoli A, Mele G, Martina F, Mazzetto S E, Tarzia A and Stifani C (2007), 'Synthesis of a novel cardanol-based benzoxazine monomer and environmentally sustainable production of polymers and bio-composites', *Green Chem,* 9, 754–759.

Campana Filho S P C, Frollini E and Curvelo A A S (1997), 'Organosolv delignification of lignocellulosic materials: Preparation and characterization of lignin and cellulose derivatives', in Leão A L, Carvalho F X and Frollini E, *Lignocellulosic-plastics Composites*, São Paulo, Brazil, USP and UNESP, 163–178.

Cardona F, Aravinthan T and Moscou C (2010), 'Modified PF resins for composite structures with improved mechanical properties', *Polym Polym Compos*, 18(6), 297–306.

Cardona F, Kin-Tak A L and Fedrigo J (2012), 'Novel phenolic resins with improved mechanical and toughness properties', *J Appl Polym Sci,* 123, 2131–2139.

Carvalho G, Pimenta J A, Santos W N and Frollini E (2003), 'Phenolic and lignophenolic closed cells foams: Thermal conductivity and other properties', *Polym-Plast Technol Eng*, 42(4), 605–626.

Cerrutti B M, de Souza C S, Castellan A, Ruggiero R and Frollini E (2012), 'Carboxymethyl lignin as stabilizing agent in aqueous ceramic suspensions', *Ind Crops Prod*, 36, 108–115.

Chawla K K (1998), *Composite Materials: Science and Engineering*, New York, Springer.

Choi M H, Jeon B H and Chung I J (2000), 'The effect of coupling agent on electrical and mechanical properties of carbon fiber/phenolic resin composites', *Polymer*, 41, 3243–3252.

Conroy A, Halliwell S and Reynolds T (2006), 'Composite recycling in the construction industry', *Compos Appl Sci Manuf*, 37, 1216–1222.

Da-Peng Z and Hong F (2008), 'Mechanical and high-temperature properties of glass fibers reinforced phenolic composites', *J Reinf Plast Compos*, 27, 1449–1460.

Doherty W, Halley P, Edye L, Rogers D, Cardona F, Park Y and Woo T (2007), 'Studies on polymers and composites from lignin and fiber derived from sugar cane', *Polym Adv Technol*, 18, 673–678.

Dzenis Y (2008), 'Structural nanocomposites', *Science,* 319, 419–420.

Economy J and Parkar Z (2011), 'Historical perspectives of phenolic resins', in: Strom E T and Rasmussen S C, *100+ Years of Plastics*: *Leo Backeland and Beyond*, ACS Symposium Series; American Chemical Society, Washington, DC.

El Mansouri N E and Salvadó J (2007), 'Analytical methods for determining functional groups in various technical lignins', *Ind Crops Prod*, 26, 116–124.

El Mansouri N E, Pizzi A and Salvadó J (2007a), 'Lignin-based polycondensation resins for wood adhesives', *J Appl Polym Sci,* 103, 1690–1699.

El Mansouri N E, Pizzi A and Salvadó J (2007b), 'Lignin-based wood panel adhesives without formaldehyde', *Holz Roh Werkst*, 65, 65–70.

El Mansouri N E, Yuan Q and Huang F (2011), 'Characterization of alkaline lignins for use in phenol-formaldehyde and epoxy resins', *BioResources*, 6, 2647–2662.

Ewanick S M, Bura R and Saddler J N (2007), 'Acid-catalyzed steam pretreatment of lodgepole pine and subsequent enzymatic hydrolysis and fermentation to ethanol', *Biotechnol Bioeng*, 98, 737–746.

Fengel D and Wegener G (1989), *Wood: Chemistry, Ultrastructure, Reactions*, New York, Walter de Gruyter.

Fink J K (2005), *Reactive Polymers Fundamentals and Applications*, Norwich, NY, William Andrew Publishing.

Forsdyke K L (2002), Phenolics 'fibreglass' meets new Euroclass B fire code**,** The Composites Processing Association, Phenolic Composites Group.

Frollini E and Castellan A (2012), 'Phenolic resins and composites', in *Encyclopedia of Composites*, 2nd edition, New York, John Wiley & Sons, 2059–2068.

Frollini E, Paiva J M F, Trindade W G, Razera I A T and Tita S P (2004), 'Plastics and composites from lignophenols', in Wallenberger F T and Weston N, *Natural Fibers, Plastics and Composites*, Dordrecht, the Netherlands, Kluwer Academic Publishers, 193–225, and references therein.

Gardziella A, Pilato L and Knop A (2000), *Phenolic Resins: Chemistry, Applications, Standardization, Safety, and Ecology*, Berlin and Heidelberg, Springer-Verlag, and references therein.

Ghosh N N, Kiskan B and Yagci Y (2007), 'Polybenzoxazines. New high performance thermosetting resins: Synthesis and properties', *Prog Polym Sci,* 32, 1344–1391.

Goto J and Santorelli M (2010), 'Recycling', in Pilato L, *Phenolic Resins: A Century of Progress*, New York, Springer, 517–524.

Grishchuk S, Mbhele Z, Schmitt S and Karger-Kocsis J (2011), 'Structure, thermal and fracture mechanical properties of benzoxazine-modified amine-cured DGEBA epoxy resins', *Express Polym Lett*, 5, 273–282, and references therein.

Gul' V E (1996), *New Concepts in Polymer Science: Structure and Properties of Conducting Polymer Composites*, Zeist, the Netherlands, VPS Verlag, 1–22.

Guo F, Zhang Z, Liu W, Su F and Zhang H (2009), 'Effect of plasma treatment of Kevlar fabric on the tribological behavior of Kevlar fabric/phenolic composites', *Tribol Int*, 42, 243–249.

Guo J, Rao Q and Xu Z (2010), 'Effects of particle size of fiberglass-resin powder from PCBs on the properties and volatile behavior of phenolic molding compound', *J Hazard Mater*, 175, 165–171.

Guzman M E, Rodriguez A J, Minaie B and Violette M (2012), 'Processing and properties of syntactic foams reinforced with carbon nanotubes', *J Appl Polym Sci*, 124, 2383–2394.

Hatakeyama T and Quinn F X (1994), *Thermal Analysis – Fundamentals and Applications to Polymer Science*, Chichester, UK, John Wiley & Sons, 1–105.

Herakovich C T (1998), *Mechanics of Fibrous Composites*, New York, John Wiley & Sons, 1–7.

Hernández-Salas J M, Villa-Ramirez M S, Veloz-Rendón J S, Rivera-Hernández K N, González-César R A, Plascencia-Espinosa M A and Trejo-Estrada S R (2009), 'Comparative hydrolysis and fermentation of sugarcane and agave bagasse', *Bioresource Technology*, 100, 1238–1245.

Hirayama T, Yamada N, Nohara M and Fukui S (1984), 'The high performance liquid chromatographic determination of total malondialdehyde in vegetable oil with dansyl hydrazine', *J Sci Food Agric*, 35, 338–344.

Hoareau W, Oliveira F B, Grelier S, Frollini E and Castellan A (2006), 'Fiberboards based on sugarcane bagasse lignin and fibers', *Macromol Mater Eng*, 291, 829–839.

Hou T H, Bai J M and Baughman J M (2006), 'Processing and properties of a phenolic composite system', *J Reinf Plast Compos*, 25, 495–502.

Iyim T B (2007), 'Modification of high ortho novolac resin with diacids to improve its mechanical properties', *J Appl Polym Sci*, 106, 46–52.

Johanson T (2005), 'Expanding possibilities without compromise', *Reinf Plast*, 49, 26–29.

Kim S J and Jang H (2000), 'Friction and wear of friction materials containing two different phenolic resins reinforced with aramid pulp', *Tribol Int*, 33, 477–484, and references therein.

Kim S S, You H N, Hwang I U and Lee D G (2009), 'Development of the carbon/phenolic composite shoulder bearing', *Compos Struct*, 88, 26–32.

Kim Y A, Kamio S, Tajiri T, Hayashi T, Song S M, Endo M, Terrones M and Dresselhaus M S (2007), 'Enhanced thermal conductivity of carbon fiber/phenolic resin composites by the introduction of carbon nanotubes', *Appl Phys Lett*, 90, 093125(1)–093125(3).

Knop A and Pilato L A (1985), *Phenolic Resins*, Berlin, Springer-Verlag.

Kowatsch S (2010), 'Formaldehyde', in Pilato L, *Phenolic Resins: A Century of Progress*, New York, Springer, 24–40.

Ku H, Rogers D, Davey R, Cardona F and Trada M (2008), 'Fracture toughness of phenol formaldehyde composites: pilot study', *J Mater Eng Perform*, 17, 85–90.

Kumar N M, Reddy G V, Naidu S V, Rani T S and Subha M C S (2009), 'Mechanical properties of coir/glass fiber phenolic resin based composites', *J Reinf Plast Compos*, 28, 2605–2613.

Lacerda T M, de Paula M P, Zambon M and Frollini E (2012), 'Saccharification of Brazilian sisal pulp: Evaluating the impact of mercerization on non-hydrolyzed pulp and hydrolysis products', *Cellulose*, 19, 351–362.

Leão A L (1997), 'Fire retardants in lignocellulosic composites', in Leão A L, Carvalho F X and Frollini E, *Lignocellulosic-plastics Composites*, São Paulo, Brazil, USP and UNESP, 111–161.

Lei H, Pizzi A and Du G (2008), 'Environmentally friendly mixed tannin/lignin wood resin', *J Appl Polym Sci*, 107, 203–209.

Lewark B A (2007), 'Composites: Past, present future: Phenolics revisited', *Composites Technology*, http://www.compositesworld.com/articles/ct.

Liu H and Laborie M G (2011), 'Bio-based nanocomposites by *in situ* cure of phenolic prepolymers with cellulose whiskers', *Cellulose*, 18, 619–630.

Ma C M, Lee C and Wu H (1998), 'Mechanical properties, thermal stability, and flame retardance of pultruded fiber-reinforced poly(ethylene oxide)-toughened novolak-type phenolic resin', *J Appl Polym Sci*, 69, 1129–1136.

Malutan T, Nicu R and Popa V I (2008), 'Contribution to the study of hydroxymethylation reaction of alkali lignin', *BioResources*, 3, 13–20.

Mathur R B, Chatterjee S and Singh B P (2008), 'Growth of carbon nanotubes on carbon fiber substrates to produce hybrid/phenolic composites with improved mechanical properties', *Comp Sci Technol,* 68, 1608–1615, and references therein.

Mathur R B, Singh B P, Dhami T L, Kalra Y, Lal N, Rao R and Rao A M (2010), 'Influence of carbon nanotube dispersion on the mechanical properties of phenolic resin composites', *Polym Compos*, 31, 321–327.

Mattioda G, Métivier B and Guetté J P (1982), 'Le glyoxal, une molécule très fonctionnelle. II. Utilisations industrielles', *L´Actualité Chimique*, June–July, 33–40.

Megiatto J D, Silva C G, Rosa D S and Frollini E (2008), 'Sisal chemically modified with lignins: Correlation between fibers and phenolic composites properties', *Polym Degrad Stab*, 93(6), 1109–1121.

Megiatto Jr J D, Silva C G, Ramires E C and Frollini E (2009), 'Thermoset matrix reinforced with sisal fibers: Effect of the cure cycle on the properties of the biobased composite', *Polym Test*, 28, 793–800.

Mosiewicki M A, Aranguren M I, Curvelo A A S and Borrajo J (2007), 'Effect of natural rubber on wood-reinforced tannin composites', *J Appl Polym Sci*, 105, 1825–1832.

Moubarik A, Pizzi A, Allal A, Charrier F and Charrier B (2009), 'Cornstarch and tannin in phenol–formaldehyde resins for plywood production', *Ind Crops Prod*, 30, 188–193.

Mouritz A P (2006), *Fire Safety of Advanced Composites for Aircraft*, Australian Transport Safety Bureau, ATSB Research and Analysis Report.

Mouritz A P and Gibson A G (2006), *Fire Properties of Polymer Composite Materials*, Dordrecht, the Netherlands, Springer.

Mu Q, Wei C and Feng S (2009), 'Studies on mechanical properties of sisal fiber/phenol formaldehyde resin *in-situ* composites', *Polym Comp*, 30, 131–137.

Mueller-Harvey I (2001), 'Analysis of hydrolysable tannins', *Anim Feed Sci Technol*, 91, 3–20.

Ogawa H (2000), 'Architectural application of carbon fibers. Development of new carbon fiber reinforced glulam', *Carbon*, 38, 211–226.

Paiva J M F and Frollini E (2000), 'Natural fibers reinforced thermoset composites', in Frollini E, Leão A L and Mattoso L H C, *Natural Polymers and Agrofibers Based Composites*, São Paulo, Brazil, USP/UNESP/EMBRAPA, 229–255.

Paiva J M F and Frollini E (2006), 'Unmodified and modified surface sisal fibers as reinforcement of phenolic and lignophenolic matrices composites: thermal analyses of fibers and composites', *Macromol Mater Eng*, 291, 405–417.

Peña C, Martin M D, Tejado A, Labidi J, Echeverria J M and Mondragon I (2006), 'Curing of phenolic resins modified with chestnut tannin extract', *J Appl Polym Sci*, 101, 2034–2039.

Pickering S J (2006), 'Recycling technologies for thermoset composite materials – current status', *Compos Appl Sci Manuf*, 37, 1206–1215.

Pilato L (2010a), 'Resin chemistry', in Pilato L, *Phenolic Resins: A Century of Progress*, Berlin and Heidelberg, Springer-Verlag, 41–91.

Pilato L (2010b), 'Future aspects', in Pilato L, *Phenolic Resins: A Century of Progress*, Berlin and Heidelberg, Springer-Verlag, 526–527.

Pilato L A and Michno M J (1994), *Advanced Composite Materials*, Berlin and Heidelberg, Springer-Verlag.

Pilato L A, Koo J H, Wissler G E and Lao S (2008), 'A review – Phenolic and related resins and their nanomodification into phenolic resin fiber reinforced plastic systems', *J Adv Mater*, 40, 5–16, and references therein.

Rajaei M, Beheshty M H and Hayaty M (2011), 'Preparation and processing characterization of glass/phenolic prepregs', *Polym Polym Compos*, 19, 789–796.

Ramires E C and Frollini E (2012), 'Tannin-phenolic resins: Synthesis, characterization, and application as matrix in biobased composites reinforced with sisal fibers', *Composites Part B*, 43(7), 2851–2860.

Ramires E C, Megiatto Jr J D, Gardrat C, Castellan A and Frollini E (2010a), 'Biobased composites from glyoxal-phenolic resins and sisal fibers', *Bioresour Technol*, 101, 1998–2006.

Ramires E C, Megiatto Jr J D, Gardrat C, Castellan A and Frollini E (2010b), 'Valorization of an industrial organosolv-sugarcane bagasse lignin: Characterization and use as a matrix in biobased composites reinforced with sisal fibers', *Biotechnol Bioeng*, 107, 612–621.

Ramires E C, Megiatto Jr J D, Gardrat C, Castellan A and Frollini E (2010c), 'Biocompósitos de matriz glioxal–fenol reforçada com celulose microcristalina', *Polímeros*, 20(2), 126–133.

Rao B S and Palanisamy A (2011), 'Monofunctional benzoxazine from cardanol for bio-composite applications', *React Funct Polym*, 71, 148–154, and references therein.

Raqueza J M, Deléglise M, Lacrampe M F and Krawczak P (2010), 'Thermosetting (bio) materials derived from renewable resources: A critical review', *Prog Polym Sci*, 35, 487–509, and references therein.

Razera I A T and Frollini E (2004), 'Composites based on jute fibers and phenolic matrices: Properties of fibers and composites', *J Appl Polym Sci*, 91, 1077–1085.

Rowell R M and Han S J (2000), 'Characterization and factors affecting fiber properties', in Frollini E, Leão A L and Mattoso LHC, *Natural Polymers and Agrofibers Based Composites*, São Paulo, Brazil, USP/UNESP/EMBRAPA, 25–48.

Sánchez Ó J and Cardona C A (2008), 'Trends in biotechnological production of fuel ethanol fromdifferent feedstocks', *Bioresour Technol*, 99, 5270–5295.

Schuh T and Gayer U (1997), 'Automotive applications of natural fiber composites', in Leão A L, Carvalho F X and Frollini E, *Lignocellulosics-plastics Composites*, São Paulo, Brazil, USP and UNESP, 181–195.

Siegmann A and Narkis M (1977), 'Thermal analysis of thermosetting phenolic compounds for injection molding', *J Appl Polym Sci*, 21, 2311–2318.

Silva C G, Beneducci D and Frollini E (2012), 'Lyocell and cotton fibers as reinforcements for a thermoset polymer', *BioResources*, 7, 78–98.

Simitzis J, Zoumpoulakis L, Soulis S, Triantou D and Pinaka C (2011), 'Electrical conductivity and mechanical strength of composites consisting of phenolic resin, carbon fibers, and metal particles', *J Appl Polym Sci,* 121, 1890–1900.

Singh K P and Palmese G R (2004), 'Enhancement of phenolic polymer properties by use of ethylene glycol as diluent', *J Appl Polym Sci*, 91, 3096–3106.

Srikanth I, Daniel A, Kumar S, Padmavathi N, Singh V, Ghosal P, Kumar A and Devi

G R (2010), 'Nano silica modified carbon–phenolic composites for enhanced ablation resistance', *Scr Mater*, 63, 200–203, and references therein.

Stewart D (2008), 'Lignin as a base material for materials applications: chemistry, application and economics', *Ind Crops Prod*, 27, 202–207.

Suddell B C and Evans W J (2005), 'Natural fiber composites in automotive applications', in Mohanty A K, Misra M and Drzal L T, *Natural Fibers, Biopolymers, Biocomposites*, Boca Raton, FL, CRC Press, 231–259.

Tai N-H, Ye M-K and Liu J-H (2004), 'Enhancement of the mechanical properties of carbon nanotube/phenolic composites using a carbon nanotube network as the reinforcement', *Carbon*, 42, 2774–2777.

Taylor J G (2010), 'Composites', in Pilato L, *Phenolic Resins: A Century of Progress*, Berlin and Heidelberg, Springer-Verlag, 263–306, and references therein.

ter Meer E (1874), 'Ueber die Verbindungen von Phenol mit Aldehyden', *Ber*, 7, 1200–1203.

Thomas S and Pothan L A (2008), *Natural Fibre Reinforced Polymer Composites: From Macro to Nanoscale*, Paris, Editions des Archives Contemporaines.

Tondi G and Pizzi A (2009), 'Tannin-based rigid foams: characterization and modification', *Ind Crops Prod*, 29, 356–363.

Tondi G, Zhao W, Pizzi A, Du G, Fierro V and Celzard A (2009), 'Tannin-based rigid foams: A survey of chemical and physical properties', *Bioresour Technol*, 100, 5162–5169.

Trindade W G, Hoareau W, Razera I A T, Ruggiero R, Frollini E and Castellan A (2004), 'Phenolic thermoset matrix reinforced with sugar cane bagasse fibers: Attempt to develop a new fiber surface chemical modification involving formation of quinones followed by reaction with furfuryl alcohol', *Macromol Mater Eng*, 289, 728–736.

Trindade W G, Hoareau W, Megiatto Jr J D, Razera I A T, Frollini E and Castellan A (2005), 'Thermoset phenolic matrices reinforced with unmodified and surface-grafted furfuryl alcohol sugar cane bagasse and curaua fibers: properties of fibers and composites', *Biomacromolecules*, 6(5), 2485–2496.

Trindade W G, Paiva J M F, Leão A L and Frollini, E (2008), 'Ionized air treated curaua fibers as reinforcement for phenolic matrices', *Macromolecular Materials and Engineering*, 293, 521–528.

Tyberg C S, Sankarapandian M, Bears K, Shih P, Loos A C, Dillard D, McGrath J E, Riffle J S and Sorathia U (1999), 'Tough, void-free, flame retardant phenolic matrix materials', *Constr Build Mater*, 1999, 13, 343–353.

Tyberg C S, Bergeron K, Sankarapandian M, Shih P, Loos A C, Dillard D A, McGrath J E, Riffle J S and Sorathia U (2000), 'Structure–property relationships of void-free phenolic–epoxy matrix materials', *Polymer*, 41, 5053–5062.

Vázquez G, González-Álvarez J, López-Suevos F, Freire S and Antorrena G (2002), 'Curing kinetics of tannin–phenol–formaldehyde adhesives as determined by DSC', *J Therm Anal Calorim*, 70, 19–28.

Vázquez G, González-Álvarez J and Antorrena G (2006), 'Curing of a phenol–formaldehyde tannin adhesive in the presence of wood', *J Therm Anal Calorim*, 84, 651–654.

Wang F-Y, Ma C-C M and Wu W-J (1999), 'Mechanical properties, morphology, and flame retardance of glass fiber-reinforced polyamide-toughened novolac-type phenolic resin', *J Appl Polym Sci*, 73, 881–887.

Weber M and Weber M (2010), 'Phenols', in Pilato L, *Phenolic Resins: A Century of Progress*, Berlin and Heidelberg, Springer-Verlage, 9–23.

Willson P (2003), *An update on phenolic resins for use in mass transport, marine, offshore*

and construction applications. Composites in Fire 3, Centre for Composite Materials Engineering, University of Newcastle, UK.

Xu P J (2012), 'Preparation of high performance polybenzoxazine resin using hyperbranched polyborate', *Adv Mater Res*, 391–392, 75–80.

Yang P and Gu Y (2012), 'Synthesis of a novel benzoxazine-containing benzoxazole structure and its high performance thermoset', *J Appl Polym Sci*, 124, 2415–2422.

Yoonessi M, Toghiani H, Wheeler R, Porcar L, Kline S and Pittman Jr C U (2008), 'Neutron scattering, electron microscopy and dynamic mechanical studies of carbon nanofiber/phenolic resin composites', *Carbon*, 46, 577–588, and references therein.

Yosomiya R (1990), *Adhesion and Bonding in Composites*, New York, Marcel Dekker, 1–4.

Zhong L X, Fu S H, Zhou X S and Zhan H Y (2011), 'Effect of surface microfibrillation of sisal fibre on the mechanical properties of sisal/aramid fiber hybrid composites', *Composites A*, 42, 244–252.

Zhou G, Movva S L and Lee J (2008), 'Nanoclay and long-fiber-reinforced composites based on epoxy and phenolic resins', *J Appl Polym Sci*, 108, 3720–3726.

3

Polyester resins as a matrix material in advanced fibre-reinforced polymer (FRP) composites

N. MISKOLCZI, University of Pannonia, Hungary

DOI: 10.1533/9780857098041.1.44

Abstract: The chapter discusses the use of one type of thermoset polymer, polyester, and its use as a matrix material in fibre-reinforced polymer (FRP) composites. It begins with an overview of FRP composites, before explaining why polyester is a particularly suitable material for this application, through discussion of its key properties and structures and the manufacturing processes involved. Composites can offer improved mechanical properties compared with pure polymers at no extra cost, meaning that they are widely used in a variety of applications, including in the transport industry (manufacturing passenger cars and other vehicles), marine and shipping uses, and as structural materials. Some examples of these applications, particularly in civil engineering, are provided in this chapter, along with discussion of potential future trends in the field.

Key words: fibre-reinforced polymer composites, polyester, thermoset polymers, composites, reinforced polymers, construction materials, mechanical properties.

3.1 Introduction

The development of human civilization depends on the availability of different construction materials. Metals, ceramics, composites, polymers and other materials have all been used, or are expected to be used in the future, as structural materials. However, the relative importance of these construction materials has changed over time. Composites are structural materials produced through the combination of different constituents. They were first discovered and used in antiquity: the first artificial composite was adobe, made of vegetable parts (such as straw) and mud. Since then other types of construction material have grown in importance, including natural composites such as wood and concrete. The latter part of the twentieth century has been described as the age of polymers. The first synthetic polymers were discovered in the last decade of the nineteenth century but their bulk application began after the 1950s, after which they became increasingly important. The first polymer-based composites consisted of glass fibres and polyesters, which were used in radar technology in the 1940s [1–3].

Although there are many ways of classifying polymeric materials, a standard classification is to divide them into thermoplastics and thermosets. Figure 3.1 shows one well-known way of classifying synthetic polymers. The main difference between the two types of polymers is that thermoplastics are chain polymers, while themosets are cross-linked, which can result in differences in their behaviour, for example when exposed to high temperatures. Thermoplastics become softer as the temperature increases and begin to degrade due to the cracking of C–C bonds. In contrast, thermoset polymers initially become harder as temperature increases until they reach a critical temperature, at which point they also start to degrade. Both thermoplastics and thermosets can be manufactured by polycondensation, polyaddition and polymerization. Polyesters, which are thermoset composites, are typically synthesized by polycondensation reactions.

3.2 Fibre-reinforced polymer (FRP) composites

Reinforced composites are the most widespread type of polymer composite used today. These structural materials use a polymer as the matrix, completely covering the reinforcements; without these reinforcements the polymer would offer relatively poor mechanical properties. Several studies have investigated the effect of the type of reinforcing material used on the properties of the final composite, looking also at related issues such as pre-treatment. There are three principal ways in which the reinforcing material can be incorporated:

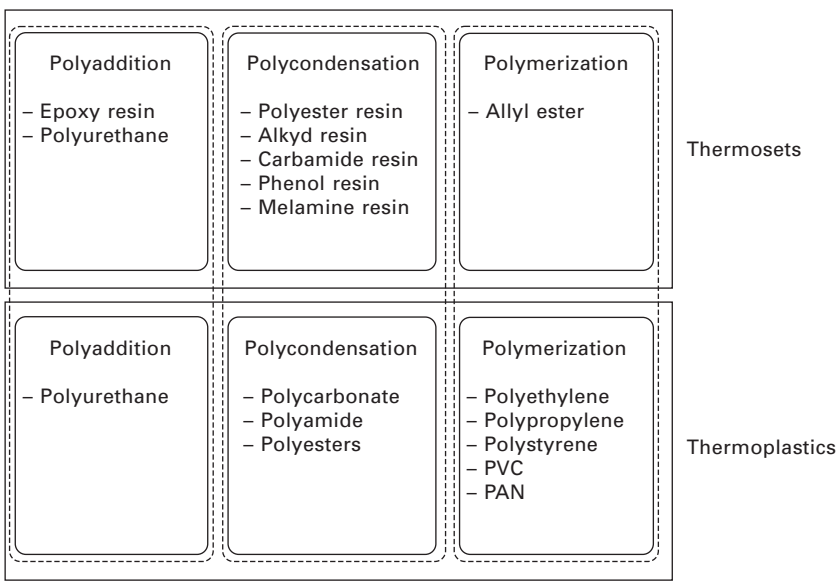

3.1 Classification of the synthetic polymers.

as grainy material (or particulates), as fibre (in the form of individual fibres embedded in the matrix) and as layers (fibres woven into mats which are laid on top of one another to create a laminate) (Fig. 3.2) [4, 5].

The reinforcing materials provide increased strength and stiffness to the composite. The matrix materials, on the other hand, are responsible not only for covering the reinforcements (thereby protecting them from environmental and chemical damage) but also for the elimination of fibre wearing and crushing that can be caused by deformation: they fix the fibres in position, which is crucial, as the reinforcing materials could otherwise easily slip out or become damaged through wear. The matrix materials also act as load-transferring media: they transfer the load in an orthogonal direction from the fibre axis. It has previously been established that the properties of reinforced composites (such as resistance against loading) vary according to the three different dimensions of space. In most construction materials, the stress pattern should be well defined, following force lines: high strength and stiffness are of primary importance close to the force lines, while lower values are suitable away from this point. This accounts for the fact that homogeneous materials with different reinforcements have a higher modulus and strength in a direction parallel to loading. The anisotropic nature of composites should facilitate the design of suitable products and structures; however, an adequate knowledge of the strength distribution lines is a prerequisite.

The relationship between the costs and mechanical properties (such as strength, E modulus, etc.) of the construction materials most commonly used in FRP composites is shown in Fig. 3.3. It has been shown that composites can offer better mechanical properties than pure polymers, and in some cases better than metals or glasses, even if expenditure is no higher; however, composite materials are often predominantly composed of the most expensive construction materials. The successful application of reinforced composites requires strong adhesion and interfacial forces (both chemical and physical) between the matrix and the reinforcements; moreover, this strong interaction must be maintained during all types of loading.

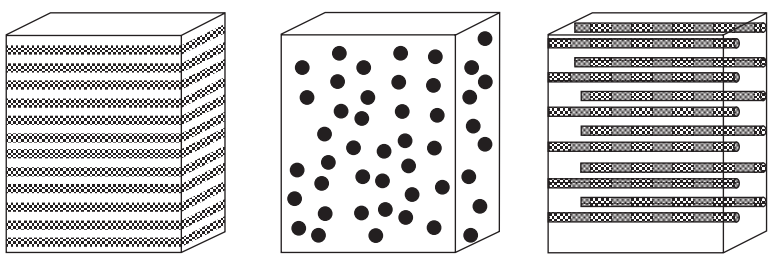

3.2 Types of composites.

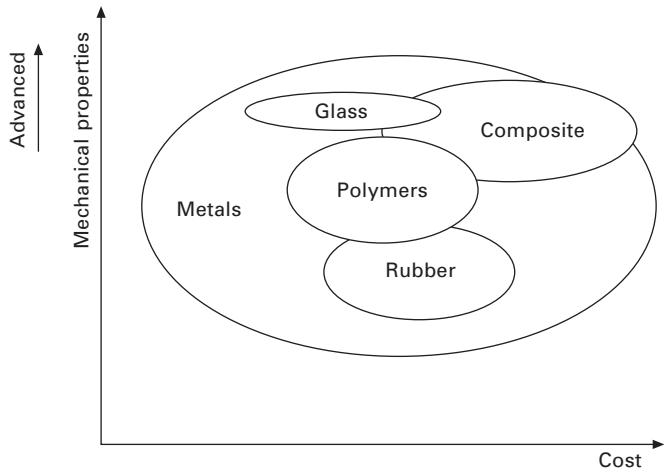

3.3 The relationship between costs and properties of the most commonly used constructional materials.

3.3 Polyesters as matrix materials

It is well known that thermoset plastics can be made from different resins. During manufacturing the monomer or oligomer resins are cross-linked by heat in the presence of a catalyst or initiator, for example. This cross-linking means that thermosets have better heat resistance, and do not soften. Unlike thermoplastics, the properties of thermosets improve as the temperature increases, but only up to a given heat value, after which they too start to degrade. However, this degradation point generally occurs at a higher temperature than the corresponding point for thermoplastics (Fig. 3.4). One advantage of thermosets is that, prior to shaping, they are liquids with low viscosity, meaning that high pressure is not required to process them; furthermore their processing costs are relatively low. On the other hand, there is one significant disadvantage, which is their reprocessing: the specific properties of thermosets mean that they are difficult to reprocess through either mechanical or chemical recycling [5–7].

Polyester is one of the earliest types of thermoset and is widely used in FRP composites, where its thermosetting properties are very valuable. Between 2000 and 2008, polyester manufacture in Europe increased rapidly, with a 4–5% annual gain. Owing to the economic crisis, the whole plastics processing sector faced a drop in both net income and industrial use; however, the polyester sector has nevertheless managed to achieve continual growth in recent years.

Unsaturated polyesters are generally in the form of polyester resins, which are viscous liquids, or even solids with low melting point, and have low molecular weights. The polymer units are linked via ester groups, and

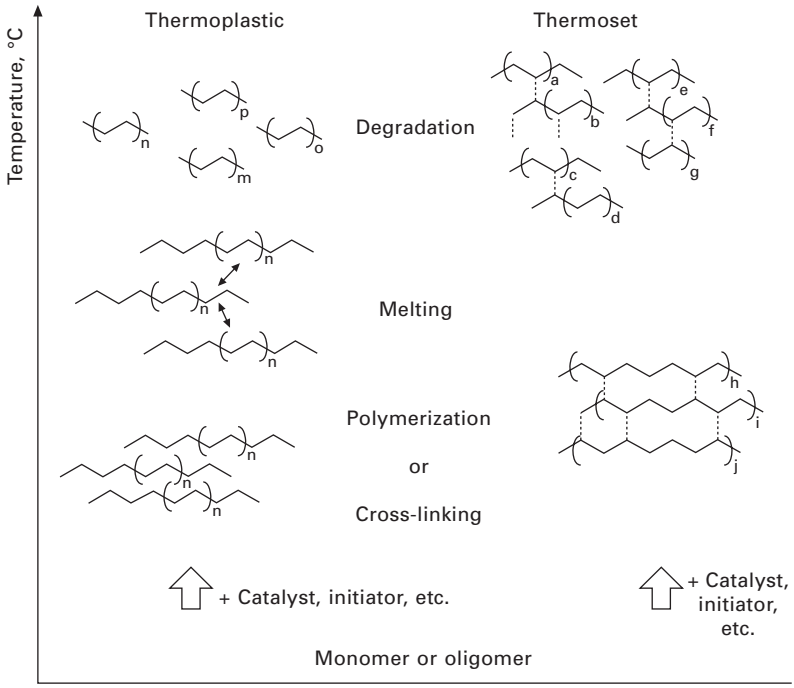

3.4 The behaviour of thermoplastics and thermosets against heat.

the unsaturated cross-linked polyesters also contain C=C bonds in the main chain, allowing cross-linking reactions. Cross-linked polyester products, such as aminoplasts or phenol-aldehyde resins, tend not be particularly rigid. One characteristic of unsaturated polyesters is that they are able to react with a vinyl group containing monomers; as noted above, the presence of C=C bonds leads to the cross-linking of the chains. It should be noted that this C=C bond does not participate in the condensation reaction that results in a polyester monomer unit, only in cross-linking reactions.

Polyesters may be formed through the reaction of dicarboxyl acids (phthalic acid, adipic acid) or carboxyl-anhydride (phthalic anhydride, maleic anhydride) and diols (ethylene diol, diethylene diol) with polycondensation reactions occurring at 180–220°C. The chemical structures of polyesters are shown in Fig. 3.5. The resulting polyester resin has a honey-like consistency, and is composed of a polyester monomer dissolved in a solvent, usually styrene, although vinyl-toluene, metacrylates and even phthalates can also be used. To ensure that the required cross-linking reactions occur, styrene and α-methyl-styrene are used as comonomers. There is therefore a high initial investment cost in the manufacture of polyesters, due not only to the cost of the solvent, but to expenses relating to recycling or reusing the products in accordance with strict environmental rules.

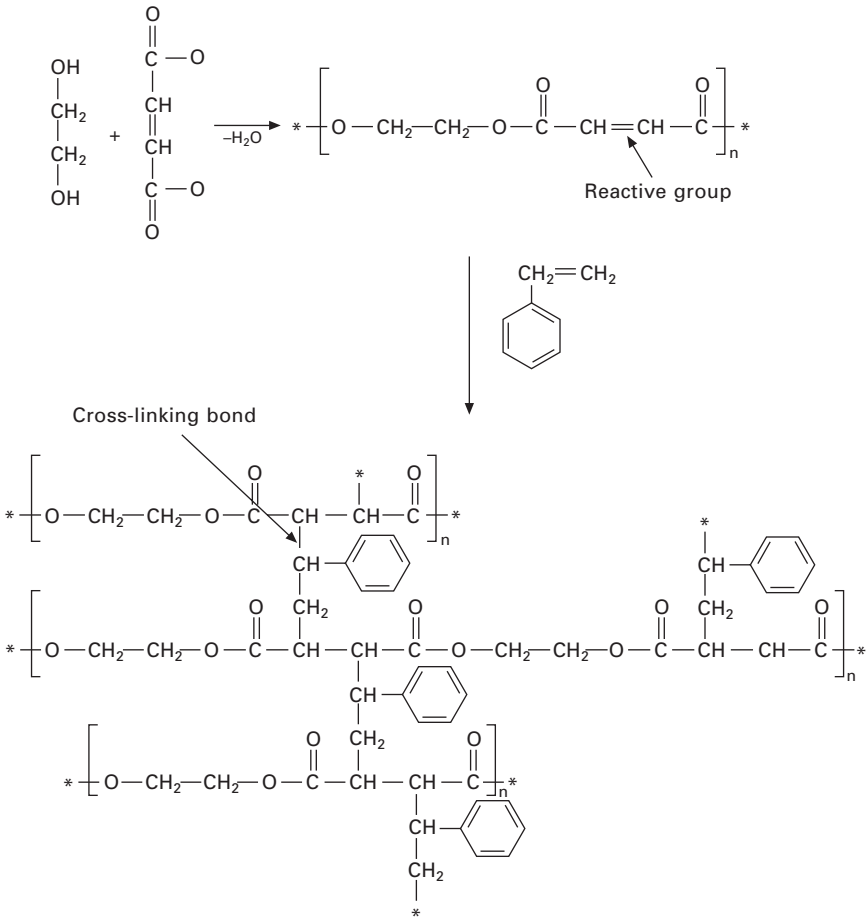

3.5 The chemical syntheses of polyesters.

The ratio of polyester to styrene in polyester resin is generally 0.5, as this has been found to offer the best properties. During the cross-linking reactions the volume of the product usually undergoes a 2–5% decrease known as die shrinkage. The reactions are initiated by the presence of oxygen, and can be maintained using paraffin. The styrene (or other solvent) plays several roles: it acts to decrease the the viscosity of the resin, which not only allows gelation during storage but also speeds up cross-linking reactions, which would otherwise be slow as the polymer molecules would be retained in the more viscous liquid; it allows cross-linking reactions without any by-products; and it also usually contains C=C bonds, meaning the number of chemical bonds in the polymer chain is increased. Although the solvent speeds up the cross-linking reactions, an initiator and accelerators (with the latter activating the former) are still needed to accelerate the reaction between the

C=C double bonds. Initiators and accelerators must be added separately to the polyester resin, usually just before the forming procedure. The initiator concentration should be 1–2%, and although the initiator plays no direct role in cross-linking and only serves to catalyse the reaction, the ratio of initiator to resin is still very important: if it is incorrect, false cross-linking may occur. The most widely used accelerators are cobalt- and manganese-based organic complex compounds.

The effect of temperature during the cross-linking of polyester resins is shown in Fig. 3.6. It has been demonstrated that cross-linking reactions are exothermic, requiring temperatures of below 150°C. In addition to the initiator and accelerator mentioned above, heat is also required to trigger the cross-linking reaction. After a slow start, the temperature is increased suddenly, meaning that the cross-linking reactions need only a relatively short time to build the final structure, such that the liquid is transformed very rapidly into a solid via a gel-like phase. The early heat treatment has a very important role not only in ensuring complete cross-linking but also in decreasing the internal stress.

Addition polymerization has a free radical mechanism, which has both advantages and disadvantages. One of the biggest problems in the use of polyester materials is ageing, since radicals can be affected by sunlight, heat and other environmental factors. The presence of free radicals can easily result in random and uncontrolled cross-linking in polyester resins, which must be avoided. One solution to this problem is the use of special additives, which are able to catch and block the free radicals, for example during long periods of storage, thereby stopping the cross-linking reactions. Other additives are

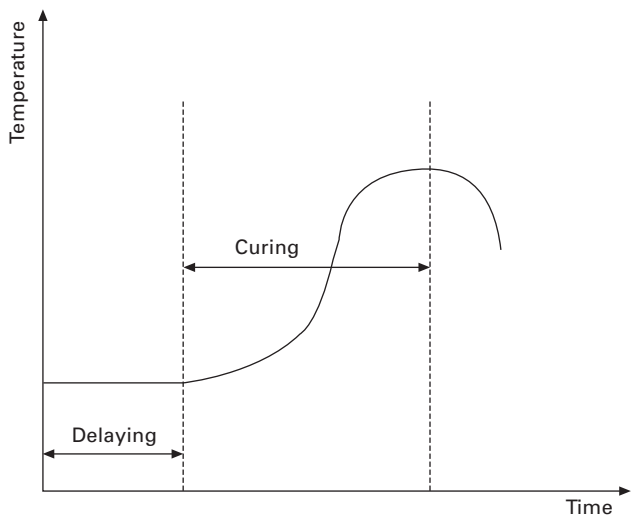

3.6 The cross-linking of thermosets.

also included during manufacture, such antioxidants, anti-ageing products, antidegradants, UV and heat stabilizers, and colouring materials.

One special type of polyester is vinylester. Vinylesters are similar in their molecular structure to polyesters (shown in Fig. 3.7) but differ in the location of their reactive sites. They have higher strength and better corrosion and chemical resistance than polyesters, as well as a higher operating temperature, but they are also more expensive. In vinylesters the cross-linking takes place via C=C double bonds positioned at the end of the polymer chain, meaning that the resulting thermoset contains fewer cross-linked bonds than polyester. The cross-linking mechanism is very similar to that of polyesters, and they experience the same problems with free radicals during long-term storage. Typical applications of vinylesters are in the wind turbine manufacture and automotive industries, among others.

Table 3.1 shows the production and application data of some polyester manufacturers. Plant capacities vary between 10,000 and 300,000 tonnes per annum. Some of the listed companies also manufacture vinylesters or epoxy thermosets as well as polyesters. The average price of polyester resin between 1999 and 2012 is demonstrated in Fig. 3.8, which shows that the price of polyester resin steadily increased until the economic crisis (2008), after which it decreases from nearly €2.5/kg to €1.6/kg. This tendency is similar to that observed for Brent crude; however, Brent crude underwent a sharper drop than polyester resin.

3.4 Manufacture of polyester-based composites

There are several well-known methods for manufacturing reinforced polyester composites, including hand lay-up, filament winding, sheet moulding, prepreg moulding, resin transfer moulding, vacuum-assisted moulding, and pultrusion. Figure 3.9 shows the use of different methods in Europe [1, 8].

Hand lay-up is one of the oldest methods of manufacturing reinforced polyesters. The first thermoset composites were manufactured in this way during World War Two. This method is particularly suitable for the manufacture of high-precision complex objects where only a limited number of items are required (100–300 yearly), or for prototypes. The process involves laying reinforcing materials into an opened die, and then laminating them with

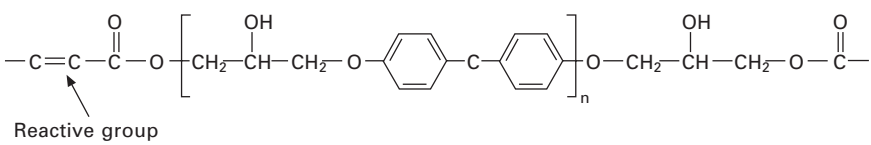

3.7 The chemical structure of vinylester.

Table 3.1 Some polyester manufacturing companies

Company	Production (tonnes p.a.)	Products/application	Source
Ashland Inc. (USA)	300,000	Pre-accelerated polyester resin. Adhesive, pigment, construction materials, additives, etc.	http://www.ashland.com/
Thai Polyester Co. Ltd	180,000	Polyester resins, polyester chip, draw textured yarn (DTY), polyester staple fibre (PSF), spin draw yarn (SDY), partially oriented yarn (POY), dope dyed yarn, mono filament	http://www.thaipolyester.com/
Shanghai New Tianhe Resin Co.	100,000	Pre-accelerated polyester resin applicable to auto parts	http://www.cnfrp.net/english/index.php?id=tianhe&web=0
Yaodonghua Furniture Boards Co. Ltd	100,000	Board, furniture, acoustic panel, chipboard, MDF panel, slot, board, plywood, particle board	http://yaodonghua.gmc.globalmarket.com
Kaiping Fuliya Composite Material Co.	30,000	Polyester resins, artificial stone, solid surface, countertop, sink	http://www.stonecontact.com
Zhejiang Guanghua Chemical Industry Co. Ltd	30,000	Polyester resin	http://zhejiang-guanghua.en.ywsp.com
Guangzhou Kinte Industrial Co.	30,000	Polyester resins, powder coatings, polyester clear powder, polyester/primid, polyester/TGIC, PU powder coating, MDF powder coating, epoxy resin epoxy/polyester, TGIC	http://www.kintepolyester.com/eng/news_details.asp?id=836&typeId=66
Anhui Huishang International Ltd	25,000	Polyester resins, raw materials for ink coating paint, raw material for powder coating, silane coupling agent, fibres for concrete	http://www.cccme.org.cn/shop/cccme10164/index.aspx
Hangzhou Showland Technology Co. Ltd	15,000	Adhesive, pigment, construction materials, pharma materials, rubber additives	http://www.showlandtech.com
Yantai Suny Chem International Co. Ltd	10,000	Aldehyde resin	http://www.sunychem.com/

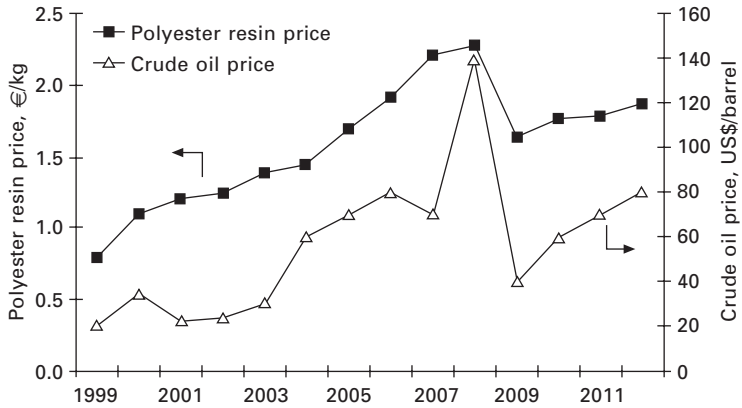

3.8 Price of polyester resin and crude oil (1999–2012) (personal discussion with Dr Gergő Lipoczi of Balatonplast Ltd) [56].

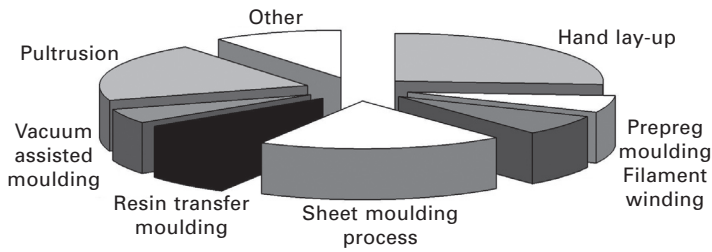

3.9 Polyester manufacturing in Europe (2008).

polyester resin, using specially designed rollers to ensure that the laminate will be free from gas or air bubbles. The composite laminate may contain up to 10 layers of reinforcing material. The outer layer of products manufactured in this way is known as the resin-rich gel layer, and offers resistance against environmental, mechanical and other types of damage.

The hand lay-up method may be followed by a prepreg moulding step, which controls the resin content of the composite. The prepreg is a mixture of resin, reinforcements, catalyst, hardener, etc. Prepreg moulding is typically used when the reinforcements are in the form of woven or unidirectional fibres, to ensure that they are aligned in the required orientation. The main disadvantage of the prepreg moulding technique is the high price of the prepreg materials; the process also requires the use of a vacuum bag, autoclave moulding or even oven curing. Owing to this high investment cost, the use of prepreg moulding is generally limited to applications such as the aerospace industry and F1 car manufacturing.

Filament winding involves the rolling of previously impregnated continuous

reinforcement fibre onto an axially symmetric base, which is in the form of a cone for easy product removal. The roving axis can be calculated and determined in advance. The resin and cut filaments are mixed in a sprinkler machine, and then moved to the surface of the die by compressed air. The diameter of the objects can be up to 40 m, with a weight of up to 15 t. The fibre content can be as high as 60–70%. The process can easily be automated, and can therefore be free from human errors, resulting in products with high reproducibility. The process is also efficient and relatively cheap; it can be used in the manufacture of pressure vessels, wind plates and train carriages.

The sheet moulding process is a very simple process for the line production of reinforced composites. It requires a hydraulic sheet moulding machine combined with a metallic high-precision die for heating. The matrix and reinforcing materials can be chopped or continuous, or a mixture of the two, and must be mixed immediately before the die is filled with resin. The process allows the manufacture of products with a short cycle time, making it particularly suitable for the automotive industry, for example. One disadvantage is that complex shapes cannot always be manufactured using this process.

In resin transfer moulding, the resin is injected into a mould containing layers of fibres or a preform at low pressure. The process cycle time is less than 3 minutes, and the fibre content of the composite product is up to 50%. The advantages of the process are design flexibility, ability to manufacture larger structures, low cost (thanks to the low pressures involved) and rapid manufacture. As with sheet moulding, resin transfer moulding is widely used in the automotive industry to manufacture a variety of parts for cars and other vehicles.

Pultrusion is a very similar process to the extrusion of thermoplastics, and is effectively the only continuous manufacturing method for thermoset composites that allows complex shapes to be produced. In the process the reinforcements are impregnated with a resin that has particularly low viscosity, and are drawn through via a die heated to a temperature of 110–160°C, which is the point at which curing reactions occur, and the fibres are permanently tensioned in the direction of the axis during curing. The profile manufacturing machines have a velocity of 1.5–60 m/h. The die should undergo several preforming steps at different temperatures, leading to a die length of as much as 1.5 m in the case of U or C profile manufacturing. Profiles have very high tensile and flexural strength only in the direction of the axis; the critical property is therefore the stiffness and strength in the cross direction, which can be improved through the use of fabric or non-fabric. Currently, pultrusion is used for the manufacture of products for use in industries including civil engineering and automotive; significant growth is also predicted, with beams, frameworks and shovel handles expected to be manufactured by this process in the future.

Vacuum-assisted moulding involves the application of a vacuum immediately before the mould is closed, and can be used to produce composites containing high levels (55–65%) of reinforcing materials. This means that the products manufactured in this way have higher strength in relation to their mass than products manufactured by other methods. The process involves a two-part die, in which one part is the negative form of the other. The product is placed between the two parts, which are pressed with a vacuum, and the resin is drawn into the hole by a second vacuum. As the die is closed, vacuum-assisted moulding is the most environmentally friendly method for manufacturing thermosets, but the initial investment and operating costs are relatively high. Moreover, vacuum-assisted moulding cannot be used in the manufacture of products with a complex shape.

3.5 Reinforcements for polyester-based composites

Owing to their low strength and weak mechanical properties, polyesters always require inorganic materials, usually in fibre or plate form, to reinforce the structure. Reinforcements are used to increase density, stiffness, tensile and flexural strength, graving resistance, water resistance, gluing ability, and even the impact properties and anisotropy. However, weldability, shrinkage during processing and the linear heat extension coefficient all decrease as a result of the addition of these reinforcing materials. The main disadvantages of reinforced polyesters are that the processing is more complicated, the costs involved are higher, and the processing machines undergo considerably greater wear compared to machines used only for pure matrix materials or other unreinforced plastics. Moreover, some reinforcements are very harmful to human health, due, for example, to their very small particle size, as is the case with the nanoparticles present in asbestos. The main properties of unreinforced and reinforced polyesters are summarized in Table 3.2.

The following standardized and non-standardized methods are used to measure the properties and structures of reinforced and unreinforced polymers and polymer composites:

- Plastics. Methods for determining the density of non-cellular plastics. Part 1: Immersion method, liquid pyknometer method and titration method (ISO 1183-1:2004)
- Plastics. Determination of tensile properties. Part 1: General principles (ISO 527-1:1993)
- Plastics. Determination of compressive properties (ISO 604:2002)
- Plastics. Determination of flexural properties (ISO 178:2001)
- Fibre-reinforced plastic composites. Determination of flexural properties (ISO 14125:1998)
- Fibre-reinforced plastic composites. Determination of apparent interlaminar shear strength by short-beam method (ISO 14130:1997)

Table 3.2 The most important properties of unreinforced and reinforced polyester

	Unreinforced	Reinforced
Tensile strength, MPa	45–95	70–150
Tensile modulus, GPa	2–5	3–6
Elongation, %	<5	<5
Flexural strength, MPa	50–150	100–200
Flexural modulus, GPa	1–4	2–6
Compressive strength, MPa	80–190	90–250
Density, g/cm^3	1.15–1.50	1.20–1.70
Advantages	Easy to use Low cost of resins	Higher mechanical properties High chemical and environmental resistance
Disadvantages	Weaker mechanical properties High styrene emissions during manufacturing Limited range of processing times High cure shrinkage	High fibre content Higher cost than unreinforced polyesters Difficult to recycle

Sources: References 1, 2, 4 and 9–13.

- Plastics. Determination of Charpy impact properties. Part 1: Non-instrumented impact test (ISO 179-1:2000)
- Plastics. Determination of Charpy impact properties. Part 2: Instrumented impact test (ISO 179-2:1993)
- Plastics. Determination of ash. Part 1: General methods (ISO 3451-1:1997)
- Plastics and ebonite. Determination of indentation hardness by means of a durometer (Shore hardness) (ISO 868:2003)
- Plastics. Methods of exposure to laboratory light sources. Part 1: General guidance (ISO 4892-1:1999)
- Plastics. Methods of exposure to laboratory light sources. Part 2: Xenon-arc lamps (ISO 4892-2:2006)
- Plastics. Methods of exposure to laboratory light sources. Part 3: Fluorescent UV lamps (ISO 4892-3:2006)
- Scanning Electron Microscopy (SEM) is used to study the structure of fractured faces of specimens and to follow the possible interaction between the polymers and reinforcements.
- For chemical composition analysis Fourier transform infrared (FTIR) or even Raman spectrometry are used.

It should be noted that thermoplastic composites also require the addition

of a filler: the main difference between the filler and the reinforcing materials is that the latter do not have the same measurements in all three dimensions. The main properties of some widely used reinforcements and fillers are shown in Table 3.3.

Reinforcements are arranged in different ways: they can be laid in one continuous direction, oriented at 0/90°, laid in different directions in different layers, or even arranged randomly, as in fact is the case with the most widely used composites. Quite often the fibres have to be combined with others in order to achieve improved properties: the resulting composites are known as hybrid, and are usually composed of thermosets, glass fibre and carbon fibre.

Glass fibre, which is a combination of different oxides, is the oldest type of reinforcing material. The physical and chemical properties of the glass fibre are significantly affected by the composition of its constituents, the diameter of the elemental fibre, and the surface treatment applied. The surfaces of most commercial glass fibres are treated with different chemicals, in a process known as sizing, in order to achieve better properties. In commercial use, the glass fibres are roving fibres, meaning that one fibre consists of 10^3–10^4 elemental fibres which have a diameter of 5–15 μm. E- and S-type glass fibres are the mostly commonly used for polyester reinforcement. In civil engineering the E-type is dominant, accounting for 80–95% of the market. E-type glass fibre contains 50–60% SiO_2, while the remaining part is Al_2O_3, B_2O_3, CaO and others (e.g. boric acid, $CaCO_3$, $MgCO_3$) [4–7, 14–16].

Carbon fibre reinforced polyesters account for a relatively small section of the market, at 8–12%, but are experiencing rapid growth and carbon fibre is the leading reinforcement material for 'high-tech' composites. The first carbon fibre was the cellulose-based Thornel-25, manufactured by Union Carbide at the end of the 1950s. Carbon fibre generally has higher tensile strength and better resistance against corrosion and fatigue than glass fibre, but has low impact strength and a tendency to brittleness. Carbon fibre

Table 3.3 The main properties of the commonly used reinforcements in polyester composites

Properties	Reinforcement				
	Cellulose	Basalt fibre	Glass fibre	Carbon fibre	Aramid
Tensile strength	+++	++++	++++	++++	++++
Flexural strength	+++	+++	++++	++++	++++
Electrical properties	+++	+++	++++	+	+++
Heat resistance	+++	++++	++++	++++	++++
Water resistance	++	++++	+++	+++	+++
Painting	+++	+	++	+	++

Key: +: weak, ++: medium, +++: good, ++++: excellent.

manufacture requires extreme heating and cooling, and a relatively recently developed technique reuses crude oil and tar for the purpose.

The manufacturing process involves first heating the material up to 200°C, causing the formation of a finned structure. The fibre has high thermal stability and does not melt during carbonization. The temperature is then increased to 250–300°C, when air is additionally added into the reaction vessel to cause the oxygenation of $—CH_2—$ groups, in order to avoid burning or degradation of the fibre at temperatures of over 1000°C. In inert atmosphere the fibres begin to cross-link, leaving behind hydrogen cyanide, water or nitrogen. The fibre strength and E-modulus suddenly increase when the temperature is raised above 400°C. In an inert atmosphere, carbonization takes places in the 1000–1500°C temperature range, while graphitization occurs between 2500 and 3000°C. The temperatures of these last two steps are responsible for the final structure and properties of the carbon fibre [17, 18]. There are two commercialized carbon fibres: HS (carbonized) and HM (graphitized).

In addition to the glass and carbon fibres discussed above, aramid and boron fibres may also be used as reinforcing materials. Aramid fibres are made from aromatic polyamide fibres and have very high strength, probably due to the orientation of the fibres during the process. There are two types of aramid fibres: para- and meta-aramids, with the former used much more widely in industrial applications. Aramid fibre reinforced composites have low density, high strength, advanced dynamic properties and good fire resistance, but also low press strength and high sensitivity to environmental factors [19]. Boron fibre is five times as strong as steel, and twice as hard. During processing, boron atoms are impregnated on the surface of tungsten or carbon fibres.

During the processing of reinforced composites, incompatibility between the reinforcements and the matrix materials can cause a variety of problems, due to the different chemical properties of the constituents, which results in very poor adhesion between them. A possible solution is the chemical modification of both the reinforcements and the matrix. A strong interfacial interaction is required for adequate load transfer. Strong adhesion between the phase and the reinforcements results in a poor phase–matrix relationship, because the phase border plays a key role in determining the properties of the composite. The efficiency of the load transfer between the reinforcement and the matrix is affected not only by molecules on the phase board, but also by other properties, such as thickness.

There are several means of modifying the surface of the reinforcements to obtain composites with improved properties, with different coupling agents and techniques needed for different composites. Table 3.4 provides some examples of reinforced thermosets with surface modifications [20–24]. With regard to coupling agents, the key factor is the chemical structure, because the strong connection that is needed to ensure load transfer in the

Table 3.4 The most used surface treating agents and their effects

Fibre	Additive	Tensile strength	Modulus	Flexural strength	Impact strength
Natural fibre	Vinyl-trimethoxy-silane	↔	↔	↓	↔
Natural fibre	γ-Metacryl-oxypropyl-trimethoxy-silane	↔	↑	↔	↓
E-glass fibre	Amino-silane	↑	↑	↑	↓
E-glass fibre	Glycidoxy-silane	↑	↑	↔	↑
E-glass fibre	Vinyl-silane	↑	↑	↓	↔
E-glass fibre	Metacryl-silane	↑	↑	↓	↑

Key: ↑: increasing, ↓: decreasing, ↔: no effect.

reinforcement phase board can only develop when chemical interaction occurs between the reinforcement and the matrix. The coupling agents are hydrocarbons containing short chains in which one end group is compatible with the reinforcement, while the other is compatible with the matrix. In case of glass fibre reinforced polyesters, siloxane-type coupling agents ($SiR_y(OR)_x$) are usually used, because the –OX groups are able to connect with the –OH groups on the glass surface. Other widely used surface treating agents are organotitanes and organic circonates, which are used for both glass and carbon fibre reinforced composites at concentrations of 0.1–0.5%.

3.6 Applications of polymer-based composites

As discussed previously, polyesters increase in hardness at high temperatures, because heat leads to the formation of cross-linked chemical bonds between the polymer chains, providing a strong permanent structure which is maintained even under extreme conditions (chemical stress, exposure to radiation, and so on). The properties of reinforced polyesters are often therefore more suitable than those of conventional structural materials for a number of applications, especially for longer use. Polymers are also more environmentally friendly than alternative materials over their whole life cycle, and can be widely reused, as well as having low maintenance costs. Their average life cycle is 40 years (with a minimum of 5 and a maximum of 90) in the construction industry.

3.6.1 Traditional applications

The different application areas of polyesters are summarized in Fig. 3.10. Polyesters and their composites are used mainly in transportation (in the manufacture of cars and other vehicles), in the marine and shipping industry,

and in structural materials. In civil engineering, sprinkler and drainage systems, water and gas pipes, bridge constructions, fittings and joints, wall covering panels, insulators (against heat and noise), roof panels, doors and window elements, can all be made from reinforced polyester composites. Figure 3.11 summarizes the relationship between the production method and the traditional application fields of polyester-based reinforced composites, which are also briefly discussed in Section 3.4. In the aerospace and construction industries, filament winding and pultrusion are the normal manufacturing methods, while the automotive sector tends to use composites formed through. resin transfer moulding and prepreg moulding. Only hand lay-up is used for non-structural applications [25].

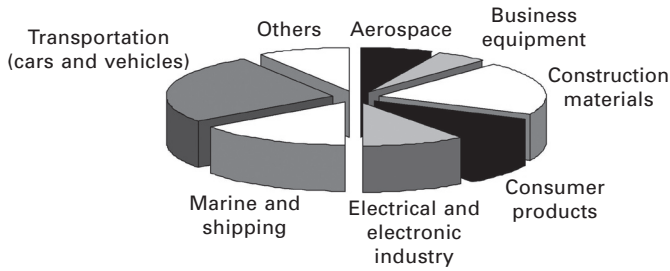

3.10 The application of polyester composites in 2009.

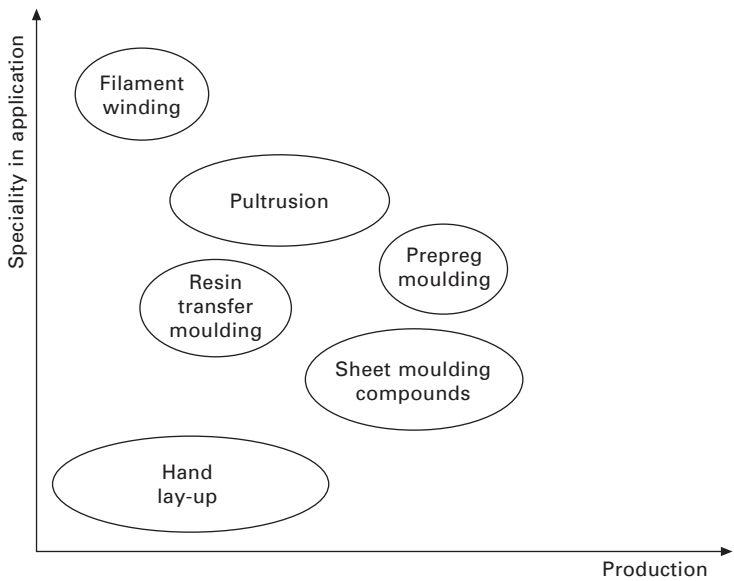

3.11 Polyester manufacturing processes (based on http://www.azom.com/article.aspx?ArticleID=352) [55].

Polymers, and particularly polyesters, are widely used in the automotive industry. Nowadays an average car contains over 100 kg of plastics; without plastics, the car would be 200–300 kg heavier, which is equivalent to an extra 0.5–0.9 litres of fuel consumption per 100 km. More than 1,000 different car parts can be made of polymers, but the types of polymers are limited, with fewer than 15 different polymers used. The Chevy Volt, a prototype of an electric car, was introduced by General Motors in 2009 and consists of a variety of polymers. Tests have shown that the car could offer fuel savings of up to 2000 litres a year. Moreover, the elements made from special polymer composites had better resistance against environmental and mechanical factors [26–30]. In the aerospace industry, Kazmerski *et al*. introduced a new use for reinforced composites in aircraft. It was demonstrated that 6000 rivets and 300 metallic parts of the Airbus A 340 aircraft could be replaced by 100 composite elements, for example, in the turbine wings, achieving a two-ton weight reduction [7, 31].

Glass fibre reinforced polyester composites are well known and widely used as construction materials in civil engineering. Biddah *et al*. (2007) investigated the possibility of using glass fibre reinforced polyester composite grids to produce 'I' form beams for bridges. The aim of this experimental work was to manufacture a composite concentrate for use in constructional parts of bridge, avoiding the use of metal-based materials and their associated corrosion problems. Different combinations of the reinforcements and matrix compositions were tested under different environmental circumstances, and the results showed that the ideal combination of thermosets and traditional constructional materials had indeed been identified [32].

In civil engineering, composites are coming to be used in areas where traditional materials have been dominant. Many elements in the construction of a house can be made from reinforced polymers, especially thermosets. Although investment in house renovation has fallen since the economic crisis, there is still interest in applications such as garage doors and so on. Companies are therefore focusing on applications of reinforced thermoset-based elements outside the house [33]. Inside the house, one area in which polyester-based polymers are being increasingly used is in the manufacturing of bathroom accessories such as WC seats, hand dryers, shower cubicles, baths, and so on [34, 35]. The main benefit of using polyester is its long life cycle, but the products remain relatively expensive.

Other specialized areas in which polyesters are used include pasted laminated wooden beams, wooden pressboards, carpet underlay, larger beams, wood covering materials, pipes, piles, traffic accessories, reinforced tables, and so on. In one specific study, Garcia-Guinea *et al*. (1998) constructed the first organ made from marble and thermoset polymer. Thermoset composites were used to connect the marble parts of the instrument and to cover certain parts of it. The instrument has the same functional properties

as an equivalent made from conventional materials, but some advantages were identified during the manufacturing process [36]. A final specialized application for functionalized polyesters is in tissue enginnering, as a corrosion inhibitor. For all applications, the ageing properties of the polymer are crucial [37–40].

3.6.2 Advanced polymers for new applications

Polymers can degrade at extremely high temperatures, meaning that materials made from polymeric compounds must contain fire retardants and heat stabilizers, but environmental concerns have led to attempts to limit the concentration of this type of additive. Barder has introduced a new type of high-temperature thermoset resin called Crestapol 1234, which was able to give better resistance against temperatures of above 300°C. The advanced properties of the new material have been assessed on the basis of the heat deflection temperature. The results have shown that Crestapol 1234 has superior properties to commercially available thermosets such as polyimide, PEI, PES and cyanide esters. The gel time is 16–17 minutes, meaning that the ideal manufacturing methods are hand lay-up or closed moulding. The proposed application areas for this new material are in civil engineering, aircraft manufacturing and the automotive industry, the electronics sector, and even the oil and gas sectors [41].

Rhodes *et al*. demonstrated a new type of thermoset (46-16-46-S BMC) with a relative temperature index of 170°C, the highest that can be achieved by reinforcing thermoset composites. The relative temperature index refers to the heat stability of the materials. The composite is ideal for outdoor lighting applications such as in car parks, for reflectors, and in tramway and runway light systems, where the hot light sources are often very close to the covering panels. The same material could also be used to replace moving machine parts where heat can be generated, such as in air conditioning systems and ventilators, and in the automotive sector The main benefits are very high strength and stability, low weight and costs and high corrosion resistance [42].

In the last decade an increasing number of scientific papers have reported the successful application of bio-based polyester composites in new areas of civil engineering. For example, soy-based polyurethanes and polyesters can be used as foam-like insulators for passenger cars and other vehicles, trains, aircraft. and farmyard machinery. In these applications the foaming procedures used, both chemical and physical, are the same as those used in conventional thermosets. These bio-based thermosets could be used as bonding agents during the manufacture of furniture, mats and rugs. They are also suitable for use as biocompatible packaging materials, and as structural materials in the manufacture of ships and boats, where they could replace

the traditionally used glass fibre reinforcements and could offer advantages in terms of strength and water resistance.

Creative Pultrusion Inc. use a compression process to manufacture parts of bridges and other products, including cables, plates, Bethlehem beams and wooden panels, and even platform coverings for public transport have been manufactured and tested. A new product has been developed, known as SuperLoc composite plate pier, which has a unique 'ball-and-stock' connection between the panels. The main application areas for this new product are in swimming pools, pedestrian walkways, docks, shipyards, and so on. Another new product is DuraSpan, which is designed for use in fibre-reinforced polymers for bridge construction [32].

3.6.3 Environmental considerations

One of the biggest challenges in today's society is the question of waste recycling. More than 4 billion tons of municipal solid wastes is produced annually worldwide, with the EU member states alone producing more than 250 million tonnes, with an annual growth of 4%. Municipal solid waste consists of plastic (approximately 15%), paper and other organic wastes. There are several methods that can currently be used to recycle or reuse waste polymers, but only a few of these constitute a real solution to the problem. One promising method is known as mechanical recycling, when waste polymers are reused in the form of plastics. Among others, Conroy, Halliwell and Reynolds have investigated the possibility of reusing thermosets for producing plastic beams, door panels, glass fibre-reinforced chipboard (13 mm and 17 mm thickness) and materials for motorway construction [5]. In addition, electromagnetic interference shadow panels for electronic equipment have been developed by reusing carbon fibre-reinforced polymers, and studies have investigated the effects of thickness, density and fibre length on the mechanical and electrical properties of the final product [31, 43–49].

In addition to waste recycling, another environmental issue relating to polymer composites is the generation of energy from alternative sources. Owing to limited fossil fuel resources, governments worldwide are focusing their attention on alternative energy, such as solar and wind power. Papers published in the last decade have shown that polyester-based structural materials can successfully be used in facilities for solar or wind energy generation [50, 51]. Natural fibre-reinforced polyester composites have shown the best properties for this and other applications from an environmental perspective [52–54].

3.7 Conclusion and future trends

Polyesters are one of the most important thermosets for use in constructional materials, being used in a variety of applications in everyday life. Fibre-

reinforced polyester composites can be manufactured using a number of methods, including hand lay-up, filament winding, sheet moulding, prepreg moulding, resin transfer moulding, vacuum-assisted moulding and pultrusion. Polyesters are able to maintain their strong structure under extreme conditions such as high temperatures and exposure to radiation; reinforced polyesters can therefore sometimes offer better properties than conventional structural materials in certain applications They have low maintenance costs and can be effectively reused throughout their whole life cycle. As a result, they have a wide range of applications in the transportation industry, shipbuilding and civil engineering, among many others.

A possible future trend in polyester-based composites is the improvement of their mechanical properties, combined with the addition of new specialized properties. Studies are currently investigating different combinations of reinforcements and developing new types of coupling agents with this aim in mind. Hybrid composites are a particular area of interest, as these allow the beneficial properties of different reinforcing materials to be combined, Soft fibres such as aramid and polyethylene are often used alongside carbon fibre in fibre-reinforced hybrid composites. The price of these carbon fibre-reinforced composites could be decreased and the impact properties increased by the use of glass fibres instead of carbon. The carbon fibre content is responsible for the good flexural modulus of these hybrid composites. The average fibre length also could be affected by the carbon fibre/glass fibre ratio; the fibres are longer if the glass content is higher, but shorter if the carbon content is higher. The advanced properties of hybrid composites are also demonstrated by their good wear resistance, which is valuable in marine applications.

A second important question for the future is the efficient use of different manufacturing processes. The main driving forces in this area of research are potential cost reduction, increased productivity, and improvements in the advanced properties of composites. Figure 3.12 shows a comparison of the different manufacturing processes. Currently, filament winding provides the highest fibre content (up to 65%), followed by pultrusion (up to 55%), resin transfer moulding (up to 45%) and sheet mould compounds (up to 35%). The main aim of research in this area is for all the manufacturing processes to be able to offer the same fibre content in the final product as filament winding, while still maintaining the same level of productivity.

3.8 Acknowledgements

The author is grateful to the TAMOP-4.2.1/B-09/1/KONV-2010-0003 Project (financially supported by both the Hungarian State and the European Union) and to the Institute of Chemical Engineering Cooperative Research Centre of the University of Pannonia.

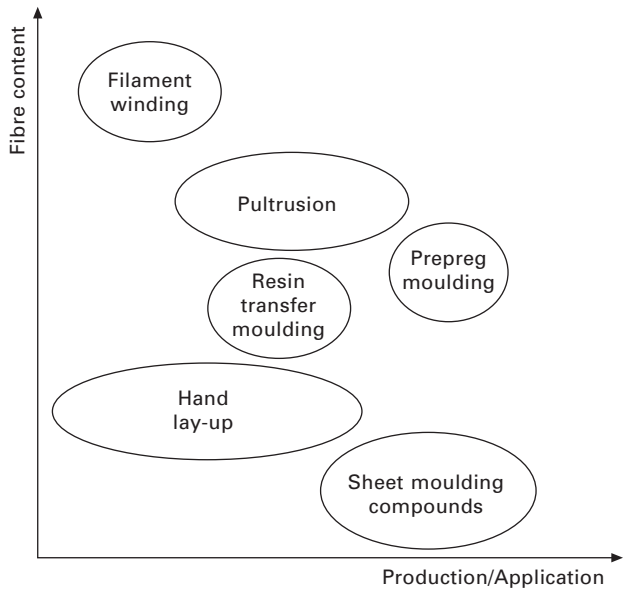

3.12 Relation between the fibre content and production data by different manufacturing processes (based on http://www.azom.com/article.aspx?ArticleID=352) [55].

3.9 References

1. Edwards K L (1998) 'An overview of the technology of fibre-reinforced plastics for design purposes', *Mater Design*, 19, 1–10.
2. Khan A S, Colak O U, Centala P (2002) 'Compressive failure strengths and modes of woven S2-glass reinforced polyester due to quasi-static and dynamic loading', *Int J Plasticity*, 18(10), 1337–1357.
3. Skrifvars M, Mackin T, Skagernerg B (1998) 'An application of experimental design to the development of glass fibre reinforced polyester laminates with enhanced mechanical properties', *Polym Test*, 17(5), 345–356.
4. Dandekar D P, Hall C A, Chhabildas L C, Reinhart W D (2003) 'Shock response of a glass-fiber-reinforced polymer composite', *Comp Struct*, 61(1–2), 51–59.
5. Manfredi L B, Rodrıguez E S, Wladyka-Przybylak M, Vazquez A (2006) 'Thermal degradation and fire resistance of unsaturated polyester, modified acrylic resins and their composites with natural fibres', *Polym Deg Sta*, 91, 255–261.
6. Zhu Y T, Valdez J A, Beyerlein I J, Zhou S J, Liu C, Stout M G, Butt D P, Lowe C T (1999) 'Mechanical properties of bone-shaped-short-fiber reinforced composites', *Acta Mater*, 47(6), 1767–1781.
7. Soutis C (2005) 'Carbon fiber reinforced plastics in aircraft construction', *Mater Sci Eng A*, 412(1–2), 171–176.
8. Varatharajan R, Malhotra S K, Vijayaraghavan L, Krishnamurthy R (2006) 'Mechanical and machining characteristics of GF/PP and GF/polyester composites', *Mat Sci Eng B*, 132(1–2), 134–137.
9. Pardo S, Baptiste D, Décobert F, Fitoussi J, Joannic R (2002) 'Tensile dynamic

behaviour of a quasi-unidirectional E-glass/polyester composite', *Comp Sci Tech*, 62(4), 579–584.
10. Mishra S, Mohanty A K, Drzal L T, Misra M, Parija S, Nayak S K, Tripathy S S (2003) 'Studies on mechanical performance of biofibre/glass reinforced polyester hybrid composites', *Comp Sci Tech*, 63(10), 1377–1385.
11. Rot K, Huskic M, Makarovic M, Mlakar T L, Zigon M (2001) 'Interfacial effects in glass fibre composites as a function of unsaturated polyester resin composition' *Composites Part A*, 32(3–4), 511–516.
12. Wan Y Z, Wang Y L, He F, Huang Y, Jiang H J (2007) 'Mechanical performance of hybrid bismaleimide composites reinforced with three-dimensional braided carbon and Kevlar fabrics', *Composites Part A*, 38, 495–504.
13. Saidpour S H, Richardson M O W (1997) 'Glass fibre coating for optimum mechanical properties of vinyl ester composites', *Composites Part A*, 28, 97l–975.
14. Sutherland L S, Soares C G (2005) 'Impact on low fibre-volume, glass/polyester rectangular plates', *Comp Struct*, 68(1), 13–22.
15. Mouzakis D E, Zoga H, Galiotis C (2008) 'Accelerated environmental ageing study of polyester/glass fiber reinforced composites (GFRPCs)', *Composites Part B*, 39, 467–475.
16. Huang G, Sun H (2007) 'Effect of water absorption on the mechanical properties of glass/polyester composites', *Mater Design*, 28(5), 1647–1650.
17. Chung D D L (1994) *Carbon Fiber Composites*, Butterworth-Heinemann, Newton, MA.
18. Bunsell A R (1988) *Fibre Reinforcements for Composite Materials*, Elsevier, Amsterdam p. 93.
19. *Ibid*., p. 120.
20. Park S J, Jin J S (2001) 'Effect of silane coupling agent on interphase and performance of glass fibers/unsaturated polyester composites', *J Colloid Interf Sci*, 242(1), 174–179.
21. Abdul Khalil H P S, Ismail H (2001) 'Effect of acetylation and coupling agent treatments upon biological degradation of plant fibre reinforced polyester composites', *Polym Test*, 20, 65–75.
22. DiBenedetto A T (2001) 'Tailoring of interfaces in glass fiber reinforced polymer composites: a review', *Mat Sci Eng A*, 302(1), 74–82.
23. Bagherpour S, Bagheri R, Saatchi A (2009) 'Effects of concentrated HCl on the mechanical properties of storage aged fiber glass polyester composite', *Mater Design*, 30, 271–274.
24. Park J M, Quang S T, Hwang B S, Lawrence DeVries K (2006) 'Interfacial evaluation of modified jute and hemp fibers/polypropylene (PP)–maleic anhydride polypropylene copolymers (PP–MAPP) composites using micromechanical technique and nondestructive acoustic emission', *Comp Sci Techn*, 66, 2686–2699.
25. Moon J I, Lee Y H, Kim H J (2012) 'Synthesis and characterization of elastomeric polyester coatings for automotive pre-coated metal', *Progr Org Coat*, 74, 125–133.
26. Schubel P J, Parsons A J, Lester E H, Warrior N A, Rudd C D (2006) 'Characterisation of thermoset laminates for cosmetic automotive applications: Part II – Cure and residual volatile assessment', *Composites Part A*, 37, 1747–1756.
27. Markarian J (2005) 'Automotive and packaging offer growth opportunities for nanocomposites', *Plastics Additives and Compounding*, November/December, 18–21.

28. Marsh G (2003) 'Next step for automotive materials', *Materials Today*, April, 36–43.
29. Stewart R (2011) 'Rebounding automotive industry welcome news for FRP', *Reinforced Plastics*, January/February, 38–44.
30. Henning F, Ernst H, Brüssel R, Geiger O, Krause W (2005) 'LFTs for automotive applications', Reinforced Plastics, February, 24–33.
31. Soutis C (2005) 'Fibre reinforced composites in aircraft construction', *Progr Aerospace Sci*, 41, 143–151.
32. Biddah A (2007) 'Structural reinforcement of bridge decks using pultruded GFRP grating', *Comp. Struct.*, 74, 80–88.
33. Westaway D (2004) 'Is there a future for composites in buildings?', *Reinforced Plastics*, June, 38–40.
34. Brady M (2008) 'Composites on the move', *Reinforced Plastics*, 52(10).
35. Stewart J, Minchin R E (2004) 'Potencial construction applications for thermoset composite scrap material', *J Constr. Eng. Mgmt.*, 130, 199–205.
36. Garcia-Guinea J, Larrea-Bellod I, Banuls V, Harffy M (1998) 'Advanced uses of thermoset-marble compounds in construction: first stone pipe organ in the world', *Constr. Build. Mater.*, 12(1), 1–8.
37. Seyednejad H, Gawlitta D, Dhert W J A, Nostrum C F, Vermonden T, Hennink W E (2011) 'Preparation and characterization of a three-dimensional printed scaffold based on a functionalized polyester for bone tissue engineering applications', *Acta Biomater*, 7, 1999–2006.
38. Alsabagh A M, Migahed M A, Awad H S (2006) 'Reactivity of polyester aliphatic amine surfactants as corrosion inhibitors for carbon steel in formation water (deep well water)', *Corrosion Sci*, 48, 813–828.
39. Beltrán J F, Williamson E B (2011) 'Numerical procedure for the analysis of damaged polyester ropes', *Eng Struct*, 33, 1698–1709.
40. Segovia F, Ferrer C, Salvador M D, Amigó V (2000) 'Influence of processing variables on mechanical characteristics of sunlight aged polyester–glass fibre composites', *Polym Deg Stab*, 71, 179–184.
41. Bader S (2011) 'High temperature thermoset resin', *Reinforced Plastics*, July/August.
42. Rhodes P (2009) 'Thermoset composites receive highest UL temperature rating', *Reinforced plastics*, June/July, 53.
43. Conroy A, Halliwell S, Reynolds T (2006) 'Composite recycling in the construction industry', *Composites Part A*, 37, 1216–1222.
44. Wong K H, Pickering S J, Rudd C D (2010) 'Recycled carbon fibre reinforced polymer composites for elektromagnetic interference shielding', *Composites Part A*, 41, 693–702.
45. Causin V, Marega C, Marigo A (2007) 'When polymers fail: A case report on a defective epoxy resin flooring', *Engineering Failure Analysis*, 14, 1394–1400.
46. van Vuure A W, Ivens J A, Verpoest I (2000) 'Mechanical properties of composite panels based on woven sandwich-fabric preforms', *Composites Part A*, 31, 671–680.
47. Cunliffe A M, Williams P T (2003) 'Characteristion of products from the recycling of glass fibre reinforced polyester waste by pyrolysis', *Fuel*, 83, 2223–2230.
48. López F A, Martín M I, Alguacil F J, Rincón J M, Centeno T A, Romero M (2012) 'Thermolysis of fibreglass polyester composite and reutilisation of the glass fibre residue to obtain a glass–ceramic material', *J Anal Appl Pyrolysis*, 93, 104–112.

49. Vargas M A, Sachsenheimer K, Guthausen G (2012) 'In-situ investigations of the curing of a polyester resin', *Polym Test*, 31, 127–135.
50. Lim Y S, Kim L C, Teh G B (2012) 'Unsaturated polyester resin blended with MMA as potential host matrix for luminescent solar concentrator', *Renewable Energy*, 45, 156–162.
51. Yang D, Tian M, Kang H, Dong Y, Liu H, Yu Y, Zhang L (2012) 'New polyester dielectric elastomer with large actuated strain at low electric field', *Mater. Lett*, 76, 229–232.
52. Sever K, Sarikanat M, Seki Y, Erkan G, Erdoğan Ü H, Erden S (2012) 'Surface treatments of jute fabric: The influence of surface characteristics on jute fabrics and mechanical properties of jute/polyester composites', *Industrial Crops and Products*, 35, 22–30.
53. Ratna Prasad A V, Mohana Rao K (2011) 'Mechanical properties of natural fibre reinforced polyester composites: Jowar, sisal and bamboo', *Mater Design*, 32, 4658–4663.
54. Sathishkumar T P, Navaneethakrishnan P, Shankar S (2012) 'Tensile and flexural properties of snake grass natural fiber reinforced isophthalic polyester composites', *Comp Sci Tech*, in press, accepted manuscript.
55. Azom – The A to Z of materials, *Thermosetting Composites – Processing*, http://www.azom.com/article.aspx?ArticleID=352
56. Balatonplast Ltd, http://www.balatonplast.hu/

4

Vinylester resins as a matrix material in advanced fibre-reinforced polymer (FRP) composites

F. SARASINI and C. SANTULLI, University of Rome 'La Sapienza', Italy

DOI: 10.1533/9780857098641.1.69

Abstract: This chapter discusses the use of vinylester resin as a matrix in polymer composite materials to be used in civil engineering applications. The chapter begins by discussing the increasing trend of composite development and use in civil engineering along with the related reasons. It then reviews the chemistry of vinylester resins together with their mechanical and chemical properties as well as the applications of vinylester resin and composites in the construction industry. The chapter includes indications on future applications of vinylester-based fibre-reinforced composites along with a section devoted to sources of further and relevant information.

Key words: vinylester resin, polymer matrix composites, fibre-reinforced plastics (FRP) in civil engineering.

4.1 Introduction

A structural composite is a material system consisting of two or more phases on a macroscopic scale, whose mechanical performance and properties are designed to be superior to those of the constituent materials acting independently. One of the phases is usually discontinuous, stiffer and stronger and is referred to as reinforcement, while the less stiff and weaker phase is continuous and is known as matrix. The properties of a composite depend on the properties of the constituents, geometry and distribution of the phases. The phases of the composite have different roles that depend on the type and application of the composite material. In the case of low to medium performance composites, the reinforcement, usually in the form of short fibres or particles, provides some stiffening but only local strengthening of the material. The matrix, on the other hand, is the main load-bearing constituent governing the mechanical properties of the material. In the case of high-performance structural composites, the continuous fibre reinforcement is the backbone of the material that determines its stiffness and strength in the direction of fibres. The matrix phase provides protection and local stress transfer from one fibre to another.

Historically, the concept of fibrous reinforcement is very old. There are biblical references to straw-reinforced clay bricks in ancient Egypt but it was in the late 1970s that applications of composites expanded widely to the aircraft, automotive and sporting goods. During the last decades, the composite industry has registered a continuous growth and, on a global basis, the composite market is forecast to grow at a rate of 3.9% between 2008 and 2013 whereas the shipments are projected to grow from 7.16 Mt in 2008 to 8.65 Mt in 2013, as can be seen in Fig. 4.1 (Lucintel, 2008). This growth can be ascribed to the fact that composite materials possess unique advantages over monolithic materials, such as high strength, high stiffness, long fatigue life, low density and adaptability to the intended function of the structure. Additional improvements can be realized in corrosion resistance, thermal insulation, thermal conductivity and acoustic insulation. The basis of the superior structural performance of composite materials lies in the high specific strength and high specific modulus and in the anisotropic and heterogeneous character of the material. The latter provides the composite system with many degrees of freedom for optimum configuration of the material.

The composites market can be broadly divided into the following categories: aerospace, transportation, construction, pipe and tank, marine, recreation/consumer products (sports, leisure), electrical/electronic and wind energy. It is to be emphasized that in the global composites industry, the construction sector represents the largest consumer of composite materials in terms of volume shipment, followed by transportation and electrical/electronics as

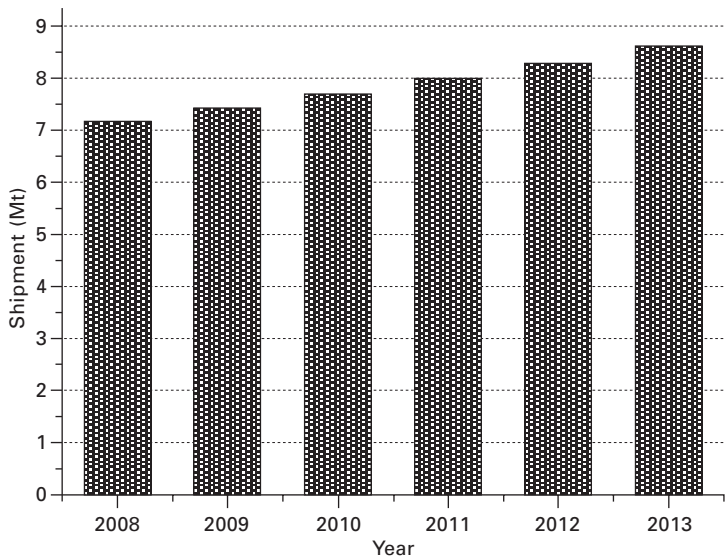

4.1 Global composites market forecast (2008–2013).

can be seen in Fig. 4.2, which reports the market breakdown among these applications (Lucintel, 2008). During 2008–2013, the construction sector will see an estimated average annual growth of 4.6%. The construction sector is considered to be the largest potential market for fibre-reinforced composites. Concrete repair and reinforcement, bridge deck repair and new installation, composite hybrid technology (the combined use of composites with concrete, wood and steel), marine piling and pier upgrade programmes are just some of the areas which are currently being explored.

4.2 Vinylester and other resins as matrix materials

Many types of resins are used in the composites industry, but the thermoset resins dominate the market. For instance, in 2007 more than 76% of the total volume was represented by thermoset composites (Lucintel, 2008). The main polymers used in construction under this heading are the epoxies, the vinylesters, unsaturated polyesters and the phenolics. Among these thermoset resins, the use of polyester resin is the highest on a volume basis whereas the use of vinylester composites is more limited (in 2007, they had a 2% share of total volumes). Currently the unsaturated polyesters are the most widely used polymers in construction. They are relatively low-cost materials, are easy to process and are an ambient temperature-cured material.

The two commonly used polyesters in construction are orthophthalic and isophthalic resins. They are both ambient-cured resins but benefit from an elevated temperature cure. The orthophthalic resins are the most widely used resins but have low thermal stability and chemical resistance. The isophthalic resins, which contain isophthalic acids as an essential ingredient, are of superior quality and have better chemical and thermal resistance and a

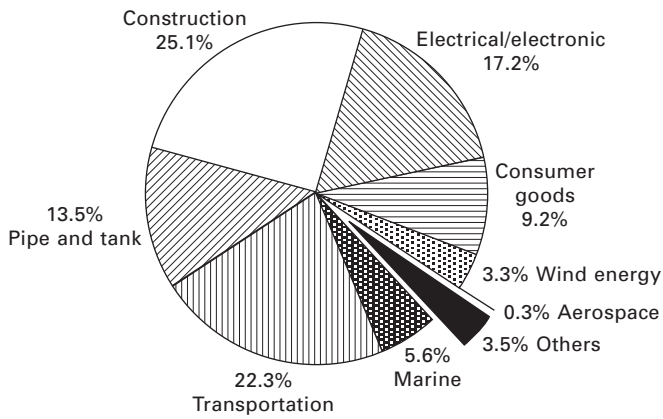

4.2 Global composites distribution (%, Mt) in 2007 by end-use application. Total shipment was 6.95 Mt.

degree of flame resistance. The common polyesters comprise low molecular weight polyhydroxyether chains with reactive groups at chain ends. Styrene in monomeric form is used as a reactive diluent in the resin in quantities between 20 and 60%. It is important to highlight, however, that the increase in styrene content results in (i) an increase in hydrophobicity, thereby effectively decreasing the level of moisture absorption, and (ii) an increase in shrinkage to levels of 5–19% by volume. This can result in significant microcracking in resin-rich areas and high residual stresses in composites having high volume fractions (Hollaway and Head, 2001).

Vinylesters are unsaturated esters of epoxy resins. They therefore offer similar mechanical and in-service properties to those of the epoxy resins and equivalent processing techniques to those of the polyesters. Indeed, they are often identified as a class of unsaturated polyester, because of the cure and processing similarity. Because of fewer cross-links, a cured vinylester resin is more flexible and has higher fracture toughness than a cured polyester one. Generally the vinylesters have good wetting characteristics and bond well to glass fibres due to the high number of OH (hydroxyl) groups which can form hydrogen bonds with similar groups on a glass fibre surface (Mallick, 2008). They possess resistance to strong acids and strong alkalis and they can be processed at both room and elevated temperatures. Compared with polyesters, vinylesters offer reduced water absorption and shrinkage as well as enhanced chemical resistance (Hollaway and Head, 2001).

4.3 Fibre-reinforced polymer (FRP) composites as structural materials

In the last two decades, there has been an increasing effort to migrate reinforced polymer composites into the construction industry for structural load-bearing applications where they have established themselves as a viable and competitive alternative for rehabilitation and retrofit of existing civil structures, as a replacement for steel in reinforced concrete and, to a lesser extent, for entirely new civil structures. There are many reasons to consider fibre-reinforced polymer (FRP) composites in civil engineering applications. This section is intended to provide a brief summary of these reasons along with the issues that have slowed down a widespread acceptance of these composites in the construction sector.

The benefits offered by fibre-reinforced composites vary depending on the choice of resin, fibre and manufacturing process. Therefore there is a strong need to optimize the design of the composite since not all of the best properties can be achieved at the same time. By way of summary, the main advantages of fibre-reinforced polymer composites are usually one or more of the following:

- High specific strength and stiffness
- Good fatigue performance
- Good creep behaviour
- Weight saving
- Time saving (this can be ascribed to their high strength to weight ratio which makes the components light and reduces the related construction and assembly time)
- Low maintenance requirements which are ideal where access is difficult or expensive
- Resistance to harsh or corrosive environments and tailorable durability
- Versatile fabrication.

As regards structural considerations, fibre-reinforced composites exhibit a number of structural properties that make them attractive alternatives to many conventional engineering materials. The tensile strength can range from about the strength of mild steel to stronger than that of prestressing steels, but it is the specific strength (which can be 40–60 times that of high-strength steel) that is often used to make comparisons between materials (Table 4.1). This property is highly appreciated in applications such as cladding panels and low-density framing materials. The low weight makes the assembly and disassembly of structures much easier and less time-consuming than for similar structures made of wood or steel and, when considering bridges, means lower deadweight which in turn can provide savings throughout the structure and the foundations. An FRP bridge deck can weigh up to 20% of the structural equivalent of a reinforced concrete deck (Hollaway, 2010). Also the specific modulus of composites is high and this can provide effective damping of vibrations in cases where this aspect is of concern. The measure of damping of a material is its damping factor and, in general, fibre-reinforced composites have a higher damping factor than metals.

4.4 Fatigue, creep and other properties of structural composites

4.4.1 Failure

Among the types of loading which civil structures have to resist, fatigue loading plays a significant role. The fatigue properties of a material represent its response to cyclic loading and it is well recognized that the strength is significantly reduced under cyclic loads. The response to this kind of loading is complex and is influenced by a number of variables, such as stress level, mode of cycling, material composition, environmental conditions and so forth. Research indicates that FRP composites exhibit good fatigue resistance in tension–tension cycling, which represents the most commonly used mode

Table 4.1 Tensile properties of some metallic and structural composite materials

Material	Density (g/cm^3)	Young's modulus (GPa)	Tensile strength (MPa)	Modulus to weight ratio (10^6 m)[a]	Tensile strength to weight ratio (10^3 m)[a]
SAE 1010 steel (cold-worked)	7.87	207	365	2.68	4.72
AISI 4340 steel (quenched and tempered)	7.87	207	1722	2.68	22.3
6061-T6 aluminium alloy	2.70	68.9	310	2.60	11.7
Ti-6Al-4V titanium alloy (aged)	4.43	110	1171	2.53	26.9
17-7 PH stainless steel (aged)	7.87	196	1619	2.54	21.0
High strength carbon fibre-epoxy matrix (unidirectional)	1.55	137.8	1550	9.06	101.9
High modulus carbon fibre-epoxy matrix (unidirectional)	1.63	215	1240	13.44	77.5
E-glass fibre-epoxy matrix (unidirectional)	1.85	39.3	965	2.16	53.2
Kevlar 49 fibre-epoxy matrix (unidirectional)	1.38	75.8	1378	5.60	101.8
Carbon fibre-epoxy matrix (quasi-isotropic)	1.55	45.5	579	2.99	38
Sheet moulding compound (SMC) composite (isotropic)	1.87	15.8	164	0.86	8.9
Glass fibre-vinylester composite (randomly oriented fibres) (fibre/matrix ratio 67%)	1.84	19.3	269	1.07	14.90
Glass fibre-vinylester composite (randomly oriented fibres) (fibre/matrix ratio 50%)	1.80	15.8	166	0.89	9.40

[a]The modulus and strength–weight ratios are obtained by dividing the absolute values with the specific weight obtained by multiplying density by the acceleration due to gravity (Mallick, 2008; Hollaway, 2010).

of loading, whereas tension–compression and compression–compression are scarcely used due to compressive buckling in thin laminates. In general, the fatigue performance of E-glass fibre-reinforced composites is inferior to those of carbon and aramid fibre-reinforced composites, which show an almost horizontal S–N curve. Long-fibre composites can retain a high proportion of their short-term strength after 10^7 cycles.

Fibre-reinforced composites seldom fail along a well-defined crack path. Instead, fatigue damage occurs at multiple locations in the form of fibre breakage, delamination, debonding and matrix cracking. Depending on the stress level, fibre orientation and constituent properties, some of these failure modes appear either individually or in combination without immediately causing the failure of the composite but, instead, causing a progressive growth until rupture. When dealing with FRP composites, it is important to take into account the effect of frequency due to the viscoelastic nature of polymers, which causes a phase difference between cyclic stresses and strains. This results in energy dissipation as heat within the material that, due to the low thermal conductivity of the polymers, is not easily dissipated, thus creating a temperature difference between the centre and surfaces of polymer composites. This temperature gradient may reduce the fatigue life of composites. Despite the great number of studies available, systematic investigations documenting the effects of temperature, moisture, compression load cycling and holes on fatigue resistance is still lacking.

4.4.2 Creep

A long-term property important for civil infrastructure composites is creep, which is defined as the increase in strain with time at a constant stress level. For polymers, the resulting creep strain increases non-linearly with increasing time. As for metals, creep strain in polymers and polymer matrix composites depends on the stress level and temperature. In general, highly cross-linked thermoset polymers (like those used in construction applications) exhibit lower creep strains than thermoplastic ones and, with the exception of aramid fibres, glass and carbon fibres do not creep (Mallick, 2008). A factor that plays a significant role in creep performance of composites is the fibre orientation: for $\theta = 0°$, creep in the longitudinal direction of a unidirectional 0° composite is negligible but, at different fibre orientations, creep strain can be quite significant.

Besides new bridge construction or complete replacement of reinforced concrete bridge sections, FRP composites are also successfully used for upgrading, retrofitting and strengthening damaged or deteriorated conventional materials, like concrete or steel (Karbhari, 2004). For these applications, the use of FRP composites can be advantageous from the standpoint of ease of installation and reduced maintenance costs. As an example, traditional techniques for external strengthening of concrete structures call for steel plates that can be substituted by wrapping them with FRP composite jackets. The low mass of these materials makes handling more convenient and their non-corrosive nature eliminates the need to protect the steel. Another advantage is represented by the tailorable anisotropy of FRP composites. Thanks to this characteristic, the fibres can be aligned primarily in the hoop direction

and, in this way, the wrapped composites do not increase the longitudinal stiffness of the columns, thus behaving in a better way than steel jackets which, being isotropic in nature, tend to stiffen the columns.

4.4.3 Operation in difficult environments

In addition to strength and stiffness requirements, FRP structural composites must possess the in-service and physical characteristics required to operate in aggressive and sometimes hostile environments found in the construction industry. The greater the degradation of structures over time, the lower will be their load-carrying capacity. It is to be noted that all materials will degrade over time, but polymers (and composites) are more resistant to degradation than many of their competitors. In fact, one of the main reasons for selecting FRP composites is their corrosion resistance and potential for long-term durability. The term 'durability', as highlighted by Hollaway (2010), is often misused. Durability of a material or structure has been defined by Karbhari *et al*. (2003) as 'its ability to resist cracking, oxidation, chemical degradation, delamination, wear, and/or the effects of foreign object damage for a specified period of time, under the appropriate load conditions, under specified environmental conditions'. The durability of a polymer composite is mainly dependent upon the matrix material. The influence of environmental factors, such as elevated temperatures, high humidity, corrosive fluids and ultraviolet (UV) rays, is of serious concern in infrastructure applications. One of the most convincing reasons to consider the use of FRP composites is their resistance to corrosive elements. FRP made of vinylester resin is one material that offers considerably higher resistance to attack in aggressive chemical environments, including various kinds of acids and caustic materials. Corrosion-resistant resins include both bisphenol-A epoxy vinylesters and epoxy novolac vinylesters. Vinylesters resins are commonly used in many applications requiring chemical resistance, such as air and water pollution treatment, for the construction of flue gas desulphurization equipment (Bogner, 2005; Taillemite and Pauer, 2009).

When exposed to humid air or water environments, many polymer matrix composites absorb moisture by surface absorption and subsequent diffusion through the matrix. This moisture absorption produces volumetric changes (swelling) in the resin and can reduce the glass transition temperature of the resin, thus impairing all the matrix-dominated properties of a polymer matrix composite. Moreover, the dilatational expansion of the matrix around the fibre reduces the residual compressive stresses at the fibre/matrix interface due to the curing shrinkage, and the mechanical interlocking between the fibre and the matrix can be relieved. In general, a high degree of cross-linking is desirable in order to decrease the permeability and to slow down the diffusion processes. The successful use of FRP composites in wet environments is

largely due to the development of coupling agents (silanes) applied to the fibres upon fabrication. Moisture and chemicals can also cause degradation at the fibre level, especially for aramid and glass fibres (Karbhari *et al.*, 2003). Another source of concern is represented by alkali attack and, in particular, degradation due to concrete pore water solution. Glass fibres are particularly prone to this degradation due to a variety of mechanisms ranging from pitting to hydroxylation and leaching. A detailed review of the durability issues of FRP rebars can be found in Ceroni *et al.* (2006). Since polymeric resins play a critical role in protecting the fibres and slowing the diffusion processes, preference should be given to epoxies and vinylesters, while the use of polyesters is not recommended (Karbhari *et al.*, 2003).

Another concern is represented by the response of composites to temperature variations and freeze–thaw cycling. The weather durability of FRP composites and how load capacity will change over time remains a major challenge, and insufficient data are available because composite structures for civil infrastructural purposes have been in service for only a relatively short time. Most of the available data are based on simulated laboratory testing (Chu *et al.*, 2004; Karbhari, 2002). There is the need to predict the long-term behaviour of FRP composites, as demonstrated by Wu and Yan (2011), who formulated a mechanics-based durability model for FRP bridge decks under accelerated freeze–thaw conditions. It was found that the reductions in strength and stiffness of glass/vinylester composites are substantial after 10,000 h of freeze–thaw cycles only when the composites are also subjected to a sustained load of 25% strain, whilst the reductions are negligible when the composites are not preloaded.

4.4.4 Flexibility of fabrication

The variety of fabrication techniques available for FRP composites – wet lay-up process, pultrusion filament winding, resin transfer moulding (Hollaway and Head, 2001) – should be considered as an advantage, because the ability to mould complex forms can provide new aesthetic possibilities and geometrically more efficient solutions. Fibres can be oriented in specific directions to better meet specialized loading conditions, and special moulding techniques allow complicated shapes to be manufactured as one unit, thus avoiding the need for joints which can represent a source of weakness for the structure. Composites offer also the ability to integrate special finishes and a wide variety of unusual effects while simulating traditional materials such as stone or granite.

4.4.5 Fire resistance

A significant concern in any application of organic matrix-based composites is fire resistance. The major health hazard derived from polymers and composites

in a fire accident is generated from the spread of flame but, most importantly, from the toxic combustion products. For these reasons, fire resistance is considered one of the most critical technical barriers to a widespread use of FRP composite in civil infrastructures. Due to its complexity, only few data and studies are available on this subject (Mouritz and Gibson, 2006). Despite these problems, polymers can be designed to meet stringent fire requirements through careful resin formulation (use of halogens, nanofillers, or passive fire protection systems).

4.4.6 Cost issues

There is little doubt that FRP composites are structurally capable but some issues have slowed down their introduction into the construction industry. Economic considerations deserve particular mention. Currently fibre composite materials are expensive when compared with conventional construction materials on an initial cost basis. There are a number of factors contributing to their high cost, including the high cost of raw materials and processing. Despite the high initial cost, there are a number of economic considerations that make the use of FRP composites attractive. Many life-cycle costs can be eliminated or significantly reduced with the use of FRP composites. To this purpose, costs of rehabilitating structures damaged by corrosion would be eliminated, periodic maintenance of structures would be reduced, and construction and transportation costs could be reduced with the use of low-density materials. All these life-cycle cost savings can offset the relatively high initial cost of FRP composites. The problem is represented by the fact that standard practice is usually to select materials not on projected life-cycle costs but rather on trying to minimize initial costs.

Another challenge to face is the presence of relatively few codes and standards for FRP composites compared to longer-established materials such as concrete and steel, and the lack of geometrical/material standardization that discourages the use of FRP composites on a routine basis.

4.5 Chemistry and properties of vinylester resins as matrix materials

This section is devoted to describing the chemistry of vinylester resins (including polymerization reactions) along with their mechanical, thermal and chemical (corrosion resistance and dimensional stability) properties. In general, vinylester resins are deemed to combine the best properties of epoxies and unsaturated polyesters: in particular, they are easily handled at room temperature, and offer mechanical properties comparable to epoxy resins (Table 4.2). Moreover, they have better chemical resistance than cheaper

Table 4.2 Comparison of properties of polyester, vinylester and epoxy resins (most diffuse ranges according to the main producers)

Resin type	Density (g/cm³)	Tensile strength (MPa)	Tensile modulus (GPa)	Flexural strength (MPa)	Flexural modulus (GPa)	Elongation (%)
Unsaturated polyester	1.1–1.2	45–90	2.5–4	80–110	3–5.5	2–3.2
Vinylester	1.05–1.2	70–90	3.5–4.5	120–150	2.7–4	2.5–6
Epoxy	1.1–1.4	30–110	2.5–10.5	90–145	2.5–10	0.8–6

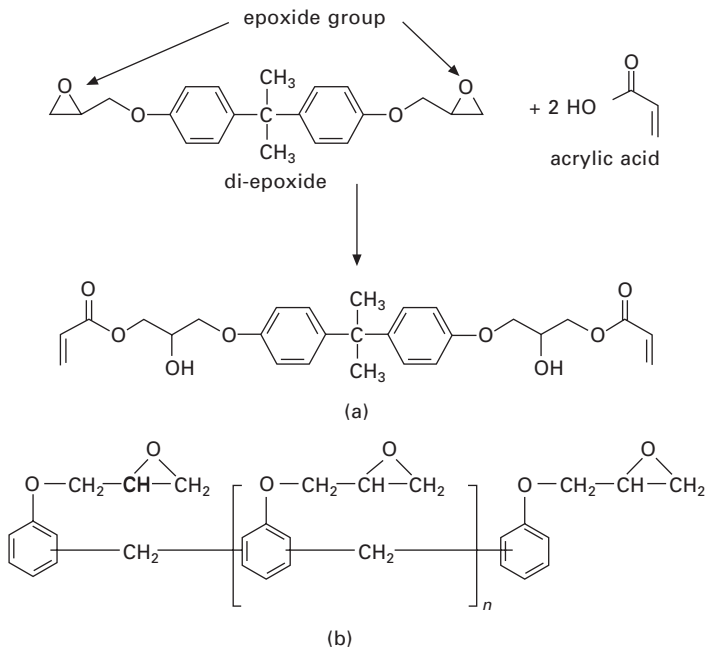

4.3 Polymerization structures of vinylester resins: (a) bisphenol-A epoxy vinylester resin; (b) novolac epoxy vinylester resin.

polyester resins, especially hydrolytic stability, offering easier control over cure rate and reaction conditions than epoxy resins.

Vinylesters are unsaturated, hence thermosetting, resins, prepared by the reaction of a monofunctional unsaturated acid, e.g. methacrylic, acrylic, crotonic or cynnamic acid, with a bisphenol diepoxide. This type of structure is referred to as bisphenol-A epoxy vinyl ester (Fig. 4.3(a)). The structural difference, which at least partially justifies the improved chemical and mechanical properties of vinylester, is the presence in vinylesters of reactive double bonds at the ends of the chains only, while unsaturated polyester resins have the reactive double bonds distributed throughout the chains.

An alternative way to obtain vinylester resins is through the novolac epoxy chemical structure (Fig. 4.3(b)). In this case, a phenol diepoxide is obtained: the novolac backbone structure is particularly suitable for improved resistance to acids in liquid and in vapour form and at higher temperatures than are allowed by bisphenol-A vinylester resins.

The resulting polymer, which is unsaturated on its terminal positions, is mixed with an unsaturated monomer, usually styrene. These reactive groups can form a cross-linked network with or without the addition of a comonomer. In many industrial products, vinylester resins include 40–50 wt% styrene, while in dental applications a common comonomer is triethylene glycol dimethacrylate. For some applications, such as filament winding, the styrene content needs to be limited (not normally exceeding 35–40%), reducing at the same time the quantity of volatile organic compounds (VOC) and therefore the environmental impact of the resin.

The dilution of vinylester oligomers with a low molecular weight comonomer, such as styrene, vinyltoluene or methyl methacrylate, is able to reduce the room temperature viscosity of the mixture and yield a solution with a typical viscosity in the range of 200 to 2000 cps. The function of the comonomer is significant in that the unsaturated bonds on the termini of the vinylester oligomers copolymerize with it to form a network with cross-link sites: this guarantees the thermosetting properties in a similar way to the curing reactions of unsaturated polyesters. Another analogy with unsaturated polyester resins lies in the fact that both systems contain styrene monomer as a reactive diluent.

To the vinylester resins, thixotropic agents are added, for example silica fume (silicon dioxide in microspheres, which is a by-product of the glass industry), to obtain a behaviour adequate to their use also in open moulds. In addition, to improve their toughness, CTBN polymers (carboxyl-terminated copolymers of butadiene and acrylonitrile) are widely employed as reactive modifiers. This occurs since the CTBN-modified vinylester oligomers act as compatibilizers for blending additional butadiene copolymer (Burchill and Pearce, 1996).

In general, vinylester resins are comparable to other resins when operating with processes such as hand spraying, resin transfer moulding, vacuum infusion and filament winding. In contrast, comparative advantages are obtained when using pultrusion processes: in this case, vinylester resins tend to saturate reinforcements more efficiently, therefore producing higher test results. They also tend to have a higher temperature capability with improved toughness and reduced corrosion. The main issue for vinylester resins used for pultrusion is possible gelation in the resin bath; to avoid this, standard heat-activated cure systems, based on peroxides, are used. Whenever styrene is diluted together with the vinylester resin, it affects both viscosity during the whole process and the extent of cure in its final part. It is worth noting

in this respect that insufficiently cured vinylester resins are particularly susceptible to significant creep and possible initiation of microcracks during early exposure to the service environment (Bradley *et al.*, 1998). It is also necessary not to have an excess of styrene, so that it does not end up being in the pultruded part, which may considerably reduce the physical properties and alter the appearance of the produced part.

4.6 Applications of vinylester-based composites in civil engineering

This section will cover the manufacturing processes of vinylester-based composites along with their applications in the civil engineering field. A summary scheme of all the applications mentioned is reported in Fig. 4.4. Some applications related to bridges are also listed with relevant references in Table 4.3. It is significant to note that in early applications GFRP composite materials were aimed more at architectural embellishment than at structural performance and durability (Hollaway, 2010). This was happening in particular because the polymer matrix has been and is still often considered the weak link in the application of FRP to civil engineering: this is true in particular when considering that for a number of applications in this field lifetimes are expected to be in excess of 50 years. In this respect, polymer composites in outdoor applications are susceptible to photo-initiated oxidation and are also known to be sensitive to hygrothermal, alkaline and saline environments (Chin *et al.*, 2001).

Civil application results also in substantial fatigue loading, in the sense that prolonged service may lead to failure at stresses largely inferior to the yield point. Fatigue may be mechanical (for example, due to vehicle traffic), thermal (from seasonal and diurnal variations in temperature) or chemical

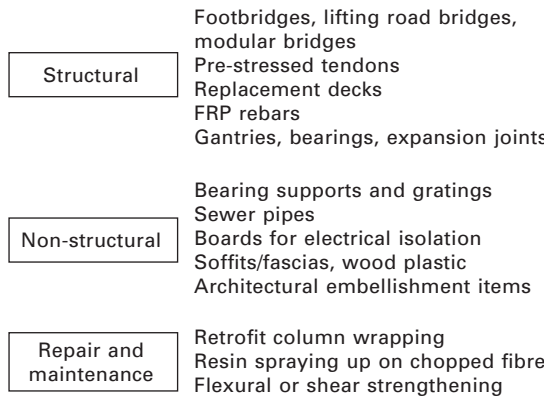

4.4 Summary scheme of applications of vinylester resin and composites in the construction industry.

Table 4.3 Short summary of applications of vinylester composites to bridges

Description	References	Location	Year
Footbridge	Nishizaki *et al.,* 2006	Okinawa (Japan)	2000
Cycle bridge	Firth and Cooper, 2001	Halgavor (UK)	2001
Lifting road bridges	http://www.infracore.nl	Oosterwolde, Rotterdam (Holland)	2010
Modular bridges	Uncredited author, 2008	Friedberg (Germany)	2007
Pre-stressed tendons	Stoll *et al.,* 2000	Various highway bridges (USA)	From 1996
Replacement decks	Black, 2003	Montgomery County, Ohio (USA)	2000

(from anti-grit road treatments, oxidation, NO_X effects by pollution, water, etc.) (Karbhari *et al.,* 2003). Among structural applications, the ability to tailor FRP design to provide high specific strength and compensate for their low stiffness, while ensuring resistance to corrosion under most environmental conditions (including, for example, contact with salt water, high concentrations of chlorides and acid rain), makes them a favourable option for the realization of bridge components. Most applications of FRP in engineering construction, such as the application of FRP rebars, require the achievement of a resistant and durable bond of the composites with concrete. This is achieved using a number of techniques, including surface deformation, sand coating, surface texture, indented grooves and helical wrapping (Lee *et al.,* 2008). In some cases, to reduce weight, hollow glass fibres have also been used as reinforcement for vinylester matrices: in this case, it was particularly evident that the bond between concrete and reinforcement is controlled by the geometry of the rebar, the embedment length and the clear cover provided by the concrete (Kachlakev and Lundy, 1999).

Structural applications include footbridges, lifting road bridges, prestressed fibre-reinforced tendons, replacement decks, modular bridges for disaster relief, gantries, bearings, expansion joints and so on. The first FRP bridge deck in New York State was installed in late 1999 to replace a deteriorated concrete deck, allowing for higher live loads on the bridge (Chiewanichakorn *et al.,* 2003). In particular, a deteriorating 25-foot long concrete bridge built in 1926 was replaced by employing glass fibre fabric and vinylester plastics in forming the sandwich structure used in the deck, which resulted in its installation in just one day (Black, 2000).

In the particular case of the application of glass-fibre reinforced vinylester composites as internal reinforcement for concrete bridge deck slabs, the results showed their superior fatigue performance and longer fatigue life when compared with the steel-reinforced ones (El-Ragaby *et al.,* 2007).

This has been applied experimentally, for example, in the construction of four highway bridge decks in the US using E-glass and vinylester resin, resulting in reduction by about an order of magnitude of the construction times and costs (Shekar *et al.,* 2003). In practical cases, a difficulty has been highlighted in the fact that the join between the deck and the girder is often not optimal and requires specific design for structural optimization, and also by the realization in continuum using pultrusion does not allow the fabrication of complex shapes (Kim *et al.,* 2004). For example, in the case of the Halgavor Bridge in Cornwall (England), installed during 2001, girder sections were hand-laminated along with the internal structure, and it is significant to observe that two different vinylester resin grades were used for the vacuum infusion process and for hand-lamination assembly work respectively (Firth and Cooper, 2001).

In addition, non-critical structural items which would not compromise safety, such as bearing supports and gratings, bearing plates, sewer pipes and boards for electrical isolation, are realized using vinylester matrix composites. Vinylester resins are being used with increasing success for the replacement of wooden structures, such as soffits and fascias, frequently both included in a system, wood plastic, and so forth. In practice, most of the above applications in construction require substantial resistance against corrosion and environmental degradation.

The repair and maintenance sector has also been a field of significant application for vinylester resins. In particular, these have been applied for retrofit column wrapping, which is a repair method able to compensate for the most frequent structural deficiencies in existing concrete columns, i.e. the lack of transverse reinforcement, leading to premature shear failure, brittle crushing of unconfined concrete and reinforcement splice failure. This is particularly true for columns situated in seismically active regions, which were designed in the absence of modern seismic codes (Seible *et al.,* 1997). An alternative method to column wrapping is spray-up using chopped short carbon or glass fibres with vinylester resin, with the advantage of having a shorter hardening time and improved flexural characteristics than when using epoxy resin for this purpose (Sen *et al.,* 2011). Other applications in this sector include strengthening of soffits, ceilings and timber, metal and brickwork. Solutions may be various, depending on the type of strengthening required, whether shear or flexural strengthening. These include, for example, the application of bidirectional or unidirectional strips at fixed intervals for flexural strengthening, bottom flange clamping of inclined strips, or U-shaped bands for shear strengthening, and plate-bonded ribs for roof elements (Hollaway, 2003). Another technique for shear strengthening in which vinylester resins have been used is near-surface mounting (NSM): in this case, the reinforcement is embedded in grooves cut onto the surface of the member to be strengthened and filled with an appropriate binding agent (De Lorenzis and Teng, 2007).

4.7 Conclusion and future trends

Vinylester resins are of increasing use in the construction industry, whenever particular resistance to corrosion and generally to exposure to the service environment is required. This justifies the large-scale use of vinylester for repair and maintenance purposes, and for replacement of damaged parts, such as bridge decks. Most structural applications, especially in the field of bridge construction, using vinylester resin composites are realized by pultrusion, and are therefore designed and assembled using relatively simple geometrical profiles. In this regard, resins are modified in order to guarantee sufficient resilience of the piece obtained and effective completion of the cure process. Future developments are particularly linked to improvements in the accuracy of process control during pultrusion and the possibility of increasing the compatibility between carbon fibres and state-of-the-art vinylester resins, which would considerably increase the possibilities for structural applications, while retaining a reasonably low 'carbon footprint' for manufactured components.

Despite the fact that FRP composites have found rapid acceptance in the construction sector, it is recognized that they have not realized their full potential. The lack of validated codes of practice, standards and guidelines for the use of these materials by the civil engineering community is definitely one of the reasons that have hindered widespread implementation of FRP in civil infrastructures. In recent years, significant steps forward have been taken as regards the publication of design codes and specifications to help engineers to design with FRP composites in Europe, the USA, Canada and Japan. A complete and up-to-date list of these key publications can be found in Hollaway (2010).

Another area where advancements are needed is represented by long-term durability data, but there is the hope that these data will become available as research and applications in this area progress. Further effort must be made in the manufacturing processes and systems, which must be suitable for high-profile production of FRP, allowing the cost-effective production of primary structural elements of repeatable and reasonably uniform quality. It has to be mentioned that often materials used in infrastructure applications are not specifically tailored for the environment and loading conditions encountered. Thus, beyond the need for cheaper raw materials, there is also the need for resins that are not sensitive to local conditions during cure, as well as for tougher systems with improved resistance to moisture and alkalinity and higher glass transition temperature (Karbhari, 2004). Progress in this field has been made through the development, for instance, of low viscosity, lower styrene and lower volatile content vinylester resins particularly suited for the pultrusion process, which is a relatively low-cost manufacturing method much used in infrastructure applications. Further improvements could be made in

terms of the fibres themselves, in particular carbon fibres, in order to lower their production costs while keeping high values of the elastic modulus. In fact, carbon fibres are particularly suited for the construction sector thanks to their chemical inertness, but their high cost and the lack of suitable and optimized surface treatments for increasing the compatibility with vinylester resins have slowed down their use so far.

In conclusion, *in situ* development of low-cost health monitoring devices and schemes, particularly to provide a level of acceptable safety when using units fabricated from composites, should be introduced into the industrial construction field. In this regard, the use of optical fibres is highly desirable since they have proved to be suitable for this purpose (Kuang and Cantwell, 2003).

4.8 Sources of further information and advice

This section is intended to provide links to additional sources of information.

Resin and composite manufacturers:

- AOC LLC – http://www.aoc-resins.com
- Ashland, Inc. – http://www.ashland.com
- Composite Building Structures, Ltd – http://www.cbs-homes.com
- Composite Rebar Technologies, Inc. – http://hollowrebar.com
- Cray Valley SA – http://www.crayvalley.com
- DSM Composite Resins AG – http://www.dsm.com
- Huachang Polymer Co. Ltd – http://www.hchp.com.cn
- Hughes Brothers, Inc. – http://www.hughesbros.com
- IDI Composites International – http://www.idicomposites.com
- Infracore – http://www.infracore.nl
- Interplastic Corporation – http://www.interplastic.com
- Kenway Corporation – http://www.kenway.com
- Marshall Composite Systems, LLC – http://www.marshallcomposite.com
- Martin Marietta Composites – http://www.martinmarietta.com
- NoVOC Performance Resins LLC – http://www.novoc.com
- Poliya Polyester Industry and Trade Co. Ltd – http://www.poliya.net
- Pultrall, Inc. – www.pultrall.com
- Reichhold, Inc. – http://www.reichhold.com
- Strongwell – http://www.strongwell.com
- Vector Construction Group – http://www.vectorgroup.com

Links to websites dealing with the use of composites in civil engineering applications:

- American Composites Manufacturers Association (ACMA) – http://www.mdacomposites.org/mda
- Composite Build – http://www.compositebuild.com
- National Composite Center – http://www.compositecenter.org
- Network Group for Composites in Construction – http://www.ngcc.org.uk
- United States Department of Transportation, Federal Highway Administration, Infrastructure – http://www.fhwa.dot.gov/bridge/frp

4.9 References

Black S (2000), 'A survey of composite bridges', *Compos Technol*, 6(2), 14–18.

Black S (2003), 'How are composite bridges performing?', *Compos Technol*, 9(6), 16.

Bogner B (2005), 'Composites for chemical resistance and infrastructure applications', *Reinforced Plastics*, 49, 30–34. doi: 10.1016/S0034-3617(05)70799-2

Bradley S W, Puckett P M, Bradley W L and Sue H J (1998), 'Viscoelastic creep characteristics of neat thermosets and thermosets reinforced with E-glass', *J Compos Technol Res,* 20(1), 51–60. doi: 10.1520/CTR10500J

Burchill P and Pearce P J (1996), in *Polymeric Materials Encyclopedia*, J C Salamone (ed.), Boca Raton, FL, CRC Press.

Ceroni F, Cosenza E, Gaetano M and Pecce M (2006), 'Durability issues of FRP rebars in reinforced concrete members', *Cement Concrete Compos*, 28, 857–868. doi:10.1016/j.cemconcomp.2006.07.004

Chiewanichakorn M, Aref A J and Alampalli S (2003), Failure analysis of fiber-reinforced polymer bridge deck system, *J Compos Techn Res*, 25, 121–129. doi: 10.1520/CTR10954J

Chin J W, Aouadi K, Haight M R, Hughes W L and Nguyen T (2001), 'Effects of water, salt solution and simulated concrete pore solution on the properties of composite matrix resins used in civil engineering applications', *Polym Compos*, 22, 282–298. doi: 10.1002/pc.10538

Chu W, Karbhari V M and Wu L (2004), 'Durability evaluation of moderate temperature cured E-glass/vinylester systems', *Compos Struct*, 66, 367–376.doi: 10.1016/j.compstruct.2004.04.058

De Lorenzis L and Teng J G (2007), 'Near-surface mounted FRP reinforcement: An emerging technique for structural strengthening', *Compos Part B,* 38, 119–143. doi: 10.1016/j.compositesb.2006.08.003

El-Ragaby A, El-Salakawy E and Benmokrane B (2007), 'Fatigue analysis of concrete bridge deck slabs reinforced with E-glass/vinyl ester FRP reinforcing bars', *Compos Part B*, 38 703–711. doi: 10.1016/j.compositesb.2006.07.012

Firth I and Cooper D (2001), 'The Halgavor Bridge – the use of glass-fibre reinforced polymer composites as the primary structural material in new bridge construction', *NGCC First Annual Conference and AGM: Composites in Construction Through Life Performance*, Watford, UK, 30–31 October, 1–11.

Hollaway L C (2003), 'The evolution of and the way forward for advanced polymer composites in the civil infrastructure', *Constr Build Mater*, 17, 365–378. doi: 10.1016/S0950-0618(03)00038-2

Hollaway L C (2010), 'A review of the present and future utilisation of FRP composites in the civil infrastructure with reference to their important in-service properties', *Constr Build Mater*, 24, 2419–2445. doi: 10.1016/j.conbuildmat.2010.04.062

Hollaway L C and Head P R (2001), *Advanced Polymer Composites and Polymers in the Civil Infrastructure*, Oxford, Elsevier.

Kachlakev D I and Lundy J R (1999), 'Performance of hollow glass fiber-reinforced polymer rebars', *J Compos Construct*, 3, 87–91. doi:10.1061/(ASCE)1090-0268(1999)3:2(87)

Karbhari V M (2002), 'Response of FRP confined concrete exposed to freeze-thaw regimes', *J Compos Construct*, 6, 35–40. doi:10.1061/(ASCE)1090-0268(2002)6:1(35)

Karbhari V M (2004), 'Fiber reinforced composite bridge systems – transition from the laboratory to the field', *Compos Struct*, 66, 5–16. doi: 10.1016/j.compstruct.2004.04.026

Karbhari V M, Chin J W, Hunston D, Benmokrane B, Juska T, Morgan R, Lesko J J, Sorathia U and Reynaud D (2003), 'Durability gap analysis for fiber-reinforced polymer composites in civil infrastructure', *J Compos Construct*, 7, 238–247. doi:10.1061/(ASCE)1090-0268(2003)7:3(238)

Kim H-Y, Kim S-M and Lee Y-H (2004), 'Design of GFRP deck and deck-to-girder connections for girder bridges', *KSCE J Civil Eng*, 8, 83–87. doi: 10.1007/BF02829084

Kuang K S C and Cantwell W J (2003), 'The use of conventional optical fibres and fibre Bragg gratings for damage detection in advanced composite structures – a review', *Appl Mech Rev*, 56, 493–513. doi: 10.1115/1.1582883

Lee J Y, Kim T Y, Kim T J, Yi C K, Park J S, You Y C and Park Y H (2008), 'Interfacial bond strength of glass fiber reinforced polymer bars in high-strength concrete', *Compos Part B*, 39, 258–270. doi:10.1016/j.compositesb.2007.03.008

Lucintel (2008), *Global Composites Market 2008–2013: Materials, Markets and Technologies*. Lucintel LLC. Dallas, TX.

Mallick P K (2008), *Fiber-Reinforced Composites: Materials, Manufacturing and Design*. Boca Raton, FL, CRC Press.

Mouritz A P and Gibson A G (2006), *Fire Properties of Polymer Composite Materials*, Dordrecht, Springer.

Nishizaki I, Takeda N, Ishizuka Y and Shimomura T (2006), 'A case study of life cycle cost based on a real FRP bridge', *Third International Conference on FRP Composites in Civil Engineering (CICE 2006)*, 13–15 December, Miami, FL.

Seible F, Priestley M J N, Hegemier G A and Innamorato D (1997), 'Seismic retrofit of RC columns with continuous carbon fiber jackets', *J Compos Construct*, 1, 52–62. doi: 10.1061/(ASCE)1090-0268(1997)1:2(52)

Sen T, Reddy H N J and Shubhalakshmi B S (2011), 'Flexural characteristic study of RCC beams retrofitted using vinyl ester bonded GFRP and epoxy bonded GFRP', *J Adv Eng Sci Technol*, 10, 70–75.

Shekar V, Petro S H and Ganga Rao H V S (2003), 'Fiber-reinforced polymer composite bridges in West Virginia', *Transportation Research Record,* 1819B, 378–384.

Stoll F, Saliba J E and Casper L E (2000), 'Experimental study of CFRP-prestressed high-strength concrete bridge beams', *Compos Struct*, 49, 191–200.

Taillemite S and Pauer R (2009), 'Bright future for vinyl ester resins in corrosion applications', *Reinforced Plastics*, 53, 34–37. doi:10.1016/S0034-3617(09)70151-1

Uncredited author (2008), 'GRP road bridge. An operational response to ageing infrastructure', *EC Composites Magazine*, November/December 45, 64.

Wu H-C and Yan A (2011), 'Time-dependent deterioration of FRP bridge deck under freeze/thaw conditions', *Compos Part B*, 42, 1226–1232. doi: 10.1016/j.compositesb.2011.02.010

5

Epoxy resins as a matrix material in advanced fiber-reinforced polymer (FRP) composites

V. FIORE and A. VALENZA, University of Palermo, Italy

DOI: 10.1533/9780857098641.1.88

Abstract: This chapter discusses the epoxy resins which, thanks to their good and versatile properties, can be considered nowadays the most important class of thermosetting polymers. In particular the chapter first reviews both the epoxy resins commonly available on the market, including a new class of bio-derived epoxy resins, and the most-used curing agents. It then describes the principal characteristics of the epoxy resins and how it is possible to enhance them by adding several fillers to the epoxy system. Finally, the chapter analyzes the main engineering fields in which epoxy resins find application today and their possible future utilization.

Key words: epoxy resins, good mechanical, chemical and thermal performance, high adhesion strength, low shrinkage and toxicity, applications.

5.1 Introduction

Epoxy resins are considered to be one of the most important classes of thermosetting polymers. They are now widely utilized as high-performance thermosetting resins in several industrial applications. Thanks to their range of useful properties, they are used as protective coatings, structural adhesives and matrix resins for fiber-reinforced polymer (FRP) composites.

Compared with other thermosetting polymers (i.e. polyester or vinyl ester resins), epoxy resins are more expensive, but show both better mechanical properties and higher resistance to moisture absorption and to corrosive liquids and environments. These good physical properties and their durability in service help to provide a favorable cost–performance ratio when compared to other thermoset plastics.

Epoxy resins also show high electrical resistivity and good performance at elevated temperatures thanks both to their higher heat deflection temperatures, compared to polyester matrices (Brent Strong, 2008), and to their high glass transition temperatures (T_g). Moreover they show optimal adhesion to several substrates (e.g. metal or plastic) and to fibers used as reinforcement in composite materials (e.g. glass, carbon and Kevlar). Another positive aspect of epoxy resins is their low shrinkage during the curing

process. Polyester and vinyl ester resins shrink up to 12% volumetrically (in particular, the shrinkage volumetric reduction is in the range of 5–12% and 5–10% for polyester and vinyl ester resins, respectively) and because the resin continues to cure over long periods of time this effect may not be immediately obvious. In contrast, epoxy resins shrink less than 5% (Zarrelli *et al.*, 2002) and an epoxy laminate is a lot more stable over a long period of time than a polyester or vinyl ester laminate.

Due to the absence of styrene, during the curing process epoxy resins have significantly less toxic emissions than polyester and vinyl ester ones, making possible their use also with 'open-mold' technology production (e.g. hand lay-up or vacuum bagging). Epoxy resins are also compatible with most composite manufacturing processes, such as vacuum bagging and infusion, autoclave molding, pressure-bag molding, compression molding, filament winding and hand lay-up.

Another characteristic that makes these systems very interesting from an engineering point of view is their great versatility: it is possible to adapt a wide number of physical, mechanical and processing properties by modifying the blend of the resin system or by adding agents (e.g. fire retardants or toughening agents). For instance, when in a given application higher electrical conductivity is required than that offered by neat resins, they can be modified by adding fillers with optimal electrical properties such as carbon nanotubes or metal powders.

Epoxy resins thus show several properties that have made them the best options among thermosetting resins for most engineering applications:

- No emission of volatile and dangerous products during the curing process reaction
- Flexibility in the choice of monomers to obtain a variety of products from low T_g rubbers to high T_g materials
- Very low or, for some blends, no volume contraction during the curing process
- High adhesion properties to several materials due to the polar groups in the structure
- Possibility of introducing different modifiers to obtain a resin system with several good properties (e.g. electrical or thermal).

However, these resins also show negative aspects such as poor resistance to crack growth, brittleness and low UV resistance (Kotnarowska, 1999; Jana and Zhong, 2007; Liu *et al.*, 2012). Furthermore, to reach their ultimate mechanical properties (i.e. to achieve 70–80% of their optimal properties), they often require a post-cure treatment of two to four hours at elevated temperature (up to 120°C), making them more difficult to use (Kelly, 1999).

5.2 Curing reactions of epoxy resins

Curing is defined as a process that involves changes of the properties of a thermosetting plastic (i.e. epoxy resin) through chemical reactions. Epoxy systems typically consist of two parts: the resin and the hardener, or curing agent, which are stable when kept separate but react to form a three-dimensional network when they are mixed together, even at room temperature. One-part epoxy systems also exist, especially those used in the aerospace and automotive industries (Sharma and Luzinov, 2011). These last are a mixture of an epoxy resin, a latent curing agent, and, in some cases, an accelerator: these blends are able to cure only at high temperature (i.e. at around 180–200°C). In these systems, the latent curing agent, which possesses a high melting temperature, gives latency to epoxy resins at room temperature while the accelerator is added if it is necessary to reduce the curing temperature (i.e. to around 100–120°C).

Each epoxy resin contains reactive groups named epoxy groups or rings: a higher heat resistance and a lower toughness of the solid state are related to the number of epoxy rings contained in the epoxy resin molecules. As shown in Fig. 5.1, the epoxy ring shows a planar geometrical structure characterized by a high stress state due to the value of the bond angles (all equal to about 60°). A tetrahedral carbon atom shows usually a bond angle equal to 109.5°, instead of a bivalent oxygen angle of 110°: the structure of the epoxy ring is highly reactive because of this angular distortion. These reactive groups, situated terminally or internally in the molecules of an epoxy resin, can react with the active hydrogen atoms of the curing agent to create covalent intermolecular bonds (i.e. cross-links) that are the basis of the curing process. By mixing molecules of resin and curing agent, a growing amount of covalent bonds between monomers forms to create the typical network structure of a thermosetting plastic, which is usually insoluble in the most common solvents.

During the curing process the cross-linking reactions (a chemical phenomenon) cause changes in the physical and chemical properties of the reagents, such as increases in molecular weight and viscosity of the resin system. As already mentioned, the properties of the solid state are related to the number of epoxy rings contained in the epoxy resin molecules: in particular they depend principally on the cross-link density (spacing between successive cross-link sites). In general the tensile modulus, glass transition temperature and thermal stability as well as chemical resistance are improved

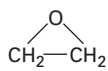

5.1 Epoxy ring.

with increasing cross-link density, but the strain to failure and fracture toughness are reduced (Mallick, 1993).

As shown in Fig. 5.2, it is possible to define two important stages associated with these changes:

- gelation
- vitrification.

Gelation can be defined as the stage of the curing process in which the resin system turns from the liquid or fluid state to the rubber one: after this time the resin system cannot flow easily due to the high number of cross-links formed. Prior to gelation time the resin system is soluble in suitable solvents; after this critical point the network cannot be dissolved but swells because it is imbibed by the solvent. Particularly at this stage of the curing process, the resin system consists of two fractions: 'sol' and 'gel'. The former is the solidified phase while the latter is the phase still liquid that can be extracted with suitable solvents: its amount decreases with the increase of the number of covalent bonds formed. The gel phase formed is still weak and, in order to obtain a structural material, the curing process has to continue until the sol fraction becomes small or almost zero: at this stage (i.e. the vitrification) most of the molecules are connected to form the three-dimensional network (solid glass in Fig. 5.2) of the epoxy resin.

During the entire curing process the T_g increases to reach the curing temperature at the onset of the vitrification stage. Figure 5.3 shows an example of the trend of T_g versus time during the curing process of an epoxy resin performed at 90°C. It is important to note that at the beginning of the curing process (prior to gel time), the difference between the cure temperature and the T_g of the resin system is still great: the reactions occur in the liquid state and the rate of cure is high since it is chemically kinetically controlled. After the gel point, this difference becomes small and the curing process, becoming diffusion controlled, decreases in rate and finally stops (Ellis, 1993). At this stage, although the resin system has reached the solid state, not all epoxy groups have reacted: to ensure complete reaction and to obtain the ultimate mechanical and physical properties of the resin, it is needed to post-cure the resin at an elevated temperature.

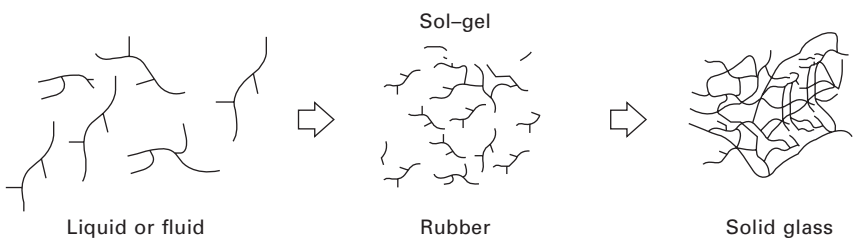

5.2 Curing reaction.

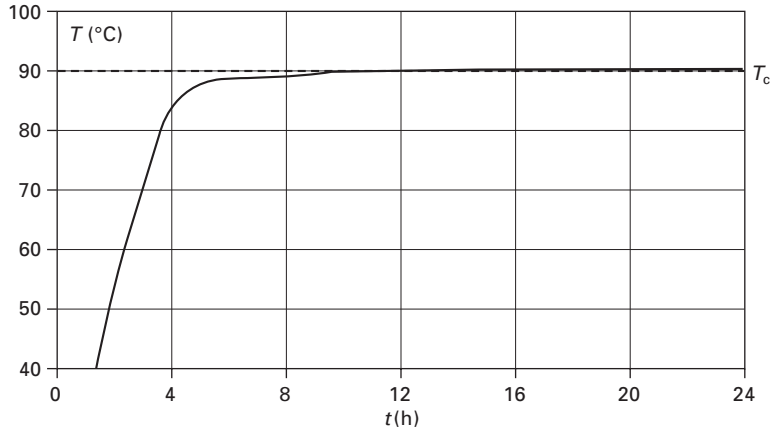

5.3 Glass transition temperature T_g versus time during the curing process of an epoxy resin.

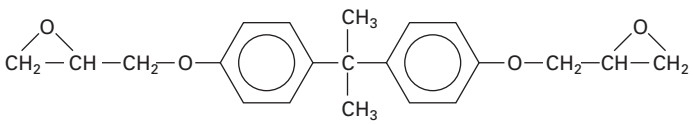

5.4 Diglycidyl ether of bisphenol-A epoxy (DGEBA).

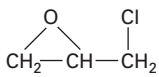

5.5 Epichlorohydrin.

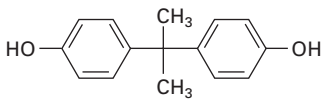

5.6 Bisphenol-A.

5.3 Common epoxy resins

5.3.1 Diglycidyl ether of bisphenol-A epoxy (DGEBA)

The diglycidyl ether of bisphenol-A (DGEBA), shown in Fig. 5.4, represents the most common type of epoxy resin. It is the product of the reaction between a large excess of epichlorohydrin (Fig. 5.5) with bisphenol-A (Fig. 5.6) with a stoichiometric amount of sodium hydroxide at about 65°C. The excess of epichlorohydrin is needed to limit the production of higher molecular weight products: in fact DGEBA can react with bisphenol-A, generating

epoxy resins with higher molecular weight (shown in Fig. 5.7, where n is the average number of repetitive units within the molecule).

DGEBA resins are available on the market with $0 < n \leq 14$. The basic commercial version of these resins has a molecular weight of 380 while purified versions ($n = 0$) show molecular weights equal to 344. On the other hand, epoxy resins with higher molecular weight ($n = 1–14$) can be produced by reducing the amount of epichlorohydrin and reacting under more alkaline conditions.

5.3.2 Diglycidyl ether of bisphenol-F epoxy (DGEBF)

Apart from bisphenol-A, other difunctional phenols can be used to react with epichlorohydrin with the aim of producing epoxy resins. The most commonly used is bisphenol-F (see Fig. 5.8). These epoxy resins are produced by using the same method as performed for DGEBA. The DGEBF epoxy resins have lower viscosity and better mechanical and chemical properties than the DGEBA ones. The DGEBA are often mixed with DGEBF both to prevent the crystallization of the system and to make them easier to handle at low temperature by lowering their viscosity.

5.3.3 Tetraglycidyl methylene dianiline epoxy (TGMDA)

By reacting epichlorohydrin with aromatic diamines, it is possible to manufacture epoxy resins with higher functionality than DGEBA or DGEBF resins. As shown in Fig. 5.9, the structure of tetraglycidyl methylene dianiline epoxy, the most important glycidyl amine, is characterized by four epoxy

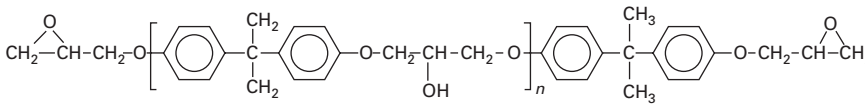

5.7 General formula of diglycidyl ether of bisphenol-A epoxy (DGEBA).

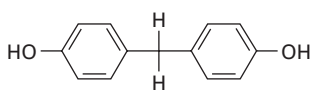

5.8 Bisphenol-F.

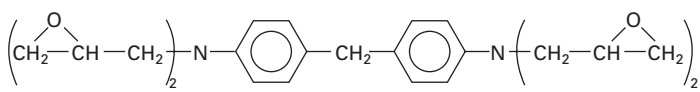

5.9 Tetraglycidyl methylene dianiline epoxy (TGMDA).

groups that confer higher strength and rigidity and better resistance to temperature (Campbell, 2010). The TGMDA are often mixed with DGEBA with the aim to confer more flexibility when an adhesive epoxy with high toughness is needed.

5.3.4 Polynuclear phenol epoxy (PNP)

These epoxy resins can be manufactured by reacting epichlorohydrin with tetrakis(4-hydroxyphenyl) ethane. As shown in Fig. 5.10, as in the TGMDA epoxy resins, the polynuclear phenol epoxy resins have four epoxy rings in their molecule.

5.3.5 Hydantoin epoxy (HY)

During recent years, various hydantoin-based heterocyclic glycidyl amine resins have been developed. These resins have low viscosity and long curing time (i.e. gel time and vitrification time) that ensure good wettability and optimal adhesion with several kind of substrates and fibers: for this last reason, the HY epoxy resins are widely used as adhesives and coatings or as a matrix for aramid fiber-reinforced composites (Charrier, 1991). As shown in Fig. 5.11, the presence of non-aromatic rings confers to these resins high resistance to UV. Moreover in comparison with other epoxy resins, the hydantoin ones possess higher heat deformation temperature and better dielectric strength.

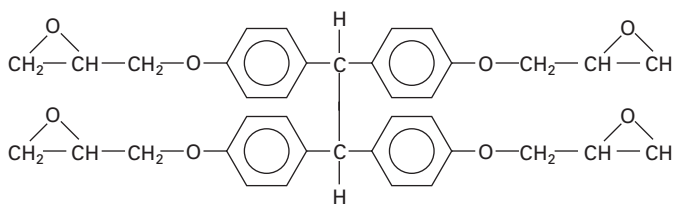

5.10 Polynuclear phenol epoxy (PNP).

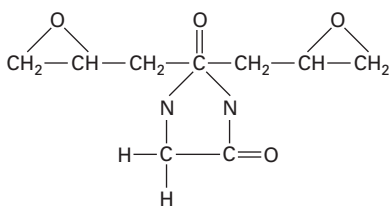

5.11 Hydantoin epoxy (HY).

5.3.6 Cycloaliphatic epoxy (CA)

These resins, characterized by a saturated cycloaliphatic ring structure without any aromatic groups, present a high heat deflection temperature and optimal electrical properties, also at high temperatures. For these reasons, in recent decades they have been considered for printed circuit board (PCB) markets and play an important role as electrical insulation for indoor and outdoor power equipment such as motors, transformers and switchgears (Kumagai and Yoshimura, 2000). Moreover these resins show low viscosity, high chemical resistance and good mechanical properties among the epoxy resins available in the market.

5.3.7 Epoxy phenol novolac (EPN)

The reaction conditions used to produce this kind of epoxy resin are similar to those used for DGEBA or DGEBF resins. In particular an excess of epichlorohydrin reacts with the organic compound (i.e. polyphenol shown in Fig. 5.12) manufactured by the reaction between phenol and an excess of formaldehyde with the use of an acid as catalyst. The structure of a phenol novolac epoxy resin is shown in Fig. 5.13. In this case, the excess of epichlorohydrin helps to minimize the reactions of phenolic hydroxyls with the epoxy groups present in the molecules, thus limiting the amount of branching that can occur. In the molecule of the EPN resin there are more epoxy rings ($n + 2$) than in that of the DGEBA resin: the greater amount of these reactive rings allows a higher density of cross-linking, so it is possible to obtain a stiff structure with better chemical resistance to solvents and better properties at high temperatures (i.e. higher T_g). In contrast, they possess higher viscosity than DGEBA resins, resulting in less workability.

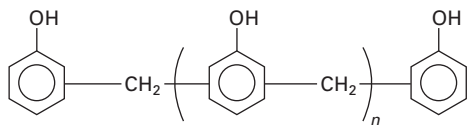

5.12 Polyphenol.

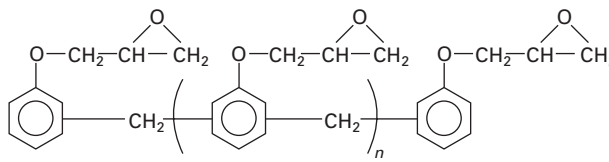

5.13 Epoxy phenol novolac (EPN).

5.4 Curing agents

The reactive groups attached to the molecules of an epoxy resin can react with several curing agents, such as amines, anhydrides, acids, mercaptans, imidazoles, phenols and isocyanates, to create covalent intermolecular bonds and thus to form a three-dimensional network. Among these compounds, due to the enhanced environmental stability of amine-cured epoxy resin (Dyakonov *et al.*, 1996), primary and secondary amines are the curing agents most commonly used: in particular aliphatic or cycloaliphatic amines for low-temperature epoxy systems as adhesives or coatings and aromatic amines to produce matrices for fiber-reinforced composites (Pascault and Williams, 2010). In Fig. 5.14 the structures of both an aliphatic and an aromatic amine are shown.

Aliphatic amines are usually blended with epoxy resins at ambient temperature, obtaining a system with higher curing rate and shorter curing life (i.e. gel and vitrification times) than in the case of cycloaliphatic or aromatic polyamines. Aliphatic amines are highly reactive curing agents that, blended with epoxy molecules, allow one to obtain dense cross-linked networks, thanks to the short distance between the active sites. As result it is possible to manufacture cured systems with high resistance to alkalis and some inorganic acids, good resistance to water and solvents (but less against many organic solvents), excellent bonding performance, and good mechanical properties, but with low flexibility. If a post-curing treatment at high temperature is performed, the properties of these epoxy systems that usually cure at room temperature are improved.

Aromatic amines react more slowly with epoxy resins than aliphatic or cycloaliphatic amines (Weinmann *et al.*, 1996). By mixing these kinds of curing agents with an epoxy resin, the resulting system shows a long curing time and needs long periods at elevated temperatures to reach optimum properties. Particularly, the curing of aromatic amine requires heating in two steps: the first heating is carried out at a rather low temperature (approximately 80°C) to reduce heat generation, and the second heating is carried out at a higher temperature (usually between 150°C and 170°C). By using aromatic amines as hardeners, the cured epoxy systems obtained show excellent heat resistance, good mechanical and electrical properties, besides excellent chemical resistance, particularly against alkalis.

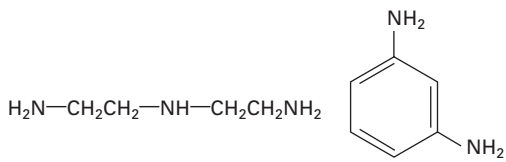

5.14 (a) Diethylenetriamine; (b) metaphenyl diamine.

Carboxylic acids and anhydrides are the second most widely used class of curing agents for epoxy resins, particularly in heat-cure applications: the acids in applications of epoxy resins as surface coatings (i.e. heat-cured surface coating), while anhydrides in most other heat-cure applications, particularly for electrical insulating materials. Anhydrides are suitable for making large moldings, since they confer long curing times to epoxy systems besides generating, during the curing process, small quantities of heat. Moreover they form cured resins characterized by well-balanced electrical, chemical and mechanical properties. In Fig. 5.15 the structure of phthalic anhydride amine is shown.

Polymercaptans are used as low-temperature curing agents: i.e. they allow the curing process of the epoxy system at between –20°C and 0°C with the addition of a tertiary amine as accelerator. On the other hand, at ambient temperature, epoxy/polymercaptan systems show a short curing time (i.e. pot life between 2 minutes and 10 minutes), rapidly reaching their optimum properties in 30 minutes.

By using imidazoles (see Fig. 5.16) as curing agents, it is possible to manufacture cured resin with a high heat deformation temperature by thermal treatment at a medium temperature (between 80°C and 120°C) for a short time. In general, imidazole-cured epoxy resins show superior physical properties compared to those cured with tertiary amines and they are widely used in the electronics industry as molding and sealing compounds (Ghaemy and Sadjady, 2006). In addition, as with tertiary amines, imidazoles are widely used as curing accelerators or co-curing agents for organic-acid anhydrides, polyhydric phenols and aromatic amines.

5.5 Bio-derived epoxy resins

Over the last decade, the synthesis of polymers starting from renewable resources has been the object of significant research efforts. This is mainly

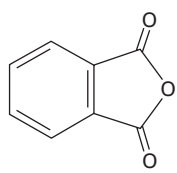

5.15 Phthalic anhydride.

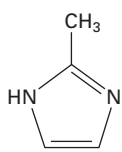

5.16 2-Methylimidazole.

due to the increasing prices of petrochemical products associated with growing environmental concerns. As for other plastic materials, the formulation and characterization of bio-derived thermosetting resins is now being studied: in particular, the substitution of bisphenol-A based epoxy resins by materials coming from natural sources represents a challenge for scientists.

For instance cardanol, a phenol-based by-product of the cashew nut industry, is one of the common precursors used to obtain different types of epoxy bio-based resins. Cardanol is an industrial grade yellow oil obtained by vacuum distillation of 'cashew nut shell liquid'(CNSL), the international name for the alkyl phenolic oil contained in the spongy mesocarp of the cashew nut shell from the cashew tree *Anacardium occidentale* L. CNSL derived from the most diffused roasted mechanical processes of the cashew industry represents nearly 25% of the total nut weight, and its production worldwide (Africa, Asia and South America being the main producer areas) is estimated to be about 300,000 tons per year (Calò *et al.,* 2007).

A thermosetting resin containing approximately 40% of cardanol by weight has been synthesized by adding an epoxy monomer and an acid-based catalyst to a resole compound (Maffezzoli *et al.*, 2004). This last was manufactured through a polycondensation reaction between cardanol and formaldehyde in the presence of a basic catalyst. The formulation characterized by adequate properties and curing temperatures was reinforced with natural fibers (i.e. short ramie, flax, hemp fibers and a jute fabric) to obtain samples which were then tested both in tensile and in flexural configurations.

Two different novolac resins (with an amount of unreacted cardanol of 35% and 20% by weight, respectively) have been used as curing agents of a DGEBA epoxy resin (Campaner *et al.*, 2009). In this work, calorimetric studies showed that novolac/epoxy resin weight ratios lower than 60/40 led to the cross-linking of the resin as a result of an increasing number of secondary hydroxyl groups available for cross-linking reactions. An improvement of the mechanical properties with the increase of the epoxy resin amount was also observed. On the other hand, the thermal resistance of the cured resin in a nitrogen atmosphere did not change significantly with varying the novolac amount, and only a one-step mass loss corresponding to a single thermal degradation process, occurring at temperatures higher than 400°C, was observed.

A paint based on an epoxy–cardanol resin has been produced and then characterized in order to compare its performance (i.e. physico-mechanical properties, chemical resistance and corrosion protection efficiency) with that of paints made with unmodified epoxy resin (Aggarwal *et al.,* 2007). It was found that the new bio-based paints show better anticorrosive properties than the unmodified paints and thus the cardanol-based epoxy resin represents an optimal binder medium for the formulation of paints.

Rosin, obtained by heating the liquid resin produced by pines and

other conifers, is an abundantly available natural product. Thanks to their chemical structure, rosin acids show molecular rigidity similar to that of the cycloaliphatic or aromatic compounds. Therefore, their derivatives may serve as alternatives to current petroleum-based rigid monomers to prepare a bio-based epoxy resin.

Some authors have synthesized a novel bio-based epoxy from a rosin acid, showing that this last possesses a high glass transition temperature (T_g = 153.8°C), a high storage modulus at room temperature and good thermal stability (Liu and Zhang, 2010). Hence the results suggest that it is possible to develop high-performance thermosetting resins from rosin.

Rosin-derived amine containing an imide structure was synthesized as a curing agent for epoxy resins (Wang *et al.*, 2011) and compared both to a commercial aromatic amine curing agent and to another type of rosin-based anhydride curing agent. The results have shown that by using this last curing agent, the epoxy system obtained has shown similar moduli, higher T_g and only slightly lower degradation temperature, compared to that cured by using the commercial amine curing agent. On the other hand, epoxy cured with the new curing agent exhibited a higher degradation temperature than that cured with a rosin-based anhydride curing agent, due to the introduction of the imide structure.

Another class of important renewable resources is represented by triglyceride plant oils. Among these vegetable oils, palm oil, soybean oil, rapeseed oil and sunflower oil are the four most important vegetable oils worldwide, holding a share of more than 80% of the market (Tan and Chow, 2010). Linseed oil and soybean oil are found to be the most popular epoxidized vegetable oils utilized today, since most of the potential vegetable oils are not available or their price is exorbitant.

Particularly, in the past decade, much effort has been dedicated to producing soybean oil-based polymeric materials. 3,4-Epoxidized soybean oil (ESO) is manufactured by the epoxidation of the double bonds of the SBO triglycerides with hydrogen peroxide, either in acetic acid or in formic acid, and it is industrially available in large volumes at a reasonable cost.

Bio-based epoxy materials containing functionalized vegetable oils, such as epoxidized linseed oil and epoxidized soybean oil, have been processed with the aid of an anhydride curing agent (Miyagawa *et al.*, 2005). In particular, those authors replaced a percentage of diglycidyl ether of bisphenol-F with each vegetable oil used. Selection of the DGEBF, vegetable oils and anhydride curing agent resulted in an excellent combination to produce a new bio-based epoxy resin characterized by both high elastic modulus and high glass transition temperature. Izod impact strength and fracture toughness were significantly improved, depending on vegetable oil content, which produced a phase-separated morphology.

Some authors have synthesized epoxy resins by partial replacement of the

synthetic DGEBA epoxy prepolymer with increasing amounts of epoxidized soybean oil, using an anhydride (i.e. methyltetrahydrophthalic) as curing agent and 1-methyl imidazole as initiator (Altuna *et al.*, 2011). Calorimetric studies have shown a drop in the reaction heat with soybean oil content because of the lower reactivity of oxirane rings due to steric constraints. The combination of DGEBA with 40% in weight of vegetable oil represents the resin cured with the best properties: particularly, E' (i.e. storage modulus) in the glass state was 93% higher than that of the neat DGEBA resin, T_g decreased by only about 11°C and the impact strength increased about 38% without loss of transparency.

A new bio-based epoxy resin system has been prepared by curing epoxidized soybean oil with tannic acid under various conditions (Shibata *et al.*, 2011): the authors have found that the most balanced properties were obtained when the system was cured at 210°C for 2 h with an epoxy/hydroxyl ratio of 1/1.4. Moreover, the authors prepared biocomposites starting from the bio-based epoxy resin using as reinforcements microfibrillated cellulose (MFC) with contents of these last from 5% to 11% in weight.

5.6 Mechanical properties

Thanks to their good mechanical properties (see Table 5.1), epoxy resins are widely used as polymer matrices for composite materials. As regards mechanical performances, the only weak point of epoxy resins is their fragile behavior. To increase the elongation at break and, consequently, the impact properties of the epoxy resins, usually small amounts of liquid rubbers with highly reactive terminal carboxyl groups are added. For instance carboxyl-terminated copolymer of butadiene and acrylonitrile liquid rubber (CTBN) can be used (Valenza and Calabrese, 2003). This rubber forms a dispersed phase bonded with the epoxy matrix that prevents crack propagation within the matrix. Particularly by adding a small amount of rubber (10–15%), the dispersed phase acts as a dissipation center of mechanical energy by cavitation and shear yielding, inducing the increase of crack growth resistance and finally excellent fracture properties. In Table 5.2 the decreases of mechanical properties such as tensile strength and modulus due to adding CTBN to epoxy resin is shown.

Table 5.1 Mechanical properties of epoxy resins

Tensile strength (MPa)	28–91
Young modulus (GPa)	2.4–4.5
Elongation at break (%)	2–6
Poisson coefficient	0.29–0.34
Izod impact strength (J/m^2)	10–50
Hardness Rockwell M	100–112

Table 5.2 Mechanical properties at varying values of CTBN content

	CTBN content [phr]			
	0	5	10	15
Tensile strength (MPa)	65.8	62.8	58.4	51.4
Young modulus (GPa)	2.8	2.5	2.3	2.1
Elongation at break (%)	4.8	4.6	6.2	8.9

Table 5.3 Effect of ATBN on the reactivity of epoxy resin

	ATBN content (phr)					
	0	5	10	12.5	15	20
Gel time (min)	13.0	12.0	10.5	11.0	10.0	10.5
Cure time [min]	19.0	17.0	16.5	16.0	16.0	17.0
Gel temperature (°C)	93.5	92.0	91.5	91.0	89.0	83.0
Exothermic peak (°C)	112.5	108.0	103.0	103.5	100.5	96.0

Source: Reprinted from *Eur Polym J*, 38, Chikhi N, Fellahi S and Bakar M, 'Modification of epoxy resin using reactive liquid (ATBN) rubber', 251–264, Copyright (2002), with permission from Elsevier.

With the same aim, an amine-terminated butadiene acrylonitrile copolymer (ATBN) can be used (Chikhi *et al.*, 2002). In this work, the authors have shown that rubber addition increases toughness but decreases the elastic modulus and the T_g of the final product (through the fraction of rubber remaining dissolved in the epoxy matrix). Moreover, adding these compounds leads to a decrease of all reactivity characteristics, due to the fact that during the reaction of ATBN with the epoxy resin some of the exothermic energy released during the epoxy cross-linking might have been consumed by ATBN. Consequently, as shown in Table 5.3, both gel time and cure time decrease as well as the exothermic peak. As discussed above, the disadvantage of adding rubber to epoxy resins is that there are decreases in properties such as glass transition temperature, Young modulus and tensile strength. To toughen epoxy resins without these decreases, epoxy resins are blended with thermoplastic polymers such as polyethersulfones, polyetherimides and polyphenylene oxides.

5.7 Chemical properties

Among thermosetting polymers, epoxy resins are characterized by the highest chemical and corrosion resistance, in addition to optimal resistance to attack from seawater. For these reasons, these thermosetting resins represent the best choice as matrices for composite structures that must retain their mechanical and physical properties and not degrade when immersed in seawater or in a

chemically aggressive environment for a long time. For the same reasons, epoxy resins are also commonly used for a wide variety of protective coatings and paints to protect metals against corrosion (Miskovic-Stankovic *et al.*, 1999; Popovic *et al.*, 2005; Armelin *et al.*, 2008).

Regarding seawater resistance, by using polyester-based composites, both the polymer matrix and the fiber/matrix interface can be degraded by hydrolysis reactions of unsaturated groups within the resin. This degradation leads to swelling and plasticization of the matrix and debonding at the fiber/matrix interface, involving great decreases in mechanical performances. To overcome this problem, it is appropriate to use vinyl ester or epoxy-based composites which, as discussed above, generally show superior chemical stability in seawater.

Some authors have studied the wet aging of four thermoset resins (orthophthalic polyester, isophthalic polyester, vinyl ester and epoxy) and their composites reinforced with glass fibers. In particular, resins and composites were aged for 18 months, under three immersion conditions: i.e. 20°C and 50°C in seawater, and 50°C in distilled water. The experimental tensile tests have shown the influence on weight changes particularly of the matrix resin and the aging medium (Davies *et al.*, 2001).

Further recent research (Mourad *et al.*, 2010) has been focused on the effects of seawater on mass change, permeation of salt and contaminants, degradation in mechanical properties and failure mechanisms of both glass/epoxy and glass/polyurethane composites composites. To this aim the laminates have been immersed in seawater for periods from three months to a year, both at room temperature and at 65°C. The experimental results have shown that high temperature accelerates the degradation mechanism in the glass/polyurethane composite. No significant changes were observed in the tensile strength of glass/epoxy and in the modulus of both glass/epoxy and glass/polyurethane composites. However, the tensile strength of the glass/polyurethane composite decreased by 19% after a year of exposure to seawater at room temperature and by 31% after a year of exposure to seawater at 65°C.

Seawater aging of epoxy and vinyl ester resins reinforced with different fibers (e.g. glass and carbon) has also been investigated (Narasimha Murthy *et al.*, 2010). The experimental results have evidenced that the vinyl ester composites retain better their mechanical properties than epoxy ones: in particular, the flexural strength and ultimate tensile strength (UTS) dropped by about 35% and 27% for glass/epoxy, by 22% and 15% for glass/vinyl ester, by 48% and 34% for carbon/epoxy, and by 28% and 21% for carbon/vinyl ester composites, respectively. In contrast, the authors have shown that the water uptake of the epoxy-based composites is lower than that of the vinyl ester ones.

5.8 Thermal and electrical properties

The thermal and electrical properties of epoxy resins are very important for many applications; due to the fact that these thermosetting materials exhibit rather low thermal and electrical conductivities, significant research efforts have been dedicated to modifying neat epoxy resins with the aim of improving these properties. Particularly, in the last decade, epoxy resins have been modified by adding fillers with optimal electrical and thermal properties such as carbon nanotubes, metal powders and inorganic microfillers. For instance, inorganic microfillers are used to improve the thermal conductivity of epoxy resins (Lee *et al*., 2008; Lee and Yu, 2005). However, to achieve the percolation threshold and obtain high thermal conductivity, very high contents of microfiller may be used, resulting in high density and poor mechanical properties.

The use of organic nanofillers allows the reduction of the filler content required to achieve high thermal conductivity. In particular, multi-walled carbon nanotubes (MWCNTs), with their one-dimensional structure, high aspect ratio and superior thermal conductivity (3000 W/mK for an individual MWCNT and 200 W/mK for bulk MWCNTs at room temperature (Yang *et al*., 1991)) have recently attracted great attention in the scientific world. The influence of different carbon nanotube types, particle content, interfacial area, surface functionalization and aspect ratio on the electrical and thermal conductivity of epoxy resins has been investigated (Gojny *et al*., 2006).

As regards different nanotube types, multi-walled carbon nanotubes (MWCNTs) exhibit the highest potential for an efficient enhancement of the electrical conductivity, due to their relatively low surface area and high aspect ratio. Some kinds of treatment lead to a reduction of the aspect ratio (i.e. functionalization, ultrasonication, etc.) with consequent increase of the percolation threshold. On the other hand, the incorporation of carbon nanotubes into epoxy resins results in a slight enhancement of the thermal conductivity. Even though multi-walled nanotubes seem to have the highest potential to improve the thermal conductivity of epoxy resins, the theoretically predicted thermal conductivities of isolated tubes cannot be transferred to epoxy resins in practice. In conclusion, Gojny *et al*. (2006) have stated that carbon nanotubes and probably further nanoparticles, which provide higher interfacial areas, are not suitable for enhancement of the thermal conductivity of polymer-based composites.

It has been shown that, by adding 6% in weight of multi-walled carbon nanotubes or 71.7% in weight of silicon carbide (SiC) microparticles to an epoxy resin, the thermal conductivity of the composites reached values that are 2.9 and 20.7 times that of the neat epoxy, respectively (Zhou *et al*., 2010). Moreover, to further improve the thermal conductivity of the composites, these authors partially replaced microfillers with nanofillers to obtain a

thermal conductivity 24.3 times that of the neat epoxy, with 5% in weight of MWCNTs and 55% in weight of microparticles of SiC.

Carbon nanotubes decorated with silver nanoparticles (Ag-CNTs) have been used as conducting fillers in epoxy resin to fabricate electrically conducting polymer (Ma *et al.*, 2008). The experimental results have shown that the electrical conductivity of composites containing 0.1% in weight of Ag-CNTs was more than four orders of magnitude higher than those containing the same content of functionalized CNTs, and this improvement was not at the expense of thermal or mechanical properties.

In recent years metallic particles have also been considered as fillers to increase the electrical and thermal conductivities of epoxy systems. The electrical and thermal conductivities of epoxy systems filled with metal (i.e. copper and nickel) powders have been studied (Mamunya *et al.*, 2002). In this work it was shown that the composite preparation conditions allow the formation of a random distribution of metallic particles in the polymer matrix. The percolation theory equation holds true for systems with a random distribution of dispersed filler, while in contrast to the electrical conductivity, the dependence of thermal conductivity on concentration shows no jump in the percolation threshold region.

Thermal, mechanical chemical and fracture properties of epoxy resins filled with alumina particles have been analyzed as a function of average filler size, size distribution, particle shape, loading and epoxy cross-link density (McGrath *et al.*, 2008). The authors have shown that the density of cross-link and the amount of filler were the most important variables, modifying all properties, while other parameters (i.e. particle size, shape and size distribution) have little impact on the final properties.

Carbon black (CB) can be considered another important filler that can be used to improve the electrical conductivity of epoxy resins because of its abundant source, low density, permanent conductivity and low cost. Nevertheless it is very important, for carbon black-filled polymer composites, to reduce the percolation threshold to as low a value as possible, since high CB volume fractions increase the melt viscosity, decrease the impact resistance, increase the final product cost and degrade the mechanical properties. Some authors have dedicated their research efforts to studying new composites with high electrical conductivities, produced by adding a low content of plasticized carbon black in an epoxy resin (Abdel-Aal *et al.*, 2008). The experimental results have shown that the conductivity of the composites at room temperature increases with carbon black content. Besides the dependence of the temperature on the electrical conductivity showing a negative temperature coefficient of conductivity behavior of the composites, the current–voltage behavior shows a switching effect, which makes the proposed composites potential candidates for a new application switching voltage and current in electronic devices, and the thermal conductivity increases with increasing CB content in composites.

5.9 Optical properties

In recent years, epoxy resins have been used to realize optical disk matrices, lenses and prisms. However, the refractive index of conventional epoxy resins is low and their applications as optical materials where a high refractive index is required are limited. For this reason, many efforts are being dedicated to synthesizing new optical epoxy resins characterized by a high refractive index, good mechanical properties and optimal thermal insulation.

To these aims, a set of novel episulfide-type optical resins with high refractive index, low dispersion and well-balanced physical properties, have been prepared (Lu *et al.*, 2003). In particular these resins, which can be considered as successors to the polythiourethane resins in wide practical applications, have been synthesized by ring-opening copolymerization of bis(β-epithiopropylthioethyl) sulfide (BEPTES) with episulfide derivative of DGEBA (ESDGEBA) and 2,4-tolylene diisocyanate (TDI), respectively. Furthermore a triethylamine has been used as curing catalyst and the episulfide monomers (i.e. BEPTES and ESDGEBA) have been synthesized from their corresponding epoxy compounds, respectively.

The experimental results have shown that the BEPTES/ESDGEBA cured resins have a high refractive index that increases linearly with the content of BEPTES. The introduction of ESDGEBA into the copolymerization system can improve both surface hardness and the T_g of the cured resins. For the BEPTES/TDI system, the refractive index increases linearly with the increase of molar ratio of BEPTES to TDI.

In order to manufacture TiO_2/epoxy resin nanocomposite films with high refractive index, some authors (Guan *et al.*, 2006) have introduced, by using a sol–gel method, amorphous titania (TiO_2) into epoxy systems. The experimental results have shown that the amorphous TiO_2 particles are uniformly dispersed in the organic polymer matrix if their size is smaller than 100 nm. Moreover, the refractive index of these kinds of materials can be increased with increase in the content of TiO_2 which is very important for applications in optical anti-refractive films.

The optical properties of a neat epoxy resin and composites prepared by its modification with two different oxime derivatives (i.e. benzaldoxime and 2-furaldoxime) in the UV-vis region (particularly from 190 nm to 680 nm wavelength) have been investigated in a recent paper (Durmus *et al.*, 2011). The experimental results have shown that oxime derivatives have not caused strong changes in the refractive index of the resin, but optical band energies greatly increase by modification. Furthermore, the absorbance in the UV region is greatly increased for the 2-furaldoxime-doped resin while it is decreased for the benzaldoxime-doped sample. In conclusion, this work has shown that the benzaldoxime-doped sample can be utilized for applications in which low absorbance in the UV region is needed, while 2-furaldoxime-

doped resin is suitable for devices requiring strong absorption in the same region.

5.10 Applications

Thanks both to their good properties and mainly to their versatility, nowadays epoxy resins find application in the following major fields: coatings, electrical and electronic insulation, adhesives and construction and as matrices for FRP automotive, nautical and aerospace applications.

5.10.1 Adhesives

In industrial manufacturing, adhesives play an important role in the production of many different kinds of product. They offer a number of advantages in comparison to the conventional joining techniques: for instance, adhesive bonds are superior in the presence of dynamic stress, due to their flexible nature. Moreover rivets or bolts can only transmit forces over a very localized area, while in an adhesive bond the stress distribution is spread over the entire area of the bond.

In addition, the parts to be bonded are weakened by the drilling of holes. In particular, when one or both substrates to be joined are made of composite material, traditional joining technologies are hardly applicable as they induce critical stresses, or composite manufacturing technology does not allow their application. Moreover, for fiber-reinforced polymer structures, the drilling process to create bolt holes breaks fibers, causing several problems such as peeling of the higher plies at the entry of the hole, resin degradation on the wall of the hole and delamination of the last plies in the laminate (Zitoune and Collombet, 2007). Such damage can initiate fatigue cracks and severely decrease the fatigue strength of mechanical joints (Matsuzaki *et al.*, 2008).

The low heat input, compared to welding, is another key criterion when joining parts that already have their final surface finish, for example painted metal or stainless steel. As non-conducting materials, cured adhesives also have an insulating effect, thus preventing contact corrosion.

Depending on the field of engineering application, various kinds of adhesives with different properties are available for structural bonding (i.e. methacrylate, polyurethanes, acrylics and silicones). Among these, epoxy-based adhesives are the most widespread class used in several applications. They are found in automotive, marine and aircraft manufacturing as well as in the building and construction industries. Their principal advantage is that they can bond both metal and plastics. Moreover, they are extremely durable, show a high creep resistance, low curing shrinkage and high chemical resistance. Depending on the type, they can withstand continuous exposure

to temperatures ranging up to 100–200°C. Epoxy-based adhesives offer a wide pot life range (from five minutes up to two hours): a long pot life can be an advantage when the parts to be joined require some time to work or when they have to be repositioned after assembling (Handwerker, 2011).

In a recent paper the performance of glass fiber-reinforced composite-to-aluminum alloy single-lap bonded joints has been studied (Valenza *et al.*, 2011). In particular, to analyze the influence of the adhesive on the mechanical behavior of the joints, the authors used two kinds of adhesives – i.e. a two-component methacrylate and an epoxy. It is important to note that the epoxy adhesive is based on the same resin and hardener mix used as the matrix of the composite laminates with the addition of two filler powders, i.e. colloidal silica and microballoons. The authors have shown that the epoxy-based joints present higher resistance than the methacrylate ones and, by pretreating the metal surface with silane coupling agent (γ-GPS), notable improvements in the failure stress of the epoxy-based joints were obtained. This is due to the chemical structure of the coupling agent used: as shown in Fig. 5.17, it has both an epoxy ring which is compatible with the epoxy adhesive and three methoxylane groups which can form covalent bonds with the metal surface.

5.10.2 Nautical

As discussed above, the nautical field is one of the most important fields in which epoxy resins are used, mainly as matrices for fiber-reinforced polymers but also as adhesives and paints. Unlike aerospace applications, in which epoxy resins have been the norm for years, in the nautical field nowadays more than 90% of pleasure boats under 60 feet are still made with polyester resin, thanks to their lower costs. In fact epoxy resins are more expensive than vinyl ester resins and the latter are about twice as expensive as polyester ones. Since the resin can constitute up to half the weight of a composite component, this price difference has a significant impact on the cost of the laminate.

Probably the most important property that the resins must have, to be useful in a marine environment, is high resistance to degradation due to water penetration. Each thermosetting resin absorbs some moisture that increases the weight of the composite structures. Moreover the absorbed

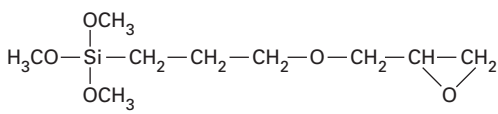

5.17 Chemical structure of γ-GPS.

water affects the three-dimensional structure of the resins (i.e. by breaking the covalent link of the network) and mainly the adhesion resistance at the interface between resin and reinforcements, leading to a gradual and long-term loss in mechanical and physical properties.

As discussed in Section 5.6.2, both polyester and also to some extent vinyl ester resins are prone to water degradation due to the presence of ester groups in their molecular structures, while epoxy resins show higher resistance to these degradation phenomena. Vinyl ester resins show much higher resistance to seawater than polyester ones thanks to the lower number of ester groups within their molecules. In particular, according to some scientific studies, vinyl ester resins have comparable resistance to seawater than epoxy ones.

It is also important to note that in the marine field, the hand lay-up technique is still today the principal production technology of composite structures, followed by the *vacuum bagging* technique. Both are defined as 'open mold' technology: consequently, the use of polyester or vinyl ester resins makes the working area very hazardous due to the high emission of dangerous volatile substances (i.e. styrene) during the curing process. In contrast, epoxy resins do not emit volatile and dangerous products during the curing process, thus keeping 'clean' the working area of the shipyard.

A further problem is due to high values of volume contraction (i.e. shrinkage) during the curing process of polyester and vinyl ester resins. In fact, as discussed in Section 5.1, polyester and vinyl ester resins shrink up to 5% volumetrically while epoxy resins shrink less than 5%. The shrinkage of thermosetting resins during their curing process is notorious for its potentially serious consequences in every application of composite materials such as, for instance, in nautical applications. Thermosetting resins are typically used in combination with stiffer reinforcements: consequently, the shrinkage is constrained and residual stresses are formed in the structure. These stresses can result in early product failure due to void formation, stress cracking, delamination and poor fiber–matrix adhesion. Moreover it is important to note that, using polyester or vinyl ester resins as matrix for a composite structure (e.g. the hull of a boat), the designers need to oversize the mold so as to take into account the volume 'lost' as a result of the high shrinkage of the resins. For all these reasons, epoxy resins represent the better choice among thermosetting materials as a matrix for composite materials used in marine applications. Nevertheless, the higher cost of epoxy resins still encourages the wide use of polyester resins and, when better chemical resistance is requested, vinyl ester reasins, in the nautical field.

5.10.3 Automotive

The automotive field has been traditionally characterized by a widespread use of metallic materials. Composite materials were introduced at the beginning

of the 1970s: initially only polyester resins reinforced with glass fibers were utilized and parts were often made by hand lay-up or spray-up technique in open molds or by using SMC – sheet molding compound. Since then many new materials and manufacturing processes have been released, so that nowadays composite part designers have at their disposal a wide range of materials and processes. Nowadays in automotive construction, around 15% to 20% of the average weight of current vehicles consists of composite materials (it was 6% in 1970).

In this field, apart from providing matrices for composite materials, epoxy resins are widely used to realize primers with the aim of coating steel, aluminum and composite surfaces before painting. These new kinds of primers show higher anti-corrosive properties than traditional ones (e.g. zinc chromate based primers) and may be applied directly over old one-part primers to provide a solvent-proof barrier coat.

One of the most important factors in corrosion prevention by protective coatings is the loss of adhesion of the coating under environmental influences. The adhesion of several epoxy primers (i.e. pigment-free, zinc-rich and chromate-based) on steel has been analyzed (Bajat and Dedic, 2007). In particular both the dry and wet adhesion strengths of primers were measured directly by a pull-off procedure and the corrosion stability of coated samples was investigated by electrochemical impedance spectroscopy. Under dry test conditions, all the samples have shown very good adhesion while, during exposure to the corrosive agent (i.e. 3% NaCl solution for 25 days), the chromate-based epoxy primer showed the lowest adhesion values and the smallest change in adhesion among all investigated samples. The electrochemical impedance measurements have confirmed the good protective properties of pigmented epoxy primers on steel surfaces.

In the past, poor attention has been given to the effect of the pre-treatment of metal surfaces on the variation of adhesive strength. Traditional treatments such as chromate treatment uses health-hazardous materials, and the phosphatation method, used particularly on aluminum alloys in the automotive industry, has the disadvantage of generating high amounts of sludge in the treatment bath.

To evaluate environmentally friendly processes for aluminum alloys, the improvement of the adhesion between a lead-free epoxy primer used in the automotive industry and aluminum alloy 6016 has been studied (Poelman *et al.*, 2005). In particular the authors have compared samples pre-treated with a commercial Zr/Ti conversion coating with no pre-treated ones.

Different aging tests (e.g. salt spray of intact and scratched samples, immersion in an aerated NaCl 0.5M solution) have been performed by using electrochemical impedance spectroscopy to evaluate both the corrosion resistance and the degree of the degradation of systems studied. Analysis of the impedance spectra has confirmed that the application of a Zr/Ti pre-

treatment before coating considerably enhances the coating to metal adhesion, reaching performance levels similar to those achieved with the traditional treatments.

5.10.4 Aerospace

In high-tech structural applications, where strength, stiffness, durability and light weight are required, epoxy resins are seen as the minimum standard of performance for the matrix of composite structures. For these reasons, in aerospace applications epoxy resins have been the norm for years: in this engineering field the main consideration for materials selection is strictly connected with performance, leaving the material cost as a detail of secondary importance.

For non-structural parts of an aircraft, aramid and glass fibers are widely used as reinforcement of epoxy resins, while for the structurally critical components such as control surfaces furniture and aircraft tail, carbon or boron fibers are preferred.

Among the largest passenger aircraft, the most important applications of composite materials have been achieved on the Boeing 767 whose fuselage, canopy and rear wing structure are entirely made of high-performance composites: 80% of the weight structure is made of graphite/epoxy. Overall, epoxy-based composites currently represent 5% of the weight of aircraft engines. As regards helicopters carrying passengers, the A139 model adopts a cockpit in sandwich Kevlar/Nomex while the tail boom and stabilizer are made of carbon/epoxy.

Finally, the most extraordinary result achieved by the aviation industry in recent years, the tiltrotor BA 609 (an aircraft which takes off and lands like a helicopter and flies like an aeroplane, thanks to its 'balancing engine' which allows it to turn the propeller into a helicopter rotor and vice versa), has its primary structure made of epoxy resin reinforced by carbon fibers. This is the only engineering solution that allows both to limit the total weight and to compensate for the weight burden due to the addition of systems for the aircraft/helicopter conversion (Sala, 2006).

The use of epoxy resins in aircraft engines is actually limited by their resistance to temperature (about 200°C), but their utilization is rapidly increasing, and already the new fans and systems containment of the early stages of the compressors are made from fiber-reinforced epoxy resins.

Another important aspect to be considered concerns the smoke that is believed to be the main hazard of fires involving epoxy resins: its production depends on many variables, principally the chemical character and the burning rate of the polymer besides the availability of oxygen. With the aim of limiting smoke production in dangerous situations, epoxy resins have been filled with flame retardants and smoke suppressors.

For instance, the effect of smoke reduction and flammability performance of zinc-based compounds (i.e. zinc borate and zinc hydroxystannate) in epoxy resin composites used in the aerospace and aeronautical industries have been analyzed (Formicola *et al.*, 2011). The flammability performance of neat and loaded systems was analyzed by using micro-combustion calorimetry, while smoke generation, in terms of CO and CO_2 production, was analyzed under dynamic conditions by using cone calorimetry. The experimental results have shown that the dispersion of zinc borate and zinc hydroxystannate within epoxy matrices leads to a significant variation in flame retardant properties: in particular the total heat release is reduced by about 25% and 30%, respectively, and the heat release capacity by about 30% and 50%, respectively. The system containing zinc hydroxystannate shows an enhancement in all smoke reduction properties, and both compounds lead to a reduction of the CO_2/CO ratio.

5.10.5 Electronic and electrical

Encapsulation is the last step in integrated circuit fabrication. Encapsulating materials must protect components from chemicals and mechanical stress, ensure good electrical insulation, and offer good thermal conductivity. Owing to their lower cost and easier processing, over 90% of encapsulation materials are polymers. Among these polymers, epoxy resins have been used most widely in electrical and electronic insulation thanks to their high resistivity and relatively low dissipation factors, as well as their good mechanical properties. Neat epoxy resins are seldom used in these applications; more commonly they are modified with fillers to improve their mechanical and thermal properties while preserving their electrical insulation. For instance, often these thermosetting materials are loaded with 70–90% silica micro- and nanoparticles (Kwon *et al.*, 2008; Rouyre *et al.*, 2010).

Nowadays, encapsulation and coating of devices such as transistors, switches, coils, insulators and integrated circuits are effected by using epoxy resins and, particularly in Europe, these thermosetting polymers have taken over from porcelain in large outdoor transformers, switching gear and high-voltage insulators. In recent years, in integrated circuits sealed with epoxy molding compounds, the chip size has been increased while the dimensions of the package have become smaller and thinner, thus needing higher resistance to thermal stress. In fact, these stresses cause numerous problems such as package cracking, passivation layer cracking, aluminum pattern deformation and delamination. Several research projects have been developed with the aim of reducing the thermal stress in epoxy molding compounds used for microelectronic packages: in particular, epoxy–silicone hybrid resins have been developed for this application.

To better withstand the thermal stress, a novolac epoxy resin has been

modified incorporating polysiloxane particles (Ho and Wang, 2001). Experimental results have shown that the dispersed silicone rubber-modified epoxy resin effectively reduces the stress of cured epoxy molding compounds by reducing the flexural modulus and the coefficient of thermal expansion, while the glass transition temperature hardly decreases. In conclusion, electronic devices encapsulated with dispersed silicone rubber-modified epoxy molding compounds have exhibited excellent resistance to the thermal shock cycling test, thus resulting in an extended use life for the devices.

An epoxy–silicone hybrid resin with epoxy–silicone oligomers incorporated into the matrix at the nanometer level by sol–gel reaction has been prepared (Takahashi *et al.*, 2005). This epoxy–silicone hybrid resin has shown excellent mechanical properties at high temperatures. Besides the thermal expansion coefficient mentioned above, the glass transition temperature was two-thirds of the conventional value.

5.10.6 Civil

The use of high-performance epoxy resin systems in the civil engineering field has greatly increased since 1960. Nowadays these thermosetting polymers are widely used in this field as matrices for fiber-reinforced materials. In particular, their principal applications are in the following fields:

- Strengthening or rehabilitation of concrete and masonry structures by confinement with epoxy laminates
- Pultruded FRP bars instead of steel ones for tensile reinforcement of concrete structural members.

As regards the confinement of concrete structures, one of the most attractive applications of FRP materials is their use as confining devices for columns, with the aim of achieving remarkable increases in strength and ductility.

In recent years, many research works have been performed to investigate the behavior of concrete columns confined with FRP composites, showing that the latter behave differently from steel-confined concrete: consequently design recommendations for steel-confined concrete columns cannot be applied to FRP-confined columns. The behavior of concrete cylinders confined with hybrid FRP composites has been studied (Wu *et al.*, 2008). In particular, the effect of different types of FRP sheets, the number of reinforced layers and different kinds of hybridization have been analyzed: i.e., five different types of FRP composites have been manufactured using as reinforcement epoxy resin carbon fibers (high strength and high modulus), aramid fibers, and glass fibers. The experimental results have shown mainly that the confinement can be effective in increasing the strength, ductility and energy absorption capacity of concrete cylinders.

A further scientific study concerns the behavior of both square-section

specimens and cylindrical ones confined by epoxy resin reinforced by unidirectional carbon fibers (Si Youcef *et al.*, 2010). The experimental results have shown a very significant advantage of circular-section specimens compared to square-section ones: consequently the confinement performance using composite laminates is better for a cylindrical specimen than for a prismatic one. As regards the influence of the number of layers, the compressive strength increases by 58% and 236% for the cylindrical test specimen and by 20% and 95% for the square specimen, using as confinement one and three layers, respectively. Moreover, the concrete has shown additional deformability proportional to the number of layers.

Some authors (Bouchelaghem *et al.*, 2011) have analyzed the behavior of cylindrical concrete specimens reinforced with external laminates made of unidirectional carbon fiber/epoxy (CFRP) and bidirectional glass/polyester (GFRP) layers. The experimental results have shown that the FRP is beneficial in providing a good resistance against axial deformations and loads, due to a reduction of the stress levels in the concrete structure. The resulting effect is an increase both in the compressive strength and in the ductility of the concrete cylinders. Moreover the CFRP-reinforced columns provide a significant increase in ultimate compression stress compared to the GFRP-reinforced ones, and the damage mechanisms of the columns wrapped by the composite layers strongly depend on the reinforcement chosen (i.e. brittle failure in the CFRP-reinforced samples, ductile in the GFRP ones). As discussed above, a further application of epoxy resins in civil engineering concerns FRP pultruded bars as internal reinforcement in concrete structural members, including for garages, multi-storey buildings and industrial structures.

As is well known, one of the most important problems regarding steel-reinforced concrete structures is their low resistance to degradation phenomena that limits their service life and increases their maintenance cost. Under normal service conditions, the corrosion of steels embedded in concrete takes place at a very low rate due to the alkaline pH that can be found inside the concrete, but several chemical processes, due to external conditions, can modify the passive state of steel reinforcements, leading to an increase in the steel corrosion rate. For instance, the attack produced by the ingress of chloride ions into concrete causes both the breaking of the passive oxide layer of the steel surface, and a progressive acidification of the environment inside the pit. As a consequence, the corrosion rate increases inside the pit due to the low pH solution created (Garcés *et al.*, 2011).

In the last decades, to overcome these problems, pultruded FRP bars instead of steel ones have been studied as tensile reinforcement of concrete structures. In this application, thanks to their better resistance to degradation phenomena in chemically aggressive environments, epoxy resins represent the best choice among thermosetting polymers as matrix for the pultruded bars.

In fact, in a fiber-reinforced polymer bar, any degradation of fibers implies the transport of the corrosive agent through the matrix: a bar produced with a high-performance matrix can have good resistance to chemical attack, i.e. the use of these resins, such as the epoxy ones, enormously improves the environmental protection of the fibers.

5.11 Toxicity, hazard and safe handling

As discussed in previous paragraphs of this chapter, epoxy resins are a complex blend of chemical compounds specially selected to achieve desired characteristics. As with any chemical, poor handling or misuse of an epoxy resin and its curing agent can be hazardous to health, and risks can be minimized by using simple precautions, appropriate care and control. In particular, the major health problems associated with use of epoxy resins are as follows:

- Epoxy systems can easily adhere to and remain on any surface, including the skin, due to their good adhesive properties.
- The curing process of an epoxy resin generates heat and some components of epoxy resin systems may be flammable.
- Both some epoxy resins and most of the curing agents can cause primary irritation of the skin, leading to its sensitization in some cases.
- Vapors produced during the curing process of some epoxy systems may be irritating to the eyes and the respiratory passages.

To deal with the problem of flammability, adequate fire precautions are necessary and reaction temperatures should not exceed those recommended for a given system. In particular, it is important to avoid preventing the heat generated by the resin-hardener reaction from escaping readily: in this case the trapped heat accelerates the reaction which in turn generates more heat and further accelerates the reaction until it becomes uncontrollable. To overcome this problem, workers should mix small amounts of resin/curing agent and transfer them to a container with a large surface area; use the mixed materials quickly enough, particularly if it is a fast resin/curing agent system (e.g. with gel time lower than 20 minutes); keep the temperature of the work area to values near the normal room temperature; and avoid leaving the components or mixed material in direct sunlight.

As noted, epoxy resins are known to be skin sensitizers while the hardeners are classified as corrosives and irritants by inhalation or when in contact with the skin. The primary skin irritation (i.e. contact dermatitis) is due to the direct action of the material on the skin and is localized only in the contact area: its degree is directly related both to the concentration of the chemical and to the duration of the exposure. In contrast, skin sensitization (i.e. allergic dermatitis) is different from contact dermatitis, even if they often appear

similar: i.e. allergic dermatitis occurs after continued or repeated contact and develops after a period of exposure to a chemical which previously had not adversely affected the worker. Once sensitization takes place, a slight or even a minimal contact with the material can lead to a violent reaction, involving other skin areas besides a local effect.

The effects of skin sensitization do not necessarily subside when contact is discontinued, i.e. a sensitized worker is permanently unfit for handling epoxy resin systems containing the sensitizing agent. Furthermore a worker who has been sensitized, for instance by an amine-curing agent, can also become sensitized to other materials such as the resins themselves. In particular, the curing process of an epoxy resin at room temperature can continue for more than two weeks from the moment of mixing with its own curing agent: once fully cured, an epoxy system can be considered inert and non-hazardous.

To isolate operators from the chemical and prevent irritation of the respiratory tract and the eyes, all work using epoxy products should be carried out in an enclosed environment but, in practice, this is difficult to achieve, particularly with the materials used in the manufacture of composite components. For this reason, ventilation of the work area (through forced extraction systems) and adequate personal protective equipment for workers (gloves, goggles, overalls, facemasks, etc.) are indispensable.

Regarding carcinogenic effects, it has been shown that older epoxy resins cause skin cancer in laboratory animals, due to their high amount of epichlorohydrin, a contaminant that can probably cause cancer also in humans. In contrast, most newer epoxy resins, which contain less epichlorohydrin, do not seem to cause cancer in animals. Besides this, diaminodiphenyl sulfone (DDS), a curing agent commonly used in some epoxy resin systems, is carcinogenic in laboratory animals and certain glycidyl ethers used in epoxy products cause genetic mutations in laboratory animals. However, it is not known if glycidyl ethers cause mutations or cancer in humans. Nowadays most other components of epoxy resin systems must be adequately tested to determine if they can cause cancer.

As regard the reproductive system, the epoxy resins and curing agents themselves probably do not affect pregnancy and reproduction in humans even if some of the diluents and solvents in epoxy resin systems may affect reproduction. In particular, two solvents sometimes found in epoxy resin systems (2-ethoxyethanol and 2-methoxyethanol) cause birth defects in laboratory animals and reduced sperm counts in men. Moreover, some glycidyl ethers also damage the testes and cause birth defects in test animals. It is not known whether they have the same effects in humans. Most other solvent additives have not been adequately tested to determine if they affect reproduction.

5.12 Future trends

In the next few years high-performance coatings will continue to be the primary application worldwide for epoxy resins, followed by electrical/electronic ones and adhesives, flooring and paving applications, composites and molding products. As regards flooring applications, since the floors of industrial buildings are usually constructed from materials such as concrete, which under adverse service conditions are likely to gradually and then rapidly disintegrate, epoxy resins are very useful in aiding the maintenance of such floors, due to their chemical resistance, high mechanical strength and easy application.

As discussed in Section 5.5, the formulation and use of bio-derived epoxy resins will represent one of the most important challenges both for the academic world and for industry in the next few years. In particular, all industrial fields where composite materials find application will aim to increase the use of epoxy matrices to reduce the environmental impact and CO_2 emissions. A further future development of epoxy resins is related to their use as matrices in composites for dental applications, substituting for methacrylate ones, thanks to their lower shrinkage.

Furthermore, epoxy resins are beginning to be used in the trenchless rehabilitation (no-dig methods) of existing pipelines. In particular the *Cured In Place Pipe* technology consists of the reconstruction of an existing pipe (or host pipe) by using a tubular liner made of polyester resin, reinforced with one or more internal layers of glass fiber pre-impregnated with fluid epoxy resin. The liner is inverted into the host pipe using water or air pressure, so as to adhere perfectly to the walls of the pipe and to solidify thanks to the curing process of the epoxy resin.

Regarding the utilization of epoxy resins throughout the world, in recent decades industrialized nations (principally the United States, Western Europe and Japan) have been by far the largest producers and consumers. However, in 2009 consumption of epoxy resins decreased in these regions whereas it increased in parts of Asia such as China and India (coupled with the increasing use of natural fibers such as basalt ones). According to some reports, the consumption of epoxy resins in the United States and Western Europe will increase in the next few years: in particular, this increase will be due to the use of adhesives in both the US and Western Europe, to the manufacture of high-performance composites in the US, and, to coatings cured by radiation in Western Europe.

5.13 Conclusion

As discussed in this chapter, epoxy resins can be considered one of the most important classes of thermosetting polymers thanks to their range of useful properties and mainly to their versatility.

In comparison with other thermosetting polymers, epoxy resins are more expensive but show better mechanical properties, lower shrinkage, and higher resistance to moisture absorption and to corrosive environments. These good physical properties and their durability in service help to provide a favorable cost–performance ratio when compared to other thermoset plastics.

For these reasons, nowadays epoxy resins find application in several fields, e.g. coatings, electrical and electronic insulation, adhesives and construction, and as matrices for FRP in automotive, nautical, aerospace and civil applications.

As regard the future trends of utilization of epoxy resins, high-performance coatings, followed by electrical/electronic ones and adhesives, flooring and paving applications, composites and molding products will continue to be their primary application worldwide. Further future developments of epoxy resins are related to their use as matrices of composites for dental applications and for trenchless rehabilitation of existing pipelines.

Finally, the formulation and use of bio-derived epoxy resins will represent one of the most important challenges both for the academic world and for industry in the next few years, in order to reduce the environmental impact and CO_2 emissions.

5.14 References

Abdel-Aal N, El-Tantawy F, Al-Hajry A and Bououdina M (2008), 'Epoxy resin/plasticized carbon black composites. Part I. Electrical and thermal properties and their applications', *Polym Compos*, 29, 511–517. doi: 10.1002/pc.20401.

Aggarwal L K, Thapliyal P C and Karade S R (2007), 'Anticorrosive properties of the epoxy-cardanol resin based paints', *Prog Org Coats*, 59, 76–80. doi: 10.1016/j.porgcoat.2007.01.010.

Altuna F I, Espósito L H, Ruseckaite R A and Stefani P M (2011), 'Thermal and mechanical properties of anhydride-cured epoxy resins with different contents of bio-based epoxidized soybean oil', *J Appl Polym Sci*, 120, 789–798. doi: 10.1002/app.33097.

Armelin E, Pla R, Liesa F, Ramis X, Iribarren J I and Aleman C (2008), 'Corrosion protection with polyaniline and polypyrrole as anticorrosive additives for epoxy paint', *Corros Sci*, 50, 721–728. doi: 10.1016/j.corsci.2007.10.006.

Bajat J B and Dedic O (2007), 'Adhesion and corrosion resistance of epoxy primers used in the automotive industry', *J Adhes Sci Technol*, 21, 819–831. doi: 10.1163/156856107781061512

Bouchelaghem H, Bezazi A and Scarpa F (2011), 'Compressive behaviour of concrete cylindrical FRP-confined columns subjected to a new sequential loading technique', *Composites Part B*, 42, 1987–1993. Doi: 10.1016/j.compositesb.2011.05.045.

Brent Strong A (2008), *Fundamentals of Composite Manufacturing: Materials, Methods and Applications*, second edition, Dearborn, MI, Society of Manufacturing Engineers, 2, 45.

Calò E, Maffezzoli A, Mele G, Martina F, Mazzetto S E, Tarzi A and Stifani C (2007), 'Synthesis of a novel cardanol-based benzoxazine monomer and environmentally

sustainable production of polymers and bio-composites', *Green Chem*, 9, 754–759. doi: 10.1039/B617180J.

Campaner P, D'Amico D, Longo L, Stifani C and Tarzia A (2009), 'Cardanol-based novolac resins as curing agents of epoxy resins', *J Appl Polym Sci*, 114, 3585–3591. doi: 10.1002/app.30979.

Campbell F C (2010), *Structural Composite Materials*, Materials Park, OH, ASM International, 68.

Charrier J M (1991), *Polymeric Materials and Processing*, Munich, Hanser Publishers.

Chikhi N, Fellahi S and Bakar M (2002), 'Modification of epoxy resin using reactive liquid (ATBN) rubber', *Eur Polym J*, 38, 251–264. doi: 10.1016/S0014–3057(01)00194-X.

Davies P, Mazéas F and Casari P (2001), 'Sea water ageing of glass reinforced composites: shear behaviour and damage modeling', *J Compos Mater*, 35, 1343–1372. doi: 10.1106/MNBC-81UB-NF5H-P3ML.

Durmus H, Safak H, Akbas H Z and Ahmetli G (2011), 'Optical properties of modified epoxy resin with various oxime derivatives in the UV-VIS spectral region', *J Appl Polym Sci*, 120, 1490–1495. doi: 10.1002/app.33287.

Dyakonov T, Chen Y, Holland K, Drbohlav J, Burns D, Velde D V, Seib L, Solosky E J, Kuhn J, Mann P J and Stevenson W T K (1996), 'Thermal analysis of some aromatic amine cured model epoxy resin systems – I: Materials synthesis and characterization, cure and post-cure', *Polym Degrad Stab*, 53, 217–242. doi: 10.1016/0141-3910(96)00085-7.

Ellis B (1993), 'The kinetics of cure and network formation', in Ellis B, *Chemistry and Technology of Epoxy Resins*, London, Blackie Academic and Professional.

Formicola C, De Fenzo A, Zarrelli M, Giordano M and Antonucci V (2011), 'Zinc-based compounds as smoke suppressant agents for an aerospace epoxy matrix', *Polym Int*, 60, 304–311. doi: 10.1002/pi.2949.

Garcés P, Saura P, Zornoza E and Andrade C (2011), 'Influence of pH on the nitrite corrosion inhibition of reinforcing steel in simulated concrete pore solution', *Corros Sci*, 53, 3991–4000. doi: 10.1016/j.corsci.2011.08.002.

Ghaemy M and Sadjady S (2006), 'Kinetic analysis of curing behavior of diglycidyl ether of bisphenol A with imidazoles using differential scanning calorimetry techniques', *J Appl Polym Sci*, 100, 2634–2641. doi: 10.1002/app.22716.

Gojny F H, Wichmann M H G, Fiedler B, Kinloch I A, Bauhofer W, Windle A H and Schulte K (2006), 'Evaluation and identification of electrical and thermal conduction mechanisms in carbon nanotube/epoxy composites', *Polymer*, 47, 2036–2045. doi: 10.1016/j.polymer.2006.01.029.

Guan C, Lü C, Liu Y F and Yang B (2006), 'Preparation and characterization of high refractive index thin films of TiO_2/epoxy resin nanocomposites', *J Appl Polym Sci*, 102, 1631–1636. doi: 10.1002/app.23947.

Handwerker H (2011), 'Structural adhesives: selection is key – Optimal bonding for industrial and marine manufacturing', *Via Mare – By Sea*, 11, 19.

Ho T H and Wang C S (2001), 'Modification of epoxy resin with siloxane containing phenol aralkyl epoxy resin for electronic encapsulation application', *Eur Polym J*, 37, 267–274. doi: 10.1016/S0014-3057(00)00115-4.

Jana S and Zhong W H (2007), 'FTIR study of ageing epoxy resin reinforced by reactive graphitic nanofibers', *J Appl Polym Sci*, 106, 3555–3563. doi: 10.1002/app.26925.

Kelly P (1999), 'Epoxy vinyl ester and other resins in chemical process equipment', in Pritchard G, *Reinforced Plastics Durability*, Cambridge, UK, Woodhead, 282–293.

Kotnarowska D (1999), 'Influence of ultraviolet radiation and aggressive media on epoxy coating degradation', *Prog Org Coat*, 37, 149–159. doi: 10.1016/S0300-9440(99)00070-3.

Kumagai S and Yoshimura N (2000), 'Impacts of thermal aging and water absorption on the surface electrical and chemical properties of cycloaliphatic epoxy resin', *IEEE Trans Dielectr Electr Insul*, 7, 424–431. doi: 10.1109/94.848931.

Kwon S C, Adachi T and Araki W (2008), 'Temperature dependence of fracture toughness of silica/epoxy composites: Related to microstructure of nano- and micro-particles packing', *Composites Part B*, 39, 773–781. doi: 10.1016/j.compositesb.2007.10.008.

Lee E S, Lee S M, Shanefield D J and Cannon W R (2008), 'Enhanced thermal conductivity of polymer matrix composite via high solids loading of aluminum nitride in epoxy resin', *J Am Ceram Soc*, 91, 1169–1174. doi: 10.1111/j.1551-2916.2008.02247.x.

Lee W S and Yu J (2005), 'Comparative study of thermally conductive fillers in underfill for the electronic components', *Diam Relat Mater*, 14, 1647–1653. doi: 10.1016/j.diamond.2005.05.008.

Liu X and Zhang J (2010), 'High-performance biobased epoxy derived from rosin', *Polym Int* 59, 607–609. DOI: 10.1002/pi.2781.

Liu F, Zhang Z, Xu L and Tang M (2012), 'Study on the resistance of ultraviolet radiation of composite materials based on epoxy resin', *Adv Mater Res,* 391–392, 812–816. doi: 10.4028/www.scientific.net/AMR.391–392.812.

Lu C, Cui Z, Wang Y, Yang B and Shen J (2003), 'Studies on syntheses and properties of episulfide-type optical resins with high refractive index', *J Appl Polym Sci*, 89, 2426–2430. doi: 10.1002/app.12459.

Ma P C, Tang B Z and Kim J K (2008), 'Effect of CNT decoration with silver nanoparticles on electrical conductivity of CNT–polymer composites', *Carbon*, 46, 1497–1505. doi: 10.1016/j.carbon.2008.06.048.

Maffezzoli A, Calò E, Zurlo S, Mele G, Tarzia A and Stifani C (2004), 'Cardanol based matrix biocomposites reinforced with natural fibers', *Compos Sci Technol*, 64, 839–845. doi: 10.1016/j.compscitech.2003.09.010.

Mallick P K (1993), *Fiber Reinforced Composites*, second edition, New York, Marcel Dekker, 2, 50.

Mamunya Ye P, Davydenko V V, Pissis P and Lebedev E V (2002), 'Electrical and thermal conductivity of polymers filled with metal powders', *Eur Polym J*, 38, 1887–1897. doi: 10.1016/S0014-3057(02)00064-2.

Matsuzaki R, Shibata M and Todoroki A (2008), 'Improving performance of GFRP/aluminum single lap joints using bolted/co-cured hybrid method', *Composites Part A*, 39, 154–163. doi: 10.1016/j.compositesa.2007.11.009.

McGrath L M, Parnas R S, King S H, Schroeder J L, Fischer D A and Lenhart J L (2008), 'Investigation of the thermal, mechanical, and fracture properties of alumina-epoxy composites', *Polymer* 49, 999–1014. doi: 10.1016/j.polymer.2007.12.014.

Miskovic-Stankovic V B, Zotovic J B, Kacarevic-Popović Z and Maksimovic M D (1999), 'Corrosion behaviour of epoxy coatings electrodeposited on steel electrochemically modified by Zn–Ni alloy', *Electrochim Acta*, 44, 4269–4277. doi: 10.1016/S0013-4686(99)00142-5.

Miyagawa H, Misra M, Drzal L T and Mohanty A K (2005), 'Fracture toughness and impact strength of anhydride-cured biobased epoxy', *Polym Eng Sci*, 45, 487–495. doi: 10.1002/pen.20290.

Mourad A H I, Beckry Mohamed A M and El-Maaddawy T (2010), 'Effect of seawater and warm environment on glass/epoxy and glass/polyurethane composites', *Appl Compos Mater*, 17, 557–573. doi: 10.1007/s10443-010-9143-1.

Narasimha Murthy H N, Sreejith M, Krishna M, Sharma S C and Sheshadri T S (2010), 'Seawater durability of epoxy/vinyl ester reinforced with glass/carbon composites', *J Reinf Plast Compos*, 29, 1491–1499. doi: 10.1177/0731684409335451.

Pascault J P and Williams R J J (2010), 'General concepts about epoxy polymers', in Pascault J P and Williams R J J, *Epoxy Polymers – New Materials and Innovations*, Weinheim, Germany, Wiley-VCH, 4.

Poelman M, Olivier M G, Gayarre N and Petitjean J P (2005), 'Electrochemical study of different ageing tests for the evaluation of a cataphoretic epoxy primer on aluminium', *Prog Org Coat*, 54, 55–62. doi: 10.1016/j.porgcoat.2005.04.004.

Popovic M M, Grgur B N and Miskovic-Stankovic V B (2005), 'Corrosion studies on electrochemically deposited PANI and PANI/epoxy coatings on mild steel in acid sulfate solution', *Prog Org Coat*, 52, 359–365. doi: 10.1016/j.porgcoat.2004.05.009.

Rouyre T, Taylor A C, Fu M, Perrot F and James I (2010), 'Nano- and micro-silica modification of epoxy polymers', *Proceedings of the 2010 IEEE International Conference on Solid Dielectrics, ICSD 2010,* art. no. 5568103. doi: 10.1109/ICSD.2010.5568103.

Sala G (2006), 'New development for composite materials in aeronautics', *Compositi Magazine*, 2, 20.

Sharma S and Luzinov I (2011), 'Ultrasonic curing of one-part epoxy system', *J Compos Mater*, 45, 2217–2224. doi: 10.1177/0021998311401075.

Shibata M, Teramoto N and Makino K (2011), 'Preparation and properties of biocomposites composed of epoxidized soybean oil, tannic acid, and microfibrillated cellulose', *J Appl Polym Sci*, 120, 273–278. doi: 10.1002/app.33082.

Si Youcef Y, Amziane S and Chemrouk M (2010), 'Geometrical effect on the behavior of CFRP confined and unconfined concrete columns', *J Reinf Plast Compos*, 29, 2621–2635. doi: 10.1177/0731684409357255.

Takahashi A, Satsu Y, Nagai A, Umino M and Nakamura Y (2005), 'Heat-resistant epoxy–silicon hybrid materials for printed wiring boards', *IEEE Trans Electron Packag Manuf*, 28, 163–167. doi: 10.1109/TEPM.2005.846831.

Tan S G and Chow W S (2010), 'Biobased epoxidized vegetable oils and its greener epoxy blends: a review', *Polym Plast Technol Eng* 49, 1581–1590. doi: 0.1080/03602559.2010.512338.

Valenza A and Calabrese L (2003), 'Effect of CTBN rubber inclusions on the curing kinetic of DGEBA–DGEBF epoxy resin', *Eur Polym J*, 39, 1355–1363. doi: 10.1016/S0014-3057(02)00390-7.

Valenza A, Fiore V and Fratini L (2011), 'Mechanical behaviour and failure modes of metal to composite adhesive joints for nautical applications', *Int J Adv Manuf Technol*, 53, 593–600. doi: 10.1007/s00170-010-2866-1.

Wang H, Wang H and Zhou G (2011), 'Synthesis of rosin-based imidoamine-type curing agents and curing behavior with epoxy resin', *Polym Int*, 60, 557–563. doi: 10.1002/pi.2978.

Weinmann D J, Dangayach K and Smith C (1996), 'Amine-functional curatives for low temperature cure epoxy coatings', *J Coat Technol*, 68, 29–37.

Wu G, Wu Z S, Lu Z T and Ando Y B (2008), 'Structural performance of concrete confined with hybrid FRP composites', *J Reinf Plast Compos*, 27, 1323–1348. doi: 10.1177/0731684407084989.

Yang D J, Zhang Q, Chen G, Yoon S F, Ahn J, Wang S G, Zhou Q and Li J Q (1991), 'Thermal conductivity of multiwalled carbon nanotubes', *Phys Rev B*, 66, 165440-1-6. doi: 10.1103/PhysRevB.66.165440.

Zarrelli M, Skordos A A and Partridge I K (2002), 'Investigation of cure induced shrinkage in unreinforced epoxy resin', *Plast Rubber Compos Process Appl*, 31, 377–384. doi: 10.1179/146580102225006350.

Zhou T, Wang X, Liu X and Xiong D (2010), 'Improved thermal conductivity of epoxy composites using a hybrid multi-walled carbon nanotube/micro-SiC filler', *Carbon*, 48, 1171–1176. doi: 10.1016/j.carbon.2009.11.040.

Zitoune R and Collombet F (2007), 'Numerical prediction of the thrust force responsible of delamination during the drilling of the long-fiber composite structures', *Composites Part A*, 38, 858–866. doi: 10.1016/j.compositesa.2006.07.009.

6

Prepreg processing of advanced fibre-reinforced polymer (FRP) composites

S. PANSART, Germanischer Lloyd,
Industrial Services GmbH, Germany

DOI: 10.1533/9780857098641.2.125

Abstract: This chapter provides some basic knowledge about FRP manufacturing processes involving prepreg materials. It contains information regarding the manufacture of prepreg semi-finished products, processing methods for obtaining structural components, and some considerations about quality. It is intended as an overview only, addressing engineering students or practitioners who have only little knowledge about composites and prepreg processing technologies.

Key words: prepreg processing, lay-up, cure, quality.

6.1 Introduction

In many industries, e.g. in aerospace, prepreg has become the standard technology for making fibre-reinforced plastic (FRP) structures; in other industries, too, its use is continuously increasing. The term prepreg is a contraction of 'pre-impregnated', which relates to the basic principle of the material. Rather than impregnating the reinforcement fibres with resin during the manufacture of the final component or structure, as is the case for the hand lamination technique, or for infusion and injection techniques, the fibres are resin-impregnated in a separate process. This pre-impregnation takes place prior to the actual component manufacture, in order to create a semi-finished product which can be transported and stored in rolls: the prepreg. In principle, part manufacture then consists of cutting pieces of prepreg from the roll, laying-up these pieces in a mould to realize the required laminate structure, and curing the resin to create the actual FRP material (Fig. 6.1).

Originally, the prepreg technology was developed as an advancement over earlier hand lamination techniques, mainly in order to improve the quality of the resulting composite material. Prepregs allow for higher mechanical strength and stiffness properties, which is in part due to the more homogeneous and straighter fibre arrangement (Pansart *et al.*, 2009). Also, the automated and continuous pre-impregnation process usually leads to less air trapped inside the composite matrix, i.e. fewer porosities, and tends to yield a higher fibre volume content of the cured part, thus increasing its weight efficiency.

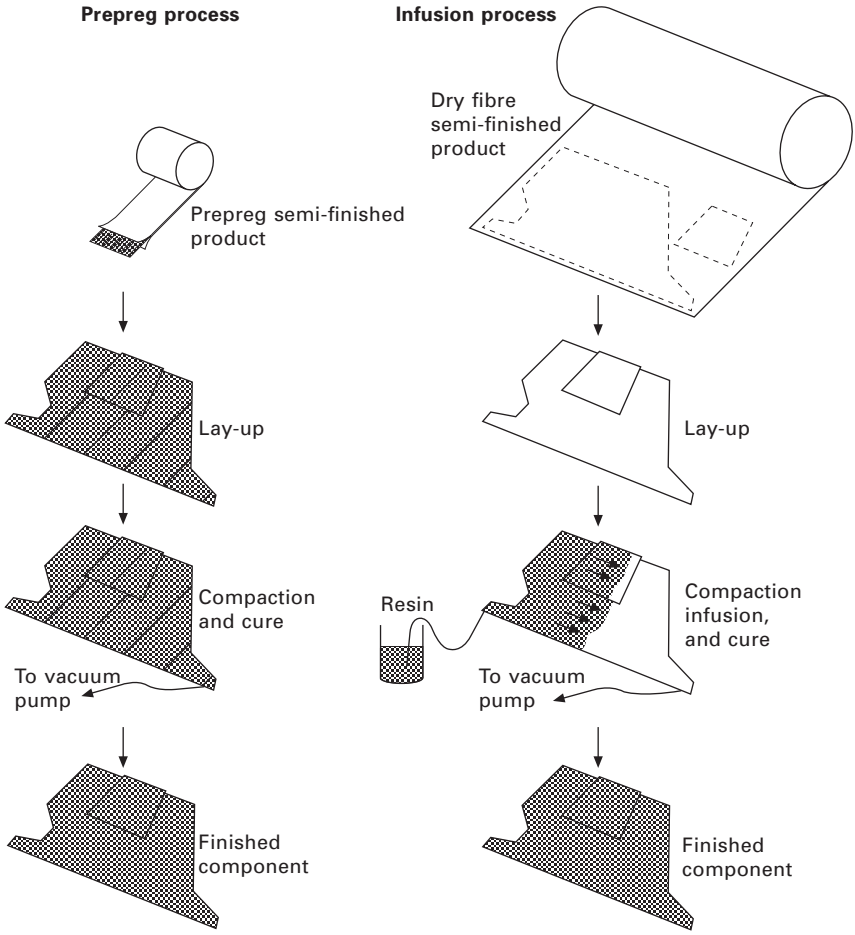

6.1 Principal manufacturing process using prepreg materials, and comparison to infusion techniques.

Usually, though, this quality improvement comes at a higher cost for materials and processing, when compared with other techniques.

This chapter provides some basic knowledge about FRP manufacturing processes involving prepreg materials. It is intended as an overview only, addressing engineering students or practitioners who have only little knowledge about composites and prepreg processing technologies. For more detailed information on any particular aspect, it is recommended to refer to more comprehensive or specialized literature and publications (e.g. Davé and Loos, 2000).

6.2 Prepreg semi-finished products

In principle, a prepreg is a semi-finished product for making FRP components, consisting of reinforcing fibres that are pre-impregnated by resin. This resin, once cured in the final component, becomes the matrix of the FRP. The matrix has, as in all types of FRP, the function of bonding the fibres together. There are various kinds of prepreg material available. The following section provides a brief overview of the different types of prepreg, how they are produced, and what needs to be taken into consideration when handling them.

6.2.1 Semi-finished product characteristics

In principle, all fibres available for FRP can also be used as reinforcement in prepregs, the most common ones being carbon and glass fibres. Polymeric fibres made from aramid or polyethylene are also quite common, as are inorganic basalt fibres, or natural fibres like hemp or flax. Often, the fibres are directly impregnated to make unidirectional (UD) tapes. Alternatively, they can first be transformed into fabric products, such as woven fabrics or non-crimp fabrics (NCF), and then impregnated to create multi-directional prepregs.

Thermoset resins used in prepregs are always already pre-mixed with their hardeners (and possibly accelerators), which means that they are ready to start their cure reaction once activated by heat. The choice of resin, together with the choice of fibre, will determine the mechanical characteristics of the composite. Of equal importance, though, is the impact of resin choice on the processing characteristics (discussed below), as well as on the maximum service temperature of the composite and its resistance to environmental influences and fire. Available chemistries are, e.g., polyesters (low cost), epoxies (higher mechanical performance), phenolics (good fire, smoke and toxicity properties) and bismaleimides, polyimides and benzoxazines (high service temperatures). In addition, resins can contain fillers or thermoplastic constituents for adjusting and improving various material properties, such as resistance to impact damage.

One important characteristic of a prepreg is its resin content. As a rule, the higher the fibre content of the cured composite, the better its weight-specific strength and stiffness. On the other hand, a higher resin content prepreg offers more robust and easy to handle manufacturing processes. Therefore, one will find relatively low resin weight contents of, e.g., 32% in aerospace-grade prepregs, and higher ones in other industries. Furthermore, many prepreg systems are designed for bleed, i.e. during cure a substantial amount of resin can be withdrawn in order to reach the target fibre content. Some prepregs, in contrast, are zero-bleed systems.

The typical conditioning for prepregs is as rolls (Fig. 6.2). To prevent the

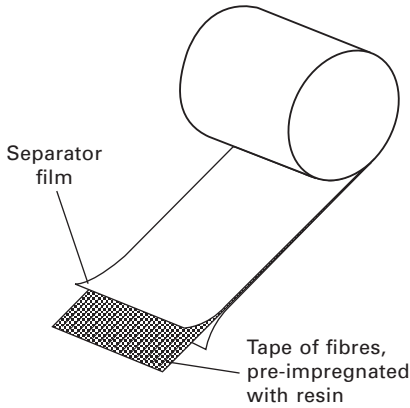

6.2 Example for a UD prepreg tape semi-finished product; typical dimensions are, e.g., a thickness of 0.125 mm to 1 mm, a width of 300 mm to 1200 mm, and a total weight of 15 kg to 100 kg.

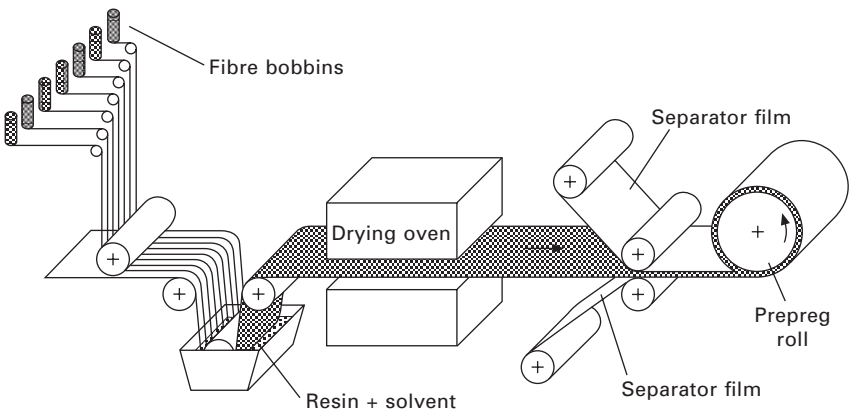

6.3 Prepreg semi-finished product manufacture by solution impregnation.

material from sticking to itself, a protective release film (separator) is used to cover both faces of the prepreg tape. The prepreg is then rolled up on a cardboard core, which can be supported at both ends for packaging, e.g. in cardboard boxes.

6.2.2 Semi-finished product manufacturing

Many prepregs are manufactured by a process called solution impregnation. This process is depicted in Fig. 6.3. First, the fibre material is introduced to the manufacturing line. For UD prepregs, this usually happens in the form of several bobbins of individual endless rovings (yarns). A roving itself

consists again of thousands of individual filaments only a few micrometres in diameter. All rovings are then aligned in parallel by a suitable arrangement of rolls, in order to constitute a tape of required width and thickness. In some cases, especially when relatively thin prepregs are produced from relatively thick rovings, a spreading operation is integrated into this process step. The fibres are then guided through a bath of solvent containing the resin, where the actual impregnation takes place. Subsequently, the impregnated fibres pass through an oven in which some heat is applied to evaporate the solvent. As a result, the resin becomes sticky and bonds the fibres together, thus creating a stable prepreg tape. Finally, this tape is equipped with its separator films, and conditioned.

As a variation on this, if textile pre-products are used as reinforcement, the fibre rovings are brought into their textile form by a separate manufacturing step rather than by introducing them directly to the impregnation line. Depending on the type of textile, this can be achieved by e.g., weaving or NCF knitting. Of course, the production of a textile pre-product takes place prior to the impregnation process – and in many cases at a different site or by a supplier.

Film impregnation, in contrast, differs from the solution impregnation process in the way the resin is introduced. The process of film impregnation is depicted in Fig. 6.4. In a first step, the resin is turned into a film pre-

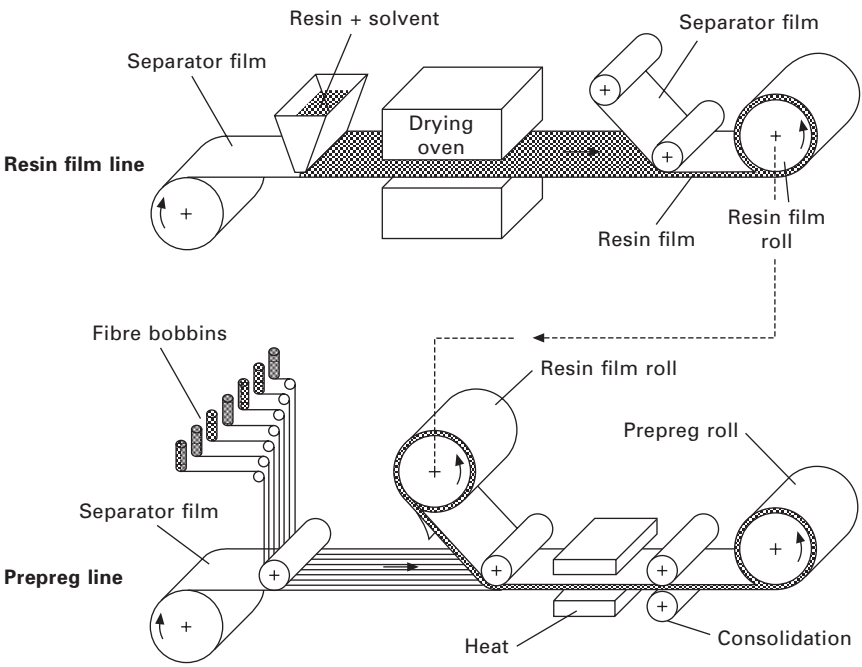

6.4 Prepreg semi-finished product manufacture by film impregnation.

product, supported by suitable release paper. In a second step, this resin film is brought together with the reinforcing fibres. This combination of fibres and resin film is then consolidated by applying roller pressure and some heat, resulting in a similarly stable prepreg tape as for the solution impregnation process.

As a special process in some industries (e.g. wind energy), it is common practice to make '*in-situ* prepregs'. In this case, the fibre rovings are impregnated by passing through a resin batch, and then, instead of being conditioned as prepreg semi-finished product rolls, immediately and directly transferred into the mould as part of the lay-up to produce a composite structure (e.g. a wind turbine rotor blade).

6.2.3 Handling and storage of prepreg rolls

When handling and storing rolls of prepreg semi-finished product, there are several constraints to be taken into account. As a rule, the lifetime of a prepreg is inherently limited, due to the self-reacting nature of the resin used in prepregs. In the context of industrial manufacturing processes, the lifetime of a prepreg roll consists of its storage life and its work life (Fig. 6.5). The storage life must be specified depending on the resin chemistry, and the requirements regarding the cured composite in terms of degree of cure. For one particular prepreg resin, it might be, e.g., 12 months when stored at –18°C; another might be stored at +4°C, or have a different storage life. After the specified storage life has expired, the resin in the prepreg will generally be so advanced in its polymerization reaction that it has become too stiff or lost too much of its tack to be processed any more. Tack is defined as the ability of a prepreg ply to stick to other prepreg plies, or to the mould surface, during lay-up (Crossley *et al.*, 2010). Also, too advanced a polymerization reaction might prevent the resin reaching its required degree of cure during the manufacturing cycle.

The work life, then, is the time a prepreg will be allowed to spend under workshop conditions (i.e. generally at room temperature). Work life is often further divided into a tack life, being the duration during which the prepreg will still have sufficient tack to be processed; and a stand-by time, being the maximum duration during which a completed lay-up will be allowed to

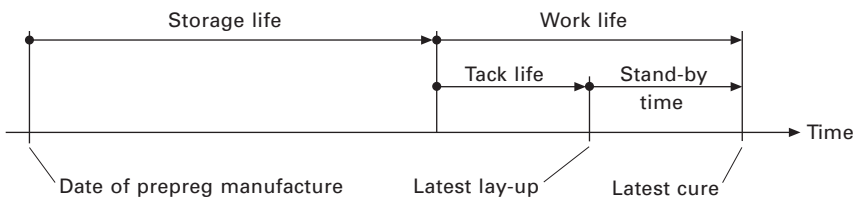

6.5 Lifetime of a prepreg roll.

remain uncured before detrimental effects on its final degree of cure are to be expected.

Obviously, the actually remaining storage life and work life of a given piece of prepreg will always depend on its temperature history. For example, a prepreg roll that has been stored at –18°C, then defrozen to room temperature during several days, and then again stored at –18°C, will have a different remaining storage life from one that has been stored uninterruptedly at –18°C. Therefore, it is usually required that, for each unit of prepreg material, its individual temperature history is precisely logged, and that storage life and work life are specified accordingly.

6.3 Manufacturing processes

When using prepreg, as for most types of fibre-reinforced plastics, the structural material is actually created during the manufacture of the final component. Therefore, its structural quality is determined not only by the quality of the used semi-finished products, but also to a significant extent by the manufacturing process itself. Consequently, manufacturing processes for prepreg structures must be well understood, and appropriately controlled, to ensure that the final component meets the structural quality requirements. In order to provide some basic knowledge in this respect, the following section gives an overview of a typical manufacturing route for structures made from prepreg.

6.3.1 Material preparation

De-freezing

As explained above, prepreg material must be stored at low temperatures, typically around 0°C or below. When a prepreg roll is to be used in a workshop for manufacturing, it has to be de-frozen first. This de-freezing must be carried out in a controlled manner, in order to avoid condensation of air humidity on the unprotected material surface. Usually, this can be obtained by allowing the fully wrapped or sealed prepreg roll to warm up and reach a temperature beyond the dew point before unwrapping it. It should be noted that the same applies, in principle, also to other materials used during lay-up and which contain uncured resin, such as pre-impregnated peel plies, or adhesive films for co-curing and co-bonding (see below).

Cutting

In most cases, the prepreg tapes then have to be cut into specific shapes as required by the component's design (i.e. its geometry and ply sequence)

before being transferred to the lay-up mould. This cutting typically takes place on a flat table. The prepreg tape, still protected by the release film on both faces, is unrolled and positioned on the table, and sometimes held in position by a vacuum system acting through a perforated table surface. Cutting can be done manually, or by a computer-controlled portal (Fig. 6.6). Common cutting tools are roller knives, scissors and ultrasonically vibrating blades. After cutting, the cut-outs are transferred to the lay-up mould. Smaller cut-outs can be handled in flat condition. Larger (i.e. longer) cut-outs are often rolled up again for transport, typically onto a cylindrical core of sufficient diameter to avoid damaging the cut-out. The cut-outs can also be stored for later processing for a limited time period. Depending on the resin characteristics, and the history of the material (time since manufacture, temperature history), this can be several days or a few weeks.

Sandwich cores

For obtaining a low-weight, high-bending-stiffness structure, sandwich constructions are a common choice for composite components. To make a sandwich, low-density materials are inserted as sandwich cores between two faces of the structural material itself (so in this case between two stacks of prepreg plies). Commonly used core materials are plastic foams (for example, made from PVC, PS, or PET) and balsa wood. Examples of core materials for more sophisticated, structured sandwich cores are honeycombs (made from aluminium, or resin-impregnated paper sheets), or fibre-reinforced foams.

When preparing sandwich cores for part manufacture, particular care should be taken to ensure that only material free of contamination is used during

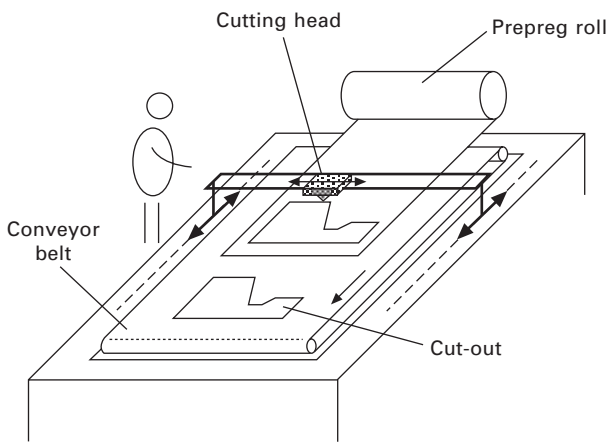

6.6 Schematic of a prepreg cutting table.

lay-up. Potential sources of contamination during core material processing are as follows:

- Dust and dirt from cutting and machining operations
- Water and oil from cutting and machining operations
- Humidity pick-up due to inappropriate storage conditions.

Therefore, when using such core materials for sandwich constructions in part manufacture, suitable procedures for cut-out preparation, cleaning, wrapping, storage and transport, as well as for humidity control (measurements, plus drying prior to lay-up), must be implemented.

6.3.2 Mould design

An appropriately designed mould is crucial for accurately controlling the process and, thus, for obtaining a qualitatively acceptable composite structure. Some of the most important criteria to be taken into account are as follows:

- Sufficient stiffness: The mould must be rigid enough to ensure the required geometrical tolerances of the part. For highly curved or otherwise complex geometries, and for heavy components, this can become quite challenging. Distortions due to the weight of the composite part and the weight of the mould itself have to be accounted for, while at the same time controlling distortions due to thermal expansion of the mould and resin shrinkage during cure and cool-down.
- Thermal management: The mould design should ensure a homogeneous heat distribution during curing, in order to obtain an evenly cured component. This will help in obtaining a laminate of constant characteristics, while at the same time reducing distortion due to resin shrink. Also, the mould should be designed to avoid harmful local overheating due to exothermic polymerization. Uncontrolled high temperature may damage the composite or the sandwich core materials. The features of a mould design affecting its thermal behaviour are, e.g., the mould material (thermal expansion coefficient and heat conductivity), locally accumulated material amounts creating thermal inertia, and integrated heating and cooling.
- Surface quality: Sometimes, specific requirements apply to certain parts of the composite structure with respect to surface quality, e.g. regarding aerodynamics or hydrodynamics, visual appearance or functional interfaces. In such cases, good surface quality of the mould is required. Also, the characteristics of the mould surface will determine the ease of first ply adhesion (see below).
- Durability: If a larger series of identical components is to be produced, it should also be taken into account that the mould will be subject to

mechanical abrasion and impacts (e.g. during cleaning, demoulding and debagging) as well as to thermal fatigue.

A wide variety of mould technologies is available, with their specific advantages and disadvantages with respect to the mentioned criteria. Common mould materials are wood, polymers, fibre-reinforced plastics, steel and Invar (low thermal expansion steel), and combinations of these. They can incorporate integrated electrical circuits for heating, hydraulics (water or oil) or air ducts for heating and cooling, as well as vacuum systems, and thermocouples for monitoring temperature. Moulds can be either machined directly from any kind of material or semi-finished product; or, in the case of fibre-reinforced plastics, moulded over a positive model of the component which in turn can be machined from an inexpensive and easy-to-machine model material. In some cases, e.g. for making straight rectangular stiffeners or plane panels, a simple mould can be assembled from off-the-shelf steel semi-finished products.

6.3.3 Mould preparation

Mould surface

Prior to the manufacture of each new component, the mould has to be prepared. First, it is mechanically cleaned of dirt, dust and all residual material from the previous manufacturing run (typically bits of cured or uncured resin and auxiliary materials, such as vacuum sealant, films, breather and the like). Often, some chemical cleaning using a solvent like acetone follows. After cleaning, a release agent is applied. Release agents prevent the prepreg resin from bonding to the mould surface during curing. Therefore, choosing an appropriate release agent is essential to ensure that the cured component is easily demoulded, and without damaging the mould surface.

Mould vacuum leak test

It is common practice to test the mould for vacuum tightness before its first use, or after repairing it. Insufficient mould tightness may result in material defects (such as pores), or insufficient compaction (and, thus, a low fibre fraction) in the final component. Typical sources of leaks are defective joints in the mould structure, such as weld lines or bonded joints.

To realize such a vacuum leak test, a vacuum set-up similar to the one used for the actual part manufacture is installed (described below), but without the part lay-up itself. Instead, only one or two plies of a glass fibre prepreg material are used. This dummy set-up is then evacuated and cured. Air leaks in the mould will cause porosities in the cured matrix. Thanks to the transparency of the glass fibres and the low thickness of the dummy

stack, these are readily visible as inhomogeneities in the cured matrix material.

6.3.4 Lay-up

Hand lay-up

Once the moulding tool is prepared, the lay-up of the part can begin. For this, the prepared cut-outs are subsequently positioned into the mould, according to the design's ply sequence. In hand lay-up, this is done manually. Before lay-up, all protective release films (separators) must be removed from the prepreg. The positioning of the individual plies can be realized using simple means such as measuring tapes, which in some cases is sufficient for the required accuracy. If complicated shapes have to be positioned, or more accurate positioning is required, it is also common practice to use a laser system, which will use numerical data of the part geometry to subsequently project the ply outlines onto the mould for each lay-up step.

During lay-up, each ply is joined as tightly as possible to the one underneath, in order to avoid large air inclusions and to ensure an accurate geometry (i.e. low bulk) during lay-up. This is typically obtained by manually applying some pressure using a roller tool or the like.

For rather simple and extensively uniform lay-ups, the prepreg tape can be directly unrolled onto the mould, skipping the intermediate step of cut-out preparation. In this case, the tape is cut directly in the mould and on top of the previously laid-up plies.

Automated lay-up

Originally developed for aerospace applications, automated tape layers (ATL) are beginning to be increasingly utilized also in other sectors. In principle, an ATL consists of a conventional portal robot equipped with a specialized tape layer head. This head contains a device carrying a roll of continuous prepreg tape, which is unrolled onto the mould, compacted by applying heat and pressure through a roller, and cut once the specified length of tape has been deposited. Lay-up and compacting usually take place in one continuous head movement. There are several variations on this basic ATL concept, such as ATL without cutters, which are charged with prepared tape cut-outs; and fibre placement machines, carrying and simultaneously depositing from multiple narrow prepreg tape rolls (slit tape) only a few millimetres in width instead of from one wide prepreg tape of several hundred millimetres.

Compared to hand lay-up, the ATL process tends to provide higher reproducibility and thus better-controlled part quality. On the other hand, investment costs can be prohibitively high, especially for large or geometrically complex components.

Surface plies

Laying up the very first ply of the component, i.e. the one that is in contact with the mould surface, often involves particular difficulties. The adhesion force for the first ply is usually much weaker than the adhesion force between two prepreg plies. Therefore, when designing the manufacturing process for a component, one must make a suitable choice of the mould surface treatment (release agent) in combination with the first ply material(s), the lay-up technique, and the geometrical arrangement of the mould surfaces (vertical or horizontal). Also, first-ply adhesion is affected by the state of ageing of the prepreg resin: the longer it has spent in storage and under shop conditions, the more its polymerization reaction is advanced. This results in the prepreg resin becoming less tacky, which means that first-ply adhesion (and ply-to-ply adhesion) becomes more difficult as the prepreg ages, eventually making a proper lay-up altogether impossible. Such loss in tack can sometimes be overcome by applying tackifiers (also called tacking promoters). Tackifiers are glue-like agents, chemically compatible with the prepreg resin and designed to provide additional tack to the lay-up surface. They are usually conditioned in a solvent and applied as liquid or by spraying.

In most cases, the lay-up schedule for a structural component will include non-structural functional plies on both surfaces:

- Smooth surfaces: If an optically, aerodynamically or otherwise functionally smooth surface is required, this is best obtained by making use of a smooth mould or caul plate surface. If this turns out to be insufficient, specialized surface ply materials can be applied to form a smooth part surface. Frequently used materials are, e.g., surface films (application as solid state resin), gel coats (application as liquid state resin), or surface prepreg plies that are low in areal weight and high in resin content.
- Bonding surfaces: If a surface area of the cured part will be subject to subsequent adhesive bonding operations, it is common practice to use a peel ply material as the outermost ply of the lay-up. Peel plies consist of pre-impregnated, or dry, fabrics made from fibres carrying a special, releasable sizing. After curing the composite part, this sizing makes it possible to separate the peel ply fabric from the cured resin by peeling it off the part surface. This operation will leave a regularly structured, rough surface (Fig. 6.7), which is generally quite suitable for subsequent bonding, often without the necessity of any further surface preparation other than cleaning.
- Other peel ply surfaces: Apart from their use for preparing bonding surfaces, peel plies are widely used as generic surface finish whenever there is no requirement for a smooth surface. During debagging, they facilitate the release of all ancillary materials that were in contact with the resin during the cure operation (e.g. breathers, bleeders, films, sealants,

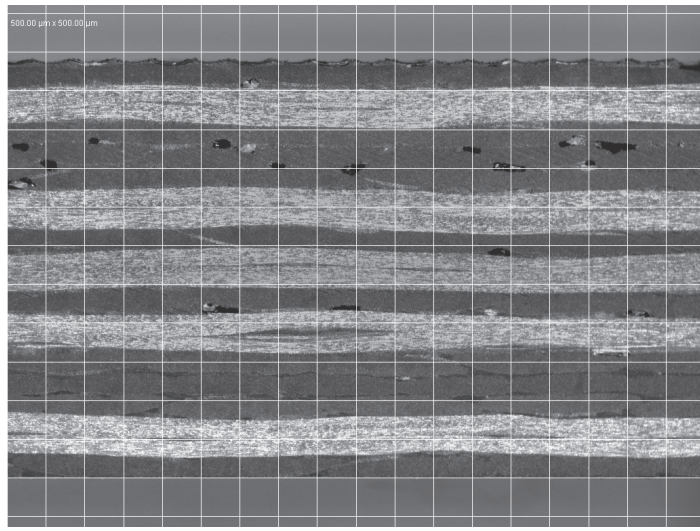

6.7 Microcut of a multi-axial laminate, approximately 5.5 mm thick, made from NCF; the upper surface reveals a typical structure after peel ply removal (in contrast, the lower surface was in direct contact with the mould); in addition, the microcut reveals some defects such as pores, resin pockets, and waviness due to the stitching yarn.

vacuum bags). Without peel plies, ripping these materials off during debagging could damage the part because of their adhesion to the part surface through the cured resin. In addition, peel plies generally improve the surface quality of a prepreg composite part: peel plies can trap small gas bubbles which tend to build up during cure at the part surface, so that the resulting porosities can be removed from the part together with the peel ply during debagging. Without peel ply, these porosities would remain in the part's first (possibly structural) ply.

- Conductive surfaces: In some applications, it will be required to ensure electrical grounding of the composite structure (or parts of it), or to shield the space inside the structure or the structure itself from electromagnetic hazards (e.g. coming from lightning strike currents). In these cases, an electrically conductive surface can be obtained by applying a pre-impregnated metallic ply or, alternatively, a dry metallic ply plus a surface film. Thermally conductive surfaces can be obtained in a similar manner if required. For such metal plies, typical materials are aluminium or copper, but commercially available products can be made from virtually any metal. Metal plies come in different forms, such as meshes, perforated foils and expanded foils.

Intermediate compaction

During prepreg lay-up, it is essential to ensure sufficient compaction at all times. Failing to do so can lead to excessive air inclusions (resulting in high porosity of the cured part) and to excessive debulking during cure (resulting in defects such as fibre waviness, wrinkles or resin pockets (Fig. 6.8). Usually, acceptable compaction is obtained by the means described above (roller consolidation during hand lay-up, or as part of the ATL process). Sometimes, though, this may not be sufficient, especially for relatively thick components and when the part geometry contains angles. In such cases, one or several intermediate compaction steps under vacuum will become necessary (debulking). The vacuum can be applied through a temporary vacuum bag set-up similar to the one used for the actual part manufacture (described below). The debulking operation can be facilitated by carefully applying some heat.

In some cases, for smaller parts manufactured in larger series, it may also be possible to use a more automated intermediate compaction tool, such as a shaped silicone bag. The silicone bag is pressed on the laid-up prepreg, thereby providing air tightness at its edges. Like this, the air underneath can be evacuated for compaction, in the same manner as with a classical vacuum bag. The advantages of this system are time savings and no need for consumable materials such as vacuum bags, sealants and the like.

Preforms

Some part geometries, such as stiffener-reinforced panels, require preparing sub-structures (preforms) prior to lay-up of the part. These could, for example, consist of a C-channel stiffener made from several prepreg plies. Such a preform can be manufactured by the same lay-up techniques as described above, e.g. by depositing ply by ply into a C-shaped mould. As an alternative, preforms can also be made by the process of hot forming.

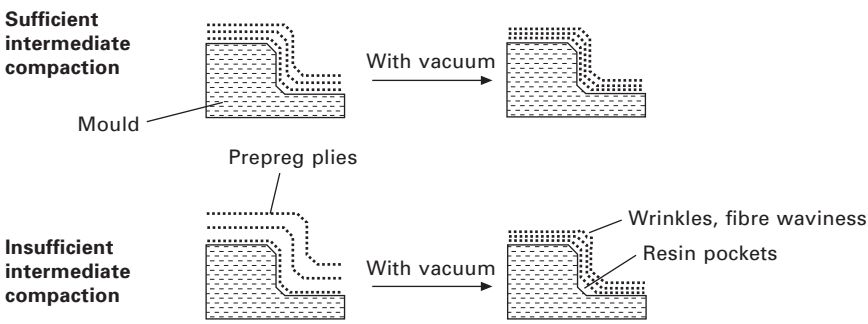

6.8 Possible defects due to insufficient intermediate compaction.

Often, hot forming is carried out as a continuous or semi-continuous process. In the case of a C-channel stiffener, a flat stack of several prepreg plies, laid up prior to the actual forming process, is moved through a series of roller arrangements which subsequently form the angles of the C-shape. At each station, an incremental deformation is added by applying localized roller pressure and heat. Furthermore, in order to obtain different shapes of preforms, it is common practice to assemble sub-preforms, e.g. by joining two C-channels into a double-T-shape, or two angles into a T-shape. Beside enabling more complex part geometries, using preforms has the additional advantage of adding flexibility to the manufacturing process from a logistics point of view. Preforms can be stored and shipped, which makes it possible to have them manufactured independently from the final part, and even in different facilities or by suppliers.

Co-curing and co-bonding

During prepreg lay-up, it is possible to add or integrate various elements to the actual prepreg ply sequence. These elements would then be bonded to the prepreg plies during the prepreg cure, in order to form an integral part of the final structural component. If the element to be integrated is an uncured or partially pre-cured ('b-staged') prepreg preform (also called a 'wet' preform), this process is called co-curing. In all other cases (already cured, or 'hard', preform, and non-curable elements), the process is called co-bonding. In many cases, films of adhesive resins are inserted at the interface of co-bonding lay-ups, in order to improve the interface strength. Some examples for co-cured and co-bonded elements are:

- Wet stringers (stiffeners) for lay-up on top of stiffened shell structures
- Previously cured bolt attachment lugs (typically with peel ply surfaces all over), inserted between prepreg plies during lay-up
- Complete sub-structures, such as the root attachment construction inserted into the lay-up of a wind turbine rotor blade
- Sandwich cores
- Watertight films (adjacent to sandwich cores, to prevent water pick-up inside the core caused by diffusion through the prepreg matrix).

6.3.5 Vacuum set-up

As soon as the lay-up of the component is completed, the material stack is wrapped up for cure. This operation is called bagging, or installing the vacuum set-up. The consumable materials used in this set-up are often referred to as ancillary materials, auxiliary materials or consumable materials. A typical vacuum set-up is depicted in Figs 6.9 and 6.10. Its

various elements, and the functions of the different ancillary materials, are described below.

- Vacuum bag, vacuum foil: The principal element to provide the airtightness needed for evacuating and compacting the prepreg stack is a plastic film (vacuum foil). This film is used to cover the entire set-up, creating what is called the vacuum bag. The film material must be strong enough to resist heat and mechanical wear, and needs to remain sufficiently elastic throughout the manufacturing process to be able to adapt to the component geometry.
- Vacuum bag sealant tape: At the edges, the vacuum foil is sealed by attaching it to the mould surface with a sealant material. Typical sealants are available as tapes of rubber-like, tacky material. As a rule, the areas of the mould to which the sealant tape is to be applied should be free of release agent; in practice these areas are often temporarily covered with adhesive tape when applying the release agent. Also, when installing the vacuum bag, sufficient excess foil should be provided for, in order to avoid tears at edges and curvatures of the composite part. This can be obtained by including additional loops of sealant together with a fold in the vacuum foil (sometimes called 'duck feet').
- Vacuum infrastructure: The evacuation of the vacuum bag is realized by vacuum pumps connected via tubes and hoses to intake valves in the vacuum set-up. The intakes can be positioned either in the vacuum bag, in which case the vacuum foil has to be perforated in order to provide a passage, or as part of circuitry integrated into the mould. For further distributing the airflow efficiently, it is usually necessary to install additional channels underneath the vacuum bag, e.g. by stacking up several narrow layers of breather fabric.
- Breathers: Typically, the entire set-up is covered with a layer of breather fabric. A breather consists of an open fabric or fleece textile which is sufficiently rigid to resist crushing under pressure, thus maintaining its open structure and permeability to air flow under all process conditions. The presence of the breather will allow for a homogeneous pressure distribution, and thereby a homogeneous compaction of the prepreg stack, over the entire surface of the set-up.
- Bleeders: If a bleed prepreg is used, an additional function of the breather is to provide the absorption capacity necessary to reach the target resin content in the cured part. In such bleed systems, the resin, liquefying under heat during the cure cycle before curing, will be squeezed out by the differential pressure in the set-up and absorbed by the breather fabric. In this case, it is necessary to carefully adjust the breather thickness according to the resin amount to be extracted from the prepreg.
- Release film: For preventing adhesion between the cured composite part

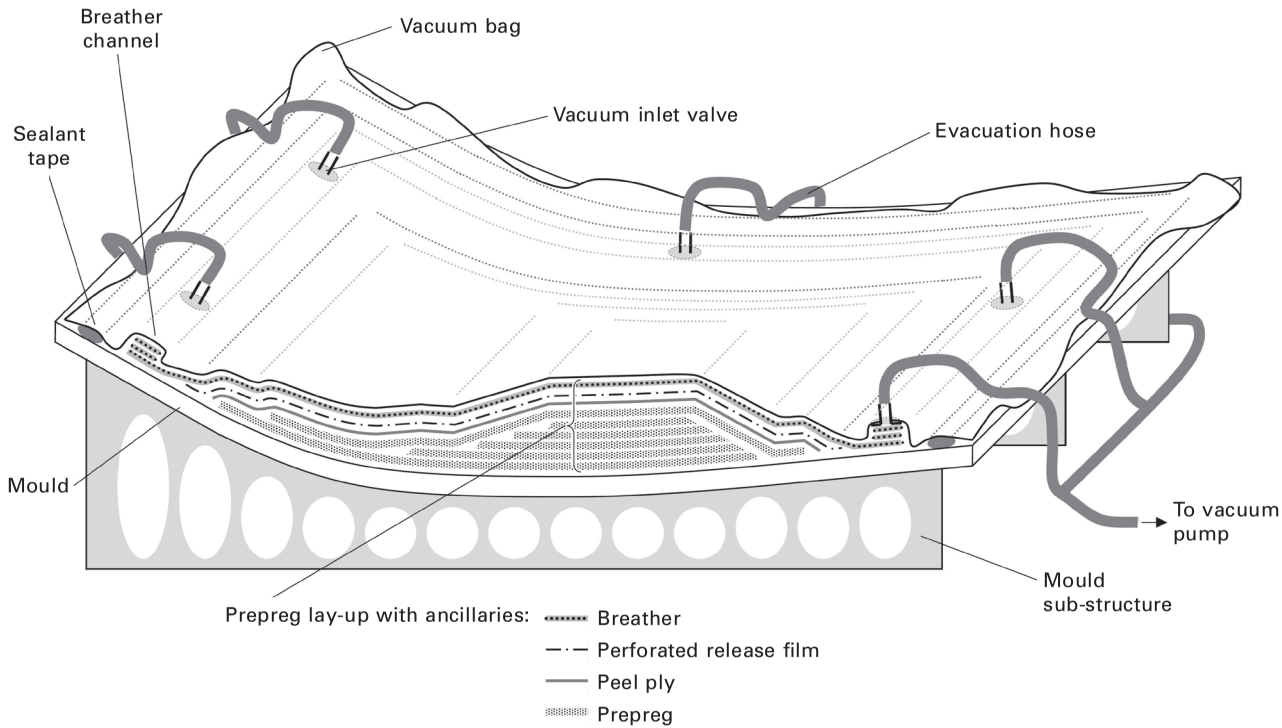

6.9 Vacuum set-up.

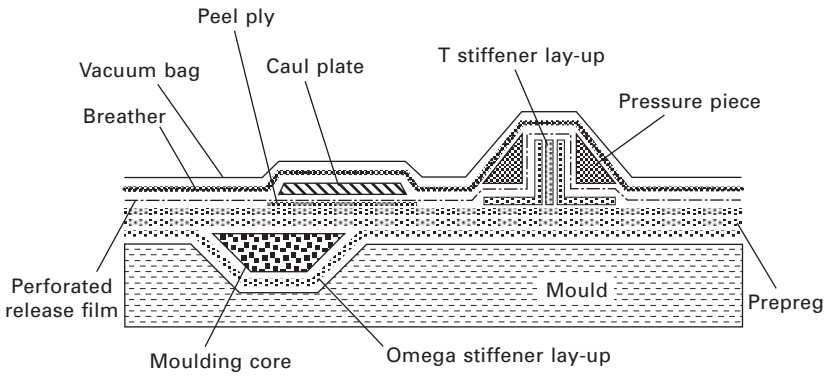

6.10 Some special features in a vacuum set-up.

and the ancillary materials in the set-up, a release film can be inserted between the two. Release films are treated such that their surface will not adhere to the resin of the prepreg. Often, this release film is perforated in order to allow resin bleed (if applicable) and gas evacuation. Release films are not necessary in places where the prepreg stack is in direct contact with the mould surface treated with release agent.

- Additional tooling pieces: For improving the part's geometrical accuracy, it is possible to use additional pressure pieces (in corners) or caul plates (on larger surfaces). Hollow structures would necessitate moulding cores, e.g. inflatable or in some other way removable ones.
- Adhesive tape: For keeping detail elements of the set-up in place during cure, it is common to use specialized, non-contaminating and heat-resistant adhesive tape.
- Sensors: For process control, thermocouples and pressure probes are often integrated directly into the vacuum set-up (or are already in the mould structure itself).

Once the bagging is finished, it is advisable to conduct an airtightness test on the entire set-up before curing. Pressure leaks due to damage in the vacuum bag itself (such as cuts, torn-off folds or wrinkles or perforations), at the vacuum bag sealant tape or at the valves and tubes can usually be repaired prior to curing, if detected in time. In contrast, if not detected, they can lead to substantial defects in the cured component.

The airtightness of the vacuum set-up can easily be verified. First, the set-up is evacuated. Then, the vacuum pump is disconnected. By monitoring the rise in pressure inside the set-up, the tightness of the system can be quantified and evaluated. The set-up would only be released for cure if the tightness complies with predefined requirements (e.g. loss in vacuum not exceeding 50 mbar during a leak test of at least 5 minutes).

It is worth mentioning that in some cases, sources of pressure leaks cannot be easily repaired. This is especially the case if the leak occurs in the mould structure, which is why vacuum leak tests on the empty mould, as described before, are so important.

6.3.6 Cure

When processing prepregs into FRP components, probably the most critical manufacturing step of all is curing the resin matrix. This is when the polymerization reaction takes place during which the component structure is consolidated and the structural materials obtain their mechanical strength and stiffness. Polymerization is irreversible, so curing will inevitably imprint all qualitative deficiencies, caused by inappropriate processing during previous steps (material preparation, mould design and preparation, lay-up and vacuum set-up) into the cured component once and for all, with little or no chance of correcting them.

For specifying a suitable cure cycle for a given component design, various aspects have to be taken into consideration (Campbell, 2003). In principle, the two main parameters that have to be controlled are the temperature and the pressure during the cure cycle (Fig. 6.11). In the following, some criteria for choosing appropriate temperature and pressure profiles are discussed.

Temperature

Although some resin systems used in FRP can cure at room temperature, i.e. without any means of controlling the temperature (heating), such resins are usually not suitable for use in prepreg materials. The reason is that the prepreg chemistry, containing both resin and hardener, is usually adjusted to allow for a sufficient work life under shop conditions. This requires very slow polymerization reaction kinetics at room temperature, which in turn would make room temperature curing prohibitively time-consuming.

As a consequence, in order to get the polymerization reaction started and to obtain a sufficiently cured matrix within a reasonable time, heating is usually required when curing components made from prepreg. Typical means of applying heat are through the mould (with integrated electrical or heated fluid circuits, or air ducts), by infrared radiation, by transferring the mould into an oven, or by installing hot air chambers over the lay-up in the mould. Other more innovative methods are currently subject to research, e.g. microwave heating, E-beam curing, and inductive heating of resins containing nano-sized metallic particles.

Some of the criteria for selecting suitable temperature parameters for the cure cycles are as follows:

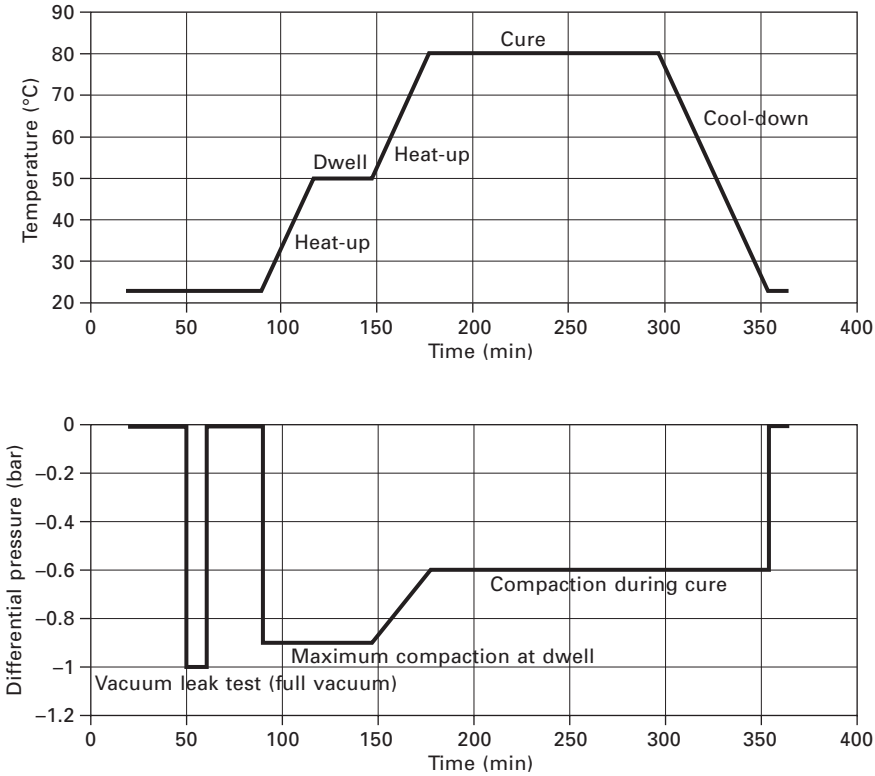

6.11 Example of a cure cycle.

- Cure temperature and cure time: In general, in order to ensure the mechanical properties required for a given structural application, it is necessary to specify both a minimum degree of cure and a minimum glass transition temperature (T_g) to be obtained after cure. As a rule, a higher cure temperature and a longer cure time will lead to a higher degree of cure and a higher T_g. Often, equivalent results can be obtained through different cure cycles, i.e. lower temperatures can be compensated for by longer durations, and vice versa (although this has certain limits; in particular, as a rule of thumb, the T_g of the cured matrix will not exceed the cure temperature). In any case, the relationship between cure temperature and cure time on the one hand, and degree of cure and T_g on the other, depends on the precise resin chemistry.
- Resin viscosity: The flow behaviour of the resin is determined by the permeability of the fibre reinforcement and ancillary materials on the one hand, and the resin viscosity on the other hand. The latter is temperature-dependent, and will also change over time due to the beginning polymerization reaction. As a consequence, resin bleed and,

thus, the obtained fibre volume content will depend on the cure cycle's temperature parameters.

- Resin shrinkage: During the cure cycle, the resin will shrink. This shrinkage occurs due to a chemical loss of volume (from the polymerization reaction), followed by thermal contraction during cool-down after cure. Since the reinforcement fibres do not chemically react, and often have a much smaller coefficient of thermal expansion than the cured matrix, this can lead to substantial geometrical distortions of the cured part, often called spring-back (Ersoy *et al.*, 2010; Stefaniak *et al.*, 2012). From the illustration in Fig. 6.12, it can be seen that the choice of cure temperature has a direct impact: a lower cure temperature will result in less resin shrinkage.
- Homogeneity of cure: Large local temperature differences during heat and cure can lead to spatial variations in resin flow (leading to higher local variations in fibre content), as well as variations in resin shrinkage (increasing the risk of uncontrollable distortions). In order to avoid this, the heat-up temperature gradient (degrees of temperature increase per minute) should be limited.
- Exothermie: The exothermic polymerization reaction releases considerable amounts of heat, which will in turn further accelerate the cure. Some

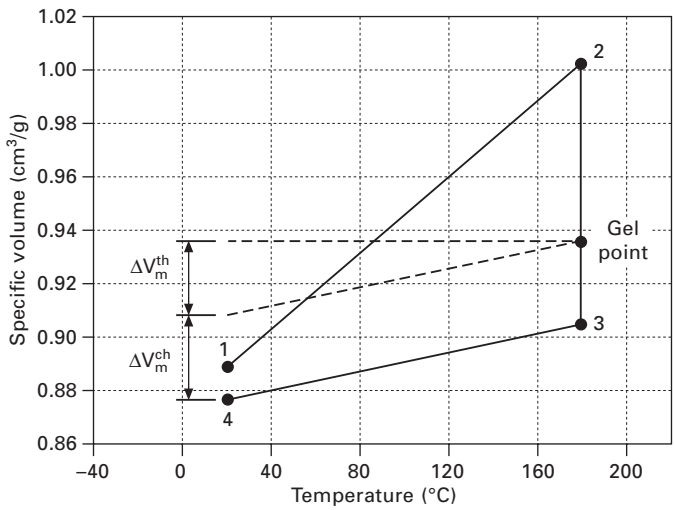

6.12 Volumetric resin shrink during cure (example values for a 180°C cure epoxy resin); line 1–2 represents the thermal expansion of the uncured resin during heat-up, line 2–3 the volumetric shrink due to the polymerization reaction, and line 3–4 the thermal shrink of the cured resin during cool-down; the gel point is defined as the moment during reaction at which the resin becomes sufficiently solid to bond to the fibres.

prepreg resin systems are designed to make use of this mechanism: by applying a relatively small amount of heat, a more or less self-maintained cure can be initiated which will continue without any further need for external heat supply. In many cases, though, the exothermie represents a risk to the process. Excessive heat can cause inhomogeneous cure (see above), and can damage the structural materials (mainly the resin itself, but also polymeric sandwich cores; or heat-sensitive fibres, such as natural fibres), as well as the ancillary materials (e.g. the vacuum bag). For mitigating the risk of excessive exothermie, the heat-up temperature gradient should be limited. Also, it is common practice to include a dwell step at intermediate temperatures in the cure cycle (Fig. 6.11). Any exothermic heat release at this stage will be less harmful, due to the overall lower temperature level, while at the same time reducing the chemical energy available for heat release at subsequent cure steps.

- Thermal stresses: During cool-down after cure, high thermal stresses can occur due to inhomogeneous cooling. In order to limit the risk of microcracking, the cool-down temperature gradient should be limited.
- Post cure: Often, it is worth considering reducing the scope of the initial cure step, by reducing either the cure temperature or the duration of cure. This can have various advantages: reducing the temperature could make it possible to use cheaper ancillary materials or cheaper tools, and can help to address some of the aforementioned issues; and reducing the cure duration will limit tool occupation time. In such cases, in order to still meet the degree of cure and T_g requirements, a post-cure by applying a second heat cycle is necessary. Post-cure can take place in the original mould, or after demoulding as a free-standing post-cure in an oven. It is also common to post-cure an assembly of several previously cured structural components.
- De-moulding: As a rule, the cured part should only be released from the mould at a temperature below the current T_g. This is particularly important when the manufacturing route includes out-of-mould post-cure.
- Further constraints: The specified cure cycle must, of course, also take into account constraints that are not directly related to the prepreg material, such as limitations in heat-up speed and maximum temperature due to the thermal inertia of the mould and the capabilities of the heating system.

Pressure

Similarly, various criteria are to be considered for selecting suitable pressure parameters for the cure cycle. Usually, the only way to control the pressure is through the evacuation of the vacuum set-up, so that the differential compaction

pressure can be adjusted to anywhere between 1 bar (full vacuum) and 0 bar (no evacuation). For high-quality components, mainly in the aerospace industry, it is standard practice to increase the applied pressure (e.g. to 7 bar) by curing inside a heated, pressurized autoclave.

One major objective of applying a differential pressure is de-gassing, i.e. evacuating any remaining air from the set-up, and in particular the air that has been trapped between individual prepreg plies during lay-up. Also, out-gassing of volatiles from the resin can occur during heat-up and cure, either due to gases dissolved in the resin, or as a by-product of the polymerization reaction. All gases have to be removed as much as possible, in order to avoid porosities in the cured composite. At the same time, this process creates the final compaction of the set-up that is needed to squeeze out any excess resin (bleed), and to ensure that the target fibre volume content is reached.

In turn, too high differential pressures can also lead to undesirable effects. Excessive bleed can cause unwetted (dry) areas in the cured part. In geometrically complex parts, e.g. at radii, too high compaction can force the prepreg plies into large deformation and create wrinkles. Also, high compaction might crush low-stiffness sandwich cores, especially when autoclave pressure is applied. And finally, depending on the precise pressure conditions within the curing part, a strong vacuum will cause gas inclusions to expand, leading to larger pores.

6.3.7 Finishing operations

After completion of the cure cycle, various operations still need to be carried out in order to obtain the final composite part. As these are common to most other composite processing methods, they are not discussed in detail here. However, it should be noted that each of these steps can add substantially to the overall component manufacturing cost, since they are time-consuming and might require expensive equipment.

Typically, the following operations are carried out after cure:

- Debagging: During cure, parts of the heated, thus liquid, resin impregnates most ancillary materials of the set-up. Once cured, this will bond the ancillary materials to each other and to the composite part. So debagging can become a delicate operation, which has to be carried out with care in order to avoid damaging the cured composite part.
- Demoulding: Especially for large components, demoulding necessitates well-designed tools. The adhesion between the cured part and the mould surface can be considerable. Therefore, moulding must always take place at sufficiently low temperature, when the material has reached its final strength and stiffness (so usually at least below its T_g).
- Machining: In many cases, mechanical machining of the outer contours of the part is necessary.

- Surface finish: All kinds of surface finish can be applied to composite parts, such as paint strippers and painting. These must fulfil various requirements, ranging from visual requirements to resistance to environmental effects such as UV radiation and mechanical wear.
- Non-destructive testing (NDT): A wide range of different NDT methods is available for inspecting the cured component. As the simplest one, visual inspection can detect surface defects, such as dry areas or wrinkles, as well as defects inside the material if glass fibres (which are translucent) are used as reinforcement. Dimensional measurements are used to detect distortions (due to spring-back), and in order to evaluate the fibre volume content through thickness measurements. In sandwich constructions, it is possible to identify insufficient adhesion between core and faces by tapping the structure and interpreting the resulting sound (tap test). As a more sophisticated but more expensive method, ultrasonic scanning in its various forms can be applied to detect internal defects such as inclusions, porosity or delaminations, as well as for measuring thicknesses. Other scanning methods, such as X-ray or CT, are also commercially available but even more costly.
- Repair: Some defects in the cured part can be repaired. Often, such repairs include a grinding or cutting operation for removing the affected material portion, followed by laying up and curing of a repair patch (either as prepreg or as dry fibres to be impregnated *in situ*).

6.3.8 Process specifications

For effectively controlling manufacturing processes for a given structural component made from prepreg, it is essential to describe these processes in all their technical details, and to define requirements that can be continuously verified. Such a description would usually consist of a set of process specifications. Table 6.1 presents an overview of some important aspects that should be covered by a process specification. At the same time, this table provides a brief summary of what has been discussed so far, and a practical starting point for manufacturing engineers who have to design and control prepreg processes.

It is worth mentioning that defining appropriate material specifications is of equal importance, because of the strong interaction some material characteristics have with the manufacturing process. Therefore, in addition to the more obvious aspects such as mechanical properties, prepreg material specifications should contain requirements regarding things like shop life, tack, viscosity behaviour over time and temperature, cure, shrinkage, etc., all of which will have an impact on the qualitative outcome of the manufacturing process. Such requirements in material specifications must be defined in close connection to the process specifications.

Table 6.1 Some aspects to be considered in process specifications

Process step	Quantity/quality to be specified
Materials	Materials allowed in this process (including ancillary materials)
Shop conditions	Cleanliness, temperature, humidity
De-freezing	Minimum temperature (dew point) to be reached before unwrapping; or minimum storage time at room temperature before unwrapping; logging of temperature history
Cutting conditions	Cutting method; blade type; cutting of prepreg stacks
Cut-out transport	Minimum diameter for roll-up cores
Intermediate storage of cut-outs	Storage conditions (temperature, humidity), maximum storage duration
Core material	Storage conditions; cleanliness; humidity content, drying
Release agent	Application method; applied quantity; drying/curing conditions
Mould vacuum leak test	Leak test method; pass/no pass criteria
Mould thermal profiling	Method; tolerances for heat homogeneity
Lay-up method and tools	Lay-up method (manual; automated); maximum lay-up speed; gap and orientation tolerances
Intermediate compaction	Conditions under which intermediate compaction is required; set-up; temperature, time, differential pressure
Preforming, hot forming	Set-up, tools; preforming time and temperature; pressure; preform storage and handling conditions
Vacuum set-up	Configuration and sequence of ancillary materials; configuration and sequence of caul plates, cores, pressure pieces; leak test conditions (differential pressure, pass/no pass criteria)
Cure	Heat-up (maximum heat-up rate); dwell (time, pressure, temperature); cure (minimum time, pressure, temperature); cool-down (max. cool down rate); tolerances; maximum demoulding temperature
Process control	Locations and requirements for witness specimens (T_g, degree of cure, fibre volume content, void content, mechanical properties); data to be logged during cure, and at which location of the mould (temperature, pressure)
Inspection	Type and requirements for NDT measures

6.4 Quality issues

As mentioned before, a composite part's quality is to a significant extent determined by the manufacturing process. Hence, thorough quality control during manufacturing is crucial to obtain satisfactory results. Beside some

common quality principles that generally apply to all sensitive manufacturing processes (such as the need for a quality management system, sufficiently qualified personnel, etc.), there are some particular aspects that are specific to the quality of prepreg manufacturing processes. This section provides an overview in this respect.

6.4.1 Workshop requirements

Due to their nature, prepregs are always more exposed to contamination during part manufacturing than other FRP semi-finished products that can be processed in closed equipment. This is why, usually, relatively strict requirements apply to the workshop conditions. Air temperature and air humidity in a prepreg-processing workshop must not exceed certain limits. The particle content in the air should be closely monitored. In high-quality workshops, temperature, humidity and cleanliness of the air are actively controlled by suitable means (air conditioning, air locks and protective clothing). Also, any potential source of greasy aerosols or silicones must be eliminated, since these can drastically reduce the adhesion characteristics of the prepreg resin.

Some publicly available information concerning workshop conditions, which is potentially useful for civil engineering applications, can be found in GL (2010).

6.4.2 Specific quality assurance measures, process control

As mentioned before, one particularly critical process step is curing the prepreg. Often, the mould has a complex thermal behaviour, due to spatially varying thermal inertia as a result of localized accumulation of mould material, and due to heating systems that are inherently incapable of delivering exactly the same amount of heat at all locations at the same time. For good part quality, though, thermal homogeneity during cure is required. One way to obtain this is to determine the thermal profile of the empty mould by heating it up and recording its thermal response at as many locations as possible. This profile can then be used to accurately tune the control loops of the heating system.

Furthermore, some of the typical quality assurance measures applied to verify an acceptable cure of a component are:

- Mechanical witness specimens (e.g. tensile strength according to ISO 527, interlaminar shear strength according to ISO 14130) retrieved from excess areas of the demoulded part
- T_g and degree of cure measurements (e.g. according to ISO 6721 and

ISO 11357) on small material samples retrieved at various locations from the demoulded part
- Fibre volume content and void content (e.g. according to ISO 1172)
- Hardness tests at various locations of the part
- Temperature and pressure readings continuously logged during cure.

6.4.3 Typical defects

Some of the defects that can occur when processing prepreg are listed in Table 6.2. This is only to provide some typical examples; in reality, the range

Table 6.2 Some typical defects in composite structures made from prepreg

Type of defect	Source	Consequence
Stacking error	Error during cutting or lay-up	Distortions, deteriorated mechanical stiffness and strength
Fibre mis-orientation	Imprecise lay-up	Deteriorated mechanical stiffness and strength
Inclusions	Contamination during lay-up; incomplete removal of separator film from prepreg	Deteriorated mechanical strength and durability
Gaps	Imprecise lay-up	Deteriorated mechanical strength
Waviness	Insufficient or excessive compaction; imprecise lay-up	Deteriorated mechanical strength and durability
Pores	Insufficient or excessive vacuum	Deteriorated mechanical strength and durability
Delamination	Insufficient ply-to-ply adhesion (due to contamination or insufficient tack); damage due to rapid cool-down from cure temperature	Deteriorated mechanical strength and durability
Surface resin shrinkage	Hindered resin flow due to inappropriate vacuum set-up configuration	Deteriorated visual appearance
Resin pockets	Insufficient compaction; imprecise lay-up; inappropriate vacuum set-up configuration	Deteriorated durability
FVC deviations	Insufficient or excessive compaction; insufficient or excessive bleeder capacity	Weight penalty; or deteriorated mechanical strength and durability; thickness deviations
Resin starvation	Excessive vacuum	Deteriorated visual appearance; deteriorated mechanical strength and durability
Uncontrolled spring-back	Inappropriate cure cycle; inhomogeneous degree of cure due to insufficient thermal management	Distortions

of possible defects is immense, and understanding the causes and effects of defects is a vast area of research; see, e.g., Piggot (1995), Wisnom and Hallet (2009), Tuminoa and Zuccarello (2011) and El-Hajjar and Petersen (2011).

The reasons for such defects to occur can be related to any of the process steps described before, e.g. lay-up, vacuum set-up or mould design. Some more generic defects may also be related to inappropriate material choices (e.g. insufficient adhesion strength of bonded assemblies due to the use of inappropriate peel ply).

Consequences of defects can be manifold, affecting various characteristics of the cured component, e.g. mechanical, optical, dimensional, weight or durability characteristics.

6.5 Conclusion and future trends

In this chapter, various aspects of a typical processing route involving prepreg material have been discussed, which might provide some useful information concerning the most common applications of prepreg technology. It is worth mentioning, though, that there are many variations and derivatives of the typical process described, some of which represent future trends or adaptations to niche applications. For instance, a special form of prepreg semi-finished product consists of chips of UD prepreg tape, which are recombined to form a planar, stochastically distributed multi-axial tape. With such a chipped prepreg tape, smaller parts of relatively complex geometries can be made that would be difficult to realize by classical prepreg techniques, such as aircraft window frames or elements in racing car seats. In this case, a closed mould is used to obtain the required compaction. Also, with classical prepreg, there are ways other than by vacuum bag to apply compaction pressure, such as by using pressurized bags pushing a hollow lay-up from the inside against a closed mould; or rod-like structures made by rolling prepreg on a mandrel, and then covering by shrink tape which exerts a compaction force when shrinking under heat influence. In the aerospace industry, a lot of effort is being spent on optimizing autoclave cure (Uçan, 2012), and indeed on getting away from the need to use an autoclave altogether.

Automation is another field of research and development activity. While closed mould injection and bulk composite moulding processes are more easily automated (and therefore often preferred, e.g. in automotive applications), prepreg processes are more complicated to automate. Even in the aerospace industry, only certain steps of the process are today fully automated, e.g. lay-up using ATL machines (Potter and Lukaszewicz, 2011; Lukaszewicz *et al.*, 2012). Others are currently being investigated, such as automated mould preparation and automated vacuum bagging, and design optimization for manufacturing (Kaufmann *et al.*, 2010). In other industries,

such as construction and wind energy, automation is even less established but is advancing (Reinforced Plastics, 2009; Crossley *et al.*, 2010; Schubel, 2012).

Finally, the continuous development of new composite materials also interacts with the manufacturing processes. Many material developments aim at improving their processing characteristics, e.g. aerospace-grade prepregs specifically designed for out-of-autoclave processes (Centea and Hubert, 2011, 2012; Garschke *et al.*, 2012; Månson *et al.*, 2009). As an altogether different group of materials, prepregs with thermoplastic matrices instead of thermosetting resin ones are emerging in the market. Such thermoplastic materials require quite a different processing route, consolidation under heat and pressure being the crucial process step rather than cure. A lot of research is currently under way in order to determine efficient and low-cost ways to properly consolidate thermoplastic composites, in either presses or autoclaves, or *in situ*.

6.6 References

Campbell F (2003), 'Curing: It's a matter of time (*t*) temperature (*T*) and pressure (*P*)', in *Manufacturing Processes for Advanced Composites*, Elsevier Science, Amsterdam, 175–221

Centea T and Hubert P (2011), 'Measuring the impregnation of an out-of-autoclave prepreg by micro-CT', *Comp Sci Technol*, 71, 593–599

Centea T and Hubert P (2012), 'Modelling the effect of material properties and process parameters on tow impregnation in out-of-autoclave prepregs', *Composites A*, doi: 10.1016/j.compositesa.2012.03.028

Crossley R, Schubel P, Warrior N (2010), 'Challenges in automated turbine blade production; Automated tape layup (ATL) of wind energy grade materials', *EWEC 2010*, EWEA Warsaw, Poland

Crossley R, Schubel P, Warrior N (2012), 'The experimental determination of prepreg tack and dynamic stiffness', *Composites A*, 43, 423–434

Davé R and Loos A (2000), *Processing of Composites*, Hanser, Munich

El-Hajjar R and Petersen D (2011), 'Gaussian function characterization of unnotched tension behavior in a carbon/epoxy composite containing localized fiber waviness', *Comp Struct*, 93, 2400–2408

Ersoy N, Garstka T, Potter K, Wisnom M, Porter D, Clegg M, Stringer G (2010), 'Development of the properties of a carbon fibre reinforced thermosetting composite through cure', *Composites A*, 41, 401–409

Garschke C, Weimer C, Parlevliet P, Fox B (2012), 'Out-of-autoclave cure cycle study of a resin film infusion process using *in situ* process monitoring', *Composites A*, 43, 935–944

GL (2010), 'Guideline for the Certification of Wind Turbines', *Germanischer Lloyd Rules and Guidelines*, IV Industrial Services, Part 1

Kaufmann M, Zenkert D, Åkermo M (2010), 'Cost/weight optimization of composite prepreg structures for best draping strategy', *Composites A*, 41, 464–472

Lukaszewicz D, Ward C, Potter K (2012), 'The engineering aspects of automated prepreg layup: History, present and future', *Composites B*, 43, 997–1009

Månson J, Sequeira Tavares S, Michaud V (2009), 'Through thickness air permeability of prepregs during cure', *Composites A*, 40, 1587–1596

Pansart S, Sinapius M, Gabbert U (2009), 'A comprehensive explanation of compression strength differences between various CFRP materials: Micro–meso model, predictions, parameter studies', *Composites A*, 40, 376–387

Piggot M (1995), 'The effect of fibre waviness on the mechanical properties of unidirectional fibre composites: a review', *Comp Sci Technol*, 53, 201–205

Potter K and Lukaszewicz D (2011), 'The internal structure and conformation of prepreg with respect to reliable automated processing', *Composites A*, 42, 283–292

Reinforced Plastics (2009), Automating wind turbine blade manufacture. Available from http://www.reinforcedplastics.com/view/695/automating-wind-turbine-blade-manufacture/ (accessed 6 December 2011)

Schubel P (2012), 'Cost modelling in polymer composite applications: Case study – Analysis of existing and automated manufacturing processes for a large wind turbine blade', *Composites B*, 43, 953–960

Stefaniak D, Kappel E, Spröwitz T, Hühne C (2012), 'Experimental identification of process parameters inducing warpage of autoclave-processed CFRP parts', *Composites A*, 43, 1081–1091

Tuminoa D and Zuccarello B (2011), 'Fatigue delamination experiments on GFRP and CFRP specimens under single and mixed fracture modes', *Procedia Engineering*, 10, 1791–1796

Uçan H (2012), 'Masterbox: How to optimize the curing process in the world's biggest laboratory autoclave', *JEC Composites Magazine*, 72, 38–40

Wisnom M and Hallet S (2009), 'The role of delamination in strength, failure mechanism and hole size effect in open hole tensile tests on quasi-isotropic laminates', *Composites A*, 40, 335–342

7

Resin infusion/liquid composite moulding (LCM) of advanced fibre-reinforced polymer (FRP)

S. BICKERTON, Q. GOVIGNON and P. KELLY,
The University of Auckland, New Zealand

DOI: 10.1533/9780857098641.2.155

Abstract: The term liquid composite moulding (LCM) encompasses a family of processes in which a dry fibrous reinforcement is impregnated by a liquid resin inside a sealed cavity. As the understanding and control of these processes improve, their field of application widens. LCM processes can be used as a replacement to decrease the environmental impact and improve the quality of composite parts made via traditional open-mould processes. They can also provide a cost-cutting alternative to prepreg techniques while maintaining a high part quality. This chapter describes the variety of processes blanketed under the class liquid composite moulding and the research advances in the monitoring and simulation of these processes. The subsequent section presents the current usage of LCM techniques in the field of civil engineering, including some case studies, before outlining some future trends and offering sources for further information.

Key words: liquid composite moulding, LCM, resin transfer moulding, closed-mould process, composite manufacturing.

7.1 Introduction

The term liquid composite moulding (LCM) describes a number of manufacturing processes in which a dry fibrous preform is placed into a mould and then impregnated with a liquid polymeric resin. These processes provide good control over harmful volatile organic compounds generated by thermoset resins, making them compliant with the tougher new environmental standards put in place in many parts of the world. By placing the dry reinforcement in an open mould, the quantity and orientation of the fibres can be precisely controlled. Application of vacuum to the cavity enables a greatly reduced porosity of the final part as compared with traditional open-mould techniques (such as wet hand lay-up or spraying of chopped fibre and resin). By applying compaction to the reinforcement throughout the process, the final V_f achieved using LCM techniques can be higher and more consistent than that obtained using an open mould.

Through variations in the processing parameters and construction of moulds, there are a high number of different designations and patents for

LCM processes. However, the LCM processes can be classified in four main categories depending on the mould construction and resin injection system: resin transfer moulding (RTM), compression RTM (CRTM), RTMLight, and resin infusion (also known as vacuum assisted RTM). These different systems are adapted to the manufacturing scenario, to provide a cost-effective solution. For large parts or small series, the use of a single-sided mould and vacuum bag allows savings on the tooling cost. The use of a heavy press and a rigid mould enables a much faster process and tighter dimensional tolerances, but requires a larger initial investment and is therefore suitable mainly for larger production numbers. The use of light, semi-rigid moulds usually made of composites provides an intermediate solution between these two extremes.

After presenting each process in more detail in the next section, the following section will detail the physics governing the process and present work on the process simulation and experimental observations. A review of the current use of these processes in civil engineering will follow, before highlighting possible future trends and research areas.

7.2 Process description

7.2.1 Resin transfer moulding

The resin transfer moulding (RTM) process, as schematically described in Fig. 7.1, is the most simple to understand and model. The fibrous reinforcement

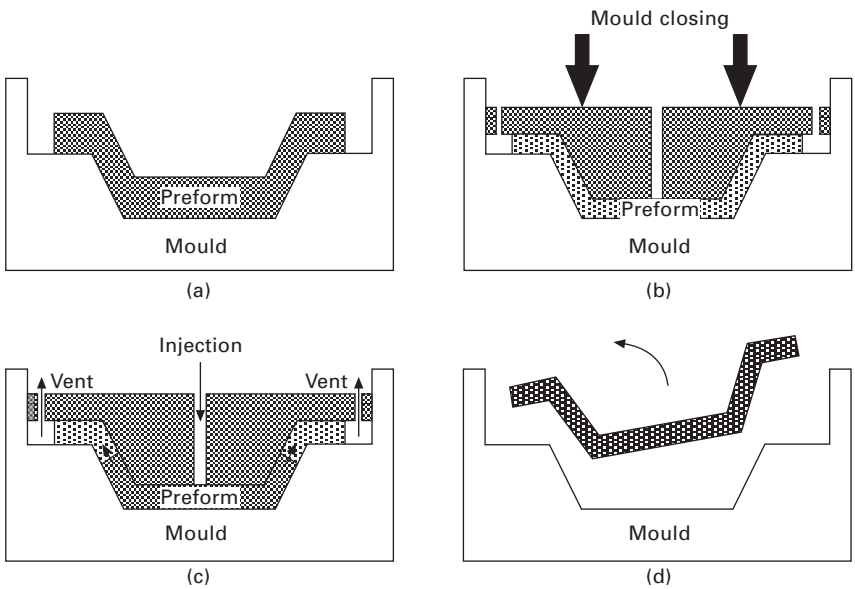

7.1 (a–d) Steps in the resin transfer moulding (RTM) process.

or preform is enclosed within a rigid mould, and resin is injected through one or more injection ports. The moulds used for RTM are typically heavy and expensive, and the process often requires a press to close the mould. As part size increases, a bigger press is required and the capital cost increases very quickly; in order to keep the cycle time low, the required injection pressures may also dramatically increase with the dimension of the part to be manufactured. Owing to the cost of tooling, RTM is preferable for large manufacturing quantities of small to medium dimension parts. Having two or more rigid matched mould pieces enables production of parts with very tight geometrical tolerances, and good surface finish on all exterior surfaces.

The RTM process can be split into four steps as depicted in Fig. 7.1. First a stack of dry reinforcements is assembled into a preform, often formed into the shape of the final part and held together with some form of binder or stitching. This preform is placed into the mould (Fig. 7.1(a)) and the mould is then closed to the desired final cavity thickness (Fig. 7.1(b)). After closing the mould, a liquid thermoset resin is injected into the preform through one or more inlet ports (Fig. 7.1(c)). Resin cure is then initiated and completed either by implementing a thermal cure cycle or by waiting the desired amount of time before demoulding the manufactured part (Fig. 7.1(d)).

RTM moulds are typically made of metal and often incorporate temperature control and part ejectors. Control of the temperature during the injection phase allows a better control of the resin viscosity and flow advancement; ramping up the temperature after the injection phase can greatly accelerate the curing of the resin and allow cycle time. The use of an injection pump capable of mixing the resin to the desired ratio, and self-flushing injection heads, can eliminate any contact of the operator with the liquid resin.

The progression of the resin flow front is highly dependent on the mould geometry and the flow properties of the reinforcement; placement of the inlet and vent ports is therefore crucial to obtain a good-quality manufactured part. Defects or material variation in the preform can also greatly affect the flow of resin. The inclusion of sensors built into the mould can help track the resin progression, and the use of multiple inlets and vents enables some control over the shape and advancement of the flow front.

7.2.2 Compression RTM

Compression resin transfer moulding (CRTM), schematically described in Fig. 7.2, is another variation of RTM, in which the rigid upper mould is partially closed, maintaining a given cavity thickness greater than the final part thickness. The desired quantity of resin is then injected. Finally the mould is closed to its final position, compacting the preform to its final thickness, and establishing a compression-driven flow which pushes the resin into the

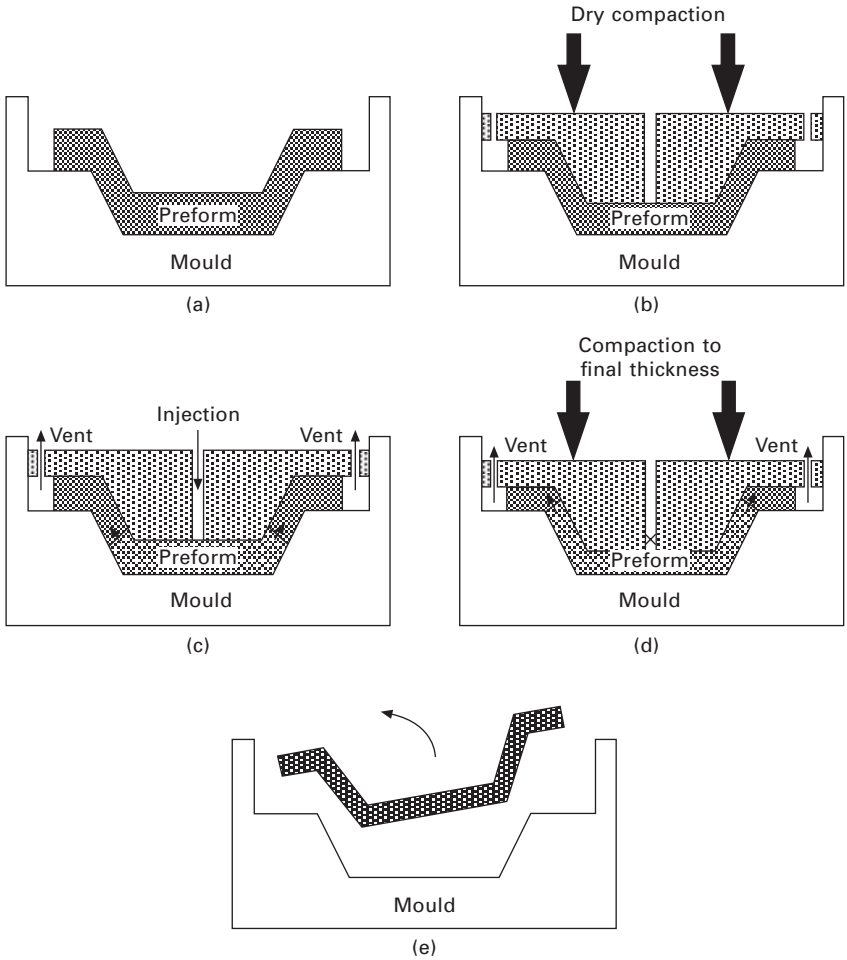

7.2 (a–e) Steps in the compression resin transfer moulding (CRTM) process.

unimpregnated portions of the preform. This process takes advantage of the higher permeability of the reinforcement when compacted to a lower V_f, in order to reduce the cycle time. With careful process design, CRTM can produce much faster cycle times than RTM. However, this is often at the expense of increased forces applied to the mould. Alternatively, it is possible to reduce the required mould clamping forces relative to RTM, while keeping the filling time constant. As for RTM, high geometric tolerances can be achieved using this process.

Possible variations of the process include leaving a gap between the top mould and the preform during the injection phase to increase speed and decrease fluid pressure during that step, and use of an articulated top mould

and sequential closing during the compaction phase in order to reduce the pressure build-up while keeping the cycle time down [1].

7.2.3 RTMLight

The RTMLight process is a variation of RTM for which the B-side mould is semi-rigid and can deform during the process. Steps in the RTMLight process are described in Fig. 7.3. The mould is usually closed using mechanical fasteners or vacuum clamping, thus greatly reducing equipment costs. However, as part size increases, the stresses applied on the mould by the preform and the resin pressure get larger and deflection of the upper mould increases. The tooling cost for RTMLight is greatly reduced compared to RTM, as the upper mould is much cheaper to manufacture. However, due to the flexibility of the upper mould, the geometrical tolerances of the part have to be increased. Also the upper mould is more subject to wear and therefore more suitable for low to medium production runs.

7.2.4 Resin infusion

Resin infusion (RI) is also known as the vacuum assisted resin transfer moulding (VARTM) process, vacuum assisted resin infusion (VARI) and Seeman's composite resin infusion moulding process (SCRIMP). In this

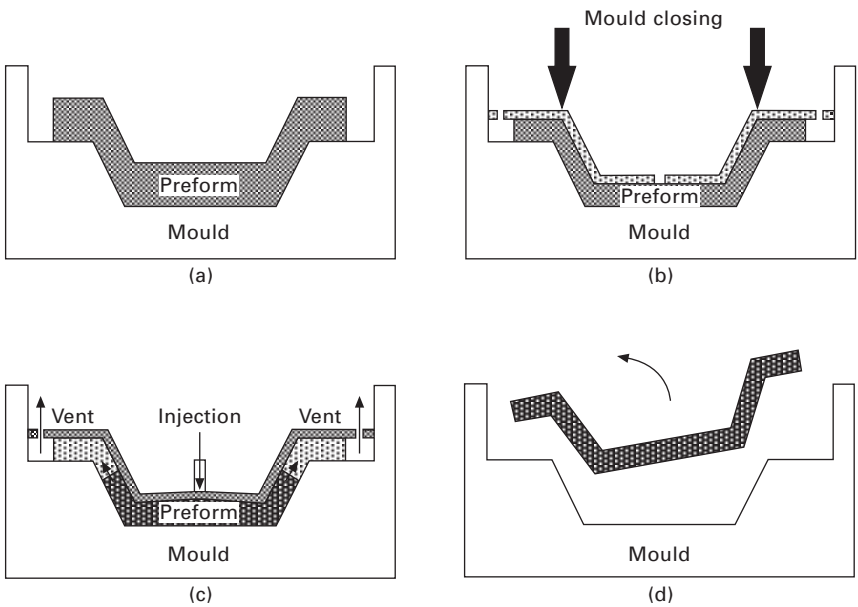

7.3 (a–d) Steps in the RTMLight process.

'sub-family' of processes, there is only one rigid mould side. The B-side is a flexible membrane sealed on the edges of the A-side mould. In this process, the preform is compacted by evacuating the cavity and using the pressure differential with the ambient pressure. As the A-side mould is subject to very little stress, the tooling costs are greatly reduced. As the vacuum bag employed during the process provides minimal rigidity, the preform thickness will vary in relation to the pressure inside the cavity, and so will the reinforcement permeability which is governed by the local reinforcement architecture. Figure 7.4 describes the components required for application of RI, and the different process stages. Initially, layers of fibrous reinforcement are laid on the mould to create the preform. A layer of peel-ply is generally laid over the preform, allowing for easy separation of the part from the consumables, and provision for a consistent part surface finish. Distribution media can be laid over the peel-ply to enhance resin flow if the reinforcement has low in-plane permeability.

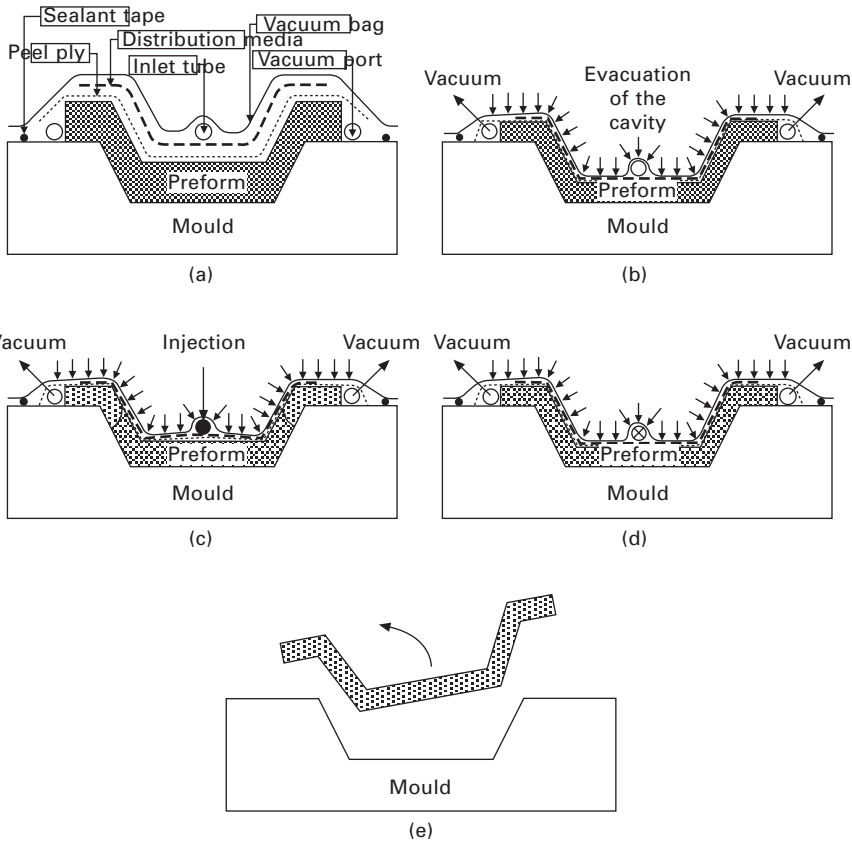

7.4 (a–e) Steps in the resin infusion (RI) process.

Once the inlet(s) and vacuum port(s) are in place, the mould is closed using a vacuum bag sealed with sealant tape. With the cavity sealed, the inlet is clamped and vacuum is applied to the vents, this stage being referred to throughout this chapter as 'pre-filling'. At the end of pre-filling, the inlet is opened and the resin penetrates the preform. During this 'filling stage', pressure inside the cavity varies in position and time. Once the resin front reaches the end of the preform, the inlet is usually clamped, stopping flow of resin into the cavity while the vents are maintained at a prescribed vacuum pressure. This 'post-filling' stage involves removal of excess resin, and allows resin pressure and laminate thickness to equilibrate within the cavity. Once the resin is fully cured, the vacuum is released and the part is lifted off the mould and separated from the consumables.

7.3 Simulation and experimental observations

During manufacture with an LCM process, the operator typically has little control over the advancement of the flow. The controllable parameters are the placement of the inlets and vents, positioning and dimensions of the flow channels, injection and vent pressure, and temperature of the mould (for control of the viscosity and cure kinetics of the resin). The type of reinforcement and its orientation are also very significant, but these will most often be decided through the functional and structural design of the product. Successful process development by trial and error therefore requires experience and can be long and expensive. Reduction of development costs requires a good understanding of the process physics, and the process designer can benefit from development of an accurate simulation tool. While the process design can be greatly aided by simulation, a simulation can also highlight the areas of the mould requiring extra attention or define where to place sensing equipment to determine the end of filling. Some flow sensing equipment can also be used to monitor directly the progression of the resin in the mould, and can be used in conjunction with fast process simulations to automate injection gate control.

7.3.1 Theory

The flow of resin through a fibrous reinforcement is usually considered to follow Darcy's law for flow through a porous medium. Assuming low Reynolds number flow, a Newtonian fluid, and that the impregnated section of the reinforcement is fully saturated, Darcy's law can be written as:

$$\boldsymbol{q} = -\frac{1}{\mu}\,\overline{\overline{\mathbf{K}}} \cdot \nabla P \qquad [7.1]$$

where $\boldsymbol{q}$ is the volume-averaged velocity vector (or Darcy velocity), μ is the fluid viscosity, $\overline{\overline{\mathbf{K}}}$ is the permeability tensor of the preform, and P is the local fluid pressure.

The conservation of solid and fluid mass for a thickness-varying process implies the following continuity equation:

$$\nabla(\boldsymbol{q} \cdot h) = -\frac{\partial h}{\partial t} \qquad [7.2]$$

where h is the local laminate thickness.

It should be noted that the Darcy velocity is different from the flow front velocity ($\boldsymbol{v}$), but they are related through the local preform porosity (ϕ):

$$\boldsymbol{v} = \frac{\boldsymbol{q}}{\phi} \qquad [7.3]$$

From these equations it can be observed that three material parameters are needed to be able to simulate and predict the infiltration of a part: the resin viscosity (μ), the reinforcement porosity (ϕ), and the permeability of the reinforcement ($\overline{\overline{\mathbf{K}}}$). The porosity of the reinforcement is related to the fibre volume fraction (Vf) as:

$$V_\mathrm{f} = 1 - \phi \qquad [7.4]$$

and the permeability of the reinforcement is also a function of the fibre volume fraction. The fibre volume fraction depends on the amount of fibre placed inside the mould and varies as an inverse function of the cavity thickness,

$$V_\mathrm{f} = \frac{\mathcal{M}N}{\rho_\mathrm{f} h} \qquad [7.5]$$

where $\mathcal{M}$ is the reinforcement areal mass, N is the number of layers, and ρ_f is the fibre density.

The balance of forces in the mould during LCM processes is typically assumed to follow Terzaghi's relation [2]:

$$\sigma_\mathrm{tot} = \sigma_\mathrm{f} + P \qquad [7.6]$$

where σ_tot is the total normal stress or normal stress applied to the mould, and σ_f is the stress applied to the preform. For a rigid mould, the stress applied to the mould is the sum of the compaction stress applied to the reinforcement and the fluid pressure. For resin infusion, as the vacuum bag provides no rigidity, the compaction of the fibre is a balance between the atmospheric pressure outside the cavity and the fluid or vacuum pressure inside the preform.

To be able to estimate the time required for the resin to fill the mould, it is necessary to know at least the permeability of the preform as well as the

viscosity of the resin. Definition of the material parameters for simulation of LCM processes therefore requires the characterisation of the relationship between v_f (or thickness) and permeability, as well as the rheological characterisation of the resin as a function of temperature and degree of cure. Knowledge of the compaction behaviour of the reinforcement is also necessary for the flexible mould processes (RTMLight and RI). For rigid mould processes the knowledge of the compaction behaviour, whilst not necessary for flow calculations, allows prediction of the tooling forces and is therefore useful for mould design and press selection.

7.3.2 Material characterisation:

Resin

While there is growing interest for the use of thermoplastic materials with LCM processes to achieve better toughness, weldability and recyclability [3], it is most common to use thermoset resins due to their lower viscosity, resulting in lower injection pressure, lower tooling forces and less possibility of deformation of the preform. There is, however, a trend towards the development of reactive thermoplastic resins, for which precursors having a much lower viscosity are injected and polymerise in the mould [3–6]. For both reactive thermoplastics and thermoset resins, over time, the components of the resin react with each other to polymerise and solidify the material. The polymeric matrix goes from a liquid state to a solid state. The resin is said to have gelled when its viscosity decreases too much for it to flow through the small interstices of the reinforcement, especially between individual fibres inside a bundle. It is important, in order to understand and simulate an LCM process, to know and be able to model the polymerisation of the resin and how it affects its viscosity to ensure a complete impregnation of the part before the resin gels. It is, however, useful to ensure that the gelling and curing of the resin happen shortly after the end of the filling stage to maximise the production rate. Extensive research is on-going into understanding the kinetics of polymerisation and its effect on the rheological properties of the resins [7–12].

Reinforcement permeability

The determination of reinforcement permeability is a requirement for any LCM simulation. Fibrous reinforcements typically have different permeability in different directions, due to the arrangement and orientation of the fibres and the presence of stitching. For most fibrous reinforcement, three principal permeability coefficients are defined: K_{11}, K_{22} and K_{33} for the three principal directions. However, for random mats, the in-plane permeability coefficients

K_{11} and K_{22} are considered equal, as the fibre orientations are randomly distributed in the plane.

While attempts have been made to analytically and numerically model the permeability of reinforcements [13–16], most LCM process simulations are performed using semi-empirical permeability models, where permeability is measured at different V_f and then fitted to an equation [17]. Many different experimental apparatuses have been designed to measure permeability [17–35], which can be characterised by the type of flow (radial or unidirectional), and whether measurement is made of in-plane or out-of-plane permeability. It is possible to further categorise measurements as those made for one value of V_f or a series (discreet or continuous) of porosity, by the type of injection (constant flow rate or constant pressure), or by the type of fluid utilised (liquid or gas). Another important distinction is that between transient unsaturated permeability and steady-state saturated permeability [26, 36, 37]. While permeability is usually measured on flat geometry, the shearing and deformation of the reinforcement placed on a non-planar mould affect the permeability and can be accounted for [38–41]. The variability of permeability due to variation in the reinforcement structure can also be evaluated [42–44]. Real parts are most often manufactured using lay-ups of multiple different reinforcements and include ply drop-off and localised reinforcement. The permeability resulting in the stacking of layers of different materials can be measured for the particular assembly, but models also allow prediction of the preform properties based on the properties of each individual material [45–48].

Reinforcement compaction

The knowledge and modelling of fibrous reinforcement compaction has multiple uses. For rigid moulds (RTM and CRTM), knowing the compaction behaviour allows prediction of the forces and stresses exerted on the mould, thus enabling optimisation of mould design. In addition, calculation of the required clamping forces through the process makes it possible to choose the press best adapted to the situation or, in the case of CRTM, to vary the process parameters in order to comply with the available press. For flexible moulds (RI) and semi-flexible moulds (RTMLight), knowledge of the compaction behaviour is essential for process modelling, as the mould stresses or applied stresses on the preform will alter the local cavity thickness and thus the permeability and flow progression.

Some efforts have been made to model the compaction of fibrous reinforcement by using beam bending theory at the fibre level [49–56]. Modelling the reinforcement at the fibre bundle scale allows prediction and evaluation of interactions between plies (also known as nesting) [57–59]. Another commonly applied approach is the use of a semi-empirical model

based on compaction characterisation experiments [60–70]. Fibre reinforcement samples are placed in a purpose-built apparatus and subjected to various loading conditions. Depending on the desired level of refinement, the compaction behaviour can then be modelled using one or multiple non-linear elastic equations or some more sophisticated models. The compaction behaviour of fibrous reinforcement was found to present a visco-elastic behaviour, including rate-dependent compaction, and stress relaxation when maintained at constant thickness [61, 65, 69–72]. Non-elastic and permanent deformation is also exhibited [62, 63, 70, 73, 74]. Differences were also observed between the compaction of wet and dry reinforcements [34, 63, 65, 68, 74–80].

While the use of standards for the determination of the behaviour of fibrous reinforcement is needed to further develop the use of LCM techniques in industrial practice, due to the complexity of the material behaviour the scientific community is still debating the development of testing standards for both permeability and compaction characterisation.

7.4 Rigid moulds

RTM has received the greatest amount of attention with regards to process simulation, as it presents the most simple case due to the constant cavity thickness. The CRTM process presents a more complex case due to the changing cavity thickness during the secondary compaction stage.

7.4.1 Experimental observation

A large amount of work has been presented on monitoring of the RTM process cycle [19, 38, 81–90]. While visualisation of the flow front progression through a transparent top mould can help understand the effect of race-tracking [38, 81, 91] and other localised effects such as inserts or converging fronts, the use of such moulds has been limited to laboratory work and they are not suitable for industrial applications. Monitoring of the process is necessary for comparison with and validation of developed simulation models, but it can also be used in industrial applications to allow process control [82, 83, 87, 92, 93]. In-mould sensors are therefore attractive, if they can be applied within, and will survive an industrial environment. Dielectric sensors, as well as monitoring flow front progression, can be used to monitor the degree of cure of the resin [85, 90, 94]. Pressure transducers can be used, and will also provide useful data of the fluid pressure in the impregnated area of the preform [86]. Thermocouples have also been used, but while cost-effective and durable, the high thermal diffusivity of metal moulds can result in a lag in the response of the sensor [95]. Ultrasonic techniques [96, 97] or X-ray radioscopy [19] can also be employed, allowing 3D monitoring of the flow front. Fibre optic sensing systems have been used to monitor flow front

progression and measure the degree of cure, and can possibly serve as strain gauges in the final part [18, 84, 98].

Very little work has been presented in the literature on the monitoring of tooling forces during RTM or LCM processes. While a load cell can easily be mounted on the hydraulic ram of a press, the local forces and ratio of reinforcement stress and fluid pressure are often ignored. By using a distributed pressure sensor placed inside the mould, Walbran and co-workers [72, 89, 99] were able to measure spatial variation in the normal stresses applied to the mould during the process cycles for RTM and CRTM, and to isolate the fluid forces from forces due to preform compaction.

Figure 7.5 presents the tooling force traces for three experiments (one RTM and two CRTM) using the same injection pressure during the injection phase and having the same final V_f. The two CRTM experiments also have the same V_f during the injection phase. For the experiment presented in Fig. 7.5(b), the secondary compaction was controlled by the mould closing velocity. For Fig. 7.5(c), the compaction was controlled through the load applied to the mould. For all experiments the time $t = 0$ was defined at the end of the primary compaction and the start of the injection.

It has been observed that for RTM the loads are usually much lower than for velocity-controlled CRTM, but the fill time is significantly longer. For RTM the initial preform compaction is to a higher V_f than for CRTM, creating a higher initial peak load. As the permeability is lower within the preform during RTM injection, it takes longer to inject the necessary amount of resin at constant pressure. For CRTM, the secondary compaction has the double effect of compacting the preform to its final thickness as well as forcing the resin through the non-saturated part of the preform. As the preform compacts, its permeability decreases, resulting in increased difficulty for the resin to flow through the reinforcement and causing an increased fluid pressure. The tooling forces are therefore seen to increase exponentially during the secondary compaction phase. The use of constant force for the secondary compaction of CRTM allows a better use of the press capacity as the peak load is achieved for a longer period of time. This results in either a reduction of cycle time for the same peak load, or a reduction of the required clamping force to the trade-off of an increased cycle time. Careful process design can therefore help determine the best compromise between press requirements and gain in productivity.

7.4.2 Simulation

The LCM operator usually has very little scope for influencing or controlling the process once initiated. While this may produce a more repeatable process than traditional open-mould techniques, it also puts more emphasis on the process design. Owing to the cost of materials used in LCM, process

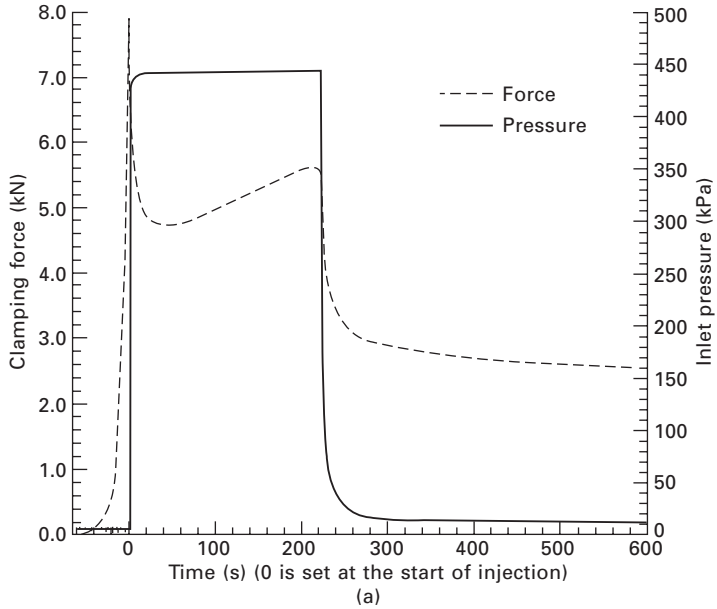

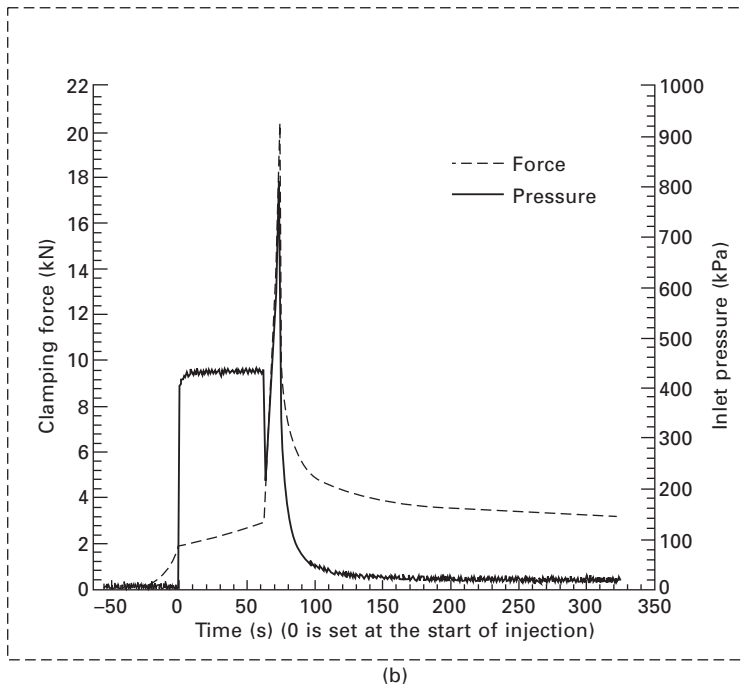

7.5 Force and injection pressure traces during the manufacturing process of a sample flat geometry using (a) RTM, (b) velocity-controlled CRTM, and (c) force-controlled CRTM.

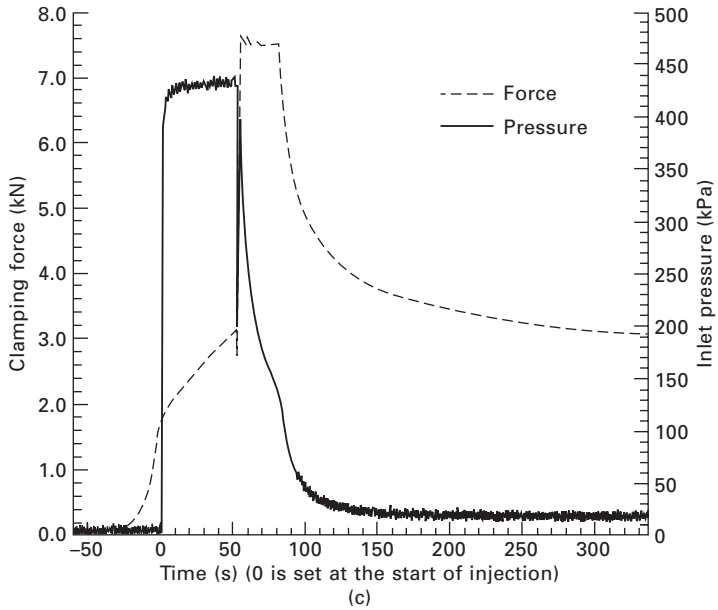

7.5 Continued

development by trial and error can be very expensive and usually relies on the experience of the tool designer. Process simulation can be used to virtualise the trial and error process, saving time and material. Beyond searching for a solution that merely works, virtual process development allows the possibility of optimising inlet and vent placement as well as the injection schedule. While the most crucial output from a simulation are the flow path and fill time, as explained earlier, it can be beneficial to predict the fluid pressure, reinforcement compaction stress and clamping forces, especially in the CRTM case. A large number of authors have developed simulations for the RTM process, but most differ only by the numerical approach taken (finite elements, finite differences, control volumes, smooth particles hydrodynamics, the lattice Boltzmann method) and by the simplifying assumptions made. A few commercial software packages are also available [100–102]. Further developments of RTM simulations now encompass void formation and dual permeability effects [103, 104], process and material variability [42, 43, 60, 105, 106] and effect of resin cure [8, 104].

Research is also on-going to simulate the CRTM process [107–112]; this process adds complication as compared to the RTM process in that part of the flow results from the reinforcement compaction. A controlled force may be employed instead of a controlled displacement during the compression flow phase, which provides an additional challenge for simulation [71, 113–116]. When the initial closing of the mould is such that an air gap remains between

the top mould and the preform, it is possible to dramatically increase the speed of the process, as the resin will flow first across the top of the preform and the flow inside the reinforcement will be mainly through the thickness. This variation also adds a challenge for simulation, as it cannot be assumed that the material flow is uniform through the thickness of the part [117, 118].

7.5 Flexible moulds

7.5.1 Experimental observation

In the RI and RTMLight processes, the combined resin pressure and reinforcement resistance to compaction are sufficient to deform the top side mould. It is therefore important to be able to measure the mould deflections resulting in variation of the reinforcement properties [119].

During pre-filling, a vacuum is applied, and as the pressure differential between the cavity and the atmospheric pressure increases, the reinforcement is subjected to dry compaction. During filling, within the saturated region, the total compaction pressure applied to the cavity is carried partly by the fluid and partly by the preform. This balance of atmospheric pressure by the fluid pressure and preform compaction stress was expressed by Terzaghi's relation [2]. As the fluid pressure increases, the top side mould deflects and the reinforcement relaxes as the cavity thickness expands. The saturated part of the reinforcement is thus subjected to a wet unloading, that is, as the local fluid pressure increases, the compaction stress on the reinforcement decreases and the local fibre volume fraction decreases. At the end of filling there is therefore a gradient of laminate thickness related to the fluid pressure gradient; some excess resin is present near the inlet and needs to be evacuated. During post-filling, the fluid pressure decreases as the excess resin is drawn out of the cavity. Therefore the preform compaction stress increases and the reinforcement is subjected to a wet compaction. Those changes in thickness will affect the local weight of the laminate as well as its mechanical properties. Monitoring of flexible mould LCM processes should therefore include mould deflection as well as flow front progression and fluid pressure as were monitored for rigid mould processes.

Owing to the transparency of most vacuum bags, the tracking of the flow front is simplified for the RI processes; when using glass fibre reinforcement it is even possible to visually monitor the through-thickness flow progression created by the use of distribution media [120]. As the vacuum bag is providing no rigidity, it can be desirable to measure the thickness variations of the preform. This can be done by using LVDTs [121–124] or laser gauges [125] but these techniques will only provide discrete point measurements. By mounting a laser on a rail it is possible to monitor the thickness of a line along the length of a part [126], but for a true measurement of the thickness

variations on the whole surface of the mould it is possible to use a 3D laser scanner [127] or stereophotogrammetry [76, 99, 128, 129].

Another specificity of flexible tooling is that the flow doesn't stop as the inlet is shut; at the end of filling there is a pressure and thickness gradient remaining that needs to equilibrate to ensure a consistent and uniform quality to the finished part [76, 127, 128, 130–133]. As the reinforcement compaction is provided by the pressure difference between the cavity and the environment, it is possible to have a limited control over the final part quality by controlling the vacuum pressure during post-filling [125, 134, 135].

Figure 7.6 presents the pressure and thickness traces of two linear infusion experiments using two different boundary conditions at the inlet, while leaving all other parameters equal; further information about these experiments can be found in [134, 135]. For these experiments, the laminate consisted of 10 plies of 400 gsm chopped strand glass mat 380 × 200 mm. While the filling conditions were kept identical for both experiments, the post-filling conditions were changed; in the experiment presented in Fig. 7.6(a) the inlet was turned into a vent at the end of filling, while in the experiment presented in Fig. 7.6(b) the inlet was clamped shut. It can be observed during filling that as the fluid pressure increases, the cavity thickness increases due to the preform relaxing. At the end of filling there is a gradient of fluid pressure and laminate thickness remaining from the inlet to the vent. The reinforcement at the inlet is almost fully uncompacted and is saturated with some excess resin that needs to be removed to allow for a higher compaction and more consistent V_f of the reinforcement. When the inlet is simply clamped at the end of filling, as is usual in industrial practice, it was observed that the pressure and thickness take a very long time to equilibrate during post-filling – about 10 times the fill time. This is because all the excess resin is located close to the inlet and needs to travel through the entire length of the preform to be evacuated through the vent. On the other hand, turning the inlet into a vent at the end of filling can tremendously speed up the post-filling phase, as the excess resin can now be removed through the inlet.

The RTMLight process is often assimilated to the RTM process and therefore very little has been published about it in the scientific literature; however, it was observed that depending on the stiffness of the B-side mould, significant deflection can be observed [132, 133, 136]. It is therefore important to monitor the process and to be able to predict the stresses applied on the mould to better understand and control this process. The same techniques as for RI can be employed to monitor the deflection of the B-side mould, but owing to the relative rigidity of the mould, simple touch sensors and contact measurements can be used as well. When the top mould is constructed with glass fibre, it can be possible to visually monitor the flow progression inside the mould; otherwise the same flow tracking techniques can be employed as

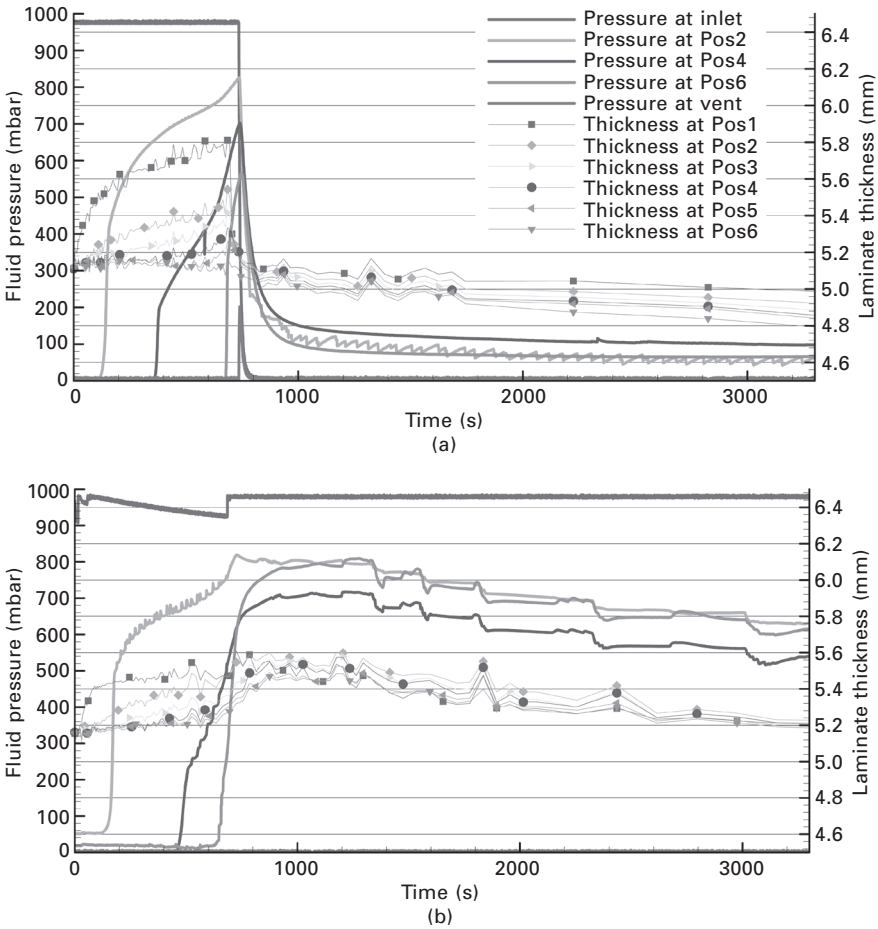

7.6 Comparison of the thickness and pressure traces during two linear vacuum assisted resin transfer moulding (VARTM) infusions (a) with inlet turned into a vent, and (b) with inlet clamped at the end of filling.

for rigid moulds. From [132], it was observed that while the fill time does not vary significantly with the varying mould stiffness, the post-filling is largely affected; when using a vacuum bag or low-stiffness top mould, there is a larger deformation of the mould close to the inlet and therefore more excess resin to draw out during post-filling.

7.5.2 Simulation

As for rigid mould processes, one of the main goals of simulation is to minimise the trial and error development for manufacturing new parts.

Positioning of the inlets and vents to ensure a fast and complete impregnation of the reinforcement is fundamental. Knowledge of the fill time and post-filling flow is also of high importance to select the cure kinetics of the resin and ensure a high-quality part throughout. While using an RTM simulation can provide reasonably good results regarding the shape of the flow front and help decide the location of the inlets and vents, the fill time predicted will most likely be quite far off and an RTM simulation will also lack any information about the post-filling phase.

Acheson *et al.* [75], Kang *et al.* [137], Joubaud *et al.* [138] and Parnas *et al.* [139] demonstrated the need for coupling the flow equation with the compaction of the reinforcement, and also with saturation of the fibre tows. In [140]; the influence of the compaction model was analysed by comparing filling simulation performed with a model based on compaction to another based on the relaxation of the reinforcement and showing a noticeable difference in fill time as well as pressure and thickness profiles at the end of filling. A $2\frac{1}{2}$ D simulation of the resin infusion was then extended from this and presented in [141]; the post-filling stage was then implemented and presented in [142]. The post-filling stage is crucial in the flexible tooling LCM processes, as it is during this phase of the process that the laminate reaches its final compaction, determining the part quality. However, so far very few papers have been published regarding the simulation of the post-filling stage.

Hsiao *et al.* [143] looked at the optimisation of the flow distribution network for complex parts, to reduce the part defects and resin wastage. Lawrence *et al.* [144] evaluated the influence of embedded impermeable inserts on the resin flow during the RI process. However, both of those studies concentrated on the flow patterns, and did not take into account the dynamic changes in preform compaction and permeability.

The RTMLight technique presents more challenges to model as compared with the RI process as the stiffness of the B-side mould has to be taken into account in the calculation of the reinforcement compaction. To the knowledge of the authors, very few studies have been published regarding the simulation of this process [132, 136, 138].

7.6 Current usage

LCM techniques are well adapted for the manufacture of wind turbine blades. While RTM is suitable for small-scale blades [145], the tooling costs and forces required to manufacture larger blades quickly become prohibitive. The RTMLight and RI techniques, requiring lower forces and enabling the use of lower-cost moulds, have proved to be competitive techniques for the manufacture of large-scale wind turbine blades [146–148]. One of their main advantages comes from the possibility of manufacturing sandwich structures in a single shot [149].

Another important use of LCM processes in civil engineering can be found in the manufacture of bridge deck sub-components [150–154], as the RI process enables the manufacture of large sandwich plates featuring lightweight corrosion resistance and low cost. RI has also been used for strengthening and repairs of concrete beams such as bridge girders [155, 156]; by using the existing concrete structure as the mould it is possible to reduce cost and improve the positioning of the fibre on the structure.

LCM techniques have also proven useful for *in-situ* maintenance of underground pipes [157, 158]; the preform is placed around an inflatable tube and dragged into place before inflating the inner tube to force the preform against the walls of the pipe to be repaired, impregnating it with liquid resin.

Another use of LCM techniques is in the manufacture of cuff links to improve the assembly of pultruded composite beams and components [159]. As part of the electrification of the rail network in New Zealand, Kiwirail is using the RTM process to manufacture screens to be placed on bridges over the rail lines to protect pedestrians and prevent any contact with the electric lines.

7.7 Case studies

7.7.1 Five Mile Road Bridges #0071, #0087, #0171 [151, 160]

As part of 'Project 100' initiated by the state of Ohio to encourage and enhance commercial growth of fibre-reinforced polymer (FRP) composite bridge decks, the deteriorated concrete deck structure of these three bridges was replaced by FRP bridge deck panels. The composite deck panel manufacturer was Hardcore Composites (HC) using a modified VARTM manufacturing technique. The advantage of VARTM over the more commonly used pultrusion technique resides in the possibility of manufacturing panels with varying width and thickness. Each bridge deck consisted of six panels that were manufactured off-site and assembled on-site with an epoxy-bonded tongue-and-groove system. The on-site installation was performed in one day by teams of 5–6 persons. While the average service life of the existing concrete bridge deck was 50 years, the service life of the replacement FRP composite deck is expected to be 100 years.

7.7.2 I-565 Highway bridge girder [156]

The I-565 highway bridge located in Huntsville, Alabama uses 23.17 m long pre-stressed concrete girders. Shortly after construction, large and unexpected cracks were observed close to the girder supports. This bridge was therefore selected by the Alabama Department of Transportation for evaluation of repair techniques. A 6.4 m^2 area was selected to carry out repair

using the VARTM technique. The area to be repaired was first prepared by sandblasting. Layers of dry unidirectional carbon fabric were then laid up at 0° and 90° for bending and shear reinforcement respectively and held in place using spray adhesive. The preform was then sealed and pressed against the concrete girder with a vacuum bag before being infused with epoxy resin. The final laminate was then coated with latex-based paint for protection against the environment. Using the VARTM technique provided good conformation of the reinforcement to the concrete girder to be reinforced, and also permitted filling and sealing the existing cracks, thus protecting the steel rods inside the concrete from corrosion. While the cost of the repair on such a small area was about double that of a bonded steel plate technique, it was estimated that for longer spans the need for welding in place of the steel plates would increase the labour, machinery and consumable cost of that technique. Maintenance cost and durability were also factors increasing the life cycle cost of the bonded steel technique.

7.8 Future trends

A possible trend for the use of infusion techniques in civil engineering applications is the use of inflatable structures to be hardened on site. By placing a preform over an inflatable bladder and then using an infusion technique to impregnate and harden the preform, a range of large-scale elements can be constructed without the need for a bulky and costly mould, and could be useful on sites with difficult or limited access. This technique has been demonstrated for the construction of bridges up to 60 ft in span [161, 162]. Another potential area of development for composites processed with LCM techniques may be in the manufacturing of façade panels for buildings. The LCM processes are well suited to manufacture panels that are strong and lightweight, with possibly complex shapes or built-in functionalities.

7.9 Conclusion

The use of LCM processes in the civil engineering industry is just in its infancy. The main hindrance to their wider use is a lack of knowledge of the behaviour of composite materials, and the mistrust of these materials due to bad experiences with the use of less repeatable processes such as wet hand lay-up or spraying of chopped fibres. However, advanced manufacturing methods such as LCM processes can allow a much improved repeatability of construction, and the mechanical performance can thus be accurately characterised and predicted. Confidence in the use of composites will also grow with growing use and experience.

Composite materials manufactured through LCM techniques have their place in a wide range of civil engineering applications, from strengthening

and repairs of existing structures to the manufacture of new structural parts or non-structural panels.

The on-going development of LCM process simulations and material characterisation techniques allows for a reduction of the development costs for new parts, and will therefore be instrumental in the cost-effective production of very small series or one-off parts using LCM techniques.

7.10 Sources of further information and advice

Books related to LCM processes

- Rudd CD *et al*. *Liquid Moulding Technologies*: Resin Transfer Moulding, Structural Reaction Injection Moulding and Related Processing Techniques, 1997, Cambridge, UK: Woodhead Publishing.
- Advani SG, Sozer EM. *Process Modeling in Composites Manufacturing*, 2002, Boca Raton, FL: CRC Press.

Journal paper concerning rigid mould processes

- Walbran WA *et al*. Prediction and experimental verification of normal stress distributions on mould tools during liquid composite moulding. *Composites Part A: Applied Science and Manufacturing*, 2012; 43(1): 138–149.

Journal papers focused on flexible mould processes

- Govignon Q, Bickerton S, Kelly PA. Simulation of the reinforcement compaction and resin flow during the complete resin infusion process. *Composites Part A: Applied Science and Manufacturing*, 2010; 41(1): 45–57.
- Timms J, Bickerton S, Kelly PA. Laminate thickness and resin pressure evolution during axisymmetric liquid composite moulding with flexible tooling. *Composites Part A: Applied Science and Manufacturing*, 2012; 43(4): 621–630.

Relevant conferences

- Flow in Processing of Composite Materials (FPCM) conference series
- International Conference on Composite Materials (ICCM) series
- International Conference on Composite Structures (ICCS) series.

7.11 References

1. Choi JH, Dharan CKH. Enhancement of resin transfer molding using articulated tooling. *Polymer Composites*, 2002; 23(4): 674–681. DOI: 10.1002/pc.10467.

2. Terzaghi K. *Theoretical Soil Mechanics*, 1943, New York: John Wiley and Sons.
3. Bittmann E. Flowing towards efficiency: LCM-compliant matrices for composites. *International AVK Meeting*, Essen, Germany, 2010.
4. Durai Prabhakaran RT, Lystrup A, Andersen TL. Attribute based selection of thermoplastic resin for vacuum infusion process: a decision making methodology. *International Journal of Manufacturing, Materials and Mechanical Engineering*, 2011; 1(3): 31–52. DOI: 10.4018/ijmmme.2011070104.
5. Pini N, Zaniboni C, Busato S, Ermanni P. Perspectives for reactive molding of PPA as matrix for high-performance composite materials. *Journal of Thermoplastic Composite Materials*, 2006; 19(2): 207–216. DOI: 10.1177/0892705706059738.
6. Rosso P, Friedrich K, Wollny A, Mülhaupt R. A novel polyamide 12 polymerization system and its use for a LCM-process to produce CFRP. *Journal of Thermoplastic Composite Materials*, 2005; 18(1): 77–90. DOI: 10.1177/0892705705041987.
7. Blest DC, McKee S, Zulkifle AK, Marshall P. Curing simulation by autoclave resin infusion. *Composites Science and Technology*, 1999; 59(16): 2297–2313. DOI: http://dx.doi.org/10.1016/S0266-3538(99)00084-6.
8. Hsiao K-T, Little R, Restrepo O, Minaie B. A study of direct cure kinetics characterization during liquid composite molding. *Composites Part A: Applied Science and Manufacturing*, 2006; 37(6): 925–933. DOI: http://dx.doi.org/10.1016/j.compositesa.2005.01.019.
9. Leroy E. Étude et modelisation des propriétés des systèmes réactifs thermodurcissable [PhD thesis]. Lyon: Institut National des Sciences Appliquées de Lyon (INSA Lyon), 2000.
10. Seifi R, Hojjati M. Heat of reaction, cure kinetics, and viscosity of Araldite LY-556 resin. *Journal of Composite Materials*, 2005; 39(11): 1027–1039. DOI: 10.1177/0021998305048738.
11. Vilas JL, Laza JM, Garay MT, Rodríguez M, León LM. Unsaturated polyester resins cure: Kinetic, rheologic, and mechanical–dynamical analysis. I. Cure kinetics by DSC and TSR. *Journal of Applied Polymer Science*, 2001; 79(3): 447–457. DOI: http://dx.doi.org/10.1002/1097-4628(20010118)79:3<447::AID-APP70>3.0.CO;2-M.
12. Vilas JL, Laza JM, Garay MT, Rodríguez M, León LM. Unsaturated polyester resins cure: Kinetic, rheologic, and mechanical–dynamical analysis. II. The glass transition in the mechanical–dynamical spectrum of polyester networks. *Journal of Polymer Science Part B: Polymer Physics*, 2001; 39(1): 146–152. DOI: http://dx.doi.org/10.1002/1099-0488(20010101)39:1<146::AID-POLB130>3.0.CO;2-A.
13. Delerue J-F, Lomov SV, Parnas RS, Verpoest I, Wevers M. Pore network modeling of permeability for textile reinforcements. *Polymer Composites*, 2003; 24(3): 344–357. DOI: http://dx.doi.org/10.1002/pc.10034.
14. Dimitrovova Z, Advani SG. Analysis and characterization of relative permeability and capillary pressure for free surface flow of a viscous fluid across an array of aligned cylindrical fibers. *Journal of Colloid and Interface Science*, 2002; 245(2): 325–337. DOI: http://dx.doi.org/10.1006/jcis.2001.8003.
15. Verleye B, Croce R, Griebel M, Klitz M, Lomov SV, Morren G, *et al*. Permeability of textile reinforcements: Simulation, influence of shear and validation. *Composites Science and Technology*, 2008; 68(13): 2804–2810. DOI: 10.1016/j.compscitech.2008.06.010.
16. Zhou F, Kuentzer N, Simacek P, Advani SG, Walsh S. Analytic characterization

of the permeability of dual-scale fibrous porous media. *Composites Science and Technology*, 2006; 66(15): 2795–2803. DOI: http://dx.doi.org/10.1016/j.compscitech.2006.02.025.

17. Sharma S, Siginer DA. Permeability measurement methods in porous media of fiber reinforced composites. *Applied Mechanics Reviews*, 2010; 63(2): 020802–020819. DOI: 10.1115/1.4001047.
18. Ahn SH, Lee WI, Springer GS. Measurement of the three-dimensional permeability of fiber preforms using embedded fiber optic sensors. *Journal of Composite Materials*, 1995; 29(6): 714–733. DOI: 10.1177/002199839502900602.
19. Bréard J, Saouab A, Bouquet G. Dependence of the reinforcement anisotropy on a three dimensional resin flow observed by X-ray radioscopy. *Journal of Reinforced Plastics and Composites*, 1999; 18(9): 814–826. DOI: 10.1177/073168449901800903.
20. Buntain MJ, Bickerton S. Compression flow permeability measurement: A continuous technique. *Composites Part A: Applied Science and Manufacturing*, 2003; 34(5): 445–457. DOI: http://dx.doi.org/10.1016/S1359-835X(03)00090-3.
21. Elbouazzaoui O, Drapier S, Henrat P. An experimental assessment of the saturated transverse permeability of non-crimped New Concept (NC2) multiaxial fabrics. *Journal of Composite Materials*, 2005; 39(13): 1169–1193. DOI: 10.1177/0021998305048746.
22. Endruweit A, Luthy T, Ermanni P. Investigation of the influence of textile compression on the out-of-plane permeability of a bidirectional glass fiber fabric. *Polymer Composites*, 2002; 23(4): 538–554. DOI: 10.1002/pc.10455.
23. Ferland P, Guittard D, Trochu F. Concurrent methods for permeability measurement in resin transfer molding. *Polymer Composites*, 1996; 17(1): 149–158. DOI: http://dx.doi.org/10.1002/pc.10600.
24. Gantois R, Jourdain E, Dusserre G. Recent patents on in-plane permeability measurement of LCM composite reinforcements. *Recent Patents on Engineering*, 2009; 3: 109–116.
25. Hoes K, Dinescu D, Sol H, Vanheule M, Parnas RS, Luo Y, *et al*. New set-up for measurement of permeability properties of fibrous reinforcements for RTM. *Composites Part A: Applied Science and Manufacturing*, 2002; 33(7): 959–969. DOI: http://dx.doi.org/10.1016/S1359-835X(02)00035-0.
26. Kuentzer N, Simacek P, Advani SG, Walsh S. Permeability characterization of dual scale fibrous porous media. *Composites Part A: Applied Science and Manufacturing*, 2006; I37(11): 2057–2068. DOI: http://dx.doi.org/10.1016/j.compositesa.2005.12.005.
27. Liu Q, Parnas RS, Giffard HS. New set-up for in-plane permeability measurement. *Composites Part A: Applied Science and Manufacturing*, 2007; 38(3): 954–962. DOI: http://dx.doi.org/10.1016/j.compositesa.2006.06.024.
28. Lundström TS, Toll S, Håkanson JM. Measurement of the permeability tensor of compressed fibre beds. *Transport in Porous Media*, 2002; 47(3): 363–380. DOI: 10.1023/a:1015511312595.
29. Luo Y, Verpoest I, Hoes K, Vanheule M, Sol H, Cardon A. Permeability measurement of textile reinforcements with several test fluids. *Composites Part A: Applied Science and Manufacturing*, 2001; 32(10): 1497–1504. DOI: http://dx.doi.org/10.1016/S1359-835X(01)00049-5.
30. Mekic S, Akhatov I, Ulven C. A radial infusion model for transverse permeability measurements of fiber reinforcement in composite materials. *Polymer Composites*, 2009; 30(7): 907–917. DOI: 10.1002/pc.20632.

31. Nedanov PB, Advani SG. A method to determine 3d permeability of fibrous reinforcements. *Journal of Composite Materials*, 2002; 36(2): 241–254. DOI: 10.1177/0021998302036002462.
32. Ouagne P, Bréard J. Continuous transverse permeability of fibrous media. *Composites Part A: Applied Science and Manufacturing*, 2010; 41(1): 22–28. DOI: DOI: 10.1016/j.compositesa.2009.07.008.
33. Scholz S, Gillespie Jr JW, Heider D. Measurement of transverse permeability using gaseous and liquid flow. *Composites Part A: Applied Science and Manufacturing*, 2007; 38(9): 2034–2040. DOI: 10.1016/j.compositesa.2007.05.002.
34. Umer R, Bickerton S, Fernyhough A. Characterising wood fibre mats as reinforcements for liquid composite moulding processes. *Composites Part A: Applied Science and Manufacturing*, 2007; 38(2): 434–448. DOI: 10.1016/j.compositesa.2006.03.003.
35. Wu X, Li J, Shenoi RA. A new method to determine fiber transverse permeability. *Journal of Composite Materials*, 2007; 41(6): 747–756. DOI: 10.1177/0021998306067012.
36. Bréard J, Henzel Y, Trochu F, Gauvin R. Analysis of dynamic flows through porous media. Part I: Comparison between saturated and unsaturated flows in fibrous reinforcements. *Polymer Composites*, 2003; 24(3): 391–408. DOI: http://dx.doi.org/10.1002/pc.10038.
37. Bréard J, Henzel Y, Trochu F, Gauvin R. Analysis of dynamic flows through porous media. Part II: Deformation of a double-scale fibrous reinforcement. *Polymer Composites*, 2003; 24(3): 409–421. DOI: http://dx.doi.org/10.1002/pc.10039.
38. Bickerton S, Sozer EM, Graham PJ, Advani SG. Fabric structure and mold curvature effects on preform permeability and mold filling in the RTM process. Part I. Experiments. *Composites Part A: Applied Science and Manufacturing*, 2000; 31(5): 423–438. DOI: http://dx.doi.org/10.1016/S1359-835X(99)00087-1.
39. Bickerton S, Sozer EM, Graham PJ, Advani SG. Fabric structure and mold curvature effects on preform permeability and mold filling in the RTM process. Part II. Predictions and comparisons with experiments. *Composites Part A: Applied Science and Manufacturing*, 2000; 31(5): 439–458. DOI: http://dx.doi.org/10.1016/S1359-835X(99)00088-3.
40. Heardman E, Lekakou C, Bader MG. In-plane permeability of sheared fabrics. *Composites Part A: Applied Science and Manufacturing*, 2001; 32(7): 933–940. DOI: 10.1016/S1359-835X(01)00006-9.
41. Louis M, Huber U. Investigation of shearing effects on the permeability of woven fabrics and implementation into LCM simulation. *Composites Science and Technology*, 2003; 63(14): 2081–2088. DOI: 10.1016/s0266-3538(03)00111-8.
42. Bickerton S, Gan JM. Accounting for reinforcement variability in liquid moulding, utilising optically measured areal weight maps, in SAMPE 2010, Seattle, WA, 17–20 May 2010. ISSN: 08910138; ISBN 9781934551073.
43. Bickerton S, Gan JM, Zhang F, Cosson B, Comas-Cardona S, Binetruy C. An optically based inverse method to measure in-plane permeability fields, in *Proceedings of the 10th International Conference on Flow Processes in Composite Materials*, Monte-Verita, Switzerland, 2010.
44. Gan JM, Bickerton S, Battley M. Automated characterisation of variability in glass fibre reinforcement architecture, in *Proceedings of the 10th International Conference on Textile Composities*, Lille, France, 2010. ISBN: 9781605950266.
45. Chen Z, Ye L, Liu H. Effective permeabilities of multilayer fabric preforms in

liquid composite moulding. *Composite Structures*, 2004; 66(1–4): 351–357. DOI: 10.1016/j.compstruct.2004.04.056.

46. Gokce A, Chohra M, Advani SG, Walsh SM. Permeability estimation algorithm to simultaneously characterize the distribution media and the fabric preform in vacuum assisted resin transfer molding process. *Composites Science and Technology*, 2005; 65(14): 2129–2139. DOI: http://dx.doi.org/10.1016/j.compscitech.2005.05.012.
47. Govignon Q, Bickerton S, Kelly PA. Homogenisation of compaction behaviour and permeability for multi-layered composite structures manufactured via LCM processes, in *16th International Conference on Composite Structures (ICCS16)*, Porto, Portugal, 2011.
48. Heider D, Simacek P, Dominauskas A, Deffor H, Advani S, Gillespie JJW. Infusion design methodology for thick-section, low-permeability preforms using inter-laminar flow media. *Composites Part A: Applied Science and Manufacturing*, 2007; 38(2): 525–534. DOI: http://dx.doi.org/10.1016/j.compositesa.2006.02.016.
49. Chen Z-R, Ye L. A micromechanical compaction model for woven fabric preforms. Part II: Multilayer. *Composites Science and Technology*, 2006; 66(16): 3263–3272. DOI: 10.1016/j.compscitech.2005.07.010.
50. Chen Z-R, Ye L, Kruckenberg T. A micromechanical compaction model for woven fabric preforms. Part I: Single layer. Composites Science and Technology. 2006;66(16):3254–3262. (DOI: 10.1016/j.compscitech.2005.07.028).
51. Curiskis JI, Carnaby GA. Continuum mechanics of the fiber bundle. *Textile Research Journal*, 1985; 55(6): 334–344. DOI: 10.1177/004051758505500602.
52. Gutowski TG, Morigaki T, Cai Z. The consolidation of laminate composites. *Journal of Composite Materials*, 1987; 21: 172–188. DOI: 0021-9983/87/02.
53. Karbhari VM, Simacek P. Notes on the modeling of preform compaction: II – Effect of sizing on bundle level micromechanics. *Journal of Reinforced Plastics and Composites*, 1996; 15(8): 837–861. DOI: 10.1177/073168449601500807.
54. Komori T, Itoh M. A new approach to the theory of the compression of fiber assemblies, *Textile Research Journal*, 1991; 61(7): 420–428. DOI: 10.1177/004051759106100709.
55. Komori T, Itoh M. Theory of the General Deformation of Fiber Assemblies. *Textile Research Journal*. 1991;61(10):588–594. (DOI: 10.1177/004051759106101005).
56. Simacek P, Karbhari VM. Notes on the modeling of preform compaction: I – Micromechanics at the fiber bundle level. *Journal of Reinforced Plastics and Composites*, 1996; 15(1): 86–122. DOI: 10.1177/073168449601500106.
57. Comas-Cardona S, Le Grognec P, Binetruy C, Krawczak P. Unidirectional compression of fibre reinforcements. Part 1: A non-linear elastic–plastic behaviour. *Composites Science and Technology*, 2007; 67(3–4): 507–514. DOI: http://dx.doi.org/10.1016/j.compscitech.2006.08.017.
58. Lomov SV, Verpoest I, Peeters T, Roose D, Zako M. Nesting in textile laminates: Geometrical modelling of the laminate. *Composites Science and Technology*, 2003; 63(7): 993–1007. DOI: 10.1016/S0266-3538(02)00318-4.
59. Yurgartis SW, Morey K, Jortner J. Measurement of yarn shape and nesting in plain-weave composites. *Composites Science and Technology*, 1993; 46(1): 39–50. DOI: 10.1016/0266-3538(93)90079-V.
60. Bickerton S, Comas-Cardona S, Razali I, Deléglise M, Walbran WA, Binétruy C, *et al*. Spatial compaction and saturated permeability variations of fibre reinforcements, in *9th International Conference on Flow Processes in Composite Materials (FPCM9)*, Montréal (Québec), Canada, 2008.

61. Bickerton S, Kelly PA, Buntain MJ. Modelling the viscoelastic compression behaviour of fibrous reinforcing fabrics, in *SAMPE Technical Conference*, Baltimore, MD, 2002.
62. Cheng JJ, Kelly PA, Bickerton S. A rate-independent thermomechanical constitutive model for fiber reinforcements. *Journal of Composite Materials*, 2012; 46(2): 247–256. DOI: 10.1177/0021998311410506.
63. Govignon Q, Bickerton S, Kelly PA. Simulation of the reinforcement compaction and resin flow during the complete resin infusion process. *Composites Part A: Applied Science and Manufacturing*, 2010; 41(1): 45–57. DOI: 10.1016/j.compositesa.2009.07.007.
64. Kelly PA, Bickerton S, Cheng J. Transverse compression properties of textile materials. *Advanced Materials Research*, 2011; 332–334: 697–701. DOI: 10.4028/www.scientific.net/AMR.332–334.697.
65. Kelly PA, Umer R, Bickerton S. Viscoelastic response of dry and wet fibrous materials during infusion processes. *Composites Part A: Applied Science and Manufacturing*, 2006; 37(6): 868–873. DOI: http://dx.doi.org/10.1016/j.compositesa.2005.02.008.
66. Pearce N, Summerscales J. Compressibility of a reinforcement fabric. *Composites Manufacturing*, 1995; 6(1): 15–21. DOI: http://dx.doi.org/10.1016/0956-7143(95)93709-S.
67. Robitaille F, Gauvin R. Compaction of textile reinforcements for composites manufacturing. I: Review of experimental results. *Polymer Composites*, 1998; 19(2): 198–216. DOI: http://dx.doi.org/10.1002/pc.10091.
68. Robitaille F, Gauvin R. Compaction of textile reinforcements for composites manufacturing. II: Compaction and relaxation of dry and H_2O saturated woven reinforcements. *Polymer Composites*, 1998; 19(5): 543–557. DOI: http://dx.doi.org/10.1002/pc.10128.
69. Somashekar AA, Bickerton S, Bhattacharyya D. An experimental investigation of non-elastic deformation of fibrous reinforcements in composites manufacturing. *Composites Part A: Applied Science and Manufacturing*, 2006; 37(6): 858–867. DOI: http://dx.doi.org/10.1016/j.compositesa.2005.06.012.
70. Somashekar AA, Bickerton S, Bhattacharyya D. Exploring the non-elastic compression deformation of dry glass fibre reinforcements. *Composites Science and Technology*, 2007; 67(2): 183–200. DOI: http://dx.doi.org/10.1016/j.compscitech.2006.07.032.
71. Walbran WA, Bickerton S, Kelly PA. Predicting stress distributions exerted on LCM tools using viscoelastic compaction models, in *SAMPE Fall Technical Conference*, Cincinnati, OH, 2007.
72. Walbran WA, Verleye B, Bickerton S, Kelly PA. Prediction and experimental verification of normal stress distributions on mould tools during liquid composite moulding. *Composites Part A: Applied Science and Manufacturing*, 2012; 43(1): 138–149. DOI: 10.1016/j.compositesa.2011.09.028.
73. Kruckenberg T, Ye L, Paton R. Static and vibration compaction and microstructure analysis on plain-woven textile fabrics. *Composites Part A: Applied Science and Manufacturing*, 2008; 39(3): 488–502. DOI: 10.1016/j.compositesa.2007.12.003.
74. Yenilmez B, Sozer EM. Compaction of E-glass fabric preforms in the vacuum infusion process, A: Characterization experiments. *Composites Part A: Applied Science and Manufacturing*, 2009; 40(4): 499–510. DOI: 10.1016/j.compositesa.2009.01.016.

75. Acheson JA, Simacek P, Advani SG. The implications of fiber compaction and saturation on fully coupled VARTM simulation. *Composites Part A: Applied Science and Manufacturing*, 2004; 35(2): 159–169. DOI: http://dx.doi.org/10.1016/j.compositesa.2003.02.001.
76. Govignon Q, Allen T, Bickerton S, Morris J. Monitoring Variations in Laminate Properties Through the Complete Resin Infusion Process, in *SAMPE: From Art to Science: Advancing Materials & Process Engineering*, Cincinnati, OH, 2007.
77. Robitaille F, Gauvin R. Compaction of textile reinforcements for composites manufacturing. III: Reorganization of the fiber network. *Polymer Composites*, 1999; 20(1): 48–61. DOI: http://dx.doi.org/10.1002/pc.10334.
78. Umer R, Bickerton S, Fernyhough A. The effect of yarn length and diameter on permeability and compaction response of flax fibre mats. *Composites Part A: Applied Science and Manufacturing*, 2011; 42(7): 723–732. DOI: 10.1016/j.compositesa.2011.02.010.
79. Walsh SM, Freese CE. Numerical model of relaxation during vacuum-assisted resin transfer molding (VARTM). *Polymer Composites*, 2005; 26(5): 628–635. DOI: http://dx.doi.org/10.1002/pc.20135.
80. Yuexin D, Zhaoyuan T, Yan Z, Jing S. Compression Responses of Preform in Vacuum Infusion Process. *Chinese Journal of Aeronautics*, 2008; 21(4): 370–377. DOI: http://dx.doi.org/10.1016/S1000-9361(08)60048-5.
81. Bickerton S, Advani SG. Experimental investigation and flow visualization of the resin-transfer mold-filling process in a non-planar geometry. *Composites Science and Technology*, 1997; 57(1): 23–33. DOI: http://dx.doi.org/10.1016/S0266-3538(96)00100-5.
82. Devillard M, Hsiao K-T, Advani SG. Flow sensing and control strategies to address race-tracking disturbances in resin transfer molding. Part II: Automation and validation. *Composites Part A: Applied Science and Manufacturing*, 2005; 36(11): 1581–1589. DOI: http://dx.doi.org/10.1016/j.compositesa.2004.04.009.
83. Hsiao K-T, Advani SG. Flow sensing and control strategies to address race-tracking disturbances in resin transfer molding. Part I: Design and algorithm development. *Composites Part A: Applied Science and Manufacturing*, 2004; 35(10): 1149–1159. DOI: http://dx.doi.org/10.1016/j.compositesa.2004.03.010.
84. Keulen CJ, Yildiz M, Suleman A. Multiplexed FBG and etched fiber sensors for process and health monitoring of 2- and 3-D TM components. *Journal of Reinforced Plastics and Composites*, 2011; 30(12): 1055–1064. DOI: 10.1177/0731684411411960.
85. Luthy T, Ermanni P. Flow monitoring in liquid composite molding based on linear direct current sensing technique. *Polymer Composites*, 2003; 24(2): 249–262. DOI: http://dx.doi.org/10.1002/pc.10026.
86. Lynch K, Hubert P, Poursartip A. Use of a simple, inexpensive pressure sensor to measure hydrostatic resin pressure during processing of composite laminates. *Polymer Composites*, 1999; 20(4): 581–593. DOI: http://dx.doi.org/10.1002/pc.10381.
87. Sozer EM, Bickerton S, Advani SG. On-line strategic control of liquid composite mould filling process. *Composites Part A: Applied Science and Manufacturing*, 2000; 31(12): 1383–1394. DOI: http://dx.doi.org/10.1016/S1359-835X(00)00060-9.
88. Turner DZ, Hjelmstad KD, LaFave JM. Three-dimensional flow visualization experiment of an RTM injection for a GFRP cuff mold. *Composite Structures*, 2006; 76(4): 352–361. DOI: http://dx.doi.org/10.1016/j.compstruct.2005.05.008.

89. Walbran WA, Bickerton S, Kelly PA. Measurements of normal stress distributions experienced by rigid liquid composite moulding tools. *Composites Part A: Applied Science and Manufacturing*, 2009; 40(8): 1119–1133. DOI: 10.1016/j.compositesa.2009.05.004.
90. Yenilmez B, Sozer EM. A grid of dielectric sensors to monitor mold filling and resin cure in resin transfer molding. *Composites Part A: Applied Science and Manufacturing*, 2009; 40(4): 476–489. DOI: 10.1016/j.compositesa.2009.01.014.
91. Bickerton S, Advani SG. Characterization and modeling of race-tracking in liquidcomposite molding processes. *Composites Science and Technology*, 1999; 59(15): 2215–2229. DOI: http://dx.doi.org/10.1016/S0266-3538(99)00077-9.
92. Bickerton S, Stadtfeld HC, Steiner KV, Advani SG. Design and application of actively controlled injection schemes for resin-transfer molding. *Composites Science and Technology*, 2001; 61(11): 1625–1637. DOI: 10.1016/s0266-3538(01)00064-1.
93. Restrepo O, Hsiao K-T, Rodriguez A, Minaie B. Development of adaptive injection flow rate and pressure control algorithms for resin transfer molding. *Composites Part A: Applied Science and Manufacturing*, 2007; 38(6): 1547–1568. DOI: 10.1016/j.compositesa.2007.01.005.
94. Ceramicomb Reusable Dieletctric Sensor, available from http://www.lambient.com/index.html (accessed 12 January 2012).
95. Tuncol G, Danisman M, Kaynar A, Sozer EM. Constraints on monitoring resin flow in the resin transfer molding (RTM) process by using thermocouple sensors. *Composites Part A: Applied Science and Manufacturing*, 2007; 38(5): 1363–1386. DOI: 10.1016/j.compositesa.2006.10.009.
96. Stöven T, Weyrauch F, Mitschang P, Neitzel M. Continuous monitoring of three-dimensional resin flow through a fibre preform. *Composites Part A: Applied Science and Manufacturing*, 2003; 34(6): 475–480. DOI: 10.1016/s1359–835x(03)00059-9.
97. Thomas S, Bongiovanni C, Nutt SR. *In situ* estimation of through-thickness resin flow using ultrasound. *Composites Science and Technology*, 2008; 68(15–16): 3093–3098. DOI: 10.1016/j.compscitech.2008.07.012.
98. Lopez-Anido R, Fifield S. Experimental methodology for embedding fiber optic strain sensors in fiber reinforced composites fabricated by the VARTM/SCRIMP process, in *4th International Workshop on Structural Health Monitoring*, Stanford, CA, 2003. ISBN: 1932078207.
99. Bickerton S, Govignon Q, Walbran WA. Observations of stress and laminate thickness variations in LCM processes, in *16th International Conference on Composite Materials (ICCM16)*, Kyoto, Japan, 2007.
100. PAM RTM, available from http://www.esi-group.com/products/composites-plastics/pam-rtm (accessed January 2012).
101. myRTM – Software for simulating the RTM process, available from http://iwk.hsr.ch/myRTM.3575.0.html?&L=4 (accessed January 2012).
102. RTM-Works FEM/CV flow simulation software, available from http://www.polyworx.com/ (accessed January 2012).
103. Bréard J, Saouab A, Bouquet G. Numerical simulation of void formation in LCM. *Composites Part A: Applied Science and Manufacturing*, 2003; 34(6): 517–523. DOI: 10.1016/S1359-835X(03)00055-1.
104. Ledru Y, Bernhart G, Piquet R, Schmidt F, Michel L. Coupled visco-mechanical and diffusion void growth modelling during composite curing. *Composites Science and Technology*, 2010; 70(15): 2139–2145. DOI: 10.1016/j.compscitech.2010.08.013.

105. Skordos AA, Sutcliffe MPF. Stochastic simulation of woven composites forming. *Composites Science and Technology*, 2008; 68(1): 283–296. DOI: 10.1016/j.compscitech.2007.01.035.
106. Gan JM, Bickerton S, Battley M. Automated characterisation of variability in glass fibre reinforcement architecture, in *10th International Conference on Textile Composites*, Lille, France, 2010. ISBN: 978–1–60595–026–6.
107. Pham X-T, Trochu F, Gauvin R. Simulation of compression resin transfer molding with displacement control. *Journal of Reinforced Plastics and Composites*, 1998; 17(17): 1525–1556. DOI: 10.1177/073168449801701704.
108. Pham X-T, Trochu F. Simulation of compression resin transfer molding to manufacture thin composite shells. *Polymer Composites*, 1999; 20(3): 436–459. DOI: 10.1002/pc.10369.
109. Bickerton S, Abdullah MZ. Modeling and evaluation of the filling stage of injection/compression moulding. *Composites Science and Technology*, 2003; 63(10): 1359–1375. DOI: http://dx.doi.org/10.1016/S0266-3538(03)00022-8.
110. Akbar S. Numerical simulation of three-dimensional flow and analysis of filling process in compression resin transfer moulding. *Composites Part A: Applied Science and Manufacturing*, 2006; 37(9): 1434–1450. DOI: 10.1016/j.compositesa.2005.06.021.
111. Deléglise M, Binétruy C, Krawczak P. Simulation of LCM processes involving induced or forced deformations. *Composites Part A: Applied Science and Manufacturing*, 2006; 37(6): 874–880. DOI: 10.1016/j.compositesa.2005.04.005.
112. Merotte J, Simacek P, Advani SG. Resin flow analysis with fiber preform deformation in through thickness direction during compression resin transfer molding. *Composites Part A: Applied Science and Manufacturing*, 2010; 41(7): 881–887. DOI: 10.1016/j.compositesa.2010.03.001.
113. Kelly PA, Bickerton S. A comprehensive filling and tooling force analysis for rigid mould LCM processes. *Composites Part A: Applied Science and Manufacturing*, 2009; 40(11): 1685–1697. DOI: 10.1016/j.compositesa.2009.07.013.
114. Walbran WA, Verleye B, Bickerton S, Kelly PA. Reducing setup costs: Tooling force prediction in resin transfer moulding (RTM) and compression RTM, in *9th Annual Automotive Composites Conference and Exhibition, ACCE 2009,* Troy, MI, 15–16 September 2009.
115. Merotte J, Simacek P, Advani SG. Flow analysis during compression of partially impregnated fiber preform under controlled force. *Composites Science and Technology*, 2010; 70(5): 725–733. DOI: 10.1016/j.compscitech.2010.01.002.
116. Verleye B, Walbran WA, Bickerton S, Kelly PA. Simulation of force and velocity controlled compression RTM, in *SAMPE 2010 Conference and Exhibition 'New Materials and Processes for a New Economy',* Seattle, WA, 17–20 May 2010. ISBN: 08910138.
117. Chang C-Y. Simulation of mold filling in simultaneous resin injection/compression molding. *Journal of Reinforced Plastics and Composites*, 2006; 25(12): 1255–1268. DOI: 10.1177/0731684406060253.
118. Simacek P, Advani SG, Iobst SA. Modeling flow in compression resin transfer molding for manufacturing of complex lightweight high-performance automotive parts. *Journal of Composite Materials*, 2008; 42(23): 2523–2545. DOI: 10.1177/0021998308096320.
119. Williams C, Summerscales J, Grove S. Resin infusion under flexible tooling (RIFT): A review. *Composites Part A: Applied Science and Manufacturing*, 1996; 27(7): 517–524. DOI: http://dx.doi.org/10.1016/1359-835X(96)00008-5.

120. Andersson HM, Lundström TS, Gebart BR, Långström R. Flow-enhancing layers in the vacuum infusion process. *Polymer Composites*, 2002; 23(5): 895–901. DOI: http://dx.doi.org/10.1002/pc.10486.
121. Grimsley BW, Hubert P, Song X, Cano RJ, Loos AC, Pipes RB. Flow and compaction during the vacuum assisted resin transfer molding process, in *SAMPE 2001*, Long Beach, CA.
122. Tackitt K, Walsh S. Experimental study of thickness gradient formation in the VARTM process. *Materials and Manufacturing Processes*, 2005; 20(4): 607–627. DOI: 10.1081/AMP-200041896.
123. Williams CD, Grove SM, Summerscales J. The compression response of fibre-reinforced plastic plates during manufacture by the resin infusion under flexible tooling method. *Composites Part A: Applied Science and Manufacturing*, 1998; 29(1–2): 111–114. DOI: http://dx.doi.org/10.1016/S1359-835X(97)00038-9.
124. Yenilmez B, Senan M, Sozer EM. Variation of part thickness and compaction pressure in vacuum infusion process. *Composites Science and Technology*, 2008; 69(11–12): 1710–1719. DOI: http://dx.doi.org/10.1016/j.compscitech.2008.05.009.
125. Daval B, Bickerton S. Exploring the potential for laminate quality control using VARTM, in *Proceedings of the 36th International SAMPE Technical*, *Conference*, San Diego, CA, 2004.
126. Kessels JFA, Jonker AS, Akkerman R. Fully $2\frac{1}{2}$D flow modeling of resin infusion under flexible tooling using unstructured meshes and wet and dry compaction properties. *Composites Part A: Applied Science and Manufacturing*, 2007; 38(1): 51–60. DOI: http://dx.doi.org/10.1016/j.compositesa.2006.01.025.
127. Li J, Zhang C, Liang R, Wang B, Walsh S. Modeling and analysis of thickness gradient and variations in vacuum-assisted resin transfer molding process. *Polymer Composites*, 2008; 29(5): 473–482. DOI: 10.1002/pc.20439.
128. Govignon Q, Bickerton S, Morris J, Kelly PA. Full field monitoring of the resin flow and laminate properties during the resin infusion process. *Composites Part A: Applied Science and Manufacturing*, 2008; 39(9): 1412–1426. DOI: http://dx.doi.org/10.1016/j.compositesa.2008.05.005.
129. Govignon Q, Bickerton S, Morris J, Lin J. A stereo photography system for monitoring full field thickness variation during resin infusion, in *FPCM8*, Douai, France, 2006.
130. Robinson MJ, Kosmatka JB. Resin bleeding simulation for the VARTM process, in *SAMPE 2008*, Long Beach, CA.
131. Simacek P, Eksik Ö, Heider D, Gillespie Jr JW, Advani S. Experimental validation of post-filling flow in vacuum assisted resin transfer molding processes. *Composites Part A: Applied Science and Manufacturing*, 2012; 43(3): 370–380. DOI: 10.1016/j.compositesa.2011.10.002.
132. Timms J, Bickerton S, Kelly PA. Laminate thickness and resin pressure evolution during axisymmetric liquid composite moulding with flexible tooling. *Composites Part A: Applied Science and Manufacturing*, 2012; 43(4): 621–630. DOI: 10.1016/j.compositesa.2011.12.012.
133. Timms J, Govignon Q, Bickerton S, Kelly PA. Observation from the filling and post-filling stages of axisymmetric liquid composite moulding with flexible tooling, in *10th International Conference on Flow Processes in Composite Materials (FPCM10)*, Monte-Verita, Switzerland, 2010.
134. Govignon Q, Kazmi SMR, Hickey CMD, Bickerton S. Control of laminate quality for parts manufactured using the resin infusion process, in *18th*

International Conference on Composite Materials (ICCM18), Jeju, South Korea, 2011.
135. Govignon Q, Bickerton S, Kelly PA. Experimental investigation into the post-filling stage of the resin infusion process. *Journal of Composite Materials*, 6 June 2012. DOI: 10.1177/0021998312448500.
136. MacLaren O, Gan JM, Hickey CMD, Bickerton S, Kelly PA. The RTM-Light manufacturing process: Experimentation and modelling, in *17th International Conference on Composite Materials (ICCM17)*, Edinburgh, 2009.
137. Kang MK, Lee WI, Hahn HT. Analysis of vacuum bag resin transfer molding process. *Composites Part A: Applied Science and Manufacturing*, 2001; 32(11): 1553–1560. DOI: 10.1016/S1359-835X(01)00012-4.
138. Joubaud L, Achim V, Trochu F. Numerical simulation of resin infusion and reinforcement consolidation under flexible cover. *Polymer Composites*, 2005; 26(4): 417–427. DOI: http://dx.doi.org/10.1002/pc.20069.
139. Parnas RS, Walsh SM, Freese CE. Vacuum-assisted resin transfer molding model. *Polymer Composites*, 2005; 26(4): 477–485. DOI: http://dx.doi.org/10.1002/pc.20121.
140. Govignon Q, Bickerton S, Kelly PA. Simulation of the complete resin infusion process, in *9th International Conference on Flow Processes in Composite Materials (FPCM9)*, Montréal (Québec), Canada, 2008.
141. Govignon Q, Verleye B, Bickerton S, Kelly PA. A 2.5D model of the resin infusion process, experiments and simulation, in *7th Asian–Australasian Conference on Composite Materials (ACCM7)*, Taipei, Taiwan, 2010.
142. Govignon Q, Maes L, Verleye B, Bickerton S, Kelly PA. A 2.5D simulation of the filling and post-filling stages of the resin infusion process, in *11th International Conference on Flow Processes in Composite Materials (FPCM11)*, Auckland, New Zealand, 2012.
143. Hsiao K-T, Devillard M, Advani SG. Simulation based flow distribution network optimization for vacuum assisted resin transfer moulding process. *Modelling and Simulation in Materials, Science and Engineering*, 2004; 12: 175–190. DOI: 10.1088/0965-0393/12/3/S08.
144. Lawrence JM, Frey P, Obaid AA, Yarlagadda S, Advani SG. Simulation and validation of resin flow during manufacturing of composite panels containing embedded impermeable inserts with the VARTM process. *Polymer Composites*, 2007; 28(4): 442–450. DOI: 10.1002/pc.20293.
145. Bechly ME, Clausen PD, Snaith H. *Structural Design, Manufacture, and Testing of Resin Transfer Moulded Blades for Small Wind Turbines*. Bury St Edmunds, UK: Mechanical Engineering Publications, 1997. ISBN: 1-86058-034-3.
146. Wind energy and vacuum infusion. *Reinforced Plastics*, 2010; 54(2): 20. DOI: 10.1016/s0034-3617(10)70060-6.
147. Schubel PJ. Technical cost modelling for a generic 45-m wind turbine blade produced by vacuum infusion (VI). *Renewable Energy*, 2010; 35(1): 183–189. DOI: 10.1016/j.renene.2009.02.030.
148. Hutchinson JR, Schubel PJ, Warrior NA. A cost and performance comparison of LRTM and VI for the manufacture of large scale wind turbine blades. *Renewable Energy*, 2011; 36(2): 866–871. DOI: 10.1016/j.renene.2010.07.025.
149. *Wind Energy Handbook*, available from http://www.gurit.com/wind-energy-handbook-1.aspx (accessed July 2012).
150. Cheng L, Karbhari VM. New bridge systems using FRP composites and concrete:

A state-of-the-art review. *Progress in Structural Engineering and Materials*, 2006; 8(4): 143–154. DOI: 10.1002/pse.221.

151. Hong T, Hastak M. Construction, inspection, and maintenance of FRP deck panels. *Journal of Composites for Construction*, 2006; 10(6): 561–572. DOI: http://dx.doi.org/10.1061/(ASCE)1090-0268(2006)10:6(561).
152. Hota GVS, Hota SRV. Advances in fibre-reinforced polymer composite bridge decks. *Progress in Structural Engineering and Materials*, 2002; 4(2): 161–168. DOI: 10.1002/pse.113.
153. Karbhari VM, Wang D, Gao Y. Processing and performance of bridge deck subcomponents using two schemes of resin infusion. *Composite Structures*, 2001; 51(3): 257–271. DOI: 10.1016/s0263-8223(00)00136-7.
154. Robinson MJ, Kosmatka JB. Light-weight fiber-reinforced polymer composite deck panels for extreme applications. *Journal of Composites for Construction*, 2008; 12(3): 344–354. DOI: http://dx.doi.org/10.1061/(ASCE)1090-0268(2008)12:3(344).
155. Karbhari VM, Zhao L. Issues related to composite plating and environmental exposure effects on composite–concrete interface in external strengthening. *Composite Structures*, 1997; 40(3–4): 293–304. DOI: 10.1016/s0263-8223(98)00031-2.
156. Nasim U, Uday V, Muhammad S, Serrano-Perez JC. Cost-effective bridge girder strengthening using vacuum-assisted resin transfer molding (VARTM). *Advanced Composite Materials*, 2004; 13(3–4): 255–281. DOI: 10.1163/1568551042580163.
157. Chin WS, Lee DG. Development of the trenchless rehabilitation process for underground pipes based on RTM. *Composite Structures*, 2005; 68(3): 267–283. DOI: 10.1016/j.compstruct.2004.03.019.
158. Yu HN, Kim SS, Hwang IU, Lee DG. Application of natural fiber reinforced composites to trenchless rehabilitation of underground pipes. *Composite Structures*. 2008; 86(1–3): 285–290. DOI: 10.1016/j.compstruct.2008.03.015.
159. Singamsethi SK, LaFave JM, Hjelmstad KD. Fabrication and testing of cuff connections for GFRP box sections. *Journal of Composites for Construction*, 2005; 9(6): 536–544. DOI: http://dx.doi.org/10.1061/(ASCE)1090-0268(2005)9:6(536).
160. Hastak M, Halpin D, Hong T. Constructability, maintainability, and operability of fiber reinforced polymer (FRP) bridge deck panels. Publication FHWA/IN/JTRP-2004/15. Joint Transportation Research Program, Indian Department of Transportation and Purdue University, West Lafayotte, IN, 2004. DOI: 10.5703/1288284313163.
161. Bannon DJ, Dagher HJ, Lopez-Anido R. Behavior of inflatable rigidified composite arch bridges, in Composites & polycon 2009, Tampa, FL, American Composites Manufacturers Association.
162. Malnati P. Bridge cost cut with inflatable arches. *Composites Technology*, April 2009.

8

Filament winding processes in the manufacture of advanced fibre-reinforced polymer (FRP) composites

A. KHENNANE, University of New South Wales at the Australian Defence Force Academy, Australia

DOI: 10.1533/9780857098641.2.187

Abstract: Despite considerable potential and many advantages over conventional materials, composites are making limited progress in the field of infrastructure applications, where the only niche market for composites is in FRP deck construction over steel girders and externally bonded FRP repair. The reasons, of course, are to be found in their high initial cost compared with conventional materials. This can only be addressed through the use of large-volume automated processes such as pultrusion and filament winding, which have the potential to lower the cost of raw materials and technologies for all applications. This chapter summarises the current level of applications of filament winding in the infrastructure industry.

Key words: filament winding, hybrid beams, bridge decks, concrete, confinement.

8.1 Introduction

At the turn of the last century, Milkovich (1994) wrote that there was a high probability that military and space industries would not be served by an adequate composite industry unless current suppliers could develop substantial markets in non-military and space areas. Now, 13 years into the new century, Milkovich's observation is still valid. Indeed, for this scenario to succeed, the civilian areas of application must provide a large market, and this can only be fulfilled through infrastructure applications. Indeed, with considerable potential for composite materials in infrastructure applications, the cost of raw material and technologies is likely to decline for all applications. Yet, composites are making limited progress in the infrastructure industry, where the only niche markets are in retrofitting of structurally deficient structures and in FRP deck construction over steel girders. In part, this is due to the relative 'newness' of the material, the high initial cost compared with concrete, timber and steel, and the low stiffness of glass fibre reinforced plastic (GFRP), which is favoured by the construction industry for its affordability as compared with aerospace-grade composites such as carbon fibre reinforced plastics (CFRP) and aramid fibre reinforced plastics (AFRP). The lack of stiffness can be

addressed through innovative design, but the problem of high initial cost can only be addressed through the use of large-volume automated processes such as pultrusion and filament winding.

8.2 Filament winding

8.2.1 Process technology

Filament winding is considered to be the oldest mechanical process for manufacturing fibre-reinforced polymer (FRP) composites. It originated in the 1950s as an advanced technique for manufacturing rocket engine cases (Koussios, 2004). It consists of winding resin-impregnated fibre or tape to a rotating mandrel as shown in Fig. 8.1. It offers a number of advantages over other manufacturing techniques. It is characterised by high fibre volume fractions (between 60 and 80%) and constant quality of the finished product. The angle at which the fibres are placed can be adjusted by controlling the speed of the payout head relative to that of the rotating mandrel and various windings could be obtained: circumferential winding and helical winding. When the mandrel has three degrees of freedom in rotation, allowing the simultaneous independent control of three rotations, a third type of winding, termed polar winding, can be obtained as shown in Fig. 8.2.

Filament winding is also the process that has benefited the most from computer technology and robotics. Nowadays, filament winding systems are available for complex axisymmetric and non-axisymmetric components.

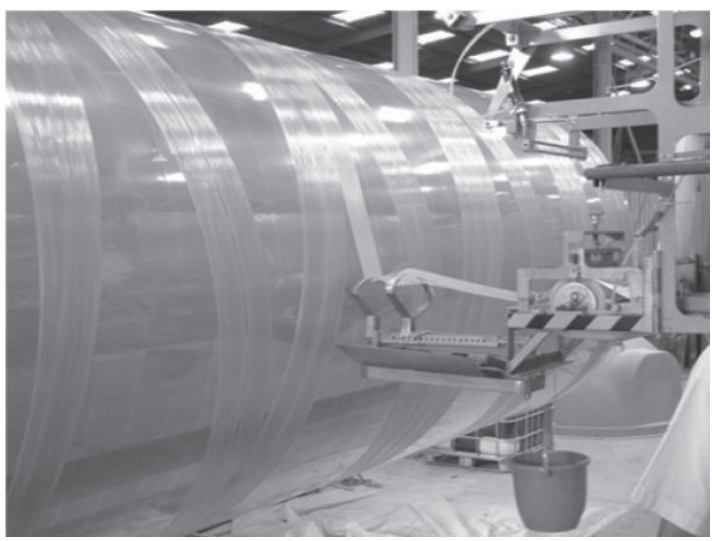

8.1 Filament winding machine (http://www.matrasurcomposites.com).

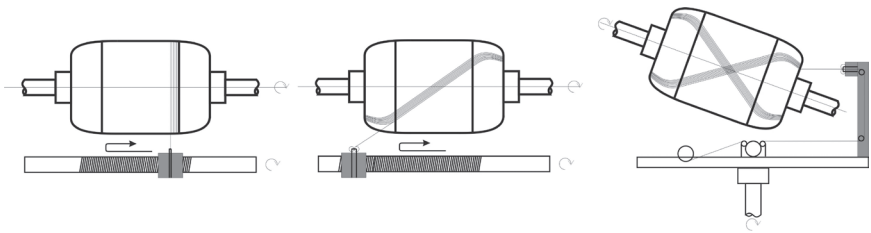

8.2 Different types of filament windings.

The placement of the fibres or rovings can be performed by CAD systems. The coordinate data of the geodesic paths, on which the fibre bands are stable and do not slip even when tensioned, are calculated and fed to the machine microcomputer for placement (Scholliers and Van Brussel, 1994). More complex configurations, such as tapered shafts, T-shaped parts, and non-axisymmetric parts could be successfully filament-wound.

Current developments, however, are focused on increasing the winding efficiency to achieve high production rates. This is motivated by the increasing demand for pressure vessels in the automotive sector (Päßler and Schledjewski, 2012). Traditional pressure vessels (350 bars) are used in many natural gas-powered vehicles, while high pressure vessels (700 bars) are required for hydrogen storage used in car prototypes.

8.2.2 Materials

Unsaturated polyester resins are by far the most widely used resins in filament winding. However, most of the thermosetting resins are suitable provided that their viscosity does not exceed 12 poises (1.2 Pa.s) at the processing temperature. The fibres are usually supplied in the form of spools of tapes or rovings. The rovings are the most widely used because they provide the fibres with their optimal tensile strength. This ensures therefore that the tension developed during the winding process to compact the fibres removes the need for an autoclave cure, which often involves significant capital expenses.

On the other hand, future developments are concentrated on developing processes to filament-wind with thermoplastics (Bannister, 2001). Indeed, thermoplastics offer a wide range of advantages such as the following:

- Superior chemical resistance
- Higher allowable strain
- 'One material concept': liner, structural layers and coating are all of the same thermoplastic material, which eliminates any interface issues
- Higher impact resistance and improved robustness
- Higher allowable operational temperature

- Speeding up the fabrication process by their ability to consolidate online.

The main difficulty, however, is ensuring proper impregnation of the fibres by resins that are an order of magnitude more viscous than their thermosetting counterparts. As a result, the wetting process is usually separate from the winding process, and intermediate products in the form of prepregs are used with the matrix being already melted to impregnate the fibres (Lauke and Friedrich, 1993). However, they are costly to produce compared to the prices of fibres and matrix (Henninger and Friedrich, 2002). In order to speed up the fabrication process and reduce the overall costs, concepts for online impregnation have been proposed. Åström and Pipes (1990) proposed a system in which the fibres were impregnated with matrix powder before being melt-impregnated in a pultrusion dye. The matrix is then kept in its molten state until it is welded to the previously wound layer. Henninger and Friedrich (2002) devised an innovative solution with the potential for improving the winding speed. The device, called the impregnation wheel, consists of a porous ring though which the molten polymer is squeezed under pressure to impregnate a bundle of fibres.

8.2.3 Processing parameters

The processing of the materials into laminates is the key to the achievement of optimum mechanical properties. The quality of the finished product depends on a large number of parameters.

For winding with thermosetting resins, Cohen (1997) and Cohen *et al.* (2001) reported that winding tension, stacking sequence, winding-tension gradient and winding time significantly affect the mechanical and physical properties of the finished product. Of these parameters, winding tension appears to be the most important one as it directly affects the fibre volume ratio. Mertiny and Ellyin (2002) reported that under fibre-dominated loading, higher fibre tension leads to an improved resistance against failure, whereas under matrix-dominated loading, failure is delayed by reducing fibre tensioning.

Because filament winding with thermoplastic resins is more complicated than wet winding with thermosetting resins, there are additional parameters that affect the quality of the final product such as temperature and roller pressure for the *in-situ* consolidation. Using prepregs, Haupert and Friedrich (1995) investigated the influence of the pre-heating and mandrel temperatures, and found out that it only took slight deviations in temperature to result in great variations in quality. A lower mandrel temperature results in poor consolidation quality, whereas a high temperature could result in the degradation of the matrix itself. Henninger *et al.* (2002) found that increasing the speed of the impregnating wheel, reduced the impregnation efficiency of the fibres, and

increasing the impregnation temperature resulted in a lower melt viscosity, thus favouring the impregnation. However, this came at a price, as an increase in the pulling force was also required.

8.3 Filament-wound structures for infrastructure applications

In civil infrastructure, filament winding is traditionally used to produce pipes, power poles and pressure vessels. Recent years, however, have seen an increase in the use of filament-wound composites in innovative structural systems. The most intuitive of these systems is the combination of filament-wound tubes with concrete to produce hybrid structural components suitable for civil infrastructure. The FRP tube not only serves as a permanent formwork for the concrete but also provides it with hoop and longitudinal reinforcement. The concrete in return provides the composite system with overall stability and stiffness.

The second major application of filament winding is in the development of lightweight, corrosion-free and strong components for use as decks for medium and long-span bridges. Figure 8.3 from Harries (2008) shows the various applications of FRP materials within the Innovative Bridge Research and Construction (IBRC) Program conducted by the United States Federal Highway Administration. About one quarter of the bridges involve the use of FRP decks as replacements for existing bridge decks on steel girders.

Parsons *et al*. (2002) developed a bridge superstructure, which consists

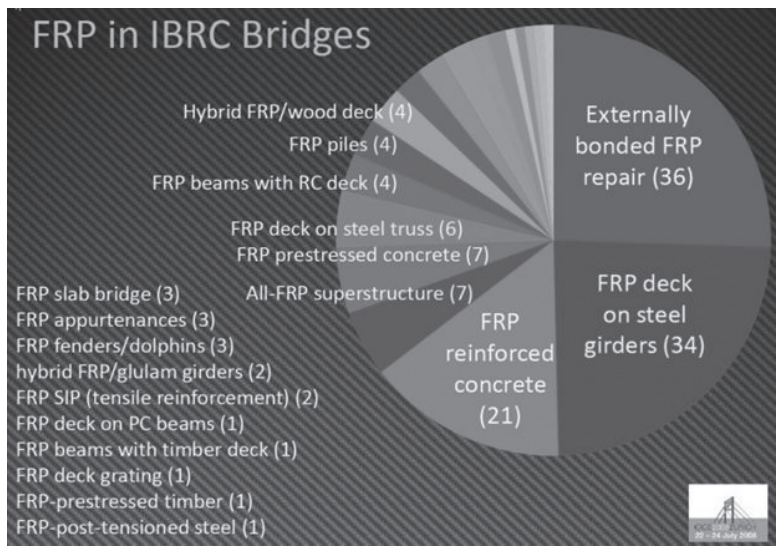

8.3 Composites in infrastructure.

of two components: a series of inner cells, lying parallel to the direction of traffic, and an outer shell. The bridge deck is manufactured in a two-stage process. First, the inner cells of the bridge deck are filament wound and cured separately using a mandrel that can be extracted after cure. After manufacturing, the inner cells are trimmed and prepared for integration with the outer shell. The outer shell structure is constructed by winding filament directly onto the inner cells as shown in Fig. 8.4. The structural tests of the manufactured specimens indicated that the structural properties of the prototypes did not deteriorate when subjected to cyclic loads.

By combining the filament winding and pultrusion techniques, Feng *et al.* (2006) tested three different configurations of an outside filament-wound FRP bridge deck. The first configuration is a GFRP modular pultruded profile deck for footbridges wound with the filament around its cross-section. The second is a combination of GFRP pultruded profiles and lay-up face plates made of E-glass strand mat and unsaturated polyester resin, all wrapped with filament winding. The third configuration, shown in Fig. 8.5, is composed of two pultruded GFRP face plates and four filament-wound square tubes bonded with epoxy adhesive, and like the previous one wrapped up using filament winding. By comparing the experimental results with those obtained on unwrapped specimens, it was found that the outside filament winding not only improved the load-carrying ability by eliminating the premature failure modes but also shifted the failure from brittle to a more ductile one.

Williams *et al.* (2003) developed three generations of hybrid FRP concrete decks using pultrusion and filament-winding techniques. The deck consisted of a number of triangular filament-wound tubes bonded with epoxy resin. GFRP plates were adhered to the top and bottom of the tubes to create one modular unit. In some of the specimens, the triangular tubes were filled with concrete as shown in Fig. 8.6. In the third generation, the whole system is

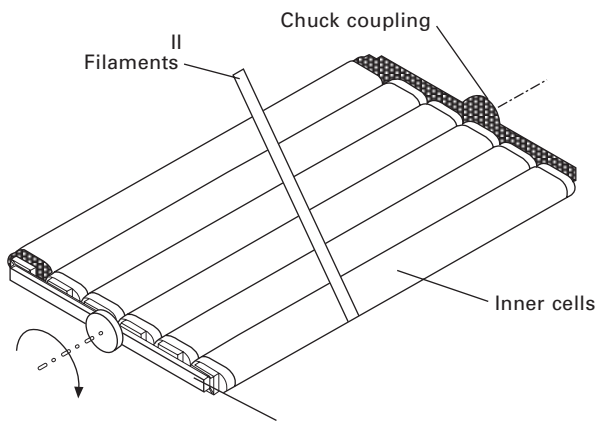

8.4 Filament-wound bridge deck (Parsons *et al.*, 2002).

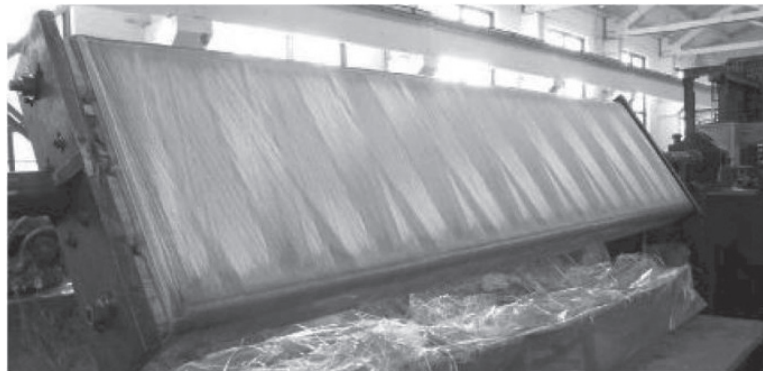

8.5 Outside filament-wound FRP bridge deck (Feng *et al.*, 2006).

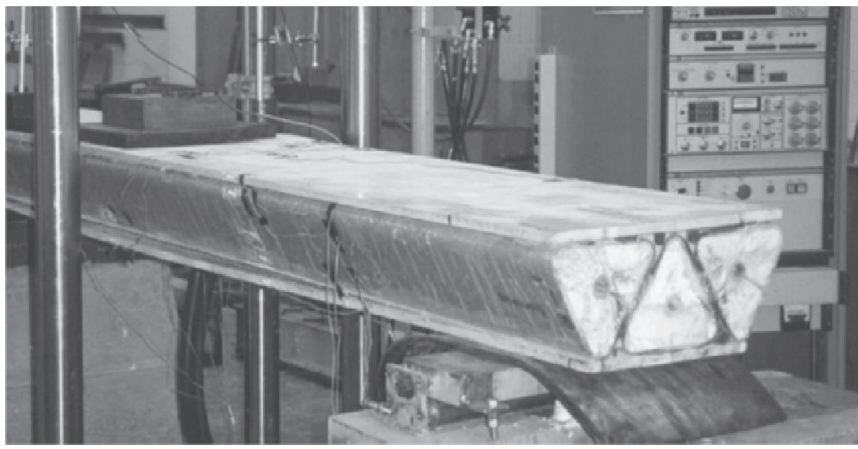

8.6 Hybrid FRP concrete deck slab using pultrusion and filament winding techniques.

externally wrapped with filament winding. The test results obtained indicated that the FRP bridge deck modules are a viable alternative to conventional reinforced concrete bridge decks. It is not surprising therefore that these lightweight, corrosion-free and strong components made with the filament winding and/or the pultrusion techniques have found a niche market in the replacement of bridge decks.

In contrast, there are very few all-composite bridges. The reason is to be found in the low stiffness of GFRP girders. Indeed, in designing with FRPs, it is the deformations and not the load-carrying capacity that are usually critical. Using GFRP typically results in a very thick girder cross-section as in the Tech 21 bridge (Fig. 8.7) or too many of them, 24 as in the two-lane Tom's Creek road bridge shown in Fig. 8.8. The girders are usually manufactured with the hand lay-up process (Farhey, 2005) or with the pultrusion process

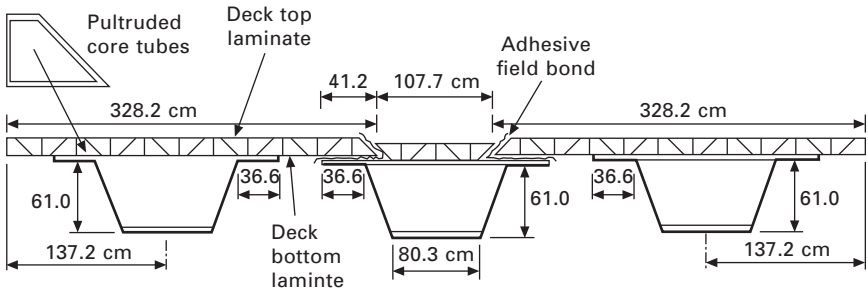

8.7 Cross-section of the Tech 21 all-composite bridge (Farhey, 2005).

(Neely *et al.*, 2004). Filament winding is hardly used because of its inability to place fibres in the 0° direction parallel to the longitudinal axis of the beam.

In addition to their inherent lack of stiffness, the major problem with all GFRP girders is their linear elastic brittle behaviour under load, in the sense that they do not display any warnings of imminent failure.

8.4 New beam design using filament winding

8.4.1 Design

In order to use FRP composites both optimally and economically, different researchers (Deskovic *et al.*, 1995; Canning *et al.*, 1999; van Erp *et al.*, 2002) have combined them with concrete in hybrid designs. Figure 8.9 shows some the concepts that have been proposed. Deskovic *et al.* (1995) (Fig. 8.9(a)), Canning *et al.* (1999) (Fig. 8.9(b)) and van Erp *et al.* (2002) (Fig. 8.9(d)) used almost similar designs, where the beams consist of a custom-made FRP box, a concrete layer, and a CFRP laminate to serve as a warning of imminent collapse. This approach simply mimics that of reinforced concrete in the sense that the CFRP failure is expected to replace steel yielding. As a result, the CFRP laminate is usually very thin, and contributes very little to the stiffness of the beam. Having recognised the inherent lack of stiffness of GFRPs, Zhao *et al.* (2000) opted for a CFRP shell filled with concrete as shown in Fig. 8.9(c). The carbon shell has both hoop reinforcement (90° from longitudinal axis) and ±10° longitudinal fibres, as well as helical ribs on the inside to ensure full-force transfer with the concrete. This design resulted in a stiff girder, but the load versus displacement curves obtained under four-point bending were linear up to failure and did not exhibit any signs of imminent failure. Correia *et al.* (2007) tested a hybrid beam which consisted of a pultruded section and a concrete layer. A preliminary test proved that the adhesion between the pultruded profile and the concrete was insignificant. As a result, the shear connection in subsequent beams had to

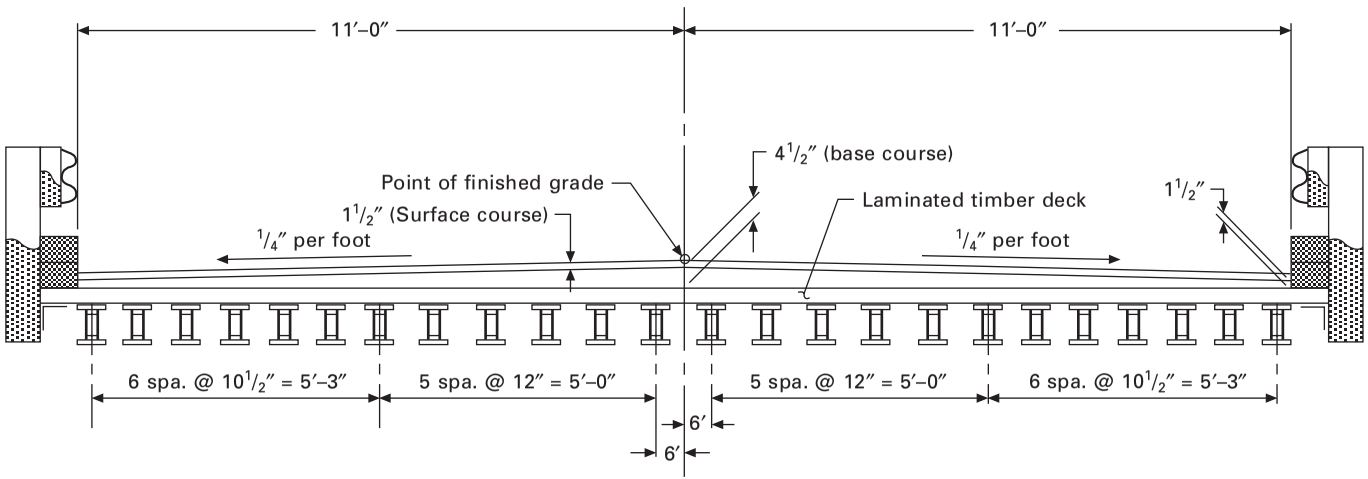

8.8 Cross-section of Tom's Creek road bridge (Neely *et al.*, 2004).

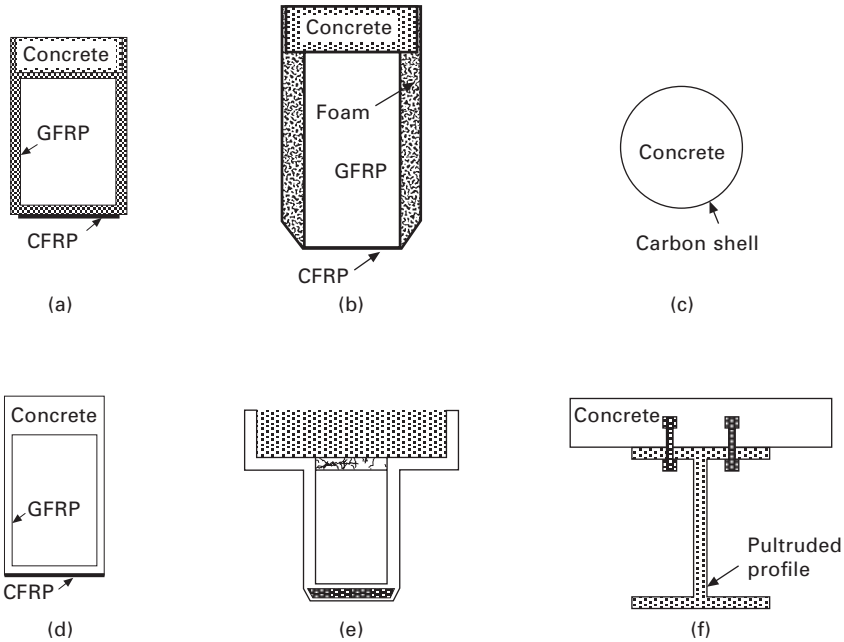

8.9 (a–f) Existing hybrid FRP–concrete beam designs.

be provided using mechanical means as shown in Fig. 8.9(f). The beams failed without warning due to shear in the GFRP profile, which occurred in the top flange junction. In summary, the shortcomings of the previously described designs can be listed as follows:

- Custom-made GFRP boxes or carbon shell have a high initial cost.
- Being very thin to serve a warning for imminent failure, the CFRP laminate contributes very little to the overall stiffness of the beam.
- When a cost-effective pultruded profile is used, mechanical means are needed to provide the shear connection with the concrete.

To address the shortcomings, Khennane (2009) and Chakrabortty *et al.* (2011) have taken this idea a stage further with the rectangular section member manufactured from pultruded GFRP composite and a CFRP laminate in the tension zone. The whole system, including the concrete in the compression zone, is confined with a wrapping consisting of external filament winding to ensure composite action between the GFRP box and the concrete block. Figure 8.10 shows a photograph of the beam and Fig. 8.11 a schematic representation of its cross-section.

To minimise the cost of the beam, a pultruded GFRP box profile, available 'off the shelf', is chosen. Thin-walled box sections are very efficient for beams and have a high resistance to lateral torsional buckling.

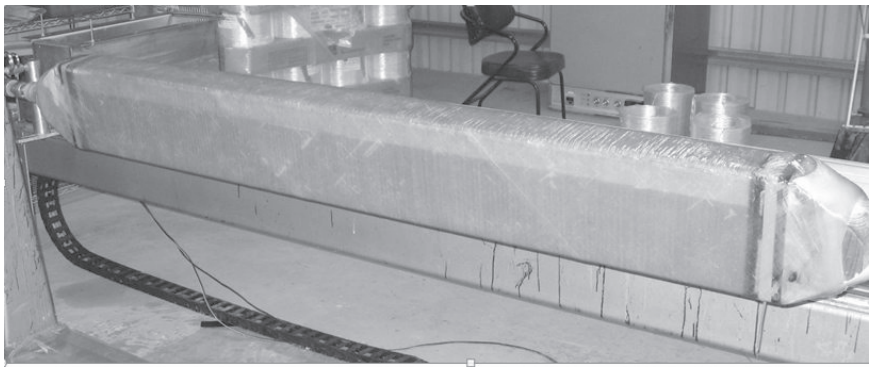

8.10 Externally filament-wound hybrid beam.

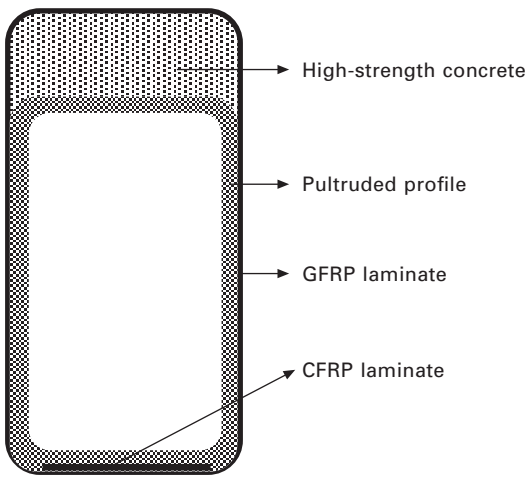

8.11 Proposed design for a hybrid FRP–concrete beam.

To address the inherent lack of stiffness of hybrid beams, the CFRP laminate is not designed to fail first to give a warning of imminent failure (Chakrabortty *et al.*, 2011). Instead, its primary role is to provide the required stiffness for the beam. As such, there is no upper limit on its thickness. Therefore, the stiffness of the beam can be tailored. The warning of imminent failure is hoped to be achieved through the crushing of the concrete.

The addition of the filament-wound outer laminate serves two purposes. Its principal role is to provide some form of confinement to the concrete block–pultruded profile system so as to ensure a composite action, thus eliminating the risk of debonding failure. The lack of composite action between the concrete and the laminates was reported as a serious shortcoming of these sections (Canning *et al.*, 1999; Correia *et al.*, 2007). Finally, with fibres oriented at ±45°, its second role is to improve the shear strength of

the pultruded profile, which has fibres predominantly in the longitudinal direction.

The subsequent experimental results reported in Chakrabortty *et al*. (2011) revealed that the filament-wound wrap induce a beneficial confinement to the concrete. What is not clear, however, was the extent of this confinement. Using finite element analysis, this effect is investigated in the following sections.

8.4.2 Analysis

Partially confined concrete model

According to Lam and Teng (2003a) and Csuka and Kollar (2010), confined concrete displays different stress–strain curves according to the amount of confinement as shown in Fig. 8.12. When the concrete is fully confined

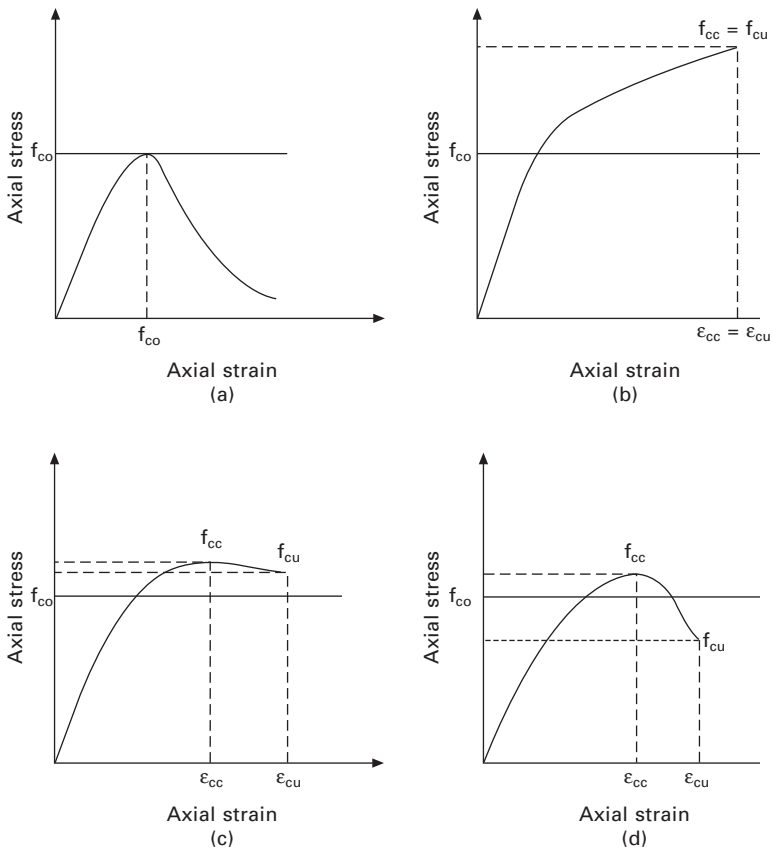

8.12 (a–d) Stress–strain curves for confined concrete.

the stress–strain curve shows a monotonically ascending bilinear shape, i.e. increasing type (Fig. 8.12(b)), which is the general case for a circular confinement as has been reported by many researchers (Lam and Teng, 2003a; Csuka and Kollar, 2010; Fam and Rizkalla, 2001; Xiao and Wu, 2003). For fully confined circular sections, the FRP confinement is able to play its role completely and provides variable confining pressures on the concrete as it maintains an appreciable amount of stiffness throughout the loading process, and ultimately fails by rupture.

Experimental evidence has also shown that such a bilinear stress–strain response cannot always be obtained, and the peak stress is reached before the rupture of FRP wrapping, i.e., a descending type (Lam and Teng, 2003b). Moreover, there are two types of descending stress–strain curves. In the first case, when the concrete is sufficiently confined, the axial stress at ultimate strain is higher than the unconfined concrete strength, i.e. $f_{cu} > f_{co}$ (Fig. 8.12(c)), and there will be a significant improvement in the strength due to confinement. In the second case, the ultimate axial stress is less than the peak unconfined concrete strength, i.e. $f_{cu} < f_{co}$ (Fig. 8.12(d)), and there will be little enhancement in the concrete strength due to the confinement. Such a concrete is insufficiently confined and is more pronounced for rectangular sections.

The concrete section in the present beams is also rectangular, and can therefore be considered as partially confined. Most importantly, the concrete in the beam crushed before FRP rupture, which is consistent with insufficient confinement as reported by Xiao and Wu (2003) and Aire *et al*. (2001). It follows therefore that, in the present case, it can be reasonably assumed that the stress-strain curve shown in Fig. 8.12(d) would be the most suitable one for this analysis. Unfortunately, there are no available models that could predict the stress–strain behaviour of this type of partially confined rectangular concrete section. Therefore a partially confined concrete material model is developed to produce the necessary curve.

Most of the FRP-confined concrete models available for evaluating the amount of increase in the concrete strength and corresponding peak axial strain are based on the confined concrete model developed experimentally by Richart *et al*. (1929), which is given by

$$\frac{f_{cc}}{f_{co}} = 1 + k_1 \left(\frac{f_1}{f_{co}} \right) \qquad [8.1]$$

$$\frac{\varepsilon_{cc}}{\varepsilon_{co}} = 1 + k_2 \left(\frac{f_1}{f_{co}} \right) \qquad [8.2]$$

where f_{cc} and ε_{cc} are the peak axial stress and corresponding strain of the confined concrete, f_1 the confining pressure, k_1 the confinement effective

coefficient, and $k_2 = 5k_1$. A wide range of other values of k_1 have been proposed both experimentally and analytically [13, 18–19]. It is a function of the confinement level and of the concrete strength (Shehata *et al.*, 2002). However, the values of k_1 available in the literature are not suitable for the present case as the concrete block is rectangular and partially confined. Therefore, it was decided to choose the value of k_1 for this analysis by trial and error.

The confining pressure, f_l, supplied by the filament-wound wrapping on the concrete of the beam is required in Eq. 8.1. It is obtained as:

$$f_l = \frac{2E_{frp}t\varepsilon_{frp}}{D'} k_s \qquad [8.3]$$

where E_{frp} is the elastic modulus of the wrapping in the hoop direction, ε_{frp} the tensile rupture strain of the wrapping, t the thickness of the wrapping, and D' the diameter of the circular section. However for square or rectangular section, D' is considered as the diagonal length of that section (Lam and Teng, 2003b; Toutanji, 1999), as shown in Fig. 8.13.

In Eq. 8.3, k_s is the shape factor that depends on the effective confining area of the cross-section, and is commonly used for both rectangular and square sections. The effective confining area for a rectangular section is the area contained by four parabolas (Fig. 8.13). Therefore, for a fully confined rectangular section, k_s is defined as the ratio of the effective confined area to the total area of the cross-section. Limiting the expression presented by Lam and Teng (2003b) to rectangular sections with round corners and plain concrete, k_s can be expressed as:

$$k_s = 1 - \frac{\frac{b}{c}(b-2r)^2 + \frac{c}{b}(c-2r)^2}{3\{bc-(4-\pi)r^2\}} \qquad [8.4]$$

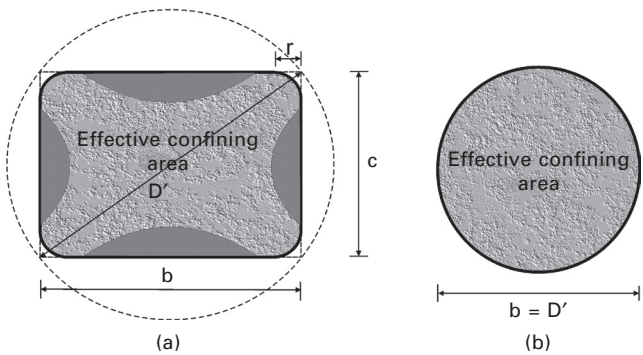

8.13 Effective confining area for fully confined rectangular (a) and circular (b) sections.

However, the concrete section in the beam is rectangular and partially confined; therefore, the effective confining area will be less than that shown in Fig. 8.13. Since the exact amount of effectively confined area for this partially confined concrete section is unknown, the minimum value of the shape factor as suggested by Pessiki *et al*. (2001) is therefore chosen for this analysis.

The stress–strain curve required for this analysis is generated from the complete stress–strain relationship given in Teng *et al*. (2007) as:

$$\sigma_c = f_{cc}\left\{\frac{(\varepsilon_c/\varepsilon_{cc})r}{r-1+(\varepsilon_c/\varepsilon_{cc})^r}\right\} \quad [8.5]$$

where ε_c is the axial strain of concrete, f_{cc} and ε_{cc} are the peak axial stress and corresponding strain of confined concrete which are given in Eqs 8.1 and 8.2, and r is a constant used to account for the brittleness of concrete (Carreira and Chu, 1985) as:

$$r = \frac{E_c}{E_c - f_{cc}/\varepsilon_{cc}} \quad [8.6]$$

From this partially confined concrete model several stress–strain curves can be generated for different values of k_1, and the suitable curve for this analysis, shown in Fig. 8.14, is obtained for a value of k_1 = 1.5 which gives the corresponding value of k_2 as 7.5. It can be seen that due to partial

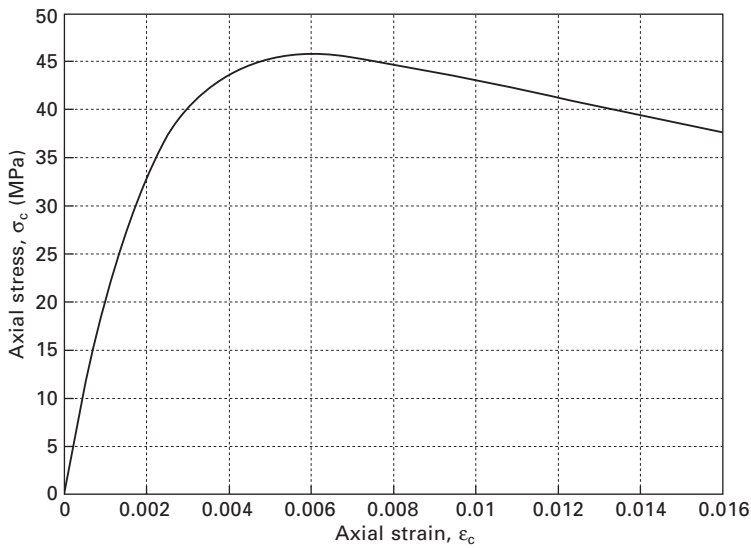

8.14 Compressive stress–strain curve for partially confined concrete.

confinement the strength enhancement is about 20%. Most importantly, the new stress–strain curve shows a more ductile behaviour.

Finite element analysis

The general-purpose finite element software ABAQUS (2009) is used to investigate the extent of the confinement introduced by the filament winding wrap (Fig. 8.15). Due to symmetry, only one quarter of the beam is modelled. The concrete block is meshed with solid eight-noded continuum three-dimensional brick elements; the pultruded profile is meshed with eight-noded continuum shell elements, and, due to relatively smaller thicknesses, both the CFRP and the outer GFRP filament-wound wrapping are meshed with four-noded conventional shell elements. The support and loading plates are also meshed using the eight-noded continuum three-dimensional brick element. The concrete damage plasticity model CDPM is used for concrete, while the FRP model including damage initiation and evolution also provided in ABAQUS is used for the composite components.

Two beams NSC-B2 and NCS-B3, made of normal concrete with a cylinder strength of 38 MPa and having different concrete block thicknesses, respectively equal to 75 mm and 90 mm, are analysed. Figures 8.16 and 8.17 show the obtained results. It can be seen that when the stress–strain curve of the concrete is used as is, that is without the effect of confinement, the predicted ultimate load-carrying abilities of the beams are less than the

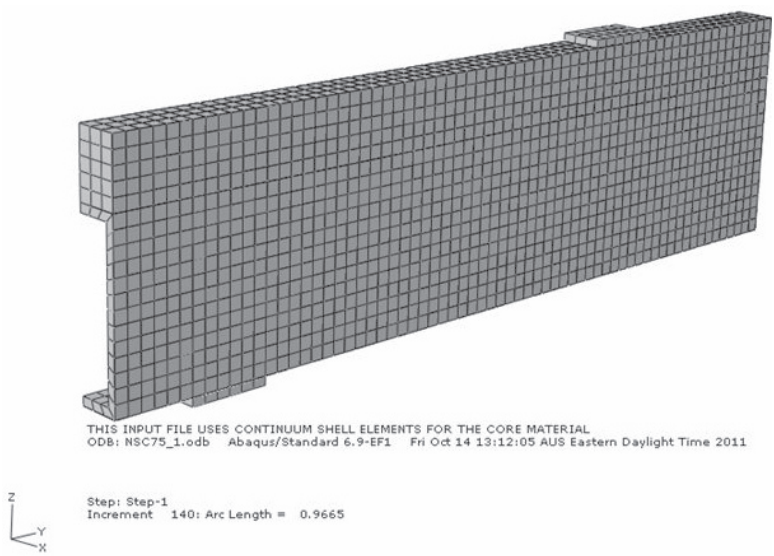

8.15 Finite element model.

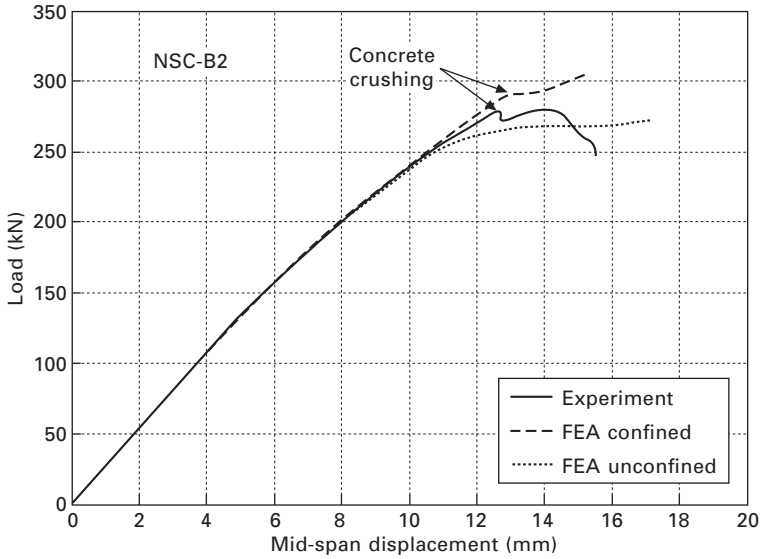

8.16 Comparison of FEA and experimental response of the NSC-B2.

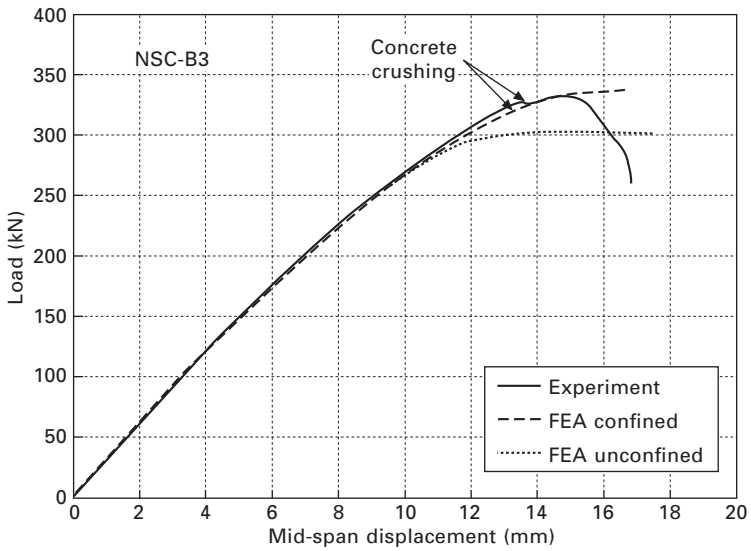

8.17 Comparison of FEA and experimental response of the NSC-B3.

recorded experimental ones. On the other hand, when the confined stress–strain curve is used, the finite element result predicted the concrete crushing and failure loads reasonably well. This indicates that the wrapping does indeed confine the concrete block, and hence provides some extra load-carrying ability.

8.5 Conclusion

The infrastructure market constitutes the most viable option for the composite industry in its push to reduce material costs. Indeed, with considerable potential for composite materials in the automotive and construction industries, the cost of raw material and technologies is likely to decline for all applications. However, this can only be achieved through the development of large-volume automated processes.

One such process is filament winding. It is the process that has benefited most from computer technology and robotics. However, because of its inherent nature, its application in infrastructure on its own is limited to axisymmetric components such as tanks and poles. Nevertheless, some innovative design philosophies have been presented to take advantage of the tension in the fibres. For instance, filament winding induces some confinement, which is very beneficial to concrete as it enhances its strength and stiffness as well as its deformational properties. This last point is particularly important to the construction industry, where design is mainly stiffness driven, and ductility is of paramount importance. Hybrid systems comprising other materials and filament winding can be tailored to address both issues as shown in the reviewed examples.

8.6 References

ABAQUS, 'Abaqus documentation', Version 6.9, 2009, http://www.simulia.com

Aire, C., Gettu, R., and Casas, J.R. (2001), 'Study of the compressive behavior of concrete confined by fiber reinforced composites', *Proc. Int. Conf. on Composites in Constructions*, Balkema, Lisse, Netherlands, 2001, 239–243

Åström, B.T., and Pipes, R.B. (1990), 'Thermoplastic filament winding with on-line impregnation', *J. Thermoplastic Comp. Mater.*, 3, 314–324

Bannister, M. (2001), 'Challenges for composites into the next millennium – a reinforcement perspective', *Composites Part A*, 32, 901–910

Canning, L., Hollaway, L., and Thorne, A.M. (1999), 'Manufacture, testing and numerical analysis of an innovative polymer composite/concrete structural unit', *Proc. Inst. Civ. Engrs Structs & Bldgs*, 134, 231–241

Carreira, D.J., and Chu, K.H. (1985), 'Stress–strain relationship for plain concrete in compression', *ACI J.*, 83(6), 797–804

Chakrabortty, A., Khennane, A., Kayali, O., and Morozov, E. (2011), 'Performance of outside filament wound hybrid FRP-concrete beams', *Composites Part B: Engineering*, 42(4), 907–915

Cohen, D. (1997), 'Influence of filament winding parameters on composite vessel quality and strength', *Composites Part A*, 28A, 1035–1047

Cohen, D., Mantell, S.C., and Zhao, L. (2001), 'The effect of fibre volume fraction on filament wound composite pressure vessel strength', *Composites Part B*, 32B, 413–429

Correia, J.R., Branco, F.A., and Ferreira, J.G. (2007), 'Flexural behaviour of GFRP-concrete hybrid beam with interconnection slip', *Composite Structures*, 77, 66–78

Csuka, B., and Kollar, L.P. (2010), 'FRP-confined circular concrete columns subjected to concentric loading', *J. Reinf. Plast. Comp.*, 29(23), 3504–3520

Deskovic, N., Triantafillou, T.C., and Meier, U. (1995), 'Innovative design of FRP combined with concrete: Short term behaviour', *ASCE J. Struct. Engrg*, 121(7), 1069–1078

Fam, A.Z., and Rizkalla, S.H. (2001), 'Confinement model for axially loaded concrete confined by circular fiber-reinforced polymer tubes', *ACI Struct. J.*, 98(4), 451–461

Farhey, N. (2005), 'Long-term performance monitoring of the Tech 21 all-composite bridge', *ASCE J. Comp. Const.*, 9(3), 255–262

Feng, P., Ye, L., Li, T., and Ma, Q. (2006), 'Outside filament-wound reinforcement: A novel configuration for FRP bridge decks', *Ninth Int. Symp. on Structural Engineering for Young Experts*, 18–21 August 2006, Fuzhou and Xiamen, China

Harries, K.A. (2008), 'FRP components for bridge superstructures – US perspective', *Fourth Int. Conf. on FRP Composites in Civil Engineering*, *CICE2008*, 22–24 July 2008, Zürich, Switzerland (PowerPoint presentation)

Haupert, F., and Friedrich, K. (1995), 'Processing-related consolidation of high speed filament wound continuous fibre/thermoplastic composite rings', *Comp. Manuf.*, 6(3–4), 201–204

Henninger, F., and Friedrich, K. (2002), 'Thermoplastic filament winding with online-impregnation. Part A: Process technology and operating efficiency', *Composites Part A*, 33, 1479–1486

Henninger, F., Hoffmann, J., and Friedrich, K. (2002), 'Thermoplastic filament winding with online-impregnation. Part B: Experimental study of processing parameters', *Composites Part A*, 33, 1677–1688

Khennane, A. (2009), 'Manufacture and testing of a hybrid beam using a pultruded profile and high strength concrete', *Aust. J. Struct. Engrg.,* 10(2), 145–155

Koussios, S. (2004), *Filament Winding: a Unified Approach*, DUP Science, Delft University Press, Delft, Netherlands, ISBN 90–407–2551–9

Lam, L., and Teng, J.G. (2003a), 'Design-oriented stress–strain model for FRP-confined concrete', *Construction and Building Materials*, 17, 471–489

Lam, L., and Teng, J.G. (2003b), 'Design-oriented stress–strain model for FRP-confined concrete in rectangular columns', *J. Reinf. Plast. Comp.*, 22(13), 1149–1186

Lauke, B., and Friedrich, K. (1993), 'Evaluation of processing parameters of thermoplastic composites fabricated by filament winding', *Comp. Manuf.*, 4(2), 93–101

Mertiny, P., and Ellyin, F. (2002), 'Influence of the filament winding tension on physical and mechanical properties of reinforced composites', *Composites Part A*, 33, 1615–1622

Milkovich, S. (1994), 'Infrastructure applications of composite materials', http://iti.acns.nwu.edu/projects/milk.html (accessed 2002)

Neely, W.D., Cousins, T.E., and Lesko, J.J. (2004), 'Evaluation of in-service performance of Tom's Creek bridge fiber-reinforced polymer superstructure', *ASCE J. Perf. Const. Facilities*, 18(3), 147–158

Parsons, I.D., White, S., Therriault, D., and Bignell, J. (2002), 'Manufacture and testing of a filament wound composite bridge superstructure', Final Report for Highway IDEA Project 63, Transportation Research Board, Washington DC http://www.nationalacademies.org/trb/idea

Päßler, M., and Schledjewski, R. (2012), 'Filament winding with increased efficiency', Institut für Verbundwerkstoffe GmbH, Kaiserslautern, Germany, www.ivw.uni-kl.de (accessed 2012)

Pessiki, S., Harries, K.A., Kestner, J.T., Sause, R., and Ricles, J.M. (2001), 'Axial

behavior of reinforced concrete columns confined with FRP jackets', *J. Comp. Const.*, 5(4), 237–245

Richart, F.E., Brandtzaeg, A., and Brown, R.L. (1929), 'The failure of plain and spirally reinforced concrete in compression', *University of Illinois Bulletin,* No. 190.

Scholliers, J., and Van Brussel, H. (1994), 'Computer-integrated filament winding: Computer-integrated design, robotic filament winding and robotic quality control', *Comp. Manuf.,* 5(1), 15–23

Shehata, I.A.E.M., Carneiro, L.A.V., and Shehata, L.C.D. (2002), 'Strength of short concrete columns confined with CFRP sheets', *Mater. Struct.*, 35, 50–58

Teng, J.G., Huang, Y.L., Lam, L., and Ye, L.P. (2007), 'Theoretical model for fiber reinforced polymer-confined concrete', *J. Comp. Const.*, 11(2), 201–210

Toutanji, H.A. (1999), 'Stress–strain characteristics of concrete columns externally confined with advanced fiber composite sheets', *ACI Mater. J.*, 96(3), 397–404

van Erp, G.M., Heldt, T.J., Cattell, C.L., and Marsh, R. (2002), 'A new approach to fibre composite bridge structures', *17th Australasian Conference on the Mechanics of Structures and Materials, ACMSM17*, Gold Coast, Queensland, Australia, 12–14, 2002. pp. 37–45

Williams, B., Shehata, E., and Rizkalla, S.H. (2003), 'Filament-wound glass fiber reinforced polymer bridge deck modules', *J. Comp. Const.*, 7(3), 266–273

Xiao, Y., and Wu, H. (2003), 'Compressive behavior of concrete confined by various types of FRP composite jackets', *J. Reinf. Plast. Comp.*, 22(3), 1187–1201

Zhao, L., Burgueño, R., Rovere, H.L., Seible, F., and Karbhari, V. (2000), 'Preliminary evaluation of the hybrid tube bridge system, Report TR-2000/04', Final Test Report submitted to California Department of Transportation under Contract No. 59AO032, San Diego, CA.

9

Pultrusion of advanced fibre-reinforced polymer (FRP) composites

J. RAMÔA CORREIA, Technical University of Lisbon, Portugal

DOI: 10.1533/9780857098641.2.207

Abstract: This chapter focuses on the properties, manufacturing processes and quality control of pultruded advanced composites used in civil engineering applications. Pultrusion technology is first briefly explained, with the main features of the raw materials used being introduced, and the philosophy underlying the development of pultruded advanced composites discussed. A detailed description of the pultrusion process then follows, covering the equipment and procedure, technical specifications and quality control. Subsequently, the types, properties, applications and sustainability of pultruded profiles, reinforcing bars and strengthening strips are described. The final part of the chapter discusses future trends for the pultrusion of the advanced composites used in civil engineering applications.

Key words: pultrusion, FRP profiles, FRP reinforcing bars, FRP strengthening strips.

9.1 Introduction

Pultrusion is a manufacturing process that converts fibre reinforcements and resin matrices into finished composite parts. Unlike other processes, pultrusion enables continuous production in a highly automated and low-labour process that uses a heated die to give shape to the composite part. These features mean that, of the different manufacturing processes developed in the last five decades, pultrusion offers the best productivity/cost ratio (Zureick and Scott, 2000).

The pultrusion manufacturing process was originally developed in the USA during the 1950s by Goldsworthy. In the early days, pultrusion was used to produce fishing rods, ski poles and golf course flag staffs, most often combining polyester resins and glass fibre rovings. The pioneering machines used then were rather different from those used today; some had a vertical design comprising an intermittent pulling mechanism (Starr and Ketel, 2000).

Since then, pultrusion technology has developed in several ways, not only in the process itself but also in the raw materials used, in particular fibre reinforcements and polymeric matrices. New types and more complex arrangements of reinforcements were introduced in the process, together with

new matrix systems, including a wide range of fillers and additives. The size and complexity of the pultruded cross-sections has evolved considerably and the composites industry is now producing a range of pultruded parts that are being used in several civil engineering applications.

The initial interest of the construction industry in composite materials dates back to the 1950s, when several dozen prototype houses were built (e.g., the Monsanto House of the Future (Phillips, 2004)), but these pioneering applications were soon abandoned for both technical and economic reasons. At the beginning of the 1980s the civil engineering industry started looking at fibre-reinforced polymer (FRP) materials with a resurgent interest, which stemmed not only from the development of the composites industry but also from the durability problems experienced by traditional materials (reinforced concrete and steel), the need for higher construction speeds and increasing functionality demands.

Since then, the pultrusion industry has been offering a response to those requirements by producing FRP materials which have high mechanical performance, but which are at the same time lighter, less prone to the degradation caused by aggressive environmental agents, and requiring less maintenance during service life, when compared to traditional materials. This chapter focuses on the properties, manufacturing processes and quality control of pultruded advanced composites used in civil engineering applications. Section 9.2 provides a brief overview of the pultrusion manufacturing process and briefly discusses the philosophy underlying the development of pultruded advanced composites. Section 9.3 describes the main features of the raw materials used in the pultrusion process, namely the fibre reinforcements and the polymeric matrixes. Section 9.4 presents the equipment that comprises a pultrusion line, describes the pultrusion process in detail, including a brief description of variants to the standard pultrusion process. Sections 9.5 and 9.6 cover the technical specifications of the pultrusion process and the quality control procedures applicable to incoming raw materials, the manufacturing process itself and the finished part, respectively. Section 9.7 addresses the joining technologies available to connect pultruded components, in particular FRP pultruded profiles. Section 9.8 describes the main features of the most frequently used pultruded composites in civil engineering applications: profiles, reinforcing bars and strengthening strips. Section 9.9 presents the most relevant physical and mechanical properties of those types of pultruded components, whereas Section 9.10 illustrates their most frequent applications. Section 9.11 presents a brief discussion about the sustainability of pultruded advanced composites in what concerns their production phase, service life and end of the life cycle. Finally, Section 9.12 presents the main conclusions of the chapter and discusses future trends for pultruded composites in civil engineering, in terms of constituent materials, manufacturing process, structural shapes and regulation.

9.2 Overview of the pultrusion process

Pultrusion is a process of continuous production of composite parts with constant cross-section. Being highly automated and requiring very little labour, it is particularly suited to the mass production of advanced composites, providing high raw material conversion efficiency (Shaw-Stewart and Sumerak, 2000). Pultrusion can produce a wide range of shapes including rebars, laminates and different types of profiles with either open (such as I, H, L or U) or closed-form cross-sections (tubular, both circular and square), including multi-cellular panels. The total length of the pultruded elements is basically limited by transportation constraints.

Standard pultrusion can generally be considered to be divided in two phases. In the first phase, the fibre reinforcement, in its various forms (*cf.* Section 9.3.1), is pulled through a bath where it is impregnated with the liquid polymeric matrix. In the second phase, the wetted reinforcement is pulled through forming guides into a heated mould in the shape of the cross-section to be produced. Here, the polymeric matrix cures due to the heat of the die, resulting in a composite part of predetermined geometry. Because fibres are pulled during the manufacturing process, for similar reinforcements the resulting strength of pultruded parts is typically higher than that obtained with other composite processing methods.

The performance of FRP pultruded composites greatly depends on the characteristics of their constituent materials (particularly the mechanical properties of the fibres and the matrix), on the composition and arrangement of the reinforcing fibres (i.e. their type, length, orientation and architecture) and also on the interaction between the fibres and the matrix, i.e. the fibre–matrix bonding.

The product development of pultruded composites offers an enormous diversity of possibilities, since a wide variety of resins, additives and fillers can be combined for use in the matrix, with several reinforcing fibres (type, content, orientation, architecture). The philosophy underlying the development of FRPs has been to design materials for specific requirements (such as mechanical performance, lightness and chemical resistance) through a judicious combination of the above-mentioned constituent materials.

It is precisely this design approach that has been used to produce a wide range of composite materials for structural applications. They have been used in various fields of application, each with its own particular requirements. One example of this tailor-made design is the production of FRP pultruded profiles with vinylester resin (instead of the standard polyester) for more aggressive environments. Likewise, the use of vinylester in the matrix of FRP pultruded bars stems from its increased resistance in alkaline environments such as concrete. Finally, stiffness can be increased by adding carbon fibres to the flanges of conventional GFRP profiles – the hybrid C/GFRP double web profiles produced by Strongwell are an example.

9.3 Fibre reinforcements and matrices used in the pultrusion of advanced composites

As with other manufacturing processes, advanced composite materials produced by pultrusion are constituted by two phases:

- The fibre reinforcement, responsible for the mechanical performance and providing most of the strength and stiffness
- The polymeric matrix, which acts as the 'glue' of the pultruded part, guaranteeing the load transfer between the fibres and also between the applied loads and the composite itself.

9.3.1 Types and properties of fibre reinforcements

The fibres most commonly used in the pultrusion of advanced composites are glass and carbon, with aramid being used only in a limited number of applications. The physical, mechanical and thermal properties of these fibres are presented in Table 9.1.

Glass fibres, used in glass fibre reinforced polymer (GFRP) pultruded profiles and bars (*cf.* Section 9.8), are the most common in civil engineering applications because they combine high strength with relatively low cost. Their main disadvantages are their relatively low elasticity modulus, their reduced long-term strength (due to susceptibility to stress rupture), and also their reduced resistance to moisture and alkaline environments (Keller, 2003). All the different types of glass fibre available (with the designations E, S, AR and C), have the same elasticity modulus, in spite of differing in terms

Table 9.1 Typical properties of most common fibres used in pultruded advanced composites

Property	Test standards	E–glass	Carbon	Aramid
Density (g/cm^3)	ISO 1889, ISO 10119, ASTM D 1577	2.6	1.7–1.9	1.4
Thermal expansion coefficient (10^{-6}/K)	ISO 7991	5.0–6.0	Axial: –1.3 to 0.1 Radial: 18.0	–3.5
Fibre diameter (μm)	ISO 1888, ISO 11567	3–13	6–7	12
Fibre structure	–	Isotropic	Anisotropic	Anisotropic
Tensile strength (MPa)	ISO 5079, ISO 11566, ASTM C 1557, ASTM D 2343, ASTM D 3379	2350–4600	2600–3600	2800–4100
Tensile modulus (GPa)		73–88	200–400	70–190
Tensile ultimate strain (%)		2.5–4.5	0.6–1.5	2.0–4.0

of strength and durability. The standard E-glass fibres are by far the most widely used, accounting for 80–90% of the FRP products commercialised (ACI Committee 440, 1996). S-fibres have better mechanical resistance but are considerably more expensive (three to four times) than E-glass fibres and so are used mainly in the aerospace industry. AR fibres, with increased zirconia content, have an improved resistance to alkalis and may be used in cementitious composites such as glass fibre reinforced concrete. C-glass fibres are more corrosion resistant (Barbero, 1998) but are not much used in civil engineering applications.

Carbon fibres, used in carbon fibre reinforced polymer (CFRP) pultruded strips, exhibit high tensile strength and elasticity modulus, high fatigue and creep resistance, excellent chemical resistance and low self-weight. The main disadvantages of carbon fibres are that they are relatively expensive and require large amounts of energy in their production (Keller, 2003). In addition to the standard carbon fibres, known as standard modulus (whose properties are listed in Table 9.1), carbon fibres can also be produced to higher grades, known as intermediate modulus, high modulus and ultra-high modulus (Bank, 2006).

Aramid fibres present very high tensile strength (on average, higher than that of carbon and E-glass) and exhibit an intermediate elasticity modulus, about 50% higher than that of E-glass (Busel and Lockwood, 2000). Furthermore, these fibres have very good tenacity and toughness properties that make them attractive for industrial products where energy absorption is needed (Bank, 2006). However, aramid fibres have relatively low compressive strength (500–1000 MPa) and reduced long-term strength due to stress rupture, and they are very sensitive to UV radiation (Keller, 2003), which lowers their potential for FRP parts used in civil engineering applications.

The above fibre reinforcements are available in several forms that include almost parallel bundles of continuous filaments, either untwisted (rovings) or twisted (yarns), and short fibres (chopped) with a length of 3 mm to 50 mm (Keller, 2003). For use in pultrusion, fibre reinforcements can be worked to obtain textile products with several reinforcing directions. There are, therefore, several products available, either with randomly oriented fibres, which can be short (chopped strand mat) or continuous (continuous strand mat), or with oriented reinforcements (such as woven and non-woven fabrics, stitched fabrics, grids and meshes), which can be biaxial (0°/90° or +45°/–45°) or triaxial (0°/+45°/–45°), the latter being considerably more expensive and less widely used in pultrusion. All these forms can be further combined to make complex textile products with continuous oriented fibres, together with randomly oriented short or continuous fibres. Figure 9.1 shows examples of forms of fibre reinforcement.

Most fibre reinforcements receive a surface chemical treatment with a sizing substance (usually starch, oil or wax), which acts as a lubricant

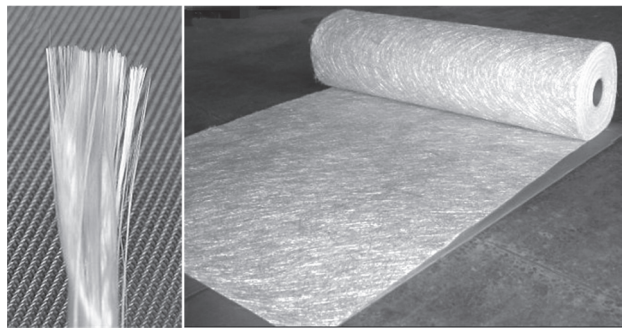

(a) (b)

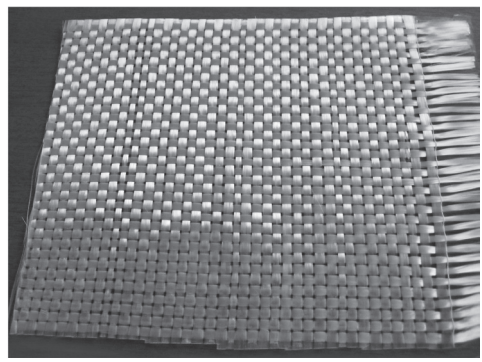

(c)

9.1 (a–c) Examples of available forms of fibre reinforcements.

and antistatic agent to protect the fibres against damage during pultrusion processing. Resinous binders are also used to help a bundle of fibres to stick together as a unit. Furthermore, surface treatment incorporates a coupling agent that promotes bonding between the fibres and the matrix. For glass fibres, the sizing also protects against moisture degradation during service life (Barbero, 1998).

9.3.2 Matrix systems

Although fibre reinforcements are responsible for most of the mechanical performance of pultruded composites, the polymeric matrices must be able to bear some of the loads, particularly those in the transverse direction and shear stresses. Furthermore, the polymeric matrix has four essential functions (Keller, 2003):

- Holding the fibres in the intended position
- Ensuring the load transfer between the fibres
- Preventing fibres from buckling when loaded in compression

- Protecting the fibres from environmental degradation agents.

In addition to the base resin, the polymeric matrices of pultruded composites contain supplementary constituents (polymerisation agents, fillers and additives), used to induce the polymerisation reaction, to improve the material processing, to modify the properties of the final FRP product or simply to reduce the cost of the part produced.

Polymeric resins

Polymeric resins are divided into thermosetting resins and thermoplastic resins, depending on how the polymer chains are connected when the polymer is in its solid form. Thermosetting resins are formed through a polymerisation chemical reaction in the presence of heat, during which an amorphous three-dimensional cross-linked molecular structure is formed. As a result of its own irreversible nature, once cured, thermosetting resins become infusible and so they cannot be reprocessed or welded. Thermosetting resins have low viscosity, which enables high processing speeds. Furthermore, they have good fibre impregnation capacity and very good adhesive properties.

Thermoplastic resins are not cross-linked; their molecular chains are held together by weak van der Waals forces or by hydrogen bonds and do not undergo any chemical change during processing. Thermoplastics can be recycled and reprocessed since they do not form an irreversible structure. However, besides being more difficult to process than thermosets because of their higher viscosity, thermoplastics exhibit worse properties of impregnation and adhesion to the fibres.

The resins used in the pultrusion of FRP composites must be selected according to four basic requirements (Moschiar *et al.*, 1998):

- Adequate viscosity (values between 500 and 2000 cP are recommended) to ensure good fibre wet-out
- Long pot life to guarantee that pultrusion can be operated for a long time
- High reactivity, so that fabrication in the die takes a short time
- Good wetting capacity to maximise mechanical properties.

The previously described properties of the resin types make thermosetting resins much more useful for civil engineering structural applications, and in fact they have been used in almost all commercially available FRP pultruded products. Table 9.2 presents the basic properties of the thermoset resins most commonly used in pultrusion: polyester, vinylester, epoxy and phenolic.

Polyester resins exhibit a good balance of their properties (mechanical, durability), dimensional stability, ease of processing due to the reduced viscosity (typically varying between 200 and 2000 cP (ACI Committee 440, 1996)) and reasonable pot life, and a relatively low cost. For these reasons,

Table 9.2 Typical properties of most common thermoset resins used in pultruded advanced composites

Property	Test standards	Polyester	Epoxy	Vinylester	Phenolic
Density (g/cm^3)	ISO 1183, ASTM D 1505	1.20–1.30	1.20–1.30	1.12–1.16	1.00–1.25
Glass transition temperature (°C)	ISO 11357–2, ISO 11359–2, ASTM E 1356, ASTM E 1640	70–120	100–270	102–150	260
Tensile strength (MPa)	ISO 527 ASTM D 638	20–70	60–80	68–82	30–50
Tensile modulus (GPa)		2.0–3.0	2.0–4.0	3.5	3.6
Tensile ultimate strain (%)		1.0–5.0	1.0–8.0	3.0–4.0	1.8–2.5

polyester accounts for approximately 75% of the resins presently used (Busel and Lockwood, 2000), and polyester resins are found in most FRP profiles and also in some FRP bars.

Epoxy resins are normally used together with carbon fibres in applications requiring high-performance materials in terms of strength, stiffness, service temperature and durability, especially in CFRP strips used in structural strengthening. Epoxy resins are more difficult to process than polyester resins due to their higher viscosity and shorter pot life; in addition they require a longer curing and tend to stick to the pultrusion die much more than polyester. However, epoxies exhibit considerably lower shrinkage than polyesters (1.2–4.0% against 8.0%, respectively), which explains their excellent adhesive properties, and they offer better environmental durability (Barbero, 1998; Bank, 2006).

Vinylester resins were developed from the other two resins to combine the improved properties of epoxy with the easier processing of polyester. As a consequence the cost of vinylester resins is a compromise between that of the epoxy and polyester resins. When improved durability is sought for FRP materials, vinylester may be preferred to polyester and today the former resins are used to make most of the commercially available FRP pultruded bars (Bank, 2006). Several FRP profiles are also available in vinylester resin.

Compared with the other thermosetting resins, phenolic resins are much less flammable and produce less smoke when submitted to fire or intense heat. Furthermore, these resins are relatively inexpensive, have good dimensional stability and retain their adhesive properties at relatively higher temperatures. However, with typical viscosity ranging from 2000 to 5000 cP (Bogner *et al.*, 2000), phenolics are much more difficult to reinforce and cure than other thermosets. Slower processing speeds are required and the water released due to polycondensation has to be properly eliminated, otherwise the bond with the fibre reinforcement will be affected. Furthermore, these resins are a brownish colour and are difficult to pigment (Bank, 2006). Because of

these difficulties, and although they are very often used in other industries, phenolics are seldom used in civil engineering structural applications.

Polymerisation agents

Polymerisation agents are used to induce the initiation of the base resin polymerisation reaction. With polyester and vinylester resins, organic peroxides (activated by heat) are typically used in quantities ranging from 0.25% to 1.50%, by weight of the resin to initiate the curing reaction. The polymerisation of epoxy resins is triggered by adding curing agents (amines, acid anhydrides and Lewis acids), often called hardeners, which are generally applied in quantities varying from 25% to 50% by weight of the resin (Bank, 2006).

Fillers

Fillers are inorganic particulates used in the polymeric matrix, both to reduce the final product cost and to improve material processing and certain properties of the pultruded part. Among the most currently used fillers are calcium carbonate, aluminium silicate (cauline), alumina trihydrate (ATH) and calcium sulphate.

Fillers may improve the fire reaction performance of pultruded composites by reducing the organic content of the matrix (e.g. ATH and calcium sulphate reduce flammability and smoke production). Furthermore, fillers may help to reduce matrix shrinkage and improve its dimensional stability, thereby preventing the development of cracking in discontinuity zones or parts with excessive resin content. Several other properties can also be improved by adding fillers to the matrix, such as the hardness, the fatigue resistance and the creep behaviour. Although some improvements may be achieved by using fillers in the resin system, it is important to bear in mind that their incorporation usually decreases the main mechanical properties and the corrosion resistance of FRP pultruded composites.

The use of fillers in non-structural FRP materials may account for as much as 40–65% of their total weight (Busel and Lockwood, 2000). However, standard pultruded FRP profiles and bars have only 10–30% by weight of filler in the matrix. Small pultruded parts, including mainly unidirectional reinforcement, usually contain less than 5% filler, while FRP strips generally do not have any (Bank, 2006).

Additives

There is a wide variety of additives that can be incorporated in the matrix to facilitate the material processing, to improve the performance of the final

product or simply to modify certain properties. The objectives usually defined include the following (Busel and Lockwood, 2000):

- Reduction of flammability and smoke production when submitted to fire – flame retardant additives are used (e.g., antimony trioxide, phosphorus compounds, aluminium trihydroxide, magnesium hydroxide, zinc borates)
- Inhibition of polymer oxidation – antioxidants
- Reduction of shrinkage – low-profile or shrink additives (usually thermoplastic polymers dissolved in styrene)
- Increase of electrical conductivity (metal and/or carbon particles) and electromagnetic interference (conductive materials)
- Increase of toughness (rubber or other elastomeric materials)
- Reduction of the tendency to attract electrical charge – antistatic agents
- Promotion of cellular structure, reducing density, cost of materials and shrinkage and improving the electrical and thermal insulation – foaming agents
- Prevention of gloss loss, discolouration, cracking or disintegration due to UV radiation – UV stabilisers
- Acquisition of a certain colour – pigments or colourants
- Facilitation of removal from moulds – release agents (most often metallic stearates, fatty acids or waxes).

Additives are used in much smaller amounts than fillers, typically less than 1% by weight of the resin. However, it must be taken into consideration that incorporating even small amounts of additives in the matrix system may also notably change the physical and mechanical properties of the final FRP product.

9.4 Pultrusion line equipment and manufacturing processes

Figure 9.2 presents a scheme of a traditional pultrusion assembly line, where six key elements can be distinguished:

- A set of spools stacked on creels
- Forming and preforming guides
- Resin impregnation system
- Forming and curing die
- Pulling system
- Cutting system.

Downstream along the production line, the rovings and mats are dispensed from a set of spools, stacked on metal racks or creels (Fig. 9.3(a)). The

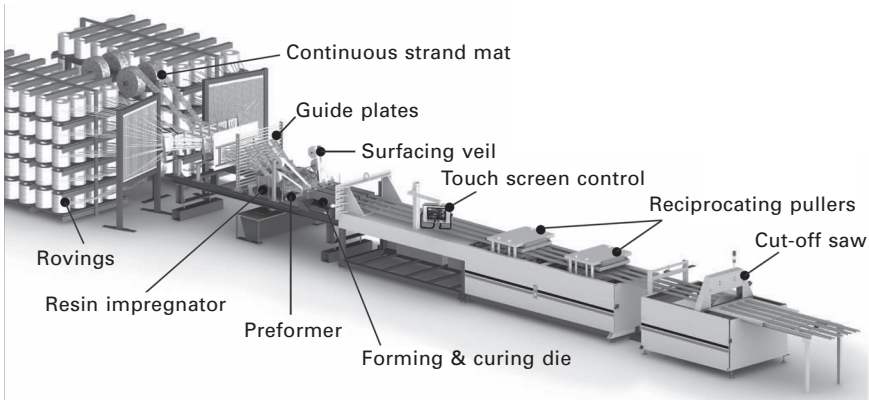

9.2 Pultrusion assembly line (courtesy of Strongwell).

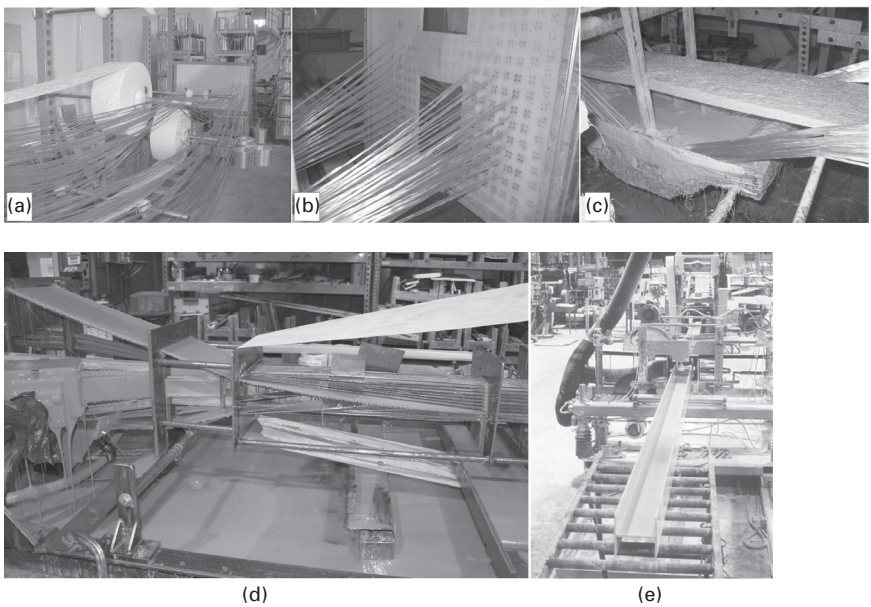

9.3 Different stages of the pultrusion process: (a) creel and mat racks for fibre handling; (b) orifice plate; (c) open bath (courtesy of ALTO); (d) preforming guides; (e) cutting system (courtesy of Strongwell).

metal creels used for fibre reinforcement handling are available in two basic configurations: table or bookshelf, the latter being more commonly used. Creels provide the initial tension and define a position from which the fibres can feed the pultrusion process. The creels must also enable spool replacement so as to ensure continuous production. Rovings can be spliced by different methods (Owens Corning, 2003), which include:

- Knots (although simple, may give rise to surface defects or breakouts in the process)
- Air splicer equipment
- Chemical adhesives
- Wrap splices.

Reinforcing mats can be spliced by inserting the tapered end of a new roll on the split tail of the old one and sewing.

The fibre reinforcement architecture (position and alignment) of a pultruded part is defined by a guiding system that consists of contact points (ceramic guidance 'eyes') and orifice plates that are usually made of polished or chromed steel or high-quality polyethylene in order not to damage the fibre reinforcement.

Resin impregnation systems are used to wet-out the fibre reinforcement. Traditional pultrusion lines comprise open baths (charged either manually or with automatic pumps), along which the reinforcement travels, over and under a series of rollers, and are impregnated with the polymeric matrix. Roving bundles are spread through guides that break them apart to allow better impregnation. The main problem of open bath systems is the evaporation of solvents (styrene) from the matrix, which raises both environmental and health concerns. After exiting the bath, the excess resin is removed when the fibres pass through the preforming guides (Fig. 9.3(b)) and is recirculated back to the open bath via a drip collection tray. When very thick composite parts are to be produced, the curing process can be improved and higher line speeds permitted if the resin and/or the impregnated fibre reinforcement is heated by means of radio-frequency and microwave before it enters the mould (Moschiar *et al.*, 1998).

In modern pultrusion machines, which are becoming more common, instead of an open bath system the dry reinforcements enter an injection chamber (which is frequently an integral part of the die), where they are impregnated with the polymeric matrix, delivered under pressure. Resin injection systems enable more accurate control of the reinforcement position, which provides greater material uniformity, and allow a higher degree of fibre impregnation. Furthermore, changes in the composition of the matrix are more rapidly introduced during the manufacturing process. Finally, resin injection reduces the evaporation of solvents from the matrix, which makes for a healthier work environment. These advantages are at the expense of higher installation and operation costs.

Regardless of the impregnation process, as the wet reinforcement travels through the die, which is heated electrically or by hot oil, the matrix is cured at very high temperatures. The curing of polyester and vinylester resins starts when the decomposition temperature of the peroxide is reached, progressing from the mould's surfaces to the centre of the part to be produced. The resin progressively changes from liquid to gel and finally to solid. As a consequence

of the curing process the composite part shrinks and separates from the internal walls of the die, exiting it as a finished product, with dimensional stability. The inner dimensions of the die often decrease gradually over its length; they are greatest at the opening. In order to withstand the repeated cycles of heating and cooling, wear abrasion and assembly and disassembly operations, the die is usually made of high-grade tool steel with a protective surface treatment (hard chrome plating or ion nitriding). Dies can be fashioned either as a single piece (less expensive, avoiding parting lines) or as multiple pieces (easier to clean and maintain). The production of tubular profiles requires a mandrel (multiple ones in the case of multicellular sections), which is usually installed with a supporting framework fastened to the entrance of the die and cantilevered along its entire length (Shaw-Stewart and Sumerak, 2000).

The cured part is generally pulled by means of urethane pads (formed to match the contour of the pultruded part being pulled) that apply a uniform clamp load, using either a caterpillar belt, or reciprocating pullers synchronised by the control system of the machine to provide a constant speed. At the end of the assembly line, an automated, moving, diamond-tipped cut-off saw is used to obtain pre-set lengths of the product (Fig. 9.3(c)). Provided the saw moves at the same speed as the pultruded part, the cut edge is straight and square and the manufacturing process does not have to be stopped.

Some pultrusion lines include dust extraction systems for reasons of both environment and tidiness; take-off systems that are used to handle and store the produced parts; and/or tunnel heaters used for post-die curing operations that improve the physical and mechanical properties of pultruded parts.

9.4.1 Variant processes

Two variants of the pultrusion process described above are:

- Pullwinding
- Pulforming.

The pullwinding technology was developed to produce tubular shapes. It basically combines standard pultrusion and continuous filament winding (Shaw-Stewart, 1988). The latter technique is added in-line with standard pultrusion equipment, making use of spools of fibre and winding them around a mandrel according to a predefined angle, prior to being pulled through the die. Most typical configurations of composite parts produced by pullwinding combine continuous longitudinal fibres (from pultrusion), which provide axial and flexural resistance, with hoop-wound continuous fibres (from winding), which provide hoop, shear and torsion strength.

The pulforming technology was developed (Goldsworthy, 1986) to produce both straight and curved parts with possible local cross-sectional changes.

It basically combines pultrusion and compression moulding. In one of the possible variations of the pulforming process, after exiting the pultrusion die the partially cured parts can be placed into moulds (negatives) which impart the designed shape. Here the cross-section can be locally changed and a curved shape can be formed by means of a rotating table with curved moulds positioned around its periphery. The curvature and/or cross-section change can be made by forcing and squeezing the part into the mould cavities using a die shoe.

9.5 Technical specifications

Regarding the plant layout, it is recommended that a pultrusion line has a minimum length of 25 m (30 to 38 m is preferable) in order to accommodate the creels, the pultrusion machine and the finished parts (Owens Corning, 2003). The width × height (the 'pulling envelope') of pultrusion machines may vary between 0.25×0.125 m^2 and 1.30×0.35 m^2 (Shaw-Stewart and Sumerak, 2000), and a free width of 1.2 m on each side of the machine is normally required.

The die is usually between 0.5 m and 1.5 m long. The polymeric matrix is cured at temperatures that mostly range from 90°C to 180°C, and depend on the resin system used (among other factors). The proper definition of temperatures at different locations along the die helps to optimise curing conditions and prevents thermal residual stresses from developing.

Pull-off forces typically vary between 30 kN and 235 kN (Shaw-Stewart and Sumerak, 2000) and the pultrusion speed varies between 0.02 and 3.0 m/min, depending on the type of machine used, the wall thickness and the complexity of the cross-section and fibre architecture. In general, mechanical properties increase with decreasing pulling speed, basically because the resin stays longer in the die at slower speeds, and achieves a higher degree of polymerisation. Cross-sections made up of thicker laminates must be produced at slower speeds so that the matrix cures properly inside the die. Thermoplastic matrices allow much faster production and speeds of up to 20 m/min have been recorded (Devlin *et al.*, 1991).

In terms of geometry of the pultruded parts, there is no theoretical limit for their length. Practical limitations are related to the plant layout and transportation requirements, which often means setting the maximum length of pultruded profiles and bars at 12 m. CFRP strips, which are very thin and flexible, are usually coiled onto long spools containing several dozen metres of material.

As already mentioned, for conventional pultrusion the composite part must have constant cross-section throughout its length (*cf.* Section 9.4.1 for variant processes). The maximum width of conventional pultruded parts is about 1500 mm and the maximum height is 350 mm. Wall thickness tends to range

between about 1.2 mm and 30 mm (Evans, 2000), but in some applications it can be as high as 60 mm. In transition zones such as web–flange junctions, radii between 0.5 and 2 mm are required and part thickness must be kept constant in order to avoid resin-rich regions.

Pultruded composites can be produced in a large variety of colours, basically in line with the RAL classic chart, using colouring additives. However, completely homogeneous pigmentation is not always possible since glass reinforcement has no pigment tolerance (Barefoot, 2007).

9.6 Quality control

This section presents some basic quality control procedures for the manufacturing process of pultruded advanced composites. The following three aspects of quality control are addressed:

- Incoming raw materials
- Manufacturing process
- Finished part.

Quality control procedures during execution on site are not covered.

Incoming raw materials, specifically the matrix constituents and the fibre rovings and mats, should be inspected. Basic inspection includes checking the delivery notes and the labels of containers when the materials arrive. Visual inspection of raw materials is also recommended: resins can be inspected for colour and the presence of contamination and gel particles (Evans, 2000); reinforcements can be checked for the presence of knots in the rovings, while simple mass measurements can be made for mats or fabrics. Some pultrusion companies have quality control and/or research and development laboratories where material characterisation tests can be performed (most often such control is executed by raw material suppliers). Fibre reinforcements can be subjected to tensile tests. The moisture content of the constituents (particularly the reinforcements and the fillers) can also be determined. The quality of incoming resins can be tested by means of thermal analysers (resin reactivity) and viscometers (resin viscosity and thixotropic index) (Owens Corning, 2003).

During the manufacturing process, quality control can include the visual checking of the components of the pultrusion line (creels, forming or preforming guides, resin bath), and the monitoring of several process parameters, as follows (Harper, 2006; Sumerak and Taymourian, 1989; Sumerak and Martin, 1991):

- Ambient temperature and humidity
- Temperature of the wet bath
- Temperature control at different points inside the die, together with the

evolution of material temperature along the die (with thermocouples)
- Machine speed
- Clamping and pulling forces (with load cells)
- Resin injection pressure and flow (when resin injection systems are used)
- Product length, to avoid wrong cut-off length.

Quality control of pultruded parts produced can be implemented according to a recognised quality control scheme and may be documented in the form of a certificate of conformity. This can include both the general obligatory properties according to a specific standard (e.g. EN 13706-2,3 (CEN, 2002)) and extra properties agreed with the customer. At this stage, quality control should address the following aspects: visual defects, dimensional tolerances, and mechanical properties.

Several defects of pultruded parts can be inspected visually. Annex A of the EN 13706-2 standard specifies the definition and the acceptance levels of the following defects, which are assessed by the unaided eye at a distance of about 0.5 m (CEN, 2002): blister, crack, crater, delamination, die parting line, dullness, exposed underlayer, fibre prominence, folded reinforcement, fracture, grooving, inclusion, internal dry fibre, internal shrinkage cracks, internal porosity (voids), surface porosity (voids), resin-rich area, saw burn, scale, stop mark, undercure and wrinkle depression. The same is recommended in the ASTM D4385 (ASTM, 2010) standard for thermosetting reinforced plastic pultruded rods, bars, shapes and sheets, in which different inspection requirements are specified for three grades of product quality.

In terms of cross-section geometry, Annex A of EN 13706-2 (CEN, 2002) specifies dimensional tolerances for the following geometrical parameters: wall thickness of open and closed profiles, flatness in the transverse direction, profile height and width of flange, size of angle, straightness and twist. Similar specifications are set out in the ASTM D3917 (ASTM, 2011) standard for standard rods, bars and pultruded shapes made of thermosetting glass-reinforced plastics.

Several pultrusion companies use Barcol hardness testers to assess the degree of cure of the produced parts. This enables the tracing of products with insufficient degree of cure of the resin matrix, which leads to lower mechanical performance. The quality control of pultruded produced parts can also include other mechanical characterisation tests which can sometimes be carried out in the laboratory facilities of pultrusion companies. EN 13706-3 (CEN, 2002) defines two grades of FRP pultruded profiles, specifying minimum values for material properties and the relevant test methods. The requirements for certain applications (e.g. petroleum and natural gas industries) can be stricter and often include aspects related to fire reaction and fire resistance behaviour, e.g. NBR 15708-1 (ABNT, 2011).

9.7 Joining technologies

FRP elements have to be connected to one another, since shape sizes are limited by production constraints and there are size limitations associated with transportation and handling operations. Connections of FRP pultruded profiles are divided into the following categories:

- Bolted
- Bonded
- Mixed (bolted and bonded)
- Interlocked
- Welded.

Mechanical fastening, adhesive bonding and combinations thereof are the most common techniques for joining FRP pultruded profiles (Zhou and Keller, 2005).

As with the structural shapes of first-generation profiles (see Section 9.8.1), which mimic the geometry of structural steel cross-sections, so the current practice of bolting FRP structural elements copies the constructive details of steel construction (Fig. 9.4). In most cases, this direct knowledge transfer of connection technology leads to oversized FRP components, since it does not consider the different behaviours of the two materials. In fact, the linear–elastic behaviour of FRP profiles is incompatible with plastic deformations and so the stress concentrations around the bolt holes are higher than those

(a) (b)

9.4 Bolted connections between GFRP profiles of (a) three-dimensional frame (courtesy of Strongwell) and (b) pedestrian bridge (courtesy of Fiberline Composites).

developed in steel, which exhibits a ductile behaviour. Furthermore, there are constraints associated with the anisotropic behaviour of the FRP profiles, since the development of transverse stresses is inevitable. As a consequence, the overall design is often governed by the load-bearing capacity of bolted connections, leading to uneconomical cross-section selection.

Adhesively bonded connections are used less often, for the following reasons: difficulty in ensuring the necessary quality control conditions, particularly on site; relatively high thickness of the FRP adherends; poor design guidance; doubts about long-term durability; and concerns about behaviour at high temperature. Nevertheless, adhesive bonding has been found to be much better adapted to the brittle and anisotropic nature of FRP materials, as it provides a smoother and more uniform load transfer. Furthermore, compared to bolting, adhesively bonded connections provide higher joint efficiency and stiffness, the latter being especially important with regard to the stiffness-governed design of structures composed of GFRP components. At the same time, bonded joints are lighter and do not require drilled holes, which facilitate the ingress of moisture in service conditions. Adhesively bonded connections have been used mainly in bridge decks to join adjacent GFRP panels (Fig. 9.5) and also to join these panels to the longitudinal girders. Adhesive bonding has also been used to assemble standard sections and thus create more complex sections than those currently provided by manufacturers.

The use of mixed connections, in which the stiffness is provided mainly by the adhesive, may be justifiable in one of the following situations: when bolts are likely to prevent the effects of a deficient bonding execution or adhesive deterioration during service life; when bonding is expected to help

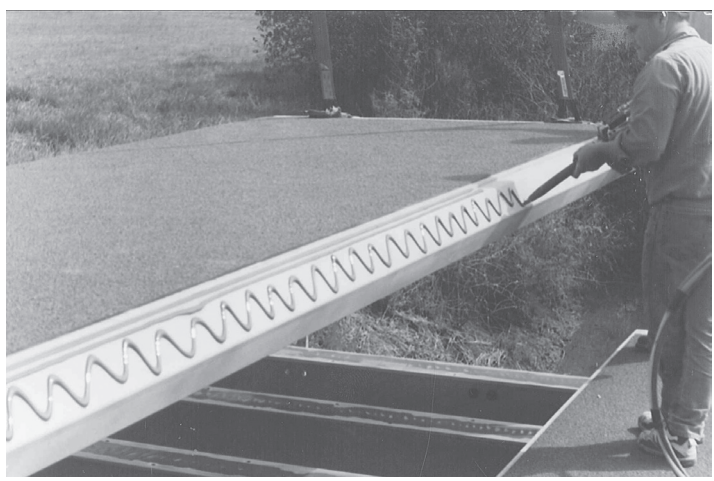

9.5 Bonded connections between GFRP panels of bridge decks (courtesy of Creative Pultrusions).

meet deformability requirements (bolts may fulfil strength requirements); or when the bonding performance is expected to be improved with the clamping pressure applied in the bolts.

In interlocking connections, the FRP materials are joined with a grooving and friction mechanism, which can be supplemented with bolting and/or bonding. This modular construction system leads to very quick erection times, since the connections are very easy to execute, but it involves a high dimensional precision of the geometry of the FRP components. The ACCS (Advanced Composite Construction System), developed by Maunsells Structural Plastic Ltd and used in several pedestrian bridge decks, is an example of such a connection method, in which plank units (multi-cellular box sections) are assembled by sliding a toggle section into the groove of each panel (Fig. 9.6). Another example is the snap-fit pultruded panel more recently developed by Kookmin Composite Infrastructure, Inc., also used in several pedestrian bridges (Fig. 9.7).

From a conceptual point of view, welded connections seem to be the most suitable method to join composite materials, with potential economic and technical advantages. However, the use of this technique is restricted to FRP materials containing thermoplastic resins which, as previously discussed, are more limited technically than thermoset resins (in terms of fibre adhesion and impregnation, processing and mechanical properties). Therefore, this technique is not often used in civil engineering applications.

9.8 Types of pultruded advanced composites

Pultruded advanced composites used in civil engineering applications are manufactured in three basic structural shapes (Bakis *et al.*, 2000; Hollaway, 2010):

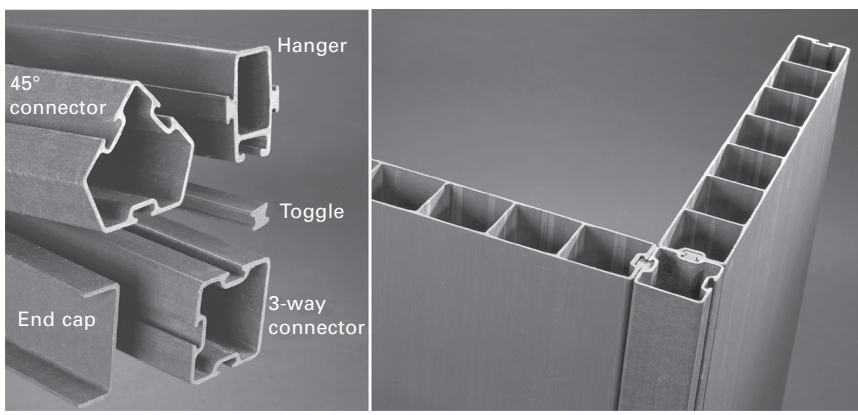

9.6 Interlocking connections in the Advanced Composite Construction System (ACCS) (courtesy of Strongwell).

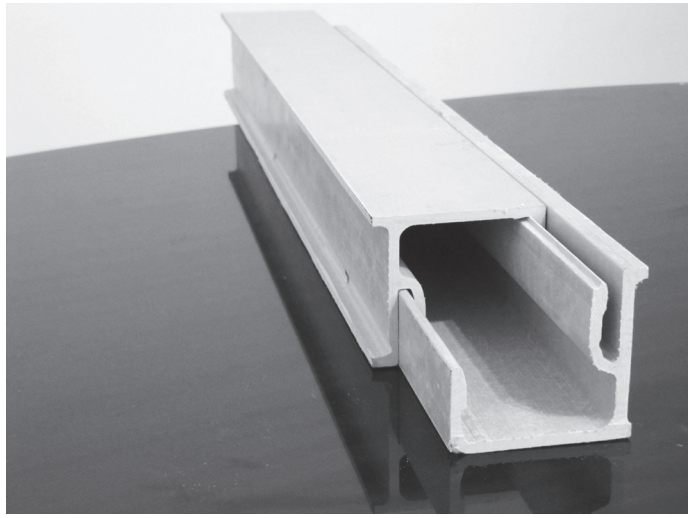

9.7 Interlocking connections in Delta Deck (Kookmin Composite Infrastructure, Inc.).

- Profiles
- Reinforcing bars
- Strengthening strips.

9.8.1 Profiles

Until quite recently, the structural shapes of pultruded profiles have been copied from steel construction, usually reproducing thin-walled open (I, H, L, C) or tubular (square, rectangular, circular) cross-sections. Figure 9.8 shows the most typical shapes of the so-called *first-generation profiles*, which are normally composed of glass fibres embedded in polyester or vinylester based resin matrix – GFRP pultruded profiles.

Figure 9.9 schematically presents the fibre architecture of the laminates that constitute the above-mentioned cross-sections of GFRP profiles. Typical architecture comprises alternating layers of rovings, to provide axial reinforcement, and mats that provide reinforcement in the transverse direction, and also to shear loading. Surface veils (thin chopped strand mats, containing short and randomly oriented glass or polyester fibres) are often positioned at the surface of the laminates. The superficial layer of the composite laminate will then exhibit increased resin content, which provides additional protection against environmental agents and creates a smooth surface finish.

Although the above shapes are used in the majority of structural applications of GFRP profiles, these first-generation shapes have several disadvantages that are essentially related to their sensitivity to impact and their stability

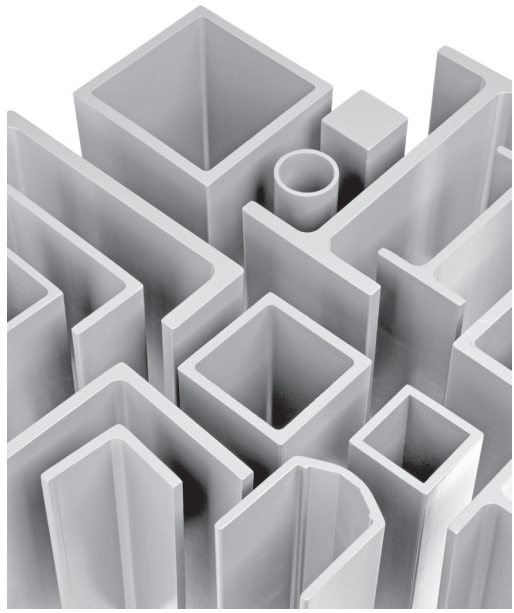

9.8 Typical shapes of the first-generation profiles (courtesy of Fiberline).

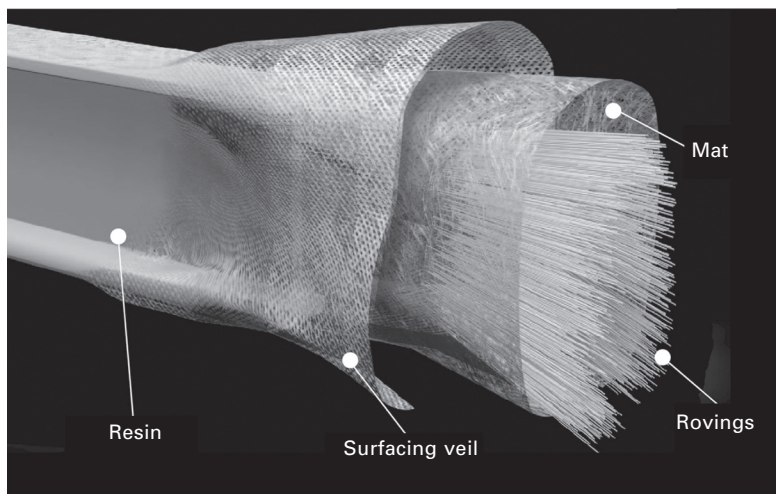

9.9 Typical fibre architecture of the laminates of pultruded profiles (courtesy of Strongwell).

when submitted to compression loads. In particular, the flanges/webs of columns or the flanges of beams often buckle well before the resistance capacity of the material is reached, which prevents the efficient exploitation

of the material's properties for most applications. Material-adapted forms are therefore needed to make better use of the GFRP pultruded material.

The use of a new structural material with shapes similar to the traditional material that it intends to replace is nothing new in the history of construction. According to Keller (1999), before the development of material-adapted forms, adapted to the specific properties of a new material, there is usually a substitution phase, firstly for technical reasons, since the material-adapted forms are simply not known, and secondly for commercial reasons, because the 'copy' induces confidence in users.

Nevertheless, several manufacturing companies have already developed *new structural systems*, which seem to be better adapted to the specific properties of FRP materials. These systems basically consist of multi-cellular pultruded panels, which can be joined together by adhesive bonding, snap-fit or fit- and -groove systems. These structural systems have been used mainly in bridge decks (Fig. 9.10), either in new construction or to replace degraded bridge decks. As they are significantly lighter than traditional solutions, these new systems lead to substantial savings in column and foundation costs and simultaneously enable higher live load levels.

9.8.2 Reinforcing bars

Commercially available pultruded bars are made of glass, carbon or aramid fibres, oriented in the axial direction and embedded in a polymeric matrix, usually made of vinylester or epoxy resin. The FRP bars most often used in civil engineering applications combine vinylester and glass fibres.

Off-the shelf FRP bars have nominal diameters of between 6 mm and 36 mm and lengths that typically vary between 10 m and 14 m. With respect to their surface, FRP bars can be produced with the following finishings

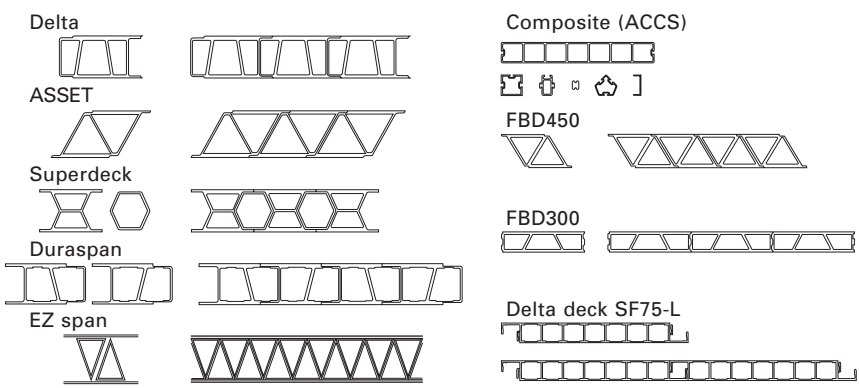

9.10 Pultruded bridge deck systems (adapted from Keller, 2002).

(textures): (i) smooth; (ii) surface formed deformations or ribs[1]; (iii) sand coatings; and (iv) exterior wound fibres, usually with additional sand coatings. The type of finishing or deformation system and the corresponding surface roughness are very important parameters in several applications, since they will strongly affect the mechanical adherence or bond of the FRP bar to the reinforced material.

In addition to straight FRP bars, produced by standard pultrusion and used in the reinforcement to axial stresses, straight bars with anchorage heads and bent bars (U-shaped) for shear reinforcement are also available (Fig. 9.11). In this last configuration, bars are bent in the pultrusion plant while the resin matrix is still uncured. Once the resin cures the bars cannot be bent or unbent, either mechanically or with heat (the latter operation would cause decomposition of the bars' resin).

9.8.3 Strengthening strips

Commercially available pultruded strips for strengthening existing structures consist of carbon or glass fibres, embedded in an epoxy or vinylester resin matrix. Most civil engineering applications make use of strengthening strips made of unidirectional carbon fibres in an epoxy matrix – CFRP strips (Fig. 9.12). CFRP strips are produced with very thin thicknesses that are generally between 1.0 mm and 2.0 mm, and with widths ranging from 50 mm to 100 mm. Standard CFRP strips with a flat cross-section are supplied in long coils and are bonded to the surface of the element to be strengthened – the externally bonded technique (EBR). CFRP strips can also be installed in grooves created in the surface of the elements to be strengthened – near surface mounted (NSM) – and in this technique the width of the strips typically varies between 3 mm and 20 mm. In addition to current strips with flat cross-section, some manufacturers also produce L-shaped strips for shear strengthening and shell segments for column/pile strengthening.

9.11 Different geometries of FRP bars: (a) straight bar; (b) bar with anchorage head; (c) bent bar (courtesy of Schöck).

[1]The ribs are cut into the hardened bars immediately after they exit the heated die, in an operation called profiling.

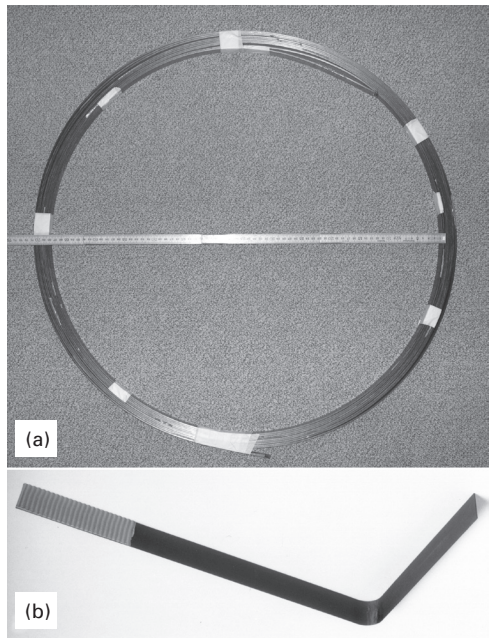

9.12 Different geometries of CFRP strips: (a) straight (roll) and (b) L-shaped (courtesy of Sika).

9.9 Properties of pultruded advanced composites

9.9.1 Profiles

The properties of FRP pultruded profiles, like all advanced composites, depend essentially on the characteristics of their constituent materials (the type, content and architecture of fibres, and the nature of the polymeric matrix) and also on the fibre–matrix interaction. Taking into consideration the numerous possibilities of combining those elements, together with the fact that FRP profiles marketed by the main manufacturers are not standardised, it is only possible to refer to typical ranges of variation for their properties. Table 9.3 lists the usual variation ranges for the most important physical and mechanical properties of GFRP profiles. According to Bank (2006), these properties tend to be based on small-scale coupon testing and correspond to a lower bound for each type of profile indicated in manufacturers' manuals. Those documents do not provide other data that would allow the statistical distributions of those properties to be determined.

Regarding the thermo-physical properties of GFRP profiles, the following behavioural aspects are outlined: (i) reduced self-weight, about four to five times less than that of steel (the main competitor within structural materials), which facilitates transport and handling operations on site; (ii) thermal

Table 9.3 Typical physical and mechanical properties of GFRP pultruded profiles

Property	Test standards	Pultrusion direction		Transverse direction
Density (g/cm^3)	ISO 1183, ASTM D 792		1.5–2.0	
Fibre content (%)	ISO 1172, ASTM D 3171		50–70	
Thermal expansion coefficient (10^{-6}/K)	ISO 11359–2, ASTM D 696	8–14		16–22
Thermal conductivity coefficient (W/m.K)	ISO 22007, ASTM D 5930		0.20–0.58	
Tensile strength (MPa)	ISO 527, ASTM D 638	200–400		50–60
Compressive strength (MPa)	ISO 14126, ASTM D 695	200–400		70–140
Shear strength (MPa)	ISO 14129, ASTM D3846		25–30	
Elasticity modulus (GPa)	ISO 527 EN 13706–2	20–40		5–9
Shear modulus (GPa)	ISO 14129 EN 13706–2		3–4	

expansion coefficient similar to steel; (iii) very reduced thermal conductivity coefficient, significantly lower than that of steel; and (iv) electro-magnetic transparency.

In terms of mechanical behaviour, GFRP profiles exhibit a linear-elastic stress–strain relationship until failure (typical of FRP composites), which contrasts with the ductile behaviour of steel. It should be noted that, given the previously shown internal constitution of the laminates, the material exhibits an anisotropic behaviour, with higher mechanical properties in the axial pultrusion direction, along which rovings are aligned, than in any other direction.[2] The tensile strength in the axial direction of GFRP profiles is higher than that of most structural steel grades, but the elasticity modulus is relatively low, about 10–20% that of steel. This results in increased deformability, to which the shear deformation may also make an important

[2]As mentioned earlier, the mechanical properties of GFRP profiles produced by the biggest manufacturers may exhibit considerable differences. In this context, in 2002, CEN published the European Standard EN 13706 (CEN, 2002), which defines the specifications for pultruded profiles. This standard establishes the test methods to determine several material properties (mechanical, physical and thermal), and it further defines two grades of profiles, specifying the minimum material properties a profile has to exhibit in order to be included in those grades.

contribution, especially in non-slender elements. In addition, for long-term deflections, the viscoelastic nature of the material has to be taken into account (Sá *et al.*, 2011a, 2011b). The design of GFRP profiles is actually often driven by serviceability requirements rather than by strength limitations. Furthermore, the low elasticity modulus is also responsible for an increased susceptibility to instability phenomena in slender members (Correia *et al.*, 2011a; Silva *et al.*, 2011).

Regarding their long-term performance, FRP profiles are non-corrodible and require very low maintenance, particularly when compared with steel. In fact, there is practical evidence of improved performance of FRP composites when submitted to several types of aggressive environments (Karbhari *et al.*, 2003). But laboratory studies show that the performance of FRP profiles is affected by several environmental agents, particularly moisture and thermal effects, so there is a need for a proper resin selection at the design stage (Schutte, 1994; Liao *et al.*, 1998; Karbhari, 2007; Cabral-Fonseca *et al.*, 2012). Another aspect that raises justifiable concerns, particularly for building applications, is the fire behaviour of FRP profiles (Mouritz and Gibson, 2006). Recent studies have shown that due to its combustible nature and the fact that mechanical properties are greatly reduced when the material is heated to moderately high temperatures (100–200°C), fire reaction (Correia *et al.*, 2010a) and fire resistance restrictions for building applications may only be fulfilled if active and/or passive fire protection systems are used (Keller *et al.*, 2006; Correia *et al.*, 2010b).

9.9.2 Reinforcing bars

Table 9.4 presents typical ranges of variation for several physical and mechanical properties of FRP bars made of glass (GFRP), carbon (CFRP) and aramid (AFRP) reinforcement. For the typical fibre content, all FRP reinforcing bars present low density, about one-sixth to one-quarter that of steel bars (again, the main competitor), which facilitates transport and

Table 9.4 Typical physical and mechanical properties of FRP reinforcing bars

Property		Test standards	GFRP	CFRP	AFRP
Density (g/cm^3)		ISO 1183, ASTM D 792	1.25–2.10	1.50–1.60	1.25–1.40
Fibre content (%)		ISO 1172, ASTM D 3171	50–60	50–60	–
Thermal expansion coefficient (10^{-6}/°C)	Axial	ISO 11359–2, ASTM D 696	6.0–10.0	–9.0 to 0.0	–6.0 to–2.0
	Transversal		21.0–23.0	74.0–104.0	60.0–80.0
Axial tensile strength (MPa)		ISO 527, ASTM D 7205	483–1600	600–3690	1720–2540
Axial elasticity modulus (GPa)			35–51	120–580	41–125
Axial ultimate strain (%)			1.2–3.1	0.5–1.7	1.9–4.4

handling operations on site. The thermal expansion coefficients of FRP bars are different in the axial and transverse directions, depending essentially on the fibres (axial) and the resin (transverse). It is also worth mentioning that the thermal expansion coefficients in the axial direction of CFRP and AFRP bars are negative.

Mechanical properties depend mainly on the type and content of the fibre reinforcement, and are also influenced by the type of curing and quality control during manufacturing. But, unlike steel, the strength of an FRP bar can vary considerably with the diameter, especially in GFRP bars. Therefore, manufacturers usually specify values of mechanical properties for all diameters commercialised.

With respect to the mechanical behaviour in tension, for all types of reinforcing fibres, FRP bars show very high tensile strengths (much higher than for current steel bars) and exhibit linear elastic behaviour up to failure without any ductility. The elasticity modulus is very much dependent on the type of fibre. For GFRP bars, the most widely used in civil engineering applications, the elasticity modulus is only about 20–30% that of steel. Therefore, when designing concrete members reinforced with GFRP bars for service limit states, the consequences of such reduced stiffness on deformability and crack pattern have to be duly taken into account.

In general, the elasticity modulus and the strength of FRP bars in compression seem to be significantly lower than their counterparts in tension, particularly for GFRP and AFRP bars. For that reason, and also because only a limited number of studies have been performed on the compressive behaviour of FRP bars, their use in columns or as compression reinforcement of members in flexure is not recommended (ACI Committee 440, 2006).

Most FRP bars exhibit relatively low interlaminar shear strength, as there is generally no reinforcement between layers of axial fibres. Therefore, the performance of FRP bars for shear loads relies mainly on the matrix properties. Shear resistance can be improved by braiding or winding fibres in the transverse direction of the bar or by introducing continuous strand mats in the fibre architecture (ACI Committee 440, 2006).

When FRP bars are used to reinforce concrete structures, a critical issue is the bond performance, which depends on several aspects such as the mechanical properties of the bar and its surface roughness. In this regard, some FRP bars now exhibit very similar bond performance to steel bars (Schöck, 2005).

In long-term applications and when subjected to constant loads, FRP bars are susceptible to creep rupture. This phenomenon, which does not occur in steel rebars, depends on the load level, environmental conditions and type of fibre reinforcement, with carbon fibres being the least and glass fibres the most susceptible (ACI Committee 440, 2006). Also regarding their long-term performance, like FRP pultruded profiles FRP bars do not corrode and are

electromagnetically transparent. However, numerous studies have shown that their mechanical performance may be affected by moisture, alkaline, acid or saline solutions (Nkurunziza *et al.*, 2005). Like FRP profiles, the mechanical performance of FRP bars is greatly reduced at high temperatures, raising a concern when FRP reinforced members have to be designed for fire (Nigro *et al.*, 2011).

9.9.3 Strengthening strips

As already mentioned, in most civil engineering strengthening applications, FRP strips are composed of carbon fibres embedded in epoxy resin. Table 9.5 presents typical ranges of variation for the physical and mechanical properties of CFRP strips. Compared to the alternative traditional strengthening solutions of concrete jacketing and, particularly, steel plate bonding (the main competitor), the main advantages of CFRP strips are very high tensile strength, high stiffness, comparable to steel, relatively high deformation capacity, lightness, which facilitates on-site application, reduces labour costs and lessens the increase of weight in the structure to be strengthened, and finally non-corrodibility.

However, CFRP strengthening systems have certain limitations (some of them similar to those already described for FRP profiles and bars, intrinsic to their nature):

- Linear-elastic behaviour up to failure, which can limit the ductility of the strengthened element
- Limited exploitation of material performance due to the occurrence of premature adherence failure mechanisms, which can be prevented to some extent by using anchorage devices

Table 9.5 Typical physical and mechanical properties of CFRP strengthening strips

Property	Test standards	Standard modulus	High modulus	Ultra-high modulus
Density (g/cm^3)	ISO 1183, ASTM D 792	1.50–1.60	1.50–1.60	1.50–1.60
Fibre content (%)	ISO 1172, ASTM D 3171	65–70	65–70	65–70
Nominal thickness (mm)	–	1.2–1.9	1.2–1.4	1.4
Width (mm)	–	50–120	50–120	50
Axial tensile strength (MPa)	ISO 527, ASTM D 638, ASTM D7565	2690–2800	1290–2800	1800
Axial elasticity modulus (GPa)		155–165	210–300	400
Axial ultimate strain (%)		1.8	1.35	0.45

- The strength, stiffness and bond properties of CFRP systems are severely deteriorated at moderately elevated temperatures – if the strengthening systems are to be exploited when designing for the fire load combination, appropriate thermal insulation is needed (Williams *et al.*, 2008; Ahmed and Kodur, 2011; Firmo *et al.*, 2012).

9.10 Applications of pultruded advanced composites

9.10.1 Profiles

FRP pultruded profiles were first used essentially in non-structural elements or in secondary structures, in applications requiring some of their potential advantages over traditional materials, such as being lightweight, showing durability in aggressive environments or having electromagnetic transparency. These advantages determined their use in diverse areas which included basic sanitation, water and waste treatment plants, the fishing industry, ports, the petrochemicals industry, thermo-electrical plants and railway transportation.

For these applications in non-structural elements or secondary structures, the pultrusion industry developed a wide variety of products made of GFRP profiles (Fig. 9.13) that included cable pathways, garden benches, doors and gates, insulated ladders with cages, banisters, stairways with handrails, gratings and plank systems for flooring, working platforms and walkways and building façade panels.

Even though they are still used far more often in non-structural elements or in secondary structures, important applications of GFRP profiles in primary structures have also started to be developed in recent years. These applications, which were initially instigated under pilot and/or research projects but are now finding their own way, concern both pedestrian and vehicular bridges, as well as buildings (Figs 9.14 and 9.15).

In addition to new construction, GFRP profiles are also being used in the rehabilitation of degraded constructions. Several bridge decks have already been replaced using the different deck systems shown in Fig. 9.10. In these solutions, the FRP bridge deck is typically bolted, bonded or dowelled to supporting longitudinal girders, as illustrated in Figs 9.16 and 9.17. These decks have greatly reduced self-weight (about 20% of a comparable concrete deck (Keller, 2002)) and improved durability and fatigue strength. They are easy to maintain and require very short installation times with minimum traffic interruption.

The use of GFRP pultruded shapes (using either profiles or deck systems) also seems to have a great potential to replace the degraded timber flooring of buildings located in old districts. In this specific application, the use of the traditional steel profiles or reinforced concrete elements is usually either

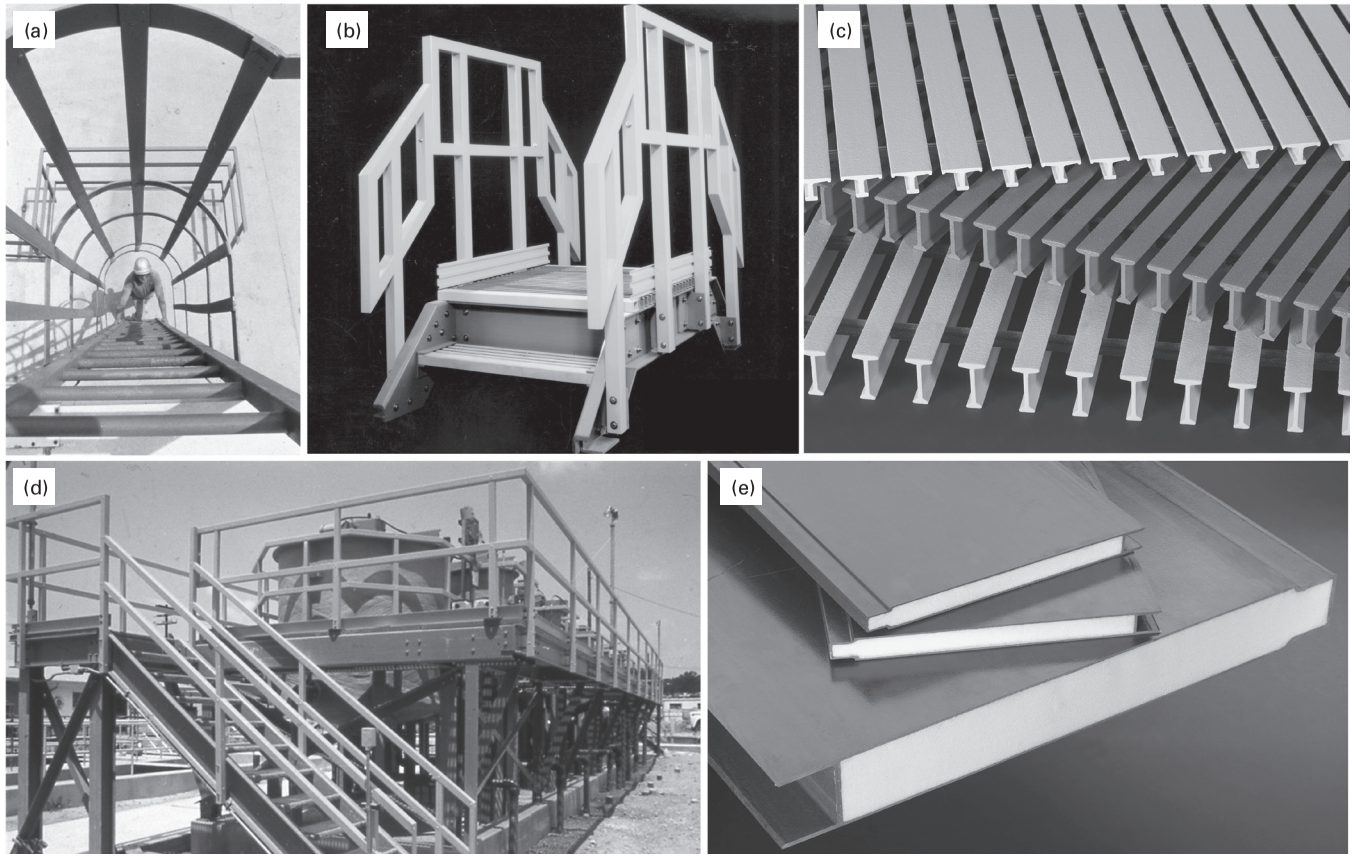

9.13 Examples of GFRP pultruded products for non-structural applications and secondary structures: (a) insulated ladders; (b) stairways with handrails; (c) floor gratings; (d) working platforms and walkways; (e) building façade panels (courtesy of Strongwell).

9.14 Lleida Bridge (courtesy of Juan Sobrino/Pedelta).

9.15 Eyecatcher building (courtesy of Thomas Keller).

not possible, due to accessibility limitations (usually it is not possible to install a crane or other lifting devices), or at least very problematic because of the constraints associated with the extra self-weight added to the existing elements of the construction.

9.10.2 Reinforcing bars

The non-corrodibility and the lack of electromagnetic interference, together with the high tensile strength, have been the main factors determining the use of FRP bars instead of steel bars. FRP bars have thus been essentially

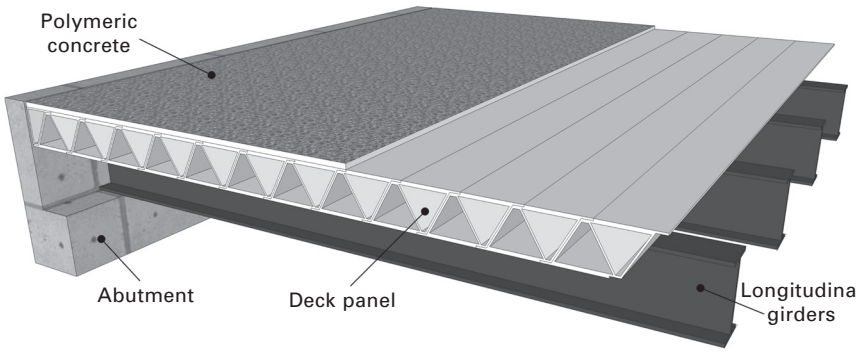

9.16 Scheme of the ASSET bridge deck system (adapted from Hollaway, 2003).

9.17 Installation of Superdeck bridge deck (courtesy of Creative Pultrusions).

used to reinforce concrete structures in maritime environments (e.g. piers), bridge decks or other structures subjected to the effect of de-icing salts, waste water treatment plants and structures enclosing equipment sensitive to electromagnetic fields, such as MRI facilities. Another field of application with some potential is underground or buried structures, where FRP bars have been used in tunnelling works (e.g. shaft walls) and retention walls (Fig. 9.18). Besides exhibiting improved corrosion resistance, the lifting and handling of FRP rebar cages is much easier than for steel ones. FRP bars also facilitate drilling operations for tunnels as they are easier to cut.

The above applications generally make use of GFRP bars, basically

(a) (b)

(c)

9.18 Application of FRP bars in the reinforcement of (a) bridge deck, Canada; (b) fish farm inlet to sea, Portugal; (c) tunnel soft eye, Belgium (courtesy of Hughes Brothers).

because they are cheaper than other types of FRP bars. CFRP bars have been used mainly in external prestressing or as strengthening elements applied according to the NSM technique, described earlier. In addition to concrete reinforcement, FRP bars have also been used in the rehabilitation of masonry and timber structural elements. As an example, GFRP bars are being increasingly used in connections (prostheses) between timber parts, fixed with epoxy resin.

In the commonest applications, the reinforcement of concrete members, FRP bars are used in roughly the same way as conventional steel bars for both handling and placement operations. Several documents (e.g. ACI 440.1R-06 (ACI Committee 440, 2006), FIB Bulletin 40 (FIB, 2007) and CAN/CSA

S806-02 (CSA, 2002)) provide guidance on the delivery, storage, handling, permitted damage tolerances, bar supports, placement tolerances and concrete cover. When needed, FRP bars can be cut with diamond blades, grinders or fine-blade saws. As already mentioned, bending operations on site are simply not possible. Therefore, the anchorages at the extremities of the rebars are often made with prefabricated hooks which overlap the longitudinal rebars. Non-metal fixings or ties are recommended (e.g. plastic-coated tie wire, nylon zip ties or plastic bar clips).

9.10.3 Strengthening strips

The use of FRP strips to strengthen existing structures is already a well-established technique with considerable commercial success in the area of rehabilitation. There are countless examples of their use in bridges and buildings, with the objective of increasing the load capacity for both static and dynamic loads (usually associated with seismic retrofitting).

Among the many structural elements that can be rehabilitated with FRP strips are beams, slabs, columns, walls, chimneys, arches, domes and tunnels. FRP strips have been used to strengthen several types of materials, among which are reinforced concrete, masonry, timber, steel and iron.

Most applications involve using CFRP strips in reinforced concrete with the following purposes: flexural strengthening of beams and slabs (Fig. 9.19); shear strengthening of beams; and axial/flexural strengthening of columns. CFRP strengthening strips are normally bonded to the external surface of the element to be strengthened with a thin layer (approximately 2 mm thick) of epoxy adhesive (the EBR technique). The surface of the substrate needs to be previously roughened to guarantee the effectiveness of the strengthening system. Manufacturers have developed several anchorage mechanisms to prevent premature debonding at the ends. In a newer alternative technique

(a) (b)

9.19 Flexural strengthening with CFRP strips of reinforced concrete (a) beam and (b) slab (prestressed strips; courtesy of S&P Clever Reinforcement).

(NSM), CFRP strips (or bars) are installed into a slot that is saw-cut to the surface of the element to be strengthened and filled with epoxy adhesive or mortar. Several documents (e.g. ACI 440.2R-08 (ACI Committee 440, 2008), FIB Bulletin 14 (FIB, 2001) and CAN/CSA S806-02 (CSA, 2002)) provide detailed guidance on the application of FRP strengthening systems.

9.11 Sustainability of pultruded advanced composites

As with other construction materials, the sustainability of pultruded advanced composites has to be analysed with respect to the different phases of their life cycle:

- The production phase
- The service life
- The end of the life cycle.

Here, it is important to consider first the environmental effects associated with producing the material, taking into account the acquisition of raw materials, the energy needed for production and any industrial waste. Then, the material use during service life, with special reference to the maintenance requirements, the long-term durability and the energy consumption, also have to be borne in mind. Finally, one has to evaluate the options at the end of the life cycle which, in decreasing order of preference, are reuse, recycling, incineration and landfill.

Concerning the production phase, it should first be noted that the resins used today are by-products of the oil industry, and the quantities needed, even if the demand for FRP materials increased considerably, would still be negligible compared to the total consumption of fossil fuels. Secondly, with respect to the fibre reinforcements, glass fibres are obtained from quartz powder and limestone, which are basically inexhaustible resources. Furthermore, an important part of the raw material can be obtained from recycled glass. Finally, it is also important to mention that GFRP pultruded composites require only one-quarter and one-sixth of the energy needed to produce steel and aluminium, respectively (Keller, 2003). The production of CFRP pultruded composites, however, requires much more energy, basically due to the significant amount of energy needed to produce carbon fibres.

With regard to the service life use, FRP pultruded composites are more environmentally friendly than most traditional materials; they need very little maintenance and, as previously discussed, exhibit improved durability even in relatively harsh environments. Furthermore, when used in building applications, the low thermal conductivity of FRPs may be associated with potential energy savings (the Eyecatcher Building stands as an example of this advantage).

Presently, the main limitation of FRP advanced composites, in terms of sustainability, arises at the end of the life cycle and has to do with the limited waste management possibilities, since thermosetting resins (by far the most commonly used for infrastructure applications), once polymerised, can no longer be reprocessed. This means that the most common option at the end of the service life is to process the FRP materials to granulates, which are then used as landfill material.

Most FRP waste is deconstruction waste, with only very low volumes arising from production waste (often resulting from trimming dust, defective items and trial runs) and building site waste (typically off-cuts) (Conroy et al., 2006). Although current volumes of FRP waste are still minimal when compared to other materials,[3] the volumes of FRP waste are expected to increase eventually, and impending European legislation on construction and demolition waste will increase landfill taxes, thereby discouraging disposal and promoting reuse and recycling. In several EU countries it is already illegal to landfill composite waste.

The practical possibilities of reuse (which is a highly rated solution in the waste hierarchy) are very limited at the present time. This is because FRP materials are often made to order and are thus usually designed for a particular application, so they do not conform to standardised shapes or material properties. The reuse of FRP pultruded members, in particular, seems quite unlikely owing to the difficulties of recalculating the residual mechanical properties and of reliably assessing material degradation or creep effects (Conroy *et al.*, 2006).

Although thermosetting resins are not recyclable, several technologies have been developed for recycling thermoset composite materials. These can be divided into two groups: mechanical recycling techniques, using mechanical comminution techniques to reduce the size of the scrap to produce recyclates; and thermal recycling techniques, which use thermal processes to break the scrap down into material and energy (fibre recovery techniques, burning in cement kilns or simple material incineration). Pickering (2006) has presented a comprehensive overview of such techniques.

With regard to the recyclates obtained from mechanical recycling, the following applications have already been investigated: replacement of filler in new thermoset compounds; incorporation in thermoplastic matrices; manufacturing of plastic lumber; reinforcement of wood particle boards; and production of road asphalt and concrete (Correia *et al.*, 2011b). Although the incorporation of recyclates in these applications may be interesting from a technical point of view, the commercial prospects are still to be achieved.

[3]According to Pickering (2006), approximately 1 million tonnes of composites are manufactured each year in Europe.

The main limitations are an insufficient throughput supply, the cost of the recyclates and the lack of developed markets (Pickering, 2006).

According to Keller (2003), the development of thermoplastic resins, presently ongoing, will enable FRP materials to be used at least as sustainably as traditional construction materials (concrete, steel and timber). These resins not only are recyclable but have already been shown to retain most of their mechanical properties after recycling (Vijay *et al.*, 2000).

9.12 Conclusion and future trends

Pultrusion technology is a well-developed method of producing advanced composite parts. The manufacturing process enables the continuous and ready conversion of fibre reinforcements and resin matrices into different types of composite parts, with very little labour and high raw material conversion, which results in competitive costs, a key factor for civil engineering applications. Among the composite parts produced by pultrusion are pultruded profiles, reinforcing bars and strengthening strips. All these advanced composites are being increasingly used in civil engineering applications to replace traditional materials, owing to their high strength-to-weight ratio, lightness, non-corrodibility, electromagnetic transparency and low maintenance.

It is envisaged that the interest in pultruded composites in the civil engineering industry will continue to grow in the years to come, especially in the rehabilitation sector, for which these products are particularly well suited. In addition, the reluctance of construction agents is expected to fade to a certain extent because some of these pultruded products already have a consistent history of application behind them and, furthermore, technical specifications and official design standards are progressively being released. Two more driving factors are the education of civil engineering agents and, of equal relevance, the capacity of the pultrusion industry to manufacture at increasingly competitive costs.

This section briefly discusses some of the possible future trends for the pultrusion of advanced composites used in civil engineering applications. Possible developments in the following topics are addressed:

- Constituent materials
- Manufacturing processes
- Structural shapes
- Technical specifications and design codes.

In terms of constituent materials, new types and forms of fibre reinforcements are likely to be introduced. In relation to this it is worth mentioning basalt fibres as an emerging alternative to the reinforcement of FRP pultruded composites. Although the manufacturing cost of basalt fibres currently exceeds that of E-glass fibres (Ross, 2006), the mechanical properties of

the former (strength and stiffness) are considerably higher (Lopresto *et al.*, 2011), in particular at high temperature, and they show improved alkaline resistance (Sim *et al.*, 2005). A future trend may also be the development of hybridised reinforcements, combining various types of fibres in different zones of the pultruded parts according to their requirements (this technique is already used today, but to a very limited degree). Fibre architecture used in pultruded parts is also likely to show considerable progress (Goldsworthy, 2000), especially in relation to the development of affordable techniques of introducing off-axis reinforcements and shifting the reinforcement planes along the length of pultruded parts. Such achievements would increase shear, interlaminar shear and off-axis strength, which are among the chief weaknesses of pultruded parts at present.

The pultrusion industry is undertaking extensive research and development regarding the introduction of polyurethane resin systems in standard pultrusion (e.g. Sumerak and Troutman, 2007; Connolly *et al.*, 2006). The following potential advantages are expected: improved matrix strength and toughness, and reduction or elimination of continuous strand mat. The main challenge of this innovation concerns the reactivity of polyurethane resins, which is difficult to deal with when producing large, heavy, wall profiles. The introduction of thermoplastic resins in the matrix of FRP pultruded parts is another promising future trend, provided that present processing and reinforcing problems are solved. If successful this will have advantages in terms of production costs (thermoplastic resins are generally less expensive and allow much faster production), work environment (elimination of emissions), connection technology (welding technique) and also in terms of sustainability (recycling prospects).

Another expected trend is the introduction of nanosized particles in the polymeric matrix to improve certain properties of pultruded parts, particularly the mechanical performance (Thunhorst *et al.*, 2011), corrosion resistance (Won *et al.*, 2012) and flammability (Ushakov *et al.*, 2009).

Regarding the manufacturing processes, according to Goldsworthy (2000), few changes to the standard pultrusion process are expected in the near future. Most of the potential adaptations are related to developments in the constituent materials, especially the fibre reinforcement architectures and the types of resin. The introduction of thermoplastic resins may require long pre-heating ovens (Goldsworthy, 2000). Traditional resin baths will continue to be replaced by resin injection systems, not only to improve the fibre wet-out, which is quite challenging in thicker pultruded parts, but also to improve health conditions at pultrusion plants.

In order to overcome some of the present limitations of pultruded parts, material-adapted forms will continue to be developed, optimising the material properties of FRP composites, with multifunctional capabilities, notably conciliating connection technology (e.g. snap-fit technology) and building

physics requirements. Some manufacturers are trying to incorporate low-density and low-cost core materials in the cross-section of pultruded parts to increase their moduli, while simultaneously maintaining lightness, thermal insulation and cost.

Fibre optic sensors are liked to be increasingly integrated in FRP pultruded parts during their manufacturing process, provided that the cost of these sensors falls considerably. This technology, which has already been successfully developed for FRP bars (Kalamkarov *et al.*, 2000), could be used during production to assess residual strains (Kalamkarov *et al.*, 1999). However, the main interest lies in its possible application in the field monitoring of relevant infrastructure (Kalamkarov *et al.*, 2005) and the remote control of smart structures which include actuators responding to the sensors.

One of the main factors delaying the widespread use of some types of FRP pultruded composites is the lack of technical specifications, design guidelines and codes. Because civil engineering is highly regulated, the lack of such documents creates a certain reluctance in construction agents, particularly with respect to the mainstream structural applications of FRP pultruded parts. Design codes and guidelines have in fact been developed for FRP strengthening strips and FRP reinforcing bars (e.g. American ACI 440.2R-08 (ACI Committee 440, 2008) and ACI 440.1R-06 (ACI Committee 440, 2006); and Canadian CAN/CSA S806-02 (CSA, 2002)). But widely accepted design codes for FRP pultruded profiles are still under development and structural designs are often based on manufacturers' guidelines. Some countries have already produced guidelines, notably the Italian design guidelines for structures made of pultruded profiles (National Research Council of Italy, 2008). The new Pre-Standard for Load and Resistance Factor Design (LRFD) of Pultruded Fiber Reinforced Polymer (FRP), an initiative of the American Composites Manufacturers Association, is likely to be released soon. These documents will certainly help to increase confidence among construction agents (owners, contactors and designers) about the use of FRP pultruded profiles.

9.13 Sources of further information and advice

Key books

- T.F. Starr, *Pultrusion for Engineers*, Woodhead Publishing, Cambridge, UK, 2000
- S.T. Peters, *Handbook of Composites*, Chapman & Hall, 1998
- A.B. Strong, *Fundamentals of Composites Manufacturing: Materials, Methods and Applications*, Society of Manufacturing Engineers, Dearborn, MI, 2008
- L.C. Bank, *Composites for Construction: Structural Design with FRP Materials*, Wiley, Hoboken, NJ, 2006

- J.G. Teng, *FRP-strengthened RC Structures*, John Wiley & Sons, 2002

Series of proceedings

- International Conference on Fiber Reinforced Polymer (FRP) Composites in Civil Engineering (CICE)
- International Symposium on Fiber Reinforced Polymer Reinforcement for Concrete Structures (FRPRCS)
- Advanced Composite Materials in Bridges and Structures (ACMBS)
- Durability of Fibre Reinforced Polymer (FRP) Composites for Construction (CDCC)
- International Conference on Composite Materials (ICCM)
- European Conference on Composite Materials (ECCM)
- Advanced Composites in Construction Conference (ACIC)
- International Conference on Composite Structures (ICCS)

Major trade/professional bodies

- American Composites Manufacturers Association (ACMA)
- European Pultrusion Technology Association (EPTA)
- ALTO, Perfis Pultrudidos Lda
- Bedford Reinforced Plastics, Inc.
- Creative Pultrusions, Inc.
- Exel Composites UK
- Fiberline Composites
- Fyfe Co. LLC
- Hughes Brothers
- Martin Marietta Composites
- Pultrall
- Schöck
- Sika
- Strongwell Corporation
- S&P Clever Reinforcement
- Top Glass, S.P.A.

Research and interest groups

- Schöck American Concrete Institute (ACI) – Committee 440 (Fiber-Reinforced Polymer Reinforcement)
- Schöck Fédération International du Béton (FIB) – Task Group 9.3 (FRP Reinforcement for Concrete Structures)
- Schöck International Association for Bridge and Structural Engineering,

IABSE – Working Commission 8 (Fibre Reinforced Composite Structures)
- Schöck International Institute for FRP in Construction (IIFC)
- ISIS Canada Research Network

Websites/online videos

- Schöck http://www.pultrusions.org/
- Schöck http://www.pultruders.com/
- Schöck http://www.compositesworld.com/
- Schöck http://www.reinforcedplastics.com
- Schöck http://www.videosurf.com/videos/pultrusion

9.14 References

ABNT (2011), *ABNT NBR 15708-1 Petroleum and Natural Gas Industries – Pultruded Shape. Part 1: Materials, Test Methods and Dimensional Tolerances*, Rio de Janeiro, Brazilian Association of Technical Standards [*in Portuguese*].

ACI Committee 440 (1996), *State-of-the-art report on fiber reinforced plastic (FRP) reinforcement for concrete structures, ACI 440 R-96*, Farmington Hills, MI, American Concrete Institute.

ACI Committee 440 (2006), *Guide for the Design and Construction of Structural Concrete Reinforced with FRP Bars, ACI 440.1 R-06*, Farmington Hills, MI, American Concrete Institute.

ACI Committee 440 (2008), *Guide for the Design and Construction of Externally Bonded FRP Systems for Strengthening Concrete Structures*, *ACI 440.2 R-08*, Farmington Hills, MI, American Concrete Institute.

Ahmed A and Kodur V K R (2011), 'Effect of bond degradation on fire resistance of FRP-strengthened reinforced concrete beams', *Composites Part B: Engineering*, 42(2), 226–237.

ASTM (2010), *ASTM D4385 Standard Practice for Classifying Visual Defects in Thermosetting Reinforced Plastic Pultruded Products*, West Conshohocken, PA, American Society for Testing and Materials.

ASTM (2011), *ASTM D3917 Standard Specification for Dimensional Tolerance of Thermosetting Glass-Reinforced Plastic Pultruded Shapes*, West Conshohocken, PA, American Society for Testing and Materials.

Bakis C E, Bank L C, Brown V L, Cosenza E, Davalos J F, Lesko J J, Rizkalla S H and Triantaffillou T C (2000), 'Fiber-reinforced polymer composites for construction – State-of-the-art review', *Journal of Composites for Construction*, 6(2), 73–87.

Bank L C (2006), *Composites for Construction: Structural Design with FRP Materials*, Hoboken, NJ, Wiley.

Barbero E J (1998), *Introduction to Composite Materials Design*, Philadelphia, PA, Taylor & Francis.

Barefoot G (2007), 'Color matching for pultruded composites. Obstacles and answers', *Composites Manufacturing*, June, 38–40, 41–42.

Bogner B R, Breitigam W V, Woodward M and Forsdyke K L (2000), 'Thermoset resins for pultrusion', in Starr T F, *Pultrusion for Engineers, Cambridge*, UK, Woodhead, 97–174.

Busel J P and Lockwood J D (2000), *Product select guide: FRP composite products for bridge application*, Harrison, NY, The Market Development Alliance of the FRP Composites Industry.

Cabral-Fonseca S, Correia J R, Rodrigues M P and Branco F A (2012), 'Artificial accelerated ageing of GFRP pultruded profiles made of polyester and vinylester resins: characterisation of physical–chemical and mechanical damage', *Strain*, 48(2), 162–173.

CEN (2002), *EN 13706: Reinforced Plastics Composites – Specifications for Pultruded Profiles. Part 1: Designation; Part 2: Methods of Test and General Requirements; Part 3: Specific requirements*, Brussels, European Committee for Standardisation.

Connolly M, King J, Shidaker T and Duncan A (2006), *Processing and Characterization of Pultruded Polyurethane Composites*, European Pultrusion Technology Association.

Conroy A, Halliwell S and Reynolds T (2006), 'Composites recycling in the construction industry', *Composites Part A: Applied Science and Manufacturing*, 37(8), 1216–1222.

Correia J R, Branco F A and Ferreira J G (2010a), 'The effect of different passive fire protection systems on the fire reaction properties of GFRP pultruded profiles for civil construction', *Composites Part A: Applied Science and Manufacturing*, 41(3), 441–452.

Correia J R, Branco F A, Ferreira J G, Bai Y and Keller T (2010b), 'Fire protection systems for floors of buildings made of GFRP pultruded profiles. Part 1: Experimental investigations', *Composites Part B: Engineering*, 41(8), 617–629.

Correia J R, Branco F A, Silva N, Camotim D and Silvestre N (2011a), 'First-order, buckling and post-buckling behaviour of GFRP pultruded beams. Part 1: Experimental study', *Computers and Structures*, 89(21–22), 2052–2064.

Correia J R, Almeida N M and Figueira J (2011b), 'Reusing fine waste from the cutting process of GFRP composites: Application to concrete mixtures', *Journal of Cleaner Production*, 19(15), 1745–1753.

CSA (2002), *Design and Construction of Building Components with Fibre-Reinforced Polymers*, *CAN/CSA S806-02*, Rexdale, Ontario, Canadian Standards Association.

Devlin B J, Williams M D, Quinn J A and Gibson A G (1991), 'Pultrusion of unidirectional composites with thermoplastic matrices', *Composites Manufacturing*, 2(3–4), 203–207.

Evans D (2000), 'Profile design, specification, properties and related matters', in Starr T F, *Pultrusion for Engineers*, Cambridge, UK, Woodhead, 66–96.

FIB (2001), *Externally Bonded FRP Reinforcement for RC Structures*, Bulletin 14, Lausanne, International Federation for Structural Concrete.

FIB (2007), *FRP Reinforcement in RC Structures*, Bulletin 40, Lausanne, International Federation for Structural Concrete.

Firmo J P, Correia J R and França P (2012), 'Fire behaviour of reinforced concrete beams strengthened with CFRP laminates: Protection systems with insulation of the anchorage zones', *Composites Part B: Engineering*, 43(3), 1545–1556.

Goldsworthy W B (1986), 'Pulforming – a continuous process for mass producing composite articles of changing shapes and volumes', *First International Conference on Automated Composites*, Plastics and Rubber Institute, Nottingham, UK.

Goldsworthy W (2000), 'The future – beyond 2000', in Starr T F, *Pultrusion for Engineers*, Cambridge, UK, Woodhead, 264–300.

Harper C A (2006), *Handbook of Plastic Processes*, Hoboken, NJ, Wiley-Interscience.

Hollaway L C (2003), 'The evolution of and the way forward for advanced polymer

composites in the civil infrastructure', *Construction and Building Materials*, 17(6–7), 365–378.

Hollaway L C (2010), 'A review of the present and future utilisation of FRP composites in the civil infrastructure with reference to their important in-service properties', *Construction and Building Materials*, 24(12), 2419–2445.

Kalamkarov A L, Fitzgerald S B and MacDonald D O (1999), 'The use of Fabry Perot fiber optic sensors to monitor residual strains during pultrusion of FRP composites', *Composites Part B: Engineering*, 30(2), 167–175.

Kalamkarov A L, Fitzgerald S B, MacDonald D O and Georgiades A V (2000), 'The mechanical performance of pultruded composite rods with embedded fiber-optic sensors', *Composites Science and Technology*, 60(8), 1161–1169.

Kalamkarov A L, Saha G, Rokkam S, Newhook J and Georgiades A (2005), 'Strain and deformation monitoring in infrastructure using embedded smart FRP reinforcements', *Composites Part B: Engineering*, 36(5), 455–467.

Karbhari V M (2007), *Durability of Composites for Civil Structural Applications*, Cambridge, UK, Woodhead.

Karbhari V M, Chin J W, Hunston D, Benmokrane B, Juska T, Morgan R, Lesko J J, Sorathia U and Reynaud D (2003), 'Durability gap analysis for fiber-reinforced polymer composites in civil infrastructure', *Journal of Composites for Construction*, 7(3), 238–247.

Keller T (1999), 'Towards structural forms for composite fibre materials', *Structural Engineering International*, 9(4), 297–300.

Keller T (2002). 'Fibre reinforced polymer materials in bridge construction', *IABSE Symposium, Towards a Better Built Environment – Innovation, Sustainability, Information Technology*, Melbourne.

Keller T (2003), *Use of fibre reinforced polymers in bridge construction*. Structural Engineering Documents, Volume 7, Zürich, International Association for Bridge and Structural Engineering.

Keller T, Tracy C and Hugi E (2006), 'Fire endurance of loaded and liquid-cooled GFRP slabs for construction', *Composites Part A: Applied Science and Manufacturing*, 37(7), 1055–1067.

Liao K, Schultheisz C R, Hunston D L and Brinson C L (1998), 'Long-term durability of fiber-reinforced polymer-matrix composite materials for infrastructure applications: a review', *Journal of Advanced Materials*, 40(4), 4–40.

Lopresto V, Leone C and De Iorio I (2011), 'Mechanical characterisation of basalt fibre reinforced plastic', *Composites Part B: Engineering*, 42(4), 717–723.

Moschiar S M, Reboredo M M and Vazques A (1998), 'Pultrusion Processing', In Cheremisinoff N P, *Advanced Polymer Processing Operations*, Westwood, NJ, Noyes Publications.

Mouritz A P and Gibson A G (2006), *Fire Properties of Polymer Composite Materials*, Dordrecht, Springer.

National Research Council of Italy (2008), *Guide for the Design and Construction of Structures Made of FRP Pultruded Elements, CNR-DT 205/2007*, Rome, Advisory Committee on Technical Recommendations for Construction.

Nigro E, Cefarelli G, Bilotta A, Manfredi G and Cosenza E (2011), 'Fire resistance of concrete slabs reinforced with FRP bars. Part I: Experimental investigations on the mechanical behavior', *Composites Part B: Engineering*, 42(6), 1739–1750.

Nkurunziza G, Debaiky A, Cousin P and Benmokrane B (2005), 'Durability of GFRP bars: a critical review of the literature', *Progress in Structural Engineering and Materials*, 7, 194–209.

Owens Corning (2003), *Pultrusion of Glass Fiber Composites. A Technical Manual*, Toledo, OH, Owens Corning Corporation.

Phillips S (2004), 'Plastics: MOHF', in Colomina B, Brennan A M and Kim J, *Cold War Hothouses: Inventing Postwar Culture, from Cockpit to Playboy,* Princeton, NJ Princeton Architectural Press.

Pickering S J (2006), 'Recycling technologies for thermoset composite materials – current status', *Composites Part A: Applied Science and Manufacturing*, 37(8), 1206–1215.

Ross A (2006), 'Basalt fibers: Alternative to glass?', *Composites Technology*, August.

Sá M, Gomes A, Correia J R and Silvestre N (2011a), 'Creep behaviour of pultruded GFRP elements – Part 1: Literature Review and Experimental study', *Composite Structures*, 93(10), 2450–2459.

Sá M, Gomes A, Correia J R and Silvestre N (2011b), 'Creep behaviour of pultruded GFRP elements – Part 2: Analytical study', *Composite Structures*, 93(9), 2409–2418.

Schöck Bauteile GmbH (2005), Technical information Schöck Combar, company brochure.

Schutte C L (1994), 'Environmental durability of glass-fiber composites', *Materials Science and Engineering, Reports*: *A Review Journal*, 13(7), 265–324.

Shaw-Stewart D E (1988), 'Pullwinding', in *Proceedings of the Second International Conference on Automated Composites*, Paper 15 (pp. 15.1–14), Plastics and Rubber Institute, Noordwijkerhout, The Netherlands.

Shaw-Stewart D and Sumerak J E (2000), 'The pultrusion process', in Starr T F, *Pultrusion for Engineers*, Cambridge, UK, Woodhead, 19–65.

Sika (2001), Shear Strengthening Sika® CarboDur® Composite Systems, company brochure.

Silva N, Camotim D, Silvestre N, Correia J R and Branco F A (2011), 'First-order, buckling and post-buckling behaviour of GFRP pultruded beams. Part 2: Numerical simulation', *Computers and Structures*, 89(21–22), 2065–2078.

Sim J, Park C and Moon D Y (2005), 'Characteristics of basalt fiber as a strengthening material for concrete structures', *Composites Part B: Engineering*, 36(6–7), 504–512.

Starr T F and Ketel J (2000), 'Composites and pultrusion', in Starr T F, *Pultrusion for Engineers*, Cambridge, UK, Woodhead, 1–18.

Sumerak J E and Martin J D (1991), 'The pulse of pultrusion – Pull force trending for quality and productivity management', *46th Annual Conference*, The Society of the Plastics Industry.

Sumerak J E and Taymourian K (1989), 'Pultrusion quality control – A comprehensive approach', *44th Annual Conference*, The Society of the Plastics Industry.

Sumerak J E and Troutman D (2007), 'Polyurethane pultrusion application successes with large profiles', *Global Pultrusion Conference – 'Composite Profiles – Save Energy*', Baltimore, MD.

Thunhorst K, Goetz D, Hine A and Sedgwick P (2011), 'The effect of nanosilica matrix modification on the improvement of the pultrusion process and mechanical properties of pultruded epoxy carbon fiber composites', *Composites 2011*, Fort Lauderdale, FL, American Composites Manufacturers Association.

Ushakov A E, Klenin U G, Sorina T G, Hayretdinov A K and Safonov AA (2009), 'Pultrusion composites and products with high fire resistance on the base on nanomodified polymers in bridge engineering', Hawaii, *Seventeenth Annual International Conference on Composites/Nano Engineering (ICCE-17)*.

Vijay P V, GangaRao H V S and Bargo J M (2000), 'Mechanical characterization of

recycled thermoplastic polymers for infrastructure applications', *Proceedings of the Third International Conference on Advanced Composite Materials in Bridges and Structures*, Ottawa.

Williams B K, Kodur V K R, Green M F and Bisby L (2008), 'Fire endurance of fiber-reinforced polymer strengthened concrete T-beams', *ACI Structural Journal*, 105(1), 60–67.

Won J-P, Yoon Y-N, Hong B-T, Choi T-J and Lee S-J (2012), 'Durability characteristics of nano-GFRP composite reinforcing bars for concrete structures in moist and alkaline environments', *Composite Structures*, 94(3), 1236–1242.

Zhou A and Keller T (2005), 'Joining techniques for fiber reinforced polymer composite bridge deck systems', *Composite Structures*, 69(3), 336–345.

Zureick A and Scott D (2000), 'Short-term behavior and design of fibre-reinforced polymeric slender members under axial compression', *Journal of Composites for Construction*, 1(4), 140–149.

10

Understanding and predicting interfacial stresses in advanced fibre-reinforced polymer (FRP) composites for structural applications

A. AL-SHAWAF, Monash University, Australia

DOI: 10.1533/9780857098641.3.255

Abstract: This chapter addresses all aspects pertaining to stresses inherent within civil applications of advanced composites, particularly the critical interfacial adhesive stresses usually controlling the design strength for externally bonded FRP composites. Informed discussions and explanations are presented on influential aspects closely affecting the distribution and magnitude of interfacial stresses along the bondline. Traditional and promising experimental methods for stress estimation are addressed, together with a corresponding brief literature review highlighting their evolution and practical advantages and disadvantages. Theoretical and numerical methods for interfacial stress analyses are also reviewed for different FRP bonding applications, and their stress prediction capabilities are verified with experimental validations. Finally, key conclusions and recommendations for future trends in the stress characterizations of adhesive joints are provided.

Key words: FRP composites, interfacial adhesive stresses, lap-shear stress distribution, numerical models, theoretical analysis.

10.1 Introduction

The recent introduction of advanced composites in retrofitting existing civil engineering infrastructure, as a cost-effective option for restoring and/or upgrading the deteriorated functional integrity of such infrastructure, has triggered a global trend of applied and experimental investigations on the behavioural and durability aspects pertinent to this technology which emerged almost 35 years ago. Yet, the turning point towards the wide utilization of fibre-reinforced polymer composite technologies in infrastructure construction and rehabilitation schemes dates back to the late 1980s when the cost of FRP (fibre-reinforced polymer/plastic) materials was constantly falling, with an unprecedented increase in the demand from various industries (Al-Shawaf, 2010).

The latter trend, together with the ongoing developments in computational processing, data-storage capabilities and numerical modelling of advanced FE (finite element) packages, have furthered more specialized and elaborate

research on all FRP strengthening aspects for civil applications. These include the effects of surface preparation, joint configuration, thermo-mechanical properties of adhesive, adherend and FRP reinforcement sheets/plies, and environmental factors reflected on the composite joint's load transfer, deformations and consequent critical stress distribution within the joint which define the bond's strength and its corresponding failure pattern and location (Al-Shawaf, 2011).

In this chapter, the above-mentioned parameters affecting the strength of adhesive joints are properly addressed in an attempt to contribute to the global research efforts that are targeting better understanding of the complexities that inherently attribute stresses within FRP composite adhesive joints utilized in civil engineering strengthening applications. Comprehensive discussions and explanations are provided for those aspects that are deemed most influential. Experimental testing for quantifying interfacial adhesive lap-shear stresses along the bondlength of double-strap FRP/steel joints, together with their theoretical and numerical modelling predictions, are presented with brief discussions of the results and their implications. A few recommendations for future trends in the stress characterizations of adhesive joints are included. Finally, the chapter concludes with a brief summary and sources of further information on this topic.

10.2 Interfacial stresses in fibre-reinforced polymer (FRP) composites

Fibre-reinforced polymers consist of two distinct phases: high-strength fibrous reinforcement impregnated or encapsulated with a continuous medium of polymeric matrix (Moy, 2001). The stiffness and strength of FRP composites are generally governed by the embedded fibres. Carbon fibres are traditionally utilized to impart the highest strength values to the FRP composites as compared with the other two types frequently used in civil applications, viz. aramid and glass fibres. The role of the polymeric matrix in fibre-reinforced composites is (a) to act as a medium binding reinforcing fibres in the predesigned orientations, (b) to transfer stresses between adjoining fibres through adhesion and provide all of the interlaminar shear strength of the composite, and (c) to protect the fibres from handling and environmental exposure (Lopez-Anido and Naik, 2000).

The weakest link in an FRP composite material strengthening application is the FRP's resin matrix/interfacial adhesive; this, indisputably, is the most vulnerable component in terms of adaptability and endurance to extreme environmental exposures. This fact has long been established and confirmed by a number of experimental and theoretical investigations (Chiew *et al.*, 2011; Hahn, 1976; Karbhari and Shulley, 1995; Kasen, 1981; Lord and Dutta, 1988; Weiss, 1982). If optimized surface preparation of the adherend is assumed,

failures of adhesive joints, for a given type of loading, are governed by key determinants of stress distribution within the joint's polymeric components, viz. the thermo-mechanical properties of the adopted adhesive and adherend, the FRP reinforcement, the extreme environmental thermal exposures, and the joint's geometrical configuration.

Typically, the adhesive and/or the matrix in FRP retrofitting applications transfers three different stress categories. These are shear, peel and thermal residual stresses. The latter occur in FRP composite joints either upon fabrication due to mismatch in the hygrothermal and elastic properties of the fibres, matrices/adhesives and adherends; or due to the difference between curing and operating temperatures of the FRP material. These three stress categories can be referred to as the good, the bad and the unavoidable, respectively.

Adhesive shear stresses originate because of different axial deformations of the adherends; whereas peel stresses primarily develop due to eccentricity in the load path, as is the case for unstabilized single-lap shear joint configurations. Considerable local stress concentrations near discontinuities in the substrate, the adhesive bond or the FRP strengthening material are the major common attribute for both shear and peel stresses, as illustrated in Fig. 10.1.

The key requirement for a well-configured adhesive joint (i.e. attaining optimum ultimate capacity) is to minimize any direct or induced peel stresses. Therefore, it should be arranged to transfer the applied load mainly in shear, since adhesively bonded joints can be strong in shear but are inevitably weak in peel (Hart-Smith, 2001). To this effect, peel stresses detract from the overall joint shear strength, hence were attributed as bad in the prelude to this section. Consequently, the double-lap shear bond configuration is

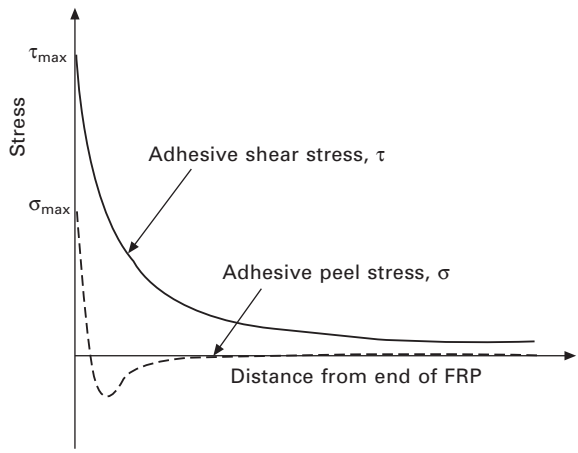

10.1 Generic trends for lap-shear and peel stresses at the adhesive layer.

considered in this chapter to demonstrate the ultimate potential lap-shear stress capacity of FRP bonds by limiting the possibility of premature failure of a joint due to the eccentricity of the applied load.

10.3 Mechanical properties of matrices and fibre reinforcements

The mechanical properties of both polymeric and fibrous components in FRP strengthening systems play an essential role in determining the load transfer mechanism, and thus the initiation and evolution of the critical stress variants responsible for controlling the failure pattern and its location within the composite joint, as detailed in succeeding sections of this chapter.

The ductility of polymeric components comes at the forefront of these properties. It has a significant effect on the mechanical response of bonded joints. Hart-Smith (1973) established that all practical adhesives exhibit some non-linear behaviour prior to failure, regardless of their environmental exposures, which has an impact in softening the shear stress peaks at the ends of the joint, and consequently increasing the potential shear strength of the bond. Kinloch (1982) and Harris and Adams (1984) reiterated the importance of considering the adhesive's plasticity for the accurate prediction of joint strength. Ever since, the incorporation of the non-linear constitutive model of the adhesive in obtaining realistic and accurate joint stress distributions and thus failure loads, has been realized and increasingly implemented in relevant theoretical and numerical investigations (Adams *et al.*, 1986; Adams and Mallick, 1992; Al-Shawaf, 2010; Angus and Cheng, 2004; Angus *et al.*, 2007; Crocombe *et al.*, 1995; Deb *et al.*, 2008; DoD, 2002; Gleich, 2002; Hart-Smith, 1986, 2001, 2002; Mortensen, 1998; Pickthall *et al.*, 1997; Yu *et al.*, 2011; Zhou *et al.*, 2001). Figure 10.2 compares bond strengths for identical double-strap CFRP/steel specimens manufactured with three different ductility and tensile modulus epoxide resins, at different environmental exposures.

The lap-shear stress distribution, the failure pattern and ultimately the bond strength of FRP joints are also functions of the mechanical properties of the FRP reinforcing fibres. This behavioural dependency is depicted in Fig. 10.3 where lap-shear stress distributions along the bondlength for two identical double-strap CFRP/steel specimens, with different elastic moduli of their reinforcing CF (carbon fibres), are presented.

In FRP composite strengthening for civil engineering applications, two generally accepted material models are utilized in the mechanical characterization and stress analysis of FRP adhesive joints, viz. microstructural and macrostructural material models. Microstructural models take into account FRP material heterogeneity, and accordingly make use of the fibre and matrix properties, individually, in analysing FRP behaviour. On the

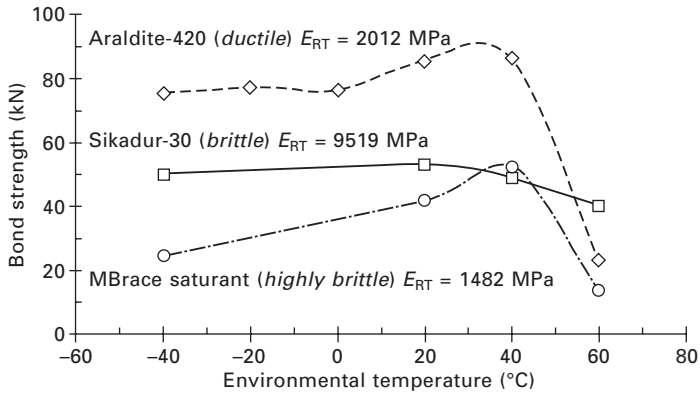

10.2 Effect of adhesive ductility on bond strength for identical double-strap CFRP/steel plate specimens at different exposure temperatures (Al-Shawaf, 2010).

other hand, in macrostructural models the individual lamina of a laminated FRP is replaced with equivalent elastic, homogeneous and anisotropic layers. These models consider the macroscopic (average) material properties of each layer in analysing the laminate behaviour (Dutta and Lampo, 1993). In terms of interfacial adhesive/FRP matrix stress predictions, the microstructural models are more accurate and reliable than the other category. The key factor which supports this fact is their efficacy in providing more realistic prediction of FRP joint stress distribution, failure criteria and capacity when the interfacial adhesive/FRP matrix plasticity and the inherent existence of shear lag deformations within the thickness of the FRP composite adherend are incorporated in the analysis of the FRP joint (Hart-Smith, 1978, 2001; Lord and Dutta, 1988; Veselovsky and Kestelman, 2002).

10.4 Structural concrete and steel adherends in civil infrastructure

Structural adherends in civil infrastructure are primarily concrete and steel structures. As such, external FRP strengthening applications target those adherends. The generic trend of localized stress concentrations shown in Fig. 10.1 is common for both adherends. In CFRP (carbon fibre-reinforced polymers/plastics)-concrete adherends, the majority of the debonding failures reported in the literature took place in the concrete substrate (Buyukozturk *et al.*, 2004). This failure pattern is clearly depicted in the double pull-pull configuration of Fig. 10.4(a), where the above-mentioned high localized stresses are likely to cause premature de-covering of the concrete due to the relatively low strength of the concrete in tension or shear-tension failure as in Mode 1 and 2, respectively, of Fig. 10.4(b) (Pham and Al-Mahaidi, 2007).

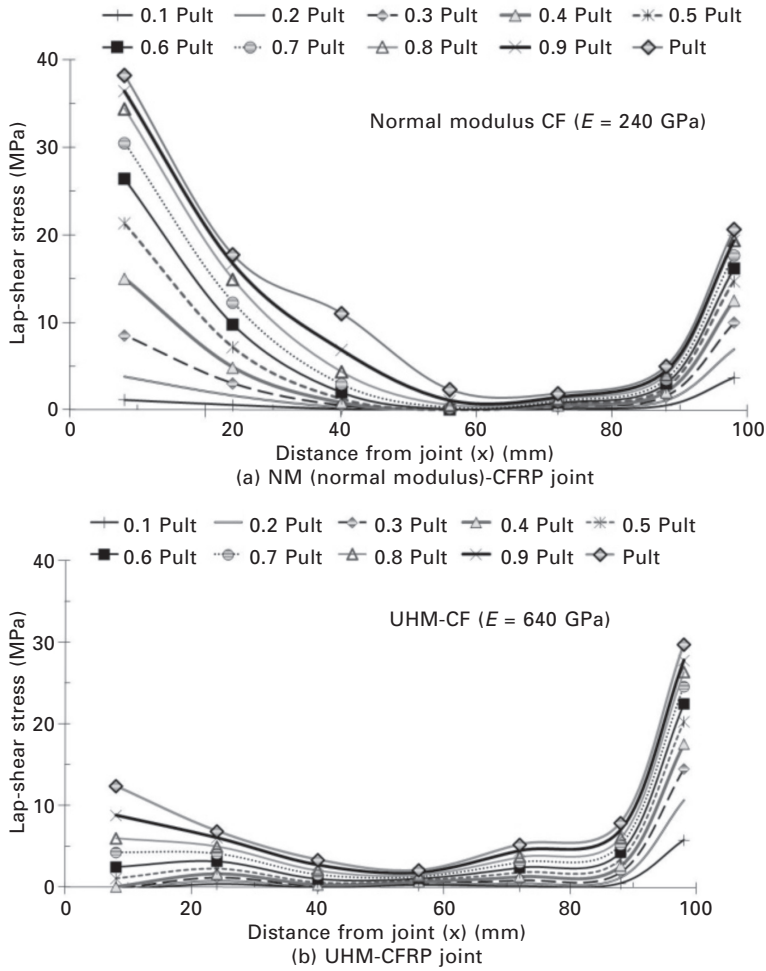

10.3 (a, b) Lap-shear stress distribution along bondlength for identical double-strap CFRP/steel plate specimens having different CF moduli (Al-Shawaf, 2010).

Consequently, the characteristic failure mode(s) for external FRP/concrete composite joints can be referred to as adherend/concrete-based.

On the other hand, the situation is more complicated in the case of steel adherends where several possible failure modes at different locations in the adhesive joint can be expected (Haghani *et al.*, 2009). In order to acquire clear understanding of the behavioural differences in terms of stress between concrete and steel adherends, likely failure modes for a CFRP/steel plate double-strap configuration are presented in Fig. 10.5. Assuming optimum surface preparation procedures, triggering failure for all modes depicted in Fig. 10.5(a)–(d) can be attributed as adhesive/matrix-based. The only exception

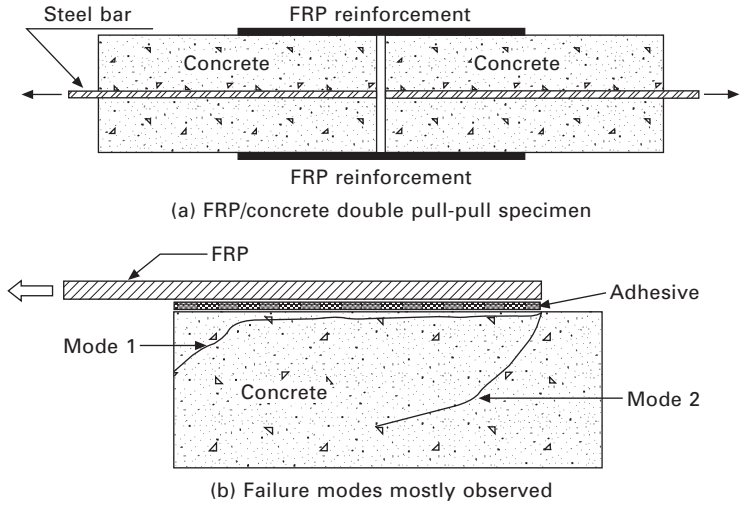

10.4 (a, b) Double lap-shear configuration for FRP and concrete adherend.

is for mode (e) of Fig. 10.5 which usually occurs in UHMCF (ultra-high modulus carbon fibre) applications with ductile adhesives, where the ultimate tensile strength of the carbon fibres in the vicinity of the simulated crack (i.e. gap between both plates) is attained prior to that of the adhesive, leading to CFRP rupture prior to adhesive/matrix failure (Al-Shawaf, 2010).

It can be implied, from the above discussion, that failure initiation and propagation mechanisms for similar configurations, adhesives and reinforcing fibres of adhesively bonded CFRP to concrete and steel adherends are utterly different, and are substantially influenced by the mechanical and microstructural properties for each adherend.

In conclusion, although the trend in stress distribution is identical for both concrete and steel adherends, adopting FRP joints with steel adherends promotes higher interfacial adhesive efficiency (i.e. higher lap-shear stress) and thus joint strength than for composite joints with concrete adherends which fail prematurely within the concrete adherend at considerably lower adhesive stresses and joint capacities. As such, a double-strap CFRP/steel adhesive joint configuration is adopted for this chapter as an optimum option in displaying the shear-stress variation and the full strength potential of FRP adhesively bonded joints.

10.4.1 Stiffness imbalance and thermal mismatch of adherends

The adherend stiffness in the terminology of adhesive joints is defined as the elastic modulus (E) times the adherend thickness (t). It is a parameter

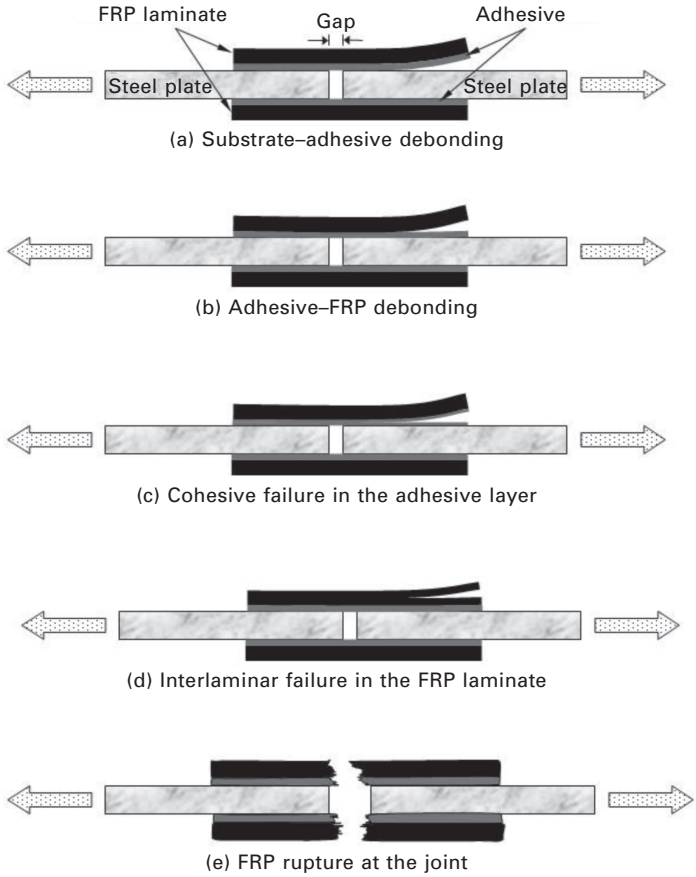

10.5 (a–e) Modes of failure for double-strap configuration of FRP/steel adherend.

used to evaluate joint efficiency for lap-shear joints of uniform-thickness adherends. Practically, the potential shear strength capacity of all types of joint geometry is unattainable due to the unequal stiffnesses of adherends (DoD, 2002). Therefore, part of sound optimum joint design is to adopt adherends with stiffness values as close as possible. Adherend stiffness imbalance for double-lap joint configurations is explained in Fig. 10.6, where the end from which the inner (soft) adherend extends exhibits more severe strains, and thus shear stresses, than at the other end from which the outer (stiff) adherend extends (i.e. $E_i t_i \ll 2E_o t_o$). The stiffer adherend's end of the joint can be only lightly loaded prior to failure at the unloaded end; hence the joint is not capable of developing the full potential strength of the adhesive at the stiffer adherend's end (Hart-Smith, 1973).

This fact is demonstrated in the lap-shear stress distribution for the CFRP/steel double-strap specimen of Fig. 10.3(a) where the outer adherend

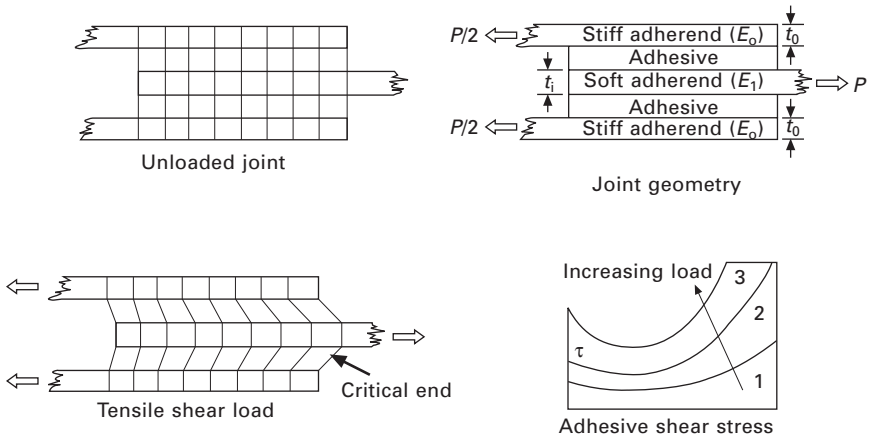

10.6 Lap-shear stress distribution for stiffness-imbalanced double-lap joint (adapted from Hart-Smith, 1973).

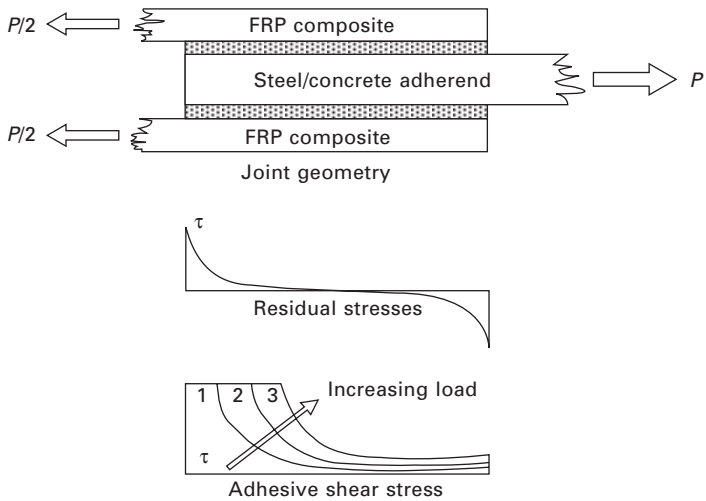

10.7 Adhesive shear stresses in thermally mismatched double-lap bonded joint (adapted from Hart-Smith, 1973).

(extending to the left) is a normal-modulus CFRP laminate with $2E_o t_o$ = 274,458 N/mm, and the inner adherend (extending to the right) is a steel plate with $E_i t_i$ = 1,100,412 N/mm (Al-Shawaf, 2010).

Thermal mismatch is another key factor to be accounted for when designing adhesive bonds in civil engineering applications, particularly for those pertinent to infrastructures where extreme environmental exposures are encountered. Figure 10.7 illustrates the effect of bonding dissimilar adherends with differences in their coefficient of thermal expansion, in the

absence of any adherend stiffness imbalance, on the adhesive's shear stress. This figure simulates FRP composite as the outer adherend and steel/concrete adherend as the inner. It is clearly shown that there are significant (no-load) residual stresses induced in the adhesive which detract from the load potential of the joint. The intensity of these stresses is directly proportional to the difference in curing and operating temperatures ($\Delta T = T_{operating} - T_{cure}$) of the FRP material, and the difference between the coefficients of thermal expansion of the inner and outer adherends ($\alpha_i - \alpha_o$) for double-lap joints. Consequently, for large-scale civil structural applications, adhesives which cure at ambient temperatures should be preferred as cost-effective alternatives (Matta, 2003). Detailed mathematical formulations of theoretical lap-shear stress models which include thermal mismatch of adherends are discussed in Section 10.6.

Figure 10.8 demonstrates experimentally the combined effect of adherend thermal mismatch, stiffness imbalance and extreme environmental exposures on the lap-shear stress distributions for identical CFRP/steel plate double-strap joints exposed to different environmental temperatures (Al-Shawaf, 2010). As shown in this figure, the generic lap-shear stress distribution along the bondlength is partly a function of the thermal environmental exposures, besides being the interaction of the other two above-mentioned parameters. It is rather difficult to separate the individual effect of any of these variables; however, the overall pattern is alleviation of the peak stresses at either one end or both ends of the bondlength, and widening the load transfer zones from the bondlength ends to the internal parts of the joint as temperatures increase from subzero to elevated ranges.

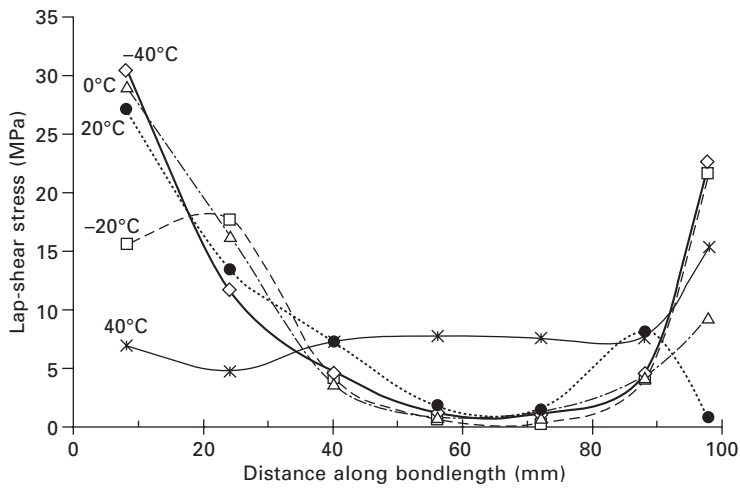

10.8 Lap-shear stress variation with exposure temperature for identical double-strap CFRP/steel plate specimens (Al-Shawaf, 2010).

10.4.2 Adhesive-joint geometrical configuration

It was stated earlier that the interfacial adhesive is the weakest link in an FRP composite strengthening system; therefore from the perspective of sound lap-joint design, it is essential to prevent joint failures occurring within the adhesive layer by ensuring that the adherends fail prior to the interfacial bond layer. This design requirement is hard to achieve in practice unless the limitations of the joint geometry are recognized and certain control on the overall thickness of the adherends is implemented (DoD, 2002). The latter concept is depicted in Fig. 10.9, which has been frequently published in the relevant literature since Hart-Smith (1974a).

Figure 10.9 sorts joint types according to their strengths in increasing order from the lowest (i.e. single-lap joint) to the highest (i.e. scarf joint). In terms of shear stress distribution and its vital correlation with joint capacity, the development in joint capacity with its geometrical configuration can be explained as follows. In a uniform-thickness lap-joint, the load transfer process takes place mostly through the narrow, highly stressed end zones (i.e. near discontinuities in the substrate, the adhesive bond or the FRP strengthening material – refer to Fig. 10.1) separated by the lightly stressed elastic trough towards the inner parts of the bondlength. As such, these parts are deprived from developing the full shear stress potential of the interfacial adhesive. As adherend thickness decreases over part or the whole of the lap bondlength,

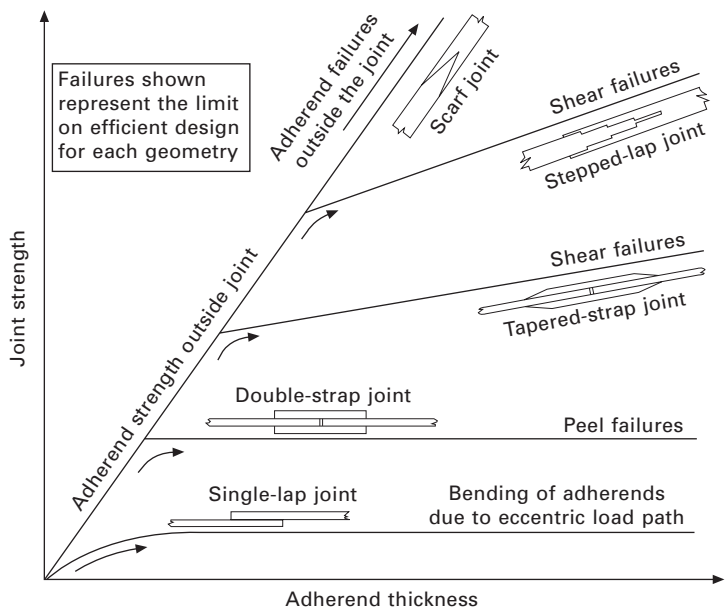

10.9 Adherend thickness effect on bonded joint strength for different joint geometries (adapted from Hart-Smith, 1974a).

the above-mentioned stress trough starts to rise up and approach the stress levels of the end zones until the whole bondlength attains a nearly uniform shear stress associated with the highest attainable joint strength, as in the case of scarf joint with identical adherends.

10.5 Measuring stresses in FRP composite bonded joints

As a prelude to the current section, it is worth mentioning that notwithstanding all the work done or yet to be done in the field of adhesively bonded FRP composite applications in general, and lap stress testing, measurement and prediction in particular, the widespread acceptance and adoption of these materials by structural designers and civil engineers are still restricted. The second prime reason for this, besides FRP durability issues, is the complexity of stress distributions and failure modes in adhesive joints and the lack of internationally accredited stress testing, measurement procedures and design codes (Al-Shawaf, 2010; Haghani, 2010; Karbhari *et al.*, 2003; Ruiz *et al.*, 2006). All currently available stress-related standards and specifications of testing methods explicitly determine τ_{avg} (the average shear stress) of the interfacial adhesive along the bondline without providing guidelines or procedures for determining lap-shear stress distribution (i.e. peak stress) (ASTM, 2004, 2007; BSI, 2011; ISO, 2001; JSA, 1999; NASI, 2011). By referring to Figs 10.1 and 10.3, it can be inferred that it is meaningless to adopt τ_{avg} in adhesive joint design, since it is the peak stress that triggers bond failure. The only method reported in the literature for measuring stresses in FRP bonded joints is via the instrumental acquisition of values for one or more strain variants within the interfacial adhesive layer, or within the adherend(s), utilizing two main measurement methodologies, viz. contact and non-contact methods, which are discussed in detail below.

10.5.1 Contact methods

The traditional contact method, and the more frequently implemented in relevant literature, is bonding ERSGs (electrical resistance strain gauges) on the outer surface of the FRP reinforcement patch (Al-Shawaf, 2010; Dawood and Rizkalla, 2007; Fawzia *et al.*, 2006; Garden *et al.*, 1998; Kim *et al.*, 2011; Pham and Al-Mahaidi, 2007; Schnerch *et al.*, 2005; Xia and Teng, 2005). A few other contact instrumentation schemes have attached ERSGs within the interfacial adhesive layer between the FRP composite reinforcement and the adherend to improve interfacial adhesive strain measurement reliability (Etman and Beeby, 2000; Fawzia *et al.*, 2006). However, it has been reported that disadvantages of the latter instrumentation method override the anticipated enhancement in strain measurement, due to the fact that strain gauges are

too large to be located at the interface without affecting interfacial properties and the overall integrity of the adhesive joint and can thus only be attached to the external surface of the laminate (Wang *et al.*, 2009). The author of this chapter has demonstrated that the strain reliability of ERSGs attached on the outer surface of the FRP strengthening laminate is not considerably compromised when strain measurement is conducted under subzero to ambient thermal exposures, since the inherent existence of shear lag deformations within the thickness of the composite adherend can be ignored due to the relatively stiff response of most structural-grade adhesives. The latter is not applicable under elevated thermal exposures where most structural adhesives exhibit gradual softening with increments in their operating temperatures as they approach their T_g (glass transition temperature) (Al-Shawaf, 2010).

The method of interfacial local lap-shear stress measurement via FRP surface-bonded ERSGs can be explained with reference to the force equilibrium of the FBD (free body diagram) of Fig. 10.10 which represents a double-strap FRP/steel joint instrumented with seven ERSGs equally spaced at $\Delta\ell$ along one bondline of total length ℓ. A tensile force (**F**) acts longitudinally on this joint from both outer ends of the inner adherend (i.e. steel plates) along its horizontal axis of symmetry, and is transferred non-uniformly to the outer adherends (i.e. FRP laminates) through the interfacial adhesive layers.

In order to maintain equilibrium of the FBD, the change in FRP laminate tensile force (Δ**F**) between any two adjacent ERSG positions (e.g. SG_4 and SG_5) due to a difference in their corresponding strain readings ($\varepsilon_4 - \varepsilon_5$)

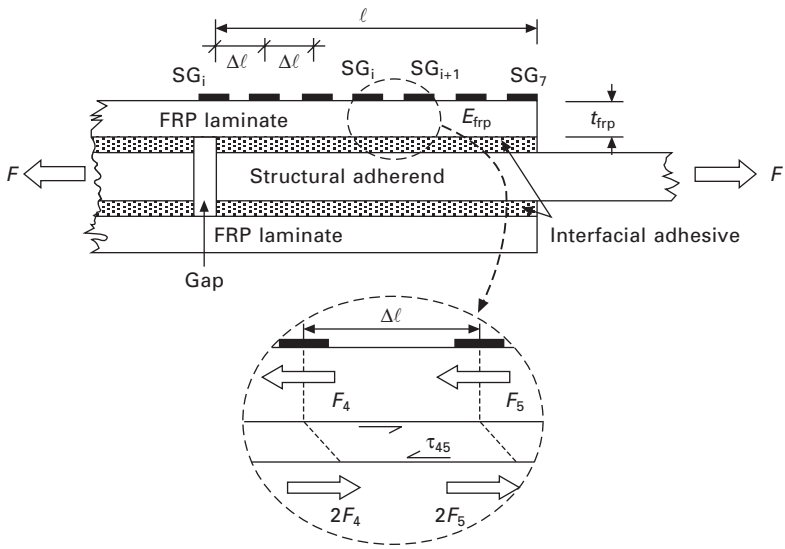

10.10 Double-strap FRP composite ERSG-instrumented joint depicting the force equilibrium for a FBD between the positions of two consecutive gauges.

over $\Delta\ell$ must be countered by an interfacial adhesive shear force between the FRP laminate and the steel plate. This difference in tensile force ($\Delta\mathbf{F}$) is given by:

$$\Delta F_{45} = F_4 - F_5 = E_{\text{frp}}(\varepsilon_4 - \varepsilon_5)t_{\text{frp}} \cdot b_{\text{frp}} \quad [10.1]$$

where ΔF_{45} is the difference in laminate tensile force between SG_4 and SG_5; F_4 and F_5 are the FRP laminate tensile forces at SG_4 and SG_5, respectively; E_{frp} is the Young's modulus of the FRP laminate; and t_{frp} and b_{frp} are the thickness and width of the FRP laminate, respectively. The balancing interfacial adhesive shear force (ΔT_{45}) is given by:

$$\Delta T_{45} = \tau_{45} \cdot \Delta l \cdot b_{\text{frp}} \quad [10.2]$$

Equating equations [10.1] and [10.2], rearranging and generalizing the lap-shear stress term, yields:

$$\tau = E_{\text{frp}} \cdot (\varepsilon_{i+1} - \varepsilon_i) \cdot t_{\text{frp}}/\Delta l \quad [10.3]$$

Accordingly, and by utilizing equation [10.3], the local lap-shear stress along the FRP bonded joint, at any loading level, can be measured between any two neighbouring ERSGs. It should be mentioned here that: (1) the resulting lap-shear stress term of equation [10.3] represents the average nominal bond shear stress value, since it is based on the average strain gradients between the centrelines of both relevant ERSGs, (2) uniform lap-shear stress is assumed across the interfacial adhesive thickness, (3) the axial strain in the FRP composite is assumed uniform across its thickness, (4) the strains in the bulk adherend are negligible, thus the adherend substrate can be considered rigid, and (5) linear-elastic bond behaviour is assumed at all load levels (i.e. up to bond failure). The lap-shear stress distributions for the double-strap CFRP/steel configurations provided earlier in Fig. 10.3 and Fig. 10.8 are estimated by utilizing equation [10.3] (Al-Shawaf, 2010).

The other contact strain-measuring method is by the use of optical fibre strain sensors. Currently, the FOS (fibre optic sensors) method is considered a prominent competitor to conventional strain gauges for strain measurement in both destructive tests in the laboratory and long-term structural health monitoring in the field, i.e. non-destructive testing (NDT) methods. The key advantage of optical fibre strain sensors over conventional ERSGs is their relatively small size (i.e. less than 250 μm) which does not influence or compromise the mechanical properties or stress conditions of the host material (Lau *et al.*, 2001a). In the same context (i.e. functioning as embedded devices), they are not susceptible to debonding from the host material and are physically protected, which promotes their durability attributes and facilitates the long-term monitoring of structures (Wang *et al.*, 2009). In addition, they are characterized by good resolution and accuracy, a wide range of operating temperatures, good signal transmission over long distances, multiplexing

capabilities, and immunity to electromagnetic fields or radio signals (Ansari, 1997; Jiang, 2007; Lau *et al*., 2001a; Tennyson *et al*., 2000).

The application of FOS in civil engineering applications has been growing over the past two decades. Pertinent civil engineering literature has mainly addressed the successful adoption of FOS with concrete structures and their relevant FRP strengthening applications (Ansari, 1997; El-Salakawy *et al*., 2003; Jiang, 2007; Kalamkarov *et al*., 2005; Lau *et al*., 2002; Li *et al*., 2004; Mufti, 2003; Tennyson *et al*., 2000; Wang *et al*., 2009; Xu *et al*., 2005; Zhang *et al*., 2002; Zhao and Ansari, 2002). On the other hand, there is tangible scarcity in civil engineering studies in terms of FOS strain measurements for steel adherends and their FRP strengthening applications (Bernini *et al*., 2006; Yamada *et al*., 2007, 2009).

Notably, all studies mentioned above focused primarily on strain acquisition and its verification with theoretical and numerical modelling without direct conclusion of the structural element/bond stress variants. However, Ansari and Libo (1998) presented a theoretical approach for estimating the shear and normal stresses within the vicinity of the gauge length for FOS embedded in a host material (e.g. the interfacial adhesive in FRP strengthening applications) by incorporating the geometrical and mechanical parameters of the FOS material in the analysis. Similar to the ERSG's shear stress equation [10.3], their model is based on some basic simplifying assumptions such as that all materials involved in the analysis (i.e. the optical fibre core, the protective coating and the host material) behave in a linear elastic manner, which is believed to restrict its validity for FRP strengthening applications to certain linear materials and low to medium working load levels. Li *et al*. (2004) have validated the latter theoretical model experimentally for the case of FOS embedded within concrete host material.

The Fabry–Perot gauge and Bragg grating are the FOS types more frequently used in civil engineering applications. The Fabry–Perot sensor, based on interferometry concepts, is particularly useful for localized strain sensing (Zhang and Hsu, 2002), yet it has the capability of being adapted in quasi-distributed strain measuring systems (Grattan and Sun, 2000). Bragg grating sensors, which provide a point measurement capability as well, have been remarkably adopted for multi-point strain measuring applications by suitable multiplexing arrangements where multiple sensors are incorporated on a single optical fibre (Green *et al*., 2000).

10.5.2 Non-contact methods

Non-contact strain measuring methods are generally based on optical principles. The principal methods addressed in the literature include MI or SI (moiré or speckle interferometry), and DIC (digital image correlation). Amongst their advantages, whole-field, non-contact or remote measurement

of surface displacement and/or deformation of structural components are of special importance in civil engineering applications.

MI utilizes optical techniques in providing contour maps of in-plane displacement fields with high sensitivity and high spatial resolution. It is based on the interference of coherent light waves (Lilleheden, 1994). The captured components of displacement are the *U* (horizontal) and *V* (vertical) that are parallel to the surface of the structural element caused by either mechanical forces, temperature changes or other environmental changes. Induced strains and stresses can then be determined from these displacements (Han *et al.*, 2001). SI is a very closely related technique to MI with comparable accuracy (Morita and Umezawa, 2011). Pioneering studies on utilizing MI in adhesively bonded joints date back to the early 1960s (Hahn and Fouser, 1962). Since then, it has evolved gradually from low-sensitivity geometric moiré with grating density of 40 lines per mm to the powerful capabilities of moiré interferometry with 4000 lines per mm grating density (Post and Han, 2008; Walker, 1994).

During the last three decades, MI/SI techniques have been implemented in measuring the in-plane surface deformation of the overlap region of FRP adhesively bonded joint specimens (Lilleheden, 1994; Post, 1993; Ruiz *et al.*, 2006, 2011; Schumacher and Hack, 2008; Tsai and Morton, 1995; Tsai *et al.*, 1998; Wood, 1985).

A few optical and laser-based NDT (non-destructive testing) methods for assessing the integrity of the materials, components or structures have been reported to be useful in producing stress/strain analysis results for the tested specimens (Karbhari and Lee, 2011). Some of the frequently applied techniques include optical holography, ESPI (electronic speckle pattern interferometry) and laser shearography. They share some common features with the MI/SI techniques such as the laser light source that illuminates the object which is interferometrically compared in two different stressed states, measuring surface deformations, and the option to stress the object mechanically, thermally (e.g. as in residual stress), via vibration-induced loading, etc. According to the author, no explicit information could be traced from all the above-mentioned optical techniques and studies concerning the utilization of the obtained strain/deformation values in FRP adhesive/adherend stress calculations.

The other widely utilized non-contact strain measuring method is DIC. Digital image techniques utilize quantitative strain data of any specimen during its loading/deformation process by capturing images of the specimen at any desired location(s). They have great potential in measuring or monitoring the 2D (two-dimensional) and 3D (three-dimensional) surface deformations and strain values of structural components at extreme environmental exposures, particularly those encountered in civil applications. Their accuracy and capabilities have been significantly improved following the

recent advanced developments in optical-electronics and computer hardware (TWI, 2011).

DIC has been frequently used in relatively recent investigations on deformation and strain mapping. It has been implemented in characterizing the mechanical properties of structural materials (Hoffmann and Vogl, 2003; Merklein and Gödel, 2009; Yang *et al.*, 2010; Zeng and Xia, 2010), strain analyses of FRP adhesively bonded concrete and steel joints (Avril *et al.*, 2004; Haghani, 2010; Haghani *et al.*, 2009; Hii and Al-Mahaidi, 2006), and interfacial adhesive lap-shear stress analyses of FRP/concrete joints (Ali-Ahmad *et al.*, 2006; Carloni and Subramaniam, 2010). According to the latter two references, the non-linear axial strain distribution along the bondline of externally bonded FRP to an adherend can be approximated from the measured DIC strains using the following expression:

$$\varepsilon_x = \varepsilon_0 + \frac{\alpha}{1 + \exp\left(-\dfrac{x - x_0}{\beta}\right)} \qquad [10.4]$$

where ε_x is the axial strain in the FRP laminate; x is the distance along the bondline where $x = 0$ coincides with the unloaded end of the FRP laminate; and α, β, ε_0 and x_0 are values determined using non-linear regression analysis of the measured DIC strains. From the measured strain ε_x, the interfacial lap-shear stress τ is calculated as (Täljsten, 1997):

$$\tau = E_{\text{frp}} \cdot t_{\text{frp}} \left(\frac{\mathrm{d}\varepsilon_x}{\mathrm{d}x}\right) \qquad [10.5]$$

It is worth mentioning that the lap-shear stress term of equation [10.5], when incrementally calculated, yields an identical form to that of equation [10.3]. In addition, all the simplifying assumptions stated previously for the latter equation are applicable for equation [10.5], as well.

10.6 Theoretical models for predicting stress in FRP composite bonded joints

Existing theoretical models for predicting stress variants of FRP strengthened structural members are basically categorized into adhesive lap-joint and FRP strengthened flexural member models. Relevant literature can be classified, in terms of the analytical problem approach, into strength/stress and fracture mechanics models. Fracture mechanics concepts do not provide realistic simulations of the stresses and strains and information on the physical cause of material failure (Sharifi and Choupani, 2008), hence the stress-based method is the only method reviewed in the current section since its prime objective is predicting both shear and normal (peel) stresses of the lap joint.

Analytical stress models involve the solution of a preset series of force equilibrium differential equations in terms of stresses and strains acting on a FBD representing a unit width of the FRP adhesive joint. Geometrical and material properties of the FRP adhesive joint, such as joint configuration, applied load pattern, adherends and adhesive thicknesses, bond length, elastic moduli, Poisson's ratios and constitutive material models are to be incorporated in the solution as relative constants in the final stress expression, with the distance along the bondlength as variable. In addition, depending on the degree of accuracy and complexity of the model, some simplifying assumptions are usually considered to facilitate the mathematical solution. It has been reported that the majority of existing analytical stress models address a relatively simple and approximate solution, while a few others involve a higher-order analysis yielding more accurate and involved solutions (Buyukozturk *et al.*, 2004).

10.6.1 Adhesive lap–joint models

A plethora of theoretical models on adhesive lap joints have been developed over the last seven decades, whether for single-lap or double-lap configuration (Adams and Mallick, 1992; Albat and Romilly, 1999; Allman, 1977; Bigwood and Crocombe, 1990; Cheng *et al.*, 1991; das Neves *et al.*, 2009; de Bruyne, 1944; Delale *et al.*, 1981; Diaz *et al.*, 2009; Goland and Reissner, 1944; Gustafson *et al.*, 2007; Hadj-Ahmed *et al.*, 2001; Hart-Smith, 1973; Mortensen and Thomsen, 2002; Pickett and Hollaway, 1985; Roberts, 1989; Sawa *et al.*, 2000; Tsai and Morton, 1994; Tsai *et al.*, 1998; Volkersen, 1938; Yang *et al.*, 2004; Yuceoglu and Updike, 1981; Zhang *et al.*, 2006). Yet, few of these models have comprehensively addressed all influential parameters to the extent necessary to achieve adequate correlation with experimental results. This is probably due to the fact that experimental verification of the analytical theories in predicting the stresses within the interfacial adhesive layer is very difficult to achieve owing to its relatively small thickness (typically in the order 0.1 to 0.5 mm), which in turn renders much of the verification to be carried out by comparison with other theoretical models (Gleich, 2002).

In this section, two analytical double-lap joint models are briefly introduced, highlighting their strengths and weaknesses in terms of accurate and realistic stress predictions, and finally validating their predicted lap-shear stress distributions for a specific double-strap CFRP/steel joint with experimentally acquired results.

In the early 1970s, Hart-Smith (1973) managed to embrace most of the influential parameters mentioned earlier in this chapter into his renowned 1D, non-linear, double lap-shear model. Addressing adhesive plasticity in his solutions is an improvement of prime significance, compared with his

predecessors, that results in alleviating the peak stresses near bondline ends, consequently predicting more reliable and realistic bond strength. In addition, adherend thermal mismatch, nature of the joint load (i.e. tensile, compressive, or in-plane lap-shear), and the effect of the peel stresses at the end(s) of the bondlength are novel inclusions that were not accounted for in preceding analyses (Hart-Smith, 1972, 1973, 1974b).

The analysis includes three mathematically distinct cases addressing all possible interfacial adhesive stress scenarios: (1) fully elastic adhesive throughout the bondline, (2) adhesive plastically strained at only one bondline end, and (3) adhesive exhibiting plastic strains at both ends of the joint. For comparison and validation purposes with the second analytical model and the experimental example provided later, only the first scenario is reviewed herein. Bond configuration and notations adopted are shown in Fig. 10.11. It should be noted that the origin of the x-coordinate is the middle of the joint only for the current mathematical lap-shear stress expressions. However, for other contexts in this chapter, the origin is located at the left end of the lap joint (i.e. near the gap of Fig. 10.10).

The general solution of the basic differential equations (Hart-Smith, 1973) yields equation [10.6] which determines the lap-shear stress along the bondline (ℓ):

$$\tau = A\sinh(\lambda x) + B\cosh(\lambda x) \qquad [10.6]$$

$$\lambda^2 = \frac{G_a}{t_a}\left(\frac{1}{E_o t_o} + \frac{2}{E_i t_i}\right) \qquad [10.7]$$

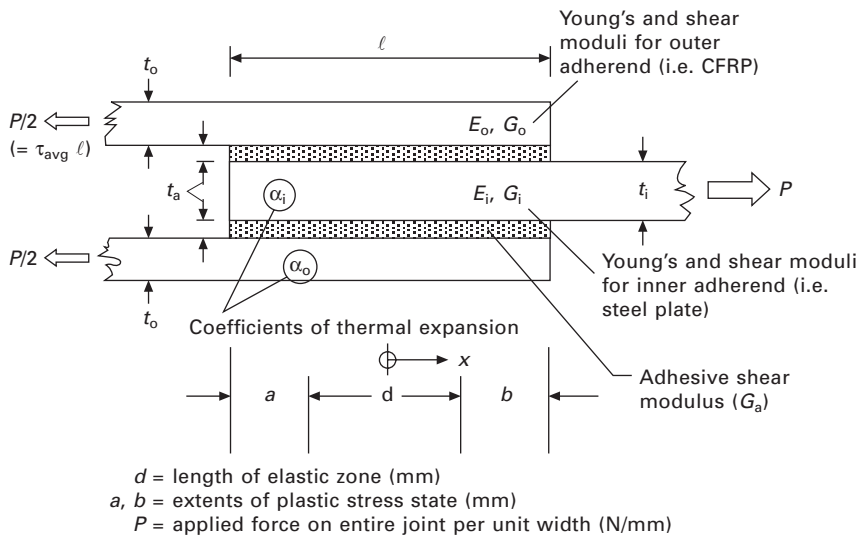

10.11 Bond geometry and notations for lap-shear stress mathematical expression.

where τ is the lap-shear stress; λ, estimated from equation [10.7], is the exponent of the elastic shear stress distribution in Hart-Smith's analytical lap-shear stress model, or the elongation parameter in the TOM (Tsai, Oplinger and Morton) analytical model (mm^{-1}); G_a and t_a are the shear modulus and thickness of the adhesive layer, respectively; and $E_{o/CFRP}$, E_i, t_o and t_i are the elastic moduli and thicknesses of the outer and inner adherends, respectively.

The constants A and B are evaluated from the boundary conditions of the joint, and their final formulae, in terms of τ_{avg} (i.e. the average lap-shear stress), are given as:

$$A = \frac{\tau_{avg}\left(1 - \frac{E_i t_i}{2E_o t_o}\right)}{\cosh\left(\frac{\lambda l}{2}\right)\left(1 + \frac{E_i t_i}{2E_o t_o}\right)} + \frac{(\alpha_i - \alpha_o)\,\lambda \Delta T}{\left(\frac{1}{E_o t_o} + \frac{2}{E_i t_i}\right)\cosh\left(\frac{\lambda l}{2}\right)} \quad [10.8]$$

$$B = \frac{\tau_{avg}\left(\frac{\lambda l}{2}\right)}{\sinh\left(\frac{\lambda l}{2}\right)} \quad [10.9]$$

where $\tau_{avg} = P/2\ell$ (refer to Fig. 10.11) (MPa); ΔT is the temperature change $T_{operating} - T_{cure}$ (°C); and α_i and $\alpha_{o/CFRP}$ are the coefficients of thermal expansion for the inner and outer adherends (i.e. steel and CFRP laminate), respectively. Accordingly, the maximum value of τ will occur at one end or the other of the joint, determined by the relative magnitude of the adherend imbalances.

Next, all geometrical and material properties and constants included in equations [10.7], [10.8] and [10.9] should be characterized correctly through experimental testing if realistic and accurate lap-shear stress predictions are sought. The following paragraphs, relevant formulas, and Fig. 10.12 explain the procedure adopted in this chapter to determine the geometrical and material parameters implemented for both theoretical and numerical lap-shear stress predictions. The current specific joint geometry and experimental testing conducted for determining the FRP material thermo-mechanical properties are reported in Al-Shawaf (2010).

The experimental validation presented later is for two geometrically identical wet lay-up CFRP/steel double-strap joints (refer to Fig. 10.10) with their measured inner adherend's thickness ($t_{i/steel}$) equal to 4.85 mm. Adhesive/matrix (i.e. Araldite®420 epoxy resin) is the same for both specimens; however, they are fabricated with different CF plies (i.e. NM and UHM) and tested under different exposure temperatures (i.e. 0°C and 20°C), respectively. Figure 10.12 portrays the assumed thicknesses for the

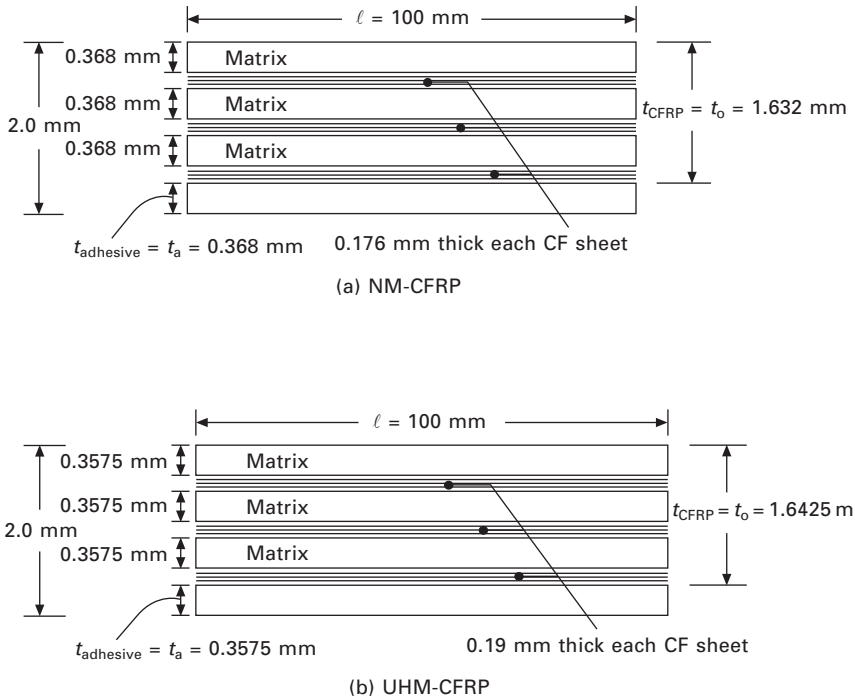

10.12 Schematic of the wet lay-up CFRP laminate and adhesive for (a) NM-carbon fibres, and (b) UHM-carbon fibres, with all assumed dimensions adopted in both theoretical and numerical validations (Al-Shawaf, 2010).

interfacial adhesive and successive matrix layers based on the controlled overall wet lay-up CFRP laminate thickness (i.e. 2 mm) and the thickness of the NM and UHM-CF plies as provided by the supplier.

The remaining tasks include determining all basic thermo-mechanical properties for the joint's constituents (i.e. adhesive, carbon fibres and steel plate), which are to be used later in estimating the global parameters for the CFRP laminates (i.e. outer adherends). The preferred method for estimating/measuring these basic properties is through direct experimental testing, though some traditional values for standard materials can be obtained from credible sources in case testing is not deemed a feasible option. These properties can be found in Table 10.1. In this table, the shear moduli for the adhesive/matrix ($G_{a/m}$), NM-CF and UHM-CF plies, and inner steel plate adherend ($G_{i/steel}$) are theoretically calculated from equation [10.10] below, utilizing their corresponding elastic moduli and Poisson's ratio (ν). In turn, the elastic moduli and Poisson's ratio for the adhesive (i.e. E_a and ν_a), and steel plate (i.e. E_i and ν_i) are experimentally determined.

From the NM and UHM-CF bond configurations of Fig. 10.12, the

Table 10.1 Basic properties of the adhesive, carbon fibres and steel plate (obtained experimentally and from the literature)

	Thermal exposure (°C)	*E* (GPa)	Poisson's ratio (ν)	*G* (GPa)	Thermal expansion coefficient α ($\times 10^{-6}$/°C)
Adhesive/ matrix	0	2.12	0.333	0.79	110
	20	2.01	0.366	0.74	
NM-CF	N.A.	240	0.270	94.50	–0.38
UHM-CF	N.A.	640	0.245	257	–0.83
Steel plate	N.A.	227	0.250	90.80	11

Source: Al-Shawaf, 2010.

calculated volume fractions for their CFRP matrix and carbon fibres (i.e. V_m and V_f) are (1) 0.68 and 0.32, and (2) 0.65 and 0.35, respectively. These values are then incorporated within equations [10.11] and [10.12] derived from the physical (rule-of-mixtures) concept to estimate the final CFRP (i.e. outer adherend) global properties.

$$G = \frac{E}{2(1+\nu)} \quad [10.10]$$

$$E_{o/CFRP} = V_f E_f + V_m E_m \quad [10.11]$$

$$\alpha_{o/CFRP} = \frac{V_f E_f \alpha_f + V_m E_m \alpha_m}{E_f V_f + E_m V_m} \quad [10.12]$$

The resulting global elastic moduli and coefficients of thermal expansion for the NM and UHM-CFRP laminate for the current experimental validation are 79.08 GPa and 223.41 GPa, and 1.62×10^{-6}/°C and -0.18×10^{-6}/°C, respectively.

The second analytical lap-shear stress model to be discussed in the current context is the TOM model (Tsai *et al.*, 1998). It incorporates adherend shear deformation in the solutions of single- and double-lap joints. In all prior models, shear deformations of the adherends were excluded, possibly due to the relatively small values compared to longitudinal normal deformations (e.g. as in metal bonding), or due to the complexity of the formulations.

During load transfer, large shear stresses are transmitted by the adhesive layer to the adherend surfaces adjacent to the adhesive layer, which entails that shear stress equilibrium at the interface is maintained. These shear stresses trigger adherend shear deformations. Shear stresses are especially significant for adherends with relatively low transverse shear modulus, such as in the case of laminated FRP composites. This theory assumes a linear shear stress distribution through the thickness of the adherend, whereas

adhesive plastic response at failure and thermal mismatch of adherends are not accounted for in its solution. The former excluded feature is believed to be of concern only at loads close to the joint's ultimate failure; nevertheless at normal service loads, incorporating shear deformation of adherends in the analysis tends to slightly underestimate peak stress values near bondlength ends (Al-Shawaf, 2010).

Based on the same notations of Fig. 10.11, the general solution for the adhesive shear stress governing equation (i.e. equation [10.13] below) is identical to that of Hart-Smith's general solution. However, the exponent of the elastic shear stress distribution (λ) in Hart-Smith's (1973) theory is called the 'elongation parameter' in Tsai *et al.*'s (1998) theory, although its mathematical formula is identical (refer to equation [10.7]). It appears in the general equation for Hart-Smith's solution instead of the current solution's β parameter of equation [10.15], which is the core difference between both theories. The parameter β is redefined by two parameters; λ and ω (refer to equation [10.15]). The latter is the 'shear deformation parameter' which accounts for the shear deformations of the adherend in its mathematical formula (i.e. equation [10.14]).

$$\tau = A \sinh(\beta x) + B \cosh(\beta x) \qquad [10.13]$$

$$\omega^2 = \left[1 + \frac{G_a}{t_a}\left(\frac{t_i}{6G_i} + \frac{t_o}{3G_o}\right)\right]^{-1} \qquad [10.14]$$

$$\beta^2 = \omega^2 \lambda^2 \qquad [10.15]$$

The constants A and B are defined as follows (Tsai *et al.*, 1998):

$$A = \frac{\left(\frac{\beta l}{2}\right)\tau_{avg}}{\cosh\left(\frac{\beta l}{2}\right)}\left[\frac{1 - \frac{E_i t_i}{2E_o t_o}}{1 + \frac{E_i t_i}{2E_o t_o}}\right] \qquad [10.16]$$

$$B = \frac{\left(\frac{\beta l}{2}\right)\tau_{avg}}{\sinh\left(\frac{\beta l}{2}\right)} \qquad [10.17]$$

The only parameter required to evaluate the general solution (i.e. equation [10.13]), besides those calculated in Hart-Smith's previous solution, is the global shear modulus of the outer adherend (i.e. CFRP laminate). The latter can be estimated from equation [10.18] (Vasiliev and Morozov, 2001):

$$\frac{1}{G_{o/CFRP}} = \frac{V_f}{G_f} + \frac{V_m}{G_{a/m}} \qquad [10.18]$$

Accordingly, the resulting global shear moduli for the NM and UHM-CFRP laminate for the current experimental validation are 1.16 and 1.10 GPa, respectively.

Lap-shear stress predictions are successfully achieved with Excel spreadsheets due to the continual iterations of parameters and formulas for each individual CFRP and adherend material, geometrical variations, and environmental preconditioning temperature usually involved in large-scale investigations. Figure 10.13(a) and (b) displays the lap-shear stress predictions

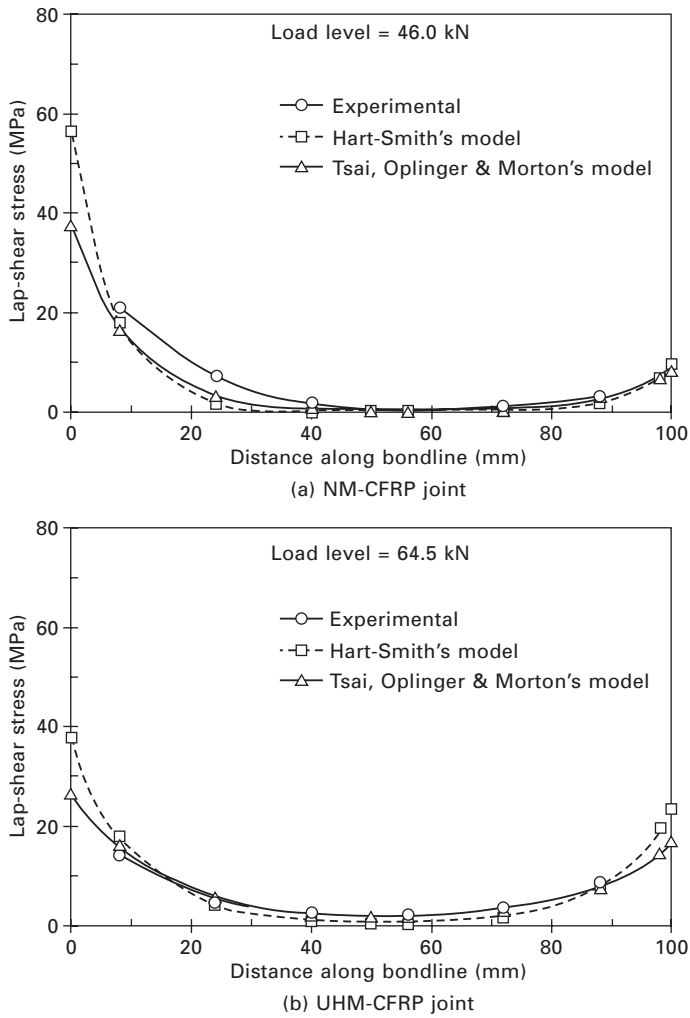

10.13 (a, b) Lap-shear stress distribution along bondlength for identical double-strap CFRP/steel plate specimens having different CF moduli (Al-Shawaf, 2010).

for both models, and for both NM-CFRP and UHM-CFRP experimental joints, respectively, along the CFRP/steel joint bondline, and validates those predictions with experimental results obtained from ERSGs bonded on the outer surface of the CFRP laminate (refer to Fig. 10.10).

10.6.2 FRP strengthened flexural member models

In the last two decades, various analytical models of FRP strengthened flexural members (either concrete or steel) have been introduced in an attempt to understand the mechanisms of load transfer through the interfacial adhesive layer and its inherent consequential shear and peel stresses and debonding failures within such members (Al-Emrani and Kliger, 2006; Benachour *et al.*, 2008; Benrahou *et al.*, 2010; Deng *et al.*, 2004; Lau *et al.*, 2001b; Limam *et al.*, 2003; Malek *et al.*, 1998; Rabinovich and Frostig, 2000; Roberts and Haji-Kazemi, 1989; Smith and Teng, 2001; Stratford and Cadei, 2006; Täljsten, 1997; Vilnay, 1988; Yang and Wu, 2007). A major commonality amongst these models is adopting closed-form solutions in order to avoid a mathematically intractable analysis. Yet, simple closed-form solutions have basically restricted the analysis to explicitly adopting linear elastic material models which may pose some uncertainty, particularly with FRP applications on steel flexural members at ultimate loads. On the other hand, what differentiates these analyses is their basic assumptions. These may include, but are not limited to, loading pattern (i.e. mechanical and thermal), variation of adherend shear deformation pattern across adherend thickness (i.e. linear or parabolic), bending stiffness of the FRP laminate relative to the flexural member, uniform or variable shear and peel stresses within adhesive thickness, FRP laminate fibre orientation, prestressing in the FRP laminate, and flexural member geometry.

Derivations for almost all analytical models for FRP strengthened flexural members are based on the typical schematic FBDs of Fig. 10.14. This particular case represents a differential segment of an FRP strengthened beam under uniformly distributed load, and the bending stiffness of the FRP laminate is assumed to be much smaller than that of the beam to be strengthened. Forces, moments and stresses acting on these basic FBDs reflect the individual assumptions preset for any analysis. The interfacial adhesive shear and normal stress are denoted by $\tau(x)$ and $\sigma(x)$, respectively. Equation [10.19] is the mathematical representation of the basic definition of shear stress $\tau(x)$ in the adhesive layer, which is directly related to the difference in longitudinal deformation between the FRP laminate at its interface with the adhesive and the beam's soffit.

$$\tau(x) = \frac{G_a}{t_a}\,[u_2(x) - u_1(x)] \qquad [10.19]$$

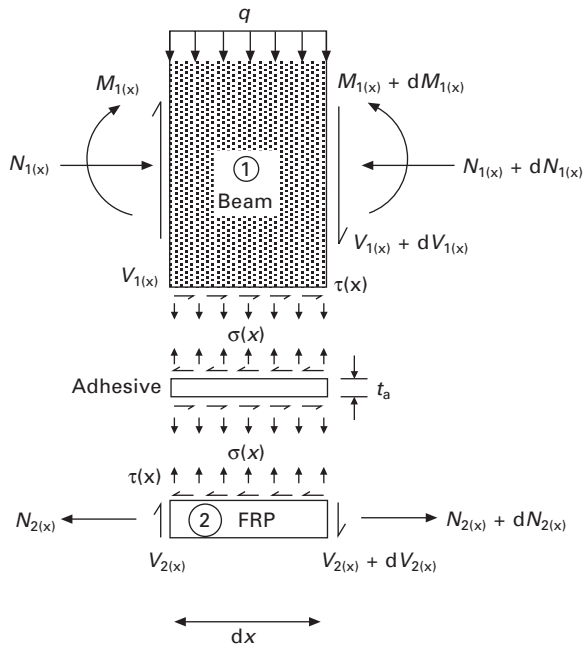

10.14 FBD for differential segments (i.e. beam, adhesive and FRP laminate) of a soffit-plated beam.

where G_a and t_a denote the shear modulus and thickness of the adhesive layer; and $u_1(x)$ and $u_2(x)$ are the longitudinal displacements at the base of adherend 1 and the top of adherend 2, respectively.

The other interfacial stress variant in the adhesive layer is the normal stress $\sigma(x)$, given in equation [10.20], created when a vertical separation occurs between adherends 1 and 2 due to the beam bending under load:

$$\sigma(x) = \frac{E_a}{t_a}[v_2(x) - v_1(x)] \qquad [10.20]$$

where $v_1(x)$ and $v_2(x)$ are the vertical displacements of adherends 1 and 2, respectively; and E_a is the adhesive's elastic modulus. Following the basic shear and normal stress equations, the mathematical solution of the governing partial differential equations (PDE) proceeds, based on the individual assumptions of each analysis and its appropriate boundary and continuity conditions, until general solutions for both stress variants are obtained and are ready to be implemented in the analytical predictions.

10.7 Finite element method (FEM) and finite difference method (FDM) models of stress in FRP composite joints

In the realm of advanced composites, and particularly adhesively bonded ones, numerical analysis methods inevitably emerge when analytical closed-form methods of solution fail to cope with complex lap-joint geometries (e.g. scarf, tapered and stepped-lap joints), finite width effects such as in 3D modelling, or material non-linearities. Numerical methods for stress predictions in advanced composites applications are customarily classified into 'finite difference methods' (FDM) and 'finite elements methods/models' (FEM). The FDM utilize pointwise approximations in lieu of the continuous variables in the governing PDEs of the otherwise closed-form algebraic solution. Finite difference expressions replace the differential terms in the differential equations, which creates a series of simultaneous equations to be solved by matrix representation with specific software (Gleich, 2002). Few FDM stress analysis investigations for adhesively bonded civil applications are found in pertinent literature (Gleich, 2002; Roberts and Haji-Kazemi, 1989; Stratford and Cadei, 2006; Varastehpour and Hamelin, 1997), compared with a multitude of FEM articles about predicting adhesive shear and peel stress (Adams *et al*., 1986; Adams and Mallick, 1992; Al-Emrani and Kliger, 2006; Al-Shawaf, 2010; Albat and Romilly, 1999; Angus *et al*., 2007; Deng *et al*., 2004; Diaz *et al*., 2009; Gleich, 2002; Harris and Adams, 1984; Lau *et al*., 2001b; Pickett and Hollaway, 1985; Pickthall *et al*., 1997; Rabinovich and Frostig, 2000; Roberts, 1989; Sharifi and Choupani, 2008; Täljsten, 1997; Tsai and Morton, 1994; Tsai *et al*., 1998). The FEM is probably the only numerical method that can viably handle and accurately predict failure loads and stresses in a structural element of almost any geometrical attributes, boundary conditions, prescribed environmental conditions and load pattern provided that model discretization, boundary conditions and the loading are applied properly (Al-Shawaf, 2010; DoT, 2005). The other salient disadvantages of the FDM compared to the FEM are the relatively long time required to set up the solution of the problem by the FDM and the less detailed stress data (e.g. peel stresses in adherends, stresses along interfaces, etc.) obtained from the solution (Gleich, 2002). For these reasons, FEM is elaborated for the remaining part of this section.

The FEM attains approximate solutions of PDEs as well as of integral equations of any structure exposed to certain loading and environmental conditions. The structure is represented as an assemblage of discrete elements interconnected at a finite number of nodal points, which collectively make a grid called a mesh. The solution approach is based on either eliminating the differential equation completely (steady-state problems) or rendering the PDE into an approximating system of ordinary differential equations, which

are then numerically integrated using standard techniques. The main finite element features that influence the accuracy of stress predictions are briefly reviewed in the following subsections.

10.7.1 FE mesh refinement

FEM literature unanimously agrees on the verified importance of refining the mesh of the FE model, particularly in regions of high stress concentrations, to obtain accurate results. In terms of FRP adhesively bonded joints, these regions include ends of the FRP strengthening bondlength (refer to Fig. 10.15), cracks in adherends, or any unintentional discontinuity in the bond due to adherend surface preparations and adhesive application procedures. Amongst these locations, high stress concentrations close to bondlength ends are unavoidable, which entails undertaking some mesh refinements to achieve acceptable stress results. However, it has been found that mesh refinement beyond a certain degree does not increase the accuracy of results within high stress concentration regions and incurs unjustifiably high computational cost (Al-Shawaf, 2010; Sharifi and Choupani, 2008).

10.7.2 FE model representability

To anticipate accurate stress predictions from the FE model, it has to be representative of the actual experimental or *in-situ* application in terms of its dimensions, material thermo-mechanical properties, prescribed environmental conditions, degrees of freedom (i.e. constraints) and loading pattern, as well as the choice of the right element formulation suitable for the simulated application. As an example, the 2D FE model of Fig. 10.15 represents half

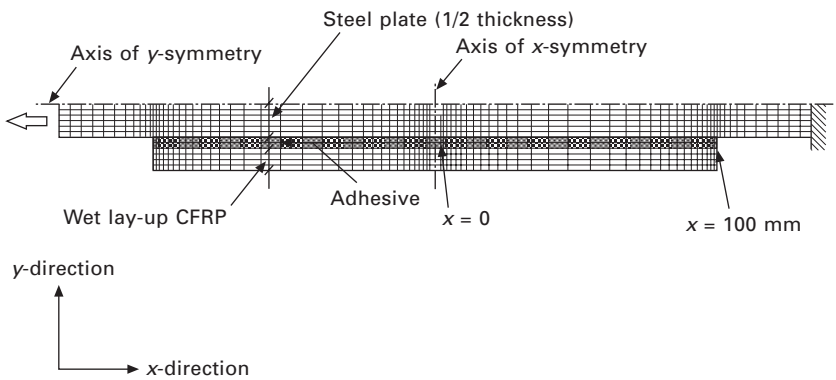

10.15 Schematic for a FE model representing half of a double-strap CFRP/steel joint experimental specimen during tensile testing (not to scale).

of an experimental double–strap joint specimen during tensile testing. The right-hand side represents the fixed grip of the testing frame; the left-hand side is the movable one controlled by either displacement or loading rate; and together with the axis of *y*-symmetry they represent the realistic features that should be simulated in the FE model. A few investigations have modelled only one-quarter of this experimental specimen by utilizing the *x*-axis of symmetry besides the *y*-axis (refer to Fig. 10.15). The latter modelling practice has been numerically proven to predict inaccurate stress values, especially at loading levels close to the ultimate joint strength (Al-Shawaf, 2010).

10.7.3 Finite element dimensionality

Generally, two types of element families are usually implemented in FEM, viz. 2D and 3D modelling. As a general rule, 2D modelling is characterized by simplicity and allows the analysis to be run on a relatively normal PC. However, it tends to yield less accurate results, particularly in large-scale structures. On the other hand, although 3D modelling yields more accurate results for these structures, it usually experiences difficulties when running on normal computers, since only the fastest computers can guarantee its smooth and effective performance. It has been demonstrated that by utilizing the stress-based analysis approach and combining the small scale of most adhesive lap-joints with the appropriate 2D elements, the accuracy of the FE model stress predictions is not compromised (Al-Shawaf, 2010).

10.7.4 Adhesive non-linearity

The effect of adhesive non-linearity on the behaviour of FRP adhesively bonded joints was adequately addressed in Section 10.3. However, it is useful to recall that considering adhesive non-linear representation in FEM has a negligible effect on the predicted shear and peel stresses at service load levels of the FRP composite joint, because their distribution along the whole bondlength is mainly linear-elastic. Interfacial adhesive non-linearity has a substantial effect on the accuracy of quantitative FEM predictions of both stresses, and thus joint capacity, only at loads nearing joint failure where all practical adhesives, even brittle ones, exhibit non-linear behaviour.

The advantage of including the adhesive's non-linear constitutive stress–strain model, in terms of the accuracy of the FE stress predictions, can be clearly demonstrated with reference to Fig. 10.16. This figure represents the stress–strain curve for a specific resin (i.e. Araldite 420® epoxy) bulk coupon tested experimentally in direct tension inside an environmental chamber where the temperature of the coupon reached –40°C. Path OAB represents the actual measured nominal stress–strain curve, which is characterized by two parts: the first part (i.e. OA) is linear, whereas the second part (AB)

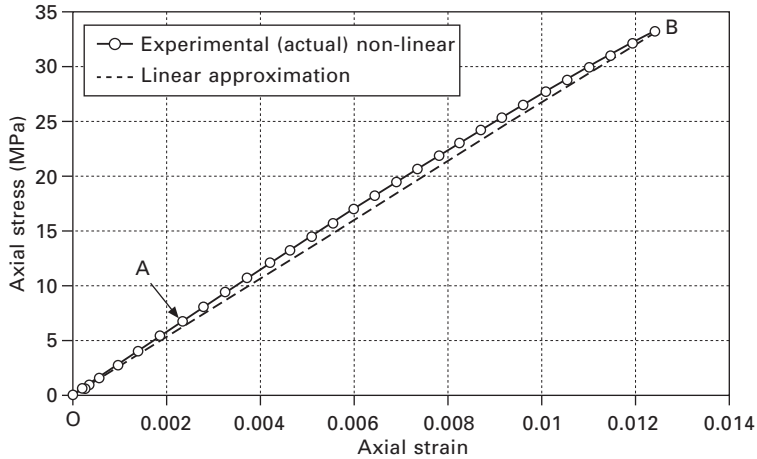

10.16 Experimental nominal stress–strain diagram for bulk Araldite 420® epoxy coupon at –40°C (Al-Shawaf, 2010).

shows slight non-linearity. On the other hand, the straight dashed line OB is a linear stress-strain approximation of curve OAB.

A FE model, simulating an experimental tensile test for a double-strap wet lay-up NM-CFRP/steel specimen fabricated with the same epoxy resin and similar geometrical dimensions to those reported in Section 10.6.1 and Fig. 10.12, and conditioned at –40°C, has been analysed twice. In the first FEM, the adhesive constitutive model is based on the slightly non-linear path OAB; while the linear approximation OB is implemented for the second model. From experimental observations and preliminary FE analyses, the critical interfacial adhesive stress locations are near either $x = 0$ or $x = 100$ mm (refer to Fig. 10.15). In this particular example, the experimental specimen fails cohesively close to the $x = 100$ mm end of the bondlength at a load of 94.8 kN.

Figure 10.17(a) and (b) represents the FE maximum principal stress–strain diagrams for two integration points lying at the mid-depth of the interfacial adhesive layer and close to the $x = 0$ and $x = 100$ mm ends of the bondlength, respectively. As can be implied from Fig. 10.17(b) and the FE post-analysis results found in Al-Shawaf (2010), the FEM based on both the linear part (OA) and the non-linear part (AB) has successfully predicted the failure location (i.e. close to $x = 100$ mm), the bulk uniaxial failure stress value of 33.88 MPa (i.e. at the turning point B' which corresponds to point B of Fig. 10.16 which has a true failure stress of 33.7 MPa), and a corresponding failure load of 94.6 kN; whereas the FEM based on the straight line (OB) is not able to predict the peak maximum principal stress, and thus the ultimate joint capacity and failure location, as it keeps ascending beyond the experimental ultimate value.

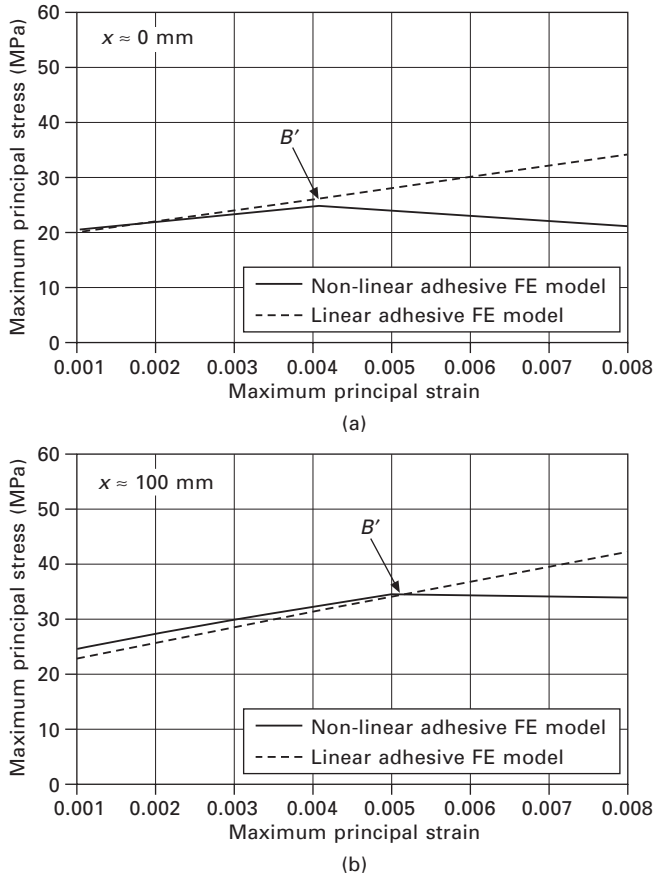

10.17 FE maximum principal stress–strain diagrams at two correspondent adhesive integration points close to (a) x = 0 mm, and (b) x = 100 mm lap ends (Al-Shawaf, 2010).

Figure 10.18(a) and (b) displays and validates the FE lap-shear stress predictions, with the same experimental double-strap CFRP/steel specimens discussed in Section 10.6.1, along the CFRP/steel joint bondline. The lap-shear stress divergence between the FE predictions and experimental results disclosed in Fig. 10.18(a) close to the x = 0 end is due to erroneous reading of the ERSG in this location, and is discussed in Al-Shawaf (2010).

For joint capacity predictions of the CFRP/steel double-strap joint model of Fig.10.15, the precise manner in which the failure criteria are applied and the consequent stress predictions extracted can be summarized as follows (Al-Shawaf, 2010):

1. For the FE simulations of experimental joints with NM-CFRP, either the maximum principal stress or the von Mises stress criterion is

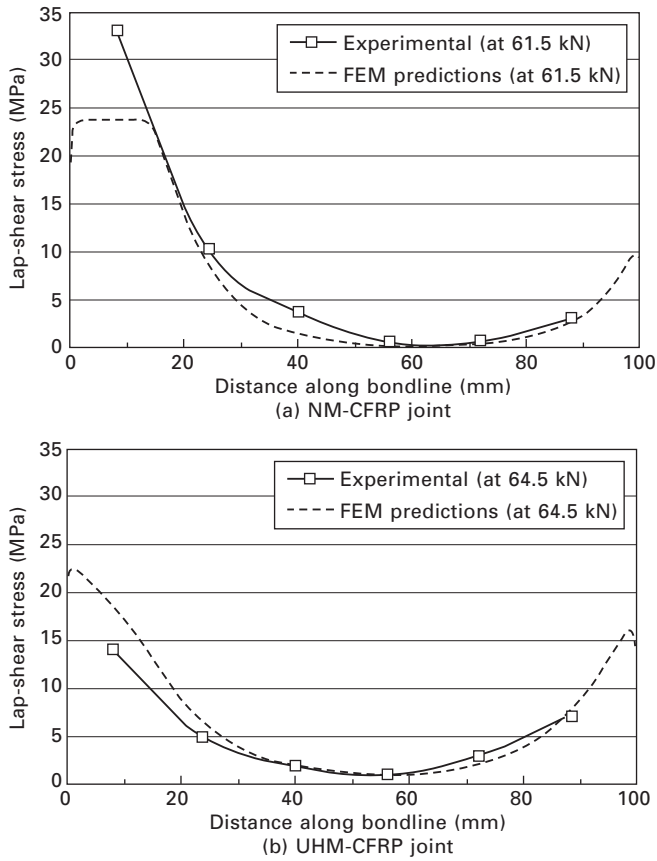

10.18 (a, b) Lap-shear stress distribution along bondlength for identical double-strap CFRP/steel plate specimens having different CF moduli (Al-Shawaf, 2010).

implemented, depending on whether the adhesive is assumed brittle or ductile, respectively. The relevant stress is plotted against the time increments (for the loading step) for the two independent integration points close to $x = 0$ and $x = 100$ mm. The selected integration points must be chosen to lie close to the mid-depth of the adhesive layer to attain accurate and reliable adhesive stress values. The integration point's curve that attains the higher peak stress is taken as the adhesive failure stress, which simulates the bulk uniaxial experimental failure stress value. The location of this integration point is the predicted triggering failure location, and the joint capacity is predicted by doubling the summation of the reaction forces at the nodes of the simulated fixed grip (refer to Fig. 10.15) recorded at the time increment corresponding to the aforementioned higher peak stress.

2. For FE simulations of experimental joints with UHM-CFRP, failure can be either adhesive-related (i.e. as in the previous point) or fibre-related (i.e. pure UHM-CF rupture at the central gap between both steel plates, as in Fig. 10.5(e)); therefore both cases should be assessed to find out the critical one (i.e. the case that satisfies its failure criterion at a smaller time increment). For the pure UHM-CF rupture, the FE maximum principal stress of the fibres is plotted with time increments for a selected integration point within the vicinity of the central gap; and since the fibre material is modelled as brittle elastic, its assumed rupture (i.e. failure) onset is predicted at the time increment when the fibre's experimental tensile strength is slightly exceeded in the aforementioned curve. The above method for ultimate stress, joint capacity and failure pattern predictions has been successfully validated in Al–Shawaf (2010).

10.8 Implications for the design of FRP composite joints

In this chapter, informative discussions, explanations and verifications have been presented on the issue of stresses, their categories, significance and characterization in FRP strengthened civil applications. Throughout the chapter, particular emphasis has been given to the lap-shear and normal stresses within the interfacial adhesive layer of externally bonded FRP/steel adherends, since this component (i.e. interfacial adhesive) and adherend (i.e. steel) of such FRP joints represent, in terms of these stresses, the most likely failure location and ultimate capacity of FRP adhesive joints, respectively. Some useful key conclusions can be drawn based on all the issues presented in this chapter:

- Typically, shear, peel and thermal residual stresses are found in FRP retrofitting applications, with the first two categories exhibiting high stresses in the adhesive layer.
- Considerable local stress concentration near both bondlength ends (or close to bond discontinuities) is the major common attribute for both shear and peel stresses.
- Optimized adhesively bonded joints are designed to transfer the applied load mainly in shear, and minimize any direct or induced peel stresses.
- Assuming adequate surface preparation, the lap-shear stress of FRP adhesive joints at the critical bond end-zones, and thus the capacities and failure patterns, are functions of the geometrical and thermo-mechanical properties of the interfacial adhesive and both adherends, besides the environmental exposure conditions.
- Ductility of the polymeric components of FRP composite joints, particularly

of the interfacial adhesive, has a significant effect on alleviating the lap-shear stress concentrations at both bond end-zones.
- Adherend stiffness imbalance and thermal mismatch have a substantial effect on the lap-shear stress distribution along the joint's bondlength.
- The experimental bond stress determination method requires instrumentally measured strains at corresponding locations via either contact or non-contact methods.
- The most established contact strain-measuring method is bonding ERSGs on the outer surface of the FRP laminate; however, strain readings and the following conversion to stresses (by utilizing the concept of FBD and equilibrium of forces) are based on a number of simplifying assumptions which compromise the accuracy of measured stresses.
- Measuring strains with the FOS method has some practical advantages over ERSGs; however, this contact method is not yet fully established in stress calculations for advanced composites.
- Moiré interferometry and digital image correlation are the most popular non-contact strain-measuring methods. Both are based on optical principles.
- MI/SI techniques have been utilized in measuring the in-plane surface deformation of the overlap region for FRP adhesively bonded joint specimens, but have not been systematically implemented for FRP adhesive/adherend stress calculations.
- The DIC method has great potential in measuring the 2D and 3D surface deformations and strain values of structural components at extreme environmental exposures. It has been adopted in a few interfacial adhesive lap-shear stress analyses of FRP–concrete joints; yet the same drawbacks of accurate stress estimation in contact methods persist in the DIC as well.
- Plenty of closed-form theoretical models for stress analysis in adhesive lap joints are available in the relevant literature, yet few of these models are capable of achieving adequate correlation with experimental results due to the preset stress calculation assumptions for both methods.
- Many closed-form analytical models for FRP strengthened flexural members exist in literature. Their potential for accurate prediction is also restricted due to the same above-mentioned assumptions.
- Numerical methods for stress predictions are classified into FDM and FEM. However, FEM is probably the only method capable of providing accurate predictions of stresses and failure loads in the field of FRP strengthening applications, basically due to its capacity in simulating geometrical and material non-linearities of the model.
- FE mesh refinement, model representability, dimensionality and adhesive non-linearity are the main influential factors that determine the accuracy of stress predictions to be anticipated from any FEM analysis.

10.9 Conclusion and future trends

The applications of advanced composites in upgrading civil engineering infrastructure are progressively increasing worldwide. This trend is justified, besides the superior advantages of advanced composites, by the ever-growing number of experimental, theoretical and numerical investigations in this field endeavouring to unveil and validate more information on pertinent parameters governing the viable implementation of these applications. Stresses inherent within these composites are indisputably the most critical parameters defining the overall structural performance of any composite strengthening scheme. This chapter started with a brief overview of the status quo in the utilization of advanced composites in civil engineering and the need to undertake more relevant specialized research. This was followed by a comprehensive explanation and discussions on issues deemed to have direct input on the quantitative and qualitative aspects of stresses within FRP adhesively bonded applications.

These issues comprised the types of stresses and adherends mainly encountered in the latter applications, besides geometrical and thermo-mechanical aspects of the adhesive joints and their constitutive materials. The next section addressed interfacial adhesive stress testing and measurement methods with pertinent detailed explanations. These included experimental, theoretical and numerical. A brief literature review for each of these methods and their sub-categories was provided with some useful comparisons to highlight their advantages and disadvantages. Practical experimental, theoretical and numerical procedures in measuring, estimating and predicting adhesive lap-shear stress were also included in this section, with supporting equations, figures and numerical examples from existing literature. The final two sections (i.e. implications and future trends) reported on important conclusions from the current chapter and future recommended suggestions for resolving current uncertainties usually encountered in FRP adhesive stress analysis and measurement.

From the issues discussed in the current chapter, a pressing need exists for future investigations to further current knowledge and resolve some of the frequently encountered uncertainties. Investigations deemed required should address the following topics:

- The existing gap in the database for adhesive materials and durability needs to be effectively bridged by conducting more thermo-mechanical characterizations on existing adhesives, at harsh environmental exposures; and by expanding this, hopefully international, database to new commercially available adhesives. This prospective database should be made readily accessible to all scholars and researchers before anticipating tangible difference in this regard.
- The introduction of more developed FRP specimen/*in-situ* fabrication and

adhesive application methods to enhance the consistency and reliability of stress results must be prioritized. This should help in excluding any sources of variations and inconsistencies in the results to enhance their credibility. A new experimental method for achieving the above desired outcome on small-scale specimens has been proposed in Al-Shawaf (2010).

- The adoption of advanced optical strain-measuring techniques in FRP advanced composite applications, based on both FOS and DIC methodologies, needs to be positively promoted. Investigations in this regard should focus on exploring novel experimental and analytical procedures to develop the current accurate strain-measuring capabilities of these methods into corresponding reliable stress values. This would substantially assist in surmounting the practical difficulties associated with ERSG measurement, especially within critical locations and infinitesimal lengths where high localized stresses reside (e.g. close to bondlength end-zones).
- Analytical and numerical models for stress predictions should rely more on information on adhesives acquired from the previously proposed material database in order to enhance their accuracy and predictability. Special emphasis on including experimentally derived adhesive stress–strain correlations in shear and direct tension should considerably contribute to the above objective.

10.10 Sources of further information and advice

Readers interested in expanding their knowledge database and acquiring more insights on the current stress topic are referred to the following publications, listed in chronological order: Hart-Smith (1973), Adams *et al*. (1986), Lilleheden (1994), Albrecht and Mecklenburg (1996), Hart-Smith (2001), Gleich (2002), Buyukozturk *et al*. (2004), Cadei *et al*. (2004), Adams (2005), DoT (2005) and Banea and da Silva (2009).

10.11 References

Adams R D (ed) (2005), *Adhesive Bonding: Science, Technology and Applications*, Cambridge, UK: Woodhead Publishing.

Adams R D and Mallick V (1992), 'A method for stress analysis of lap joints', *J Adhesion*, 38, 199–217.

Adams R D, Atkins R W, Harris J A and Kinloch A J (1986), 'Stress analysis and failure properties of carbon-fibre-reinforced-plastic/steel double-lap joints', *J Adhesion*, 20(1), 29–53.

Al-Emrani M and Kliger R (2006), 'Analysis of interfacial shear stresses in beams strengthened with bonded prestressed laminates', *Compos Part B – Eng*, 37(4–5), 265–272.

Al-Shawaf A (2010), 'Characterization of bonding behaviour between wet lay-up carbon fibre reinforced polymer and steel plates in double-strap joints under extreme environmental temperatures', Doctorate PhD thesis, Monash University, Melbourne, Australia.

Al-Shawaf A (2011), 'Modelling wet lay-up CFRP–steel bond failures at extreme temperatures using stress-based approach', *Int J Adhes Adhes*, 31(6), 416–428.

Albat A M and Romilly D P (1999), 'A direct linear-elastic analysis of double symmetric bonded joints and reinforcements', *Compos Sci Technol*, 59(7), 1127–1137.

Albrecht P and Mecklenburg M F (1996), 'Predicting cohesive strength of a bonded joint from properties of bulk adhesive', in: Saadatmanesh H and Ehsani M R (eds), *1st International Conference on Composites in Infrastructure*, Tuscon, AZ: NSF and University of Arizona, 152–177.

Ali-Ahmad M, Subramaniam K and Ghosn M (2006), 'Experimental investigation and fracture analysis of debonding between concrete and FRP sheets', *J Eng Mech – ASCE*, 132(9), 914–923.

Allman D J (1977), 'A theory for elastic stresses in adhesive bonded lap joints', *Q J Mech Appl Math*, 30(4), 415–436.

Angus C C L and Cheng J J R (2004), 'Study of the tensile strength of CFRP/steel double lap joints', *ACMBS 2004*, 20–23 July, Calgary, Alberta, Canada.

Angus C C L, Cheng J J R, Michael C H Y and Gaylene D K (2007), 'Repair of steel structures by bonded carbon fibre reinforced polymer patching: experimental and numerical study of carbon fibre reinforced polymer–steel double-lap joints under tensile loading', *Can J Civil Eng*, 34(12), 1542–1553.

Ansari F (1997), 'State-of-the-art in the applications of fiber-optic sensors to cementitious composites', *Cement Concrete Comp*, 19(1), 3–19.

Ansari F and Libo Y (1998), 'Mechanics of bond and interface shear transfer in optical fiber sensors', *J Eng Mech – ASCE*, 124(4), 385–394.

ASTM (2004), D3528-96 (reapproved 2002), 'Standard test method for: Strength properties of double lap shear adhesive joints by tension loading', *in*: *Annual Book of ASTM Standards*, 2004 edn, West Conshohocken, PA: ASTM International.

ASTM (2007), D5656-04E01, 'Standard test method for: Thick-adherend metal lap-shear joints for determination of the stress–strain behaviour of adhesives in shear by tension loading', *in: Annual Book of ASTM Standards*, 2007 edn, West Conshohocken, PA: ASTM International.

Avril S, Ferrier E, Vautrin A, Hamelin P and Surrel Y (2004), 'A full-field optical method for the experimental analysis of reinforced concrete beams repaired with composites', *Compos Part A – Appl Sci*, 35(7–8), 873–884.

Banea M D and da Silva L F M (2009), 'Adhesively bonded joints in composite materials: An overview', *P I Mech Eng L – J Mat*, 223(1), 1–18.

Benachour A, Benyoucef S, Tounsi A and Adda bedia E A (2008), 'Interfacial stress analysis of steel beams reinforced with bonded prestressed FRP plate', *Eng Struct*, 30(11), 3305–3315.

Benrahou K H, Ameur M, Tounsi A, Benyoucef S and Adda bedia E A (2010), 'Influence of adhesive characteristics on the interfacial stress concentrations in externally FRP plated steel beams', *Compos Interface*, 17(4), 283–300.

Bernini R, Fraldi M, Minardo A, Minutolo V, Carannante F, Nunziante L and Zeni L (2006), 'Identification of defects and strain error estimation for bending steel beams using time domain Brillouin distributed optical fiber sensors', *Smart Mater Struct*, 15(2), 612.

Bigwood D A and Crocombe A D (1990), 'Non-linear adhesive bonded joint design analyses', *Int J Adhes Adhes*, 10(1), 9.

BSI (2011), BS EN 14869–2:2011 *Structural adhesives. Determination of shear behaviour of structural bonds. Thick adherends shear test*, 2011 edn. London: British Standards Institution.

Buyukozturk O, Gunes O and Karaca E (2004), 'Progress on understanding debonding problems in reinforced concrete and steel members strengthened using FRP composites', *Constr Build Mater*, 18(1), 9–19.

Cadei J M C, Stratford T J, Hollaway L C and Ducket W G (2004), 'Strengthening metallic structures using externally bonded fibre-reinforced polymers C595', London: CIRIA.

Carloni C and Subramaniam K V (2010), 'Direct determination of cohesive stress transfer during debonding of FRP from concrete', *Compos Struct*, 93(1), 184–192.

Cheng S, Chen D and Shi Yu (1991), 'Analysis of adhesive-bonded joints with nonidentical adherends', *J Eng Mech – ASCE*, 117(3), 605–623.

Chiew S P, Yu Y and Lee C K (2011), 'Bond failure of steel beams strengthened with FRP laminates – Part 1: Model development', *Compos Part B – Eng*, 42(5), 1114–1121.

Crocombe A D, Richardson G and Smith P A (1995), 'A unified approach for predicting the strength of cracked and non-cracked adhesive joints', *J Adhesion*, 49(3–4), 211–244.

das Neves P J C, da Silva L F M and Adams R D (2009), 'Analysis of mixed adhesive bonded joints. Part I: Theoretical formulation', *J Adhes Sci Technol*, 23(1), 1–34.

Dawood M and Rizkalla S H (2007), 'Bond and splice behaviour of CFRP laminates for strengthening steel beams', *International Conference on Advanced Composites in Construction (ACIC 07)*, 2–4 April, University of Bath, Bath, UK.

de Bruyne N A (1944), 'The strength of glued joints', *Aircraft Eng*, 16, 115–118.

Deb A, Malvade I, Biswas P and Schroeder J (2008), 'An experimental and analytical study of the mechanical behaviour of adhesively bonded joints for variable extension rates and temperatures', *Int J Adhes Adhes*, 28(1–2), 1–15.

Delale F, Erdogan F and Aydinoglu M N (1981), 'Stresses in adhesively bonded joints: A closed-form solution', *J Compos Mater*, 15(3), 249–271.

Deng J, Lee M M K and Moy S S J (2004), 'Stress analysis of steel beams reinforced with a bonded CFRP plate', *Compos Struct*, 65(2), 205.

Diaz A D, Hadj-Ahmed R, Foret G and Ehrlacher A (2009), 'Stress analysis in a classical double lap, adhesively bonded joint with a layerwise model', *Int J Adhes Adhes*, 29(1), 67.

DoD (USA) (2002), 'Structural behaviour of joints', *in: Military Handbook – MIL-HDBK-17-3F: Composite Materials Handbook, Volume 3 – Polymer Matrix Composites Materials Usage, Design, and Analysis*, Washington DC: US Dept of Defense.

DoT (USA) (2005), 'Methods of analysis and failure predictions for adhesively bonded joints of uniform and variable bondline thickness', Washington DC: Federal Aviation Administration, Report no. DOT/FAA/AR-05/12.

Dutta P K and Lampo R G (1993), Behaviour of fibre-reinforced plastics as construction materials in extreme environments, *in: Third (1993) International Offshore and Polar Engineering Conference*, Singapore: The International Society of Offshore and Polar Engineers, 339–344.

El-Salakawy E, Benmokrane B and Desgagné G (2003), 'Fibre-reinforced polymer composite bars for the concrete deck slab of Wotton Bridge', *Can J Civil Eng*, 30(5), 861–870.

Etman E E and Beeby A W (2000), 'Experimental programme and analytical study of bond stress distributions on a composite plate bonded to a reinforced concrete beam', *Cement Concrete Comp*, 22(4), 281–291.

Fawzia S, Al-Mahaidi R and Zhao X L (2006), 'Experimental and finite element analysis of a double lap shear connection between steel plates and CFRP', *Compos Struct*, 75(1–4), 156–162.

Garden H N, Quantrill R J, Hollaway L C, Thorne A M and Parke G A R (1998), 'An experimental study of the anchorage length of carbon fibre composite plates used to strengthen reinforced concrete beams', *Constr Build Mater*, 12(4), 203–219.

Gleich D (2002), *Stress analysis of structural bonded joints*, Doctorate PhD thesis, Technical University of Delft, Delft, the Netherlands.

Goland M and Reissner E (1944), 'The stresses in cemented joints', *J Appl Mech*, 11, A17–A27.

Grattan K T V and Sun T (2000), 'Fiber-optic sensor technology: an overview', *Sensor Actuator*, 82, 40–61.

Green A K, Zaidman M, Shafir E, Tur M and Gali S (2000), 'Infrastructure development for incorporating fibre-optic sensors in composite materials', *Smart Mater Struct*, 9(3), 316.

Gustafson P A, Bizard A and Waas A M (2007), 'Dimensionless parameters in symmetric double lap joints: An orthotropic solution for thermomechanical loading', *Int J Solids Struct*, 44(17), 5774–5795.

Hadj-Ahmed R, Foret G and Ehrlacher A (2001), 'Stress analysis in adhesive joints with a multiparticle model of multilayered materials (M4)', *Int J Adhes Adhes*, 21(4), 297–307.

Haghani R (2010), 'Analysis of adhesive joints used to bond FRP laminates to steel members – A numerical and experimental study', *Constr Build Mater*, 24(11), 2243–2251.

Haghani R, Al-Emrani M and Kliger R (2009), 'Interfacial stress analysis of geometrically modified adhesive joints in steel beams strengthened with FRP laminates', *Constr Build Mater*, 23(3), 1413–1422.

Hahn H T (1976), 'Residual stresses in polymer matrix composite laminates', *J Compos Mater*, 10, 266–278.

Hahn K F and Fouser D F (1962), 'Methods for determining stress distribution in adherends and adhesives', *J Appl Polym Sci*, 6(20), 145–149.

Han B, Post D and Ifju P (2001), 'Moiré interferometry for engineering mechanics: Current practices and future developments', *J Strain Anal Eng*, 36(1), 101–117.

Harris J A and Adams R D (1984), 'Strength prediction of bonded single lap joints by non-linear finite element methods', *Int J Adhes Adhes*, 4(2), 65–78.

Hart-Smith L J (1972), 'Design and analysis of adhesive-bonded joints', *Airforce Conference on Fibrous Composites in Flight Vehicle Design*, 26–28 September, Dayton, OH.

Hart-Smith L J (1973), 'Adhesive-bonded double-lap joints', Hampton, VA, NASA Langley Research Centre, Report no. NASA CR-112235.

Hart-Smith L J (1974a), 'Advances in the analysis and design of adhesive-bonded joints in composite aerospace structures', *Proceedings of the 19th National SAMPE Symposium and Exhibition,* 23–25 April, Buena Park, CA: Society for the Advancement of Material and Process Engineering (SAMPE), 722–737.

Hart-Smith L J (1974b), 'Analysis and design of advanced composite bonded joints', Hampton, VA, Douglas Aircraft Company, Report no. CR-2218.

Hart-Smith L J (1978), 'Adhesive bond stresses and strains at discontinuities and cracks in bonded structures', *J Eng Mater – Trans ASME*, 100, 15–24.

Hart-Smith L J (1986), *Joints in advanced composite and bonded metal aircraft structures*, Doctor of Engineering PhD thesis, Monash University, Melbourne, Australia.

Hart-Smith L J (2001), 'Bolted and bonded joints', *in*: Miracle D B and Donaldson S L (eds), *Composites*, Materials Park, OH: ASM International.

Hart-Smith L J (2002), 'Adhesive bonding of composite structures – Progress to date and some remaining challenges', *J Comp Tech Res*, 24(3), 133–151.

Hii A K Y and Al-Mahaidi R (2006), 'An experimental and numerical investigation on torsional strengthening of solid and box-section RC beams using CFRP laminates', *Compos Struct*, 75(1–4), 213–221.

Hoffmann H and Vogl C (2003), 'Determination of true stress–strain-curves and normal anisotropy in tensile tests with optical strain measurement', *Cirp Ann – Manuf Techn*, 52(1), 217–220.

ISO (2001), ISO 11003–2: 2001, 'Adhesives – Determination of shear behaviour of structural adhesives – Part 2: Tensile test method using thick adherends', 2001 edn. Geneva, Switzerland: The International Organization for Standardization.

Jiang G (2007), *Self-monitoring fiber reinforced polymer retrofits*, Doctorate PhD thesis, North Carolina State University, Raleigh, NC.

JSA (1999), JIS K 6868-2:1999, 'Adhesives – Determination of shear behaviour of structural bonds – Part 2: Thick-adherent tensile-test method', 1999 edn. Tokyo: The Japanese Standards Association.

Kalamkarov A, Saha G, Rokkam S, Newhook J and Georgiades A (2005), 'Strain and deformation monitoring in infrastructure using embedded smart FRP reinforcements', *Compos Part B – Eng*, 36(5), 455–467.

Karbhari V M and Lee L S (2011), *Service Life Estimation and Extension of Civil Engineering Structures*, Cambridge, UK: Woodhead Publishing.

Karbhari V M and Shulley S B (1995), 'Use of composites for rehabilitation of steel structures – determination of bond durability', *J Mater Civil Eng*, 7(4), 239–245.

Karbhari V M, Chin J W, Hunston D, Benmokrane B, Juska T, Morgan R, Lesko J J, Sorathia U and Reynaud D (2003), 'Durability gap analysis for fiber-reinforced polymer composites in civil infrastructure', *J Compos Constr*, 7(3), 238–247.

Kasen M B (1981), 'Cryogenic properties of filamentary-reinforced composites: an update', *Cryogenics*, 21(6), 323–340.

Kim Y J, Hossain M and Chi Y (2011), 'Characteristics of CFRP–concrete interface subjected to cold region environments including three-dimensional topography', *Cold Reg Sci Technol*, 67(1–2), 37–48.

Kinloch A J (1982), 'Review. The science of adhesion: Part 2 Mechanics and mechanisms of failure', *J Mater Sci*, 17(3), 617–651.

Lau K T, Chan C C, Zhou L M and Jin W (2001a), 'Strain monitoring in composite-strengthened concrete structures using optical fibre sensors', *Compos Part B – Eng*, 32(1), 33–45.

Lau K T, Dutta P K, Zhou L M and Hui D (2001b), 'Mechanics of bonds in an FRP bonded concrete beam', *Compos Part B – Eng*, 32(6), 491–502.

Lau K T, Zhou L M, Tse P C and Yuan L B (2002), 'Applications of composites, optical fibre sensors and smart composites for concrete rehabilitation: An overview', *Appl Compos Mater*, 9(4), 221–247.

Li Q, Li G, Wang G and Yuan L (2004), 'CTOD measurement for cracks in concrete by fiber optic sensors', *Opt Laser Eng*, 42(4), 377–388.

Lilleheden L (1994), 'Mechanical properties of adhesives *in situ* and in bulk', *Int J Adhes Adhes*, 14(1), 31–37.

Limam O, Foret G and Ehrlacher A (2003), 'RC beams strengthened with composite material: a limit analysis approach and experimental study', *Compos Struct*, 59(4), 467–472.

Lopez-Anido R and Naik T R (2000), *Emerging Materials for Civil Infrastructure / State of the Art*, Reston, VA: American Society of Civil Engineers,

Lord H W and Dutta P K (1988), 'On the design of polymeric composite structures for cold regions applications', *J Reinf Plast Comp*, 7, 435–458.

Malek A M, Saadatmanesh H and Ehsani M R (1998), 'Prediction of failure load of R/C beams strengthened with FRP plate due to stress concentration at the plate end', *ACI Struct J*, 95(1), 142–152.

Matta F (2003), 'Bond between steel and CFRP laminates for rehabilitation of metallic bridges', Masters MS, University of Padova, Padova, Italy.

Merklein M and Gödel V (2009), 'Characterization of the flow behavior of deep drawing steel grades in dependency of the stress state and its impact on FEA', *IJMF*, 2, 415–418.

Morita M and Umezawa O (2011), 'Analysis of crystal rotation by Taylor theory', *in*: Proulx T (ed.) *Optical Measurements, Modeling and Metrology*, Bethel, CT: Springer Science + Business Media.

Mortensen F (1998), 'Development of tools for engineering analysis and design of high-performance FRP-composite structural elements', Doctorate PhD thesis, Aalborg University, Aalborg East, Denmark.

Mortensen F and Thomsen O T (2002), 'Analysis of adhesive bonded joints: a unified approach', *Compos Sci Technol*, 62(7–8), 1011–1031.

Moy S S J (ed) (2001), *FRP Composites: Life Extension and Strengthening of Metallic Structures*, London: Thomas Telford Publishing.

Mufti A A (2003), 'FRPs and FOSs lead to innovation in Canadian civil engineering structures', *Constr Build Mater*, 17(6–7), 379–387.

NASI (2011), I.S.EN 14869–2:2011, 'Structural adhesives – Determination of shear behaviour of structural bonds – Part 2: Thick adherends shear test', 2011 edn. Dublin: National Standards Authority of Ireland.

Pham H B and Al-Mahaidi R (2007), 'Modelling of CFRP-concrete shear-lap tests', *Constr Build Mater*, 21(4), 727–735.

Pickett A K and Hollaway L (1985), 'The analysis of elastic–plastic adhesive stress in bonded lap joints in FRP structures', *Compos Struct*, 4(2), 135–160.

Pickthall C, Heller M and Rose L R F (1997), 'Finite element analysis of the double lap joint with an elastic–plastic adhesive', Melbourne, Australia, DSTO Aeronautical and Maritime Research Laboratory, Report no. DSTO-TR-0528.

Post D (1993), 'Moiré interferometry', *in*: Kobayashi A S (ed) *Handbook on Experimental Mechanics*, New York and London: VCH Publishers.

Post D and Han B (2008), 'Moiré interferometry', *in*: Sharpe W N (ed) *Springer Handbook of Experimental Solid Mechanics*, New York: Springer Science + Business Media.

Rabinovich O and Frostig Y (2000), 'Closed-form high-order analysis of RC beams strengthened with FRP strips', *J Compos Constr*, 4(2), 65–74.

Roberts T and Haji-Kazemi H (1989), 'Theoretical study of the behaviour of reinforced concrete beams strengthened by externally bonded steel plates', *ICE Proc Part 2*, 87(1).

Roberts T M (1989), 'Shear and normal stresses in adhesive joints', *J Eng Mech – ASCE*, 115(11), 2460–2479.

Ruiz P D, Jumbo F, Seaton A, Huntley J M, Ashcroft I A and Swallowe G M (2006),

'Numerical and experimental investigation of three-dimensional strains in adhesively bonded joints', *J Strain Anal Eng*, 41(8), 583–596.

Ruiz P D, Jumbo F, Huntley J M, Ashcroft I A and Swallowe G M (2011), 'Experimental and numerical investigation of strain distributions within the adhesive layer in bonded joints', *Strain*, 47(1), 88–104.

Sawa T, Liu J, Nakano K and Tanaka J (2000), 'A two-dimensional stress analysis of single-lap adhesive joints of dissimilar adherends subjected to tensile loads', *J Adhes Sci Technol*, 14(1), 43–66.

Schnerch D, Stanford K, Sumner E A and Rizkalla S H (2005), 'Bond behaviour of CFRP strengthened steel bridges and structures', *in:* Chen J F and Teng J G (eds) *Bond Behaviour of FRP in Structures (BBFS 2005),* 7–9 December, Hong Kong, xi, 566.

Schumacher A and Hack E (2008), 'Comparison of measured and calculated interfacial strains at CFRP plate end', *in: 4th International Conference on FRP Composites in Civil Engineering (CICE2008)*, 22–24 July, Zürich, Switzerland, 1–6.

Sharifi S and Choupani N (2008), 'Stress analysis of adhesively bonded double-lap joints subjected to combined loading', *Proceedings of World Academy of Science, Engineering and Technology,* July 2008, Vienna, 759–764.

Smith S T and Teng J G (2001), 'Interfacial stresses in plated beams', *Eng Struct*, 23(7), 857–871.

Stratford T J and Cadei J M C (2006), 'Elastic analysis of adhesion stresses for the design of a strengthening plate bonded to a beam', *Constr Build Mater*, 20(1–2), 34–45.

Täljsten B (1997), 'Strengthening of beams by plate bonding', *J Mater Civil Eng*, 9(4), 206–212.

Tennyson R C, Coroy T, Duck G, Manuelpillai G, Mulvihill P, Cooper D J F, Smith P E, Mufti A A and Jalali S J (2000), 'Fibre optic sensors in civil engineering structures', *Can J Civil Eng*, 27(5), 880–889.

Tsai M Y and Morton J (1994), 'An evaluation of analytical and numerical solutions to the single-lap joint', *Int J Solids Struct*, 31(18), 2537–2563.

Tsai M Y and Morton J (1995), 'The effect of a spew fillet on adhesive stress distributions in laminated composite single-lap joints', *Compos Struct*, 32(1–4), 123–131.

Tsai M Y, Oplinger D W and Morton J (1998), 'Improved theoretical solutions for adhesive lap joints', *Int J Solids Struct*, 35(12), 1163–1185.

TWI (2011), 'Non contact strain measurement, Cambridge', available from http://www.twi.co.uk/technologies/structural-integrity/numerical-modelling/non-contact-strain-measurement/ (accessed 24 December 2011).

Varastehpour H and Hamelin P (1997), 'Strengthening of concrete beams using fiber-reinforced plastics', *Mater Struct*, 30(3), 160–166.

Vasiliev V V and Morozov E V (2001), *Mechanics and Analysis of Composite Materials*, 1st edn, New York: Elsevier Science.

Veselovsky R A and Kestelman V N (2002), *Adhesion of Polymers*, New York: McGraw–Hill.

Vilnay O (1988), 'The analysis of reinforced concrete beams strengthened by epoxy bonded steel plates', *Int J Cem Compos Lightweight Concr*, 10(2), 73–78.

Volkersen O (1938), 'The rivet-force distribution in tension-stressed riveted joints with constant sheet thickness', *Luftfahrtforschung*, 15, 41–47.

Walker C A (1994), 'A historical review of moiré interferometry', *Exp Mech*, 34(4), 281–299.

Wang B, Teng J G, De Lorenzis L, Zhou L M, Ou J, Jin W and Lau K T (2009), 'Strain monitoring of RC members strengthened with smart NSM FRP bars', *Constr Build Mater*, 23(4), 1698–1711.

Weiss W (1982), 'Low temperature properties of carbon fibre reinforced epoxide resins', *in:* Hartwig G and Evans D (eds) *Proceedings of the 2nd ICMC Symposium on Non-metallic Materials and Composites at Low Temperatures*, New York: Plenum Press, 293–309.

Wood J (1985), 'Detection of delamination onset in a composite laminate using moiré interferometry', *J Compos Tech Res*, 7, 121–128.

Xia S H and Teng J G (2005), 'Behaviour of FRP-to-steel bonded joints', *International Symposium on Bond Behaviour of FRP in Structures – BBFS 2005*, 7–9 December, Hong Kong, 419–426.

Xu Y, Leung C K Y, Tong P, Yi J and Lee S K L (2005), 'Interfacial debonding detection in bonded repair with a fiber optical interferometric sensor', *Compos Sci Technol*, 65(9), 1428–1435.

Yamada S, Yoshida Y, Saito S, Yamada S and Komiya I (2007), 'Fibre optic sensing for the delamination behaviour of FRP reinforced steel structures', *Asia-Pacific Conference on FRP in Structures (APFIS 2007)*, 12–14 December, Hong Kong, 587–592.

Yamada S, Nakajima S, Matsumoto Y, Yamada S and Komiya I (2009), 'Delamination of the bond interface between FRP and steel plate and its structural health monitoring', *2nd Official International Conference of International Institute for FRP in Construction for Asia-Pacific Region*, 9–11 December, Seoul, South Korea, 505–510.

Yang C, Huang H, Tomblin J S and Sun W (2004), 'Elastic–plastic model of adhesive-bonded single-lap composite joints', *J Compos Mater*, 38(4), 293–309.

Yang J and Wu Y F (2007), 'Interfacial stresses of FRP strengthened concrete beams: Effect of shear deformation', *Compos Struct*, 80(3), 343–351.

Yang L, Smith L, Gothekar A and Chen X (2010), *Measure strain distribution using digital image correlation (DIC) for tensile tests*, Oakland, New Zealand Department of Mechanical Engineering, Oakland University.

Yu Y, Chiew S P and Lee C K (2011), 'Bond failure of steel beams strengthened with FRP laminates – Part 2: Verification', *Compos Part B – Eng*, 42(5), 1122–1134.

Yuceoglu U and Updike D P (1981), 'Bending and shear deformation effects in lap joints', *J Eng Mech Div – ASCE*, 107(EM1), 55–76.

Zeng D and Xia Z (2010), 'Extending tensile curves beyond uniform elongation using digital image correlation: Capability analysis', *SAE Int J Mater Manuf*, 3(1), 702–710.

Zhang B, Benmokrane B, Nicole J and Masmoudi R (2002), 'Evaluation of fibre optic sensors for structural condition monitoring', *Mater Struct*, 35(6), 357–364.

Zhang J, Bednarcyk B A, Collier C, Yarrington P, Bansalk Y and Pindera M J (2006), 'Analysis tools for adhesively bonded composite joints, Part 2: Unified analytical theory', *AIAA J*, 44(8), 1709–1719.

Zhang Z and Hsu C T T (2002), 'Shear strengthening of RC beams using carbon fiber reinforced polymer strips', *in: 15th ASCE Engineering Mechanics Conference*, New York, 1–8.

Zhao Y and Ansari F (2002), 'Embedded fiber optic sensor for characterization of interface strains in FRP composite', *Sensor Actuat A – Phys*, 100(2–3), 247–251.

Zhou T Q, Li Z X and Jia J B (2001), 'Elasto-plastic interface stress analysis of FRP retrofitted beam', *in:* Teng J G (ed.) *Proceedings of the International Conference on FRP Composites in Civil Engineeering*, Hong Kong: Elsevier, 527–536.

11

Understanding and predicting stiffness in advanced fibre-reinforced polymer (FRP) composites for structural applications

R. M. GUEDES, University of Porto, Portugal and
J. XAVIER, CITAB/UTAD, Portugal

DOI: 10.1533/9780857098641.3.298

Abstract: This chapter describes the elastic qualities of advanced fibre-reinforced composites, in terms of characterization, measurement and prediction from the basic constituents, i.e. the fibre and matrix. The elastic analysis comprises applying micromechanics approaches to predict the lamina elastic properties from the basic constituents, and using classical lamination theory to predict the elastic properties of composite materials composed of several laminae stacked at different orientations. Examples are given to illustrate the theoretical analysis and give a full apprehension of its prediction capability. The last section provides an overview on identification methods for elastic proprieties based on full-field measurements. It is shown that these methodologies are very convenient for elastic characterization of anisotropic and heterogeneous materials.

Key words: elastic modulus, orthotropic, micromechanics, classical lamination theory, digital image correlation, optical methods.

11.1 Introduction

Polymer matrix-based composites are essentially composed of fibres embedded in polymeric matrices. Polymeric matrices are divided into thermoplastic and thermoset resins. The fibres play an important role by their reinforcing character, enhancing the mechanical performance of these composites to high levels. These arrangements are more than simple combinations of fibres and polymeric matrices, since the synergistic effects are important in their global mechanical performance. In the case of continuous reinforcement, fibres are disposed mainly on the surface ply, either unidirectional or woven fabric, resulting in superior mechanical properties in the ply surface directions. Consequently, in the thickness direction the mechanical properties of composites are low. The complexity of these systems poses some challenges on the models used to predict stiffness evolution, when general loading conditions are applied, including the environmental effects.

The reinforcements can have different geometries – particulate, flake or fibres. The fibres can be continuous, discontinuous and oriented, or randomly

distributed (see Fig. 11.1). The polymer matrices have much lower stiffness compared with the reinforcements. The matrix holds the reinforcements, protecting them against environmental and external aggression. Simultaneously the matrix allows an effective stress transfer to the reinforcements. This relies on good adhesion between the matrix and the reinforcement. The mechanical performance of fibre-reinforced polymers depends on different factors such as fibre length, fibre orientation and fibre shape. The circular shape is more usual since it is easier to produce, but other shapes are possible.

This chapter is devoted to the analysis of the elastic properties and their characterization for laminated advanced composites. It starts with a general overview of composite stiffness and then moves to lamina analysis focused on unidirectional reinforced composites. The analysis of laminated composites is addressed through the classical lamination theory (CLT). The last section describes full-field techniques coupled with inverse identification methods that can be employed to measure the elastic constants.

11.2 General aspects of composite stiffness

Composite materials consist of two or more constituents mixed at a nano-, micro- or macroscopic level. These constituents are not soluble and form distinct phases. The reinforcing phase is embedded in the other phase, designated the matrix. Usually the reinforcing material is in the form of continuous or short fibres or particles. Actually, composites provide a more efficient way for using materials in structural applications. For example, they allow mass reduction without decreasing the stiffness and strength of components, by

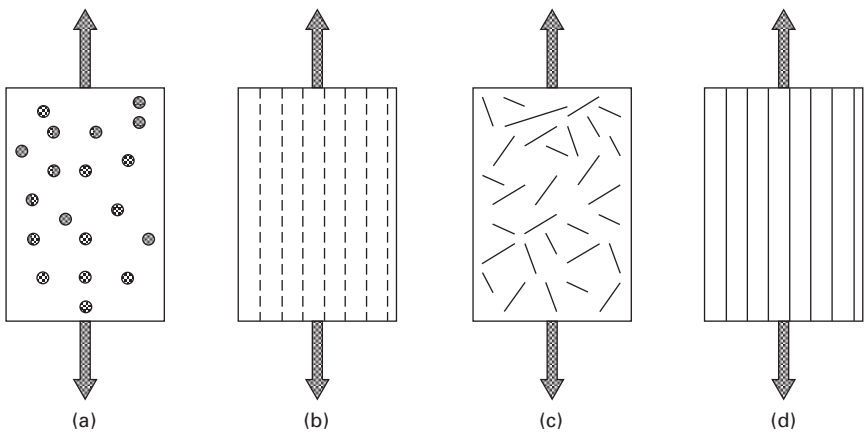

11.1 (a) Particulate, (b) oriented discontinuous fibres, (c) randomly distributed discontinuous fibres, (d) continuous fibres.

replacing conventional metal alloys with composite materials. The reduction in weight and number of parts in an assembly largely compensates for the higher composite material costs. Moreover, composite systems often present improved fatigue, impact resistance, thermal conductivity and corrosion resistance.

The lightest structural component for a specified deformation, i.e. strain or deflection, under a specified load is the one with the highest specific modulus. This is calculated as the ratio of the Young's modulus to the density of the material. For comparison purposes in Fig. 11.2 is plotted the specific modulus for several materials, including typical reinforcing fibres. Carbon-reinforced composites possess higher specific modulus when compared against aluminium and steel [1].

The stiffness of polymer-based composite systems depends on numerous factors such as the stiffness of constituents, the volume fraction of each component, and the size, shape and orientation of reinforcements. As a whole there are three distinct types of polymer composites: continuous fibre-reinforced polymer composites, short fibre-reinforced polymer composites, and polymer nanocomposites. Theoretical models based on micromechanical models are well developed and provide an adequate representation of composite stiffness. These micromechanical models are formulated based on assumptions of continuum mechanics. However, for nanocomposite materials, with fillers of size approximately 1 nm compared to the typical carbon fibre diameter of 50 μm, the rules and requirements for continuum

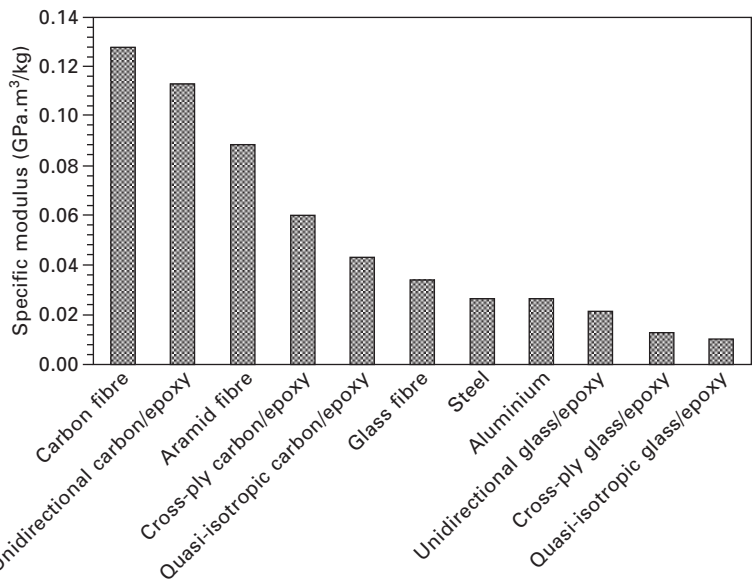

11.2 Specific modulus of different materials.

modelling are not satisfied. Several studies have attempted to address the applicability of continuum micromechanics to nano-reinforced polymer composites, by taking into account the effects associated with the significant size difference between nano fillers and typical carbon fibre. Nonetheless the classical approach can capture the main effects of nanoparticles on the elastic properties of nanocomposites. Particle clustering is the phenomenon mainly responsible for deviations of experimental data from theoretical predictions.

Since the reinforcements possess higher modulus and strength than the polymer matrix, internal mismatches are induced, leading to local stress concentrations. Depending on the loading direction, fibre-aligned cracks may start to form. In the literature the terms matrix microcracks, microcracks, intralaminar cracks, ply cracks and transverse cracks often describe the same phenomenon [2]. These are observed during tensile loading, fatigue loading and thermocycling. Microcracks appear predominantly in plies off-axis to loading directions. This phenomenon leads to degradation in all effective moduli, Poisson's ratios, thermal expansion coefficients [3] and moisture diffusion coefficients [3, 4]. Furthermore, the nucleation of microcracks may induce delamination [2].

The application of damage mechanics enables one to model matrix degradation in fibre-reinforced polymers due to cracking [5]. This damage is quantified in terms of crack density, i.e. the reciprocal of crack spacing. The model used by Roberts *et al*. [6], based on the previous work of Zang and Gudmundson [7, 8], applies to microcracks with crack surfaces parallel to the fibre direction and perpendicular to the lamina plane.

The viscoelastic and viscoplastic nature of polymeric materials that constitutes the composite matrix makes their mechanical behaviour time- or rate-dependent. Polymers are also temperature- and moisture-dependent displaying, in certain cases, large stiffness variations. Physical ageing is also an important issue that is often ignored for simplification purposes. A recent overview concerning these important matters is given elsewhere [9].

11.3 Understanding lamina stiffness

The typical building block of a composite structure is the lamina, with a typical thickness of 0.125 mm. The lamina stress–strain relationships are described for orthotropic, transverse isotropic and isotropic materials. When a lamina is reinforced with unidirectional fibres it can be assumed to be a transversely isotropic material. In this chapter, theoretical determination of lamina elastic properties, assumed to be a transversely isotropic material, using micromechanics approaches is presented and illustrated with experimental data.

11.3.1 The representative volume element (RVE)

Knowledge of the exact configuration of fibres and matrix in a composite structure is impractical for structural analysis. Observation of a typical micrograph of a cross-section of a unidirectional glass or carbon/epoxy lamina makes it clear that the fibre distribution is not uniform but is fairly random [10]. This provokes irregular gaps and contiguity, i.e. fibres touching in some locations. Similar cross-sections can be computationally randomly generated as shown in Fig. 11.3. Detailed discussion on this subject can be found elsewhere [11–13].

The effective properties of a composite material correspond to properties averaged over a repeating representative volume element (RVE). This element should be large enough to represent the microstructure yet sufficiently smaller than the macroscopic structural dimensions. In fibre-reinforced composites, the RVE length scale is several times the fibre diameter. If the RVE dimension is small compared with the characteristic dimensions of the structure, the material can be assumed as homogeneous. Figure 11.4 depicts a schematic example of a RVE with other examples of elements that cannot be considered RVEs.

11.3.2 Generalized Hooke's law

The most general linear elastic relationship between the stresses and strains is given as

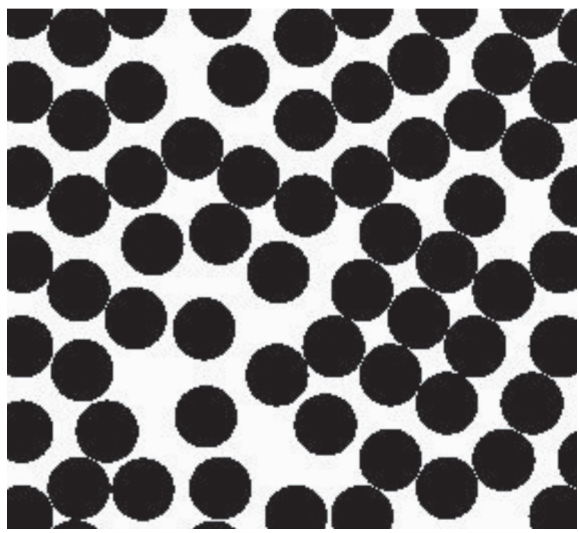

11.3 Example of randomly distributed fibres computationally generated over a lamina cross-section.

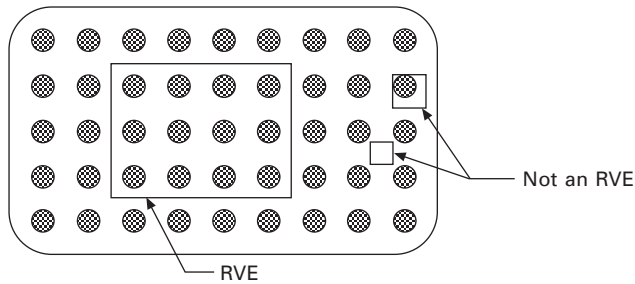

11.4 Example of a representative volume element (adapted from [14]).

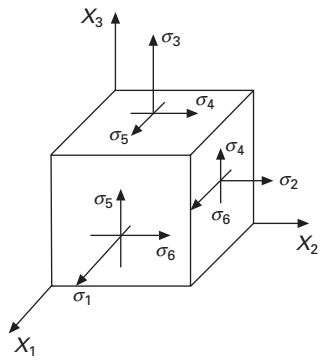

11.5 Three-dimensional representation of the stresses.

$$\sigma_{ij} = C_{ijkl}\varepsilon_{kl} \qquad [11.1]$$

where σ_{kl} represent the stresses and ε_{kl} the strains, and C_{ijkl} is a fourth-order tensor with 81 constants called the elastic moduli. This linear elastic stress–strain constitutive law is called the Generalized Hooke's law.

Inverting (11.1) the strains are given in terms of stresses in the form

$$\varepsilon_{ij} = C^{-1}_{ijkl}\sigma_{kl} \qquad [11.2]$$

where the compliance $S_{ijkl} = C^{-1}_{ijkl}$ is defined as the inverse of the stiffness.

When the stresses and strains are symmetric the number of independent constants is reduced to 36. Hooke's law can be written in a contracted notation:

$$\sigma_i = C_{ij}\varepsilon_j \ (i, j = 1, 2, \ldots, 6) \qquad [11.3]$$

A three-dimensional representation of the stresses in contract notation is presented in Fig. 11.5.

If there exists a strain density function such as

$$W = \tfrac{1}{2}\, C_{ij}\varepsilon_i\varepsilon_j \qquad [11.4]$$

and it verifies

$$\sigma_i = \frac{\partial W}{\partial \varepsilon_i} \qquad [11.5]$$

then c_{ij} is symmetric and the number of independent elastic constants is reduced to 21. A material with 21 independent constants is called anisotropic. The stiffness matrix is written as

$$[C_{ij}] = \begin{bmatrix} C_{11} & C_{12} & C_{13} & C_{14} & C_{15} & C_{16} \\ & C_{22} & C_{23} & C_{24} & C_{25} & C_{26} \\ & & C_{33} & C_{34} & C_{35} & C_{36} \\ & & & C_{44} & C_{45} & C_{46} \\ & & & & C_{55} & C_{56} \\ Sym. & & & & & C_{66} \end{bmatrix} \qquad [11.6]$$

The inverted matrix gives the symmetric compliance,

$$[S_{ij}] = [C_{ij}]^{-1} = \begin{bmatrix} S_{11} & S_{12} & S_{13} & S_{14} & S_{15} & S_{16} \\ & S_{22} & S_{23} & S_{24} & S_{25} & S_{26} \\ & & S_{33} & S_{34} & S_{35} & S_{36} \\ & & & S_{44} & S_{45} & S_{46} \\ & & & & S_{55} & S_{56} \\ Sym. & & & & & S_{66} \end{bmatrix} \qquad [11.7]$$

11.3.3 Material symmetry: orthotropic, transversely isotropic and isotropic materials

Consider a material that is symmetric about two planes: the x_1–x_2 and x_2–x_3 planes as shown in Fig. 11.6. It must be expected that the elastic constants in both coordinate systems (unprimed and primed) are identical, i.e. $C_{ij} = C'_{ij}$.

The definition of the coordinate systems leads to

$$\begin{aligned} &\sigma_1 = \sigma'_1 \; \sigma_4 = -\sigma'_4 \\ &\sigma_2 = \sigma'_2 \; \sigma_5 = -\sigma'_5 \\ &\sigma_3 = \sigma'_3 \; \sigma_6 = -\sigma'_6 \\ &\varepsilon_1 = \varepsilon'_1 \; \varepsilon_4 = -\varepsilon'_4 \\ &\varepsilon_2 = \varepsilon'_2 \; \varepsilon_5 = -\varepsilon'_5 \\ &\varepsilon_3 = \varepsilon'_3 \; \varepsilon_6 = -\varepsilon'_6 \end{aligned} \qquad [11.8]$$

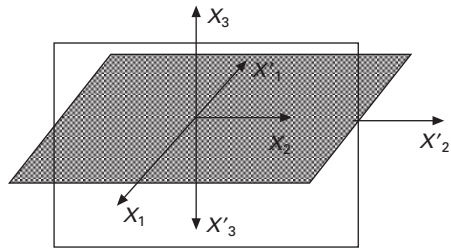

11.6 Symmetry about the $x_1 - x_2$ and $x_2 - x_3$ planes.

Expressing $\sigma_1 = \sigma'_1$ in terms of strains and elastic constants using the Generalized Hooke's law,

$$C_{11}\varepsilon_1 + C_{12}\varepsilon_2 + C_{13}\varepsilon_3 + C_{14}\varepsilon_4 + C_{15}\varepsilon_5 + C_{16}\varepsilon_6$$
$$= C'_{11}\varepsilon_1 + C'_{12}\varepsilon'_2 + C'_{13}\varepsilon'_3 + C'_{14}\varepsilon'_4 + C'_{15}\varepsilon'_5 + C'_{16}\varepsilon'_6 \quad [11.9]$$

Now using the previous relationships, the following is obtained:

$$C_{14} = C_{15} = C_{16} = 0 \quad [11.10]$$

Using similar procedures, it is possible to conclude that

$$C_{24} = C_{25} = C_{26} = C_{34} = C_{35} = C_{36} = C_{45} = C_{46} = C_{56} = 0 \quad [11.11]$$

The obtained stiffness matrix corresponds to an orthotropic material with nine independent constants. The constitutive equation can be written in matrix form as

$$\begin{Bmatrix} \sigma_1 \\ \sigma_2 \\ \sigma_3 \\ \tau_{23} \\ \tau_{13} \\ t_{12} \end{Bmatrix} = \begin{bmatrix} C_{11} & C_{12} & C_{13} & 0 & 0 & 0 \\ & C_{22} & C_{23} & 0 & 0 & 0 \\ & & C_{33} & 0 & 0 & 0 \\ & & & C_{44} & 0 & 0 \\ & & & & C_{55} & 0 \\ Sym. & & & & & C_{66} \end{bmatrix} \begin{Bmatrix} \varepsilon_1 \\ \varepsilon_2 \\ \varepsilon_3 \\ \gamma_{23} \\ \gamma_{13} \\ \gamma_{12} \end{Bmatrix} \quad [11.12a]$$

or by inversion

$$\begin{Bmatrix} \varepsilon_1 \\ \varepsilon_2 \\ \varepsilon_3 \\ \gamma_{23} \\ \gamma_{13} \\ \gamma_{12} \end{Bmatrix} = \begin{bmatrix} S_{11} & S_{12} & S_{13} & 0 & 0 & 0 \\ & S_{22} & S_{23} & 0 & 0 & 0 \\ & & S_{33} & 0 & 0 & 0 \\ & & & S_{44} & 0 & 0 \\ & & & & S_{55} & 0 \\ Sym. & & & & & S_{66} \end{bmatrix} \begin{Bmatrix} \sigma_1 \\ \sigma_2 \\ \sigma_3 \\ \tau_{23} \\ \tau_{13} \\ t_{12} \end{Bmatrix} \quad [11.12b]$$

where $\tau_{23} = \sigma_4$, $\tau_{13} = \sigma_5$, $\tau_{12} = \sigma_6$ and $\gamma_{23} = \varepsilon_4$, $\gamma_{13} = \varepsilon_5$, $\gamma_{12} = \varepsilon_6$.

The stiffness and compliance matrices are described in a very simple manner by the elastic constants. However, the elastic constants are not measured directly. Hence it is important to write the stiffness and compliance matrices as functions of the measured constants called engineering constants.

The compliance matrix for an orthotropic material in terms of engineering constants is given as

$$\mathbf{S} = \begin{bmatrix} \frac{1}{E_1} & -\frac{\nu_{21}}{E_2} & -\frac{\nu_{31}}{E_2} & 0 & 0 & 0 \\ -\frac{\nu_{12}}{E_1} & \frac{1}{E_2} & -\frac{\nu_{32}}{E_3} & 0 & 0 & 0 \\ -\frac{\nu_{31}}{E_1} & -\frac{\nu_{23}}{E_2} & \frac{1}{E_3} & 0 & 0 & 0 \\ 0 & 0 & 0 & \frac{1}{G_{23}} & 0 & 0 \\ 0 & 0 & 0 & 0 & \frac{1}{G_{13}} & 0 \\ 0 & 0 & 0 & 0 & 0 & \frac{1}{G_{12}} \end{bmatrix} \quad [11.13]$$

Since the matrix is symmetric $S_{ij} = S_{ji}$ then it must be true that

$$\frac{\nu_{ij}}{E_i} = \frac{\nu_{ji}}{E_j} \; (i, j = 1, 2, 3 \quad [11.14]$$

The correspondent stiffness matrix is given as

$$\mathbf{C} = \begin{bmatrix} \frac{1-\nu_{23}\nu_{32}}{\Delta} E_1 & \frac{\nu_{21}+\nu_{23}\nu_{31}}{\Delta} E_1 & \frac{\nu_{31}+\nu_{21}\nu_{32}}{\Delta} E_1 & 0 & 0 & 0 \\ \frac{\nu_{12}+\nu_{13}\nu_{32}}{\Delta} E_2 & \frac{1-\nu_{31}\nu_{13}}{\Delta} E_2 & \frac{\nu_{32}+\nu_{12}\nu_{31}}{\Delta} E_2 & 0 & 0 & 0 \\ \frac{\nu_{13}+\nu_{23}\nu_{12}}{\Delta} E_3 & \frac{\nu_{23}+\nu_{13}\nu_{21}}{\Delta} E_3 & \frac{1-\nu_{21}\nu_{12}}{\Delta} E_3 & 0 & 0 & 0 \\ 0 & 0 & 0 & G_{23} & 0 & 0 \\ 0 & 0 & 0 & 0 & G_{13} & 0 \\ 0 & 0 & 0 & 0 & 0 & G_{12} \end{bmatrix} \quad [11.15]$$

where $\Delta = 1 - (\nu_{31}\nu_{13} + \nu_{21}\nu_{12} + \nu_{23}\nu_{32} + \nu_{23}\nu_{31}\nu_{12} + \nu_{21}\nu_{13}\nu_{32})$

Figure 11.7 gives an example of an orthotropic fibre-reinforced material where the cross-section of the fibres is oval.

When the cross-section of fibre-reinforced composite is a plane of isotropy, it is called a transversely isotropic material, as described in Fig. 11.8.

Since the elastic properties are isotropic in the plane transverse to the fibres, the plane x_2–x_3 (Fig. 11.8), additional simplifications on elastic constants are obtained as follows:

$$C_{22} = C_{33},\ C_{12} = C_{13},\ C_{55} = C_{66},\ C_{44} = (C_{22} - C_{23})/2 \qquad [11.16]$$

The stiffness matrix corresponds to a transversely isotropic material with five independent constants. The constitutive equation can be written in matrix form as

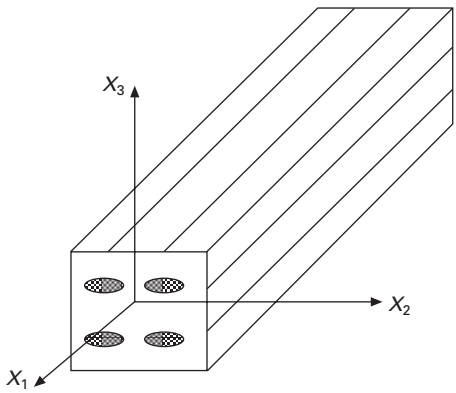

11.7 Example of an orthotropic composite (adapted from [14]).

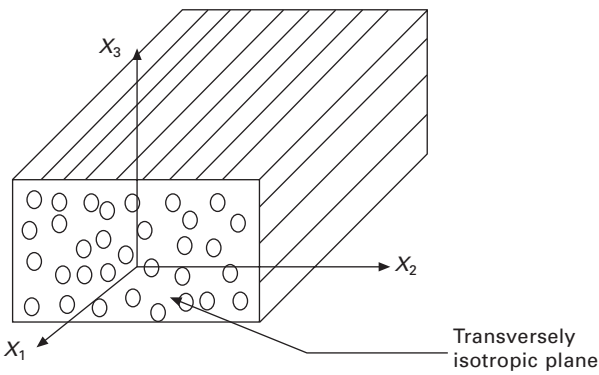

11.8 Transversely isotropic composite (adapted from [14]).

$$\begin{Bmatrix} \sigma_1 \\ \sigma_2 \\ \sigma_3 \\ \tau_{23} \\ \tau_{13} \\ \tau_{12} \end{Bmatrix} = \begin{bmatrix} C_{11} & C_{12} & C_{13} & 0 & 0 & 0 \\ & C_{22} & C_{23} & 0 & 0 & 0 \\ & & C_{22} & 0 & 0 & 0 \\ & & & \frac{C_{22}-C_{23}}{2} & 0 & 0 \\ & & & & C_{66} & 0 \\ \textit{Sym.} & & & & & C_{66} \end{bmatrix} \begin{Bmatrix} \varepsilon_1 \\ \varepsilon_2 \\ \varepsilon_3 \\ \gamma_{23} \\ \gamma_{13} \\ \gamma_{12} \end{Bmatrix} \quad [11.17]$$

The compliance matrix for a transversely isotropic material in terms of engineering constants is given as

$$\mathbf{S} = \begin{bmatrix} \frac{1}{E_1} & -\frac{\nu_{12}}{E_2} & -\frac{\nu_{12}}{E_1} & 0 & 0 & 0 \\ & \frac{1}{E_2} & -\frac{\nu_{23}}{E_2} & 0 & 0 & 0 \\ & & & \frac{1}{E_2} & 0 & 0 \\ & & & \frac{2(1+\nu_{23})}{E_2} & 0 & 0 \\ & & & & \frac{1}{G_{12}} & 0 \\ \textit{Sym.} & & & & & \frac{1}{G_{12}} \end{bmatrix} \quad [11.18]$$

The correspondent stiffness matrix is given as

$$\mathbf{C} = \begin{bmatrix} \frac{1-\nu_{23}}{\Delta_1}E_1 & \frac{\nu_{12}}{\Delta_1}E_2 & \frac{\nu_{12}}{\Delta_1}E_2 & 0 & 0 & 0 \\ & \frac{E_1-\nu_{12}^2E_2}{\Delta_2} & \frac{E_1\nu_{23}+\nu_{12}^2E_2}{\Delta_2} & 0 & 0 & 0 \\ & & \frac{E_1-\nu_{12}^2E_2}{\Delta_2} & 0 & 0 & 0 \\ & & & \frac{1}{2}\frac{E_2}{1+\nu_{23}} & 0 & 0 \\ & & & & G_{12} & 0 \\ & & & & & G_{12} \end{bmatrix} \quad [11.19]$$

where

$$\Delta_1 = \frac{E_1(1-\nu_{23}) - 2\nu_{12}^2 E_2}{E_1},\ \Delta_2 = \frac{E_1(1-\nu_{23}^2) - 2\nu_{12}^2(1+\nu_{23})E_2}{E_2}$$

If all planes are planes of isotropy then the material is called isotropic. The respective stiffness matrix has two independent constants. The additional simplifications on elastic constants are obtained as follows:

$$C_{11} = C_{22},\ C_{12} = C_{23},\ C_{66} = (C_{22} - C_{23})/2 = (C_{11} - C_{12})/2 \quad [11.20]$$

The constitutive equation can be written in matrix form as

$$\begin{Bmatrix} \sigma_1 \\ \sigma_2 \\ \sigma_3 \\ \tau_{23} \\ \tau_{13} \\ \tau_{12} \end{Bmatrix} = \begin{bmatrix} C_{11} & C_{12} & C_{12} & 0 & 0 & 0 \\ & C_{11} & C_{12} & 0 & 0 & 0 \\ & & C_{11} & 0 & 0 & 0 \\ & & & \frac{(C_{11}-C_{12})}{2} & 0 & 0 \\ & & & & \frac{(C_{11}-C_{12})}{2} & 0 \\ \textit{Sym.} & & & & & \frac{(C_{11}-C_{12})}{2} \end{bmatrix} \begin{Bmatrix} \varepsilon_1 \\ \varepsilon_2 \\ \varepsilon_3 \\ \gamma_{23} \\ \gamma_{13} \\ \gamma_{12} \end{Bmatrix} \quad [11.21]$$

The compliance matrix for an isotropic material in terms of engineering constants is given as

$$\mathbf{S} = \begin{bmatrix} \frac{1}{E} & -\frac{\nu}{E} & -\frac{\nu}{E} & 0 & 0 & 0 \\ & \frac{1}{E} & -\frac{\nu}{E} & 0 & 0 & 0 \\ & & \frac{1}{E} & 0 & 0 & 0 \\ & & & \frac{2(1+\nu)}{E} & 0 & 0 \\ & & & & \frac{2(1+\nu)}{E} & 0 \\ \textit{Sym.} & & & & & \frac{2(1+\nu)}{E} \end{bmatrix} \quad [11.22]$$

The correspondent stiffness matrix is given as

$$\mathbf{C} = \begin{bmatrix} \frac{(1-\nu)E}{(1-2\nu)(1+\nu)} & \frac{\nu E}{(1-2\nu)(1+\nu)} & \frac{\nu E}{(1-2\nu)(1+\nu)} & 0 & 0 & 0 \\ & \frac{(1-\nu)E}{(1-2\nu)(1+\nu)} & \frac{\nu E}{(1-2\nu)(1+\nu)} & 0 & 0 & 0 \\ & & \frac{(1-\nu)E}{(1-2\nu)(1+\nu)} & 0 & 0 & 0 \\ & & & \frac{E}{2(1+\nu)} & 0 & 0 \\ & & & & \frac{E}{2(1+\nu)} & 0 \\ & & & & & \frac{E}{2(1+\nu)} \end{bmatrix} \quad [11.23]$$

The relationships between elastic constants which must be satisfied for an isotropic material impose restrictions on the possible range of values for the Poisson's ratio of $-1 < \nu < \frac{1}{2}$. In a similar manner, there are restrictions in orthotropic and transversely isotropic materials. These constraints are based on considerations of the first law of thermodynamics [15]. Moreover, these constraints imply that both the stiffness and compliance matrices must be positive-definite, i.e. each major diagonal term of both matrices must be greater than 0.

11.4 Micromechanical analysis of a lamina

The engineering properties of interest are the elastic constants in the principal material coordinates. If we restrict ourselves to transversely isotropic materials, the elastic properties needed are E_1, E_2, ν_{12}, G_{12} and G_{23}, i.e. the axial modulus, the transverse modulus, the major Poisson's ratio, the in-plane shear modulus and the transverse shear modulus, respectively. All the elastic properties can be obtained from these five elastic constants. Since experimental evaluation of these parameters is costly and time-consuming, it becomes important to have analytical models to compute these parameters based on the elastic constants of the individual constituents of the composite. The goal of micromechanics here is to find the elastic constants of the composite as functions of the elastic constants of its constituents, as

$$C_{ij}^{*} = C_{ij}^{*}(E_1^f, E_2^f, \nu_{12}^f, \nu_{23}^f, G_{12}^f, V_f, E^m, \nu^{m,} V_m) \quad [11.24]$$

assuming that the fibres are transversely isotropic and the matrix isotropic. In practice, glass fibres are isotropic and carbon fibres are transversely isotropic.

The superscripts *f* and *m* over the elastic constants stand for fibre and matrix, respectively. The theoretical formulas to compute the elastic properties of a lamina are also dependent on fibre and matrix volume fractions. The fibre volume fraction and the matrix volume fraction are noted as V_f and V_m, respectively. The sum of volume fractions is

$$V_f + V_m = 1 \qquad [11.25]$$

As a consequence of the manufacturing process of a composite, voids are created in the composite. This causes the theoretical volume of the composite to be lower than the actual volume. Moreover, the void content of a composite decreases the matrix-dominated strengths and the compression strength.

Simple models based on the mechanics of materials approach, semi-empirical approaches, and other methods based on advanced topics such as elasticity, will be presented in this section, which is focused mainly on a unidirectional continuous fibre-reinforced lamina. This forms the basic building block of a composite structure which in general is composed of several unidirectional laminae stacked at different angles. A unidirectional lamina is not homogeneous, but it can be assumed homogeneous if the average response of the lamina to mechanical loads is of interest. In this case the elastic properties are assumed to be constant along the lamina, i.e. not depending on the specific location in the lamina.

11.4.1 Strength of materials approximations

Approximate formulae for four (E_1^*, E_2^*, ν_{12}^*, G_{12}^*) of the five elastic properties of a transversely isotropic composite can be developed using simple approaches based on the strength of materials concepts. These concepts do not necessarily satisfy in full all the elasticity requirements. The RVE considered consists of a uniform arrangement of straight, continuous fibres.

Effective axial modulus, E_1^*

Let us assume a transversely unidirectional lamina under uniform axial loading $\bar{\varepsilon}_1$, as depicted in Figure 11.9. Assuming that the fibres and matrix are perfectly bonded with no slip, i.e. the axial strain of the composite is uniform,

$$\bar{\varepsilon}_1 = \frac{\delta H_m}{H} = \frac{\delta H_f}{H} \qquad [11.26]$$

or

$$\bar{\varepsilon}_1 = \varepsilon_{m=}\varepsilon_f$$

The axial force equilibrium condition requires that the average axial composite stress $\bar{\sigma}_1$ be given as

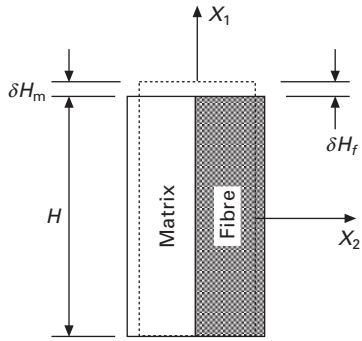

11.9 Axial displacements (adapted from [14]).

$$\overline{\sigma}_1 A = \sigma_m A_m \, \sigma_f A f \qquad [11.27]$$

with $A = A_m + A_f$ where, A, A_m and A_f represent the composite area, matrix area and fibre area, respectively. These are naturally related to the respective volumes. Invoking Hooke's law, the composite axial modulus is given as

$$\begin{aligned} E_1^* &= \frac{\overline{\sigma}_1}{\overline{\varepsilon}_1} = \frac{\sigma_m}{\varepsilon_m}\frac{A_m}{A} + \frac{\sigma_f}{\varepsilon_f}\frac{A_f}{A} = E^m V_m + E_1^f V_f \\ &= E^m(1 - V_f) + E_1^f V_f \end{aligned} \qquad [11.28]$$

This result is often designated the rule of mixtures. The effective axial modulus is a linear function of the fibre volume fraction.

Effective axial Poisson's ratio, ν_{12}^*

The effective axial Poisson's ratio is defined as the negative ratio of lateral strain $\overline{\varepsilon}_2$ when under axial strain $\overline{\varepsilon}_1$ and $\overline{\sigma}_1 \neq 0$ and all the other stresses are identically zero,

$$\nu_{12}^* = -\frac{\overline{\varepsilon}_2}{\overline{\varepsilon}_1} \qquad [11.29]$$

Based on the RVE depicted in Fig. 11.10, the following is obtained:

$$\overline{\varepsilon}_2 = \frac{\delta H}{H} = \frac{\delta H_f + \delta H_m}{H} = \frac{-(\nu_f \overline{\varepsilon}_1 V_f H + \nu_m \overline{\varepsilon}_1 V_m H)}{H} \qquad [11.30]$$

Therefore the effective axial Poisson's ratio is given as

$$\nu_{12}^* = \nu^m V_m + \nu_{12}^f V_f = \nu^m(1 - V_f) + \nu_{12}^f V_f \qquad [11.31]$$

As before, this result is often designated the rule of mixtures. The effective axial Poisson's ratio is a linear function of the fibre volume fraction.

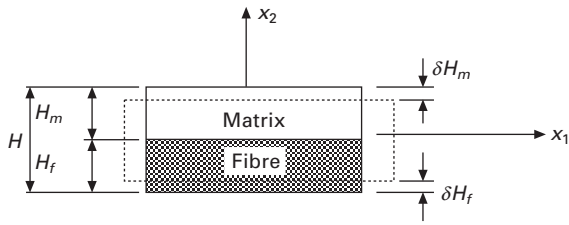

11.10 Transverse displacements (adapted from [14]).

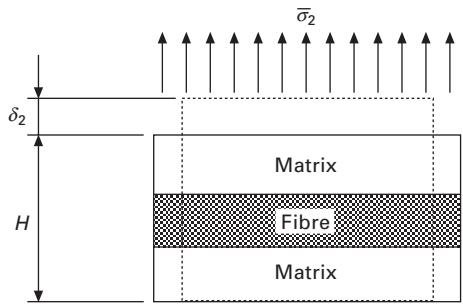

11.11 Transverse loading (adapted from [14]).

Effective transverse modulus, E_2^*

The effective transverse modulus can be determined assuming that the composite is subjected to a uniform transverse stress $\overline{\sigma}_2$, as depicted in Fig. 11.11. In this case the transverse stress is constant across the composite; therefore the total transverse deformation for a thickness H is given as

$$\delta_2 = \overline{\varepsilon}_2 H = \varepsilon_f V_f H + \varepsilon_m V_m H \qquad [11.32]$$

Therefore

$$\overline{\varepsilon}_2 = \varepsilon_f V_f + \varepsilon_m V_m \qquad [11.33]$$

Consequently the effective transverse modulus is given as

$$\overline{\varepsilon}_2 = \frac{\overline{\sigma}_2}{E_2^*} = \frac{\overline{\sigma}_2}{E_2^f} V_f + \frac{\overline{\sigma}_2}{E_m} V_m \qquad [11.34]$$

and

$$\frac{1}{E_2^*} = \frac{V_f}{E_2^f} + \frac{V_m}{E^m} \qquad [11.35]$$

or

$$E_2^* = \frac{E^m}{V_f\left(\frac{E^m}{E_2^f} - 1\right) + 1} \qquad [11.36]$$

The effective transverse modulus is a nonlinear function of the fibre volume fraction.

Effective in-plane shear modulus, G_{12}^{*}

The effective in-plane shear modulus can be determined assuming that the composite is subjected to a uniform shear stress $\bar{\tau}_{12}$, as depicted in Fig. 11.12. In this case the shear stress is uniform across the composite; the shear strains in the fibre and matrix are

$$\gamma_m = \frac{\bar{\tau}_{12}}{G^m},\ \gamma_f = \frac{\bar{\tau}_{12}}{G_{12}^f} \qquad [11.37]$$

The average composite shear strain is given by

$$\tan \bar{\gamma}_{12} \cong \bar{\gamma}_{12} = \frac{\bar{\delta}}{H} \qquad [11.38]$$

From Fig. 11.12 the following is obtained:

$$\bar{\delta} = \delta_f + \delta_m = \frac{\bar{\tau}_{12}}{G_{12}^f} V_f H + \frac{\bar{\tau}_{12}}{G^m} V_m H \qquad [11.39]$$

Therefore

$$\frac{1}{G_{12}^*} = \frac{\bar{\tau}_{12}}{\bar{\gamma}_{12}} = \frac{V_f}{G_{12}^f} + \frac{V_m}{G^m} \qquad [11.40]$$

or

$$G_{12}^* = \frac{G^m}{V_f\left(\frac{G^m}{G_{12}^f} - 1\right) + 1} \qquad [11.41]$$

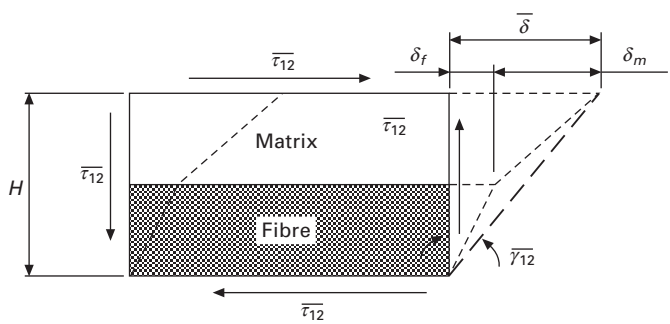

11.12 Shear deformations (adapted from [14]).

As before, the effective in-plane shear modulus is a nonlinear function of the fibre volume fraction.

11.4.2 Improvements to the strength of materials approximations

The strength of materials approach provides four of the five elastic properties of transversely isotropic unidirectional composites. Two properties (E_1^*, ν_{12}^*) are well predicted by this simple approach, i.e. using the law of mixtures. The other two (E_2^*, G_{12}^*) require more accurate micromechanics models. The main reason for this is that E_1^* and ν_{12}^* are independent of fibre packing while d E_2^* and G_{12}^* depend strongly on fibre arrangement.

The maximum volume fraction of fibres to incorporate in a composite has both theoretical and practical limitations. The possible fibre arrangements lead to these limitations. Some examples of fibre packing geometry are shown in Fig. 11.13.

A theoretical maximum fibre volume fraction can be calculated for each packing geometry. For the square array and close packing shown in Fig. 11.14, the maximum fibre volume fraction is given as

$$\begin{aligned}\text{Square array: } (V_f)_{\max} &= \frac{\pi D^2/4}{D^2} = 0.785 \\ \text{Close packing: } (V_f)_{\max} &= \frac{\pi D^2/4}{\sqrt{3}D^2/4} = 0.907\end{aligned} \qquad [11.42]$$

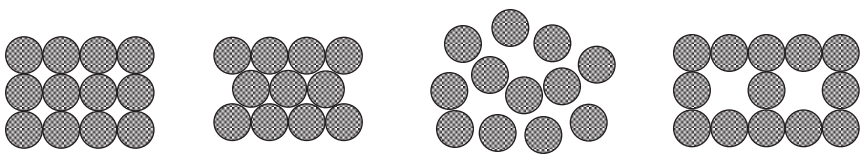

11.13 Examples of fibre packing.

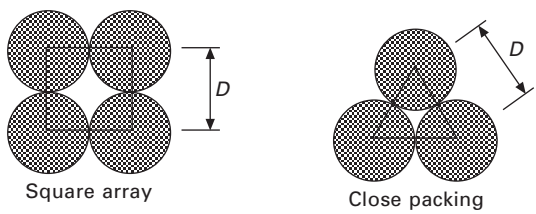

11.14 Geometry of fibre packing for two cases: square array and close packing.

The approach employed to improve the formulas for the two elastic properties is based on the square array. Referring to the RVE represented in Fig. 11.15, since the theoretical fibre volume fraction is given by Equation (11.42) we must have $s = d$.

Now it is possible to proceed to divide the RVE into two regions [15], according to Fig. 11.16. The square dimension of the fibre becomes

$$s_f = \sqrt{\frac{\pi}{4}}\, d \qquad [11.43]$$

Therefore the RVE dimension becomes

$$s_f = \sqrt{\frac{\pi}{4V_f}}\, d \qquad [11.44]$$

Noting that

$$\frac{s_f}{s} = \sqrt{V_f} \qquad [11.45]$$

then

$$\frac{s_m}{s} = 1 - \sqrt{V_f} \qquad [11.46]$$

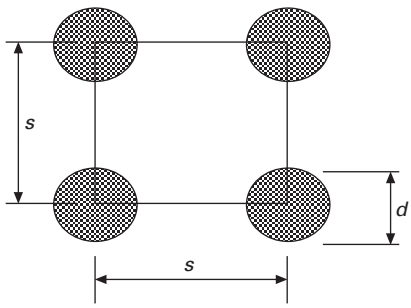

11.15 Representative volume element used for square array.

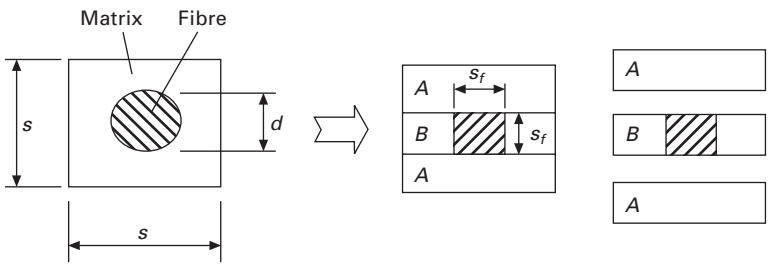

11.16 Division of RVE into two regions (*A* and *B*).

In region B the effective transverse modulus is obtained by strength of materials analysis:

$$\frac{1}{E_{B2}} = \frac{s_f/s}{E_2^f} + \frac{s_m/s}{E^m} = \frac{1 - \sqrt{V_f}(1 - E^m/E_2^f)}{E^m} \qquad [11.47]$$

A parallel combination of regions A and B is under a transverse normal stress, where the rule of mixtures can be applied to allow the determination of the effective transverse modulus:

$$E_2^* = E_{B2}\,\frac{s_f}{s} + E^m\,\frac{s_m}{s} = \frac{E^m}{1 - \sqrt{V_f}(1 - E^m/E_2^f)}\,\sqrt{V_f} + E^m\,(1 - \sqrt{V_f}) \qquad [11.48]$$

and finally

$$E_2^* = E^m \left[\frac{\sqrt{V_f}}{\sqrt{V_f}\;E^m/E_2^f + (1 - \sqrt{V_f})} + (1 - \sqrt{V_f}) \right] \qquad [11.49a]$$

For G_{12}^* a similar expression can be found. These results are close to the Chamis formulae [16],

$$E_2^* = \frac{E^m}{\sqrt{V_f}\;E^m/E_2^f + (1 - \sqrt{V_f})} \qquad [11.49b]$$

11.4.3 Spencer's approach

Another approach to improve the accuracy of the formulae for E_2^* and G_{12}^* was suggested by Spencer [17]. The proposed model was also based on a square array but included the stress concentration effects at the points where the fibres were closer. The formulae are given as

$$E_2^* = E^m \left[\frac{\Gamma - 1}{\Gamma} + \frac{1}{k_E} \left(\frac{2\Gamma}{\sqrt{\Gamma^2 - k_E^2}} \arctan \frac{\sqrt{\Gamma + k_E}}{\sqrt{\Gamma - k_E}} - \frac{\pi}{2} \right) \right] \qquad [11.50]$$

and

$$G_{12}^* = G^m \left[\frac{\Gamma - 1}{\Gamma} + \frac{1}{k_G} \left(\frac{2\Gamma}{\sqrt{\Gamma^2 - k_G^2}} \arctan \frac{\sqrt{\Gamma + k_G}}{\sqrt{\Gamma - k_G}} - \frac{\pi}{2} \right) \right] \qquad [11.51]$$

where

$$k_E = 1 - \frac{E^m}{E_2^f},\; k_G = 1 - \frac{G^m}{G_{12}^f},\; \Gamma = \frac{s}{d} = 1 \qquad [11.52]$$

Spencer [17] also suggested that Γ can be given for a large variety of fibre packing geometries and respective volume fractions V_f by

$$\Gamma = \frac{1}{\sqrt{V_f(1.1V_f^2 - 2.1V_f + 2.2)}} \qquad [11.53]$$

The evolution of Γ is plotted in Fig. 11.17. The deviations from unity become significant for lower fibre volume fractions.

11.4.4 Continuous approaches

In a critical review by Chamis and Sendeckyj [18], it was proposed to classify the variety of micromechanical approaches as follows: netting analysis, mechanics of materials (or strength of materials), self-consistent model, variational, elasticity, statistical, discrete element and semi-empirical methods, and theories accounting for microstructure. After this Mori and Tanaka [19, 20] proposed an original method which assumes that the average strain in the fibre is related to the average strain in the matrix by a fourth-order tensor. Another approach, designated the method of cells (MOC), was initiated by Aboudi [21] and later extended as the generalized method of cells (GMC) [22]. More recently, a new micromechanics model was developed to overcome the shortcomings of GMC. This model, based on a higher-order theory, is designated the high fidelity generalized method of cells (HFGMC) [23]. All these methods, except netting analysis and mechanics of materials, use some or all of the principles of elasticity to different extents.

11.4.5 Elasticity model

The arrangement of fibres in the matrix influences the transverse elastic properties. In a real case this cannot be known precisely and various

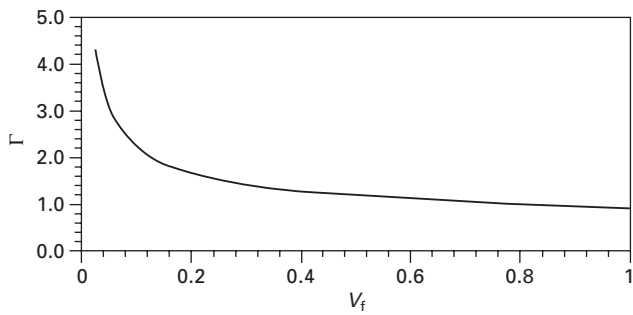

11.17 Dependence of Γ on fibre content.

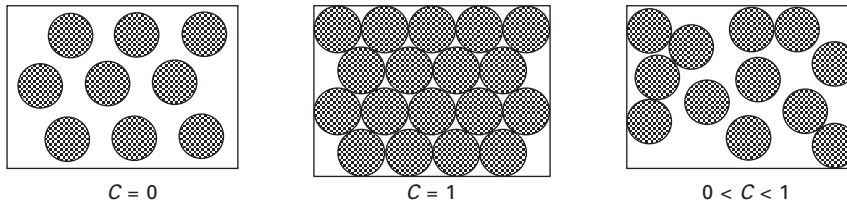

11.18 Contiguity models for calculating transverse elastic properties.

approaches can be used. Tsai [24] used models of fibre contiguity as depicted in Fig. 11.18.

Two extreme cases can be recognized from Fig. 11.18: when fibres have the maximum number of neighbours touching them ($C = 1$) and when fibres are isolated in the matrix ($C = 0$). Most composites have partial contiguity, therefore $0 < C < 1$.

The transverse Young's modulus based on an elasticity solution using the contiguity models is given as

$$E_2^* = 2[1 - \nu_{12}^f + (\nu_{12}^f - \nu^m)V_m]E^m \left[\begin{array}{l} (1-C)\dfrac{K_f(2K_m + G^m) - G_m(K_f - K_m)V_m}{(2K_m + G^m) + 2(K_f - K_m)V_m} \\ \quad + C\dfrac{K_f(2K_m + G_{12}^f) + G_{12}^f(K_m - K_f)V_m}{(2K_m + G_{12}^f) - 2(K_m - K_f)V_m} \end{array} \right] \quad [11.54]$$

where

$$K_f = \frac{E_2^f}{2(1 - \nu_{12}^f)}, K_m = \frac{E^m}{2(1 - \nu^m)}, G_{12}^f = \frac{E_2^f}{2(1 + \nu_{12}^f)}, G^m = \frac{E^m}{2(1 + \nu^m)} \quad [11.55]$$

In this solution the fibres are assumed isotropic, i.e. $E_1^f = E_2^f = E_3^f$ and $\nu_{12}^f = \nu_{23}^f$.

The effective planar shear modulus is

$$G_{12}^* = G^m \frac{2G_{12}^f - (G_{12}^f - G^m)V_m}{2G^m + (G_{12}^f - G^m)V_m} (1 - C) + G_{12}^f \frac{G^m + G_{12}^f - (G_{12}^f - G^m)V_m}{G^m + G_{12}^f + (G_{12}^f - G^m)V_m} C \quad [11.56]$$

The Poisson's ratio is

$$\nu_{12}^{*} = (1 - C)\frac{K_f \nu_{12}^{f}(2K_m + G^m)V_f + K_m \nu^m(2K_f + G^m)V_m}{K_f(2K_m + G^m) - G^m(K_f - K_m)V_m} + C\frac{K_m \nu^m(2K_f + G_{12}^{f})V_m + K_f \nu_{12}^{f}(2K_m + G_{12}^{f})V_f}{K_f(2K_m + G_{12}^{f}) + G_{12}^{f}(K_m - K_f)V_m} \quad [11.57]$$

11.4.6 Halpin–Tsai equations

Due to the inherent complexity of previous developments and the uncertainty associated with the contiguity parameter, a simplified approach was obtained from the elasticity. The elastic constants E_1^{*} and ν_{12}^{*} are given by the law of mixtures which proved to be accurate enough. The remaining elastic constants, E_2^{*}, G_{12}^{*} and ν_{23}^{*}, are given by

$$E_2^{*} = E^m \frac{1 + \xi\eta V_f}{1 - \eta V_f} \text{ with } \eta = \frac{E_2^f/E^m - 1}{E_2^f/E^m + \xi}$$
$$G_{12}^{*} = G^m \frac{1 + \xi\eta V_f}{1 - \eta V_f} \text{ with } \eta = \frac{G_{12}^f/G^m - 1}{G_{12}^f/G^m + \xi} \quad [11.58]$$
$$\nu_{12}^{*} = \nu^m \frac{1 + \xi\eta V_f}{1 - \eta V_f} \text{ with } \eta = \frac{\nu_{23}^f/\nu^m - 1}{\nu_{23}^f/\nu^m + \xi}$$

The parameter ξ is a measure of fibre reinforcement of the composite materials that depends on several factors, such as fibre geometry and fibre arrangement. The exact elasticity calculations predict the moduli to rise faster with increasing fibre volume fraction above 0.7 as compared to the Halpin–Tsai equation [25]. The following empirical expressions were suggested by others [26]:

$$\xi_{E_2} = 1 + 40V_f^{10},\ \xi_{G_{12}} = 2 + 40V_f^{10} \quad [11.59]$$

11.4.7 Additional approaches

As discussed before, the rule of mixtures proved to give accurate predictions for the longitudinal modulus and Poisson's ratio. The plane shear modulus can be predicted with good accuracy by the self-consistent model [10, 27]:

$$G_{12}^{*} = G^m\left[\frac{G^m(1 - V_f) + G_{12}^f(1 + V_f)}{G^m(1 + V_f) + G_{12}^f(1 - V_f)}\right] \quad [11.60]$$

For the other elastic properties, the self-consistent model is only able to give accurate predictions for the plane-strain bulk modulus,

$$k_{23}^{*} = \frac{k^{m}(k_{23}^{f} + G^{m})(1 - V_{f}) + k_{23}^{f}(k^{m} + G^{m})V_{f}}{(k_{23}^{f} + G^{m})(1 - V_{f}) + (k^{m} + G^{m})V_{f}} \quad [11.61]$$

The plane-strain bulk modulus is related to the other elastic properties by [14]:

$$k_{23}^{*} = \frac{1}{2}(C_{22}^{*} + C_{23}^{*}) = \frac{E_{1}^{*}E_{2}^{*}}{2(E_{1}^{*} - E_{1}^{*}\nu_{23}^{*} - 2E_{2}^{*}(\nu_{12}^{*})^{2})} \quad [11.62]$$

In a similar fashion the plane bulk modulus of the matrix (isotropic) and fibre (transversely isotropic) are given by

$$k^{m} = \frac{E^{m}}{2(1 + \nu^{m})(1 - 2\nu^{m})},\ k_{23}^{f} = \frac{E_{1}^{f}E_{2}^{f}}{2(E_{1}^{f} - E_{1}^{f}\nu_{23}^{f} - 2E_{2}^{f}(\nu_{12}^{f})^{2})} \quad [11.63]$$

In this context Morais [27] derived a closed-form equation for the transverse modulus using a relatively simple mechanics-of-materials model. The method employed is a sophistication of the technique presented in Section 11.4.2. The formula obtained for the transverse modulus is given by

$$E_{2}^{*} = E^{m}\left[\frac{\sqrt{V_{f}}}{\sqrt{V_{f}}\ E^{m}/E_{2}^{f} + (1 - \sqrt{V_{f}})(1 - (\nu^{m})^{2})} + \frac{(1 - \sqrt{V_{f}})}{1 - (\nu^{m})^{2}}\right] \quad [11.64]$$

From these results it becomes straightforward to obtain the transverse Poisson's ratio modulus:

$$\nu_{23}^{*} = 1 - E_{2}^{*}\left(\frac{2(\nu_{12}^{*})^{2}}{E_{1}^{*}} + \frac{1}{2k_{23}^{*}}\right) \quad [11.65]$$

and then the transverse shear modulus:

$$G_{23}^{*} = \frac{E_{2}^{*}}{2(1 + \nu_{23}^{*})} \quad [11.66]$$

Another model based on ideas similar to those presented in section 11.4.2 was obtained by Fu *et al*. [28] for the transverse modulus:

$$\frac{1}{E_{2}^{*}} = \frac{1}{E^{m}}\left[\frac{\sqrt{4V_{f}/\pi}}{\sqrt{\pi V_{f}/4}\,E_{2}^{f}/E^{m} + (1 - \sqrt{\pi V_{f}/4})} + (1 - \sqrt{4V_{f}/\pi}\right] \quad [11.67]$$

Neither formula provides coherent results for the extreme values of fibre volume fraction V_f, i.e. $\lim_{V_f \to 0} E_{2}^{*} = \frac{E^{m}}{1 - (\nu^{m})^{2}} \neq E^{m}$ for Equation (11.64), and $\lim_{V_f \to 1} \frac{1}{E_{2}^{*}} = \frac{1}{E^{m}}\left[\frac{4}{\pi\ E_{2}^{f}/E^{m} + (2\sqrt{\pi} - \pi)} + \left(1 - \frac{2}{\sqrt{\pi}}\right)\right] \neq \frac{1}{E_{2}^{f}}$ for Equation (11.67).

In this field there are several other related works. Among them and not so well known is the work of Puck in which models were developed to predict elastic properties of unidirectional fibre-reinforced composites [29]. His work was based on glass fibre-reinforced composites and therefore assumes that both constituents, fibre and matrix, are isotropic materials.

11.4.8 Bridging model

A unified micromechanics model named the Bridging Model was developed by Huang [30]. The main feature of the model is to correlate the averaged stress states in the constituent fibre and matrix through a bridging matrix. This matrix depends only on the constituent properties and on the fibre packing geometry in the matrix. The model recovers the rule of mixtures formulae for the axial modulus and the major Poisson's ratio (E^*_1, ν^*_{12}). The formula for the in-plane shear modulus (G^*_{12}) recovers the result obtained by the self-consistent model. The differences arise for the remaining elastic constants – the transverse modulus,

$$E_2^* = \frac{(V_f + (1 - V_f)a_{11})(V_f + (1 - V_f)a_{22})}{(V_f + (1-V_f)a_{11})(V_f S_{22}^f + (1-V_f)a_{22}S_{22}^m) + V_f(1-V_f)a_{12}(S_{12}^m - S_{12}^f)} \quad [11.68]$$

and the transverse shear modulus,

$$G_{23}^* = \frac{1}{2}\frac{(V_f + (1 - V_f)a_{22}}{V_f(S_{22}^f - S_{23}^f) + (1 - V_f)a_{22}(S_{22}^m - S_{23}^m)} \quad [11.69]$$

where

$$a_{11} = E^m/E_1^f,\ a_{22} = \frac{1}{2}(1 + E^m/E_2^f),\ a_{12} = \frac{(S_{12}^f - S_{12}^m)}{(S_{11}^f - S_{11}^m)}(a_{11} - a_{22})$$
$$S_{11}^f = 1/E_1^f,\ S_{22}^f = 1/E_2^f,\ S_{12}^f = -\nu_{12}^f/E_2^f,\ S_{23}^f = -\nu_{23}^f/E_2^f$$
$$S_{11}^m = S_{22}^m = 1/E^m,\ S_{12}^m = S_{23}^m = -\nu^m/E^m \quad [11.70]$$

11.5 Comparing micromechanical models with experimental data

Results obtained from the literature are used to assess the prediction capabilities of the micromechanics approaches. In this case a unidirectional composite made using isotropic glass fibres and epoxy matrix with E^f = 73.1 GPa, ν^f = 0.22, E^m = 3.45 GPa and ν^m = 0.35 [30] is used. The predicted transverse

modulus E_2^* is shown in Fig. 11.19. The simple formula given by Chamis [16] proves to give accurate predictions. The rule of mixtures (ROM) prediction underestimates the composite transverse modulus.

Experimental data were obtained for the in-plane shear modulus G_{12}^* of another unidirectional composite made of isotropic glass fibres and epoxy matrix with G^f = 30.2 GPa and G^m = 1.8 GPa [31]. The predicted in-plane shear modulus G_{12}^* is shown in Fig. 11.20. Again, in this case, the simple

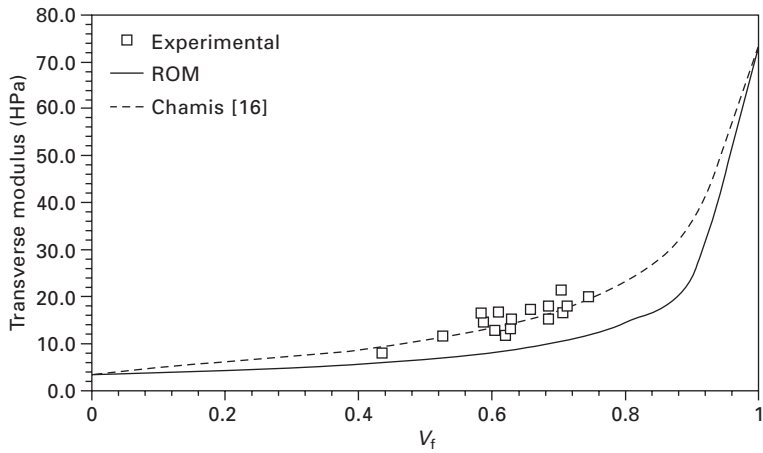

11.19 Transverse modulus E_2^* of unidirectional glass/epoxy composite as a function of fibre volume fraction (E^f = 73.1 GPa, ν^f = 0.22, E^m = 3.45 GPa, ν^m = 0.35).

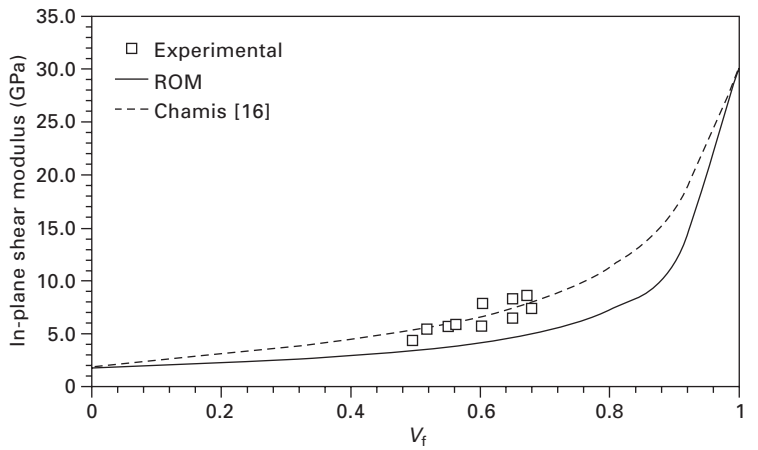

11.20 In-plane shear modulus G_{12}^* of unidirectional glass/epoxy composite as a function of fibre volume fraction (G^f = 30.2 GPa, G^m = 1.8 GPa).

formula given by Chamis [16] proves to give accurate predictions. Again, the rule of mixtures (ROM) prediction underestimates the composite in-plane shear modulus.

Kriz and Stinchcomb [32] published experimental data for unidirectional graphite/epoxy composites. These results illustrate the case when the fibres are transversely isotropic. The elastic properties of the matrix are E^m = 5.28 GPa and ν^m = 0.354, and for the fibres E_1^f = 232 GPa, E_2^f = 15 GPa, G_{12}^f = 24 GPa, ν_{12}^f = 0.279 and ν_{23}^f = 0.49. In Figs 11.21–11.25 are plotted the predictions against the experimental data for E_1^*, E_2^*, G_{12}^*, G_{23}^* and ν_{23}^*, i.e. the longitudinal or axial modulus, the transverse modulus, the in-plane shear modulus, the transverse shear modulus and the transverse Poisson's ratio, respectively.

For the transverse shear modulus, the approach designated self-consistent was based on the formula obtained by the self-consistent method for the plane-strain bulk modulus (11.61), on the transverse modulus calculated using the Chamis approach (11.49b) and the in-plane Poisson's ratio given by the rule of mixtures. Except when used to predict the axial modulus and the major Poisson's ratio, the rule of mixtures underestimates the remaining composite elastic properties. The Bridging Model proved to be a very effective theory to account for all five elastic properties for unidirectional composites that are transversely isotropic.

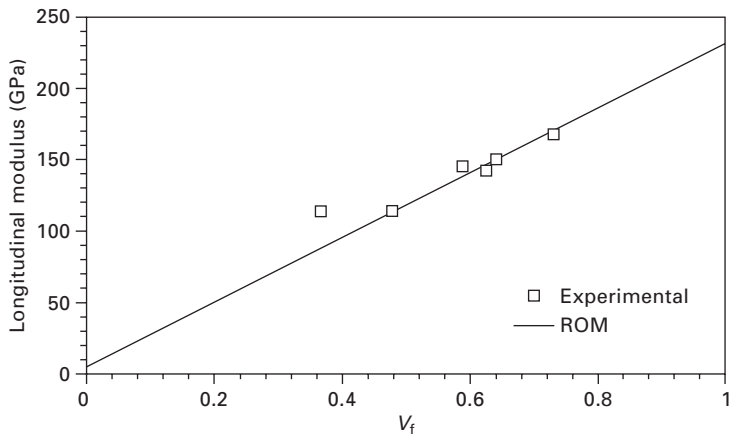

11.21 Longitudinal modulus E_1^* of unidirectional carbon/epoxy composite as a function of fibre volume fraction (E^m = 5.28 GPa, ν^m = 0.354, E_1^f = 232 GPa, E_2^f = 15 GPa, G_{12}^f = 24 GPa, ν_{12}^f = 0.279, ν_{23}^f = 0.49).

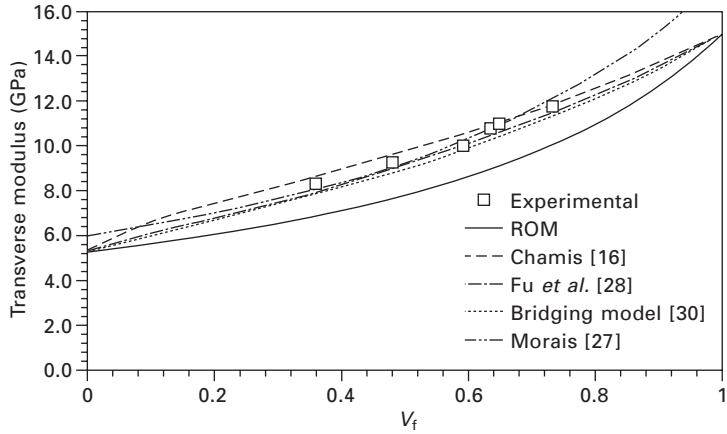

11.22 Transverse modulus E_2^* of unidirectional carbon/epoxy composite as a function of fibre volume fraction (E^m = 5.28 GPa, ν^m = 0.354, E_1^f = 232 GPa, E_2^f = 15 GPa, G_{12}^f 24 GPa, ν_{12}^f = 0.279, ν_{23}^f = 0.49).

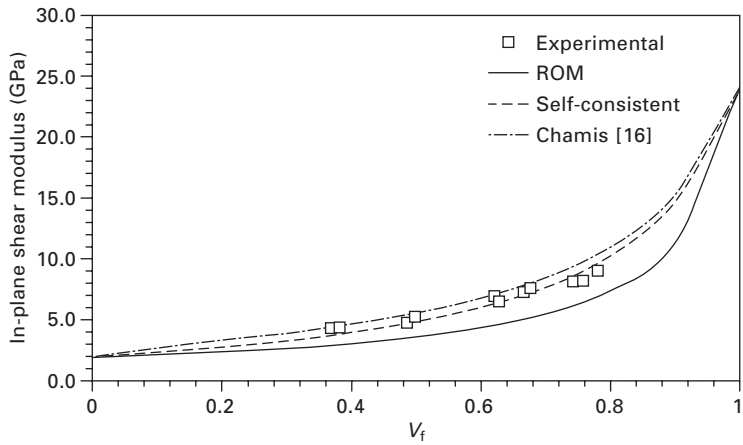

11.23 In-plane shear modulus G_{12}^* of unidirectional carbon/epoxy composite as a function of fibre volume fraction (E^m = 5.28 GPa, ν^m = 0.354, E_1^f = 232 GPa, E_2^f = 15 GPa, G_{12}^f = 24 GPa, ν_{12}^f = 0.279, ν_{23}^f = 0.49).

11.6 Stiffness and compliance transformations

Stress and strain are second-order tensors while stiffness and compliance are fourth-order tensors [14]. Hence these entities are ruled by the tensor transformation laws that establish the relationships between the components

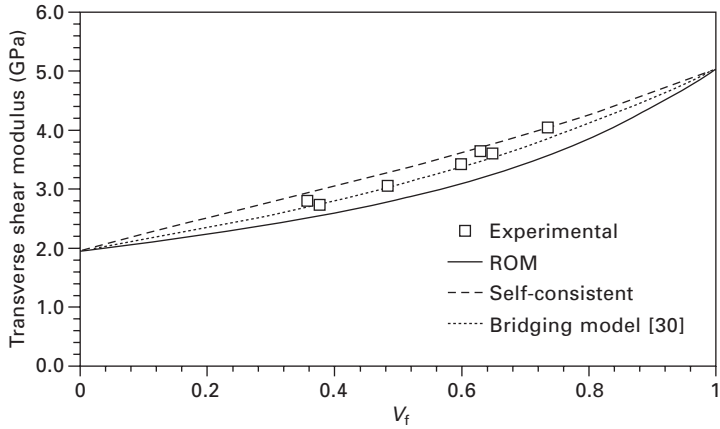

11.24 Transverse shear modulus G_{23}^{*} of unidirectional carbon/epoxy composite as a function of fibre volume fraction (E^m = 5.28 GPa, ν^m = 0.354, E_1^f = 232 GPa, E_2^f = 15 GPa, G_{12}^f = 24 GPa, ν_{12}^f = 0.279, ν_{23}^f = 0.49).

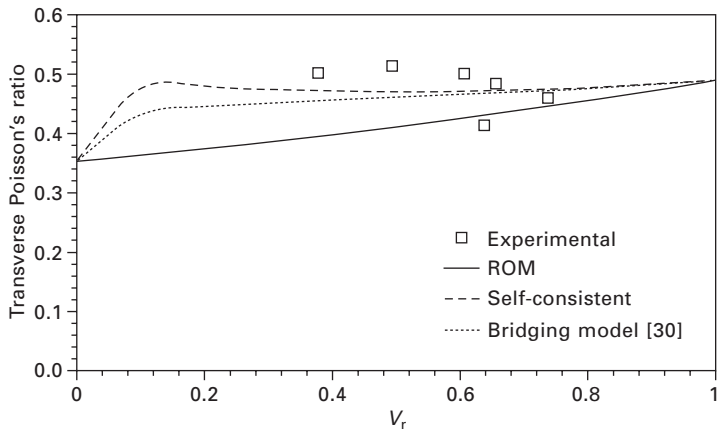

11.25 Transverse Poisson's ratio ν_{23}^f of unidirectional carbon/epoxy composite as a function of fibre volume fraction (E^m = 5.28 GPa, ν^m = 0.354, E_1^f = 232 GPa, E_2^f = 15 GPa, G_{12}^f = 24 GPa, ν_{12}^f = 0.279, ν_{23}^f = 0.49).

in rotated coordinated systems. The stiffness and compliance tensors are readily obtained from the five independent elastic constants, for the case of transversely isotropic materials. These tensors are obtained for the principal material coordinate system. In the principal material coordinate system,

formed by the 1–2–3 axes as shown in Fig. 11.26(a), the 1-axis is associated with the maximum lamina stiffness, while the 2-axis corresponds to the direction of minimum lamina stiffness. In laminated composites the laminae are stacked sequentially with different orientations. In this case the material's coordinate system may no longer coincide with the global coordinate system formed by the x–y–z axes as shown in Fig. 11.26(b). This arrangement is designated the off-axis configuration. The angle θ is measured positive counterclockwise from the x-axis to the 1-axis. In the case of Fig. 11.26(b) the angle is negative, i.e. $\theta < 0$.

Therefore it becomes necessary to use the transformation laws which relate the tensors in one coordinate system to another in a rotated coordinate system. Briefly, the relationship between the stresses in the principal material and global coordinates [14] is given by

$$\{\sigma\}_1 = [T_1]\{\sigma\}_x \qquad [11.71]$$

where the transformation matrix is

$$[T_1] = \begin{bmatrix} m^2 & n^2 & 0 & 0 & 0 & 2mn \\ n^2 & m^2 & 0 & 0 & 0 & -2mn \\ 0 & 0 & 1 & 0 & 0 & 0 \\ 0 & 0 & 0 & m & -n & 0 \\ 0 & 0 & 0 & n & m & 0 \\ -mn & mn & 0 & 0 & 0 & m^2 - n^2 \end{bmatrix} \text{ with } m = \cos\theta \text{ and } n = \sin\theta$$

The strain transformation is

$$\{\varepsilon\}_1 = [T_2]\{\varepsilon\}_x \qquad [11.72]$$

where the transformation matrix is

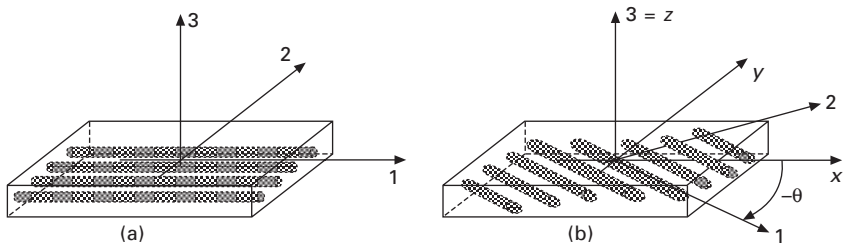

11.26 Schematic representation of (a) principal material coordinate system (1–2–3) and (b) lamina coordinated system (x–y–z).

$$[T_2] = \begin{bmatrix} m^2 & n^2 & 0 & 0 & 0 & mn \\ n^2 & m^2 & 0 & 0 & 0 & -mn \\ 0 & 0 & 1 & 0 & 0 & 0 \\ 0 & 0 & 0 & m & -n & 0 \\ 0 & 0 & 0 & n & m & 0 \\ -2mn & 2mn & 0 & 0 & 0 & m^2 - n^2 \end{bmatrix}$$

Therefore the transformed stiffness $[\overline{C}]$ may be determined using the relationships obtained for the stress and strain transformation,

$$\{\sigma\}_1 = [C]\{\varepsilon\}_1 \Leftrightarrow [T_1]\{\sigma\}_x = [C][T_2]\{\varepsilon\}_x \Leftrightarrow \{\sigma\}_x$$
$$= [T_1]^{-1}[C][T_2]\ \{\varepsilon\}_x \qquad [11.73]$$

Therefore,

$$[\overline{C}] = [T_1]^{-1}[C][T_2], \text{ noting that}$$
$$[T_i(\theta)]^{-1} = [T_i(-\theta)](i = 1, 2) \qquad [11.74]$$

For transformed compliance a similar relationship is established:

$$[\overline{S}] = [T_2]^{-1}[S][T_1] \qquad [11.75]$$

From these transformations it is possible to obtain the elastic properties in any direction. For example, the off-axis elastic modulus is given by

$$E_x = \frac{E_1}{m^4 + m^2n^2(-2\nu_{12} + E_1/G_{12}) + n^4E_1/E_2} \qquad [11.76]$$

the Poisson's ratio by

$$\nu_{xy} = -\frac{\overline{S}_{12}}{\overline{S}_{11}} = \frac{(n^4 + m^4)\nu_{12} - m^2n^2(1 + E_1/E_2 - E_1/G_{12})}{m^4 + m^2n^2(-2\nu_{12} + E_1/G_{12}) + n^4E_1/E_2} \qquad [11.77]$$

and the shear modulus by

$$G_{xy} = -\frac{1}{\overline{S}_{66}} = \frac{E_1}{4m^4n^2(1 + 2\nu_{12} + E_1/E_2) + (n^2 - m^2)^2E_1/G_{12}} \qquad [11.78]$$

The determination of the in-plane elastic properties involves four values E_1, E_2, ν_{12} and G_{12}. The measurement of longitudinal and transverse moduli and Poisson's ratio (E_1, E_2, ν_{12}) is made using tensile coupons oriented at 0° and 90°. These tests are quite straightforward to perform and to analyse when measuring the elastic properties. For the in-plane shear modulus (G_{12}) off-axis, ±45° and Iosipescu test coupons are used, but these tests are not so straightforward to analyse since a complex stress/strain state is induced in the coupons; further details on this subject are well documented in the literature [33–37].

Using experimental data from three different unidirectional composites, a comparison is made between the theory and measured values from off-axis tensile tests. Table 11.1 presents the in-plane elastic properties for unidirectional composites [14].

The comparisons are made using the four in-plane elastic properties (E_1, E_2, ν_{12}, G_{12}) and the relationships throughout given by Equations (11.76–(11.78) for different off-axis angles. The results are plotted throughout Figs 11.27–11.35.

The theory compares quite well with experimental data, as should be expected. The experimental values for the off-axis shear modulus G_{xy} were computed from the respective G_{12} measured for each off-axis angle. The deviations found are related to experimental errors, which are much more critical and pronounced in the case of the off-axis tensile tests. However, the measurement of the in-plane shear modulus requires the use of off-axis specimens. Although consistent values of in-plane shear modulus may be obtained, specimen geometry must be optimized to reduce the errors provoked by the end-constraint effect [34].

Table 11.1 In-plane elastic properties of unidirectional composites

Unidirectional composite	E_1 (GPa)	E_2 (GPa)	ν_{12}	G_{12} (GPa)	Fibre volume fraction
Aramid/epoxy	61.1	4.1	0.435	1.48	0.55
Carbon/epoxy (T300/5208)	136.5	9.8	0.350	5.65	0.62
Carbon/polyimide (Celion 6000/PMR-15)	136.5	9.8	0.350	4.92	0.57

Source: Herakovich [14].

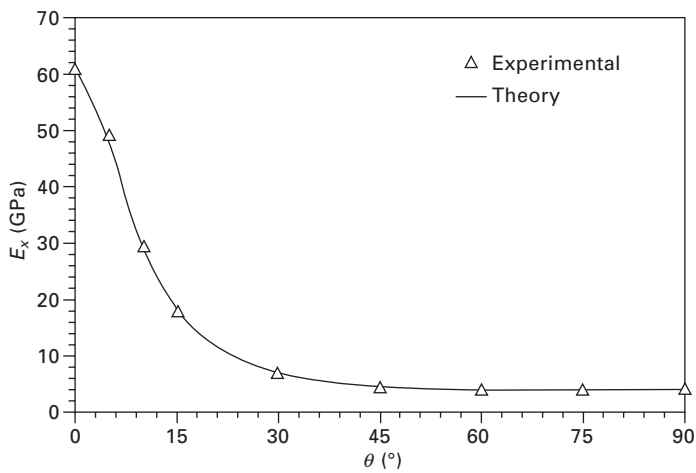

11.27 Off-axis modulus for aramid/epoxy (after [14]).

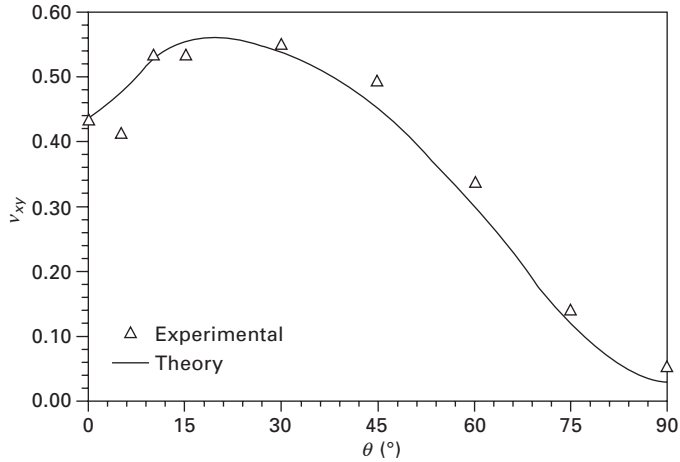

11.28 Off-axis Poisson's ratio for aramid/epoxy (after [14]).

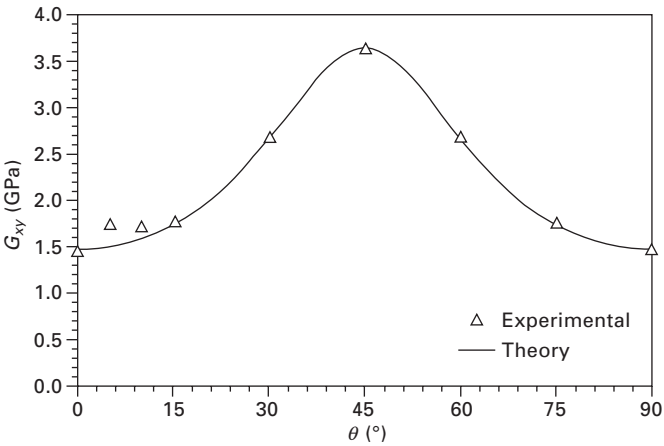

11.29 Off-axis in-plane shear modulus for aramid/epoxy.

11.7 Laminate plate and shell stiffness: classical lamination theory (CLT)

Many composite structures can be described and analysed as thin laminated shells or plates composed of several laminae stacked sequentially, each aligned at a specific angle with respect to a material reference axis, by convention the *x*-axis. Classical lamination theory is quite suitable for analysing thin laminated plates or any thin laminated shell that can be reduced to an equivalent plate.

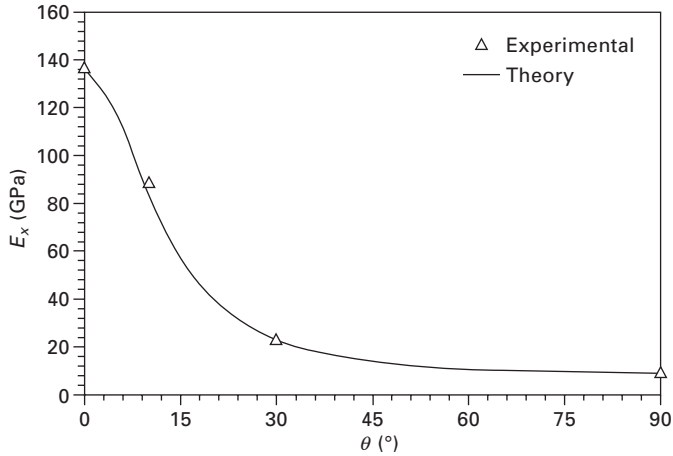

11.30 Off-axis modulus for carbon/epoxy (after [14]).

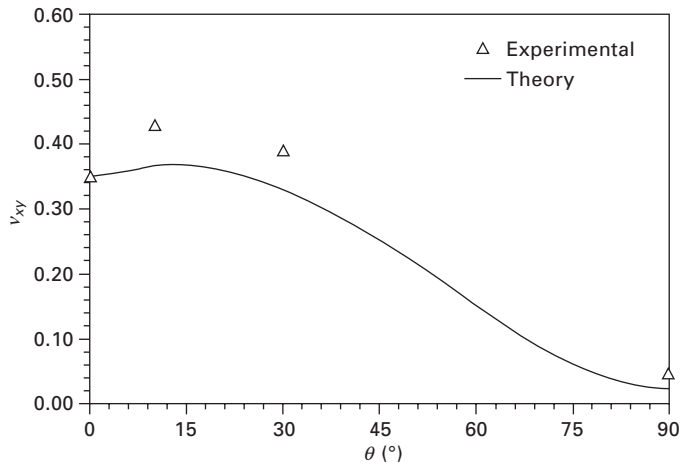

11.31 Off-axis Poisson's ratio for carbon/epoxy (after [14]).

11.7.1 Laminate code

The elastic properties of a laminate depend on elastic moduli, stacking position, thickness and angle of orientation of each lamina [14, 15, 38, 39]. Figure 11.36 gives a schematic of the [0/+θ/90/–θ/0] laminate. The code represents each lamina by the angle separated from other plies by a slash sign. The code also implies that each ply is made of the same material and is of the same thickness. For hybrid composites, letters are used after the ply angle to distinguish different materials. The first ply is the top ply of the laminate.

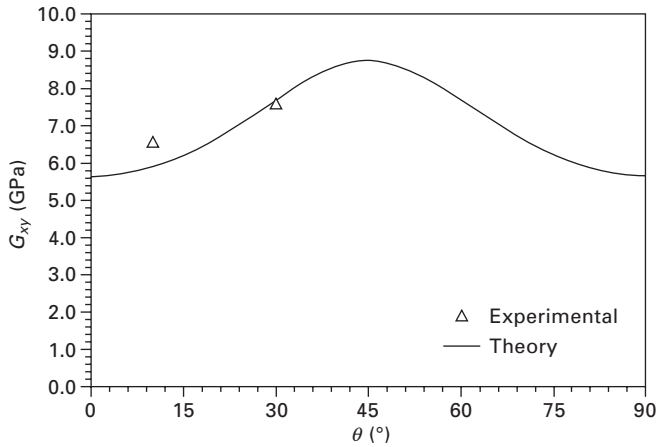

11.32 Off-axis in-plane shear modulus for carbon/epoxy.

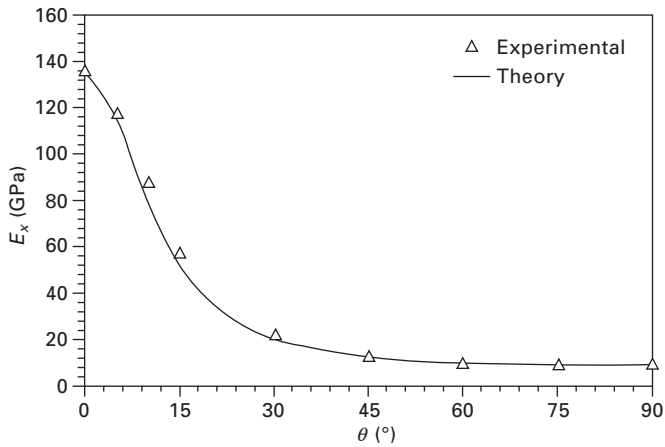

11.33 Off-axis modulus for carbon/polyimide (after [14]).

Special notations are used for symmetric laminates, laminates with adjacent laminae of the same orientation or of opposite angles, and so on.

Figure 11.37 shows four examples of usage of the special notation. The subscript T outside the brackets stands for total laminate, and the subscript S stands for symmetry, implying that the total laminate, i.e. the plies in brackets, are repeated in the reverse order. When the number of plies is odd and symmetry exists at the mid-surface, the last ply does not repeat in reverse order and is denoted with a bar on the top. A notation of $\pm\theta$ indicates that the $+\theta°$ angle ply is followed by a $-\theta°$ angle ply.

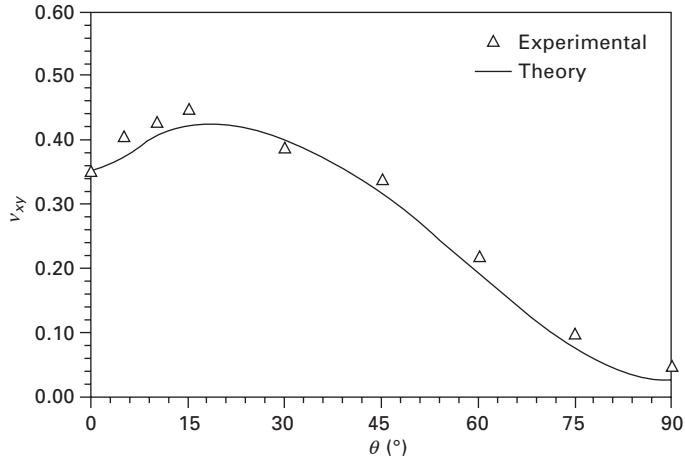

11.34 Off-axis Poisson's ratio for carbon/polyimide (after [14]).

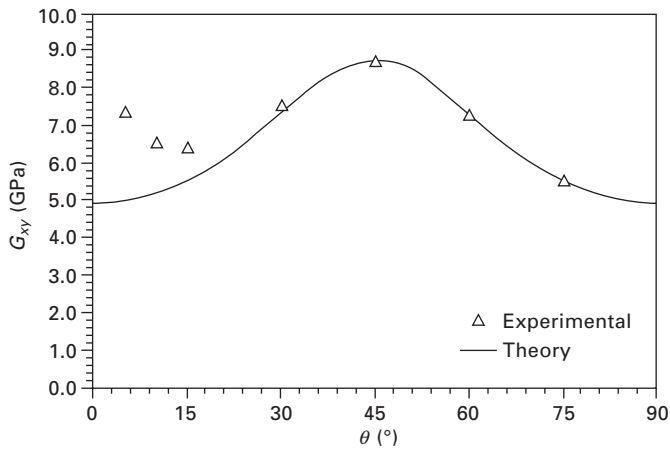

11.35 Off-axis in-plane shear modulus for carbon/polyimide.

11.7.2 Strain–displacement relationships

For thin plates subjected to small deformations, the Kirchhoff hypotheses for plates or the Kirchhoff–Love hypotheses for thin plates and shells are assumed [40]. These are as follows:

1. Normals to the mid-plane remain straight and normal to the deformed mid-plane after deformation.
2. Normals to the mid-plane do not change length.

These assumptions lead to the following simplifications. Assumption 1 requires that the shear strains $\gamma_{zx} = \gamma_{zy} = 0$. Assumption 2 requires that the

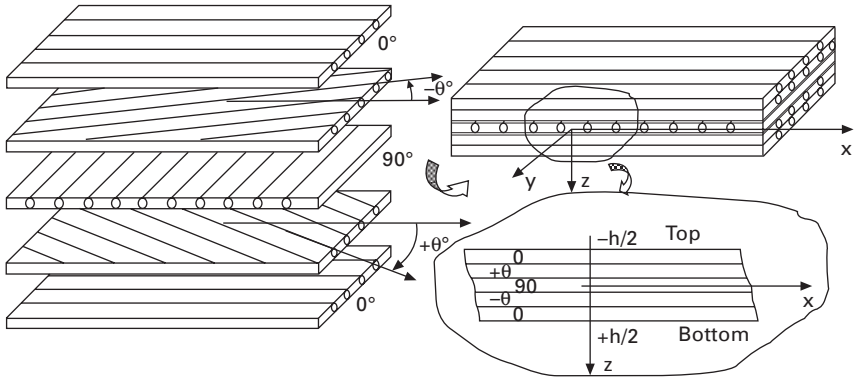

11.36 Schematic of a [0/ + θ/90/ – θ/0] laminate to illustrate the laminate code.

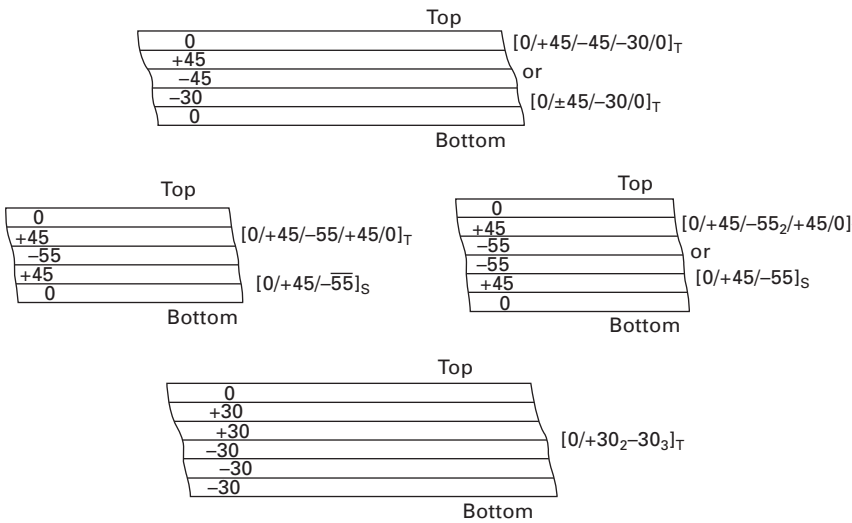

11.37 Examples of the laminate code notation usage.

deflection of the mid-plane depends only on x and y coordinates, i.e. $w = w(x, y)$. Hence this requires that $\varepsilon_z = 0$.

In Fig. 11.38 the mid-plane deformation is shown schematically. If the displacements are assumed small, the slope, tanα, of the deformed mid-plane will also be small. Since for small angles the approximation tan$\alpha \cong \alpha$ can be used,

$$\tan \alpha = \frac{\partial w}{\partial x} \cong \alpha \qquad [11.79]$$

The total displacement of a generic point in the x-axis direction is given by

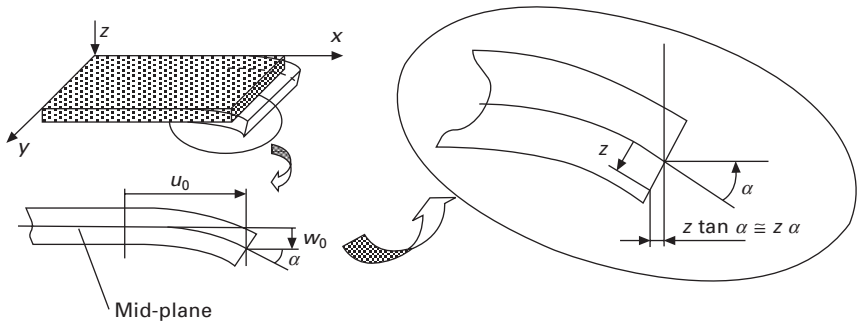

11.38 Schematic description of displacements through the thickness of a plate.

the sum of the mid-plane u^0 and the displacement produced by the rotation α of the normal to the mid-plane (see Fig. 11.38):

$$u = u^0 - z \tan \alpha \cong u^0 - a\alpha = u^0 - z \frac{\partial w}{\partial x} \qquad [11.80]$$

Similarly, the total displacement of a generic point in the y-axis direction is given by

$$v = v^0 - z \frac{\partial w}{\partial y} \qquad [11.81]$$

The plane deformations can be readily obtained, from the displacements

$$\begin{Bmatrix} \varepsilon_x \\ \varepsilon_y \\ \gamma_{xy} \end{Bmatrix} = \begin{Bmatrix} \dfrac{\partial u}{\partial x} \\ \dfrac{\partial v}{\partial y} \\ \dfrac{\partial u}{\partial y} + \dfrac{\partial v}{\partial x} \end{Bmatrix} = \begin{Bmatrix} \dfrac{\partial u^0}{\partial x} \\ \dfrac{\partial v^0}{\partial y} \\ \dfrac{\partial u^0}{\partial y} + \dfrac{\partial v^0}{\partial x} \end{Bmatrix} - z \begin{Bmatrix} \dfrac{\partial^2 w}{\partial x^2} \\ \dfrac{\partial^2 w}{\partial y^2} \\ 2\dfrac{\partial^2 w}{\partial y \partial x} \end{Bmatrix} = \begin{Bmatrix} \varepsilon_x^0 \\ \varepsilon_y^0 \\ \gamma_{xy}^0 \end{Bmatrix} - z \begin{Bmatrix} \kappa_x \\ \kappa_y \\ \kappa_{xy} \end{Bmatrix} \qquad [11.82]$$

where ε_x^0, ε_y^0 and γ_{xy}^0 represent the mid-plane strain state and κ_x, κ_y and κ_{xy} represent the curvatures.

11.7.3 Stress–strain relationships and transformation by rotation

The lamination theory assumes also that each layer is in a state of plane stress. Furthermore it assumes that each lamina is a homogeneous material

that can be isotropic, transversely isotropic or orthotropic. In the state of plane stress the condition $\sigma_z = \gamma_{zx} = \gamma_{zy} = 0$ is verified. The stress–strain relationships are devolved from the 3D relationships to obtain the reduced compliance and stiffness [14]. In the principal material coordinate system, the plane stress–strain relationship is

$$\begin{Bmatrix} \varepsilon_1 \\ \varepsilon_2 \\ \gamma_{12} \end{Bmatrix} = \begin{bmatrix} S_{11} & S_{12} & 0 \\ S_{21} & S_{22} & 0 \\ 0 & 0 & S_{66} \end{bmatrix} \begin{Bmatrix} \sigma_1 \\ \sigma_2 \\ \tau_{12} \end{Bmatrix} \quad [11.83]$$

or

$$\begin{Bmatrix} \varepsilon_1 \\ \varepsilon_2 \\ \gamma_{12} \end{Bmatrix} = \begin{bmatrix} \frac{1}{E_1} & -\frac{\nu_{21}}{E_2} & 0 \\ -\frac{\nu_{12}}{E_2} & \frac{1}{E_2} & 0 \\ 0 & 0 & \frac{1}{G_{12}} \end{bmatrix} \begin{Bmatrix} \sigma_1 \\ \sigma_2 \\ \tau_{12} \end{Bmatrix} \quad [11.84]$$

where $\frac{\nu_{21}}{E_2} = \frac{\nu_{12}}{E_1}$.

Inverting the former relationships,

$$\begin{Bmatrix} \sigma_1 \\ \sigma_2 \\ \tau_{12} \end{Bmatrix} = \begin{bmatrix} Q_{11} & Q_{12} & 0 \\ Q_{21} & Q_{22} & 0 \\ 0 & 0 & Q_{66} \end{bmatrix} \begin{Bmatrix} \varepsilon_1 \\ \varepsilon_2 \\ \gamma_{12} \end{Bmatrix} \quad [11.85]$$

or

$$\begin{Bmatrix} \sigma_1 \\ \sigma_2 \\ \tau_{12} \end{Bmatrix} = \begin{bmatrix} \frac{E_1}{1-\nu_{12}\nu_{21}} & \frac{\nu_{12}E_2}{1-\nu_{12}\nu_{21}} & 0 \\ \frac{\nu_{21}E_1}{1-\nu_{12}\nu_{21}} & \frac{E_2}{1-\nu_{12}\nu_{21}} & 0 \\ 0 & 0 & G_{12} \end{bmatrix} \begin{Bmatrix} \varepsilon_1 \\ \varepsilon_2 \\ \gamma_{12} \end{Bmatrix} \quad [11.86]$$

where $\frac{\nu_{12}E_2}{1-\nu_{12}\nu_{21}} = \frac{\nu_{21}E_1}{1-\nu_{12}\nu_{21}}$.

The 2D transformations for the rotations are obtained readily from the 3D transformations. The stress transformation, by rotation from the principal material coordinates to the global coordinates, is

$$\{\sigma\}_1 = [T_1]\{\sigma\}_x \qquad [11.87]$$

where the transformation matrix is

$$[T_1] = \begin{bmatrix} m^2 & n^2 & 2mn \\ n^2 & m^2 & -2mn \\ -mn & mn & m^2 - n^2 \end{bmatrix} \text{ with } m = \cos\theta \text{ and } n = \sin\theta$$

The strain transformation, by rotation from the principal material coordinates to the global coordinates, is

$$\{\varepsilon\}_1 = [T_2]\{\varepsilon\}_x \qquad [11.88]$$

where the transformation matrix is

$$[T_2] = \begin{bmatrix} m^2 & n^2 & mn \\ n^2 & m^2 & -mn \\ -2mn & 2mn & m^2 - n^2 \end{bmatrix}$$

Therefore the transformed stiffness $[\overline{Q}]$ may be determined using the relationships obtained for the stress and strain transformation,

$$[\overline{Q}] = [T_1]^{-1}[Q][T_2] = \begin{bmatrix} \overline{Q}_{11} & \overline{Q}_{12} & \overline{Q}_{16} \\ \overline{Q}_{12} & \overline{Q}_{22} & \overline{Q}_{26} \\ \overline{Q}_{16} & \overline{Q}_{26} & \overline{Q}_{66} \end{bmatrix} \qquad [11.89]$$

noting that $[T_i(\theta)]^{-1} = [T_i(-\theta)](i = 1, 2)$.

For transformed compliance a similar relationship is established:

$$[\overline{S}] = [T_2]^{-1}[S][T_1] = \begin{bmatrix} \overline{S}_{11} & \overline{S}_{12} & \overline{S}_{16} \\ \overline{S}_{12} & \overline{S}_{22} & \overline{S}_{26} \\ \overline{S}_{16} & \overline{S}_{26} & \overline{S}_{66} \end{bmatrix} \qquad [11.90]$$

11.7.4 In-plane forces and bending moments per unit length

The in-plane forces or membrane forces and bending moments per unit length, depicted in Fig. 11.39, are defined as through-thickness integrals of planar stresses, assuming that the laminate consists of perfectly bonded laminae or layers.

Using a condensed form, the following is obtained:

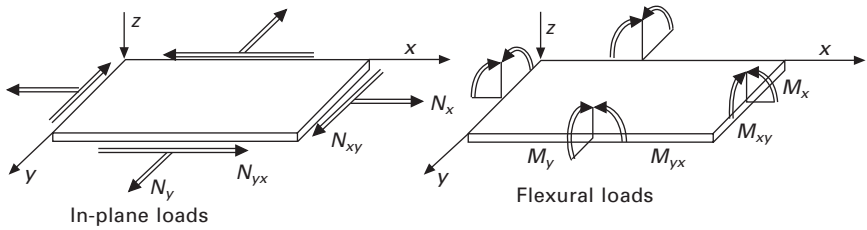

11.39 Resultant forces and moments on a laminate.

$$\begin{Bmatrix} N \\ M \end{Bmatrix} = \begin{Bmatrix} \int_{-h/2}^{+h/2} \{\sigma\}_x \, \mathrm{d}z \\ \int_{-h/2}^{+h/2} \{\sigma\}_x \, z\mathrm{d}z \end{Bmatrix} \quad [11.91]$$

or

$$\begin{Bmatrix} N \\ M \end{Bmatrix} = \begin{Bmatrix} \int_{-h/2}^{+h/2} [\bar{Q}]^k \{\varepsilon^0\} \, \mathrm{d}z + \int_{-h/2}^{+h/2} [\bar{Q}]^k \{\kappa\} \, z\mathrm{d}z \\ \int_{-h/2}^{+h/2} [\bar{Q}]^k \{\varepsilon^0\} \, z\mathrm{d}z + \int_{-h/2}^{+h/2} [\bar{Q}]^k \{\kappa\} \, z^2\mathrm{d}z \end{Bmatrix}$$

$$= \begin{bmatrix} \int_{-h/2}^{+h/2} [\bar{Q}]^k \mathrm{d}z & \int_{-h/2}^{+h/2} [\bar{Q}]^k \, z\mathrm{d}z \\ \int_{-h/2}^{+h/2} [\bar{Q}]^k \, z\mathrm{d}z & \int_{-h/2}^{+h/2} [\bar{Q}]^k \, z^2\mathrm{d}z \end{bmatrix} \begin{Bmatrix} \varepsilon^0 \\ \kappa \end{Bmatrix} \quad [11.92]$$

where the superscript k stands for the ply number. The integration can be replaced by a summation, since for each ply $[\bar{Q}]^k$ is constant. Finally, the fundamental equation of classical lamination theory is obtained:

$$\begin{Bmatrix} N \\ M \end{Bmatrix} = \begin{bmatrix} A & B \\ B & D \end{bmatrix} \begin{Bmatrix} \varepsilon^0 \\ \kappa \end{Bmatrix} \quad [11.93]$$

where N_c is the total number of laminae and

$$A = \int_{-h/2}^{+h/2} [\bar{Q}]^k \, \mathrm{d}z = \sum_{i=1}^{N_c} [\bar{Q}]^k (z_k - z_{k-1})$$

$$B = \int_{-h/2}^{+h/2} [\bar{Q}]^k \, z\mathrm{d}z = \frac{1}{2} \sum_{i=1}^{N_c} [\bar{Q}]^k (z_k^2 - z_{k-1}^2)$$

$$D = \int_{-h/2}^{+h/2} [\bar{Q}]^k \, z^2\mathrm{d}z = \frac{1}{2} \sum_{i=1}^{N_c} [\bar{Q}]^k (z_k^3 - z_{k-1}^3)$$

are the submatrices of the laminate stiffness matrix. The laminate stiffness matrix is symmetric. Matrix [A] represents the in-plane stiffness and matrix [D] represents the flexural stiffness. Matrix [B] represents the coupling between in-plane deformations and bending. When the laminate is symmetric, [B] is null, i.e. the in-plane deformations are decoupled from the bending. Matrix [A] does not depend on the stacking sequence, which is not the case for matrix [B] and matrix [D]. When matrix [B] is not null, in-plane loading simultaneously induces in-plane deformations and curvatures. Matrices [A], [B] and [D] are called the extensional, coupling and bending stiffness matrices, respectively. Figure 11.40 gives examples of relationships between in-plane and flexural loads and mechanical behaviour, through the **ABD** matrix elements.

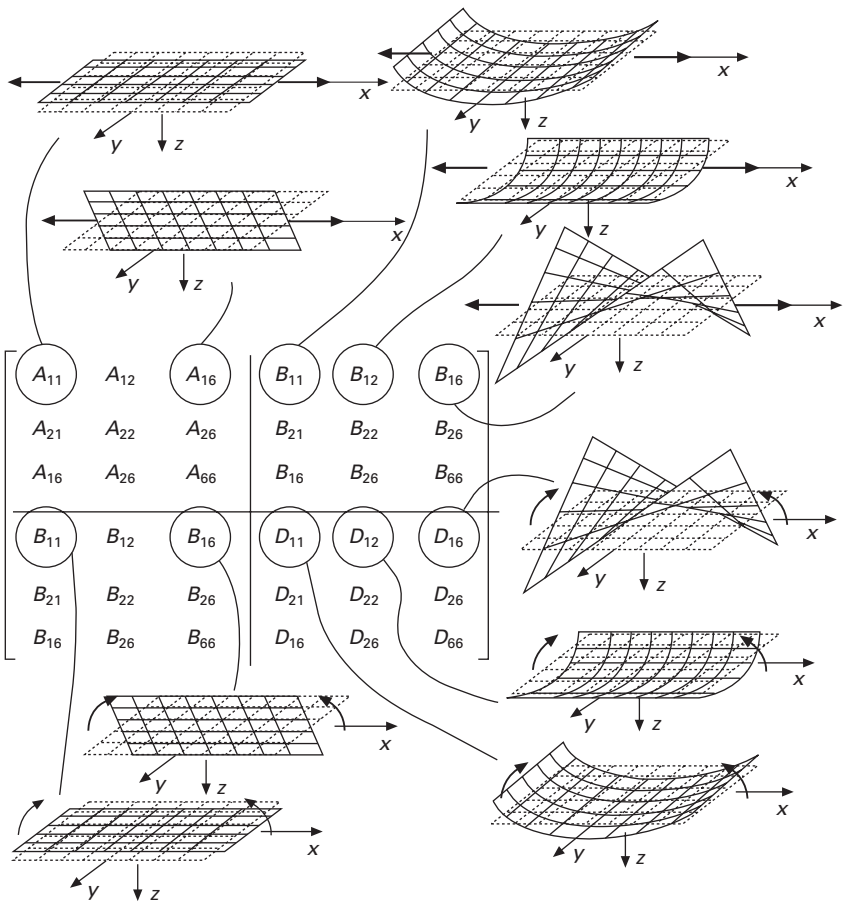

11.40 ABD stiffness matrix and mechanical deformation for in-plane and flexural loading.

The inversion of Equation (11.93) gives the compliance matrix:

$$\begin{Bmatrix} \varepsilon^0 \\ \kappa \end{Bmatrix} = \begin{bmatrix} A' & B' \\ B'^{\mathrm{T}} & D' \end{bmatrix} \begin{Bmatrix} N \\ M \end{Bmatrix} \qquad [11.94]$$

where $[A'] = [A]^{-1} + [A]^{-1}[B][D'][B][A]^{-1}$, $[B'] = [A]^{-1}[B][D']$, $[C'] = [D'][B][A]^{-1}$ and $[D'] = ([D] - [B][A]^{-1}[B])^{-1}$, also noting that $[B'^{\mathrm{T}}] = [B']$ and the laminate compliance matrix $A'B'D'$ is symmetric. This comes directly from matrix algebra; the inverse matrix of a symmetric matrix is also symmetric. The $[A']$, $[B']$ and $[D']$ matrices are called the extensional compliance matrix, coupling compliance matrix, and bending compliance matrix, respectively.

After calculating the strains $\{\varepsilon^0\}$ and curvatures $\{\kappa\}$, the stresses can be readily calculated for the kth lamina as

$$\begin{aligned} \{\sigma\}^k &= [\overline{Q}]^k \{\varepsilon^0\} + [\overline{Q}]^k z\{\kappa\} \\ &= [\overline{Q}]^k([A']\{N\} + [B']\{M\} + z([B']\{N\} + [D']\{M\})) \end{aligned} \qquad [11.95]$$

where z represents the distance of the kth lamina centre plane to the laminate mid-plane.

11.8 Properties of different types of laminate

11.8.1 Symmetrical laminates

In the case of symmetric laminate, the in-plane deformations become uncoupled from bending, i.e. $[B] = \mathbf{0}$. The fundamental equation of classical lamination theory reduces to

$$\begin{Bmatrix} N \\ M \end{Bmatrix} = \begin{bmatrix} A & \mathbf{0} \\ \mathbf{0} & D \end{bmatrix} \begin{Bmatrix} \varepsilon^0 \\ \kappa \end{Bmatrix} \Leftrightarrow \{N\} = [A]\{\varepsilon^0\} \wedge \{M\} = [D]\{\kappa\} \qquad [11.96]$$

and

$$\begin{Bmatrix} \varepsilon^0 \\ \kappa \end{Bmatrix} = \begin{bmatrix} A^{-1} & \mathbf{0} \\ \mathbf{0} & D^{-1} \end{bmatrix} \begin{Bmatrix} N \\ M \end{Bmatrix} \Leftrightarrow \{\varepsilon^0\} = [A]^{-1}\{N\} \wedge \{\kappa\} = [D]^{-1}\{M\} \qquad [11.97]$$

11.8.2 Specially orthotropic laminates

Laminates with $A_{16} = A_{26} = 0$ are designated specially orthotropic because there is no coupling between in-plane extensions and shear deformation. This does not imply necessarily that $D_{16} = D_{26} = 0$ because the designation is solely related to the in-plane response.

11.8.3 Cross-ply laminates

Cross-ply laminates are uniquely composed of laminae with fibre orientations of 0° and 90°. Since for these orientations both $\overline{Q}_{16} = \overline{Q}_{26} = 0$, independently of thickness and stacking sequence, for these laminates $A_{16} = A_{26} = 0$, i.e. the laminates are specially orthotropic. Moreover, these cases also verify that $D_{16} = D_{26} = 0$.

The in-plane stiffness or extensional matrix of a cross-ply laminate of the type $[0_{n_1}/90_{n_2}]_s$, since $\overline{Q}_{11}(0) = \overline{Q}_{22}(90) = Q_{11}$, $\overline{Q}_{22}(0) = \overline{Q}]_{11}(90) = Q_{22}$, $\overline{Q}_{12}(0) = \overline{Q}_{12}(90) = Q_{12}$ and $\overline{Q}_{66}(0) = \overline{Q}_{66}(90) = Q_{66}$, is given as

$$[A] = 2t \begin{bmatrix} n_1Q_{11} + n_2Q_{22} & (n_1 + n_2)Q_{12} & 0 \\ (n_1 + n_2)Q_{12} & n_2Q_{11} + n_1Q_{22} & 0 \\ 0 & 0 & (n_1 + n_2)Q_{66} \end{bmatrix} \quad [11.98]$$

Assuming that all laminae have the same thickness t, then the total thickness h is given by $h = 2t(n_1 + n_2)$. In terms of engineering constants, the equation for $[A]$ is written as

$$[A] = \frac{2t}{1 - \nu_{12}\nu_{21}} \begin{bmatrix} n_1E_1 + n_2E_2 & \nu_{12}(n_1 + n_2)E_2 & 0 \\ (n_1 + n_2)Q_{12} & n_2E_1 + n_1Q_2 & 0 \\ 0 & 0 & (1 - \nu_{12}\nu_{21})(n_1 + n_2)G_{12} \end{bmatrix} \quad [11.99]$$

11.8.4 Angle-ply laminates

Angle-ply laminates have an equal number of laminae at $+\theta$ and $-\theta$ fibre orientations with equal thickness. It is quite easy to demonstrate that angle-ply laminates verify $A_{16} = A_{26} = 0$, based on the fact that $\overline{Q}_{16}(-\theta) = -\overline{Q}_{16}(\theta)$ and $\overline{Q}_{26}(-\theta) = -\overline{Q}_{26}(\theta)$. Hence angle-ply laminates are specially orthotropic. Contrary to cross-ply laminates, $D_{16} \neq 0 \wedge D_{26} \neq 0$, because the $+\theta$ and $-\theta$ laminae are not at the same distance from the mid-plane. Since $\overline{Q}_{11}(-\theta) = \overline{Q}_{11}(\theta)$, $\overline{Q}_{12}(-\theta) = \overline{Q}_{12}(\theta)$, $\overline{Q}_{22}(-\theta) = \overline{Q}_{22}(\theta)$ and $\overline{Q}_{66}(-\theta) = \overline{Q}_{66}(\theta)$, the in-plane stiffness or extensional matrix can be written as

$$[A] = h \begin{bmatrix} \overline{Q}_{11}(\theta) & \overline{Q}_{12}(\theta) & 0 \\ \overline{Q}_{12}(\theta) & \overline{Q}_{22}(\theta) & 0 \\ 0 & 0 & \overline{Q}_{66}(\theta) \end{bmatrix} \quad [11.100]$$

where h is the total thickness.

11.8.5 Balanced laminates

In a balanced laminate the laminae with positive angles are balanced by equal laminae with negative angles. Contrary to angle-ply laminates which are restricted to one pair of matched angles, balanced laminates can contain several pairs, including 0° and 90°. Like angle-ply laminates, for balanced laminates $A_{16} = A_{26} = 0$ and $D_{16} \neq 0 \wedge D_{26} \neq 0$.

11.8.6 Quasi-isotropic laminates

There is an important group of laminates that exhibit in-plane isotropic elastic response. These laminates are called quasi-isotropic. This group includes all symmetric laminates with $2N$ ($N > 2$) laminae with the same thickness and N equal angles between fibre orientations ($\Delta\theta = \pi/N$), i.e. $\Delta\theta = 60°$ for $N = 3$, $\Delta\theta = 45°$ for $N = 4$, $\Delta\theta = 30°$ for $N = 6$ and so on. It is possible to prove that the in-plane stiffness or extensional matrix of quasi-isotropic laminates is given in reduced form as [14]

$$[A] = h \begin{bmatrix} U_1 & U_4 & 0 \\ U_4 & U_1 & 0 \\ 0 & 0 & U_5 \end{bmatrix} \qquad [11.101]$$

where h is the total thickness and U_1, U_4 and U_5 are invariants, i.e. only functions of the material, given by [14]

$$\begin{aligned} U_1 &= \frac{3Q_{11} + 3Q_{22} + 2Q_{12} + 4Q_{66}}{8} \\ U_4 &= \frac{Q_{11} + Q_{22} + 6Q_{12} - 4Q_{66}}{8} \\ U_5 &= \frac{Q_{11} + Q_{22} - 2Q_{12} + 4Q_{66}}{8} \end{aligned} \qquad [11.102]$$

These laminates are also specially orthotropic since $A_{16} = A_{26} = 0$. Hence there is no coupling between in-plane normal and shear responses in these laminates. The designation quasi-isotropic is used because the bending response of these laminates is not isotropic.

11.9 In-plane and flexural engineering constants of a laminate

For symmetric laminates it is possible to define effective in-plane moduli in terms of the in-plane stiffness or extensional compliance matrix, since there is no coupling between in-plane and bending response. The effective

in-plane engineering constants for a laminate with thickness h are readily obtained from the extensional compliance matrix [1],

$$E_x = \frac{1}{hA'_{11}},\ E_y = \frac{1}{hA'_{22}},\ G_{xy} = \frac{1}{hA'_{66}},\ \nu_{xy} = -\frac{A'_{12}}{A'_{11}},\ \nu_{yx} = -\frac{A'_{12}}{A'_{22}} \quad [11.103]$$

which represent the effective in-plane longitudinal modulus, the effective in-plane transverse modulus, the effective in-plane shear modulus and the two effective in-plane Poisson's ratios, respectively. It should be noted that $\nu_{xy}/E_x = \nu_{yx}/E_y$.

Similarly, the flexural elastic moduli of symmetric laminates are readily obtained from the bending compliance matrix,

$$E_x^f = \frac{12}{h^3 D'_{11}},\ E_y^f = \frac{12}{h^3 D'_{22}},\ G_{xy}^f = \frac{12}{h^3 D'_{66}},\ \nu_{xy}^f = -\frac{D'_{12}}{D'_{11}},\ \nu_{yx}^f = -\frac{D'_{12}}{D'_{22}} \quad [11.104]$$

which represent the effective flexural longitudinal modulus, the effective flexural transverse modulus, the effective flexural shear modulus and the two effective flexural Poisson's ratios, respectively. It should also be noted that $\nu_{xy}^f/E_x^f = \nu_{yx}^f/E_y^f$.

11.9.1 Examples

Examples of angle-ply and quasi-isotropic laminated T300/5208 (carbon/epoxy) are analysed in terms of in-plane and flexural engineering constants. The lamina engineering constants were given in Table 11.1. Table 11.2 shows the longitudinal modulus and Poisson's ratio for different laminates experimentally measured [14]. The measured data compare quite well with calculated values from CLT.

Table 11.2 Experimental and calculated engineering constants for T300/5208 laminates

Laminate	Experimental		Calculated			
	E_x (GPa)	ν_{xy}	E_x (GPa)	E_y (GPa)	ν_{xy}	G_{xy} (GPa)
$[10_2/-10_2]_S$	127	0.59	126	9.92	0.672	9.1
$[\pm 10_2]_S$	123	0.56	126	9.92	0.672	9.1
$[\pm 30_2]_S$	45	1.12	50.4	11.9	1.30	27.8
$[\pm 45_2]_S$	16	0.76	19.7	19.7	0.745	35.2
$[0/\pm 45/90]_S$	52	0.27	53.4	53.4	0.309	20.4
$[90/-45/0/45]_S$	51	0.30	53.4	53.4	0.309	20.4

Source: experimental constants are from Herakovich [14]

Using the angle-ply laminates from Table 11.2, the in-plane and flexural engineering constants, functions of orientation, were calculated and compared through the plots in Figs 11.41–11.43. For all three laminates, $[\pm 10_2]_S$, $[\pm 30_2]_S$ and $[\pm 45_2]_S$, it is quite clear that the differences between in-plane and flexural engineering constants are small. The effect of the stacking sequence on the flexural elastic constants is more evident for the $[\pm 30_2]_S$ laminate. For this laminate the Poisson's ratio becomes negative for directions between 35° and 55°.

Using the two quasi-isotropic laminates from Table 11.2, the flexural engineering constants, functions of orientation, were calculated and compared

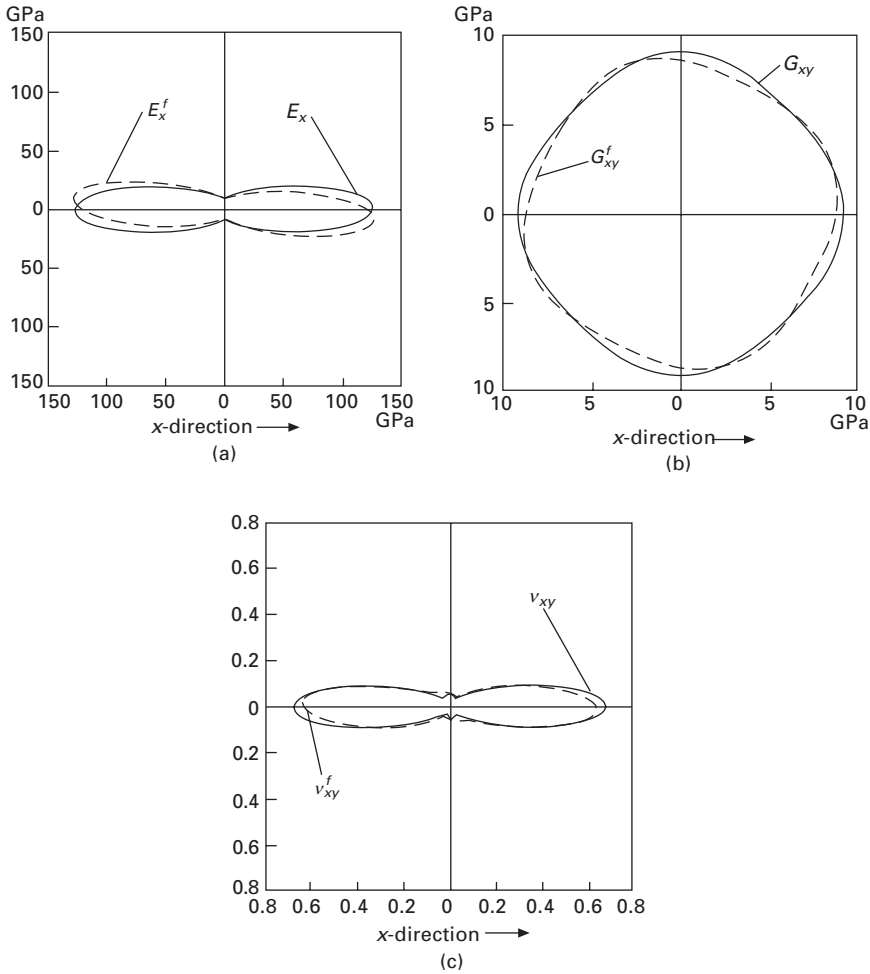

11.41 Polar variation for the $[\pm 10_2]_S$ laminate of (a) longitudinal modulus, (b) shear modulus and (c) Poisson's ratio.

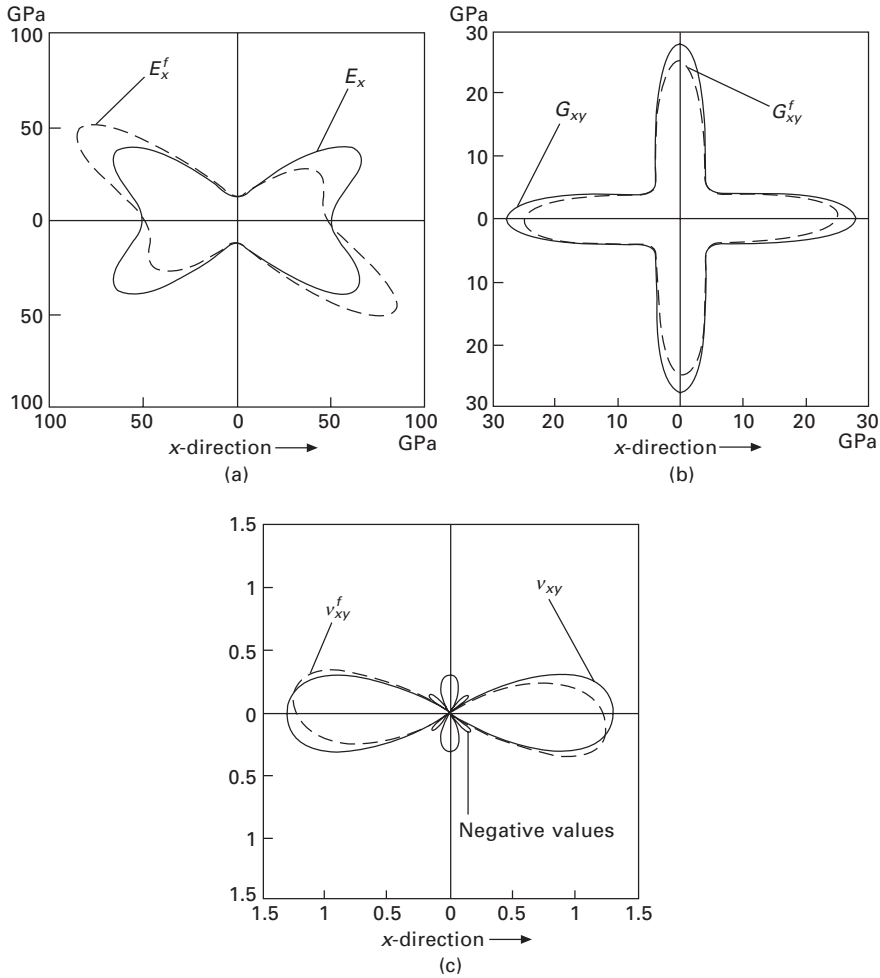

11.42 Polar variation for the $[\pm 30_2]_S$ laminate of (a) longitudinal modulus, (b) shear modulus and (c) Poisson's ratio.

through the plots in Fig.11.44. It is quite clear that the flexural behaviour is far from being isotropic. The effect of the stacking sequence on the flexural elastic constants is evident from the plots.

The Engineering Sciences Data Unit (ESDU) [41] offers a classification system which uses the **ABD** stiffness matrices with an extended subscript notation to describe their form, i.e. subscripts 0 if all elements are zero, F if all elements are not zero (finite), S if the matrix has the specially orthotropic form and, additionally proposed by York [42], I if it has the isotropic form. Accordingly it is quite easy to describe the **ABD** stiffness matrix for the following:

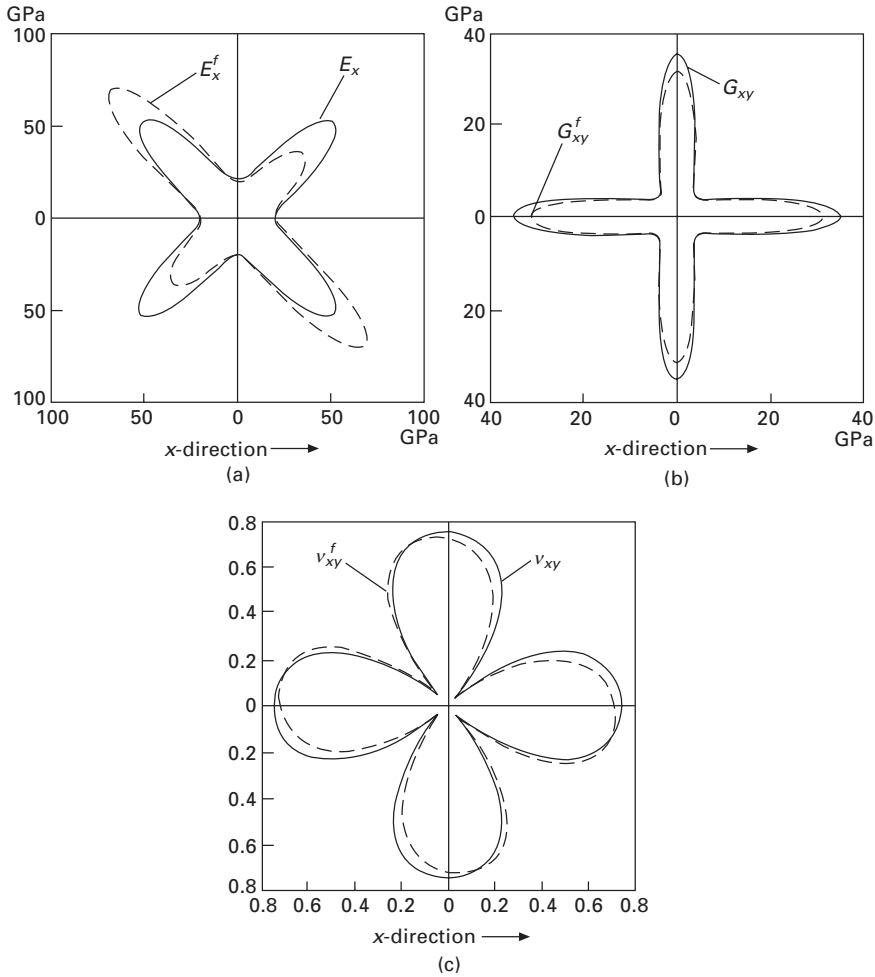

11.43 Polar variation for the $[\pm 45_2]_S$ laminate of (a) longitudinal modulus, (b) shear modulus and (c) Poisson's ratio.

- Balanced and symmetric laminates: $\mathbf{A}_S\mathbf{B}_0\mathbf{D}_F$
- Unbalanced laminates: $\mathbf{A}_F\mathbf{B}_0\mathbf{D}_S$
- Fully orthotropic angle-ply laminates: $\mathbf{A}_S\mathbf{B}_0\mathbf{D}_S$
- Extensionally isotropic laminates: $\mathbf{A}_I\mathbf{B}_0\mathbf{D}_S$
- Fully isotropic laminates: $\mathbf{A}_I\mathbf{B}_0\mathbf{D}_I$.

For brevity, the examples given before were restricted to symmetric laminates. However, unsymmetric laminates provide a unique structural behaviour not found in conventional materials. Depending on the prevalent loading conditions and on the specific structural requirements, the selection of the most effective laminate may lead to unsymmetric laminates.

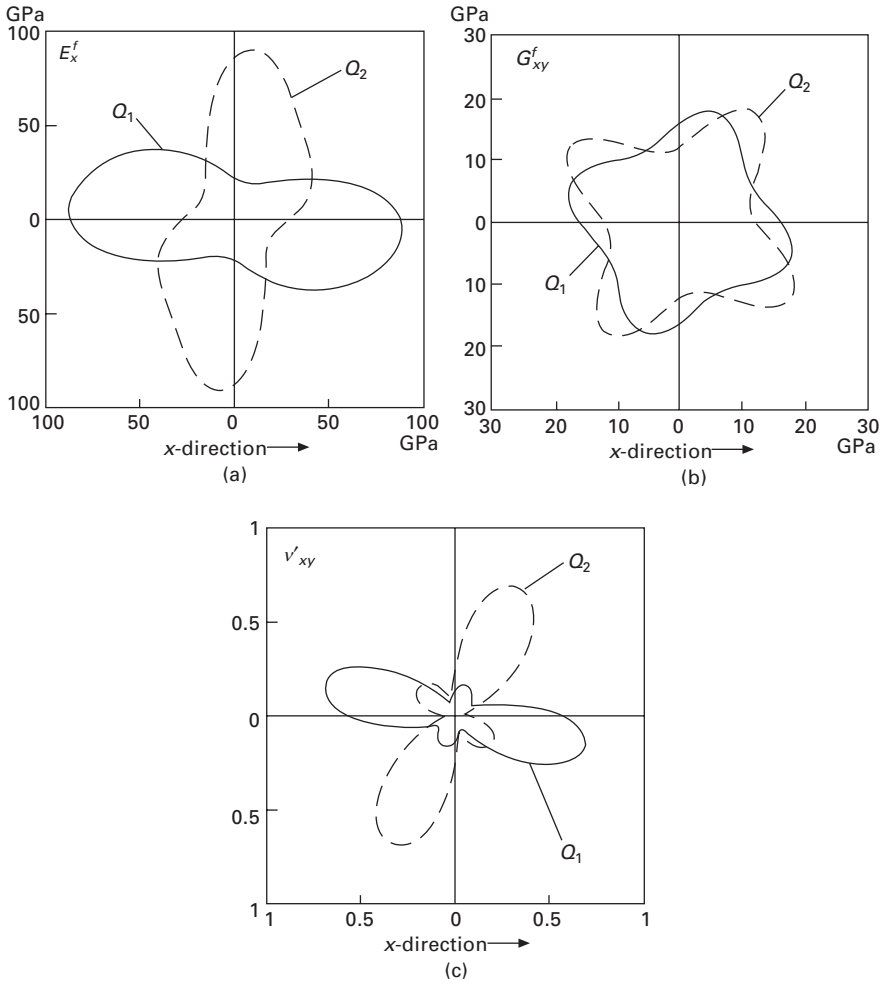

11.44 Polar variation for the Q1 ($[0/\pm45/90]_S$) and Q2 ($[90/-45/0/45]_S$) laminates of (a) flexural longitudinal modulus, (b) flexural shear modulus and (c) flexural Poisson's ratio.

Examples showing that the zero coupling does not require any symmetry were given by Caprino and Crivelli–Visconti [43]. For instance, the uncoupled antisymmetric 8-ply laminate $[\theta/-\theta/-\theta/\theta/-\theta/\theta/\theta/-\theta]$, with θ an arbitrary angle, is a fully orthotropic angle-ply laminate, i.e. $\mathbf{A}_S\mathbf{B}_0\mathbf{D}_S$. Finally for practical design there is specific software that can be very helpful to assist the CLT calculations. A list is included at the end of this chapter.

11.10 New optical methods for measuring laminate stiffness

Conventionally, experimental mechanics is based on surface deformation measurements (plane stress, plane strain or kinematic assumptions). Mechanical test methods are typically carried out using strain gauges (punctual) or extensometers (average). Data reduction schemes (closed-form solutions) are then proposed for determining material properties as a function of load, specimen dimensions and kinematic (e.g., displacement or strain) measurements. However, in the last decades thanks to the progress of computer science, automated image processing and digital cameras, a photomechanics approach has been emerging. It relies on the use of photonics (the science and technology of generating, controlling and detecting radiant energy) for measuring kinematic quantities (displacement, strain, slope, rotation, etc.) in the branch of mechanics.

Several full-field optical methods have been proposed in solid mechanics [44]. These techniques can be classed according to the physical phenomenon involved in the measurements as white-light (e.g., moiré, grid and digital image correlation methods) and interferometric (e.g., speckle and moiré interferometry, holography and shearography) (Table 11.3). The choice of a given technique can be driven by several criteria such as, for instance, cost, set-up apparatus (simplicity, flexibility, sensitivity to vibrations, etc.), performance (resolution, spatial resolution, etc.), measuring quantity (displacement, strain, etc.), and length scale of observation (from structural

Table 11.3 Optical methods in experimental mechanics

White-light techniques		
Measurand	Periodic pattern	Speckle pattern
u_x, u_y	Geometrical moiré Grid method Feature tracking method	Digital speckle photography Digital image correlation –
u_z	Shadow and projection moiré Grid projection	– –
u_x, u_y, u_z	–	Stereo-correlation
θ_x, θ_y	Reflection moiré Deflectometry	– –
Interferometric techniques		
Measurand	Diffuse light	Diffracted light
u_x, u_y, u_z ε_x, ε_y, ε_{xy}	Speckle interferometry Speckle shearography	Moiré interferometry Grating shearography

Source: after Rastogi [44] and Grédiac [45].

down to micro or nano). Contrasting with punctual devices (e.g. strain gauges and extensometers) these methods provide full-field data and are contact-free. The access of this type of information has allowed new insights into different engineering problems, such as, for instance, non-destructive testing, validation of constitutive models and multi-parameter identification from single test configurations [45].

Novel methods have been proposed for material parameter identification, based on full-field measurements (Table 11.4) [46]. This approach has opened new perspectives over classical data reduction schemes. The underlying idea is that a single specimen can be loaded in such a way that several parameters can be simultaneously involved in its mechanical response, yielding complex and heterogeneous stress/strain fields. Providing that these fields are measured by a suitable optical method, the whole set of active parameters can be determined afterwards by a given identification strategy. This approach seems to be particularly convenient for anisotropic and heterogeneous materials.

11.10.1 Individual optical methods

In white-light optical techniques the deformation of a material is described by means of the geometrical deformation of a target texture which is assumed to be perfectly attached to the material surface. Moreover, the local luminance of each source point of the imaged pattern is assumed constant throughout the material deformation (optical flow constraint). The analysis is then focused on the spatial variation of the light intensity distribution reflected across the textured pattern. This class of methods can be sorted with regard to periodic (phase-measuring techniques), random (image correlation techniques) or marked (image processing techniques) textures (Table 11.3). A periodic pattern is usually a network of parallel and evenly spaced dark and bright lines, such as the one used in geometrical moiré and grid methods. A random pattern can be imaged by a detector when a rough diffuse surface (roughness > light wavelength) is illuminated by coherent light. In this case, the light is scattered in all directions. Its spatial interference forms a granular pattern, called speckle, which is used as a metrological carrier in digital speckle photography. In digital image correlation, a white-light source is used and the

Table 11.4 Identification methods

• Finite Element Model Updating Method (FEMU)
• Virtual Fields Method (VFM)
• Constitutive Equation Gap Method (CEGM)
• Equilibrium Gap Method (EGM)
• Reciprocity Gap Method (RGM)

Source: after Avril *et al.* [46].

speckle pattern can be either the natural contrasted texture of the surface of interest or an artificial texture obtained by spraying a black-to-white paint.

An image-based feature tracking method can also be used for measuring displacements. This method requires only a few marks (i.e., local features with suitable colour, shape and size) over the region of interest, which can be transferred (painted) to a background surface. Normally, this technique does not have the same spatial resolution as counterpart DIC and grid methods, but can be suitable for measuring strains over uniform or moderate gradient fields.

Optical interferometry techniques are based on the phenomenon of interference of light waves. These techniques rely on monochromatic and coherent light illumination. Considering the way light interacts with a target surface of interest, these methods can be sorted into diffused light (speckle) and diffracted light (grating) interferometric techniques (Table 11.3). Speckle interferometry is based on the diffuse reflection of light from an optical rough surface, whereas grating interferometry is based on the diffraction of light by a grating attached to the object surface. Several configurations can be set up in which the interference phase variation is given as the dot product of the displacement to the sensitivity vector, given by the difference of illumination and observation wave vectors. Therefore, there are speckle interferometry techniques for both in-plane and out-of-plane displacement measurements. Moiré interferometry is a technique based on grating metrology allowing the measurement of both in-plane and out-of-plane displacements. Finally, there are also different shearography set-ups (Table 11.3) that provide directly the measurement of the (optical) derivatives of the displacement.

Among optical techniques (Table 11.3), digital image correlation (DIC) has become widely used in experimental solid mechanics to study material deformation and fracture mechanics [47, 48]. On the one hand, with regard to counterpart methods, this technique requires neither specific and expensive optical devices (e.g., lasers and anti-vibration tables) nor time-consuming surface preparation. On the other hand, DIC can be flexibly coupled with mechanical testing machines. Moreover, it can be conveniently applied from the structural to the micro or nano scale. In mechanical tests DIC-2D is usually used, whilst in structural applications DIC-3D (stereovision) can be preferable. In contrast with interferometric methods, phase analysis of the fringe images and phase unwrapping process are not required. Nevertheless, DIC measurements are usually unreliable near boundaries or discontinuities, since subsets (continuous shape functions) in the image are typically used for displacement evaluation through mathematical correlation (local approach) [49, 50]. In the following a review of the DIC method is presented.

11.10.2 Digital image correlation

A schematic representation of the 2D digital image correlation technique coupled with a mechanical test is shown in Fig. 11.45. A (quasi-)planar object is imaged by a camera-lens optical system connected to a computer for real-time visualisation. It is assumed that the surface of interest has a random textured pattern uniquely characterizing the material surface. The magnification of the imaging system is assumed constant during image acquisition (i.e., out-of-plane movements are neglected and the object undergoes only in-plane deformation). Besides, geometrical distortions induced by optical aberrations are assumed to be either negligible (differential measurements) or taken into account by a distortion correction method. A matching process is carried out between images taken before and after deformation, as shown schematically in Fig. 11.46. The reference (undeformed) image is divided by square or rectangular subsets defining a given domain (Ω in Fig. 11.46). In order to enhance the displacement spatial resolution (defined as the smaller distance separating two independent displacement measurements), subsets can slightly overlap by sharing some pixels. In this case, the subset step (f_d) will be smaller than the subset size (f_s). Adjacent ($f_s = f_d$) or spaced ($f_s < f_d$) subsets can also be selected, depending on the purpose. The selection of these measuring parameters is a key issue, because they will contribute to the spatial resolution (Δu) and the resolution (σ_u) associated with DIC measurements. Therefore, they should be carefully chosen with regard to the application, in a compromise between correlation (small subsets) and interpolation (large subsets) errors. By locally minimizing the difference in light intensity distribution between pairs of images, subset mapping

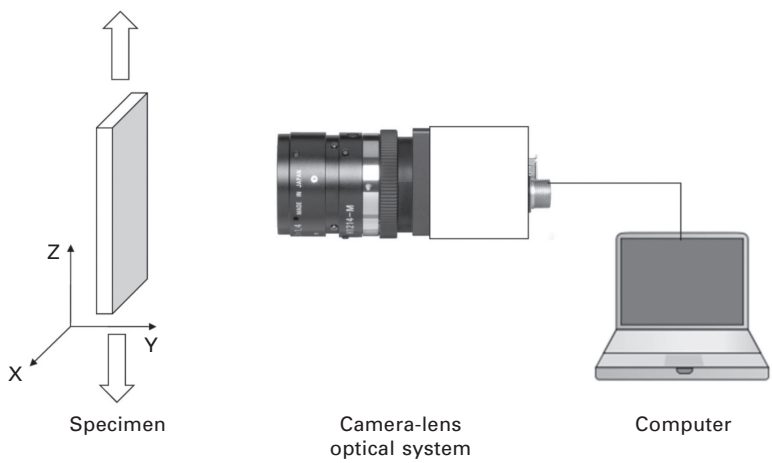

11.45 Photo-mechanical setup of the digital image correlation.

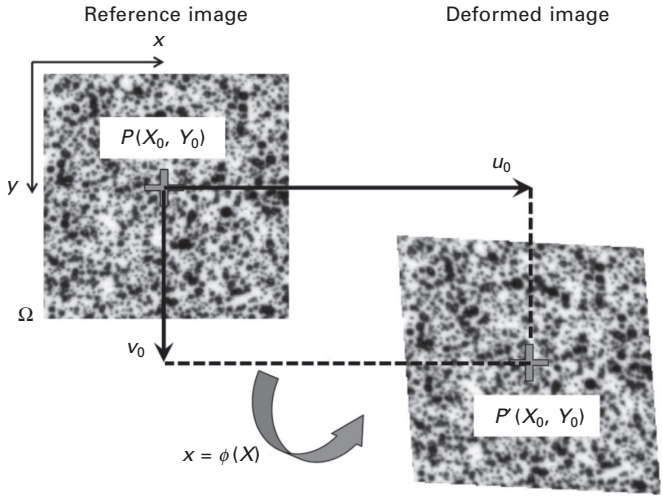

11.46 Schematic representation of the principle of digital image correlation.

in the deformed image is calculated, allowing the definition of full-field displacements.

Several mathematical correlation criteria have been proposed for estimation of the displacement fields in the subset matching process. It has been shown that the zero-normalized sum of squared differences (ZNSSD) is a robust algorithm, since it takes into account offset and linear scale variations of light intensity [48]:

$$c_{\mathrm{ZNSSD}}(\mathrm{p}) = \sum_{\Omega}\left[\frac{f(x_i, y_i) - y_m}{\sqrt{\sum_{\Omega}(f(x_i, y_i) - f_m)^2}} - \frac{g(x_i', y_i') - g_m}{\sqrt{\sum_{\Omega}(g(x_i', y_i') - g_m)^2}}\right]^2 \quad [11.105]$$

where Ω is the subset domain, $f(x_i, y_i)$ is the pixel grey level at (x_i, y_i) in the reference image, $g(x_i', y_i')$ is the pixel grey level at (x_i', y_i') in the deformed image, and f_{m} and g_m are the mean grey-level values over the subset in the reference and deformed images, respectively.

A given deformation mapping function is to be chosen whose constants define the design parameters ($\mathbf{p}$) to be identified in the matching optimization problem. Both first-order and second-order shape functions have been commonly used [48]. As an example, the first-order transfer is written as:

$$\begin{cases} x_i' - x_i = u_0 + \mathbf{u}_{\mathrm{I}}^{\mathrm{T}}\mathbf{d} \\ y_i' - y_i = v_0 + \mathbf{v}_{\mathrm{I}}^{\mathrm{T}}\mathbf{d} \end{cases} \quad [11.106]$$

with

$$\mathbf{u}_1 = \left\{\frac{\partial u}{\partial x}, \frac{\partial u}{\partial y}\right\}^{\mathrm{T}}, \mathbf{v}_1 = \left\{\frac{\partial v}{\partial x}, \frac{\partial v}{\partial y}\right\}^{\mathrm{T}}, \mathbf{d} = \{x_i - x_0, y_i - y_0\}^{\mathrm{T}}$$

An iterative algorithm, e.g. Newton–Raphson or Levenberg–Marquardt, can then be used for finding the optimal deformation parameter optimizing the correlation coefficient [48, 51].

11.10.3 Identification methods

The material parameters governing the relevant constitutive equations are determined experimentally through suitable mechanical tests. In the field of solid mechanics, this issue is presented as an inverse problem where the constitutive parameters are to be determined knowing the specimen geometry, the boundary conditions and the strains (or displacements). Conventionally, the identification is carried out on mechanical tests in which geometry and loading conditions yield a homogeneous or simple state of strain/stress across the gauge area. The concept behind this assumption is useful for theoretical analyses because closed-form solutions exist, relating the unknown material parameters to load and strain measurements (statically determined tests). However, the practical implementation of these tests can be difficult, for instance due to end-effects, especially for anisotropic and heterogeneous materials.

The recent development of full-field optical techniques has enabled a new glance on mechanical tests for material characterization [45]. The basic idea underlying this new approach is that a single specimen can be loaded in such a way that several parameters are activated in its mechanical response, yielding heterogeneous and complex strain fields (statically undetermined tests). By means of a suitable identification strategy, all the active parameters can be determined afterwards. A few approaches exist in the literature for addressing this problem (Table 11.4) [46]. The most familiar may be the finite element model updating method (FEMUM). It consists in building a finite element model of the mechanical test and considering a cost function of the difference between numerical and experimental data (displacement or strain) over the region of interest. The minimization of this cost function with respect to the unknown material parameters (design variables), iteratively updated in the model, provides the solution to the problem. This method is flexible and does not specifically require full-field measurements. However, as it is iterative, it can be time-consuming and the convergence can depend on the initial guess of parameters. Moreover, accurate boundary conditions need to be modelled to avoid a bias on the identified parameters. The presence of noise in the measurements will also affect the robustness of the updating routine. To overcome the drawbacks associated with the FEMUM,

alternative approaches have been proposed, among them the virtual fields method (VFM) [52].

The VFM is based on the fundamental equations of solid mechanics: the equilibrium equation, through the principle of virtual work (PVW), the constitutive equations and the strain–displacement relationships. For an arbitrary solid in equilibrium, the PVW can be written as

$$\int_V \sigma : \varepsilon^* \, \mathrm{d}V = \int_{S_\mathrm{f}} \mathbf{T} \cdot \mathbf{u}^* \, \mathrm{d}S + \int_V \mathbf{f} : \mathbf{u}^* \, \mathrm{d}V + \int_V \rho\gamma \cdot \mathbf{u}^* \mathrm{d}V \quad [11.107]$$

where σ is the stress tensor, ε^* the virtual strain tensor, V the volume of the solid, $\mathbf{T}$ the distribution of external tractions applied over S_f, $\mathbf{u}^*$ the virtual displacement, $\mathbf{f}$ the distribution of volume forces acting over V, ρ the mass per unit volume and γ the acceleration. Equation (11.107) is valid for any kinematically admissible (K. A.) virtual field (i.e., continuous, differentiable and equal to the prescribed displacements at the displacement boundary conditions). A macroscopic constitutive model of the material must be assumed *a priori* at this point. In a general case this equation may be written as

$$\sigma = g(\varepsilon, p) \quad [11.108]$$

where g is a given function of the actual strain components (ε) and of the constitutive parameters (p). By replacing (11.108) into the PVW (11.107) and by neglecting body forces and accelerations, the following relationship is obtained:

$$\int_V g(\varepsilon, p) : \varepsilon^* \, dV = \int_{S_\mathrm{f}} \mathbf{T} \cdot \mathbf{u}^* \, \mathrm{d}S \quad [11.109]$$

in which the material parameters are related to some kinematic response over a region of interest, geometric characteristics and virtual displacement and strain functions. Generically, the VFM then consists in building up a system of equations by choosing as many independent virtual fields as unknown material parameters. The solution of this system yields the identification of the material properties. In linear elasticity one clear advantage of this method is the direct identification of the unknown constitutive parameters. However, a key issue of the VFM is the selection of such virtual fields yielding to the solution. These functions can be selected either intuitively (*a priori* choice) or by some automatic process. Polynomial and finite element basis functions have been proposed for automatically generating the virtual fields. Since a large number of possible virtual fields exist, a constrained optimization scheme has also been proposed for selecting virtual fields that minimize the sensitivity of the VFM to noise (maximum likelihood solution). Such strategy was found to significantly improve the robustness of the method.

The design of statistically determined mechanical tests, for which the actual

state of stress across the gauge area can be deduced directly from the applied load, is most often restricted to simple geometries and loading cases. The main advantage is that simple data reduction can be achieved in these cases. Conversely, more complex tests giving rise to heterogeneous mechanical responses can be carried out for material characterization, providing that full-field measurements are available by a suitable optical method. For that purpose, redesign of mechanical tests is needed. Several test configurations have already been proposed in the literature (Table 11.5) [53]. Most of these tests aim at identifying the linear-elastic properties of orthotropic materials through either in-plane or bending tests. However, some attempts were also made to redesign test methods for identifying elasto-plastic constitutive parameters (Table 11.5). In test design, the configurations must be optimized with regard to the identifiability of the whole set of constitutive parameters to be determined. A general procedure is to build up a cost function that penalizes unbalanced strain components. Generically, this condition may be considered as sufficient to guarantee that several (or all) parameters contribute to the global response of the specimen. Consequently, they can be recovered by a suitable identification strategy afterwards.

11.11 Conclusion

This chapter began by describing briefly the elasticity of anisotropic materials, providing the fundamental relationships and the allowed simplifications by the existence of material planes of symmetry. The current unidirectional composites are usually classified as transversely isotropic materials. In this case, only five independent elastic constants are necessary to fully characterize unidirectional composites. The micromechanics provides the analytical and numerical approaches to predict the elastic constants based on the elastic properties of the composite constituents. Several classical closed formulas are revisited and compared with experimental data. Finally, stiffness and compliance transformations are given in the context of unidirectional composites. Experimental data are used to assess theoretical predictions and illustrate the off-axis in-plane elastic properties.

The classical lamination theory was then briefly presented. This is an analytical tool suitable for modelling thin laminated plates in an effective way. Laminate examples were given to illustrate the dependence of in-plane and flexural engineering constants on direction.

The subsequent sections presented an overview of full-field optical techniques and material parameter identification methods. Recent developments in optical methods have allowed a new perspective on the mechanical characterization of advanced composite materials. Several redesigned mechanical tests are summarized, yielding complex and heterogeneous stress/strain fields. By coupling a full-field optical method with a suitable identification strategy,

Table 11.5 Some heterogeneous mechanical tests for the identification of constitutive parameters

1. Unnotched Iosipescu test	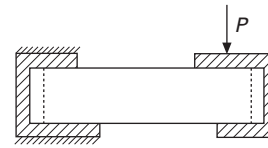
2. Open-hole tensile test	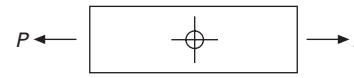
3. Ring compression test	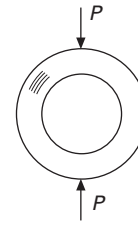
4. Biaxial tensile tests on cruciform specimen	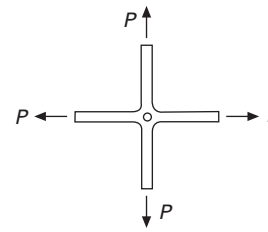
5. Tensile test on flat dog-bone like specimens	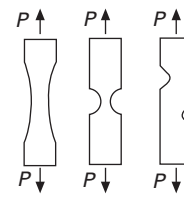
6. Bending test on a plate	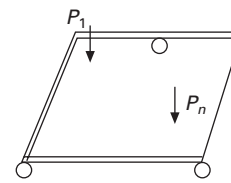

Source: after Xavier [53].

several constitutive parameters can be simultaneously determined on single test configurations. This new approach seems particularly suitable for anisotropic and heterogeneous materials.

This chapter has focused on the elastic qualities of advanced fibre-reinforced composites, in terms of characterization, measurement and prediction from the basic constituents, i.e. the fibre and matrix. Unidirectional fibre-reinforced polymers were the material selected for these brief elastic analyses. These comprised the micromechanics approaches which were applied to predicting the lamina elastic properties from the basic constituents and the classical lamination theory which was used to predict the elastic properties of composites materials composed of several laminae stacked at different orientations. The theoretical predictions were compared against available experimental data, illustrating the predictive capability of the theoretical analysis. Finally, a brief overview was delivered on the identification methods for elastic properties based on full-field measurements. This approach proved to be suitable for anisotropic and heterogeneous materials.

11.12 Software available

- Alfalam: Laminate theory, MS Excel, [ABD] matrix, Puck failure criteria, http:/www.klub.tu-darmstadt.de
- CADEC: Computer Aided Design Environment for Composites, Laminate theory, [ABDH] matrix, FEM application, http://www.mae.wvu.edu/barbero/cadec.html
- eLamX: Laminate theory, Java, [ABD] matrix, 3D failure envelope plots, http://tu-dresden.de
- ESAcomp: Laminate theory, [ABDH] matrix, FEM application http://www.esacomp.com/
- Genlam: Laminate theory, [ABD] matrix, failure criteria, http://www.thinkcomposites.com/
- LamiCens: Laminate theory, MS Excel, [A] Matrix, Graphics, http://www.r-g.de.

11.13 References

1. Kaw A. K. (2006) *Mechanics of Composite Materials*, CRC Taylor & Francis, Boca Raton, FL.
2. Nairn J. A. (2006) in Talreja R. and Manson J.-Å. E., eds *Polymer Matrix Composites*, Elsevier Science, Amsterdam, the Netherlands, pp. 403–432.
3. Roy S., Xu W., Patel S. and Case S. (2001) *International Journal of Solids and Structures*, 38, 7627–7641 (2001).
4. Roy S. and Xu W. (2001) *International Journal of Solids and Structures*, 38, 115–125.
5. Frost S. R. (2008) Ageing of composite in oil and gas applications, in Martin R., ed. *Ageing of Composites*, Woodhead Publishing, Cambridge, UK.
6. Roberts S. J., Evans J. T., Gibson A. G. and Frost S. R. (2003) The effect of matrix microcracks on the stress–strain relationship in fibre composite tubes, *Journal of Composite Materials*, 37(17), 1509–1523.

7. Zang W. and Gudmundson P. (1993) An analytical model for the thermoelastic properties of composite laminates containing transverse matrix cracks, *International Journal of Solids and Structures*, 30, 3211–3231.
8. Gudmundson P. and Östlund S. (1992) Numerical verification of a procedure for calculation of elastic constants in microcracking composite laminates. *Journal of Composite Materials*, 26(17), 2480–2492.
9. Guedes R. M. (ed.) (2011) *Creep and Fatigue in Polymer Matrix Composites*, Woodhead Publishing, Cambridge, UK.
10. Hashin Z., Rosen B. W., Humphreys E. A., Newton C. and Chaterjee S. (1997) Fibre composite analysis and design: composite materials and laminates, Volume I. Report No. DOT/FAA/AR-95/29,Federal Aviation and Administration, William J. Hughes Technical Center, COTR.
11. González C. and LLorca J. (2007). Mechanical behavior of unidirectional fibre-reinforced polymers under transverse compression: Microscopic mechanisms and modeling, *Composites Science and Technology*, 67(13), 2795–2806.
12. Romanowicz M. (2010) Progressive failure analysis of unidirectional fibre-reinforced polymers with inhomogeneous interphase and randomly distributed fibres under transverse tensile loading, *Composites – Part A: Applied Science and Manufacturing*, 41(12), 1829–1838.
13. Melro A. R., Camanho P. P. and Pinho S. T. (2008) Generation of random distribution of fibres in long-fibre reinforced composites, *Composites Science and Technology*, 68(9), 2092–2102.
14. Herakovich C. T. (1997) *Mechanics of Fibrous Composites*, Wiley.
15. Staab G. H. (1999) *Laminar Composites*, Elsevier.
16. Chamis C. C. (1984) Simplified composite micromechanics equations for hygral, thermal, and mechanical properties, *SAMPE, Quarterly*, 15(3), 14–23.
17. Spencer A. (1986) The transverse moduli of fibre-composite material. *Composites Science and Technology*, 27(2), 93–109.
18. Chamis C.C. and Sendeckyj G. P. (1968) Critique on theories predicting thermoelastic properties of fibrous composites, *Journal of Composite Materials*, 2, 332–358.
19. Mori T. and Tanaka K. (1973) Average stress in matrix and average elastic energy of materials with misfitting iclusions. *Acta Metallurgica*, 21, 571–574.
20. Benveniste Y. (1987) A new approach to the application of Mori–Tanaka's theory in composite materials, *Mechanics of Materials*, 6(2), 147–157.
21. Aboudi J. (1991) *Mechanics of Composite Materials: A Unified Micromechanical Approach*, Elsevier, Amsterdam.
22. Paley M. and Aboudi J. (1992) Micromechanical analysis of composites by the generalized cells model, *Mechanics of Materials*, 14(2), 127–139.
23. Aboudi J., Pindera M.-J. and Arnold S. M. (2002) High-fidelity generalized method of cells for inelastic periodic multiphase materials, NASA TM-2002–211469.
24. Tsai S. W. (1964) Structural behavior of composite materials, NASA CR-71, July.
25. Halpin J. C. (1969) Effects of environmental factors on composite materials, AFML-TR-67-423.
26. Halpin J. C. and Kardos J. L. (1976) The Halpin–Tsai equations: a review *Polymer Engineering and Science*, 16(5), 344–352.
27. Morais A. B. D. (2000) Transverse moduli of continuous-fibre-reinforced polymers, *Composites Science and Technology*, 60(7), 997–1002.
28. Fu S., Hu X. and Yue C. (1998) A new model for the transverse modulus of

unidirectional fibre composites, *Journal of Materials Science*, 33(20), 4953–4960.
29. Nijhof A. H. J. (1990) *Ontwerpen in vezelversterkte Kunststoffen*, TU Delft, the Nethedands.
30. Huang Z. M. (2000) Unified micromechanical model for the mechanical properties of two constituent composite materials. Part I: Elastic behavior, *Journal of Thermoplastic Composite Materials*, 13(4), 252–271.
31. Tsai S. W. and Hahn H. T. (1980) *Introduction to Composite Materials*, Technomic Publishing, Lancaster, PA. pp. 377–431.
32. Kriz R. D. and Stinchcomb W. W. (1979) Elastic moduli of transversely isotropic graphite fibres and their composites – Equations used to calculate the complete set of elastic transversely isotropic properties for unidirectional fibre-reinforced materials having transversely isotropic fibres are experimentally verified by using improved ultrasonic techniques, *Experimental Mechanics*, 19(2), 41–49.
33. Pindera M.-J. and Herakovich C. T. (1986) Shear characterization of unidirectional composites with the off-axis tension test, *Experimental Mechanics*, 26(1), 103–112.
34. Pindera M., Choksi G., Hidde J. S. and Herakovich C. T. (1987) A methodology for accurate shear characterization of unidirectional composites. *Journal of Composite Materials*, 21(12), 1164–1184.
35. Tsai C. L. and Daniel I. M. (1990) Determination of in-plane and out-of-plane shear moduli of composite materials, *Experimental Mechanics*, 30(3), 295–299.
36. Marín J. C., Cañas J., París F. and Morton J. (2002) Determination of G_{12} by means of the off-axis tension test. part I: Review of gripping systems and correction factors, *Composites – Part A: Applied Science and Manufacturing*, 33(1), 87–100.
37. Marín J. C., Cañas J., París F. and Morton J. (2002) Determination of G_{12} by means of the off-axis tension test. Part II: A self-consistent approach to the application of correction factors, *Composites – Part A: Applied Science and Manufacturing*, 33(1), 101–111.
38. Jones R. M. (1975), *Mechanics of Composite Materials*, Hemisphere Publishing, New York.
39. Tsai S. W. (1992) *Theory of Composites Design*, Think Composites, Dayton, OH.
40. Love A. E. H. (1906) *A Treatise on the Mathematical Theory of Elasticity*, 2nd edition, Cambridge University Press, Cambridge, UK.
41. ESDU (1994) Stiffnesses of laminated plates. No. 94003, Engineering Sciences Data Unit, London.
42. York C. B. (2010) Unified approach to the characterization of coupled composite laminates: Benchmark configurations and special cases, *Journal of Aerospace Engineering*, 23(4), 219–242
43. Caprino G. and Crivelli Visconti I. (1982) A note on specially orthotropic laminates, *Journal of Composite Materials*, 16(5), 395–399.
44. Rastogi P. K. (2000) *Photomechanics*, Springer-Verlag, Berlin, p. 472.
45. Grédiac M. (2004) The use of full-field measurement methods in composite material characterization: Interest and limitations, *Composites–Part A: Applied Science and Manufacturing*, 35(7–8), 751–761.
46. Avril S., Bonnet M., Bretelle A. S., Grédiac M., Hild F., Ienny P., Latourte F., Lemosse D., Pagano S., Pagnacco E. and Pierron F. (2008) *Experimental Mechanics*, 48, 381–402.

47. Sutton M. A., Orteu J.-J. and Schreier H. (2009) *Image correlation for Shape, Motion and Deformation Measurements: Basic Concepts, Theory and Applications*, Springer, New York.
48. Pan B., Qian K., Xie H. and Asundi A. (2009) Two-dimensional digital image correlation for in-plane displacement and strain measurement: a review, *Measurement Science and Technology*, 20(6), 062001.
49. Sousa A. M. R., Xavier J., Morais J. J. L., Filipe V. M. J. and Vaz M. (2011) Processing discontinuous displacement fields by a spatio-temporal derivative technique, *Optics and Lasers in Engineering*, 49(12), 1402–1412.
50. Xavier J., Sousa A. M. R., Morais J. J. L., Filipe V. M. J. and Vaz M. (2012) Measuring displacement fields by cross-correlation and a differential technique: experimental validation, *Optical Engineering*, 51, 043602.
51. Pan B., Xie H., Xu B. and Dai F. (2006) Performance of sub-pixel registration algorithms in digital image correlation, *Measurement Science and Technology*, 17, 1615–1621.
52. Pierron F. and Grédiac M. (2012) *The Virtual Fields Method*, Springer, New York.
53. Xavier J. (2007) Characterisation of the wood stiffness variability within the stem by the virtual fields method: Application to *P. pinaster* in the LR plane. Ph.D. Thesis, Arts et Métiers ParisTech, Châlons-en-Champagne, France.

12

Understanding the durability of advanced fibre-reinforced polymer (FRP) composites for structural applications

K. BENZARTI, Université Paris-Est/IFSTTAR, France and
X. COLIN, Arts et Métiers ParisTech, France

DOI: 10.1533/9780857098641.3.361

Abstract: Fibre-reinforced polymer (FRP) composites are increasingly being used in the field of civil engineering, either for the rehabilitation/retrofitting of existing infrastructures or for the construction of new structural elements. However, such applications are still recent and there are still unresolved questions regarding the long-term durability of FRP reinforcements or structural elements under service conditions, and their behaviour under accidental fire events as well. In this chapter, it is proposed to highlight the basic mechanisms involved in the environmental degradation of FRP composites, with a large emphasis on ageing mechanisms of the polymer matrix and their consequences on the mechanical properties. The last section is specifically devoted to the fire behaviour of polymer composites and also recalls existing fire-proofing solutions.

Key words: FRP composites, matrix, reinforcing fibres, interphase, ageing mechanisms, degradation, mechanical properties, fire behaviour.

12.1 Introduction

Composite materials have been used successfully for many decades in various industrial sectors (aerospace, automotive, rail, defence, telecommunication, sport and leisure, etc.). Their outstanding properties combined with decreasing production costs continue to drive a growing demand for their use in place of traditional materials such as metal. Key advantages of composites over metal alloys include low density, high specific stiffness and strength, good fatigue life, excellent corrosion resistance, good thermal insulation and low thermal expansion. There has been extensive research to adapt raw materials and manufacturing processes to meet the durability requirements for these industrial applications.

The use of FRP composites in civil engineering and construction is more recent. When faced with increasing problems of ageing concrete infrastructure and traffic growth, civil engineers realized the potential of composite materials for strengthening structural components and started to develop practical applications in the 1980s. Good mechanical performance, resistance to

corrosion, light weight and ease of installation have made these materials very attractive. Some of these applications (e.g. strengthening of concrete structures by externally bonded FRP systems) are now used routinely around the world and their effectiveness is well recognized. However, the long-term behaviour of FRP composites under service conditions still remains a crucial issue.

FRP materials used in civil infrastructure have a number of specific features compared with composites designed for other sectors:

- They may differ in terms of manufacturing process (manual operations are often necessary for on-site implementation) and in terms of constitutive materials (cold-curing thermoset matrices/adhesives are often used during on-site implementation). These factors can affect the overall quality of the FRP material and hence its durability.
- They can be exposed to various and complex environments during service life, such as harsh and changing weather conditions or contact with alkaline media, with possible additional sustained mechanical loads. Such environments play a key role in the mechanisms and kinetics of ageing and consequently in changes in material properties.
- The lifespan of FRPs is ideally expected to match the usual design life of civil infrastructure, typically in the range 50–100 years or more. However, predicting durability over such long periods of time is a difficult challenge, and traditional methods based on accelerated ageing tests may not be representative of actual environmental ageing conditions.
- There is still a lack of well-developed standard testing methods and experimental procedures for FRP materials used in construction.

These specific features may explain why only limited information can be found on the durability of FRP composites in civil engineering and, when available, data from different studies can be contradictory. As a result, concern about durability remains a barrier to the widespread acceptance of FRP materials in construction. Another critical concern is the behaviour of FRP materials or structures in the case of fire. These materials are very vulnerable to fire and their combustion may produce large amounts of toxic gases which are a direct threat to life. Civil engineers should take this issue into account when choosing materials used in FRP composites, and should implement adequate fireproofing solutions.

This chapter begins by briefly describing the multiphase structure of FRP composites. The main applications of these composites in civil engineering are outlined in order to identify environmental factors which may induce physical/chemical changes in materials under normal service conditions. The following sections describe in more detail the various ageing mechanisms involved in the environmental degradation of FRP constituents (with a special focus on the polymer matrix), and the consequences of these degradation

mechanisms on mechanical properties. Finally, the fire behaviour of polymer composites is discussed in a separate section at the end of the chapter.

12.2 Structure and processing of fibre-reinforced polymer (FRP) composites

Advanced polymer composites are heterogeneous materials resulting from the combination of different constituents, including high-performance fibres, a polymer matrix and various fillers and additives. Due to synergistic effects, polymer composites are expected to perform better at the macroscopic scale than the individual constituents taken separately. The reinforcing elements (fibres) determine the mechanical properties of the FRP composite (elastic modulus, strength, etc.) whereas the polymer matrix is the continuous phase that binds the fibres together, transfers loads to the fibres and protects them from abrasion and environmental degradation. The role of the interfaces between the different phases is also of paramount importance and a good level of adhesion is usually required to ensure both optimal load transfer and durability. Fillers and additives are also used to reduce the cost and confer specific properties (for instance toughness, flame resistance, etc.) to the FRP composite. When investigating the durability of a composite structure, it is usually necessary to take into account this multiphase structure as well as the manufacturing process used to combine the raw materials.

12.2.1 Fibres

Fibres are the dominant constituents of composite systems as they control the mechanical performance of the material (stiffness and strength) as well as other physical properties such as thermal and electrical conductivity. Key parameters are the fibre content (usually in the range 30–70 vol%, depending on the manufacturing process) and the arrangement of the fibre network within the composite. The orientation of fibres (unidirectional, multidirectional or multiple configurations) is usually adapted for optimizing the load-carrying capacity of the composite structure.

FRP composites used in construction are mainly based on glass, carbon and aramid fibres. The suitability of these fibres for a specific application depends on the required mechanical performance, the cost and the required durability. Glass fibres are inexpensive, exhibit high tensile and compressive strength and present both good compatibility with conventional polymer matrices and good processability. However, their drawback is a low elastic modulus which restricts the range of applications, and their high sensitivity to hydrolysis when exposed to alkaline environments (in a concrete medium, for instance). Carbon fibres are more expensive, but also much stiffer and lighter than glass fibres. They are appropriate for applications requiring a

high performance-to-weight ratio and are very popular in strengthening systems for civil infrastructure. They also show a very good resistance to environmental attack (e.g. UV radiation and moisture) and exhibit a good thermal stability up to 450°C. Aramid fibres are less used than the previous types of reinforcements and show intermediate properties between glass and carbon fibres. Their main advantages are their low density (even lower than carbon) and excellent toughness. However, they are known to be sensitive to UV radiation and moisture.

12.2.2 Polymer matrices

Polymer matrices used in composite materials are either thermosetting systems or thermoplastics. Thermoset polymers are usually formulated from a resin, a curing agent and a catalyst or initiator. A solvent is also introduced to lower viscosity and improve fibre impregnation. The polymerization process involves irreversible chemical cross-linking reactions and produces a three-dimensional network of macromolecular chains which cannot be reversibly softened and has high temperature resistance. Physical and mechanical properties of thermoset networks are generally dependent upon the achieved cross-link density. In contrast, thermoplastic matrices are composed of long molecular chains that are only bonded together by weak van der Waals interactions. They can be processed in the melted state at elevated temperature, and become solid and retain their shape as they are cooled to room temperature.

Polymer matrices used in civil engineering are almost exclusively based on thermosetting systems, due to their good thermal stability, chemical resistance, low creep and relaxation properties and their better ability to impregnate the fibre reinforcements in comparison with thermoplastic matrices. Depending on the type of application and the aggressiveness of the surrounding environment, either unsaturated polyesters, vinylesters or epoxies are selected for the thermosetting matrix. Polyester resins are traditionally used with glass fibres to yield low-cost structural composite elements. These resins consist of low molecular weight unsaturated polyester chains dissolved in styrene. Polymerization of styrene forms cross-links across unsaturated sites of the polyester chains. These reactions are highly exothermic and the excessive heat generated may damage the final laminate. Other major drawbacks of unsaturated polyesters are substantial shrinkage, production of toxic vapours (styrene), and sensitivity to hydrolysis when exposed to alkaline environments (for instance in contact with concrete).

Vinylester resins differ from polyesters in that the unsaturation is located at the end of the molecule and not along the chain. They exhibit a much better resistance to hydrolysis and are stable in aqueous environments. They are thus preferred to unsaturated polyesters for specific applications requiring alkali resistance, and are commonly used in the composition of FRP reinforcing bars

for concrete structures. In epoxy systems, cross-linking reactions generally involve polycondensation between a prepolymer containing reactive oxirane functions (diglycidyl ether of bisphenol-A is the most common) and a polyamine hardener. Due to their good wetting ability and adhesion to most building materials, epoxies are often used as adhesives for the bonding of external FRP reinforcements. In this case, cold-curing epoxies are usually chosen for the sake of practicality. Durability characteristics may be affected by the low glass transition temperature or an incomplete curing of these systems (Mays and Hutchinson, 1992; Benzarti *et al*., 2011). For specific cases requiring composites with high thermal or fire resistance, advanced thermosetting matrices are also available on the market, such as phenolic resins manufactured from phenol and formaldehyde or bismaleimide resins prepared by reaction of maleic anhydride with primary amines. However, these materials are characterized by their brittleness and low toughness.

Thermoplastic matrices (mainly polypropylene, polyethylene, polyethylene teraphthalate) have sometimes been used with short-length glass fibres to produce FRP elements for civil structures. The attractiveness of these materials is due to the possibility of joining elements by heat welding, and theoretically, the possibility of recycling at the end of their service life. However, they are difficult to process and show lower strength and stiffness than thermoset composites, although they are tougher and more ductile (Bank, 2006).

12.2.3 Interfacial areas

Interfacial areas between the bulk matrix and the reinforcing fibres can be characterized by a gradient of physical and mechanical properties (Theocaris, 1987; Thomason, 1990; Vasquez *et al*., 1998). In this region, which is often called the interphase or mesophase, the structure and properties of the polymer network differ from those of the bulk matrix, due to several possible phenomena such as:

- diffusion of the fibre sizing (using silane coupling agents, lubricant agents like fatty acids or esters, etc.) into the polymer, that may induce a local plasticization of the matrix in the vicinity of the fibres,
- influence of the fibres on the polymerization kinetics of the matrix, due either to the presence of humidity at the fibre surface or to an alteration in thermal properties, and leading to a local variation of the cross-link density of the thermoset network (Amdouni, 1989),
- effects of residual thermal stresses due to the curing cycle (Theocaris, 1987).

The interphase has a significant effect on the mechanical properties and the failure mode of FRP composites (Benzarti *et al*., 2001). It may also affect long-term behaviour by controlling resistance to hydrothermal degradations,

for instance (Chateauminois *et al.*, 1994). An optimization of the fibre sizing composition may thus help to increase composite durability.

12.2.4 Manufacturing processes

There are various techniques for manufacturing polymer composites used in civil engineering. Each method involves a specific curing cycle (for instance, cure at ambient temperature or at elevated temperature, or a possible additional post-curing period) and a particular level of compaction. These parameters influence both the cross-link density of the polymer matrix and the structure of the composite material (distribution and alignment of the reinforcing fibres, volume fraction of voids, etc.), which can impact the long- term performances of FRP elements under service conditions. Manufacturing processes are of three types (Hollaway, 2001):

- Manual processes, such as the *wet lay-up* (fabricated in the factory or on site) and the pressure bag method. In these methods, the matrix is usually cold cured (at ambient temperature).
- Semi-automated processes, like resin injection and moulding of pre-impregnated sheets (cured under pressure at elevated temperature).
- Fully automated methods, such as pultrusion (hot curing cycle), filament winding (cold or hot cured), injection moulding, etc.

Amongst these methods, pultrusion produces a broad range of thermoset FRP products (pipes, profiles, rods, plates, panels, box girders) with high fibre contents (up to 80 wt%) and which can be directly used as structural elements or reinforcements in civil infrastructure. These products have a more consistent quality and compaction compared to FRP composites prepared by manual techniques, and are thus expected to behave better in the long term under normal or severe service conditions.

12.3 Applications of FRP composites in civil engineering

Structural applications of composite materials in civil engineering can be sorted into three main categories (Hollaway, 2010):

- Repair/strengthening of existing infrastructures with externally bonded FRP composites
- Internal reinforcement of concrete structures using FRP bars in replacement of steel gratings
- All-FRP structural members and all-FRP infrastructures.

12.3.1 External FRP strengthening systems

The rehabilitation or upgrading of concrete infrastructures by externally bonded FRP composites is a well-established technique developed in the 1990s. It is considered to be an efficient and inexpensive alternative to the replacement of damaged or structurally deficient RC elements. This method covers several specific applications:

- Flexural or shear strengthening of concrete elements (beams) can be performed using the wet lay-up process, in which fabrics or sheets are saturated with a cold-curing epoxy resin and applied directly to the concrete surfaces, or using an epoxy adhesive or putty to bond a prefabricated FRP laminate (Fig. 12.1(a)). In the wet lay-up process, the dry fabric or sheet is impregnated on-site and the epoxy resin serves both as matrix for FRP laminate and as adhesive joint. Carbon fibres are most often chosen as they provide high stiffness and strength to the reinforcing laminates. This method of flexural and shear strengthening is also applicable for metal, timber or masonry structures.
- An alternative or complementary technique based on 'near surface mounted' reinforcements and called NSM consists in inserting FRP rods with an epoxy adhesive or cement grout into grooves cut in the concrete member (De Lorenzis and Teng, 2007).
- A specific technique for the seismic retrofit of concrete columns consists in wrapping these elements by resin-impregnated fabrics or sheets (Fig. 12.1(b)). Installation of composite jackets or rigid shells can also be used for the rehabilitation of severely corroded or degraded concrete piles, as they both restore the integrity of the structure and act as a protective barrier against further penetration of deleterious species (chloride, moisture, etc.).

For external strengthening applications, the durability of the adhesive bond between the FRP composite and the infrastructure member is a crucial issue, as any degradation of the bond properties may affect severely the effectiveness of the FRP reinforcement (Benzarti *et al.*, 2011). Several guidelines for the design of externally bonded FRP reinforcements have been published worldwide, in particular ACI 440.2R-08 (2008) in the United States, JSCE recommendations (2001) in Japan, Italian and French guidelines in Europe (CNR, 2004; AFGC, 2011), etc.

12.3.2 Internal reinforcement of concrete structures

Passive FRP bars are increasingly being used as internal reinforcement for concrete structures (beams, slabs, columns, decks), especially in Canada and in the United States where the weather conditions can be very harsh.

(a)

(b)

12.1 FRP external strengthening of concrete structures: (a) flexural strengthening of a concrete beam using carbon FRP laminates; (b) wrapping of a concrete column with resin-impregnated carbon fabrics.

A major advantage of these materials over traditional steel bars is that they are not subject to electrochemical corrosion, and the reinforced elements require very limited maintenance. Most FRP rebars used in civil engineering

are based on vinylester/glass fibre composites, as these materials are less expensive than other high-performance FRPs and vinylester matrices show relatively good resistance to hydrothermal ageing and alkaline environments (Robert *et al.*, 2009). However, their low stiffness compared to steel and their brittle behaviour must be taken into account in the design of the reinforced structures. Some of the main related guidelines are ACI Committee 440.1R-06 (2006) in the United States, and the Canadian (CSA, 2002) and Japanese (JSCE, 1997) guidelines. Pre- or post-tensioned FRP tendons have also been used as effective reinforcements of concrete structural elements. In this case, there are still unresolved problems due to creep/relaxation phenomena which induce loss of pre-stress and limit the wide diffusion of this technique.

12.3.3 All structural members

The production of high-quality profiles at a competitive cost by the pultrusion process has opened new horizons for the development of all-FRP members, and even full composite infrastructures. Composite materials have been used, for instance, to construct various types of structural elements, such as cables for cable-stayed bridges (epoxy/carbon fibres), box girders and bridge deck panel systems (usually based on polyester/glass fibre composites), all-FRP piles, modular building systems, etc. As regards full composite structures, the first realizations were initially restricted to relatively small-scale structures and demonstrators like pedestrian bridges (cf. the Aberfeldy bridge in Scotland) and short-span FRP bridges, but larger projects are currently under study. A major issue is related to the connection of FRP structural members: the current practice of bolting generally leads to a large oversizing of the structural elements and requires very conservative design, whereas adhesive bonding would be more appropriate (it favours more uniform load transfer and lowers the stress concentrations) and may widen the design possibilities (Keller, 2006). However, in the latter case, the durability characteristics of the adhesive bond under combined mechanical and environmental loads become a critical issue.

12.3.4 Durability concerns

In the above-mentioned civil engineering applications, FRP materials and adhesive joints are exposed to weathering conditions and may also be in contact with alkaline concrete medium, whilst being simultaneously subjected to sustained load or fatigue cycles due to the infrastructure dead load or to traffic. In this context, durability of FRP composites has been defined by Karbhari *et al.* (2003) as 'the ability of these materials to resist cracking, oxidation, chemical degradation, delamination, wear and/or the effects of foreign object damage for a specified period of time, under the appropriate

load conditions, under specified environmental conditions'. Although FRP materials are not susceptible to electrochemical corrosion like steel, they may indeed deteriorate under the combined action of environmental factors related to outdoor exposure and physical factors, such as:

- *Moisture diffusion* from the surrounding medium (concrete pore solution, wet environment)
- Effect of *an alkaline environment*, if embedded in concrete (FRP rebars) or in contact with cementitious materials (FRP external strengthening)
- Effects of *temperature variations* during the manufacturing process or the installation procedure or under service conditions
- Impact of *ultraviolet radiation* (photo-oxidation)
- Effect of *fire*
- Influence of *sustained mechanical loads* (creep/relaxation) and *fatigue cycles*.

These factors may affect the properties of the polymer matrix, the fibres and the interfacial areas to differing degrees, depending on the chemical nature and volume fraction of these components in the FRP material, and on the manufacturing process of the composite as well (cf. Section 12.2.1). It is usually recognized that the matrix-related properties of the FRP composite are affected more than fibre-related characteristics. Information on ageing kinetics and changes in properties are commonly obtained from field testing or from laboratory-accelerated ageing tests (Karbhari, 2007; Hollaway, 2010). Significant data have been collected during the two last decades. These are sometimes contradictory due to the broad range of FRP products tested and the various ageing procedures and characterization methods involved.

To account for the material evolutions, guidelines dedicated to the external or internal reinforcements of concrete structures using FRP composites usually introduce substantial durability parameters (reduction factors on FRP tensile properties and on shear characteristics of FRP/concrete bonded interfaces, creep stress levels and fatigue limits); see, for instance, ACI 440.2R-08 (2008) and ACI 440.1R-06 (2006). However, further research is still needed to refine the design codes and better calibrate the durability reduction factors taking into account synergistic effects between various environmental factors.

The next sections do not review the various durability studies available in the literature, since there are recent reviews by Karbhari (2007) and Benmokrane *et al*. (2006). Instead they assess the main environmental ageing mechanisms involved in the degradation of FRP components (especially polymer matrices, but also reinforcing fibres) under normal service conditions, as well as their consequences on the mechanical properties of the overall composite. The influence of creep and fatigue loading will not be discussed in this chapter.

12.4 Physical ageing: mechanisms and stabilization techniques

Physical ageing can result from the spatial reorganization of polymer chains or segments (relaxation of enthalpy, volume, orientation or stress; crystallization; etc.), transport phenomena (penetration of a solvent, migration of additives) and superficial phenomena (e.g. cracking in a tension-active medium).

12.4.1 Structural reorganization

Transition from liquid to glass and crystallization are both phenomena responsible for polymer solidification at the end of a processing operation. Since they are kinetic phenomena, they lead to an out-of-equilibrium thermodynamic state: glassy polymers present an excess of unstable conformations and free volume; semi-crystalline polymers are not totally crystallized, their melting point being largely lower (usually some dozens of degrees) than the equilibrium value.

If, in their use conditions, polymers are subjected to a residual molecular mobility (β motions in glassy polymers, α motions in the rubbery amorphous phase of semi-crystalline polymers), they will undergo a molecular reorganization towards the thermodynamic equilibrium, characterized by:

- a compaction of polymer chains or segments, and a loss in enthalpy;
- an increase in yield stress;
- a decrease in creep compliance.

The variation against time of creep compliance, $J(t)$, has been the subject of significant research, in particular in the case of organic glasses (Struik, 1978). As an example, the general shape of creep curves of samples aged for three different durations: t_a, $10 \times t_a$ and $100 \times t_a$, is presented in Fig. 12.2.

The shift factor of creep curves along the logarithmic scale of time, defined by $a_c = \log(t_{1c}/t_{2c})$, and corresponding to a variation $a_a = \log(t_{1a}/t_{2a})$ in ageing time, is such that $a_a/a_c \approx 1$. In other words, one decade increase in ageing time leads to about one decade increase in the creep characteristic time. This is a general trend of the physical ageing by structural relaxation observed for polymers or molecular organic materials (glucose), as well as for granular solids like sand, or emulsions.

The decrease in creep compliance (i.e. increase in Young's modulus), as well as the increase in yield stress, can be viewed as advantages for many industrial applications. Unfortunately, these changes are counterbalanced by a catastrophic decrease in ductility/toughness, as schematized in Fig. 12.3. Thus, the consequence of structural relaxation can be understood as an increase in the polymer brittleness.

The increase in yield stress (typically, up to 30% of its initial value

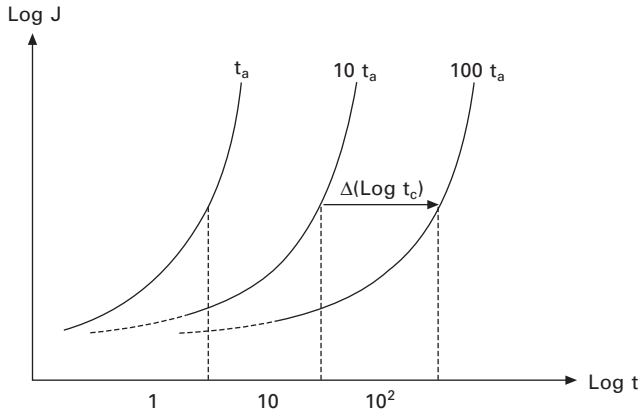

12.2 Creep curves (in a log–log scale) of samples aged in their glassy state during t_a, $10 \times t_a$ and $100 \times t_a$.

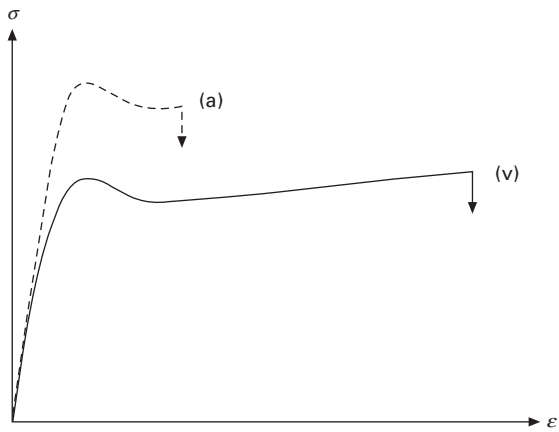

12.3 Shape of stress (σ) vs. strain (ε) curves before (v) and after (a) structural relaxation. Vertical arrows symbolize sample failure.

for a polycarbonate (PC)), the loss in ductility without any variation of the molecular weight distribution, plus the appearance of an endothermic peak close to the glass transition temperature (T_g) (Fig. 12.4) in differential scanning calorimetry (DSC) thermograms allow one to unambiguously identify the structural relaxation from any other type of physical ageing in amorphous glassy polymers. Another direct effect of the decrease in free volume induced by structural relaxation is about one decade decrease in the diffusion coefficient of gases in amorphous polymers (Tiemblo *et al.*, 2001).

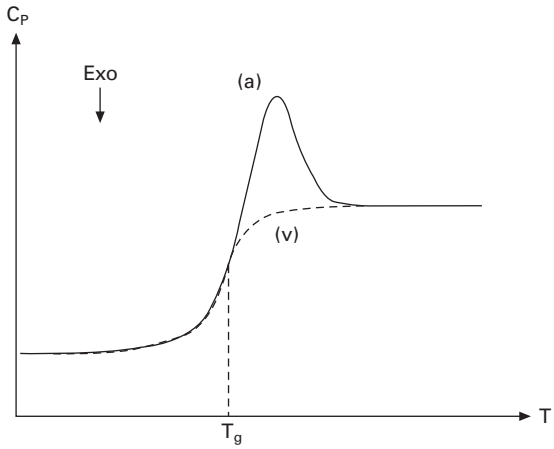

12.4 Shape of DSC thermograms around the glass transition temperature (T_g) before (v) and after (a) structural relaxation.

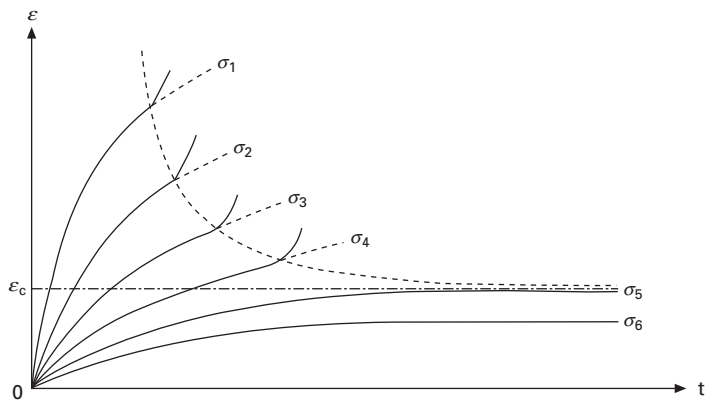

12.5 Shape of creep curves (time variation of strain) for different stress levels ($\sigma_1 > \sigma_2 > \sigma_3$, etc.) in the presence of a solvent. Black points indicate the appearance of damage. Their envelope follows a horizontal asymptote for $\varepsilon = \varepsilon_C$.

12.4.2 Solvent absorption

Solvents plasticize polymers and thus lead to a decrease in T_g and yield stress (if the polymer is initially ductile). However, the most significant effects, in practice, are observed when the polymer is subjected to a mechanical loading. In this case, plasticization favours damage, in particular by crazing. As an example, let us consider a creep test during which damage is detected by an optical technique. The resulting behaviour can be schematized by Fig. 12.5.

One can see that there is a critical strain ε_C below which the material does not damage. The value of ε_C is a function of the polymer–solvent couple. In simplest cases, for moderately polar polymers such as poly(2,6-dimethyl oxyphenylene) (PPO) (Bernier and Kambour, 1968), ε_C depends on the solvent solubility parameter as shown in Fig. 12.6. The dashed zone corresponds to values of ε_C determined in air. In the case of polar polymers, e.g. poly(methyl methacrylate) (PMMA), the behaviour can be more complex: the curve $\varepsilon_C = f(\delta_S)$ can exhibit several minima.

Let us remember that some peculiar vapours and gases (e.g. water and carbon dioxide) can play an important role in physical ageing. Moreover, plasticizers can migrate from one polymer to another and induce damage under mechanical loading. In components of complex geometries using FRP composites, solvent vapours can create residual stresses by generating localized damage.

The penetration of solvents into a polymer leads to swelling, but also to stress gradients induced by hindered swelling during the transient regime of diffusion. Numerous problems of damage of FRP structures induced by water diffusion have been reported in the literature of the past half-century, in particular in aeronautics (McKague *et al.*, 1975; Shen and Springer, 1976; Whitney and Browning, 1978).

12.4.3 Loss of additives

Most technical polymers contain additives like antioxidants, plasticizers or processing agents that do not form chemical bonds with macromolecules.

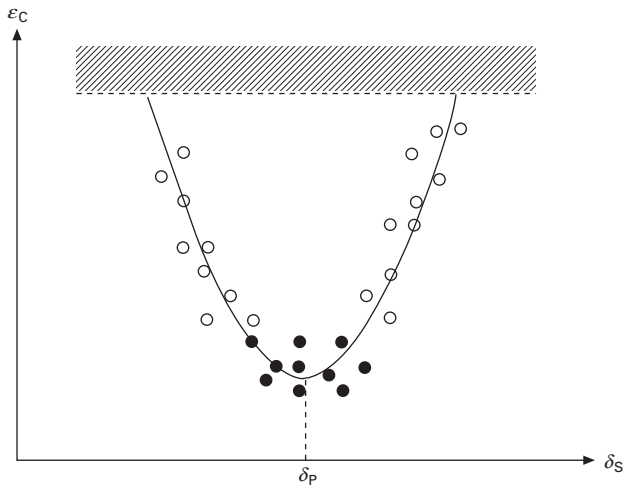

12.6 Shape of the variation, against a parameter of solvent solubility (δ_S), of critical strain (ε_C) for PPO (Bernier and Kambour, 1968). Minimum of curve corresponds to $\delta_S = \delta_P$, δ_P being the parameter of polymer solubility. *Legend*: (○) crazes; (●) open cracks.

These molecules can migrate within the host polymer with a rate depending on their size, their solubility and diffusivity among other parameters. The following discussion reviews the limiting steps in additive migration.

A polymer–additive mixture is out of thermodynamic equilibrium. Since the additive concentration in the environment is equal to zero, there is no equality between its chemical potentials in the environment and in the polymer. Additive molecules tend to migrate outside the polymer in order to reach an equilibrium. This migration is composed of two elementary steps (see Fig. 12.7):

1. The first step corresponds to the passing of some additive molecules into a medium of molecules close to the polymer surface, that is to say the crossing of the polymer–external medium interface. It is an additive evaporation in the case of an external gaseous medium (e.g. atmosphere), or an additive dissolution in the case of an external liquid medium (e.g. water),
2. The additive molecule exchange between the polymer and the external medium leads to a gradient of concentration in a region adjacent to the material surface. This latter is the 'driving force' for the diffusion of additive molecules from the core towards the sample surface. If diffusion obeys the second Fick's law, the diffusion distance (ℓ) is proportional to the square root of time (t_d):

$$t_d = \frac{\ell^2}{D} \qquad [12.1]$$

where D is the coefficient of additive diffusion into the polymer.

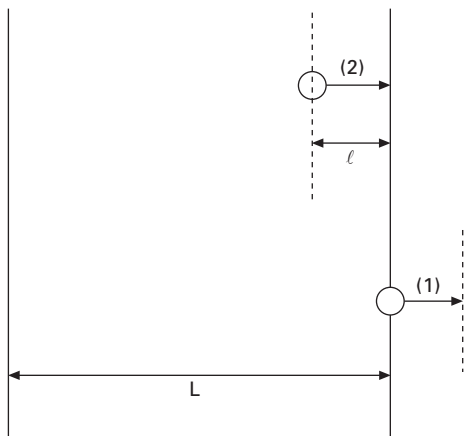

12.7 Schematization of a two-step migration of molecular species outside the polymer. *L* is the sample thickness.

For the sake of simplicity, we only consider here the Fickian diffusion process which may occur in the glassy state far from T_g. But there are exceptions to this process and we invite the reader to refer to extensive literature reviews for the treatment of other transport modes of small molecules into polymers (Müller-Plathe, 1994; Masaro and Zhu, 1999; George and Thomas, 2001).

One can see from Equation [12.1] that t_d is an increasing function of the sample thickness L. As a result, one can distinguish two distinct kinetic regimes, depending on the relative predominance of the previous steps:

1. *Regime 1: Evaporation (or dissolution)-controlled kinetics*. In the case of thin samples (fibres, films, coatings) and high additive diffusivity, additive evaporation (step 1 in Fig. 12.7) is the slowest step and thus controls the global migration kinetics. Its concentration C (into the polymer) decreases proportionally with time (see Fig. 12.8(a)):

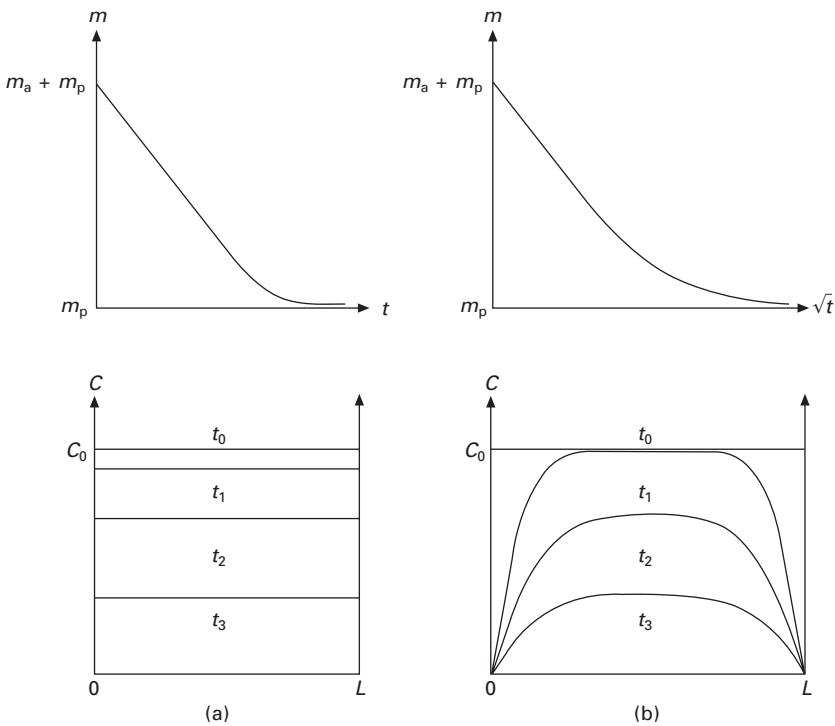

12.8 Additive migration governed by (a) evaporation and (b) diffusion. *Top*: shape of weight changes as a function of time. Sample weight (m) corresponds to polymer weight (m_p) plus additive weight (m_a). *Bottom*: distribution, in the sample thickness, of additive concentration (C) for different times of exposure: $t_0 < t_1 < t_2 < t_3$. The initial concentration is $C = C_0$ (at $t = t_0$).

$$\frac{dC}{dt} = -H \qquad [12.2]$$

The evaporation rate H is a decreasing function of the additive molar mass and the cohesive energy density.

2. *Regime 2: Diffusion-controlled kinetics*. In the case of relatively thick samples (typically a few millimetres) and low additive diffusivity, diffusion in the bulk (step 2 in Fig. 12.7) controls the global migration kinetics. In the simplest case, the second Fick's law can be successfully applied. It is found that, in the early period of exposure, the sample weight m decreases proportionally with the square root of time (see Fig. 12.8(b)):

$$\frac{\partial m}{\partial t} = D\,\frac{\partial^2 m}{\partial z^2} \qquad [12.3]$$

where z is the spatial coordinate in the sample thickness.

Thus, a gradient of the additive concentration appears in the sample thickness. Figure 12.8 shows the shape of the time variation of sample mass and concentration profile in the cases of evaporation- and diffusion-controlled additive migration.

If the additive molar mass is relatively high, its evaporation (or, more generally speaking, its crossing of the polymer–medium interface) is slow. Then, its concentration at the sample surface takes an intermediate value between C_0 and zero. It is thus necessary to take into account this variation in the boundary conditions for solving Equation [12.3]. If the additive concentration is high (in the case of plasticizers), it modifies the polymer properties. Then, its diffusivity becomes concentration dependent (an increasing function of the plasticizer concentration). Complications appear when a phase transition takes place during the additive migration. As an example, in case of diffusion of plasticizers in PVC, a dramatic increase in T_g occurs in regions of low plasticizer concentration. The resulting T_g profile can have the shape illustrated in Fig. 12.9.

One can see that, in the sample bulk, the polymer remains in a rubbery state. On the contrary, in the superficial layer of thickness ℓ_a, the polymer vitrifies and thus becomes brittle. Since the coefficient of plasticizer diffusion varies by at least one order of magnitude on both sides of the glass transition, the real gradient will display rather the shape of Fig. 12.10. In such cases, the diffusion 'front' is very abrupt and the sample weight decreases proportionally with time.

From the mechanical point of view, the loss in additives leads to a loss in the specific properties targeted by the introduction of these additives: long-term durability in the case of antioxidants, flexibility in the case of plasticizers, etc. If the additive concentration is high (in the case of plasticizers), their

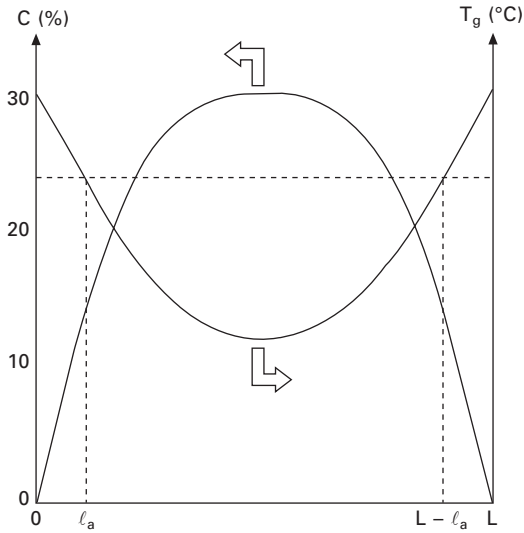

12.9 Shape of distribution, in the sample thickness, of plasticizer concentration (*C* expressed in weight fraction) and resulting local glass transition temperature (T_g) for a plasticized PVC aged at room temperature (Wypych, 2004).

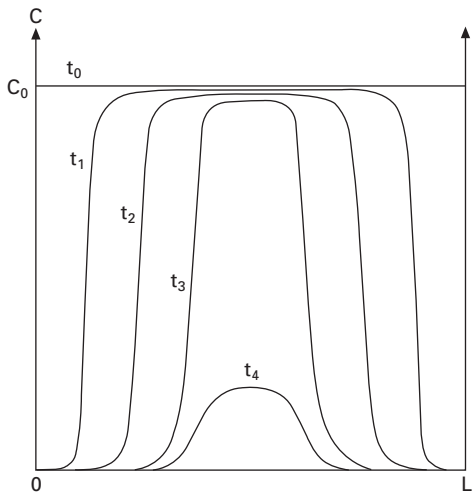

12.10 Correction of the hypothetical curve (right) presented in Fig. 12.8. Real shape of the distribution, in the sample thickness, of plasticizer concentration (*C*) for different times of exposure: $t_0 < t_1 < t_2 < t_3 < t_4$.

loss induces a volume shrinkage (of the same order of magnitude than the weight loss, but slightly lower). This shrinkage can generate local stresses and thus lead to crack initiation in the brittle superficial layer.

12.4.4 Stabilization against physical ageing

One can envisage ways of stabilizing polymer matrices against at least two types of physical ageing:

- After processing, annealing at a temperature below T_g for glassy polymers, or between T_g and T_m for semi-crystalline polymers, can be made to allow the polymer chains and segments to reorganize in a relatively short duration. However, such post-processing operation can be difficult to achieve in some industries, in particular in civil engineering, for which composite materials are generally processed directly on site.
- Increasing the molar mass of additives, such as plasticizers and stabilizers, by grafting a long aliphatic chain on the active function allows one to increase their compatibility with weakly polar polymers and reduce significantly their loss rate by diffusion and evaporation (or dissolution by a solvent).

12.5 Mechanisms of chemical ageing: introduction

This section focuses on two main types of chemical ageing processes covering the great majority of deterioration problems encountered in civil engineering: 'hydrolytic ageing' and 'oxidative ageing'. Both processes result from the chemical interaction between the polymer matrix and the environmental reagents, especially water, oxygen and alkalis. Moreover, they have two important common characteristics. First, they induce random chain scission, which is the cause of deep embrittlement at low conversion of the chemical ageing process. Second, they are diffusion-controlled, affecting a more or less thick superficial layer and inducing gradients of degradation.

This part of the chapter will be divided into four main sections. This first section will be devoted to common aspects of chemical ageing processes. The second section will be devoted to reaction-diffusion coupling, and the last two will focus on hydrolytic and oxidative ageing respectively. Durability problems will be considered essentially from the 'material science' point of view rather than the 'chemical mechanism' point of view. Emphasis will be put on the consequences of chemical ageing on mechanical properties.

Structural changes induced by chemical ageing can be ranged into four categories depending on the affected structural scale (see Table 12.1). The 'target' of water, oxygen or alkali attack is always the molecular scale, i.e. a region of sub-nanometric dimension. Some examples of chemical transformations at this scale are presented in Fig. 12.11. One can distinguish two categories of chemical events: those which do not affect the structure at the macromolecular scale and those (chain scissions, cross-linking) which do affect the structure at this scale. This distinction is based on a simple rule: only the structural changes at the macromolecular scale can induce

Table 12.1 The four scales of structure and the corresponding tools of investigation

Structural scale	Entity	Main analytical tools	Theoretical tools
Molecular	Group of atoms Monomer unit	IR and NMR spectrometry	Organic chemistry
Macromolecular	Chain Network strand Cross-link	Viscosimetry SEC Sol-gel analysis	Macromolecular physico-chemistry
Morphological	Crystalline lamellae Spherulite	SAXS, WAXS, DSC SEM, TEM, AFM	Materials science
Macroscopic	Skin–core structure	Visible microscopy Modulus profiling Nano- and macro-indentation	Materials science

dramatic consequences on the polymer mechanical properties at reasonably low conversions of the chemical ageing process.

Hydrolysis without chain scission occurs only in acrylic and vinylic polymers with ester side groups. These polymers are not frequently used as composite matrices. Oxidation leads to a predominating chain scission process in the majority of cases, and to a predominating cross-linking in few cases such as polybutadiene (Coquillat *et al*., 2007). An important quantity is the yield of chain scission or cross-linking expressed as the number of broken chains or cross-links formed per oxygen molecule absorbed. There is, to our knowledge, no case of industrial polymer for which this quantity is null.

12.5.1 Changes of side-groups

As previously seen, a change of side-groups, e.g. the replacement of an ester by an acid (case A in Fig. 12.11), or the replacement of a methylene by a ketone or an alcohol (case C in Fig. 12.11), has no effect on mechanical properties. However, it can affect other physical properties, for instance:

- Colour, if the new group is a chromophore. In general, hydrolysis does not affect colour, but oxidation induces yellowing in most aromatic polymers, because it can transform some aromatic nuclei into quinonic structures absorbing in the violet-blue part of the visible spectrum.
- Replacement of a non-polar group by a polar group, e.g. an ester by an acid (case A in Fig. 12.11) or a methylene by an alcohol (case C in Fig. 12.11). Such modifications are expected to have the following consequences: increase in dielectric permittivity; increase in the refractive index; growth of dielectric absorption bands; and increase in hydrophilicity and wettability.

Case A: Hydrolysis of an acrylic polymer

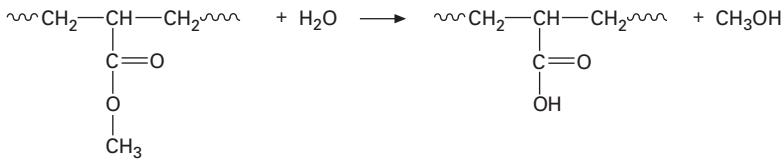

Case B: Hydrolysis of PET

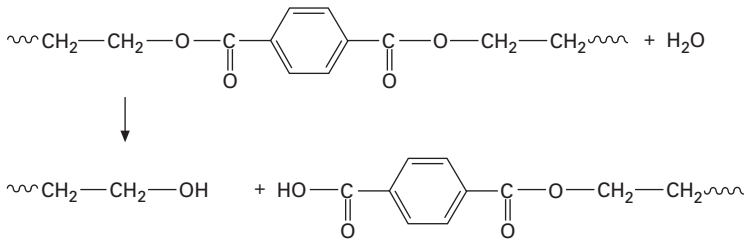

Case C: Oxidation of a polymer containing an aliphatic segment

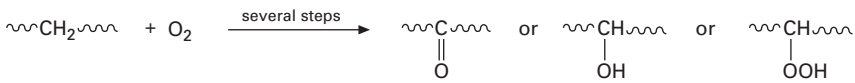

Case D: Oxidation of a polymer containing an aliphatic segment (case B)

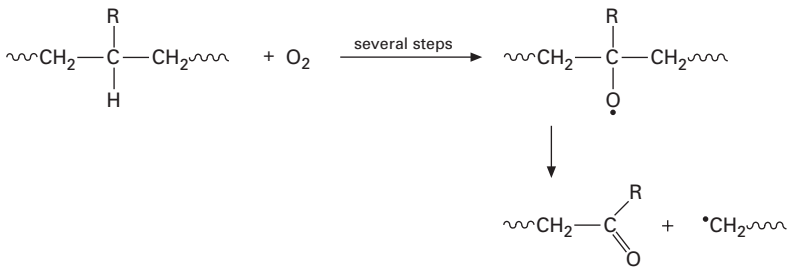

12.11 Examples of hydrolysis (A, B) or oxidation (C, D) processes leading (B, D) or not (A, C) to a chain scission.

However, these chemical changes are rarely decisive in the case of composites.

12.5.2 Random versus selective chain scissions

Chain scissions can occur at peculiar sites of high reactivity (selective chain scissions). They may also be randomly distributed if all the repeat units are equi-reactive (random chain scissions). Both types of scissions are schematized in Fig. 12.12. For composite matrices, in the context of long-term hydrolytic

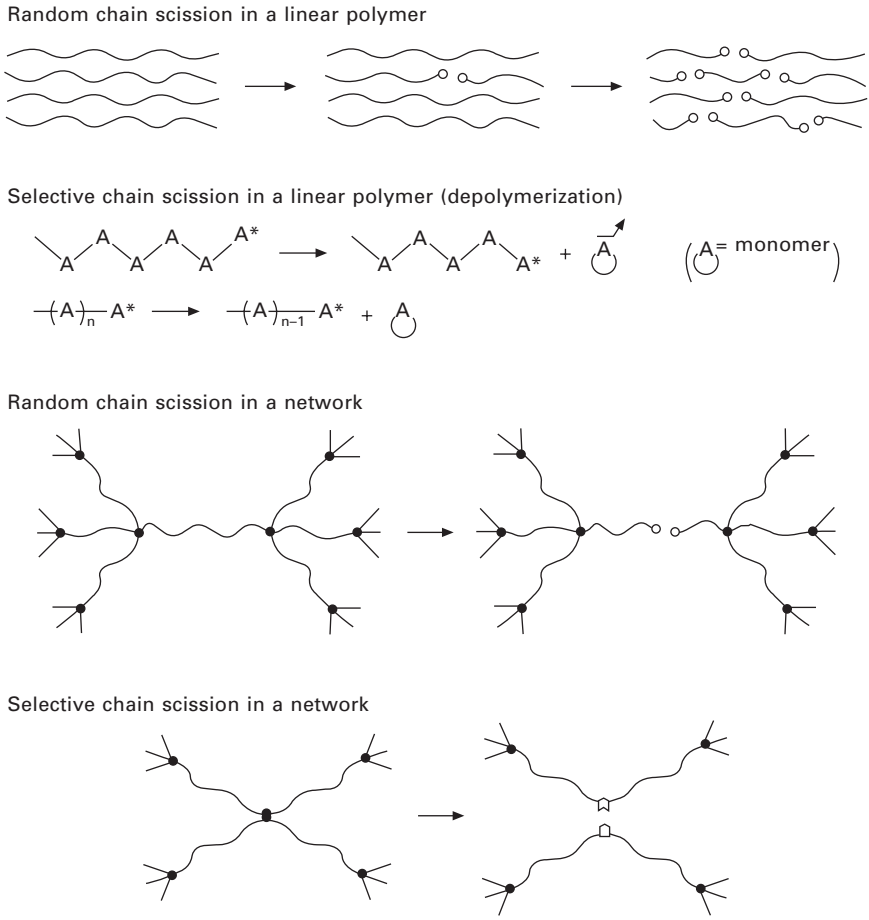

12.12 Random and selective chain scissions in linear and tridimensional polymers.

or oxidative ageing, random chain scissions predominate over all the other processes in the great majority of cases.

Depolymerization (or reversion) occurs essentially at high temperatures, only in linear polymers having weak monomer–monomer bonds, or in tridimensional polymers having weak cross-link junctions (see Table 12.2). These are linear polymers containing the weakest aliphatic C–C bonds, i.e. involving tetrasubstituted carbon atoms, e.g. polyisobutylene (PIB), poly(methyl methacrylate) (PMMA), poly(α-methyl styrene) (PαMS), etc. These are also linear polymers containing heteroatoms, e.g. poly(oxy methylene) (POM), poly(ethylene terephthalate) (PET), poly(vinyl chloride) (PVC), etc., but also sulphur vulcanized elastomers. Cross-linking predominates mainly in unsaturated linear polymers, i.e. essentially polybutadiene and its

Table 12.2 Order of magnitude of the dissociation energy (E_D) of main polymer chemical bonds

Chemical bond	E_D (kJ.mol^{-1})	Chemical bond	E_D (kJ.mol^{-1})
Aromatic C–C	510	C–Cl	320
C–F	470	C–Si	300
Aromatic C–H	465	C–N	290
Aliphatic C–H	325–425	C–S	275
Aliphatic C–C	300–380	S–S	260
C–O	340	O–O	150

copolymers (Coquillat *et al.*, 2007), and in poorly cross-linked elastomers and thermosets. Some exceptions are known for composite matrices, and will be examined in a later short paragraph.

12.5.3 Random chain scissions in linear polymers

The random character results from the fact that all the reactive groups of the macromolecules have an equal probability to react. This means that the probability for a chain to react is an increasing function of its length. The number (M_n) and weight (M_W) average molar masses are linked to the number S of chain scissions per mass unit by the following relationships (Saito, 1958a, 1958b):

$$\frac{1}{M_n} - \frac{1}{M_{n0}} = S \qquad [12.4]$$

$$\frac{1}{M_w} - \frac{1}{M_{w0}} = \frac{S}{2} \qquad [12.5]$$

The polydispersity index PI varies as follows:

$$PI = PI_0 \frac{1 + SM_{n0}}{1 + \frac{PI_0}{2} SM_{n0}} \qquad [12.6]$$

One sees that PI increases when $PI_0 < 2$, decreases when $PI_0 > 2$, but in all cases tends towards 2 when S increases (Fig. 12.13). This characteristic is generally used to recognize a random chain scission.

Steric exclusion chromatography (SEC) can be used to determine the molar mass distribution and the average values M_n and M_W. M_W can also be determined by viscosimetry using a power law:

$$\eta = KM_w^a \qquad [12.7]$$

In the case of dilute polymer solution, η is the intrinsic viscosity: $a \approx 0.7$ and K depends on temperature and solvent nature. In contrast, in the case

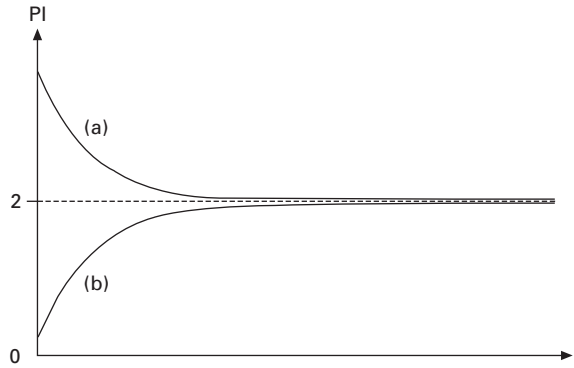

12.13 Shape of the variation of polydispersity index (PI) as a function of ageing time for a linear polymer undergoing a random chain scission: (a) $PI_0 > 2$; (b) $PI_0 < 2$.

of molten polymer, η is the Newtonian viscosity: $a = 3.4$ and K depends on temperature and polymer chemical structure.

According to Fox and Flory (1954), in linear polymers, the glass transition temperature T_g is a decreasing function of the number of chain ends:

$$T_g = T_{g\infty} - \frac{K_{FF}}{M_n} \quad [12.8]$$

where K_{FF} and $T_{g\infty}$ are parameters depending on the polymer chemical structure.

Both parameters are increasing functions of the chain stiffness. According to Richaud *et al*. (2010), they would be closely related:

$$K_{FF} \propto T_{g\infty}^2 \quad [12.9]$$

From Equations [12.4] and [12.8], one obtains:

$$T_{g0} - T_g = K_{FF}\, S \quad [12.10]$$

One can see that T_g is a decreasing function of the number of chain scissions S. The effect of these latter is an increasing function of the chain stiffness. Indeed, in flexible polymers having typically T_g values lower than 100°C, T_g changes are negligible. In contrast, they can be measured in stiff polymers, especially in those having aromatic groups in their macromolecular chain.

In semi-crystalline polymers, chemical ageing is accompanied by morphological changes (see below) and it is not easy to separate the (small) effects of molecular mass decrease from the effects of morphological changes. To summarize, chemical ageing induces only small variations of melting point and the sense of this variation can vary from one polymer to another. Melting point measurement is thus not an adequate method to monitor random chain scissions.

At conversions of practical interest, random chain scissions have no significant effect on elastic properties of linear polymers. The effect of molar mass on toughness of linear polymers is schematized in Fig. 12.14. Let us notice that the same type of curve can be obtained for the ultimate elongation. For all the polymers, one can distinguish two regimes separated by a relatively sharp transition at a critical molar mass M_F. At molar masses lower than M_F, polymers are extremely brittle, their toughness being due only to van der Waals interactions. Polymers behave like a wax or an eggshell, depending on their stiffness. They cannot be used in mechanical applications owing to their extremely high brittleness. On the contrary, at molar masses higher than M_F, polymers often have toughness in the range of 10^3–10^4 J.m^{-2}, i.e. almost independent of the molar mass.

In amorphous polymers, M_F is mainly linked to the entanglement density. Indeed, plastic deformations, responsible for the high toughness, are linked to chain drawing and this latter is only possible if the chains participate in a network, here the entanglement (topological) network. In contrast, in semi-crystalline polymers, the critical quantity is the interlamellar spacing l_a. As an example, PE is brittle when $l_a \leq 6$ nm (Kennedy *et al.*, 1994). Since l_a is sharply linked to molar mass, it can be considered, for these polymers also, that there is a critical molar mass M_F separating the brittle from the ductile domains (Fayolle *et al.*, 2008).

It can be interesting to establish a relationship between M_F and the entanglement molar mass M_E, this latter being sharply linked to the chemical structure (Fetters *et al.*, 1999). It appears that:

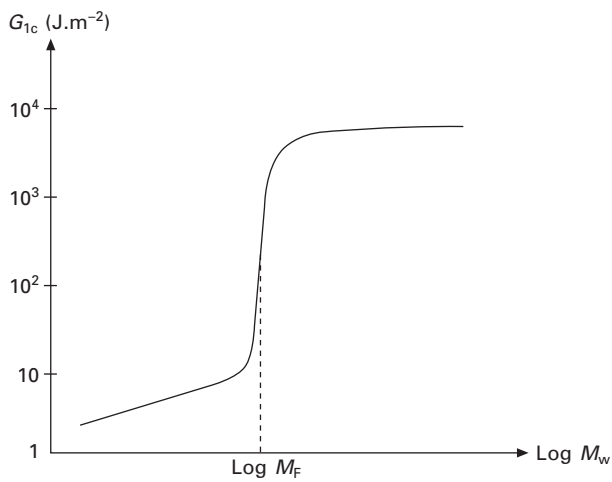

12.14 Shape of the variation of toughness (G_{1C}) for a linear polymer as a function of its weight average molar mass (M_W) (according to Greco and Ragosta, 1987).

- For amorphous polymers (e.g. PC, PS and PMMA) and semi-crystalline polymers having initially their amorphous phase in the glassy state (e.g. PA11 and PA6-6) (Kausch *et al.*, 2001):

$$\frac{M_F}{M_E} \approx 2 \text{ to } 5 \qquad [12.11]$$

- For semi-crystalline polymers having their amorphous phase in the rubbery state (e.g. PE, PP and PET) (Fayolle *et al.*, 2008):

$$\frac{M_F}{M_E} \approx 50 \qquad [12.12]$$

According to the shape of Fig. 12.14, the effect of random chain scissions on fracture properties must display three characteristics:

1. If the initial molar mass is high enough, chain scissions are expected to have no effect on fracture properties in the initial period of exposure, before molar mass reaches the critical value M_F.
2. Toughness must decay abruptly by one to three decades when molar mass reaches M_F.
3. Beyond the ductile–brittle transition, the toughness decreases continuously but very slowly.

Let us consider a chain scission process occurring at a constant rate: $r = dS/dt$. Assuming that PI $\approx$ PI$_0 \approx 2$, Equation [12.6] can be rewritten as:

$$M_w = \frac{2M_{w0}}{2 + r_r M_{w0} t} \qquad [12.13]$$

The changes in molar mass M_W and ultimate elongation ε_R with time are schematized in Fig. 12.15. One can see that, although S is a linear function of time, M_W is a hyperbolic function of time. As expected, ε_R falls abruptly when $M_W = M_F$.

The critical number of chain scissions S_F for embrittlement is given by:

$$S_F = 2\left(\frac{1}{M_F} - \frac{1}{M_{w0}}\right) \qquad [12.14]$$

In any case $M_F > 10$ kg.mol^{-1}, so that:

$$S_F \leq \frac{2}{M_F} \approx 0.2 \text{ mol.kg}^{-1} \qquad [12.15]$$

In common industrial linear polymers, the monomer concentration $[m]$ is such that:

$$[m] > 2 \text{ mol.kg}^{-1} \qquad [12.16]$$

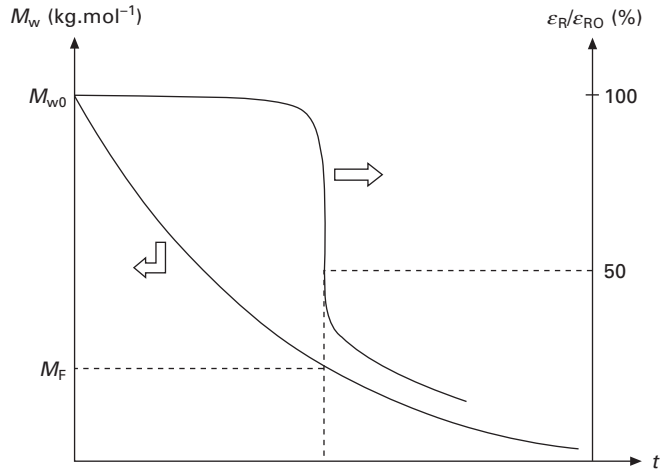

12.15 Shape of the changes with ageing time of weight average molar mass (M_W) and ultimate elongation (ε_R) for a linear polymer subjected to a random chain scission process.

It appears that embrittlement occurs always at a small conversion degree of the chain scission process. In certain cases, e.g. PP (Fayolle *et al.*, 2002), embrittlement occurs while no structural change is observable by spectrophotometry IRTF.

12.5.4 Random chain scissions in networks

Let us consider an ideal network in which every chain is connected to cross-link nodes at both extremities. Such chains are called 'elastically active chains' (EACs). Their concentration ν_0 is linked to the concentration x_0 of nodes by:

$$\nu_0 = \frac{f}{2} x_0 \qquad [12.17]$$

where f is the node functionality, i.e. the number of EACs connected to a node.

If the network undergoes a small number of random chain scissions such that $S << \nu_0$, each chain scission occurs in an EAC, so that new cross-link density is given by (Pascault *et al.*, 2002):

$$\nu = \nu_0 - jS \qquad [12.18]$$

with $j = 3$ for $f = 3$, and $j = 1$ for $f > 3$ (see Fig. 12.16).

Each chain scission creates two dangling chains. Indeed, chain scissions transform an ideal network into a non-ideal one, and the probability of

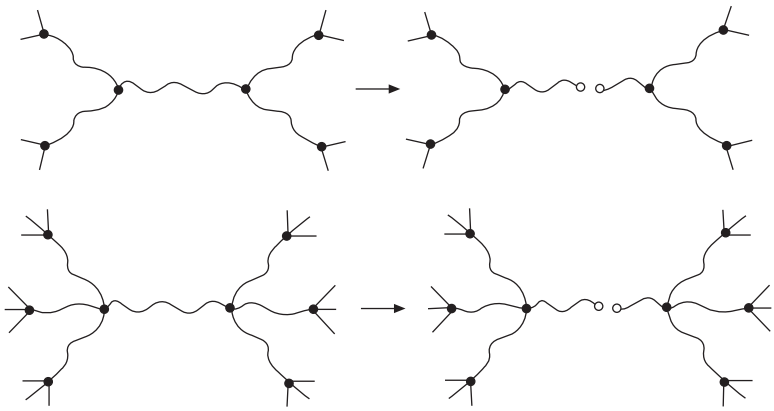

12.16 Schematization of a random chain scission in a network with trifunctional (above) and tetrafunctional (below) nodes.

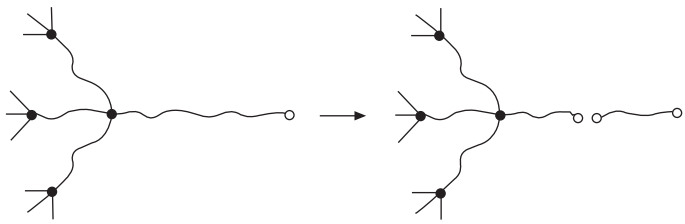

12.17 Schematization of a chain scission in a dangling chain.

having a chain scission in a dangling chain increases with the number of chain scissions (see Fig. 12.17).

At a given state of degradation, the mass fraction w_e of EAC is:

$$w_e = \nu M_e \qquad [12.19]$$

Let us consider a chain scission process at a constant rate: $r = dS/dt$, e.g. in a network having nodes of functionality $f > 3$. The probability of breaking an EAC is expected to be proportional to the EAC mass fraction, so that:

$$\frac{d\nu}{dt} = -rw_e = -rM_e\nu \qquad [12.20]$$

It follows that:

$$\nu = \nu_0 \exp(-rM_e t) \qquad [12.21]$$

One can see that, although chain scission is an apparent zero-order process, the cross-link density decreases in an apparent first-order process. In practice, the mechanical behaviour is strongly altered at relatively low conversions of the chemical ageing process, before the probability of having a scission in

a dangling chain has reached a significant value. It is noteworthy that chain scissions on dangling chains create free chains. The amount of the latter corresponds to the extractable fraction in solvents.

Analytical methods for the determination of the number of chain scissions S per mass unit are scarce. When elastic properties in the rubbery state are measurable, one can use the theory of rubber elasticity (Flory, 1953), according to which:

$$\frac{\mathrm{d}G}{\mathrm{d}S} = \frac{\mathrm{d}G}{\mathrm{d}\nu}\frac{\mathrm{d}\nu}{\mathrm{d}S} = -jRT\rho \qquad [12.22]$$

where G is the shear modulus at $T > T_g$ and ρ is the specific weight (kg.m^{-3}) of the polymer.

The glass transition temperature T_g is also dependent on cross-link density. According to Di Marzio (1964):

$$T_g = \frac{T_{gl}}{1 - K_{DM}F\nu} \qquad [12.23]$$

where T_{gl} and F are parameters depending on chain stiffness, and K_{DM} is a universal constant ($K_{DM} \approx 3$).

$$\frac{\mathrm{d}T_g}{\mathrm{d}S} = -j\frac{T_g}{\mathrm{d}\nu} = \frac{jK_{DM}FT_{gl}}{(1 - K_{DM}F\nu)^2} = jK_{DM}F\frac{T_g^2}{T_{gl}} \qquad [12.24]$$

The effect of chain scissions is thus an increasing function of T_g. Let us consider, for instance, an epoxy network based on the triglycidyl derivative of *p*-aminophenol (TGAP) cross-linked by diaminodiphenylmethane (DDM) in stoichiometric proportion. The characteristics are (Pascault *et al.*, 2002) T_g = 494 K, F = 23 g.mol^{-1}, T_{gl} = 293 K and j = 3 (trifunctional cross-links). Then, it follows that:

$$\frac{\mathrm{d}T_g}{\mathrm{d}S} = 172 \text{ K.kg.mol}^{-1} \qquad [12.25]$$

Effects of random chain scissions on elastic properties depend on the amplitude of the dissipation peak related to the β relaxation. For polymers having a weak β transition, e.g. styrene cross-linked polyesters or vinylesters, chain scissions have a minor effect on elastic properties in the glassy state. In contrast, for polymers having a strong β transition, e.g. diamine-cross-linked epoxies, chain scissions lead to an increase in the modulus plateau between the β transition and the glass transition (Fig. 12.18). This phenomenon is called 'internal antiplasticization' (Rasoldier *et al.*, 2008). It can be evidenced through nano- or micro-indentation profiles that characterize degradation gradients in the sample thickness (Olivier *et al.*, 2009). Chain scissions induce a decrease in fracture toughness (or ultimate elongation).

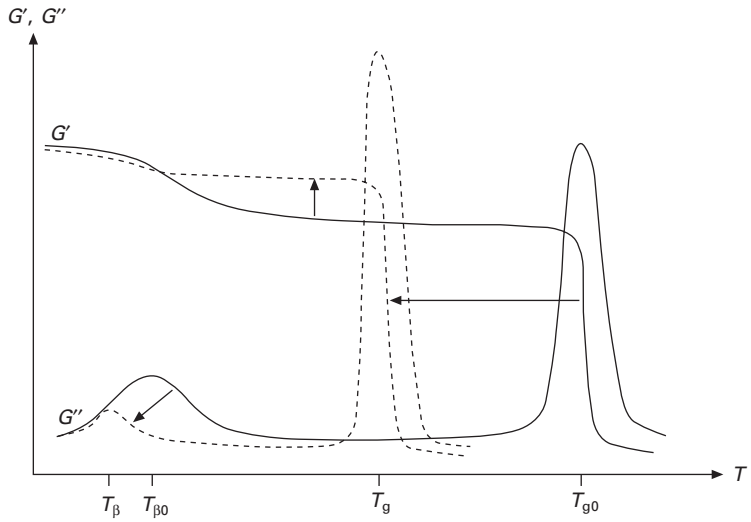

12.18 Storage (*G′*) and dissipation (*G″*) modulus against temperature for a network having a strong β transition before (full line) and after (dashed line) a chain scission process.

From this point of view, degraded networks differ from ideal networks in which fracture properties are generally a decreasing function of cross-link density (Crawford and Lesser, 1999; Pascault *et al.*, 2002). Little is known on the quantitative relationships between chain scission and embrittlement in networks.

12.5.5 Simultaneous random chain scissions and cross-linking

In linear polymers, Saito's equations become (Saito, 1958a, 1958b):

$$\frac{1}{M_n} - \frac{1}{M_{n0}} = S - X \qquad [12.26]$$

$$\frac{1}{M_W} - \frac{1}{M_{W0}} = \frac{S}{2} - 2X \qquad [12.27]$$

where X is the number of cross-links and S the number of chain scissions.

There is an 'equilibrium' corresponding to the constancy of M_W for:

$$S = 4X \qquad [12.28]$$

For $X > S/4$, cross-linking predominates over chain scissions. Polymer gelation occurs when $M_W \to 0$, i.e. when:

$$\frac{S}{2} - 2X = -\frac{1}{M_{W0}} \quad [12.29]$$

i.e. in the absence of chain scission for:

$$X_g = -\frac{1}{2M_{W0}} \quad [12.30]$$

Beyond the gel point, an insoluble fraction appears. According to Charlesby and Pinner (1959), the soluble fraction w_S is related to the number of chain scissions and cross-links by:

$$w_s + w_s^{1/2} = \frac{S}{2X} + \frac{1}{M_{W0}X} \quad [12.31]$$

In linear polymers, cross-linking affects mainly rheological properties in the molten state. Indeed, long branching is responsible for the disappearance of the Newtonian plateau (Fig. 12.19).

Cross-linking induces an increase in the glass transition temperature. In the case of simultaneous chain scission and cross-linking, it can be written, in a first approach, that:

$$T_g = T_{g0} + k_S S + k_X X \quad [12.32]$$

k_S is significantly higher than k_X. As an example, in bisphenol-A polysulphone, $k_S/k_X \approx 2.1$ (Richaud *et al.*, 2010). In other words, cross-linking has less influence than chain scissions on T_g.

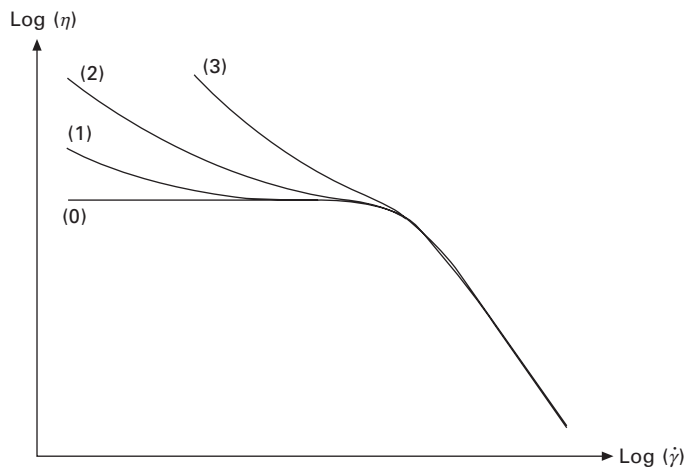

12.19 Shape of the curve of log(viscosity) versus log(shear rate) for a linear polymer before (0) and after ageing leading to an increase in degree of branching (0 < 1 < 2 < 3).

The effects of cross-linking on fracture properties are not well known. In most cases, cross-linking is expected to induce embrittlement according to the following causal chains:

1. Cross-linking → Increase in T_g → Increase in yield stress → Ductile (plastic) deformation less and less competitive with brittle deformation.
2. Cross-linking → Shortening of EAC → Decrease in drawability of EAC → Reduction in plastic zone at crack tip → Decrease in toughness.

12.5.6 Effects of post-curing

In most industrial thermosets and especially for cold-cured systems used in construction, cure is not complete and reactive groups remain trapped at the end of processing operations. In ageing conditions, they can recover enough mobility to react, because they are heated at temperatures close to T_g or the polymer is plasticized by a solvent, e.g. water. Cure reactions are then reactivated; the cross-link density increases in an auto-retardated way and stops when all the available reactive groups have been consumed. Except for scarce cases, e.g. epoxides cross-linked by unsaturated anhydrides (Le Huy *et al.*, 1993), oxidative ageing is dominated by chain scission, so that, for thermosets, cross-link density variations during thermal ageing have the shape of Fig. 12.20.

These curves can be decomposed into two components, i.e. post-cure and degradation (see Fig. 12.21). In the simplest cases, there is no interaction between both processes, so that their effects on cross-link density are additive.

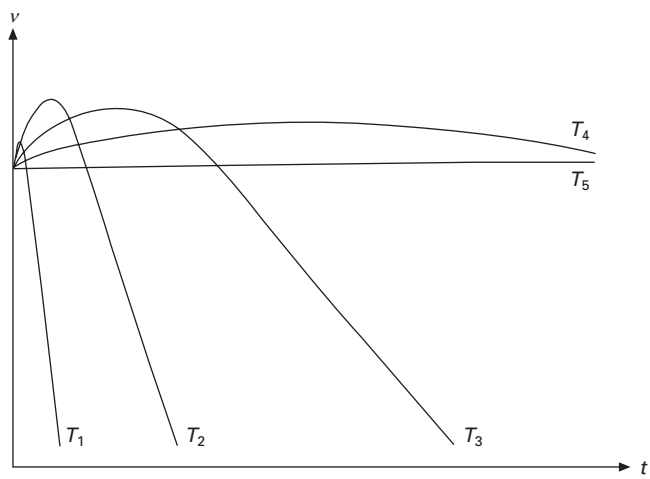

12.20 Shape of kinetic curves of cross-link density variations during the thermal ageing (in air) of a thermoset at various temperatures: $T_1 > T_2 > T_3 > T_4 > T_5$.

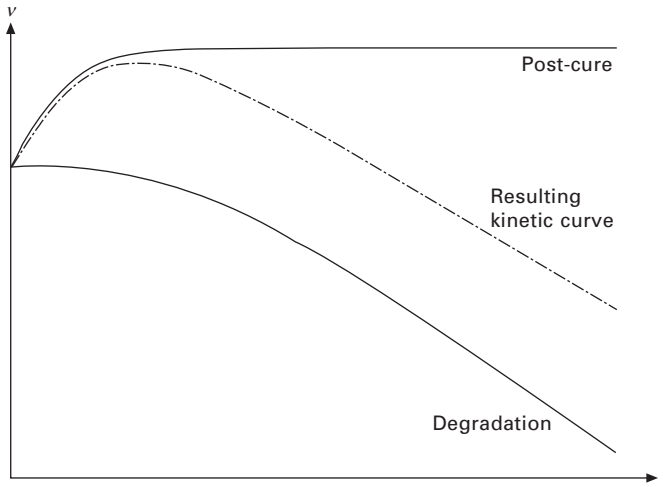

12.21 Schematization of combined effects of post-cure and degradation.

In other cases, however, oxygen or water can inhibit post-cure and a more complex behaviour can be expected.

12.6 Mechanisms of chemical ageing: reaction–diffusion coupling

In both oxidation and hydrolysis, the polymer matrix reacts with a small molecule coming from the environment (oxygen or water, for instance). In a thin elementary layer at a distance z from the sample surface, the reactant concentration balance can be ascribed as follows: reactant concentration change = rate of reactant supply by diffusion – rate of reactant consumption by reaction.

In the case of unidirectional diffusion, far from the sample edges, this balance equation can be written:

$$\left(\frac{\partial C}{\partial t}\right)_z = D\,\frac{\partial^2 C}{\partial z^2} - r(C) \qquad [12.33]$$

where C is the reactant concentration, D is the coefficient of reactant diffusion in the polymer matrix and $r(C)$ is the rate of reactant consumption expressed as a function of the reactant concentration.

Resolution of Equation [12.33] requires the knowledge of two physical quantities: the equilibrium concentration C_S of the reactant and its coefficient of diffusion D in the polymer matrix; and one item of chemical data: the concentration dependence of the reactant chemical consumption $r(C)$.

There are various works (Crank and Park, 1968; Hopfenberg, 1974; Bicerano, 2002; Van Krevelen and Te Nijenhuis, 2009) devoted to transport properties of gases and vapours in polymer matrices and their relationships with polymer structure. The main differences between oxygen and water properties can be summarized as follows: oxygen solubility in polymers is always low, typically $\leq 10^{-3}$ mol.l^{-1}, and practically insensitive to small structural changes. The coefficient of oxygen diffusion is of the order of $10^{-11 \pm 2}$ m^2.s^{-1} at ambient temperature and its apparent activation energy is located in the 30–60 kJ.mol^{-1} interval. Oxygen transport properties are practically always determined from permeability measurements. It can be reasonably assumed that, during an ageing experiment at a constant temperature, D is independent of C and reaction conversion at reasonably low conversions of the oxidation process, e.g. before and just after embrittlement. In contrast, relationships between polymer structure and water transport characteristics are obviously more complicated, as illustrated by Table 12.3.

The main trends of structure–property relationships can be briefly summarized as follows:

- Three main types of groups can be distinguished:
  - G1: Hydrocarbon and halogenated groups of which the contribution to hydrophilicity is negligible. Polymers containing only these groups (polyethylene, polypropylene, polystyrene, elastomers, etc.) absorb less than 0.5 wt% water.

Table 12.3 Molar mass of the constitutive repeat unit, water mass fraction at equilibrium at 50°C and 50% RH, coefficient of water diffusion in the same conditions, and number of moles of water per constitutive repeat unit

Polymer	Code	M (g.mol^{-1})	m_{equ} (%)	$D \times 10^{12}$ (m^2.s^{-1})	n (mol.mol^{-1})
Poly(methyl methacrylate)	PMMA	100	1.28	0.36	0.071
Poly(ethylene terephthalate)	PET	192	0.55	0.54	0.059
Polycarbonate	PC	254	0.25	5.4	0.035
Polyamide 11	PA11	183	1.5	0.13	0.153
Poly(bisphenol-A) sulphone	PSU	442	0.52	8.97	0.128
Polyethersulphone	PES	232	1.8	2.79	0.232
Polyetherimide	PEI	592	1.4	0.97	0.460
Polypyromellitimide	PPI	382	5.0	0.1	1.061
Polyimide	IP960	486	4.2	0.83	1.134
Epoxy	DGEBA–Etha	858	2.0	1.03	0.953
Epoxy	DGEBD–Etha	578	6.8	0.11	2.183
Unsaturated polyester	UP	334	0.83	0.88	0.154
Vinylester	VE(D)	980	1.7	0.6	0.926
Vinylester	VE(C)	550	0.5	0.5	0.153

Source: data compiled from Bellenger *et al.* (1994), Tcharkhtchi *et al.* (2000) and Gaudichet-Maurin *et al.* (2008).

  - G2: Groups of relatively low polarity (ethers, ketones, esters, etc.). Polymers containing only these groups (with hydrocarbon ones) absorb generally less than 2 wt% water. Physical effects of water absorption (plasticization, swelling) are generally negligible. Polymers containing ester groups (polyalkylene terephthalates, unsaturated polyesters, anhydride crosslinked epoxies, etc.) are, however, susceptible to hydrolysis (see below). Polymers containing methacrylic esters (polymethyl methacrylate, vinylesters, etc.) are generally resistant to hydrolysis.
  - G3: Highly polar groups able to establish strong hydrogen bonds with water (sulphones, alcohols, amides, acids, etc.). These polymers can absorb up to 5 wt% water, which can induce considerable physical changes, e.g. T_g decreases by about 10 K per percent of water absorbed, and swelling and damage by swelling stresses occur during the sorption or desorption transients.
- In each polymer family containing one type of hydrophilic group, e.g. polyamides, polysulphones, polyimides, epoxies, etc., the equilibrium water concentration increases non-linearly with the concentration of polar groups. A theory based on the hypothesis that water is doubly bonded was proposed to explain this trend (Tcharkhtchi *et al.*, 2000; Gaudichet-Maurin *et al.*, 2008).
- The relationships between diffusion coefficient and polymer structure are not fully understood, but it is clear that in a given family, D is a decreasing function of the water equilibrium concentration (Thominette *et al.*, 2006). Such dependence indicates that water-polymer hydrogen bonds slow down diffusion in polyethylenes (McCall *et al.*, 1984) and in epoxies (Tcharkhtchi *et al.*, 2000).
- Diffusion is thermally activated and apparent activation energies are generally in the 20–60 kJ.mol^{-1} interval. Equilibrium water concentrations depend only slightly on temperature, which can be explained by considerations on heat of solubility (Merdas *et al.*, 2002).

Let us consider now the term representing the chemical reactant consumption in the reaction–diffusion equation (Equation [12.33]). In the simplest case of hydrolysis, $r(C)$ is a simple first-order equation:

$$r(C) = kE_0\, C \qquad [12.34]$$

where k is the second-order rate constant of the water–polymer reaction, and E_0 is the concentration of hydrolysable groups, considered constant at reasonably low conversions.

A more complex equation is needed when hydrolysis is equilibrated by the reverse condensation reaction (see next paragraph). When Equation [12.34] is an acceptable approximation, the integration of Equation [12.33], for a symmetric sheet of thickness L, gives:

$$C = C_S \frac{\cosh J\left(z - \frac{L}{2}\right)}{\cosh \frac{JL}{2}} \quad [12.35]$$

where $J = kE_0/D$. The origin of z has been taken at one sample edge.

The water concentration and then the hydrolysis rate decrease in a pseudo-exponential way from the sample edges, where $C = C_S$ (maximum value), to the middle of the sample, where $C = C_m$ (minimum value). Note that, when $L = 6J^{-1}$, $C_m/C_S \approx 0.1$. Thus, for $L >> 6J^{-1}$, the sample behaves as a sandwich made of an undegraded core surrounded by two degraded superficial layers. In the case of an equilibrated hydrolysis, e.g. for PA11 (Jacques *et al*., 2002) or PA6-6 (El Mazry *et al*., 2012), a degradation gradient appears at the beginning of exposure, but the sample tends to homogenize as the hydrolysis rate slows down.

The case of oxidation is more complex because the mechanism is a branched radical chain of which the kinetic modelling was considered out of reach for a long time. The first attempts were made at the beginning of the 1980s by Seguchi *et al*. (1981, 1982) and Cunliffe and Davis (1982) by applying a series of simplifying assumptions: constant initiation rate, existence of a steady state for radical concentration, long kinetic chain, and low conversion of the oxidation process. All these assumptions are more or less valid in some cases of photochemical and radiochemical oxidation, but they are questionable in the case of thermal oxidation. Assuming their validity, the rate of oxygen consumption can be expressed by a hyperbolic function of oxygen concentration:

$$r(C) = \frac{aC}{1 + bC} \quad [12.36]$$

where a and b can be expressed in terms of rate constants of the elementary reactions involved in the oxidation mechanistic scheme.

There is no analytical solution for Equation [12.33], but approximations can be obtained for extreme cases:

- When $C >> b^{-1}$:

$$r(C) = \frac{a}{b} = r_S \quad [12.37]$$

- In contrast, when $C << b^{-1}$:

$$r(C) = aC \quad [12.38]$$

In the second case, the same solution as for hydrolysis is obtained (Equations [12.34] and [12.35]). However, in the first case, integration of Equation

[12.33] for a symmetric sheet of thickness L leads to a parabolic shape of the oxygen concentration profile:

$$C = C_S + \frac{r_S}{2D}(z - L)z \qquad [12.39]$$

The concentration in the middle of the sample is:

$$C = C_S - \frac{r_S L^2}{8D} \qquad [12.40]$$

12.6.1 Reaction–diffusion coupling in composite laminates

In the case of composite laminates, new problems linked to the anisotropy of diffusion paths, the eventual role of interfacial diffusion and the role of pre-existing or swelling-induced damage appeared in the mid-1970s. The interest was mainly focused on the effect of humidity on carbon fibre/amine crosslinked epoxy composites of aeronautical interest. For the pioneers of this research (Shen and Springer, 1976), the determination of diffusion kinetic laws appeared as the key objective. Various studies revealed that, in certain cases, diffusion in composites cannot be modelled by a simple Fick's law and that Langmuir's equation is more appropriate. Carter and Kibler (1978) proposed a method for the parameter identification. At the end of the 1970s, the kinetic analysis of water diffusion into composites became a worldwide research objective. Related experimental results can be summarized as follows.

Concerning the effect of fibre anisotropy on diffusion, a model for unidirectional composites was proposed by Kondo and Taki (1982). This model takes full account of the fact that water diffusivity is more privileged in the fibre direction than in the transverse one:

$$D_{//} = \frac{1 - V_f}{1 - a\sqrt{V_f}} D_{\perp} \qquad [12.41]$$

where $D_{//}$ and $D_{\perp}$ are the respective diffusion coefficients in the longitudinal and transverse fibre directions, V_f is the volume fraction of fibres, and a is a parameter depending on the fibre arrangement:

- For a cubic stacking (Kondo and Taki, 1982; Hahn, 1987):

$$a = \frac{2}{\sqrt{\pi}} \qquad [12.42]$$

- For a compact hexagonal stacking (Woo and Piggot, 1988):

$$a = \sqrt{\frac{2\sqrt{3}}{\pi}} \qquad [12.43]$$

Examples of values of water and oxygen diffusivity determined in unidirectional composites are reported in Tables 12.4 and 12.5 respectively. Colin *et al*. (2005) showed that such models can also be used to predict oxygen diffusivity in composites. More recently, Roy and Singh (2009) showed that these models can be improved to take into account physical discontinuities such as highly permeable fibre/matrix interface or fibre/matrix debonding due to oxidative shrinkage and erosion.

Concerning Langmuir's mechanisms, it was assumed, for a long time, that water was trapped in 'defects' resulting from damage or pre-existing, eventually located at the interface. Tcharkhtchi *et al*. (2000) found that unreacted epoxide groups undergo a reversible hydrolysis:

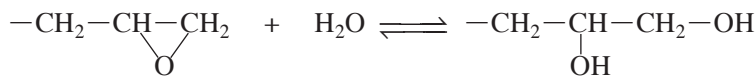

Epoxide groups appear thus as 'water traps' and are responsible for a Langmuir component in diffusion kinetic curves. Since industrial composites are rarely fully cured, it can be assumed that epoxide hydrolysis was often the cause of Langmuir's behaviour in previous studies. Recently, however, Derrien and Gilormini (2006) found that Langmuir's behaviour could be simply linked to the stress state induced by water diffusion.

Table 12.4 Values of oxygen diffusivity for carbon fibres/epoxy matrix in the longitudinal ($D_{//}$) and transverse ($D_{\perp}$) directions of fibres

Temperature (°C)	*D* for carbon/epoxy ($m^2.s^{-1}$)	
	$D_{//} \times 10^{-12}$	$D_{\perp} \times 10^{-12}$
70	2.24	1.36

Note: The epoxy matrix is an aromatic diamine (DDS) cross-linked epoxy. The volume fraction of carbon fibres is 65% (Didierjean, 2004).

Table 12.5 Values of oxygen diffusivity for glass and carbon fibres/epoxy matrix in the longitudinal ($D_{//}$) and transverse ($D_{\perp}$) directions of fibres

Temperature (°C)	D for glass/epoxy ($m^2.s^{-1}$)		D for carbon/epoxy ($m^2.s^{-1}$)	
	$D_{//} \times 10^{-12}$	$D_{\perp} \times 10^{-12}$	$D_{//} \times 10^{-12}$	$D_{\perp} \times 10^{-12}$
180	3.75	0.70	2.59	0.70
200	5.36	1.10	3.70	1.10

Note: The epoxy matrix is an anhydride cross-linked epoxy. The volume fractions of glass and carbon fibres are 64% and 69% respectively (Barjasteh *et al.*, 2009).

Concerning eventual interfacial processes, there is an abundance of literature. Various techniques have been used to characterize interfaces/interphases (Schradder and Block, 1971; Di Benedetto and Scola, 1980; Ishida and Koenig, 1980; Rosen and Goddard, 1980; Ishida, 1984; Di Benedetto and Lex, 1989; Thomason, 1990; Hoh *et al.*, 1990; Schutte *et al.*, 1994). Round-robin tests showed that no analytical method is able to provide unquestionable results (Pitkethly *et al.*, 1993). Even in cases where the interface response to humid ageing has been unambiguously identified from studies on model systems (Kaelble *et al.*, 1975, 1976; Salmon *et al.*, 1997), it seems difficult, at this stage, to build a non-empirical kinetic model of the water effects on interfaces/interphases in composites.

12.7 Mechanisms of chemical ageing: hydrolytic processes

Hydrolytic processes are especially important in two main polymer matrix families containing ester or amide groups in the chain. In these cases, each hydrolysis event is a chain scission:

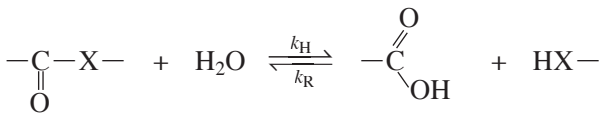

where X = –O– (polyesters) or –NH– (polyamides).

Taking [–CO–X–] = E, [–COOH] = [HX–] = b, and S = number of chain scissions (mole per mass unit), one can write:

$$\frac{dS}{dt} = k_H C(E_0 - S) - k_R (b_0 + S)^2 \qquad [12.44]$$

where C is the water concentration, and k_H and k_R are rate constants depending only on temperature.

Two cases can be distinguished:

1. *Equilibrium occurs at high conversions* ($S_\infty/E_0 \approx 1$). Since embrittlement occurs at low conversions, far from equilibrium, one can neglect the reverse reaction. Then, the rate of chain scissions is well approximated by:

$$\frac{dS}{dt} = -\frac{dE}{dt} = k_H E_0 C = K \qquad [12.45]$$

where K is a pseudo-zero-order rate constant of which some typical values are given in Table 12.6.

Polymers containing ester groups (linear or cross-linked polyesters, anhydride-cured epoxies, urethane cross-linked polyesters, polycarbonate, etc.) belong to this category.

Table 12.6 Approximate value of the pseudo zero-order rate constant of hydrolysis for ester-containing polymers

Polymer	Temperature (°C)	$K \times 10^8$ (mol.l^{-1}.s^{-1})	E_{act} (kJ.mol^{-1})
PET	99	6	107
PET	60	0.08	107
PC	85	0.2	75
PC	100	0.7	75
Unsaturated polyesters	100	20–150	70 ± 10
Vinylesters	100	0.2–1.0	–

Source: Bellenger *et al.*, 1995.

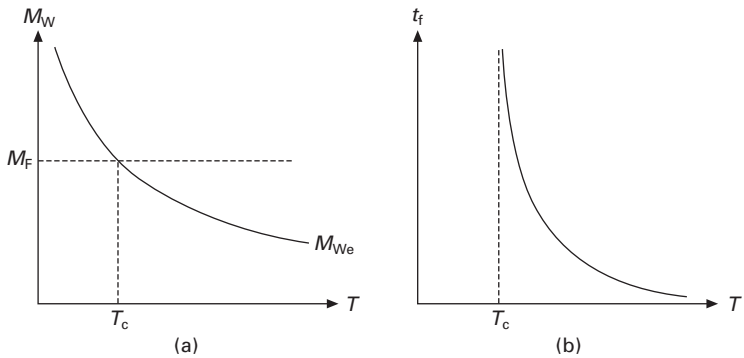

12.22 (a) Molar mass–temperature map; (b) lifetime versus temperature.

2. *Equilibrium occurs at low conversions* (typical case of PA11 and PA6-6). Then, the reverse reaction cannot be neglected and the kinetic model is somewhat more complicated (Jacques *et al.*, 2002; El Mazry *et al.*, 2012), especially when acids are present (Merdas *et al.*, 2003). It can be easily shown that the equilibrium molar mass M_{We} (when $t \to \infty$) is given by:

$$M_{We} = 2\left(\frac{k_R}{k_H E_0 C}\right)^{1/2} \quad [12.46]$$

The molar mass is a decreasing exponential function of temperature (Fig. 12.22). One can thus distinguish two important cases:

- If $T > T_C$, then $M_{We} < M_F$. The material becomes brittle.
- If $T < T_C$, then $M_{We} > M_F$. The material never becomes brittle, but reaches an equilibrium. Lifetime is theoretically infinite. In the case of PA11, $T_C \approx 80$°C.

In composites, interphase hydrolysis can occur, e.g. in the case of silane

coupling agents (Ishida and Koenig, 1980; Hoh *et al.*, 1990; Salmon *et al.*, 1997). The level of knowledge in this field remains far from what would be needed to predict lifetime from mechanical criteria.

Since hydrolysis is a chain scission process, it always induces embrittlement. In initially ductile linear polymers, such as PET or PA11, toughness falls off by two or three decades when the weight average molar mass reaches a critical value M_F of the order of 10–20 mol.kg^{-1}, corresponding to a small multiple of the entanglement molar mass (Fayolle *et al.*, 2008). In the frame of second-order kinetics (rate constant k_H), it is possible to determine a lifetime value corresponding to the time to embrittlement:

$$t_F = \left[\frac{2}{E_0}\left(\frac{1}{M_F} - \frac{1}{M_{W0}}\right)\right]\left[\frac{1}{k_H}\right]\left[\frac{1}{C}\right] \qquad [12.47]$$

This non-empirical quantity can be decomposed into three almost independent factors: the first linked to the polymer structure, the second to temperature through the Arrhenius law, and the third to water activity through the sorption isotherm equation. Note that this last factor can also slightly depend on temperature.

In thermosets, which are often initially brittle, chain scissions induce also a decrease in fracture properties, but the structure–property relationships are not yet well established in this domain.

12.7.1 Hydrolysis-induced osmotic cracking

In the most economically important class of hydrolysable thermosets, e.g. unsaturated polyesters (decks, swimming pools, tanks, etc.), failure comes generally from a specific consequence of hydrolysis: osmotic cracking. In laminates, subcutaneous cracks propagate preferentially parallel to the surface, giving blisters. This phenomenon was catastrophic for the composite boat industry in the 1970s and 1980s. It was later understood why cracks propagate. Indeed, they contain water in which solutes, coming from the polyester matrix, create an osmotic pressure which increases until stress concentration at crack tips induces propagation. Then, the pressure decreases until the crack stops, but new solutes are released by the polymer, the osmotic pressure increases again, etc. (Ashbee *et al.*, 1967; Ashbee and Wyatt, 1969). The mechanism of crack initiation was elucidated by Gautier *et al.* (1999): it is due to the accumulation of small highly hydrophilic molecules (diacids, dialcohols) resulting from hydrolysis events near the end of dangling chains (these latter pre-existing or being formed by hydrolysis events on elastically active chains). The composite resistance to osmotic cracking would be thus linked to three factors having additive effects on the initiation rate: the initial presence of solutes linked to the polymerization catalysts; the initial presence of dangling chains (which is a decreasing function of the prepolymer molar

mass); and the polyester hydrolysis rate. If, by a proper optimization of the above factors, the rate of small molecules release is lowered enough, then they can eventually disappear (at least partially) by diffusion, and the time to cracking increases considerably, or even becomes infinite.

In the case of glass fibre/unsaturated polyester matrix composites, the kinetic curve of weight changes can present a peculiar shape revealing the presence of osmotic cracking (see Fig. 12.23). Such behaviour can be explained as follows:

- At time t_1, sorption equilibrium is reached.
- At t_2, cracks initiate and the sorption capacity of the sample increases.
- At t_3, cracks coalesce and organic molecules, resulting from polymer hydrolysis and dissolved in water contained in the cracks, are extracted. The weight begins to decrease.

Note that the phenomena of sorption and cracking are distinguishable if the sample thickness L is low enough to have $t_D < t_C$, where $t_D = L^2/D$ is the characteristic time of diffusion, D is the diffusion coefficient of water in the material, and t_C is the characteristic time of osmotic cracking, mainly linked to the hydrolysis rate and independent of thickness (Gautier *et al.*, 1999).

12.8 Mechanisms of chemical ageing: oxidation processes

Oxidation processes are especially important in hydrocarbon polymer matrices. These processes result from a radical chain reaction established

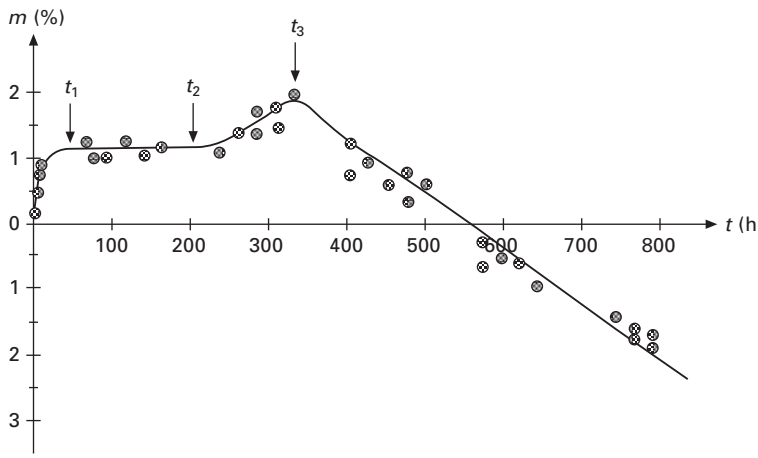

12.23 Osmotic cracking in a polyester for boat hulls, as revealed by the kinetic curve of weight changes after immersion in boiling water (according to Mortaigne *et al.*, 1992).

for the first time by Semenov (who was awarded a Nobel Prize in 1956) and co-workers in the 1930s (Semenov, 1935). However, in the polymer community of western countries, this mechanism remained ignored until the end of the Second World War, when it was rediscovered by a British team (Bolland and Gee, 1946) and then called the 'standard oxidation scheme'. In its general form, it involves six elementary steps:

1. Polymer $\rightarrow \mu P^{\bullet}$ (r_1)
2. $P^{\bullet} + O_2 \rightarrow PO_2^{\bullet}$ (k_2)
3. $PO_2^{\bullet}$ + polymer $\rightarrow$ Per + $P^{\bullet}$ (k_3)
4. $P^{\bullet} + P^{\bullet} \rightarrow$ inactive products (k_4)
5. $P^{\bullet} + PO_2^{\bullet} \rightarrow$ inactive products (k_5)
6. $PO_2^{\bullet} + PO_2^{\bullet} \rightarrow$ inactive products + O_2 (k_6)

where Per, $P^{\bullet}$ and $PO_2^{\bullet}$ refer respectively to peroxides and alkyl and peroxy radicals, r_1 is the initiation rate, k_i are rate constants, and μ is the yield of radicals formation in initiation.

Oxidation propagates in two elementary steps:

1. Oxygen addition to alkyl radicals. This is a very fast process and thus practically structure and temperature independent. The corresponding rate constant is very high: $k_2 = 10^8$–10^9 l.mol^{-1}.s^{-1} (Kamiya and Niki, 1978).
2. Peroxyl radical reaction with the polymer. This is a generally much slower process, which is structure dependent. In saturated hydrocarbon polymers, e.g. polyethylene (PE) and polypropylene (PP), it is exclusively a hydrogen atom abstraction. In this case, Per is a hydroperoxide group (POOH). The corresponding rate constant is very low: $k_3 = 10^{-3}$–10^{-1} l.mol^{-1}.s^{-1} at ambient temperature (see Table 12.7). In polyenic elastomers, e.g. polybutadiene (PBD) and polyisoprene (PIP), step 3 can also be an addition to double bonds. In this case, Per is a peroxide bridge (POOP). The corresponding rate constant is also very low: typically $k_3 = 10^{-1}$–10 l.mol^{-1}.s^{-1} at ambient temperature for an intramolecular addition (see Table 12.7).

In the absence of antioxidants, radicals terminate according to bimolecular processes (steps 4, 5 and 6). At relatively low temperature, close to ambient temperature, the corresponding termination rate constants classify in the following order (Gillen *et al.*, 1995):

$$k_4 > k_5 >> k_6 \qquad [12.48]$$

whereas the corresponding activation energies classify in the reverse order, mainly because $P^{\bullet}$ radicals can propagate by hydrogen abstraction:

Table 12.7 Propagation reactions of oxidation and corresponding value of the rate constant (k_3) at ambient temperature in some common hydrocarbon polymers: polypropylene (PP), polyethylene (PE), polybutadiene (PBD) and polyisoprene (PIP)

Type of propagation	Polymer	k_3 ($l.mol^{-1}.s^{-1}$ or s^{-1})	Reference
Hydrogen atom abstraction	PP	1.0 × 10–3	Korcek *et al.*, 1972
	PE	2.4×10^{-3}	Korcek *et al.*, 1972
	PBD	4.9×10^{-3}	Coquillat *et al.*, 2007
	PIP	5.2×10^{-2}	Colin *et al.*, 2007
Intramolecular addition to double bonds	PBD	6.1×10^{-1}	Coquillat *et al.*, 2007
	PIP	2.7	Colin *et al.*, 2007
Intermolecular addition to double bonds	PBD	5.8×10^{-4}	Coquillat *et al.*, 2007
	PIP	–	Colin *et al.*, 2007

$$P^{\bullet} + PH \rightarrow PH + P^{\bullet}$$

This transfer reaction does not influence the whole oxidation kinetics (except for polyenic elastomers), but provides a simple explanation for a relatively high mobility of alkyl radicals and thus for a high k_4 value.

However, at moderate to high temperature, elementary steps 5 and 6 lead mainly to unstable peroxide bridges (POOP). As a result, Equation [12.48] is no longer valid. As an example, when $T > 200°C$, it is instead observed that (Colin and Verdu, 2003; Assadi *et al.*, 2004; Nait-Ali *et al.*, 2011):

$$k_4 > k_5 \approx k_6 \qquad [12.49]$$

The most debated aspect of the subject during the past half-century has been the initiation of oxidation. Initiation processes can be very varied and complex. They depend on both the polymer nature (PH) and the way that energy is brought to organic material (by temperature or radiation). Although the intermediate steps are not always totally known and understood (mainly because of the lack of sufficiently sensitive analytical methods to elucidate the corresponding structural changes), this problem simplifies considerably because all initiation processes lead finally to the formation of $P^{\bullet}$ and/or $PO_2^{\bullet}$ radicals.

For the sake of simplicity, we will consider only the case of oxygen excess (a relatively thin polymer sample exposed to a relatively high oxygen pressure). In this case, all the $P^{\bullet}$ radicals are almost instantaneously transformed into $PO_2^{\bullet}$ ones and then, their probability of participating in reactions other than reaction 6, in particular reactions 4 and 5, is negligible. As a result, the 'standard oxidation scheme' reduces to four elementary steps (1, 2, 3 and 6). One can distinguish two important initiation processes according to the type of oxidative ageing under consideration.

12.8.1 Initiation of oxidation: initiation at a constant rate (Case 1)

In the case of radiochemical ageing (high energy provided), the main source of radicals is the polymer radiolysis, i.e. the breakdown of lateral bonds of the monomer unit. As an example, in the case of PE, radiolysis leads to the formation of very reactive radicals $H^{\bullet}$ which recombine rapidly by hydrogen atoms abstraction:

$$\sim\!\sim CH_2-CH_2-CH_2\sim\!\sim + h\nu \rightarrow \sim\!\sim CH_2-\dot{C}H-CH_2\sim\!\sim + H^{\bullet}$$

$$H^{\bullet} + \sim\!\sim CH_2-CH_2-CH_2\sim\!\sim \rightarrow \sim\!\sim CH_2-\dot{C}H-CH_2\sim\!\sim + H_2$$

Thus, the corresponding balance initiation can be written:

$$PH \rightarrow P^{\bullet} + \tfrac{1}{2}H_2 \ (r_1)$$

where the initiation rate r_I is proportional to the dose rate I according to:

$$r_1 \approx 10^{-7}\, G_1 I \qquad [12.50]$$

and G_1 is the radical yield expressed in number of radicals $P^{\bullet}$ per 100 eV absorbed, of the order of magnitude of 1–10 for saturated hydrocarbon polymers (Colin *et al.*, 2010). In this case, the reaction rapidly reaches a steady state and oxidation products accumulate with a constant rate (Fig. 12.24).

One can easily demonstrate that initiation and termination products form with a rate proportional to r_1. As an example, if ketones are formed with a yield γ_K in termination:

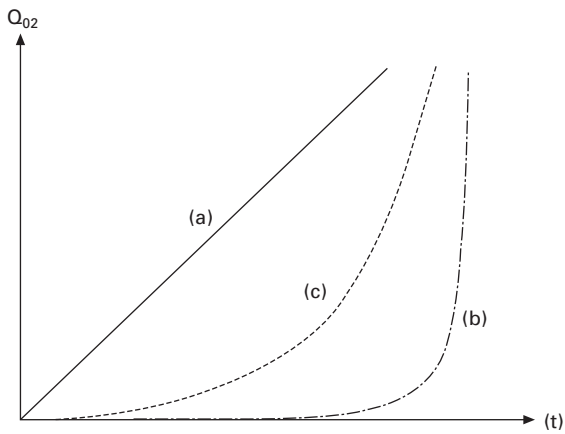

12.24 Shape of oxidation kinetic curves in the case of initiation (a) at constant rate (case of radiochemical ageing); (b) by bimolecular Per decomposition (thermal ageing); and (c) by unimolecular Per decomposition (case of many photochemical ageings).

$$r_K = \gamma_K k_6 [PO_2^\bullet]^2 = \frac{\gamma_K}{2} r_1 \quad [12.51]$$

On the contrary, propagation products form with a rate proportional to the square root of r_1, e.g. for peroxides:

$$r_{Per} = k_3 [PO_2^\bullet][PH] = k_3 [PH] \left(\frac{r_1}{2k_6} \right)^{1/2} \quad [12.52]$$

Finally, oxygen is consumed with a rate:

$$r_{O2} = k_2 [O_2][P^\bullet] - k_6 [PO_2^\bullet]^2 = \frac{r_1}{2} + k_3 [PH] \left(\frac{r_1}{2k_6} \right)^{1/2} \quad [12.53]$$

12.8.2 Initiation of oxidation: initiation by decomposition of peroxides (Case 2)

In the case of thermal and photochemical ageing (lower energy provided), the problem is significantly more complex. Chemical bonds of common industrial polymers rarely have a dissociation energy lower than 260 kJ.mol^{-1} (Table 12.2) and thus decompose only at high temperatures (typically, at $T > 250°C$) or at high irradiation intensities (e.g. under gamma-irradiation in a nuclear environment). However, it has been seen, in the previous sections, that oxidation leads to the formation of two main propagation products: hydroperoxide groups (POOH) and peroxide bridges (POOP), noted as Per, of which the activation energy of the O–O bond is very low: $E_D \approx 150$ kJ.mol^{-1}. Such chemical groups are thermally and photo-chemically unstable, in particular in common use conditions.

It cannot be totally excluded that 'extrinsic species' generate also primary radicals (e.g. decomposition of structural irregularities or direct oxygen–polymer reaction). But it can be easily demonstrated that their contribution to initiation is very limited: the corresponding initiation rate is initially very low and vanishes rapidly (as soon as the 'extrinsic species' concentration vanishes). As a result, in all cases, initiation by Per decomposition rapidly becomes the main source of radicals. From a kinetic modelling point of view, the following approach is usually adopted: the initially present 'extrinsic species' are replaced by a kinetically equivalent initial Per concentration: $[Per]_0$. Thus, initiation involves two important reactions:

$$\delta_{Per} \rightarrow \alpha P^\bullet + \beta PO_2^\bullet \ (k_1)$$

with $\alpha = 2$ and $\beta = 0$ for unimolecular decomposition ($\delta = 1$), and $\alpha = 1$ and $\beta = 1$ for bimolecular decomposition ($\delta = 2$).

Then, the initiation rate depends on Per concentration:

$$r_1 = k_1[\text{Per}]^{\delta} \quad [12.54]$$

This oxidation mechanism is called a 'close-loop mechanism', as it produces its own initiator product (Per). The resulting kinetic curves present an induction period followed by a sharp auto-acceleration, preceding a steady state. The auto-acceleration step is much more progressive in its initial phase when Per decomposition is unimolecular (the case for many photochemical ageings) (see Fig. 12.23).

According to analytical models, the duration of the induction period for a unimolecular decomposition is given by:

$$t_i \approx \frac{5}{2k_1} \quad [12.55]$$

and for a bimolecular decomposition by:

$$t_i \approx \frac{1 - \ln Y_0}{K} \quad [12.56]$$

where $K = k_3[\text{PH}](k_1/k_6)^{1/2}$ and $Y_0 = [\text{Per}]_0/[\text{Per}]_s$

Moreover, in steady state, the Per concentration is:

$$[\text{Per}]_s = -\delta k_1[\text{Per}]^{\delta} + k_3[\text{PO}_2^{\bullet}][\text{PH}] = \left[\frac{k_3^2[\text{PH}]^2}{\delta^2 k_1 k_6}\right]^{1/\delta} \quad [12.57]$$

and the rate of oxygen consumption is:

$$r_{O_2S} = k_2[O_2][\text{P}^{\bullet}] - k_6[\text{PO}_2^{\bullet}]^2 = \frac{2}{\delta^2}\frac{k_3^2[\text{PH}]^2}{k_6} \quad [12.58]$$

12.8.3 Prediction of polymer oxidizability

From the previous kinetic analysis of the 'standard oxidation scheme', it is possible to state that the oxidation kinetic behaviour of a given hydrocarbon polymer matrix depends on two main factors:

- An extrinsic factor (i.e. an external factor to the polymer structure): initiation rate r_1 or initiation rate constant k_1
- An intrinsic factor: ratio $k_3[\text{PH}]/\sqrt{k_6}$.

According to some authors (Korcek *et al.*, 1972), there is a linear relationship between log k_3 and the dissociation energy E_D of CH bonds. Thus, in a first approach, the polymer oxidizability can be roughly estimated from the reactivity of the CH bonds involved (see Table 12.8).

The following global trends can be deduced:

Table 12.8 Order of magnitude of the dissociation energy (E_D) of CH bonds

CH bond	E_D (kJ.mol^{-1})
	465
—CH_3	414
⩽CH_2—CH_2—	393
—CH—	378
—O—CH_2— or ⩽N—CH_2—	376
⩽C=CH—CH_2—	335

- Polymers without CH bonds, e.g. poly(tetrafluoroethylene) (PTFE), or containing exclusively aromatic CH bonds, e.g. poly(ether ether ketone) (PEEK), poly(ether sulfone) (PES) and polyimides (PI), are stable to oxidation.
- Polymers containing exclusively methyl CH bonds, e.g. poly(dimethyl siloxane) (PdMS), or containing methyl and methylene CH bonds, e.g. poly(methyl methacrylate) (PMMA), polycarbonate (PC) and polyethylene (PE), are moderately stable.
- Polymers containing methyne CH bonds, e.g. polypropylene (PP), or methylene CH bonds in the α position of a heteroatom, e.g. poly(methylene oxide) (POM), polyamides (PA) and amine cross-linked epoxy (ACE), are relatively unstable.
- Finally, polymers containing allylic CH bonds, e.g. polyisoprene (PIP) and polybutadiene (PBD), are highly unstable.

The above section has treated oxidation kinetics only through polymer intrinsic stability. But there are other factors of determining importance to take into account, for instance:

- Oxygen diffusivity allows oxygen transport into deeper layers of the material. It is about three orders of magnitude higher in elastomers than in glassy polymers. Thus, at equal reactivity, glassy polymers appear much more stable than elastomers, because their superficial oxidized layer is considerably thinner.
- Polymer sensitivity to macromolecular changes resulting from oxidation is a key factor from the mechanical point of view. As an example, mechanical embrittlement occurs in polypropylene (PP) for a number of chain scissions 10 times lower than in an amorphous polymer. Thus, at equal reactivity, according to this mechanical endlife criterion, PP will be 10 times less stable than an amorphous polymer.

12.8.4 Oxidation-induced spontaneous cracking

Oxidation is kinetically controlled by oxygen diffusion in FRP composites. In other words, in relatively thick FRP structures (typically 2 mm thick), oxidation is restricted to a superficial layer of thickness ℓ_{ox}. As shown previously in this chapter, ℓ_{ox} can be determined from Equation [12.33]. But it can also be estimated from a simple scaling law (Audouin *et al.*, 1994):

$$\ell_{ox} = \left(\frac{DC_S}{r_S}\right)^{1/2} \quad [12.59]$$

where D is the coefficient of oxygen diffusion in the polymer matrix, and C_S and r_S are respectively the equilibrium concentration and consumption rate of oxygen in the superficial layer of the material.

As shown previously, C_S is generally temperature independent, whereas the diffusion coefficient D obeys an Arrhenius law:

$$D = D_0 \exp\left(-\frac{E_D}{RT}\right) \quad [12.60]$$

where D_0 and E_D are respectively the pre-exponential factor and activation energy of oxygen diffusion.

Moreover, the temperature effect on r_S can be satisfyingly approximated by an Arrhenius law:

$$r_S = r_{S0} \exp\left(-\frac{E_r}{RT}\right) \quad [12.61]$$

where r_{S0} and E_r are respectively the pre-exponential factor and activation energy of reactant consumption.

Finally, one can see that ℓ_{ox} also obeys an Arrhenius law:

$$\ell_{ox} = \ell_0 \exp\left(-\frac{E_\ell}{RT}\right) \quad [12.62]$$

where $\ell_0 = (D_0 C/r_{S0})^{1/2}$ and $E_\ell = \frac{1}{2}(E_D - E_r)$.

In most cases of thermal oxidation and hydrolysis, $E_D < E_r$ so that E_ℓ is negative. Thus, ℓ_{ox} is a decreasing function of temperature.

In the case of irradiation-induced chemical ageing, e.g. radio- and photo-oxidation, C_S and D are light intensity independent (Equation [12.60] remains valid). At the opposite, it can be demonstrated that the effect of light intensity I on r_S can be satisfyingly approximated by a simple power law:

$$r_S \propto I^{\alpha} \quad [12.63]$$

with $\alpha = \frac{1}{2}$ in the simplest models.

Thus, ℓ_{ox} is a slowly decreasing function of dose rate given by:

$$\ell_{ox} \propto I^{-\alpha/2} \qquad [12.64]$$

The fact that the thickness of the degraded layer is, in general, a decreasing function of the 'severity' of ageing conditions has been systematically observed by many authors.

Degradation gradients, resulting from diffusion control of chemical reaction kinetics, play an important role from a mechanical point of view. Schematically, an initially ductile/tough and homogeneous polymer sample is progressively transformed into a binary structure, the sample core remaining ductile/tough, whereas the superficial layer becomes brittle and thus highly sensitive to cracking (Colin *et al.*, 2005). A superficial crack can rapidly cross the whole superficial layer thickness and reach the skin–core interface. At this stage, two scenarios can take place (Fig. 12.25):

1. The crack tip blunts and remains restricted to the sample superficial layers.
2. The crack crosses the interface and propagates in the core. Since cracks are a preferred path for penetration of small reactive molecules, the degradation front moves towards deeper layers. A secondary degraded layer, of the same thickness as the primary one, forms beyond the crack tip, and so on. Following this scheme, failure will ultimately occur, even without external loading.

In a first approach, one can consider that the brittle superficial layer is equivalent to a 'natural' notch with the same depth. Fracture mechanics

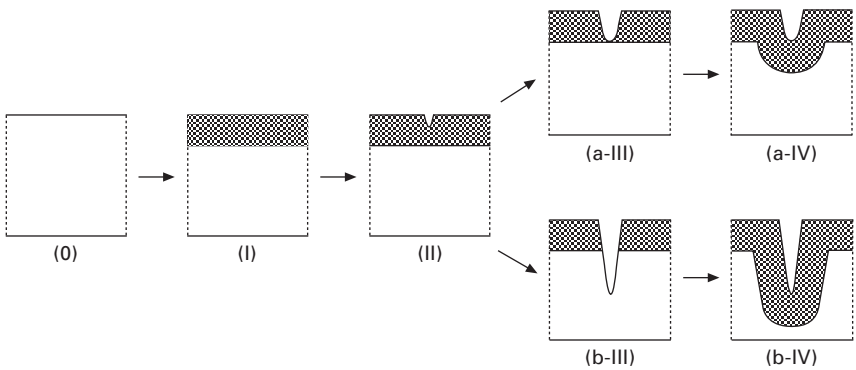

12.25 Schematization of chemical ageing-induced cracking. Sample zones where the polymer chemical structure has been changed are represented in grey. (0) Initial (virgin) sample; (I) superficial degraded layer below its embrittlement threshold; (II) superficial degraded layer close to its embrittlement threshold; (a-III) crack having reached the skin–core interface and having blunted; (b-III) crack having crossed the interface; (a-IV) and (b-IV) propagation of oxidation front towards deeper layers.

(Griffith, 1921) predicts that there is a critical notch depth below which the notch does not initiate the material failure. This depth depends on the material toughness, this latter depending, in turn, on the rate of crack propagation. As an example, in the case of PE oxidation, this depth is of the order of magnitude of 100 μm (Audouin and Verdu, 1991). It is thus expected that rapid chemical ageing, leading to very small thicknesses of degraded layer, will have less effect on the material fracture behaviour than slower ones. This general trend has also been observed by many authors.

12.9 Chemical ageing: stabilization techniques

One can envisage two possible ways of stabilization of the polymer matrix against chemical ageing:

- Internal stabilization will consist in modifying the polymer chemical structure by copolymerization, grafting or substitution, in order to reduce significantly the concentration of unstable groups (ester or amide groups in the case of hydrolysis, aliphatic CH groups in the case of oxidation).
- External stabilization will consist in adding appropriate additives into the polymer matrix either to restrict access by the chemical reactant or to inhibit the chemical reaction.

During the past three decades, many research works have shown a significant improvement in the gas barrier properties of nanofiller reinforced polymer membranes (Espuche, 2011). It was demonstrated that the adding of nanofillers (layered clays, carbon blacks or nanotubes, etc.) into a polymer matrix increases significantly the tortuosity of diffusion paths. Unfortunately, this physical way of external stabilization is still often ignored by practitioners.

In contrast, chemical ways of external stabilization, in particular for inhibiting the chain reaction such as by thermal or photo-oxidation, have long been well known by practitioners. They have been the subject of an abundant literature and reviews (Reich and Stivala, 1969; Hawkins, 1971; Kamiya and Niki, 1978; Zweifel, 2001). There are two main families of antioxidants which can be combined in a polymer matrix in order to constitute efficient synergistic blends of antioxidants:

- F1: Organic sulphides and phosphites decompose hydroperoxides (POOH) into non-radical species and thus reduce significantly the initiation rate of oxidation.
- F2: Hindered phosphites or secondary aromatic amines transform peroxy radicals ($PO_2^{\bullet}$) into hydroperoxides and thus interrupt efficiently the propagation of oxidation.

Except for carbon black, antioxidants are synthetic products. They are relatively expensive and moderately soluble into polymers. Therefore, their

use makes sense only if they are efficient stabilizers at low concentration. The existence of such a property can be attributed to the 'auto-accelerated' character of thermal oxidation kinetics. Indeed, in the induction period, thermal oxidation involves very low concentrations of reactive species (POOH, $PO_2^{\bullet}$) which can thus be efficiently scavenged by low concentrations of antioxidants (Verdu *et al.*, 2003).

12.10 Fibre and interfacial degradation

Although the reinforcing fibres are protected from direct exterior aggression by the embedding polymer matrix, they may experience substantial chemical and physical attack due to the ingress of moisture, alkaline or salt solutions in the FRP composite. In addition, these effects may be emphasized if additional sustained loads are applied to the composite materials. In this section, the various degradation mechanisms are briefly recalled for the main types of fibres used in construction.

12.10.1 Corrosion of glass fibres

Glass fibres are very sensitive to corrosion induced by moisture and aqueous environments (acidic, basic or neutral). The degradation mechanisms are well known and have been extensively reported by various authors (Charles, 1958; Metcalfe *et al.*, 1971; Michalske and Frieman, 1983; Smets, 1985). When a glass fibre is exposed to an aqueous solution, the water first wets the surface and then diffuses into the glass network. Several chemical reactions may then occur between the glass and reactive species from the aqueous solution (H_2O, H_3O^+, OH^- and metal ions produced by dissolving metal hydroxides in water), depending on both the pH of the solution and the composition of the glass:

- A leaching process, i.e. an ion exchange process or the selective removal of soluble constituents, is the predominant phenomenon in acidic media.
- An etching process involving a dissolution of the glass is a common feature in alkaline media.

Corrosion of glass fibres in acidic environments

The degradation of glass in contact with an acidic solution is characterized by an exchange of ions between the surface of the glass and the solution, and is known as a desalkalinization or leaching process. The accepted mechanism involves the replacement of metal ions associated with the glass surface by H^+ from the acid medium, according to the following reaction (Metcalfe and Schmitz, 1972):

$$\overline{M^{n+}} + nH^+ \rightleftharpoons \overline{nH^+} + M^{n+} \quad [12.65]$$

where the bars indicate the species associates with glass. Since protons are smaller in size than the replaced cations, tensile stresses are induced in the surface of the glass and can become large enough to promote cracking. As a result, the composite material may fracture under relatively low mechanical stress, or even spontaneously in the absence of mechanical stress (Jones and Chandler, 1984).

It was originally presumed that the corrosion effect was mainly related to the acidic strength of the solution (H^+ concentration), but later studies showed that the associated anion can also play a significant role if it can form complex or insoluble species with the cations of the glass (Jones and Chandler, 1984). Such complex formation will consume leached cations and drive Equation [12.65] to the right, hence emphasizing the leaching process. This particular phenomenon may explain the severe corrosion effects observed with relatively weak acids such as oxalic acid.

In addition, the tendency of an ion to deplete would be related to the characteristics of this ion (bond energy in the glass network, valence state, hydrated volume). More generally, the extent of corrosion depends on the nature and concentration of the acid, on the glass composition and on the manufacturing process of the glass fibres (Kumosa, 2001).

Corrosion of glass fibres in neutral aqueous solutions

The diffusion of chemical species is the predominant mechanism driving corrosion in neutral solutions. After water diffusion into the glass network, hydration of alkaline oxides present in all glass formulations (even the most resistant) leads to the diffusion of Na^+ and OH^- ions towards the surface and the aqueous medium (Equation [12.66]). Hydroxide ions may then lead to the hydrolysis of siloxane bonds (etching) without being consumed, as shown in Equations [12.67] and [12.68] (Ishai, 1975). This is an autocatalytic process, as the rate of dissolution of the glass increases with time.

$$Si–O–Na + H_2O \rightarrow SiOH + (Na^+, OH^-) \quad [12.66]$$

$$Si–O–Si + OH^- \rightarrow SiOH + SiO^- \quad [12.67]$$

$$SiO^- + H_2O \rightarrow SiOH + OH^- \quad [12.68]$$

Corrosion of glass fibres in alkaline media

The predominant mechanism over pH 10 is the degradation of the silica network (etching). In this case, hydroxide ions of the alkaline solution lead directly to the break-up of Si–O–Si linkages (Equation [12.67]). This effect

is exacerbated by elevated temperatures and prolonged exposures. In the case of civil engineering applications, FRP materials may be embedded in concrete (internal rebars) or in contact with concrete (external strengthening of concrete structures). The concrete pore solution has a pH value in the range 12–13.5, depending on cement formulation. It can severely affect the glass fibres (loss in strength, embrittlement), due to combination of the chemical attack and the growth of hydration products between the glass filaments. Hydroxylation can cause fibre surface pitting, which acts as flaws and degrades the overall mechanical properties (Benmokrane *et al.*, 2006). Several solutions are available for improving the chemical resistance of glass fibres in concrete:

- Alkali resistant (AR) glass fibres have been developed with a specific formulation that includes a substantial amount of zirconia (ZrO_2). The higher the zirconia content, the better the resistance to alkali attack of the fibres.
- The application of a surface coating (styrene acrylic copolymer emulsions, for instance) on individual glass filaments may also protect the glass surface and enhance its alkali resistance.

12.10.2 Corrosion of aramid and carbon fibres

Aramid fibres are also known to be affected by moisture and alkaline environments. Due to the presence of amide functions on the polymer chain, Twaron or Kevlar fibres based on poly(*p*-phenylene terephthalamide) or PPTA, and Technora fibres based on copoly(paraphenylene/3,4'-oxydiphenylene terephthalamide) can all be subjected to hydrolysis. For instance, the hydrolysis mechanism of PPTA fibres involves a scission of the amide N–C linkage and yields acid and amine end-functions, as shown below by Equation [12.69] (Morgan *et al.*, 1984). These chain scissions are responsible for the deterioration of the mechanical strength of the fibres, and such an effect is emphasized by both temperature and exposure time. The pH of the environment is also a crucial parameter: the higher the deviation from neutrality (towards the acid or basic domains), the higher the rate of degradation. Under alkaline conditions, Technora fibres are usually considered more stable than PPTA-based fibres. For instance, following immersion in NaOH solution at 95°C for 100 hours, Technora fibres retain 75% of their tensile strength while PPTA fibres retain only 20% (Imuro and Yoshida, 1986).

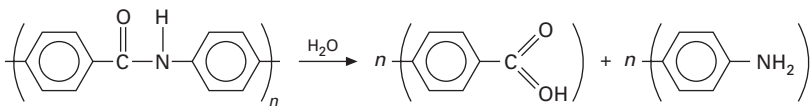

[12.69]

In contrast, carbon fibres are inert under normal service temperatures: they are usually considered insensitive to moisture and only little affected by alkaline environments. Therefore, apparent degradations of carbon fibre-reinforced composite are in general exclusively due to the interaction between the matrix and the environment. Besides, it is of note that galvanic corrosion may occur if CFRP composites are adventitiously placed in contact with metal elements, which usually contributes to accelerated corrosion of the metal components (Tavakkolizadeh and Saadatmanesh, 2001).

12.10.3 Interfacial degradation

The fibre–matrix interphase may be considered the most susceptible component of FRP composites in terms of degradation. First, it must be underlined that this interphase is the locus of many pre-existing defects that were created during the manufacturing process, such as air bubbles or local disbonds related to imperfect wetting of the reinforcing fibres by the polymer, or micro-cracks caused by residual stresses. These defects may grow and coalesce under the action of external loading (for instance, temperature or fatigue cycles), ultimately leading to transverse cracking and fibre–matrix debonding. In the case of hydrothermal ageing, the interphase is a privileged path for the penetration of the water and solutes by capillary action (the contribution of the interphase to the diffusion process in polymer composites has been discussed previously in Section 12.6). Water molecules may then break chemical and physical bonds between the fibres and the matrix by reacting, for instance, with the sizing or coupling agents, hence favouring interfacial debonding. In the case of alkali attacks on the reinforcing fibres, chemical reactions are also initiated from the fibre–matrix interface.

12.11 Flammability of FRP composites

The polymer phase of composite materials used in construction contains large amounts of carbon, hydrogen and nitrogen, which are all flammable to various extents if conditions of ignition are met (arson, vehicle accident, fire caused by cigarettes, adventitious ignition of spilt oil, etc.). In a fire situation, the main health hazard is caused by the release of smoke and toxic gases produced by the combustion of organic compounds; another crucial issue is also the structural integrity of the burning composite structure, as this may prematurely collapse, causing severe injuries to the occupants. Consequently, the problem of fire is a major concern for civil engineers who are planning to use composite materials, and the fire properties should be taken into account in the early design process, while choosing the material constituents (matrix and fibres).

After recalling the basic mechanisms involved in the combustion of

polymer composites, the following sections will describe the main fire reaction properties of these materials and the different fireproofing solutions which can be implemented to enhance their flame resistance. The last part briefly discusses the degradation of the load-bearing capacity of composite-containing structures exposed to fire in the framework of various civil engineering applications (full-composite structures, FRP strengthening/retrofitting, and concrete structures reinforced by FRP rebars).

12.11.1 Combustion principles

A general scheme which summarizes the necessary conditions for combustion to occur is represented by the fire triangle (Fig. 12.26). This scheme involves three factors: the fuel materials (polymer matrix, and in some cases organic fibres), the combustive element (oxygen) and an additional heat source. If one of these factors is removed, the combustion phenomenon will not take place.

Combustion of polymer composites is a complex phenomenon (Fig. 12.27) which is largely governed by the chemical processes involved in the thermal decomposition of the organic phases, i.e., the polymer matrix and the organic fibres (if the latter are used as reinforcing materials). These chemical reactions may occur in three interdependent regions: within the condensed phase, at the interface between the condensed and the gas phase, or in the gas phase. It is generally admitted that combustion involves four main stages, which are *heating*, *thermal decomposition*, *ignition* and *propagation* (Cullis and Hirschler, 1981; Troitzsch, 2004; Mouritz and Gibson, 2006):

1. The initial phase consists in the *heating* of the FRP composite under the effect of an external heat flux produced by a pre-existing fire or a radiant source. The resulting temperature increase leads to the softening or even the melting of the polymer matrix in the case of thermoplastic systems. Thermosetting systems are less affected, due to their cross-

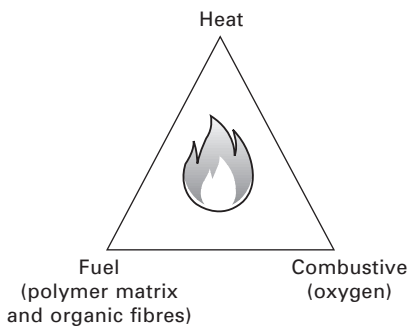

12.26 Representation of the fire triangle.

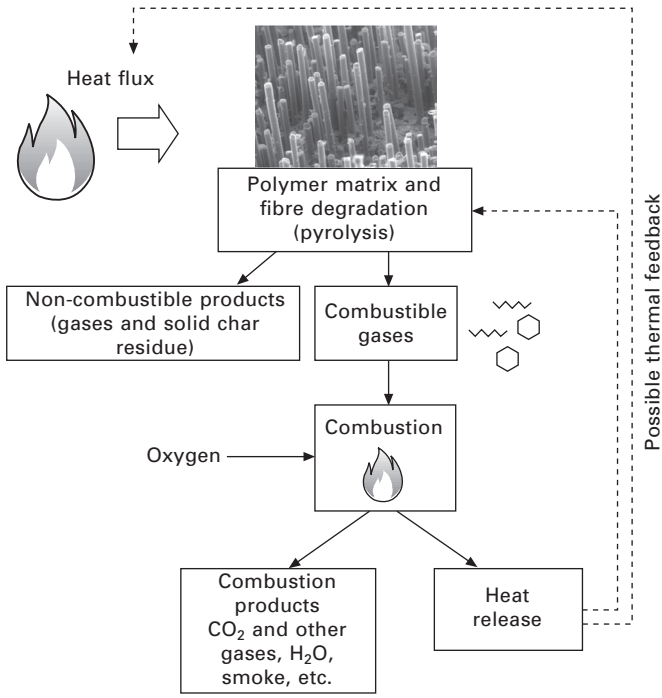

12.27 Schematic diagram of polymer composite combustion.

linked molecular structure, but they experience a substantial drop in mechanical properties over the glass transition temperature (typically in the range 70–180°C for composites used in construction). Globally, the evolution of the polymer composite depends on thermal properties of both polymer matrix and fibres (heat conductivities, thermal diffusivities, heat capacities, etc.).

2. Over a critical temperature (usually between 250 and 400°C), the *degradation* of the polymer composite begins and different types of chemical reactions enter into competition: chain-end scission or depolymerization, random chain scission and degradation of side groups. The weakest chemical bonds are the first to break, followed by bonds of higher dissociation energies as the temperature increases. These degradations generate fragments of low molecular weight, such as monomer, oligomers and other species. This thermal decomposition yields non-flammable products on the one hand (solid carbonaceous char and soot particles), and flammable volatiles on the other hand, including a large amount of hydrocarbon gases. Those volatiles then diffuse across the degraded polymer matrix into the fire environment.
3. The third step involves the *ignition* of the combustible gases, provided

the release rate of the volatile products is high enough to produce a favourable gas mixture with air. This combustion produces highly reactive $H^{\bullet}$ radicals which may combine with oxygen to form $OH^{\bullet}$ radicals, finally leading to the formation of combustion products (CO, CO_2, water and soot particles).

4. The heat released at this level and the subsequent heat transfers (by convection, conduction and radiation) maintain the decomposition process of the polymer composite and may also feed the main fire source. The combustion process is therefore self-sustained.

This cycle stops when one of the parameters involved in the 'fire triangle' is suppressed, usually when the polymer composite has been completely decomposed or when the oxygen content in the fire atmosphere becomes too low.

It is of note that the respective amounts of char and flammable volatiles produced by the thermal decomposition of the composite are highly dependent on the chemical nature of the organic phases, i.e., the polymer matrix and synthetic fibres, if present (Levchnick and Wilkie, 2000; Mouritz, 2007). As regards the main thermosetting polymers used in construction (i.e., polyesters, vinylesters and epoxies), pyrolysis yields a large amount of volatiles but retains a small amount of char (10–20% of the initial mass). FRP composites based on these thermoset matrices are thus highly flammable materials.

In some cases, non-flaming combustions can occur in the form of smouldering or glowing combustions, which propagate within the material by a thermal front or wave. Glowing combustion usually occurs after the initial charring and involves pale flames of carbon burning that forms carbon monoxide. Smouldering combustion generates smoke due to pyrolysis at or near the surface of the material.

12.11.2 Flammability of polymer composites

The fire response of a polymer composite can be described by several reaction properties which determine both the flammability and the fire hazard of the material under consideration (Mouritz and Gibson, 2006; Mouritz, 2007):

- The *flammability* addresses the following questions: (1) how readily the material ignites when exposed to a flame or heat source; (2) once ignited, whether it continues to burn; (3) how rapidly the fire spreads across a surface; and (4) how much heat is released by the combustion and how fast. The main reaction properties that quantify these various parameters are the time-to-ignition, the limiting oxygen index (LOI), the flame spread rate and the heat release rate (HRR).
- The *fire hazard* depends on the characteristics (density, composition and toxicity) of the smoke and toxic gases released during stages of a fire.

Besides, one can also define the *fire resistance* of a composite material or a composite structure as its ability to restrict the spread of fire and to retain mechanical and physical integrity. Key fire resistance parameters include heat transfer, burn-through resistance and structural integrity.

Different tests and standards are available worldwide to assess the fire reaction properties and the fire resistance. They vary from small bench-scale procedures to large-scale room tests. The most popular fire reaction tests remain bench-scale tests because they are quick and inexpensive and yield generally reproducible data. However, such small-scale tests are known to be limited because they do not reproduce exactly the conditions existing in a real fire and they ignore the effects due to fire growth (Babrauskas, 2000). In the following, a brief focus is given to the main fire reaction properties and their most common determination methods.

Time-to-ignition

The time-to-ignition (t_{ig}) characterizes the ease of ignition of the material by defining how quickly the flaming combustion occurs when the material is exposed to a heat source at a given incident heat flux and in an oxygen-controlled environment. It reflects various phenomena, such as the time necessary for the specimen's surface to reach the pyrolysis temperature, as well as the ability of the material to produce a critical concentration of flammable volatile gases during the thermal decomposition process. It is therefore a rough indicator of the flammability resistance. The time-to-ignition can be determined using experimental methods such as the cone calorimeter (ISO 5660-1, 2002; ASTM E 1354, 1990) or the ignitibility test (ISO 11925-2, 2002). As regards composite materials used in construction, tests are usually performed at an incident heat flux of about 50 kW/m^2, which corresponds to the intensity commonly released by a room fire (Mouritz, 2007) and produces a maximum temperature of 700°C at the surface of the material. If tests are reproduced for different heat flux values, time-to-ignition is found to increase as the heat flux is reduced; a linear relationship is usually obtained between t_{ig} (in the case of thermally thin materials with a uniform temperature across the specimen) or $\sqrt{t_{ig}}$ (in the case of thermally thick materials with a gradient of temperature from the surface to the interior) and the external heat flux (Tewarson, 2007). As an illustration, time-to-ignition values found in the literature for several thermoset composites are given in Table 12.9.

Limiting oxygen index

The *limiting oxygen index* (LOI) is defined as the minimum oxygen concentration (in vol%) that is necessary to sustain a stable combustion of the specimen after ignition; it is therefore considered a measure of the ease

Table 12.9 Fire reaction properties of common thermoset composites for an incident heat flux of 50 kW/m^2

Materials	Time-to-ignition (s)	LOI index at 25°C	Peak HRR (kW/m^2)	Total heat released (MJ/m^2)	Flame spread index	Reference
Vinylester/glass:						
– non-fire-retarded	85	–	276	59	156	Sorathia, 2004
– fire-retarded (brominated)	278	–	75	11	27	
Polyester/glass	52	23	299	–	–	Mouritz, 2007
Epoxy/glass	48	–	266	48	11	Sorathia, 2004
	70	38	350	–	11	Mouritz, 2007
Epoxy/carbon	94	–	171	–	–	Sorathia, 2004
	79	41	240		11	Mouritz, 2007
Phenolic/glass:						Sorathia, 2004
– RT cured laminate	121	–	66	18	1	Mouritz, 2007
	146	54	73	–	5.5	
Bismaleimide/glass	141	–	176	60	–	Sorathia, 2004

of extinguishment. LOI tests are performed under standard conditions as specified by ISO 4589 (1996) or ASTM D 2863-70 (1970), with specimens of dimension 80 × 10 × 4 mm^3 placed vertically at the centre of a glass chimney. The test consists in subjecting the sample to a flame ignition in environments containing different oxygen concentrations, then finding the lowest concentration which just allows the specimen to burn with a candle-like flame. The higher the LOI of a polymer material, the lower the heat flux provided by its flame and the higher the flammability resistance. The LOI test is simple to carry out and shows high repeatability and reproducibility. However, it is generally performed at room temperature and does not reproduce a realistic fire environment; it is thus mainly used to compare the relative flammability and rank polymer and composite materials. Table 12.9 reports LOI values taken from the literature for common thermoset composites used in civil engineering. Most of these present LOI indexes between 20 and 40. Besides, the LOI value usually increases when using thermally stable or aromatic matrices (phenolic or bismaleimide) and high glass or carbon fibre contents (Mouritz, 2007; Tewarson, 2007).

Heat released rate

The *heat released rate* (HRR) is considered the most important variable in a fire, since heat release may contribute to the growth and spread of the fire (Babrauskas and Peacock, 1992). HRR mainly depends on the combustion of hydrocarbon volatiles produced during the thermal decomposition of the polymer composite, as shown in Fig. 12.28. It is therefore correlated to the amount of volatiles released by the burning material. The HRR varies continuously during the stages of the fire development (Mouritz and Gibson, 2006). An initial induction period is observed, during which no heat is generated because the surface temperature remains below the decomposition temperature. It is then followed by a sharp increase in the HRR due to the combustion of volatiles released from the sample's surface. The curve then reaches a peak HRR value and starts to decrease progressively, as the formation of char limits both heat transfers towards the underlying substrate and diffusion of combustible gases in the fire environment. Based on this HRR evolution profile, one can define several parameters (Fig. 12.28):

- The *peak heat release rate* (*PHRR*), expressed in W/m^2, corresponds to the maximum release rate during the combustion process. It is generally considered one of the best indicators of flammability; materials with large PHRR values are thus considered to be highly flammable.
- The *total heat released* (*THR*), expressed in J/m^2, is the total amount of energy released by the combustion. Materials which exhibit large THR values contribute to the temperature and the development of the fire.

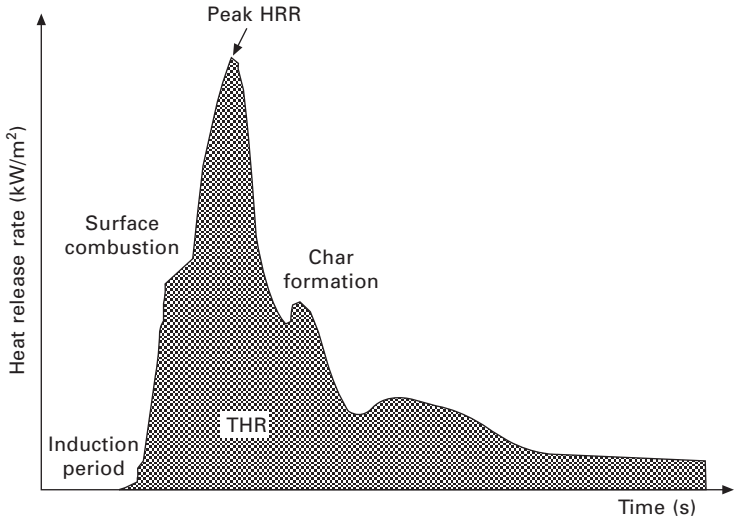

12.28 Profile of the heat release rate versus time for a polymer composite exposed to a constant incident heat flux, after Mouritz and Gibson (2006).

- The *average heat release rate*, expressed in J/m^2, corresponds to the total heat release averaged over a specific period of time (usually 5 minutes); it can be understood as a measure of the heat contribution to a sustained fire.

HRR parameters can be assessed using bench-scale methods or large fire test rooms, depending on the size of the representative specimen (small sample or large structural element). Among bench-scale tests, the cone calorimeter makes it possible to determine both the peak and average HRR, the total heat released, and the ignition properties previously mentioned. The test protocol is standardized according to ASTM E 1354 and ISO 5660-1: specimens of dimensions 100 × 100 × 4 mm^3 are placed on a load cell and exposed to a preset radiant heat flux in the range 0–100 kW/m^2. An electric spark ignition source is used for piloted ignition of the pyrolysis gases. HRR is then calculated from the oxygen concentration and mass flow rate measurements, considering it is proportional to the amount of oxygen consumed. The Ohio State University (OSU) calorimeter is an alternative method used in the United States for measuring the heat release rate, which is covered by ASTM E 906 (1984). Although it generates a greater error than the cone calorimeter (Babrauskas, 2000), several regulatory authorities such as the Federal Aviation Administration have adopted this technique as a standard method.

Table 12.9 reports values of HRR parameters found by various authors for the common thermoset composites used in civil engineering. Values of

the peak HRR and THR are usually ranked in the following order: phenolic/glass << epoxy/glass < vinylester/glass < polyester/glass, suggesting that FRP materials based on phenolic matrices exhibit a much lower flammability and are suitable in the design of fire-safe infrastructures. In addition, it is usually admitted that increasing the amount of glass or carbon fibres leads to a decrease in the HRR properties. This feature can be ascribed to the reduced content of the organic phase, which limits the amount of flammable volatiles (Le Bras *et al.*, 1998).

Spread of flames

The *spread of flames* over the burning material plays an important role in the fire growth. In fires where large surfaces of very flammable materials are involved, the increase in the heat release rate with time is mainly due to the increase in burning area. The flame spread ability of polymer composites can be assessed by several experimental methods. The radiant panel test (ASTM D 3675 for polymer material and ASTM E 162 for other building materials) is probably the most popular and involves subjecting a panel of the test material to a fixed heat flux. The panel itself is angled at 45° to the heater, directed at the panel's top edge. During the test, the rate at which the flame travels down the panel along with the temperature rise are recorded. From these, a Flame Spread Index (FSI) is determined and used to compare different materials to each other; the lower the value of the FSI, the lower the flame spread ability. However, the downward direction of the flame spread is considered unrealistic of a real fire where flame spread is predominately upwards, hence more rapid. Therefore the relevance of the radiant panel test is still a matter of discussion. It can be seen from Table 12.9 that highly flammable thermoset systems such as polyester or epoxy composites present low FSI values associated with rapid flame propagation. In contrast, composites based on phenolic or bismaleimide matrices present a reduced flame spread (high FSI values), in agreement with the superior fire resistance of these polymers shown previously by ignition and heat release rate tests.

12.12 Improving the fire retardancy of FRP composites

As shown in the previous section, most polymer composites used in construction involve highly flammable matrices, such as polyester, vinylester or epoxy resins. Besides, if glass and carbon fibres are generally considered heat resistant, other type of fibres used for specific applications may also exhibit poor fire behaviour (aramid, polyolefins or other polymer fibres, for instance). Therefore, to meet the safety requirements specified in building codes and

standards, it can be necessary to improve the overall fire resistance of the composite material through adequate fire-proofing solutions.

Flame-retardant systems are intended to inhibit or to stop the combustion cycle of the polymer composite. After such a treatment, the material does not become non-combustible, but it is more resistant to ignition, takes more time to burn and generates less heat compared to the original composite. As a function of their nature, flame-retardant systems act either chemically or physically (Troitzsch, 2004; Horrocks and Price, 2001; Laoutid *et al.*, 2009). They can interfere with the various processes involved in the combustion cycle (heating, pyrolysis, ignition and propagation stages) which were previously discussed in Section 12.4.1.

Chemical action of fire retardants may involve:

- *A gas phase mechanism* (also called flame poisoning): flame retardants acting in the gas phase are able to react with $H^{\bullet}$ and $OH^{\bullet}$ radicals present in the gas phase to form inert molecules, thus leading to a marked decrease in the heat balance and a reduction in the fire development. These systems are most often based on halogenated or phosphorus chemicals.
- *Condensed phase mechanisms* (charring effect): at high temperatures, specific silicon- or phosphorus-containing chemicals can initiate cross-linking reactions in the polymer matrix that create a vitreous or ceramic layer with effective barrier properties against both heat transfer and diffusion of volatiles. Another condensed phase mechanism is the intumescence effect in which other additives may favour the formation of a porous carbonaceous char, which also acts as a thermal insulating layer.

Fire retardants may also operate physically, according to the following mechanism:

- *Cooling effect* (heat sink effect): flame retardants that decompose in endothermic reactions are able to cool the fire environment and therefore to slow down the reaction pathway. These additives are usually hydrated minerals or metal hydroxide fillers.
- *Fuel dilution*: by releasing inert gases (H_2O, CO_2, NH_3) during their thermal decomposition, other flame retardants lead to a decrease in the oxygen concentration of the combustible gas mixture. This effect limits the concentration of reagents and decelerates the reaction pathway.
- *Protective layer effect*: some flame-retardant additives lead to the formation of a protective coating or gaseous layer between the combustion medium and the condensed phase. This barrier effect tends to decrease the rate of thermal decomposition and the diffusion of flammable volatiles.

Fire retardants can be sorted in two main categories: (1) additives which are generally incorporated during the manufacturing process and consist of

inorganic filler particles, and (2) reactive chemicals which are introduced at the synthesis stage to modify the chemical structure and reduce the flammability of the polymer matrix. Beside these conventional methods, examples of other fire-proofing solutions receiving increasing interest include (3) the introduction of nanoparticles in the polymer matrix, (4) the application of passive fire-protection systems like insulating coatings, and (5) the use of inorganic matrices. Those various fire-retardant methods will be briefly detailed in the following sections.

12.12.1 Fire-retardant fillers

An efficient and easy way of reducing the flammability of polymer composites consists in dispersing flame-retardant fillers in the liquid matrix during processing. A first catergory of flame-retardant fillers involves inert mineral particles such as calcium carbonate, silica/sand or carbon black. These particles operate mainly through a fuel dilution effect, as a significant part of the flammable polymer matrix is replaced by the non-combustible fillers. The effectiveness of this method is very dependent on the quality of dispersion of the flame-retardant fillers and on their loading content (Horrocks and Price, 2001; Mouritz, 2007); the latter should be preferably higher than 50–60 wt%, so as to reduce substantially the fraction of flammable polymer. On the other hand, one has to keep in mind that such a large amount of filler particles may significantly affect the ultimate mechanical properties of the composite material.

A second type of filler, called active flame-retardant fillers, is considered more effective than inert particles. Its operating mode involves not only fuel dilution, but also an additional cooling or heat sink effect. Indeed, these compounds are able to decompose at elevated temperature via endothermic reactions which absorb energy and tend to slow down thermal degradation of the composite. Besides, inert gases (water vapour, carbon dioxide) are formed by the filler decomposition and contribute to diluting the concentration of combustible volatiles in the flame-environment. Common active flame retardant fillers are:

- Metal hydroxides, in particular aluminium trihydroxide (ATH), which is a low-cost filler, and magnesium dihydroxide (MDH). The endothermic decomposition of $Al(OH)_3$ occurs between 180 and 200°C and leads to the release of water and the formation of an insulating ceramic layer of alumina (Al_2O_3). The use of ATH also reduces the HRR peak and the smoke production. $Mg(OH)_2$ acts in a similar way but its endothermic degradation occurs at a higher temperature (over 300°C) and a protective layer of MgO is formed at the composite surface.
- Zinc borates ($2ZnO.3B_2O_3.3.5H_2O$), which decompose between 300

and 450°C and release water, boric acid and boron oxide (B_2O_3). The later flows at high temperature (over 500°C) form a vitreous protective layer.

Here again, these metal hydroxides and borates must be incorporated in large quantities (around 60%) to obtain a significant effect on the flame properties, hence the possible degradation of mechanical performance.

12.12.2 Flame-retarded matrices

Another fireproofing method consists in modifying the molecular structure of the polymer by introducing organohalogen compounds containing bromine or chlorine during the synthesis or polymerization stages: these compounds can be incorporated in a blend with the polymer, used as polymerization monomers, or grafted on the polymer chains. The acting principle of halogenous derivatives is the interruption of the radical chain mechanism in the gas phase, either by transfer or by recombination reactions (Papazoglou, 2004). Brominated derivatives are considered the most effective halogenous flame retardants, as they can release HBr hydracids very easily; some usual compounds are tetrabromobisphenol-A (TBBPA), which is mainly used with epoxy resins, and polybromodiphenyl ethers (PBDE), which are generally incorporated in polyester and polyolefin matrices (Laoutid *et al.*, 2009). Most but not all halogenated flame retardants are used in conjunction with a synergist to enhance their efficiency. Antimony trioxide is widely used, but other forms of antimony such as the pentoxide and sodium antimonate are also used. An important feature is that fire degradation of halogenated polymer composites generates large amounts of toxic gases in the atmosphere, which is a major concern for both human health and the environment (Horrocks and Price, 2001). This has led many countries to restrict the use of halogenous flame retardants and replace them by more environmentally friendly products such as hydrated mineral fillers, for instance.

Another class of reactive chemical with effective fire-retardant properties is based on phosphorous derivatives (phosphorus, phosphates, etc.). It is mainly used with oxygen or nitrogen-rich polymers like polyesters and polyamides, as it promotes the formation of char during the decomposition of these matrices (Horrocks and Price, 2001; Mouritz, 2007; Laoutid *et al.*, 2009).

12.12.3 Nanoparticles

The potential of nanoparticles for increasing the fire resistance of polymer matrices has been known since the end of the 1990s. Organoclays of the montmorillonite type were the first nanoparticles to be used as flame retardants in polymers. Introducing a low amount of these nanofillers (1 to

5 wt%) in the matrix may improve its fire behaviour, due to the formation of a protective layer during combustion according to various mechanisms (Laoutid *et al.*, 2009):

- Upon heating, the viscosity of the molten nanocomposite decreases, thus facilitating the migration of clay nanoparticles towards the surface of the material.
- Thermal decomposition of surfactants present at the surface of clay creates catalytic sites favouring the formation of a stable char residue.

The accumulation of clay at the surface acts thus as a barrier which limits heat transfers and reduces the release of combustible volatiles into the flame. A substantial decrease in the peak heat release rate of the nanocomposite (25 to 50%) can be achieved compared to the neat polymer (Bourbigot *et al.*, 2006). However, this effect is very dependent on the quality of dispersion of the nanoparticles within the host matrix, and a high degree of exfoliation is usually targeted in order to maximize both the mechanical and fire properties (Hackman and Hollaway, 2006). Other types of nanoparticles, such as silica (SiO_2), titanium dioxide (TiO_2), carbon nanotubes or silesquioxane, have also proven to have significant flame-retardant properties (Laoutid *et al.*, 2009).

Nervertheless, it is admitted that nanofillers are globally less effective than conventional fire retardants (halogenous/phosphorus compounds or metal hydroxides) and nanocomposites are generally unable to meet fire performance standards. Research efforts are currently underway on the combination of nanoparticles with usual fire retardants, preferably non-halogenated, in order to promote synergistic effects (Horrocks and Price, 2001; Laoutid *et al.* 2009). Another promising strategy consists in the surface modification of nanoparticles with surfactants having effective flame-retardant properties instead of conventional ammonium salts.

12.12.4 Protective coatings

Another effective solution for protecting composites against fire involves the use of flame-resistant paints or coatings. Such coatings can be classified among the following categories (Mouritz, 2007):

- *Intumescent coatings*: Under the action of heat, these systems evolve gases and swell to form a voluminous foamed char. Thanks to its high porosity content, this char acts as an insulative barrier and protects the underlying substrate from heat. These coatings are very effective for delaying ignition and reducing the heat release rate properties. A typical intumescent system consists of charring agents (carbon donors such as polyalcohols) and blowing agents (whose thermal decomposition yields CO_2 or NH_3, such as melamine) (Papazoglou, 2004).

- *Ceramic coatings*: Based on silica, zirconia, alumina, etc., they provide high heat insulation to the underlying material and are non-flammable,
- *Flame-retardant films*: These are based on fire-resistant polymers that contain halogenous or phosphorous flame retardants which act in the gas phase.

12.12.5 Mineral matrices

Over the past years, significant researches have been conducted to develop inorganic matrices as an alternative to thermosetting polymers in composite materials. For instance, fibre-reinforced cement matrix (FRCM) composites were developed for the strengthening/retrofitting of concrete or masonry structures (Triantafillou and Papanicolaou, 2006; Bournas *et al*., 2007; Faella *et al*., 2010; De Caso y Basalo *et al*., 2012). These mineral matrix composites exhibit very similar outstanding mechanical properties to their organic counterparts (Bournas *et al*., 2007). In addition, they present many advantages over polymer composites, such as improved thermal and fire resistance, no emission of toxic smoke in fire events, no release of hazardous compounds (solvents, aromatic volatiles) during the manufacturing process and the in-service period, enhanced compatibility with concrete and other mineral substrates, and lower price.

Geopolymers are another class of inorganic materials with very interesting prospects for the composite industry (Davidovits, 2008). These materials, based on the chemistry of polysialates $(–Si–O–Al–O–)_n$, are a particular type of alumino-silicates. In specific conditions (usually in an alkaline environment), these silicate molecules can react by polycondensation at low temperatures (room temperature to 150°C) and form a mineral macromolecular network very similar to that of an organic polymer. Depending on the atomic ratio of Si:Al, one can obtain either linear molecular structures comparable to that of thermoplastic polymers (high ratios over 15), or tridimensional networks analogous to that of thermosetting polymers (low Si:Al ratios). Geopolymer matrices are compatible with various types of fibres (aramid, basalt, carbon, glass and even ceramic fibres) and can be processed to form composite laminates. This type of matrix can withstand temperatures higher than 1000°C without producing any smoke, and carbon fibre-reinforced geopolymer composites can retain about 63% of their original strength after long-term exposure to 800°C (Lyon *et al*., 1997).

12.13 Structural integrity of FRP composites exposed to fire

As previously mentioned, mechanical properties of polymer composites degrade at elevated temperatures. This degradation is more pronounced for

resin-dominated properties (compression and shear) than for fibre-dominated properties (tension), since the polymer matrix is the first component to be affected by viscoelastic softening and pyrolysis processes.

Around the glass temperature of the polymer matrix (typically in the range 70–150°C for composites used in construction) FRP materials soften, creep and distort. Over T_g, both stiffness and strength rapidly decrease with temperature. This drastic weakening of the mechanical properties often leads to buckling failure of load-bearing composite structures (Mouritz, 2007). At higher temperatures (in the range 300–500°C), the matrix starts to decompose and fibres may also experience softening (for glass fibres) and oxidative degradation (carbon fibres).

As regards thick structural elements exposed to fire, it is to be noted that the temperature is not uniform through the composite section due to the low thermal conductivity. Only a part of the structure is over T_g and the thermal front advances gradually over time. Mechanical loads are thus supported by the part of the structure which remains below T_g, so long as these loads do not exceed the capacity of the active region. A critical issue is to ensure that the mechanical functions of the structure are not compromised during the fire scenario (at least for 30 minutes), so as to permit the intervention of firefighters (Sorathia, 2004). Mouritz and Gibson (2006) have developed a simple modelling approach for evaluating the time-to-failure of such load-bearing structures in fire; however, due to the complexity and the non-linearity of the composite response, full-scale testing is usually required.

With regard to civil concrete structures externally reinforced by bonded FRP composites, the load-carrying capacity under fire conditions is primarily influenced by the thermo-mechanical behaviour of the adhesive (Ahmed and Kodur, 2011). When the temperature of the adhesive layer reaches T_g, bond properties (shear and bond strength) of the glue drop considerably, which affects the load transfer in the adhesive joint and compromises the effectiveness of the reinforcing technique, ultimately leading to debonding of the FRP composite (Di Tommaso *et al.*, 2001; Gamage *et al.*, 2006). In this context, ACI guidelines (ACI Committee 440 2R-08, 2008) consider no contribution from the FRP reinforcements to the load-carrying capacity of reinforced concrete elements in the case of fire events. It is thus recommended to ensure a convenient thermal insulation to prevent the temperature of the FRP reinforcement from reaching T_g.

For concrete structures reinforced by FRP rebars, exposure to fire also induces a progressive rise of the internal temperature. As FRP rebars are embedded in concrete, the lack of oxygen will inhibit their burning. However, if temperature within the structure exceeds T_g, softening of the polymer matrix may compromise the stress transfer at the concrete/rebar interface and lead to bond failure (Saafi, 2002). This may result in increased load deflection and ultimately to the collapse of the structure. It has been demonstrated that

the temperature of the rebars is dependent upon the concrete cover (Saafi, 2002); recommendation on minimal concrete covers may be included in future guidelines to ensure fire resistance, but further research is still needed at this stage (ACI Committee 440.1R-06, 2006).

12.14 Conclusion and future trends

During the last decade, there have been continuous improvements in the selection of constitutive materials, in the manufacturing processes and the field implementation of polymer composites for civil engineering applications. The use of FRP materials as externally bonded reinforcement is now an attractive solution to increase the lifespan of existing concrete infrastructures, while their use as internal reinforcing bars or as structural members is intended to prevent corrosion problems and increase the overall durability of new constructions exposed to severe environments. Nevertheless, key issues regarding the long-term durability of FRPs for infrastructure applications have been only partially addressed, and there remain considerable needs for research and development in this field:

- Durability test methods lack standardization and are not always representative of realistic service conditions; it is therefore essential to develop standard accelerated ageing tests that correspond to actual *in-situ* environments. In particular, significant effort should be undertaken to study the synergistic effects between environmental factors (moisture, temperature, alkalinity, chemical attacks) and mechanical loads (sustained loads, fatigue) at both the material and structural scales.
- As the durability of FRP materials is largely dependent on the environmental resistance of the polymer matrix, and as existing cold-curing polymers used in construction are more vulnerable to environmental degradation than high-temperature systems, development of appropriate cold-curing formulations or alternative polymer-based systems is an important means of improvement. Specific degradation mechanisms involved in the case of partially cured or undercured polymer matrices/adhesives should also be investigated in greater detail.
- Besides, it is necessary to improve service life models in order to accurately predict the long-term behaviour of FRP systems used in infrastructure applications. In this line, the development of theoretical approaches coupling both mechanical aspects and physico-chemical degradation processes is of primary interest. Moreover, methods for extrapolating service life predictions from short-term tests are also required. In the end, the challenge is always to determine appropriate reduction or knockdown factors that could be implemented in the design guidelines.

Another important durability-related issue is the fire behaviour of FRP

materials used in construction, which remains partially unknown. In particular, the relationships between the fire reaction properties at the material scale and the full-scale structural performance under fire events still require further investigation. Predictive models must also be developed in order to better evaluate the fire behaviour of FRP structures.

12.15 Sources of further information and advice

Design guidelines related to FRP composites in civil engineering

ACI Committee 440.1R-06 (2006), *Guide for the Design and Construction of Concrete Reinforced with FRP Bars*, ACI, Farmington Hills, MI, USA.

ACI Committee 440.2R-08 (2008), *Guide for the Design and Construction of Externally Bonded FRP Systems for Strengthening Concrete Structures*, ACI, Farmington Hills, MI, USA.

AFGC (2011), *Réparation et renforcement des structures en béton au moyen des matériaux composites*, Technical report, Bulletin scientifique et technique de l'AFGC, in French.

CNR (2004), *Guide for the Design and Construction of Externally Bonded FRP Systems for Strengthening Existing Structures – Materials, RC and PC Structures, Masonry Structures*, CNR-DT 200/2004, Italian National Research Council, Rome, Italy.

CSA (2002), *Design and Construction of Building Components with Fibre-reinforced Polymers*, CSA-S806-02 (R2007), Canadian Standards Association (CSA) International, Toronto, Canada.

JSCE (1997), Recommendation for Design and Construction of Concrete Structures using Continuous Fibre Reinforcing Materials, *Concrete Engineering Series 23*, Japan Society of Civil Engineers, Tokyo, Japan.

JSCE (2001), Recommendation for Upgrading of Concrete Structures with Use of Continuous Fibre Sheets, *Concrete Engineering Series 41*, Japan Society of Civil Engineers, Tokyo, Japan.

Standard test methods

ASTM D 2863-70 (1970), *Standard Test Method for Measuring the Minimum Oxygen Concentration to Support Candle-like Combustion of Plastics (Oxygen Index)*, The American Society for Testing and Materials, Philadelphia, USA.

ASTM D 3675-98 (1998), *Standard Test Method for Surface Flammability of Flexible Cellular Materials Using a Radiant Heat Energy Source*, The American Society for Testing and Materials, Philadelphia, USA.

ASTM E 1354–90 (1990), *Standard Test Method for Heat and Visible Smoke*

Release Rates for Materials and Products Using an Oxygen Consumption Calorimeter, The American Society for Testing and Materials, Philadelphia, USA.

ASTM E 906-83 (1984), *Standard Test Method for Heat and Visible Smoke Release Rates for Materials and Products*, The American Society for Testing and Materials, Philadelphia, USA.

ISO 11925-2 (2002), *Reaction to Fire Tests – Ignitability of Building Products Subjected to Direct Impingement of Flame – Part 2: Single-flame Source Test*, International Organization for Standardization, Geneva, Switzerland.

ISO 4589 (1996), *Plastics – Determination of Burning Behaviour by Oxygen Index*, International Organization for Standardization, Geneva, Switzerland.

ISO 5660-1 (2002), *Reaction to Fire Tests – Heat Release, Smoke Production and Mass Loss Rate – Part 1: Heat Release Rate (Cone Calorimeter Method)*, International Organization for Standardization, Geneva, Switzerland.

12.16 References

Ahmed, A., Kodur, V.K.R. (2011). Effect of bond degradation on fire resistance of FRP-strengthened reinforced concrete beams, *Composites Part B*, 42, 226–237. doi:10.1016/j.compositesb.2010.11.004

Amdouni, N. (1989). Caractérisation et role d'une interphase élastomère au sein de matériaux composites polyépoxy/renforts de verre, PhD thesis, University of Lyon, France.

Ashbee, K.H.G., Wyatt, R.C. (1969). *Proceedings of the Royal Society*, A312, 553–564. doi:10.1098/rspa.1969.0175

Ashbee, K.H.G., Frank, F.C., Wyatt, R.C. (1967). *Proceedings of the Royal Society*, A300, 415–419. doi:10.1098/rspa.1967.0179

Assadi, R., Colin, X., Verdu, J. (2004). *Polymer*, 45(13), 4403–4412. doi:10.1016/j.polymer.2004.04.029

Audouin, L., Verdu, J. (1991). In: *Radiation Effects on Polymers*, Clough, R.L., Shalaby, S.W. (eds), ACS Symposium Series 475, American Chemical Society, Washington DC, 473–484.

Audouin, L., Langlois, V., Verdu, J., De Bruijn, J.C.M. (1994). *Journal of Materials Science*, 29(3), 569–583. doi: 10.1007/BF00445968

Babrauskas, V. (2000). Fire test methods for evaluation of fire retardant efficacy in polymeric materials. In: *Fire Retardancy of Polymeric Materials*, Grand, A.F., Wilkie, C.A. (eds), Marcel Dekker, New York.

Babrauskas, V., Peacock, R.D. (1992). Heat release rate: the single most important variable in fire hazard, *Fire Safety Journal*, 18, 255–272. doi:10.1016/0379-7112(92)90019-9

Bank, L.C. (2006). *Composites for Construction: Structural Design with FRP Materials*, John Wiley & Sons, Hoboken, NJ.

Barjasteh, E., Bosze, E.J., Tsai, Y.I., Nutt, S.R. (2009). *Composites Part A: Applied Science and Manufacturing*, 40, 2038–2045. doi:10.1016/j.compositesa.2009.09.015

Bellenger, V., Verdu, J., Ganem, M., Mortaigne, B. (1994). *Polymer and Polymer Composites* 2, 17–25.

Bellenger, V., Ganem, M., Mortaigne, B., Verdu, J. (1995). *Polymer Degradation and Stability*, 49(1), 91–97. doi:10.1016/0141-3910(95)00049-R

Benmokrane, B., Wang, P., Pavate, T., Robert, M. (2006). Durability of FRP composites for civil infrastructure applications. In: *Durability of Materials and Structures in Building and Civil Engineering*, Wu, C.W., Bull, J.W. (eds), Whittles Publishing, Dunbeath, UK, 300–343.

Benzarti, K., Cangemi, L., Dal Maso, F. (2001). Transverse properties of unidirectional glass/epoxy composites: influence of fibre surface treatments, *Composites Part A: Applied Science and Manufacturing*, 32, 197–206. doi:10.1016/S1359-835X(00)00136-6

Benzarti, K., Chataigner, S., Quiertant, M., Marty, C., Aubagnac, C. (2011). Accelerated ageing behaviour of the adhesive bond between concrete specimens and FRP overlays, *Construction and Building Materials*, 25(2), 523–538. doi:10.1016/j.conbuildmat.2010.08.003

Bernier, G.A., Kambour, P. (1968). *Macromolecules,* 1, 393–400. doi: 10.1021/ma60005a005

Bicerano, J. (2002). *Prediction of Polymer Properties*, 3rd edition, Marcel Dekker, New York.

Bolland, J.L., Gee, G. (1946). *Transactions of the Faraday Society*, 42, 236–252. doi: 10.1039/TF9464200236

Bourbigot, S., Duquesne, S., Jama, C. (2006). Polymer nanocomposites: how to reach low flammability? *Macromolecular Symposia*, 233, 180–190. doi: 10.1002/masy.200690016

Bournas, D.A., Lontou, P.V., Papanicolaou, C.G., Triantafillou, T.C. (2007). Textile-reinforced mortar versus fibre-reinforced polymer confinement in reinforced concrete columns, *ACI Structural Journal*, 104, 740–748.

Carter, H.G., Kibler, K.G. (1978). *Journal of Composite Materials*, 12, 118–131. doi: 10.1177/002199837801200201

Charles, R.J. (1958). Static fatigue of glass Part I, *Journal of Applied Physics*, 29, 1549–1560. doi.org/10.1063/1.1722991

Charlesby, A., Pinner, S.H. (1959). *Proceedings of the Royal Society*, A249, 367–386. doi:10.1098/rspa.1959.0030

Chateauminois, A., Vincent, L., Chabert, B., Soulier, J.P. (1994). Study of the interfacial degradation of a glass-epoxy composite during hygrothermal ageing using water diffusion measurements and dynamic mechanical thermal analysis, *Polymer*, 35, 4766–4774. doi:10.1016/0032-3861(94)90730-7

Colin, X., Verdu, J. (2003). Plastics rubber and composites, *Macromolecular Engineering*, 32(8/9), 349–356.

Colin, X., Mavel, A., Marais, C., Verdu, J. (2005). *Journal of Composite Materials*, 39, 1371–1389. doi:10.1177/0021998305050430

Colin, X., Audouin, L., Verdu, J. (2007). *Polymer Degradation and Stability*, 92, 886–897, 898–905, 906–914. doi:10.1016/j.polymdegradstab.2007.01.017, doi.org/10.1016/j.polymdegradstab.2007.01.004, doi.org/10.1016/j.polymdegradstab.2007.01.013

Colin, X., Richaud, E., Verdu, J., Monchy-Leroy, C. (2010). *Radiation Physics and Chemistry*, 79, 365–370. doi.org/10.1016/j.radphyschem.2009.08.019

Coquillat, M., Verdu, J., Colin, X., Audouin, L., Nevière, R. (2007). *Polymer Degradation and Stability*, 92, 1326–1333, 1334–1342, 1343–1349. doi:10.1016/j.polymdegradstab.2007.03.020, doi:10.1016/j.polymdegradstab.2007.03.019, doi.org/10.1016/j.polymdegradstab.2007.03.018

Crank, J., Park, G.S. (1968). *Diffusion in Polymers*, Academic Press, London.

Crawford, C.D., Lesser, A.J. (1999). *Polymer Engineering and Science*, 39, 385–392. doi: 10.1002/pen.11425

Cullis, C.F., Hirschler, M. (1981). *The Combustion of Organic Polymers*, Clarendon Press, Oxford, UK.

Cunliffe, A.V., Davis, A. (1982). *Polymer Degradation and Stability*, 4, 17–37. doi:10.1016/0141-3910(82)90003-9

Davidovits, J. (2008). *Geopolymer Chemistry and Applications*, Institut Géopolymère, Saint-Quentin, France.

De Caso y Basalo, F.B., Matta, F., Nanni, A. (2012). Fibre reinforced cement-based composite system for concrete confinement, *Construction and Building Materials*, 32, 55–65. doi:10.1016/j.conbuildmat.2010.12.063

De Lorenzis, L., Teng, J.G. (2007). Near-surface mounted FRP reinforcement: An emerging technique for strengthening structures, *Composites Part B: Engineering*, 38, 119–143. doi:10.1016/j.compositesb.2006.08.003

Derrien, K., Gilormini, P. (2006). In: *Proceedings of the DSL 2006 Conference*, *Defect and Diffusion Forum*, 258/260, 447–452.

Di Benedetto, A.T., Lex, P.J. (1989). *Polymer Engineering and Science*, 29, 543–555. doi: 10.1002/pen.760290809

Di Benedetto, A.T., Scola, D.A. (1980). *Journal of Colloid and Interface Science*, 74, 150–162. doi:10.1016/0021-9797(80)90178-2

Di Marzio, E.A. (1964). *Journal of Research of the National Bureau of Standards: Section A: Physics and Chemistry*, 68, 611–617.

Di Tommaso, A., Neubauer, U., Pantuso, A., Rostasy, F.S. (2001). Behaviour of adhesively bonded concrete–CFRP joints at low and high temperatures, *Mechanics of Composite Materials*, 37, 327–338. doi: 10.1023/A:1012392703519

Didierjean, S. (2004). Etude du comportement de matériaux composites carbone/epoxy en environnement hygrothermique, PhD thesis, University of Paul Sabatier, Toulouse, France.

El Mazry, C., Correc, O., Colin, X. (2012). A new kinetic model for predicting polyamide 6–6 hydrolysis and its mechanical embrittlement, *Polymer Degradation and Stability*, 97, 1049–1059. doi:10.1016/j.polymdegradstab.2012.03.003

Espuche, E. (2011). Gas diffusion in multiphase polymer systems. In: *Handbook of Multiphase Polymer Systems*, vol. 2/2, Boudenne, A., Ibos, L., Candau, Y., Thomas, S. (eds), John Wiley & Sons, Chichester, UK, Chapter 21, 749–775.

Faella, C., Martinelli, E., Nigro, E., Paciello, S. (2010). Shear capacity of masonry walls externally strengthened by a cement-based composite material: An experimental campaign, *Construction and Building Materials*, 24, 84–93. doi:10.1016/j.conbuildmat.2009.08.019

Fayolle, B., Audouin, L., Verdu, J. (2002). *Polymer Degradation and Stability*, 75, 123–129. doi:10.1016/S0141-3910(01)00211-7

Fayolle, B., Richaud, E., Colin, X., Verdu, J. (2008). *Journal of Materials Science*, 43, 6999–7012. doi: 10.1007/s10853–008-3005-3

Fetters, L.J., Lohse, D.J., Graessley, W.W. (1999). *Journal of Polymer Science: Part B: Polymer Physics*, 37, 1023–1033. doi: 10.1002/(SICI)1099-0488(19990515)37:10<1023::AID-POLB7>3.0.CO;2-T

Flory, P.J. (1953). *Principles of Polymer Chemistry*, Cornell University Press, Ithaca, NY.

Fox, T.G., Flory, P.J. (1954). *Journal of Polymer Science*, 14, 315–319. doi: 10.1002/pol.1954.120147514

Gamage, J., Al-Mahaidi, R., Wong, M.B. (2006). Bond characteristics of CFRP plated concrete members under elevated temperatures, *Composite Structures*, 75, 199–205. doi :10.1016/j.compstruct.2006.04.068

Gaudichet-Maurin, E., Thominette, F., Verdu, J. (2008). *Journal of Applied Polymer Science*, 109, 3279–3285. doi: 10.1002/app.24873

Gautier, L., Mortaigne, B., Bellenger, V., Verdu, J. (1999). *Polymer*, 41, 2481–2490. doi :10.1016/S0032-3861(99)00383-3

George, S., Thomas, S. (2001). *Progress in Polymer Science*, 26, 985–1017. doi:10.1016/S0079-6700(00)00036-8

Gillen K.T., Wise J., Clough R.L. (1995). General solution for the basic autoxidation scheme, *Polymer Degradation and Stability*, 47 (1), 149–161.

Greco, R., Ragosta, G. (1987). *Plastics and Rubber Processing and Applications*, 7, 163–171.

Griffith, A.A. (1921). *Philosophical Transactions of the Royal Society, Series A*, 221, 163–198. doi:10.1098/rsta.1921.0006

Hackman, I., Hollaway, L. (2006). Epoxy-layered silicate nanocomposites in civil engineering. *Composites Part A: Applied Science and Manufacturing*, 37, 1161–1170. doi:10.1016/j.compositesa.2005.05.027

Hahn, H.T. (1987). *Journal of Engineering Materials and Technology*, 109, 3–11. doi:10.1115/1.3225930

Hawkins, W.L. (1971). *Polymer Stabilization*, Wiley-Interscience, New York.

Hoh, K.-P., Ishida, H., Koenig, J.L. (1990). *Polymer Composites*, 11(3), 192–199. doi: 10.1002/pc.750110308

Hollaway, L.C. (2001). Part 7: Fibre composites. In: *Construction Materials: Their Nature and Behaviour*, Illstone, J.M., Domone, P.L.J. (eds), Spon Press, London, 369.

Hollaway, L.C. (2010). A review of the present and future utilisation of FRP composites in the civil infrastructure with reference to their important in-service properties, *Construction and Building Materials*, 24, 2419–2445. doi.org/10.1016/j.conbuildmat.2010.04.062

Hopfenberg, H.B. (1974). *Permeability of Plastic Films and Coatings in Gases, Vapors, and Liquids*, Plenum Press, New York.

Horrocks, A.R., Price, D. (2001). *Fire Retardant Materials*, CRC Press, Boston, MA.

Imuro, H., Yoshida, N. (1986). Differences between HM-50 and PPTA-aramides, *Proceedings of the 25th International Man Made Fibres Congress*, Dornbirn, Austria, 1–23.

Ishai, O. (1975). Environmental effects on deformation, strength, and degradation of unidirectional glass-fibre reinforced plastics. I. Survey, *Polymer Engineering and Science*, 15, 486–490. doi: 10.1002/pen.760150703

Ishida, H. (1984). *Polymer Composites*, 5, 101–123. doi: 10.1002/pc.750050201

Ishida, H., Koenig, J.L. (1980). *Journal of Polymer Science: Part B: Polymer Physics*, 18, 1931–1943. doi: 10.1002/pol.1980.180180906

Jacques, B., Werth, M., Merdas, I., Thominette, F., Verdu, J. (2002). *Polymer*, 43, 6439–6447. doi:10.1016/S0032-3861(02)00583-9

Jones, R.L., Chandler, H.D. (1984). Strength loss in E-glass fibres treated in strong solutions of mineral acids, *Journal of Materials Science*, 19, 3849–3854. doi: 10.1007/BF00980747

Kaelble, D.H., Dynes, P.J., Crane, L.N., Maus, L. (1975). *Journal of Adhesion*, 7, 25–54. doi:10.1080/00218467508078896

Kaelble, D.H., Dynes, P.J., Maus, L. (1976). *Journal of Adhesion*, 8, 121–144. doi:10.1080/00218467608075078

Kamiya, Y., Niki, E. (1978). In: *Aspects of Degradation and Stabilisation of Polymers*, Jellinek, H.H.G. (ed.), Elsevier, New York, Chapter 3, 79–147.

Karbhari, V. (2007). *Durability of Composites for Civil Structural Applications*, Woodhead Publishing, Cambridge, UK.

Karbhari, V.M., Chin, J.W., Hunston, D., Benmokrane, B., Juska, T., Morgan, R. *et al*. (2003). Durability gap analysis for fibre-reinforced polymer composites in civil infrastructure, *Journal of Composites for Construction*, 7, 238–247. doi:10.1061/(ASCE)1090-0268(2003)7:3(238)

Kausch, H.H., Heymans, N., Plummer, C.F., Decroly, P. (2001). *Matériaux Polymères. Propriétés Mécaniques et Physiques*, Presses Polytechniques et Universitaires Romandes, Lausanne, Switzerland.

Keller, T. (2006). *Material Tailored Use of FRP Composites in Bridge and Building Construction*, Swiss Federal Institute of Technology, Lausanne, Switzerland.

Kennedy, M.A., Peacock, A.J., Mandelkern, L. (1994). *Macromolecules*, 27, 5297–5310. doi: 10.1021/ma00097a009

Kondo, K., Taki, T. (1982). *Journal of Composite Materials*, 16, 82–93. doi:10.1177/002199838201600201

Korcek, S., Chenier, J.H.B., Howard, J.A., Ingold, K.U. (1972). *Canadian Journal of Chemistry* 50, 2285–2297. doi: 10.1139/v72-365

Kumosa, M. (2001). Fracture analysis of composite high voltage insulators, *Centre for Advance Materials and Structures*, 67, 269.

Laoutid, F., Bonnauda, L., Alexandreb, M., Lopez-Cuestac, J.-M., Dubois, P. (2009). New prospects in flame retardant polymer materials: from fundamentals to nanocomposites, *Materials Science and Engineering: R: Reports*, 63, 100–125. doi:10.1016/j.mser.2008.09.002

Le Bras, M., Bourbigot, S., Mortaigne, B., Cordellier, G. (1998). Comparative study of the fire behaviour of glass fibre insaturated polyesters using a cone calorimeter, *Polymers and Polymer Composites*, 6, 535–539.

Le Huy, H.M., Bellenger, V., Verdu, J., Paris, M. (1993). *Polymer Degradation and Stability*, 41, 149–156. doi:10.1016/0141-3910(93)90037-J

Levchnick, S., Wilkie, C.A. (2000). Char formation. In: *Fire Retardancy of Polymeric Materials*, Grand, A.F., Wilkie, C.A. (eds), Marcel Dekker, New York, 171–215.

Lyon, R.E., Balaguru, P., Foden, A.J., Sorathia, U., Davidovits, J. (1997). Fire resistant aluminosilicate composites, *Fire and Materials*, 21, 67–73. doi: 10.1002/(SICI)1099-1018(199703)21:2<67::AID-FAM596>3.0.CO;2-N

Masaro, L., Zhu, X.X. (1999). *Progress in Polymer Science*, 24, 731–775. doi:10.1016/S0079-6700(99)00016-7

Mays, G.C., Hutchinson, A.R. (1992). *Adhesives in Civil Engineering*, Cambridge University Press, Cambridge, UK.

McCall, D.W., Douglass, D.C., Blyler Jr, L.L., Johnson, G.E., Jelinski, L.W., Bair, H.E. (1984). *Macromolecules*, 17, 1644–1649. doi: 10.1021/ma00139a001

McKague, E.L., Halkias, E., Reynolds, J.D. (1975). *Journal of Composite Materials*, 9, 2–9. doi:10.1177/002199837500900101

Merdas, I., Thominette, F., Tcharkhtchi, A., Verdu, J. (2002). *Composites Science and Technology*, 62, 487–492. doi:10.1016/S0266-3538(01)00138-5

Merdas, I., Thominette, F., Verdu, J. (2003). *Polymer Degradation and Stability*, 79, 419–425. doi:10.1016/S0141-3910(02)00358-0

Metcalfe, A.G., Schmitz, G.K. (1972). Mechanisms of stress corrosion in E-glass filaments, *Glass Technology*, 13, 5–16.

Metcalfe, A.G., Gulden, M.E., Schmitz, G.K. (1971). Spontaneous cracking of glass filaments, *Glass Technology*, 12, 15–23.

Michalske, T.A., Frieman, S.W. (1983). A molecular mechanism for stress corrosion in vitreous silica, *Journal of the American Ceramic Society*, 66, 284–288. doi: 10.1111/j.1151-2916.1983.tb15715.x

Morgan, R.J., Pruneda, C.O., Butler, N., Kong, F.-M., Caley, L., Moore, R.L. (1984). The hydrolytic degradation of Kevlar 49 fibres, *Proceedings of the 29th National SAMPE Symposium*, 891–900.

Mortaigne, B., Bellenger, V., Verdu, J. (1992). *Polymer Networks and Blends*, 2, 187–195.

Mouritz, A.P. (2007). Durability of composites exposed to elevated temperature and fire. In: *Durability of Composites for Civil Structural Applications*, Karbhari, V.M. (ed.), Woodhead Publishing, Cambridge, UK, 98–125.

Mouritz, A.P., Gibson, A.G. (2006). *Fire Properties of Polymer Composite Materials*, Springer, Dordrecht, The Netherlands.

Müller-Plathe, F. (1994). *Polymerica Acta*, 45, 259–293. doi: 10.1002/actp.1994.010450401

Nait-Ali, K.L., Colin, X., Bergeret, A. (2011). *Polymer Degradation and Stability*, 96, 236–246. doi : 10.1016/j.polymdegradstab.2010.11.004

Olivier, L., Baudet, C., Bertheau, D., Grandidier, J.-C., Lafarie-Frenot, M.-C. (2009). *Composites: Part A: Applied Science and Manufacturing*, 40, 1008–1016. doi:10.1016/j.compositesa.2008.04.015

Papazoglou, E.S. (2004). Flame retardants for plastics. In: *Handbook of Building Materials for Fire Protection*, Harper, C.A. (ed.), McGraw-Hill, New York Chapter 4.

Pascault, J.-P., Sautereau, H., Verdu, J., Williams, R.J.J. (2002). In: *Thermosetting Polymers*, Marcel Dekker, New York, Chapter 10, 282–321, and Chapter 14, 420–467.

Pitkethly, M.J., Favre, J.-P., Gaur, U., Jakubowski, J., Mudrich, S.F., Caldwell, D.L., Drzal, L.T., Nardin, M., Wagner, H.D., Di Landro, L., Hampe, A., Armistead, J.P., Desaeger, M., Verposet, I. (1993). *Composites Science and Technology*, 48, 205–214. doi:10.1016/0266-3538(93)90138-7

Rasoldier, N., Colin, X., Verdu, J., Bocquet, M., Olivier, L., Chocinski-Arnault, L., Lafarie-Frenot, M.-C. (2008). *Composites: Part A: Applied Science and Manufacturing*, 39, 1522–1529. doi:10.1016/j.compositesa.2008.05.016

Reich, L., Stivala, S.S. (1969). *Autooxidation of Hydrocarbons and Polyolefins*, Marcel Dekker, New York.

Richaud, E., Ferreira, P., Audouin, L., Colin, X., Verdu, J., Monchy-Leroy, C. (2010). *European Polymer Journal*, 46, 731–743. doi :10.1016/j.eurpolymj.2009.12.026

Robert, M., Cousin, P., Benmokrane, B. (2009). Durability of GFRP reinforcing bars embedded in moist concrete, *Journal of Composites for Construction*, 13, 66–73. doi: 10.1061/(ASCE)1090-0268(2009)13:2(66)

Rosen, M.R., Goddard, E.D. (1980). *Polymer Engineering and Science*, 20, 413–425. doi: 10.1002/pen.760200607

Roy, S., Singh, S. (2009). *Composites Science and Technology*, 69, 1962–1967. doi:10.1016/j.compscitech.2009.04.019

Saafi, M. (2002). Effect of fire on FRP reinforced concrete members, *Composite Structures*, 58, 11–20. doi:10.1016/S0263-8223(02)00045-4

Saito, O. (1958a). *Journal of the Physical Society of Japan*, 13, 198–206. doi: 10.1143/JPSJ.13.198

Saito, O. (1958b). *Journal of the Physical Society of Japan*, 13, 1451–1464. doi: 10.1143/JPSJ.13.1451

Salmon, L., Thominette, F., Pays, M.-F., Verdu, J. (1997). *Composites Science and Technology*, 57, 1119–1127. doi:10.1016/S0266-3538(97)00038-9

Schradder, M.E., Block, A. (1971). *Journal of Polymer Science: Part C: Polymer Symposia*, 34, 281–291. doi: 10.1002/polc.5070340126

Schutte, L.L., McDonough, W., Shioya, M., Mcauliffe, M., Greenwood, M. (1994). *Composites*, 25, 617–624. doi:10.1016/0010-4361(94)90193-7

Seguchi, T., Arakawa, K., Hayakawa, W., Watanabe, Y., Kuryama, I. (1981). *Radiation Physics and Chemistry*, 17, 195–201. doi:10.1016/0146-5724(81)90331-9

Seguchi, T., Arakawa, K., Hayakawa, W., Watanabe, Y., Kuryama, I. (1982). *Radiation Physics and Chemistry*, 19, 321–327. doi:10.1016/0146-5724(82)90116-9

Semenov, N.N. (1935). *Chemical Kinetics and Chain Reactions*, Oxford University Press, London.

Shen, C.H., Springer, G.S. (1976). *Journal of Composite Materials*, 10, 2–20. doi:10.1177/002199837601000101

Smets, B.M.J. (1985). On the mechanism of the corrosion of glass by water, *Philips Technical Review*, 42, 59–64.

Sorathia, U. (2004). Materials in military applications. In: *Handbook of Building Materials for Fire Protection*, Harper, C.A. (ed.), McGraw-Hill, New York, Chapter 9.

Struik, L.C.E. (1978). *Physical Ageing in Amorphous Polymers and Other Materials*, Elsevier, Amsterdam.

Tavakkolizadeh, M., Saadatmanesh, H. (2001). Galvanic corrosion of carbon and steel in aggressive environments, *Journal of Composites for Construction*, 5, 200–210. doi:10.1061/(ASCE)1090-0268(2001)5:3(200)

Tcharkhtchi, A., Bronnec, Y., Verdu, J. (2000). *Polymer*, 41, 5777–5785. doi :10.1016/S0032-3861(99)00801-0

Tewarson, A. (2007). Flammability. In: *Physical Properties of Polymers Handbook*, Mark, J. E. (ed.), Springer Science + Business Media, New York, 889–925.

Theocaris, P.S. (1987). *The Mesophase Concept in Composites*, Springer Verlag, Berlin (1987).

Thomason, J.L. (1990). Investigation of composite interphase using dynamic mechanical analysis: artifacts and reality, *Polymer Composite*, 11, 105–113. doi: 10.1002/pc.750110206

Thominette, F., Gaudichet-Maurin, E., Verdu, J. (2006). In: *Proceedings of the DSL 2006 Conference*, *Defect and Diffusion Forum*, 258/260, 442–446.

Tiemblo, P., Guzman, J., Riande, E., Mijangos, C., Reinecke, H. (2001). *Polymer*, 42, 4817–4823. doi:10.1016/S0032-3861(00)00922-8

Triantafillou, T.C., Papanicolaou, C.G. (2006). Shear strengthening of reinforced concrete members with textile reinforced mortar (TRM) jackets, *Materials and Structures*, 39, 93–103. doi: 10.1007/s11527-005-9034-3

Troitzsch, J. (2004). *Plastics Flammability Handbook: Principles, Regulations, Testing and Approval* (3rd edn), Carl Hanser Verlag, Munich, Germany.

Van Krevelen, D.W., Te Nijenhuis, K. (2009). *Properties of Polymers. Their Estimation and Correlation with Chemical Structure* (4th edn), Elsevier, Amsterdam, Chapter 18, 655–702.

Vasquez, A., Ambrustolo, M., Moschiar, S.M., Reboredo, M.M., Gerard, J.F. (1998). Interphase modification in unidirectional glass-fibre epoxy composites, *Composite Science and Technology*, 58, 549–558. doi:10.1016/S0266-3538(97)00172-3

Verdu, J., Rychly, J., Audouin, L. (2003). Synergism between polymer antioxidants. Kinetic modelling, *Polymer Degradation and Stability*, 79(3), 503–509. doi:10.1016/S0141-3910(02)00366-X

Whitney, J.-M., Browning, C.E. (1978). *Advanced Composite Materials: Environmental Effects*, ASTM STP 658, American Society for Testing and Materials, 43–60.
Woo, M., Piggot, M.R. (1988). *Journal of Composites Technology and Research*, 10, 20–24. doi: 10.1520/CTR10271J
Wypych, G. (2004). *Handbook of Plasticizers*, ChemTec Publishing, Toronto, Canada, 151–170.
Zweifel, H. (2001). *Plastics Additives Handbook* (5th edn), Hanser Publishers, Munich, Germany.

13

Testing of pultruded glass fibre-reinforced polymer (GFRP) composite materials and structures

G. J. TURVEY, Lancaster University, UK

DOI: 10.1533/9780857098641.3.440

Abstract: An overview is presented of four groups of static load tests to determine the mechanical properties of pultruded GFRP materials and structures. The first group includes standard and non-standard tests on material samples. The second group encompasses bending, buckling and collapse load tests on structural elements. The third and fourth groups include tests on bolted joints and sub-structures/full-scale structures, respectively. Throughout the overview, the difficulties of simulating practical support and loading conditions and monitoring deformations are emphasised. Future developments are mentioned briefly in the final section. It is noted that dynamic load testing and monitoring of static/dynamic deformations by means of full-field and other novel techniques are likely to receive much greater attention.

Key words: GFRP, materials testing, pultrusions, structural testing.

13.1 Introduction

It is often suggested that glass fibre-reinforced polymer (GFRP) is the most common so-called *advanced* fibre-reinforced composite material used in today's construction industry. For example, it is used extensively in lightweight sandwich panel cladding of high-rise buildings, as reinforcing bars in concrete slabs and walls, and in thin-walled flat, cylindrical and hemispherical panels of tanks and other types of storage structures.

Straight prismatic structural-grade profiles are another form of GFRP composite material which is being used with increasing frequency in both primary and secondary civil and military infrastructure. The most common examples are replacement bridge decks, lightweight footbridges, rapid-assembly kits for temporary accommodation, elevated storage platforms, walkways and staircases. These profiles are usually manufactured by a process known as pultrusion. This is a long-line process in which raw materials (fibres, polymer matrix and filler) enter at one end of the line and the finished profile emerges at the other (see Fig. 13.1). Moreover, pultrusion is one of the most economical composites manufacturing processes. Detailed descriptions of the process are provided on several pultruders' websites (see, for example, Anon.,

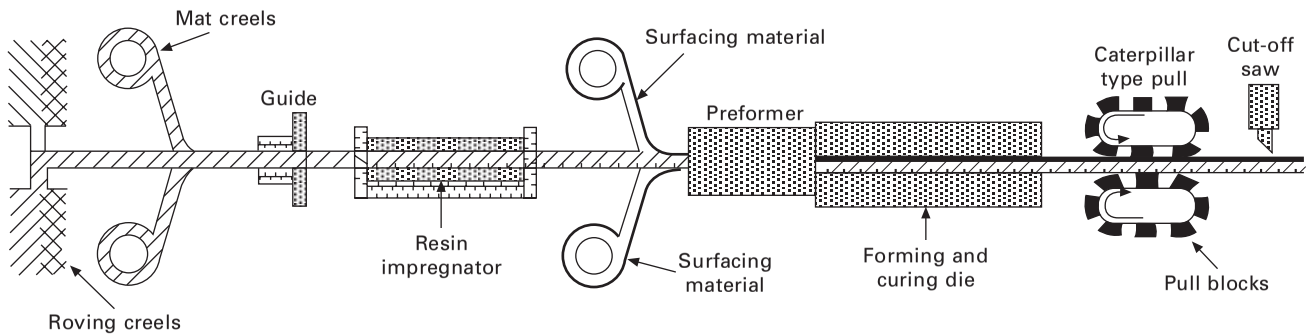

13.1 The pultrusion process (reproduced with permission from Strongwell, www.strongwell.com).

1989). With the exception of the bridge deck profiles, most pultruded GFRP structural-grade profiles have simple open or closed cross-sectional shapes that are similar to structural steel and aluminium profiles (see Fig. 13.2). Nonetheless, it should be appreciated that composite material profiles with more complicated cross-sectional shapes may be pultruded. These profiles, known as *custom* profiles, are used less frequently in construction and will not be considered herein.

In comparison to steel and aluminium profiles, structural-grade pultruded GFRP profiles have a much shorter history of use in civil engineering, probably amounting to not much more than 30 years. In view of this relatively short time scale, it is not altogether surprising that codes of practice for the design of GFRP structures are not well developed, unlike the situation for ductile steel and aluminium structural materials. During the late 1980s only a few documents were available to assist structural engineers with the design of pultruded GFRP structures. These were predominantly pultruders' design handbooks (see, for example, Anon., 1988, 1989). It was not until 1996 that the first design guidance based on *limit state* philosophy was published (Clarke, 1996). Moreover, even in their later editions, the pultruders' handbooks are still based on *factor of safety* rather than limit state design philosophy. The former design philosophy has long been abandoned in Europe and elsewhere for the design of metallic and timber structures. Unfortunately, at the time when the EUROCOMP design code and handbook (Clarke, 1996) was published, the total amount of test work underpinning the design clauses and guidance given therein was limited. Hence, in order to overcome knowledge gaps in the code and to achieve *deemed to satisfy status* for the design of pultruded GFRP structures, it has often been necessary to undertake additional test

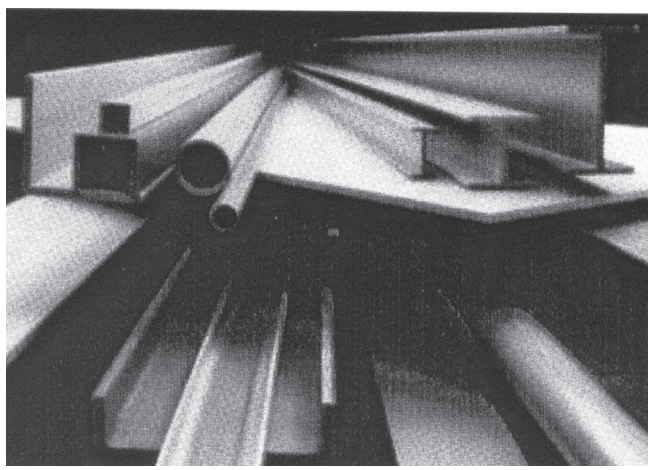

13.2 Pultruded GFRP structural grade profiles (reproduced with permission from Strongwell, www.strongwell.com).

work on the GFRP material, structural elements, joints, sub-structures and, to a lesser extent, full-scale structures.

At this juncture, it is perhaps appropriate to point out that the situation with respect to design codes has begun to change for the better. A design code (albeit in Dutch) was published in the Netherlands in 2003 (CUR96, 2003) and is currently being updated with publication of the revised edition expected in 2013. An Italian design code for pultruded GFRP structures was also published in 2008 (CNR-DT 205, 2008). The most recent design code for pultruded GFRP structures is the American Society of Civil Engineers (ASCE) draft load and resistance pre-standard (ASCE, 2010). It was submitted to the American Composites Manufacturers Association (ACMA) for approval in November 2010 and it is expected that it will be published in 2013. To conclude this digression, it is also worth mentioning that Technical Committee 250 (Working Group 4) of the European Standards Organisation (CEN) started work in late 2011 on the development of design guidance for *Fiber Reinforced Polymer Structures* which could eventually form the basis of a future Eurocode. Also in the UK in 2011, work started on the development of *Guidance for the Design of FRP Bridges* under the auspices of a Steering Group set up by the Network Group for Composites in Construction (NGCC).

Although the absence of design standards approved by the building regulatory authorities has stimulated a significant amount of testing of pultruded GFRP materials, profiles, joints and structures, several other factors have provided additional stimulus. They include: (1) lack of knowledge and understanding of the orthotropic elastic–brittle nature of pultruded GFRP material, (2) limited design experience with composite profiles of inherently low flexural stiffness (one-seventh to one-tenth that of similar-sized steel profiles), and (3) inadequate appreciation of the impact on design of the material's high strength to stiffness ratio. An important consequence of the second and third factors is that, compared to metallic profiles, the relative importance of stiffness and strength design criteria are different for pultruded GFRP profiles. Thus, serviceability rather than strength criteria dominate design, i.e. deflection and buckling have to be considered first in design and strength is checked after these stiffness criteria have been satisfied.

Having explained the reasons why material and structural testing has played such an important role in advancing the use of pultruded GFRP structures in infrastructure, the remainder of this chapter will be concerned with selected descriptions of the wide range of *static* load tests that have been undertaken. In so doing, an attempt will be made to highlight important and novel features that arise in these tests as a consequence of the factors, identified in the preceding paragraph, which distinguish the response of pultruded GFRP profiles from their metallic counterparts.

It is both convenient and logical to sub-divide the descriptions and

discussions of the various types of tests that have been undertaken on pultruded GFRP composites as follows: materials, structural elements, joints and structures. Thus, mechanical property tests are introduced first. They are followed by descriptions of flexural, buckling and failure tests on structural profiles. Thereafter, testing of bolted and bonded joints in tension and bolted joints in bending and shear are addressed. The penultimate sub-section is concerned with presenting two examples of tests on sub-structures and two on full-scale structures. In each of the aforementioned sub-sections, the consequences of the differences between GFRP and metallic materials are highlighted in terms of their impact on test set-ups, loading arrangements and deformation measurement techniques. The chapter is concluded with some comments about full-field deformation and load measurement techniques that are expected to be used more frequently in future test work and the need for more testing in order to enhance knowledge and understanding of the dynamic and impact response of pultruded GFRP structures.

13.2 Tests to characterise the mechanical properties of pultruded glass fibre-reinforced polymer (GFRP) material

13.2.1 Coupon tests in accordance with standards and other guidance documents

From the standpoint of structural design, tests to characterise the mechanical properties of the pultruded GFRP material constitute the smallest-scale load tests that are undertaken. Such tests are carried out on coupons of material cut out of the constituent parts of the profiles (typically webs, flanges and flat plate). For metallic structures, such as steel, it is usually sufficient to carry out a number of tension tests on coupons specified in accordance with the relevant standard, e.g. BS EN ISO 6892-1:2009, to determine the elastic modulus and yield strength. In fact, the structural designer does not generally have to be involved with the determination of these properties – they are provided by the supplier of the steel sections, or values are given in the structural steel design code (EN 1993-1-1, 2006).

The situation is much more complicated for pultruded GFRP materials because they are inherently orthotropic. Consequently, it is, at the very least, necessary to cut out rectangular coupons parallel and transverse to the length of a flange or web in order to determine the profile's longitudinal and transverse elastic moduli and strengths. Moreover, because of the nature of the profile's fibre architecture, the tensile and compressive strengths differ, and so much more testing has to be undertaken to determine these properties for pultruded GFRP materials than for steel or aluminium.

There are a number of standards, which describe in detail how such coupon

tests have to be undertaken. The American Society for Testing and Materials (ASTM) has developed standards for tensile and compression testing of fibre-reinforced polymer composite materials (ASTM D 3039M-08, 2008; ASTM D 695-08, 2008). They prescribe the coupons' overall shapes and dimensions, end tab details, the minimum number of coupons to be tested and how the moduli and strengths are to be determined from the load versus deformation responses. Moreover, for the compression tests, descriptions of anti-buckling devices are also included. Similar standards have also been developed by other organisations (see, for example, EN 13706-2, 2002).

Figures 13.3(a) and (b) show respectively the tensile failure modes of rectangular coupons cut out of a 203 × 203 × 9.5 mm pultruded GFRP Wide Flange (WF) profile parallel and transverse to the pultrusion direction. Both sets of coupons were tested without end tabs. It is of interest to note the extensive delaminations in the longitudinal coupons compared to the more localised failure in the transverse coupons. The failure modes of longitudinal compression coupons cut out of the same WF profile are shown in Fig. 13.4(a). There is clear evidence of buckling at the outer surfaces and through-thickness shear failure in the interior of the coupons. These coupons, all of which required bonded aluminium end tabs, were tested in a modified Illinois Institute of Technology Research Institute (IITRI) fixture without anti-buckling guides (see Figure 13.4(b)). Typical load versus strain plots for longitudinal tension and transverse compression are shown in Figs 13.5(a) and(b) respectively for the 203 × 203 × 9.5 mm WF profile. The response of the longitudinal tension coupon is linear up to the failure strain of about 13,000 microstrain, whereas the transverse compression coupon's response is non-linear up to a similar failure strain. In Table 13.1 some of the moduli and strength values obtained from these coupon tests are compared with the pultruder's *minimum* values. It is evident that the latter values vary between 59% and 92% of the former values.

For steel, the elastic shear modulus and shear yield strength are usually determined by calculation, based on the tensile properties, rather than by

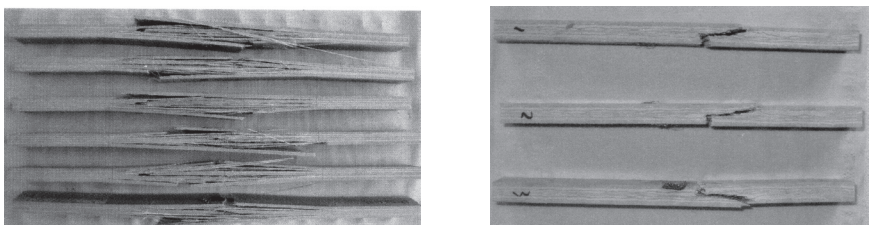

(a) Ib)

13.3 Failure modes of tension coupons cut out of a 203 × 203 × 9.5 mm WF profile: (a) longitudinal flange coupons; (b) transverse web coupons.

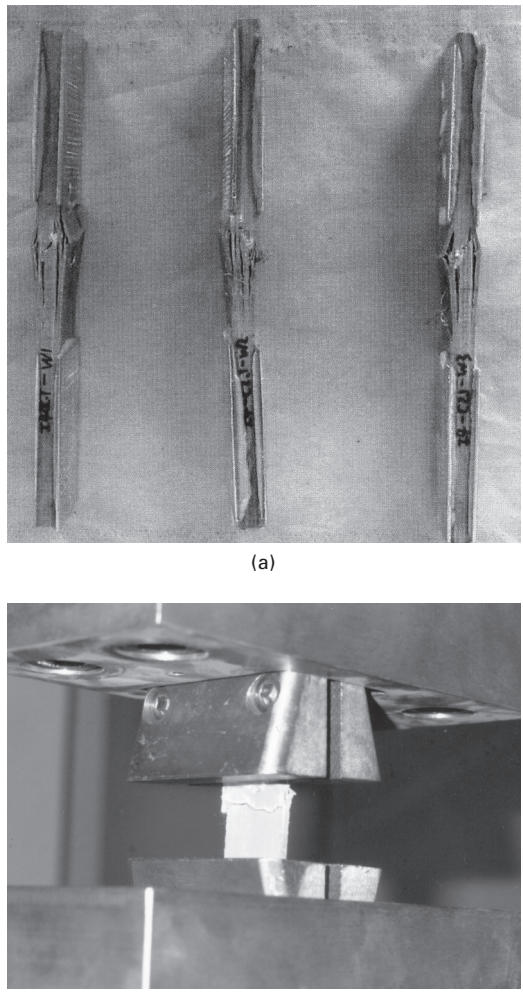

(a)

(b)

13.4 (a) Failure modes of longitudinal compression coupons cut out of the web of a 102 × 102 × 6.4 mm WF profile; (b) compression coupon under test in a modified Illinois Institute of Technology Research Institute (IITRI) test fixture.

testing. However, for pultruded GFRP materials the situation is, again, more complicated, because there are three (one in-plane and two mutually orthogonal through-thickness) shear moduli and strengths that may need to be quantified. Furthermore, there are several test configurations that may be used to determine the in-plane shear modulus and shear strength. They include the v-notched, asymmetric, four-point bending or Iosipescu test, the rail shear test, the diagonally opposite corner-loaded and supported plate

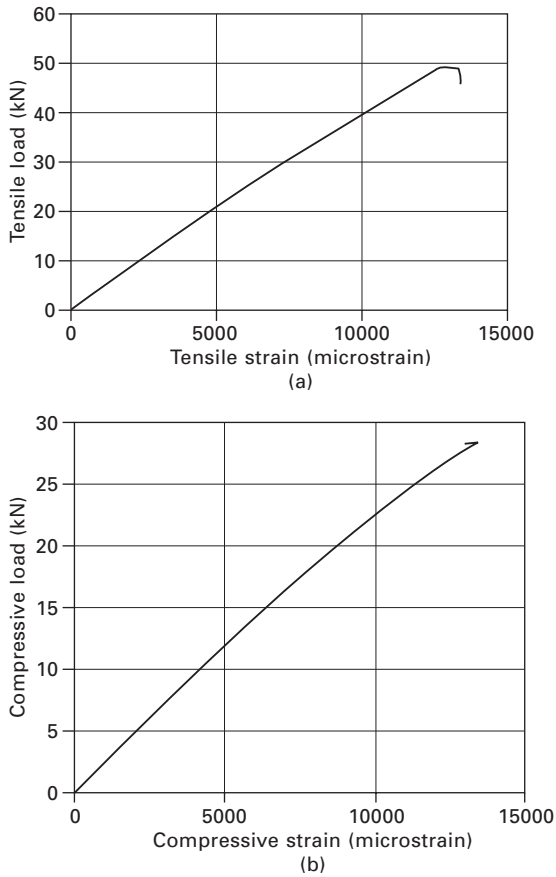

13.5 Load versus strain responses obtained from tests on coupons cut out of a 203 × 203 × 9.5 mm WF profile: (a) longitudinal flange coupon tested in tension; (b) transverse web coupon tested in compression.

bending test, and the axial torsion test. Test standards and other documents provide detailed guidance on how to carry out these tests (see, for example, ASTM D 5379-05 (2005), ASTM D 4255M-01 (2007) and Sims *et al*. (1994)). However, it is unclear as to which is the preferred test for pultruded GFRP materials, though restrictions on available specimen size and the availability of a particular test set-up may be the deciding factors.

A v-notched asymmetric four-point bending test on a pultruded GFRP coupon is shown in Fig. 13.6(a). The coupon is somewhat larger than is prescribed in the relevant ASTM standard (see ASTM D 5379-05, 2005). In addition, it also includes end stabilisers to prevent the coupon tipping sideways whilst it is being installed in the test fixture. A strain gauged,

Table 13.1 Comparison of average elastic moduli and strengths obtained from coupon tests with pultruder's minimum values (Anon., 1989) for pultruded GFRP WF profiles

Cross-section dimensions (mm)	Longitudinal modulus (GPa)	Longitudinal strength (MPa)	Transverse modulus (GPa)	Transverse strength (MPa)	Load type
203 × 203 × 9.5	20.3 (17.2)	246 (207)	9.43 (5.52)	63.2 (48.3)	Tension
102 × 102 × 6.4			9.16 (5.52)	78.9 (48.3)	
203 × 203 × 9.5	20.9 (17.2)	226 (207)	9.65 (6.90)	126 (103)	Compression
102 × 102 × 6.4	22.4 (17.2)	294 (207)	10.1 (6.90)	135 (103)	

Note: The bracketed values are the pultruder's values.

v-notched coupon is shown prior to and after testing in Figs 13.6(b1) and (b2) respectively in order to illustrate its failure mode. A typical shear stress versus shear strain plot is shown in Fig. 13.6(c).

Test set-ups for the plate bending (Sims *et al.*, 1994) and axial torsion tests (Turvey, 1998), which may also be used to determine the shear stress versus shear strain responses of pultruded GFRP specimens, are shown in Figs 13.7 and 13.8(a) respectively. A pultruded GFRP plate coupon twisted through 66° in the axial torsion test rig shows the onset of edge delamination failure in Fig. 13.8(b). A typical shear stress versus shear strain plot obtained from this type of test on a rectangular coupon cut in the direction of pultrusion out of the flange of a 102 × 102 × 6.4 mm WF profile is depicted in Fig. 13.8(c).

It should be appreciated that standards have been developed to determine several other mechanical properties of fibre-reinforced polymer composites, for example, the through-thickness tensile stiffness and strength (ASTM D 7291/D 7291M-07, 2007) and the short-beam strength (ASTM D 2344/D 2344M-00, 2006). Moreover, it should also be recognised that many of these standard tests were developed originally for laminated fibre-reinforced composite material used in aerospace applications. Consequently, they are not always applicable to pultruded GFRP materials without minor deviation(s) from the recommended coupon specification or modification(s) of the test fixtures. The most common reason for this is that material thicknesses of aerospace composites (predominantly CFRP), because of the overriding importance of weight-saving, are generally thinner than pultruded GFRP composites used in civil engineering.

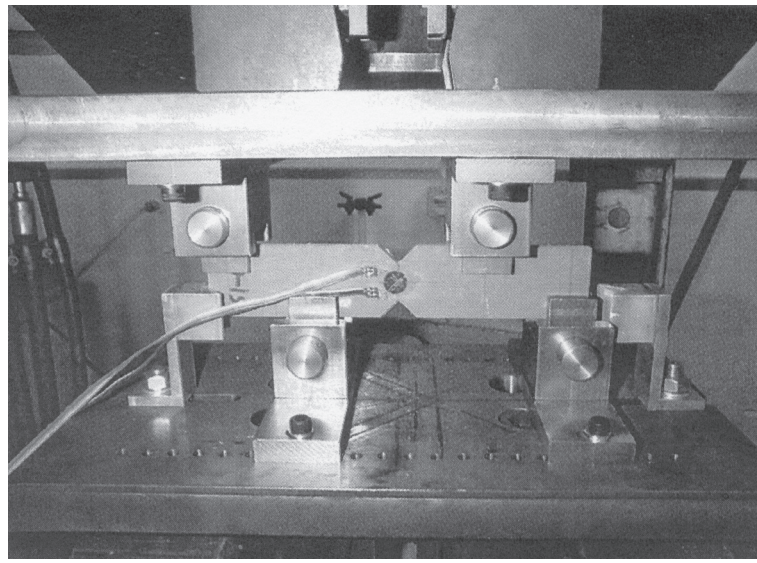

(a)

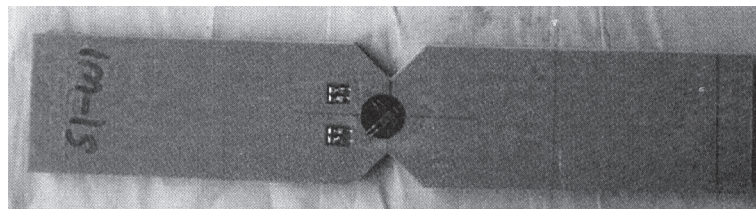

(b) (1)

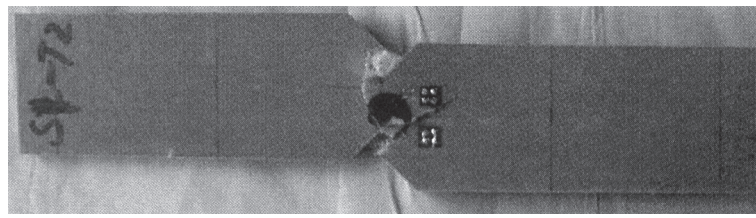

(b) (2)

13.6 (a) A v-notched pultruded GFRP coupon under test in an asymmetric four-point bending (Iosipescu) test fixture to determine its shear stress versus shear strain response; (b) Iosipescu coupon with a biaxial strain gauge bonded to its centre (gauge's principal axes oriented at ±45° to the longitudinal centreline): (1) coupon before testing and (2) coupon after testing to failure; (c) typical shear stress versus shear strain plot obtained from an Iosipescu test on a coupon cut out of the web of a 102 × 102 × 6.4 mm WF profile.

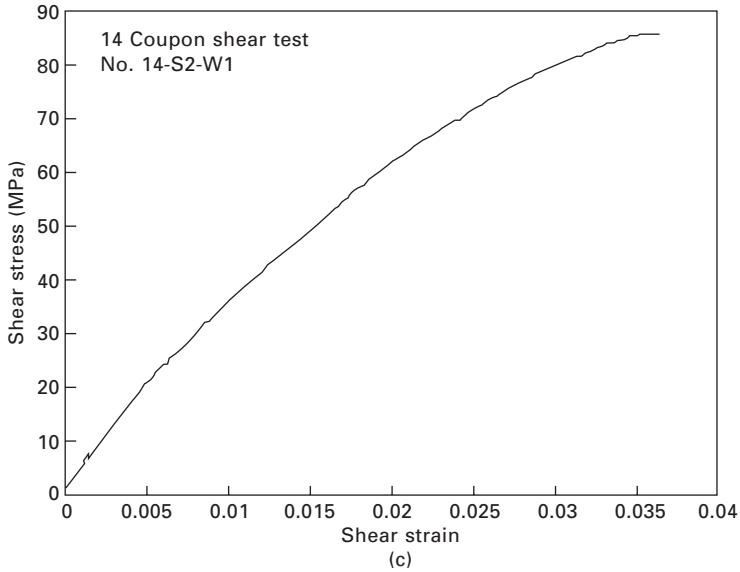

13.6 Continued

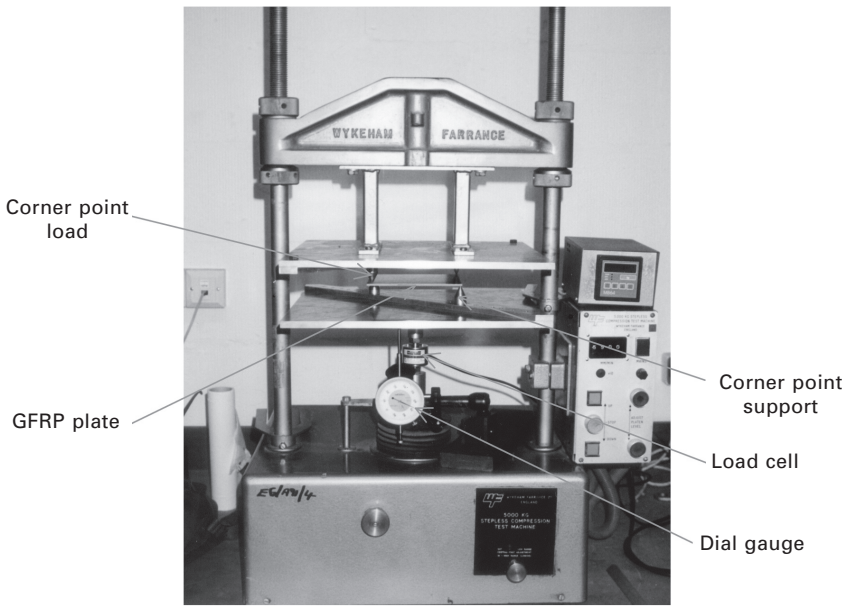

13.7 Diagonally opposite corner-supported and corner-loaded plate bending test rig used to determine the in-plane shear modulus of pultruded GFRP plate (note that the test rig is able to accommodate plates of different sizes and thicknesses).

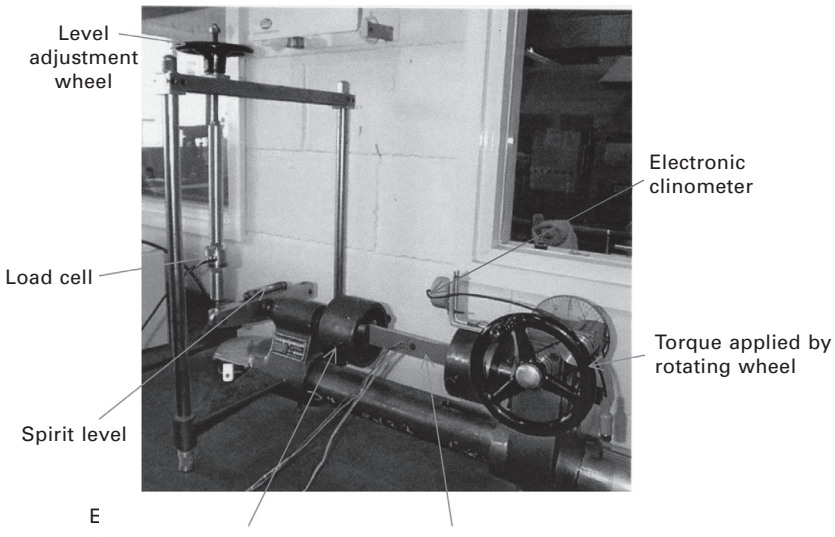

(a)

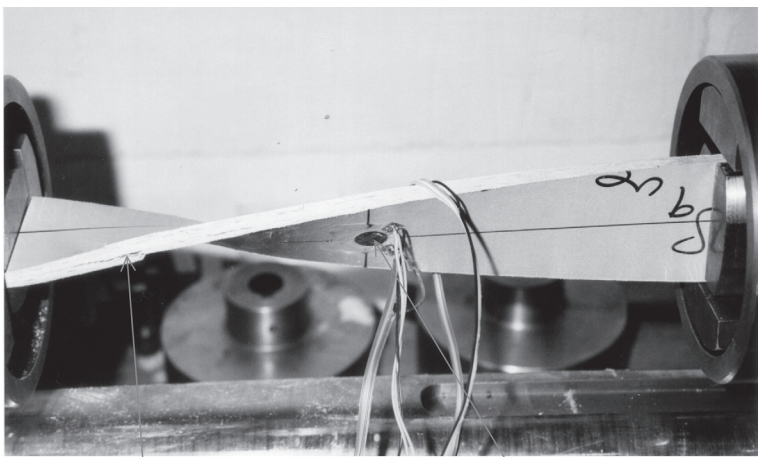

(b)

13.8 (a) Axial torsion test rig used to determine the in-plane shear modulus and ultimate shear strength of pultruded GFRP plate (note that the rig accommodates other end fixtures which allow axial torsion tests to be carried out on pultruded circular cross-section rods, small equal angles and channels up to 2 m long); (b) axial twist applied to a 6.4 mm thick pultruded GFRP flat plate coupon with rovings transverse to the torsion axis: first signs of edge delamination failure at 66° angle of twist; (c) typical shear stress versus shear strain plot obtained from an axial torque versus twist test on a rectangular coupon (plate) cut out of the flange of a 102 × 102 × 6.4 mm pultruded GFRP WF profile.

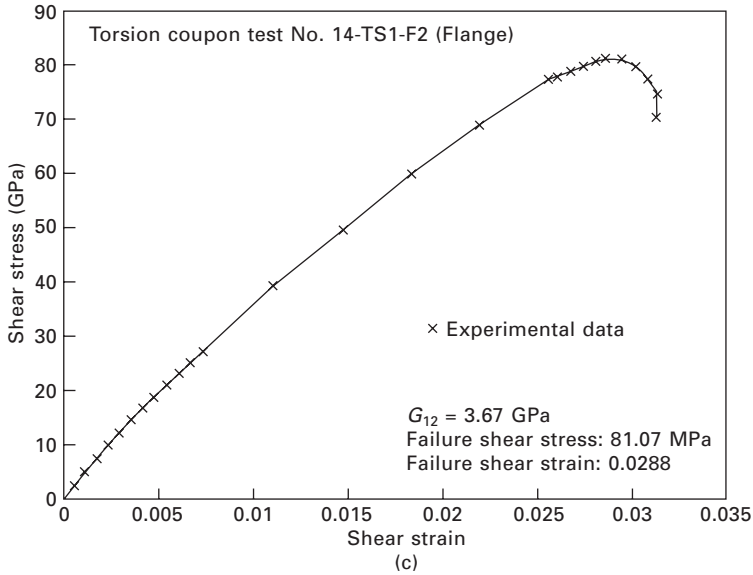

13.8 Continued

13.2.2 Non-standard tests for profile coupons

Although a number of standard tests based on coupon specimens, e.g. the four-point bending test to determine the flexural modulus and strength of the GFRP material, were not included in Sub-section 13.2.1, several important stiffness and strength properties have to be determined without recourse to standardised test procedures. They are the focus of the descriptions in this sub-section.

Tests on WF beams and columns have shown that final collapse is generally triggered by localised cracking and/or separation of one or both flanges from the web. This mode of collapse occurs within the post-buckled regime, so that at the instant of collapse the so-called *web-flange* junction is subjected to a combined stress state. However, within the web-flange junction the fibre architecture differs from that in the web and flanges. Consequently, strength data derived from standardised testing of web or flange coupons does not adequately reflect the strengths of the profiles' web-flange junctions. Recognition of this situation has led to the development of a number of non-standard tests on profile coupons. The tests have been developed in order to quantify the tensile, shear and flexural moduli and the strengths of the junctions of WF and equal-leg angle profiles. The strengths may then be used to formulate failure criteria for the junctions. These tests will now be presented and discussed.

The simplest of the tests is used to determine the tensile strength of the

web-flange junctions of a WF profile. The test uses a short length of the profile, which is cut longitudinally along the centre-line of its web to form two identical T-specimens for testing. The flange of the T-specimen is clamped to the moveable grip of a universal test machine and the web is clamped in the fixed grip. The specimen is then loaded in tension until tearing failure occurs at the web-flange junction. Two T-specimens, each with a small strain gauge bonded to its junction, are shown in Fig. 13.9(a). A schematic diagram of the test set-up is shown in Fig. 13.9(b) and Fig. 13.9(c) depicts a T-specimen being tested. Further details, including test data for two sizes of WF profile, are given in Turvey and Zhang (2005a). Similar tensile failure tests have been reported for the leg junctions of equal angle profiles (see Turvey and Wang, 2009a).

A rather more complicated test set-up has been developed to determine the shear strength of the web-flange junctions of WF profiles. The test set-up is based on the WF profile specimen being supported as a short, propped cantilever loaded by a vertical concentrated load applied close to the clamped support (see Fig. 13.10(a)). Although the dominant stress applied to the junction is shear, there is, nevertheless, a small parasitic bending stress present. An advantage of this particular test set-up is that it utilises a very short length of WF profile, as shown in Fig. 13.10(b). A typical (approximately trilinear) load versus displacement response for this test is shown in Fig. 13.10(c) and sketches of the modes of failure within the junctions are illustrated in Fig. 13.10(d). Further details of the test set-up, the underlying theory and test data are given in Turvey and Zhang (2004a).

The third type of web-flange junction test is a test to determine the flexural or rotational strength of the junction. Two versions of the test have been developed. The first version uses a short length of WF profile, i.e. similar to that used in the shear test. In this version, equal and opposite tensile forces are applied normal to the top and bottom flanges on one side of the profile, thereby subjecting the top and bottom web-flange junctions to *opening-mode* bending. Figure 13.11(a) shows a schematic diagram of the loading and instrumentation on a WF specimen. In order to measure the rotations of the web-flange junctions, two electronic clinometers, each with a resolution of 0.001° over the first few degrees of rotation, are attached to the unloaded, top and bottom flange. A specimen under test is shown in Fig. 13.11(b). Further details of this test and test data are given in Turvey and Zhang (2005b).

An alternative flexural strength test has been developed specifically for the leg junctions of different sizes of equal angle profile. In this test the angle profile specimen – akin to a *cranked* beam in the vertical plane – is subjected to three-point bending. The junction is subjected a vertical line load and the edges of the angle's legs are supported on two steel platforms which are able to translate horizontally with minimal frictional resistance. The latter are supported by the lower platen of the test machine and the

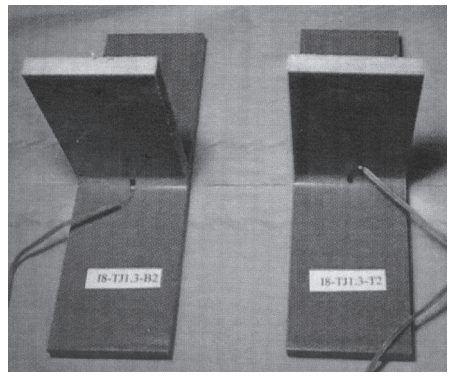

(a)

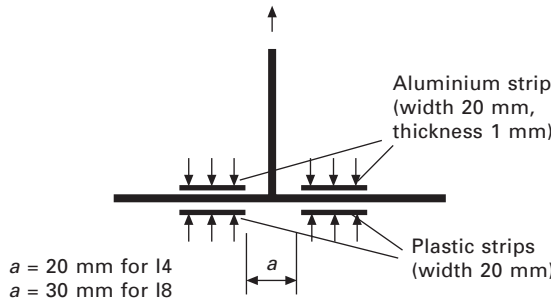

(b)

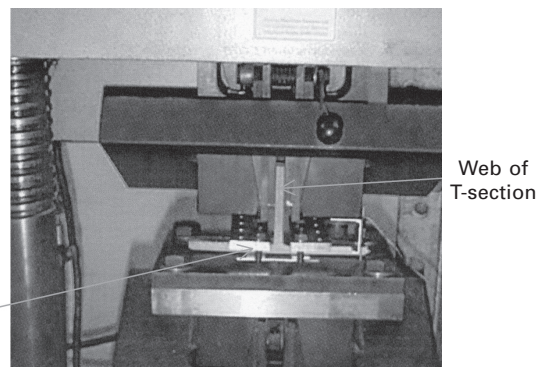

(c)

13.9 (a) Two T-profile specimens cut out of a 203 × 203 × 9.5 mm pultruded GFRP WF profile (note that uniaxial strain gauges are bonded to the centres of their web-flange junctions); (b) schematic diagram of the clamping and loading arrangement for testing the web-flange junction of a T-profile specimen in tension; (c) web-flange junction of a T-profile specimen cut out of a 203 × 203 × 9.5 mm pultruded GFRP WF profile being tested in tension (reproduced with permission from Elsevier (Turvey and Zhang, 2005a)).

line load is applied via a rigid steel plate attached to the upper platen. A schematic diagram and an image of an angle profile specimen under test are shown in Figs 13.12(a) and(b) respectively. In the latter image, internal delamination in the junction region is clearly visible. Detailed test results are given in Turvey and Zhang (2007).

It is pertinent to draw attention to the fact that both flexural tests for the junctions of WF and equal angle profiles are only able to measure *opening-mode* stiffnesses and strengths. However, it should be relatively simple to devise test set-ups which allow the junctions' *closing-mode* flexural stiffnesses and strengths to be determined.

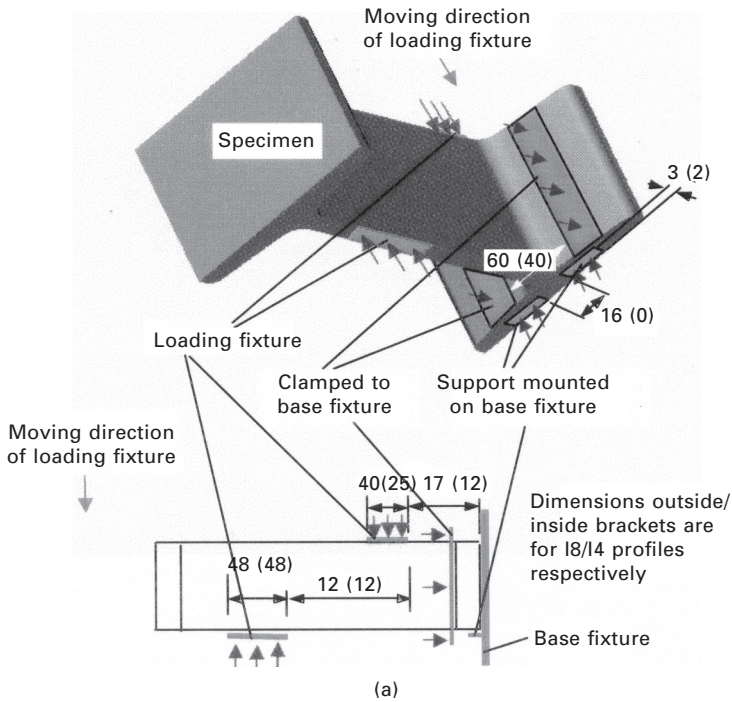

13.10 (a) Schematic diagrams showing the loading and support arrangements used in the web-flange junction shear test of a WF profile specimen (all dimensions in mm); (b) shear test on the web-flange junction of a 203 × 203 × 9.5 mm pultruded GFRP WF profile specimen; (c) shear load versus shear displacement response of the web-flange junction of a 203 × 203 × 9.5 mm pultruded GFRP WF profile specimen; (d) sketches of typical crack patterns in web-flange junctions of pultruded GFRP WF profile specimens failed in shear (reproduced with permission from Woodhead Publishing Limited (Turvey and Zhang, 2004a)).

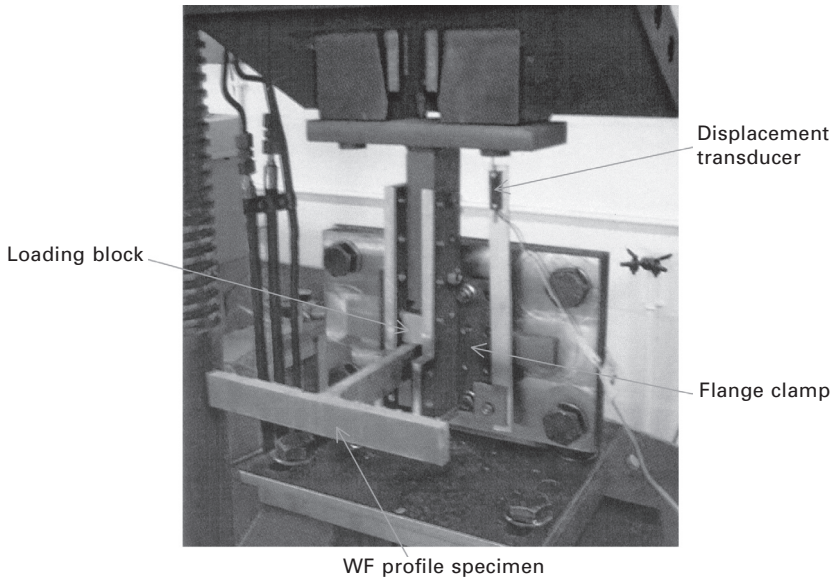

(b)

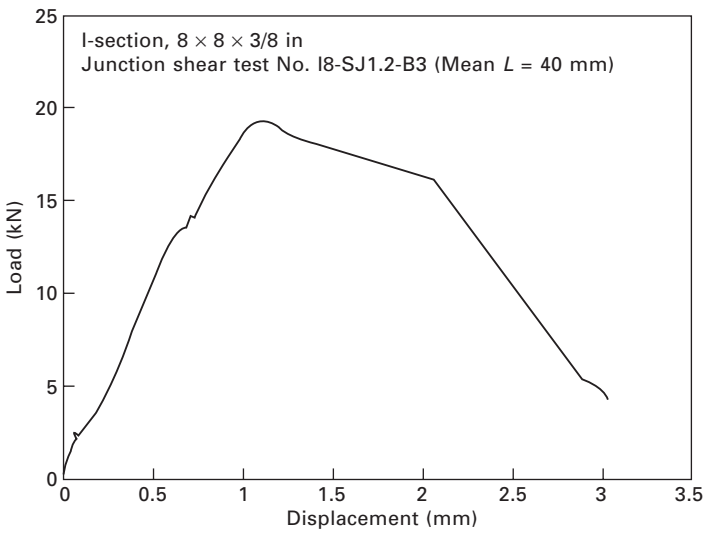

(c)

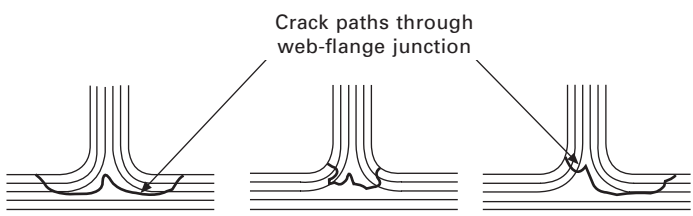

(d)

13.10 Continued

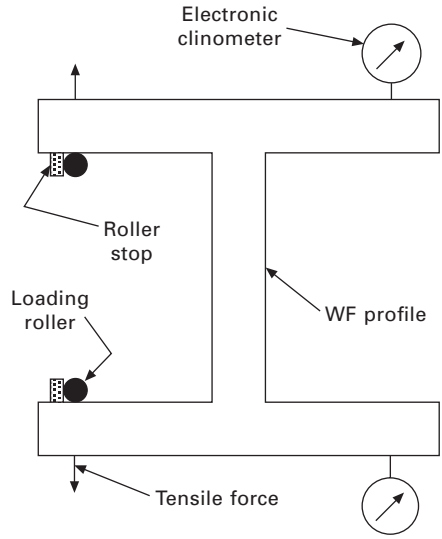

(a)

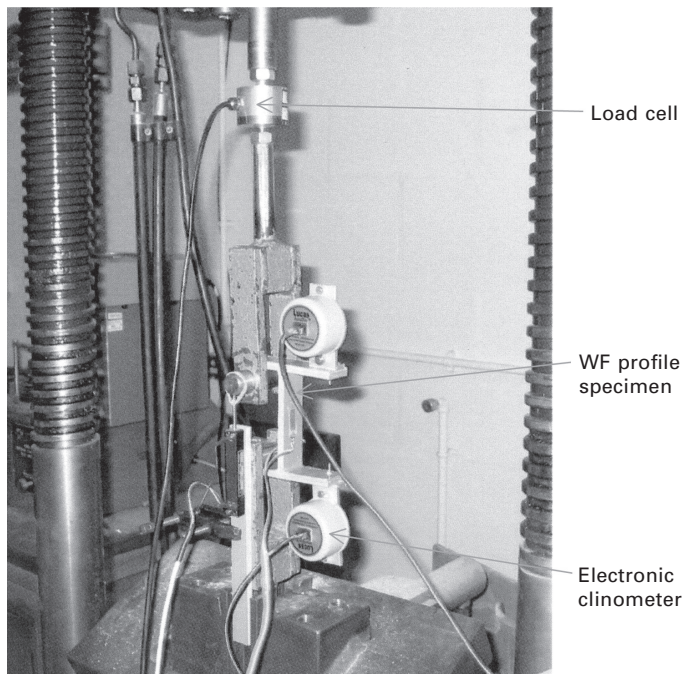

(b)

13.11 (a) Schematic diagram of the test set-up for an *opening-mode* flexure test on the web-flange junctions of a pultruded GFRP WF profile specimen; (b) an *opening-mode* flexure test on the web-flange junctions of a pultruded GFRP WF profile specimen (reproduced with permission of the Institution of Civil Engineers (Turvey and Zhang, 2005b)).

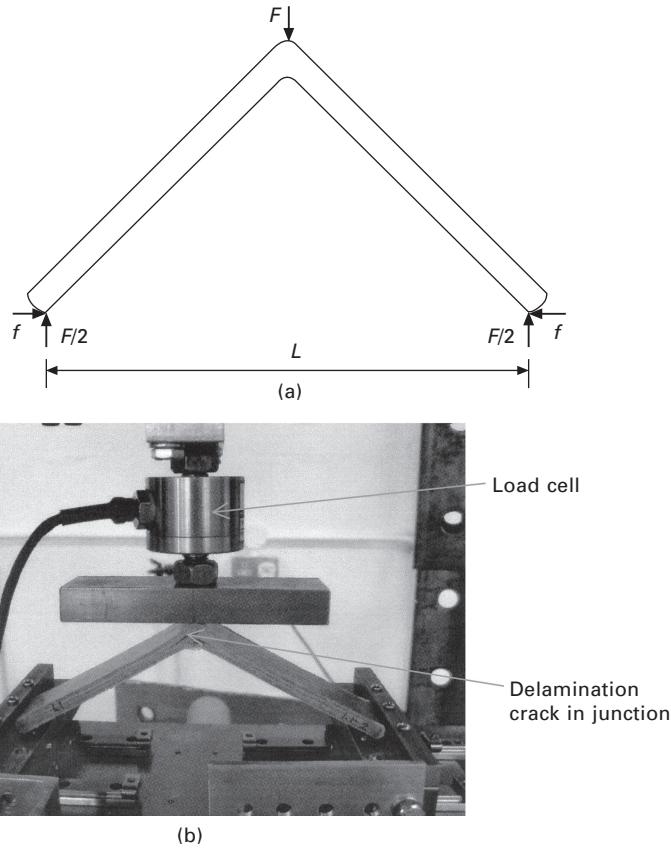

13.12 (a) Schematic diagram of the test set-up used to determine the *opening-mode* flexural stiffness and strength of the leg-junction of a pultruded GFRP equal-angle profile specimen (note that the forces *f* represent the friction acting on the sliding supports); (b) *opening-mode* test on an equal-leg angle (note that there is significant internal delamination within the junction) (reproduced with permission of the University of Bath (Turvey and Zhang, 2007)).

13.3 Tests to characterise the flexural, torsional, buckling and collapse responses of pultruded GFRP structural grade profiles

13.3.1 Flexural response of pultruded GFRP beams

It appears that the first three-point, beam bending tests on structural-grade pultruded GFRP profiles were reported by Sims *et al.* (1987) and Bank (1989). The purpose of these tests was not to demonstrate *directly* that linear, first-order shear deformation beam theory could be used to predict the flexural

response of simply supported beams, but rather to determine the elastic longitudinal flexural and transverse shear moduli for the particular profiles tested. They measured the centre deflections (w) of simply supported beams with different spans (L) which were subjected to the same mid-span point load (P). By rearranging the classical equation for the centre deflection of a shear-deformable, simply supported beam in symmetric three-point flexure, they were able to show that by plotting w/PL versus L^2 or w/PL^3 versus $1/L^2$, the responses were linear. In the former plot the slope of the *best fit* straight line through the test data was proportional to the elastic longitudinal flexural modulus of the profile, and in the latter case it was proportional to the transverse shear modulus.

There have been a number of other investigations concerned with testing pultruded GFRP beams with various end support conditions. The primary purpose of these tests was to demonstrate that first-order shear deformation beam theory may be used to predict their small deflection response and to quantify its accuracy relative to classical shear-rigid beam theory.

Simply supported end conditions are relatively easy to simulate for WF profiles. For example, in its simplest form, the lower flange of the profile may be supported on a transverse circular steel rod (see Fig. 13.13(a)). Alternatively, a similar rod may be slotted through a roller bearing on the neutral axis of the profile's web. The ends of the rod may then be supported either on flat surfaces or on roller bearings in mountings. An image of the type of roller bearing used is shown in Fig. 13.13(b). Fig. 13.13(c) shows a beam with the simpler type of simple support being tested in four-point bending.

Unfortunately, the clamped end condition is much more difficult to simulate. Several different clamping arrangements have been used. They include rigid concrete blocks with hardwood packing pieces clamped together with steel bolts (see Fig. 13.14(a)), adjustable steel clamping plates and hardwood blocks (see Fig. 13.14(b)) and bolted steel plates (used for the rectangular cross-section cantilever shown later in Fig. 13.17(a)). None of these arrangements has been particularly successful.

Recently, an alternative approach has been used to obtain test data for beams with one clamped support which could be used to verify both shear-rigid and shear-flexible beam theory. The approach exploits structural and loading symmetry to identify equivalent simply supported, single and multi-span beams and loading configurations, which may be tested to provide the required deformation data. Thus, Turvey (2008) used data from simply supported, symmetric three-point, flexure tests on unstiffened and CFRP stiffened pultruded GFRP WF beams to validate the deformation equations for tip-loaded cantilevers (see Fig. 13.15(a)). Subsequently, he used the same approach (Turvey, 2011) to validate the deformation equations for propped cantilevers subjected to a point load at mid-span using deformation data

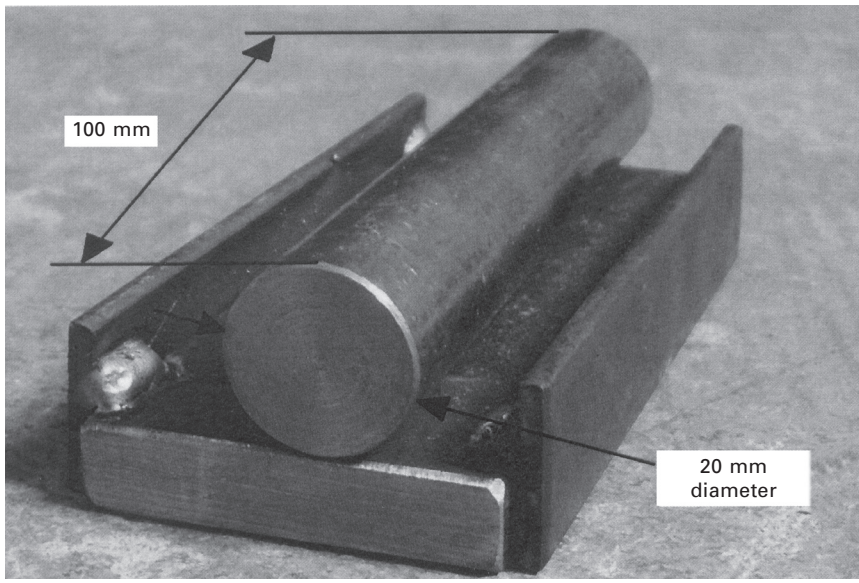

(a)

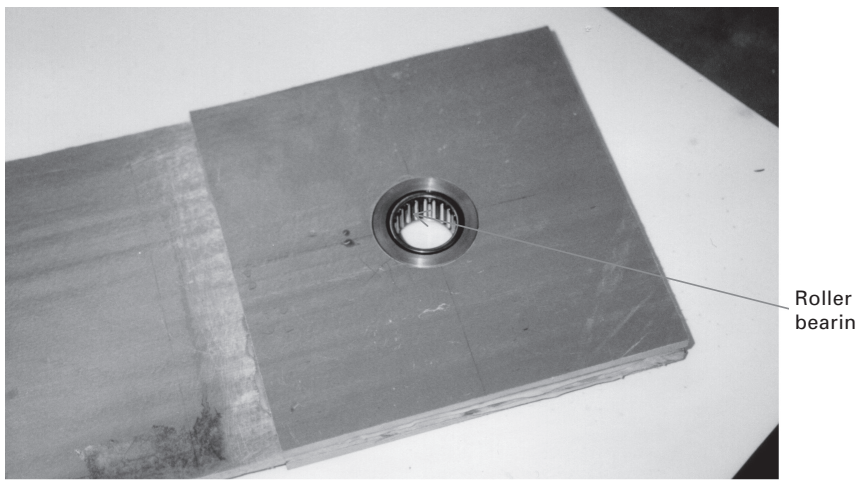

(b)

13.13 (a) Solid steel cylindrical roller used to simulate a simple support; (b) roller bearing simple support on the neutral axis of a locally reinforced member of rectangular cross-section; (c) four-point flexure test on a simply supported pultruded GFRP beam with solid steel cylindrical roller supports.

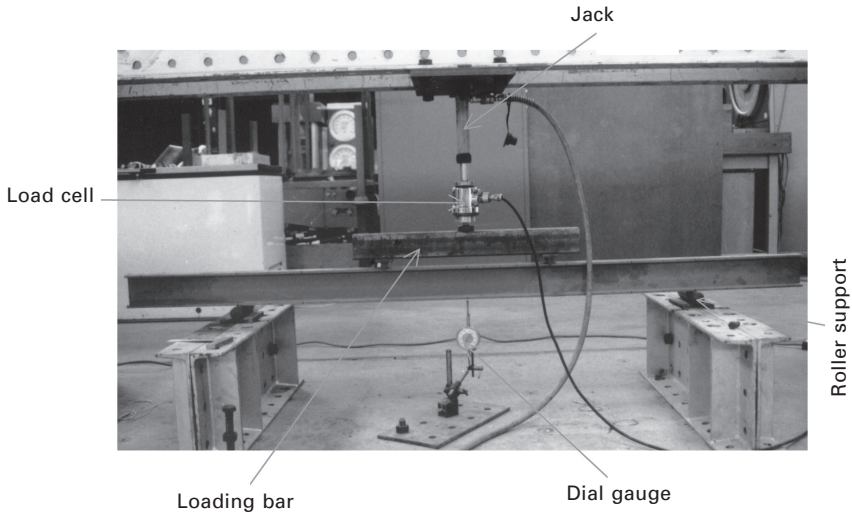

(c)

13.13 Continued

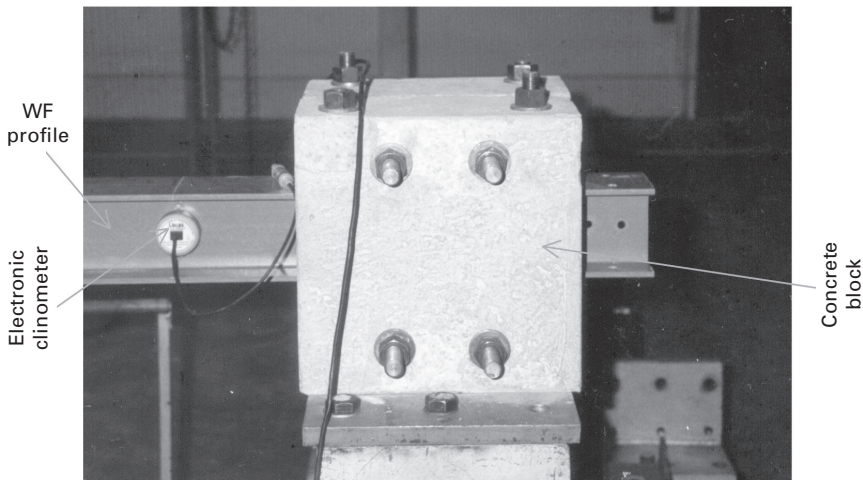

(a)

13.14 Different methods used to simulate clamped end conditions for beams: (a) concrete blocks and internal timber packing bolted together by means of torqued horizontal and vertical bolts; (b) adjustable steel plates and timber packing used together with bolted steel plates.

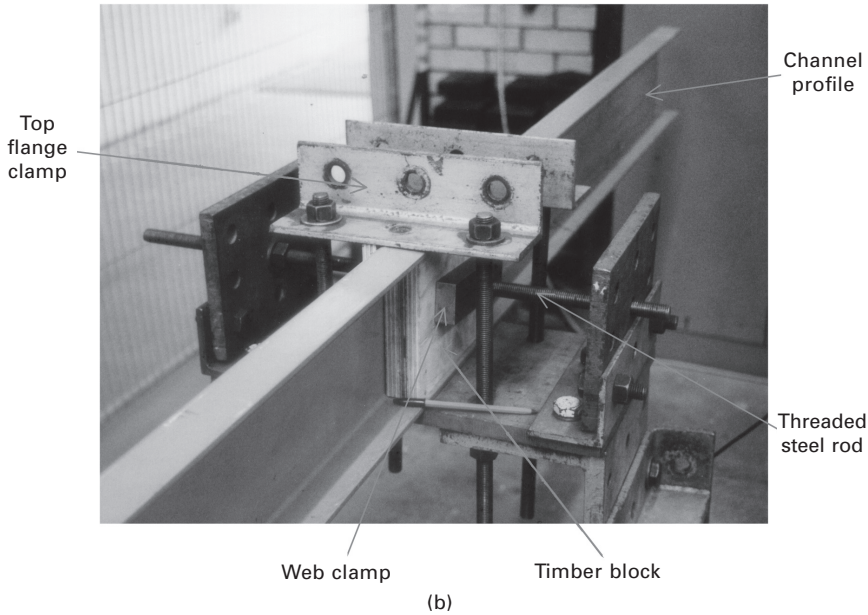

13.14 Continued

derived from tests on a simply supported continuous beam with two equal spans and point loads applied at their centres (see Fig. 13.15(b). It is evident from Fig. 13.15(c) that the rotation recorded by the electronic clinometer at the interior support B during the third test on a simply supported, continuous, 102 × 102 × 6.4 mm WF beam with 2.5 m spans is zero. This verifies that the interior support B is behaving as a rigidly clamped support for each span.

Tests have also been carried out on unstiffened and CFRP stiffened pultruded GFRP beams with CFRP stiffened flanges and bolted end connections to check whether first-order, semi-rigid, shear deformation beam theory may be used to predict their deformation responses (see Turvey and Brooks (2002) and Turvey (2007)). Good correlation between theory and experiment was demonstrated.

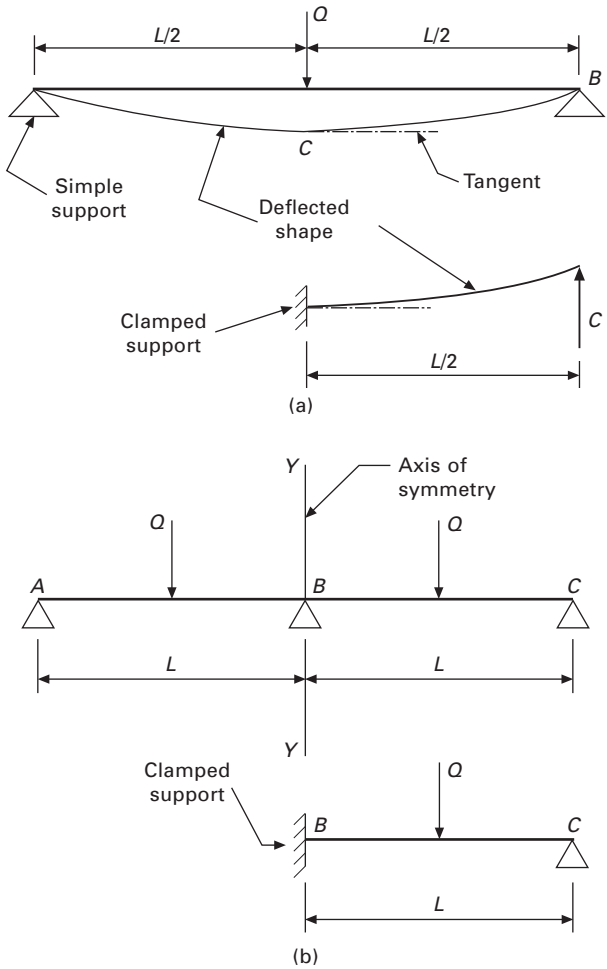

13.15 The use of structural and loading symmetry to show that a beam with one clamped support is equivalent to another beam with only simple supports: (a) a tip loaded cantilever beam is equivalent to a simply supported beam; (b) a propped cantilever beam is equivalent to a two-span simply supported beam; (c) load versus support rotation response of a two-span, simply supported continuous 102 × 102 × 6.4 mm pultruded GFRP WF beam (reproduced with permission of Net Composites Ltd (Turvey, 2011)).

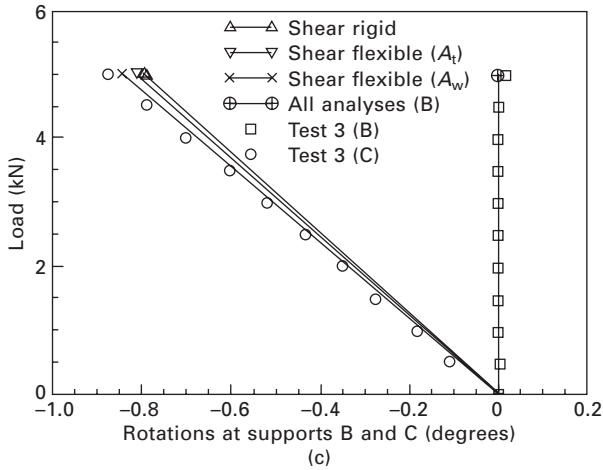

13.15 Continued

13.3.2 Torsion testing of pultruded GFRP beams

It appears that there has not been a great deal of test work undertaken to quantify the torsional stiffness characteristics of *open-section* pultruded GFRP structural-grade profiles. The reason for this may be that the design of the test fixture(s) is not straightforward. Figure 13.16(a), which shows one means of applying a torque to the mid-span of a pultruded GFRP WF profile, illustrates the point. It consists of a two-part aluminium disk which encloses the profile so that the centre of the disk and the axis of the profile are coincident. Two pin-jointed tension/compression members have their ends connected to diametrically opposite points on the disk's circumference. Their other ends are connected to a lever-loading device. The load applied to the end of the lever-loading device is determined from the deformation of a calibrated proving ring and the pin-jointed members are also strain gauged. The angle of twist of the beam is recorded by an electronic clinometer attached to the rear of the aluminium disk. Concrete blocks with hardwood packing and steel bolts, similar to that shown in Fig. 13.14(a), were used to simulate rigidly clamped end conditions. Some tests were also undertaken with bolted end connections formed from pultruded GFRP angle profiles connected to the I-profile's web and transverse steel side plates, as shown in Fig. 13.16(b).

An alternative test set-up that has been used to apply an axial torque to a pultruded GFRP WF profile is described in Turvey and Zhang (2004b). It is essentially a scaled-up version of that shown in Fig. 13.8(a). One end of the beam is connected to a rigid steel support by bolted GFRP web and flange cleats, as shown in Fig. 13.16(c). The other end of the beam is similarly connected to a thick steel plate. Attached to the rear of the plate is

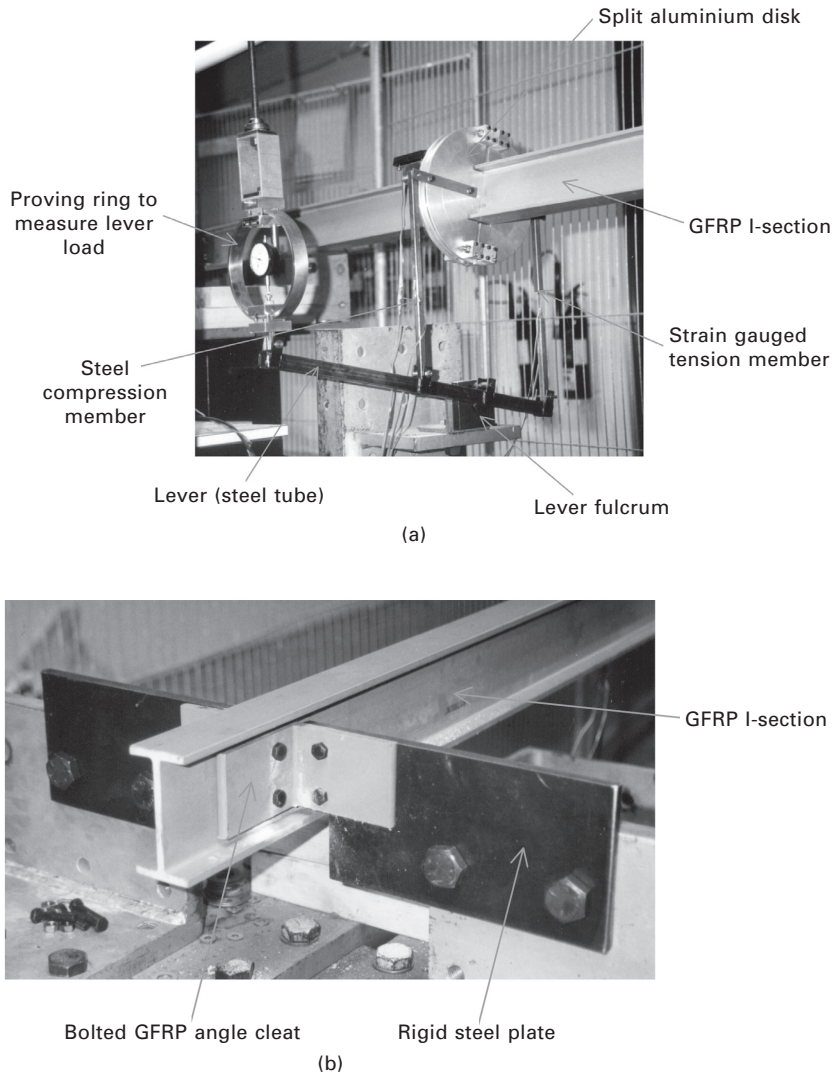

13.16 Test rig used to carry out torsion tests on beams: (a) lever loading arrangement for applying and measuring the torque and rotation at the mid-span of a 102 × 51 × 6.4 mm pultruded GFRP I-beam; (b) bolted cleat end support conditions for the same beam. Photographs (c) and (d) show parts of an alternative test rig for torsion tests on beams: (c) bolted flange cleats connected to a rigid steel support at one end of the beam; (d) rigid steel plate at the other end of the beam connected to a pulley wheel supported by a short steel spindle; the torque is applied by means of a loading hanger (not shown) at the end of a wire which is attached to the pulley wheel (reproduced with permission of the Canadian Society for Civil Engineering (Turvey and Zhang, 2004b)).

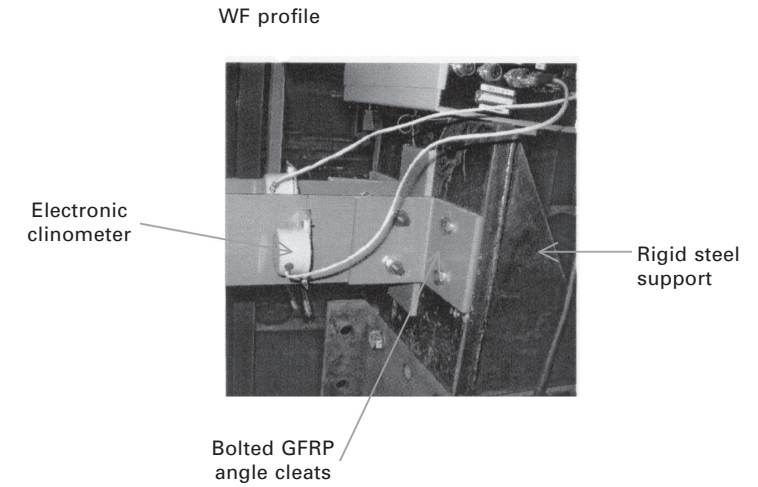

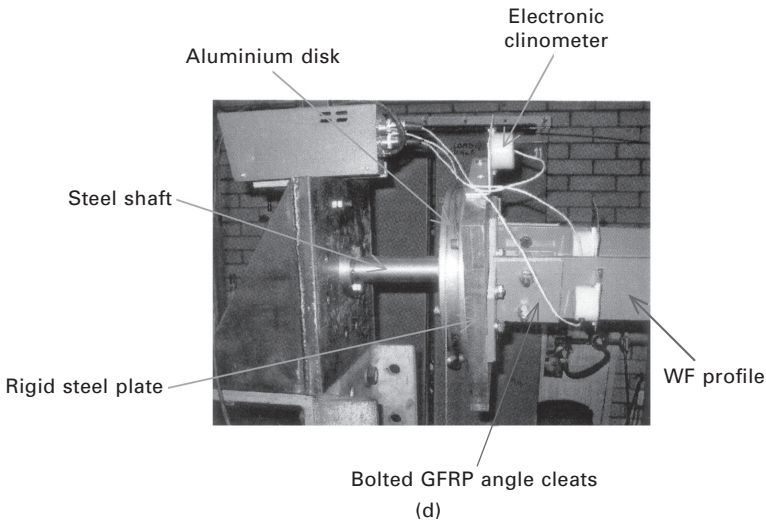

13.16 Continued

an aluminium pulley. The pulley is fixed at its centre to a short steel shaft, the other end of which is supported by a bearing housed in a rigid steel support (see Fig. 13.16(d)). An axial torque is applied to the WF profile by means of a hanger carrying dead weights (not shown) which is connected tangentially to the pulley by a steel cable. Three clinometers were used to monitor rotations – one attached to each of the WF profile's flanges to detect cross-section distortion, and the third attached to the steel plate to record the angle of twist. The test rig has been used to carry out torsion tests on pultruded GFRP 102 × 102 × 9.5 mm WF beams with bolted web, flange

and web and flange connections. Further details, i.e. torque versus twist plots and torsional stiffnesses, are given in Turvey and Zhang (2004b).

13.3.3 Lateral buckling of pultruded GFRP beams

Although it is important to know that classical first-order shear deformation beam theory may be used to predict the deflection of unstiffened/stiffened beams with various end support conditions, it is equally important to appreciate that beams may also buckle laterally before the deflection serviceability limit is reached. Of course, this potential consequence has been appreciated for a long time and several researchers have carried out tests on pultruded GFRP beams in order to provide load and deformation data to verify lateral buckling analyses. It appears that Mottram (1992) was the first to report lateral buckling tests on a simply supported, pultruded GFRP I-beam. Subsequently, lateral buckling tests have been reported by Brooks and Turvey (1995), Turvey (1996a, 1996b) and Shan and Qiao (2005) on tip-loaded flat strip, WF and channel profile cantilevers, by Barbero and Raftoyiannis (1994), Davalos *et al*. (1997), Roberts (2002) and Insausti *et al*. (2009) on simply supported WF and I-profiles subjected to mid-span point loads, and by Turvey and Brooks (1996) on WF profiles subjected to end moment loading.

Figure 13.17(a) depicts the consequences of gradually increasing the load applied at the free end of a cantilevered, rectangular cross-section, pultruded GFRP profile. The load has exceeded the lateral buckling load and the cantilever has assumed a stable post-buckled state. It is self-evident that, in reaching this state, the loaded end cross-section of the cantilever has undergone large horizontal and vertical translations as well as a large rotation. Furthermore, the applied load, whilst remaining vertical, has followed these large translations. It is the size of these translations which are the cause of difficulty when planning lateral buckling tests on pultruded GFRP beams. How are the large deformations to be measured and how can the verticality of the applied load be maintained whilst following the large translations?

These difficulties have, of course, been resolved in a number of ways, one of which is partially illustrated for the pultruded GFRP cantilever shown in Fig. 13.17(a). In this case, dead-loading has been applied to the free end of the cantilever, so the load moves with the free end and gravity ensures that it remains vertical. The dead-load is in the form of weights slotted onto a hanger. The hanger is supported at the lowest point of a wire loop. The uppermost point of the loop is in contact with the inner surface of an annular steel insert, which is positioned on the neutral axis close to the free end of the cantilever. The loop wire is kept inclined by a horizontal steel compression member with slotted ends, so that when the cantilever buckles laterally, and the end cross-section rotates, it does not touch the wire. This loading arrangement is, however, only satisfactory for long slender pultruded GFRP

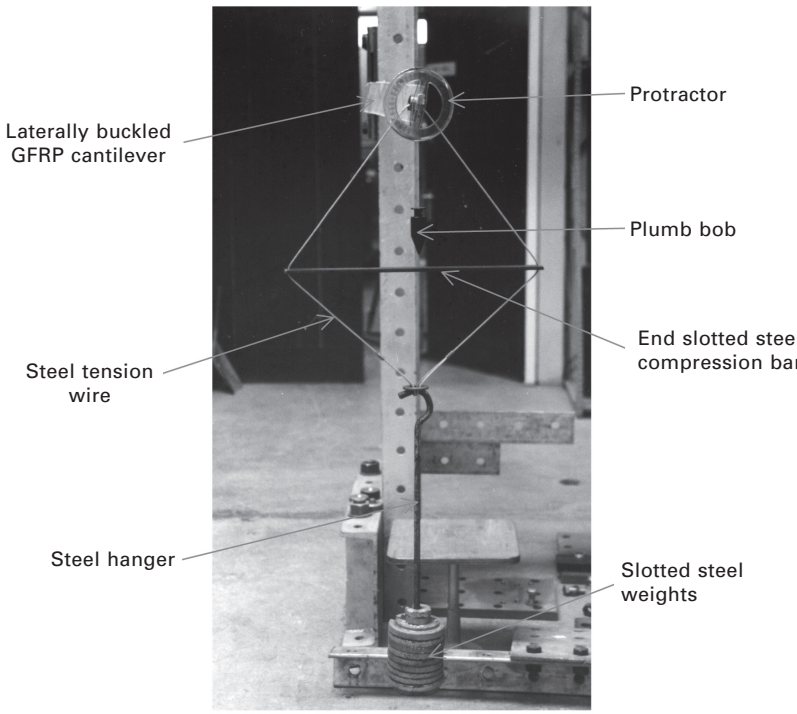

(a)

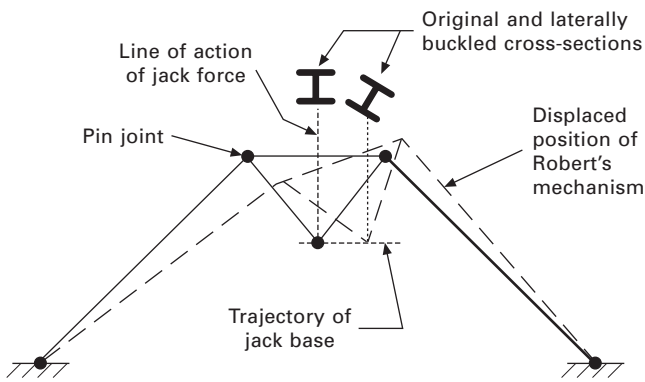

(b) (1)

13.17 (a) A tip-loaded rectangular cross-section pultruded GFRP cantilever beam in a stable post-laterally buckled state showing the loading arrangement, (b1) schematic diagram of a Roberts mechanism which translates whilst keeping the lowest vertex of the pin-jointed triangle at a constant height above the base, (b2) a prototype Roberts four-hinged mechanism for applying gravity loading to a pultruded GFRP beam; (c) air-bearing supported jack.

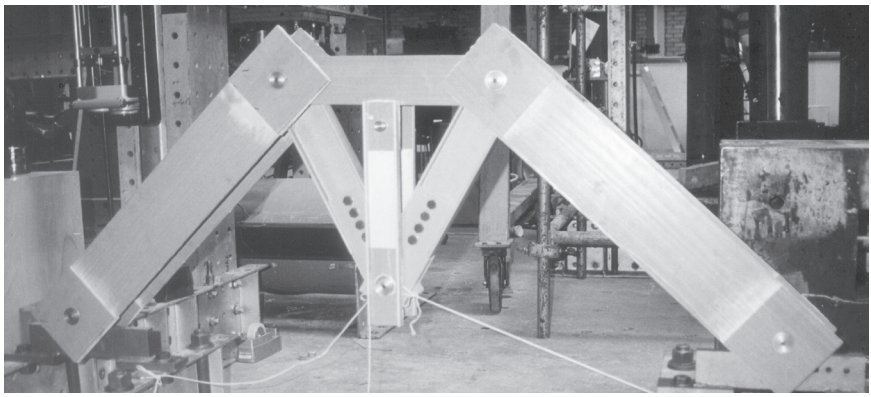

(b) (2)

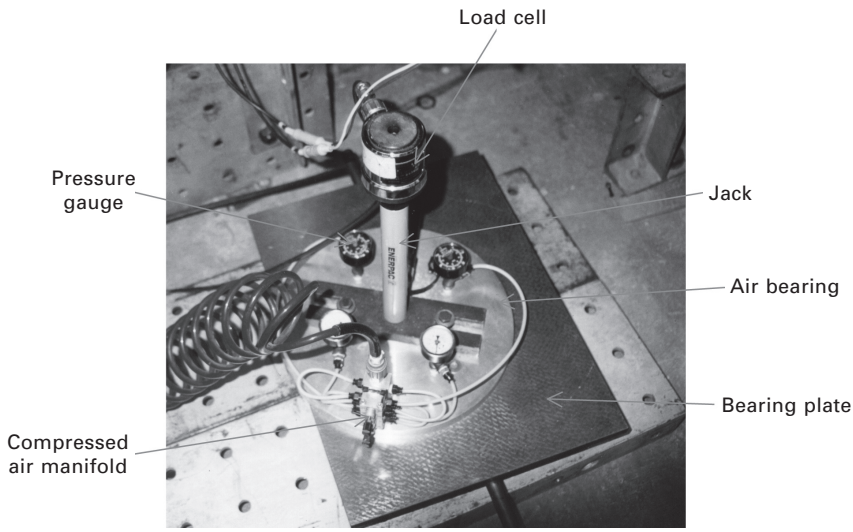

(c)

13.17 Continued

beams, which buckle laterally under relatively low loads. It is unsuitable for shorter span beams, which buckle at much higher loads, because the length of the hanger will have to increase substantially to accommodate the required number of slotted weights. Moreover, there are safety issues to contend with, in so far as it is undesirable to have large dead-weight loads undergoing relatively large vertical and horizontal displacements. Furthermore, should the beam collapse suddenly and without warning (GFRP is, after all, an elastic brittle material) whilst a slotted weight is being added to those already on the hanger, the whole dead-loading would be released, possibly resulting in personal injury.

As mentioned above, the other major difficulty with carrying out lateral buckling tests on beams is how to measure the large translations and rotations. For the beam test shown in Fig. 13.17(a), which was carried out some 20 years ago, a large protractor and a plumb bob were attached to the end of the cantilever to enable rotations to be measured. In addition, two theodolites (not shown) were set up facing each other (one behind the clamped support and the other at a known, reasonably large distance in front of the free end of the cantilever). The theodolite behind the clamped support was used to align the one in front with the *true* longitudinal centreline of the cantilever. The latter theodolite was used to determine the initial and subsequent translations and rotations of the free end of the cantilever during the test. Although somewhat cumbersome, this method of recording deformations was effective.

For lateral buckling tests on stiffer pultruded GFRP beams, i.e. WF profile beams with both ends supported, dead-weight loading (for the reasons already given) is not practical and it is necessary to use hydraulic jacks. The jacks tend to be of lower capacity than those generally used to test metallic or concrete structures – typically 10 to 50 kN capacity. Moreover, they need long extensions, i.e. 125–250 mm. In order to simulate gravity loading, the jacks have to translate with the beam as it buckles laterally. In his lateral buckling tests on simply supported beams subjected to symmetric three-point flexure, which were carried out in a universal testing machine, Mottram (1992) used a fixed roller bearing to allow the beam's loaded flange to translate laterally under the applied load. However, with this arrangement the lateral translation was very limited and could have acted as a restraint as the lateral deformation of the beam increased.

Two other means of allowing the applied load to translate with the beam have been used successfully. One involves supporting the jack in a four-bar mechanism, which is illustrated schematically in Fig. 13.17(b1), and the other uses an air bearing. Generally, it is easier to accommodate higher loads with four-bar mechanisms than with air bearings. However, the four-bar mechanism can only be used when the plane of lateral translation is known *a priori*, whereas the air bearing automatically adjusts to the direction of lateral translation.

The four-bar mechanism depicted in Fig. 13.17(b2) is a prototype mechanism fabricated from pultruded GFRP plate and I-profiles. It was used to prove the design requirements, namely that a jack load of 45 kN could translate through ±150 mm whilst ensuring that the jack's pivot point (the lower vertex of the triangle) always remained at the same elevation above the base of the mechanism. On the other hand, the air bearing supporting the jack shown in Fig. 13.17(c) is only able to accommodate jack loads up to about 20 kN and radial translations in the horizontal plane of ±100 mm. One drawback with the air bearing is its proneness to vibration if the air leakage becomes unsteady.

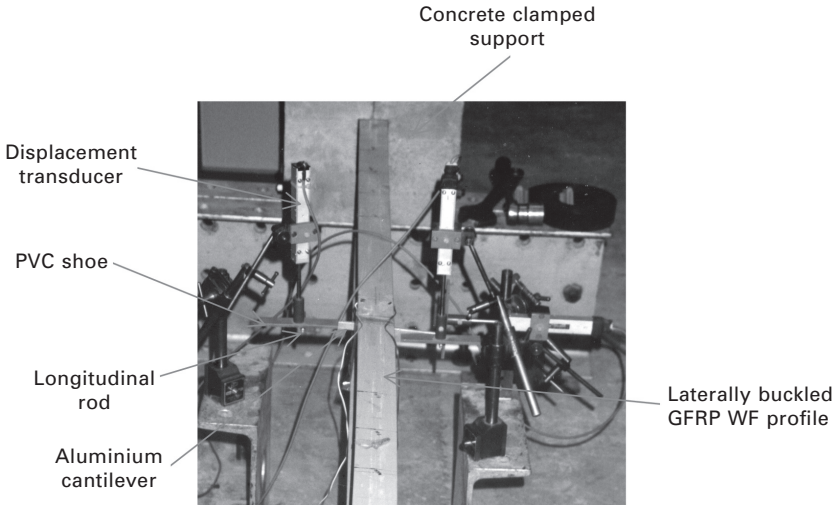

13.18 Laterally buckled beam showing the vertical and horizontal displacement transducers with PVC shoes in contact with the longitudinal rods at the ends of the aluminium cantilevers bonded to the web of the beam.

In lateral buckling tests on pultruded GFRP WF profile beams with both ends supported, the deformations within the post-buckled regime are generally smaller than those of the cantilever shown in Fig. 13.17(a). Nevertheless, they are sufficiently large to require special attention. One method of measuring lateral buckling deformations, used by Stoddard (1997), was to attach the ends of braided, pre-tensioned fishing line to the edges of the flanges (one to the top and two to the bottom flange) of a WF beam. The other ends of the lines were connected to the cables of three string potentiometers, which recorded their extensions as the beam buckled laterally. Trigonometry was then used to decompose the extensions into the vertical and horizontal deflections and the rotation of the beam's cross-section.

An alternative approach, used by Turvey and Brooks (1996), involved bonding two small aluminium cantilevers normal to the web of the WF beam. Aluminium rods at the ends of the cantilevers extended for a short distance parallel to the web of the beam. These rods provided the lines of contact for long, PVC *shoes* placed over the ends of three extensometers (two vertical and one horizontal). Figure 13.18 shows an image of the cantilevers and the transducers with their PVC shoes. The two vertical transducers enabled the vertical deflection and the cross-section rotation to be determined and the horizontal transducer recorded the lateral translation of the beam directly. In later lateral buckling tests an electronic clinometer was also attached either to one of the beam's flanges or to its web to record the cross-section rotation directly.

13.3.4 Buckling and collapse of columns

Testing of columns has attracted a lot of attention from researchers. In the USA buckling tests on axially compressed, slender WF and angle profile columns have been carried out by Zureick and Scott (1997) and Zureick and Steffen (2000) respectively. Barbero and Tomblin (1992, 1993) have also tested long WF profile columns. In Europe Mottram *et al*. (2003) have carried out similar tests on long and intermediate length WF profile columns. In the latter case, the columns were tested horizontally rather than vertically. Although not cited here, there are a number of other researchers who have undertaken column tests on channel, angle and circular hollow section profiles. The earlier test work has led to the development of column buckling curves for WF profiles (see Barbero and Tomblin, 1994).

Long columns tend to buckle in an overall or long-wavelength mode (often referred to as the Euler buckling mode), as shown in the right-hand image of Fig. 13.19(a), whereas short columns buckle in a local or short-wavelength mode (see Fig. 13.19(b)). At intermediate lengths buckling mode interaction may arise, i.e. the buckled mode is a combination of the two modes. Although it was not mentioned specifically in Sub-section 13.3.3, lateral buckling of beams is a long-wavelength buckling mode. Furthermore, the local or short-wavelength buckling mode may also arise in the compression flanges of beams, particularly WF profile beams. In addition, it is also possible for the interactive buckling mode to arise in beams (see Fig. 13.19(c)).

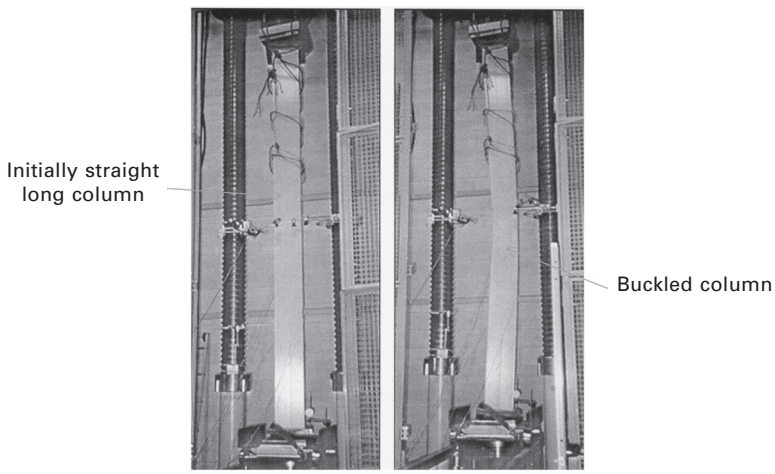

13.19 (a) Buckling of a long column: straight column set up ready for an axial load test (left-hand image) and long wavelength (Euler) buckling mode of the same column (right-hand image) (reproduced with permission of S. Russo, Iuav University of Venice, Italy, 2011); (b) local buckling of a short column, (c) image showing buckling mode interaction of a tip-loaded pultruded GFRP cantilever.

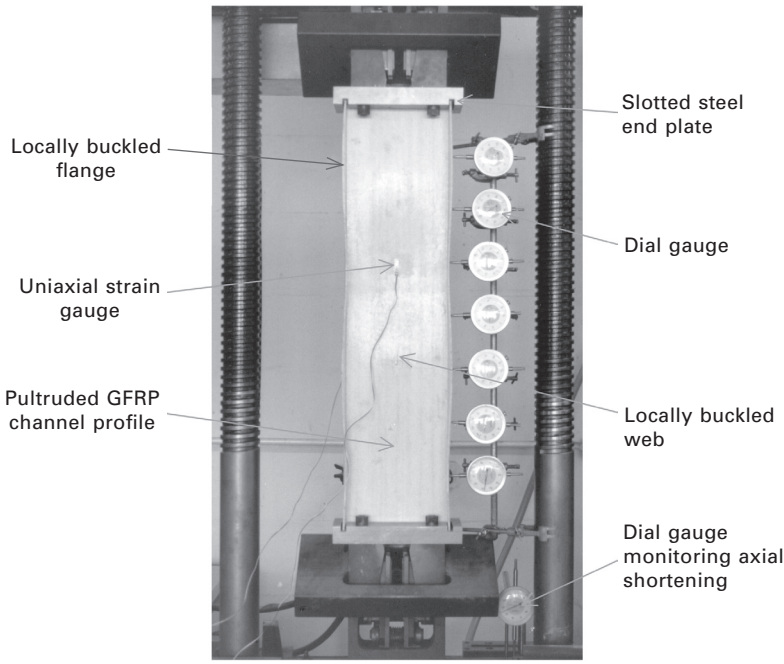

13.19 Continued

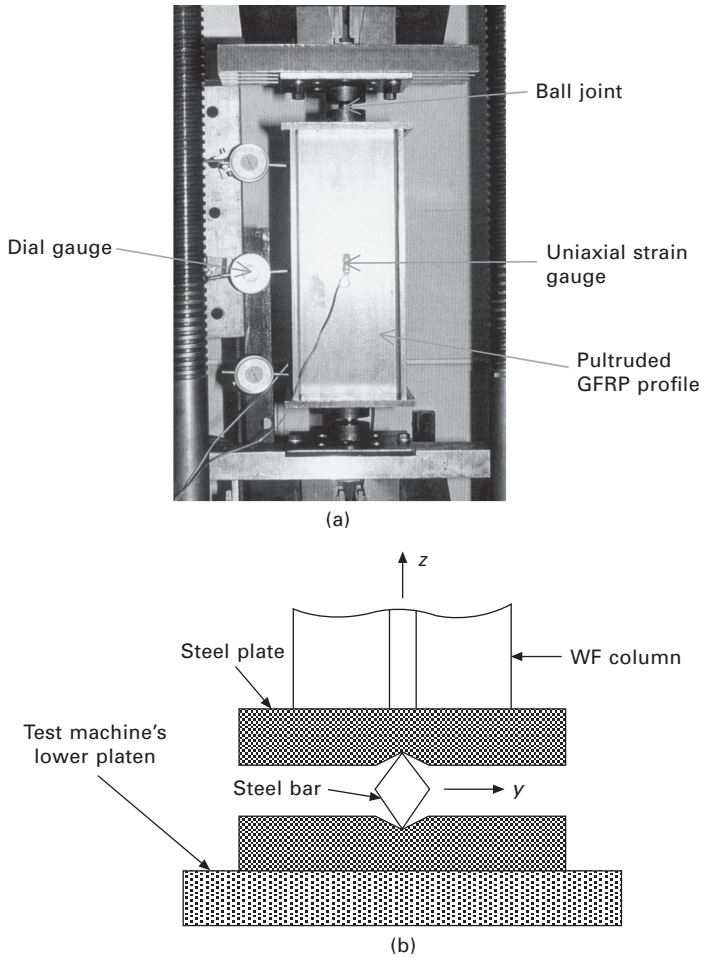

13.20 (a) A pultruded GFRP WF column with the load applied axially through hardened steel ball joints; (b) schematic diagram of a diamond-shaped rocker between two steel plates with shallow v-recesses which simulates simply supported end conditions with respect to one principal plane and clamped conditions with respect to the other principal plane.

In column buckling tests particular care has to be taken with setting up the column's end support conditions and with the axial or eccentric alignment of the end compressive forces. In order to reduce force alignment difficulties, buckling tests are often carried out in universal testing machines with extended *daylights*. Simply supported end conditions have been simulated in some tests by means of a steel ball located between two thick steel plates, as shown in Fig. 13.20(a). For column tests which require simply supported

end conditions with respect to one of the profile's principal planes, and clamped conditions with respect to the other, a diamond-shaped steel bar located between v-notches in upper and lower thick steel plates may be used, as shown schematically in Fig. 13.20(b). Many column tests have also been carried out with the load applied through flat steel plates bearing directly on the ends of the profile. Plates with recesses machined in the shape of the profile's cross-section have also been used. In both cases it is necessary to machine the ends of the column profile both flat and parallel to each other.

In general, short pultruded GFRP columns buckle in a local mode. Figure 13.21(a) shows a WF profile column subjected to axial end compression in which the local buckles in the flanges and web are clearly visible. A finite element (FE) eigenvalue analysis of the buckling test has been carried out; the similarity between the experimental and computed buckling modes is self-evident in Fig. 13.21(a), and good correlation between the FE computed and experimental load versus surface strain responses is also evident in Fig. 13.21(b) (see Turvey and Zhang, 2006, for further details).

It is well known that imperfections can lower the buckling loads of columns, especially for intermediate length columns, where mode interaction may arise. In general, there are two types of imperfection: residual stresses and geometric imperfections. At the present time, it appears that little is known about the former type of imperfection in pultruded GFRP structural-grade profiles. However, this may not be of too much concern, because buckling is stiffness rather than strength dominated. Moreover, it is possible that initial residual stresses within the profiles may dissipate due to creep effects within the matrix of the GFRP composite material. On the other hand, geometric imperfections are likely to be significant. There are three types of geometric imperfection, which may affect the buckling behaviour of pultruded GFRP long and intermediate length columns, namely out-of-straightness with respect to the column cross-section's principal axes and twist about the column's longitudinal axis. The latter imperfection is rarely considered in hot rolled steel columns, though residual stresses are considered to be important. In their design handbooks (see, for example, Anon., 1989) the manufacturers quantify upper limits on the magnitudes of the geometric imperfections (tolerances) per metre length of their pultruded GFRP structural-grade profiles. However, it is unclear as to how these values have been determined. Another type of geometric imperfection that may be of importance for local buckling of pultruded GFRP WF profiles is *flange droop*, which is believed to be a consequence of residual curing of the polymer matrix (the profile is not fully cured on exiting the pultrusion die).

As far as the author is aware, the effects of real geometric imperfections in column buckling analyses of pultruded GFRP profiles have not been investigated thoroughly. As mentioned above, only maximum values of

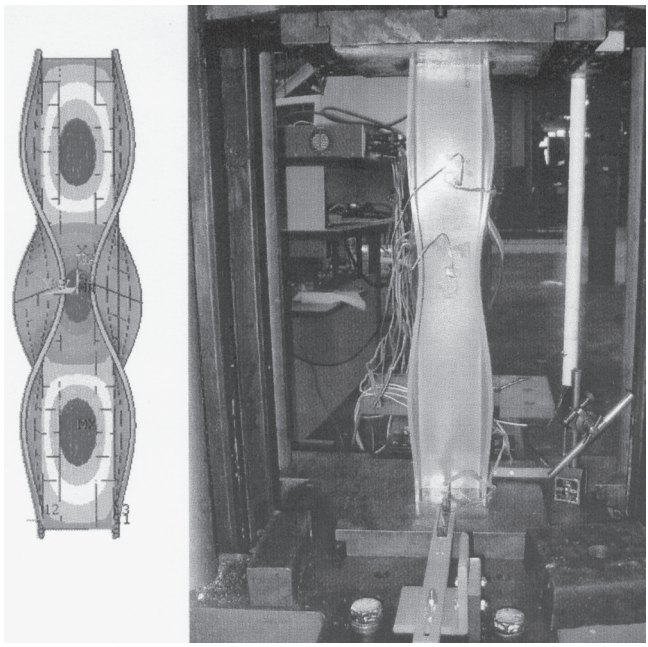

(a)

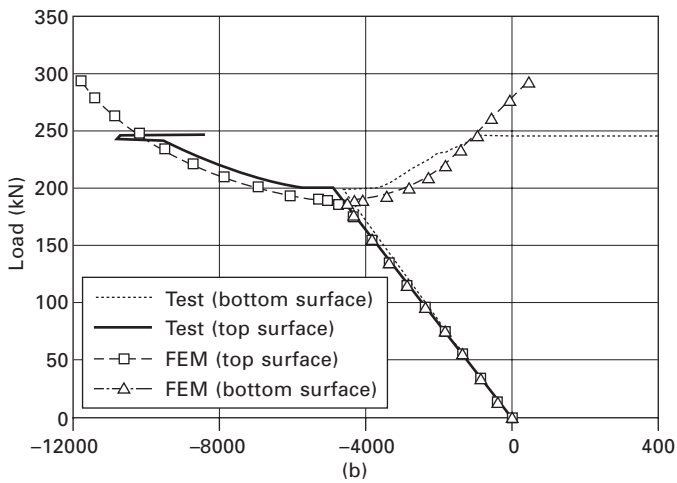

(b)

13.21 (a) An axially loaded, short, post-locally buckled, pultruded GFRP WF column showing the short wavelength buckles in the web and flanges and a finite element (FE) eigenvalue analysis of the same column (note the strong similarity between the local buckling modes); (b) comparison of the experimental and FE predicted pre and post-buckling axial compression load versus surface strain responses of a short WF column (reproduced with permission of Elsevier (Turvey and Zhang, 2006)).

tolerances on out-of-straightness, etc., are given in the manufacturer's design handbook (Anon., 1989). The measurement of actual geometric imperfections remains to be investigated thoroughly. However, some progress has been made towards addressing this situation. A test rig has been developed for measuring the geometric imperfections of pultruded GFRP WF profiles. An image of the rig is shown in Fig. 13.22(a). It incorporates two systems for measuring geometric imperfections. One comprises six linear displacement potentiometers, which travel up the length of the column on an aluminium frame driven by an electric motor. The other comprises four video cameras fixed to the same frame. A close-up view of the frame and instrumentation is shown in Fig. 13.22(b), and an image of the measured shape of a 2.5 m long WF profile column is shown in Fig. 13.22(c). The maximum values of the translations at the top of the column (relative to the bottom) were 17 mm and 7 mm in the minor and major principal planes respectively. Likewise, the maximum axial rotation was 0.0083 radians. It should, however, be recognised that the process of setting up a long column in a test machine is likely to modify the values of the *free-standing* imperfections. Consequently, it is desirable to re-measure them *in-situ* prior to commencing the column test. Unfortunately, the rig shown in Fig. 13.22(a) could not be used with the long column test machine available to the author.

Although a large number of column buckling tests have been carried out on pultruded GFRP profiles, and in many instances the columns have been loaded to failure, their post-buckled reserve of strength has not been adequately quantified. Moreover, their modes of failure/collapse remain poorly understood. This is due in no small part to the orthotropic elastic, brittle nature of the GFRP composite material, which dictates that collapse occurs suddenly and extremely rapidly – being effectively a dynamic process. Consequently, it is not at all easy to discern, from the usually extensively cracked and delaminated remains, what triggered collapse and how it progressed in such a short time interval (less than one thousandth of a second).

In the belief that collapse of pultruded GFRP columns is a dynamic process, high-speed video imagery has been used to try to *capture* failure initiation and progression during axial compression tests on short WF columns. Three images of the failure event from one such test are shown in Fig. 13.23. Figure 13.23(a) shows the column in a stable post-buckled state. Figure 13.23(b), taken about a two-thousandth of a second later, shows that failure initiates at the column's left-hand web-flange junction. This image is particularly significant, not least because many structural analysts tend to overlook the fact that, even in the presence of macro-scale structural and loading symmetry, composite material structures generally fail unsymmetrically. The reason is simply that, at the micro-scale, the fibres and matrix are not distributed symmetrically, especially in web-flange junctions. Figure 13.23(c) shows the further development of the collapse mode. In this image, failure

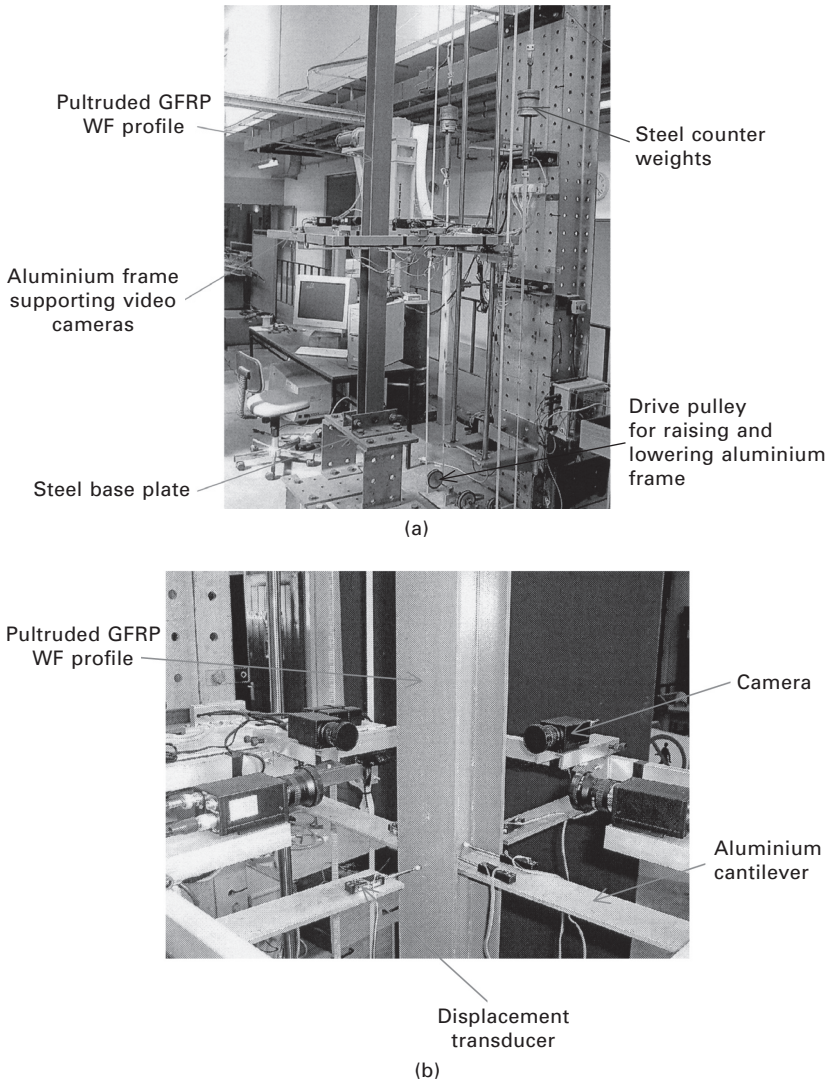

13.22 (a) An overall view of a test rig used to measure the geometric imperfections of a pultruded GFRP WF column; (b) a close-up view of the frame used to support the linear displacement transducers and the four cameras used to record the geometry of the WF profile; (c) an image of the measured shape of a WF profile.

has developed at the left-hand and right-hand web-flange junctions and both flanges have started to collapse as a result of local tearing of the web-flange junctions. It is also evident that the web is also starting to bulge locally due to tearing of the right-hand web-flange junction.

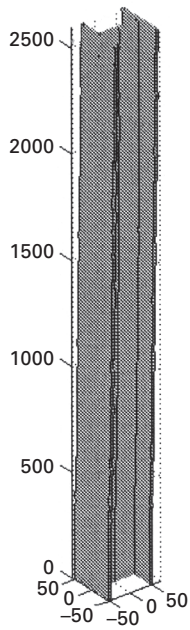

(c)

13.22 Continued

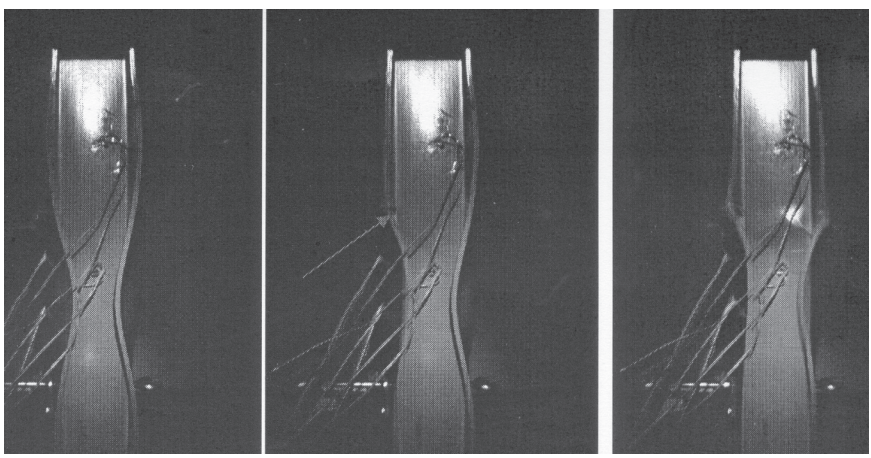

(a) (b) (c)

13.23 High-speed video images of the sequence of buckling and failure of a short, pultruded GFRP WF column subjected to axial compression: (a) the post-locally buckled state immediately prior to failure initiation, (b) the instant of failure initiation at the left web-flange junction (see arrow head) and (c) development of further failure at both web-flange junctions and in the web.

13.4 Tests to characterise the stiffness and strength of pultruded GFRP joints

In this sub-section consideration is given to some of the features of tests that have been carried out on axially loaded bolted and bonded joints. These joints arise predominantly in truss-type structures or in bracing systems used to resist sway of simply connected beam and column frame structures.

The other type of bolted joint considered here is that used to connect beams to columns, and columns to column bases. These joints usually involve additional connection components in the form of angle or flat plate profiles. Consequently, both the bolts and the angles/plates participate in the transfer of bending moments and shear forces between beams and columns and between columns and their bases, and in the latter case also uplift forces.

It is convenient to consider axially loaded joints first. Furthermore, as only minimal testing of such joints in compression has been reported (see Erki, 1995), consideration will be restricted to tension testing of such joints.

13.4.1 Tests on plate-to-plate joints in tension

At the outset, it should be appreciated that there are no standardised tests for bolted and bonded tension joints. There are, however, standardised tests for the determination of a composite material's pin bearing strength (ASTM D 953-02 (2002), ASTM D 5961/D 5961M-05 (2005) and EN 13706-2 (2002)). Only the third standard mentioned is specifically intended for use with pultruded GFRP composite profiles. In addition, there are standardised tests for the determination of the shear strength of adhesives (ASTM D 5868-01 (2008)). Clearly, the pin bearing strength standards are relevant to the testing and design of bolted tension joints and the standard for adhesive shear strength is relevant to bonded joints.

The standardised pin bearing test methods specify the test fixture geometry, material specimen, pin and hole dimensions and their tolerances as well as details of the test procedure. Bearing compression failure is induced at the pin–hole contact interface within the composite material specimen by means of axial tension applied to the rig and specimen. A schematic diagram of the test set-up and test specimen is shown in Fig. 13.24(a).

Two versions of an alternative, non-standardised test – a direct compression test – for the determination of the pin bearing strength of pultruded GFRP composite material have been developed by Mottram (1994) and Mottram and Zafari (2011). A schematic diagram of the test configuration of both versions of the test is shown in Fig. 13.24(b). An important advantage of the test set-up is that it uses less material than is required by the test set-up shown in Fig. 13.24(a). However, this is only achieved by eliminating material above the horizontal cross-section through the centre of the pin, which would otherwise

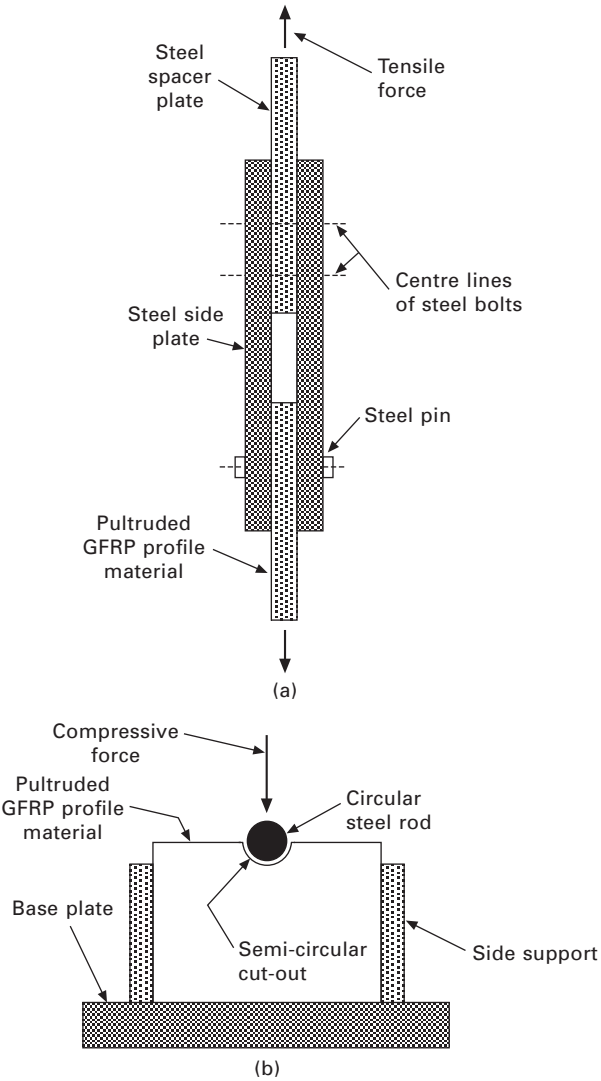

13.24 (a) Schematic diagram of the ASTM test set-up to determine the pin bearing strength of a composite material; (b) schematic diagram of the non-standard test set-up to determine the pin bearing strength of a pultruded GFRP composite material.

be stressed in tension. Consequently, the stress distribution around the hole is different from that in the test set-up shown in Fig. 13.24(a), which may be regarded as being closer to that which arises in practice.

Turning now to tests on bolted joints in tension, the test set-up is straightforward and similar to tension coupon testing, but with the addition

of displacement transducers to monitor the axial displacement of the bolt(s). The majority of tests undertaken have been on single-bolt joints in pultruded GFRP plate profile. Moreover, most of them have used the symmetric, double-lap configuration with the bolt shank being sheared along two planes and only the smooth surface of the shank in contact with the GFRP material. A schematic diagram of the test configuration is shown in Fig. 13.25(a). This configuration may be used in three forms: (1) with pultruded GFRP inner and outer laps, (2) with pultruded GFRP outer laps and a steel inner lap, and (3) with steel outer laps and a pultruded GFRP inner lap. Moreover, it is not necessary for the inner and outer laps to be of equal thickness, as indicated in Fig. 13.25(a). It appears that most joint tests have used either configuration (2) (see Rosner and Rizkalla, 1995) or configuration (3) (see Cooper and Turvey, 1995). When configuration (2) is used, two nominally identical single-bolt joints are tested in parallel, and, moreover, the through-thickness compression around the bolt hole due to the bolt torque is limited to the surface areas of the washers under the bolt head and nut. However, when configuration (3) is used, only one joint is tested. Moreover, the through-thickness compression around the bolt hole due to bolt torque is likely to be low because it is distributed over a large area by the relatively rigid steel outer laps. There is a further difference between test configurations (2) and (3). In the latter case, the failure mode is only revealed after the outer steel plates have been removed, whereas in the former case, failure due to cracking/delamination has only to progress beyond the outer circumference of the washers to be visible during the test.

Similar test configurations have also been used to undertake tension tests on multi-bolt joints (see Hassan *et al.*, 1997; Turvey and Wang, 2009b). Moreover, the latter authors have also carried out both single and multi-bolt tension tests on pultruded GFRP plate profile which, prior to testing, was subjected to environmental conditioning (immersion in water at ambient/elevated temperature for up to three months) (see Turvey and Wang, 2007; 2009b; 2009c). It has been shown that elevated temperature causes a substantial reduction in load capacity, and that it may also change the mode of failure from that which would occur in a joint with the same geometry when tested at ambient temperature (approximately 20–25°C) (see Turvey and Wang, 2009b). The reduction in load capacity of single-bolt joints with increasing temperature is shown in Fig. 13.25(b1 and b2) and some images of the effects of adverse environmental conditions on the failure modes of multi-bolt tension joints are depicted in Fig. 13.25(c1–c4). It is evident that these modes are combinations of the basic modes of bearing, net tension and shear-out that are observed in single-bolt joints with specific ratios of end distance (E) to bolt diameter (D) and of joint width (W) to bolt diameter.

In practice, it is not always possible to use the preferred double-lap joint configuration. Instead, the single-lap configuration, shown schematically in

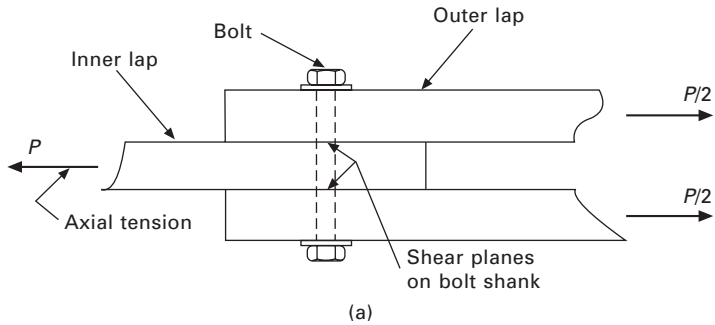

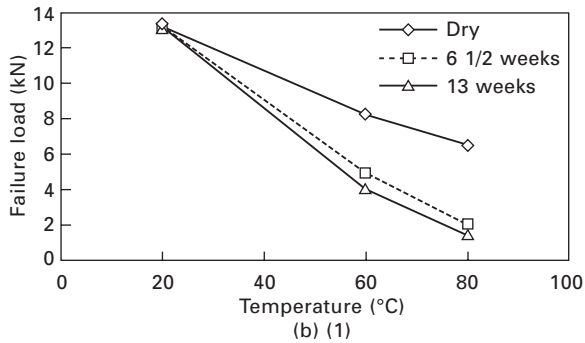

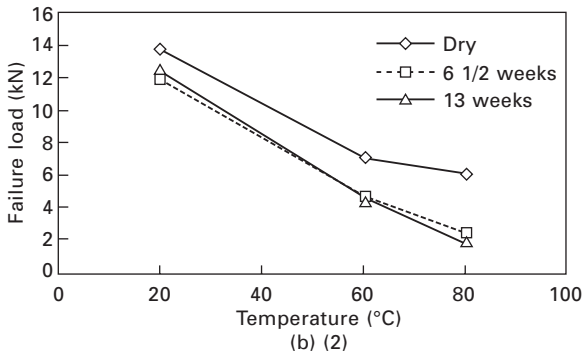

13.25 (a) Schematic diagram of the symmetric double-lap bolted joint test set-up (single-bolt case shown); (b) ultimate load capacity versus temperature for single-bolt, double-lap tension joints: (1) bearing failure design (E/D = 5, W/D = 7), (2) tension failure design (E/D = 7, W/D = 3); (c) failure modes of double-lap two-bolt tension joints subjected to various adverse conditions: (1) ambient temperature (~20°C), (2) hot (60°C), (3) wet (6.5 weeks in water) and (4) hot–wet (60°C plus 6.5 weeks in water).

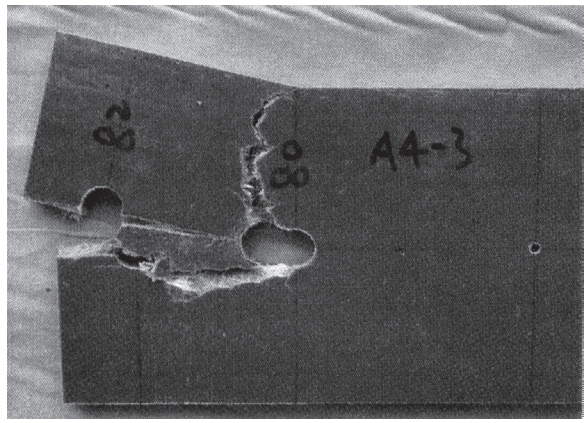

(c) (1)

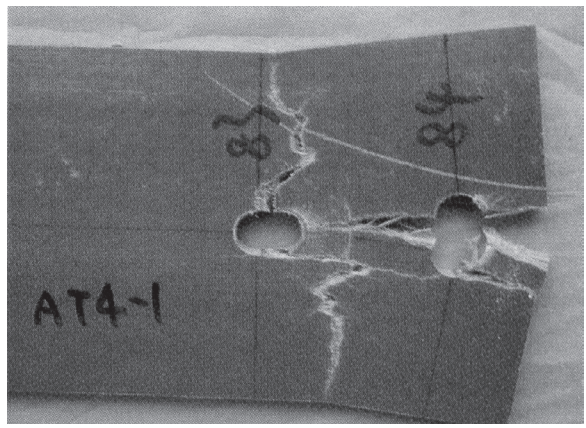

(c) (2)

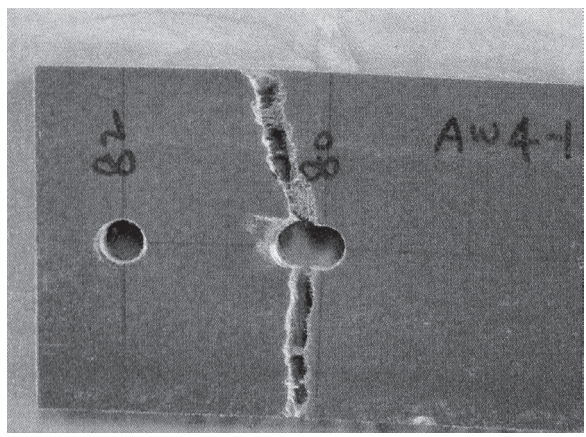

(c) (3)

13.25 Continued

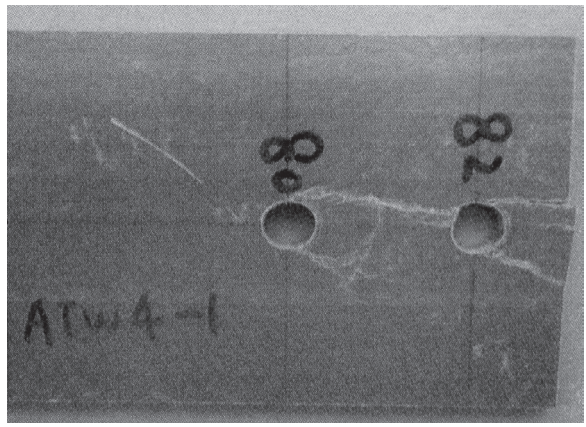

(c) (4)

13.25 Continued

Fig. 13.26(a) for the single-bolt case, has to be adopted. Unfortunately, the equal and opposite tensile forces are not co-axial. Consequently, the joint is also subjected to a *parasitic* bending moment, which lowers the joint's ultimate load capacity and promotes a different mode of failure. The two images, depicted in Figs 13.26(b) and (c), show, respectively, a single-bolt single-lap joint set up ready for testing and a similar joint after failure in tension. The latter figure also illustrates the significant joint rotation at failure and the flexural cracking and extensive delamination of the pultruded GFRP plate. A typical load versus extension plot for a single-bolt single-lap joint exhibits a short region of reduced stiffness, which does not arise in the response plots of double-lap joints prior to failure. This is believed to correspond to slip due to hole clearance and/or the onset of rotation of the single-lap joint during the test.

With regard to the testing of bonded lap joints, it is apparent that most of the test work has been undertaken on symmetric double-lap joints. A sketch of a typical joint configuration is shown in Fig. 13.27. No special test rig is required to conduct the tests. Indeed, they are tested in much the same way as tension coupons. Most of the early tension tests on pultruded GFRP profile joints were carried out under ambient temperature conditions (see, for example, Keller and Vallée, 2005a, 2005b; Vallée and Keller, 2006; Zhang *et al*., 2010a). The main differences in the test configurations are (1) whether or not a gap is left between the joint ends of the inner adherends, and (2) whether or not the ends are bonded together. In the case of bonded ends with only a bondline thickness separating them, it may be anticipated that the stress concentrations at those ends may differ somewhat from when there is a gap and no adhesive. In most of the aforementioned tests, there was a gap between the ends of the inner adherends, so their ends were unbonded. In

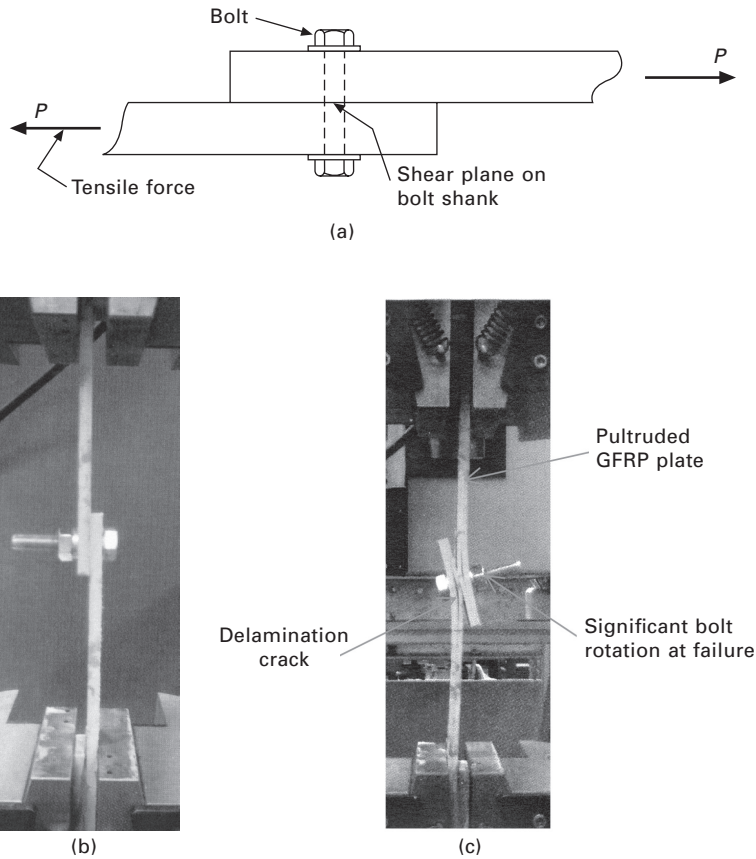

13.26 (a) Schematic diagram of a single-bolt, single-lap tension joint; (b) single-bolt, single-lap joint set up ready for testing; (c) single-bolt, single-lap joint after failure in tension.

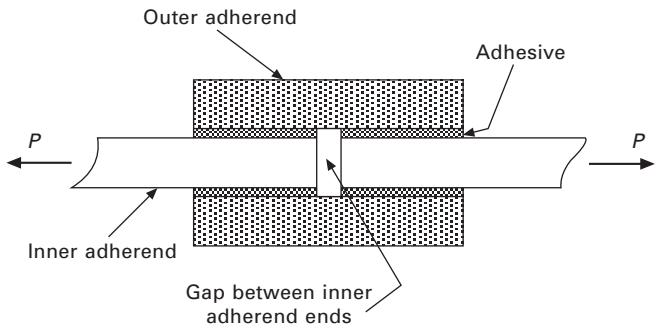

13.27 Schematic diagram of a double-lap bonded tension joint.

some of the tests, uniaxial strain gauges were bonded across the width and near to the ends of the outer faces of the outer adherends in order to detect first failure of the adhesive bond. In addition, crack propagation gauges were bonded to the sides of some of the joints in order to monitor failure progression within the adhesive.

Zhang *et al*. (2010b) have also carried out tension tests on symmetric double-lap bonded joints at temperatures below and above ambient in order to quantify their effects on joint stiffness and strength. However, the data obtained must be regarded as preliminary or exploratory, because a single-joint geometry was used. Moreover, at some temperatures, too few nominally identical joints were tested.

13.4.2 Tests on beam-to-column and column-to-base joints

Although a few tests on bonded pultruded GFRP WF profile beam-to-column joints have been reported (see Sanders *et al*., 1996), in practice mechanical fastening is the preferred means of connecting beams to columns in frame structures made of these materials. Consequently, only tests on bolted configurations of these joints are considered in this sub-section.

It comes as no surprise to realise that standardised procedures for carrying out such tests do not exist. Indeed, most of the test configurations are similar to those that have been used in the past to test bolted joints between hot rolled steel columns and beams.

The simplest type of test set-up that has been used is based on a tip-loaded semi-rigidly connected cantilever beam. One leg of each angle profile (the cleats) forming the joint is bolted to the web and/or flanges at one end of the pultruded GFRP WF profile beam. The other leg is then bolted to a rigid vertical support (typically a thick steel plate) to complete the joint (see Fig. 13.28). The cantilever beam is loaded either by weights or by a tension jack connected to the lower horizontal member of a rectangular steel frame placed over its free end. The upper horizontal member of the frame pivots on a ball-bearing located between two steel disks. The upper disk is welded to the centre of the underside of the upper horizontal member and the lower disk is bonded to the upper flange of the beam by *Isopon* adhesive. The advantage of this adhesive is that it is easily removed from the flange once testing is finished. The test rig has been used to determine the moment versus rotation response of bolted web, flange and web and flange cleat joints with the cleats cut out of pultruded GFRP and stainless angle profiles. One disadvantage with this test set-up is that the effect of the flexibility of the column's web or flange (depending on the vertical orientation of the column) on the joint's load versus rotation response is not taken into account. In order to record the joint rotation, an electronic clinometer was attached to

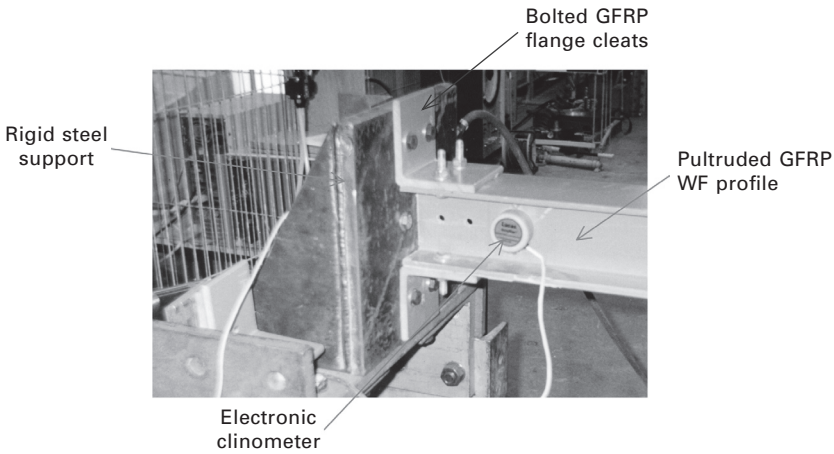

13.28 Image of the bolted cleat arrangement of the cantilever beam set-up for determining the joint's moment versus rotation response.

the centreline of the beam's web close to the toe of one of the web cleats. An additional clinometer was also attached to the back of the vertical steel support to check that it did not rotate during the test.

Another simple test set-up for beam-to-column joints is shown in Fig. 13.29(a). The test applies co-axial tensile forces across the ends of the stub beam and column forming the joint. The test is attractive, because it can be carried out in a universal test machine. However, it suffers from a number of drawbacks. In particular, the loading arrangement induces an axial load in the stub beam, which would not arise in practice. As depicted in Fig. 13.29(a), only the *opening-mode* load versus rotation response of the joint may be determined. In order to determine the *closing-mode* response, co-axial compressive forces would have to be applied and bracing would be required to prevent the joint buckling. An image of the opening-mode failure obtained from a test on a similar joint is shown in Fig. 13.29(b) (Note that the joint shown has an extra angle cleat bolted to the internal flanges of the stub column and beam.)

A third type of test set-up, used to quantify the moment versus rotation response of beam-to-column joints, is shown in Fig. 13.30. The set-up comprises two half-beams and a stub column. One end of each half-beam is connected to the flange (or web) of the stub column using the bolted cleat configuration to be tested. The other ends of the half-beams rest on roller supports. The two nominally identical joints may be loaded either by applying an upward/downward force along the vertical centreline of the stub column or by a pair of point loads applied to the half-beams equidistant from the stub column's vertical axis. The former loading configuration (three-point bending) has the advantage that by adjusting the positions of the roller support the joints

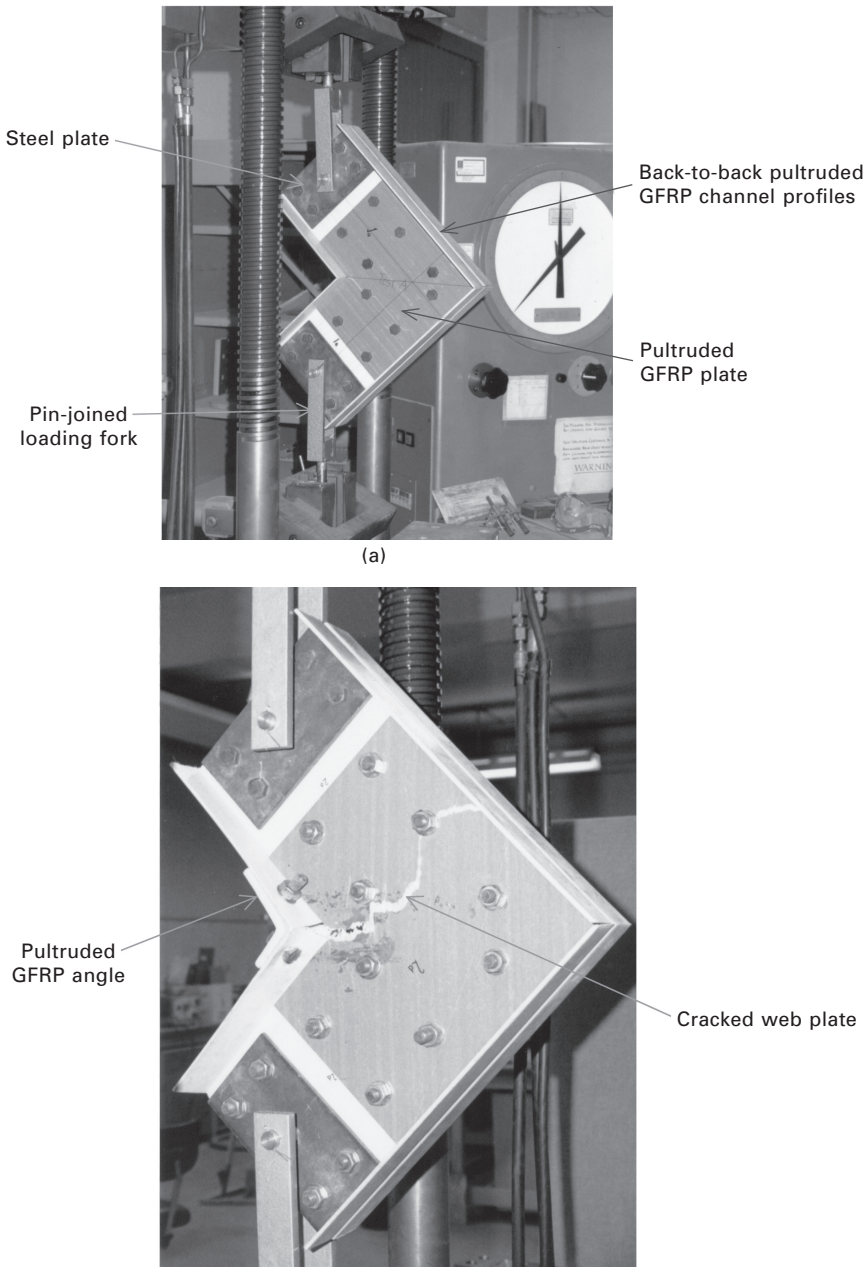

13.29 (a) Image of the co-axial tension test on a bolted, plated stub beam-to-stub column joint; (b) failure mode of a bolted, plated stub beam-to-stub column joint (note that this joint has an additional pultruded GFRP angle profile bolted to the internal flanges).

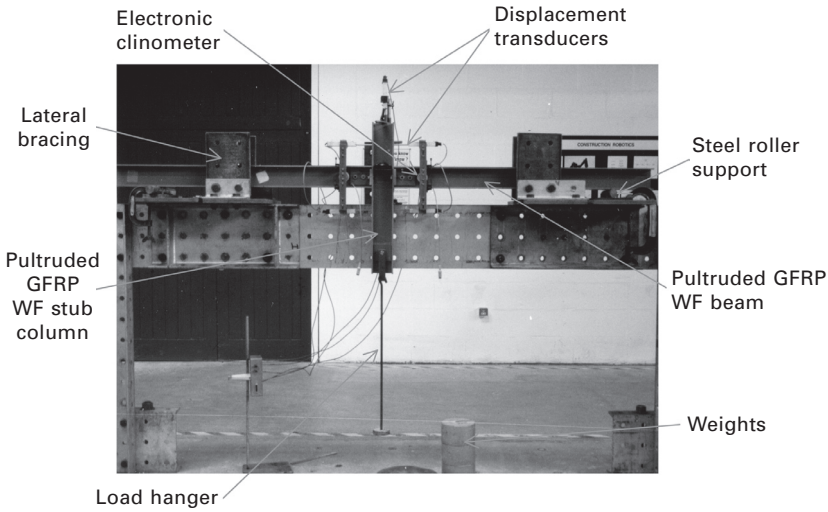

13.30 Image of the test set-up for determining the moment versus rotation responses of beam-to-column joints using two simply supported half-beams connected to a vertically loaded stub column.

may be subjected to varying ratios of bending moment to shear force. On the other hand, the latter loading configuration (four-point bending) subjects the joints to pure bending. Another redeeming feature of these test set-ups is that *two* nominally identical joints are tested. It is prudent to provide lateral bracing with these test set-ups, because lateral buckling may arise when the span is long and the joint is flexible (as with web cleats).

The fourth type of test set-up is based on a short column and two identical short beams cantilevering from the column. The two nominally identical bolted joints to be tested connect the cantilevers to either the column's flanges or its web. The base of the column is often a pinned joint, which means the configuration is potentially unstable and, therefore, needs to be provided with both in-plane and out-of-plane props. The cantilevers are loaded at their free ends by means of tension jacks. However, if the base of the column is clamped, then instability problems are avoided and the test set-up may be used with one cantilever and one joint or with two cantilevers and two joints. An image of the former test set-up is shown in Fig. 13.31(a) (note that dental plaster was used to ensure full contact between the flanges of the pultruded GFRP WF profile and the steel clamps). The mode of failure observed from such a test is shown in Fig. 13.31(b) (note that there is considerable flexing of the column's compression flange, as well as *opening up* of the joint).

Two types of test have been used to determine the load–deformation response of bolted column-to-base joints. The first type is used to determine the response to *uplift* loading and may be carried out on a stub column in a universal test machine. An image of the bolted web and flange cleat joint at

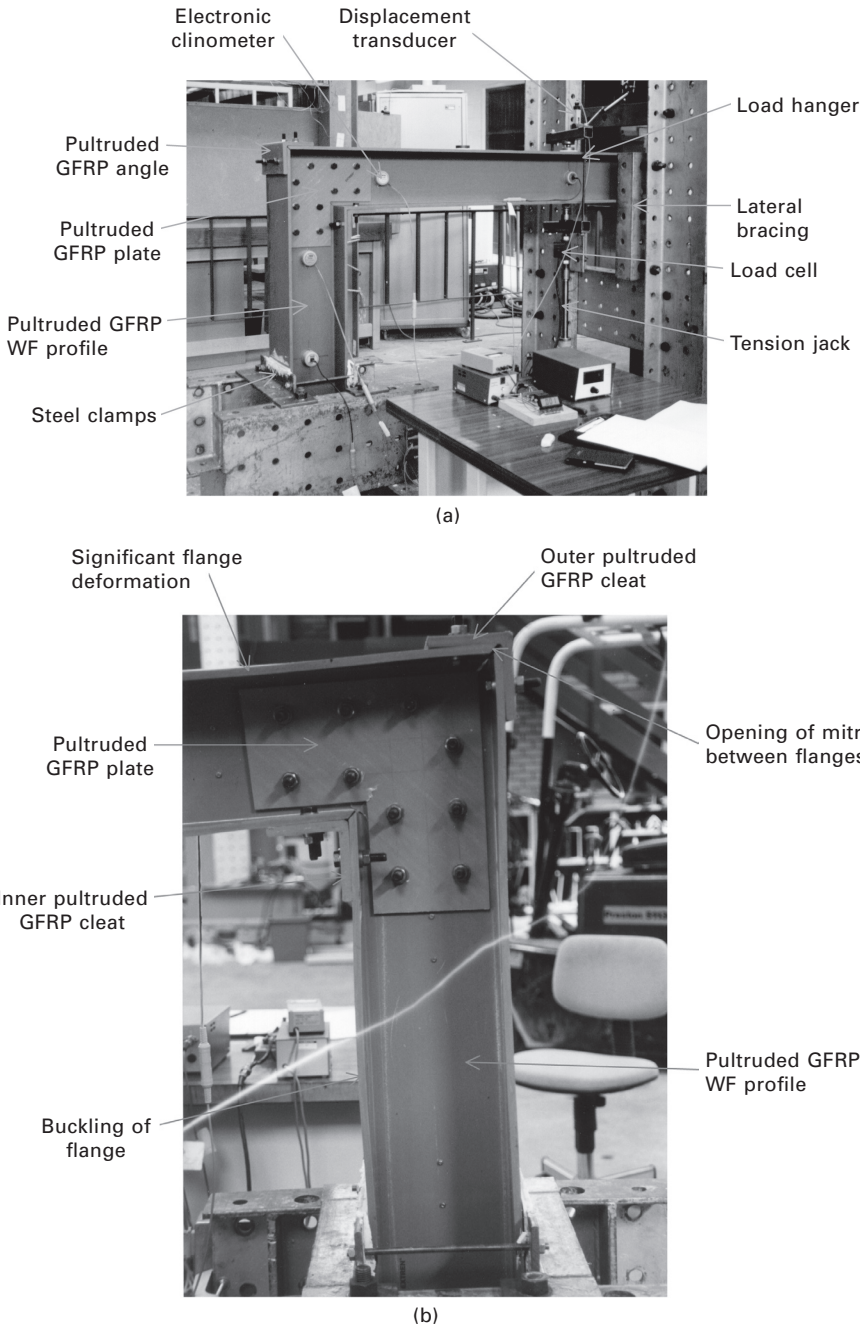

13.31 (a) Test set-up for determining the moment versus rotation response of a bolted, plated beam-to-column joint using a clamped base column and an end loaded beam; (b) failure mode of the plated beam-to-column joint.

the base of the WF profile stub column and the linear potentiometers, used to record the uplift displacements, are shown in Fig. 13.32(a). Figure 13.32(b) shows the uplift mode of joint failure, i.e. cracking across the width of the horizontal leg and along the instep, and delamination at the edge of the web cleat.

The second type of test on a column-to-base joint is a bending test to determine the joint's moment versus rotation response. The test is the vertical equivalent of the beam-to-column joint test shown in Fig. 13.28. An overall view of a moment versus rotation test on a bolted web and flange cleat joint at the base of a pultruded GFRP WF profile is shown in Fig. 13.33(a). The method of applying the horizontal load and the positioning of the long travel, linear potentiometer, used to record the horizontal displacement at the top of the column, are also shown in the figure. Figure 13.33(b) shows the extent of uplift of the heel and opening rotation of the legs of the angle cleat on the tension side of the column. The surface crack across the full width of the instep of the angle cleat is also clearly visible, as is the internal delamination around the web-flange junction and in the angle cleat's horizontal leg.

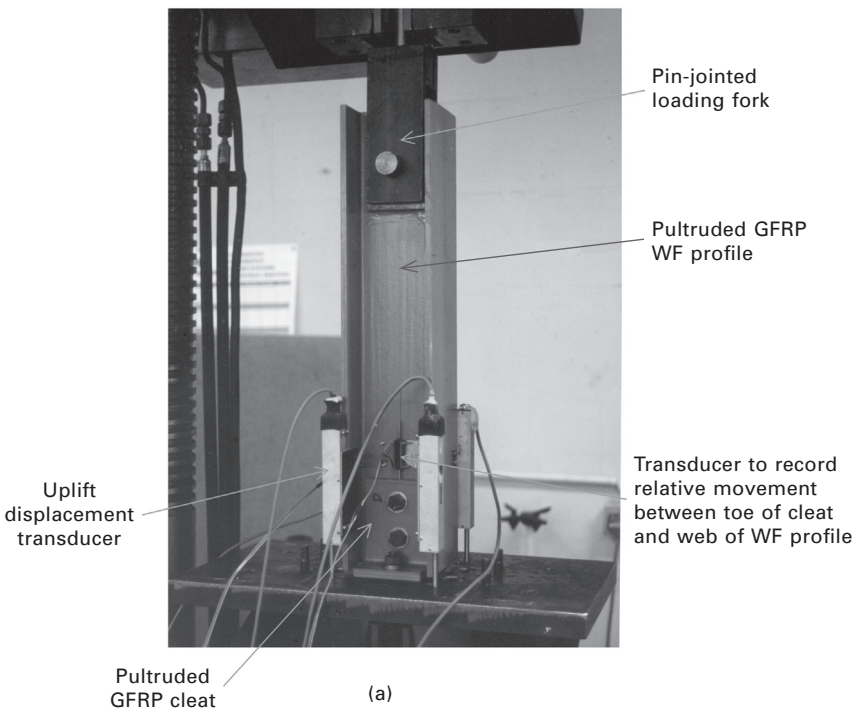

13.32 (a) Test set-up used to determine the uplift stiffness of a bolted angle cleat joint at the base of a WF profile column; (b) uplift failure mode in the bolted angle cleat at the base of a WF profile column.

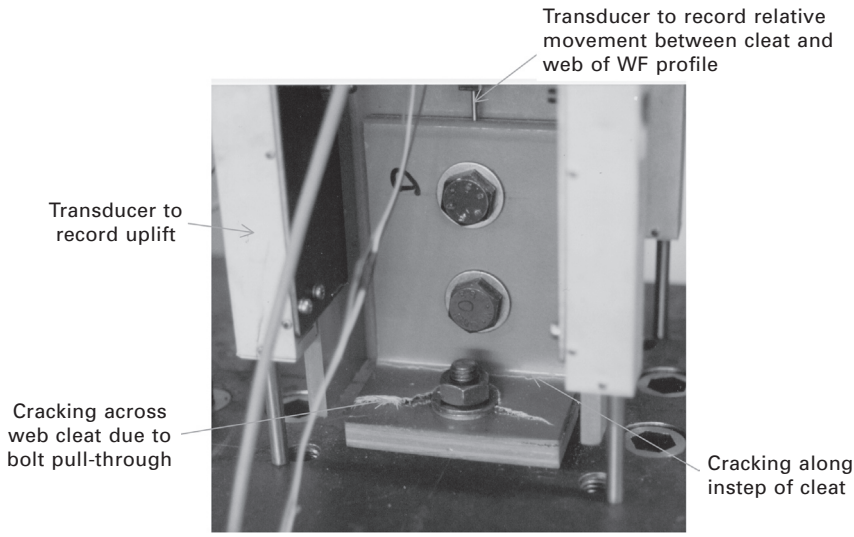

(b)

13.32 Continued

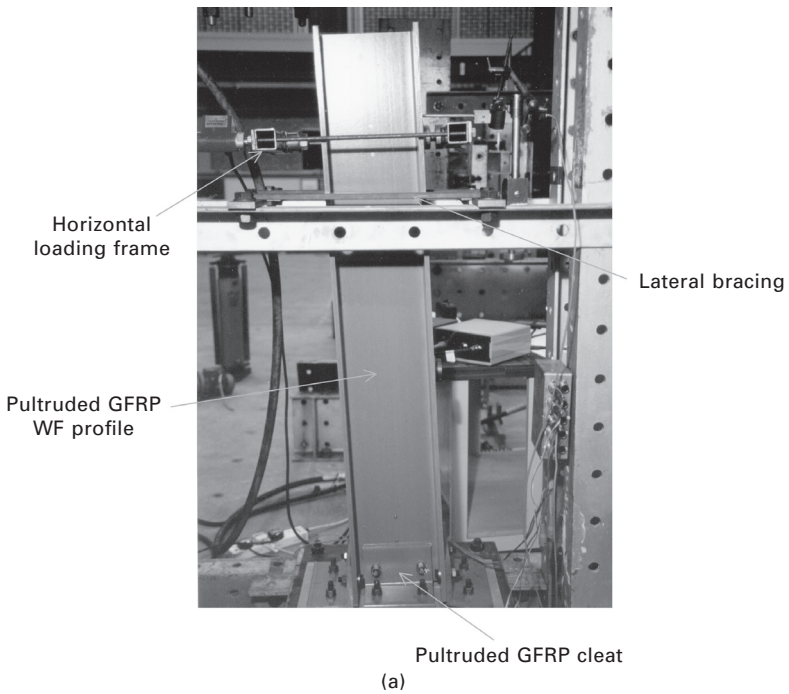

(a)

13.33 (a) Test set-up used to determine the moment versus rotation response of a WF profile's bolted column base joint; (b) uplift and internal delamination/cracking observed in a bending test on a bolted column base joint.

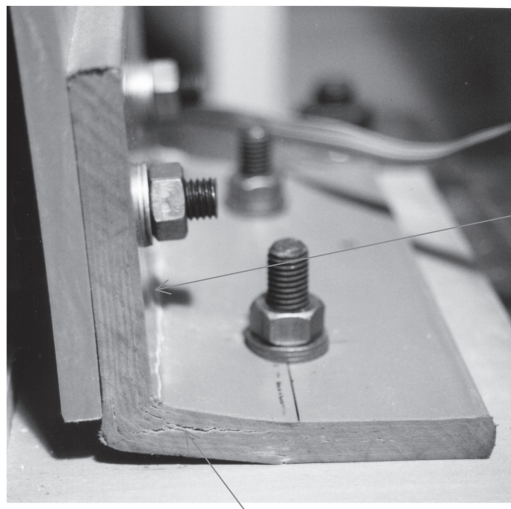

13.33 Continued

13.5 Tests on pultruded GFRP sub- and full-scale structures

In this sub-section on testing of pultruded GFRP structures and materials, attention is focused on testing of sub-structures and full-scale structures. Two examples of each are presented briefly to give the reader some idea of the range and scope of the tests that have been undertaken.

13.5.1 Tests on sub-structures

The first sub-structure example is part of a grillage, consisting of one longitudinal and one transverse pultruded GFRP WF profile beam which are joined by means of a pair of pultruded GFRP bolted angle profiles (web cleats) at the mid-span of the longitudinal beam. The two ends of the longitudinal beam and the end of the transverse beam were supported on pedestals bolted to the laboratory strong floor. In Fig. 13.34(a) the grillage sub-structure is shown with simple supports and in Fig. 13.34(b) the longitudinal and transverse beams are shown with clamped ends, formed by concrete blocks and packing pieces bolted together transversely and vertically to the pedestals. The grillage sub-structure was tested by applying dead-weight loading at the centre of the top flange of the longitudinal beam, and deflections were

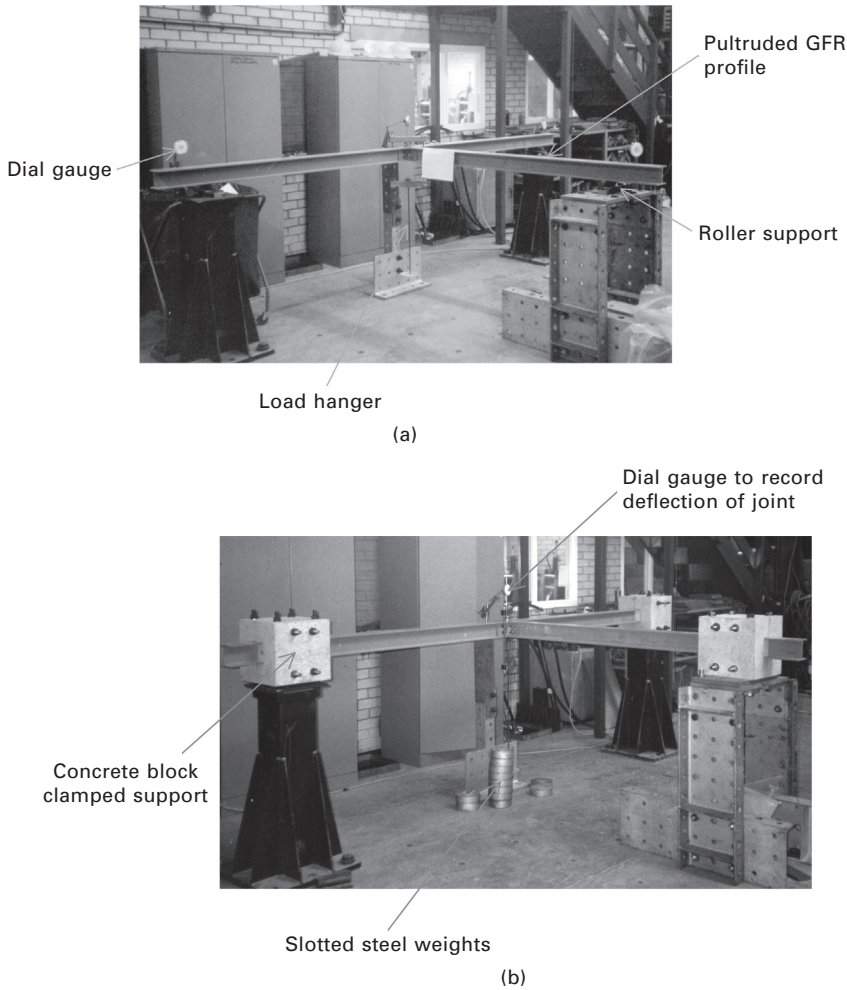

13.34 (a) A simply supported grillage sub-structure with a bolted web cleat joint at the mid-span of the longer beam; (b) a similar grillage sub-structure with clamped ends.

recorded at the same location. Different spans were investigated by moving the pedestals and their supports along the beams towards the common joint. At the time the tests were carried out, the test data was compared only with classical rigid-jointed grillage theory.

The second sub-structure that has been tested is a tapered, cantilevered, pultruded GFRP, plane truss. The motivation for undertaking the test work was that it could provide potentially useful insights into the possible application of these materials to the space trusses which are used to support the insulators

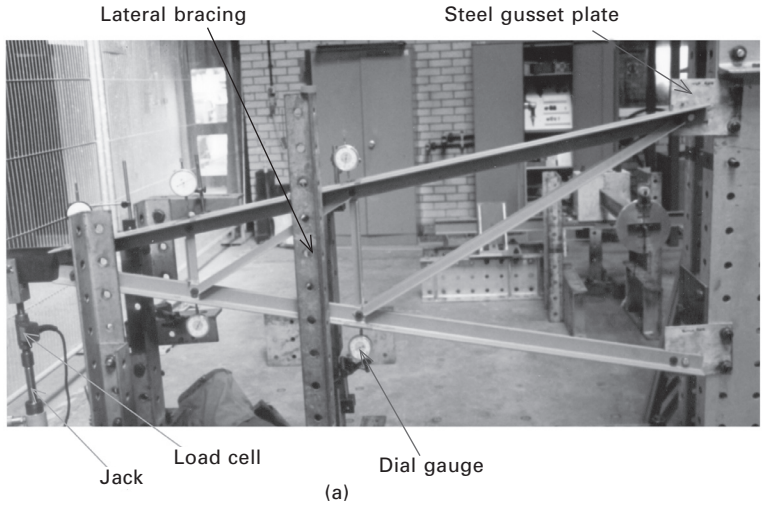

(a)

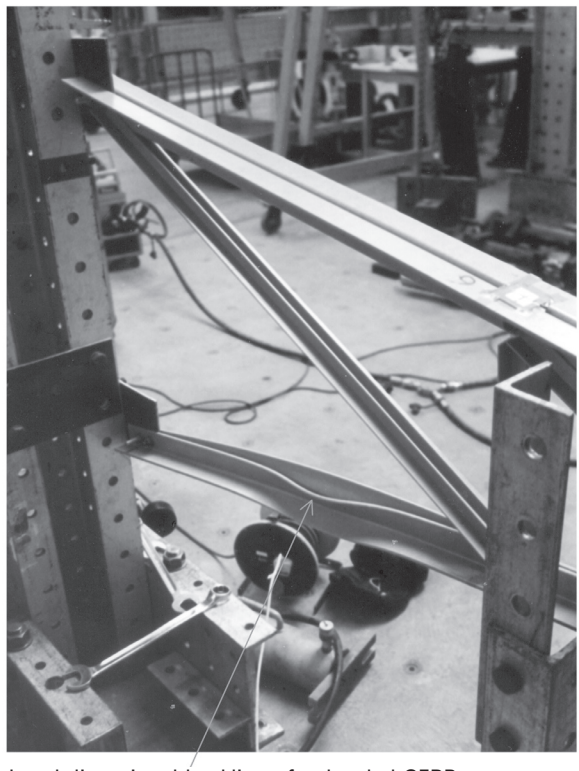

(b)

13.35 (a) Typical truss sub-structure set up for testing under a vertical point load applied at its free end; (b) buckling failure of the compression chord of the truss sub-structure.

and electrical conductor cables, and prevent them from contacting the legs of the steel transmission towers.

The truss, shown in Fig. 13.35(a), was one of a pair fabricated from two sizes of pultruded GFRP equal-leg angle profile. Each main tension and compression member of the truss comprised two back-to-back angles. All of the trusses' joints were bolted, with one or two bolts through the vertical legs of the angles. Both trusses were subjected to vertical point loads, which, for practical reasons, were applied through a loading plate at their tips. The only difference between the two trusses was that one used single-bolt joints throughout, whereas the other used two bolts in the main tension/compression members. Each truss was subjected to serviceability loading prior to loading to failure. Bracing was provided to inhibit the possibility of lateral buckling. Simple pin-jointed truss analysis gave reasonable predictions of the measured joint deflections up to the serviceability limit load, but could not be used to predict the truss collapse load. An image of the failure mode – compression buckling of the most highly loaded part of the compression chord – is shown in Fig. 13.35(b).

13.5.2 Tests on full-scale structures

Serviceability and ultimate load tests on a pultruded GFRP post and rail structure constitute the first example of testing at full-scale. The four posts and two rails were cut out of lengths of 51 × 51 × 3.2 mm tube. The connections between the tubes comprised solid resin blocks bonded into their ends. The blocks were drilled through their centres so that pultruded GFRP rods could be inserted and bonded in to complete the connection. Resin blocks were also bonded inside the tubes forming the top rails at the loading points. The *feet* of the posts were bolted and bonded into steel shoes which were welded to base plates through which two holes were drilled to accommodate holding-down bolts.

The test programme specified two serviceability load cases to be applied to the top rail normal to the plane of the post and rail system: (1) a uniform load over an outer bay, and (2) a uniform load over an inner and an outer bay. From a practical standpoint, it was decided to use dead-weight loading and, therefore, the post and rail system was cantilevered horizontally from a rigid steel framework. Three equal point loads were used to simulate uniform loading applied to the outer and inner bays of the top rail. Deflections at the joints and the centres of the bays of the top rail were recorded with dial gauges. Figure 13.36(a) shows the load case (1) test underway.

The ultimate load test of the post and rail system used jack rather than dead-weight loads for safety reasons. Hence, upward rather than downward loading was applied to the top rail, as shown in Fig. 13.36(b). However, because the structure was flexible and the ram extensions of the jacks were

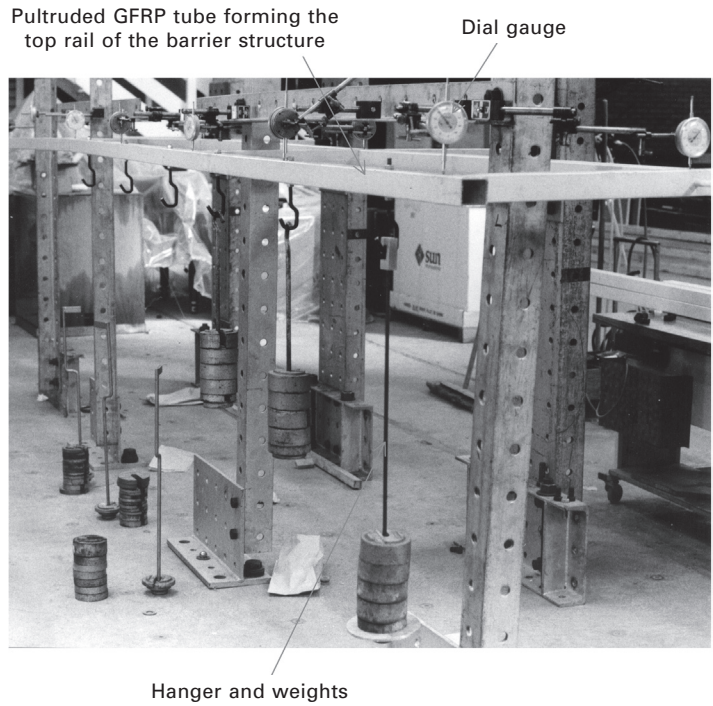

13.36 (a) Three-bay post and rail structure with serviceability loading applied to the top rail of an outer bay; (b) ultimate load test on the top rail of the outer bay of the post and rail structure.

limited, it was necessary to prop the structure and reset the jacks and dial gauges each time the maximum ram extension was reached. This situation provides further evidence of the need to be able to apply loads through large displacements and to be able to record these displacements (circumstances which do not usually arise to the same extent when testing steel structures) for the successful testing of pultruded GFRP composite structures. The post and rail system eventually failed by shear and bearing in the top rail at one of the props adjacent to a load point. This occurred whilst resetting the jacks for the second time, because the resin insert at the load point did not extend to the position of the adjacent prop.

The second and final example of testing a full-scale pultruded GFRP structure is that of a 12 m span footbridge based on two parallel Warren trusses. Back-to-back unequal angles formed the T-section tension and compression chords of each truss and single angle profiles were used for the diagonal members. The footbridge was designed to comply with a county council footbridge design specification.

A significant part of the initial test work undertaken was concerned with testing the angle profiles with various bolted end connections. The aim of the tests was to identify the most suitable joint configuration that could accommodate the compression load applied along the centreline of one leg. In order to carry out these tests a vertical test rig was set up. Unfortunately, it proved time-consuming to adjust for testing different lengths of angle profile. An alternative, more readily adjustable, test rig in which the angles were tested horizontally was developed. Figure 13.37(a) shows an angle undergoing large post-buckling deformations.

After the angle tests had been completed and the layout of their two-bolt end connections had been decided, the design of the trusses was finalised. The footbridge was then constructed and prepared for testing. It was subjected to a series of vertical and horizontal load tests in order to determine whether the design complied with the load and deflection criteria of the county council's footbridge design specification.

Seven plastic water tanks were used to apply a *uniform* vertical load to the footbridge. Water levels were marked in each tank so that the vertical load could be applied incrementally. Three jacks were used to apply the required horizontal load to the lower chord. Figure 13.37(b) shows the seven full water tanks on the footbridge, which produced a total uniform vertical load of 17.5 kN. The addition of 10 people (distributed as uniformly as possible) increased the vertical load to 25.5 kN but was still less than the 31.5 kN required by the specification. Sand-filled bags could have been used instead to meet the specified load, but would have been more costly and labour intensive (water was freely available, its mass was determined accurately with a flow meter, and the tanks were filled under mains pressure and emptied to a drain).

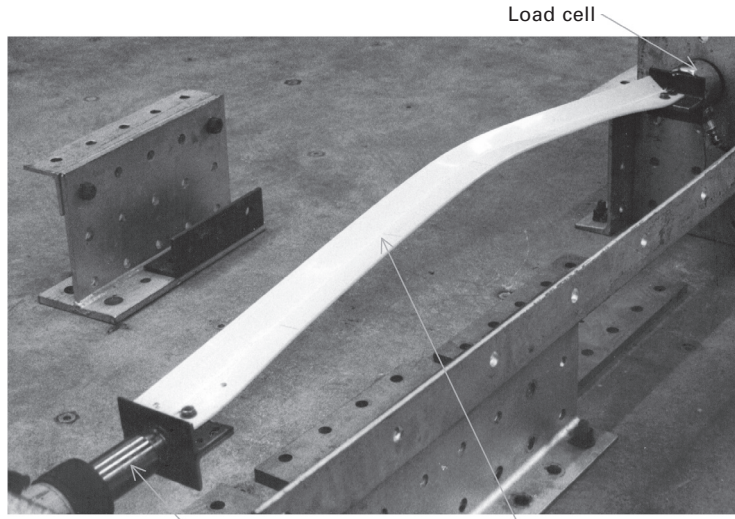

(a)

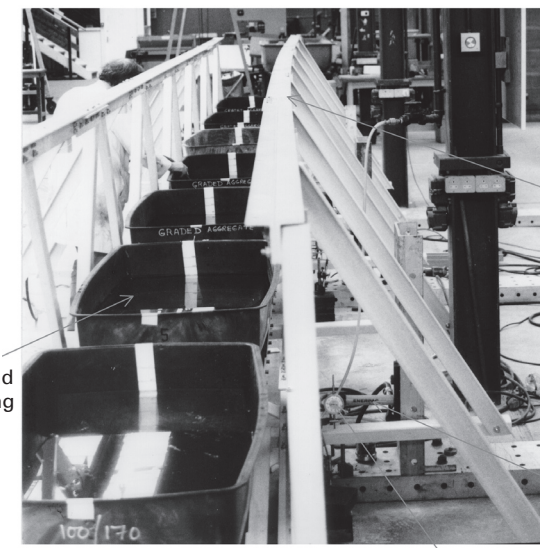

(b)

13.37 (a) Buckling failure test on a pultruded GFRP angle with two-bolt end connections; (b) vertical load test using water-filled plastic tanks on a pultruded GFRP footbridge (note the *inward* bowing of the compression chord of the right-hand truss) (reproduced with permission of P. Wynn).

Even though it was not possible to apply the full load to the footbridge, the mid-span deflection data obtained from the incrementally applied vertical loading could be extrapolated and compared with the corresponding deflection obtained from computer analysis for the maximum design load. The extrapolated mid-span deflection was about 80% of the computed value.

The horizontal load tests proved to be unsatisfactory because of problems with slippage at the supports. Nevertheless, the process of designing, fabricating and testing the truss footbridge was a valuable exercise and highlighted where design, fabrication and testing needed to be improved. Furthermore, it should not be forgotten that this footbridge was completed 21 years ago and, most probably, was the first of its kind to be designed, fabricated and tested in the UK from pultruded GFRP composite components.

13.6 Conclusion

This tour of test methods and associated instrumentation that have been deployed to establish the mechanical properties and response characteristics of pultruded GFRP materials, structural elements, joints and sub- and full-scale structures to a variety of load types has endeavoured to show some of what has been accomplished during the past three decades. The test work has helped to promote the use of these materials in civil engineering. It has also helped to compensate for the absence of statutory design codes, which has been a significant impediment to progress. However, this latter impediment is set to disappear within a relatively short time-scale. As indicated in the introductory sub-section, new design codes are expected to emerge during the next few years. However, it is the author's opinion that their emergence will *not* lead to the *total* demise of structural testing.

The test methods described in this chapter have all been concerned with response to *static* loading. Moreover, some of the instrumentation may be regarded as *well established*. Consequently, it is probably fair to conclude that our understanding of the *static* response of these materials and structures has reached a reasonable state of maturity (perhaps this is one of the reasons why design codes are emerging?). However, by comparison, *dynamic* response of pultruded GFRP materials and structures is much less well understood. It is, therefore, not unreasonable to expect that there will be increased emphasis on vibration, fatigue and impact testing in the future. Likewise, one may expect to see much more use of the newer instrumentation/monitoring techniques: acoustic emission, digital image correlation, laser vibrometry, thermography and high-speed video, all of which should lead to a better understanding of how these materials and structures fail. Unfortunately, in some situations with pultruded GFRP components, failure initiates internally rather than at the surface. In order to monitor and study internal failure initiation, and

indeed progression, some of the full-field techniques mentioned above may not be applicable and new, or yet to be developed techniques will be required. Perhaps tomographic techniques, nano-technology and/or other future technologies may have a role to play? Nevertheless, however the future unfolds, it is the author's firm belief that testing and monitoring test outcomes will always have a role to play in the development of pultruded GFRP composite material structures in civil engineering.

13.7 Acknowledgements

The foregoing *snapshot* descriptions (excuse the pun) of testing pultruded GFRP composite materials and structures are based on the author's experience, derived from initiating, supervising or otherwise contributing to approximately 80 projects during the past 25 years. As with nearly all projects, especially those with a substantial experimental content, the outcome depends on contributions from many individuals, even though only one individual has taken responsibility for writing this chapter. Therefore, the author wishes to take the opportunity to acknowledge his indebtedness and grateful thanks to all his former postdoctoral research assistants, postgraduate research students, undergraduate project students, visiting summer internees, academic colleagues, technical staff, and staff of the major UK and US pultruders (Exel Composites UK and Strongwell). In addition, he wishes to record his thanks to Lancaster University's Engineering Department for providing access to the all-important test equipment and instrumentation. Without such help and assistance, this chapter could not have been started, let alone finished. And last, but by no means least, he wishes to acknowledge several research grants from the UK's Engineering and Physical Sciences Research Council (EPSRC) which have supported his research on pultruded composite materials and structures.

13.8 Sources of further information and advice

This section lists selected information sources on pultruded composite materials, processing and structures.

Books

Bank L C (2006), *Composites for Construction – Structural Design with FRP Materials*, John Wiley & Sons, Hoboken, NJ, pp. 551.

Barbero E J (2011), *Introduction to Composite Materials Design*, CRC Press, Boca Raton, FL, pp. 520.

Journals

American Society of Civil Engineers' journals:
Journal of Composites for Construction
Journal of Structural Engineering

Elsevier's journals:
Composite Structures
Composites Engineering and *Composites Part B: Engineering*
Composites and *Composites Part A: Applied Science and Manufacturing*
Composites Science and Technology

Institution of Civil Engineers' journals:
Structures and Buildings
Technomic publishing's journals:
Journal of Reinforced Plastics and Composites
Journal of Composite Materials

Conference proceedings

Conferences on Advanced Composites for Construction (ACIC) (2002–)
Conferences on FRP Composites in Civil Engineering (CICE) (2001–)
Conferences on Advanced Composite Materials in Bridges and Structures (ACMBS) (1992–)
European Pultrusion Technology Association (EPTA) Conferences (1990–)
American Composites Manufacturers Association (ACMA) Conventions (annually)
European Conference on Composite Materials (ECCM) Conferences (1982–).
International Conference on Composite Materials (ICCM) Conferences (1975–)

Design handbooks/manuals

Creative Pultrusions, Alum Bank, PA (see http://www.creativepultrusions.com/)
Fiberline Composites A/S, Middlefart, Denmark (see http://www.fiberline.com/)
Strongwell, Bristol, VA (see http://www.strongwell.com/)
Clarke J L (ed.) (1996), *Design of Polymer Composites*, *EUROCOMP Design Code and Handbook*, E & F N Spon, London, pp. 751.

Mosallam A S (2011), *Design Guide for FRP Composite Connections*, ASCE Manuals and Reports on Engineering Practice No. 102, ASCE, Reston, VA, pp. 601.

Common Interest Groups

American Composites Manufacturers Association (ACMA) (see www.cfa-hq.org)
Composites UK (see http://www.compositesuk.co.uk/)
European Pultrusion Technology Association (EPTA) (see http://www.pultruders.com)
Network Group for Composites in Construction (NGCC) (see http://www.ngcc.org.uk/)
International Institute for FRP in Construction (IIFC) (see http://www.iifc-hq.org/)

Literature database on R&D with Pultruded Fibre Reinforced Polymer Shapes and Systems

See http://www2.warwick.ac.uk/fac/sci/eng/staff/jtm/

13.9 References

Anon. (1988), *Creative Pultrusions Design Guide*, Creative Pultrusions, Inc., Alum Bank, PA.
Anon. (1989), *EXTREN Design Manual*, Strongwell, Bristol, VA.
ASCE (2010), *Pre-Standard for Load and Resistance Factor Design (LRFD) of Pultruded Fiber Reinforced Polymer (FRP) Structures (Final)*, ASCE, Reston, VA.
ASTM D 953-02 (2002), Standard test method for bearing strength of plastics, ASTM, West Conshohocken, PA.
ASTM D 5379-05 (2005), Standard test method for shear properties of composite materials by the notched beam method, ASTM, West Conshohocken, PA.
ASTM D 5961/D 5961M-05 (2005), Standard test method for the bearing response of polymer matrix composite laminates, ASTM, West Conshohocken, PA.
ASTM D 2344/D 2344M-00 (2006), Standard test method for short-beam strength of polymer matrix composite materials and their laminates, ASTM, West Conshohocken, PA.
ASTM D 4255/D 4255M-01 (2007), Standard test method for in-plane shear properties of polymer matrix composite materials by the rail shear method, ASTM, West Conshohocken, PA.
ASTM D 7291/D 7291M-07 (2007), Standard test method for through-thickness "flatwise" tensile strength and elastic modulus of a fiber-reinforced polymer matrix composite material, ASTM, West Conshohocken, PA.
ASTM D 695-08 (2008), Standard test method for compressive properties of rigid plastics, ASTM, West Conshohocken, PA.

ASTM D 3039M-08 (2008), Standard test method for tensile properties of polymer matrix composite materials, ASTM, West Conshohocken, PA.

ASTM D 5868-01 (2008), Standard test method for lap shear adhesion for fiber reinforced plastic (FRP) bonding, ASTM, West Conshohocken, PA.

Bank L C (1989), Flexural and shear moduli of full-section fiber reinforced plastic (FRP) pultruded beams, *Journal of Testing and Evaluation*, Vol. 17, No. 1, pp. 40–45.

Barbero E J and Raftoyiannis I G (1994), Lateral and distortional buckling of pultruded I-beams, *Composite Structures*, Vol. 27, No. 3, pp. 261–268.

Barbero E and Tomblin J (1992), Buckling testing of composite columns, *AIAA Journal*, Vol. 30, No. 11, pp. 2798–2800.

Barbero E and Tomblin J (1993), Euler buckling of thin-walled composite columns, *Thin-Walled Structures*, Vol. 17, No. 4, pp. 237–258.

Barbero E J and Tomblin J S (1994), A phenomenological design equation for FRP columns with interaction between local and global buckling, *Thin-Walled Structures*, Vol. 18, No. 2, pp. 117–131.

Brooks R J and Turvey G J (1995), Lateral buckling of pultruded GRP I-section cantilevers, *Composite Structures*, Vol. 32, Nos. 1–4, pp. 203–216.

BS EN ISO 6892-1:2009 (2009), Metallic materials. Tensile testing. Method of test at ambient temperature. British Standards Institution, London.

Clarke J L (ed.) (1996), *Design of Polymer Composites*, *EUROCOMP Design Code and Handbook*, E & F N Spon, London, pp. 751.

CNR-DT 205 (2008), *Guide for the Design and Construction of Structures Made of Pultruded FRP Elements,* CNR, Rome.

Cooper C and Turvey G J (1995), Effects of joint geometry and bolt torque on the structural performance of single bolt tension joints in pultruded GRP sheet material, *Composite Structures*, Vol. 32, Nos. 1–4, pp. 217–226.

CUR96 (2003), *Recommendation 96: Fibre-Reinforced Polymers in Civil Load-bearing Structures*, CUR commission C124, CUR, Gouda, The Netherlands (in Dutch).

Davalos J F, Qiao P and Salim H A (1997), Flexural-torsional buckling of pultruded fiber reinforced plastic composite I-beams, *Composites Structures*, Vol. 38, Nos. 1–4, pp. 241–250.

EN 13706-2 (2002), Reinforced plastic composites – specification for pultruded profiles – part 2: methods of test and general requirements, CEN, Brussels.

EN 1993-1-1 (2006), Eurocode 3 design of steel structures – Part 1 – 1: General rules and rules for buildings, CEN, Brussels.

EN ISO 527-4 (1997), Plastics – determination of tensile properties – Part 4: Test conditions for isotropic and orthotropic fibre-reinforced plastic composites, CEN, Brussels.

Erki M A (1995), Bolted glass-fibre reinforced plastic joints, *Canadian Journal of Civil Engineering*, Vol. 22, No. 4, pp. 736–744.

Hassan N K, Mohamedien M A and Rizkalla S H (1997), Multibolted joints for GFRP structural members, *Journal of Composites for Construction*, Vol. 1, No. 1, pp. 2–9.

Insausti A, Puente I and Azkune M (2009), Interaction between local and lateral buckling on pultruded I-beams, *Journal of Composites for Construction*, Vol. 13, No. 4, pp. 315–324.

Keller T and Vallée T (2005a), Adhesively bonded lap joints from pultruded GFRP profiles. Part I: Stress–strain analysis and failure modes, *Composites Part B: Engineering*, Vol. 36, No. 4, pp. 331–340.

Keller T and Vallée T (2005b), Adhesively bonded lap joints from pultruded GFRP profiles. Part II: Joint strength prediction, *Composites Part B: Engineering*, Vol. 36, No. 4, pp. 341–350.

Mottram J T (1992), Lateral-torsional buckling of a pultruded I-beam, *Composites*, Vol. 23, No. 2, pp. 81–93.

Mottram J T (1994), Compression strength of pultruded flat sheet material, *Journal of Materials in Civil Engineering,* Vol. 6, No. 2, pp. 185–200.

Mottram J T and Zafari B (2011), Pin bearing strengths for bolted connections in fibre-reinforced polymer structures, *Proceedings of the Institution of Civil Engineers: Structures and Buildings*, Vol. 164, No. SB5, pp. 291–305.

Mottram J T, Brown N D and Anderson D (2003), Physical testing for concentrically loaded columns of pultruded glass fibre reinforced plastic profile, *Proceedings of the Institution of Civil Engineers: Structures and Buildings*, Vol. 152, No. 2, pp. 205–219.

Roberts T M (2002), Influence of shear deformation on buckling of pultruded fiber reinforced plastic profiles, *Journal of Composites for Construction*, Vol. 6, No. 4, pp. 241–248.

Rosner C N and Rizkalla S H (1995), Bolted connections for fiber-reinforced composite structural members: experimental program, *Journal of Materials in Civil Engineering*, Vol. 7, No. 4, pp. 223–231.

Sanders D H, Gordaninejad F and Mundi S (1996), FRP beam-to-column connections using adhesives. In *Proceedings of the International Conference on Composites in Infrastructure*, Tucson, AZ, pp. 596–607.

Shan L Y and Qiao P Z (2005), Flexural-torsional buckling of fiber-reinforced plastic composite open channel beams, *Composite Structures*, Vol. 68, No. 2, pp. 211–224.

Sims G D, Johnson A F and Hill R D (1987), Mechanical and structural properties of a GFRP pultruded section, *Composite Structures*, Vol. 8, No. 3, pp. 173–187.

Sims G D, Nimmo W, Johnson A F and Ferriss D H (1994), Analysis of plate twist test for in-plane shear modulus of composite materials, *NPL Working Draft*, National Physical Laboratory, Teddington, UK.

Stoddard W P (1997), Lateral-torsional buckling behaviour of polymer composite I-shaped members, PhD thesis, Georgia institute of Technology, Atlanta, GA.

Turvey G J (1996a), Lateral buckling tests on rectangular cross-section pultruded GRP cantilever beams, *Composites B*, Vol. 27B, No. 1, pp. 35–42.

Turvey G J (1996b), Effect of load position on the lateral buckling response of pultruded GRP cantilevers – comparison between theory and experiment, *Composite Structures*, Vol. 35, No. 1, pp. 33–47.

Turvey G J (1998), Torsion tests on pultruded GRP sheets, *Composites Science and Technology*, Vol. 58, No. 8, pp. 1343–1351.

Turvey G J (2007), Analysis of bending tests on CFRP-stiffened pultruded GRP beams, *Proceedings of the Institution of Civil Engineers: Structures and Buildings*, Vol. 160, No. 1, pp. 37–49.

Turvey G J (2008), Bending of tip-loaded CFRP stiffened pultruded GRP cantilevers: comparison between theory and experiment. In *Proceedings of the 13th European Conference on Composite Materials (ECCM 13)*, Kungliga Tekniska Högskolan, Stockholm (Paper 1202, pp. 10 in CD-Rom Proceedings).

Turvey G J (2011), Pultruded GFRP continuous beams – comparison of flexural test data with analysis predictions. In *Proceedings of the 5th International Conference on*

Advanced Composites in Construction (ACIC 2011), University of Warwick, Coventry, UK, pp. 470–481.

Turvey G J and Brooks R J (1996), Lateral buckling tests on pultruded GRP I-section beams with simply supported–simply supported and clamped–simply supported end conditions. In *Proceedings of the 1st International Conference on Composites in Infrastructure (ICCI'96)*, University of Arizona, Tucson, AZ, pp. 651–664.

Turvey G J and Brooks R J (2002), Semi-rigid–simply supported shear deformable pultruded GRP beams subjected to end moment loading: comparison of measured and predicted deflections, *Composite Structures*, Vol. 57, Nos. 1–4, pp. 263–277.

Turvey G J and Wang P (2007), Failure of PFRP single-bolt tension joints under hot-wet conditions, *Composite Structures*, Vol. 77, No. 4, pp. 514–520.

Turvey G J and Wang P (2009a), Failure of pultruded GRP angle leg junctions in tension. In *Proceedings of the 17th International Conference on Composite Materials (ICCM 17)*, Edinburgh (Paper A1.1, pp. 11 in CD-Rom Proceedings).

Turvey G J and Wang P (2009b), Environmental effects on the failure of GRP multi-bolt joints, *Proceedings of the Institution of Civil Engineers: Structures and Buildings*, Vol. 162, No. 4, pp. 275–287.

Turvey G J and Wang P (2009c), Failure of pultruded GFRP joints: a Taguchi analysis, *Proceedings of the Institution of Civil Engineers: Engineering and Computational Mechanics*, Vol. 162, No. 3, pp. 145–153.

Turvey G J and Zhang Y (2004a), Shear failure of web–flange junctions in pultruded GRP profiles. In *Proceedings of the 2nd International Conference on Advanced Polymer Composites for Structural Applications in Construction (ACIC 2004)*, Woodhead Publishing, Cambridge, UK, pp. 553–560.

Turvey G J and Zhang Y (2004b), Torsion of a pultruded GRP WF beam with bolted end connections: test results and FE analysis. In *Advanced Composite Materials in Bridges and Structures*, El-Badry M M and Dunaszegi L (eds), The Canadian Society for Civil Engineering, Montreal (abstract p. 99; CD-Rom Proceedings).

Turvey G J and Zhang Y (2005a), Tearing failure of web–flange junctions in pultruded GRP profiles, *Composites Part A: Applied Science and Manufacturing*, Vol. 36, No. 2, pp. 309–317.

Turvey G J and Zhang Y (2005b), Stiffness and strength of web-flange junctions of pultruded GRP sections, *Proceedings of the Institution of Civil Engineers: Structures and Buildings*, Vol. 158, No. 6, pp. 381-391.

Turvey G J and Zhang Y (2006), A computational and experimental analysis of the buckling, postbuckling and initial failure of pultruded GRP columns, *Computers and Structures*, Vol. 84, Nos. 22–23, pp. 1527–1537.

Turvey G J and Zhang Y-S (2007), Opening mode failure of pultruded GRP angle leg junctions. In *Proceedings of the 3rd International Conference on Advanced Composites in Construction (ACIC 07)*, Darby A P and Ibell T J (eds), University of Bath, UK, pp. 389–393.

Vallée T and Keller T (2006), Adhesively bonded lap joints from pultruded GFRP profiles. Part III: Effects of chamfers, *Composites Part B: Engineering*, Vol. 37, Nos. 4–5, pp. 328–336.

Zhang Y, Vassilopoulos A P and Keller T (2010a), Mode I and mode II fracture behavior of adhesively-bonded pultruded composite joints, *Engineering Fracture Mechanics*, Vol. 77, No. 1, pp. 128–143.

Zhang Y, Vassilopoulos A P and Keller T (2010b), Effects of low and high temperatures on tensile behavior of adhesively-bonded GFRP joints, *Composite Structures*, Vol. 92, No. 7, pp. 1631–1639.

Zureick A and Scott D (1997), Short-term behavior and design of fiber-reinforced polymeric slender members under axial compression, *Journal of Composites for Construction*, Vol. 1, No. 4, pp. 140–149.

Zureick A and Steffen R (2000), Behavior and design of concentrically loaded pultruded angle struts, *ASCE Journal of Structural Engineering*, Vol. 126, No. 3, pp. 406–416.

14

Advanced fiber-reinforced polymer (FRP) composites to strengthen structures vulnerable to seismic damage

M. F. M. FAHMY, Assiut University, Egypt

DOI: 10.1533/9780857098641.4.511

Abstract: To ensure better performance for a range of existing reinforced concrete structures in seismic regions with substandard structural details, seismic retrofit is an economical solution. Hence, this chapter presents some of the available results in which fiber-reinforced polymer (FRP) composites can be used for damage-controllable structures. For example, the performance of existing reinforced concrete structures whose components are vulnerable to shear failure, flexural-compression failure, joint reinforcement bond failure, or longitudinal reinforcement lap splice failure and retrofitted with FRPs is described. Novel concepts of modern constructions with controllability and recoverability using FRP composites are addressed.

Key words: damage-controllable structures, existing RC structures, seismic retrofit, FRP; steel–fiber composite rebars.

14.1 Introduction

Civil infrastructure includes bridges, buildings, transportation systems, and other life-supporting facilities such as water supply and distribution, waste and wastewater systems, electricity, oil and gas installations. These networks deliver essential services, provide shelter, and support social interactions and economic development. Essentially, the sustainable economic growth, productivity, and the well-being of a nation depend heavily on the functionality, reliability, and durability of its civil infrastructure systems. However, in most parts of the world, civil infrastructure is ageing and in constant need of maintenance, repair and upgrading. Moreover, in the light of our current knowledge and of modern codes for seismic design, in many countries existing reinforced concrete (RC) structures that were designed according to pre-1970s codes often have inadequate reinforcement detailing, which results not only in deficient lateral load resistance, but also in insufficient energy dissipation, rapid strength deterioration and improper hinging mechanisms during earthquakes, leading to excessive drifts and ultimately to structural collapse. Non-ductile detailing is generally manifested through deficient joint shear resistance, deficient column shear capacity, deficient column main reinforcement lap splices, deficient anchorage of

beam positive reinforcement at the beam–column joint, and deficient beam shear resistance. (Said and Nehdi, 2004). Hence, the devastating social and economic impacts of recent earthquakes in urban areas have resulted in an increased awareness of the potential seismic risk and the corresponding vulnerability of the built environment. As a result, major advances in seismic engineering have been made in the last decade with further refinements of performance-based seismic design philosophies. The target performance is to maintain structural integrity and avoid collapse. In order for structures to be able to sustain a design-level earthquake with limited or negligible damage, the rapid development of material, design, and construction techniques has been applied to improve the seismic performance of RC structures.

To successfully decide on the appropriate upgrading/repair systems for the existing deficient structures based on the requirements of the current code provisions, a clear picture of the desired performance during and after an earthquake from all the elements composing the structural system is critical. This would ultimately produce structural systems that can withstand large earthquake forces without compromising life-safety. The recent progress of experimental and analytical studies on retrofitting of deficient RC structures has brought the challenge of designing a quickly recoverable structure to the research forefront. In the study of Fahmy (2010) a mechanical model for a damage-controllable structure is proposed. Figure 14.1 shows the mechanical model of the proposed structure, where the lateral response proceeds along O-A-B-C-D-E-F. The behavior of a general RC flexural structure whose lateral response is along O-A′-B′-C′-D′-F′. is also given for comparison. It is obvious that the most remarkable difference occurs after the yielding of the steel reinforcement: after point C and C′. For the general RC structure, the deformation increases dramatically almost without any increase in load-carrying capability: along line C′D′ no post-yield stiffness is demonstrated. However, with the proposed approach, the structure can still carry the load even after the steel reinforcement yields and hardening behavior has been exhibited along line CD. The stiffness K_2 between points C and D is termed the 'secondary stiffness' in this chapter. Due to the existence of secondary stiffness, the dramatic increase in deformation and residual deformation can be effectively controlled after the reinforcement yields, and the load-carrying capacity can be further improved. Based on the codes requirements for ductile structures to withstand strong earthquakes, the proposed structure is characterized by the part DE after the hardening zone, where favorable ductility is demonstrated. The ultimate drift (δ_u) corresponding to point F or F′ for the proposed structure and the general RC structure, respectively, is defined for both structures to be at 20% strength decay. The use of 20% strength decay as the failure criterion is consistent with that employed by previous researchers, since it is reasonable to accept some strength decay

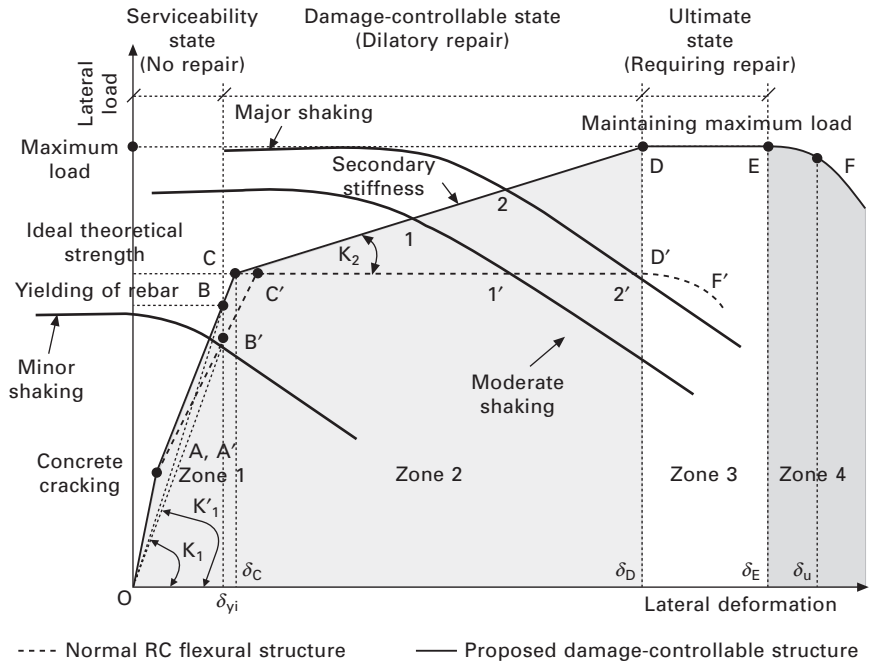

14.1 Idealized load–deformation behavior of proposed damage-controlled structures.

Table 14.1 Comparison between the performance of the normal RC structure and the damage-controllable structure

Earthquake level	Normal RC structure		Damage-controllable structure	
Minor shaking	Limit state	Performance level	Limit state	Performance level
Moderate shaking	Serviceability	Fully operational	Serviceability	Fully operational
Major shaking	Ultimate	Requiring repair	Damage-controllable	Dilatory repair
	Failure	Unstable	Ultimate	Requiring repair

during seismic response of a structure before it can be considered to have failed (Park and Paulay, 1975).

According to the mechanical behavior shown in Fig. 14.1, Table 14.1 summarizes the limit states and the corresponding performance levels under the action of three different levels of earthquakes for both normal RC structure and damage-controllable structure. It is clear that the proposed structure can be kept in place for a relatively long time without collapse during a large

earthquake, though severe damage may occur. The original function of the structures may be recovered through the replacement of some elements.

The proposed mechanical model can satisfy a seismic design philosophy that holds that the structure suffers no damage under a small earthquake, exhibits prompt recoverability under medium earthquake, and does not collapse under a large earthquake.

In the last four decades, fiber-reinforced polymers (FRPs) have received interest in a wide range from many researchers in the field of civil engineering because of the numerous advantages of their mechanical properties, so this chapter exhibits how fiber composites could be successfully applied to enhance the behavior of concrete structures (existing and new constructions) to achieve damage-controllable structures withstanding strong earthquakes. Firstly, the behavior of columns, beams, and joints of existing RC structures (bridges and buildings), which could not meet the requirements of the current code provisions because of their inadequate reinforcement detailing, is demonstrated. After that, the impacts of strengthening deficient structural components of RC bridges and buildings using fiber composite are addressed: successful retrofitting techniques achieving the aim of RC structures with controllability and recoverability under the action of massive seismic loads are defined. Ultimately, this chapter represents innovative FRP-RC constructions achieving the required restorability.

14.2 Seismic behavior of reinforced concrete (RC) structures

Throughout the world, many RC structures such as bridges and buildings have been deteriorated and/or distressed to such a degree that strengthening such structures or reducing the load limit on them is becoming necessary to extend their service life (Li *et al.*, 2002). Further, extensive human and economic losses in recent major earthquakes (Kashmir in 2005; China in 2008; Indonesia and Italy in 2009; Haiti and Chile in 2010; and Japan in 2011) have highlighted the seismic vulnerability of substandard RC structures. In this section, the general performance of existing deficient RC structures is briefly presented.

14.2.1 Damage to RC columns

In RC bridge piers, the three locations where failure is likely to occur include the end of columns, the bent cap, and the joint region between the column and the bent cap. The common type of structural failure of bridges in earthquakes is bridge pier column failure (Kawashima and Unjoh, 1997; Hsu and Fu, 2004). In Japan, the Kobe Earthquake (Hyogo-ken Nanbu Earthquake) occurred on 17 January 1995, exactly one year after the Northridge, USA, Earthquake.

It resulted in destructive damage to bridges (Fig. 14.2). Reinforced concrete columns suffered failure in shear. Premature shear failure at terminations of longitudinal bars with insufficient development lengths resulted in collapse of many bridges. In the study of Seible *et al*. (1997) it was reported that lap splice failure at the connection between the footing and the column, shear failure, and confinement failure of the flexural plastic hinge region are the failure modes observed in existing reinforced concrete bridge columns under a seismic load/deformation input. Xiao and Ma (1997), Chang and Chang (2004) and Harries *et al*. (2006) related these failure modes to poor detail in the longitudinal lap splices, improper transverse confinement, and insufficient shear strength. In China, after the 2008 earthquake, a field investigation for over than 320 bridges was carried out by Qiang *et al*. (2009). Their survey divided the failure modes of the highway bridges into two categories, i.e. bending failure and bending–shear brittle damage (Fig. 14.3).

Because a large number of existing RC buildings around the world were originally designed to carry only gravity loads, the most significant failures in past earthquakes (low to moderate earthquake motions) have been attributed to column failures. Typically, columns have minimum cross-sectional dimensions and their longitudinal steel reinforcement is inadequate to satisfy flexural and shear demand generated during an earthquake; i.e. they lack the ductility and the hierarchy of strength that induce a global failure mechanism appropriate for seismic conditions. Furthermore, the lack of appropriate size and spacing of column ties increases the risk of brittle and local failure mechanisms such as the collapse of the column end, resulting in crushing of the unconfined concrete, instability of the longitudinal steel reinforcing bars in compression, and pullout of those in tension when spliced. The associated failure mode is characterized by a brittle and catastrophic structural failure (Bracci *et al*., 1992; Harries *et al*., 2006). Several collapses of one or more stories of buildings have been attributed to column failures (see Fig. 14.4).

14.2.2 Damage to RC beam–column joints

Recent earthquakes worldwide have also illustrated the vulnerability of existing RC beam–column joints to seismic loading. Under a severe earthquake, there may be a large amount of shear stress concentrated on the beam–column joint area while the shear capacity of the joint was not sufficient due to a non-ductile reinforcement detailing in the beam-column joint area in terms of inadequate transverse reinforcement. Figure 14.5 shows the beam–column damage in one of the investigated highway bridges by Qiang *et al*. (2009), where the column and beam joints and the lateral braces were damaged as a result of strong shear force during the earthquake. It was reported also in this study that the crack width was as large as 50 mm, which also implying insufficient shear reinforcement.

(a)

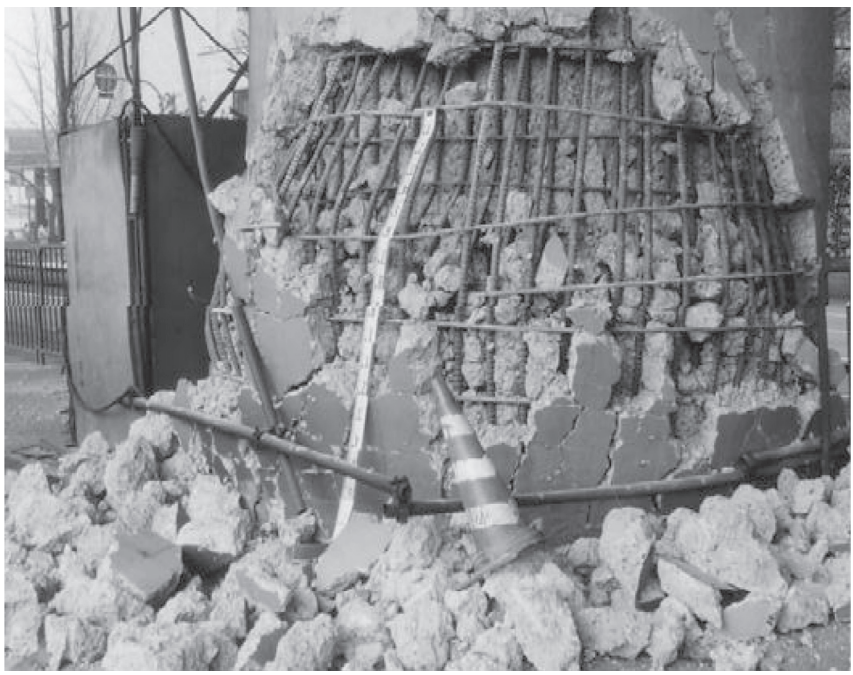

(b)

14.2 Different damage levels after the Kobe earthquake of 1995: (a) complete collapse; (b) very severe damage; (c) severe damage; (d) moderate damage.

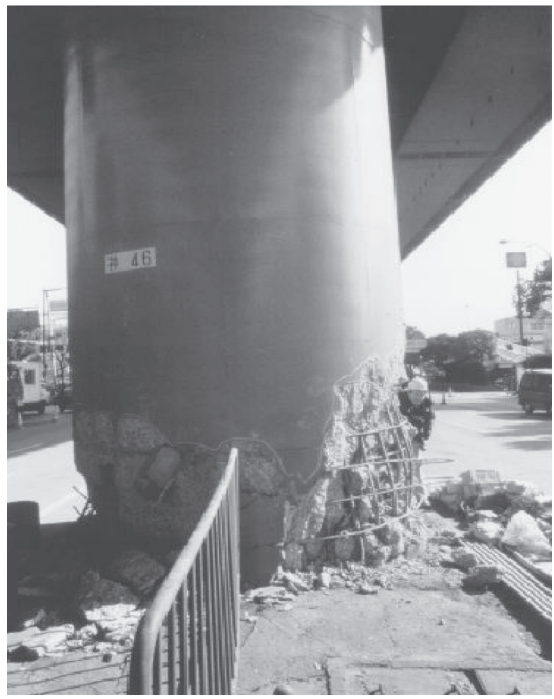

(c)

(d)

14.2 Continued

(a)

(b)

14.3 (a, b) Bending failure and bending–shear brittle damage after the China earthquake of 2008.

Additionally, post-earthquake examinations of RC buildings in several countries located in high seismicity zones showed also that one of the weakest links in the lateral load-resisting system is the beam–column joint. That is, in RC frames, the beam–column connection is one of the critical components in the lateral load path. Column load is vertically transmitted through the

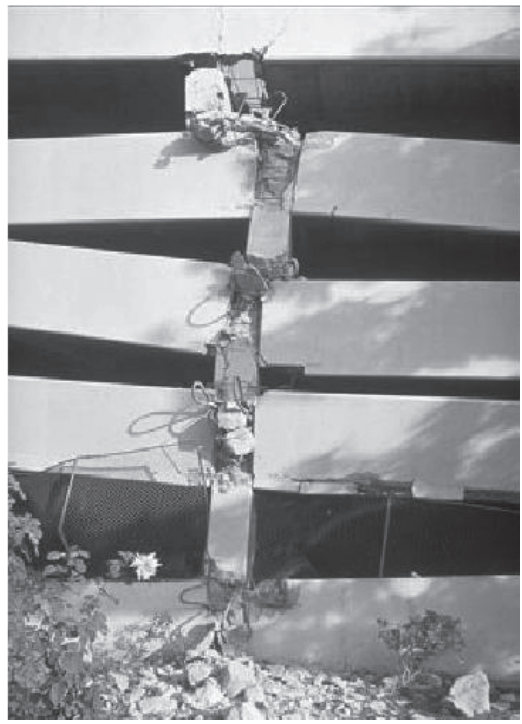

14.4 Column failures (Northridge earthquake, 1994, USA).

14.5 Beam–column damage after China, 2008, earthquake.

joint; hence the failure of a beam–column joint may lead to the collapse of the building, because hinging in the joint allows excessive rotations in both the beam and the column in conjunction with a loss of load-carrying capacity of the column. Bedirhanoglu *et al*. (1997) reported that the use of low-strength concrete, smooth (plain) reinforcing bars in beam–column joints may cause severe damage to buildings during earthquakes. In the study of Ghobarah and Said (2002), inadequate transverse reinforcement in the joint and weak-column/strong-beam design are the main reasons for the observed joint shear failures during recent earthquakes. Figure 14.6(a) shows RC structures that collapsed during the 1999 Kocaeli earthquake in Turkey, and Figs 14.6(b) and (c) present those damaged or collapsed during the earthquake and tsunami of Thailand and Indonesia in 2004 (Ghobarah *et al*., 2004). Joint failures appear to be the major contributor to such collapse. Such a dangerous failure mechanism is unacceptable and must be prevented in design (Said and Nehdi, 2004).

14.3 FRP composite retrofitted bridges

14.3.1 Acceptable damage zones in RC bridges

In some major earthquakes in the past, a large number of bridges suffered damage and collapsed due to failure of the foundation (structural and geotechnical), substructure, superstructure, and superstructure–substructure and substructure–foundation connections. Unlike the damage to buildings in earthquake-affected regions, where a large number of injuries or deaths would be directly caused by building collapse, bridge damage will isolate the affected area by preventing the transport of lifeline supplies and denying access by rescuers. Of course, this would generate a larger impact to society. The severe damage to bridges and the difficulty in repairing or retrofitting them will lengthen the rescue process to such an extent that wounded people may lose their lives due to the lack of access to medical care. Bridge foundations are not easily accessible for inspection and retrofitting after an earthquake, and any inelastic action or failure of the superstructure renders the bridge dysfunctional for a long period. Besides, connection failure is generally brittle in nature and hence should be avoided. Therefore, the substructure is the only component where inelasticity (plastic hinge formation) can be allowed to dissipate the input seismic energy and that too in flexural action. In addition, a flexurally damaged pier can be more easily retrofitted.

14.3.2 Residual deformation as a recoverability measure

In recent years, the downside of permanent displacements in RC structures has focused researchers' attention on the issue related to both the control of

(a) (1)

(a) (2)

14.6 (a–c) Corner and exterior joint failure during 1999 Turkey earthquake.

(b)

(c)

14.6 Continued

the structural integrity and resistance conservation against static incipient collapse in the aftermath of earthquake events. For RC bridges, in fact, large residual inclination makes placement of the bridge girders difficult and causes visual uneasiness even if the repercussions of overall or partial structural damage are not serious. Elevated bridges usually consist of four

main elements: girder, bearing, piers, and foundation. Among these, the piers and foundation can be a cause of the residual inclination of the pier. Another possible cause is the rigid body rotation of the bridge, that is, residual deformation of the ground. In Japan after the Kobe earthquake of 1995, one of the measurements checked during the investigation of the reconstruction and repair of the damaged bridges was the amount of inclination of the columns (residual drift ratio) (Fujino *et al*., 2005). Although, in the Kobe route, many single RC piers suffered from flexural mode damage and some piers with rectangular cross-sections suffered from shear failure, the observed large residual inclination was not attributed to the flexural residual deformation or residual deformation of the ground, but primarily to the pulling out of the reinforcing bars (Hashimoto *et al*., 2005). Hence, the JSCE Earthquake Engineering Committee (2000) defined that the residual deformation of RC bridge piers should not exceed 1% of the piers height for rapid restoration of structural functions after an earthquake.

14.4 Recoverability of FRP composite-RC bridge piers

The inadequacy in the performance of existing bridges under the influence of earthquakes has triggered the attention of researchers to upgrade existing older RC piers using fiber composites to current seismic design standards in regions with high seismicity. The following subsections address successful FRP-retrofitting approaches achieving the performance of damage-controllable systems.

14.4.1 FRP-confined bridge piers

The use of FRP represents an innovative and effective technology for strengthening, retrofitting, and upgrading of existing concrete structures (Seible *et al*., 1997; Xiao *et al*., 1999; Lacobucci *et al*., 2003). In view of that, extensive studies have investigated the seismic behavior of columns with square, rectangular, and circular cross-sections wrapped with FRP composites, to test the enhanced ductility of bridge columns under the seismic action. In the study of Fahmy *et al*. (2009, 2010a), the inelastic performance of 109 FRP confined columns with lap-splice deficiency (Xiao and Ma, 1997; Seible *et al*., 1997; Elsanadedy, 2002; Chang and Chang, 2004; Haroun and Elsanadedy, 2005b; Ghosh and Sheikh, 2007; Brena and Schlick, 2007; Harajli and Dagher, 2008), flexural deficiency (Seible *et al*., 1997; Chang *et al*., 2003; Kawashima, 2000; Sheikh and Yau, 2002; Lacobucci *et al*., 2003; Memon and Sheikh, 2005; Shan *et al*., 2006), or shear deficiency (Seible *et al*., 1997; Masukawa *et al*., 1997; Chang *et al*., 2003; Li and Sung, 2004; Haroun and Elsanadedy, 2005a; Xiao *et al*., 1999;

G. Wu *et al*., 2006a, 2007; Z. S. Wu *et al*., 2006b) were scrutinized. Sixty-one columns exhibited idealized lateral performance with stable post-yield stiffness. The hysteretic responses of these 61 samples were represented by the moment–curvature relationship for six samples, the skeleton curve of the load–deformation relationship for 16 samples, and complete hysteretic load–deformation response for 39 samples. To categorize columns, which successfully achieved secondary stiffness, in accordance with the required recoverability after an earthquake, the residual deformations were applied as a seismic performance index measuring the required recoverability of FRP-retrofitted bridges. The residual deformation, which is defined as the displacement of zero-crossing at unloading on the hysteresis loop from the endpoint of post-yield stiffness, should not exceed 1% of the column height for rapid restoration of structural functions after an earthquake.

Figure 14.7 shows the lateral drifts of 39 scale-model tests at the recoverability limit in comparison with the maximum achieved drifts (point D or E of Fig. 14.1 according to column response). Figure 14.7(a) displays columns with flexural and lap-splice deficiencies, and columns with shear deficiencies are depicted in Fig. 14.7(b). Below the line representing the lateral drifts of the columns at the recoverability limit, columns are within the recoverable state; and beyond this line, columns residual drifts are over 1%, which means columns enter into the irrecoverable state. Although lateral deformation at the recoverability limit of any of these samples does not correspond to a specific point on the idealized lateral load–deformation relationship of the FRP-RC damage-controllable structure, it is noticeable that most columns could not stay recoverable until point D of Fig. 14.1 (the end point of the achieved post-yield stiffness).

Based on the nonlinear pushover test results, it is clear that a residual drift ratio of 1% does not correspond to a specific column drift ratio, since many parameters affect the performance of these columns. However, it is interesting to stress that there is a zone of the drift ratio between 2 and 3.5% within which the recoverability limit state could be checked. Hence, the endpoint of the recoverable state can be defined by evaluating the residual inclination value within this zone. Ultimately, Fahmy *et al*. (2009) recommend three limit states for FRP-RC bridge columns as shown in Fig. 14.8. The first state is the state of pure recoverability whose end corresponds to column drift ratio 2% as shown Fig. 14.8. Here, the residual deformation of all the represented columns is below the recoverability limit. The second state is the state of recoverability limit check which falls between the 2% and 3.5% column drift ratios. The third state is the irrecoverable one, where the residual deformations exceed the recoverability limit.

In the study of Fahmy *et al*. (2010a), suitable FRP design assumptions and concepts certifying the reality of post-yield stiffness are defined and summarized as follows:

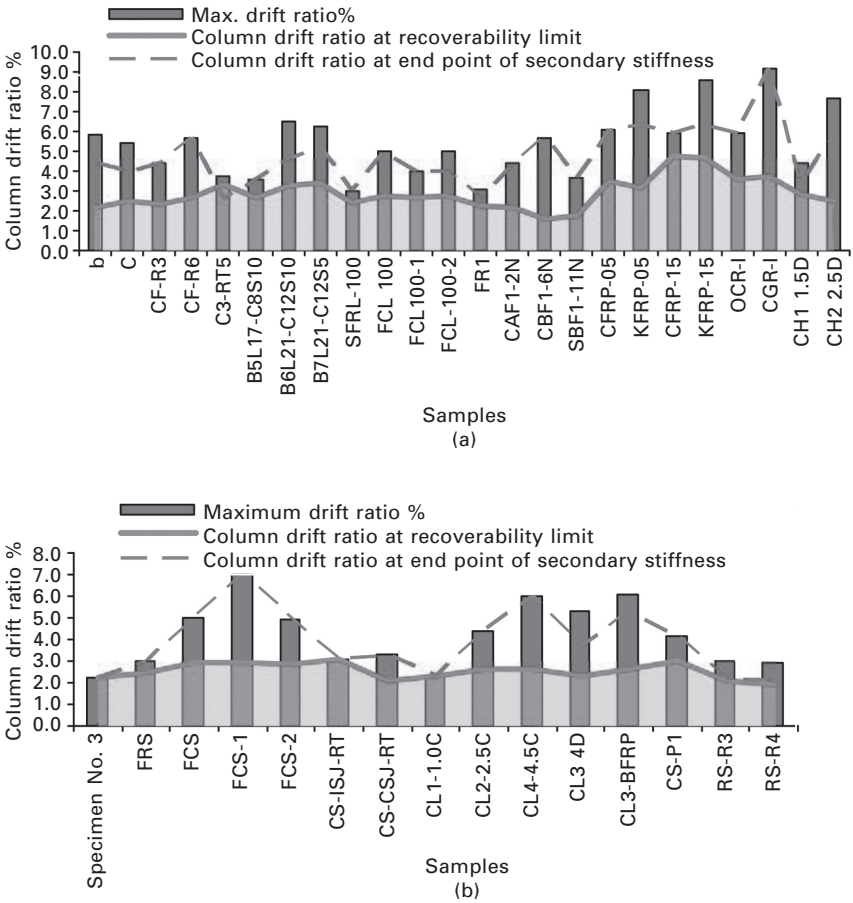

14.7 Recoverability limit of FRP-retrofitted RC bridge columns with (a) flexural and lap-splice deficiencies and (b) shear deficiencies.

1. The minimum design level of the FRP confinement ratio should be ≥0.12 for columns with continuous reinforcement, and it should be ≥0.25 in case column reinforcement is lap-spliced at the plastic hinge zone.
2. To avoid shear failure, horizontal FRP wrapping should limit the column dilation in the loading direction up to a dilation strain <0.004.
3. To postpone the onset of splitting of deficiently lap-spliced reinforcements and to reduce the severity of the subsequent deterioration, a hoop strain of 1,000 $\mu\varepsilon$ is appropriate for the design of the composite jacket for circular and rectangular columns. Also steel plates should be used in the wrapper region of rectangular columns.
4. In case different fibers are offered for retrofitting of a deficient column, these fibers should be designed to equivalent lateral stiffnesses, then the

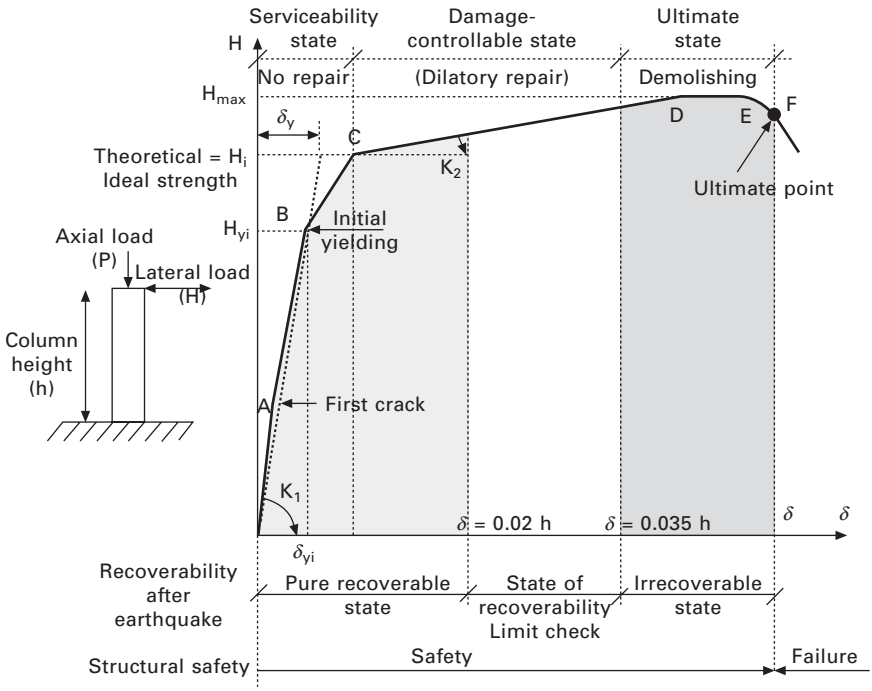

14.8 Recoverable and irrecoverable states of damage-controlled FRP-RC columns.

one with the highest confinement ratio would be selected for a ductile-recoverable structure.

14.4.2 Damage-controlled RC bridges using near-surface mounted (NSM) FRP rebars

The effect of the FRP type and stiffness and the axial load ratio on the residual deformation of the tested columns was studied by Fahmy *et al.* (2009). The axial load ratio is the only factor showing a clear effect on the residual deformation. For instance, an increase of the axial load ratio causes a reduction in the residual deformation, but without any significant effect on the final drift ratio. In addition, the achieved post-yield stiffness in an FRP-confined column could not be directly controlled, since its appearance is dependent on the enhancement of the confined concrete and the strain-hardening behavior of the steel reinforcement used. This is an indication that controlling the irrecoverable deformations and post-yield stiffnesses of existing structures using FRP composites is a future challenge toward achieving the aim of ductile-recoverable structures.

The near-surface mounted (NSM) technique is based on installing laminates

into precut grooves executed on the concrete cover of the elements to strength, and has been used to increase the flexural strength of beams (Hacha and Rizkalla, 2004; Barros and Fortes, 2005; De Lorenzis and Teng, 2007) and slabs (Bonaldo *et al.*, 2008). In RC buildings, NSM proved to be very effective in terms of increasing column flexural resistance, as long as the NSM bars can be effectively anchored in the adjacent elements (Barros *et al.*, 2006; Bournas and Triantafillou, 2009; Perrone *et al.*, 2009).

Fahmy and Wu (2012) adopted the NSM technique using basalt FRP (BFRP) rebars (produced by Zhejiang GBF Basalt Fiber Co.) as a retrofitting system for deficient RC bridge columns, where bond conditions between NSM BFRP rebars and the surrounding material were considered to find out how the recoverability indices (post-yield stiffness and residual deformation) of RC bridge columns could be controlled. Two specimens (CF-S and CF-R) were strengthened using the NSM technique. The strengthening process was provided by BFRP rebars, where two 6-mm-diameter bars were symmetrically placed on each of two opposite sides of the column (those with highest tension/compression). Figure 14.9 shows the strengthening system using NSM reinforcement (Fahmy and Wu, 2012).

To determine the effectiveness of the proposed retrofitting technique using NSM BFRP rebars (with different textures), the apparent damage, residual deformations, and the force–displacement curves were compared for the three test models.

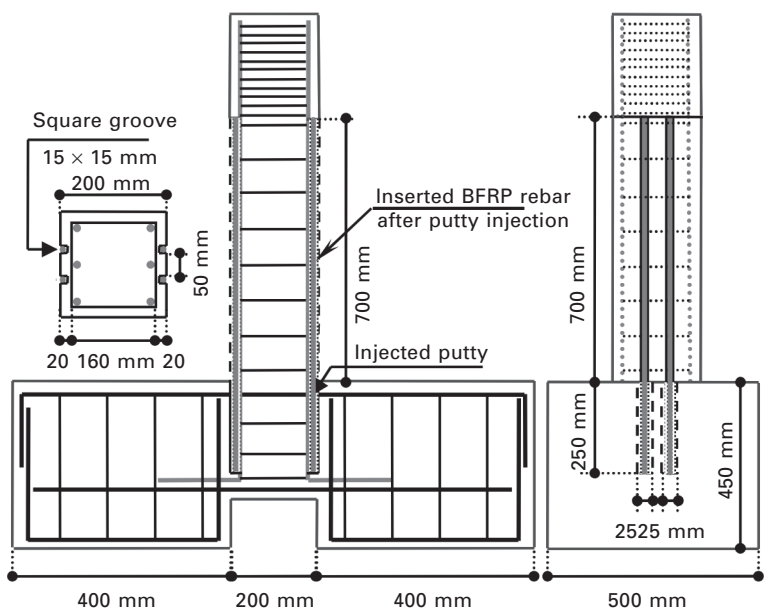

14.9 Strengthening procedure using NSM BFRP rebars.

The apparent damage

The apparent damage on one side (north side) of the tested columns by Fahmy and Wu (2012) under the effect of pull loadings is shown in Fig. 14.10. The observed damage at 0.5, 1.0, 2.0 and 3.0% drifts was compared among the models. Cracks shown in grey were developed at the achieved level of lateral drift, but cracks in black appeared at the previous loading cycles.

At 0.5% drift, the extent of cracking was the highest in CF-S and the lowest in CF-R. Furthermore, at all drifts, the extent of cracking was higher in CF-S than in CF-R. Both observations could be attributed to the rough texture of the BFRP rebars in CF-R which, to some extent, controls the appearance and propagation of cracks on the unconfined concrete (concrete cover). Figure 14.10 shows also that the number of cracks in CF-S exceeded those of CF-R up to 2.0% drift; however, at 3.0% drift many cracks were developed in the first 250 mm of the column CF-R.

Force–displacement relationship

The lateral force–drift relationships of the three models are shown in Fig. 14.11, and the envelopes of these responses were superimposed on the same figure. The measured response of CF showed a ductile behavior and after yielding the column was still carrying load over the ideal theoretical strength (29 kN) up to a lateral drift of 2.0 and 2.5% in the push and pull loading directions, respectively. On the other hand, the proposed retrofitting technique successfully enhanced the inelastic performance of the existing column without any significant effect on column elastic stiffness, where both CF-S and CF-R realized the existence of post-yield stiffness and the end points of the achieved stiffnesses were 4% and 4.5%, respectively. This result reflects the significance of adopting the bond between NSM rebars and the surrounding material as a design parameter that can be employed to control the column post-yield stiffness.

Residual deformation

The effect of the texture of NSM rebars on the column residual displacements was evaluated in the study of Fahmy and Wu (2012). Figure 14.12 shows the normalized residual displacements of CF-S and CF-R versus the column drift. It is clear that the reduction in the residual drift in CF-R was considerably higher than that of CF-S, indicating the beneficial effect of using deformed NSM BFRP rebars rather than smooth rebars. For instance, residual displacement of the column retrofitted with smooth BFRP rebars reduced by 25% at 1% drift, and mitigation by 10% was only achieved beyond 2% drift; the corresponding values were 37% and 20% respectively

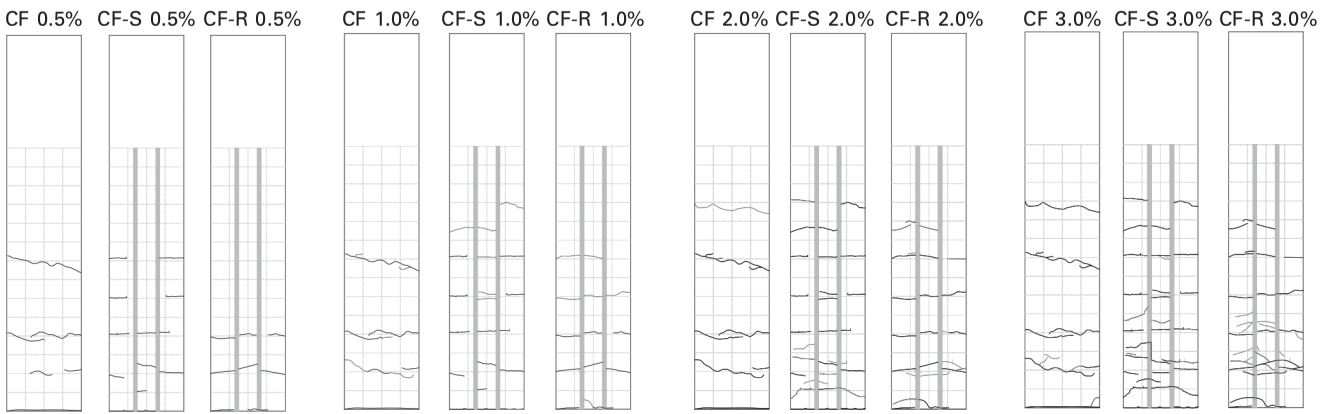

14.10 Damage of CF, CF-S, and CF-R at 0.5, 1.0, 2.0, and 3.0% drifts.

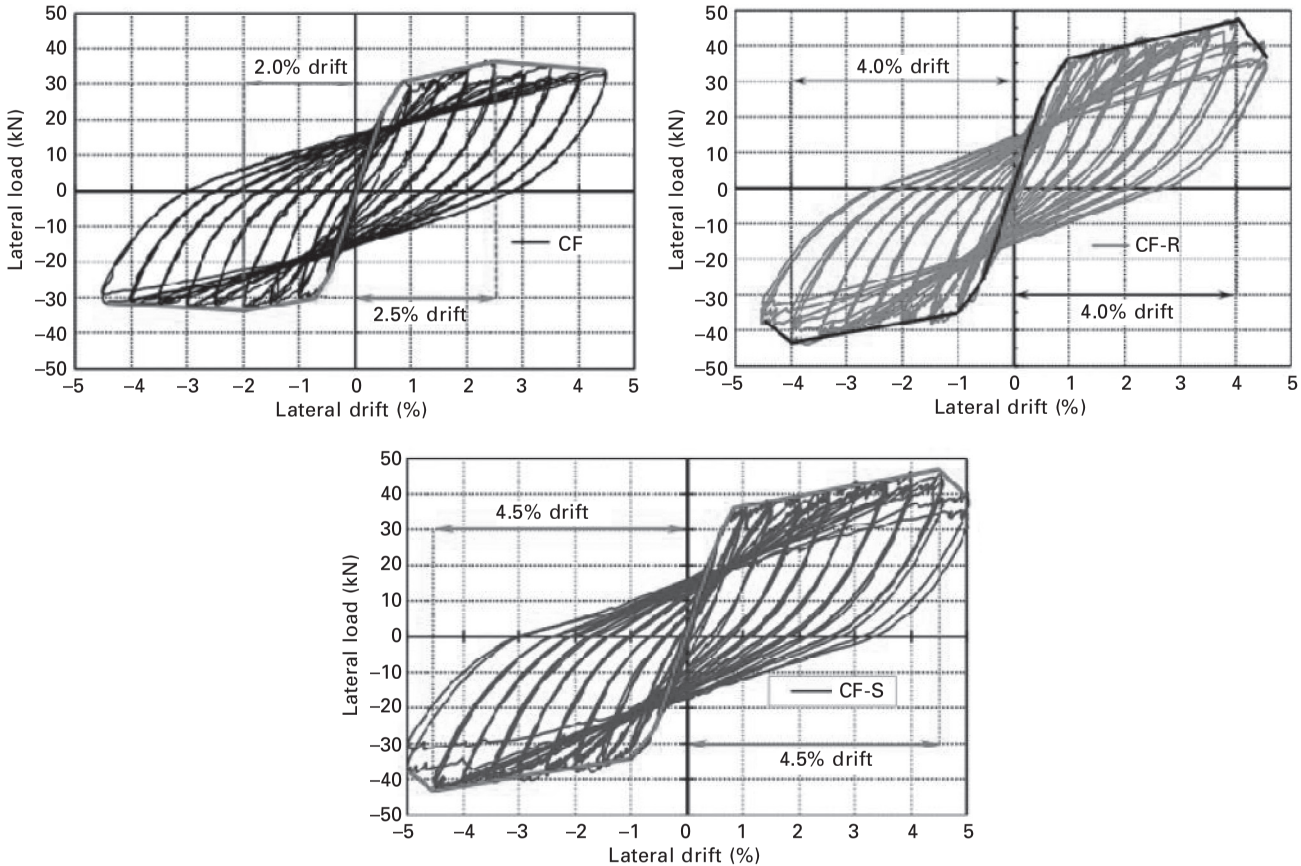

14.11 Lateral load versus drift for CF, CF-S, and CF-R.

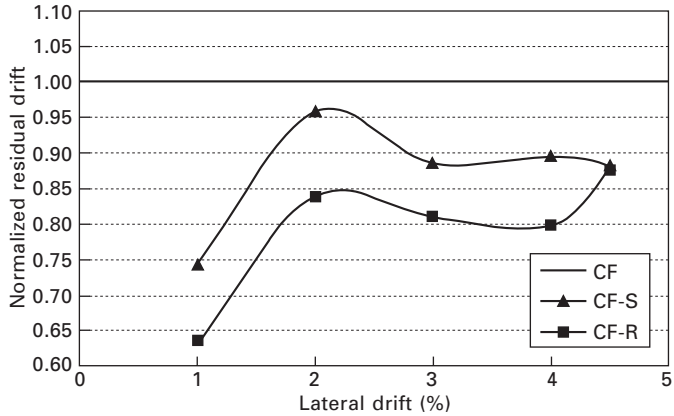

14.12 Reduction in column residual deformation after retrofitting with NSM technique.

where the retrofitting rebars had a rough texture. The practical application of the major reduction in residual drift is that the structure is more likely to remain serviceable after strong earthquakes when the reasonable bond-based NSM technique is applied.

14.5 Performance of FRP composite-retrofitted beam–column joints in RC bridges

According to the modern seismic design methodology of RC bridges, the ductile flexural failure in columns is desirable so long as significant inelastic deformation can be developed; therefore the other parts of the bridge piers should remain elastic by providing them with strength greater than the capacity of the plastic hinges. In the previous section, it was shown that FRP-retrofitting of existing RC bridge columns was applied successfully to prevent several deficiencies and guarantee the required recoverability and controllability. However, to accomplish the main aim of a recoverable structure, it is critical to strengthen the other deficient regions (bent cap and column/bent cap joint), which must behave elastically.

Strengthening of RC joints is a challenging task that poses major practical difficulties. Chen *et al*. (2005) investigated the overall performances of three different retrofitting schemes with five-test units. One of the tested units was strengthened with carbon fiber-reinforced polymer (CFRP) sheets prior to testing. Bridge specimens were designed to reproduce the behavior of a prototype bridge under simulated seismic loads. The FRP jacket thickness for column shear deficiency is defined initially, and then the FRP jacket thickness for confinement of the plastic hinge region is determined based on the designed curvature ductility (Chen *et al*., 2005). Afterwards, a CFRP

retrofit model was proposed for the strengthening of a bridge column/bent cap joint subjected to applied lateral loads. A total of three CFRP sheet plies were required and placed in the diagonal direction of the joint. In order to enhance the clamping resistance for the diagonal sheets and to enhance the flexural capacity of the bent cap layers, six additional sheets were placed in the other directions, as shown Fig. 14.13. GFRP anchors made of glass fibers and subsequently epoxied into holes predrilled in the concrete member were also used. The main objective for installation of these anchors was to aid in the development of the mechanical bond transfer mechanism between the CFRP sheets and the concrete, thereby reducing the propensity for the CFRP delamination.

The CFRP retrofit scheme was adequate for column shear strengthening and generally acceptable for joint shear strengthening. The bent cap did not experience the onset of a shear cone failure surrounding the column longitudinal bars at increased ductility levels. Although some shear cracks occurred in the joint, the CFRP sheets successfully prevented the cracks from further developing. In the lateral load–displacement relationship, the lateral load increased with displacement to a displacement ductility between 4.5 and 6. Therefore, the retrofit technique was successful in preventing the complete joint shear failure.

14.6 Overall performance of *in-situ* carbon fiber-reinforced polymer (CFRP) composite retrofitted RC bridges

It was fortunate for interested readers that Gergely *et al*. (1998) got the opportunity to test two bents of an old freeway (the Interstate-15 bridges

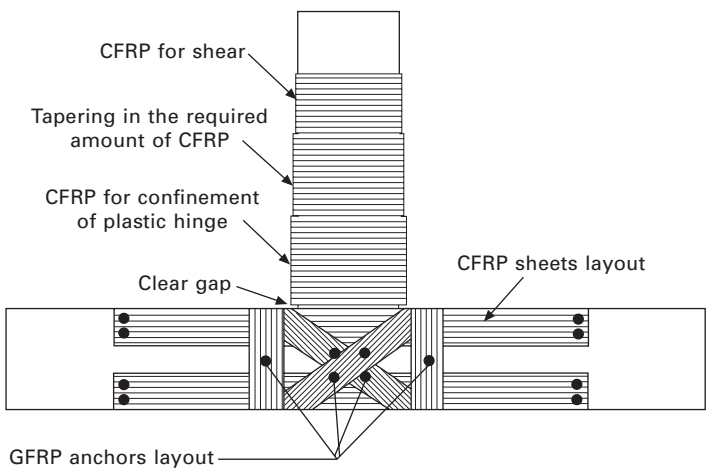

14.13 Column/bent cap strengthening details.

along the Wasatch front): one test served as reference and the second was retrofitted with CFRP. This bridge under consideration was designed and built in 1963, before the 1971 San Fernando earthquake, and was missing the basic reinforcement details necessary to provide adequate lateral load capacity and ductility. Gergely *et al*. conducted a pushover analysis based on the actual conditions of those bridge bents, and they concluded that the bent had deficiencies in the following areas: the confinement of the column lap-splice region, the confinement of the plastic hinges, the column shear, the shear in the joint region, and the anchorage of the column longitudinal reinforcement into the cap beam.

A complete design of the seismic retrofit of the bridge bent using CFRP composite was presented in detail by Pantelides and Gergely (2002). Based on the lateral load–displacement hysteretic response of the as-built and FRP-retrofitted bents (Pantelides and Gergely, 2008), a comparison between the experimental performances of the structure in the two configurations is given in Fig 14.14. It is clear that externally CFRP composites did not significantly affect the initial stiffness; this is an advantage of the applied retrofitting technique because the amount of fibers used will not attract additional force due to the seismic input (Saiidi *et al*., 2009). Also, it is evident that the applied retrofitting technique was able to increase the displacement ductility significantly. That is, the bent-cap column joint shear capacity was enhanced, and overall damage was controlled.

Figure 14.15 shows the relationship between the bent lateral displacement and residual deformation for both tested bents. Superimposing the recoverability limit on this figure confirms the finding of Fahmy *et al*. (2009); that is, that

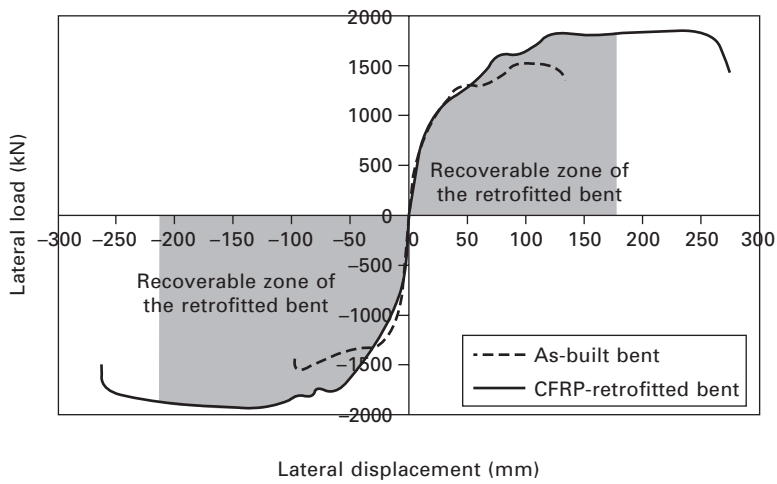

14.14 Envelope curves of the lateral load–displacement response of both tested bents.

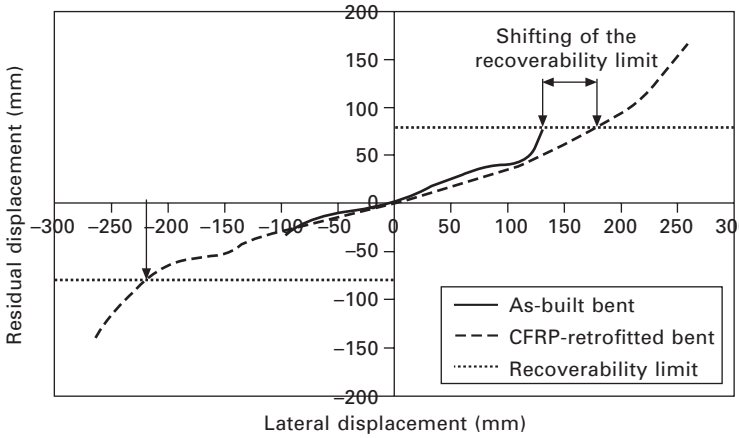

14.15 Comparison between residual displacement of the as-built bent and the CFRP retrofitted one.

the end of the recoverable zone of the FRP-retrofitted system falls between 2 and 3.5% drift ratio. For instance, the ends of the recoverable zones of the CFRP-retrofitted bent are 2.3% and 2.8% in the push and pull directions of loading, respectively (see Figs 14.14 and 14.15). Also, it is interesting to note that the applied technique successfully shifted the recoverability limit to 2.3% drift, which was 1.68% in the as-built bent (Fig. 14.15).

14.7 Retrofitting and recoverability of FRP composite-RC buildings

Poor seismic performance of most RC buildings designed and constructed prior to the current code provisions has raised concern and interest in retrofitting of those most vulnerable to collapse. That is, there is an urgent need to upgrade the vast numbers of existing RC structures to prepare society for the next destructive earthquake. In RC structures, a large stiffness is needed in order to limit structural deformation for service load conditions. When a severe earthquake strikes, however, the energy dissipation demands are imposed and inelastic deformations should be permitted in special detailed regions of structures. A failure in the beam is usually less critical than that in the column, and the latter is less critical than a failure in the beam–column joint (Said and Nehdi, 2004). Further, to prevent the possible collapse of RC structures, columns are supposed to remain elastic to maintain vertical load-carrying capacity (Qazi *et al*., 2006). In a RC frame structure, the story drift consists of the deflection in beams and columns themselves, the shear deformation in joints and the rigid-body rotation of beams at the joint faces (Joh *et al*., 1991). Hence, in particular for deficient structures, the ideal frame deformation mechanism is that the moment resisting frame

should be retrofitted to behave according to the strong column/weak beam concept in which the beams are expected to undergo inelastic deformations by forming plastic hinges.

Figure 14.16 shows the damage sequence in the components of RC structures to achieve the required recoverability after a massive earthquake. For instance, under the action of a minor shaking, the structure will behave elastically and concrete cracking in RC beams is probable; at point B, main reinforcement of the RC beams starts for yielding. When earthquake motion is stronger, the structure comes into the damage-controllable state wherein the plastic hinges form at the detailed regions of the RC beams; so, both the slope and the end of the post-yield stiffness are dependent on the performance of the RC beams. At point D, ductile behavior after hardening initiates (ultimate state), where favorable formation of plastic hinges commences at the column bases of the first floor and thus deformation would increase dramatically and the structure would not be able to carry additional load. The structure can be kept in place for a relatively long time without collapse during a large earthquake, though severe damage may occur. The original function of the structures may be recovered through the replacement of some elements. Ultimately, during a very severe earthquake, the structure may exceed the ultimate state when the beam–column joints fail.

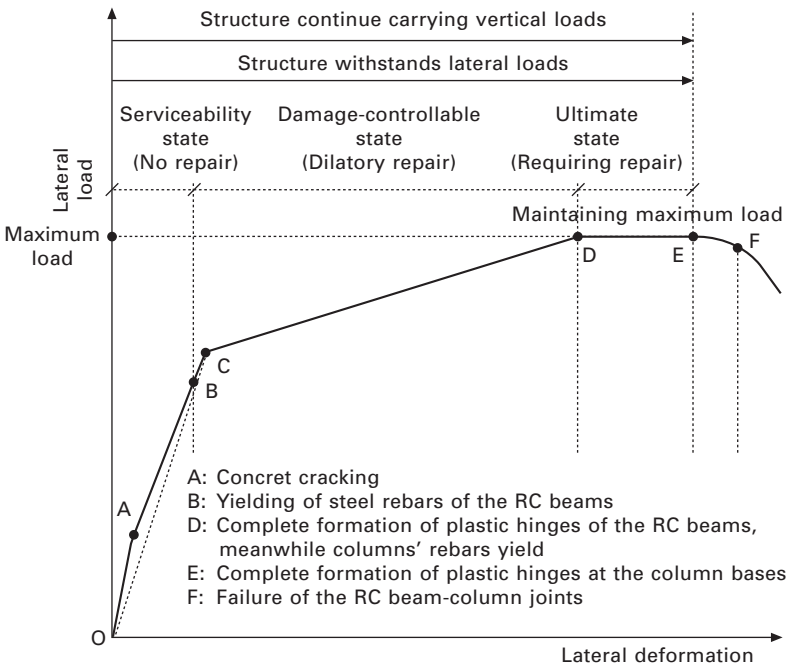

14.16 Sequence damage in the components of RC structures during severe earthquake.

In the following sections, the author addresses some aspects on efficient solutions for retrofitting RC-framed structures using FRP composites to prevent their collapse; in addition, the required recoverability and controllability are examined.

14.7.1 Performance of FRP-retrofitted beam–column joints

Several studies were conducted in order to develop retrofitting schemes for beam–column joints. To be successful, retrofitting schemes for deficient beam–column joints should achieve a shift from a brittle mode of failure (joint or column hinging) to a ductile beam flexural hinging mechanism of failure (Said and Nehdi, 2004). So, retrofitting is targeted at overcoming deficiencies such as usage of low-strength concrete, insufficient column sections, absence of stirrups in the joint, and poor anchorage of beam longitudinal bars at the joint.

Since 1998, research efforts on upgrading existing beam–column joints have focused on the use of FRP composites in the form of epoxy-bonded flexible sheets, shop-manufactured strips, or NSM rods (Bedirhanoglu *et al.*, 1997; Prota *et al.*, 2001, 2004; El-Amoury and Ghobarah, 2002; Ghobarah and Said, 2002; Engindeniz *et al.*, 2005; Anil, 2006; Tsonos, 2008; Trung *et al.*, 2010; Mahini and Ronagh, 2011). They are most attractive for their tailorability; the fiber orientation in each ply can be adjusted so that specific strengthening objectives such as increasing the strength only, the confinement only, or both, can be achieved.

Bedirhanoglu *et al.* (1997) tested three large-scale specimens to investigate the behavior of reference and retrofitted beam–column joints against simulated earthquake excitation. The specimens were designed to represent the exterior joint of a column and two beams at a corner of an intermediate floor in a RC building. In all specimens, the longitudinal reinforcement of the column was continuous and the longitudinal reinforcement of the beam was anchored in the joint using 90° hooks. In the FRP-retrofitted specimen, to prevent the slip of beam longitudinal bars in the joints, the hooks of top longitudinal bars were welded to the hooks of bottom bars in the joint. And to prevent brittle shear failure of the joint, FRP sheets were bonded over the external surface of the joint (Fig. 14.17). The test result established that through adequate design and detailing of FRP retrofitting of joint core together with rehabilitation of the anchorage of beam longitudinal bars through welding, the specimen could reach its flexural capacity and could keep its strength up to the drift ratio of 7%.

Four different rehabilitation techniques were tested by Ghobarah and Said (2002) for one-way exterior joints, originally designed to fail in joint shear. One system consists of wrapping the reinforced concrete joint area with

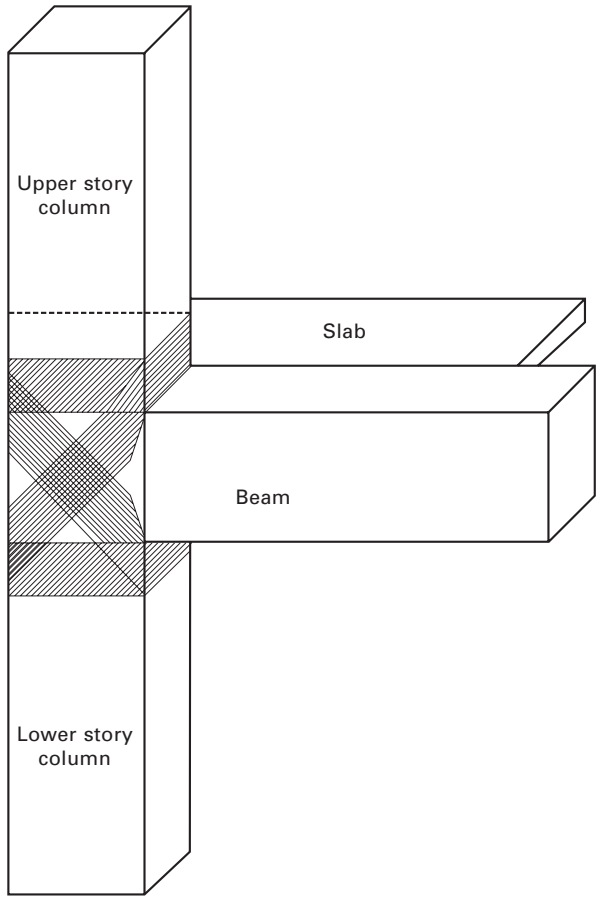

14.17 FRP application details of the FRP-retrofitting specimen (Bedirhanoglu *et al.,* 1997).

one layer of GFRP sheets in the form of a 'U'. The free ends of the 'U' at the beam were left unanchored. The GFRP used was bidirectional (±45°) (Fig. 14.18(a)). Another sample was retrofitted with the same system but the free ends of the 'U'-shaped GFRP were tied together using steel plates and threaded steel rods driven through the joint section. In both retrofitted specimens, the height of the FRP wrapping was limited to the depth of the beam at the joint (Fig. 14.18(b)). To strengthen the joint and the column, in the third system (Fig. 14.18(c)), two layers of GFRP fabric were extended above and below the joint and wrapped around the column; in addition, similar to the second system, bolted steel plates were used in the joint area. In the last sample, three layers of unidirectional GFRP were wrapped in the direction of diagonal tension forces in the joint at ±45°, with the vertical (Fig. 14.18(d)). The results from testing the first retrofitting system are very

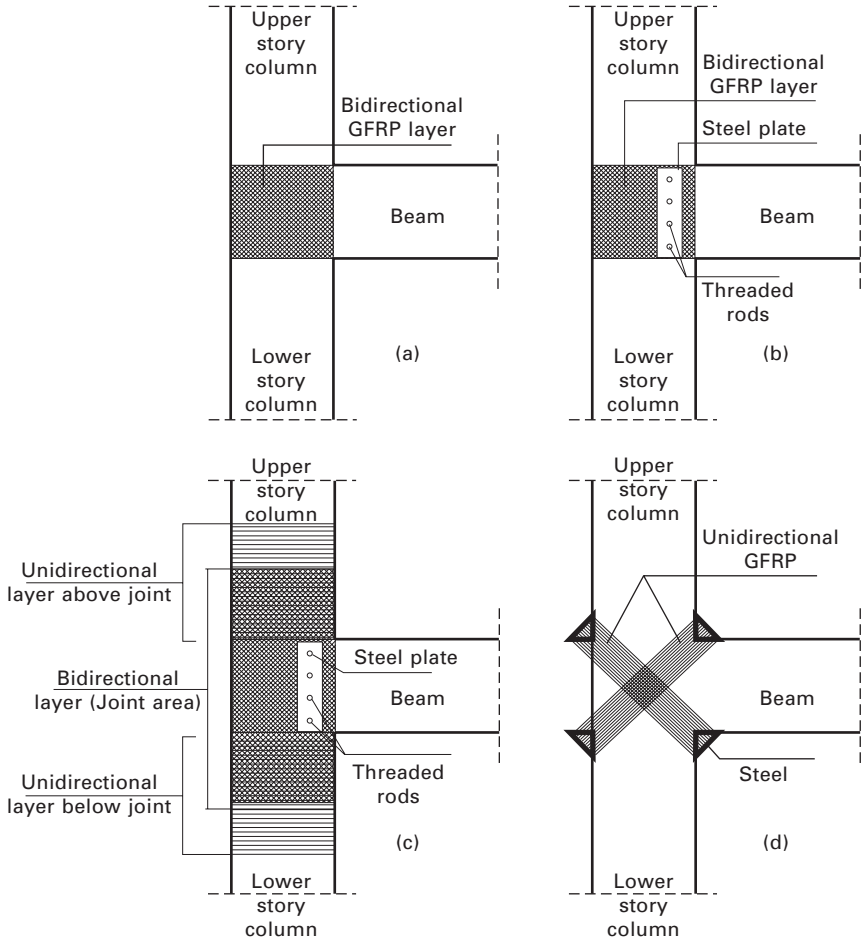

14.18 (a–d) Retrofitting schemes (Ghobarah and Said, 2002).

similar to the deficient sub-assemblage. On the other hand, the presence of the bolted plate in the second system prevented the premature failure of the joint and hence a flexural plastic hinge in the beam developed starting from the face of the column. Ductile plastic flexural hinging in the beam was the failure mode of the third system. This rehabilitation system was successful in preventing the beam–column joint shear failure. In the last rehabilitation system, the beam flexural strength and joint shear capacity were the same, so ultimately the joint failed in shear.

Trung *et al*. (2010) tested eight specimens made to simulate the exterior beam–column joints on the second floor of the building. Two of these samples served as references, and six remaining specimens were retrofitted by CFRP sheets. The main experimental outcome in their study is that, at the same

number of layers of CFRP sheets, seismic performance of the retrofitted specimens was most improved when the fiber direction was inclined at 45° from the beam axis (in an X-shaped configuration of wrapping).

When plastic hinging in beams is located away from the column faces, the effects of shear and bond stresses in the joint core are less severe. That is, the degradation of shear carried by the concrete diagonal compression strut and bond strength during reversals of seismic loading will not be so great if yielding of the beam longitudinal steel is forced to occur away from the faces of the joint core (Paulay *et al.*, 1978; Abdel-Fattah and Wight, 1987; Wong *et al.*, 1990). Mahini and Ronagh (2011) adopted that fact to control plastic hinging and implement the strong-column weak-beam concept through the use of a web-bonded FRP retrofitting system. The experimental investigation has proved that web-bonded CFRP-retrofitting technique can be applied to relocate the beam plastic hinging zone away from the column face, where the inelastic deformations occurred between 150 mm and 300 mm away from the column.

In conclusion, the use of an FRP retrofitting system in the direction of diagonal tension forces in the joint at ±45° assures the strong-column weak-beam concept. In addition, the damaged zone location can be controlled through the utilized FRP retrofitting system.

14.7.2 Performance of FRP-retrofitted columns

One of the main deficiencies in existing RC buildings is the poor design of columns. As indicated previously, the design of columns based on pre-1970 codes has many potential deficiencies, such as insufficient shear strength, lack of confinement and ductility as well as improper lap-splice details. In order to prevent the brittle shear failure and increase the ductility of the deficient columns, several FRP-retrofit approaches, such as fiber glass composite jacketing or carbon fiber composite winding, composite strips, as well as prefabricated composite jacketing, have been developed (Ma *et al.*, 2000; Ye *et al.*, 2003; Galal *et al.*, 2005; Verderame *et al.*, 2008; Yalcin *et al.*, 2008; Tao *et al.*, 2008; and Dai *et al.*, 2012).

To investigate the seismic performance of RC columns strengthened with CFRP sheets, Ye *et al.* (2003) tested eight specimens under constant and lateral cyclic load, including two strengthened after being loaded to yield level to imitate strengthening with some damage and one strengthened under a sustained axial load to imitate strengthening under service conditions. In the other samples, different strip widths and center-to-center strip distances were employed to provide different amounts of CFRP strengthening. Due to a low shear capacity, the control column failed in shear mode, and when the amount of wrapped fibers was not enough, the CFRP strips finally ruptured due to large shear deformation of diagonal shear cracks. When the amount

of CFRP sheet was sufficient to suppress the shear failure mode, the lateral load capacities after yielding were almost constant with zero post-yield stiffness due to flexural failure at the bottom section of the column, while ductility was increased with the amount of CFRP.

A new retrofitting method has been developed in the study of Tao *et al*. (2008) to retrofit large RC rectangular columns. They utilized the combined function of FRP-confinement and anchorage of embedded bars for concrete, and five RC square columns were tested to examine its validity and feasibility for enhancing the ductility of rectangular RC columns. The test results showed that the new retrofit method of GFRP bars and CFRP sheets can improve the anti-seismic behavior greatly by increasing the displacement ductility ratio, keeping the moment at the column bottom unreduced greatly during the test, and never increasing the stiffness of the columns.

The study of Dai *et al*. (2012) has been concerned with the seismic retrofit of square RC columns with polyethylene terephthalate (PET) FRP composites, which is a new type of FRP with a larger strain capacity and lower tensile stiffness compared to conventional FRPs. The hysteretic behavior and failure mode of PET FRP-jacketed column specimens under cyclic lateral loading has been explored and compared with those of unjacketed reference specimens and a specimen jacketed with high-strength aramid FRP (AFRP) in the plastic hinge zone. The results showed that PET FRP is a promising alternative to conventional FRPs for the seismic retrofit of RC columns. It improves the displacement ductility of RC columns significantly and does not rupture at the ultimate limit state.

In some instances, the formation of plastic hinges at the column bases may not be so critical regarding the safety of the structure; nevertheless this formation requires extensive rehabilitation efforts. Furthermore, the frame does not possess the recentering ability after undergoing severe lateral drift during strong shaking (Qazi *et al*., 2006). Residual deformations can result in the partial or total loss of a building if static incipient collapse is reached, or the structure appears unsafe to occupants. Furthermore, they can also result in increased cost of repair or replacement of non-structural elements as the new at rest position of the building is altered (Christopoulos and Pampanin, 2004). Consequently, it is imperative to control the plastic hinges formation at column bases, that is, columns should keep their integrity and residual deformations should be limited.

Barros *et al*. (2006) investigated the response of RC columns strengthened with NSM laminate strips and submitted to static axial compression load and cyclic horizontal increasing load. Three series of reinforced concrete columns were tested: series NON consisted of non-strengthened columns, series PRE was composed of concrete columns strengthened with CFRP laminate strips before testing, and series POS consisted of previously tested columns of series NON which were post-strengthened. The envelope curves for the first

and second series are superimposed on Fig. 14.19 for comparison. With the applied retrofitting technique, the column was able to carry additional load with the increase in the column deformation after yielding. In addition, the final residual deformation is the same for both columns and its value did not pass the recoverability limit (equal to 8.25 mm in this case) (Fig. 14.19). However, the achieved lateral drift (2.47%) highlights the significance of examining the possibility of achieving the required ductile-recoverable performance using this technique.

14.8 Novel damage-controllable structures using FRP composites

The demand for efficient and effective damage-controllable systems has received strong attention in the last decade, where the main goal is the alleviation of the damage at the plastic hinge zones along with substantial mitigation of the static residual deformations (Sakai *et al.*, 2006; Zatar and Mutsuyoshi, 2002; Ikeda *et al.*, 2002; Saiidi *et al.*, 2009). However, the most fundamental challenge is to improve the integrity of the structure in terms of its construction cost, age and usage, and its level of safety to withstand massive earthquakes.

14.8.1 Steel–fiber composite rebars for damage-controllable structures

Because the advantages of advanced composite materials (FRPs) include light weight, high strength or stiffness-to-weight ratio, corrosion resistance and,

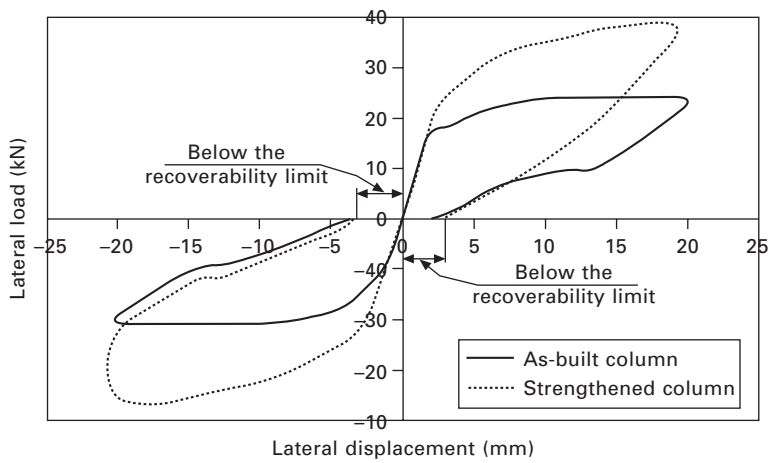

14.19 Hysteretic response of shear-deficient column and FRP-retrofitted column.

in particular, elastic performance, steel bars hybridized in the longitudinal direction with FRPs are proposed in the study of Fahmy *et al*. (2010b) as an innovative reinforcement method for recoverable structures, where the strain-hardening behavior of the innovative bars can be controlled based on both the amount and type of fibers used. Also, the use of the innovative rebars, i.e., steel fiber composite bars (SFCBs), will increase the life spans of structures because the inner steel bar is protected against corrosion (Fig. 14.20). Uniaxial and cyclic tensile behaviors of the innovative rebars were experimentally tested by Wu *et al*. (2010). Accordingly, the study of Fahmy *et al*. (2010b) investigates the controllability and recoverability of bridge columns reinforced with SFCBs: post-yield stiffness and residual deformations of columns reinforced with SFCBs were examined experimentally, where basalt FRPs (BFRPs) and carbon FRPs (CFRPs) were the fibers used for the production of SFCBs.

An experimental program was prepared and tested to verify the adopted concept of using SFCBs for bridge columns in place of the ordinary reinforcement. So, the objectives of this program were to test the possibility of increasing column lateral strength capacity through the existence of post-yield stiffness using additional longitudinal fibers, rather than by increasing the amount of reinforcement, and to enhance column restorability by shifting the lateral column drift at the recoverability limit. The reliability of applying this concept was measured by testing three columns. Two samples, CS10-B30 and CS10-C40, were reinforced with SFCBs, whereby the longitudinal reinforcement included twelve SFCBs consisting of 10-mm-diameter inner steel rebar and outer fibers, i.e., 30 bundles of basalt fibers and 40 bundles of carbon fibers. The third column (CS14) was reinforced with 12 ordinary, 14-mm-diameter rebars. Relevant details can be found in Fahmy *et al*. (2010b). The envelopes of the measured force–drift relationships are shown in Fig. 14.21. The curves are the average of the envelopes for the push-and-pull loadings. Additionally, for comparison, the calculated response of RC columns reinforced with 12 ordinary, 10-mm-diameter rebars (CS10) is superimposed

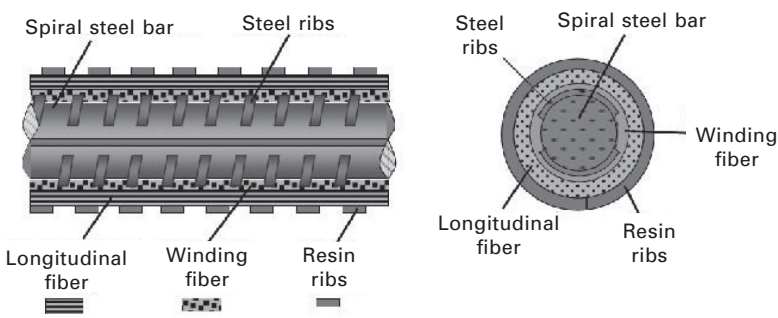

14.20 Details of steel fiber composite bar (SFCB).

on Fig. 14.21. It is clear from this figure that the yield stiffness is the same among the three columns reinforced with 10-mm-diameter ordinary rebars or SFCBs, and it is lower than that of column CS14. After yielding, CS10-B30 and CS10-C40 also showed a close similarity in the relation between column drifts and the corresponding lateral load until a lateral drift of 15 mm was reached, at which point a light rupture sound of the carbon fibers of column CS10-C40 was noticed. Further, a louder sound of the ruptured fibers was heard at 25 mm and was continuous at the column base until the end of the test. Column CS10-B30 was still carrying a load until a lateral deformation of about 30 mm was reached, and then louder sounds at a 35-mm lateral drift were heard due to the continuous rupture of basalt fibers at the column base. The deformation of column S14 increased without any increase in load-carrying capability, and strength degradation began at a lateral displacement of 35 mm due to buckling of longitudinal steel bars at the plastic hinge zone.

Although the amount of the inner steel reinforcement of the innovative columns was almost 50% of that used to reinforce CS14, the fulfilled strength of column CS10-B30 with the existence of a post-yield stiffness was 115 kN, which is nearly 92% of that achieved by the ordinary column. However, column CS10-C40 could not achieve a lateral strength of more than 110 kN due to the early rupture of carbon fibers. The second main objective of this study was to evaluate the effect of SFCBs on residual displacements of the innovative columns in comparison with conventionally reinforced columns. Figure 14.22 shows the residual drift versus the lateral drift for the three columns, where the plotted values are based on lateral push-and-pull

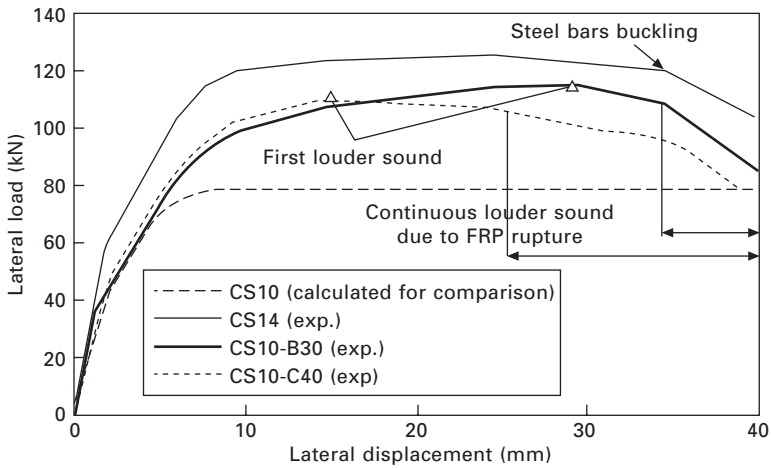

14.21 Comparison between lateral load–displacement relationships of the three tested columns and the calculated column CS10.

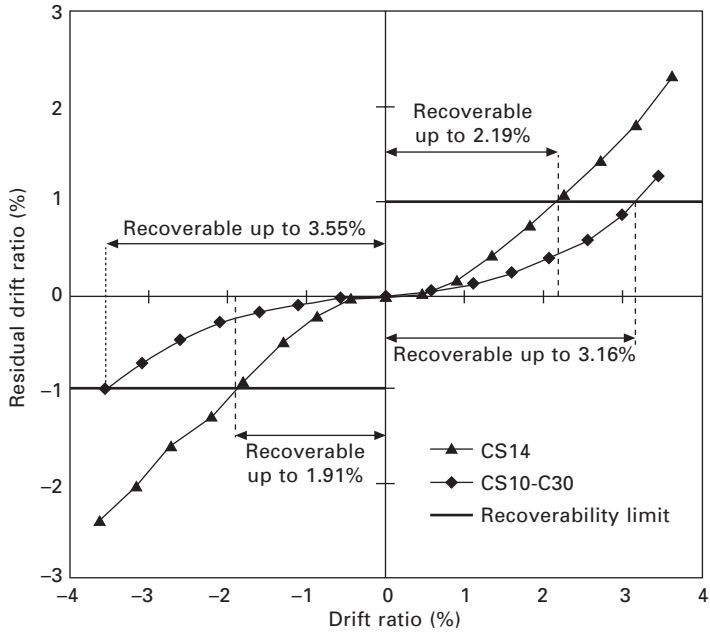

(a)

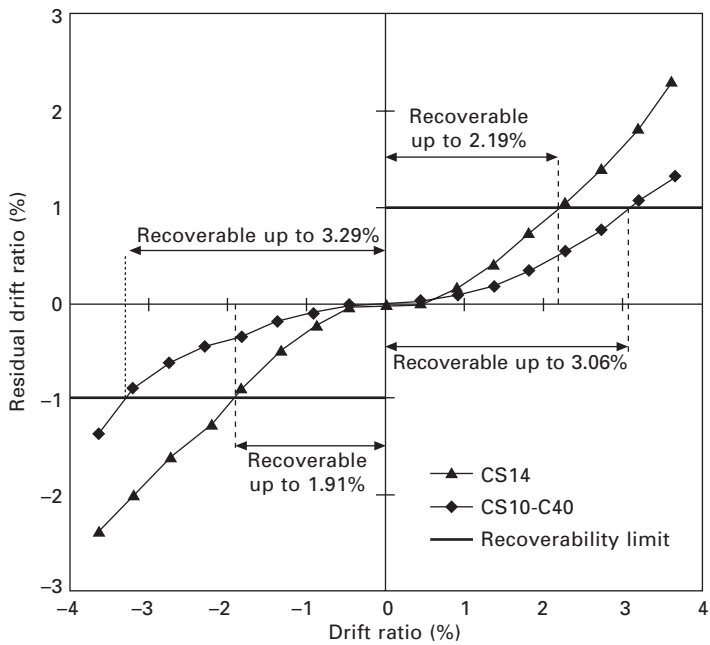

(b)

14.22 Comparison between residual drift ratios of the conventionally reinforced column (CS14) and innovative columns: (a) CS10-B30 and (b) CS10-C40.

loadings. It is clear that the residual drift in columns reinforced with SFCBs was considerably lower than that of CS14, indicating the beneficial effect of replacing conventional reinforcement with the SFCBs. For instance, the conventionally reinforced column CS14 could not achieve a lateral drift at the recoverability limit of over 1.91%, but hybridization of the longitudinal steel reinforcement with FRPs shifted the end of the recoverable state of columns CS10-B30 and CS10-C40 to 3.16% and 3.06%, respectively. Overall, the performance of the innovative columns revealed that the replacement of ordinary rebars with basalt SFCBs was effective in increasing column strength and in substantially reducing the residual drift.

14.9 Conclusion and future trends

Existing RC structures that were designed according to pre-1970s codes often have inadequate reinforcement detailing, which results not only in deficient lateral load resistance, but also in insufficient energy dissipation, rapid strength deterioration and improper hinging mechanisms during earthquakes, leading to excessive drifts and ultimately to structural collapse. Hence, this chapter discussed the recoverability and controllability of FRP-retrofitted RC structures (bridges and buildings). The following conclusions are reached.

1. Results of the experimental studies have indicated very clearly for both RC bridges and buildings that fiber composites (FRP sheets and rebars) are promising strengthening tools that can be used to alter the critical failure modes in deficient elements of the existing structures. Furthermore, fiber composites can be employed to control the behavior of those deficient elements; hence, the required seismic performance of the entire structure could be achieved.
2. The FRP-RC structures (existing RC bridges and buildings and modern constructions) can realize the seismic design goal of no damage during a small earthquake, prompt recoverability during a medium or strong earthquake, and no collapse during a huge earthquake.
3. Some studies have shown the success of the NSM retrofitting technique to reach the desired seismic behavior, raising attention to the importance of an intensive search in this direction to establish the suitable recommendations to be taken at strengthening the deficient elements to achieve the aim of ductile-recoverable structures.
4. The bond between FRP reinforcement and concrete plays an important role in the definition of the required performance from structures during and after earthquakes; thus, comprehensive studies on how to control bond behavior between FRP reinforcement and adjoining concrete should be a focus of future research efforts.

14.10 Proceedings

The major series of proceedings for this chapter are listed in the following.

Asia-Pacific Conference on FRP in Structures (APFIS, 2009), Seoul, Korea.

Fourth International Conference on FRP Composites in Civil Engineering (CICE 2008), Zurich, Switzerland.

Fifth International Conference on Advanced Composite Materials in Bridges and Structures (ACMBS, 2008), Winnipeg, Manitoba, Canada.

Ninth International Symposium on Fiber Reinforced Polymer Reinforcement for Concrete Structures (FRPRCS, 2009), Sydney, Australia.

Ninth US National and 10th Canadian Conference on Earthquake Engineering: Reaching Beyond Borders, 2010, Toronto, Canada.

Seventh International Conference on Urban Earthquake Engineering (7CUEE) and Fifth International Conference on Earthquake Engineering (5ICEE), 2010, Tokyo Institute of Technology, Tokyo, Japan.

14.11 References

Abdel-Fattah, B., and Wight, J.K. (1987). 'Study of moving beam plastic hinging zones for earthquake-resistant design of RC buildings'. *ACI Structural Journal*, 84(1): 31–39.

Anil, Ö. (2006). 'Improving shear capacity of RC T-beams using CFRP composites subjected to cyclic load'. *Cement and Concrete Composites Journal*, 28: 638–649.

Barros, J.A.O., and Fortes, A.S. (2005). 'Flexural strengthening of concrete beams with CFRP laminates bonded into slits'. *Cement Concrete Composites Journal*, 27(4): 471–480.

Barros, J.A.O., Ferreira, D.R.S.M., Fortes, A.S., and Dias, S.J.E. (2006). 'Assessing the effectiveness of embedding CFRP laminates in the near surface for structural strengthening'. *Construction and Building Materials*, 20(7): 478–491.

Bedirhanoglu, I., Ilki, A., and Kumbasar, N. (1997). 'Innovative techniques for seismic retrofitting of RC joints'. *ACES Workshop*, DOI 10.1007/978-94-007-1997-2_15

Bonaldo, E., Barros, J.A.O., and Lourenço, P.B. (2008). 'Efficient strengthening technique to increase the flexural resistance of existing RC slabs'. *Journal of Composites for Construction*, 12(2): 149–159.

Bournas, D.A., and Triantafillou, T.C. (2009). 'Flexural strengthening of reinforced concrete columns with near-surface-mounted FRP or stainless steel'. *ACI Structural Journal*, 106(4): 495–505.

Bracci, J.M., Reinhorn, A.M., and Mander, J.B. (1992). 'Evaluation of seismic retrofit of reinforced concrete frame structures'. Technical report NCEER-92-0031, State University of New York at Buffalo, Buffalo, NY, pp. 3–7.

Brena, S.F., and Schlick, B.M. (2007). 'Hysteretic behavior of bridge columns with FRP-jacketed lap splices designed for moderate ductility enhancement'. *Journal of Composites for Construction*, 11(6): 565–574.

Chang, K.C., and Chang, S.P. (2004). 'Seismic retrofit study of rectangular RC columns lap spliced at plastic hinge zone'. In: *Proceeding Joint NSC/NRC Workshop on Construction*, Taipei, Taiwan, IRC Research Report RR-192, pp. 27–34.

Chang, K.C., Chung, L.L., Lee, B.J., Tsai, K.C., Hwang, J.S., and Hwang, S.J. (2003). 'Seismic retrofit study of RC bridge columns'. *International Training Program for Seismic Design of Structures*, National Center for Research on Earthquake Engineering, pp. 57–76.

Chen, G., Anderson, N., Luna, R., Stephenson, R., Engebawy, M., Silva, P., and Zoughi, R. (2005). 'Experimental study on seismic retrofit technique for cap beams, columns and their connections of highway bridges'. Report No. UTC R89, US Department of Transportation, Research and Special Programs Administration, Washington, DC 20590–0001.

Christopoulos, C. and Pampanin, S. (2004). 'Towards performance-based seismic design of MDOF structures with explicit consideration of residual deformations'. *ISET Journal of Earthquake Technology*, 41(1): 53–73.

Dai, J.-G., Lam, L., and Ueda, T. (2012). 'Seismic retrofit of square RC columns with polyethylene terephthalate (PET) fiber reinforced polymer composites'. *Construction and Building Materials*, 27(1): 206–217. doi:10.1016/j.conbuildmat.2011.07.058.

De Lorenzis, L., and Teng, J.G. (2007) 'Near-surface mounted FRP reinforcement: An emerging technique for strengthening structures'. *Composites, Part B*, 38: 119–142.

El-Amoury, T., and Ghobarah, A. (2002). 'Seismic rehabilitation of beam–column joint using GFRP sheets'. *Engineering Structures*, 24: 1397–1407.

Elsanadedy, H.M. (2002). 'Seismic performance and analysis of ductile composite-jacketed reinforced concrete bridge columns'. Thesis (PhD), University of California at Irvine.

Engindeniz, M., Kahn, L.F., and Zureick, A.-H. (2005). 'Repair and strengthening of reinforced concrete beam–column joints: state of the art'. *ACI Structural Journal*, 102(2): 187–197.

Fahmy, M.F.M. (2010). 'Enhancing recoverability and controllability of reinforced concrete bridge frame columns using FRP composites'. Thesis (PhD), Ibaraki University, Hitachi, Ibaraki, Japan.

Fahmy, M.F.M., and Wu, Z.S. (2012). 'Seismic performance of RC bridge columns retrofitted with smooth and deformed near-surface-mounted basalt FRP rebars'. *6th Int. Conf. on FRP Composites in Civil Engineering (CICE 2012)*, Rome.

Fahmy, M.F.M., Wu, Z.S., and Wu, G. (2009). 'Seismic performance assessment of damage-controlled FRP-retrofitted RC bridge columns using residual deformations'. *Journal of Composites for Construction, ASCE*, 13(6): 498–513.

Fahmy, M.F.M., Wu, Z.S., and Wu, G. (2010a). 'Post-earthquake recoverability of existing RC bridge piers retrofitted with FRP composites'. *Construction and Building Materials*, 24(6): 980–998.

Fahmy, M.F.M., Wu, Z.S., Wu, G., and Sun, Z.Y. (2010b). 'Post-yield stiffnesses and residual deformations of RC bridge columns reinforced with ordinary rebars and steel fiber composite bars'. *Journal of Engineering Structures*, 32: 2969–2983.

Fujino, Y., Hashimoto, S., and Abe, M. (2005). 'Damage analysis of Hanshin expressway viaducts during 1995 Kobe earthquake. I: Residual inclination of reinforced concrete piers'. *Journal of Bridge Engineering*, 10(1): 45–53.

Galal, K., Arafa, A., and Ghobarah, A. (2005). 'Retrofit of RC square short columns'. *Engineering Structures*, 27: 801–813.

Gergely, I., Pantelides, C.P., Nuismer, R.J., and Reaveley, L.D. (1998). 'Bridge pier retrofit using FRP composites'. *Journal of Composites for Construction, ASCE*, 2(4): 165–174.

Ghobarah, A., and Said, A. (2002). 'Shear strengthening of beam–column joints'. *Engineering Structures*, 24(7): 881–888.

Ghobarah, A., Saatcioglu, M., and Nistor, I. (2004). 'The impact of the 26 December 2004 earthquake and tsunami on structures and infrastructures'. *Engineering Structures*, 28: 312–326.

Ghosh, K.K., and Sheikh, S.A. (2007). 'Seismic upgrade with carbon fiber reinforced polymer of columns containing lap-spliced reinforcing bars'. *ACI Structural Journal*, 104(2): 227–236.

Hacha, R., and Rizkalla, S.H. (2004). 'Near-surface-mounted fiber reinforced polymer reinforcements for flexural strengthening of concrete structures'. *ACI Structural Journal*, 101(5): 717–726.

Harajli, M.H., and Dagher, F. (2008). 'Seismic strengthening of bond-critical regions in rectangular columns using fiber reinforced polymer wraps'. *ACI Structural Journal*, 105(1): 68–76.

Haroun, M.A., and Elsanadedy, H.M. (2005a). 'Behavior of cyclically loaded squat reinforced concrete bridge columns upgraded with advanced composite-material jackets'. *Journal of Bridge Engineering*, 10(6): 741–748.

Haroun, M.A. and Elsanadedy, H.M. (2005b). 'Fiber-reinforced plastic jackets for ductility enhancement of reinforced concrete bridge columns with poor lap-splice detailing'. *Journal of Bridge Engineering*, 10(6): 749–757.

Harries, K.A., Ricles, J.R., Pessiki, S., and Sause, R. (2006). 'Seismic retrofit of lap splices in nonductile square columns using carbon fiber-reinforced jackets'. *ACI Structural Journal*, 103(6): 874–884.

Hashimoto, S., Fujino, Y., and Abe, M. (2005). 'Damage analysis of Hanshin expressway viaducts during 1995 Kobe earthquake. II: Damage mode of single reinforced concrete piers'. *Journal of Bridge Engineering*, 10(1): 54–68.

Hsu, Y.T., and Fu, C.C. (2004). 'Seismic effect on highway bridges in Chi Chi earthquake'. *Journal of Performance of Constructed Facilities*, 18(1): 47–53.

Ikeda, S., Nonaka, S., Hirose, S., and Yamagushi, T. (2002). 'Seismic performance of concrete piers prestressed in the critical section'. In: *Proceedings of the First FIB Congress*, Osaka, Japan, 47–48.

Japan Concrete Institute. *Handbook for Retrofitting of Existing Reinforced Concrete Structures*. Gihodo-shuppan (in Japanese).

Joh, O., Goto, Y., and Shibata, T. (1991). 'Behavior of reinforced concrete beam–column joints with eccentricity'. Special publication of American Concrete Institute (ACI, SP 123–12), pp. 317–357.

JSCE Earthquake Engineering Committee (2000). *Earthquake Resistant Design Codes in Japan*. Japan Society of Civil Engineers (JSCE), Tokyo, Japan, 150 pp.

Kawashima, K. (2000). 'Seismic design and retrofit of bridges'. In: CD-ROM of 12th World Conference on Earthquake Engineering (WCEE), Auckland, New Zealand, paper no. 1818.

Kawashima, K., and Unjoh, S. (1997). 'The 1996 Japanese seismic design specifications of highway bridges and performance based design'. In: Fajfar, P. and Krawinkler, H. (eds), *Seismic Design Methodologies for the Next Generation of Codes*, Balkema, Rotterdam.

Lacobucci, R.D., Sheikh S.A., and Bayrak, O. (2003). 'Retrofit of square concrete columns

with carbon fiber-reinforced polymer for seismic resistance'. *ACI Structural Journal*, 100(6): 785–794.

Li, J., Samali, B., Ye, L., and Bakoss, S. (2002). 'Behavior of concrete beam–column connections reinforced with hybrid FRP sheet'. *Composite Structures*, 57: 357–365.

Li, Y.-F., and Sung, Y.-Y. (2004). 'A study on the shear-failure of circular sectioned bridge column retrofitted by using CFRP jacketing'. *Journal of Reinforced Plastics and Composites*, 23(8): 811–830.

Ma, R., Xiao, Y., and Li, K.N. (2000). 'Full-scale testing of a parking structure column retrofitted with carbon fiber reinforced composites.' *Construction and Building Materials*, 14: 63–71.

Mahini, S.S., and Ronagh, H.R. (2011). 'Web-bonded FRPs for relocation of plastic hinges away from the column face in exterior RC joints'. *Composite Structures Journal*, 93: 2460–2472.

Masukawa, J., Akiyama, H., and Saito, H. (1997). 'Retrofit of existing reinforced concrete piers by using carbon fiber sheet and aramid fiber sheet'. In: *Proceedings of the Third International Symposium on Non-Metallic (FRP) Reinforcement for Concrete Structures*, Vol. 1.

Memon, M.S., and Sheikh, S.A. (2005). 'Seismic resistance of square concrete columns retrofitted with glass fiber-reinforced polymer'. *ACI Structural Journal*, 102(5): 774–783.

Pantelides, C.P., and Gergely, J. (2002). 'Carbon-fiber-reinforced polymer seismic retrofit of RC bridge bent: design and *in situ* validation'. *Journal of Composites for Construction*, 6(1): 52–60.

Pantelides, C.P., and Gergely, J. (2008). 'Seismic retrofit of reinforced concrete beam-column T-joints in bridge piers with FRP composite jackets'. ACI special publication SP 258–1, American concrete Institute.

Park, R., and Paulay, T. (1975). *Reinforced Concrete Structures*. John Wiley & Sons, New York, 769 pp.

Paulay, T., Park, R., and Priesley, M.J.N. (1978). 'Reinforced concrete beam–column joints under seismic actions'. *ACI Journal, Proceedings*, 75: 585–593.

Perrone, M., Barros, J.A.O., and Aprile, A. (2009) 'CFRP-based strengthening technique to increase the flexural and energy dissipation capacities of RC columns'. *Journal of Composites for Construction*, 13(5): 372–383.

Prota, A., Nanni, A., Manfredi, G., and Cosenza, E. (2001). 'Selective upgrade of of beam–column joints with composites'. In: *Proceedings of the International Conference on FRP Composites in Civil Engineering*, Hong Kong.

Prota, A., Nanni, A., Manfredi, G., and Cosenza, E. (2004). 'Selective upgrade of underdesigned reinforced concrete beam–column joints using carbon fiber reinforced polymers'. *ACI Structural Journal*, 101(5) 699–707.

Qazi, A.U., Lieping, Y.E., and Xinzheng, L.U. (2006). 'Passive control reinforced concrete frame mechanism with high strength reinforcements and its potential benefits against earthquakes'. *Tsinghus Science & Technology Journal*, 11(6)L 640–647.

Qiang, H., Xiuli, D., Jingbo, L., Zhongxian, L., Liyum, L., and Jianfeng, Z. (2009). 'Seismic damage of highway bridges during the 2008 Wenchuan earthquake'. *Journal of Earthquake Engineering and Engineering Vibration*, 8(2): 263–273.

Said, A.M., and Nehdi, M.L. (2004). 'Use of FRP for RC frames in seismic zones: Part I. Evaluation of FRP beam–column joint rehabilitation techniques'. *Journal of Applied Composite Materials*, 11: 205–226.

Saiidi, M.S., O'Brein, M., and Sadrossadat-Zadeh, M. (2009). 'Cyclic response of concrete bridge columns using superelastic nitinol and bendable concrete'. *ACI Structural Journal*, 106(1): 69–77.

Sakai, J., Jeong, H., and Mahin, S.A. (2006). 'Reinforced concrete bridge columns that re-center following earthquakes'. In: *Proceedings of the 8th National Conference on Earthquake Engineering*, San Francisco, CA, paper no. 1421.

Seible, F., Priestley, M.J.N., Hegemier, G.A., and Innamorato, D. (1997). 'Seismic retrofit of RC columns with continuous carbon fiber jackets'. *Journal of Composites for Construction*, 1(2): 52–62.

Shan, B., Xiao, Y., and Guo, Y. (2006). 'Residual performance of FRP-retrofitted RC columns after being subjected to cyclic loading damage'. *Journal of Composites for Construction*, 10(4): 304–312.

Sheikh, S.A., and Yau, G. (2002). 'Seismic behavior of concrete columns confined with steel and fiber-reinforced polymers'. *ACI Structural Journal*, 99(1): 72–81.

Tao, L., Wei, F., Zhi-mei, Z., and Yu, O. (2008). 'Experimental study on ductility improvement of reinforced concrete rectangular columns retrofitted with a new fiber reinforced plastics method'. *Journal Shanghai University*, 12(1): 7–14. doi: 10.1007/s 11741-008-0102-1.

Trung, K.L., Lee, K., Lee, J., Lee, D.H., and Woo, S. (2010). 'Experimental study of RC beam-column joints strengthened using CFRP composites'. *Composites: Part B*, 41: 76–85.

Tsonos, A.G. (2008). 'Effectiveness of CFRP-jackets and RC-jackets in post-earthquake and pre-earthquake retrofitting of beam–column subassemblages'. *Engineering Structures*, 30: 777–793.

Verderame, G.M., Fabbrocino, G., and Manfredi, G. (2008). 'Seismic response of r.c. columns with smooth reinforcement. Part II: Cyclic tests'. *Engineering Structures*, 30: 2289–2300.

Wong, P.K.C., Priestley, M.J.N., and Park, R. (1990). 'Seismic resistance of frames with vertically distributed longitudinal reinforcement in beams'. *ACI Structural Journal*, 87(4): 488–498.

Wu, G., Wu, Z.S., Lu, Z.T., and Gu, D.S. (2006a). 'Seismic retrofit of large scale circular RC columns wrapped with CFRP sheets'. In: CD-ROM of Third International Conference on FRP Composites in Civil Engineering (CICE 2006), Miami, FL, 547–550.

Wu, G., Gu, D.S., Wu, Z.S., Jiang, J.B., and Hu, X.Q. (2007). 'Comparative study on seismic performance of circular concrete columns strengthened with BFRP and CFRP composites'. In: *Proceeding of Asia-Pacific Conference on FRP in Structures (APFIS 2007)*, Hong Kong, Vol. 1: 199–204.

Wu, G., Wu, Z.S., Luo, Y.B., Sun, Z.Y., and Hu, XQ. (2010). 'Mechanical properties of steel fiber composite bar (SFCB) under uniaxial and cyclic tensile loads'. *Journal of Materials in Civil Engineering, ASCE*, 22(10): 1056–1066.

Wu, Z.S., Gu, D.S., Wu, G., and Hirahata, H. (2006b). 'Seismic performance of RC columns strengthened with Dyneema fiber-reinforced polymer sheets'. In: *Proceedings of the Fourth International Conference of Earthquake Engineering*, Taipei, Taiwan.

Xiao, Y., and Ma, R. (1997). 'Seismic retrofit of RC circular columns using prefabricated composite jacketing'. *Journal of Structural Engineering*, 123(10): 1357–1364.

Xiao, Y., Wu, H., and Martin, G.R. (1999). 'Prefabricated composite jacketing of RC columns for enhanced shear strength'. *Journal of Structural Engineering*, 125(3): 255–264.

Yalcin, C., Kaya, O., and Sinangil, M. (2008). 'Seismic retrofitting of R/C columns having

plain rebars using CFRP sheets for improved strength and ductility'. *Construction and Building Materials*, 22: 295–307.

Ye, L.P., Zhang, K., Zhao, S.H., and Feng, P. (2003). 'Experimental study on seismic strengthening of RC columns with wrapped CFRP sheets'. *Construction and Building Materials*, 17: 499–506.

Zatar, W.A., and Mutsuyoshi, H. (2002). 'Residual displacement of concrete bridge piers subjected to near field earthquakes'. *ACI Structural Journal*; 99(6): 740–749.

Zhejiang GBF Basalt Fiber Co. Ltd (GBF), http://www.chinagbf.com/en/index.asp

15

High performance fibre-reinforced concrete (FRC) for civil engineering applications

T. H. PANZERA and A. L. CHRISTOFORO, Federal University of São João del Rei (UFSJ), Brazil and P. H. RIBEIRO BORGES, Federal Centre for Technology Education of Minas Gerais (CEFET/MG), Brazil

DOI: 10.1533/9780857098641.4.552

Abstract: Portland cement concrete is a brittle material. The main reason for incorporating fibres into a cement matrix is to improve the cracking deformation characteristics, increasing not only the toughness, impact and tensile strength, but also eliminating temperature and shrinkage cracks. Several different types of fibres have been used to reinforce cement-based materials. This chapter briefly discusses the characteristics of fibre-reinforced concrete (FRC), reporting the effect of the fibres on the physico-chemical and mechanical properties. It also presents some of the recent research and future perspectives of FRC.

Key words: fibre-reinforced concrete (FRC), mechanical strength, toughness, impact resistance, shrinkage.

15.1 Introduction

Brittle materials are known to have no significant post-cracking ductility; therefore, fibrous composites have been developed to provide improved mechanical properties to otherwise brittle materials. When subjected to tension, unreinforced brittle matrices initially deform elastically. The elastic responses are then followed by microcracking, localized macrocracking and finally fracture. Introduction of fibres into brittle matrices usually results in changes in the post-elastic properties, which can range from subtle to substantial, depending upon a number of factors. Those factors include matrix strength, type and amount of fibre, fibre strength and orientation, among others. Fibres may be inert or reactive; their inertness or reactivity with the matrices will determine the bonding characteristics of fibre-reinforced composites (Brown *et al.*, 2002; Shah and Ribakov, 2011).

Fibres may also prevent the occurrence of large cracks, thus preventing percolation of water and contaminants into ceramic materials such as Portland cement mortars and concretes. So, corrosion of steel reinforcement or potential deterioration of concrete may be reduced with the addition of a variety of fibres to the Portland cement matrices. In addition, other enhanced

properties are observed, such as tensile and compressive strength, elastic modulus, crack resistance, crack control, fatigue life, impact and abrasion resistance, shrinkage, expansion, thermal characteristics and fire resistance (ACI report, 2002).

The employment of fibres to reinforce brittle materials dates from the Egyptian and Babylonian era. Baked clay reinforced with straw and masonry mortars reinforced with animal hair are good early examples of fibre-reinforced composites employed as construction materials (Johnston, 2001). However, the modern concept of fibre reinforcement emerged with the development of asbestos-cements. Those composites were made of a mix of asbestos fibres and slurry (cement and water) to produce thin-section flat and corrugated plates for roofing, pipes and other elements. That technology, known as the Hatschek, Magnani or Mannville processes, started about 1900 and has been widely used in construction materials for many years. Asbestos-cement declined in the 1970s when it was discovered that breathing asbestos represented a severe hazard to human health. In the meantime, however, other fibre-reinforced composites have been developed.

Romualdi first proposed fibres as dispersed reinforcement for concrete in his two papers in 1963 and 1964. Later on, Biryukovichs proposed the employment of glass fibres into concrete, which were originally not resistant and durable in the highly alkaline Portland cement paste. It was Majumdar and Ryder (1968) who invented the alkali-resistant (AR) glass fibres with the addition of zirconium oxide (Brandt, 2008).

The main role of fibres is to bridge the cracks that develop in concrete and increase the ductility of concrete elements. Fibres increase the strain at peak load, as well as provide additional energy absorption ability of reinforced concrete elements and structures. It was recently reported that they also considerably improve the static flexural strength of concrete as well as its impact strength, tensile strength, ductility and flexural toughness (Shah and Ribakov, 2011; Pacheco-Torgal and Jalali, 2011).

The ACI report (2002) defines fibre-reinforced concrete (FRC) as concrete made of hydraulic cements containing fine or fine and coarse aggregates mixed with discontinuous discrete fibres. The categories of employed fibres are steel, alkali-resistant glass, synthetic, and natural fibre materials. Naturally occurring asbestos fibres and a wide range of vegetable fibres (e.g. sisal, jute, bamboo, etc.) are also used for reinforcement. There is a great variety of fibre-reinforced mortar and concrete formulations, depending on particular applications. In general, the length and diameter of the fibres used for fibre-reinforced concrete do not exceed 3 in. (76 mm) and 0.04 in. (1 mm), respectively (Ohama, 1989; ACI, 2002). Continuous meshes, woven fabrics and long rods are not considered to be discrete fibre-type reinforcing elements. In all cases, the most convenient numerical parameter to describe a fibre is the aspect ratio, i.e. fibre length divided by an equivalent diameter

(the equivalent fibre diameter being the diameter of a circle with an area equal to the cross-sectional area of the fibre). For concrete, the typical fibre aspect ratios used range from 30 to 150 for fibre lengths of 0.25–3.0 in. (6.3–76.2 mm) (Majumdar, 1975).

Figure 15.1 (Brown *et al*., 2002) shows the behaviour of fibre-reinforced concrete under loading. The plain concrete (with no fibre reinforcement) cracks into two pieces when the structure is subjected to the peak tensile load and cannot withstand further load or deformation. An analogous fibre-reinforced concrete (FRC) structure cracks at the same peak tensile load; however, it usually maintains large deformations as a single element. The area under the curve represents the energy that the FRC absorbed when subjected to tensile load, usually described as the 'post-cracking response' of FRC. The best performance of fibre addition takes place when fibres not only bridge the cracks but also undergo pullout processes. In those cases, the deformation continues only with employment of further loading energy (Brown *et al*., 2002; ACI, 2002).

It is possible to see from Fig. 15.1 that FRC works as non-reinforced until it reaches the so-called 'first crack strength'. From that moment on, the fibre reinforcement takes over and holds the concrete together. The fibre pull-out will determine the maximum load capacity. It is important to note that concrete reinforcing bars have a rough surface, which helps adhesion to the paste and mechanical bonding. Short fibres, on the other hand, are smooth. This condition limits performance to a point far less than the yield strength of the fibre itself. As a consequence, some fibres pull out easier than others when used as reinforcing, affecting the toughness of the concrete, i.e. the total energy absorbed prior to complete failure (Brown *et al*., 2002).

FRC has started to find application in many areas of civil engineering, especially when repairing and when increased durability is required. The

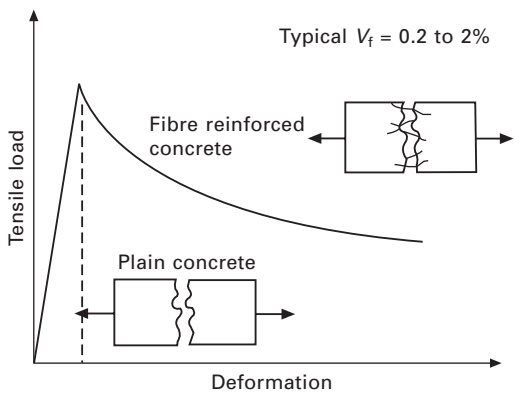

15.1 Tensile load versus deformation for plain and fibre-reinforced concrete (adapted from Brown *et al.,* 2002).

synthetic fibres have been employed mostly to maximize prevention of corrosion in concrete structures. FRC is also suitable for minimizing cavitation/erosion damage in structures such as sluice-ways, navigational locks and bridge piers where high-velocity flows are encountered. Other applications comprise lightweight structures, where relatively thin FRC elements have the equivalent strength of thicker plain concrete. Special applications of fibre in concretes as well as the future trends are detailed in Section 15.4 of this chapter.

FRC may present some disadvantages. Depending on the fibre categories, the reinforced concrete may exhibit high permeability, which can lead to carbonation and chloride ion attack, resulting in corrosion problems (Glasser *et al*., 2008; Bentur and Mitchell, 2008). The fabrication processes represent another disadvantage associated with FRC. The incorporation of fibres into the cement matrix is labour intensive and costs more than the production of the plain concrete. However, the overall advantages gained by the use of FRC override the disadvantages (Brown *et al*., 2002).

15.2 Physical and chemical effects of fibres in concrete

15.2.1 Workability of the mixes

Despite the benefits of fibre reinforcement, fibres usually affect the workability of fresh concrete significantly. The reason for this is the incorporation of an extra needle-like shape ingredient, which has high specific surface and may absorb part of the mixing water. Thus, concretes incorporating fibres are more difficult to mix, transport, place and compact. Inadequate compaction may lead to excessive voids in hardened concrete, which are of course undesirable. Investigation of fresh fibre-reinforced concrete is therefore very important to prevent adverse rheological and hardened properties of FRC. The slump test has been known to be a poor indicator of FRC, especially steel fibre-reinforced concrete (SFRC). In fact, the V-B test has been found to be more suitable for assessment of workability of FRC. This latter test is, however, empirical in nature and cannot define fresh concrete properties in terms of yield stress and plastic viscosity (Tattersall and Banfill, 1983). The ACI report (2009) recommended the use of the inverted slump cone test for workability of FRC. Review of literature shows that there is limited information on the effect of fibres on the rheological behaviour of high-strength concrete in terms of yield stress and plastic viscosity. Tattersall (1991) observed that increasing the steel fibre content in SFRC resulted in increasing yield stress and plastic viscosity. Increasing the fibre length yields mainly an increase in plastic viscosity. Increasing the fibre volume fraction to its maximum packing density led to greater yield stress and plastic

viscosity in fibre-reinforced mortar. There are other factors that affect the rheology of FRC, such as total surface area, modulus of elasticity of fibre, rheological behaviour of concrete without fibre, and processing techniques (Shah and Ribakov, 2011).

Fibres with higher aspect ratios give rise to increasing flexural strength; however, workability of FRC is adversely affected by an increase in the aspect ratios of fibres. Hence, the aspect ratio is generally limited to an optimum value to achieve good workability and strength. Chunxiang and Patnaikuni (1999) suggested that aspect ratios of less than 60 are best from the point of handling and mixing of fibres, but an aspect ratio of about 100 is desirable from a strength point of view. Song and Hwang (2004), however, suggested that aspect ratios between 50 and 70 are more practicable for ready-mix concrete.

Despite the reduced workability of FRC, recent studies have shown that it is possible to produce fibre-reinforced self-compacted concrete (FR-SCC), with good flow properties and suitable properties. Akcay and Tasdemir (2012) have studied steel fibre in FR-SCC and found that the main parameter affecting the flowability of FR-SCC is the geometry of fibres, rather that the fibre strength. El-Dieb and Taha (2012) show that suitable workability of FR-SCC depends on the fibre content. For polypropylene fibres, the maximum fibre content should be 1000, 1200 and 1300 g/m^3 for SCC mixtures with cement content 350, 400 and 500 kg/m^3 respectively. For steel fibres, one should limit the fibre aspect to 50, 90 and 100 kg/m^3 for SCC mixtures with cement content of 350, 400 and 500 kg/m^3 respectively.

15.2.2 Hydration and shrinkage of FRC

Despite the changes in the rheological properties, hydration of cement in FRC is not expected to alter to a great extent, as long as the fibres do not absorb large amounts of water required to cement hydration. This could be a problem, especially with natural fibres; they must not absorb water for two main reasons: (1) to ensure complete hydration of cement grains, and (2) to ensure fibre durability over time. Saturation of fibres may be an alternative if water absorption is an issue; however, for durability purposes, impregnation may be a better option.

As cement hydrates, autogenous and drying shrinkage takes place. Autogenous shrinkage has become an important issue with the development of high-performance concrete (Bentz and Jensen, 2004). Fibres may be used to improve matrices prone to cracking due to excessive shrinkage. According to Torgal and Jalali (2011), the natural fibres appear to delay restrained plastic shrinkage, controlling crack development at early ages. Apparently, the control of shrinkage does not require large amounts of fibre. Filho *et al.* (2005) found that only 0.2 vol% of 25 mm sisal fibres reduce free plastic

shrinkage in FRC. Saje *et al*. (2011) state that 0.25 vol% of polypropylene fibres are effective to control concrete autogenous shrinkage; further fibre addition shows negligible improvements. Kawashima and Shah (2011) have shown that small amounts of saturated cellulose fibres (1% by mass of cement) significantly improve the shrinkage control, as well as provide some internal curing of fibre-reinforced cementitious materials.

Studies on the effect of short and long steel and polypropylene fibres on autogenous shrinkage of FRC have shown that steel fibres are more effective in controlling early autogenous shrinkage. However, both types of fibre equally control later autogenous and drying shrinkage of reinforced concrete (Saje *et al*., 2012).

The work of Aly *et al*. (2008) shows different results. The authors studied the reinforcement of slag concrete incorporating 0.2–0.5 vol% of polypropylene (PP) fibres and found that increasing dosage of fibres caused small but consistent increases of the overall total shrinkage of the concretes, compared with unreinforced concrete. They explained the results by the fact that concretes with PP fibres were more permeable and, consequently, more prone to drying. In that study, the lower cracking resistance of PP reinforced slag concretes resulted from the combined effect of higher elastic modulus and higher drying shrinkage.

It is well known that shrinkage of concrete may be reduced with the employment of shrinkage reducing admixtures (SRA). Passuello *et al*. (2009) has shown that the combination of SRA and PVA fibres led to a better cracking behaviour of concrete. Short fibres from recycled PET bottles appear to be an alternative to restrain plastic shrinkage in concrete and building cement materials (Pelisser *et al*., 2010).

15.2.3 Durability of fibre-reinforced cement-based materials

Portland cement-based materials like concrete have long been used for civil engineering construction. However, the deterioration of civil infrastructure all over the world has proved that cement-based materials must be improved in terms of their engineering properties and durability. The employment of pozzolanic materials, such as blastfurnace slag, metakaolin or silica fume, is a well-established method to improve those properties (Mindess *et al*., 2003). The utilization of fibres may act as additional reinforcement to improve certain properties of concrete elements, such as ductility, toughness, flexural strength, fatigue and impact resistance (Banthia *et al*., 1987a; Balaguru and Shah, 1992; Nawy, 2001; Lawler *et al*., 2002; Voigt *et al*., 2004). However, FRC is not necessarily a durable material. The long-term durability depends on (1) the fibre–matrix bonding properties, (2) the durability of the matrix, and (3) the durability of the fibre in the high-pH environment of the cement paste.

The durability of the fibre under a high-pH environment is treated as one of the main issues regarding FRC. Synthetic reinforcements, such as polypropylene or carbon fibres, may be attractive because they are inert in the highly alkaline environment and their chemical inertness also allows for accelerated curing (e.g. autoclaving), without degradation of fibres. Steel fibres are durable in high pH, but they may present rust stain problems on concrete surfaces. Alkali resistant (AR) glass fibres have been developed with incorporation of 16–20 wt% zirconium dioxide in the fibre formulation. AR glass fibres are meant to be durable in cement paste, but the increasing temperature and pH in the pore solution may cause degradation of the fibre (Mechtcherine, 2012).

In general, the durability of natural fibres is definitively the main concern, given that this type of fibres must resist both external (temperature and humidity variations, sulphate or chloride attack, etc.) and internal damage (compatibility between fibres and cement matrix, volumetric changes, etc.). The main degradation of natural fibres is caused by the high alkaline environment, which dissolves the lignin and hemicellulose phases, thus weakening the fibre structure. Fibre degradation has been evaluated by exposing them to alkaline solutions and subsequent measurement of the variations in tensile strength. Results have shown a deleterious effect of Ca^{2+} ions on fibre degradation, as well as the better durability of fibres where pH is lower, e.g. areas of carbonated concrete (ACI report, 2009).

Toledo Filho *et al*. (2000) investigated the durability of sisal and coconut fibres to alkaline solutions. Sisal and coconut fibres maintained, respectively, 72.7% and 60.9% of their initial strength after 420 days of exposure to NaOH solution. The behaviour of those fibres was different when exposed to $Ca(OH)_2$, as both types of fibre completely lost their initial strength after 300 days. The explanation for the higher attack by $Ca(OH)_2$ can be related to the crystallization of lime in the fibre pores. Natural fibres also absorb water and this is another way to decrease the durability of FRC, as water absorption leads to volume changes and cracking (Ghavami, 2005; Tonoli *et al*., 2007).

Results show that the addition of pozzolanic materials is effective in preventing fibre degradation, as they lower the pH of cement pastes (Mohr *et al*., 2007). D'Almeida *et al*. (2009) replaced 50% of Portland cement with metakaolin to produce a matrix totally free of $Ca(OH)_2$ that prevented migration of calcium hydroxide to the fibre lumen, middle lamella and cell walls, thus avoiding embrittlement behaviour. But in some cases the low alkalinity of blended pastes is not sufficient to prevent lignin from being decomposed (John *et al*., 2005). Another alternative may be the employment of artificial carbonation as a curing method to (1) increase the strength, (2) reduce water absorption, and (3) reduce the pH of cured pastes (Agopyan *et al*., 2005; Tonoli *et al*., 2010).

Coating of natural fibres may also avoid penetration of water and free alkalis. Some of the methods employ water-repellent agents (e.g. silanes) or fibre impregnation with sodium silicate, sodium sulphite or magnesium sulphate; the objective is to prevent swelling of the fibres in the presence of moisture. Ghavami (1995) studied bamboo fibres impregnated with water-repellents and has shown that water absorption was reduced to 4%. Pimentel *et al*. (2006) have used organic compounds like vegetable oils to reduce the embrittlement process, but with partial success. Toledo *et al*. (2003) recommend the immersion of the fibre in silica fume slurry before adding it to the mix. Pre-treatment of fibres (e.g. high temperature and compression) improve the fibre stiffness and consequently decrease the fibre moisture absorption (Agopyan *et al*., 2005). Pre-treatment of natural fibres is found to increase FRC performance. Pulping is one of the fibre treatments that improve fibre adhesion to the cement matrix and also resistance to alkaline attack (Savastano *et al*., 2003).

Some authors have shown that not only the durability of the fibre but also the fibre–matrix adhesion may be improved with fibre treatment (Ghavami, 1995; Coutts, 2005; Tonoli *et al*., 2009). This is the case for natural fibres. The bonding of synthetic fibres (nylon, polyester and polypropylene) within the concrete matrix is essentially mechanical, as there is no chemical bond. In this case, the modulus of elasticity and Poisson's ratio of each material will govern the bonding properties as will the fibre geometry.

The durability of the fibres is paramount on the development of ultra-high-performance fibre-reinforced concrete (UHPFRC). These new composites represent the future of FRC and are treated in Section 15.5.

Scanning electron microscopy (SEM) has been used to characterize the physical and chemical interaction of fibres in FRC, as well as to address the durability of fibres. Microstructural analysis provides information on the corrosion of fibres, deposits of Portlandite surrounding fibres and the interaction between fibres and matrix (Purnell *et al*., 2000). Other techniques may be used as alternative to SEM. Uygunoğlu (2008) has shown that polarizing microscopy is a suitable technique to assess the bond characteristics of steel fibres in SFRC, which is also related to durability of the composite.

15.3 Mechanical effect of fibres in concrete

The mechanism of fibre reinforcement of the cementitious matrix in concrete has been extensively studied in terms of the resistance of the fibres, pullout from the matrix and as a result from the breakdown of the fibre–matrix interfacial bond. Undoubtedly, the knowledge of the individual phases as well as the interface between fibre and matrix is paramount in understanding the mechanical behaviour of FRC. There are a huge number of studies on the mechanical effect of fibres in concrete. The following sections will only

cover some basic concepts of this subject. Good reviews may be found in Zollo (1997) and Brandt (1987, 2008).

15.3.1 Strength and stiffness

Fibres may improve the mechanical properties of concrete not as a replacement of the continuous reinforcement bars but in addition to them. The reinforcement bars are not designed to stop the development of microcracks, but the randomly distributed fibres can prevent the propagation or widening of microcracks, thus controlling the overall cracking. Attempts have been made to predict the first cracking strength of FRC either by applying linear elastic fracture mechanics or by employing the mixture rules for composite materials. In both cases, the ultimate strength of these materials appeared to depend on the properties of the fibres – mainly the content, aspect ratio and bond characteristics (Majumdar, 1975).

Romualdi and Batson (1963) have shown that the tensile strength of FRC at the proportional limit is higher than that of the unreinforced matrix. Closely spaced fibres act as crack arrestors and reduce the stress intensity. In other words, the strength is related to the spacing between the fibres, as shown in Fig. 15.2. The average fibre spacing is calculated from Eq. [15.1]:

$$s = 13.8d\sqrt{\frac{1}{p}} \qquad [15.1]$$

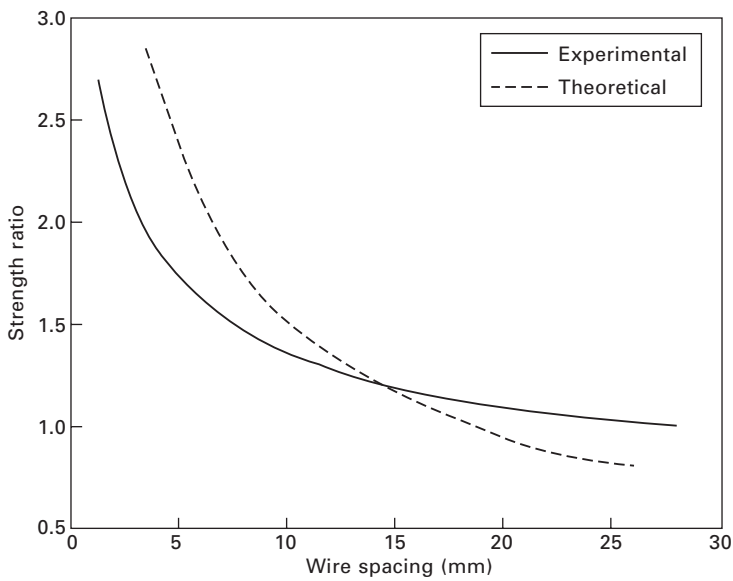

15.2 Theoretical and experimental strength ratio as a function of fibre spacing (adapted from Romualdi and Batson, 1963).

where s is the spacing between centroids of fibres, d is the fibre diameter and p is the volume percentage of the reinforcement. The matrix and the fibre behave elastically up to the proportional limit. The Young's modulus of the reinforced composite is represented by Eq. [15.2], where E is the Young's modulus, V is the volume fraction and c, f and m represent the composite, fibre and matrix phase respectively. Furthermore, the ultimate strength of reinforced composites (S_c) may be estimated, based on experimental results for steel fibre and as a function of the strength of the matrix, S_m, the volume fraction of the fibre, V_f, and the aspect ratio of the fibre, l/d. The other terms of Eq. [15.3], A and B, are constants whose values can be determined from graphs in which composite strengths are plotted against $V_f.l/d$. The relationship of Eq. [15.3] is claimed to be applicable for both flexural and indirect tensile strengths of FRC containing fibres with aspect ratios of up to 150 (Majumdar, 1975).

$$E_C = E_f V_f + E_m V_m \quad [15.2]$$

$$S_C = AS_m(1 - V_f) + BA_f\frac{l}{d} \quad [15.3]$$

The length of the fibres also affects the crack bridging and consequently the mechanical properties of the composites. Fine fibres control opening and propagation of microcracks, given that they are densely dispersed in cement matrix. Longer fibres (50-80 mm) tend to control larger cracks and contribute to increase the final strength of fibre-reinforced concrete, as shown in Fig. 15.3 (Betterman *et al.*, 1995).

FRC may be classified in conventional fibre-reinforced concrete (FRC) and high-performance fibre-reinforced concrete (HPFRC). They are composites that present a distinct stress–strain response in tension (Fig. 15.4). The

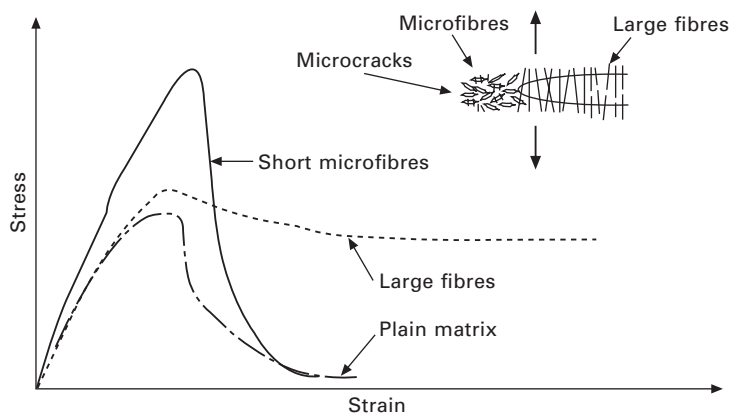

15.3 Structures of long and short fibres controlling crack propagation (adapted from Betterman *et al.,* 1995).

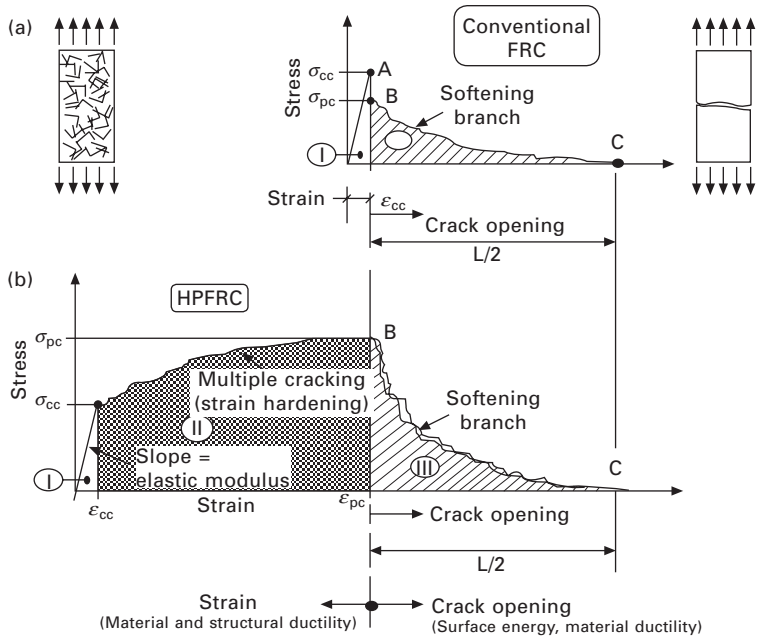

15.4 Comparison of typical stress–strain response in tension of (a) conventional FRC with (b) HPFRC (adapted from Naaman, 2003).

conventional FRC element is characterized by initial linear increase of stress; after the first crack opening there is a slow decrease of tension, usually called the softening branch. In contrast, where the reinforcement is sufficient (HPFRC), there is a strain hardening stage after the first crack, accompanied by multiple cracking and a considerable amount of absorbed energy, which is proportional to the area under the curve. The softening branch follows that stage.

Steel fibre may significantly improve tensile strength, with increases of the order of 30–40% for the addition of 1.5 vol% of fibres in mortar or concrete; therefore steel fibre-reinforced concrete can be categorized based on its tensile behaviour after first cracking (Parra-Montesinos, 2005). When strain-hardening behaviour is observed, the mixture is categorized as steel fibre-high strength concrete (SFHSC). When strain-softening behaviour is observed, the mixture is categorized simply as steel fibre concrete (SFC).

Natural fibres have a high tensile strength as well as low modulus of elasticity. However, one of the disadvantages of using natural fibres is that they have a high variation on their properties, usually leading to unpredictable concrete properties (Li *et al.*, 2006).

In general, compressive strength is not significantly affected by the addition of fibres, while tensile and flexural strength and toughness are all substantially

increased. Ultimate compressive strength is only slightly affected by the presence of fibres, with observed increases ranging from 0 to 15% for up to 1.5 vol% of fibres (ACI report, 2002). Some authors, however, have found that the effect of addition of steel fibres on compressive strength ranges from negligible to marginal and sometimes up to 25% (Chunxiang and Patnaikuni, 1999; Khaloo and Kim, 1996). However, Silva and Rodrigues (2007) studied the addition of sisal fibres to concrete and reported that compressive strength was lower than in concrete samples without the fibres.

Increases in the flexural strength of FRC are substantially greater than in tension or compression because the ductile behaviour of the FRC on the tension side of a beam alters the normally elastic distribution of stress and strain over the member depth. Khaloo and Kim (1996) showed that the flexural strength of FRC is about 50–70% higher than for unreinforced concrete, based on a third-point bending test. According to the ACI report (2002), higher fibre volume fractions, or centre-point loading, or small specimens and long fibres with significant fibre alignment in the longitudinal direction will produce greater percentage increases up to 150%. Figure 15.5 shows the flexural strength (or modulus of rupture) for SFHSC at various fibre volume fractions.

It has been shown that the addition of fibres increases both the fatigue life and fatigue loading of FRC beams, as well as decreases the crack width under fatigue loading. For a non-reversible type of loading, fatigue strengths of the order of 90% of the first crack strength have been obtained after 2×10^6 cycles with fibre concrete containing 2–3 vol% of steel wire. At 10×10^6 cycles, the fatigue strength is approximately 50% of the first crack strength. For a reversal type of loading, slightly poorer results have been reported by Majumdar (1975).

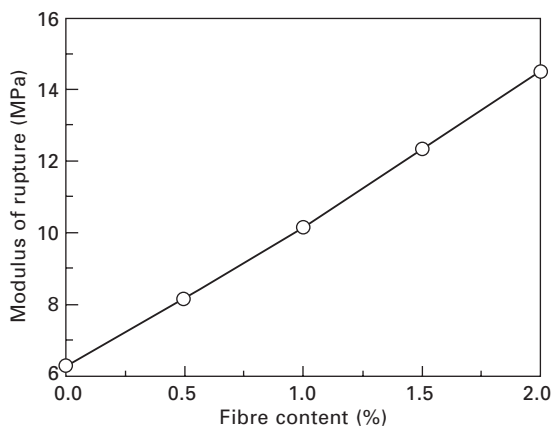

15.5 Effect of fibre volume on flexural strength or modulus of rupture for SFHSC (adapted from Khaloo and Kim, 1996).

The flexural fatigue strengths and endurance limits have been reported for polypropylene FRC with various fibre contents. Specifically, the addition of polypropylene fibres, even in small amounts, has increased the flexural fatigue strength. Using the same basic mixture proportions, the flexural fatigue strength was determined for three fibre contents (0.1, 0.2, and 0.3 vol%) and it was shown that the endurance limit for two million cycles had increased by 15–18% (Ramakrishnan *et al.*, 1989).

Even though polymer additions to alkali-resistant GFRC have been shown to reduce the rate at which GFRC composites lose strength and ductility, commercially available GFRC composites will experience reduction in tensile and flexural strengths and ductility with age if exposed to an outdoor environment. The strength of fully-aged GFRC composites will decrease to about 40% of the initial strength prior to aging. However, strain capacity (ductility or toughness) will decrease to about 20% of the initial strain capacity prior to aging. This loss in strain capacity is often referred to as composite embrittlement. Two basic theories have been suggested to explain loss in strength and strain capacity in GFRC composites. One theory is that alkali attack on the glass fibre surfaces results in the reduction of the fibre tensile strength and, subsequently, reduction of composite strength (Proctor *et al.*, 1982). The second and most accepted theory suggests that ongoing cement hydration in water-stored or naturally weathered GFRC results in hydration products penetrating the fibre bundles, filling the interstitial spaces between glass filaments, thereby increasing the bond to individual glass filaments. This phenomenon can lead to lack of fibre pull-out and results in a loss in tensile strength and ductility (Stucke and Majumdar, 1976; Bentur *et al.*, 1985).

15.3.2 Toughness and impact resistance

Since the early development of FRC, toughness was recognized as the outstanding characteristic of this material. Fibres in most cases will not improve the mechanical strength, but rather improve the toughness, or energy absorption capacity. Toughness is related to the growth of cracks; therefore when fibres are present the cracks cannot extend easily without stretching or de-bonding the fibres (Fig. 15.6). Additionally, FRC requires large amounts of energy in fibre pull-out processes. As a result, considerable energy has to be expended before complete fracture of the material. According to Majumdar (1975), the fibre volume governs the toughness of FRC, which is at least an order of magnitude greater than that of their unreinforced counterparts (Fig. 15.7). However, other parameters, such as orientation of the fibres, their aspect ratio and the stress/strain relationship, control the ultimate strength of the composite, consequently influencing toughness. In general, fibres with large diameters tend to be inefficient in enhancing toughness of FRC. Given that

15.6 Fracture surface of steel fibre-reinforced concrete (ACI report, 2002).

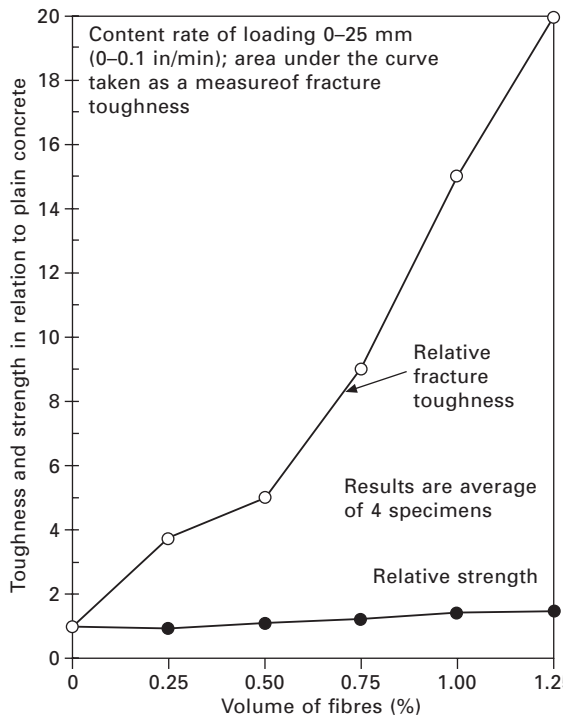

15.7 The effect of volume of steel fibres on toughness in flexure (adapted from Majumdar, 1975).

low-diameter fibres are expensive to produce, Banthia and Sappakittipakorn (2007) propose hybridization of fibres (mixture of fibres of high diameters with others of low diameter) as a means of improving the toughness of FRC. The mechanisms of toughening in fibre-reinforced cement composites are thoroughly discussed by Li and Maalej (1996).

Steel fibres improve the ductility of concrete under all modes of loading, but their effectiveness in improving strength varies among compression, tension, shear, torsion, and flexure (Shah and Winter, 1966; Edgington *et al*., 1974; Holschemacher *et al*., 2010; Shah and Ribakov, 2011). According to Banthia *et al*. (1987b), steel fibres increased the fracture energies by a factor of about 5 for normal strength concrete and by a factor of about 4 when compared to high-strength concrete. SFRC has approximately 2.5–3.5 times fracture energy under impact than concretes without fibre reinforcement. However, the improvement observed in the peak load and the fracture energy under impact in some cases was considerably smaller than that obtained in static loading, which may be explained by the fracture of fibres under impact loading.

Ali *et al*. (1972) studied the effects of carbon fibre orientation and distribution in carbon fibre-reinforced concrete (CFRC). Instrumented impact test results using low-modulus carbon fibres demonstrated substantial increases in impact strength and fracture energy in proportion to the volume fraction of fibres used. Also, the impact strength increases as fibre content is increased. Improvement in fracture energy for polypropylene FRC was reported between 33 and 1000% (Mindess and Vondran, 1988; Banthia *et al*., 1987a).

Ohama *et al*. (1985) studied the effect of fibre content on the impact resistance of CFRC containing silica fume (Fig. 15.8). Results have shown that the impact resistance of CFRC is markedly improved with a rise in the fibre content, irrespective of the fibre length. In his experiments, a steel ball was used to evaluate the impact resistance of conventional and CFRC. Non-reinforced concrete fractured at one blow of the steel ball, whereas CFRC with a fibre content of 5–10% withstood 3,000 blows or more.

Synthetic polymeric fibres (e.g. nylon and polypropylene) improve the impact strength of brittle cementitious materials even at small amounts; they tend to behave similarly to horse hair or sisal in gypsum plaster and straw in sun-dried bricks – applications known to mankind for centuries. When added to cement and concrete, nylon fibres have given as much as 26-fold and polypropylene 32-fold increases in the impact strength. The polymer fibres are chemically inert and therefore suitable for the highly alkaline environment of Portland cement pastes. However, they suffer from the disadvantages of a low elastic modulus and a poor bonding surface (Majumdar, 1975). Sridhara *et al*. (1971) employed 0.5 wt% of nylon in FRC and found that the impact strength increased for times, compared to plain concrete. In addition, at a

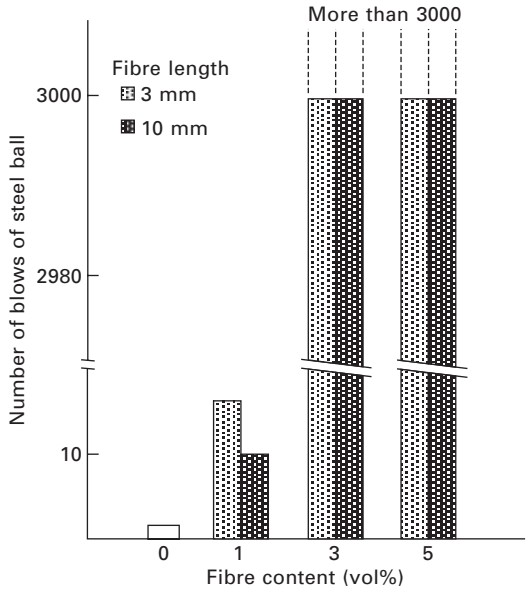

15.8 Carbon fibre content vs. impact resistance of CFRC using silica fume (adapted from Ohama, 1989).

fibre content of 1wt%, the impact strength was 17 times greater than for non-reinforced concrete (Fig. 15.9).

Al-Oraimi and Seibi (1995) reported that using a low percentage of natural fibres improved the mechanical properties and the impact resistance of concrete and had similar performance when compared to synthetic FRC. Ramakrishna and Sundararajan (2005) also presented results of impact resistance using natural fibres: fibre inclusion increased impact resistance 3–18 times when compared to non-reinforced concrete.

15.4 Types of fibre used in fibre-reinforced concrete (FRC)

This section will present some well-established applications of fibre-reinforced mortars and concretes, as well as the developments in recent years and future trends.

15.4.1 Steel fibres

Steel fibres continue to have a wide range of applications in civil engineering materials. There are some structural applications where they have been used in concrete without any conventional reinforcing bars. These have been short span, elevated slabs, for example a parking garage at Heathrow Airport

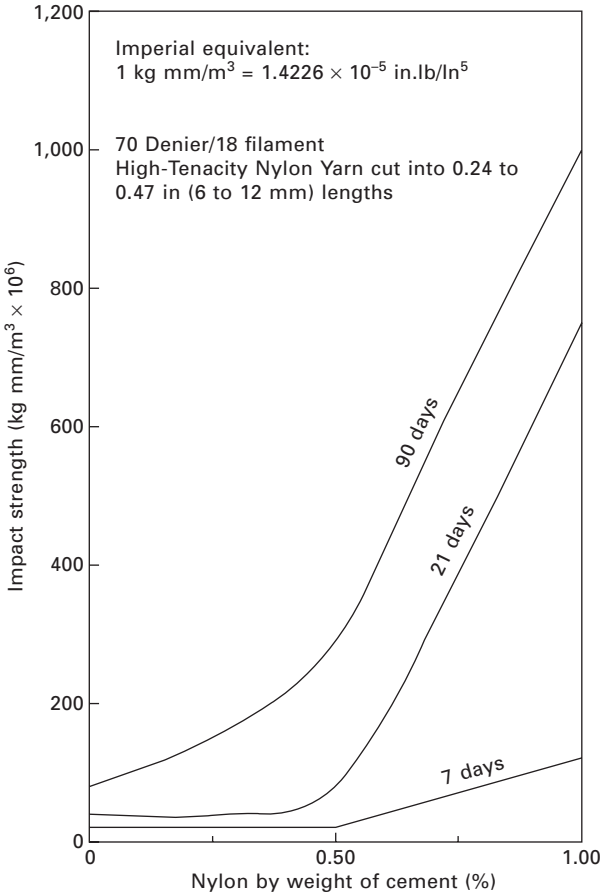

15.9 Nylon content versus impact strength at different ages (adapted from Sridhara *et al.,* 1971).

(London, UK) with slabs 3 ft 6 in. (1.07 m) square by 4 in. (10 cm) thick, supported on four sides. In cases like that, load tests should be performed and the fabrication of the elements should employ rigid quality control (ACI report, 2002). Steel fibre concrete (SFC) has also been employed as slabs, bridge decks, airport pavements, parking areas, and cavitation/erosion environments, as well as worldwide for the production of highway slabs. Steel fibre high-strength concrete (SFHSC) is an option for the design of critical regions in earthquake-resistant structures exposed to impact and fatigue (Brandt, 2008). It was reported that ductility and adequate structural seismic response could be achieved without additional seismic reinforcement detailing. Work is required, however, so that building officials accept FRC as a structural material (Shah and Ribakov, 2011).

Steel fibre-reinforced refractories have shown excellent performance in

a number of refractory application areas including ferrous and nonferrous metal production and processing, petroleum refining applications, and rotary kilns used for producing Portland cement and lime, among numerous other applications (ACI report, 2002)).

Shah and Ribakov (2011) recently presented a good review of steel fibre-reinforced concrete. Some future trends in the development of FRC involve (1) changing the fibre amount during the casting process, so that fibres are employed only in some parts of the structure where they are required; (2) using modern non-destructive techniques to monitor the casting and to obtain a feedback for online prediction of hardened properties; and (3) controlling the corrosion of fibres with age, by altering their chemical composition.

15.4.2 Synthetic fibres

The current high cost of carbon fibres somewhat limits their application. Nevertheless, carbon fibre-reinforced concrete has been used in corrugated units for floor construction, single and double curvature membrane structures, boat hulls, and scaffold boards. The overall cost may be reduced if other fibres are used in combination with carbon fibre.

Polypropylene and nylon FRC have been applied to non-structural and non-primary load-bearing applications. They are commonly employed in residential, commercial, and industrial products, such as slabs for composite metal deck construction, floor overlays, shotcrete for slope stabilization and pool construction, precast units, slip form curbs, and mortar applications involving sprayed and plastered Portland cement stucco (Krenchel and Shah, 1985; Zollo and Hays, 1991).

Glass fibre-reinforced concrete (GFRC) has found the largest application in the manufacture of external claddings, façade plates and other elements where their strengthening effects are required particularly during construction. GFRC is also present in other applications, such as electrical utility products, e.g. trench systems and distribution boxes, as well as in surface bonding and floating dock applications (Brandt, 2008).

15.4.3 Natural fibres

The employment of natural fibres, such as cellulose pulp, sisal, bamboo, hemp, flax, jute, ramie fibres, etc., is restricted to countries where these fibres are easily available. They are important constituents of structural elements used for construction of inexpensive buildings in developing regions of the world (Coutts, 2005). In Africa, sisal fibre-reinforced concrete has been used extensively for making roof tiles, corrugated sheets, pipes, silos, and gas and water tanks. Subrahmanyam (1984) cited the application of elephant grass

fibre-reinforced mortar and cement sheets in Zambia for low-cost house construction. In addition, wood and sisal fibres are constituents of cement composite panel lining, eaves, soffits, and insulation construction materials. Silva *et al*. (2010a, 2010b, 2011) have recently studied the physical and mechanical properties of long sisal-reinforced cement composites, as well as the influence of fibre shape and morphology on the cracking behaviour. Kraft pulp fibre-reinforced cement has found major commercial applications in the manufacture of flat and corrugated sheet, non-pressure pipes, cable pit, and outdoor fibre-reinforced cement paste or mortar products for gardening (Tait and Akers, 1989). These products appear to be considerably durable, given that nearly 10 years have passed since the beginning of commercial use.

Cellulose fibres have been commercially used in asbestos-free fibre cement for many years. Most of the current research still deals with durability aspects of cellulose fibres and other alternative fibres. Improved durability of natural fibre composites has been achieved with the employment of mineral admixtures, such as rice husk ash or metakaolin in order to reduce the alkalinity of the cement paste [Rodrigues *et al*., 2006, 2010).

15.4.4 Hybrid high-performance fibre-reinforced concrete

The blending of different types of fibre, usually referred to as hybrid systems, presents some advantages for FRC (Qian and Stroeven, 2000): (1) providing a system in which a strong and stiff type of fibre improves the first crack stress and ultimate strength, whereas a more flexible and ductile fibre improves the toughness; (2) providing a system in which a small fibre controls microcracking and a large fibre reduces the propagation of macrocracks; and (3) improving durability of FRC, by partial replacement of a less durable fibre with a durable one. Hybrid systems are not a new subject; they have been used since the 1990s. Nevertheless, much research still considers the blending of different types of fibres to enhance the properties of FRC.

Banthia and Nandakumar (2003) have employed secondary polypropylene micro-fibres to enhance the deformation of steel fibre-reinforced concrete. More recently, Dawood and Ramli (2012) proposed the combination of steel fibres with synthetic and palm fibres as a means of reducing the corrosion problems of fibres and improving the flowing and mechanical properties of concrete. Lee *et al*. (2012) have shown that the blending of nylon and polypropylene fibres improves the spalling protection of FRC subjected to fire. Azhari and Banthia (2012) have blended carbon fibres and nanotubes in the development of smart structure materials, such as strain sensors.

15.5 Ultra-high-performance fibre-reinforced concrete (UHPFRC) and other new developments

Ultra-high-performance fibre-reinforced concrete is a recently developed low-porosity ceramic material with excellent mechanical performance, such as 28-day compressive and flexural strength around 150 MPa and 40 MPa, respectively, and modulus of elasticity of about 90 GPa. It is essentially a low water to-cement (~0.24) superplasticized silica fume concrete, reinforced with fibres. UHPFC has improved homogeneity, given that the traditional aggregates are replaced with very fine aggregates (Corinaldesi and Moricani, 2012). These new materials find applications in various areas; some examples are (1) reliable containers for chemical and hazardous liquids and solids; (2) high impact-resistant products and high abrasion-resistant dies in the molding processing of metals; and (3) extremely high-performance structureal elements in buildings.

Some recent studies are related not only to the mechanical performance of UHPFRC (Habel and Gauvreau, 2008) but also to the production of UHPFRC with blended fibres (Kim *et al*., 2011; Park *et al*., 2012), i.e. hybrid systems. Lee *et al*. (2012) presented interesting results from a hybrid system containing polypropylene, nylon and steel fibres to produce full-scale columns with compressive strength of approximately 200 MPa and effective spalling protection when subjected to severe fire. Much work has been carried out at Cardiff University (UK) in the last decade on the development of CARDIFRC, an ultra-high-performance fibre-reinforced cement-based composite (Benson and Karihaloo, 2005a, 2005b; Benson *et al*., 2005; Nicolaides *et al*., 2010). Mechtcherine (2012) presents a good review of UHPFRC, where both mechanical properties and durability issues are taken into consideration.

15.5.1 Other emerging applications

Hybrid systems will continue to be the subject of future research on the development of ultra-high-performance fibre-reinforced concrete for many applications. However, two other research topics on FRC have emerged in recent years: (1) utilization of waste fibres as reinforcement, and (2) development of fibre-reinforced alkali-activated binders (also known as geopolymers).

The employment of waste fibres aims to contribute to the development of sustainable concretes. Indeed, the production of manufactured fibres (mainly synthetic ones) is responsible for an environmental impact that, at some extent, could be reduced if waste materials were used instead. The future of waste fibres as reinforcement for FRC is subjected to the maintenance of suitable properties and durability of those fibres under the high-alkaline environment of

cement paste. Nevertheless, the waste materials also require some preparation to be employed as reinforcement (washing, drying, grinding, etc.); therefore, the environmental impact caused by the preparation procedures of waste fibres need to be taken into consideration when assessing the pro and cons of employing those wastes. Some recent publications on waste fibres for FRC have studied the following materials: recycled plastic bottles, rubber tyres, alloy cans (Sholihin *et al.*, 2011); pulp paper waste (Hosseinpourpia *et al.*, 2012); glass fibre-reinforced polymer (GFRP) waste (Asokan *et al.*, 2009; Correia *et al.*, 2011); recycled polyethylene terephthalate (PET) (Won *et al.*, 2010) and by-products of the production of metallic and polypropylene fibre (Meddah and Bencheikh, 2009).

Alkali-activated binders (AAB) or geopolymers are new materials with potential to replace Portland cement for some applications. These materials are based on the alkaline activation of aluminosilicates, such as pulverized fly ash, blastfurnace slag and metakaolin. Most of the research so far has confirmed that AAB are materials with great advantages over Portland cement. First of all the aluminosilicates may be wastes or natural materials processed at temperatures much lower than that to which limestone and clay need to be submitted to the production of Portland cement clinker, i.e. 1400–1500°C. So, the production of AAB may be eco-friendlier than Portland cement concrete. Also, in theory 100% waste materials may be alkali- activated, as long as they are silica- and alumina-based. Other advantages of geopolymers are high early strength (usually achieved at one day of curing) as well as the high chemical durability. Despite presenting advantages over Portland cement-based materials, AAB are brittle materials like the former. Whilst much research in AAB is still related to the chemistry and reactions during the activation processes, others have focused on the application of these new materials. In this respect, recent publications have shown interesting results on the development of fibre-reinforced geopolymer concrete. Silva and Thaumaturgo (2002) and Dias and Thaumaturgo (2005) have shown that geopolymers reinforced with wollastonite microfibres and reinforced with basalt fibres, respectively, presented better fracture properties than conventional Portland cement concrete. Other studies presented results of geopolymers reinforced with carbon fibres (Lin *et al.*, 2008, 2009, 2010) as well as with carbon and glass fibres (Pernica *et al.*, 2010).

15.6 Case studies

This section will briefly present some recent case studies of high-performance fibre-reinforced concrete. The main idea is to highlight the application of different types of fibre into concrete structures or elements.

Steel fibre high-performance concrete has been recently employed in the new runway (D-Runway) and connecting taxiway of the Tokyo International

Airport (Haneda Airport). The runway was completed in 2010; its pier area incorporated super-high-strength steel fibre high-performance concrete slabs. The concrete employed, designed with 180 MPa and also known as SUQCEM – abbreviation for super high-quality cementitious material – was composed of cement, superplasticizers, aggregates and a combination of two different length steel fibres, which provided high strength and ductility. The slabs also contained prestressing steel strands (SEI, 2010).

Renault's new automotive plant in Tangier, Morocco (annual capacity of 170,000 vehicles with possible increase to 400,000) also employed steel-fibre concrete for jointless floor slabs. 165,000 m^2 of SFRC was the technical solution to (1) comply with the fast-track construction programme demanded by Renault, as reinforcement was added directly in the concrete; and (2) eliminate the need for sawcut contraction joints and dramatically reduced year-to-year maintenance costs. Class C25/30 and C30/37 concretes were used with 35–40 kg/m^3 dosages of steel fibres (Lazzari, 2012).

Glass fibre-reinforced concrete panels gave an impressive effect on the façade of the Soccer City Stadium, host of the South Africa 2010 FIFA World Cup. The biggest challenge for architects was to design unusual curved panels and a chequerboard of colours and textures that echo the appearance of a calabash gourd. The architects addressed all of those issues by covering the stadium with concrete panels reinforced with alkali-resistant (AR) glass fibres, which created the necessary sculpted forms without compromising strength and resilience. The AR glass-reinforced panels are 1.2×1.8 metres with a thickness of only 13 mm. In total, more than 2,100 moudules, each having 16 panels, were prefabricated in a field factory. The panels are solid, moldable and durable like concrete, but also thin-walled, fire resistant and much lighter, thanks to the glass fibres. Glass fibres allow the construction of very slim elements with good tensile strength. Glass-reinforced concrete (GRC) panels reduce the weight and thickness of the concrete by up to 10 times compared to conventional steel-reinforced concrete panels. This allows the building or renovation of façades with the excellent reproduction of complex details and fine texture (Owens Corning, 2010).

Carbon fibre has been used in hundreds of projects in the USA, mainly as reinforcement of concrete precast panels for façades. Recent examples are the Symphony House, a 32-storey, $145-million condominium in Philadelphia; and wall insulation panels on dorms at Georgia State University. The benefits of carbon fibre-reinforced concrete depend on the application but, in most cases, they represent improvements over conventional steel reinforcing while maintaining the generally accepted benefits of precast concrete. Probably the main advantage is the fact that the wall panels reinforced with carbon fibre weigh much less than conventional six-inch-thick precast (40% less weight in the façade of the Symphony House in Philadelphia). In fact, as carbon fibre will not oxidize, it causes no rusting, staining or spalling as

can occur with steel reinforcing. Consequently, precasters can reduce the amount of concrete cover – three inches or more in the case of some wall panels – required to protect the reinforcing. The use of carbon fibre grid also enables significant improved thermal performance. As carbon fibre has low thermally conductivity, it reduces the transfer of heat or cold from outside to inside and vice versa. For the dorms at Georgia State Univeristy, it is estimated that the carbon fibre insulating panels gave $700,000 savings on heating, ventilation and air-conditioning (Pitly, 2009).

15.7 Conclusion

At present, FRC is specified especially when repair and increased durability is required for many non-conventional structures or concrete subjected to special conditions. The main role of fibres is to control cracking due to plastic shrinkage and drying shrinkage, providing additional energy absorption capability. It has also been reported that fibres may improve the static flexural strength of concrete as well as its impact strength, tensile strength, ductility and flexural toughness. Many modern reinforced concrete structures contain a wide range of reinforcing materials, made of either steel, polymers or alternative composite materials; they may or may not be combined with traditional steel reinforcement. The final composite will have a particular failure mechanism, which depends on the combination of the employed materials. Needless to say, these new design techniques are required to ensure the long-term durability of these special concretes. The successful experimental and theoretical methods will certainly be used in future concrete R&D activities.

15.8 Acknowledgements

The authors would like to thank all editors who have permitted the reproduction of the figures included in this chapter.

15.9 References and further reading

ACI Report, 1978. Measurement of Properties of Fibre Reinforced Concrete. *ACI Journal*, Title no. 544.2R 78.

ACI Report, 2002. State-of-the-Art Report on Fibre Reinforced Concrete. *ACI Journal*, Title no. 544.1–96.

ACI Report, 2009. Measurement of Properties of Fibre Reinforced Concrete. *ACI Journal*, Title no. 544.2R 89.

Agopyan, V., Savastano, H., John, V., Cincotto, M., 2005. Developments on vegetable fibre–cement based materials in São Paulo, Brazil: an overview. *Cement & Concrete Composites*, 27(5), pp. 527–536.

Akcay, B., Tasdemir, M.A., 2012. Mechanical behaviour and fibre dispersion of hybrid

steel fibre reinforced self-compacting concrete. *Construction and Building Materials*, 28(1), pp. 287–293.

Akihama S., Suenaga, T., Nakagawa, H., 1988. *Concrete International*, 10, 40.

Al-Oraimi S., Seibi A., 1995. Mechanical characterization and impact behavior of concrete reinforced with natural fibres. *Composite Structures*, 32, pp. 165–171.

Ali, M.A., Majumdar, A.J., Rayment, D.L., 1972. Carbon-fibre reinforcement of cement. *Cement & Concrete Research*, 2, pp. 201–212.

Aly, T., Sanjayan, J.G., Collins F., 2008. Effect of polypropylene fibres on shrinkage and cracking of concretes. *Materials and Structures*, 41(4), pp. 1741–1753.

Asokan, P., Osmani, M., Price, A.D.F., 2009. Assessing the recycling potential of glass fibre reinforced plastic waste in concrete and cement composites. *Journal of Cleaner Production*, 17, pp. 821–829.

ASTM A820/A820M. 2006. Standard Specification for Steel Fibres for Fibre Reinforced Concrete. American Society for Testing and Materials, Annual Book of ASTM Standards.

ASTM C 1018. 2002. Standard Test Method for Flexural Toughness and First-Crack Strength of Fibre Reinforced Concrete. American Society for Testing and Materials, Annual Book of ASTM Standards.

Azhari, F., Banthia, N., 2012. Cement-based sensors with carbon fibres and carbon nanotubes for piezoresistive sensing. *Cement & Concrete Composites*, doi: 10.1016/j.cemconcomp.2012.04.007

Balaguru, P.N., Shah, S.P., 1992. *Fibre-reinforced Cement Composites*. New York: McGraw-Hill.

Banthia, N., Nandakumar, N., 2003. Crack growth resistance of hybrid fibre reinforced cement composites. *Cement & Concrete Composites*, 25(1), pp. 3–9.

Banthia, N., Sappakittipakorn, M., 2007. Toughness enhancement in steel fibre reinforced concrete through fibre hybridization. *Cement and Concrete Research*. 37 (9), pp. 1366–1372.

Banthia, N., Mindess, S., Bentur, A., 1987a. Impact behavior of concrete beams. *Materials and Structures*, 20(119), pp. 293–302.

Banthia, N., Mindess, S., Bentur, A., 1987b. Steel fibre reinforced concrete under impact. *Proceedings of International Symposium on Fibre Reinforced Concrete (ISFRC-87)*, Madras, India.

Barr, B., 1987. The fracture characteristics of FRC materials in shear. *Fibre Reinforced Concrete Properties and Applications*, SP-105, pp. 27–53.

Benson, S.D.P., Karihaloo, B.L., 2005a. CARDIFRC1 – Development and mechanical properties. Part I: Development and workability. *Magazine of Concrete Research*, 57(6), pp. 347–352.

Benson, S.D.P., Karihaloo, B.L., 2005b. CARDIFRC1 – Development and mechanical properties. Part III: Uniaxial tensile response and other mechanical properties. *Magazine of Concrete Research*, 57(8), pp. 433–443.

Benson, S.D.P., Nicolaides, D., Karihaloo, B.L., 2005. CARDIFRC1 – Development and mechanical properties. Part II: Fibre distribution. *Magazine of Concrete Research*, 57(7), pp. 421–432.

Bentur, A., Mitchell, D., 2008. Material performance lessons. *Cement Concrete Research*, 38, pp. 259–272.

Bentur, A., Ben-Bassat, M., Schneider, D., 1985. Durability of glass fibre reinforced cements with different alkali resistant glass fibres. *Journal of American Ceramic Society*, 68(4), pp. 203–208.

Bentz, D.P., Jensen, O.M., 2004. Mitigation strategies for autogenous shrinkage cracking. *Cement & Concrete Composites*, 26(6), pp. 677–685.

Betterman, L.R., Ouyang, C., Shah, S.P., 1995. Fibre–mortar interaction in microfibre-reinforced mortar. *Advanced Cement Based Materials*, 2(2), pp. 53–61.

Brandt, A.M., 1987. Present trends in the mechanics of cement based fibre reinforced composites. *Construction & Building Materials*, 1(1), pp. 28–39.

Brandt, A.M., 2008. Fibre reinforced cement-based (Fibre Reinforced Concrete) composites after over 40 years of development in building and civil engineering. *Composite Structures*, 86, pp. 3–9.

Brown, R., Shukla, A., Natarajan, K.R., 2002. Report: Fibre Reinforcement of Concrete Structures, University of Rhode Island.

Canbolat, B.A., Parra–Montesinos, G.J., Wight, J.K., 2005. Experimental study on the seismic behavior of high performance fibre reinforced cement composite coupling beams. *ACI Structural Journal*, 102(1), pp. 159–166.

Choi, O.C., Lee, C., 2003. Flexural performance of ring-type steel fibre-reinforced concrete. *Cement Concrete Research*, 33(6), pp. 841–849.

Chunxiang, Q., Patnaikuni, I., 1999. Properties of high strength steel fibre reinforced concrete beams in bending. *Cement and Concrete Composites*, 21(1), pp. 173–181.

Corinaldesi, V., Moriconi, G., 2012. Mechanical and thermal evaluation of ultra high performance fibre reinforced concretes for engineering applications. *Construction and Building Materials*, 26(1), pp. 289–294.

Correia J.R., Almeida, N.M., Figueira, J.R., 2011. Recycling of FRP composites: reusing fine GFRP waste in concrete mixtures. *Journal of Cleaner Production*, 19, pp. 1745–1753.

Coutts, R.S.P., 2005. A review of Australian research into natural fibre cement composites. *Cement & Concrete Composites*, 27, pp. 518–526.

Coutts, R.S.P., Michell, A.S., 1983. Wood pulp fibre cement composites. *Journal of Applied Polymer Science*, Applied Polymer Symposium 37, John Wiley & Sons, pp. 829–844.

D'Almeida, A., Melo Filho, J., Toledo Filho, R., 2009. Use of curaua fibres as reinforcement in cement composites. *Chemical Engineering Transactions*, 17, pp. 1717–1722.

Dawood, E.T., Ramli, M., 2012. Mechanical properties of high strength flowing concrete with hybrid fibres. *Construction and Building Materials*, 28(1), pp. 193–200.

Dias, D.P., Thaumaturgo, C., 2005. Fracture toughness of geopolymeric concretes reinforced with basalt fibres. *Cement & Concrete Composites*, 27(1), pp. 49–54.

Edgington, J., Hannant, D.J., Williams, R.I.T., 1974. *Steel Fibre Reinforced Concrete*. Building Research Establishment. CP69, pp. 17.

El-Dieb, A.S., Taha, R.M.M., 2012. Flow characteristics and acceptance criteria of fibre-reinforced self-compacted concrete (FR-SCC). *Construction and Building Materials*, 27(1), pp. 585–596.

Erdem, S., Dawson, A.R., Thom, N.H., 2011. Microstructure-linked strength properties and impact response of conventional and recycled concrete reinforced with steel and synthetic macro fibres. *Construction and Building Materials*, 25 (10), pp. 4025–4036.

Filho, R., Ghavami, K., Sanjuán, M., England, G., 2005. Free, restrained and drying shrinkage of cement mortar composites reinforced with vegetable fibres. *Cement & Concrete Composites*, 27(5), pp. 537–546.

Firas, S.A., Gilles, F., Robert, L.R., 2011. Bond between carbon fibre-reinforced polymer (CFRP) bars and ultra high performance fibre reinforced concrete (UHPFRC): Experimental study. *Construction and Building Materials*, 25(2), pp. 479–485.

Ghavami, K., 1995. Ultimate load behaviour of bamboo-reinforced lightweight concrete beams. *Cement and Concrete Composites*, 17(4), pp. 281–288.

Ghavami, K., 2005. Bamboo as reinforcement in structure concrete elements. *Cement & Concrete Composites*, 27(6), pp. 637–649.

Gjorv, O.E., 1994. Steel corrosion in concrete structures exposed to Norwegian marine environment. *Concrete International*, 16(4), pp. 35–39.

Glasser, F., Marchand, J., Samson, E., 2008. Durability of concrete. Degradation phenomena involving detrimental chemical reactions. *Cement and Concrete Research*, 38(2), pp. 226–246.

Habel, K., Gauvreau, P., 2008. Response of ultra-high performance fibre reinforced concrete (UHPFRC) to impact and static loading. *Cement & Concrete Composites*, 30(10), pp. 938–946.

Hannant, D.J., 1978. *Fibre Cements and Fibre Concretes*, New York: John Wiley & Sons.

Holschemacher, K., Mueller, T., Ribakov, Y., 2010. Effect of steel fibres on mechanical properties of high strength concrete. *Materials & Design*, 31(5), pp. 2604–2615.

Hosseinpourpia, R., Varshoee, A., Soltani, M., Hosseini, P., Tabari H.Z., 2012. Production of waste bio-fibre cement-based composites reinforced with nano-SiO_2 particles as a substitute for asbestos cement composites. *Construction and Building Materials*, 31, pp. 105–111.

Hsu, L.S., Hsu, T., 1994. Stress–strain behavior of steel–fibre high-strength concrete under compression. *ACI Structural Journal*, 91(4), pp. 448–457.

John, V., Cincotto, M., Sjotrom, C., Agopyan, V., Oliveira, C., 2005. Durability of slag mortar reinforced with coconut fibre. *Cement & Concrete Composites*, 27(5), pp. 565–574.

Johnston, C.D., 1974. Steel fibre reinforced mortar and concrete – A review of mechanical properties. *Fibre Reinforced Concrete*, SP-44, pp. 127–142.

Johnston, C.D., 2001. Fibre reinforced cements and concretes. *Advances in Concrete Technology*, 3, pp. 111–134.

Kawashima, S., Shah, S.P., 2011. Early-age autogenous and drying shrinkage behavior of cellulose fibre-reinforced cementitious materials. *Cement & Concrete Composites*, 33(2), pp. 201–208.

Khaloo, A.R., Kim, N., 1996. Mechanical properties of normal to high strength steel fibre-reinforced concrete. *Cement, Concrete and Aggregates*, 18(2), pp. 92–97.

Khare, L., 2005. Performance evaluation of bamboo reinforced concrete beams. Master of Science in Civil Engineering, University of Texas.

Kim, D.J., Park, S.H., Ryu, G.S., Koh, K.T., 2011. Comparative flexural behavior of hybrid ultra high performance fibre reinforced concrete with different macro fibres. *Construction and Building Materials*, 25, pp. 4144–4155.

Kormeling, H.A., Reinhardt, H.W., Shah, S.P., 1980. Static and fatigue properties of concrete beams reinforced with continuous bars and with fibres. *ACI Journal*, 77(1), pp. 36–43.

Krenchel, H., Shah, S.P., 1985. Applications of polypropylene fibres in scandinavia. *Concrete International*, 7(3), pp. 32–34.

Kucharska, L., Brandt, A.M., 1997. Pitch-based carbon fibre reinforced cement composites: A review. *Architecture and Civil Engineering*, 43(2), pp. 165–187.

Lawler, J.S., Zampini, D., Shah, S.P., 2002. Permeability of cracked hybrid fibre-reinforced mortar under load. *ACI Materials Journal*, 4(99), pp. 379–385.

Lazzari, J., 2012. Driving forward steel-fibre concrete. *Concrete Engineering International*, January, pp. 49.

Lee, G., Han, D., Han, M.C., Han, C.G., Son, H.J., 2012. Combining polypropylene and nylon fibres to optimize fibre addition for spalling protection of high-strength concrete. *Construction and Building Materials*, 34, pp. 313–320.

Li, V.C., Maalej, M., 1996. Toughening in cement based composites. Part II: Fibre reinforced cementitious composites. *Cement & Concrete Composites*, 18(4), pp. 239–249.

Li, V.C., Wang, S., 2006. Microstructure variability and macroscopic composite properties of high performance fibre reinforced cementitious composites. *Probabilistic Engineering Mechanics*, 21(3), pp. 201–206.

Li, Z., Wang, X., Wang, L., 2006. Properties of hemp fibre reinforced concrete composites. *Composites Part A*, 37(3), pp. 497–505.

Lin, T., Jia, D., He, P., Wang, M., Liang, D., 2008. Effects of fibre length on mechanical properties and fracture behavior of short carbon fibre reinforced geopolymer matrix composites. *Materials Science and Engineering A*, 497(1–2), pp. 181–185.

Lin, T., Jia, D., Wang, M., He, P., Liang, D., 2009. Effects of fibre content on mechanical properties and fracture behaviour of short carbon fibre reinforced geopolymer matrix composites. *Bulletin of Materials Science*, 32(1), pp. 77–81.

Lin, T., Jia, D., Wang, M., He, P., Liang, D., 2010. *In situ* crack growth observation and fracture behavior of short carbon fibre reinforced geopolymer matrix composites. *Materials Science and Engineering A*, 527(9), pp. 2404–2407.

Majumdar, A.J., 1975. Fibre cement and concrete a review. *Composites*, 6(1), pp. 7–16.

Majumdar, A.J., Ryder, J.R., 1968. Glass fibre reinforcement of cement products. *Glass Technology*, 9(3), pp. 78–84.

Mechtcherine, V., 2012. Towards a durability framework for structural elements and structures made of or strengthened with high-performance fibre-reinforced composites. *Construction and Building Materials*, 31, pp. 94–104.

Meddah, M.S., Bencheikh, M. 2009. Properties of concrete reinforced with different kinds of industrial waste fibre materials. *Construction and Building Materials*, 23, pp. 3196–3205.

Mindess, S., Vondran, G., 1988. Properties of concrete reinforced with fibrillated polypropylene fibres under impact loading. *Cement and Concrete Research*, 18(1), pp. 109–115.

Mindess, S., Young, J.F., Darwin, D., 2003. *Concrete*. Upper Saddle River, NJ: Prentice Hall, Pearson Education.

Mohr, B., Biernacki, J., Kurtis, K., 2007. Supplementary cementitious materials for mitigating degradation of kraft pulp fibre cement-composites. *Cement & Concrete Research*, 37(11), pp. 1531–1543.

Naaman, A.E., 2003. Strain hardening and deflection hardening fibre reinforced cement composites. In: *Proceedings of the International RILEM Workshop – High Performance Fibre Reinforced Cement Composites – HPFRCC4*, Ann Arbor, MI, pp. 95–113.

Nawy, E.G., 2001. *Fundamentals of High-performance Concrete*, 2nd edn. New York: John Wiley & Sons.

Nicolaides, D., Kanellopoulos, A., Karihaloo, B.L., 2010. Fatigue life and self-induced volumetric changes of CARDIFRC. *Magazine of Concrete Research*, 62(9), pp. 679–683.

Ohama, Y., 1989. Carbon-cement composites. *Carbon*, 27(5), pp. 729–737.

Ohama, Y., Amano, M., Endo, M., 1985. Properties of carbon fibre reinforced cement with silica fume. *Concrete International*, 7(3), pp. 58–62.

Owens Corning, 2010. Façade Reinforced with Cem-FIL AR Glass is Enduring Image of 2010 FIFA World Cup, Publication No. 10013096.

Pacheco-Torgal, F., Jalali, S., 2011. Cementitious building materials reinforced with vegetable fibres: A review. *Construction and Building Materials*, 25(2), pp. 575–581.

Park, S.H., Kim, D.J., Ryu, G.S., Koh, K.T., 2012. Tensile behavior of ultra high performance hybrid fibre reinforced concrete. *Cement & Concrete Composites*, 34(2), pp. 172–184.

Parra-Montesinos, G., 2005. High-performance fibre reinforced cement composites: a new alternative for seismic design of structures. *ACI Structural Journal*, 102(5), pp. 668–675.

Passuello, A., Moriconi, G., Shah, S.P., 2009. Cracking behavior of concrete with shrinkage reducing admixtures and PVA fibres. *Cement & Concrete Composites*, 31(10), pp. 699–704.

Pelisser, F., Neto, A.B.S.S., La Rovere, H.L., Pinto, R.C.A., 2010. Effect of the addition of synthetic fibres to concrete thin slabs on plastic shrinkage cracking. *Construction and Building Materials*, 24(11), pp. 2171–2176.

Pernica, D., Reis, P.N.B., Ferreira, J.A.M, Louda. P., 2010. Effect of test conditions on the bending strength of a geopolymer-reinforced composite. *Journal of Materials Science*, 45, pp. 744–749.

Pimentel, L., Beraldo, A., Savastano, H., 2006. Durability of cellulose–cement composites modified by polymer. *Engenharia Agricola*, 26, pp. 344–353.

Pitly, D., 2009. Carbon fibre growing as reinforcing material in precast concrete. Carbon Fibre Gear website (http://www.carbonfibregear.com/author/davidpitlyuk/).

Proctor, B.A., Oakley, D.R., Litherland, K.L., 1982. Developments in the assessment and performance of GRC over 10 years. *Composites*, 13(2), pp. 173–179.

Purnell, P., Short, N.R., Page, C.L., Majumdar, A.J., 2000. Microstructural observations in new matrix glass fibre reinforced cement. *Cement and Concrete Research*, 30(11), pp. 1747–1753.

Qian, C.X., Stroeven, P., 2000. Development of hybrid polypropylene-steel fibre-reinforced concrete. *Cement and Concrete Research*, 30, pp. 63–69.

Ramakrishna, G., Sundararajan T., 2005. Impact strength of a few natural fibre reinforced cement mortar slabs: a comparative study. *Cement and Concrete Composites*. 27, pp. 547–553.

Ramakrishnan, V., Wu, G.Y., Hosalli, G., 1989. Flexural behavior and toughness of fibre reinforced concretes. *Transportation Research*, pp. 69–77.

Razak, A., Ferdiansyah T., 2005. Toughness characteristics of *Arenga pinnata* fibre concrete. *Journal of Natural Fibres*, 2(2), pp. 89–103.

Reis, J., 2006. Fracture and flexural characterization of natural fibre-reinforced polymer concrete. *Construction Building Materials*, 20, pp. 673–678.

Rodrigues, C.S., Ghavami, K., Stroeven, P., 2006. Porosity and water permeability of rice husk ash-blended cement composites reinforced with bamboo pulp. *Journal of Materials Science*, 41(21), pp. 6925–6937.

Rodrigues, C.S., Ghavami, K., Stroeven, P., 2010. Rice husk ash as a supplementary raw material for the production of cellulose–cement composites with improved performance. *Waste Biomass Valorization*, 1(2), pp. 241–249.

Romualdi, J.P., Batson, G.B., 1963. Mechanics of crack arrest in concrete. *Proceedings of the American Society of Civil Engineers*, 89 EM3, pp. 147–168.

Saadatmanesh, H., Ehsani, M.R., Li, M.W., 1994. Strength and ductility of concrete columns externally reinforced with fibre composite straps. *ACI Structural Journal*, 91(4), pp. 434–447.

Saje, D., Bandelj, B., Šušteršič, J., Lopatič, J., Saje, F., 2011. Shrinkage of polypropylene fibre-reinforced high-performance concrete. *Journal of Materials in Civil Engineering*, 23(7), pp. 941–953.

Saje, D., Bandelj, B., Šušteršič, J., Lopatič, J., Saje, F., 2012. Autogenous and drying shrinkage of fibre reinforced high-performance concrete. *Journal of Advanced Concrete Technology*, 10(2), pp. 59–73

Savastano, H., Warden, P., Coutts, R., 2003. Mechanically pulped sisal as reinforcement in cementitious matrices. *Cement & Concrete Composites*, 25, pp. 311–319.

Sedan, D., Pagnoux, C., Smith, A., Chotard, T., 2008. Mechanical properties of hemp fibre reinforced cement: influence of the fibre/matrix interaction. *Journal of the European Ceramic Society*, 28, pp. 183–192.

SEI – Sumitomo Electric Industries, 2010. Super high strength fibre reinforced concrete SUQCEM, *Newsletter 'SEI NEWS'*, v. 398.

Shah, A.A., Ribakov, Y., 2011. Recent trends in steel fibreed high-strength concrete. *Materials and Design*, 32(7), pp. 4122–4151.

Shah, S.P., Winter, G., 1966, Inelastic behavior and fracture of concrete. *ACI Journal*, 63(9), pp. 925–930.

Sholihin, A.A., Purnawan, G., Alaydrus M.S., 2011. Fresh state behavior of self compacting concrete containing waste material fibres. *Procedia Engineering*, 14, pp. 797–804.

Silva, J., Rodrigues, D., 2007. Compressive strength of low resistance concrete manufactured with sisal fibre. *51st Brazilian Congress of Ceramics*, Salvador, Brazil.

Silva, F.J., Thaumaturgo, C., 2002. Fibre reinforcement and fracture response in geopolymeric mortars. *Fatigue and Fracture of Engineering Material and Structures*, 26, pp. 167–172.

Silva, F.A., Mobasherb, B., Filho, R.D.T., 2010a. Fatigue behavior of sisal fibre reinforced cement composites. *Materials Science and Engineering A*, 527(21–22), pp. 5507–5513.

Silva, F.A., Filho, R.D.T., Filho, J.A.M., Fairbairn, E.M.R., 2010b. Physical and mechanical properties of durable sisal fibre–cement composites. *Construction and Building Materials*, 24(5), pp. 777–785.

Silva, F.A., Mobasherb, B., Soranakom, C., Filho, R.D.T., 2011. Effect of fibre shape and morphology on interfacial bond and cracking behaviors of sisal fibre cement based composites. *Cement & Concrete Composites*, 33(8), pp. 814–823.

Song, P.S., Hwang, S., 2004. Mechanical properties of high-strength steel fibre-reinforced concrete. *Construction and Building Materials*, 18(9), pp. 669–673.

Soroushian, P., Bayasi, Z., 1991. Fibre-type effect on the performance of steel fibre reinforced concrete. *ACI Materials Journal*, 88(2), pp. 129–134.

Sridhara, S., Kumar, S., Sinare, M.A., 1971. Fibre reinforced concrete, *Indian Concrete Journal*, pp. 428–442.

Stucke, M.J., Majumdar, A.J., 1976. Microstructure of glass fibre reinforced cement composites. *Journal of Material Science*, 11(6), pp. 1019–1030.

Subrahmanyam, B.V., 1984. Bamboo reinforcement for cement matrices. *New Reinforced Concretes*, pp. 141–194.

Tait, R.B., Akers, S.A.S., 1989. Micromechanical studies of fresh and weathered fibre cement composites, Part 2: Wet testing. *International Journal of Cement Composites and Lightweight Concrete*, 11(2), pp. 125–131.

Tattersall, G.H., 1991. *Workability and Quality Control of Concrete*, London: E&FN Spon.

Tattersall, G.H., Banfill, P.F.G., 1983. *The Rheology of Fresh Concrete*, London: Pitman.

Toledo Filho, R., Scrivener, K., England, G., Ghavami, K., 2000. Durability of alkali sensitive sisal and coconuts fibres in cement mortar composites. *Cement & Concrete Composites*, 22(2), pp. 127–143.

Toledo, R., Ghavami, K., England, G., Scrivener, K., 2003. Development of vegetable fibre–mortar composites of improved durability. *Cement & Concrete Composites*, 25(2), pp. 185–196.

Tonoli, G., Joaquim, A., Arsene, M., Bilba, K., Savastano, H., 2007. Performance and durability of cement based composites reinforced with refined sisal pulp. *Materials and Manufacturing Processes*, 22(1–2), pp. 149–156.

Tonoli, G.H.D., Rodrigues Filho, U.P., Savastano, H., Bras, J., Belgacem, M.N., Lahr, F.A.R., 2009. Cellulose modified fibres in cement based composites. *Composites Part A*, 40, pp. 2046–2053.

Tonoli, G., Santos, S., Joaquim, A., Savastano, H., 2010. Effect of accelerated carbonation on cementitious roofing tiles reinforced with lignocellulosic fibre. *Construction and Building Materials*, 24(2), pp. 193–201.

Torgal, F.P., Jalali S., 2011. Cementitious building materials reinforced with vegetable fibres: A review. *Construction and Building Materials*, 25, pp. 575–581.

Uygunoğlu, T., 2008. Investigation of microstructure and flexural behavior of steel-fibre reinforced concrete. *Materials and Structures*, 41(8), pp. 1441–1449.

Voigt, T., Bui, K.B., Shah, S.P., 2004. Drying shrinkage of concrete reinforced with fibres and welded-wire fabric. *ACI Materials Journal*, 2(101), pp. 233–241.

Walton, P.L., Majumdar, A.J., 1978. Properties of cement composite reinforced with Kevlar fibres. *Journal of Materials Science*, 13(5), pp. 1075–1083.

Won, J.P., Jang, C., Lee, S.W., Lee, S.J., Kim, H.Y., 2010. Long-term performance of recycled PET fibre-reinforced cement composites. *Construction and Building Materials*, 24, pp. 660–665.

Zollo, R.F., 1997. Fibre-reinforced concrete: an overview after 30 years of development. *Cement and Concrete Composites*, 19(2), pp. 107–122.

Zollo, R.F., Hays, C.D., 1991. Fibres vs. WWF as non-structural slab reinforcement. *Concrete International*, 13(11), pp. 50–55.

16

Advanced fibre-reinforced polymer (FRP) composite materials in bridge engineering: materials, properties and applications in bridge enclosures, reinforced and prestressed concrete beams and columns

L. C. HOLLAWAY, University of Surrey, UK

DOI: 10.1533/9780857098641.4.582

Abstract: Chapters 16 and 17 discuss the development of the advanced polymer composite material applications in bridge engineering. They demonstrate the innovative types of components and structures which have been developed from FRP composite materials and the most advantageous way to employ composites in bridge engineering. Given the importance of bridge infrastructure, the discussion of this topic has been split over two chapters. This chapter focuses on the type of FRP composite materials used in bridge engineering, their in-service properties and their applications in bridge enclosures and the rehabilitation of reinforced and prestressed concrete bridge beams and columns. Chapter 17 covers rehabilitation of metallic bridge structures, all FRP composite bridges and bridges built with hybrid systems.

Key words: FRP composites, in-service properties, FRP bridge enclosures, FRP bridge decks, bridge beams and columns.

16.1 Introduction

There is a growing concern with respect to the deterioration of reinforced concrete and steel bridges over the entire world. Therefore, cost-effective and durable technologies are needed for bridge repair, rehabilitation, replacement and new bridge structures. Advanced fibre-reinforced polymer (FRP) composite materials can be a viable alternative for bridge construction and repair. The advanced polymer composite is a hybrid material consisting of two main components, the fibre and the polymer. The unique properties of this material suggest their suitability for integration into the civil/building infrastructure to form 'All FRP composite' structures and hybrid structural systems. Hybrid structures are fabricated from dissimilar material units which when connected together will complement each other. The hybrid systems range from open or closed stay-in-place formwork to systems incorporating FRP and traditional construction materials.

During the 1970s progressive consulting structural engineers (mainly

concerned with cladding to structures/buildings) began to consider FRP composites as a structural material (initially mainly concerned with cladding to structures/buildings) and to design composite building structures. Fabricating firms that had experience in the manufacture of large FRP composite units for other industries entered the building industry, but it was not until the mid-1980s that there was a desire by structural engineers to use FRP composites as a structural material in civil engineering. This was driven by the need for durable, high strength and high stiffness materials that could replace the more traditional civil engineering materials exposed to aggressive and hostile environments that are invariably encountered in civil engineering applications. Thus private research laboratories, universities and consulting civil/structural engineers investigated the possibility of using automated manufacturing methods for the production of structural components. The main fabricating technique to form structural components was the pultrusion method and this technique lent itself conveniently to the manufacture of structural building blocks which could be combined to form structural systems. There was one economic problem associated with manufacturing these units by pultrusion: each different cross-section required a new steel mould.

For FRP bridge systems and the repair/rehabilitation of old bridges to be successful, components should be modular and assembly should be rapid and simple and have reliable connections; the material should be durable. FRP composite materials are durable and can be readily made in modular forms; consequently, they fulfil these requirements provided the design of the basic structural building modular system is properly undertaken and the units are properly installed. Furthermore, these materials can provide significant advantages over conventional materials for the construction of bridges, such as reduction in dead load and subsequent increase in live load rating, rehabilitation of old bridge structures, faster installation, and enhanced service life even under harsh environments. However, higher initial cost of materials is a concern, but the whole-life costs do even out the initial cost of the material.

Complete structural components made from FRP composites for bridge constructions are generally manufactured under factory conditions; these are then readily transported to site and installed. FRP components are available as elements in the form of rebars (for reinforcing concrete beams); strips and sheets for flexural, rehabilitation and shear strengthening of reinforced concrete beams; and rods for prestressing concrete members. Furthermore, during the manufacture of the FRP structural components fibre-optic sensors for continuous monitoring can be integrated in the materials; in addition, adhesives are being increasingly used for joining components.

Arguably the greatest utilisation of FRP composites in civil engineering has been in the area of ‘all-FRP’ composite bridge fabrication/construction, strengthening/rehabilitating existing bridges, retrofitting bridge columns and replacing bridge decks, which have deteriorated over time. Given its

importance, the discussion of this topic is split over two chapters. This chapter focuses on materials used in FRP composites; it discusses briefly their important mechanical and in-service properties and their applications in bridge enclosures, the rehabilitation of concrete bridge beams and columns. Important mechanical and in-service properties will be discussed in more detail in areas where these properties have a significant importance to the bridge structural system. Chapter 17 covers rehabilitation of metallic bridge structures, 'all FRP' composite bridges, and bridges built with hybrid systems. These chapters were completed in January 2012 and will require updating in five years' time or so.

16.1.1 The combination of FRP composites with other materials to form hybrid systems

In current bridge engineering infrastructure there are a number of areas in which FRP composites are used, although they do have a material cost premium. Each application takes advantage of the material's light weight to meet the design, erection and operational objectives and its durability, its corrosion resistance, and its long life cycle.

The areas to be covered are:

- An access enclosure to an existing structure for maintenance purposes, to protect the structure from hostile environments and for aerodynamics of the structure, namely a bridge enclosure and aerodynamic fairings using FRP units.
- FRP bridge decks.
- The rehabilitation of RC beams by the techniques of (i) external plate bonding (EPB) and (ii) Near Surface Mounted (NSM) FRP rods.
- The retrofitting of RC columns by using unidirectional FRP composites.
- The FRP rebars used to reinforce concrete beams and slabs.
- The construction of a hybrid structural member to enable two or more structural materials to take full advantage of their superior properties.
- The rehabilitation of steel beams by the techniques of EPB.
- 'All FRP' composite bridge superstructure.

The last three items will be discussed in Chapter 17.

16.2 Fibre-reinforced polymer (FRP) materials used in bridge engineering

16.2.1 The matrix material

Fibre-reinforced composite materials are made by the controlled distribution of two materials: (i) the continuous matrix phase (phase1) and (ii) the fibre

reinforcement phase (phase 2). In addition, there is the boundary between the matrix and the reinforcement (the interface area, phase 3), which controls the properties of the given materials. The three major types of matrices (polymers) which are used in bridge construction are the thermosetting, the thermoplastic and the elastomeric; each requires different procedures for their manufacture. The matrix polymer material requires two components, the resin and curing agent (hardener). In bridge engineering there are two types of curing procedures; one uses an *ambient cure* resin and the other uses an *elevated temperature cure* system. The former would be utilised *in-situ* in the field to form either a composite material or an adhesive. The ambient temperature of the site (the cure temperature) would determine the length of the polymerisation period. It is advisable when using an ambient cure resin to post-cure the material through the use of a heating blanket on site, or by reflective heating, ovens and hot rooms in a laboratory or factory area. It is also possible in the case of some elevated temperature cure systems to substitute the hardener for an ambient temperature one to enable room temperature cure; the performance characteristics and rate/degree of polymerisation of the resin will be different from that of an elevated temperature one. The elevated temperature cure resin products would invariably be manufactured in a factory area by automated techniques, such as the pultrusion method (Starr, 2000), or fibre pre-impregnation under controlled conditions of temperature and pressure (Hollaway and Head, 2001). The problems of surface finish of a carbon fibre reinforced polymer (CFRP) composite with a rapid curing procedure are discussed by Herring and Fox (2011). The ambient and elevated temperature cured resins have different formulations; generally, these systems are interface ones. Attention must be given to the site temperature when using the ambient cure polymers; the environmental temperature under working conditions should be some 20°C below the *glass transition temperature* (T_g) of the composite material (T_g is the mid-point of the temperature range over which an amorphous material changes from (or to) a brittle, vitreous state to (or from) a plastic state).

The thermosetting polymer is invariably used in bridge construction, or in bridge maintenance, in conjunction with a fibre array to form the structural composite. The thermosetting polymer consists of long chain molecules, which are cross-linked in a curing reaction. The network so formed and the length and the density of the molecular units are a function of the chemicals used in the manufacture of the polymers, and the cross-linking is a function of the degree of cure of the polymer. Both the network and the cross-linking will have an influence on the mechanical and in-service properties of the material. Furthermore, the degree of cure is a function of the temperature and the length of the polymerisation (curing) period. The main thermosetting polymers used for structural components in bridge engineering are the epoxies, the vinylesters, and occasionally the iso-polyesters. Epoxies generally

out-perform most other resin types in terms of mechanical properties and resistance to environmental degradation. The most important epoxy resins for the bridge engineer are the low molecular weight polymers (oligomers), which are produced from the reaction of bisphenol-A and epichlorohydrin. The vinylester is a hybrid form of polyester resin which has been toughened with epoxy molecules within the main molecular structure. Its molecule has fewer ester groups compared with the polyester resin and, as the ester groups are susceptible to water, degradation by hydrolysis would result; thus vinylesters exhibit better resistance to water and also many other chemicals compared with their polyester counterparts. Furthermore, as vinylesters have unsaturated esters of epoxy resins, they have similar mechanical and in-service properties to those of the epoxies, but they have similar processing techniques to those of the polyesters. Iso-polyesters are sometimes used to manufacture pultrusion sections for structural components for bridges; they are also used in the production of automated pultrusion components for bridge furniture. They are readily processed and cured at ambient temperatures using a wet lay-up procedure; these ambient cured polymers must be post-cured.

For polymers to perform their in-service and mechanical properties efficiently they should have reached near 100% polymerisation. It is essential that the correct mix ratio is obtained between the resin and its curing agent to ensure that a complete reaction takes place, as the curing agent molecules 'co-react' with the thermosetting resin molecules in a fixed ratio. This process bonds together repeating molecular building blocks, known as monomers, through a variety of reaction mechanisms to form large chainlike or network molecules of relatively high molecular mass known as a polymer. Thermosetting resins are formed under the influence of heat and once formed they do not melt or soften upon reheating, and do not dissolve in solvents; they can be made by either addition or condensation polymerisation.

16.2.2 The fibre material

A wide range of amorphous and crystalline materials can be used to form fibres, but in bridge engineering the three fibres which are generally used are the glass fibre, the aramid fibre and the carbon fibre. The fibres may be used separately or as a hybrid of two or three different fibres. The hybrid system will be used when, say, the major fibre is the glass fibre but the stiffness is required to be increased somewhat and this could be achieved by introducing some carbon fibres into the system. Hollaway (2008) has discussed the various fibres which are used in the construction industry and it is recommended that this publication be referred to for the manufacturing techniques, in-service and mechanical properties of the three major civil engineering fibres. It is noted that there are two precursors that may be used to form the carbon fibre, namely the polyacryonitrile (PAN) fibre

which is used in the manufacture of the standard and high-moduli carbon fibre (and the Ultra High-Modulus carbon fibre used by the aero and space industry), and the PITCH fibre which is produced from the by-product of the destructive distillation of coal. This fibre is used in the manufacture of ultra high-modulus carbon fibres for the construction industry. As this fibre can have a very high modulus of elasticity value, greater than 400 GPa, its strain to failure will be very low, of the order of 0.4%.

The majority of the carbon fibres currently commercially available for bridge engineering are manufactured from the PAN precursor; the aerospace industry also uses these fibres. After the carbonisation stage of the production of carbon fibres is completed, only about 50% of the original fibre mass remains. Furthermore, the higher the heat treatment of the fibre during the graphitisation stage of the manufacturing process the higher is the stiffness of the fibre; clearly this property will be directly proportional to the cost of the fibre.

The carbon fibre produced from the PITCH precursor is relatively low in cost and high in carbon yield compared to the PAN fibre, but from batch to batch the fibres tend to be non-uniform in their final cross-section. This does not generally cause a problem in the civil engineering industry but they are not used in the aerospace industry.

Carbon fibres are available as 'tows' and a 12K tow has 12,000 filaments. The fibres are commonly sold in a variety of modulus categories:

- Standard or modulus $\simeq$200 GPa
- High strength $\simeq$3 GPa and modulus $\simeq$220 GPa
- High modulus $\simeq$220–300 GPa (this category is also known as intermediate modulus in some parts of the world)
- Ultra-high modulus >450 GPa (this category is also known as high modulus in some parts of the world).

The production of aramid fibre, an aromatic polyamide fibre, is by an extrusion and spinning process (Hollaway, 2008). There are two grades of stiffness available:

- The higher modulus of elasticity and tensile strength fibre (typical values 130 GPa and 3,000 MPa respectively with an ultimate strain of the order of 2.4%) is the fibre used in construction.
- The lower modulus of elasticity and tensile strength fibre (typical values 70 GPa and 2,900 MPa respectively with an ultimate strain of the order of 4%) is used in bullet-proof systems.

Aramid fibres are available under a variety of grades and trade names. Kevlar is manufactured by Du Pont and Twaron is manufactured by Akzo; they may differ slightly in their physical structure but have a very similar chemical structure. Further reading on the subject may be obtained from Schaefgen

(1983), Burgoyne (1992), Hollaway and Head (2001), Giannopoulos (2009) and the Kevlar Technical Guide (undated).

The production of glass fibres is by the direct melt process in which fine filaments diameter 3–24 μm are produced by continuous and rapid drawing from the melt (Hollaway, 2008). The two most important fibres which are used in bridge engineering are:

- E-glass, which has a low alkali content of the order of 2%; it is used for general-purpose structural applications. The elastic modulus and tensile strength values are of the order of 72 GPa and 2.46 MPa respectively.
- S-glass fibres which are stronger and stiffer compared to those of the E-glass fibre, the modulus of elasticity and tensile strength values are 88 GPa and 4.6 GPa respectively.

Other glass fibres that might be used under certain circumstances are E-CR glass, R-glass and AR-glass.

16.3 In-service and physical properties of FRP composites used in bridge engineering

FRP engineering structural composites must possess sufficient strength and stiffness properties to resist the full superimposed and self-weight loads to which the structure is exposed. Furthermore, the materials must possess the relevant in-service and physical characteristics required to function in their exposed environments. The greater the degradation of the material over time the lower will be the load-carrying capacity of the structure. Consequently, the most important properties of the matrix (the polymer), which protects the load-carrying fibre component of the composite, are its physical and in-service characteristics and these will be briefly discussed in the next two sections. As the basic mechanical properties of the component parts and the combination of these to form the whole FRP composite material have been discussed many times in publications (Kim, 1995; Hollaway and Head, 2001; Karbhari, 2007; Hollaway, 2009), they will not be dealt with in this chapter. However, it is noted that currently the literature evaluating the rehabilitation of bridge structures rarely addresses, from a theoretical or an experimental consideration, the time-dependent degradation of FRP composites when they are exposed to severe and changing environmental conditions. The introduction to creep characteristics of polymers has been mentioned in Hollaway (2008).

16.3.1 The influence of temperature on polymers

The influence of temperature on polymers can be separated into two effects:

- Short-term
- Long-term.

The short-term effect is generally physical and is reversible when the temperature returns to its original state, whereas the long-term effect is generally dominated by chemical change and is not reversible; this effect is referred to as ageing. As the temperature varies, all properties of the polymer will change; consequently, to fully characterise the temperature-dependent material, properties must be measured over a range of temperatures. To study one or more of the properties as a function of temperature, a thermal analyser (differential scanning calorimeter (DSC)) is used; it scans property change over a wide temperature range. Particular cases of the effects of temperature on polymers are:

1. Their glass transition temperature T_g and their melting point (Hollaway, 2008; Hansen and McDonald, 2007; Hollaway, 2010)
2. Their thermal expansion (Hollaway, 2010; Hansen and McDonald, 2007)
3. Their thermal conductivity (Hollaway, 2008)
4. Their exposure to ultraviolet light, although this is not strictly a temperature property (Hollaway, 2010)
5. Their resistance to fire (Mouritz and Gibson, 2007; Hollaway and Head, 2001).

16.3.2 The long-term in-service properties of the thermosetting polymers

The polymer serves a number of functions besides being the binder to hold the fibres together in their required positions. It provides environmental and damage protection to the fibres and toughness to the composite. The long-term stability of the polymer will be dependent upon its durability in the environment into which it is placed. As mentioned already, the stiffness of the polymer is a function of its degree of cure, which in turn is a function of the degree of cross-linking of the three-dimensional network of polymer chains; however, the stiffness and strength of the polymer are not critical in terms of the composite as the fibres are the components that assess these properties. What is important is the ability of the material under load to resist the particular civil engineering environments; this topic comes under the heading of *durability* of the polymer (Karbhari *et al.*, 2000, 2003), Karbhari, 2007) which covers two main properties of the polymer:

- Polymer permeability/barrier property
- Corrosion resistance property.

Moisture will diffuse into all organic polymers, leading to changes in their mechanical, chemical and thermophysical characteristics. By improving the barrier property of the polymer a reduction of the ingress of moisture, aqueous and salt solutions will be achieved; a successful method of improving the barrier properties is to apply an additive to the matrix at the time of manufacture. Silanes (organofunctional trialkoxysilanes) or organotitanates are two agents which have been used as a barrier against moisture ingress (van Ooij *et al*., 2005). Teng *et al*. (2003) undertook field monitoring and laboratory tests to investigate the performance of new bridge columns wrapped with GFRP exposed to aggressive environmental conditions. They found that GFRP wraps provide excellent protection against aggressive environmental conditions. Furthermore, epoxy-layered silicate nanocomposites introduced into the polymer at the time of manufacture have the potential to lower its permeability, thus improving its barrier properties and its mechanical strengths (Haque *et al*., 2003; Sangaj and Malshe, 2004; Liu *et al*., 2005; Hackman and Hollaway, 2006; Choudalakis and Gotsis, 2009).

The resistance of a thermosetting polymer to chemical attack depends upon its chemical composition and the bonding in its monomer. These polymers can degrade by several mechanisms, but degradation may be divided into two main categories, physical and chemical:

- Physical corrosion is the interaction of a thermosetting polymer with its environment causing an alteration in its properties but with no chemical reaction.
- Chemical corrosion is when the bonds in the polymer are broken by a chemical reaction with the polymer's environment. During this process the polymer may become embrittled, softened, charred, delaminated, discoloured or blistered; these are usually non-reversible reactions. A correct curing procedure of the polymer is important to reduce these degrading effects.

However, the corrosion resistance of polymers in a civil engineering environment is generally superior to that of most other construction materials.

16.4 FRP bridge enclosures

The concept of 'bridge enclosure' was developed jointly by the Transport Research Laboratory (TRL, formerly TRRL) and Maunsell civil engineering consultants (now AECOM), Beckenham, UK, in 1982 to provide a solution for regular inspections and maintenance of bridge structures. The enclosures provide a 'floor' underneath bridges. They were developed initially for steel bridges but have been used with concrete bridges mainly for the purpose of aesthetic or aerodynamic profile; enclosures allow greater freedom of expression independent of the strength requirements. The 'floor' is

sealed onto the underside of the edge girders to enclose bridges, and to protect them from further corrosion. Research work undertaken at the TRL (McKenzie, 1991, 1993) showed that once the enclosures are erected the rate of corrosion for uncoated steel in the protected environment within the enclosure is 2–10% of that of painted steel in the open; no dehumidifying equipment is needed to prevent corrosion. Although enclosure spaces have high humidity, chloride and sulphur pollutants are excluded by seals so that when condensation does occur (as in steel girders) the water drops onto the enclosure 'floor' and there it escapes through small drainage holes. The floor and fixings are non-corrosive and no water is able to pond against the steel, and hence corrosion of the latter material is prevented. The advantages of enclosure systems include:

- Corrosion rates are drastically reduced.
- Enclosure provides safe permanent access for future inspection and maintenance.
- Traffic disruption below the deck is minimised during inspection and maintenance.
- Any paint or debris from maintenance work is contained within the enclosure.
- Maintenance work may be carried out in controlled conditions during sociable hours.

In spite of the numerous advantages, there are relatively few examples of bridge enclosures in the UK. The probable reasons are the lack of historical cost data to justify the economic case for enclosures, and the reduction of headroom or increase in structural depth required to accommodate the system. Most bridge enclosures which have been erected in the UK have utilised polymer/fibre composites; these are ideal materials for enclosure floors because they add little weight to the bridge and are highly durable. As the composite material is under the bridge and therefore out of the direct influence of the sun, there is no need to protect it against UV radiation. The first major example of this technique was in 1988–1989, when the A19 Tees Viaduct at Middlesborough, UK, was fitted with the Maunsell 'caretaker' system (Hollaway and Head, 2001). Since then there have been some other examples of bridge enclosures erected under bridges, namely at Botley, Oxford (1990) where the hand lay-up GFRP method was used, and at Nevilles Cross (1990) near Durham where the pultruded GFRP system was fitted to an existing bridge over the main east coast railway line. Two bridges were then built with enclosures. One was at Bromley in South London (1992) which utilised the Maunsell 'caretaker' system; the Composolite panels were produced with a brickwork appearance to complement the piers and abutment. The other was in 1993, at Winterbrook, which carries the A4130 Wallingford by-pass over the river Thames and was designed by the Bridge Department

of Oxford County Council; the enclosure was designed by Mouchel, West Byfleet (now Sinclair Knight Merz (SKM)).

In 1996 the UK Highways Agency published the design standard for Bridge Enclosures, BD 67/96 (1996); the requirements for wind loading are covered by BD 37 or 38/88 (1988). When enclosures are placed under railway bridges, aerodynamic pressure caused by the displacement of air due to the passage of a train is significant, and therefore the allowable deflection and the design of the fixings for the enclosure must be carefully considered.

16.5 FRP bridge decks

The bridge deck is the most vulnerable element in the bridge system because it is exposed to the direct actions of wheel loads, chemical attack, and temperature/moisture effects including freeze and thaw, shrinkage and humidity. Owing to the advantageous FRP material properties such as high specific strength and stiffness, a tolerance to frost and de-icing salts, short installation times with minimum traffic interference and, in addition, lower or competitive life-cycle cost, this material has matured to become a valuable alternative structural material for bridge deck structures. Compared with cast-in-place concrete decks, FRP bridge decks typically weigh 80% less, can be erected twice as fast and have a service life that can be two to three times longer. By utilising FRP material to form a bridge deck replacement, it is possible to increase the live load or deck width of existing bridge superstructures. Furthermore, during the manufacture of the structural FRP components, fibre-optic sensors for continuous monitoring on site can be integrated into the materials.

In addition to their transverse load-carrying function, concrete decks usually form part of the top chords of the main girders in the longitudinal axis of the bridge. Thus the stiffness and load-carrying capacity can be increased compared with a simple steel or concrete girder. The shear stud or stirrup connections provide full composite action over the cross-section. Therefore, in order to be a competitive option, FRP decks must offer a transverse load-carrying component and a longitudinal top chord function.

However, there are certain disadvantages to the use of FRP bridge decks:

- *Cost*. Highway authorities responsible for construction and maintenance of the nation's bridges are under considerable pressure to maintain the significant number of substandard bridges, all of which are competing for the limited amount of monies for such purposes. Under these conditions officials are compelled to maximise the number of bridges in serviceable condition at any given time and rarely have the latitude to consider the life-cycle cost advantages of initially more expensive

materials. Consequently, any decision to use a more expensive material (first cost) must be justified based on superior performance or specific project requirements (Berg *et al*., 2006); nevertheless, the utilisation of FRP bridge decks is growing.

- *Standard specifications*. Specifications for the procurement and construction of FRP decks must be developed so that bridge owners can obtain the decks within their procurement process.

On a unit area basis, FRP decks are more expensive compared to those of conventional materials but applications need to be selected on some criterion other than initial cost. Situations where their value might be recognised include the following.

- *Life-cycle cost*. The expected service life of the composite deck exceeds 75 years with little maintenance; this is about three times the expected life of a concrete bridge deck.
- *Weight advantage*. FRP bridge decks weigh only 15–20% of a structurally equivalent reinforced concrete deck; therefore, load-rated bridges may be re-rated to their original design capacity or an ageing bridge may be kept in service longer before being replaced. Lightweight bridge decks provides a direct benefit from the point of view of:
  - The utilisation of lightweight cranes for lifting the deck into position
  - In new construction the superstructure of the bridge can be smaller, likewise its foundations.
- *Corrosion resistance*. FRP materials can resist corrosion effects of de-icing salts and corrosive chemical environments; this resistance provides long life and low maintenance.
- *Time-dependent deterioration*. The deterioration over time of the various components of FRP bridge decks will degrade at different rates. To investigate the effects of this degradation Wu and Yan (2011) have developed a mechanics model to simulate the changes in load capacity and stiffness of FRP decks over time; they have also included a quantitative effect of sustained loads and environmental exposure to determine deterioration rates of the stiffness and strength. The results indicated that the reductions in strength and stiffness of glass fibre/vinylester composites were substantial after 10,000 hours of freeze/thaw cycles and a sustain load of 25% strain, although the reductions were insignificant when the composite was not loaded. Further references on the time-dependent deterioration of composites may be obtained from Hollaway and Head (2001), Karbhri *et al*. (2003), Helbling *et al*. (2006) and Wu *et al*. (2006).
- *Rapid installation*. Traffic management costs are relatively low during construction due to the rapid installation of the FRP deck. Furthermore,

construction projects over railways where possession is costly benefit FRP technology.

- *The versatility of FRP composites*. Their high strength to weight ratio and the wide range of material properties achievable offer opportunities for FRP to be used in innovative and more efficient structural forms with lighter and longer spans.

Lightweight bridge decks are also valuable in the case of the historic steel or timber truss bridges. Many steel truss bridges were constructed in the first half of the twentieth century and are of historic value. Many of these bridges are load-rated since they were not designed for current vehicles; FRP decks are an option for reducing the dead load on these bridge superstructures and thus increasing the loading capacity of the bridge.

16.5.1 The construction of the FRP bridge deck

The FRP bridge decks commercially available at the present time can be classified according to two types of construction: (i) adhesively bonded pultruded shapes, and (ii) sandwich construction. In both cases quality control of the product is enabled by standardised fabrication procedures within individual manufacturing facilities. The adhesively bonded FRP pultruded bridge deck structures are typically made from vinylester polymer and E-glass fibre; occasionally the deck is moulded. These shapes can be economically produced in continuous lengths using well-established processing methods. The deck replacement can be fabricated in conjunction with the FRP superstructure replacement of the bridge; the deck would be transported from the factory with the final fabrication undertaken on site, and when the bridge structure is completed the wearing surface is added. An example of a complete replacement bridge is given in Luke *et al*. (2002).

FRP sandwich constructions have been used to manufacture bridge decks. Characterisation studies have recognised that FRP bridge deck systems are highly stiffness driven and to date several novel sandwich FRP deck systems have been proposed; these have been categorised into two types: cellular structure and sandwich construction. These structural forms imply the use of strong, stiff face sheet materials that carry the flexural loads and a low specific weight core material. Cellular materials are the most efficient core materials for weight-sensitive applications. Owing to the ease with which face sheets and core materials can be changed in manufacturing, sandwich construction presents tremendous flexibility in designing for various depths and deflection requirements. Face sheets of sandwich bridge decks are primarily composed of E-glass mats and/or rovings infused with a polyester or vinylester resin. Currently core materials are rigid foams or thin-walled cellular FRP materials.

FRP bridge decks are required to meet the same design requirements as conventional bridge decks. Unless waived or modified by the bridge owner, typical design criteria are given in Daly and Duckett (2002), AASHTO (2002), AASHTO LRFD (2004) and BD 90/05. Most of the bridge decks which have been built use proprietary experimental systems and details; consequently, the lack of geometrical/material standardisation is a challenge to bridge engineers, who traditionally are accustomed to standard shapes, sizes and material properties.

One of the first fibre-reinforced polymer sandwich deck, installed on a truss bridge in New York State, was load tested to study its behaviour (Alampalli and Kunin, 2002, 2003; Alampalli, 2006). The test data indicated that localised bending effects may play a role in the strain distribution of FRP decks and should be appropriately considered. Several other researchers have considered modelling and characterisation of fibre-reinforced plastic honeycomb sandwich panels for highway bridge applications (Davalos and Qiao, 2001). Most of the research on cellular FRP deck panels initially considered them to act as beams and thus they were tested as a three-point load system (Harik and Alagusundaramoorthy, 1999); punching shear and edge delamination were reported as the failure mode.

The first public highway advanced polymer composite bridge to be built in Western Europe was constructed over the River Cole in Oxfordshire; it was officially opened on 29 October 2002. It was developed and built by a consortium of seven European companies led by Mouchel Consulting, West Byfleet (now Sinclair Knight Merz (SKM)), UK; the deck and superstructure replacement was demonstrated by the innovative ASSET Project (Luke *et al.*, 2002). The beam and deck structures were manufactured by the pultrusion technique (Zhang and Canning, 2009). The span of the bridge was 10 metres with a width of 6.8 metres; the bridge carries two lanes of traffic and a footpath. The beams of the superstructure have unidirectional carbon fibre-reinforced polymer composite plates bonded to the flanges of the I cross-section of GFRP beams to provide the required global flexural rigidity; the wearing surface of the bridge is of polymer concrete composite construction. The bridge incorporated an optical fibre Bragg grating sensor-based structural monitoring system using fluorescent fibre as the optical source with a tunable, fibre-coupled, Fabry–Perot filter, actuated by piezoelectric transducers and operated over the bandwidth of the source at up to 250 scans per second. Light from the source was filtered and reflected back from the Bragg gratings, through optical couplers, to eight photodiode detectors. These detected the resulting time-domain spectra of the sensors in each of the serially connected sensor arrays.

The first highway bridge in the UK with a FRP bridge deck to span a railway was constructed at Standen Hey, near Clitheroe, Lancashire. Figure 16.1 shows the deck being lifted on to its abutments; it replaced the over-

16.1 The first UK highway FRP bridge deck to span over a railway being lowered on to the abutments at Standen Hey, near Clitheroe, Lancashire. Image courtesy of Network Rail. Acknowledgements to TPG and Partners (the designers) and to Birse Rail Ltd (the contractors).

line bridge. The bridge has a span of 10 metres, weighs 20 tonnes and was completed in March 2008 (TGP, 2008); this was the first of Network Rail's six trial sites in the country. The bridge deck comprised three layers of ASSET panel deck units which were made from E-glass fibres in the form of biaxial mats within a UV-resistant resin matrix.

The 40-year-old Garstang Mount Pleasant Highways Agency Bridge over the M6 motorway was replaced with a new innovative single carriageway road bridge; this was the first FRP/steel composite bridge in the UK and was completed in 2008. The bridge elements were fabricated on site at the roadside and then the assembled structure was lifted into position. The superstructure comprises a novel prefabricated FRP deck; it was supported and adhesively bonded to the two longitudinal steel plate girders and reinforced concrete abutments. Simple and robust connection details were provided between the FRP deck and other bridge components. The FRP bridge deck was designed by Mouchel Group (now Sinclair Knight Merz (SKM)), Manchester, UK, and was constructed from ASSET construction and provides general vehicular access to an equestrian centre; it was designed for unrestricted traffic loading (Canning, 2008).

There have been many deck replacements in the UK. Some have been mentioned above, and others include the following:

- A5 Nesscliffe Bypass Wilcott Footbridge, Shropshire, England (John, 2003).

- St Austell footbridge, Cornwall, England, GFRP composite deck carrying pedestrian traffic over the railway (Shave *et al.*, 2009).
- Standen Hey Bridge, Blackburn, England, GFRP composite bridge deck carrying farm traffic (Dawson and Farmer, 2009).
- Calder Viaduct, Cumbria, England, the world's first application of FRP composites for structural re-decking of a railway bridge for full railway and derailment load; it was chosen by Network Rail, UK, as a pilot project. The deck is supported on a series of girders constructed from 1922 manufactured steel, carrying unrestricted railway traffic (Canning *et al.*, 2009). Figure 16.2(a) shows the arrangement in one of the three spans of the viaduct where the ballast depth was critical. The GFRP deck was supported on new steelwork, which in turn was supported on the existing cross-girders, to form a level surface no higher than the existing cross-girder top flange; consequently, the decking had to be under-slung. In the other two spans where ballast was less critical the arrangement used was that in Fig.16.2(b). Figure 16.2(c) shows the FRP decking (Fig. 16.2(b) arrangement) installed, ready for the ballast and track to be replaced.

In 2008, an innovative GFRP composite bridge was constructed over the new German B3 Highway in Friedberg near Frankfurt. The bridge serves a small country lane over a federal road with a span of 21.5 m, a width of 5.0 m and a total length of 27.0 m; its weight is approximately 8 tonnes. It comprises a superstructure of two steel beams supporting innovative multi-cellular FBD 600 GFRP deck profiles constructed of the ASSET pultruded technique and manufactured by Fiberline, Denmark; the FRP sections are bonded to the steel girders. The lightweight composite material and fabrication enabled the bridge to be erected quickly and with minimum disruption to road and, in addition, to reduce long-term maintenance work over the busy road. A typical cross-section of the Friedberg bridge is given in Knippers and Gabler (2007) and the description is given in GFRP road bridge (2008). Figure 16.3 shows the bridge being lowered onto its abutments.

There have been many bridge deck replacements built in the USA. One of these was the new Eight Mile Road Bridge, in Hamilton County, near Cincinnati, Ohio, that became the first site in the USA to receive the integrated composite superstructure. The original bridge was built in 1940, and in 2008 the bridge was replaced by a deck and bridge 'drop-in-place' superstructure structural system SuperFiberSPAN™, which is an integrated fibre-reinforced polymer bridge system produced by Composite Advantage using TYCOR® fibre-reinforced composite core material; the polymer was a corrosion-resistant vinylester resin with pigment additives and a UV inhibitor. The bridge beams and deck were integrally moulded and manufactured by the infusion process; this eliminated the connection joints between deck

and beams. In addition to replacing the deck and bridge superstructure, the abutments required rehabilitation to extend their life. Figure 16.4 shows the unit bridge deck being lowered onto its supporting beams. The span

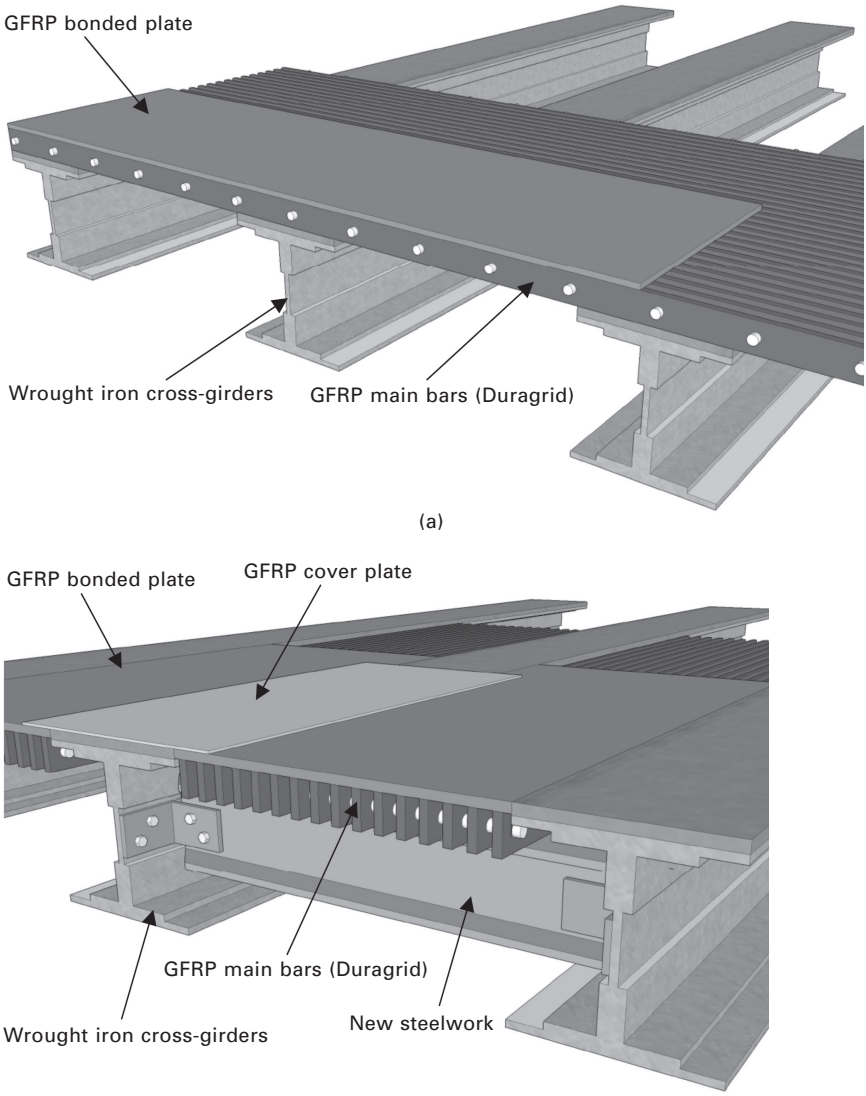

16.2 (a) The under-slung girder and the FRP deck arrangement to maximise ballast depth (image courtesy of Network Rail and Mouchel/SKM); (b) bonded/bolted GFRP components (image courtesy of Network Rail and Mouchel/SKM); (c) the installed FRP deck panels (image courtesy of Network Rail and Mouchel/SKM).

(c)

16.2 Continued

of the bridge is 6.7 metres and the width is 19 metres. It was designed to specifications which included the standard AASHTO HS 20 loading, L/800 deflection criteria, a skew bridge design, and an asphalt wearing surface.

As the integrated system is able to prefabricate a number of components of the bridge at one time, the cost premium for using high-performance composite material is reduced. Furthermore, the manufacturer claims that the overall cost of the integrated system is less than that of a conventional FRP bridge deck and separate beams, due to the fabrication and assembly of the panels taking place under one roof, thus minimising production costs. The above information is based upon the company's website: www.compositeadvantage.com, and *Composite Advantage Newsletter* (2008).

16.6 The rehabilitation of reinforced concrete (RC) and prestressed concrete (PC) bridge beams using external FRP plate bonding (EPB)

A substantial number of RC and PC bridges in Europe are more than 40 years old; many were built during the construction boom after the Second World War from the 1950s to the 1970s. A large number of these structures now require repair or strengthening due to several reasons ranging from damage due to collision by overheight vehicles or construction equipment, inadequacy to new and heavier loads, degradation due to fatigue, corrosion and obsolescence. Approximately 42% of the bridges in the USA in the mid-1980s were considered to be structurally deficient (Klaiber *et al*., 1987). The majority of these bridges require continuous maintenance and strengthening due to lack of stiffness, strength, ductility and durability.

16.3 GFRP composite bridge being lowered on to its abutments over the new German B3 Highway in Friedberg near Frankfurt. Image courtesy of Fiberline, Composites A/S.

16.4 Bridge deck replacements to the Eight Mile Road Bridge, in Hamilton County, near Cincinnati, Ohio, USA. Image courtesy of Composite Advantage LLC.

The key issues affecting FRP composites in the rehabilitation and retrofitting of concrete structures have been cited by Hollaway (2011). The two primary sources of deterioration are corrosion and vehicle impact; Kasan and Harries (2009) have cited and demonstrated the combination of these effects as being critical.

The above alarming statistics emphasise the importance of developing reliable and cost-effective repair and strengthening techniques for existing bridge structures. Traditional repair strategies include external post-tensioning, internal strand splices, and steel jackets. However, such repair strategies are in many cases only partially satisfactory in restoring the ultimate capacity of the damaged member and are particularly vulnerable to future corrosion. Amongst the available rehabilitation techniques was the application of steel plates bonded to the tensile region of the beam; this technique was pioneered simultaneously in South Africa and Germany in the 1960s (L'Hermite and Bresson, 1967; Flemming and King, 1967; Lerchenthal, 1967). The use of steel plates has many disadvantages, such as corrosion, difficulty in handling the plates at the construction site, deterioration of bond at the steel-concrete interface, and restrictions on length of steel plate (Triantafillou and Plevris, 1991; Meier, 2000; Karbhari and Seible, 2000). In order to develop an alternative to bonding steel plates, the use of FRP composites for strengthening RC structures was first investigated at the Swiss Federal Laboratory for Materials Testing and Research (EMPA) where tests on RC beams strengthened with CFRP plates were conducted in 1984 (Meier, 1987; Meier and Kaiser, 1991; Meier and Deuring, 1992). From these early tests FRP composites are considered to be the most favoured material in many strengthening applications. A state-of-the-art paper was presented by Motavalli and Czaderski (2007), for strengthening existing civil engineering structures in Europe using the advanced polymer composites; discussed in this paper are existing techniques for flexural and shear strengthening, near surface mounting reinforcement as well as column confinement of RC structures. In addition, the prestressing techniques of FRP for the rehabilitation of existing structures are presented; this is a well-established market in Europe and the USA.

Unlike steel, FRP is unaffected by electrochemical deterioration and can resist the corrosive effects of acids, alkalis, salts and similar aggressive substances under a wide range of temperatures. In addition, they have high specific strength and can be tailored to performance requirements, by volume fraction and fibre orientation (Meier, 2000; Karbhari and Seible, 2000; Takács and Kanstad, 2000). Experimental studies conducted on both virgin and damaged beams strengthened with externally bonded FRP plates showed this technique to be very effective (Saadatmanesh and Ehsani, 1991; Meier and Kaiser, 1991; Ross *et al*., 1994). The increase in strength exhibited by beams strengthened with FRP plates can be as high as three

times their original capacity depending on the steel ratio, concrete strength, FRP ratio and FRP mechanical properties, the bonding agent properties and the existing level of damage to the beams.

CFRP composite strips and sheets are used for strengthening RC structural slabs by the externally bonded technique. This chapter will not be discussing this topic but the following references on this topic, are given: for initially unstressed CFRP strips, Shahawy and Beitelman (1999), Teng *et al*. (2002), Kotynia and Kaminska (2003) and Longworth *et al*. (2004); and for prestressed CFRP strips, Kotynia *et al*. (2011). Within the scope of rehabilitation of structures, it is essential that differentiation is made between 'repair', 'strengthening' and 'retrofit', terms which are often erroneously used when describing EPB. In 'repairing' a structure, the composite material is used to upgrade a structural or functional deficiency such as a crack or a severely degraded structural component. In contrast, the 'strengthening' of structures is specific to those cases wherein the addition or application of the FRP composite plate would enhance the existing design performance level, for instance to increase the load rating (or capacity) of a bridge superstructure through the application of composite plates to the soffit of the beams. The term 'retrofit' is specifically used to relate to the seismic upgrade of structures, such as the use of composite jackets for the confinement of columns, or the repair of a damaged beam.

16.6.1 The rehabilitation of RC bridge beams in flexure using unstressed FRP plates.

The strengthening of concrete structures by the technique of externally bonding FRP composites is now routinely considered a viable alternative to the rather costly replacement of these structures. Furthermore, the high strength-to-weight ratio and good corrosion resistance of FRP materials provide considerable advantages over that of steel for rehabilitation. Moreover, the effectiveness of flexural strengthening of RC beams with FRP is evident from the large database of experiments reported by Smith and Teng some 10 years ago (Smith and Teng, 2002).

The FRP composite plate material used for upgrading RC bridges is generally the high-modulus CFRP (the European definition), the AFRP (Kevlar 49) or the GFRP composite materials. These would be fabricated by one of four methods, namely:

1. The pultrusion technique, in which the factory-made rigid pre-cast FRP plate is bonded onto the degraded member on site with ambient cure adhesive polymer. The pultrusion method is described in Hollaway (2008) and Starr (2000).
2. The factory-made rigid fully cured FRP prepreg plate bonded to the degraded member on site with ambient cure adhesive polymer.

3. The factory-made cold-melt FRP prepreg and compatible adhesive film both of which are wrapped onto the structural member and cured simultaneously on site under 1 bar pressure and elevated temperature of 60°C for 16 hours or 80°C for 4 hours (Hollaway, 2008); the elevated temperatures on site would be realised by using a heat blanket. The site erection bonding/curing work takes no longer than that for methods 1 and 2.
4. The wet lay-up process, where the polymer matrix also acts as the adhesive of the upgrading composite (Hollaway, 2008).

The third method mentioned is superior to those of the precast plates and ambient cure adhesive systems, as the site compaction and cure procedure of the prepreg and film adhesive ensures a low void ratio in the composite and an excellent join to the concrete. The drawback to this method currently is the cost; it is about twice as expensive as the first two methods. The current preferred manufacturing system for upgrading is either the first or the second method. The implementation of either of these two methods means that:

- The plate material cannot be reformed to cope with any irregular geometries of the structural member, unlike method 3.
- A two-part, ambient cure epoxy adhesive is used to bond the plate onto the substrate. The ambient cured adhesive is the Achilles heel of the system, particularly if it is cured at a low ambient temperature and without post-cure. In this case the polymer may not be completely polymerised and therefore the durability of the composite may be affected.

The design procedures for the tensile flexural strengthening and the repair of RC members with FRP composites are analogous to the design of RC sections (Triantafillou and Antonopoulos, 2000; Täljsten, 2002; Teng *et al.*, 2003, 2008a, 2008b). Currently, strengthening the beam on its compressive side is not usually considered. When strengthening RC beams utilising FRP composites the design assumptions are:

- Plane sections remain plane after bending.
- There is complete bond to ensure complete composite action between materials.
- Cracked concrete retains no tensile strength.
- FRP composite is linear up to failure.

There are seven failure modes associated with FRP composite-strengthened RC members (Hollaway and Head, 2001), which should be considered during the design stage:

- Concrete crushing
- Yielding of the tensile reinforcing rebars
- Yielding of the compressive reinforcement

- FRP tensile failure
- Shear failure in concrete which initiates peel failure at the crack
- Peel failure at the termination of the plate due to high normal stresses to the plate. These will cause the plate to peel off towards the centre of the beam; this is known as end anchorage peel and will generally become a concrete cover separation.
- There are a number of other possible but unlikely modes of failure which have been identified in the literature such as delamination of the composite plate or of the area within the glue line, but these have not generally been experienced; the strength of these materials is higher than that of concrete and the failures will only happen if the installation has been poorly performed or there is a defect in the manufacture of the plate.

The flexural design procedure for a RC beam using FRP composites must consider the above possible failure modes. After designing for flexure a check on the shear capacity of the original beam design must be undertaken to confirm that this has not been exceeded. Further information regarding the failure modes for FRP composite strengthened RC members may be found in Hollaway and Head (2001), Hollaway and Leeming (1999) and Bank (2006).

There have been many research investigations during the last two decades to understand the behaviour of externally bonded FRP composites (Teng *et al.*, 2002; Chen and Teng, 2003; Prota *et al.*, 2004; Buyukozturk *et al.*, 2004; Barnes and Mays, 2006; Eyre *et al.*, 2006). Chen and Teng (2008) have also reviewed existing strength proposals and have highlighted their deficiencies. Resulting from these investigations there have been a number of design codes and design guidelines published covering this area, namely:

- ACI (2008a)
- CAN/CSA (2002)
- CAN/CSA (2006)
- CIDAR (2006)
- fib 9.3 'FRP (Fibre Reinforced Polymer) Reinforcement for Concrete Structures', the European task group. fib was one of the first to publish a guideline in the field of externally bonded reinforcement (fib, 2001). The fib TG 9.3 group forms part of Commission 9 'Reinforcing and Prestressing Materials and Systems'. The work of fib TG 9.3 is organised in two subgroups: (i) FRP reinforcement (RC/PC) and (ii) Externally bonded reinforcement (EBR). An updated bulletin of fib (2001) for EBR is being undertaken currently.
- BD 85/08, 'Strengthening Highway Bridges Using Externally Bonded Fibre Reinforced Polymer', Design Manual for Roads and Bridges, UK Highways Agency, May 2008.

- The design guidelines for FRP strengthened RC structures (Teng *et al.*, (2008b).
- ACI 440.2R-08: 'Guide for the Design and Construction of Externally Bonded FRP Systems for Strengthening Concrete Structures', American Concrete Institute, Farmington Hills, MI 48331.
- ISIS (2001), 'Strengthening Reinforced Concrete Structures with Externally-Bonded Fibre Reinforced Polymers', Design Manual, ISIS-M05-00, ISIS Canada.
- AASHTO – Manual for Condition Evaluation of Bridges – 1994, American Association of State Highway and Transportation Officials, Washington, DC, 2nd edition, 2000.
- AASHTO – Standard Specifications for Highway Bridges, American Association of State Highway and Transportation Officials, Washington, DC, 16th edition, 1996.
- American Association of State Highway and Transportation Officials, Washington, DC, 'Guide Specification and Commentary for Vessel Collision Design of Highway Bridges', 149 pp.

The ductility of a flexural member generally decreases as a result of strengthening, especially if the controlling failure mode is debonding or FRP rupture. To guarantee adequate ductility of a strengthened cross-section, the strain level of the internal steel reinforcement at ultimate should exceed the steel yield strain, as indicated by available design recommendations, for example, fib Task Group 9.3 (2007) and ACI 440.2R-08 (2008). ACI 440.2R-02 (2002) also suggests that the lower ductility should be compensated with a higher reserve of strength through the use of a lower overall strength reduction factor.

Canning (2011) has discussed the upgrading of the Minsterley Bridge, Shropshire, UK, which is a 101-year-old, Grade II listed structure carrying the main access road into Minsterley village over the Minsterley Brook. The 10 m span reinforced concrete arch bridge is an early example of the Hennebique system and was originally designed by Louis Gustave Mouchel. The original structure was assessed having a capacity of 7.5 tonnes live load in accordance with BD21/01; no weight restrictions were imposed. This bridge required an upgrade to HA loading.

Several proposals were investigated but the one that was finally accepted was replacement of the existing fill with a composite concrete saddle, and CFRP strengthening to the intrados of the arch to raise the structure to full HA loading. The proposal included the installation of a cathodic protection system to minimise the risk of steel reinforcement corrosion in the future, and replacement of the existing substandard parapets with new concrete parapets.

The strengthening system comprised a thin *in-situ* concrete saddle acting

compositely with the existing arch barrel with bespoke shear connectors, together with CFRP fabric and pultruded plates bonded to the arch intrados. Other associated repair/refurbishment works included passive cathodic protection, concrete repairs, highway and drainage works.

The CFRP strengthening comprised a transverse carbon fibre *in-situ* laminated fabric (to provide additional transverse flexural capacity), and after the installation of this fabric had been installed and cured, the surface cleaned and roughened, 112 pultruded CFRP plates were installed. Figure 16.5 shows the installation of the CFRP strengthening (plates and fabric) system to the arch intrados of Minsterley Bridge.

During the site operations test specimens including bulk adhesive samples and lap-shear samples were taken (the adhesive/resin tensile strength was greater than 15 MPa, the adhesive/resin tensile modulus was 2–10 GPa, the adhesive/resin glass transition temperature was greater than 55°C, and single lap-shear strength was greater than 8 MPa). It is noted that the bonding of the CFRP composite is to a curved concave surface; this is one of the first upgrading to a curved structure. It is similar to that undertaken in a research exercise by Eshwar *et al*. (2005).

Further information on the technique and analysis of rehabilitating RC bridge structures using FRP composites to reinforced concrete may be obtained from Hollaway and Leeming (1999), Teng *et al*. (2002, 2004), Oehlers and Seracino (2004), Anania *et al*. (2005), Pešić and Pilakoutas (2005), Lu *et al*. (2007), Hollaway and Teng (2008), Bogas and Gomes (2008), Parke and

16.5 Installation of CFRP strengthening (plates and fabric) to arch intrados, Minsterley Bridge. Image courtesy of Mouchel/SKM.

Hewson (2008), Forde (2009) and Hollaway and Chen (2009) and Wu *et al*. (2010).

16.6.2 The rehabilitation of PC bridge beams in flexure using unstressed FRP plates

Shanafelt and Horn (1980) reported that approximately 160 PC bridge overheight impacts were reported each year by transportation departments in the United States. Impact damage to PC girders can range from simple scrapes to large section loss and severed prestressing strands. Shanafelt and Horn (1980) also detailed information concerning damage evaluation and repair methods for PC bridges. One of the results of their work was a set of guidelines for inspectors and engineers to classify various levels of damage; they classified four different levels:

- Minor damage
- Moderate damage
- Severe damage
- Critical damage.

Feldman *et al*. (1996) developed another set of guidelines for classifying impact damage. They classified damage to PC girders on three different levels:

- Minor damage
- Moderate damage
- Severe damage.

Although there are many research articles and case studies addressing repair of PC bridge girders, there is little comprehensive guidance available for designers. The original and traditional PC repair methods outlined in Shanafelt and Horn (1980, 1985) have remained the most comprehensive US study to address the evaluation and repair of prestressed bridge members; the NCHRP Reports 226 (1985a) and 280 (1985b) sponsored by the AASHTO have incorporated their findings. The two basic methods for restoring prestressing force according to the two reports are internal splices and external post-tensioning. The first method involves internal strand splices using mechanical devices that consist of standard prestressing chucks and high-strength turnbuckles to restore the original prestressing force to the severed strands. After the splices are installed and fully tensioned, a preload (by hydraulic jacks) is applied to the beam followed by concrete repair. After the patch has attained sufficient strength the preload is removed. The second method involves post-tensioning with external tendons. This technique requires jacking corbels located outside the damage area. Traditional PC repair methods such as installation of internal splices, external post-tensioning,

and steel jacket systems have a number of disadvantages; they can be time consuming and are susceptible to corrosion. Another problem with internal splices and external post-tensioning is that it is possible for a piece of the patch to dislodge, causing damage to passing vehicles.

The above extant studies do not address the more recent rehabilitation methods, namely the application of composite materials which use CFRP and prestressed CFRP composites, which could be used to repair impact and corrosion damaged PC girders; the experimental data on full-scale PC girders strengthened by using FRP laminates are very limited. CFRP composites have been adopted in several practical cases, for instance (i) the Highway Appia near Rome, (ii) Bridge A10062, St Louis County, Missouri, and (iii) Bridge A5657, south of Dixon, Missouri. Nanni (1997), Nanni *et al*. (2001) and Parretti *et al*. (2003) have discussed cases where PC girders were accidentally damaged and restored to their original flexural strengths.

PC members are susceptible to steel strand fatigue and may require strengthening to prevent further loss of prestress (Hollaway and Leeming, 1999; Schiebel *et al*., 2001), Hassan and Rizkalla, 2002). Reed and Peterman (2004) showed that both flexural and shear capacities of a 30-year-old damaged prestressed concrete girder could be substantially increased with externally bonded CFRP composite sheets. They used CFRP U-wraps as shear reinforcement along the length of the girder to delay debonding failure.

Balaguru *et al*. (2009) have discussed the fundamentals and design of FRP for the repair and rehabilitation of reinforced and prestressed concrete structures. Kasan and Harries (2009) undertook experimental and analytical analyses on three prototype PC bridge girders of different sections, namely adjacent boxes, spread boxes and AASHTO-type I-girders, and having four different levels of damage. Twenty prototype repair designs were presented using five variants of CFRP-based repair systems. They concluded that whilst active repairs utilise the CFRP material efficiently, the difficulties in construction are more significant than the CFRP material savings. PC/CFRP repairs are potential alternatives to conventional external post-tensioned steel repairs, but are somewhat cumbersome to apply in the field.

Di Ludovico *et al*. (2010) experimentally tested five full-scale, PC I-sectioned girders with a reinforced concrete slab; their length and height were 13,000 mm and 1,050 mm respectively. Two beams simulated overheight vehicle damage and two simulated normally degraded beams. All were upgraded by utilising CFRP composite U-wraps and installed by using a wet manual lay-up technique. To obtain full bond the wraps were eventually anchored. This study was intended as an extension of a previous experimental work conducted by Di Ludovico *et al*. (2005) on three full-scale PC specimens. The authors concluded that the experimental outcome qualified the application of FRP technique as an effective tool to restore the flexural capacity of PC girders.

16.6.3 The rehabilitation of RC and PC bridge beams in flexure using stressed FRP plates

When bonding unstressed FRP composite plates to the soffit of RC or PC bridge beams in order to rehabilitate them, only about 25% of their ultimate strain capacity is used. In order to utilise their maximum strain to increase their efficiency, they have to be prestressed before being bonded; in this situation special consideration must be given to the transfer of shear stresses from the plate end to the concrete. The practical operation of bonding the FRP prestressed plates is not straightforward as each end of the plate has to be anchored; the prestressing operation is generally reacted against the beam which is being upgraded. During the Robust project (Hollaway and Leeming, 1999; Quantrill and Hollaway, 1998) a jacking system was developed for research purposes and this was further modified by Mouchel Consulting (now Sinclair Knight Merz (SKM)) for prestressing CFRP plates against RC, PC and steel beams. Technical papers were written by Saadatmanesh and Ehsani (1991), Triantafillou *et al*. (1992), Char *et al*. (1994) and Garden and Hollaway (1998) for upgrading RC beams, and El-Hacha *et al*. (2001) also undertook work on prestressed FRP plates to upgrade both RC and PC beams.

Prestressing the strips before they are bonded to RC or PC beams offers several advantages:

- Improving the serviceability conditions such as flexural crack control, reducing deflections at service load level and delaying the onset of yielding of the steel reinforcement
- Reducing the stress in the internal steel, and possibly increasing the fatigue resistance
- Increasing the upper range of the stress and strain.

In the investigations undertaken by Deuring (1993) and Hollaway and Leeming (1999) for RC beams, mechanical anchorages were used to transfer the prestress forces from the sheets to the concrete beams. Another method of undertaking this transfer without using anchors was developed and tested at EMPA, Switzerland (Meier *et al*., 2002); this method is known as the gradient end anchorage, in which the prestressing force in the CFRP plate is gradually transferred to the concrete; the force gradient is produced by sector-wise heating of the adhesive and a step-wise release of the force (Stöcklin and Meier, 2001, 2002, 2003; Meier and Stöcklin, 2005).

Czaderski and Motavalli (2007) reported on a 17-metre PC beam taken from a bridge in southern Switzerland which was subsequently flexurally strengthened for experimental investigations using prestressed CFRP plates; the prestressing level was 32%. The anchorage of the prestressed CFRP plates was undertaken by the ‘EMPA method’ of gradient end anchorage.

Thus no permanent anchorage was required and this method was found to be feasible.

The advantage of prestressed CFRP plates for strengthening of the beam are:

- Lower deflections
- Lower strains at top and bottom face of the girder due to loading
- Fewer cracks and/or crack widths
- Less debonding length between CFRP plates and concrete at mid-span
- Higher maximum load.

Aram *et al*. (2008) tested four PC beams to investigate the effectiveness of flexural post-strengthening with prestressed CFRP strips. Prestressing the strips caused no significant decrease in the deflection of beam and in crack width compared to an unstressed beam, but the failure load could not be increased, and the deformation ductility was smaller. The gradient anchorage method was not effective as the gradient was in the region of shear stresses from the superimposed load. The short beams resulted in high shear stresses between the CFRP strips and concrete in the shear span. It was concluded that this method would be more effective for large-span beams, and it was recommended that the sum of the initial and additional shear stress from loading between the CFRP strips and the concrete should be limited to the shear stress given in Approach 3 in fib (2001).

Lees and Winistörfer (2011) reviewed the non-laminated CFRP strap systems and their potential for the use of self-anchored FRP tension elements with a variety of civil engineering materials. It was shown that when the strap is non-laminated, as opposed to laminated, higher efficiencies can be achieved. Ascione *et al*. (2011) have discussed and produced a model for the long-term behaviour of PC beams externally plated with prestressed FRP composites. The studies have shown a marked influence of the composite viscous properties on the long-term behaviour of the PC elements strengthened with FRP composites. More specifically, a stress variation has been found in the case of AFRP composites characterised by a high sensitivity to creep phenomena. Motavalli *et al*. (2011) have reviewed the recent developments at EMPA; their paper focuses on the prestressing of FRP composite sheets bonded to RC beams, the developments in flexural and shear strengthening of beams and column confinement.

16.6.4 The flexural strengthening of RC bridge beams by the technique of Near Surface Mounted (NSM) FRP rods

An alternative technique to the externally bonded FRP composite plates and sheets is that of Near Surface Mounted (NSM) reinforcement. The

reinforcement used in the NSM technique is generally manufactured by the pultrusion method and is similar to that of FRP rebars; they can have circular or square cross-section. These reinforcing bars are embedded and bonded into grooves cut into the soffit of the beam; the adhesive used for bonding is a high-viscosity epoxy or cement paste. CFRP composite rebar materials are generally the most suitable material but GFRP and AFRP can be and have been used. The technique of NSM is applicable only if the cover to the internal steel rebars is sufficiently thick for the groove size to be accommodated. State-of-the-art reviews on NSM reinforcement are given by De Lorenzis and Teng (2007) and Badawi (2007). NSM reinforcement can significantly increase the flexural capacity of RC beams as reported by De Lorenzis *et al*. (2002) and El-Hacha and Rizkalla (2004); the degree of bonding of the FRP rods into the grooves may be the limiting factor on the efficiency of this technology (Kotnia, 2006). However, to achieve a superior bond it is possible for the reinforcement to be anchored to adjacent members. The advantages of the (NSM) FRP technique are:

- The opportunity exists for upgrading elements in their negative moment region.
- The reinforcement is not exposed to potential mechanical damage typical of floor or deck systems.
- The (NSM) FRP technique does not require extensive surface preparation work and after the groove has been cut there is minimal installation time compared with the externally bonded FRP composites.
- The NSM reinforcement technology has a great advantage in seismic retrofit of RC column–beam joints, thus providing additional strength or ductility when transferring the failure zone from the column to the beam (Prota *et al*., 2001).
- The rods are protected from the external environments in that they are completely surrounded in adhesive paste. This assumes that concrete structures which have alkaline or other salts in the cements will not attack the paste; consequently, the rods will not be affected by the alkaline-initiated corrosion in a concrete environment.

As with FRP plated flexural beams, NSM reinforcement may be prestressed prior to anchoring and bonding to the concrete beam. The main advantage of the NSM prestressing technique is to improve serviceability conditions such as flexural crack control, to reduce defections at service load levels and to delay the onset of yielding steel reinforcement. Nordin and Täljsten (2006) applied a NSM prestressed system to RC beams using an external anchor system; the prestressing level was within the 10–27% level of the ultimate strength of the rebar rod; the latter were not anchored. They found that the ultimate load-carrying capacity and the serviceability were greatly improved and that the force transfer from the FRP rebar to the structure was

satisfactory. Jung *et al*. (2007) tested prestressed NSM beams with anchors at levels of 20% of the ultimate strength of the CFRP and compared the test results to non-prestressed beams. The authors concluded that the prestressed beams increased the cracking load and the stiffness; consequently, premature debonding failure could be prevented. Gaafer and El-Hacha (2007) and Badawi (2007) also found that serviceability and the ultimate load-carrying capacity were improved by increasing the level of the prestressing force. Choi *et al*. (2011) studied the effect of partial debonding of the CFRP reinforcement on the flexural behaviour of a Tee beam; the variables were the level of prestressing force in the CFRP bars and the unbonded length at mid-span. They concluded that all the prestressed strengthened beams effectively improved the ultimate load-carrying capacity and the serviceability performance compared with the unstrengthened beam. The deformability index μ (defined as the ratio of the ultimate deflection δ_u to the deflection at steel yield δ_y) of the fully bonded beams and the partially bonded beams were 2.60 and 3.67 respectively. The improvement provided by partial debonding was more effective at higher levels of prestressing force.

16.7 FRP rebars/grids and tendons as an alternative to steel for reinforcing concrete beams in highway bridges

FRP reinforcements for structural concrete members are used in two areas:

1. FRP rebars or grids for reinforcing concrete.
2. FRP tendons for prestressed concrete.

16.7.1 FRP rebars or grids for reinforcing concrete

The material has many advantages over the conventional structural steel. When structural members are exposed to aggressive environmental combinations of moisture, temperature and chlorides the alkalinity of the concrete is reduced; this combination of attack together with freeze–thaw and de-icing salts on the steel through cracks in the concrete will result eventually in the corrosion of the steel reinforcement and a loss of structural serviceability. To overcome these corrosion problems the use of FRP composite rebars would be an advantageous option; but the composite material intrinsically lacks ductility. The main reason for the use of FRP bars in some countries (such as the United Kingdom, Northern Europe, Northern USA, Canada and Switzerland) in bridge decks and highway structures is due to the seasonal use of de-icing salts. A review of the practical application of FRP rebars can be found in Rizkalla and Nanni (2003).

The FRP rebars are generally manufactured by the pultrusion technique from thermosetting resins such as continuous carbon, glass or aramid fibres embedded in polyester, vinylester or epoxy matrix (Nanni, 1997; ACI, 1996; Pilakoutas, 2000; Bank, 2006). Their geometric cross-sections are typically round, square or rectangular and have smooth surfaces; these must be modified to improve the bond characteristics between the concrete and the rebar. The improvements in bond characteristics are effected by forming:

- Ribbed bars – manufactured from a combination of a pultrusion and compression moulding method.
- Sand-blasted bars – manufactured by applying a sand-blasted finish to the pultrusion.
- Spirally wound and sand-coated bars – manufactured by spirally winding the pultrusion rod with a sand-coated fibre tow.
- Applying a peel-ply to the surface of the pultruded bar during the manufacturing process; the peel-ply is removed before encasing the bar with concrete, thus leaving a rough surface on the pultruded rod.

Other systems for improving the bond between the FRP composite and concrete are given in Pilakoutas (2000).

Features and benefits of using FRP rebars are as follows:

- Non-corrosive – it will not corrode when exposed to a wide variety of corrosive elements including chloride ions and it is not susceptible to carbonation-initiated corrosion in a concrete environment.
- Non-conductive – it provides good electrical and thermal insulation.
- Fatigue resistance – it performs well in cyclic loading situations.
- Impact resistance – it resists sudden and severe point loading.
- Magnetic transparency – it is not affected by electromagnetic fields.

16.7.2 FRP tendons for prestressed concrete

FRP composite tendons have been proposed as an alternative to steel tendons in post-tensioning applications. A number of studies have been undertaken into the rehabilitation of prestressed concrete (PC) and cable stay bridges utilising prestressing bars and tendons manufactured from FRP composites (Arockiasamy *et al.*, 1996; Fam *et al.*, 1997; Shehata *et al.*, 1997; Rizkalla *et al.*, 1998; Grace (1999, 2000); Lu *et al.*, 2000). Burke and Dolan (2001) undertook experimental studies on certain Canadian precast concrete bridges that had been upgraded using prestressed FRP composite tendons and presented the advantages of this system for upgrading. Nordin (2004) has reviewed a number of existing concrete bridge girders which have been rehabilitated and strengthened with external FRP tendons. FRP composites are weak in the transverse direction; therefore they are highly vulnerable to premature

failure at the anchor zone if any notching in the tendon occurs during the post-tensioning process or during service.

16.8 Seismic retrofit of columns and shear strengthening of RC bridge structures

16.8.1 Seismic retrofit of columns

Performance of bridges during earthquakes has demonstrated that many structural failures could be attributed to inadequate seismic design of bridge columns. Lack of transverse reinforcement and splicing of longitudinal reinforcement in potential hinge regions constitute the primary reasons for poor performance. Whilst it is not financially feasible to replace all deficient bridges with seismically critical columns, it is possible to retrofit them with fibre-reinforced polymer jackets. FRP jackets provide additional shear capacity, confinement of the compression concrete and improved bond between the steel and concrete, enhancing column performance in all three areas of design deficiency. The material generally used for column jacketing consists of continuous carbon fibre prepreg tows which have extremely low weight-to-strength ratios, high elastic modulus values, resistance to corrosion and ease of application. The main purpose of seismic retrofit of RC columns is to achieve a sufficient level of deformation ductility to dissipate seismic energy before one of the failure modes becomes critical. Unidirectional CFRP wrapping can improve column ductility without excessive stiffness amplification, thereby maintaining the bridge dynamic properties (Haroun and Elsanadedy, 2005). FRP-confined concrete models have been developed; extensive reviews of the literature on FRP-confined concrete have been undertaken (Lam and Teng, 2002; Teng *et al*., 2002). Most of these models are empirical in nature and employ best-fit expressions. Other analytical models (Binici, 2005; Kazunori *et al*., 2004; Spoelstra and Monti, 1999) define the axial and lateral stress–strain relationships of concrete for different levels of confinement. A state-of-the-art for the repair and strengthening techniques for reinforced concrete beam–column joints can be found in Engindeniz *et al*. (2005).

FRP retrofit systems can be effective for both circular and rectangular columns. Circular jackets provide the column with a continuous confinement pressure, whilst rectangular jackets only provide confinement pressure at the corners of the column. In such cases to avoid stress concentrations at these points, Seible *et al*. (1995), in their Advanced Composites Technology Transfer Consortium, Report No. ACTT-95/08, have suggested the use of oval-shaped FRP jackets in design; these can be expected to prevent slippage of lapped bars within the retrofitted region. Columns with oval-shaped FRP composite material produce ductile column performance. The FHWA (January

2006) has provided design guidelines for application to circular columns; ACI 440 (2006) uses similar equations to the FHWA guidelines but applies additional safety factors. The International Federation for Structural Concrete (fib) (2006) produced a bulletin for the retrofitting of concrete structures by externally bonded FRPs, with emphasis on seismic applications.

Choi *et al*. (2011) have reviewed and studied the problems of old Korean bridges in areas of frequent seismic disturbance. The bridges were constructed with plain concrete gravity piers which support an open steel plate girder (OSPG); the concrete piers have now developed severe corrosion degradation. Some of the bridges were built in the period between the 1910s and the 1930s, and the overturning problem together with the tensile cracking of concrete piers have caused problems; a cold joint at half the height of the piers also adds to the cracking due to the tensile stresses introduced by lateral loading such as the braking of traffic or from seismic loading. The possibility of pier-overturning due to lateral loading is high as the piers are not founded on piles. The problem of overturning of the columns was solved by introducing an anchoring system using prestressed strands situated at the base of the pier and anchored to the bedrock or equivalent beneath. The problem of concrete cracking was investigated by utilising several seismic retrofit methods. Three confinement techniques were considered: the use of (1) steel, (2) FRP composites, and (3) Shape Memory Alloy (SMA) wire jackets. Choi *et al*. (2008, 2010) had investigated the possibility of using the SMA technique to confine concrete; it was shown to be effective. However, the three independent methods were not appropriate for plain concrete piers supporting OSPG bridges as the piers required reinforcement in the longitudinal direction as well as in the lateral one. The final solution was to fabricate a 'sandwich' plate made from FRP composites as the face materials and a steel sheet as the core material. The bending retrofit with the sandwich systems provided an effective retrofit system for the plain concrete piers.

16.8.2 Shear strengthening of RC bridge structures

When a beam is flexurally strengthened, it may be necessary also to increase its shear capacity; this may be undertaken effectively by FRP composites. Since the beginning of the 1990s many research studies on shear strengthening of RC beams have been undertaken using FRP composites (Uji, 1992; Al-Sulaimani *et al*., 1994; Chaallal *et al*., 1998; Triantafillou, 1998; Khalifa *et al*., 1998; Khalifa and Nanni, 2000; Pellegrino and Modena, 2002; Chen and Teng, 2001, 2003; Monti and Liotta, 2003; Zhang *et al*., 2004; Bousselham and Chaallal, 2008; Hollaway and Teng, 2008). Resulting from these studies several design equations and analytical models have been developed and have been implemented into code format to predict the shear contribution of externally bonded FRP composites. Nevertheless, there remain major

parameters relating to shear strengthening that have not yet been solved by existing theoretical predictive tools, including the codes and guidelines (Bousselham and Chaallal, 2008), for instance:

- The existing design codes assume that the FRP effective strain remains constant whether the RC beam has transverse steel or not. However, Chaallal *et al*. (2002), Pellegrino and Modena (2002) and Bousselham and Chaallal (2004) have shown that the contribution of the FRP composites to the shear resistance (i.e. the effective strain) of the beam decreases as the internal steel-reinforcement ratio increases.
- A number of debonding models have been developed and have been incorporated into design guidelines (ACI, 2008; CAN/CSA, 2006), but Holzenkämpfer (1994), Neubauer and Rostásy (1997) and Chen and Teng (2001) had undertaken theoretical studies on bond models and a question is now raised, 'how well do the results of these bond models compare with the predictions of the debonding models?'

Lees *et al*. (2002) proposed a system which used carbon fibre reinforced thermoplastic tape straps as external post tensioned shear reinforcement for concrete. The tape was thin (typically between 0.12 and 0.16 mm thick) and was composed of high strength carbon fibres oriented in the longitudinal direction. It was shown that a concrete beam strengthened with CFRP straps exhibited a significantly higher load capacity than an unstrengthened beam. This system has been further studied by Yapa and Lees (2009) by investigating the optimum shear strengthening of reinforced concrete beams with prestressed CFRP straps.

Mofidi and Chaallal (2011) have discussed shear strengthening of RC beams with externally bonded FRP composites; their paper also reviews the design provisions of the latest versions of the major design guidelines related to shear strengthening of RC beams with FRP, which are:

- CAN/CSA-S6 (2006) (this Canadian Highway Bridge Design Code has adopted design provisions similar to those in ACI 440 2R-08(2008))
- fib-TG 9.3 (2001) (based on the regression of experimental results carried out by Triantafillou and Antonopoulos, 2000)
- ACI 440.2R (2008) (based on a research study by Khalifa *et al*., 1998)
- CNR-DT200 (2004) (the Italian guidelines are based on a research study by Monti and Liotta, 2003)
- CIDAR (2006) (the Australian guidelines are based on a research study carried out by Chen and Teng, 2003).

Hollow bridge piers, particularly those built before the 1970s, often have insufficient shear capacity due to inadequate transverse reinforcement. Consideration must be given to this aspect when RC piers with hollow

sections are rehabilitated. Delgado *et al*. (2012) undertook experimental cyclic shear failure tests and design procedures for the rehabilitation of square hollow piers using CFRP sheets along their entire height. Various transverse reinforcement detailing scenarios were assessed to determine their shear-failure efficiency. It was shown that shear rehabilitation developed a 40% increase over the original flexural column load with satisfactory ductile behaviour.

16.9 Conclusion and future trends

This chapter and Chapter 17 review advanced polymer composites in bridge engineering and cover many aspects for the utilisation of this material within bridge engineering infrastructure. It is suggested that the reader refers to Section 17.6 of Chapter 17 which covers the future trends of fibre-reinforced polymer composites used in all types of bridge engineering.

16.10 Sources of further information and advice

Regulatory/trade/professional bodies

1. *CEN-TC250* – EUR 22864 EN, 2007 – http://eurocodes.jrc.ec.europa.eu
2. *European Organisation for Technical Approvals* (EOTA): Discussions between the European Commission Joint Research Centre (JRC) and EOTA, on the works for new codes and standards regarding the use of FRP composites in civil engineering.
3. Industrial organisations:
   - *European Construction Technology Platform* (ECTP).
   - *European Composites Industry Association* (EuCIA).
     The JRC has contacted both the above organisations with a view to ensuring that their main concerns and needs are addressed by any proposed standards.
   - *The Directorate General Enterprise and Industry* (DG ENTR) of the European Commission in 2005 committed the JRC to assist in the implementation, harmonisation and further development of the Eurocodes. This will enable the European composites industry to be more aware of the impact that new Eurocodes, specifically tailored for FRPs, would have on their core business.

Professional bodies

The following is based upon the Network Group for Composites in Construction (NGCC), 11 May 2012.

1. *Composites UK*. The mission of Composites UK, as the representative body of the UK composites industry, is to promote the use of composite materials to the widest market spectrum.
2. *British Composites Society* (BCS). This is one of the technical arms of the Institute of Materials, Minerals and Mining. The British Composites Society provides a focus for the exchange of knowledge on all aspects of composite materials. It is a national contact point for communication with similar bodies on a worldwide basis.
3. *The Institute of Materials*, *Minerals and Mining* (IOM3), recognised by the UK's Privy Council on 26 June 2002. It was created from the merger of The Institute of Materials (IOM) and The Institution of Mining and Metallurgy (IMM). The Institute is potentially the leading international professional body for the advancement of materials, minerals and mining to governments, industry, academia, the public and the professions.
4. *International Institute for FRP in Construction* (IIFC). The aim of the Institute is to advance the understanding and the application of FRP composites in the civil infrastructure, in the service of the engineering profession and society.
5. *Welsh Composites Consortium* (WCC). The consortium acts as a Technology Transfer Network consisting of a number of partner organisations with a wide range of expertise in the field of composites, particularly to SMEs in Wales in the form of advisory visits.
6. *Construction Industry Research and Information Association* (CIRIA).
7. *The Italian Association for Composites in Construction* (AICO). AICO was formed in 1996. It is active in the field with membership from industry and universities.
8. *European Composites Industry Association* (EuCIA). The primary goal of EuCIA is to unite the composites industry at European level into one single European association.
9. *COBRAE*. The objective of COBRAE is to promote research, development, standardisation and application of fibre reinforced polymer composites in rehabilitation, upgrade and new build bridge constructions and infrastructure applications.
10. *European Construction Technology Platform* (ECTP). It is hoped that the ECTP will raise the sector to a higher world-beating level of performance and competitiveness. This will be achieved by analysing the major challenges that the sector faces in terms of society, sustainability and technological development. Research and innovation strategies will be developed to meet these challenges, engaging with and mobilising the wide range of leading skills, expertise and talent available to us within our industry over the coming decades, in order to meet the needs of society.

11. *Intelligent Sensing for Innovative Structures* (ISIS), Canada.
12. *Canadian Association for Composite Structures* (CACS). The CACS is a network of individuals and corporate members (suppliers, fabricators, equipment manufacturers, distributors, consultants, technologists, research centres, materials specialists, researchers, teachers, and government employees) working to develop and enhance new and existing applications for composite structures and materials.

16.11 References

AASHTO (1994), 'Standard Specifications for Structural Supports for Highway Signs, Luminaires and Traffic Signals', American Association of State Highway and Transportation Officials, Washington, DC.

AASHTO (1996), 'Standard Specifications for Highway Bridges', 16th edn, American Association of State Highway and Transportation Officials, Washington, DC.

AASHTO (2002), 'Standard Specifications for Highway Bridges', 17th edn, American Association of State and Highway Transportation Officials, Washington, DC.

AASHTO LRFD (2004), 'Bridge Design Specifications', 3rd edn, American Association of State Highway and Transportation Officials, Washington, DC.

ACI, American Concrete Institute (1996), ACI 440R 1996, 'State-of-the-art Report on Fiber Reinforced Plastic Reinforcement for Concrete Structures', Committee 440, American Concrete Institute, Farmington Hills, MI.

ACI, American Concrete Institute (2002), ACI 440.2R-02, 'Guide for the Design and Construction of Externally Bonded FRP Systems for Strengthening Concrete Structures', Committee 440, American Concrete Institute, Farmington Hills, MI.

ACI, American Concrete Institute (2008a), ACI 318-08, 'Building Code Requirements for Structural Concrete and Commentary', American Concrete Institute, Farmington Hills, MI.

ACI, American Concrete Institute (2008b), ACI 440.2R-08, 'Guide for the Design and Construction of Externally Bonded FRP Systems for Strengthening Concrete Structures', Committee 440, American Concrete Institute, Farmington Hills, MI.

ACI, American Concrete Institute (2006), ACI 440 2006, 'The Seismic Retrofit of Columns', Committee 440, American Concrete Institute, Farmington Hills, MI.

Alampalli, S. (2006), 'Field performance of an FRP slab bridge', *Composite Structures*, Vol. 72, Issue 4, pp. 494–502.

Alampalli, S. and Kunin, J. (2002), 'Rehabilitation and field testing of an FRP bridge deck on a truss bridge', *Composite Structures*, Vol. 57, Issues 1–4, pp. 373–375.

Alampalli, S. and Kunin, J. (2003), 'Load testing of an FRP bridge deck on a truss bridge', *Applied Composite Materials*, Vol. 10, Issue 2, pp. 85–102.

Al-Sulaimani, G. J., Sharif, A. M., Basunbul, I. A., Baluch, M. H. and Ghaleb, B. N. (1994), 'Shear repair for reinforced concrete by fiberglass plate bonding', *ACI Structural Journal*, Vol. 91, Issue 3, pp. 458–464.

Anania, L., Badala, A. and Failla, G. (2005), 'Increasing the flexural performance of RC beams strengthened with CFRP materials', *Construction and Building Materials*, Vol. 19, Issue 1, pp. 55–61.

Aram, M. R., Czaderski C. and Motavalli, M. (2008), 'Effects of gradually anchored prestressed CFRP strips bonded on prestressed concrete beams', *Journal of Composites for Construction*, *ASCE*, Vol. 12, Issue 1, pp. 25–34.

Arockiasamy, M., Shahawy, M.A., Sandepudi, K. and Zhuang, M. (1996), 'Application of high strength composite tendons in prestressed concrete structures', *Proceedings of the First International Conference on Composites in Infrastructure: Fiber Composites in Infrastructure*, University of Arizona, Tucson, AZ, pp. 520–535.

Ascione, L., Berardi, V. P. and D'Aponte, A. (2011), 'Long-term behavior of PC beams externally plated with prestressed FRP systems: A mechanical model', *Composites Part B: Engineering*, Vol. 42, Issue 5, pp. 1196–1201.

Badawi, M. (2007), 'Monotonic and fatigue flexural behaviour of RC beams strengthened with prestressed NSM CFRP rods', PhD thesis, University of Waterloo, Waterloo, Ontario, Canada.

Balaguru, P., Nanni, A. and Giancaspro, J. (2009), *FRP Composites for Reinforced and Prestressed Concrete Structures: A Guide to Fundamentals and Design for Repair and Retrofit,* Taylor & Francis, New York.

Bank, L. C. (2006), *Composites for Construction: Structural Design with FRP Materials*, John Wiley & Sons, Hoboken, NJ.

Barnes, R. A. and Mays, G. C. (2006), 'Strengthening of reinforced concrete beams in shear by the use of externally bonded steel plates: Part 1 – Experimental programme', *Construction and Building Materials*, Vol. 20, Issue 6, pp. 396–402.

BD 21/01, *The Assessment of Highway Bridges and Structures*, Design Manual for Roads and Bridges, The Highways Agency, 2001.

BD 37 or 38/88, *Loads for Highway Bridges*, Design Manual for Roads and Bridges, HMSO, London, 1988.

BD 67/96, *Bridge Enclosures*, *Highway Structures: Design (Substructures and Special Structures) Materials*, Volume 2, Section 2, Parts 7 and 8, 1996.

BD 85/08, *Strengthening Highway Bridges using Externally Bonded Fibre Reinforced Polymer*, Design Manual for Roads and Bridges, The Highways Agency, 2008.

BD 90/05, *Design of FRP Bridges and Highway Structures*, Design Manual for Roads and Bridges, Vol. 1, Section 3, Part 17, 2005.

Berg, A. C., Bank, L. C., Oliva, M. G. and Russell, J. S. (2006), 'Construction and cost analysis of an FRP reinforced concrete bridge deck', *Construction and Building Materials*, Vol. 20, pp. 515–526.

Binici, B. (2005), 'An analytical model for stress–strain behaviour of confined concrete', *Engineering Structures*, Vol. 27, Issue 7, pp. 1040–1051.

Bogas, J. A. and Gomes, A. (2008), 'Analysis of the CFRP flexural strengthening reinforcement approaches proposed in fib bulletin 14', *Construction and Building Materials*, Issue Vol. 22, 10, pp. 2130–2140.

Bousselham, A. and Chaallal, O. (2004), 'Shear strengthening reinforced concrete beams with fiber-reinforced polymer: Assessment of influencing parameters and required research', *ACI Structural Journal*, Vol. 101, Issue 2, pp. 219–227.

Bousselham, A. and Chaallal, O. (2008), 'Mechanisms of shear resistance of concrete beams strengthened in shear with externally bonded FRP', *Journal of Composites for Construction*, Vol. 12, Issue 5, pp. 499–512.

Burgoyne, C. J. (1992), 'Aramid fibres for civil engineering applications', in *Construction Materials Reference Book*, ed. D. K. Doran, Butterworths, Oxford, UK.

Burke, C. R. and Dolan, C. W. (2001). 'Flexural design of prestressed concrete beams using FRP tendons', *PCI Journal*, Vol. 46, Issue 2, pp. 76–87.

Buyukozturk, O., Gunes, O. and Karaca, E. (2004), 'Progress on understanding debonding problems in reinforced concrete and steel members strengthened using FRP composites', *Construction and Building Materials*, Vol. 18, pp. 9–19.

CAN/CSA (2002), 'Design and construction of building components with fiber-reinforced polymer', S806-02, Canadian Standards Association, Rexdale, Ontario, Canada.

CAN/CSA-S6 (2006), 'Canadian highway bridge design code', S6–06, Canadian Standards Association, Mississauga, Ontario, Canada.

Canning, L. (2008), 'Mount pleasant FRP bridge deck over M6 motorway', *Proceedings of the 4th International Conference on FRP Composites in Civil Engineering (CICE 2008)*, 22–24 July 2008, Zurich, Switzerland, pp. 243–249.

Canning, L. (2011), 'Minsterley Bridge strengthening using novel methods', *Proceedings of ACIC 2011*, 6–8 September 2011, University of Warwick, UK, pp. 21–29.

Canning, L., Speight, N., Stephens, R. and Dobson, Y. (2009), 'Calder Viaduct FRP re-decking', *Fourth International Conference on Advanced Composites in Construction (ACIC 2009)*, 1–3 September 2009, University of Edinburgh, Edinburgh, Scotland, pp. 127–134.

Chaallal, O., Nollet, M. J. and Perraton, D. (1998), 'Strengthening of reinforced concrete beams with externally bonded fiber-reinforced-plastic plates: Design guidelines for shear and flexure', *Canadian Journal of Civil Engineering*, Vol. 25, Issue 4, pp. 692–704.

Chaallal, O., Shahawy, M. and Hassan, M. (2002), 'Performance of reinforced concrete T-girders strengthened in shear with CFRP fabrics', *ACI Structural Journal*, Vol. 99, Issue 3, pp. 335–343.

Char, M. A. S., Saadatmanesh, H. and Ehsani, M. R. (1994), 'Concrete girders externally prestressed with composite plates', *PCI Journal*, May–June 1994, pp. 128–134.

Chen, J. F. and Teng, J. G. (2001), 'Anchorage strength models for FRP and steel plates bonded to concrete', *Journal of Structural Engineering*, Vol. 127, Issue 7, pp. 784–791.

Chen, J. F. and Teng, J. G. (2003), 'Shear capacity of FRP-strengthened RC beams: FRP debonding', *Construction and Building Materials*, Vol. 17, Issue 1, pp. 27–41.

Chen, J. F. and Teng, J. G. (2008), 'Shear strengthening of reinforced concrete (RC) beams with fibre-reinforced polymer (FRP) composites', in *Strengthening and Rehabilitation of Civil Infrastructures Using Fibre-reinforced Polymer (FRP) Composites*, eds L. C. Hollaway and J. G. Teng. Woodhead Publishing in Materials, Cambridge, UK.

Choi, E., Nam, T. H., Cho, S. C., Chung, Y. S. and Park, T. (2008), 'The behaviour of concrete cylinders confined by shape memory alloy wires', *Smart Materials and Structures*', Vol. 17, pp. 1–10.

Choi, E., Chung, Y. S., Choi, J. H., Kim, H. T. and Lee, H. (2010), 'The confining effectiveness of NiTiNb I and NiTi SMA wire jackets for concrete', *Smart Materials and Structures*, Vol. 19, pp. 1–8.

Choi, H. T.,West, J. S. and Soudki, K. A. (2011), 'Effect of partial unbonding on prestressed near-surface-mounted CFRP-strengthened concrete T-beams', *Journal of Composites for Construction*, Vol. 15, pp. 93–102.

Choudalakis, G. and Gotsis, A. D. (2009), 'Permeability of polymer/clay nanocomposites: A review', *European Polymer Journal*, Vol. 45, Issue 4, pp. 967–984.

CIDAR (2006), 'Design guideline for RC structures retrofitted with FRP and metal plates: Beams and slabs', Draft 3 – Submitted to Standards Australia, University of Adelaide, Australia.

CNR-DT 200 (2004), 'Guide for the Design and Construction of Externally Bonded FRP Systems for Strengthening Existing Structures', CNR, Rome (13 July).

Composite Advantage Newsletter (2008), 'Composite Advantage builds new drop-in-place FRP superstructure', press release, 1 May 2008.

Czaderski, C. and Motavalli, M. (2007), '40-year-old full-scale concrete bridge girder strengthened with prestressed CFRP plates anchored using gradient method', *Composites Part B: Engineering*, Vol. 38, pp. 878–886.

Daly, A. F. and Duckett, W. G. (2002), 'The design and testing of an FRP highway bridge deck', *Proceedings of the Advanced Polymer Composites for Structural Applications in Construction (ACIC 2002)*, 20–22 April 2003, University of Surrey, Guildford, UK, eds L. C. Hollaway, M. K. Chryssanthopolus and S. J. Moy. Woodhead Publishing, Cambridge, UK, pp. 483–492.

Davalos, J. F. and Qiao, P. (2001), 'Modeling and characterization of fiber-reinforced plastic honeycomb sandwich panels for highway bridge applications', *Composite Structures*, Vol. 52, Issues 3–4, pp. 441–452.

Dawson, D. G. and Farmer, N. S. (2009), 'Replacement FRP bridge deck for vehicle loading', *Proceedings of the ICE – Engineering and Computational Mechanics*, Vol. 162, Issue 3, pp. 141–144.

Delgado, P., Arêde, A., Pouca, N. V., Rocha, P., Costa, A. and Delgado, R. (2012), 'Retrofit of RC hollow piers with CFRP sheets', *Composite Structures*, Vol. 94, Issue 4, pp. 1280–1287.

De Lorenzis, L. and Teng, J. G. (2007), 'Near-surface mounted reinforcement: an emerging technique for structural strengthening', *Composites Part B: Engineering*, Vol. 38, Issue 2, pp. 119–143.

De Lorenzis, L., Micelli, F. and La Tegola, A. (2002), 'Passive and active near surface mounted FRP rods for flexural strengthening of RC beams', *Proceedings of the International Conference on Fibre Composites in Interface – ICCI-02*, 10–12 June 2002, San Francisco, CA (CD ROM).

Deuring, M. (1993), 'Verstärken von Stahlbeton mit gespannten Faserverbundwerkstoffen [Strengthening of reinforced concrete using prestressed FRP]', Diss. ETH No. 10199, EMPA Bericht Nr. 224, Empa Dübendorf, 279 (in German).

Di Ludovico, M., Nanni, A., Prota, A. and Cosenza, E. (2005), 'Repair of bridge girders with composites: Experimental and analytical validation', *ACI Structural Journal*, Vol. 102, Issue 5, pp. 639–648.

Di Ludovico, M., Prota, A., Manfredi, G. and Cosenza, E. (2010), 'FRP strengthening of full-scale PC girders', *Journal of Composites for Construction*, Vol. 14, Issue 5, pp. 510–520.

El-Hacha, R. and Rizkalla, S. H. (2004), 'Near-surface-mounted fibre-reinforced polymer reinforcements for flexural strengthening of concrete structures', *ACI Structural Journal*, Vol. 101, Issue 5, pp. 717–726.

El-Hacha, R., Green, M. and Wight, G. (2001), 'Experimental and analytical investigation of concrete beams post-strengthened with prestressed carbon fibre reinforced polymer sheets', *9th International Conference and Exhibition*, 4–6 July 2001, London.

Engindeniz, M., Kahn, L. F. and Zureick, A.-H. (2005), 'Repair and strengthening of beam-column joints: State-of-the-art', *ACI Structural Journal*, Vol. 102, Issue 2, pp. 1–14.

Eshwar, N., Ibell, T. and Nanni, A. (2005), 'Effectiveness of CFRP strengthening on curved soffit RC beams', *Advances in Structural Engineering*, Vol. 8, Issue 1, pp. 55–68.

Eyre, J. M., Ibell, T. J. and Nanni, A. (2006), 'Strengthening choices for the repair and retrofit of concrete bridge structures with FRP', *Proceedings of the International Institute for FRP in Construction (IIFC)*, *CICE 2006*, 13–15 December 2006, Miami, FL, pp. 623–626.

Fam, A. Z., Rizkalla, S. H. and Tadros, G. (1997), 'Behaviour of CFRP for prestressing

and shear reinforcements of concrete highway bridges', *ACI Structural Journal*, Vol. 94, Issue 1, pp. 77–86.

Feldman, L. R., Jirsa, J. O., Fowler, D. W. and Cassasquillo, R. L. (1996), 'Current practice in the repair of prestressed bridge girders', Research Report 1370-1, University of Texas at Austin, June 1996.

FHWA (January 2006), *Seismic Retrofitting Manual for Highway Structures: Part 1 – Bridges*, Federal Highway Administration, Washington, DC.

fib (2001), 'Externally bonded FRP reinforcement for RC structures', Bulletin 14, TG 9.3, International Federation for Structural Concrete, Lausanne, Switzerland.

fib (2006), 'Retrofitting of concrete structures by externally bonded FRP's, with emphasis on seismic applications', Bulletin 35, International Federation for Structural Concrete, Lausanne, Switzerland.

fib Task Group 9.3 (2007) homepage: http://www.labomagnel.ugent.be/fibTG9.3/.

Flemming, C. J. and King, G. E. M. (1967), 'The development of structural adhesives for three original uses in South Africa', *Proceedings of RILEM Symposium on Resins in Building Construction*, Paris, September 1967, pp. 75–92.

Forde, M. (ed.), (2009), *ICE Manual of Construction Materials*, Vols I and II, Thomas Telford, London.

Gaafer, M. A. and El-Hacha, R. (2007), 'Prestressing concrete beams using NSM FRP technique', *Proceedings of the 8th International Symposium on Fibre-Reinforced Polymer Reinforcement for Concrete Structures (FRPRCS-8)*, Patras, Greece, 16–18 July 2007 (CD-Rom, 8p).

Garden, H. N. and Hollaway, L. C. (1998), 'An experimental study of the failure modes of reinforced concrete beams strengthened with prestressed carbon fibre composite plates', *Composites: Part B Engineering*, Vol. 29, Issue 4, pp. 411–424.

GFRP road bridge (2008), 'An operational response to ageing infrastructure', *EC Composites Magazine*, November/December 2008, no. 45, p. 64.

Giannopoulos, I. P. (2009), 'Creep and creep–rupture behaviour of aramid fibres', PhD thesis, University of Cambridge, UK.

Grace, N. F. (1999), 'Continuous CFRP prestressed concrete bridges', *Concrete International*, Vol. 21, Issue 10, pp. 42–47.

Grace, N. F. (2000), 'Transfer length of CFRP/CFCC strands for double-T girders', *PCI Journal*, Vol. 45, Issue 5, pp 110–126.

Hackman, I and Hollaway, L. C. (2006), 'Epoxy-layered silicate nanocomposites in civil engineering', *Composites Part A*, Vol. 37, Issue 8, pp. 1161–1170.

Hansen, J.-P. and McDonald, I. R. (2007), *Theory of Simple Liquids*. Elsevier, pp. 250–254.

Haque, A., Shamsuzzoha, M., Hussain, F. and Dean, D. (2003), 'S2-glass/epoxy polymer nanocomposites: manufacturing, structures, thermal and mechanical properties', *Journal of Composite Materials*, Vol. 37, Issue 20, pp. 1821–1837.

Harik, I. E. and Alagusundaramoorthy, P. (1999), 'Static testing on FRP bridge deck panels', *International SAMPE Symposium and Exhibition (Proceedings)* 44 (pt 2), pp. 1643–1654.

Haroun, M. A. and Elsanadedy, H. M. (2005), 'Fiber-reinforced plastic jackets for ductility enhancement of reinforced concrete bridge columns with poor lap splice detailing', *ASCE Journal of Bridge Engineering*, Vol. 1, Issue 6, pp. 749–757.

Hassan, T. and Rizkalla, S. (2002), 'Flexural strengthening of post-tensioned bridge slabs with FRP systems', *PCI Journal*, Vol. 47, Issue 1, pp. 76–93.

Helbling, C., Abanilla, M., Lee, L. and Karbhari, K. M. (2006), 'Issues of variability and

durability under synergistic exposure conditions related to advanced polymer composites in the civil infrastructure', *Composites: Part A*, Vol. 37, Issue 8, pp. 1102–1110.

Herring, M. L. and Fox, B. L. (2011), 'The effect of a rapid curing process on the surface finish of a carbon fibre epoxy composite', *Composites*, *Part B: Engineering*, Vol. 42, Issue 5, pp. 1035–1043.

Hollaway, L. C. (2008), 'Advanced fibre polymer composite structural systems used in bridge engineering', in *ICE Manual of Bridge Engineering*, 2nd edition, eds G. Parke and N. Hewson. Thomas Telford, London, pp. 503–530.

Hollaway, L. C. (2009), 'Advanced polymer composites', Chapters 51 and 52, of Section 7, Sub. Editors, L. C. Hollaway and J. F. Chen in *ICE Manual of Construction Materials*, ed. M. Forde. Thomas Telford, London.

Hollaway, L. C. (2010), 'A review of the present and future utilisation of FRP composites in the civil infrastructure with reference to their important in-service properties', *Construction and Building Materials*, Vol. 24, Issue 12, pp. 2419–2445.

Hollaway, L. C. (2011), 'Key issues in the use of fibre reinforced polymer (FRP) composites in the rehabilitation and retrofitting of concrete structures', in *Service Life Estimation and Extension of Civil Engineering Structures*, eds V. M. Karbhari and L. S. Lee. Woodhead Publishing, Cambridge, UK, Chapter 1.

Hollaway, L. C. and Chen, J.-F. (2009), Chapters 55 and 56 of Section 7, 'Polymer fibre composites in civil engineering', Sub. Editors, L. C. Hollaway and J. F. Chen, in *ICE Manual of Construction Materials*, ed. M. Forde. Thomas Telford, London.

Hollaway, L. C. and Head, P. R. (2001), *Advanced Polymer Composites and Polymers in the Civil Infrastructure*. Elsevier, Oxford, UK.

Hollaway, L. C. and Leeming, M. B. (1999), *Strengthening of Reinforced Concrete Structures Using Externally-bonded FRP Composites in Structural and Civil Engineering*. Woodhead Publishing, Cambridge, UK.

Hollaway, L. C. and Teng, J. G. (2008), *Strengthening and Rehabilitation of Civil Infrastructures Using Fibre-reinforced Polymer (FRP) Composites*. Woodhead Publishing, Cambridge, UK.

Holzenkämpfer, P. (1994), 'Ingenieurmodelle des Verbundes Geklebter Bewehrung für Betonbauteile', Dissertation, TU Braunschweig, Germany.

ISIS Canada (2001), Design Manual No. 3, *Strengthening Reinforcing Concrete Structures with Externally Bonded Fiber Reinforced Polymers*, Canada Network of Centers of Excellence on Intelligent Sensing for Innovative Structures, ISIS Canada Corporation, Winnipeg, Manitoba, Canada (Spring 2001).

John, C. (2003), 'The Nesscliffe Bypass Wilcott Footbridge – A triumph of FRP', *Concrete*, June, p. 37.

Jung, W. T., Park, J. S. and Park, Y. H. (2007), 'A study on the flexural behavior of reinforced concrete beams strengthened with NSM prestressed CFRP reinforcement', *Proceedings of the International Symposium on Fibre-reinforced Polymer Reinforcement in Concrete Structures (FRPRCS-8)*, Patras, Greece, 16–18 July 2007 (CD-Rom, 8p).

Karbhari, V. M. (2007), 'Fabrication, quality and service-life issues for composites in civil engineering', in *Durability of Composites for Civil Structural Applications*, ed. V. M. Karbhari. Woodhead Publishing, Cambridge, UK, Chapter 2.

Karbhari, V. M. and Seible, F. (2000), 'Fiber reinforced composites – Advanced materials for the renewal of civil infrastructure', *Applied Composite Materials*, Vol. 7, pp. 95–124.

Karbhari, V. M., Chin, J.W., Hunston, D., Benmokrane, B., Juska, T. and Morgan, R.,

(2000). 'Critical gaps in durability data for FRP composites in civil infrastructure', *International SAMPE Symposium and Exhibition* (Proceedings) 45 (I), pp 549–563.

Karbhari, V. M., Chin, J. W., Hunston, D., Benmokrane, B., Juska, T. and Morgan, R. (2003), 'Durability gap analysis for fiber-reinforced polymer composites in civil infrastructure', *ASCE Journal of Composites for Construction*, Vol. 7, Issue 3, pp. 238–247.

Kasan, J. L. and Harries, K. A. (2009), 'Repair of impact-damaged prestressed concrete bridge girders with carbon fiber reinforced polymers', *Proceedings of the 2nd International Conference of the International Institute for FRP in Construction for Asia-Pacific Region*, Seoul, Korea, 9–11 December 2009, pp. 157–162.

Kazunori, F., Mindness, S. and Xu, H. (2004), 'Analytical model for concrete confined with fiber reinforced polymer concrete', *ASCE Journal of Composites for Construction*, Vol. 8, Issue 4, pp. 341–351.

Kevlar Technical Guide, prepared and published by DuPont (undated).

Khalifa, A. and Nanni, A. (2000), 'Improving shear capacity of existing RC T-section beams using CFRP composites', *Cement and Concrete Composites*, Vol. 22, pp. 165–174.

Khalifa, A., Gold, W. J., Nanni, A. and Aziz, A. (1998), 'Contribution of externally bonded FRP to shear capacity of RC flexural members', *ASCE Journal of Composites for Construction*, Vol. 2, Issue 4, pp. 195–203.

Kim D.-H. (1995), *Composite Structures for Civil and Architectural Engineering*, E & FN Spon, London.

Klaiber, F. W., Dunker, K. F., Wipf, T. J. and Sanders, Jr, W. W. (1987), 'Methods of Strengthening Existing Highway Bridges', NCHRP 293, Transportation Research Board, 1987, 114 pp.

Knippers, J. and Gabler, M. (2007), 'New design concepts for advanced composite bridges – The Friedberg Bridge in Germany', *IABSE Report*, Vol. 92, pp. 332–333.

Kotynia, R. (2006), 'Flexural behavior of reinforced concrete beams strengthened with near surface mounted CFRP strips', in *CICE 2006*, Miami, FL, pp. 619–622.

Kotynia, R. and Kaminska, M. (2003), 'Ductility and failure mode of RC beams strengthened for flexure with CFRP', Report No. 13, Department of Concrete Structures, Technical University of Łódź, 2003, 51pp.

Kotynia, R., Walendziak, R., Stoecklin, I. and Meier, U. (2011), 'RC slabs strengthened with prestressed and gradually anchored CFRP strips under monotonic and cyclic loading', *Journal of Composites for Construction*, Vol. 15, Issue 2, pp. 168–180.

Lam, L. and Teng, J. G. (2002), 'Strength models for fiber-reinforced plastic-confined concrete', *ASCE Journal of Structural Engineering*, Vol. 128, Issue 5, pp. 612–623.

Lees, J. M. and Winistörfer, A. U. (2011), 'Nonlaminated FRP strap elements for reinforced concrete, timber, and masonry applications', *Journal of Composites for Construction*, Vol. 15, Issue 2, pp. 146–155.

Lees, J. M., Winistörfer, A. U. and Meier, U. (2002), 'External prestressed carbon fiber-reinforced polymer straps for shear enhancement of concrete', *Journal of Composites for Construction*, Vol. 6, Issue 4, pp. 249–256.

Lerchenthal, C. H. (1967), 'Bonded sheet metal reinforcement for concrete slabs', *Proceedings of the RILEM Symposium on Synthetic Resins in Building Construction*, Paris, September 1967, pp. 165–174.

L'Hermite, R. and Bresson J. (1967), 'Beton armé d'armatures collées', *Proceedings of the RILEM Symposium on Resins in Building Construction*, Paris, September 1967, pp. 175–203.

Liu, W., Hoa, S. and Pugh, H. (2005), 'Epoxy-clay nanocomposites: dispersion, morphology and performance', *Composites Science and Technology*, Vol. 65, pp. 307–316.

Longworth, J., Bizindavyi, L., Wight, R. G. and Erki, A. (2004), 'Prestressed CFRP sheets for strengthening two-way slabs in flexure', in *Advanced Composite Materials in Bridges and Structures*, Canadian Society for Civil Engineering, 8 pp.

Lu, X. Z., Teng, J., Ye, L. P. and Jiang, J. J. (2007), 'Intermediate crack debonding in FRP-strengthened RC beams: FE analysis and strength model', *Journal of Composites for Construction*, Vol. 11, Issue 2, pp. 161–174.

Lu, Z., Boothby, T. E., Bakis, C. E. and Nanni, A. (2000), Transfer and development lengths of FRP prestressing tendons', *PCI Journal*, Vol. 45, Issue 2, pp. 84–95.

Luke, S., Canning, L., Brown, P., Knudsen, E. and Olofsson, I. (2002), 'The development of an Advanced Composite Bridge Decking System – Project ASSET', *Structural Engineering International*, Vol. 12, Issue 2, pp. 76–79.

McKenzie, M. (1991), 'Corrosion protection: The environment created by bridge enclosure', Research Report 293, TRRL, 1991.

McKenzie, M. (1993), 'The corrosivity of the environment inside the Tees Bridge Enclosure: Final year results', Project Report PR/BR/10/93, TRRL, 1993.

Meier, U. (1987), 'Bridge repair with high performance composite materials', *Mater. Technik*, Vol. 15, pp. 125–128. (in French and German)

Meier, U. (2000), 'Composite material in bridge repair', *Applied Composite Materials*, Vol. 7, pp. 75–94.

Meier, U. and Deuring, M. (1992), 'Strengthening of structures with CFRP laminates: Research and applications in Switzerland', *1st International Conference on Advanced Composite Materials in Bridges and Structures*, Sherbrooke, Quebec, Canada, p. 243.

Meier, U. and Kaiser, H. (1991), 'Strengthening structures with CFRP laminates', *Proceedings of Advanced Composite Materials in Civil Engineering Structures*, ASCE, Las Vegas, NV, pp. 224–232.

Meier, U. and Stöcklin, I. (2005), 'A novel carbon fiber reinforced polymer (CFRP) system for post-strengthening', *International Conference on Concrete Repair, Rehabilitation and Retrofitting (ICCRRR)*, Taylor & Francis, London, pp. 477–479.

Meier, U., Stöcklin, I. and Winistörfer, A. (2002), 'Method and device for applying pretensed tension-proof reinforcing strips to a construction', US Patent No. 6,464,811 B1, 15 October 2002.

Mofidi, A. and Chaallal, O. (2011), 'Shear strengthening of RC beams with EB FRP: Influencing factors and conceptual debonding model', *Journal of Composites for Construction*, Vol. 15, Issue 1, pp. 62–74.

Monti, G., and Liotta, M. (2003), 'Tests and design equations for FRP strengthening in shear', *Construction and Building Materials*, Vol. 21, pp. 799–809.

Motavalli, M. and Czaderski, C. (2007), 'FRP composites for retrofitting of existing civil structures in Europe: State-of-the-art review', *Composites & Polycon, American Composites Manufacturers Association*, 17–19, October 2007, Tampa, FL, pp. 1–9.

Motavalli, M., Czaderski, C. and Pfyl–Lang, K. (2011), 'Prestressed CFRP for strengthening of reinforced concrete structures: recent developments at EMPA, Switzerland', *Journal of Composites for Construction*, Vol. 15, Issue 2, pp. 194–205.

Mouritz, A. P. and Gibson, A. G. (2007), *Fire Properties of Polymer Composite Materials*, Solid Mechanics and its Applications series. Springer, Dordrecht, the Netherlands.

Nanni, A. (1997), 'Carbon FRP strengthening: New technology becomes mainstream', *Concrete International*, Vol. 19, Issue 6, pp. 19–23.

Nanni, A., Huang, P. C. and Tumialan, J. G. (2001), 'Strengthening of impact damaged bridge girder using FRP laminates', *Proceedings of the 9th International Conference on Structural Faults and Repair*, Engineering Technics, Edinburgh, UK.

National Cooperative Highway Research Program (NCHRP) (1985a), Report 226, 'Damage Evaluation and Repair Methods for Prestressed Concrete Bridge Members'.

National Cooperative Highway Research Program (NCHRP) (1985b), Report 280, 'Guidelines for Evaluation and Repair of Damaged Prestressed Concrete Bridge Members'.

Neubauer, U. and Rostásy, F. S. (1997), '*Design aspects of concrete structures strengthened with externally bonded CFRP plates*', ECS Publications, Edinburgh, pp. 109–118.

Nordin, H. (2004), 'Strengthening structures with externally prestressed tendons', Technical Report, University of Luleå, Sweden.

Nordin, H. and Täljsten, B. (2006), 'Concrete beams strengthened with prestressed near surface mounted CFRP', *Journal of Composites for Construction*, Vol. 10, Issue 1, pp. 60–68.

Oehlers, D. J. and Seracino, R. (2004), *Design of FRP and Steel Plated RC Structures: Retrofitting Beams and Slabs for Strength, Stiffness and Ductility*, Elsevier, Oxford, UK, 288 pp.

Parke, G. and Hewson, N. (eds) (2008), *Manual of Bridge Engineering*, Thomas Telford, London.

Parretti, R., Nanni, A., Cox, J., Jones, C. and Mayo, R. (2003), 'Flexural strengthening of impacted PC girder with FRP composites', in *Field Applications of FRP Reinforcement: Case Studies*, SP-215, eds S. Rizkalla and A. Nanni, American Concrete Institute, Detroit, pp. 249–262.

Pellegrino, C. and Modena, C. (2002), 'Fiber reinforced polymer shear strengthening of RC beams with transverse steel reinforcement', *Journal of Composites for Construction*, Vol. 6, Issue 2, pp. 104–111.

Pešić, N. and Pilakoutas, K. (2005), 'Flexural analysis and design of reinforced concrete beams with externally bonded FRP reinforcement', *Materials and Structures*, Vol. 38, Issue 2. pp. 183–192.

Pilakoutas, K. (2000), 'Composites in concrete construction', in *Failure Analysis of Industrial Composite Materials*, eds E.E. Gdoutos, K. Pilakoutas and C. A. Rodopoulos. McGraw-Hill, New York, Chapter 10.

Prota, A., Nanni, A., Manfredi, G. and Cosenza, E. (2001), 'Design criteria for RC beam–column joints seismically upgraded with composites', *Proceedings of the International Conference on FRP Composites in Civil Engineering (CICE 2001)*, ed. J. G. Teng, Hong Kong, Vol. 1, pp. 919–926.

Prota, A., Nanni, A., Manfredi, G. and Cosenza, E. (2004), 'Selective upgrade of underdesigned RC beam–column joints using CFRP', *ACI Structural Journal*, Vol. 101, Issue 5, pp. 699–707.

Quantrill, R. J. and Hollaway, L. C. (1998), 'The flexural rehabilitation of reinforced concrete beams by the use of prestressed advanced composite plates', *Composites Science and Technology*, Vol. 58, pp. 1259–1275.

Reed, C. E. and Peterman, R. J. (2004), 'Evaluation of prestressed concrete girders strengthened with carbon fiber reinforced polymer sheets', *ASCE Journal of Bridge Engineering*, Vol. 9, Issue 2, pp. 185–192.

Rizkalla, S. H. and Nanni, A. (2003), 'Field applications of FRP reinforcement: case studies', American Concrete Institute (ACI) special publication SP–215.

Rizkalla, S., Shehata, E., Abdelrahman, A. and Tadros, G. (1998), 'The new generation:

Design and construction of a highway bridge with CFRP', *Concrete International*, Vol. 20, Issue 6. pp. 35–38.

Ross, C. A., Jerome, D. M. and Hughes, M. L. (1994), 'Hardening and rehabilitation of concrete structures using carbon fiber reinforced plastics (CFRP)', Final Report, Wright Laboratory Armament Directorate, Eglin Air Force Base, Florida.

Saadatmanesh, H. and Ehsani, M. R. (1991), 'RC beams strengthened with GFRP plates, I: Experimental study', *ASCE Journal of Structural Engineering*, Vol. 117, Issue 11, pp. 3417–3433.

Sangaj, N. S. and Malshe, V. C. (2004), 'Permeability of polymers in protective organic coatings', *Progress in Organic Coatings*, Vol. 50, Issue 1, pp. 28–39.

Schaefgen, J. R. (1983), 'Aramid fibres: structures, properties and applications', in *The Strength and Stiffness of Polymers*, eds. A. E. *Zachariades* and R. S. Porter. Marcel Dekker, New York, pp. 327–335.

Schiebel, S., Parretti, R. and Nanni, A. (2001), 'Repair and strengthening of impacted PC girders on bridge A4845', Report No. RDT01-017, Sponsoring Organization MoDOT Research Development and Technology, Jefferson City, MO.

Seible, F., Priestley, M. J. N. and Chai, Y. H. (1995), 'Earthquake retrofit of bridge columns with continuous carbon fiber jackets', Report No. ACTT-95/08, Advanced Composites Technology Transfer Consortium, La Jolla, CA.

Shahawy, M. and Beitelman, T. E. (1999), 'Static and fatigue performance of RC slabs strengthened with CFRP laminates', *ASCE Journal of Structural Engineering*, Vol. 125, Issue 6, pp. 613–621.

Shanafelt, G. O. and Horn, W. B. (1980), 'Damage evaluation and repair methods for prestressed concrete bridge members', National Cooperative Highway Research Program (NCHRP) Report 226, Project No. 12–21, Transportation Research Board, Washington, DC.

Shanafelt, G. O. and Horn, W. B. (1985), 'Guidelines for evaluation and repair of prestressed concrete bridge members', National Cooperative Highway Research Program (NCHRP) Report 280, Project No. 12-21(1), Transportation Research Board, Washington, DC.

Shave, J. D., Denton, S. R. and Frostick, I. (2009), 'St Austell Footbridge: The first fibre reinforced polymer structure on the UK rail network', *Fourth International Conference on Advanced Composites in Construction (ACIC 2009)*, 1–3 September 2009, University of Edinburgh, Edinburgh, Scotland.

Shehata, E., Abdelrahman, A., Tadros, G. and Rizkalla, S. (1997). 'FRP for large span highway bridge in Canada', *Proceedings of the US–Canada–Europe Workshop on Bridge Engineering*: Recent Advances in bridge Engineering, EMPA Switzerland, Dubendorf and Zurich, Switzerland, pp. 247–254.

Smith, S. T. and Teng, J. G. (2002), 'FRP strengthened RC beams II – Assessment of de-bonding strength models', *Engineering Structures*, Vol. 24, No. 4, pp. 397–417.

Spoelstra, M. R. and Monti, G. (1999), 'FRP-confined concrete model', *ASCE Journal of Composites for Construction*, Vol. 3, Issue 3, pp. 143–150.

Starr, T. F. (ed.) (2000), *Pultrusion for Engineers*. Woodhead Publishing, Cambridge, UK.

Stöcklin, I. and Meier, U. (2001), 'Strengthening of concrete structures with prestressed and gradually anchored CFRP strips', *5th International Conference on Fibre-reinforced Plastics for Reinforced Concrete Structures (FRPRCS-5)*, Cambridge, UK. Thomas Telford, London, pp. 291–296.

Stöcklin, I. and Meier, U. (2002), 'Strengthening of concrete structures with prestressed

and gradually anchored carbon fibre reinforced plastic (CFRP) strips', *1st International Conference on Bridge Maintenance, Safety, and Management (IABMAS)*, Barcelona, International Centre for Numerical Methods in Engineering, Barcelona, Spain, pp. 1–8.

Stöcklin, I. and Meier, U. (2003), 'Strengthening of concrete structures with prestressed and gradually anchored CFRP strips', *6th International Symposium on Fibre-reinforced Polymer (FRP) Reinforcement for Concrete Structures (FRPRCS-6)*, Singapore, World Scientific, Singapore, pp. 1321–1330.

Takács, P. E. and Kanstad, T. (2000), 'Strengthening pre-stressed concrete beams with carbon fiber reinforced polymer plates', NTNU Report R-9-00, Trondheim, Norway.

Täljsten, B. (2002), 'FRP strengthening of existing concrete structures – design guidelines', Luleå University Printing Office, Luleå, Sweden.

Teng, J. G., Chen, J. F., Smith, S. T. and Lam, L. (2002), *FRP Strengthened RC Structures*. John Wiley & Sons, Chichester and New York.

Teng, J. G., Lu, X. Z., Ye, L. P. and Jiang, J. J. (2004), 'Recent research on intermediate crack de-bonding in FRP-strengthened RC beams', *Proceedings of 4th International Conference on Advanced Composite Materials in Bridges and Structures (ACMBS IV)*, Calgary, Alberta, Canada, July 2004 (CD-ROM).

Teng, J. G., Smith, S. T. and Chen, J. F. (2008a), 'Flexural strengthening of reinforced concrete (RC) beams with fiber-reinforced polymer (FRP) composites', in Strengthening and Rehabilitation of Civil Infrastructures Using Fibre-reinforced Polymer (FRP) Composites, eds L. C. Hollaway and J. G. Teng. Woodhead Publishing in Materials, Cambridge, UK, Chapter 4.

Teng, J. G., Smith, S. T. and Chen, J. F. (2008b), 'Design guidelines for fibre-reinforced polymer (FRP)-strengthened reinforced concrete (RC), in *Strengthening and Rehabilitation of Civil Infrastructures Using Fibre-reinforced Polymer (FRP) Composites*, eds L. C. Hollaway and J. G. Teng. Woodhead Publishing in Materials, Cambridge, UK, Chapter 7.

Teng, M., Sotelino, E. and Chen, W. (2003), 'Performance evaluation of reinforced concrete bridge columns wrapped with fiber reinforced polymers', *Journal of Composites for Construction*, Vol. 7, Issue 2, pp. 83–92.

TGP (2008), 'Birse Rail and TGP complete the UK railway network's first vehicle carrying FRP bridge deck over a railway', Newsletter, March 2008.

Triantafillou, T. C. (1998), 'Shear strengthening of reinforced concrete beams using epoxy-bonded FRP composites', *ACI Structural Journal*, Vol. 95, Issue 2, pp. 107–115.

Triantafillou, T. C. and Antonopoulos, C. P. (2000), 'Design of concrete flexural members strengthened in shear with FRP', *Journal of Composites for Construction*, Vol. 4, Issue 4, pp. 198–205.

Triantafillou, T. C. and Plevris, N. (1991), 'Post-strengthening of RC beams with epoxy bonded fiber composite materials', *Proceedings of the Specialty Conference on Advanced Composite Materials in Civil Engineering Structures*, Las Vegas, NV 31 January – 1 February 1991, pp. 245–256.

Triantafillou, T.C., Deskovic, N. and Deuring, M. (1992), 'Strengthening of concrete structures with prestressed fiber reinforced plastic sheet', *ACI Structural Journal*, Vol. 89, Issue 3, pp. 235–244.

Uji, K. (1992), 'Improving shear capacity of existing reinforced concrete members by applying carbon fiber sheets', *Transactions of the Japanese Concrete Institute*, Vol. 14, pp. 253–266.

van Ooij, W. J., Zhu, D., Stacy, M., Seth, A., Mugada, T., Gandhi J. and Puomi, P.

(2005), 'Corrosion protection properties of organofunctional silanes – an overview', *Tsinghua Science and Technology*, Vol. 10, Issue 6, pp. 639–664.

Wu, H. C. and Yan, A. (2011), 'Time-dependent deterioration of FRP bridge deck under freeze/thaw conditions', *Composites Part B: Engineering*, Vol. 42, Issue 5, pp. 1226–1232.

Wu, H. C., Fu, G., Gibson, R. F., Warnemuende, K., Yan, A. and Anumandla, V. (2006), 'Durability testing of FRP material in low temperature weathering condition', *CD Proceedings of 21st Annual Technical Conference*, Dearborn, MI, American Society of Composites, 2006.

Wu, Z., Kim, Y. J., Diab, H. and Wang, X. (2010), 'Recent developments in long-term performance of FRP composites and FRP–concrete interface', *Advances in Structural Engineering*, Vol. 13, Issue 5, pp. 891–903.

Yapa, H. D. and Lees, J. M. (2009), 'Optimum shear strengthening of reinforced concrete beams with prestressed carbon fibre reinforced polymer (CFRP) straps', *Proceedings of the 4th Advanced Composites in Construction (ACIC 09)*, eds S. Halliwell and C. Whysall, NetComposites, pp. 214–226.

Zhang, C. and Canning, L. (2009), 'A successful model for introducing non-conventional materials in construction', *Proceedings of the 11th International Conference on Non-conventional Materials and Technologies (NOCMAT 2009)*, 6–9 September 2009, Bath, UK.

Zhang, Z., Hsu, C.-T. and Moren, J. (2004), 'Shear strengthening of reinforced concrete deep beams using carbon fiber reinforced polymer laminates', *Journal of Composites for Construction*, Vol. 8, Issue 5, pp. 403–414.

17

Applications of advanced fibre-reinforced polymer (FRP) composites in bridge engineering: rehabilitation of metallic bridge structures, all-FRP composite bridges, and bridges built with hybrid systems

L. C. HOLLAWAY, University of Surrey, UK

DOI: 10.1533/9780857098641.4.631

Abstract: This chapter continues the discussions of the development of advanced polymer composite material applications associated with bridge engineering. It focuses on the rehabilitation of metallic bridge structures, all-FRP composite bridges and bridges built with hybrid systems. Chapter 16 covered the materials used in FRP composites, in-service properties and applications of FRP composites in bridge enclosures, the rehabilitation of reinforced and prestressed concrete bridge beams and columns.

Key words: FRP composites, metallic bridge beams, FRP rebars/grids, FRP tendons, all FRP structures, hybrid systems.

17.1 Introduction

As discussed in the previous chapter, advanced FRP composites have a key role to play in the repair and construction of bridge structures. They have been used in the rehabilitation of both ageing concrete and metallic bridge structures. The unique in-service and mechanical properties, viz. durability, high specific stiffness and strength, etc., of advanced FRP composites for the civil infrastructure suggest their suitability for integration in hybrid structural systems as well as the development of all advanced FRP composite structures.

17.2 The rehabilitation of metallic bridge beams

17.2.1 The rehabilitation of metallic bridge beams using unstressed FRP plates

The upgrading of metallic bridge structures is not as widespread as that for the upgrading or retrofitting of RC bridges, as it possesses a different and a more difficult set of problems; these problems have been discussed by Mertz and Gillespie (1996) and Mertz *et al*. (2001). At the beginning

of the 2000s only a limited amount of research had been conducted on the application of FRP composite materials to metallic structures, but this situation has now changed (Mosallam and Chakrabarti, 1997; Tavakkolizadeh and Saadatmanesh, 2003; Cadei *et al*., 2004; Luke and Canning, 2004, 2005; Photiou *et al*., 2006a; Hollaway *et al*., 2006; Zhang *et al*., 2006; Schnerch and Rizkalla, 2008). Bell (2009) has discussed the series of high-level requirements relating to the use of FRP in bridge strengthening developed by Network Rail UK. From 2001 to 2009 Network Rail UK considered in detail and accepted over 25 steel bridges for FRP strengthening; many other bridges were considered but, following a preliminary site visit, were rejected either on the basis of condition or because the capacity increase required was considered to be excessive.

The technique for strengthening and stiffening of metallic structures could involve the addition of steel plates to the structure by the methods of bolting, riveting, welding, clamping and adhesively bonding, or utilising the method of adhesively bonding FRP composite plates to the structural member. Both these techniques have been shown to be successful in practice but there are disadvantages with the first system in particular when bonding is undertaken. Considering only the adhesively bonded steel plates, the main disadvantages are as follows:

- Uncertainty remains regarding any durability and corrosion effects.
- There are situations where contaminants on structural members remain prior to bonding.
- Plates must be subjected to careful surface preparation including the application of resistant priming systems.
- A minimum thickness of plate is typically 5 mm to prevent distortion during the grit blasting operation; plates are restricted to lengths of 6–8 metres.
- It is difficult to shape and fit complex profiles.
- The weight of plates makes transportation and installation difficult.
- Elaborate and expensive falsework is required to maintain steelwork in position during bonding.

The advantages of using FRP composites compared with steel plate bonding can be stated as follows:

- The fibres can be introduced in a certain position, volume fraction and direction in the matrix to obtain maximum efficiency, allowing the composites to be tailor-made to suit the required shape and specification.
- The resulting materials have high strength and stiffness in the fibre direction at a fraction of the weight of steel.
- They are easier to transport and handle.
- As the plates are lightweight there is not the requirement for heavy

support equipment during the period of polymerisation of the adhesive, thus requiring less falsework than steel plates.
- They can be used in areas of difficult access.
- Traffic disruption is kept to a minimum.
- The material has good durability characteristics.

In addition, CFRP and AFRP composites exhibit excellent fatigue and creep properties and require less energy per kilogram to produce and to transport than steel. However, there are drawbacks to the use of FRP:

- Its intolerance to uneven bonding surfaces, which may cause peeling of the plate away from the substrate surface, and the possibility of brittle failure modes (Swamy and Mukhopadhyaya, 1995).
- The material costs, which can be between four and 20 times as expensive as steel in terms of unit volume. However, consider that:
  - Two kilograms of FRP material could replace 47 kg of steel on an equal strength basis (Peshkam and Leeming, 1994).
  - In a rehabilitation project the installation savings can offset the higher material costs, which rarely exceed 20% of the overall project (Meier, 1992). The exception to this percentage value is the ultra high modulus carbon fibre for which case the percentage value could be as high as 50%.
  - When traffic management, traffic delays and maintenance costs are included, the use of FRP provides a cost saving in the region of 17.5% over steel.
  - Peshkam and Leeming (1994) presented a cost comparison of bridge replacement against strengthening with FRP, in which possible savings of 40% were demonstrated.

The appropriate method of analysis and design for FRP composite plate bonding of metallic structures is dependent upon the material of the bridges and their geometric cross-sections. The material is likely to be one of the following, (a) grey cast iron, (b) wrought iron, (c) ductile cast iron or (d) carbon steel; all their basic properties are given in Cadei *et al.*, 2004.

The FRP composite plate material used for the bonding operation is either the ultra-high-modulus (European definition) or the high-modulus (European definition) CFRP composite, and the manufacture and installation of the CFRP composite onto the site structure would be by one of the following methods:

- Pultrusion technique and components bonded on to site structure with an ambient cured adhesive.
- Prepreg sheets preformed into a plate in the factory, elevated temperature cured, delivered to site and bonded onto the structure with an ambient cured adhesive.

- Factory made cold-melt pre-impregnated fibre (prepreg) and compatible film adhesive which are simultaneously wrapped onto the bridge and cured under an elevated temperature (heat blanket) of 60°C for 16 hours or 80°C for 4 hours under a 1 bar pressure (Hollaway, 2008).
- Vacuum infusion (the Resin Infusion under Flexible Tooling (RIFT) process).
- Dry mats which are placed on the structure and impregnated with polymer and heat assisted (wet lay-up) followed by post-cure at an elevated temperature; in this case the polymer acts as the matrix material of the composite as well as the adhesive.

The various methods of fabrication have been discussed in Hollaway and Head (2001).

It should be noted that the ultra-high-modulus carbon fibre composite has a low strain to failure of the order of 0.4% strain, and a modulus of elasticity value of the composite of about 28 GPa, so the system will fail with a small inelastic characteristic. The high-modulus CFRP composites have an equivalent value of ultimate strain of the order of 1.6% for a value of modulus of elasticity of 220 GPa. This implies that the material is ductile and is unlikely to fail in a rehabilitation situation by ultimate strain but by some other criteria (Photiou, 2005).

Figure 17.1 illustrates a typical Network Rail-owned cast iron beam/brick jack arch carrying a public road over the railway in Irlam, Greater Manchester: the supports to hold the FRP composites in position whilst the adhesive cures are clearly shown; these were removed after about one week

17.1 Illustrates the upgrading of Network Rail CI brick arch bridge (New Moss Road Bridge, on the CLC Liverpool to Manchester railway, Greater Manchester). Image courtesy of Network Rail.

when full polymerisation had been achieved. The original bridge, constructed in 1873, was a single-span structure comprising six simply supported cast iron beams with brick masonry jack arches spanning between the beams. In 1956, the bridge was extended to the south by the provision of a second span of reinforced concrete construction; the track under this span has now been removed. The cast iron beams in the bottom flanges of the northern span were under-strength and also tie-bar replacements were required as part of the strengthening work; the southern reinforced concrete span was under-strength in flexure. Ultra-high-modulus (UHM) CFRP plates (tensile modulus in excess of 320 GPa) were selected to strengthen the cast iron beams in the bottom flange. To increase the flexural capacity of the reinforced concrete span, CFRP composite plates with modulus values of 150 GPa were utilised; these upgrades strengthen the structure to the 40 tonne assessment load. The pultrusion technique was used to manufacture the plates.

FRP strengthening has been applied to struts and columns carrying compression. Moy *et al*. (2004) reported on the strengthening of cast iron cruciform-section struts in a ventilation shaft on the London Underground using ultra-high-modulus CFRP composites, where the CFRP composite was designed to increase the capacity of the tensile zone of the strut during buckling. Moy and Lillistone (2006) have discussed the strengthening of cast iron using FRP composites. Shaat and Fam (2004) have discussed the use of FRP sheets to increase the local buckling strength of hollow square-section columns.

Further information on the technique, analysis and design of the rehabilitation of CFRP composites to metallic structures may be obtained from Hill *et al*. (1999), Liu *et al*. (2001), Moy (2001), Moy *et al*. (2001), Moy and Nikoukar (2002), Leonard, (2002), Photiou *et al*. (2006a, 2006b), ISIS design guide (2001), Cadei *et al*. (2004), Schnerch and Rizkalla (2004), and Dawood and Rizkalla (2006).

17.2.2 The rehabilitation of metallic bridge beams using stressed FRP plates

The application of prestressed FRP plates bonded on to steel girders is similar to that employed for RC beams; the anchors for the prestressed FRP plates are achieved by the use of steel anchorages bolted in predrilled holes in the flanges of the steel girders. It is not advisable to drill into some metallic beams, for instance into cast iron, due to the risk of cracking the beam. To overcome this problem the prestressing force may be transferred to the metallic element by a combination of clamps, using high friction bolts and adhesive bonding. To improve the durability of the prestressing anchorage system, grout is applied to it on completion. One of the first cast iron bridges to be strengthened using stressed FRP plates in the UK was the historic Hythe

Bridge, Oxford, constructed in 1861 and serving a major arterial route into Oxford. Assessment of the existing structure showed that it was capable of carrying only 7.5 tonnes and therefore it was required to be strengthened to 40 tonnes. A feasibility study was undertaken by Mouchel Consulting (now Sinclair Knight Merz (SKM)) to evaluate all possible options for the bridge including reconstruction. The final conclusion was that the most cost-effective way of strengthening the bridge, was to use prestressed CFRP plates (Luke, 2001). A jacking system was developed for research purposes during the ROBUST Project (Hollaway and Leeming, 1999) and this was further modified by Mouchel Consulting for prestressing CFRP plates against RC, PC and metallic beams. The description of upgrading the bridge may be found in Luke (2001).

17.2.3 Joining of concrete, metallic and FRP composite components

There are two techniques for joining polymer composites to concrete:

- By adhesive bonding, which will form one of the subjects of this section.
- By mechanical fasteners (i.e. nails), which will not be covered here but is covered in Bank *et al*. (2003) and Bank (2006).

Adhesive bonding is used for joining polymer composites to metallic adherents.

There are a wide range of adhesives which can be used to join concrete and metallic materials to FRP composite adherents, including epoxies, polyurethanes, acrylics and cyanoacrylate, but the one that is generally used for polymer composite plate bonding to concrete and metallic substrates is one of the epoxy group of adhesives. There are a number of epoxies on the market but the one selected must be compatible with the two adherents and the curing conditions; the manufacturers' advice should be sought for the most relevant adhesive to use in particular circumstances.

Concrete adherents

Most structural adhesives depend upon the formation of chemical bonds (mainly covalent but some ionic and static attractive bonds may also be present) between the adherent surface atoms and the compound constituting the adhesive (Kinloch, 1987). Prior to the rehabilitation or retrofitting of RC and PC structures their surfaces to be bonded must be prepared, and likewise the surface of the FRP composite. The purpose of the surface preparation of concrete is to remove the outer, weak and potentially contaminated skin together with poorly bound material, in order to expose small- to medium-

sized pieces of aggregate. This must be achieved without causing micro-cracks or other damage in the layer behind, which would lead to a plane of weakness and hence a reduction in strength of the adhesive connection. The basic steps in this process are given by Hutchinson (2008, 2009). It may be necessary to use a suitable solvent to remove contaminants and to apply an adhesive-compatible epoxy primer. After the surface preparation is completed the concrete substrate is grit blasted; a possible procedure in the UK is by 'Turbobead' grade 7 angular chilled iron grit (Guyson, 1989). A particle size of nominal 0.18 mm is generally used and the surface is then solvent degreased. This operation is important as it removes contaminants, which inhibit the formation of the chemical bonds (Kinloch, 1987).

Hashemi and Al-Malaidi (2012) conducted experimental tests and FE analyses on the utilisation of cementitious mineral-based bonding agents such as modified concrete to produce a fire-resistant strengthening system; they concluded that considerable composite action can be achieved by using this adhesive. Compared to CFRP composite material, the CFRP textile has a greater compatibility with the adherent and is therefore more efficient in bonding the composite plate to concrete beams. In another study by Wu and Sun (2005), the application of FRP sheets impregnated with cementitious mortar was suggested but it was found to be impractical for large-scale projects. Other investigations in this area have been undertaken by Wiberg (2003), Triantafillou *et al*. (2006), Täljsten and Blänksvard (2007), Bournas *et al*. (2007) Hashemi and Al-Malaidi (2008, 2010).

Metal adherents

The formation of chemical links is the load transfer mechanism between the adherents. Solvent degreasing is an important procedure in metal/FRP plate bonding as it removes contaminant materials, which inhibit the formation of the chemical bonds; a ketone, such as methyl ethyl ketone, or trichloroethylene are generally acceptable solvents for cleaning metals. However, while solvent degreasing provides a clean surface, it does not promote the formation of acceptable surface conditions for longer-term bond durability; thus cleaning pretreatment should precede any abrasive or chemical surface treatment. For an effective adhesive bonding process, a fresh, chemically active surface is essential. This may be achieved by either grit blasting for metal surfaces or acid etching for some steels or aluminium substrates using an aqueous acid solution to remove any loose layer of oxide from the surfaces. Grit blasting produces an active surface mainly because it is a non-contact process with a visible measure of effectiveness; after this procedure, solvent cleaning is undertaken again. Davis and Bond (1999) have stated that the basic principles for surface preparation are that the surfaces to be bonded must be (a) free

from contamination, (b) sufficiently chemically active to enable the formation of chemical bonds between the adhesive and the adherents, and (c) resistant to environmental deterioration in service, especially due to hydration.

FRP composite adherents

When the FRP composite plate is manufactured by the pultrusion or the prepreg techniques it would normally contain a peel-ply on either one or both surfaces. One of the peel-ply layers is removed immediately prior to bonding to the adherent, thus providing a clean, textured surface to the composite unit; the peel-ply is a sacrificial layer of glass fibre and polymer material. Most peel-plies are coated with a release agent to ensure that their removal does not damage the underlying plies of the plate. Hollaway and Leeming (1999) recommended the use of the peel-ply method, particularly when long-span beams (e.g. 18-metre span beams) are to be upgraded using strips of CFRP composite manufactured by the pultrusion or prepreg techniques. If the polymer composite did not contain a peel-ply, the surface preparation procedure would be to abrade the bond-side of the plate using medium sandpaper or a sand blaster and to wipe clean with a dry cloth to remove any residue, and finally the surface would be wiped with acetone or equivalent. The adhesive is then applied to the pretreated girder surface and to the CFRP plate.

For FRP composite strengthened steel structures, an important concern is the potential bond failure between the FRP laminate and the steel surface. Tong and Steven (1999) suggested that the dominant failure mode for composite bonded metal joints is adhesive failure rather than adherent failure; the failure strengths of steel and FRP are both higher than the adhesive bond. The research topics covered on FRP/steel joints are (1) stress analysis (Deng *et al*., 2004), (2) ultimate strength (El Damatty and Abushagur, 2003; Fawzia *et al*., 2004), and (3) fatigue behaviour (Liu *et al*., 2005; Yu and Chiew, 2007). In addition, some methods have been proposed to predict the bond failure of FRP bonded steel structures. The most straightforward method is to use the maximum stress in the bond-line as the failure criterion (Deng *et al*., 2004; Cadei *et al*., 2004). The advantage of this method is that the bond failure load of a FRP strengthened steel beam can be found explicitly if the bond strength of the FRP–steel joint is known. However, this method is only applicable for the case of elastic deformation and the effects of different geometries of the bondline are not considered.

Chiew *et al*. (2011) and Yu *et al*. (2011) developed a model to estimate the bond failure of steel beams strengthened with FRP composites. The first paper (Part 1) proposed a bond failure model and the second paper (Part 2) predicted the bond strength of the FRP–steel joint. Full-scale experiments on FRP strengthened steel beams were initially undertaken to study the bond

failure behaviour under static loading, followed by numerical analyses on the strengthened steel beams; the validity of the model was then assessed by comparing the experimental and the numerical results. The advantage of this equivalent strain energy density based bond failure model was demonstrated by comparing the results predicted by the proposed model with those predicted by using the traditional maximum value based model. In the case of joints subjected to in-plane loading the increase of bond strength was not synchronous with that of bond length. There exists a critical bond length beyond which the bond strength will not increase further. The most important factor influencing the final bond failure is the concentration at the end of the bond line.

17.3 Composite patch repair for metallic bridge structures

Composite material patching is a novel technique and a very promising method for repairing and/or reinforcing metallic structures. By bonding CFRP strips to military aircraft after they have become fatigue damaged, it has been possible to extend the service life of aluminium aerospace components. The method is now of interest to the civil engineering industry to repair cracked metallic materials, particularly to ageing metallic bridges. However, the same benefits may not apply to bridge patching as apply to aircraft patching, as there are several fundamental differences between the aerospace applications and that of steel bridges; these two applications dictate separate approaches to the investigation of the problem. These differences include:

- The steel is considerably stiffer compared with the aluminium.
- The different geometries between the thicker steel plate and larger steel bridge structure and the thinner aluminium plate structure of the aerospace systems.
- The different loading cases and the different in-service operating and environmental conditions.

Furthermore, there are larger differences between the normal repair cost of an aerospace structure and that of the steel bridge counterpart. However, research has been conducted to investigate the bonding of CFRP patches to reinforce cracked steel sections relevant to highway bridges.

Righiniotis *et al*. (2004) investigated the potential fatigue life improvement that may be achieved in using CFRP patches on cracked steel members. They showed that composite patches prevented crack growth and extended the lifetime of the repaired structure; the patch acts as a crack arrestor by decreasing the stress in the area of the crack tip and extending the lifetime of the repaired structure. Aggelopoulos *et al*. (2011) have investigated the debonding of adhesively bonded composite patch repairs of cracked steel members.

It is also possible to prestress the composite patch to increase the reinforcement effectiveness. Experimental tests were performed by Bassetti *et al*. (2000a) on a 91-year-old cross-girder in order to prove the effectiveness of prestressing CFRP-strips to stop fatigue cracks. Colombi *et al*. (2003) have shown by experimental testing that by applying pre-stress to the patch the fatigue life is increased by a factor of about 5. Prestressing the CFRP composite patch introduces compressive stresses that produce a crack closure effect. Furthermore, it modifies the crack geometry by bridging the crack faces and so reducing the stress intensity range at the crack tip. Bassetti *et al*. (2000b) undertook a two-dimensional finite element analysis of steel members repaired by prestressed composite patches. They observed that the stress range at the crack tip is reduced, patches that are perpendicular to the crack path limit the crack opening, and the dominant parameter is the intensity factor range and not its maximum value.

Composite patch repairs overcome some of the traditional disadvantages of normal rehabilitating methods used currently to upgrade bridge structures. These advantages are:

- There are minimal temporary falsework requirements.
- Patches can be applied directly on to corroded steel members by performing a simple surface preparation procedure.
- Patches can be applied quickly to the bridge structure.
- Patches exhibit good fatigue resistance.
- Patches do not cause stress concentrations.
- Patches result in low added weight.

17.4 All-fibre-reinforced polymer (FRP) composite bridge superstructure

There are two types of FRP bridge concepts: (1) the traditional bridge one with material substitution, and (2) the new material one. The number of bridges being built utilising the second concept with 'all-FRP' composite material is small, although it is growing.

Ideally, all-FRP composite bridge components should be modular and their assembly should be rapid and simple and have reliable connections; the material should be durable. The advanced polymer composite materials fulfil these requirements as they are durable and lightweight; they have high specific stiffness and strength and they may readily be constructed in modular form. The early advanced polymer composite bridges manufactured from modular components were the Aberfeldy Footbridge, Aberfeldy, Perthshire, UK (1992), the Bonds Mill Road Bridge, Gloucestersire, UK (1994) and the Fiberline Bridge in Kolding, Denmark (1997).

The first bridges that were manufactured and built using the Advanced

Composite Construction System (ACCS) Plank, known as the Maunsell Plank, were the Aberfeldy Footbridge and the Bonds Mill Road Bridge. The Maunsell Plank was developed by Maunsell Structural Plastics (now AECOM), Beckenham, Kent, UK, and consisted of a number of interlocking fibre-reinforced polymer composite units which could be assembled into a large range of different high-performance structural units for use in the construction industry. The panels were connected to each other by bonded connectors, and GFRP toggles were used to hold the parts together while the adhesive polymerised; these toggles stayed in position after polymerisation. The details of the Maunsell Plank are shown in Hollaway and Head (2001). (Strongwell, Bristol, VA and Chatfield, MN, USA, now hold the manufacturing licence for the plank and produce similar panels under the trade name of COMPOSOLITE®.) The production of the ACCS commenced in 1987 and it was first used in the construction of the bridge enclosure (see Chapter 16, Section 16.4) to the A19 Tees Viaduct at Middlesborough, UK (Constable, 1997). The Aberfeldy Footbridge was the first cable-stay GFRP bridge to use the Maunsell Plank as the decks and the pylons to the bridge. The cables were manufactured from Parafil (aramid fibre-reinforced polymer (AFRP)). A description of the bridge has been discussed in Skinner (2009) and its design and construction are given in Cadei and Stratford (2002). The durability performance of this bridge over the first 16 years of service has been very satisfactory (Stratford, 2008). The bridge was erected by students from the University of Dundee during their summer vacation under the supervision of staff from Maunsell Structural Plastics (AECOM).

The Bonds Mill Road Bridge, Gloucestershire, UK, crosses the Stroudwater Navigation canal near Stonehouse. It is constructed from 10 ACCS units which form an integral 3D multi-cellular box structure 8.5 m in span, and 4.25 m wide and 0.8 m in depth, and weighs 4.5 tonnes; the units are bonded together with cold-cure epoxy adhesive in a similar way to that of the Aberfeldy Maunsell planks. It is a single carriageway and is able to support vehicles up to 44 tonnes in weight. The bridge is operated hydraulically to allow water traffic to pass underneath.

West Mill Bridge over the River Cole, Oxfordshire, UK, was the first highway bridge in Western Europe to be constructed entirely of advanced polymer composites; it was opened in 2002. It was developed and built by a consortium of seven European companies within the Advanced Structural Systems for Tomorrow's Infrastructure (ASSET) project. Fiberline construction profiles of rectangular section in GFRP composites formed the four longitudinal main beams; these were stiffened by CFRP plates bonded throughout the length of the tensile and compressive flanges of the beams. The deck systems were manufactured from 34 GFRP ASSET bridge deck profiles bonded together and bonded to the four longitudinal GFRP composite beams. The side panelling consisted of corrosion-resistant 550 mm high

composite profiles (Canning and Luke, 2002); Mouchel Consulting (now SKM) were the lead partners. Further information may be obtained from Canning and Luke (2005) and www.fiberline.com.

Potyrala (2011) has provided a very useful table naming all-composite and hybrid bridges around the world from the oldest to the newest. The table gives basic details and the type of FRP composites used. Some of the more recent examples of the construction of all-composite bridges throughout the world are in Spain and Russia.

17.4.1 Spain

Sobrino and Pulido (2002) have discussed the design aspects of the GFRP footbridge crossing the Madrid–Barcelona high-speed rail link at Lleida, Spain (Fig. 17.2). The bridge is manufactured from E-glass fibres combined with woven and complex mats; the minimum glass fibre is 50% by volume. The bridge is a twined-tied arch and has a 38 m span with a rise of 6.2 m and a width of 3 m; it has a total weight of 19 tonnes. The bridge was designed by the Spanish engineering consultants Pedelta and built using structural components supplied by Fiberline, Kolding, Denmark. The key issues in choosing GRP material were that (1) the material is an electrical insulator which eliminates magnetic interference with the electrified railway, and (2) the bridge could be assembled at the site and then manoeuvred into position by crane. The assembly of this bridge was undertaken by eight operatives

17.2 Lleida Bridge, Spain, over an electrified railway line. Image courtesy of Fiberline, Composites A/S.

working over three months. The bridge won international acclaim in the form of the 'Footbridge Award 2005'.

Vink (2011) described the 44 m long, 5 m wide and 1.2 m deep Manzanares FRP footbridge which was design and constructed in 2010 by Acciona Infrastructures and Huntsman; as the bridge has no joints the designers claim it is the longest such bridge in the world. The bridge is a U-shaped beam with transversal ribs and weighs 25 tonnes; the bridge spans the Manzanares River, Madrid. It is a load-bearing, jointless, single structure manufactured using carbon fibre-reinforced epoxy polymer; it utilised 12 tonnes of carbon fibre. The bridge was designed, manufactured and constructed as a monolithic single piece by an injection infusion process with lay-up to fill and reinforce the epoxy-bonded prefabricated ribs of the bridge; the epoxy adhesive system used had enhanced toughness, chemical thixotropy and low exotherm. As the bridge was designed as a lightweight structure it was possible to meet the transportation, logistics and installation requirements defined for the project. Acciona is currently constructing a 200 m long single-beam bridge in Cuenca, Spain. Acciona and Huntsman won the JEC civil engineering award for 2011.

17.4.2 Russia

Ushakov *et al.* (2008) described the first Russian composite bridge manufactured by vacuum infusion technology for small rivers with spans of 15 to 30 metres and an expected life cycle of 100 years; the structure was designed by Lightweight Structures BV, the Netherlands, and by Applied Advanced Technology (ApATeCh), Russia, who installed it (Fig. 17.3). The vacuum-infused system enabled a reduction in the manufacturing stages, thus avoiding assembling activities on site; the possibility of using one mould for bridges of different dimensions allowed for a reduction in the cost of the structure. Furthermore, the bridge production technology provides aesthetic design possibilities and the creation of new unusual forms. It consisted of a central arch and two end spans leading to the two abutments; it was erected in 2008 at the park '50 years of October'. The only parts of the bridge which are not manufactured from FRP composites are the metal hinges and fence fasteners. The authors won the best innovative construction paper award from the American Society of Civil Engineers (ASCE) for their paper on this structure.

A number of sophisticated FRP composite footbridges have been constructed in Russia during the last few years. For example:

- Pedestrian bridge near the platform 'Chertanovo', Promishlennaya Street, Chertanovo, Moscow (October 2004).
- Pedestrian passage over the platform 'Kosino', developed and installed

17.3 The first Russian composite bridge manufactured by vacuum infusion technology (for small rivers with spans of 15 to 30 metres). Image courtesy of Infra Composites B.V., ApATeCh Co. Ltd., Moscow, and Lightweight Structures, The Netherlands.

within the frame of reconstruction of the Moscow railroad. The structure is the first bridge in Russia with stair flights, all the elements of which are made of composite materials. The location is in Kaskadnaya street, Kosino, Moscow (July 2005).

- Pedestrian passage at the 23rd km of the highway 'Leningradskoe', Moscow region (December 2005).
- Pedestrian bridge near the 586th km of the South-East Railway haul Otrozhka-Pridacha of the South-East Railway (June 2008).
- Pedestrian bridge Kuskovo at the second Karachaev driveway, Moscow.
- Footbridge erected in the Khimki, Moscow region. One of the most recent bridge projects to be designed and erected by ApATeCh was a lightweight pedestrian footbridge, shaped to form a cross; the four spans, each of length 33 metres, are integrated into one unit, the footbridge load-bearing elements consists of two intersecting steel beams supported at the centre of the cross by steel tubular members and at the end by four vertical towers; the towers contain pedestrian stairs and lifts. A decorative spiral grid made from GFRP composite embraces both the spans and towers; the spiral grids are a set of curved thin-walled tubes which are joined at their intersection. The main loads are carried by the steel and concrete elements of the structure but the spiral grid is exposed

to a number of environmental loads including wind, snow and ice. The grid is a curved tube 2800 mm long with a 200 mm diameter and wall thickness from 3 mm to 5 mm, depending on the magnitude of the load. The tubes are fabricated onto the bridge deck and tower structure; the two systems are joined by bonding or by a combination of bonding and mechanical joints. The total number of composite elements in the bridge structure is 1777 with a total weight of 13,689 kg. The elements of the grid are manufactured from multi-axial quasi-isotropic GFRP by the vacuum infusion technique. Figure 17.4 shows this bridge.

All the above bridges were designed by ApATeCh–Applied Advanced Technologies, Moscow, www.apatech.ru.

17.5 New bridge construction with hybrid systems

This section will describe the possibility of joining the advanced polymer composites and conventional construction materials to form a new hybrid structural system which could be used in bridge engineering. For instance, combining concrete, which is weak in tension but strong in compression, with FRP composites in plate form, which are strong in tension but will buckle under low compressive loads, could take advantage of the dominant properties of both by joining the two to form a hybrid structural member.

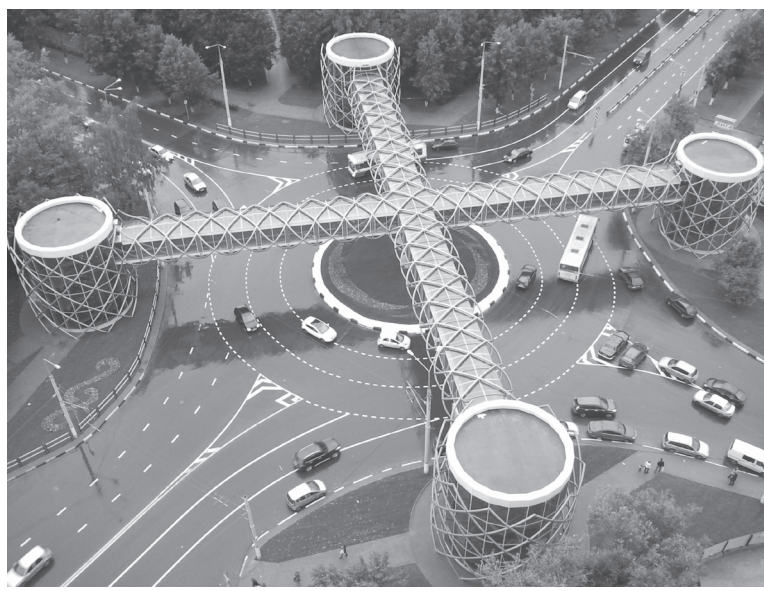

17.4 Footbridge erected in the Khimki, Moscow region. Image courtesy of ApATeCh Co. Ltd., Moscow, Russia.

Hybrid systems may be classified as (1) structural composite products with hybrid fibres or (2) structural systems consisting of hybrid composites and conventional materials. The first category involves a product-level definition that is made by the combination of fibres and polymers to form unidirectional structural elements such as composite plates, rods, tendons and strands. The second category involves a system level that is defined by incorporating FRP composite components into a structural member made from the more traditional materials.

The first category (the high product system), where the FRP composites are fabricated to form rebars, gratings or flat plates, is the subject matter of this chapter and Chapter 16. When designing for the second category the aim of the designer is to place the two (or more) component materials in their most strategic position in the structural system to take full advantage of their unique superior properties, i.e. the high compressive strength and/or high stiffness of traditional materials and the high tensile strength and stiffness of the FRP composite. The hybrid structural system will then be optimally combined, but the successful applications of these systems require that the following three criteria should be met:

- The FRP material should ideally be used in areas subjected to tension, for instance in wrapping columns and on the tension soffit of beams.
- Fire resistance should not be critical, for instance where the structure is in an open space (e.g. bridges) or the FRP is not required to make any contribution to structural resistance during a fire. Research is currently being undertaken to modify polymers to be more resistant to fire. For example, Advanced Composites Group Ltd (ACG now Cytec), Derbyshire, UK, have recently launched a new a phenolic resin system (MTM 82S-C), available as a prepreg, which has been designed to offer outstanding fire performance to mass transit, industrial and construction applications. Cytec claims that the new prepreg has excellent mechanical properties in combination with exceptional fire performance, where the operating temperature is within the range –55°C to 80°C.
- Cost-effectiveness in terms of the most advantageous combination of whole-life cost and high quality and performance.

Some examples of hybrid structures are discussed in the following sections.

17.5.1 Hybrid columns

Hybrid FRP/concrete structural columns filled with concrete with or without internal reinforcement have been investigated by many researchers including Fam and Rizkalla (2001a) Mirmiran (2003) and Xiao (2004). This work was extended to two concentric FRP tubes where the annulus was filled with

concrete (Fam and Rizkalla, 2001b); in all cases the majority of fibres were placed in the hoop direction, providing confinement to the concrete and with only minimal fibre volume fraction being arranged longitudinally, basically to hold the circumferential fibres in position.

In practice the FRP columns have largely superseded the concrete-filled steel jackets. The former hybrid systems have many advantages over steel-jacketed systems:

- Lightweight
- Corrosion resistant
- Resistant to lateral forces on column
- Retains the cracking of the concrete.

The disadvantages of the FRP/concrete hybrid columns are:

- Brittle failure in bending
- Difficulty in detailing connection details when joining column to beam
- Poor fire resistance, but this is not significant with respect to bridge columns.

Teng *et al*. (2007) have suggested a new form of hybrid column consisting of an outside FRP tube and a concentric steel tube inside; the annulus is filled with concrete. Likewise, the fibres in the outside tube are mainly placed in the hoop direction and only a small volume fraction are positioned in the longitudinal direction, thus providing confinement to the concrete and enhanced ductility and an additional shear resistance. The 'Teng' column aims to achieve a high-performing structural member by combining the benefits of the three materials and to provide the advantages mentioned above. The 'Teng' column may readily be converted to a beam by displacing the inner steel tube nearer to the FRP outer tube (Teng *et al*., 2007). Figure 17.5 shows a series of possible column cross-sections for confining the concrete and a section for the beam.

A confinement technique using non-laminated *thermoplastic* CFRP straps was investigated and applied to 2 m high RC columns. The results from tests were encouraging, although practical and theoretical problems remain to be solved before these techniques can be applied in practice (Motavalli *et al*., 2011).

17.5.2 Hybrid bridge beams

One of the earlier hybrid bridge structures was the King Stormwater Channel Bridge which was a demonstration bridge on California State Route 86 near the Salton Sea, USA. The bridge was a project sponsored by the Defense Advanced Research Projects Agency (DARPA) Bridge Infrastructure Renewal

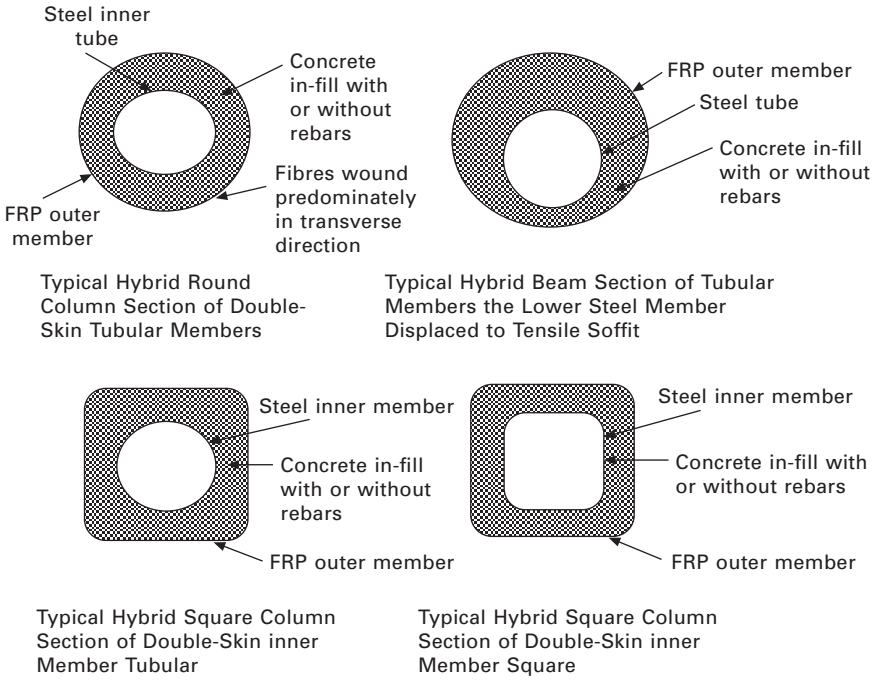

17.5 A series of possible column cross-sections for confining the concrete and a section for the beam, utilising steel, composite and concrete. Adapted from Teng *et al.*, 2007.

Program. It was administered and studied extensively by the University of California at San Diego (UCSD) for the California Department of Transport (CALTRAN). The carbon shell bridge design, known as the Composite Shell System (CSS), consisted of a 20.1 m two-span continuous beam-and-slab bridge with a five-column intermediate pier. The six concrete-filled carbon tubes were 10 mm thick and had an inside diameter of 343 mm. They formed the longitudinal beams and were connected along their tops to a structural slab consisting of an E-glass GFRP deck system. The superstructure depth requirement was that it should be shallow. This was determined primarily by geometric constraints and structural performance; the final dimension was 762 mm. Zhao *et al*. (2000) provided the Final Test Report submitted to the California Department of Transportation under Contract No. 59AO032.

An innovative hybrid beam of rectangular cross-section composed of concrete placed in its compressive region and a high specific strength/stiffness FRP composite situated in the tensile region was presented by Triantafillou and Meier (1992), Deskovic and Triantafillou (1995) and Triantafillou (1995), Canning *et al*. (1999). This system was extended to form a composite/concrete duplex beam for both a standard rectangular and a Tee beam cross-section

(Hulatt *et al.,* 2001); the webs of both sections were constructed as a GFRP plate or as a sandwich plate section and a CFRP plate was incorporated into the soffit of the beam. Further developments of this beam system have been discussed in Hulatt *et al*. (2003a, 2003b, 2004). The VTM260 series epoxy resin, glass and carbon fibre prepregs supplied by ACG (now Cytec), Heanor, UK, were used in this research at the University of Surrey. Using a similar hybrid structural beam system and ACG's VTM264 variant epoxy/carbon fibre prepreg material, NECSO Entrecanales Cubiertas, Madrid, Spain, undertook a R&D project and developed an advanced composite/concrete beam element. This system was utilised as the motorway bridge on the highway at Cantabrico in Spain; Hollaway (2008) shows the completed bridge. This system resulted in a new structural concept which is corrosion free with excellent damping and fatigue properties.

There are, in the offing, one or two further designs for bridges in Spain using this method of construction. In recognition of the development of the hybrid structural beam system used on the motorway bridge at Cantabrico in Spain and for the prepreg composite technology, ACG was awarded the JEC Composites Award 2005 for Construction, Reinforced Plastics (2005).

The Knockerbocker Bridge in Boothbay, Maine, USA, is another variation on the hybrid beam system. It was originally a 38-span timber bridge built in the 1930s and was replaced in 2011 with a hybrid composite beam manufactured by Hybrid Composite Beams (HCB), Wilmette, Illinois, USA. Figure 17.6(a) shows the elevation of the composite bridge and Fig. 17.6(b) shows its soffit. The HCB consisted of an FRP shell which was shaped in the form of a U and was manufactured by the vacuum infusion technique; the beam interior is lined with interlocking sections of two to four 3 mm thick fibreglass textile fabric. This FRP shell was then combined with tension reinforcement using high-strength steel galvanised prestressing strand placed along the bottom of the beam with 90° bends at the ends of the box acting as anchors. The compression reinforcement is composed of an arch made from GFRP composite and filled with a self-consolidating concrete which is placed in the void of the FRP shell. The remaining void around the arch is filled with low-density polyiso foam; Fig. 17.6(c) shows the cross-section of the bridge. The HCBs were designed to match the recommended 838 mm depth box beams in order to maintain the required vertical under-clearance; the HCB framing system was limited to two 18.3 m end spans and six 21.3 m interior spans, resulting in an eight-span bridge with a total length of 164.3 m. The above information is based upon the company's website, www.hcbridge.com.

A number of sophisticated hybrid bridge structures have been constructed in Europe during the last few years. For example in the Netherlands, Infra Composite B.V., Delft and Breukelen, have designed and manufactured:

(a)

(b)

17.6 (a) Elevation of Knockerbocker Bridge, Boothbay, Maine, USA (image courtesy of HC Bridge Company, LLC, Wilmette, Illinois, USA); (b) soffit of Knockerbocker Bridge, Boothbay, Maine, USA (image courtesy of HC Bridge Company, LLC, Wilmette, Illinois, USA); (c) cross-section of the Knockerbocker Bridge, Boothbay, Maine, USA.

- A hybrid bridge of steel girders and a GFRP/balsa sandwich deck, bonded with a non-epoxy adhesive, located at Kadijkweg, Andijk, the Netherlands.

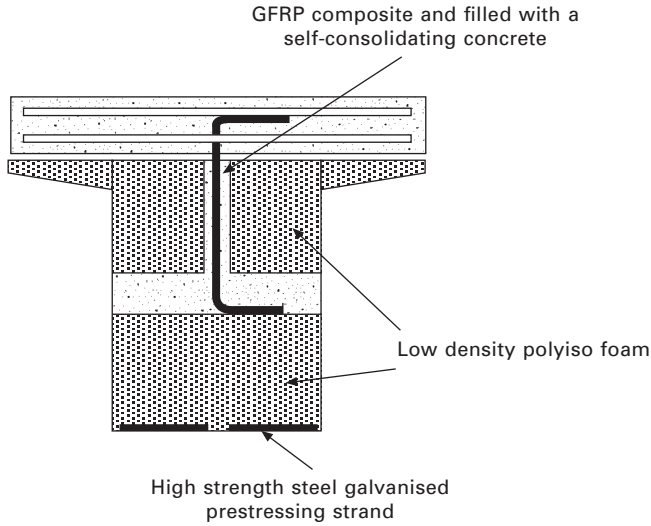

17.6 Continued

- A hybrid bridge (Fig. 17.7) of steel girders and a GFRP sandwich deck including GFRP sheer webs, joined with bolts; this bridge is located at Rijksstraatweg, De Meerin, the Netherlands.

Their website is https://www.infracomposites.com.

17.6 Conclusion and future trends

Chapters 16 and 17 have covered many aspects of the utilisation of advanced polymer composites in bridge engineering. The advantages of FRP composites are realised from their physical characteristics and their potential to develop structural systems with their service lives exceeding those of traditional materials. The light weight of the composite can result in lower construction costs and increased speed of construction. In the case of FRP composite materials, their high strength and stiffness characteristics will require less material to achieve similar performance criteria as that of traditional materials, thus resulting in minimising resource use and waste production. In general, the advantage of FRP composites in bridge engineering is their potential to extend the service life of existing structures, and to develop new structures that are far more resistant to hostile civil engineering environments and are better able to withstand the effects of ageing, weathering and degradation compared with the more traditional materials. It is noted from these chapters that in the foreseeable future it is likely that most new-build bridge beams when using composites will be fabricated from a hybrid material of FRP

17.7 Hybrid bridge of steel girders and a GFRP sandwich deck including GFRP sheer webs, joined with bolts, Rijksstraatweg, De Meerin, The Netherlands. Image courtesy of Infra Composites B.V., The Netherlands.

composites in conjunction with the more traditional materials. These two dissimilar materials are, and will be, combined in such a way within the structure that benefits will be evident in terms of the mechanical and in-service properties and the economics of the complete system.

Bridge engineering continues to face numerous challenges, for instance from increasing growth in heavier vehicle weights, preserving ageing and delaying the deterioration of highway and rail bridges. The strategy of the civil engineer is to use high-performance structural materials and innovative quality designs for more durable and reliable structures.

In the twenty-first century, composite fabricators and suppliers are actively developing products for the civil engineering infrastructure, which is considered to be the largest potential market for FRP composites. The development of databases in bridge performance applications, covering long-term durability issues, long-term integrity of bonded joints and components, and cyclic fatigue loading in hostile environments, is gradually being defined. The worldwide bridge application demonstrator structures and the FRP composite rehabilitation/strengthening technologies are serving as field study exercises which will develop greater confidence in the use of FRP composite structures in future decades.

Standardised bridge components and systems design for the 'all composite' bridge structure would allow more focused research, development and competitiveness. More efficient manufacturing and effective production

methods for large-volume panels and higher-modulus materials are required to make it more cost-effective for composites to compete in the bridge engineering infrastructure.

An excellent example of an effective application for FRP composite material is the bridge deck system. An important feature of this technology is its rapid deployment and installation on site; this reduces congestion in the work zone, improves site safety and minimises expensive lane/road closures considerably.

A major advance has been made in the development of smart FRP components where it has been shown that pultrusion technology can be modified to incorporate fibre optic sensors. Instead of using FRP reinforcements with external sensors, the necessary composite components can now arrive at the work site with fibre optic sensors already embedded as an integral part of the unit members.

The bridge construction technology and philosophy is based largely on a first-cost basis. Since FRP composite materials have a higher first-cost than most traditional materials used in construction, hybrid FRP systems that combine the high stiffness and strength of the material with the compression strength of concrete, metallic and timber materials have been shown to be effective. When designing hybrid structures an important requirement is to strategically place the FRP composites where their high tensile strength and/or high stiffness can be exploited, while taking advantage of the high compressive strength of the traditional materials.

It will have been seen from Chapters 16 and 17 that the main future utilisation of FRP materials is in conjunction with the more traditional materials. These two dissimilar materials are combined in such a way within the structure that the benefits are clearly seen in terms of the mechanical and in-service properties and the economics of the complete system. The FRP composite material has now become one of the competing materials in bridge engineering; it is an exciting time for bridge engineers, consultants, researchers and the FRP composites industry. With FRP composites, the world is already changing the way it builds and maintains its bridges.

17.7 Sources of further information and advice

Regulatory/trade/professional bodies

1. *CEN-TC250* – EUR 22864 EN, 2007 – http://eurocodes.jrc.ec.europa.eu
2. *European Organisation for Technical Approvals* (EOTA): Discussions between the European Commission Joint Research Centre (JRC) and EOTA, on the works for new codes and standards regarding the use of FRP composites in civil engineering.

3. Industrial organisations:
   - *European Construction Technology Platform* (ECTP).
   - *European Composites Industry Association* (EuCIA).
     The JRC has contacted both the above organisations with a view to ensuring that their main concerns and needs are addressed by any proposed standards.
   - *The Directorate General Enterprise and Industry* (DG ENTR) of the European Commission in 2005 committed the JRC to assist in the implementation, harmonisation and further development of the Eurocodes. This will enable the European composites industry to be more aware of the impact that new Eurocodes, specifically tailored for FRPs, would have on their core business.

Professional bodies

The following is based upon the Network Group for Composites in Construction (NGCC), 11 May 2012.

1. *Composites UK*. The mission of Composites UK, as the representative body of the UK composites industry, is to promote the use of composite materials to the widest market spectrum.
2. *British Composites Society* (BCS). This is one of the technical arms of the Institute of Materials, Minerals and Mining. The British Composites Society provides a focus for the exchange of knowledge on all aspects of composite materials. It is a national contact point for communication with similar bodies on a worldwide basis.
3. *The Institute of Materials, Minerals and Mining* (IOM3), recognised by the UK's Privy Council on 26 June 2002. It was created from the merger of The Institute of Materials (IOM) and The Institution of Mining and Metallurgy (IMM). The Institute is potentially the leading international professional body for the advancement of materials, minerals and mining to governments, industry, academia, the public and the professions.
4. *International Institute for FRP in Construction* (IIFC). The aim of the Institute is to advance the understanding and the application of FRP composites in the civil infrastructure, in the service of the engineering profession and society.
5. *Welsh Composites Consortium* (WCC). The consortium acts as a Technology Transfer Network consisting of a number of partner organisations with a wide range of expertise in the field of composites, particularly to SMEs in Wales in the form of advisory visits.
6. *Construction Industry Research and Information Association* (CIRIA).

7. *The Italian Association for Composites in Construction* (AICO). AICO was formed in 1996. It is active in the field with membership from industry and universities.
8. *European Composites Industry Association* (EuCIA). The primary goal of EuCIA is to unite the composites industry at European level into one single European association.
9. *COBRAE*. The objective of COBRAE is to promote research, development, standardisation and application of fibre reinforced polymer composites in rehabilitation, upgrade and new build bridge constructions and infrastructure applications.
10. *European Construction Technology Platform* (ECTP). It is hoped that the ECTP will raise the sector to a higher world-beating level of performance and competitiveness. This will be achieved by analysing the major challenges that the sector faces in terms of society, sustainability and technological development. Research and innovation strategies will be developed to meet these challenges, engaging with and mobilising the wide range of leading skills, expertise and talent available to us within our industry over the coming decades, in order to meet the needs of society.
11. *Intelligent Sensing for Innovative Structures* (ISIS), Canada.
12. *Canadian Association for Composite Structures* (CACS). The CACS is a network of individuals and corporate members (suppliers, fabricators, equipment manufacturers, distributors, consultants, technologists, research centres, materials specialists, researchers, teachers, and government employees) working to develop and enhance new and existing applications for composite structures and materials.

17.8 References

Aggelopoulos, E. S., Righiniotis, T. D. and Chryssanthopoulos, M. K. (2011), 'Debonding of adhesively bonded composite patch repairs of cracked steel members', *Composites Part B: Engineering*, Vol. 42, Issue 5, July 2011, pp. 1262–1270.

Bank, L. C. (2006), *Composites for Construction: Structural Design with FRP Materials*, John Wiley & Sons, Hoboken, NJ.

Bank, L. C., Borowicz, D. T., Arora, D. and Lamanna, A. J. (2003), 'Strengthening of concrete beams with fasteners and composite material strips – Scaling and anchorage issues', US Army Corps of Engineers, Final Report, Contract Number DACA42-02-P-0064.

Bassetti, A., Nussbaumer, A. and Hirt, A. (2000a), 'Fatigue life extension of riveted bridge members using pre-stress carbon fibre composites', in: *Steel Structures of the 2000s*, ECCS, Istanbul, pp. 375–380.

Bassetti, A., Colombi, P. and Nussbaumer, A. (2000b), 'Finite element analysis of steel members repaired by prestressed composite patch', *Proceedings of the IGF 2000, XV Congresso Nazionale del Gruppo Italiano Frattura*, Bari, Italy, 3–5 May 2000.

Bell, B. (2009), 'Fibre-reinforced polymer in railway civil engineering', *Engineering and Computational Mechanics*, Vol. 162, Issue 3, pp. 119–126.

Bournas, D. A., Lontou, P. V., Papanicolaou, C. G. and Triantafillou, T. C. (2007), 'Textile-reinforced mortar versus fiber-reinforced polymer confinement in reinforced concrete columns', *ACI Structural Journal*, Vol. 104, Issue 6, pp. 740–748.

Cadei, J. M. C. and Stratford, T. J. (2002), 'The design, construction and in-service performance of the all-composite Aberfeldy Footbridge', *Proceedings of the First International Conference*, held at Southampton University, UK, 15–17 April 2002, eds R. A. Shenoi, S. S. J. Moy and L. C. Hollaway. Thomas Telford, London, pp. 445–455.

Cadei, J. M. C., Stratford, T. J., Hollaway, L. C. and Duckett, W. G. (2004), 'Strengthening metallic structures using externally-bonded fibre-reinforced polymers', CIRIA Report RP 645, CIRIA, London.

Canning, L. and Luke, S. (2002), 'Development of FRP bridges in the UK – An overview', *Advances in Structural Engineering*, Vol. 13, Issue 5, pp. 823–835.

Canning, L. and Luke, S. (2005), 'West Mill Bridge – Comparison of initial and long-term structural behaviour', *Composites in Construction 2005 – 3rd International Conference*, Lyon, France, 11–13 July 2005, pp. 1–8.

Canning, L., Hollaway, L. and Thorne, A. M. (1999), 'Manufacture, testing and numerical analysis of an innovative polymer composite/concrete structural unit', *Proc. Instn Civ. Engrs Structs & Bldgs*, Vol. 134, pp. 231–241.

Chiew, S. P., Yu, Y. and Lee, K. C. (2011), 'Bond failure of steel beams strengthened with FRP laminates – Part 1: Model development', *Composites Part B: Engineering*, Vol. 42, Issue 5, pp. 1114–1121.

Colombi, P., Bassetti, A. and Nussbaumer, A. (2003), 'Analysis of cracked steel members reinforced by pre-stress composite patch', *Fatigue and Fracture of Engineering Materials and Structures*, Vol. 26, pp. 59–66.

Constable, P. A. (1997), 'Bridge modification approach – a value for money approach', Paper 3, *Proceedings of Stronger and Safer Bridges – Bridge Modification*, 2, 21.

Davis, M. and Bond, D. (1999), 'Principles and practice of adhesive bonded structural joints and repair', *International Journal of Adhesion and Adhesives*, Vol. 19, pp. 91–105.

Dawood, M. and Rizkalla, S. (2006), 'Bond and splice behaviour of high modulus CFRP materials bonded to steel structures', *Proceedings of Third International Conference on FRP Composites in Civil Engineering (CICE 2006)*, eds A. Mirmiran and A. Nanni. University of Miami, FL, pp. 705–706.

Deng, J., Lee, M. M. K. and Moy, S. S. J. (2004), 'Stress analysis of steel beams reinforced with a bonded CFRP plate', *Composite Structures*, Vol. 65, Issue 2, pp. 205–215.

Deskovic, N. and Triantafillou, T. C. (1995), 'Innovative design of FRP combined with concrete: short-term behaviour', *Journal of Structural Engineering*, Vol. 121, Issue 7, pp. 1069–1078.

El Damatty, A. and Abushagur, M. (2003), 'Testing and modelling of shear and peel behaviour for bonded steel/FRP connections', *Thin Walled Structures*, Vol. 41, Issue 11, pp. 987–1003.

Fam, A. Z. and Rizkalla, S. H. (2001a), 'Confinement model for axially loaded concrete confined by circular fiber-reinforced polymer tubes', *ACI Structural Journal*, Vol. 98, Issue 4, pp. 451–461.

Fam, A. Z. and Rizkalla, S. H. (2001b), 'Behavior of axially loaded concrete-filled circular fiber-reinforced polymer tubes', *ACI Structural Journal*, Vol. 98, Issue 3, pp. 280–289.

Fawzia, S., Zhao, X. L. and Al-Mahaidi, R. (2004), 'Investigation into the bond between CFRP and steel tubes', *Second International Conference on FRP Composites in Civil Engineering*, Adelaide, Australia, pp. 733–739.

Guyson (1989), 'Manual of Blast media', Guyson Data Sheets.

Hashemi, S. and Al-Mahaidi, R. (2008), 'Cement based bonding material for FRP', Proceedings of the *11th International Inorganic-Bonded Fiber Composites Conference (IIBCC)*, 5 – November 2008, Madrid, Spain, pp. 267–271.

Hashemi, S. and Al-Mahaidi, R. (2010), 'Investigation of bond strength and flexural behaviour of FRP-strengthened reinforced concrete beams using cement-based adhesives', *Australian Journal of Structural Engineering*, Vol. 11, Issue 2, pp. 129–139.

Hashemi, S. and Al-Malaidi, R. (2012), 'Experimental and finite element analysis of flexural behavior of FRP-strengthened RC beams using cement-based adhesives', *Construction and Building Materials*, Vol. 26, Issue 1, pp. 268–273.

Hill, P. S., Smith, S. and Barnes, F. J. (1999), 'Use of high modulus carbon fibres for reinforcement of cast iron compression struts within London Underground: project details', *Conference on Composites and Plastics in Construction*, November 1999, BRE, Watford, UK. RAPRA Technology, Shawbury, Shrewsbury, UK, paper 16 1–6.

Hollaway, L. C. (2008), 'Advanced fibre polymer composite structural systems used in bridge engineering', in *ICE Manual of Bridge Engineering*, 2nd edition, eds G. Parke and N. Hewson. Thomas Telford, London, pp. 503–530.

Hollaway, L. C. and Head, P. R. (2001), *Advanced Polymer Composites and Polymers in the Civil Infrastructure*, Elsevier, Oxford, UK.

Hollaway, L. C. and Leeming, M. B. (1999), *Strengthening of Reinforced Concrete Structures Using Externally-bonded FRP Composites in Structural and Civil Engineering*, Woodhead Publishing, Cambridge, UK.

Hollaway, L. C., Zhang, L., Photiou, N. K., Teng, J. G. and Zhang, S. S. (2006), 'Advances in adhesive joining of carbon fibre/polymer composites to steel members for repair and rehabilitation of bridge structures', *Advances in Structural Engineering*, Vol. 9, Issue 6, pp. 791–803.

Hulatt, J., Hollaway, L. C. and Thorne, A. M. (2001), 'Developing the use of advanced composite materials in the construction industry', *Proceedings of the International Conference, FRPRC-5*, Cambridge, UK, July 2001, pp. 1133–1142.

Hulatt, J., Hollaway, L. C. and Thorne, A. (2003a), 'The use of advanced polymer composites to form an economic structural unit', *International Journal of Construction and Building Materials*, Vol. 17, Issue 1, pp. 55–68.

Hulatt, J., Hollaway, L. and Thorne, A. (2003b), 'Short term testing of a hybrid T-beam made from a new prepreg material', *ASCE, Journal of Composites for Construction*, Vol. 7, Issue 2, pp. 135–145.

Hulatt, J., Hollaway, L. C. and Thorne, A. M. (2004), 'A novel advanced polymer composite/concrete structural element', *Proceedings of the Institution of Civil Engineers*, Special Issue: Advanced Polymer Composites for Structural Applications in Construction, February 2004, pp. 9–17.

Hutchinson, A. (2008), 'Surface preparation of component materials', in: *Strengthening and Rehabilitation of Civil Infrastructures Using Fibre-reinforced Polymer (FRP) Composites*. Woodhead Publishing, Cambridge, UK, Chapter 3.

Hutchinson, A. (2009), 'Adhesives for externally bonded FRP reinforcement', Chapter 57, Section 7, Sub. Editors, L.C. Hollaway and J.-F. Chen, *ICE Manual of Construction Materials*, Vol. II, ed. M. Forde. Thomas Telford, London, pp. 667–673.

ISIS Canada (2001), Design Manual No. 3, *Strengthening Reinforcing Concrete Structures with Externally Bonded Fiber Reinforced Polymers*, Canada Network of Centers of Excellence on Intelligent Sensing for Innovative Structures, ISIS Canada Corporation, Winnipeg, Manitoba, Canada (Spring 2001).

Kinloch, A. J. (1987), *Adhesion and Adhesives*, Chapman & Hall, London, p. 78.

Leonard, A R. (2002). 'The design of carbon fibre composite strengthening for cast iron struts at Shadwell Station vent shaft', *Proceedings of the International Conference 'Advanced Polymer Composites for Structural Applications in Construction'*, eds R. A. Shenoi, S. J. Moy and L. C. Hollaway, University of Southampton, UK, 15–17 April 2002, pp. 219–227.

Liu, H. B., Zhao, X. L. and Al-Mahaidi, R. (2005), 'The effect of fatigue loading on bond strength of CFRP bonded steel plate joints', *Proceedings of International Symposium on Bond Behaviour of FRP in Structures (BBFS 2005)*, eds F. J. Chen and J. G. Teng, 7–9 December 2005, Hong Kong, pp. 459–464.

Liu, X., Silva, P. R. and Nanni, A. (2001), 'Rehabilitation of steel bridge members with FRP composite materials', *Proceedings of CCC 2001, Composites in Construction, Porto*, Portugal, October 2001, eds J. Figueiras, L. Juvandes and R Furia, pp. 613–617.

Luke, S. (2001), 'Strengthening structures with carbon fibre plates. Case histories for Hythe Bridge, Oxford and Qafco Prill Tower', *NGCC First Annual Conference and AGM – Composites in Construction through Life Performance*, 30–31 October 2001, Watford, UK.

Luke, S. and Canning, L. (2004), 'Strengthening highway and railway bridge structures with FRP composites – case studies', in L. C. Hollaway, M. K. Chryssanthopoulos and S. S. Moy (eds), *Advanced Polymer Composites for Structural Applications in Construction: ACIC 2004*, Guildford, UK. Woodhead Publishing, Cambridge, UK, pp. 747–754.

Luke, S. and Canning, L. (2005), 'Strengthening and repair of railway bridges using FRP composites', *Proceedings of the 5th International Conference on Bridge Management*, eds G. A. R. Parke and P. Disney, University of Surrey, Guildford, UK, 13–15 April 2005. Thomas Telford, London, pp. 549–556.

Meier, U. (1992), 'Carbon fiber-reinforced polymers: modern materials in bridge engineering', *Structural Engineering International*, Vol. 1, pp. 7–12.

Mertz, D. R. and Gillespie, J. W. (1996), 'Rehabilitation of steel bridge girders through the application of advanced composite materials', Final Report to the Transportation Research Board, Washington, DC, Project NCHRP-IDEA, 93-ID11, pp. 1–20.

Mertz, D. R., Gillespie, J. W., Chajes, M. J. and Sabol, S. A. (2001), 'The rehabilitation of steel bridge girders using advanced composite materials', IDEA Program, Final Report for the period Feb. 1999 to Aug. 2000, Contract Number: NCHRP-98-ID051.

Mirmiran, A. (2003), 'Stay-in-place FRP form for concrete columns', *Advances in Structural Engineering*, Vol. 6, Issue 3, pp. 231–241.

Mosallam, A. S. and Chakrabarti, P. R. (1997), 'Making connection', *Civil Engineering*, ASCE, pp. 56–59.

Motavalli, M., Czaderski, C. and Pfyl-Lang, K. (2011), 'Prestressed CFRP for strengthening of reinforced concrete structures: Recent developments at Empa, Switzerland', *Journal of Composites for Construction*, Vol. 15, Issue 2, pp. 194–205.

Moy S. S. J., ed. (2001), *FRP composites – Life Extension and Strengthening of Metallic Structures*, Institution of Civil Engineers, London, pp. 33–35.

Moy, S. S. J. and Lillistone, D. (2006), 'Strengthening cast iron using FRP composites', *Proceedings of the ICE – Structures and Buildings*, Vol. 159, Issue 6, pp. 309–318.

Moy, S. S. J. and Nikoukar, F. (2002), 'Flexural behavior of steel beams reinforced with carbon fibre reinforced polymer composite', *Proceedings of the First International Conference on Advanced Polymer Composites for Structural Applications in Construction*, Southampton University, UK, 15–17 April 2002, pp. 195–202.

Moy, S. S. J., Hill, P., Moriarty, J., Dier, A. F., Kenchington, A. and Iverson, B. (2001), 'Strengthening of tunnel supports using carbon fibre composites', *Proceedings of the Institution of Mechanical Engineers, Part L, Journal of Materials: Design and Applications*, Vol. 215, November 2001, pp. 235–243.

Moy, S. S. J., Clark, J. and Clarke, H. (2004), 'The strengthening of wrought iron using carbon fibre reinforced polymer composites', *Advanced Polymer Composites for Structural Applications in Construction, (ACIC 2004)*. L. C. Hollaway, M. K. Chryssanthopoulos and S. S. J. Moy (eds). Woodhead Publishing, Cambridge, UK, pp. 258–265.

Peshkam, V. and Leeming, M. (1994), 'Application of composites to strengthening of bridges: Project ROBUST', *Proceedings of the 19th British Plastics Federation Composites Congress*, Birmingham, UK, 22–23 November 1994, British Plastics Federation.

Photiou, N. K. (2005), 'Rehabilitation of steel members utilising hybrid FRP composite material systems', PhD Thesis, University of Surrey, Guildford, Surrey, UK, March 2005.

Photiou, N. K., Hollaway, L. C. and Chryssanthopoulos, M. K. (2006a), 'Selection of carbon-fibre-reinforced polymer systems for steelwork upgrading', *Journal of Materials in Civil Engineering*, Vol. 18, Issue 5, pp. 641–649.

Photiou, N. K., Hollaway, L. C. and Chryssanthopoulos, M. K. (2006b), 'Strengthening of an artificially degraded steel beam utilising a carbon/glass composite system', *Construction and Building Materials*, Vol. 20, Issues 1–2, pp. 11–21.

Potyrala, P. B. (2011), 'Use of fibre reinforced polymer composite bridge construction – State-of-the-art in hybrid and all composite structures', Project of the Polytechnic University of Catalonia, Spain.

Righiniotis, T. D., Aggelopoulos, E. S. and Chryssanthopoulos, M. K. (2004), 'Fracture mechanics 2D-FEA of cracked steel plate with a CFRP patch', *Advanced Polymer Composites for Structural Applications in Construction (ACIC 2004)*, eds L. C. Hollaway, M. K. Chryssanthopoulos and S. S. J. Moy. Woodhead Publishing, Cambridge, UK.

Schnerch, D. and Rizkalla, S. (2004), 'Strengthening of scaled steel–concrete composite girders and steel monopole towers with CFRP', *Proceedings of the FRP Composites in Civil Engineering – CICE 2004*, ed. R. Seracino. Balkema, London, Leiden, New York and Singapore.

Schnerch, D. and Rizkalla, S. (2008), 'Flexural strengthening of steel bridges with high modulus CFRP strips', *ASCE Journal of Bridge Engineering*, Vol. 13, Issue 2, pp. 192–201.

Shaat, A. and Fam, A. (2004), 'Strengthening of short HSS steel columns using FRP sheets', *ACMBS-IV, Proceedings* (CD-ROM).

Skinner, J. M. (2009), 'A critical analysis of the Aberfeldy footbridge, Scotland', *Proceedings of Bridge Engineering 2 Conference 2009*, April 2009, University of Bath, Bath, UK.

Smith, S. T. and Teng, J. G. (2002), 'FRP strengthened RC beams II – Assessment of debonding strength models', *Engineering Structures*, Vol. 24, Issue 4, pp. 397–417.

Sobrino, J. A. and Pulido, M. D. G. (2002), 'Towards advanced composite material footbridges', *Structural Engineering International*, Vol. 2, Issue 2, pp. 84–86.

Stratford, T. (2008), 'Aberfeldy Footbridge after 16 years', *Long Term In-service Performance of FRPs in Construction Seminar*, 1 July 2008, Arup Campus, Birmingham, UK.

Swamy, R. N. and Mukhopadhyaya, P. (1995), 'Role and effectiveness of non-metallic plates in strengthening and upgrading concrete structures', in *Non-Metallic (FRP) Reinforcement for Concrete Structures*, ed. L. Taerwe. E & FN Spon, London, pp. 473–481.

Täljsten, B. and Blänksvard, T. (2007), 'Mineral-based bonding of carbon FRP to strengthen concrete structures', *Journal of Composites for Construction*, Vol. 11, Issue 2, pp. 120–128.

Tavakkolizadeh, M. and Saadatmanesh, H. (2003), 'Strengthening of steel–concrete composite girders using carbon fibre reinforced polymer sheets', *Journal of Structural Engineering, ASCE*, Vol. 129, Issue 1, pp. 30–40.

Teng, J. G., Yu, T., Wong, Y. L. and Dong, S. L. (2007), 'Hybrid FRP–concrete–steel tubular columns: Concept and behaviour', *Construction and Building Materials*, Vol. 21, Issue 4, pp. 846–854.

Tong, L. N. and Steven, G. P. (1999), *Analysis and Design of Structural Bonded Joints*, Kluwer Academic Publishers, Boston, MA.

Triantafillou, T. C. (1995), 'Composite materials for civil engineering construction', *Proceedings of the First Israeli Workshop on Composite Materials for Civil Engineering Construction*, Haifa, Israel, May 1995, pp. 17–20.

Triantafillou, T. C. and Meier, U. (1992), 'Innovative design of FRP combined with concrete', *Proceedings of the 1st International Conference on Advanced Composites for Bridges and Structures, (ACMBS)*, Sherbrooke, Quebec, Canada, pp. 491–499.

Triantafillou, T. C., Papanicolaou, C. G., Zissimopoulos, P. and Laourdekis, T. (2006), 'Concrete confinement with textile-reinforced mortar jackets', *ACI Structural Journal*, Vol. 103, Issue 1, pp. 28–37.

Ushakov, A. E., Dunbinsky, S. V. and Ozerov, S. N. (2008), 'Development of modular arched bridge design', *Proceedings of the 5th International Engineering and Construction Conference (IECC'5)*, 27–29 August 2008, paper 116.

Vink, D. (2011), 'Composite materials bridge the divide', *European Plastics News*, 31 May 2011. (Accessed from the Internet on 6 December 2011)

Wiberg, A. (2003), 'Strengthening of concrete beams using cementitious carbon fibre composites', PhD degree thesis, KTH Royal Institute of Technology, Stockholm.

Wu, H. C. and Sun, P. (2005), 'Fibre reinforced cement based composite sheets for structural retrofit', *Proceedings of the International Symposium on Bond Behaviour of FRP in Structures (BBFS 2005)*, 7–9 December 2005, Hong Kong, pp. 351–356.

Xiao, Y. (2004), 'Applications of FRP composites in concrete column', *Advances in Structural Engineering*, Vol. 7, Issue 4, pp. 335–343.

Yu. Y. and Chiew, S. P. (2007), 'Fatigue behaviour of CFRP bonded steel plates', *Proceedings of the 5th International Conference on Advances in Steel Structures – ICASS*, Singapore, 2007.

Yu, Y., Chiew, S. P. and Lee, C. K. (2011), 'Bond failure of steel beams strengthened with FRP laminates – Part 2: Verification', *Composites Part B: Engineering*, Vol. 42, Issue 5, pp. 1122–1134.

Zhang, L., Hollaway, L. C., Teng, J.-G. and Zhang, S. S. (2006), 'Strengthening of steel bridges under low frequency vibrations', *Proceedings of the 3rd International Conference on FRP Composites in Civil Engineering (CICE 2006)*, 13–15 December 2006, Miami, FL.

Zhao, L., Burgueño, R., La Rovere, H., Seible, F. and Karbhari, V. (2000), 'Preliminary evaluation of the hybrid tube bridge system', Report No. TR-2000/04, Final Test Report Submitted to California Department of Transportation under Contract No. 59AO032, February 2000.

18

Advanced fiber-reinforced polymer (FRP) composites for the manufacture and rehabilitation of pipes and tanks in the oil and gas industry

F. TAHERI, Dalhousie University, Canada

DOI: 10.1533/9780857098641.4.662

Abstract: There is strong evidence that the oil and gas industry has become increasingly interested in using pipes and risers made of fiber-reinforced polymer (FRP) composite materials. Moreover, oil and gas exploration nowadays has to be conducted in much deeper water depths (500–1500 m and deeper), thus requiring more resilient and lighter materials. In this section various applications of FRP in relation to pipes and risers are discussed to familiarise the reader with various FRP and hybrid pipes. The issues affecting the long-term performance of these materials, as well as issues involved with joining pipes and risers are also covered. Finally, the recent trends related to the use of FRP for repair and rehabilitation of deteriorated metallic pipes are presented.

Key words: fiber-reinforced polymer composites, pipes, risers, bonded joints, composite repair systems.

18.1 Introduction

Fiber-reinforced polymer (FRP) composite materials have been used for over a half a century in various demanding structural applications in the aerospace and automotive industries, as well as in boatbuilding and sporting goods. Nevertheless, their usage in the oil and gas industry has been relatively less. Some of the main barriers for the relatively slow progress into the widespread usage of FRP in the industry have been the lack of regulatory requirements, specific design procedures, standards and relevant performance information. Some of these impediments have been addressed to a great extent in recent years. As a result, more recently, composite materials have made a significant impact in the oil and gas and drilling industries, as well as in municipal infrastructures.

As has been fully documented and substantiated in the previous chapters of this book, FRP offer many advantages over the traditional materials used to form the structural components used by the oil and gas industry and municipalities. Light weight, corrosion resistance, and tailorability to

various configurations and fittings are some of the advantages one could gain by considering FRP. These materials are currently being used either to reinforce the congenitally formed metallic pipes and other related structures, or to create new structural components used by these industries (i.e., pipes, risers, well liners and caps, to name a few), thereby reducing the maintenance cost and ensuring integrity and longer life for such structures.

Another important reason for the consideration of FRP for pipe formation is the fact that natural resources traditionally found in accessible water depths are becoming progressively and rapidly depleted, thus forcing oil and gas exploration to take place in very deep waters. The significantly larger depths often impede the use of traditional steel alloys, because their inherent high density makes their use prohibitive. As a result, several researchers and companies have explored the use of newly termed 'sandwich' pipes or 'pipe-in-pipes' to overcome the obstacles. These pipes, although made primarily of high-grade steel, have a sandwich configuration (which renders a greater stiffness to the pipe), which is achieved through the use of polymeric materials, and also works as a coupling agent, placed in between steel pipes, thus generating 'composite' structures. It is also believed that as the requirement for energy increases (hence more demand for its exploration), the trend of market expansion for the use of FRP would also steadily increase.

From the historical perspective, the glass fiber-based polymer composites have been the more popular FRP materials used for construction of pipes and platform components for onshore and offshore applications. However, in recent years, subsea applications (especially those in deep waters) have focused more on high performance composites, such as carbon-fiber and steel strip based composites.

In this section various applications of fiber-reinforced polymer composites in relation to pipes and risers, as well as the other applications relevant to the petrochemical and oil and gas industries, will be discussed. The discussion will primarily cover the structural components that are essentially load-bearing components (such as actual pipes and risers).

We will start by introducing the more conventionally used glass fiber-based pipes, followed by hybrid pipes, such as steel strip laminate pipe (SSLP) technology, composite reinforced line pipe (CRLP) and sandwich pipe technologies. A discussion will also be presented, exploring the advantages of the various types of pipes, from the perspectives of their performance and utility, as well as their cost. We will also cover the issues related to long-term performance of these materials, discuss joining of FRP pipes, and finally, introduce the most recent trends in the use of FRP for repair and rehabilitation of deteriorated metallic pipes.

18.2 Glass fiber-reinforced polymer (GFRP) pipes

Glass fiber-reinforced polymer (GFRP) pipes are produced by combining fiberglass reinforcement with a thermosetting resin. Various additives are also incorporated to enhance specific function(s) of the pipe. Successful production of such pipes can only be achieved when the appropriate combinations of all ingredients used to form the pipes meet or exceed design requirements. Some of the key features and performance characteristics of GFRP are:

- They are highly resistant to corrosion, which could be caused by a wide variety of chemical and environmental effects; as a result, GFRP pipes do not require protective coatings on their outer or inner surfaces.
- GFRP pipes have high strength to weight ratio. They are considerably lighter than steel or concrete pipes of comparative strength.
- GFRP pipes are tailorable; as a result, their strength and weight can be optimized based on critical stress locations.
- GFRP pipes can be made as rigid or spoolable; spoolable pipes are generally more easily transportable, especially to hard-reached areas, since a great length of such pipes can be more conveniently transported by either ground or air (i.e., by a helicopter).
- GFRP pipes are normally nonconductive; however, being tailorable, conductive GFRP pipes can be practically and easily manufactured as required.
- GFRP pipes can maintain the required critical tolerances, such as strength and stiffness, dimensional tolerance, weight and cost.
- GFRP pipes require minimal maintenance, since they do not rust and do not need environmental protection. GFRP pipes provide excellent resistance to water and chemicals and unlike metallic pipes they are not affected by corrosion attack. Furthermore, unlike their carbon fiber-reinforced polymer counterparts, they are not susceptible to galvanic corrosion. However, they can be susceptive to certain chemical attacks (such as alkaline), though this aspect can be mitigated by adopting appropriate remedies during the design stage.
- GFRP pipes also offer good thermal resistance. Certain polyester and phenolic resins provide excellent resistance to fire. Moreover, additives such as nano-clays can also be added to resins during the production of the GFRP structure to further enhance fire resistance capacity of these pipes (Bensadoun *et al.*, 2011). Antimony compounds have also been widely used for this purpose (see NYACOL, 2011).
- GFRP pipes also offer excellent resistance to abrasion. The abrasion resistance of GFRP pipes can also be further enhanced by use of additives such as silica, ceramic beads, or carborundum.
- GFRP pipes have excellent resistance against biological attacks (e.g., bacteria, fungi or other microorganisms). With the appropriate choice

of resin additives, GFRP pipes can actually decelerate marine growth, when used offshore.

To achieve the positive attributes noted above, however, the design of GFRP pipes requires a thorough understanding of the mechanics of composite materials, so that one could optimize the design of such pipes based on cost and performance characteristics. For instance, while GFRP pipes in general do offer good weather resistance attributes, their resistance toward ultraviolet UV rays is moderate. UV rays cause resins brittleness, in turn leading to creation of microcracks. This Achilles' heel can, however, be overcome by choosing appropriate UV inhibitors, pigments and dyes.

Although the description of the constituents used to form GFRP pipes as well as the general design principles have been discussed in detail in the earlier chapters, additional design-related facts and hints are further presented below.

18.2.1 Strength

Within a given volume, the strength of GFRP increases with the increase in amount of glass fibers, but to a certain limit, after which not only would the increase in fiber volume produce no additional benefit, but in fact it could degrade the other characteristics of the composite (e.g., its interlaminar shear capacity, toughness, etc.). This is due to the fact that the increase of fiber volume beyond the critical value would leave limited space to the matrix, thus contributing to a decrease in the strength of composite in shear and compression.

18.2.2 Fiber type

As explained in earlier chapters, glass fibers come in a variety of forms from both mechanical and configuration perspectives. Depending upon the application and location in which a pipe is being utilized, one can choose conventional glass (commonly known as E-glass, where the 'E' reflects 'good insulation properties and high temperature resistance' of the fiber), or S-glass (for high tensile strength and stiffness), or some special type of glass fibers, such as 'ECR' and 'C' (for improved acid and chemical resistance, respectively).

18.2.3 Configuration of reinforcements

As also seen in earlier chapters, fiberglass reinforcements can be obtained in various forms, such as continuous roving, woven roving and chop-strand mats. The choice of configuration would largely depend on the selected

manufacturing method. For example, if the pipe is being produced by an automated filament winding process, then continuous roving will be used, while in the case of the pultrusion process, a combination of continuous, woven roving and CSM could be utilized. Chopped strands are also used in the production of medium-strength pipe applications.

Glass fibers also come in 'surface veil' configuration. These veils are lightweight fiberglass reinforcement mats, customarily used to provide extra environmental protection and a smooth appearance, especially when used in conjunction with gel-coats (a special resin used to provide a high-quality finish on the visible surface of a fiber-reinforced composite material).

18.2.4 Resins

As stated, thermosetting resins are commonly used in production of fiberglass pipes, as noted in the earlier chapters. They are basically polymeric resins that are cured by heat or chemical additives. Once cured, the resin cannot be 're-melted' for reuse.

The most commonly used thermosetting resins in production of fiberglass pipes are polyester and epoxy resins. Polyester resins offer good resistance to water and chemicals. They are also recognized for their excellent acid resistance characteristic. Polyester resins are generally used in the manufacture of larger diameter water and wastewater pipes. These resins are cured by organic peroxide catalysts. On the other hand, epoxy resins are used in water and hydrocarbon piping systems of smaller diameter (usually less than 800 mm), intended for service at high pressures. They also have a relatively higher glass transition temperature; therefore, they are also good at withstanding high temperatures.

There are several catalysts used in industry; more commonly used ones are MEKP methyl ethyl ketone peroxide), BPO (benzoyl peroxide), CHP (cumene hydrogen peroxide), DMA (dimethyl aniline), and CoNap (cobalt naphthenate). The correct amount of the catalyst for use with a given resin is usually specified by resin suppliers; the user must assure the exact amount of the specified catalyst when fabricating composites.

Epoxies are generally cured by two commonly used curing agents, namely amine and bisphenol. Heat-curing the resin with bisphenol-A usually provides a good temperature and chemical resistance.

It should be noted that FRP mechanical properties are influenced by the curing agent, therefore a very carefully calculated selection of curing agent is required. This is because a faster cure agent would produce greater shrinkage, which could in turn develop shrinkage microcracks. While microcracks could be tolerated in several structural applications, however, when a pipe carries a volatile liquid, the existence of microcracks could not be tolerated for obvious reasons.

18.2.5 Other materials used in production of GFRP pipes

Besides reinforcements, resins and curing agents used in forming GFRP pipes, there are also some other materials and chemicals that are used in pipe production. The following briefly outlines some such materials.

- Inorganic filler materials, such as hydrated alumina, glass microspheres, clay, talc, calcium carbonate, calcium silicate and sand, are sometimes used to increase the economic benefit and/or performance of GFRP pipes.
- Accelerators are also used to reduce the processing time, while inhibitors are used to decelerate the cure cycle. Inhibitors become useful in lengthening the gel time of resins (usually in conjunction with unsaturated polyester resins), to accommodate slow cure under high-temperature circumstances. For example, pentanedione, which is used to retard resin gel-time, is customarily used when large pipes are manufactured.
- Thixotropes (which are generally silica-based products) are added to resins to minimize resin drain-out.
- Pigments are added to GFRP to generate a desired color and surface finish, as well as providing resistance to UV degradation.

18.2.6 Drawbacks of GFRP pipes

The following are some of the issues that are considered as drawbacks in relation to GFRP pipes.

- The cost of basic constituents (though reduced considerably in recent years) still impedes wider usage of GFRP applications. Nevertheless, once the life cycle of GFRP pipes is considered, this issue becomes less relevant. Nevertheless, relatively higher fabrication cost is still the main impediment to the more widespread use of GFRP pipes.
- GFRP pipes have anisotropic properties; these properties are a function of the fiber orientation and the lay-up sequence used to form the pipe. In comparison to isotropic metals, this aspect makes the design somewhat more complex, thus requiring not only a comprehensive understanding of the basic mechanics of the materials, but also an understanding of the intricacies involved in the fabrication methods and chemistry of the materials (e.g., the role of various chemicals in the curing process, etc.).
- Quality assurance and testing of GFRP pipes is more involved than with metallic pipes, therefore increasing the overall cost of GFRP pipes.
- Buried GFRP pipelines are difficult to detect. However, if need be, metal lines could accompany the pipes for the purpose of finding their location during their service life.

18.3 Steel strip laminate pipes (SSLP)

A combination of composite materials in conjunction with steel was introduced into the pipeline industry in the 1980s, when the application of composites overlaying steel sleeve became a standard for pipeline repairs. One of the most notable applications is that resulting from the collaborative efforts of Enron and the Gas Research Institute (GRI) in 1991, which resulted in installation of SSLP in their system. After eight years in service, the SSLP was inspected, and was verified to be in the same condition as in its initial state. Later on, TransCanada Pipelines Inc. also ventured into the use of SSLP pipes in several projects in 1998, 2001 and 2002 (Stephen, 2005).

Another version of SSLP is the composite reinforced line pipe (CRLP), in which glass-reinforced composite (at the wet and uncured stage) is circumferentially wound around a steel pipe. The composite provides increased pressure capacity and environmental protection against corrosion. Depending upon the requirement, the ratio of steel and composite (in terms of their thicknesses) can be adjusted during manufacturing.

One of the major safety issues in steel pipes is the potential for development of fatigue cracking and propagation due to corrosion or stress corrosion cracking (SCC). A notable advantage of combining FRP to steel pipe is the inherently superior fatigue resistance of FRP that would be harnessed to arrest any crack that may develop in the steel pipe.

Figure 18.1 illustrates the variation of hoop stress developed in steel and composite in a typical CRLP pipe.

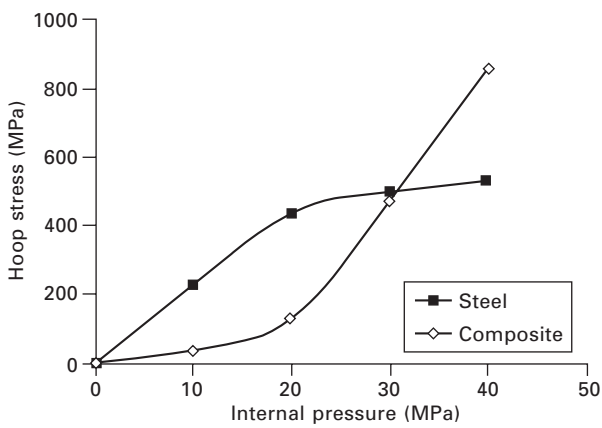

18.1 Typical variation of hoop stress as a function of internal pressure in steel and composite pipes.

18.4 Design procedures

ASTM D2992 provides an excellent procedure for design of GFRP pipes. The standard provides two methods, for static or cyclic loading conditions, for an estimated service life of 100,000 hours (per the static test method) or 150 million cycles (per the cyclic test method). The procedure involves determining the hoop stress (or strain) on the basis of 'hydrostatic design' philosophy, also known as the HDB method. According to HDP, the pressure rating of the pipes is typically based on the hydrostatic capacity offered by the individual layers (laminae) forming the GFRP pipe. On the other hand, under the pressure design philosophy (PDB), the entire pipe wall thickness is assumed to contribute to resisting the pressure. The procedure allows the designer to establish the wall thickness of GFRP pipes based on the internal pressure, the diameter of the pipes and the GFRP specified strength, as well as incorporation of a safety factor.

When designing GFRP pipes, in some cases, the designers would also specify a corrosion barrier (liner) layer. The thickness of the layer would then be added to the pipe's wall thickness as established based on the above-mentioned design methods. In less hostile environments, however, the designer may choose to include the corrosion barrier (or some portion thereof) in the structural calculations. In some cases, the pipe wall thickness is further increased to accommodate other design requirements, such as additional stiffness required for special loading conditions (e.g., in the presence of vacuum in a pipe).

The following simple procedure can be use as the basis for the preliminary design of GFRP pipes. As an example, we consider the design of a 200 mm diameter pipe, subject to 5 MPa internal pressure, using a safety factor (FS) of 6.

According to the basic mechanics of materials, the hoop stress/unit thickness of the pipe can be calculated by:

$$\sigma_{hoop} = \text{pressure} \times \text{diameter} \times FS/2 = 5 \times 200 \times 6/2$$
$$= 3000 \text{ N/mm}$$

The axial stress per unit thickness is calculated by:

$$\sigma_a = \text{Pressure} \times \text{diameter} \times FS/4 = 5 \times 200 \times 6/4 = 1500 \text{ N/mm}$$

Several possible lay-up sequences can be selected to provide the required strength against the above calculated stresses. One possible combination could be obtained by using 12 layers of 13.5 oz/yd^2 chopped strand glass mat (CSM) (with strength of 47.25 N/mm) and six layers of 45 oz/yd^2 woven roving (biaxial) E-glass fabric (with strength of 406 N/mm):

12 layers of chopped strand @ 47.25 N/mm = 567 N/mm

6 layers of woven roving @ 406 N/mm = 2436 N/mm

Total strength = 567 + 2436 = 3003 N/mm.

This would satisfy both the hoop and longitudinal strength. This pipe would have a total thickness of (12 × 0.015″ + 6 × 0.043″) = 0.438″ or 11.125 mm (the data are selected from Vectorply.com).

It should be noted that a more optimum lay-up could have been selected by selecting a biaxial roving woven fabric with biased amount of longitudinal to transfer fibers, so as to overcome the hoop and transverse stresses by approximately equal amounts. Such biased fabrics are commercially available from several vendors.

18.5 Other design considerations

18.5.1 Fittings

It should be noted that in several practical applications the fittings used in conjunction with GFRP pipes are often subjected to higher stresses due to their geometric configuration. For example, a tee-connection becomes subjected to a pressure typically twice that of the same diameter pipe. The designer should therefore use 'pressure stress multipliers' to account for the extra pressure (i.e., increasing the hoop stress by a factor of 2) when specifying such parts. Compensation of such locally induced stress states is crucial and should be considered carefully on a case-by-case basis. In many cases, the designer may be required to conduct a finite element analysis and/or specify appropriate testing to address the situation.

18.5.2 Design considerations for pipes under vacuum

In many practical situations, pipes may be subjected to vacuum or externally applied hydrostatic loadings. In such cases, aside from the strength perspective, one should also consider the stiffness-related issues. Under such loading conditions, a GFRP pipe's wall may locally buckle if appropriate design considerations are not adopted at the design stage. The traditional resolution has been to increase the wall thickness to provide the required stiffness. This is, however, a reasonable means when considering pipes with relatively small diameters that encounter low to moderate external pressure or vacuum. In the case of larger diameter pipes, the above remedy would not be an economical solution, and hence ribs (stiffeners) should be designed and specified to ensure pipe stability under such loading conditions.

The collapse pressure of a GFRP pipe having no stiffener may be computed by the following equation (Ragab and Bayoumi, 1998):

$$P_{CR} = \frac{2E_h t^3}{(1 - \nu_{TL}/\nu_{LT})D^3} \quad [18.1]$$

where E_h is the flexural modulus of the pipe in the hoop direction, t is the wall thickness, ν_{TL} is Poisson's ratio resulting from the strain caused in the axial direction due to the hoop stress, ν_{LT} is Poisson's ratio resulting from the strain caused in the hoop direction due to the axial stress, and D is the outer diameter of the pipe.

For the cases when a pipe should need ribs, its buckling capacity can be calculated by the following equation (DNV, 2010):

$$P_{CR\text{-ribbed}} = K_p P_{CR} = \frac{5.5K_p D_{\theta\theta}}{LR^{3/2}t^{1/2}} \left[\frac{(A_{xx}A_{\theta\theta} - A_{x\theta}^2)t^2}{A_{\theta\theta}D_{\theta\theta}}\right]^{0.25} \quad [18.2]$$

where K_p accounts for geometric imperfection (often referred to as the 'knock–down' factor), usually taken as 0.75, unless a larger value can be justified; L, R and t are the pipe length, radius and thickness, respectively; laminate elastic constants for in-plane deformations $A_{xx}A_{\theta\theta}$ and $A_{\theta\theta}D_{\theta\theta}$ are the stiffness terms, where A refers to in-plane stiffness, D refers to flexural stiffness of the FRP forming the pipe, and X and θ refer to the longitudinal and circumferential (hoop) directions, respectively.

It should be noted that the above equation is valid when the pipe has a symmetric lay-up and the following condition is satisfied:

$$\left(\frac{D_{\theta\theta}}{D_{xx}}\right)^{1.5} \left[\frac{(A_{xx}A_{\theta\theta} - A_{x\theta}^2)t^2}{12A_{\theta\theta}D_{xx}}\right]^{0.5} \frac{2L^2}{Dt} \geq 500 \quad [18.3]$$

A more elaborate equation for calculating the buckling capacity of pipe, accounting for the liquid buoyancy and base flexibility, can be found in the Fiberglass Pipe Design Manual produced by the American Water Works Association (AWWA, 1996).

18.5.3 Practical considerations

As discussed earlier, in comparison to steel pipes, a GFRP pipe with the same thickness as the steel pipe would have lower stiffness, as well as other differences in its mechanical and physical properties that must be considered in practical situations. For instance, due to the relatively more flexible nature of GFRP (in comparison to steel pipes), the support span would be shorter than those specified for steel pipes. In addition, since their tensile strength is relatively lower than that of steel, the consideration of longitudinal load induced by thermal loads, long support span, heavy valves and water hammer must be carefully considered when GFRP pipes are used. For instance, heavy

valves used in conjunction with GFRP pipes are generally independently supported.

In consideration of the fact that GFRP behaves linearly elastic up to its failure (i.e., no yielding), stress concentration in GFRP pipes (e.g., those generated due to support or concentrated loads) should also be carefully compensated for. Other issues, such as the vulnerability of GFRP (and other FRP, in general) to impact, especially under cold service temperature, should also be given particular consideration when designing GFRP pipes.

18.6 Risers

One cannot discuss composite pipes without discussing risers, which are also a form of pipes. Indeed, a riser is one of the major and primary load-bearing structural components involved in exploration of subsea oil and gas. A riser essentially connects the drilling platform to the exploration hole on the seabed. The role of a riser has become even more important and critical in recent years, as the increasing demand for energy and depletion of the traditional resources have forced the oil and gas industry to explore resources in deep and ultra-deep water depths (from the oil and gas industry's perspective, deep waters refer to water depths of between 500 and 1499 meters, while ultra-deep water refers to water depths of 1500 meters and greater). In Brazil, for example, there are some 1200 flexible risers in service, which are responsible for the transportation of approximately 80% of all the oil and gas produced in Brazil. Outside Brazil, there are more than 1000 flexible risers in use in the UK section of the North Sea alone (Elman and Alvim, 2008). In Norway the accumulated number of dynamic flexible risers increased from 30 to 270 from the early 1990s to 2005 (Seaflex, 2011).

Traditionally, steel alloys have been used to form risers; such risers are often referred to as 'rigid risers'. During recent years, however, flexible risers, made of a combination of metallic and polymeric materials, have become more prevalent. The main advantage of flexible risers in comparison to rigid steel risers is the relatively lower bending stiffness of the former, thus rendering the riser to have smaller radii of curvature, yet offering the same pressure capacity. Flexible risers can also naturally undergo larger deformations than their steel counterparts when subjected to the loads from sea currents, vortex-induced vibrations and the motion of the floating vessel and those induced during installation, thus making them more resilient.

A typical flexible riser's cross-section from the inside to the outside layers consists of a steel carcass, a polymer internal sheath, a pressure armor layer, tensile armor layers, and an external sheath. The flexible riser cross-section essentially depends on polymer layers to provide sealing and metallic layers to provide strength. Figure 18.2 shows the cross-section of a typical

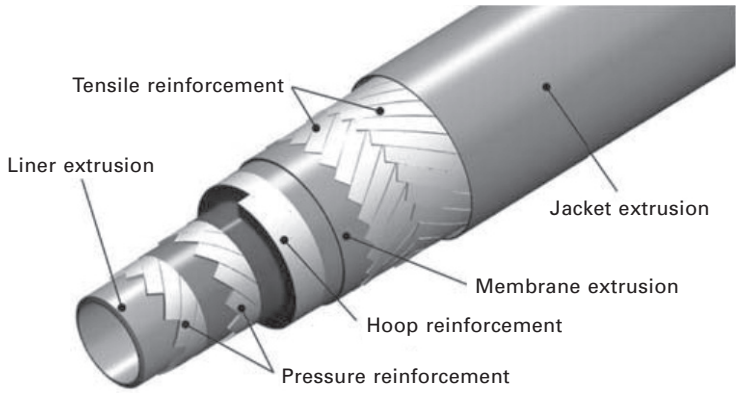

18.2 Unbounded flexible riser layers (*Offshore Magazine,* May 2008).

flexible riser, with more details of each specific layer and constituent given in Table 18.1.

As flexible as these risers are, nevertheless, they become subjected to very large loads at an area near the top section of the riser, close to the bend stiffener (Elman and Alvim, 2008). The resulting critical stresses often cause damage to the external sheathing of the riser, thus promoting corrosion and/or fatigue of the tensile armors, and torsional instability associated with tensile armor rupture. Recent surveys have stated that damage to such risers can also be initiated during their installation phase, since the external polymer sheath can be accidentally torn (reports have indicated that this type of failure is the most prevalent failure type in risers used in the North Sea). Once the sheath is damaged, water can ingress and reportedly reduce the predicted service life of the riser from 20 years to 2 years (Health and Safety Laboratory, 2009). The aforementioned report also tabulates the most frequent failure modes in unbounded flexible risers, and the associated probability.

18.6.1 Riser design standards

There are essentially two main standards that are commonly used in design and operation of flexible risers: ISO 13628-2 and API 17J. These standards offer valuable information regarding the design, test and inspection of risers. As an example, ISO 13628-2 illustrates the riser design criteria. Table 5 of the same publication outlines the load combination to be used for riser design.

Further aspects of the environmental effects on the mechanical and physical properties of GFRP are discussed in the following section.

Table 18.1 Unbounded flexible riser layer functionality and material

Layer	Function	Material
Carcass	Provides collapse resistance to external pressure loads, with a seawater-flooded annulus.	Carcass is manufactured from thin metallic strip, typically stainless steel, fabricated into an interlocked or corrugated tube.
Internal pressure sheath	Contains process fluid within pipe bore.	Polymer materials such as PA, PVDF, PE, and XLPE
Pressure armor wires	Supports internal sheath and internal pressure loads.	Pressure armor layers are manufactured from interlocked metallic layer.
Intermediate sheath	Provides bore collapse resistance in event of breach of outer sheath or end fitting outer sheath seal leakage.	Polymer materials such as PA, PVDF, PE, and XLPE.
Antifriction layer	Prevents metal-to-metal contact.	Antifriction layers are manufactured from polymer materials and are applied as tape or extruded layer.
Tensile armor wire	Provides tensile strength and contains end cap loads.	Tensile armor layers are manufactured from thin rectangular high strength metallic wires in two or four layers, cross-wound for torsional balance.
Anti-birdcaging/ lateral buckling tapes	Provides resistance against radial expansion/compression of the tensile armor wires.	Anti-birdcage layers are manufactured from high strength composite material, such as Kevlar.
External sheath	Prevents ingress of seawater into the annulus of flexible pipe.	External sheath is manufactured from polymer material extruded over tensile armor layers.
Insulation	Provides thermal insulation for bore fluid.	Insulation layers are manufactured from foam tapes or solid insulation.

Source: BP Group Engineering, 2011.

18.7 The influence of the aqueous environment

In the earlier chapters, various authors have provided basic issues regarding the mechanical and physical properties of composites. An issue that may not have been fully covered, which could be considered as an important factor affecting the durability of pipes and risers made of composite, is the issue of long-term durability of GFRP when in contact with an aqueous environment, especially in the presence of relatively high temperatures. GFRP pipes and risers are subjected to harsh environments; the environments

could be water, acidic or alkaline. Even benign environments like water can impact the long-term durability of GFRP, if adequate resin coverage is not insured for the surfaces of GFRP. In such cases, even if adequate resin coverage is provided, the potential presence of microcracks (due to either large deformations or UV rays among many other possible reasons) could facilitate moisture ingress into the GFRP, thus compromising the long-term performance of the material.

18.7.1 Liquid infusion under no externally applied stress

In GFRP, the fiber–matrix interface is the medium for transferring the applied loads from one fiber to another, and hence, it plays an important role in controlling the strength of composites. Several investigators (for example, Bao and Yee, 2011, and Assarar *et al.*, 2011) have shown that humidity diffusion through the matrix is accomplished inherently slowly; nonetheless, moisture would diffuse along the fiber/matrix interface more easily and in turn would degrade the interface-bond. In addition, the fiber cross-section shape has been found to affect the moisture diffusion rate (Aditya and Sinha, 1996). For instance, fibers with regular cross-section (like glass fibers) provide more diffusivity in comparison to fibers with arbitrary cross-section (such as most carbon fibers). It has also been commented that glass fibers possess more permeable nature when subjected to moisture in comparison to carbon fibers (Aditya and Sinha, 1996).

Although it has been argued that the absorption behavior of some polymeric resins is non-Fickian (Berketis *et al.*, 2008), in general it has been demonstrated that Fick's solution can be used to establish the amount of moisture intake in composites formed by epoxy resins with reasonable accuracy. The following equation was developed to estimate the amount of moisture absorbed, at a given time t, by tubular-shaped specimens (Springer, 1981):

$$\frac{M_{\%}}{M_{\infty}} = 1 - \frac{8}{\pi^2} \sum_{n=0}^{\infty} \frac{1}{(2n+1)^2} \exp\left[-D(2n+1)^2\pi^2 t/h^2\right] \qquad [18.4]$$

After some manipulations, we obtain:

$$\frac{M_{\%}}{M_{\infty}} \approx 1 - \exp\left[-7.3\left(\frac{Dt}{h^2}\right)^{0.75}\right] \qquad [18.5]$$

where $M_{\%}$ is the percent moisture absorbed at time t, M_{∞} is the percent moisture absorbed at saturation, h is the specimen thickness and D is the diffusion coefficient.

It should be noted that admissibility of the use of the above equation for estimating moisture absorption in tubular FRP specimens has been examined

and confirmed by several researchers (see, for example, Ellyin and Maser, 2004; d'Almeida *et al*., 2008).

By plotting the graph of moisture content versus time, one can calculate the magnitude of D through the slope of the linear portion of the curve; mathematically, it can be calculated by:

$$D = \pi\left(\frac{h}{4M_\infty}\right)^2\left(\frac{M_2 - M_1}{\sqrt{t_2} - \sqrt{t_1}}\right)^2 \quad [18.6]$$

where t_2 and t_1 are arbitrary times selected along the linear portion of the curve, and M_1 and M_2 are the corresponding amounts of absorbed moisture, respectively.

Moreover, d'Almeida *et al*. (2008) reported that the following equation would better fit the experimental data when fiberglass pipes were tested:

$$\frac{M_\%}{M_\infty} = \tanh\left(\frac{4}{h}\sqrt{\frac{Dt}{\pi}}\right) \quad [18.7]$$

It should be noted that moisture-induced degradation of the fiber/matrix interface could significantly reduce the stiffness of the FRP pipes when subjected to bending, shear and compression loading conditions, while the hoop strength would not be as significantly affected. This is because a debonded fiber/matrix interface acts mainly as interlaminar cracks, and therefore would induce less impact on the strength of the pipes, especially when subject to purely internal pressure.

The moisture saturation duration for a composite can be calculated according to the equation provided in ASTM D5229. The following equation, for example, can be used to estimate the time necessary for a completely dry GFRP to reach 99.9% moisture at a given temperature, regardless of the ambient moisture exposure level:

$$t_{\max}(T) = \frac{0.93h^2}{D(T)} \quad [18.8]$$

where $t_{\max}$ is the time required (in seconds) for a completely dry specimen to reach 99.9% moisture equilibrium, h is the thickness of the composite material (inches), and D is the through-the-thickness Fickian material diffusion constant of the material (in^2/s).

18.7.2 Stress cracking corrosion

Aside from the diffusion issue discussed above, another factor affecting the long-term performance of GFRP, especially when under constant sustained loading (the common loading case for GFRP pipe) is the phenomenon of

stress cracking corrosion (SCC). SCC could significantly reduce the stiffness of GFRP.

Although several power-law type equations have been suggested by various researchers for establishing the reduction in the stiffness of GFRP due to SCC (see, for example, Pauchard *et al.*, 2002), such relations require values of several constants that should be obtained through various tests. Fahmy and Hurt (1980) developed an equation based on the concept of free volume in polymers and explained the effect of stress on the diffusion of water into epoxy. Their equation simply modifies the diffusion coefficient of the materials in the unstressed state, D_0, to obtain the stressed (SCC related) diffusion coefficient), D_σ, based on the following equation:

$$D_\sigma = D_0\left(1 + A\frac{\sigma}{G}\right) \qquad [18.9]$$

where σ, G and A are the applied stress, shear modulus and an experimentally obtained constant, respectively. It should be noted that once a composite host becomes perforated, the rate of water absorption and SCC in such composites becomes greater than in non-perforated situations.

Figures 18.3 and 18.4, obtained through experiment conducted by the author of this chapter, present an interesting insight into the impact of

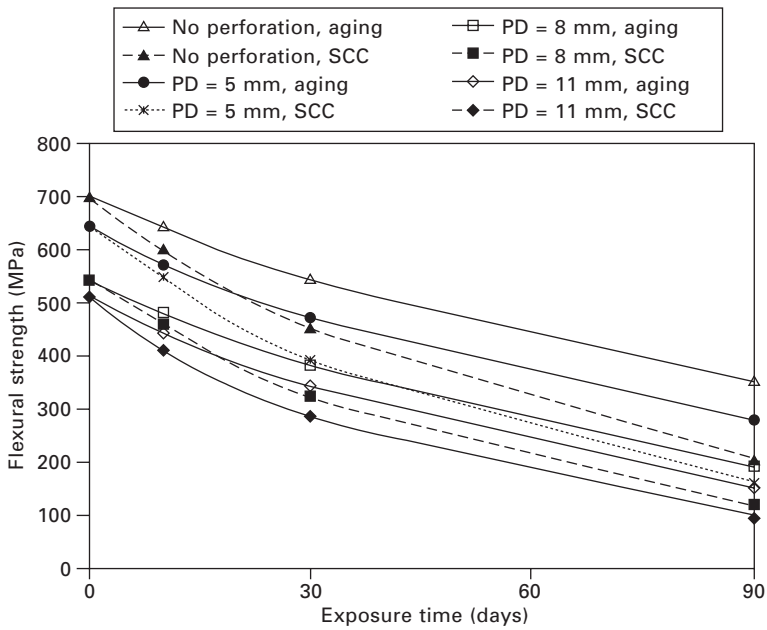

18.3 Degradation in the flexural strength of the perforated specimens as a function of time and perforation diameter (aged in water specimens and those subject to SCC).

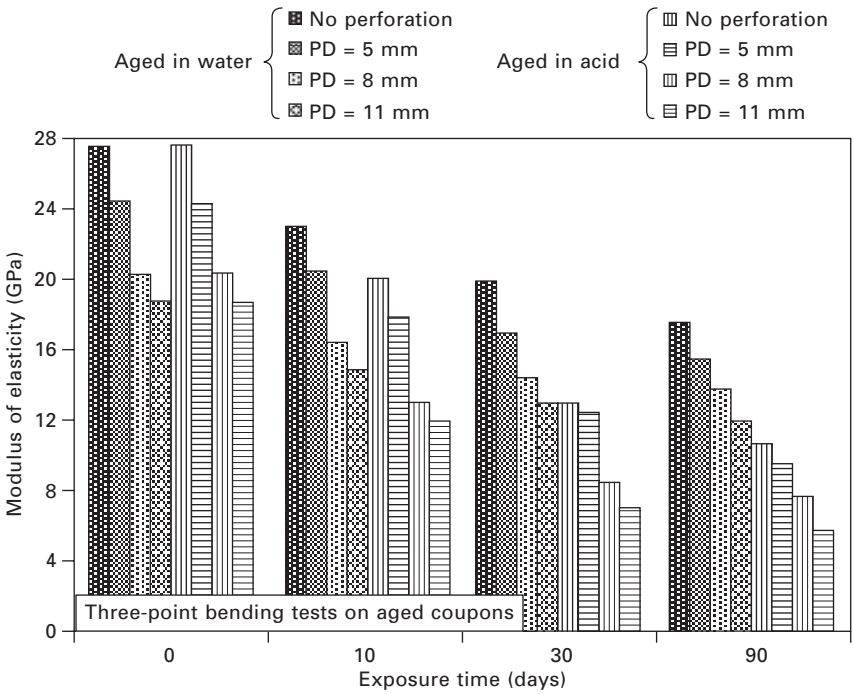

18.4 Degradation in the flexural modulus of elasticity of the perforated specimens as a function of time and perforation diameter (aged in water specimens and those subject to SCC).

immersion of GFRP, in both non-perforated and perforated configurations, in water and acidic environments. The behaviors have been experimentally investigated under no load (aging) and under constant stress situation (SCC). In these figures, PD signifies the perforation diameters; moreover, each curve represents the average response of three specimens.

18.8 Sandwich pipes and pipe-in-pipe design

In this section, the basic design equations will be presented. A major portion of this section will be devoted to sandwich pipes (SP) and pipe-in-pipe (PIP) design technology. This is an important and novel topic, merely due to the fact that explorations for oil and gas are continually being extended into ultra-deep waters, since the volume of crude available in accessible regions has been continually depleting. While the trend in the past decade has been exploration in so-called deep waters, exploration in ultra-deep waters has been deemed as a key element in the continued expansion of the offshore oil and gas industry (Salama *et al.*, 2000). This would indicate that pipe

design must be improved to withstand the very large hydrostatic pressure at such great depths.

In order to facilitate the above requirements in a cost-effective manner, one should resort to a more robust piping system, such as the sandwich pipe technology, since the incorporation of the traditionally used single-wall steel pipes can no longer be considered feasible for such applications.

18.8.1 Design equations

An important factor that governs the design of SP and PIP used in ultra-deep waters is their buckling collapse capacity. The anatomy of a SP is shown in Fig. 18.5.

Sato and Patel (2007) proposed an analytical solution for calculating the buckling capacity by simplifying the problem and determining the buckling pressure of a ring, supported internally by an elastic foundation. They proposed the following equation:

$$P_{cr} = P_{crs} + \frac{1}{n^2 - 1} k \qquad [18.10]$$

where n is the buckling mode number and

$$k = E_c \frac{2n(\nu_c - 1) - 2\nu_c + 1}{4\nu_c^2 + \nu_c - 3} \qquad [18.11]$$

and P_{crs} is the buckling pressure of the external pipe, obtained by:

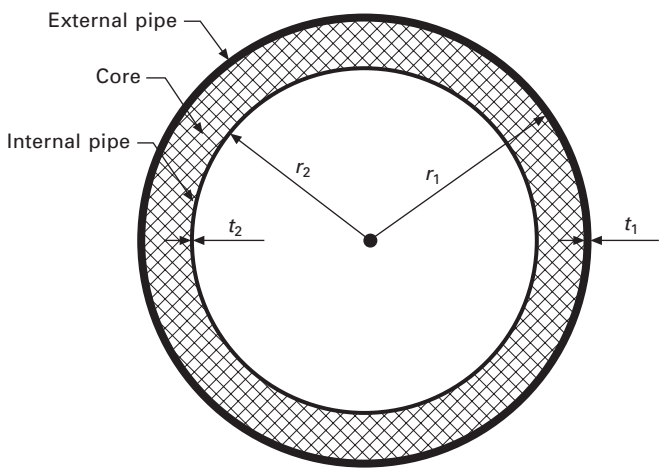

18.5 Idealized geometry of the sandwich pipes.

$$P_{\text{crs}} = \left(\frac{t_1}{r_1}\right)^3 \frac{E_{\text{p}}(n^2 - 1)}{(1 - \nu_{\text{p}}^2)\left(\left(\frac{t_1}{r_1}\right)^2 + 12\right)} \quad [18.12]$$

In the above equations, E_{c}. and E_{p}. are the internal and external pipes' elastic moduli, ν_{c}. and ν_{p} are the core's and pipe's Poisson's ratios, and the other parameters are illustrated graphically in Fig. 18.5.

An in-depth investigation carried out recently by Arjomandi and Taheri (2011b) illustrated that the above equation's prediction of the buckling pressure involves relatively large error margins, especially in SPs with a relatively thick and soft core material. In order to improve the accuracy of the equation, Arjomandi and Taheri proposed a modified solution, which significantly improves the prediction of the buckling capacity of SP in comparison to the Sato and Patel solution presented above. The simplified equation takes the following form:

$$P_{\text{cr-AT}} = \frac{\xi_1}{\xi_2} \quad [18.13]$$

where $P_{\text{cr-AT}}$ signifies the critical buckling capacity based on Arjomandi and Taheri's solution, and

$$\begin{aligned}\xi_1 = {} & 192E_{\text{c}}^2 a_1 r_1^3(\nu_{\text{p}}^2 - 1)^2 + E_{\text{p}}^2 t_1^4 n^2 \Lambda(n^2 - 1)(\Lambda + 7)^2 \\ & + 2E_{\text{c}}E_{\text{p}} r_1 t_1(\nu_{\text{p}}^2 - 1)(\Lambda + 7)\{t_1^2 n^2[n(\Lambda - 1) - \Lambda - 1] \\ & - 6t_1 r_1[(n + 1)^2 + (n - 1)^2 \Lambda] - 12r_1^2[n(\Lambda - 1) - \Lambda - 1]\}\end{aligned} \quad [18.14]$$

$$\begin{aligned}\xi_2 = {} & r_1(\nu_{\text{p}}^2 - 1)(\Lambda + 7)\{-12E_{\text{c}} r_1^2 a_1(\nu_{\text{p}}^2 - 1)[n(\Lambda - 1) - \Lambda - 1] \\ & + E_{\text{p}} t_1 n^2 \Lambda(t_1^2 + 12r_1^2)(\Lambda + 7)\}\end{aligned} \quad [18.15]$$

where $a_1 = r_1 - t_1/2$, and parameter Λ is defined as:

$$\Lambda = 4\nu_{\text{c}} - 3 \quad [18.16]$$

Figure 18.6 compares the predicted external pressure capacity of pipes with different *t*/*r* ratios based on various approaches. The results indicate that Sato and Patel's solution (i.e., equation [18.10] significantly overpredicts the elastic buckling pressure in comparison with the FE linear perturbation analysis results and that the error margin becomes larger as a relatively thicker core layer is used. Moreover, the results indicate that the more simplified solution proposed by Arjomandi and Taheri (2011a) better predicts the elastic buckling pressure capacity with improved accuracy. Moreover, both produce predictions with considerably large error margins when compared with the

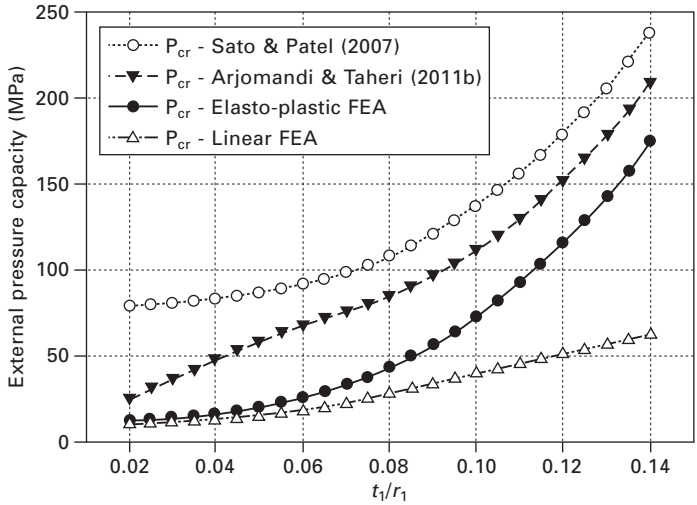

18.6 Comparison of the pressure capacity calculated through different approaches for a sandwich pipe with $t_2/r_2 = 0.03$, $r_2/r_1 = 0.85$ and X60 grade steel internal and external pipes.

linear perturbation FE results. However, when the results are compared with those obtained through elasto-plastic finite element analysis, then the error margins are significantly lowered for the results obtained through Arjomandi and Taheri's solution.

18.9 Manufacturing and assembly of composite pipes and tanks

18.9.1 Manufacturing-related issues

When designing pipes, tanks or risers made of various grades of steel, the designers are more or less ambivalent to the actual manufacturing-related issues. On the contrary, when designing with FRPC materials, the designer must be fully familiar with how the designed parts would be manufactured, so that an effective and economical design could be rendered. For instance, if a hybrid pipe of metal and FRP is being contemplated, the designer should understand the fundamentals of the most effective manufacturing techniques pertinent to formation of such a pipe (in this case, filament winding). Understanding of the automated FRPC manufacturing schemes would directly impact the design of composites, and in certain cases, it could limit the values of mechanical properties that a designer would have assumed in his or her design.

Composite pipes are mainly produced by automated manufacturing methods such as filament winding and pultrusion. It is assumed that the reader has

consulted the detailed descriptions of various composite manufacturing methods given in Chapters 6–9 of this book; as a result, no more discussion on the manufacturing topic is provided in this chapter.

18.9.2 Joining of FRPC pipes

One of the most important design aspects when dealing with FRP structural components is their joining methodology. A majority of failures occurring in FRPC structures as well as in structures made of other traditional materials has been documented to initiate from the joints, where various components are mated. Whether welded (or adhesively bonded in the case of FRPC components) or mechanically fastened (by bolts or rivets), joining is one of the most critical aspects of a design when FRP materials are concerned. That is because, for instance, unlike their metallic counterparts, bolted joints in composites create different values of stress concentration. In other words, while the usual stress concentration at a hole in steel or aluminum components usually takes a value approximately three orders of magnitude larger than that in far-field (i.e., experienced by the non-perforated part of the material), in contrast, in FRP components, the stress concentration increase would vary between 1.6 and 6-fold, depending on the fiber orientation and lay-up sequence of the FRP. Other disadvantages associated with the use of mechanical fasteners that are unique to FRP materials include the high interlaminar stresses induced by the fasteners and the holes accommodating them. Excessive inter-laminar stresses, as well as bolt hole machining, could lead to delamination of FRP plies. FRP members with bolt holes experience a steep reduction in strength. In fact, the most carefully designed FRP fastened joints will attain only half the strength of their base laminates (Hart-Smith, 1987). Moreover, due to the abrasive nature of certain fibers (e.g., carbon and boron), machining of FRP laminates can be an expensive venture. Therefore, the use of mechanical fasteners is less desirable in joining composites.

Adhesively bonded joint is a more preferred means of joining FRP members when disassembly is not necessary. Adhesively bonded joints distribute the load over a larger area than their mechanical counterparts and eliminate the need for holes in FRP members, thereby reducing the risk of delamination. The structurally attractive attributes of bonded joints also enhance their popularity.

The most commonly used adhesively bonded joining methods for composite pipes are (1) adhesive-bonded socket joints, (2) tubular lap joints, (3) heat-activated coupling joints (similar to (1)) and (4) flanged joints (see Fig. 18.7). The first three configurations are considered as permanent joints, while the flanged joints provide the opportunity and ease of quick assembly/disassembly for installation, inspection, and repair. Nevertheless, most composite flanges are

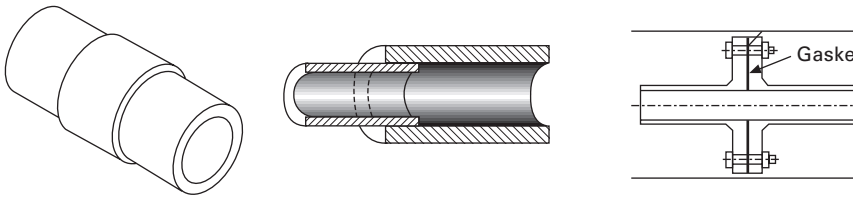

18.7 Commonly used joint types in piping.

connected to composite pipes with one of the aforementioned three permanent joining methods. The same joint mechanism is found in adhesive-bonded socket joints, butt-and-strap joints, and heat-activated coupling joints. In all these joints there are essentially two pieces of composite pipes to be joined, a coupling to carry the load at the connection, and a medium (adhesive) to transfer the load from the pipes to the coupling.

As for bonded joints, adhesively bonded joints are also more susceptible to environmental condition and fatigue loading in comparison to their metallic counterparts, also governed by the lay-up of the FRPC adherends. The aforementioned issues, coupled with the paucity of relevant engineering data, make the design of adhesively bonded joints of pipes more critical.

18.9.3 Design aspects of adhesively bonded tubular joints

Without going into too much mathematical and analytical detail, it suffices to state that the axial strength of tubular bonded joints can be estimated by the traditional analytical approaches, such as that developed by Volkersen in 1938 (Adams *et al.*, 1997). According to Volkersen, the maximum adhesive shear stress in a lap joint can be estimated by:

$$\overline{\tau}_{\max} = \sqrt{\frac{\phi}{2}} \coth \sqrt{\frac{\phi}{2}} \qquad [18.17]$$

where

$$\phi = \frac{GL_{\text{bond}}^2}{Et_{\text{adhesive}}t_{\text{adherend}}} \qquad [18.18]$$

in which G is the shear modulus of the adhesive, L_{bond} is the bond length and E is Young's modulus of the adherends (which are assumed to have equal thicknesses).

Later on, Goland and Risner considered the rotation that takes place in the bonded section of single lap joints as a result of non-collinearity of

the forces applied by the adherends; they developed a new formulation for evaluating the maximum shear stress. However, the phenomenon would not be a critical issue in bonded tubular joints.

A critical issue when designing adhesively bonded joints mating pipes is when the joint undergoes torsion, which could often be experienced by pipes and risers in their service lives. Again, without elaborate mathematical derivations, the distribution of the shear stress in the adhesive with reference to the geometry shown in Fig. 18.8 can be evaluated by the following equation:

$$\tau_{\mathrm{a}} = \frac{T\alpha}{2\pi a^2}\left[\left(\frac{1-\psi(1-\cosh \alpha L)}{\sinh \alpha L}\right)\cosh \alpha x - \psi(\sinh \alpha x)\right] \qquad [18.19]$$

In the above equation, $T = \frac{\tau_{2i} J_2}{r_{2i}}$ and $\alpha = \left(\frac{\delta}{\psi}\right)^{\frac{1}{2}}$, in which $\delta = \frac{2\pi a^2 G_{\mathrm{a}} r_{1o}}{\eta G_1 J_1}$ and $\psi = \frac{G_2 J_2 r_{1o}}{r_{2i} G_1 J_1 + r_{1o} G_2 J_2}$ and J_1 and J_2 are the polar moments of inertia of the adherends; G_{a}, G_1 and G_2 and the shear moduli of the adhesive and the adherend, respectively; and a is the adhesive thickness and L is the bond length.

A more exact formulation for assessing the stress distribution in tubular bonded single-lap and socket joints is provided by Zou and Taheri (2006).

Hosseinzadeh *et al*. (2006) provided a simple equation for establishing the effective bond length. Effective bond length is defined as the bond

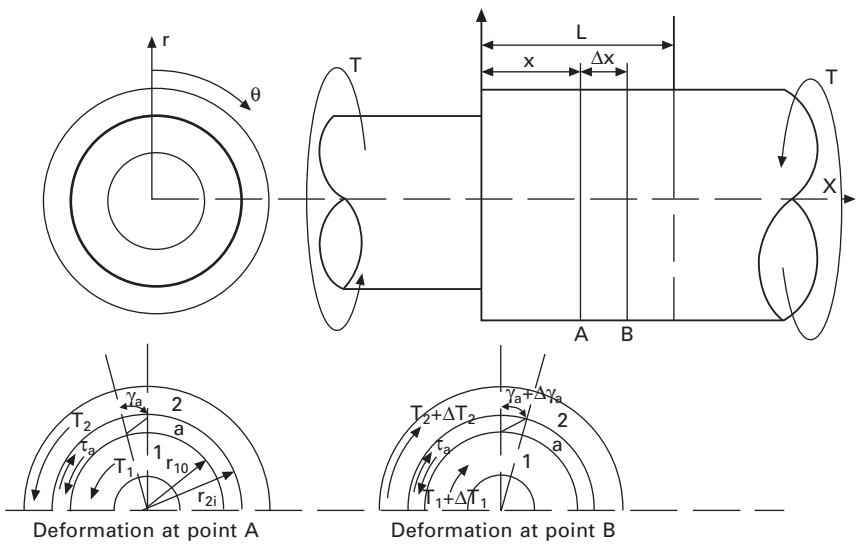

18.8 Deformation in tubular lap joint under torsion.

length within which the shear stress distribution is more or less constant, as opposed to that created in usual (longer) length joints, where the shear stress is a maximum on the edges of the bond line and very low elsewhere (see Fig. 18.9).

The equation for establishing the effective bond length is as follows:

$$\left(\frac{\tau_{\max}}{\tau_{\text{avg}}}\right) = \left(\frac{\pi D_{\text{avg}}^2 \tau_{\max}}{2T}\right) L = \xi L \qquad [18.20]$$

In the above equation, D_{avg} is the average diameter (half-way through the thickness of the adhesive), T is the applied torque, and ξ is a coefficient related to the adhesive's thickness.

18.10 Repair and rehabilitation of composite pipes

Although various pipeline repair techniques, such as the steel sleeve, have been in use for several decades, the introduction of FRP repairs has been widely recognized as a remarkable advancement. Indeed, since the initial development of the composite repair techniques in the early 1990s, the use of FRP in pipeline rehabilitation has been gaining increasing popularity in the pipeline industry. This is because FRP repairs offer a high strength to weight ratio, excellent chemical and corrosion resistance, transparency to electromagnetic radiation, and strong resistance to fatigue. The main benefit of the composite repair method over other conventional repair methods is in its ability to maintain operations without interruption during the repair. In addition, the safety, economic feasibility and anti-corrosion attributes

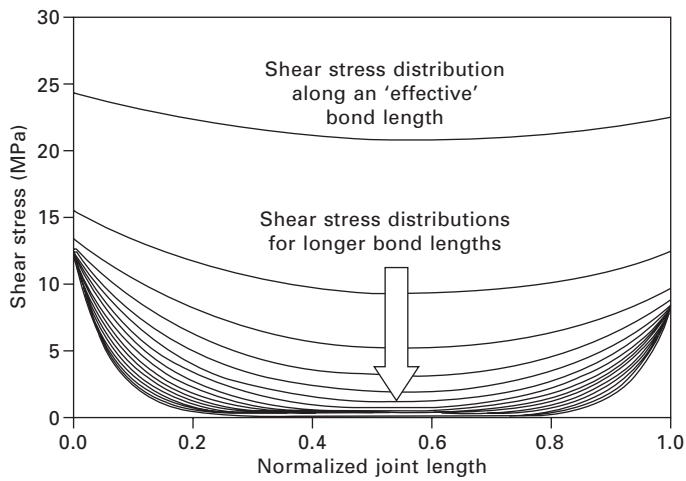

18.9 Shear stress distribution along various joint lengths.

associated with the use of FRPC repair make it a highly attractive option. FRPC repair can be easily implemented, and it provides adequate strength as compared to other traditional methods (e.g., the steel sleeve repair method). To date, extensive research works have been performed on the development of FRP composites, with some regulatory authorities approving these composite repair methods as 'permanent repair methods'. Moreover, when considering the overall cost of traditional pipeline repair techniques in comparison, FRP repair would be deemed as more economical and feasible.

In this section of the chapter, the basics of pipe repair techniques using FRP materials will be discussed. Design equations for selecting the appropriate thickness of FRPC repair wrap will be provided. Various commercially available repair kits will be introduced. The advantages and specific attributes of the various repair techniques will also be discussed.

18.10.1 Advantages of the use of FRP for repair of pipelines

Nowadays, the use of FRP materials instead of the traditionally used steel sleeves for repair and rehabilitation of pipes has become quite popular. The most commonly used FRP pipeline repair materials consist of fibers such as glass and carbon, whereas the most commonly used resin is epoxy. FRP, with a combination of glass fibers and epoxy resin, is mostly used in the pipeline industry due to the following characteristics:

- Excellent corrosion resistance
- High strength-to-weight ratio
- Light weight compared to most metals
- Non-conductive to electricity
- Dimensional stability
- Low maintenance cost
- Unlimited shape/size configurations
- Orthotropic in nature (different properties in different directions)
- Relatively lower material cost (in comparison to carbon).

18.10.2 Types of FRP repair systems

FRP repair systems for pipelines can be categorized into two main categories depending upon the way in which they are delivered and installed *in-situ*. These systems are either 'wet lay-up' or 'post-cured' wrap systems. Some of the commonly used commercially available repair systems are introduced in the following sections.

Wet lay-up systems products in the market

The wet lay-up systems most commonly used in the industry are Aqua-Wrap, Armor Plate wrap, BlackDiamond wrap and StrongBack systems.

Aqua-Wrap

Aqua-Wrap (California, US) is manufactured commercially in compliance with the US Department of Transportation (DOT). Aqua-Wrap (see Fig. 18.10) uses water-activated polyurethane resin, which cures in wet conditions and under water. Thus, it can be applied and fully cured in water.

Armor Plate

Armor Plate (Texas, US) is another pipe repair system that uses multipurpose fiberglass/epoxy wraps and different curing agents (see Fig. 18.11). The difference between Armor Plate and StrongBack composite repair systems (discussed below) is that Armor Plate uses chemicals instead of water as the catalyst agent.

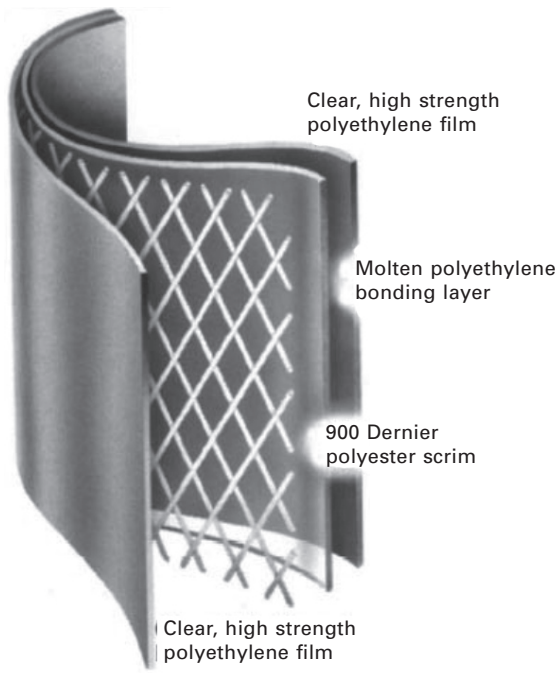

18.10 AquaWrap pipe repair system (Advanced Waterproof Technologies, 2005).

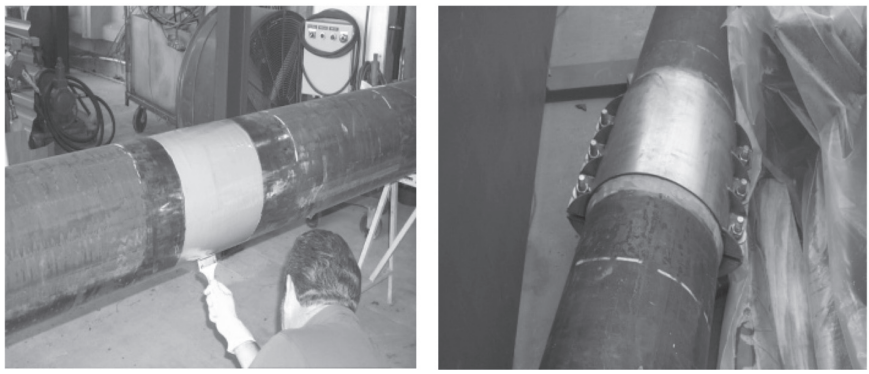

18.11 Installation of Armor Plate Pipe Wrap and armor clamp installed on a dented pipe (Alexander, 2008).

18.12 BlackDiamond wrap (Citadel Technologies, 2007).

Recommended for low levels of corrosion and mechanical damage, Armor Plate is monolithic in nature and can be applied to various pipe configurations under different environmental conditions such as high temperatures or pressures, below-freezing temperatures and on irregular pipeline surfaces.

BlackDiamond

The BlackDiamond (Oklahoma, US) repair system (Fig. 18.12) is a combination of solid epoxy primer, bidirectional carbonfiber and polymeric epoxy resin. The epoxy primer ensures the complete bonding and load transfer repair and substrate. The bidirectional carbonfiber material provides reinforcements in

the hoop and axial directions. The epoxy resin allows the uniform loading throughout the wrap. The BlackDiamond system offers reduced thickness solutions and shows minimal creep, and its stiffness is almost equal to that of steel. It can be used to repair complex geometries like branches, tees, elbows, valve boxes and reducers.

StrongBack systems

StrongBack (Texas, US) repair systems (Fig. 18.13) are manufactured by StrongBack Corporation. StrongBack systems use glass reinforcements that are resin impregnated and activated by water and use glass fiber remediation materials (Alexander, 2008). The main feature of the StrongBack repair system is that it uses a biaxially woven glass cloth, which functions to provide reinforcement in both the hoop and transverse directions. Some of the system's properties are presented in Table 18.2.

StrongBack composite wrap systems can be applied to wet lines (under water), as it has the ability to displace the water from wet surfaces in order to make a permanent wrap. This tape-wrap reinforcement system can be used in the repair of low corrosion levels or mechanical damage.

Post-cure repair systems

Post-cure repair systems involve bonding a post-cured system, which is held together using an adhesive, which is applied in the field. A variation in strain is noted between different layers of this system. Research shows that

18.13 StrongBack composite repairs (Integ Pipeline Services, 2006).

Table 18.2 Technical specifications of the StrongBack repair system

Mechanical properties		
Tensile strength (73°F)	ASTM-D-3039: Modified	61,220 psi
Flexural strength (77°F)	ASTM-D-790	53,100 psi
Compression strength	ASTM-D-695	32,800 psi
Interlaminar shear (77°F)	ASTM-D-2344	4500 psi
Glass transition temperature	ASTM-D-831	
Temperature cycle test	16 layers cycled from 75 to 450°F with no delamination or loss of bond	
Technical specifications		
Number of plies required	8 min. to 10″ OD, 10 min. over 10″ OD	
Application methods	Water activated wet lay-up	
Cure time	30–60 minutes	
Shore D hardness (24 hour cure)	80	
Heat resistance (24 hour cure)	500°F	
Maximum installation temperature	350°F	

Source: StrongBack, 2007.

mostly the inner layers are responsible for carrying the bulk of the load and the outer layers provide redundancy in terms of overall reinforcement. The application of these systems is limited to straight sections of pipes. Examples of post-cured systems are ClockSpring and PermaWrap.

ClockSpring

The ClockSpring pipeline reinforcement system consists of a coil wrap of high-strength composite material. It is a three-part system consisting of a high-strength composite structure, a high-performance two-part resin system, and an extremely high-compressive-strength proprietary load transferring component or filler (Mohitpour *et al*., 2005). In this technology, the pipe with a defect is wrapped with a fiberglass composite-reinforced coil, locked in position with a specially designed adhesive. These three components, when bonded together, form a strong durable repair. The adhesive plays an important role in the three-part component. It is resilient enough to maintain its integrity for at least 50 years in varying conditions (Mohitpour *et al*., 2005). A typical ClockSpring installation uses eight complete wraps of the pipe to form a 0.50-in-thick monolithic structure. The strength of this wrap actually exceeds the yield strength of the original pipe. The glass component in the ClockSpring system maintains its strength, which also gives extra resistance against corrosion. Figure 18.14 shows a typical ClockSpring pipe repair.

Research conducted by the Gas Research Institute (GRI) concluded that if the ClockSpring system is properly installed on the defected area, it can permanently restore the pressure-containing ability of the pipe. The purpose

18.14 A typical ClockSpring pipe repair (Tecma Pipeline Services, 2009).

of the filler is to level up the defect (i.e., corrosion, mechanical damage or dents, etc.). Also, the filler helps to support and load transfer before ClockSpring is installed. However, the use of ClockSpring has certain limitations; for instance, it is not recommended for rehabilitating pipes having sharp cracks or internal defects. Furthermore, since its reinforcement has a unidirectional fiber configuration, it is not recommended for repair of girth-weld/circumferential defects.

PermaWrap

PermaWrap uses a two-part adhesive system and a rigid fiberglass sleeve (Fig. 18.15). The adhesive system bonds the PermaWrap sleeve to the pipe surface. High compressive strength putty is used to fill the cavities and dented areas; it serves to transfer the load from the pipe surface to the PermaWrap repair sleeve. The sleeves come in various widths (from 6″ (150 mm) to 18″ (457 mm)). The main feature of PermaWrap sleeve repair is that it can be detected by a 'smart pig' or magnetic flux leakage tool.

18.10.3 Design of FRP wrap systems

Design considerations

As stated earlier, the purpose of a composite repair system is to reinforce the damage caused as a result of corrosion or mechanically related forces causing

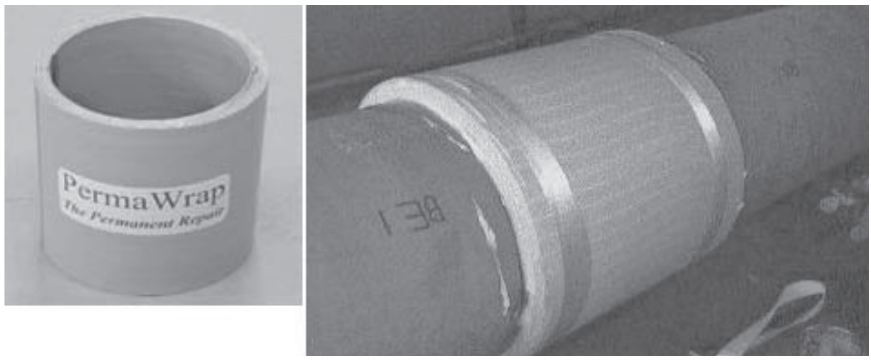

18.15 PermaWrap repair systems (Russell NDE Systems, 2010).

dents and gouges. In evaluating the repair system, beside the establishment of the appropriate thickness for the reinforcing wrap system, several other factors require careful consideration (Alexander and Fracini, 2006; Shouman and Taheri, 2011):

- The effect of the surrounding environment (such as the ambient temperature and/or whether the surroundings are acidic or alkaline)
- The strength of the composite materials at elevated or sub-freezing temperatures
- The effect of different pressure conditions, like static and cyclic pressures
- The effect of moisture and liquid diffusion
- The mechanics of load transfer from pipe to wrap
- Careful assessment of the long-term performance of FRP, especially when adhesively bonded joints are also involved
- Consideration of the consistency in application and the importance of quality control in manufacturing and installation of the system.

FRP repair wrap thickness calculations

Prior to calculation of the appropriate thickness of the FRP wrap, it would be prudent to conduct a preliminary calculation to assess the integrity of the pipe in its present condition.

Assuming that the pipe hosts a gouge, the hoop failure capacity of the pipe, σ_f, hosting an axially oriented gouge can be calculated according to the following equation provided by ASME B31G (2009):

$$\sigma_f = \sigma_{flow}\left(\frac{1-\frac{2}{3}\left(\frac{d}{t}\right)}{1-\frac{2}{3}\left(\frac{d}{t}\right)\left(\frac{1}{M}\right)}\right) \qquad [18.21]$$

where $\sigma_{flow} = \frac{SMYS + S_{ult}}{2}$ is the flow stress, SMYS is the specified minimum yield strength of the pipe material, S_{ult} is the ultimate tensile strength in the hoop direction of the pipe material, t is the pipe wall thickness, d is the depth of the gouge (taken usually as 80% of the wall thickness, this being the maximum allowable gouge depth that such repair strategy can be applied to), and $M = \sqrt{1 + 0.80\left(\frac{L^2}{Dt}\right)}$ with L defined as the length of the gouge and D being the outer diameter of the pipe.

Once σ_f is calculated, the burst pressure P_f of the damaged pipe can be calculated by the following equation:

$$P_f = 2\sigma_f\left(\frac{t}{D}\right) \quad [18.22]$$

According to ASME PCC-2 (2006), the main purpose of FRP wrap repair is to strengthen an undamaged section of the pipe to carry the additional loads caused by the damaged or weakened section. Assuming that the repair is applied at zero internal pressure and the pipe material behaves elastic–perfectly plastic (i.e. no strain hardening), the minimum composite repair thickness, t_{repair}, can be calculated by:

$$t_{repair} = \frac{1}{S_c}\left(\frac{PD}{2} - SMYS \times t_s\right) \quad [18.23]$$

where S_c is the tensile strength of the glass FRP composite material in the circumferential direction, $P = \frac{2 \times SMYS \times t_s}{D}$ is the internal design pressure based on the yield criterion, and t_s is the minimum remaining wall thickness of the pipe.

The burst pressure of the repaired pipe can be estimated by the following equation, which is obtained based on a pseudo rule-of-mixture:

$$P_{fail} = \left(\frac{2S_{ult}t_s}{D}\right)_{steel} + \left(\frac{2S_c t_{repair}}{D}\right)_{composite} \quad [18.24]$$

It is therefore clear that a great enhancement in the pipe burst pressure could be achieved by using FRP repair, as the burst pressure of the repaired pipe can be increased significantly in comparison to its capacity in its damaged state (usually more than twice the capacity).

18.11 Case studies

As stated earlier, FRP pipes have been used in a variety of applications. A few notable applications are listed below.

18.11.1 Imperial Oil composite flowlines

In 2005, Imperial Oil completed the placement of over 1760 km of FRP flowlines in the Norman Wells oil field in the Northwest Territories of Canada (*Oil & Gas Journal*, June 2005). These lines replaced some of the corroded steel lines in that location. The FRP pipes offered 50% less wall thickness compared to the steel lines. Star 2000 Manufacturers of San Antonio manufactured the pipes. Installation cost was estimated at 25–40% less than that of steel. Moreover, 1000 m of the FRP pipe could be laid in two hours, half of the time required to lay steel pipes.

Another advantage of using the FRP was the longer support span (which went as high as 10 m in comparison to the 3–4 m counterparts usually used for steel pipes). At the time, the FRP pipe cost was only 8% more than steel (since the steel price had increased by 80% in one year).

18.11.2 TransCanada Pipeline

TransCanada Pipeline Limited (TCPL) is a leader in natural gas and crude oil transportation and storage in North America. It started its first task in the mid-1950s, when systems of pipes, with diameters as large as 48″ (1219 mm), spanned thousands of kilometers through Alberta, Saskatchewan, Manitoba, Ontario and Quebec provinces in Canada. Currently, it maintains the longest pipeline array in Canada (nearly 57,000 kilometers).

Although TransCanada Pipeline had been involved in developing and testing a hybrid product called the composite reinforced line pipe (CRLP) since the mid-1990s, they demonstrated the practicality in the application of CRLP in western Alberta in 2005 (*Oil & Gas Journal*, March 2003). This initiative was started due to the growing trend in the natural gas transportation industry for using costly high-strength pipelines capable of transporting fluids at high pressure. At the time, X70 grade steel pipes with diameters as large as 48″ with 0.461″ wall thickness were being used. The industry chose to wrap the steel pipes with isopolyester resin–glass fiber composite. The selected GFRP offers high mechanical and corrosion resistance properties and is stable under high temperatures. The hybrid CRLP was estimated to offer resistance to internal pressure of 3600 psi (240 MPa). The hybridization also increased the resistance against dents and gouges.

A glass fiber layer in isopolyester resin has a tensile strength of 120,000-140,000 psi which makes the composite layer twice as strong as its underlying steel layer.

An important attribute of CRLP is the relative safety they offer. One of the major safety issues of pipelines is fracture propagation in pipes. Even a minute crack developed on the pipe surface can be enough to fail a high-pressure pipeline. Unlike steel, CRLP is a multi-layered pipe which has the

ability to arrest any fracture developed due to corrosion or stress corrosion cracking (SCC) on the steel liner or the outer composite layer.

To demonstrate the added safety offered by CRLP, a burst test was conducted on a pipe section which hosted an initial crack. This section was first isolated from the rest of the pipe by installing composite material over the pipe sections, one upstream and the other downstream of the fractured pipe. CO_2, which produces the highest crack driving force in pipes, was used to pressurize the pipe section during this test. It was observed that the fracture propagated through the pipe section quickly when pressurized to burst; nevertheless, the fracture was arrested by the composite layer on both ends. This test indicated a fracture arrest capability of CRLP beyond the expectation.

Moreover, Zimmerman *et al*. (2002) also reported that the hybrid pipe's mechanical properties improved markedly, e.g., ultimate strength of 483–1034 MPa compared to 485–655 MPa, as well as an elastic modulus of 48 GPa compared to 207 GPa of steel pipes. Thermal expansion was reported to be 12×10^{-6}/°C compared to $7–9 \times 10^{-6}$/°C, and Poisson's ratio was 1.2–2.7 compared to 0.3, both with respect to the steel counterpart, respectively.

In addition, the use of CRLP gave a cost saving of 10–20% in material cost when compared against X100 steel pipe. The associated 30–40% weight reduction offered by CRLP reduced transportation costs. There was also an estimated saving of 40% in welding, since thinner steel pipe was used. In all, it was reported that the hybrid CRLP could offer an overall cost-saving of approximately 20% in comparison to the conventional steel pipe.

18.11.3 Four-inch diameter 5000 ft (1.5 km) producing line

In order to connect one of its wells to its facility in the Badin district of Pakistan, British Petroleum Pakistan planned to construct 5000 ft (1524 m) of 4-inch diameter spoolable reinforced composite pipe (SRCP). Python series 1500 cross-linked polyethylene (PEX) spoolable pipe was selected, offering a maximum operating temperature of 180°F (80°C). Table 18.3 reports the physical properties of the spoolable reinforced composite pipe.

Table 18.3 Mechanical proposers of the SRCP

Property	Value
Axial elastic modulus	2.0×10^6 psi
Hoop elastic modulus	4.1×10^6 psi
Axial coefficient of thermal expansion	1.0×10^{-5} in/in/°F
Poisson's ratio	0.40
Average density	0.052 lb/in^3
Flow factor coefficient	150 Hazen Williams Coefficient

Source: Kham *et al.,* 2005.

The type of pipe used was selected in response to the challenge caused by the very rough terrain and the related environmental concerns (i.e., handling water tables, etc.). Valuable lessons were learnt in relation to mainly the configuration of the trenches (it was found that they should be made as straight as possible, with relatively wide turn radii). In addition, the tension in the pipe (especially when laying or pulling the pipe) should be carefully monitored.

18.11.4 Oil gathering line

Thermoflex tubes with diameter of 1.75″ were used to form the gathering line in an operation in North-western West Virginia (PolyFlow, 2012). The lines, produced by PolyFlow Inc. of Oaks, PA, accommodate 200 bbl/day capacity flow with no brine content. Due to the hilly area, the line had to accommodate an operating pressure up to 500 psi. These tubes incorporated a Fortron liner to eliminate the potential for paraffin build-up in the pipe and were rated for 1000 psi operating pressure. Since these pipes were connected to steel lines, it was found that appropriate measures should be taken to protect the FRP section in the transition region, so that the weld temperature propagation would not exceed 120°C.

18.12 Conclusion and future trends

The emergence of advanced FRP composites in recent years has revolutionized the possibilities of design methodologies for composites. These design methodologies can be potentially used in producing composite structures that could withstand various demanding and complex loadings and physical and environmental conditions. There has also been an exciting new niche in the application of composites, which involves the use of composites for repair and rehabilitation of pipelines. Various real-life applications have demonstrated that FRP can be used to repair and prolong the life cycle of pipelines in a very cost-effective and non-intrusive manner.

This chapter outlined various applications of FRP in relation to pipes and risers, and those relevant to the petrochemical and oil and gas industries. It introduced various hybrid applications of FRP and its hybrid, such as the steel strip laminate pipe (SSLP) technology and the composite reinforced line pipe (CRLP) technology, and sandwich pipes as well as their pertinent design procedures. The issues affecting the long-term performance of these materials, as well as the issues involved in joining them, were also discussed.

Recent and future trends in the context of application of FRP in the above-mentioned structures involve various innovative and exciting developments, mainly with the aim of overcoming the complex and extreme conditions imposed on pipes and risers at very large depths. For example, as stated in

the chapter, since the world's energy resources are fast becoming depleted, the need for exploration in deep and very deep waters has become a new reality and, of course, a great challenge. The challenge is in developing not only resilient structural components that could withstand the harsh loading and environmental conditions in deep waters, but also effective methods for monitoring the health of the structures under such complex and harsh conditions.

In another effort, researchers have been working towards effective solutions for health monitoring of pipelines. As a result, for instance, there have been great strides in recent years in developing advanced monitoring systems for assessing the integrity of pipelines. Indeed, advancements in electronic technology and material sciences have established a new trend in 'smart structural health monitoring systems' (SSHMS). The main components of such smart systems include new materials that can sense appropriate elements (e.g., stress, temperature and pH), as well as new techniques that enable the effective assessment of such parameters. For instance, one of the recent advances in SSHMS involves the use of piezoelectric sensors, along with the most recent signal processing technique (i.e., Empirical Mode Decomposition (EMD)), used to develop a robust technique for detection of damage and real-time heath monitoring of pipelines and various types of joining systems used to mate pipelines (Cheraghi and Taheri, 2007; Rezaei and Taheri, 2010; Esmaeel *et al*., 2012). The technique allows nondestructive and real-time monitoring of structural components. The new advances in electronics have further allowed the advancement of remote SSHMS, wirelessly (see Razi *et al*., 2012).

Another example of such advancement is the use of fiber-optic cables that have been incorporated through the entire length of pipes, thereby enabling the operator to measure temperatures and stresses at thousands of points along the pipe in a very short time. Such systems are used to detect pipeline leakages, verify pipeline operational parameters, prevent failures of pipelines constructed in landslide zones, optimize oil production from wells and detect hot-spots in high power cables. In essence, this advancement increases safety, decreases economic losses and optimizes maintenance cost.

A newly developed sensing system called DiTeSt (Distributed Temperature and Strain monitoring system) produced by SMARTEC of Switzerland (see http://smartec.ch/index.htm for more details) incorporates a distributed sensing device with linear measurement basis (Inaudi and Glisic, 2010). The sensors used in the component have a single optical fiber distributed all along the length and a low fiber attenuation allowing for monitoring of long lengths.

Moreover, today's reservoir drilling and exploration requires more advanced intelligent technology. One such technology could be in so-called 'electric coil tubing', where composite coil tubing could be considered as a viable

answer. Recently, a special composite pipe with high pressure and temperature rating, equipped with the capability of power and data transmission (PDT-COIL), has been developed by SMARTEC of Switzerland, incorporating an embedded electrical power and fiber-optic cable for sensing, monitoring and data transmission, wound by a structural layer of carbon and glass fibers embedded in high-performance thermoplastic polymers. An electric cable is used to supply power to submersible pumps and drilling motors, while SMART fiber-optic sensing and monitoring cables measure the relevant well parameters, monitor the structural integrity of the PDT-COIL and can be used for data transmission as shown in Fig. 18.16.

The most recent trends also involve the use of nanocomposites in developing more resilient pipes/risers. As stated earlier, the use of hybrid composites has enabled us to develop very strong and lightweight structures, such as risers, thus facilitating exploration in deeper waters. A great example is the relatively recent development by Lincoln Composites, which produced a hybrid composite riser, composed of carbon and S-glass fibers in an epoxy matrix, possessing an average burst pressure of ~80 MPa, with an axial load capacity of 4190 kN. The in-air riser's weight was 41% less than that of the comparable steel riser, but its in-water weight was 68% lighter. However, even this advanced technology encounters problems as the demand for exploration in deeper waters advances. An important factor (in other words, the weak link) that impedes further gains in strength and stiffness that are offered by fibers like glass and carbon is the relatively much lower strength of the resins used to form the composites. As a result, not only cannot the inherent

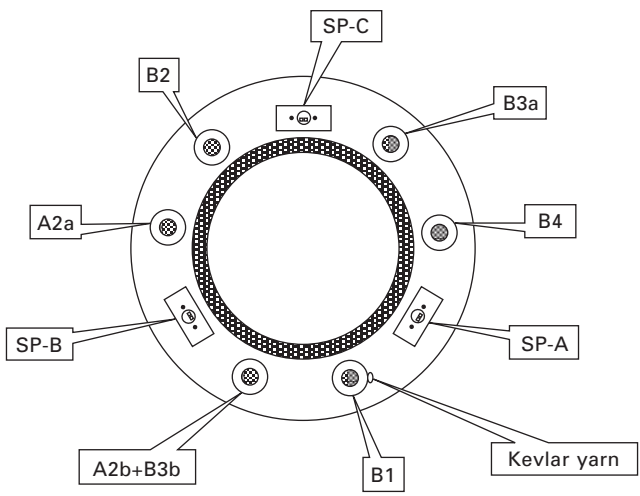

18.16 PDT-COIL's cross-section. The fiber optics sensing SMART profiles are designated by SP-A, SP-B and SP-C (Inaudi and Glisic, 2010).

strength of the fibers be fully harnessed due to this weak link, but this factor necessitates the incorporation of very large safety factors (often higher than 10) when designing FRP risers. Therefore, the need for an effective agent that can reduce this shortfall is of paramount and urgent importance.

The recent emergence of multifunctional nanoparticles has practically revolutionized the possibilities of design methodologies that could be used in producing such demanding and complex systems. As an example, single-wall carbon nanotubes (SWCNT) offer elastic modulus and tensile strength in the order of 1 TPa and 60 GPa, respectively. Furthermore, they can carry the highest current density of any known materials (i.e., 10^9 A/cm^2). These particles can effectively be added to FRP to enhance their properties. SWCNT are, however, quite expensive.

The utilization of graphite nanoplatelets (GNP) in the resin, as a potentially viable means of resolving the above-mentioned issue, is therefore being currently explored by the author's research group. It has been hypothesized that not only would the use of GNP improve the strength of the resin, but, being a highly conductive material, it would enable one to devise a concurrent robust health monitoring system.

18.13 Sources of further information and advice

Although there are several resources available to readers in relation to fiber-reinforced composites, especially with respect to their applications in aerospace and civil infrastructure, the material related to application of FRP in pipes, risers and storage tanks is relatively scarce. Nevertheless, there are several valuable reading resources that are usually underexplored. The following provides a list of some relevant reading resources that could be further explored by readers. Of course, of equal importance is the Internet.

Product specifications and classifications

ASTM D2310 Standard Classification for Machine-Made 'Fiberglass' (Glass-Fiber-Reinforced Thermosetting-Resin) Pipe

ASTM D2513 Standard Specification for Thermoplastic Gas Pressure Pipe, Tubing and Fittings

ASTM D2517 Standard Specification for Reinforced Epoxy Resin Gas Pressure Pipe and Fittings

ASTM D2996 Standard Specification for Filament-Wound 'Fiberglass' (Glass-Fiber-Reinforced Thermosetting-Resin) Pipe. Applicable to epoxy, polyester, and furan resins in sizes from 1 in. to 16 in. (25 mm to 400 mm)

ASTM D2997 Standard Specification for Centrifugally Cast 'Fiberglass'

	(Glass-Fiber-Reinforced Thermosetting-Resin) Pipe. Applicable for 1 in through 14 in. (25 mm through 350 mm) pipe of polyester or epoxy resins
ASTM D3262	Standard Specification for 'Fiberglass' (Glass-Fibre-Reinforced Thermosetting-Resin) Sewer Pipe. Applicable for pipes 8 in. through 144 in. (200 mm through 3600 mm) diameter, with or without siliceous sand, and polyester or epoxy resin
ASTM D3517	Standard Specification for 'Fiberglass' (Glass-Fiber-Reinforced Thermosetting-Resin) Pressure Pipe. Applicable for pipes 8 in. through 144 in. (200 mm through 3600 mm) diameter, with or without siliceous sand, and polyester or epoxy resin
ASTM D3754	Standard Specification for 'Fiberglass' (Glass-Fiber-Reinforced Thermosetting-Resin) Sewer and Industrial Pressure Pipe. Applicable for 8 in. through 144 in. (200 mm through 3600 mm) diameter, with or without siliceous sand, and polyester or epoxy resin
ASTM D4024	Standard Specification for Machine made 'Fiberglass' (Glass-Fiber-Reinforced Thermosetting-Resin) Flanges. Applicable from ½ in. through 24 in. (13 mm through 300 mm) ANSI B16.5 150 lb (70 kg) bolt circle flanges
ASTM D4161	Standard Specification for 'Fiberglass' (Glass-Fiber-Reinforced Thermosetting-Resin) Pipe Joints Using Flexible Elastomeric Seals
ASTM F1173	Standard Specification for Thermosetting Resin Fiberglass Pipe and Fittings to be Used for Marine Applications
API 15LR	Specification for High Pressure Fiberglass Line Pipe. Applicable to 2 in. through 12 in. (50 mm through 300 mm) diameter pipe of epoxy or polyester resin for use at cyclic pressures to 1000 psi (6895 kPa)
API 15HR	Specification for High Pressure Fiberglass Line Pipe. Applicable to 1 in. through 8 in. (25 mm through 200 mm) pipe and fittings for operating pressures over 1000 psi (6895 kPa)
API 15AR	Specification for Fiberglass Tubing. Applicable to tubing through 4½ in. (115 mm) diameters
API 15 S	Qualification of Spoolable Reinforced Plastic Line Pipe
AWWA C950	AWWA Standard for Fiberglass Pressure Pipe
CSA Z662	Section 13.1 – Fiber glass pipelines

US military specifications

MIL P24608 Specification for epoxy resin pipe from ½ in. through 12 in. (13 mm through 300 mm) diameters for 200 psig (1379 kPa) for service at 150°F (66°C) for US Navy shipboard applications

MIL P28584A Specification for epoxy resin pipe and fittings from 2 in. through 12 in. (50 mm through 300 mm) diameter for use as Steam Condensate Return Lines in continuous service at 125 psig (862 kPa) and 250°F (121°C)

MIL P29206A Specification for epoxy or polyester pipe and fittings 2 in. through 12 in. (50 mm through 300 mm) in diameter for POL services to 150°F (66°C) and 150 psig (1034 kPa) with surges to 250 psig (1724 kPa)

Recommended practices for product listings, approvals, and piping codes

NSF International – Standard Nos. 14 and 61. This document provides recommendation for testing fiberglass pipes, fittings, and adhesives for use in conveying potable water. In addition, Standard No. 14 serves as the relevant document for testing and certifying FRP products.

Underwriters Laboratories Inc. is another entity that provides set standards for testing and listing fiberglass pipe for use as underground fire water mains and underground transport of petroleum products. It also provides great documentation for the design and certification of above-ground GFRP oil tanks, etc.

ANSI/ASME B31.1 – Power Piping Code and ANSI/ASME B31.3 – Chemical Plant and Petroleum Refinery Piping Code. These codes list some of the acceptable ASTM, AWWA, and API fiberglass pipe specifications for use along with the code to establish criteria for their installation and use.

ANSI/ASME B31.8 – Gas Transmission and Distribution Piping Systems Code. This code states fiberglass pipe manufactured in compliance with ASTM D2517 as acceptable for use within the code.

ASME Boiler and Pressure Vessel Code Case N155. This code also provides rules for the construction of FRP piping systems for use in nuclear power plant applications.

18.14 References

Adams R D, Comyn J, Wake W C (1997) *Structural Adhesive Joints in Engineering*. 2nd Edition, Chapman & Hall, London.

Aditya P K, Sinha P K (1996) 'Moisture diffusion in variously shaped fibre reinforced composites', *Computers and Structures*, 59, 157–166.

Advanced Waterproof Technologies (2005) AqauWrap pipeline repair (online). Available at http://ridwater.com/aqua-wrap.htm, retrieved October 2011.

Alexander C (2008) 'Repair of pipelines, piping, and structures using composite materials'. Technical Report, Stress Engineering Services.

Alexander C, Fracini B (2006) 'State of the art assessment of composite systems used to repair transmission pipelines', *Proceedings of the 6th International Pipeline Conference*, Calgary, Alberta, Canada.

Arjomandi K, Taheri F (2011a) 'A new look at the external pressure capacity of sandwich pipes. *Marine Structures,* 24(1), 23–42.

Arjomandi K, Taheri F (2011b) 'Stability and post-buckling response of sandwich pipes under hydrostatic external pressure', *International Journal of Pressure Vessels and Piping*, 88(4), 138–148.

ASME B31G (2009) *Manual for Determining the Remaining Strength of Corroded Pipelines*. American Society of Mechanical Engineers, New York.

ASME PCC-2 (2006) *Repair of Pressure Equipment and Piping Standard*. American Society of Mechanical Engineers, New York, 2006 edition.

Assarar M, Scida D, El Mahi A, Poilane C, Ayad R (2011) 'Influence of water aging on mechanical properties and damage events of two reinforced composite materials: flax fibres and glass fibres', *Materials and Design*, 32, 788–795.

AWWA (1996) *Fiberglass Pipe Design Manual*, American Water Works Association, Denver, CO.

Bao L R, Yee L F (2002) 'Moisture diffusion and hygrothermal aging in bismaleimide matrix carbon fiber composites: part II – Woven and hybrid composites', *Composites Science and Technology*, 62, 111–119.

Bensadoun F, Kchit N, Billotte C, Bickerton S, Trochu F, Ruiz E (2011) 'A study of nanoclay reinforcement of biocomposites made by liquid composite molding', *International Journal of Polymer Science*, Article ID 964193.

Berketis K, Tzetzis D, Hogg P J (2008) 'The influence of long term water immersion aging on impact damage behaviour and residual compression strength of glass fibre reinforced polymer (GFRP)', *Materials and Design*, 29, 1300–1310.

BP Group Engineering (2011) 'Design of unbonded flexible pipe risers and flowlines', BP Group Engineering Technical Practice GP 65–75, available online: ftp://213.42.230.54/Exchange/ADMAOPCO/Tender%20Bulletin/TB-05/CD 2/BP%20ETPs/ETP/files/65%20Floating%20Production%20Systems/Riser%20Systems/GP%2065-75%209th%20November%202007.pdf, retrieved September 2011.

Cheraghi N, Taheri F (2007) 'A damage index for structural health monitoring based on the empirical mode decomposition', *Journal of Mechanics of Materials and Structures*, 2(1), 43–62.

Citadel Technologies (2007) BlackDiamond pipeline repair, available online: http://www.cittech.com/prdblackdiamond.html, retrieved October, 2011.

d'Almeida J R M, de Almeida R C, de Lima W R (2008) 'Effect of water absorption of the mechanical behavior of fiberglass pipes used for offshore service waters', *Composite Structures*, 83, 221–225.

DNV-RP-F202 (2010) *Composite Risers, Recommended Practice*, Det Norske Veritas, October 2010.

Ellyin F, Maser R (2004) Environmental effects on the mechanical properties of glass-fiber epoxy composite tubular specimens', *Composites Science and Technology,* 64, 1863–1874.

Elman J, Alvim R (2008) 'Development of a failure detection system for flexible risers', *Proceedings of the Eighteenth International Offshore and Polar Engineering Conference*, Vancouver, BC, Canada, 6–11 July 2008.

Esmaeel R A, Briand J, Taheri F (2012) 'Computational simulation and experimental verification of a new vibration-based structural health monitoring approach using piezoelectric sensors', *Journal of Structural Health Monitoring*, 11(2), 237–250.

Fahmy A A, Hurt J C (1980) 'Stress dependence of water diffusion in epoxy resin' *Polymer Composites*, 1(2), 77–80.

Hart-Smith L J (1987) 'Design and empirical analysis of bolted or riveted joints', in *Joining of Fibre-reinforced Plastics*, ed. Matthews F L, Elsevier Applied Science, 1987.

Health and Safety Laboratory (2009) 'Reinforcing wire corrosion in flexible pipe', Health and Safety Laboratory Literature Survey ES/MM/09/07, available online: http://www.hse.gov.uk/research/hsl_pdf/2009/esmm0907.pdf, retrieved September 2011.

Hosseinzadeh H, Cheraghi N, Taheri F (2006) 'An engineering approach for design and analysis of metallic pipe joints under torsion by finite element method', *Journal of Strain Analysis for Engineering Design*, 41(6), 443–452.

Inaudi D, Glisic B (2010) 'Long-range pipeline monitoring by distributed fiber optic sensing', *Journal of Pressure Vessel Technology, Transactions of the ASME*, 132(1), 0117011–0117019.

Integ Pipeline Services (2006) Available online: www.integpipelineservices.com, retrieved October 2011.

Khan A A, Naeem M, Asif M (2005) 'Use of Spoolable Reinforced Composite (SRP) Pipe for Transfer of Low Pressure Oil and Gas in BP Pakistan', British Petroleum Pakistan, Islamabad.

Mohitpour M, Szabo J, Hardeveld T V (2005) *Pipeline Operations and Maintenance*, American Society of Mechanical Engineers, New York.

NYACOL Nanotechnology, Inc. (2011) Available on line: http://www.nyacol.com/ap50-1-98.htm, retrieved October 2011.

Offshore Magazine (2008) 'High performance flexible pipe can be designed to fit', May 2008.

Pauchard V, Grosjean F, Campion-Boulharts H, Chateauminois A (2002) 'Application of a stress corrosion cracking model to the analysis of the durability of glass/epoxy composites in wet environments', *Composites Science and Technology*, 62, 493–498.

PolyFlow Inc. (2012) 'Thermoflex Oil Gathering Line Installation'. Retrieved May 2012, from Polyflowinc: http://www.polyflowinc.com/docs/Case_Study_WV.pdf

Ragab A R A, Bayoumi S A (1998) *Engineering Solid Mechanics, Fundamentals and Applications*. CRC Press, Boca Raton, FL.

Razi P, Esmaeel R A, Taheri F (2012) 'Improvement of a vibration-based damage detection approach for health monitoring of bolted flange joints in pipelines', *Journal of Structural Health Monitoring*, under review, May 2012.

Rezaei D, Taheri F (2010) Health monitoring of pipeline girth weld using empirical mode decomposition, *Smart Materials and Structures*, 19(5), doi:10.1088/0964-1726/19/5/055016.

Russell NDE Systems (2010) PermaWrap pipeline repair', available online: http://www.russelltech.com/PipelineProducts/PermaWrap.html, retrieved October 2011.

Salama M M, Storhaug T, Martinussen E, Lindefjeld O (2000) 'Application and remaining challenges of advanced composites for water depth sensitive systems', paper presented at Deep Offshore Technology Conference, 2000.

Sato M, Patel M H (2007) 'Exact and simplified estimations for elastic buckling pressures

of structural pipe-in-pipe cross sections under external hydrostatic pressure', *Journal of Marine Science and Technology*, 12(4), 251–262.

Seaflex (2011) 'Failure modes, inspection, testing and monitoring', Seaflex Technical Report P5996-RPT01-REV02, prepared for Petroleum Safety Authority (PSA) Norway, online at: http://www.ptil.no/getfile.php/PDF/P5996RPT01REV02cSeaflex_JanMuren.pdf, retrieved September 2011.

Shouman A, Taheri F (2011) 'Compressive strain limits of composite repaired pipelines under combined loading states', *Composite Structures*, 93(6), 1538–1548.

Springer G S (1981) *Environmental Effects on Composite Materials,* vol. 3, Chapter 1, Technomic Pub. Co., Lancaster, PA.

Stephen G L (2005) 'Composite reinforced line pipe for hydrogen pipeline transmission', presentation at 2005 ASME-IPC Conference, Calgary, Alberta, Canada.

StrongBack Corp. (2007) 'Repair sleeves. Kemah, Texas, US', Available at: http://www.Strongbackcorp.com, retrieved October 2011.

Tecma Pipeline Services (2009) 'Clockspring pipeline repair', available at: http://www.tecma.it/EN/clock.php, retrieved October 2011.

Zimmerman T, Stephen G, Glover A (2002) 'Composite reinforced line pipe (CRLP) for onshore gas pipelines', *Proceedings of the International Pipeline Conference, IPC*, 467–473.

Zou G P, Taheri F (2006) 'Stress analysis of adhesively bonded sandwich pipe joints subjected to torsional loading', *International Journal of Solids and Structures*, 43(20), 5953–5968.

19

Sustainable energy production: key material requirements

L. C. HOLLAWAY, University of Surrey, UK

DOI: 10.1533/9780857098641.4.705

Abstract: Sustainable energy contributes to reducing the dependence on the use of fossil fuel resources, thus providing the opportunity to reduce greenhouse gases. The renewable technologies may be divided into three generations. The first commenced in the nineteenth century and was hydro-, biomass- and geothermal-power. The second stage started during the 1980s and consists of wind power, tidal and wave power, and solar power. The third stage is under development and is gasification, bio-refinery and ocean power. This chapter describes and discusses the second generation of renewable technologies and the phase to which each has currently progressed; these developments have been rapid. It also forms an introduction to Chapter 20 which considers the significance of equipment made from advanced polymer composite materials in obtaining sustainable energy.

Key words: sustainable energy, wind turbines, tidal energy, wave energy, solar power, advanced polymer/fibre composites.

'If historians now see the turn of the 19th century as the dawn of the industrial revolution, I hope they will see the turn of the 21st century as the dawn of the energy revolution.' Bentham, J.B. (2007)

19.1 General introduction

Environmental pollution is of considerable concern throughout the world. Moreover, as demand on finite petroleum reserves and the price of fuels derived from them continue to rise, renewable forms of energy are becoming more attractive and cost-effective. Over the centuries, energy has been supplied by wood, coke, coal, oil and natural gas, as well as by uranium (nuclear energy). The early sources (i.e. wood) were natural in the sense that they renewed themselves over a short time period (tens of years), while the later energy supplies were trapped in layers in the crust of the earth from sources established millions of years ago. The increasing energy demands in the world today, due to expanded civilisations and thus to increasing populations, have led to concerns over the limited energy resources. The demand has focused attention on a sustainable energy supply, which implies optimised use of energy, minimised pollution and reduction in fossil fuel energy consumption. These aspects have led to an increasing focus on the

short-term stored energy resources, which could be derived from wind power, hydro power, solar power, biomass and geothermal heat power. The fastest growing segment of sustainable energy is the wind; however, the other mainstream forms such as hydro power and solar power are in the prototype form or at the research and development stage. These three forms of power production will be discussed in this chapter and Chapter 20.

A quarter of the UK's generating capacity is to be shut down over the next 10 years as the old coal and the nuclear power stations close. According to the UK government in 2011, more than £110bn in investment is required by 2020 to build the equivalent of 20 large power stations and upgrade the grid. Responding to these challenges, on 12 July 2011 the UK government published 'Planning our electric future: a White Paper for secure, affordable and low-carbon electricity'. The White Paper sets out key measures to attract investment, reduce the impact on consumer bills, and create a secure mix of electricity sources including gas, new nuclear and coal-fired power stations with carbon capture and storage (CCS) and renewables.

The package of reforms outlined in the White Paper should mean that by 2030 the UK will have a flexible, smart and responsive electricity system, powered by a diverse and secure range of low-carbon sources of electricity, with a full part played by demand management, storage and interconnection. Competition between low-carbon technologies should keep costs down, and will support a network that will be able to meet the increasing demand from the electrification of transport and heating systems. Furthermore, the future electricity system will also contain more intermittent generation (such as wind) and inflexible generation (such as nuclear). Before discussing the utilisation of fibre/polymer composites in renewable energies, it is necessary to introduce the various generating techniques available for securing this energy currently and in the future. This chapter and Chapter 20 will discuss the types of sustainable energies that may be obtained from generators currently available or at the 'drawing board' stage; the generators are constructed from components some of which are manufactured from advanced fibre/polymer composites. The chapter will also attempt to estimate the degree to which these systems have been developed and their likely success in future in providing sustainable energy to all countries of the world. The techniques utilised in producing sustainable energy are rapidly expanding and industrial firms are introducing further innovative systems; this chapter, which was completed in January 2012, will require updating at regular intervals.

A definition of sustainable energy

Sustainable energy is the provision of energy such that it meets the needs of the present without compromising the ability of future generations to meet their needs (Lemaire, 2004). This means that sustainable energy is power

which is able to be replenished within a human lifetime and so cause no long-term damage to the environment. Sustainable energy includes all renewable energy sources, such as hydroelectricity, biomass, geothermal, wind, wave, tidal and solar energies. Only wind, wave, tidal and solar energies, which are currently utilising advanced polymer composites, will be considered in this chapter and in Chapter 20.

19.2 Introduction to wind turbines

The concept of harnessing the wind's energy has been around for thousands of years. It is estimated that the Chinese built the first wind turbines in 200 BC to pump water and grind grain. The world's first wind turbine to generate electricity was in July 1887; it was developed in Scotland by Professor James Blyth of Anderson's College, Glasgow, and gained a UK patent four years later. Since then, the technology of wind turbines has made great progress. Williamson (2011a) stated that the UK's wind power generation has exceeded 3 GW of electricity exported to the National Grid, and on 6 September 2011 this generation peaked at 3021 MW, which was 7.2% of the total amount of electricity on the grid.

A wind turbine transforms the kinetic energy of the wind into mechanical energy and then into electrical energy and/or heat. There are four components forming the turbine, viz. the rotor (an aerodynamic device and a rotor blade with an aerodynamic shape for rotation), the nacelle (containing the gearbox and generator), the yaw mechanism (sensors to monitor and rotate the turbine directly into the wind in order to generate maximum power), and the tower. Generally, the rotors of the turbine consist of three blades; however, they can have two or just one blade. The blades rotate around a horizontal hub which is connected to a gearbox and generator located inside the nacelle. The latter houses the electrical components and is mounted at the top of the tower (column of the turbine). This type of turbine is referred to as a 'horizontal axis' machine and is the commonest of all turbines. Sensors are used to monitor wind direction and to rotate the tower head horizontally into the direction of the wind; in addition, the blades also 'pitch' (angle to the vertical); both rotations ensure that the optimum amount of power is extracted from the wind. Wind turbines are not physically staffed, although each will have periodic mechanical checks. The onboard computers also monitor the performance of each turbine component, and will automatically shut the turbine down if any problems are detected, alerting an engineer that an onsite visit is required. The information from the onboard computers is transmitted to a control centre, which can be many miles away. The current height of towers for onshore wind turbines is typically between 25 m and 75 m and they are generally cylindrical in cross-section and manufactured in steel; lattice towers are used in some locations. Advanced polymer composite

materials play an important part in the fabrication of the rotor blades; research is being undertaken to ascertain whether FRP composites could be used to manufacture the tower in the form of a lattice structure.

To harness the force of the wind a converter (the rotor blades) is required to turn the kinetic energy of the wind into operational energy) (mechanical energy) and this into electricity and/or heat. The rotor blades have aerodynamic shapes, to enable them to rotate efficiently, and thus extract a power of:

$$P = \alpha\rho\, Av^3 \qquad [19.1]$$

where α is an aerodynamic efficiency constant, ρ is the density of air, A is the area of the rotor-plane, and v is the wind velocity.

There are practical limits to the amount of power that can be extracted from wind streams. Some of these limits relate to the design of the wind devices and others to the characteristics of the resource.

The rotor blade diameters range between 30 m and 80 m although some of the offshore wind turbines which are currently being designed have rotor blades up to 150 m. The blades rotate at about 10–30 revolutions per minute at constant speed, although an increasing number of machines operate at a variable speed (Renewable UK 2010). The power is controlled automatically as the wind speed varies, and if the speed is too great brakes are applied to control the rotational speed of the fan blades; at very high wind speeds the shaft and machine are stopped to protect them from damage.

Commercial onshore turbines range in capacity from a few hundred kilowatts to over 2 megawatts (MW). The crucial parameter for the production capacity is the diameter of the rotor blade; the longer the blade, the greater is the area 'swept' by the rotor and the larger is the energy output. This is particularly relevant to offshore turbines where the larger size of blades and thus the larger overall size of the turbine are a more economic consideration when concerned with energy output and the shipment of the blade to its final position; the transportation of offshore blades is far less problematic compared with onshore wind turbines but the erection of the blades offshore is considerably more harassing than that for onshore blades. However, the trend is towards these larger machines as they can produce electricity at a lower price.

One of the complaints against wind power is the intermittent energy resource as there are periods of zero wind velocity. However, this situation does not reduce the value of wind as a source of power. The variable output from wind energy poses no special difficulty for power system operation. Electricity demand is constantly fluctuating, and supply and demand have to be matched on a minute-to-minute basis, throughout the year. The fluctuation caused by the introduction of wind energy to the National Grid system is not discernible above normal fluctuations; it is likely that it will remain until electricity generated from wind turbines reaches approximately 20% of the

total system supply (Wind Power, 2011). When this situation is reached a dual system of sustainable energy production would be required and it is possible by then that a method of storing electrical power will have been developed; the intermittent nature of wind power means that the demand must be managed. The real issue is a potential future scenario where the wind energy penetration into the market is very high at a situation of high energy demand at a low wind speed; this situation will result in insufficient energy capacity to cope with such a demand (it would require a wind penetration at 30–40%, rather than currently at 5–10%). In this case, it would be necessary to pay for spare generation capacity to cope with the lack of wind power generation.

19.2.1 The two types of wind turbine

There are two basic types of wind turbines determined by the way the turbine rotates: those which rotate around a horizontal axis and those which rotate around a vertical axis; the former are generally used in practice. The main rotor shaft and electrical generator of the horizontal axis turbines are situated at the top of the column and point into the wind. The vertical axis wind turbines have the main rotor shaft arranged vertically. These are mainly relevant to offshore wind turbines (see page 710). The main advantage of this arrangement is that there is no need for the wind turbine to be pointed into the wind direction, but the disadvantage is that it is difficult to mount the vertical axis turbine on its tower. Consequently, the blades of these turbines are invariably installed near to the base on which they rest, but the drawback of this system is that the wind speed at a lower altitude is lower than that at higher altitudes. However, it will be shown on page 714 that with an offshore vertical axis turbine it is an advantage to install the base near to the surface of the water as the centre of gravity of that system will be lower compared with that of the horizontal axis turbine, see page 714, regarding the 'Aerogenerator X' turbine. With the exception of the 'Aerogenerator X' turbine, the following discussions will involve horizontal axis wind turbines. Wind turbines can be situated onshore or offshore.

Onshore wind turbines

The onshore wind turbine blades and the hubs are currently supported on a steel column, although there are examples where reinforced concrete material has been used (see Chapter 20, Section 20.5.6). The production area of the turbines is generally referred to as a wind farm, which is a group of wind turbines in the same location. A large wind farm may consist of several hundred individual wind turbines, which could cover an area of hundreds of square kilometres, but generally an onshore wind farm of 20

turbines might extend over an area of 4 square kilometres but only 2% of the land area would be used to house the turbines, electrical infrastructure and access roads; the remainder could be used for other purposes, such as farming, public amenities or as natural habitat. A typical turbine installation could consist of:

- Foundations
- Turbine base
- Switchgear house
- Access road.

Individual onshore turbines are interconnected with a medium voltage (usually 34.5 kV) power collection system and communications network by underground cables. At a substation, the medium-voltage electrical current is increased in voltage via a transformer for connection to the high-voltage National Grid system.

The 'QuietRevolution' wind turbine

A unique onshore wind turbine is the 'QuietRevolution' wind turbine conceived by QuietRevolution which was designed and developed by XCO2 in conjunction with Aviation Enterprises Ltd. The rotating section is 5 metres high and 3.1 metres in diameter and is designed to withstand a maximum wind speed of 120 mph. It is vital that this wind turbine's weight is kept to a minimum due to the developed centrifugal forces of up to 200g. XCO2 states that the operation of the turbine is more efficient compared with the traditional turbine as it does not have to constantly change direction with the wind; this advantage reduces the vibrations and the aerodynamic noise. A further advantage is that the cylindrical structure with the vertical 'S' blades occupies less space than the conventional turbine, and is able to integrate into the urban environment; aesthetically it is very pleasing. The above information has been based upon the company's website: www.quietrevolution.com. Figure 19.1 shows an image of the 'QuietRevolution' wind turbines which are placed upon the roof of City House Building in Croydon.

The composite blades of the turbine will be discussed in Chapter 20, Section 20.5.5.

Offshore wind turbines

Technology development in the largest unit sizes of conventional wind turbines has been particularly stimulated by the offshore market (Roney, 2012) and many of the most innovative wind energy systems proposed in recent years target that market. Clearly, offshore is the ideal position for wind turbines, but the environment can be hostile. The technology for this

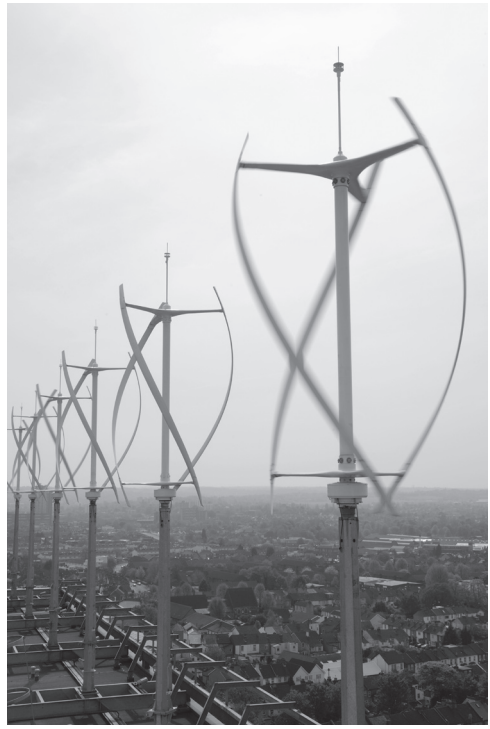

19.1 Image of the 'QuietRevolution' wind turbines placed upon the roof of City House Building, Croydon, Surrey, UK (by kind permission of QuietRevolution, XCO2 and Aviation Enterprises Ltd).

type of turbine is based on the same principles as that for onshore turbines; the offshore winds tend to flow at higher speeds than those onshore, thus allowing turbines to produce more economical power.

There are several ways of supporting the superstructure of the turbine, illustrated in Fig. 19.2:

- *A fixed foundation for the superstructure*. There are a number of different construction designs; most have piled foundations. The top of the foundations is painted in a bright colour to make the structure visible to shipping and an access platform provides access for maintenance teams. The power developed by the turbines is transmitted via subsea cables to an offshore transformer, where it is converted into electricity with a high voltage (normally between 33 kV and 132 kV) before connecting to the grid at a substation on land.
- *Floating platforms*. As the name suggests, the platform floats on the surface of the waves. There are construction designs which are under investigation by different firms involved in the offshore wind farms

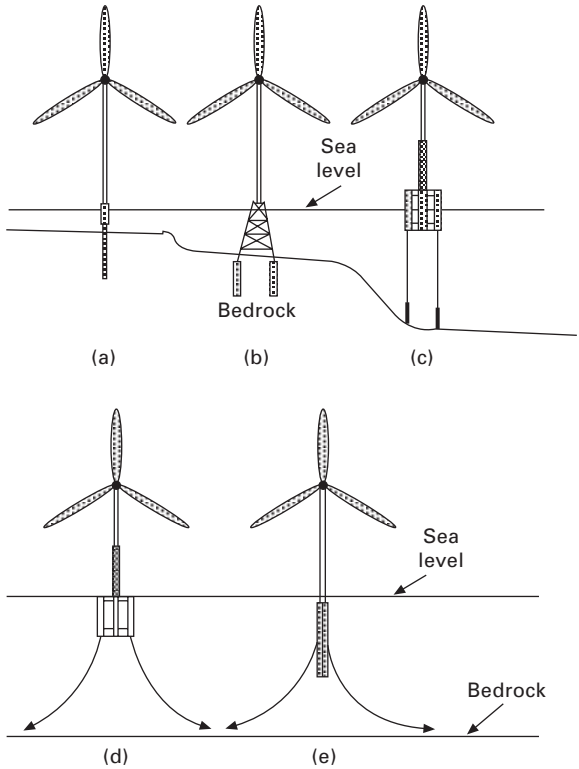

(a) Monopile (piled), depth ≃ 30 m (output 1–2 MW)
(b) Jack Tripod (piled), depth ≃ 30–50 m (output 2–5 MW)
(c) Mooring line stabilised – Tension Leg Platform (TLP) with suction pile anchors (floating), depth >50m (output 5–10 MW)
(d) Buoyancy stabilised barge with catenary mooring lines (floating), depth >50m (output 5–10 MW)
(e) Ballast stabilised 'spar-buoy' with catenary mooring drag embedded anchors (floating), depth 50–200 m (output 5–10 MW)

19.2 (a–e) Typical offshore wind turbine platforms.

industry. The three methods that can be used for the foundations of floating offshore wind turbines are ballast stabilisation, mooring line stabilisation and buoyancy stabilisation. The installation of the foundations depends on the type of platform: the foundations are built first, then the turbine's tower is erected and lastly the nacelle and rotor are placed in position. The installation is done from either a jack-up barge or a floating crane vessel.

Floating offshore wind turbines have great potential as they are not limited by the same conflicts of interest as the onshore and the near-shore 'offshore' turbines. Furthermore, wind farm developers have greater

flexibility when it comes to wind farm designs in terms of considering bird migration, shipping lanes, etc. Floating wind farms can be taken further offshore, thus reducing their visibility from the shoreline (Larsen, 2010).

An example of a floating wind turbine is the Hywind, which is a 2.3 MW floating offshore turbine; it was installed and moored in 2009. Developed by the Norwegian Oil and Gas Company StatoilHydro, Siemens and Technip, it is tethered by slack cables to three giant concrete blocks that sit on the seafloor off the coast of Norway. These allow the turbine to drift by 8 metres in any direction. It is undergoing a two-year sea trial which will provide valuable knowledge on how to perfect the technology; the firm hopes that the trial will lead to a financially viable alternative to other energy sources.

Another type of floating wind turbine is one which is fitted with patented water entrapment (heave) plates at the base of each column; these plates dampen the water effects and allow this type of turbine to operate in deep as well as in shallow waters. WindFloat is a semi-submersible structure and is an example of this type of turbine. The heave plates reduce the size of the structure and minimise the pitch and yaw motions of the system, thus enabling the siting of these offshore wind turbines in waters exceeding 50 metres in depth. In addition, the WindFloat has an active ballast system to further optimise energy production efficiency. The mooring system uses conventional components such as chain and polyester lines. WindFloat is developed in collaboration with Key Account EDP and the American offshore rig designer Principle Power. It will be transported by tug to a distance of 350 kilometres from the coast of Agucadoura on the Portuguese west coast; here it will be tested for at least a year.

To illustrate the rapid increase in size of offshore wind turbine blades, LM Wind Power Group, Denmark, have recently developed a 73.5 metre blade manufactured in polymer composites which it was hoped would be installed at Alstom's prototype sites in Europe over the winter 2011–2012; the blades will travel at a speed of more than 320 km/h. A special prototype mould has been produced with a transparent surface that allows the full-scale manufacturing trials to be followed by visual inspection of the critical polyester infusion production (see Chapter 20, Section 20.4.2 for infusion techniques). When LM Wind Power began to produce wind turbine blades in 1978 the blades were 5 metres in length.

Constructing offshore wind farms is expensive: each turbine costs at least 50% more than one built on land (*The Economist*, 2008). However, the stronger winds out at sea can, as stated before, generate more electricity. Wind speeds of 10 m/s can produce five times more electricity as wind speeds of 5 m/s; this greatly favours the building of offshore wind farms.

The 'Aerogenerator' system

As an example of the rapid development of wind turbine technology, the 10 MW 'Aerogenerator' is a revolutionary design for a vertical axis offshore wind turbine, conceived by Wind Power Ltd in conjunction with architects Grimshaw, Cranfield University, Rolls Royce, Arup, BP and Shell; the 'Aerogenerator' is shown in Fig. 19.3. In its present conceived form it is twice the size and power of any conventional wind turbine and because of its economies of scale its capacity could transform the global energy market. It is believed the first turbines will be built in 2013–14 following two years of testing (*The Engineer*, 2011); this is probably an optimistic forecast. It is different from the typical wind turbine as it features a set of blades that are mounted on a vertical axis with a blade span of just over 270 m. The structure floats and as the weight is concentrated at its base it gives it a low-level centre of gravity; it could, therefore, reduce the costs of deepwater offshore wind energy. It mimics a spinning sycamore leaf and uses techniques developed for semi-submersible oil platforms. This development is by an all-British team and was in competition with US wind company Clipper Wind, which had close ties with the US Department of Energy's National Renewable Energy Laboratory; the UK subsidiary (Clipper Windpower Marine) announced plans in the summer of 2010 to build the 10 MW Britannia turbines in north-east

19.3 10 MW 'Aerogenerator X' © Wind Power Ltd and Grimshaw (image courtesy of Grimshaw Architects and Wind Power Ltd).

England that would have probably been positioned in the location of the Dogger Bank, North Sea; Williamson (2011b) has reported that this scheme has been withdrawn due to financial difficulties.

Floating wind turbines

The Norwegian firm Sway Power and Clipper Marine, UK, are developing an ingenious system of floating wind turbines, anchored by a single flexible tether, which have their backs to the wind. The main advantage of these large turbines is their economies of scale, which will be an important factor for developers to consider as the UK looks to meet future renewable energy targets (http://www.theengineer.co.uk/news/wind-power).

Blade performance

The part to be played by advanced polymer composite materials to form the blades and other components is discussed in Chapter 20, Section 20.5.

Improving the performance of wind turbine blades, and therefore increasing the energy capture of the system, will depend upon enhancing the reliability of the component materials of the blades; future designs will utilise larger rotors with longer blades fabricated from advanced composite materials with high strength and stiffness-to-weight ratios (Hayman *et al.*, 2008). Consequently, a thorough knowledge of composite materials and their safety factors will be required. In particular, a basic understanding of their damage and failure mechanisms and the effects and interpretation of stochastic loadings, multiple stress states, environmental effects, size effects and thickness effects must be known.

WindFloat wind turbine

Principle Power, Inc. and Energias de Portugal (EDP) have deployed the first full-scale, 2 MW offshore WindFloat (i.e. a floating turbine: see Section 19.2.1). The machine is a new technological system for offshore wind turbines to be constructed on land including assembly, installation and pre-commissioning. It is then loaded onto a dry-dock and towed to its final position offshore. The project is thought to be the first offshore wind deployment worldwide which does not require the use of any heavy lift equipment offshore. The first deployment of this semi-submersible structure is currently being commissioned off the coast of Aguçadoura, Portugal some 350 km into the Atlantic Ocean; this system could be the first of many offshore wind turbines in open Atlantic waters. Deep-water offshore wind technology will allow WindFloat to harness the stronger and more stable winds and in the medium term deliver sustainable energy into an electrical

system. WindFloat is being developed by WindPlus JV partners, including EDP, Principle Power, A. Silva Matos (ASM), Vestas Wind Systems A/S, InovCapital and Fundo de Apoio à Inovação (FAI).

There are clearly tremendous advances being made in the development of offshore wind turbines and it is likely that the blades of these turbines will continue to be manufactured from advanced polymer composite industries; this provides extra stimulus to the manufacturers of polymer composites to develop new and improved polymers to resist the ocean environments.

19.2.2 The advantages and disadvantages of using wind turbine energy

There are advantages and disadvantages in using wind power to provide green energy. The advantages are as follows:

- Wind energy is 'clean' to the surrounding environment, as no fossil fuels are burnt.
- Wind turbines take up less space than the average power station. (This has been discussed above.)
- New technologies are making the extraction of the free wind energy much more efficient. ExxonMobil's yearly review of energy statistics and trends have estimated that by 2030 wind will be the second cheapest power supply with energy from gas the cheapest (Paris, 2011).
- Wind turbines are a resource to generate energy in remote locations, such as mountain communities and remote countryside areas. As mentioned above, wind turbines have a range of different sizes in order to support varying population levels.
- If wind energy is combined with another sustainable energy supply, e.g. solar power, these combined sources of power would be ideal for developed and developing countries to provide a steady, reliable supply of electricity.

The disadvantages of using wind turbine energy with a comment against each are given as follows:

- Wind turbines suffer from the variability of the wind speed, but it is predictable.
  Comment: This disadvantage suggests that in some areas of the world the wind strengths are too low to support a wind turbine or a wind farm. In these areas clearly wind turbines are not an option and other forms of green energy would be used such as solar power or geothermal power. The problems of variable wind speeds have been discussed previously in the last paragraph of Section 19.2.

- Wind turbines generally produce a lower electrical output compared with the average fossil-fuelled power station, requiring multiple wind turbines to be built in order to make an impact.
  Comment: Modern wind turbines produce electricity 70–85% of the time, but they generate different outputs depending on the wind speed. Over the course of a year, a turbine will typically generate about 30% of the theoretical maximum output; this is known as its load factor. The load factor of conventional power stations is on average 50% (DTI, 2004). A modern wind turbine will generate enough energy to meet the electricity demands of more than 1000 homes over the course of a year.
- The cost of energy produced by wind turbines is expensive.
  Comment: (1) The cost of generating electricity from wind fell dramatically over the years between 1990 and 2002; in addition, the world wind energy capacity doubled every three years and with every increase the prices fell by 15% (Milborrow, 2003). (2) Wind energy is competitive with new coal and with new nuclear capacity, even before any environmental costs of fossil fuel and nuclear generation are taken into account (ExternE, 2003). (3) A yearly review of energy statistics and trends from ExxonMobil has given a positive estimate of costs of wind power compared with other forms of producing power (Paris, 2011); a graph showing the various estimated costs of power for 2025 is shown in Fig. 19.4. It is perhaps over-simplistic to suggest that the chart shows that wind is likely to be the cheapest form of electricity generation in 2025, since that is only the case in the second scenario depicted in the chart; it is clear that the chart does not include the costs of providing back-up generating capacity for those times when there is no wind. Furthermore, if carbon emissions from coal and gas-fired power stations were taxed the economies of these two production methods would change, but even with no taxation, wind production still appears to be the cheaper option.
- Wind turbines are noisy (Rogers and Manwell, 2002).
  Comment: The major noise nuisance is the low-frequency, penetrating sound that is emitted when the rotating blades pass the turbine tower; low-frequency noise travels further than the audible. So far there has been no success in eliminating this low-frequency noise, which can continue day and night for extended periods. The closest that a wind turbine is typically placed to a home is 300 metres or more. At that distance, a turbine will have a sound pressure level of 43 decibels. To put that in context, the average air conditioner can reach 50 decibels of noise, and most refrigerators run at around 40 decibels.
- There are reports of bird mortality at wind turbine sites. The scale of the ecological impact is uncertain and will depend upon specific circumstances. The site and the operation of the wind turbines can prevent and mitigate the fatalities of wildlife.

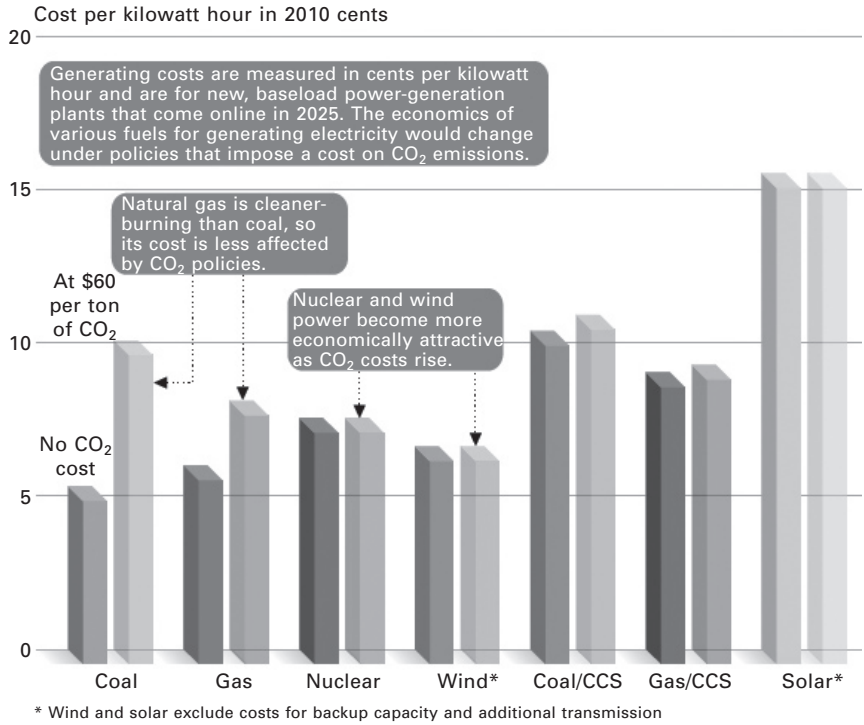

19.4 Average USA cost of electricity generation in 2025 (from ExxonMobil's yearly review of energy statistics and trends, called *Energy Outlook: A View to 2030*, Paris, 2011) (image courtesy of ExxonMobil, Leatherhead, Surrey, UK).

19.3 Introduction to hydropower

Modern ocean wave energy conversion machines use new technologies that are designed to operate in (1) high-amplitude waves (using wave energy converters which harness the vertical motion of waves) and (2) tidal/river/ocean currents (hydrokinetic machines use new technologies that are designed to operate in fast-moving currents). Both of these emerging technologies have the potential to provide significant amounts of affordable electricity with low environmental impact, given proper care in siting, deployment and operation.

In the next 20 years, hydrokinetic power drawn from the earth's oceans and rivers could account for more than 10% of the world's global electricity market (Wood, 2010). The renewable energy resources from ocean wave, tidal stream, ocean and river current and ocean thermal resources are expected to be the major growth area over the next decade (Marsh, 2009).

19.3.1 Types of hydro-generators

There are three main types of hydro turbines: (1) hydroelectric power, (2) tidal power, and (3) wave power.

1. Hydroelectric power is the most common form of hydropower and makes up the majority of all renewable energy produced. Electricity is produced in hydroelectric dams where the force of falling water drives massive turbines. This is not covered in this chapter.
2. Tidal power is the second most popular type of hydropower; tidal power generates electrical power through the harnessing of the ebb and flow of the tides, which is due to the gravitational attraction of the earth and the moon. The tides cause a protuberance of water on earth that creates high and low water levels at different times.
3. Wave power is the youngest of the three hydropower solutions. Wave power is created by the wind blowing across the surface of the water, thus forming ripples; the stronger these winds become the larger and stronger will be the waves. When the waves propagate at a slower speed than the speed of the wind adjacent to the waves, there is an energy transfer from the wind to the waves. Both air pressure differences between the upwind side and the leeward side of a wave crest (as well as friction on the surface of the water by the wind) will cause a shear stress to be set up at the surface of the water, thus causing the growth of the waves.

A range of different prototype technologies for tidal and wave power is currently being developed or has been installed. Some have progressed as far as full-scale deployment and testing, and several UK-based companies are presently actively involved in constructing devices, supported by various financial means, including government and private investors.

The kinetic energy of a flowing tidal stream per unit time obeys the same power law as that for the wind turbine and is given at any instant in the tidal cycle as equation [19.2]:

$$P = \tfrac{1}{2}\rho\, A\, v^3 \qquad [19.2]$$

where v is the velocity of the stream, A is the cross-sectional area perpendicular to the flow direction, and ρ is the density of water.

This function is convenient for undertaking a quick estimation of a tidal stream resource, but as the velocity changes constantly, a time-weighted calculation is needed to determine the energy resource.

The cubic relationship between velocity and power is the same as that underlying the power curves of wind turbines, and likewise there are practical limits to the amount of power that can be extracted from tidal streams. Some of these limits relate to the design of the tidal stream devices and others to the characteristics of the resource.

Tidal power and wave power have a lower cost and lower ecological impact compared with tidal barrages; however, they are young technologies and their progress has not been as rapid as other forms of renewable energy. Tidal energy is about 15 years behind wind energy, and wave energy is another five years behind tidal energy (Royle, 2009).

19.3.2 The types of tidal energy power generators

There are two types of tidal energy that are able to produce electricity:

- The tidal stream system uses the kinetic energy from the ebbing and surging tides.
- Tidal barrages are designed to utilise the potential energy from the difference in height of the tidal waves.

The first system is the one with which this chapter is concerned; it remains the primary method of generating electricity.

The following statistics have been based on Black & Veatch (2005). The UK has a significant tidal stream energy resource representing about 50% of the European resource and around 10–15% of the known global resource that could be economically exploited. Of the total technically extractable resource, about 63% is at sites with depths of water greater than 40 metres and 30% at sites with depths between 30–40 metres; there is limited resource at the sites of shallow water less than 30 metres in depth. Approximately 50% of the UK resource is at deep sites greater than 40 metres where the velocity of flow is relatively high.

It is clear that the UK has by far the highest potential in the European Union for converting tidal energy into electricity. It has been estimated that the amount of energy in tidal form around the UK is more than the energy currently used to meet people's demand for electricity; Scotland has a particularly high potential with much of the western coastline being exposed to the Atlantic Ocean. The advantage of offshore tidal generators is that tidal currents are sub-surface, so tidal generators have minimum visual impact, unlike wind farms or estuary barrage schemes.

Three tidal energy generators will be discussed in the following section.

SeaGen tidal energy turbine

In 2010 the SeaGen tidal stream generator was the largest tide-harnessing turbine in the world. It captures the energy of the tide by placing the generator into the path of flowing water and is currently known as the 1.2 MW SeaGen which is installed in Strangford Narrows, Northern Ireland. Figure 19.5 shows an image of SeaGen. It was the first tidal turbine to produce

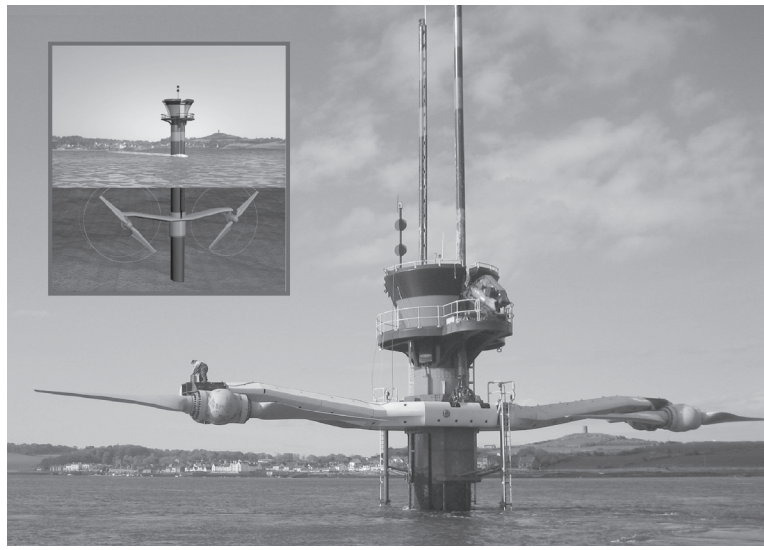

19.5 SeaGen, the first tidal turbine to produce energy on a commercial scale (image courtesy of Marine Current Turbines).

energy for the National Grid on a commercial scale and in March 2011 it passed the British Marine Current Turbines, the UK government's operating performance criteria for emerging tidal and wave energy technologies. It has the capacity to deliver about 10 MWh per tide which is equivalent to 6000 MWh per year (Fraenkel, 2011). It consists of twin axial-flow rotors 16 metres in diameter, each driving a generator through a gearbox similar to the wind turbine; each twin rotor sweeps over 200 square metres of flow. These generators have a patented feature by which the rotor blades can be pitched through 180°, allowing them to operate in both flow directions (on the ebb and the flood tides). The power units of each system are mounted on arm-like extensions on either side of a tubular steel monopile some 3 metres in diameter; the arms, and the power units, can be raised above the surface for maintenance access; Fig. 19.5 shows the blades acting under water. Each blade of the SeaGen rotor comprises a hollow carbon fibre composite box spar as the main load-bearing member, along with carbon ribs, and a glass fibre composite envelope bonded to this skeleton. The tubular steel monopile system is situated on piles drilled into bedrock of the seabed; SeaGen weights 300 tonnes (Rush, 2008). Sea Generation Ltd is the project company, which is a wholly owned subsidiary of Marine Current Turbines (MCT) Ltd, based in Bristol, and SeaGen was developed and manufactured by Marine Current Turbines.

Douglas *et al*. (2008) have presented an analysis of the life cycle energy use and CO_2 emissions associated with the first generation of SeaGen turbines and have assessed the environmental impact. The detailed assessment covered

the embodied energy and CO_2 emissions in the materials and manufacturing of components, device installation, and operation along with those for decommissioning. They have concluded that the embodied energy and carbon showed limited sensitivity to assumptions, with the environmental performance remaining excellent even under the most adverse scenarios considered. Materials used were identified as the primary contributors to embodied energy and carbon with transportation shipping also significant. They suggested that improvements in the environmental impact of SeaGen can be achieved primarily by increased structural efficiency and the use of alternative installation methods to increase recovery of steel at decommissioning. In addition, they stated that each rotor blade was made up of 800 kg of composite material for the blade spar and skin, which amounted to 2% of the total mass of the material used.

Many pre-production tidal stream devices are now in operation or are currently being installed in several locations around the British Isles. SeaGeneration (Wales) Ltd, a development company, has been set up by Marine Current Turbines (MCT) and RWE npower renewables to develop a 10.5 MW tidal energy farm in 'The Skerries' off the coast of Anglesey; it was anticipated that construction would commence in 2012.

Atlantis tidal generator

The AK1000™ tidal turbine is currently the world's largest tidal turbine and was installed on the sea bed and connected to the grid at a dedicated berth at the European Marine Energy Centre in Orkney, Scotland, during the late summer of 2011; it was developed by Atlantis Resources Corporation, a developer of electricity-generating tidal current turbines. AK1000™ is a horizontal axis turbine designed for open ocean deployment in the harshest environments on earth. It is a series turbine featuring a unique twin rotor set with fixed pitch blades eliminating the requirement for subsea nacelle rotation to improve operational reliability; it has a height of 22.5 metres off the seabed with an 18 metre rotor diameter and weighs 1300 tonnes. The two sets of blades are manufactured from GFRP and generate power from both ebb and flood tides. Figure 19.6 shows an image of the AK1000™ tidal turbine on the deck of Aker Wayfarer before it was lowered onto its subsea foundation; it was installed by the Aker Wayfarer, which is as an offshore construction vessel designed for ultra-deep water with state-of-the-art equipment.

Pulse Tidal generator

Pulse Tidal has developed a system whereby tidal streams move horizontal blades up and down to drive a generator. The test system shows that

19.6 AK1000™ tidal turbine on the deck of the Aker Wayfarer (image courtesy of Atlantis Resources Corporation).

predictable energy can be produced close to shore where it is needed, reducing massively the investment required to install, connect and maintain devices compared with those in remote locations. Power Take Off (PTO) has proved to be too inefficient and they are now planning to use a mechanical PTO where the device will remain fully submerged with the blades oscillating above a 'base' which is on the sea bed. Its 100 kW test rig in the Humber estuary currently feeds power into a chemicals company on the banks of the river. Figure 19.7 shows the demonstration machine.

Sheffield-based Pulse Tidal is now developing the Pulse Stream 1.2 MW tidal energy converter which can operate in a mean water level of 9 metres, with a 4-metre tidal range on either side of the 9 metres; this machine shows the potential for tidal stream energy from shallow waters. It features a 'flat' design based on twin composite hydrofoils positioned across the tidal flow, thus imposing no physical limit on blade length. The system harvests the energy created by the tidal streams flowing alternately over the hydrofoils, thus creating an upward and downward force as the machinery changes the angle of the blade-foil; this is similar to the air moving over a wing of an aircraft to provide uplift. This motion is converted to rotate a driveshaft that turns a conventional generator. The full-scale concept is based on four blades approximately 20 m in length. The blades are instrumented, enabling Pulse Tidal to verify actual loads during operation. Figure 19.8 illustrates

19.7 Pulse Tidal device; it is intended to be fully submerged in order to avoid surface conditions in exposed sites (image courtesy of Pulse Tidal Ltd).

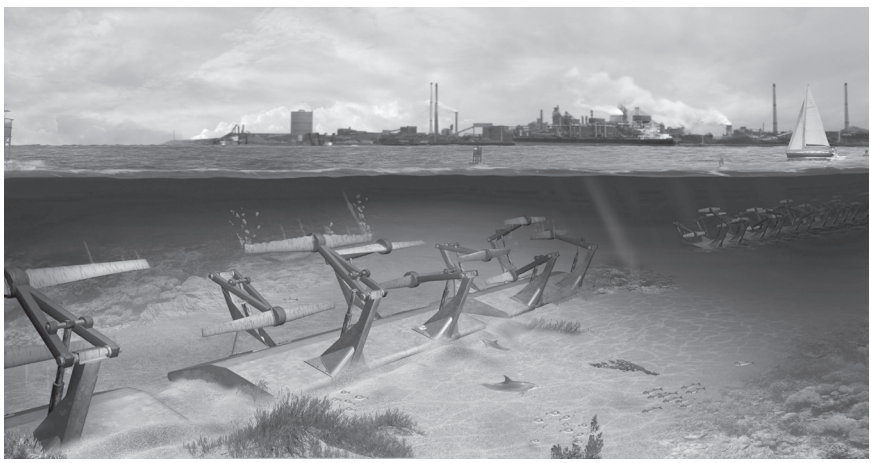

19.8 The blades for Pulse Tidal Pulse Stream 1 MW demonstrator, by Sheffield-based Pulse Tidal. Pulse Tidal has signed contracts with a group of international companies to form a secure supply chain for volume production. The partners are Gurit, Bosch Rexroth, Herbosch Kiere, DNV, IT Power, Niestern Sander, and the Fraunhofer Institute (image courtesy of Pulse Tidal Ltd).

the commercial machine. Pulse Tidal believes its approach will surpass the wind turbine as the most economic source of offshore power.

There have been several proposed generator systems relying on floating buoys that rise and fall with passing waves, the resulting vertical motions being converted via internal oscillating water columns to electrical energy. In another type of scheme, energy is derived from the differential motions of adjacent floating elements connected together via articulating joints that incorporate power take-off systems.

In all systems that rely upon tidal energies, composites have an inherent advantage over metal wherever buoyancy is required. This can also be exploited in devices that profile the waves, whether they employ foils, hemispherical floats or buoys.

19.3.3 The advantages and disadvantages of tidal renewable energy

Advantages of tidal energy:

- Tidal energy is renewable, does not lead to any pollution of the air and does not lead to any carbon emissions like fossil fuels.
- Tidal energy requires flowing water for the generation of electricity in its catchment area; it requires no fuel.
- Tidal energy power plant operating costs are extremely low.
- The tidal turbines are up to 80% efficient in converting tidal energy to usable electricity.
- The wave energy is very predictable as tides rise and fall with great uniformity.

Disadvantage of tidal energy:

- The effect on marine life may be disruptive in terms of the movement and growth of fish and other marine life.

19.3.4 Wave energy

McCormick (2007) has described wind waves as a form of solar energy, as the primary source of wind energy is the sun and solar radiation which are collected by both land and water masses; the water is the more efficient collector of the two. For a more detailed discussion of the meteorological aspects of wind generation it is recommended that reference should be made to Voss (1972) and Dietrich (1963).

At present wave power generation is not a widely employed commercial technology, although there have been attempts at using it since 1890 (Miller, 2004); however, there are a number of projects in the development stages.

One of the first turbines to generate electricity was the Pelamis Machine P2 which has five tube sections linked by hinged joints and floating on the sea surface, in offshore water of depths greater than 50 m; it is anchored at one end. Incoming waves cause the tube sections to move relative to one another, causing bending movements at the joints of the machine that are resisted by hydraulics which pump oil through a hydraulic motor; this converts the wave motion to electricity by powering electrical generators. All equipment is housed inside the machine and power is transmitted to shore using standard subsea cables. Several machines can be connected together and linked to shore through a single subsea cable. The first Pelamis machine was installed on its moorings at the European Marine Energy Centre in Orkney on 10 October 2010; the initial period of its operation, lasting five days, was to prove the installation and removal process and confirm satisfactory operation of all machine systems. Currently, five Pelamis machines have been produced. The sixth machine was launched on 14 April 2011 and is currently being commissioned for sea trials and testing; it will be towed to the berth of the first Pelamis at the European Marine Energy Centre in Orkney where it will generate to the National Grid. At the moment the main structure of the Pelamis machine is manufactured in steel, fabricated into steel cans and welded into specific tube sections at the site of Pelamis Wave Power at Edinburgh. However, the firm is investigating alternative methods of producing the body of the machine and no doubt will be analysing the advantages of composites in the hostile environment in which the Pelamis machine has to operate.

In all systems which rely upon buoyancy, such as in the production of tidal and wave energies, polymer composite materials used to manufacture the components of the systems have inherent advantages over metals due to their corrosion resistance, fatigue-life and durability requirements. The advantage of composites can also be exploited in devices that profile the waves, whether they employ foils, hemispherical floats or buoys. To become cost-competitive with metals requires volume production of components, thus tidal and wave systems are an emerging new market for composites.

19.4 Introduction to solar power

19.4.1 Introduction

Solar power has great potential. It is the largest energy source available to mankind for consumption on earth and is limitless; if utilised it could supply energy to mankind to meet many times the present demand (International Energy Agency, 2008). The basic idea of space-based solar power was first investigated in the 1970s, when solar panels were positioned on a satellite to beam the collected energy from the sun to a receiver on Earth to be

converted into electricity. If the sunlight were collected in the vacuum of space it would indicate that the solar panels can harvest the sun's intense energy without losses due to atmospheric absorption. When a satellite is placed in geostationary orbit it can be exposed to sunlight for 24 hours per day with no interruptions due to cloud cover. Microwave transmission at frequencies up to about 10 gigahertz can move through Earth's thick atmosphere with little absorption, allowing most of the power collected to travel from the solar collector to the receiver on Earth. However, microwaves tend to spread out as they travel, so for great distances large receivers are required to capture the energy being beamed. Consequently, solar collectors at a geostationary orbit would require a microwave receiver on Earth to cover hundreds of square miles; this clearly is not a practicable option. Little (2011) has outlined a design for a space-based solar platform that first beams a laser from a solar-collecting satellite to another satellite positioned some 20 kilometres above the surface of the Earth. This satellite would be equipped to transform the laser to microwaves and would then beam that energy to a ground receiver.

In the past the drawback to space-based power has been the cost of setting up the infrastructure. With cheaper commercially developed rockets, such as the SpaceX Falcon Heavy, which are now being developed as the US successors to the retired space shuttle fleet for delivering cargo to low-Earth orbit, these rockets will be able to launch payloads much more cheaply. A reusable version of the Falcon rocket family is also under development, which could further reduce launch costs (Strickland, 2011).

The International Academy of Astronautics conducted during 2008–10 the first broadly based international assessment of the concept of solar power satellites, collecting solar energy in space and delivering it to markets on Earth via wireless power transmission (Mankins, 2011). The study found that the Solar Power Satellites concept has significant potential to meet global requirements for largely carbon-neutral energy during this century. One of the conclusions of this study was that 'Solar Power Satellites appear to be technically feasible within the next 20 to 30 years using laboratory technologies that currently exist (at low- to moderate-technology readiness level) that could be developed/demonstrated (depending upon the systems concept details).'

Earth-based solar power (EBSP) technology

Earth-based solar power (EBSP) is abundantly available, but it is variable and intermittent; it is less effective in overcast or cloudy conditions and cannot generate electricity at night. Its conversion tends to be material-intensive, leading to high investment costs; these are decreasing as more experience is gained in this area (Wiser *et al.*, 2009).

The two most frequently discussed solar technologies for the production of electricity are solar photovoltaics (PV), which uses semiconductor materials to convert sunlight into electricity, and Concentrating Solar Power (CSP), which concentrates sunlight on a fluid to produce steam and to drive a turbine, thus producing electricity. Solar PV currently accounts for about twice as much installed capacity as CSP (US Energy Information Administration (EIA), 2009). Both solar PV and CSP are expensive relative to other forms of electricity generation, but technological improvements have helped to bring these costs down in recent years.

The solar receiver systems concentrate the solar radiation for large-scale energy production, including distribution. CSP systems use lenses or mirrors and tracking systems to focus a large area of sunlight into a small beam. The concentrated heat is then used as a heat source for a conventional power plant. One technology, and the most advanced, uses rows of parabolic troughs to focus the small beam onto a central-pipe receiver which runs above the troughs. Pressurised water and other fluids, generally molten salts, are heated in the pipe and are used to generate steam to drive a turbogenerator for electricity production or to provide industry with heat energy.

BrightSource Energy, Inc., Oakland, California, manufacture power plants to generate power from solar thermal technology by creating high-temperature steam to turn a turbine. Their solar thermal system uses proprietary software to control thousands of heliostats, each of which consists of two flat glass mirrors, supported by a lightweight steel support structure, that are mounted on a single pylon equipped with a computer-controlled drive system. Composites could readily be used as the support structure for the mirrors and would be an advantage in hostile environments due to their resistance to corrosion. The largest solar thermal power plant in the world is currently being built by BrightSource Energy, Inc., at Ivanpal, California.

One of the advantages of solar thermal systems compared with the conventional photovoltaics is that heat can be stored cheaply and used when required to generate electricity. In all solar thermal plants, some heat is stored in the fluids circulating through the system. This tends to balance any short-term fluctuations in the rays from the sun and allows the plant to generate electricity for some time after the sun sets. Increasing the storage systems would allow the plant to continue to operate during longer periods of cloud cover and generate power well into, or even throughout, the night. Such long-term storage could be needed if solar is to provide a large share of the total power supply.

EBSP requires a considerable acreage of land for collection and production of electricity, therefore this technology competes with agriculture and forestry; consequently the availability of land is a limiting factor in the development of EBSP energy.

The space-based solar power (SBSP) method

Considering an outline design as suggested by Little (2011) (see Section 19.4.1), the collected electrical energy from solar collectors supported by satellite no. 1 at geostationary orbit would be beamed to Earth by laser onto satellite no. 2 positioned some 20 kilometres above the Earth. Satellite no. 2 would support the equipment to transform the laser to microwaves which would be beamed to a ground receiver. Ideally both satellites 1 and 2 would be fabricated from a polymer/fibre composite skeletal space structure to support the collectors and equipment. Figure 19.9 illustrates the components that would be required for the SBSP system.

Currently, there are two techniques for placing large backing frames in space to support collectors and equipment; it is suggested that these are manufactured from polymer composite material systems as (1) a rigid deployable skeletal system, (2) an inflatable and flexible continuum structure.

1. Rigid deployable skeletal system. The unit building blocks of the rigid deployable skeletal structure and its deployment mechanisms would be manufactured on Earth and collapsed into a minimum volume as compact packages, stowed in the cargo bay of the space transporter in their operating configurations for launch and deployment at low earth orbit (LEO). One method for deployment of the space skeletal structure could

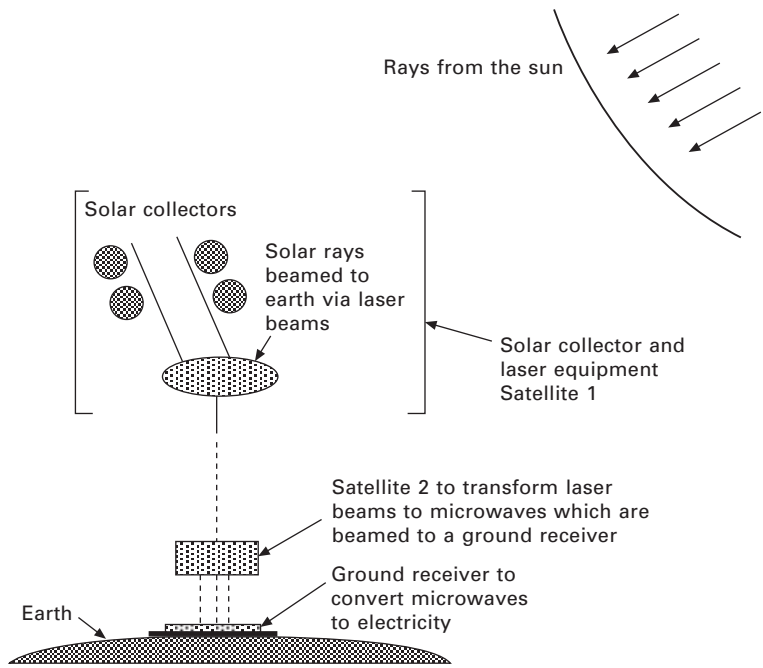

19.9 The components that would be required for a SBSP system.

be achieved by releasing potential energy which would be stored in the joints and in the centre of certain members of the skeletal structure in the stowed configuration of the structure. An alternative method could be by external means such as electrically driven motors or inflatable devices; the former system will be discussed in this chapter. If necessary the various unit building blocks after deployment at LEO would be joined in space by extra vehicular activity (EVA) and also any equipment that would be used in geostationary orbit (GEO) would be joined at LEO; this would involve either astronauts or specifically designed robots. The completed structure could then be taken, if required, to geostationary orbit by space tug (Wingo, 2004) or under its own method of propulsion. The skeletal space structure positioned at LEO 20 kilometres above the earth would be manufactured in a similar way. The fibre/matrix composite technique is described in Chapter 20, Section 20.7.

2. *Inflatable and flexible continuum structure*. The unit elements of the inflatable continuum structure would be stowed into a minimum volume in the cargo bay of the space transporter, launched and deployed at LEO. The various unit elements would be inflated and joined by EVA. Any equipment required would be connected at LEO and the whole would be transported to geostationary orbit. The system is described in Chapter 20, Section 20.7.4.

19.4.2 The rigid deployable skeletal structure to support the solar collectors

The requirements for the backing space structures are that they should be light in weight and have high specific strength and stiffness; in addition, their physical properties must be able to resist the hostile environments of space. Polymer composites have the required mechanical and in-service attributes and, if necessary, the polymers can be modified to provide properties to resist the hostile space environments for a finite length of time.

Chapter 20, Section 20.7.3, will discuss the unit building block manufactured in advanced polymer composites and the deployment mechanism by stored potential energy for the skeletal structure. Figure 20.4 of Chapter 20 illustrates the unit building block backing frame of a nine-cluster node point of 21 tubular members. Hollaway and York (1995) have discussed a suitable deployment system.

19.4.3 The rigidised inflatable flexible continuum structure to support the solar collectors

Inflatable structures were originally investigated in the early space programmes to reduce the weight and volume of onboard items and hence the cost of

the space flight. Recent advances in materials technology have introduced another group of polymers which are distinct from those originally used for inflatable structures; they are known as rigidised inflatables (RI). These systems require a shape memory polymer (SMP) material for the space trusses; this specific structural form of self-deployable truss would use the thermoplastic material SMP/carbon fibre composite. These systems have been used for experimentation in a number of development programmes for various applications (Ji *et al.*, 2006; Scarborough and Cadogan, 2006) and an actual RI flight was reported by Cooper *et al. (*2009).

SMPs change their shapes in response to an external stimulus; the most common ones are temperature and thermo-responsive. They typically consist of two polymer components and two phases, one with a higher melting temperature than the other. The glass transition temperature (T_g) is the reference point where the higher-temperature component starts to become flexible. When heated above their T_g (typically 20°C above T_g) SMPs become soft and rubbery and readily change shape. When subsequently cooled below T_g, they will retain the given shape (shape fixing characteristic). When heated again above T_g, the materials autonomously return to the original 'parent' shape. SMPs have gained substantial interest in the designers' community of deployable space structures, due to their superior structural versatility, lower manufacturing cost, easier pre-treatment procedure, larger recoverable deformation and lower recovery temperature. Section 20.7.4 of Chapter 20 describes the SMP material characteristics in greater detail.

The flexibility of the SMP composite material is important for folding the structure into the spacecraft for transfer to space; the folding temperature is highly dependent on both the resin and fibre properties. Once the structure is packed into its folded position, it is constrained in that position until cooled to approximately 15°C, or lower below T_g at which point the SMP composite structure will remain locked or frozen in the packed position unrestrained until it is again heated above the T_g. When the SMP structure is heated, internal strain energy will cause it to return to its initial cured shape. The speed and the accuracy of the shape return are a function of the shape memory recovery force of the composite.

Chapter 20 will introduce the materials which can be used for the construction of the two structural systems and will compare them for possible use in space.

19.5 Introduction to biomass and geothermal energies

Biomass (plant material) is a renewable energy source because the energy it contains comes from the sun. Through the process of photosynthesis, plants capture the sun's energy. When the plants are burned, they release the sun's

energy that they contain. In this way, biomass functions as a type of natural battery for storing solar energy (Pigott, 2009). As long as biomass is produced in a sustainable way, with only as much used as is grown, the 'battery' will last indefinitely (Union of Concerned Scientists, 2009). In general there are two main approaches to using plants for energy production: (1) growing plants specifically for energy use, and (2) using the residues from the plants that are used for other commodities. The best approach varies from region to region according to climate, soils and geography (Union of Concerned Scientists, 2009).

Johnson and Linke-Heep (2007) have suggested that jute-based composites will be used in the biomass energy source, which is one of the younger technologies that have not progressed sufficiently for discussion; therefore, this energy technique will not be discussed further.

Geothermal energy comes from the earth's interior. The heat is generated in the earth's core some 4000 miles below the earth's surface and seeps up through faults and cracks in the earth's surface. When the heat reaches the surface, it is released naturally in the form of volcanoes, hot springs and geysers. Depending on the geology, it is possible to access this heat by drilling into the earth's surface or tapping into the hot springs. The most active site of geothermal energy is in the Pacific Ocean in an area called The Ring of Fire.

Likewise, composites will be used in plants performing geothermal energy capture but again this is one of the young technologies; consequently, this energy system will not be discussed further.

19.6 Discussion

The energy system a century from now will be very different from that of today; the question is how the transitions will emerge over the next few decades. If fossil fuels were to maintain their current share of the energy mix and, in addition, respond to the increased demands in future years, CO_2 emissions would be on a course that could severely threaten human well-being. Even with the moderation of fossil fuel use and effective CO_2 management, the path forward is still highly challenging. Remaining within desirable levels of CO_2 concentration in the atmosphere will become increasingly difficult. CO_2 can be stored underground (in aquifers or in certain oil and gas fields), or used in some industrial processes. However, capturing and storing CO_2 is energy intensive and expensive. It is, therefore, clear that the engineering society must develop systems and materials which incorporate sustainable energy supplies. Consequently, new technology combinations are being developed such as intermittent renewable sources being integrated into existing power supply systems; new infrastructures, such as CO_2 capture and storage are required and older inefficient ones need to be decommissioned. This period is

an exciting one for the development of sustainable electricity supplies which could be derived from wind power, wave power, hydro power, solar power, biomass and geothermal heat power. With the advantageous mechanical and in-service properties of advanced fibre/polymer composites, this material is the preferred one for many of the structural units of systems associated with sustainable power.

Even with the moderation of fossil fuel use and effective CO_2 management, the path forward is still highly challenging and therefore to remain within the desirable levels of CO_2 concentration in the atmosphere will become increasingly difficult.

19.7 Conclusion

This chapter has introduced the various systems which are supplying or could supply the future energy for mankind and where advanced polymer composites have been and could be used in the machinery to supply renewable energy. Some of these systems may be the way forward into the future; some will undoubtedly disappear from the scene. At the very least, they illustrate the huge stimuli for advanced polymer composites and for creative engineering which have arisen from the challenges in harnessing renewable energy sources.

To show how important renewable power is, the Spanish utility company Iberdrola, S.A. (one of the leading private electric utilities worldwide and the largest renewable energy operator in the world) has stated that the commissioning of the West of Duddon Sands (WoDS) offshore wind farm to be located 14 km south-west of Walney Island off the coast of Cumbria, in the Irish Sea, 'marks the start of one of the most important technological missions in the company's history; to take the lead in the future development of this technology, which is considered "*a second renewable-energy revolution*"'.

Chapter 20 will discuss the types of polymers and fibres and the manufacturing techniques which are used to produce the composites that are utilised in parts of the machines to develop renewable energy.

19.8 Acknowledgements

The author would like to express his thanks to the many engineers and scientists employed by firms associated with advanced polymer composites in the field of sustainable energy; their help is greatly appreciated. These firms include ACG, Derbyshire, UK; Gurit, Isle of Wight, UK; Solent Composite Systems, Isle of Wight, UK; Pulse Tidal, Sheffield, UK; Wind Power Ltd, Bury St Edmunds, Suffolk, UK; Aviation Enterprise, Lambourn, UK; Marine Turbines, Bristol, UK; Exxonmobil, Leatherhead, UK; and Grimshaw, Architects, London, UK. The author would also like to thank the editor of

the *International Journal of Reinforced Plastics*, Amanda Jacob, for her help, and the various authors of journal articles associated with sustainable energy, many of whom have been acknowledged in the text.

19.9 References

Bentham, J.B. (2007), 'Shell energy scenarios to 2050', published by Shell International BV.

Black & Veatch (2005), 'Tidal stream energy resource and technology summary', Report – *Marine Energy Challenge*, published by Black & Veatch for the Carbon Trust, 4 July 2005.

Cooper, B.J., Black, J.T., Swenson, E.T. and Cobb, R.G. (2009), 'Rigidizable Inflatable Get-Away-Special Experiment (RIGEX) space flight data analysis', *50th IAA/ASME/ASCE/AHS/ASC Structures, Structural Dynamics, and Materials Conference*, 4–7 May 2009, Palm Springs, CA.

Dietrich, G. (1963), *General Oceanography*, Wiley-Interscience, New York.

Douglas, C.A., Harrison, G.P. and Chick, J.P. (2008), 'Life cycle assessment of the Seagen marine current turbine', *Proc. IMechE, Part M: Journal of Engineering for the Maritime Environment*, Vol. 222, Issue 1, pp. 1–13.

DTI (2004), Digest of United Kingdom Energy Statistics 2004, Table 5.10 Plant loads, demand and efficiency, available online at http://www.dti.gov.uk/energy/inform/energy_stats/electricity/dukes5_10.xls (accessed 20 March 2011).

ExternE (2003), 'External costs – Research results on socio-environmental damages due to electricity and transport (EUR 20198)', Office of Publications of the European Communities, available online at http://www.externe.info/exterpr.pdf.

Fraenkel, P. (2011), 'Underwater windmills – Harnessing the world's marine currents', *Ingenia* (The Royal Academy of Engineering, quarterly online magazine), Issue 46, March 2011, ISSN 9768 (www.ingenia.org.uk).

Hayman, B.J., Wedel-Heinen, J. and Brøndsted, P. (2008), 'Materials challenges in present and future wind energy', *Materials Research Society Bulletin*, Vol. 33, Issue 4, pp. 343–353.

Hollaway, L.C. and York, D. (1995), 'Numerical analysis of an energy loaded joint for a deployable satellite structure', *International Journal of Space Structures*, Vol. 10, Issue 1, pp. 47–55.

International Energy Agency (2008), *Energy Technology Perspectives*, OECD/IEA, Paris.

Ji, F., Zhu, Y., Hu, J., Liu, Y., Yeung, L. and Ye, G. (2006), 'Smart polymer fibers with shape memory effect', *Smart Materials and Structures*, Vol. 15, Issue 6, pp. 1547–1554.

Johnson, F.X. and Linke-Heep, C. (2007), 'Industrial biotechnology and biomass utilisation – Prospects and challenges for the developing world', Report for United Nations Industrial Development Organisation (UNIDO) Vienna 2007, based upon EGM Programme 14–16 December 2005 meeting of an Expert Group on 'Industrial Biotechnology and Biomass Utilisation: Prospects and Challenges for the Developing World', convened at UNIDO headquarters, Vienna, Austria, in December 2005.

Larsen, K. (2010), 'Hywind floating offshore wind turbine foundation', *Wind Power, Renewable Energy Focus Magazine*, 22 March 2010, (accessed 14 March 2011).

Lemaire, X. (2004), 'Renewable energy and efficiency partnership (August 2004) –

Glossary of terms in sustainable energy regulations', items sent privately to X. Lemaire at Warwick Business School, University of Warwick, Coventry, UK (accessed 1 September 2011).

Little, F.E. (2011), 'Meeting the challenges of implementing portable space-based solar power', *Proceedings of 30th General Assembly and Scientific Symposium of the International Union of Radio Science*, Istanbul, Turkey, 13–20 August 2011, Paper CHGBDJK.3.

Mankins, J.C. (editor) (2011), *Space Solar Power – The First International Assessment of Space Solar Power: Opportunities, Issues and Potential Pathways Forward*, International Academy of Astronautics, Paris, 248 pp.

Marsh, G. (2009), 'Wave and tidal power – an emerging new market for composites', *Reinforced Plastics*, Vol. 53, Issue 5, pp. 20–24.

McCormick, M.E. (2007), *Ocean Waves Energy Conversion*, Dover Publications, Mineola, NY.

Milborrow, D. (2003), 'Wind energy – Top myths about wind energy', Renewable UK, London.

Miller, C. (2004), 'A brief history of wave and tidal energy experiments in San Francisco and Santa Cruz', Western Neighbours Projects, San Francisco, CA. (accessed from the Internet on 14 June 2011).

Paris, J. (2011), 'ExxonMobil says wind is cheapest form of electricity generation', in *Energy Outlook: A View to 2030*, published by ExxonMobil.

Pigott, J. (2009), 'Biomass supply economics: managing the supply cost of raw materials', *TAPPI International Bioenergy and Bioproducts Conference*, 14–16 October 2009, Memphis, TN.

Renewable UK (2010), 'Wind energy technology', text and figures based on a fact-sheet produced by the European Wind Energy Association accessed 2 August 2011).

Rogers, A.L. and Manwell, J.F. (2002) (amended 2004), 'Wind turbine noise issues', White Paper prepared by the Renewable Energy Research Laboratory, Center for Energy Efficiency and Renewable Energy, University of Massachusetts, Amherst, MA.

Roney, J.M. (2012), 'Offshore wind development picking up pace', published by Earth Policy Institute, in *Wind Power*, 16 August 2012 (accessed 1st November 2012).

Royle, T. (2009), 'Gurit offers composite materials for ocean energy market', ReinforcedPlastics.com, 15 April 2009.

Rush, J. (2008), 'Power generation: the new wave', Channel 4, 31 March 2008, http://www.channel4.com/news/articles/science_technology/power+generation+the+new+wave/1907547 (accessed 21 March 2011).

Scarborough, S.E. and Cadogan, D. (2006), 'Applications of inflatable rigidisable structures', Technical Paper published by ILC Dover, Frederica, DE, 16 pp.

Strickland, J. (2011), 'The SLS: too expensive for exploration?', *The Space Review*, 28 November 2011 (accessed 9 December 2011).

The Economist (2008), 'Wind power – Blowing at sea', *The Economist*, 7 May 2008 (accessed 2 February 2010).

The Engineer (2011), 'Wind power reveals 10MW turbine design', *The Engineer*, 26 July 2010, http://www.theengineer.co.uk/news/wind-power-reveals-10mw-turbine-design/1003935.article#ixzz1ISWKqPKT (accessed 4 April 2011).

Union of Concerned Scientists (2009), 'How biomass energy works', Union of Concerned Scientists Cambridge, MA (accessed 29 March 2011).

U.S. Energy Information Administration (EIA) (2009), *Annual Energy Outlook 2008*, U.S. EIA, Washington, DC, March 2009.

Voss, G.L. (1972), *Oceanography*, Golden Press, New York.
Williamson, K. (2011a), 'Wind produces "record" amount of UK electricity', *Reinforced Plastics*, 16 September 2011 (accessed 2 September 2011).
Williamson, K. (2011b), 'Giant 10 MW Britannia wind turbine scrapped', *Reinforced Plastics*, 25 August 2011 (accessed 17 September 2011).
Wind Power (2011), information provided by the British Wind Energy Association, www.bwea.com (accessed 2 August 2011).
Wingo, D.R. (2004), 'Orbital recovery's responsive commercial space tug for life extension missions', *2nd Responsive Space Conference*, 19–24 April 2004, Los Angeles, CA, 9 pp.
Wiser, R., Barbose, G. and Peterman, C. (2009), 'Tracking the Sun – The installed cost of photovoltaics in the US from 1998–2007', Environmental Energy Technologies Division, Lawrence Berkeley National Laboratory, Berkeley, CA.
Wood, K. (2010), 'Composites-enabled tidal stream energy projects lead the way as new forms of hydrokinetic power generation move towards commercialization', *Composites Technology, Composites World*, 30 September 2010.

20

Advanced fibre-reinforced polymer (FRP) composite materials for sustainable energy technologies

L. C. HOLLAWAY, University of Surrey, UK

DOI: 10.1533/9780857098641.4.737

Abstract: This chapter will introduce advances in properties, production and manufacturing techniques of the advanced polymer/fibre composite materials that are utilised in the manufacture of machines that produce sustainable energy. Chapter 19 discussed the various methods of transferring wind, tidal, wave and solar energies into electrical power and this chapter will show how advanced composites are utilised in these various machines. Furthermore, it will suggest methods for the repair, maintenance and recycling of advanced polymer composite wind turbine blades. Finally, the future trends of sustainable energy systems and the role that polymers and polymer/fibre composites will have in their manufacture/fabrication will be evaluated.

Key words: thermoplastic and thermosetting polymers, carbon-, aramid-, glass-fibre and nano-fibre composites, land, sea and space environments, composite manufacturing technologies, wind, tidal and space generators.

20.1 Introduction: current use of composite materials in sustainable energy technology

This chapter should be read in conjunction with Chapter 19; it will discuss the role that fibre/matrix composites have and will have in the manufacture of structural component parts used in the developed and in the developing systems for sustainable power. It will discuss the types of in-service and mechanical properties of the fibres, the matrix and the composite materials that are required in the harsh environments of earth, sea and space in which the material will operate; the methods of manufacture of the composites used will be presented. Furthermore, it will suggest fibre/matrix composite systems that could be used in the emerging tidal and wave power technology systems. It will be realised that the confidentiality of some of the technologies being developed to produce power will prevent a full discussion of the fibre/matrix composites which will be used. Finally, the future of fibre/polymer composites in and the trends of sustainable energy will be discussed. Owing to the rapid advances in the topic of sustainability, this chapter, which was completed in January 2012, will require updating in a few years' time.

20.1.1 Introduction to advanced FRP composites

Composites are made up of individual materials; these are referred to as constituent materials. The purpose of a composite is to create a material that combines the constituent parts of it in some beneficial way. The two main categories of constituent materials are the matrix and the reinforcement. The matrix materials are either thermoplastic or thermosetting resins. These polymers bind the reinforcement together and determine the physical in-service properties of the composite material. Polymers can also act as reinforcing material in composites; Kevlar, for instance, is a polymer fibre that is very strong and imparts toughness to a composite.

Thermosetting resins are the polymers (polyester, vinylester, epoxies) that are generally used to manufacture parts of the machines to produce sustainable energy generators. In addition, thermoplastic resins such as polyether ether ketone (PEEK), polyether sulphone (PES) and various liquid crystal polymers (LCP) are also used. The latter high-performance polymers also meet stringent out-gassing (relevant to space environments) and flammability requirements.

In any composite, fibres (such as glass, carbon or Kevlar fibres) carry the load, and their type, volume fraction, orientation and straightness determine their effectiveness; they are the dominant contributor to the mechanical properties of the composite. Glass fibre, the generic name given to this class of material, is used for applications where toughness, electrical non-conductivity or abrasion resistance is required. From this statement it will be clear that there are a number of different types of glass fibre, all with specific mechanical and physical properties (Hollaway and Head, 2001). Carbon fibre is used for applications requiring high strength and stiffness; likewise there are a number of specific carbon fibres which may be selected having required properties (Smith, 2000). The resin transfers loads between fibres, protects them, and holds them in the correct location and orientation in the composite. Moreover, the type of resin used in the composite determines the resistance of the composite to water and chemical absorption and sensitivity, mechanical properties at elevated temperatures, and compressive strengths and stiffness. In addition, the resin type determines the method of fabrication of the final structural component and its cost relative to alternative resin types and fabrication methods.

20.1.2 Recently developed polymers

There are several firms that specialise in producing composite materials for machinery which generates sustainable energy, such as Advanced Composite Group (ACG, now Cytec), Gurit, and Hexcel.

Cytec has developed several prepreg materials, for instance the resin

Variable Temperature Moulding (VTM) systems forming the resin VTM®260 series prepreg, which was used on the SeaGen generator blades (see Section 20.6.2) and on the initial construction of the blades of the 'QuietRevolution' but was later superseded by the resin MTM®57 systems (see Section 20.5.5). Based on this latter superior system, Cytec have developed two new 80°C to 120°C curing variants; these are the MTM®57-2 and the MTM®57-3. These systems, used with the heavyweight unidirectional (UD) carbon reinforcement prepregs, could be used in future to form an integrated spar of a very large turbine blade. The skins of the future blades could be manufactured from the resin MTM®57-2 on a 1200 gsm glass ZPREG® rapid lay-up format which would be combined with an in-mould surface primer film, MTF246.

For the repair of wind turbine blades, Gurit has developed the prepreg, SPRINT™, SparPreg™, which requires no debulking. They have also developed the RENUVO™ blade repair system (see Section 20.5.7) for the repair and maintenance of wind turbine blades. SparPreg™ material is said to provide the following benefits in spar manufacture:

- Fast material deposition rates
- Single debulk vacuum processing
- 95°C curing and low exotherm
- Very low void content and material wrinkling in thick sections (e.g. 80 mm)
- Wide range of industrial-grade fibre choice.

GFPMS is a European composites distributor and has established a strong portfolio of advanced composites products, including Advanced Composites Group's prepregs and Sigmatex's carbon fibre materials; they do not manufacture polymers.

Hexcel (2005) has published an article on their prepreg technology. Since then Hexcel has developed the unidirectional carbon fibre Hexcel HexPly M9G® which is a standard cure prepreg product. The unidirectional carbon fibre prepreg HexPly M19G cures in 15–20% less time than the HexPly M9G whilst having the same handling and mechanical properties. Both prepregs have been certified by Germanischer Lloyd (GL)[1] for use in the manufacture of wind turbine blades. Both Hexcel prepregs are suitable for shells, spars and the root end of wind turbine blades. Hexcel has also developed a new surfacing prepreg for wind energy applications. HexPly® XF2P provides a

[1]Certification of wind turbines or components to harmonised requirements is a necessity and therefore it is important for manufacturers, banks and insurers of wind turbines and components to know the different certification processes and guidelines as well as the keystones of their development. Consequently, Germanischer Lloyd, Hamburg, Germany has developed a new standard and innovations in certification of wind turbines; this is the latest version (Woebbeking, 2007, 2010).

ready-to-paint surface; they claim it is tough and durable without the need for a gel coat.

Renewergen Ltd is a tidal energy device developer but as an offshoot to the firm's activity undertakes blade repair using Gurit and Cytec materials; their application method is by squeegees. The repair area is ground with an angle grinder and is scarified to an angle of between 25:1 and 40:1. The peel-ply is laid on the repair area and is covered with a perforated release film, and breather absorber. The whole repair area is vacuum bagged and a vacuum is applied by means of a vacuum pump to consolidate the repair whilst the peel-ply is cured.

Scott Bader Co. Ltd. of Wollaston, England, has recently launched Crystic Permabright, a high-performance gel coat designed to provide long-term UV weathering performance by providing strong colour stability. This gel coat is designed for marine, construction, wind-energy and transportation applications.

20.2 The use of nanoparticles in composites

As with the advanced polymer composite, a nanocomposite is formed from a combination of two or more materials; however, one of the materials has dimensions in the nanoscale (<100 nm). Nanoparticles can be classified into three categories depending on their number of nanoscale dimensions: (a) nano-spheres, (b) nano-fibres and (c) nano-plates, having three, two and one nanoscale dimension respectively (Thostenson *et al.*, 2005). Paul and Robeson (2008) have given a comprehensive review of nanoparticles. Only nano-fibres and nano-plates will be mentioned in this chapter as these are relevant to possible structures concerned with sustainability energy.

20.2.1 Nano-fibres

The paper of Iijima (1991) has generated unprecedented interest in carbon nanostructures and has fuelled intense research in the area of nanotechnology.

Carbon nanotubes (CNTs) consist of molecular cylinders of pure, hexagonally arranged carbon atoms with a diameter of a few nanometres and a length of many microns. They occur in two main types, the single-wall carbon nanotube (SWNT) composed of a single lattice cylinder of carbon, and the multi-wall version (MWNT) consisting of concentric lattice cylinders of carbon; they resemble one cylinder within the other. The ends of the tubes are usually closed off by a carbon end-cap, also in lattice form.

The strength of the sp^2 carbon–carbon bonds provides carbon nanotubes with extraordinary mechanical properties. The nature of the bonding of a nanotube is described by applied quantum chemistry, specifically by orbital

hybridisation, the chemical bonding of nanotubes being composed entirely of sp^2 bonds, similar to those of graphite. The scale size, aspect ratio and properties of carbon nanotubes provide advantages in a variety of applications, including electrostatically dissipative materials, advanced materials with combined stiffness, strength and impact for aerospace, space, composite mirrors and components with enhanced mechanical properties. Consequently, CNTs are a promising new material for blending with polymers and having the potential to obtain low-weight nanocomposites with exceptionally good mechanical, electrical, thermal and multifunctional properties ideal for use in the manufacture of structural components to produce sustainable energy.

The mechanical properties of various types of nanotubes have been extensively studied by both experimental and computational means (Thostenson *et al*., 2001; Qian *et al*., 2002; Ruoff *et al*., 2003). Their tensile strength can vary between 100 and 600 GPa, which is about two orders of magnitude higher than that of current high-strength carbon fibres (Sennett *et al*., 2003; Koziol *et al*., 2007), and their density is around 1.3 g/cm^3, lower than the density of commercial carbon fibres (1.8–1.9 g/cm^3). The enhancement in strength implies that, for the same performance, replacing commercial carbon fibres with CNTs will lead to significant reduction in the density and volume of the structural composite parts (Breuer and Sundararaj, 2004). The compressive strength of CNTs is approximately two orders of magnitude higher than the compressive strength of any known fibre (Louriel *et al*., 1998; Salvetat *et al*., 1999). CNTs are also one of the stiffest material structures ever made; compared to carbon fibres, which typically have a modulus of elasticity of up to 750 GPa, the modulus of elasticity of nanotubes ranges between 1 and 5 TPa (Iijima, 1991; Sennett *et al*., 2003).

Loos (2011) reported that investigators from Bayer Material Science LLC, USA and Moulded Fibre Glass, Cleveland, USA have developed a prototype wind turbine blade 0.74 metre long manufactured from polyurethane reinforced with carbon nanotubes (CNT PU). The researchers claim that the advanced material has a specific tensile strength of five times and 60 times that of carbon fibre composite and aluminium respectively and is tougher than CFRP; furthermore, the stiffer but thinner blades enable maximum energy to be produced.

20.2.2 Nano-plates

Nano-plates are generally naturally occurring layered materials such as layered silicates (montmorillonite plates, a type of clay) which is dispersed within polymers for nanocomposite formation (Hackman and Hollaway, 2006; Tran *et al*. (2006); initially man-made materials such as silicate acids were used (Wang *et al*., 1996). The objective in a nanocomposite produced from plate-like fillers is to disperse the latter in a polymer to take advantage of

the large surface area of the plate and thus modify the polymer properties. The nano-plates were first produced by a group of Toyota researchers when they dispersed clay within Nylon-6 (Kojima *et al*., 1993a); the nano-plate composites possessed considerable mechanical and permeability property advantages (Kojima *et al*., 1993b). A number of extensive reviews have been published that cover various areas of nanocomposite processing, behaviour and properties with respect to numerous types of polymer (Le Baron *et al*., 1999; Ray and Okamoto, 2003; Utraki, 2004).

The advantages of incorporating nano-plates into FRP composites include the following:

- *Barrier properties*. At a high aspect ratio which can be achieved in nanocomposites (with exfoliated clay) significant decreases in permeability are predicted and observed in practice (Hollaway and Hackman, 2004). The barrier properties of polymers can be significantly altered by inclusion of inorganic platelets with sufficient aspect ratio to alter the diffusion path of the penetrant molecules.
- *Flammability resistance*. An increase in flammability resistance has been noticed as an important property enhancement involving nano-platelets incorporated into polymers involving exfoliated clay; this involves the formation of a stable carbon/nano-platelet or nanofibre surface. This surface exhibits analogous characteristics to intumescent coatings whereby the resultant 'char' provides protection to the interior of the specimen by preventing continual surface regeneration of available fuel to continue the combustion process. The primary advantage noted with nano-filler incorporation is the reduction in the maximum heat release rate.

Hydrogen is a promising alternative to fossil fuels due to its clean combustion compared with that of fossil fuels; the only combustion by-product of hydrogen is water. Compared to petrol, hydrogen is lightweight, can provide a higher energy density and is readily available. However, to replace petrol as a fuel, hydrogen must be safely and densely stored, but easily accessed; storage of hydrogen is a potential problem. Scientists at the U.S. Department of Energy, Lawrence Berkeley National Laboratory, have designed a composite material for hydrogen storage consisting of nano-particles of magnesium metal sprinkled through a matrix of polymethyl methacrylate, a polymer related to Plexiglas. This nanocomposite rapidly absorbs and releases hydrogen at modest temperatures without oxidising the metal after cycling; this technology has been designed specifically for hydrogen storage, batteries and fuel cells. This work shows an ability to design composite nanoscale materials that can overcome fundamental thermodynamic and kinetic barriers to realise a materials combination. The unique properties of both the polymer and the nanoparticle to form a composite material may be applicable to related problems in other areas of energy research.

An area where nanocomposites could achieve a dramatic commercial prominence is in the advanced polymer composites. CFRP composites have a limit on the achievable properties, particularly in cross-ply composites due to the low modulus and strength of the matrix phase. Modification of the matrix with carbon nanotubes at the lower scale of dimensions and with carbon nanofibres at a higher dimensional scale would allow for significant increase in the modulus and strength contributions of the matrix to the overall composite properties. Whilst this would offer some improvement in unidirectional composites, it could be dramatic in the case of cross-ply composites which are the major type of composite structure utilised in some advanced composite applications.

Whilst there have been some components which have been manufactured using carbon nanotubes and nano-plates in development, the nano-particle markets have been constrained by three main issues:

- A lack of commercially available material of consistently high quality.
- The nano-particle technologies are in the early stages of industrial development. Whilst they are expensive compared to a fully commoditised product, such as carbon fibre, the price will fall as demand increases. Currently, they are probably too expensive for the field of sustainable energy but their potential cannot be ignored.
- The incredibly small scale of the material poses some interesting challenges for advanced material and coatings science.

Such teething problems in developing new materials are not unfamiliar; for instance, carbon fibres took many years to be widely accepted in the materials world from both a cost and a performance aspect.

20.3 In-service requirements of advanced fibre-reinforced polymer (FRP) composites for sustainable energy applications

20.3.1 Land environments

The properties of the fibres, the matrices and the fibre arrangement within the composite and the fibre volume fraction govern the final strength and stiffness value properties of the composites. These parameters have been illustrated in Hollaway and Teng (2008) and Smith and Yeomans (2002). The matrices for the composites that could be used in the manufacture of wind turbine blades would be polyester, vinylester or epoxies. Glass, Kevlar or carbon fibres can be used with any of the polymers mentioned, but as the rotor blades become larger a hybrid construction of glass and carbon is used. The hybrid concept is often a compromise between the improved

performance of carbon fibres and their high cost. Few rotor blades have been made completely of carbon fibre composites.

The rotor blades, both onshore and offshore, are exposed to various hostile conditions such as extreme temperatures, humidity, rain, hail impact, snow, ice, solar radiation, lightning and salinity. In order to withstand these external conditions without diminishing the safety, a sound knowledge of the fatigue behaviour of the material and structural properties is needed.

The cyclic loading of the structure of a wind turbine could cause failure if some critical level of damage is exceeded. Once initiated, the damage will grow with the load cycling until failure occurs. The failure process would occur for one of the following reasons:

- The net section stress, accounting for the loss of section caused by the damage, exceeds the ultimate strength of the material.
- A critical crack forms by the accumulation of damage.

Forces relevant to fatigue

The S–N curves provide an indication of the relevant fatigue properties; they do not take into account the complex effects of the large number of different cyclic forces which act on a wind turbine blade during operation. These forces arise due to the self-mass of the blade and the force of the wind acting upon it and include:

- The gravitational force, which leads to compression and tension through each cycle.
- The centrifugal force due to the rotation of the blade.
- The wind thrust which is a force that is perpendicular to the plane of the rotor blade; it varies relatively slowly.
- Other rapidly varying forces arise from the wind turbulence which increases as the stall conditions are approached.

Research workers have concluded that the relatively low-frequency high-amplitude wind thrust forces primarily contribute to fatigue damage.

Environmental factors affecting fatigue

Environmental attack can rapidly reduce the material's fatigue strength. This could happen in two ways:

- *Blade topography*. The topography of the surface of the blade may be modified by minute erosive and corrosive pits from sand or rain impingement. These would act as stress concentrations during cyclic loading, causing localised cracking to be initiated. The erosion attack

can occur near the blade tips where the rotational velocities can reach the equivalent of 100 m/s.

- *Bulk material properties*. The bulk material properties may be altered, thus reducing fatigue strength through the blade wall thickness or through the surface layers. To overcome this problem, protective coatings are applied initially at the manufacturing stage and if necessary during maintenance procedures. The leading edge of wind turbine blades will require a special finish.

The fatigue properties of composite materials depend on the inherent strength and stiffness of their component materials as well as on their structure. Experimental full-scale simulations on GFRP turbine blades have been conducted and the results indicate a satisfactory service life under normal conditions. However, laboratory test data show a steadily decreasing S–N curve indicating a finite service life; it is advisable to monitor rotor blades under operational conditions. Composite materials containing higher-modulus or stiffer fibres possess better fatigue properties, if the cyclic stress is applied parallel to the fibre orientation. CFRP composites exhibit excellent fatigue performance when compared to GFRP composites, particularly when subjected to tension fatigue in the fibre direction.

20.3.2 Seawater environments

Fibre/polymer composites have a long history of use in marine vessels, piping, corrosion equipment and underground storage tanks; anecdotal evidence and limited testing show that they can be successfully engineered to have a long service life in contact with moisture and aqueous solutions (Helbling and Karbhari, 2007).

Durability and dynamic failure properties are critical parameters for fibre/polymer composite in seawater. In general, all carbon fibre/epoxy engineering composite structures are subject to a multiaxial stress state. Furthermore, carbon/epoxy composites are susceptible to environmental degradation from long-term saltwater exposure. It is important that the long-term effects of saltwater on the multiaxial fatigue behaviour of these composites are understood but research results of impact resistance of composite materials when immersed in seawater are sparse and not well documented. Chiou and Bradley (1997) investigated the fatigue and static edge delamination on $[45/0/–45/90]_s$ CFRP laminates both in the dry state and in pre-soaked seawater specimens to examine any effect moisture absorption had on the fatigue crack development; the results were monitored by optical microscopy and ultrasonic C-scan. They found that seawater changed the dominant edge-cracking mode from the –45/90 interlaminar delamination in the unaged specimen to intralaminar cracking in 90° plies in the aged saturated seawater specimens. The edge-crack growth rates in both unaged

and aged specimens were similar. Monaghan and Wang (2004) studied the long-term saltwater effects on multiaxial fatigue degradation, failure modes, and stress–life relationship. A series of tension–torsion fatigue experiments were conducted on hoop-wound carbon/epoxy tubes in a variety of saltwater environments. They concluded that the composite elastic properties degrade slightly during cycling. Long-term soaking in saltwater provides the most significant reduction in fatigue life, modulus and monotonic strength. Xu (2010) tested more than 50 specimens for 21 months under saturated seawater exposure; he shows that after impact the compression strengths of the wet specimens reduced less than 9% compared to the dry baseline specimens. From these results he concluded that the durability of composites exposed to seawater was much better than had previously been realised.

20.3.3 Space environment

Space Based Solar Power (SBSP) structural systems would be exposed to harsh environments and therefore the physical properties of the composite materials must resist such loadings.

The basic criteria for a wholly space-resistant, space-tailored composite are that it must possess:

- Atomic oxygen and atomic nitrogen resistance
- Radiation resistance
- Low out-gassing (it is important that the out-gassing is low as the volatile compounds can migrate from the polymers and condense onto nearby surfaces)
- Fatigue resistance
- Vacuum stability
- High specific strength and stiffness
- The thermal differential stresses mentioned above.

Hollaway (2011) has discussed the various environments of space.

The type of environment encountered in Low Earth Orbit (LEO) (approximately 250 km above the earth's surface) to which space-systems would be exposed is characterised by:

- High levels of magnetic flux and trapped solar radiation. This environment may degrade a composite quite quickly, with polymer cross-linking embrittlement occurring as a consequence of the high ionisation levels that exist in this orbit.
- Residual atmospheric drag effects and chemical attack from highly energetic atoms, principally from atomic oxygen (AO) and atomic nitrogen (AN) radicals (Leger *et al*., 1986, 1987).
- Incessant and rapidly varying thermal fluctuations as it undergoes excursions through the earth's umbra (Annandale, 1986).

The environments of LEO would be experienced for a period of time, albeit a short period during the space structure's fabrication and deployment (see Section 20.7.4).

At the higher altitude of GEO, at 36,000 km above the earth, the space structure is exposed to a different loading regime. The type of environments encountered in GEO to which space-systems would be exposed are:

- The solar wind, which is hydrogen plasma of varying intensity and is dependent on solar flare activity; its velocity is approximately 400 km/s. The effect of this plasma can be expected to lead to substantial degradation of the space structure's material thermal properties over its lifetime.
- The essentially beneficial warming influence of planetary infra-red (IR) radiation.
- The earth-albedo is greatly diminished at these high altitudes.
- The space-system will not be attacked by AO at these heights.

20.4 Manufacture of FRP composite materials for sustainable energy systems

20.4.1 Wet lay-up

The process is one of the open-mould processes for the manufacture of fibre/polymer composite. Initially the mould cavity is coated with either polyvinyl alcohol or a non-silicon wax to aid component release. If a resin-rich smooth surface to the final composite is required for environmental protection purposes, a gel coat is applied to the mould surface. Furthermore, for an improved surface finish and corrosion resistance of the composite, a surface veil is used, which is applied with an embedded fabric for reinforcement. Each layer of the designed fibres is positioned on the mould. An accelerator and a catalyst are mixed in with the resin and the whole is applied to the fibres by brush or poured onto the fibres and rolled to ensure complete wetting of the fibres; during this process air bubbles are removed. For large mouldings the cold-cured resin is polymerised at room temperature for a period of 16 hours at 40°C, but these figures depend upon the resin system used; if the temperature is lower than 40°C the composite must be post-cured for a further time, the length of time being dependent upon the post-cure temperature. If a hot-cured resin is used an accelerator would not be employed. From health and safety considerations care must be taken at the time of manufacture of the composite due to styrene emissions. This method is not suitable for a strength- or weight-critical primary structure as the fibre orientation and local resin content cannot be well controlled.

To improve the quality of the final composite by reducing the voids caused by air becoming trapped in the laminate and improving the consolidation

at the wet lay-up stage, a vacuum-assisted technique can be applied. The wet composite is sealed within a bagging material and a vacuum is applied to the wet composite using a vacuum pump to extract the enclosed air; the polymer is then cured.

20.4.2 Resin infusion technology

Resin infusion technology is a process in which a dry fibre laminate preform is used. A dry stack of fabric material is placed into a mould tool; the fabric is sometimes pre-stressed to the shape of the mould and held together by a binder. A second mould is then clamped over the first and the resin component is added by an infusion methodology; alternatively a flexible film membrane can be placed over the composite material. The thermosetting polymer enters the space between and around the dry fibre laminate preform through feeder pipes and a runner system; the composite is then cured in place. A high quality dimensionally accurate polymer composite is formed with a high quality surface finish. Typical polymers used are epoxies, vinylester, polyester or phenolic with glass or carbon fibre preform reinforcement which are stitched.

The process of resin infusion is often divided into two distinct categories based on the manner in which the resin is infused into the preform and mould cavity, though the divisions are not universally accepted:

- Resin Transfer Moulding (RTM) or its recent invention Light Resin Transfer Moulding (LRTM), in which the resin is introduced into the mould and the preform at a pressure higher than atmospheric
- Vacuum Infusion Process (VIP), generally referred to as Vacuum Assisted Resin Transfer Moulding (VARTM), in which the resin is introduced into the mould and the preform under a pressure lower than atmospheric (i.e. a vacuum).

Process innovations have led to a number of advances in this field which have improved the process or have developed a process to meet structural or design needs. Examples of these are:

- The Seeman Composite Resin Infusion Moulding Process (SCRIMP™) system which was developed to infuse very large and complex structures more quickly than other RTM methods, by taking advantage of an increased rate of flow through the porous media over large surface areas such that infusion travelled the minimum distance (e.g. through the thickness).
- Resin Film Infusion (RFI) where dry fibres are laid up interleaved with layers of semi-solid resin film supplied on a release paper. The lay-up is vacuum bagged to remove the air through the dry fabrics and then heated to allow the resin to first melt and flow into the air-free fabrics, and then to cure.

- Autoclave pressure, temperature-time sequencing and vacuum draw similar to conventional prepreg procedures are utilised to cause the resin to flow through the minimum thickness direction.

20.4.3 Prepreg technology

A pre-impregnated (prepreg) laminate consists of a specially formulated pre-catalysed resin system, using machinery designed to ensure consistency; the resin is combined with fibre or fabric reinforcement.

One of the most common methods of preparing a composite prepreg is to draw a sheet of woven fibre through a bath, or to impregnate it through gravity from a container, containing the pre-catalysed resin system. A heating chamber removes the solvent through evaporation and partially cures the resin. Ideally, the resin has reacted with the cross-linking agent to form short polymer chains producing a viscoelastic solid, but has not cross-linked or vitrified it into a glassy solid. The prepreg should be slightly tacky so layers do not slip over each other during lay-up, and it should be sufficiently pliable such that it forms (drapes) to the mould plate. Controlling the extent of cure is extremely important. The prepregs are then covered by a flexible backing paper, and can be readily handled and remain pliable for a certain time period (out-life) at room temperature. Curing of prepreg laminates is achieved by heating at elevated temperatures under pressure according to the manufacturer's specifications. Conventional prepregs are formulated for autoclave curing, whilst low-temperature prepregs can be fully cured by using vacuum bag pressure alone at much lower temperatures. Before use, prepregs are typically stored at sub-freezing temperatures (generally –20°C) to prolong their usable life. The prepreg technology, including the manufacturing method for the production of the prepreg, is discussed in EPTA Publication (2008).

20.4.4 SPRINT technology

When using prepreg materials in thick laminates (greater than 3 mm) it becomes difficult to remove entrapped air between plies, and around laminate details such as ply overlaps, during the curing procedure. To overcome this problem in traditional prepreg materials a number of warm debulking stages are introduced during lay-up to remove the trapped air and thus significantly reduce the manufacturing times. Gurit has patented a number of modified prepreg products that enable the manufacture of high quality (low void content) thick laminates in one processing step; two of these are:

- SPRINT® materials consist of a resin film sandwiched between two dry fibre layers. Once placed in the mould, a vacuum is applied to extract all of the air in the laminate (monolithic and/or sandwich) before heat is

applied to allow the resin to soften and impregnate the dry fibre layers and then cure.

- SparPreg™ is a UD prepreg also for use with thick laminate sections. The excellent 'breathability' of the material produces laminates of exceptional quality with low void content, without the need for debulking or additional dry fabric reinforcement to aid air removal during the application of vacuum and the subsequent curing process.

The main advantages of the SparPreg™ technique are:

- High fibre volumes can be accurately achieved with low void contents for very thick laminates (100 mm).
- High resin mechanical properties due to the solid state of the initial polymer material and the elevated temperature cure.
- It enables the use of lower-cost heavyweight materials (e.g. 1600 gsm) and allows fast deposition rates, reducing component manufacturing costs.
- It is a very robust and repeatable process as the resin content is accurately controlled and the complexity of the infusion process is very low.
- It is environmentally safe, as the resin has already been mixed, and there is no emission of volatile gases typically present when mixing two component resin systems.

The main disadvantages are:

- The cost of materials is higher than for non-pre-impregnated fabrics.
- Tooling needs to be able to withstand higher temperatures compared to the infusion processes (typically 80–140°C).

20.4.5 Film-stacking technology under elevated temperature and pressure

Prepreg sheets of thermoplastic aromatic polymers (a polyethersulphone or polyetheretherketone) can be moulded by the use of a hot press using vacuum or compressed air. The equipment consists of a fixed frame that can be heated and a two-step heating system for providing a uniform temperature distribution to the surface and cross-section of the sheet. The heater is designed so that the temperature will reach 270° to 280°C within 40 to 50 seconds. To form tubes, a film stacking and compression moulding technique is used. It consists of steel moulds and an expandable mandrel (a suitable material would be PTFE) of the correct size for the finished internal diameter of the rods; the initial cure temperature of a carbon-fibre polyethersulphone (CF-PES) would be 290°C and a pressure of 3 MPa would be applied to the mould. To fabricate the tubes the prepreg films are wrapped on to the PTFE mandrel at the correct fibre orientation and stacking sequence. The cure temperature must remain at the constant value (i.e. 290°C) for half

an hour, when it is reduced to room temperature. The PTFE material has a coefficient of thermal expansion much greater than that of the steel moulds and this leads to a high compaction of the polymer against the metal mould and a low void ratio.

20.4.6 Pultrusion

The pultrusion technique is a closed-mould system and is a fully automated continuous process. Continuous fibrous reinforcement rovings and strand mat, or other designed reinforcement, are pulled through a reservoir of resin and a heated die. Alternatively the fibres can be impregnated with resin by injecting it through port holes in the heated die as the fibres pass through the die. The fibre placement, resin formulations, catalyst level, die temperature and pull speed are all critical process variables. These variables must be established during the design of the product and during its manufacture; continuous monitoring must be undertaken to ensure that the finished pultruded unit has the correct appearance and specific physical and chemical properties. The pultrusion technology has been discussed in European Pultrusion Technology Association publication, EPTA Publication (2008).

20.5 Composite materials/fabrication techniques used for wind turbines

20.5.1 Introduction

Fibre/polymer composites are the material of choice for rotor blades in wind turbines as these have the best balance between stiffness and density for the application (Brøndsted *et al.*, 2005), although there are other composite materials which could be used for wind turbine blades (Griffin and Ashwill, 2003). As mentioned before, the most common design is a thermosetting matrix (polyester, vinylester or carbon) with glass fibres. Although glass reinforcements are not as stiff and strong as carbon fibres, they provide similar reinforcements at a reduced cost, albeit at an increased volume content. Different volume fractions of fibre, matrix and fibre arrays can be employed to provide different mechanical strengths and stiffnesses. The stiffness of the composite can be determined from the simple equation [20.1]:

$$E_c = \eta V_f + V_m E_m \qquad [20.1]$$

where V_f and V_m represent the molar volumes of the fibre and the matrix respectively, and η represents the orientation factor.

From equation [20.1] it can be seen that the stiffness of a composite material is dependent on the stiffness of the polymer matrix and the orientation of the fibres.

Carbon fibre-reinforced load-bearing spars have been identified as a cost-effective means for reducing weight and increasing stiffness.

20.5.2 Wind turbine blade construction

The requirements for wind turbine blades are:

- Wind turbine blades are subject to static and dynamic lift, drag and inertial loads over a wide range of temperatures and other severe environmental conditions during a typical 20-year service life.
- Blades must possess:
  - Low weight and rotational inertia (a standard 35–40 metre blade for a 1.5 MW turbine weighs 6 to 7 tonnes)
  - High rigidity
  - Resistance to fatigue and wear
  - High resistance to the hostile environment.

A typical blade of large wind turbines consists of outer skins supported by a main spar and stiffeners. The blades are generally constructed using fibre/polymeric matrix composites and may have a sandwich construction with low density polymer foam or balsa wood cores. The epoxy-based composites are of greatest interest to wind turbine manufacturers because they deliver a combination of environmental, production and cost advantages over other resin systems. Epoxies also improve wind turbine composite blade manufacture by allowing a shorter cure cycle, increased durability and improved surface finish. The utilisation of epoxy infusion or prepreg manufacture (see Sections 20.4.2 and 20.4.3) further improves cost-effective operations by reducing processing cycles, and therefore manufacturing time, compared with the former method of the wet lay-up procedure. However, vinylester, phenolic and high-temperature polymers such as polyimides, cyanate esters and bismaleimides have also been used.

The majority of the medium-sized blades utilise glass fibre reinforcement (70–75% by weight) impregnated with epoxy or unsaturated polyester resin. The larger blade designs incorporate carbon fibres, particularly for the spars. The primary motivation for the use of carbon fibres is their lower density, higher stiffness and tensile strengths relative to glass fibres. With the increase in the very large rotor diameters currently being developed it could be expected that there will be an increase in the utilisation of carbon fibres in the spars and selected regions of the aero-shell.

Figure 20.1 illustrates a typical section of fibre lay-up through a Gurit-manufactured wind turbine blade. Further information on the manufacture of turbines blades, the materials used, their description and properties may be obtained from *Gurit Handbook – Materials for Wind Turbine Blades*.
Materials for infusion blades:

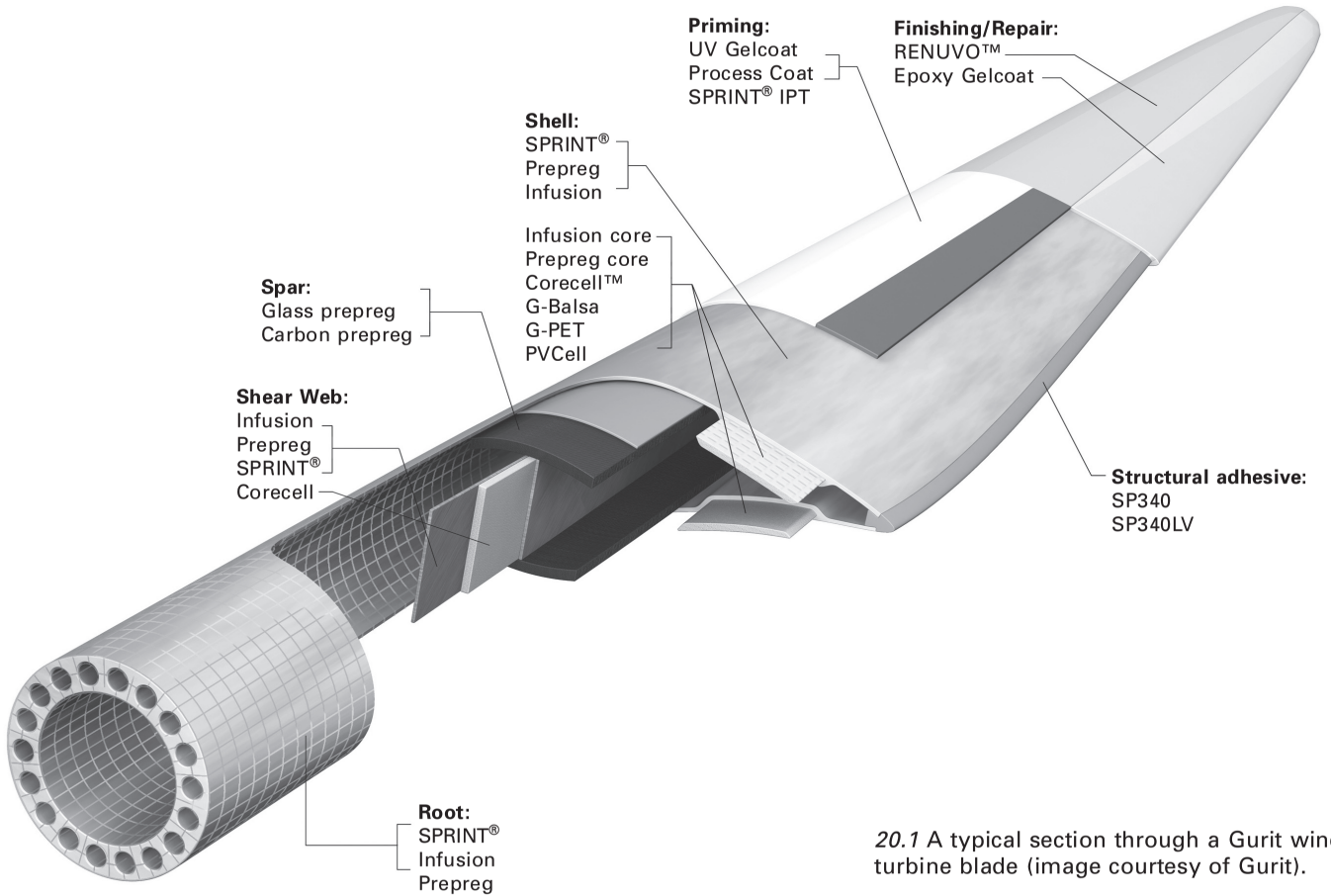

20.1 A typical section through a Gurit wind turbine blade (image courtesy of Gurit).

- Infusion resin: PRIME™ Infusion Family
- Structural adhesives: Spabond 340™LV
- Structural core: G-Balsa, PVCell, Corecell™ T-Foam

Materials for prepreg blades:

- Advanced prepregs: SPRINT™, SparPreg™
- Structural adhesives: Spabond 340™LV
- Structural core: Corecell™ T-Foam

20.5.3 Fabrication techniques for the manufacture of the moulds for wind turbine blades

Metal moulds on which the blades are formed are still used by some manufacturers of smaller blades, but polymer composites are invariably used for the multi-megawatt (MW) wind turbines; the following description of the manufacture of FRP composite moulds has been derived from Marsh (2007). The moulds are manufactured using epoxy (although vinylester or polyester polymers can be used), reinforced with glass fibres and/or carbon fabric, woven rather than stitched. The blade is manufactured by moulding two half-shells in a pair of composite moulds. These mould materials are much lighter than all-steel ones and have less thermal inertia, and their coefficients of thermal expansion are then matched with those of the wind turbine blade materials; a mismatch between two unlike materials could create difficulties during in-mould thermal cycling. The composite moulds are supported on mild steel support frames. The complete tool pair for, say, a 40 m wind turbine blade can weigh about 16–18 tonnes; the polymer composite in the tool would weigh about 4 tonnes and the rigid steel backing frame would weigh about 12 tonnes (Marsh, 2007). It is possible to achieve a smooth FRP mould surface containing a high vacuum integrity with the infusion technique, which is rapidly becoming the process of choice for moulds for significant series production; it is also possible to use prepreg material. Polymer composite mould tools are generally rated to produce 300–400 wind turbine blade sets, but they rarely achieve this value before the blade design becomes obsolete.

A set of tools are required for the manufacture of a turbine blade; these include the two half-shells in a pair of moulds, the web stiffeners and the spar cap. Further moulds may be associated with blade edges and root ends.

A spar cap, web stiffeners and other details are installed in one of the halves of the blade mould and adhesive is applied to the exposed bonding edges of these units. The second half of the mould, containing the half-shell, is then turned over and lowered onto the first; the adhesive is then allowed to cure, thus joining the two halves of the wind turbine blade together. The steel support frames are hinged together at one side to enable the mould to

open clamshell-fashion. A gel coat can be used on the inner mould surface to obtain a blade surface free of voids that can be present in mouldings produced by wet lay-up or from prepregs. Figure 20.2 shows an image of a composite mould opened.

To obtain the configuration of one of the outer surfaces of the turbine blade, which will be formed from one of the inner surfaces of the mould, a polystyrene plug is first shaped to the exact profile of the outer blade surface. The plug is generally about 6 metres long and can be readily joined to and separated from its neighbour as required, which provides the flexibility to change individual modules as modifications are made to the blade design. The plug is then reversed and the other face is machined to the profile of the second face of the turbine blade; the two faces of the plug are shaped to fine tolerances and are then ready for the application of the release system and subsequent lamination of the mould.

The composite characteristics vary along the blades: the tip of the blade is thin and at its root end it is thick, consequently a considerable exotherm is experienced at the root end and normal curing with little exotherm at the tip end; this must be taken into account in the design of the composite tool. The lightest fabrics are laid first and the heaviest fabrics last. Most of the

20.2 An image of the composite mould in the open position for the manufacture of the wind turbine (courtesy of Solent Composite Systems (SCS); the system uses the SCS SmartMould™).

fabrics are laid across the plug, although some will be placed longitudinally; this then profiles the outside surface of the blade. Electrical heating is applied to cure the polymer, but its intensity will vary along the length of the mould due to variations in the characteristics of the composite profile. Finally, stiffeners are laminated onto the back of the wind turbine blade mould; these serve to spread loads during blade demoulding operations. A highly critical component in a wind turbine blade tooling system is the tool surface, which interfaces with the blade surface and influences the latter's ultimate aerodynamic qualities. To gain a fuller understanding of the manufacture of composite tooling for large wind turbine blades and in particular the curing procedure of the mould, it is recommended that reference to Marsh (2007) should be made.

20.5.4 Composite materials/fabrication techniques used to form the blades of the Aerogenerator system

The Aerogenerator, Chapter 19, page 714, has been a collaborative feasibility study project on a 5–10 MW offshore vertical axis wind turbine; the first stage has been funded by the Energy Technologies Institute, and it is hoped that the second stage of the contract to design and to test the novel areas of the system and structure will commence shortly.

The two arms and the two sail (blades) design comprise a steel hub and the lower arm sections. The two upper arms are 140 metres long and are manufactured from carbon fibre fabric skin as are the spar and rib box structures. The glass fabric composite leading and trailing edge fairings are bonded to this. The sails use similar materials selection with the structures connected by steel pinned fittings. The composite parts of the structure have a total mass of about 150 tonnes.

The manufacturing approach features a novel automated fabric laminating system for the one-piece skin and spar components. For ease of construction the *in situ* resin infusion technique and the curing of the composite assembly will be undertaken in a factory which will be located at a dockside.

The size of the structure presents some structural and manufacturing challenges, in particular the strut and cable stay joints, the structural box adhesive bonding, the carbon fibre tow supply and the mass of the components and structure during assembly.

The description of the Aerogenerator system is given in Chapter 19, page 714.

20.5.5 The QuietRevolution wind turbine

The blades of the QuietRevolution wind turbine were originally manufactured from ACG's resin VTM system but were changed to ACG's resin MTM®57

systems to reduce costs. The blades are now manufactured using a prepreg system which is similar to the MTM®57 system.

The description of the QuietRevolution is given in Chapter 19, page 710.

20.5.6 Composite materials/fabrication techniques to form the columns of the wind turbines

As wind speeds increase with increasing height above the ground, the blades of turbines are mounted on tall towers, thus leading to a more efficient production of energy. Wind turbine towers have been traditionally constructed of steel, although the 7 MW (20 million kilowatt hours per year) Enercon E-126 wind turbine, which in 2009 was the largest and most efficient turbine in the world, has a 131-metre tower and is composed of 35 tapering concrete rings and one steel connector to accommodate the yaw bearing. The diameter at the foot is 14.5 metres, narrowing to 4.1 metres at the top. The turbine rotor diameter of 127 metres and the 135-metre hub height give a cumulative 198.5-metre installation height. The total installation height of 200 metres (hub height + rotor radius) is the maximum for which permission can be obtained in many European countries; the E-126 is just within this limit. It was installed at Estinnes, Belgium, in 2009.

Considering the above construction it may be seen that columns of the wind turbines are large and therefore composite construction is currently not cost-competitive with steel or concrete for tower structures, but with innovative designs and manufacturing processes of the composite materials it may be possible in future to construct composite towers utilising skeletal configurations.

20.5.7 Repair and maintenance of wind turbine blades

Maintenance of wind turbine blades is a critical element in the lifecycle cost of turbines and the efficient running of the system; poor maintenance will lead to erosion and an inefficient wind turbine. Damage to the blades may occur during transportation of the blade to its final site, during erection of the complete nacelle on to the tower, or during operation in hostile environments such as rain, wind erosion and lightning strikes. Wind turbulence and changes in wind direction will have been taken into account during the design, but these loads will have a severe impact on the fatigue of the blades and can lead to early wear and tear damage. In the past the repair systems used were specific to the original blade substrate construction (polyester, vinlyester or epoxy) and were fabricated by a wet process and thus limited to use in a narrow temperature window during curing. The utilisation of this process when maintaining blades in their fixed position is difficult, particularly in high wind speeds and cold temperatures.

Gurit has developed and launched the RENUVO™ blade repair system (see Section 20.1.2) which overcomes the above disadvantages (Cripps, 2011). Depending on the thickness of the composite laminate, a high intensity ultraviolet (UV) cure of 60–180 seconds cures the material to its full value. The RENUVO™ materials are specially formulated and exhibit excellent handling, adhesion and cured properties at temperatures as low as +5°C and at high humidity levels. It has been because of the combination of the low temperature operating window and fast UV cure system that the RENUVO™ blade repair has received certification by the Germanischer Lloyd (see Section 20.1.2 for definition).

Further information may be obtained from Marsh (2011).

20.5.8 Recycling of wind turbine blades

Currently there are three possible routes for disposing of thermosetting polymer/fibre wind turbine blades: (1) to send the waste to landfill, (2) to incinerate it or (3) to recycle it. As countries are seeking to reduce the landfill option generally and in particular of GFRP due to its high organic content, the first disposable option is losing its credibility. The most popular option is to incinerate the material to create electricity; however, this route has objections. After incineration of the GFRP about 60% of residue remains, and due to the possible inorganic pollutant nature of this residue, two courses of action would be considered: (1) if it were a pollutant it would go to landfill, and (2) if it were not a pollutant it could be recycled as a substitute construction material. Furthermore, the inorganic material emits hazardous flue gases and the small glass fibres in the residue may cause problems in the flue gas cleaning stages. Before the blades are recycled they have to be crushed, which places a further strain on the environment in terms of energy used.

20.6 Composite materials/fabrication techniques for tidal energy power generators

20.6.1 Introduction

Converting tidal energy current to electrical current poses a major polymer composite materials challenge. The hydrosphere is seen to be a particularly hostile environment when one realises that water is some 830 times denser than air; the exact value will depend upon its depth. The flow is varying and often turbulent and will reverse in direction with the ebb and flow of the tide. Moisture ingress is a constant hazard exacerbated by device motion and equipment maintenance; the latter event has to take place infrequently as generally the access to submerged installations is limited. Furthermore,

fatigue, not often a significant consideration with composites, becomes an important one when a typical service life of 20–25 years in a turbulent environment is proposed.

Three tidal wave systems will be discussed in the next section.

20.6.2 Composite materials/fabrication techniques used to form the blades of the SeaGen generator

Aviation Enterprises Ltd, Lambourn, UK, was responsible for manufacturing the blade assemblies of SeaGen (Chapter 19, page 720). The advanced composite – material Cytec's Variable Temperature Moulding, VTM®266, carbon fibre/epoxy polymer prepreg – was selected for the manufacture of the 65 mm thick structural spars, which run down the full length of the inside of the blade; the spar is the critical element that adds strength and rigidity to the 8-metre-long blades. The spar and blades were manufactured separately. The blade skins were manufactured in two halves using the VTM260 prepregs, and the spar and two half-blade skins were bonded in one operation. The spar was bonded to a steel root fitting to transfer the loads from the composite spar into the hub. The standard high strength carbon fibre, with a tensile strength greater than 4000 MPa and a modulus of elasticity value of 230 GPa, was used; the polymer was a modified bisphenol-A/epoxy cured with an accelerated dicyandiamide (dicy) system. The 8-metre-long spars had to be made using a material that possessed the requisite design qualities, performance and high strength and stiffness characteristics with minimum mass. From the processing standpoint, the chemistry of the VTM 266 provided a safe, low temperature cure processing route, thus making these prepregs ideally suited for this particular application where the overall composite thickness could result in severe exothermic reaction. The out-of-autoclave vacuum bag system and a large zone controlled oven were used for curing and processing the prepreg material; the vacuum-only route was particularly suitable for this size of component. Figure 19.5 of Chapter 19, page 721 shows an image of SeaGen.

20.6.3 The Atlantis tidal generator

The blades of the Atlantis tidal generator (Chapter 19 page 722 and Fig. 19.6) were manufactured from non-woven E-glass multi-axial fabric and epoxy resin composites using the vacuum infusion technique; this method presented a number of challenges and the blades for the next generator will most likely be made using the prepreg technique. Figure 20.3 shows the manufacturing procedure of the blade with the composite material under vacuum during curing; the top half of the blade is manufactured

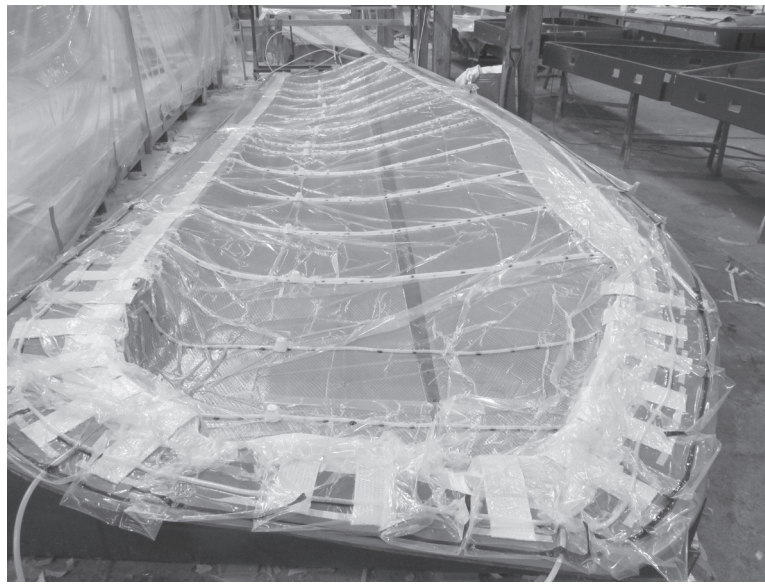

20.3 The manufacturing procedure of the Atlantis tidal generator blade with the composite material under vacuum during curing (courtesy of Atlantis Resources Corporation).

separately from the bottom one and the two halves are then bonded together.

The fibres of the AK 1000 blade are oriented along its length to provide an axial stiffness at its root of 24 GPa and 15 GPa in the chord. At the junction between the main hydrodynamic profile and the root, the fibres are aligned to give an axial laminate modulus of 29 GPa and 13 GPa in the chord.

Due to limitation in time constraints and the availability of materials, only E-glass fibre was considered and the laminates were constructed from multiple layers of the commonly available 600 gsm unidirectional fibres and ±45 fabrics.

On completion of the blades' manufacturing procedures static uniformly distributed load tests of 40 tonnes were applied to the blades.

20.6.4 Composite materials/fabrication techniques used to form the blades of the Pulse Tidal generator

The Pulse Stream 100 tidal generator (Chapter 19, page 722), was the first pulse tidal generator to be under sea trials; the programme of the development of Pulse Tidal generators is very much in the development stage but great advances are being made. The shells of the blades of the Pulse Stream 100 tidal generator were manufactured in glass fibre/epoxy polymer composites

and the spar was fabricated in carbon fibre/epoxy polymer composites. The spar, which is thick compared with the shell, was manufactured by the infusion technique but for subsequent generators the prepreg technique will be used to make the spars.

20.7 Composite materials/fabrication techniques for solar energy applications

20.7.1 Introduction

The following discussion refers only to Satellite 1 positioned in GEO (Fig. 19.9, Chapter 19, page 729); it is suggested that Fig. 19.9 should be referred to whilst reading this section. The two types of support structures that will be considered are the Rigid Deployable Skeletal (RDS) structure and the Rigidised Inflatable Flexible Continuum (RIFC) structure. Both types of structure need to be lightweight and rigid and in the case of the skeletal structure high modulus composite materials would be used. In addition, the structures must be able to be folded to a minimum volume to be placed in the cargo bay of the launch vehicle.

As already stated in Section 20.3.3, the environment of space to which SBSP support structural systems would be exposed is harsh. Full account must be taken of the environmental loadings to which the composite materials are to be subjected when in orbit. Primary among these loading situations are thermal differential-induced stresses which can be either gradually varying due to member self-shadowing in a planet-orientated orbit or abruptly periodic, as during passage through the earth's shadow (Hollaway and O'Neill, 1991). Hence, an accurate understanding of the thermal response characteristics of candidate composite materials is important before any complete assessment as to their suitability for orbital applications can be made.

The space frame would be permanently placed in Geostationary Orbit (GEO) at the altitude of 36,000 km above the earth and would remain in LEO for a short length of time whilst the collectors and equipment were fixed. At GEO the whole structure is exposed to a different loading regime from that of LEO. Although safe from AO attack at GEO heights, the structures would be exposed to the effects of solar wind. This wind is hydrogen plasma of varying intensity and is dependent on solar flare activity; its velocity is approximately 400 km/s. The effect of this plasma can be expected to lead to degradation of the space structure's material thermal properties over its lifetime; to overcome this problem it would require a protective gel coat to be applied to the polymer surface. However, the essentially beneficial warming influence of planetary infrared (IR) radiation and earth-albedo is greatly diminished at these high altitudes. Annandale (1986) has discussed the environment in GEO including the thermal shocks during the vernal and

autumnal equinoxes when the structure will be shadowed by the earth for up to 72 minutes per day for some 50 days. The environment in GEO is not nearly as hostile as that in LEO.

20.7.2 Carbon fibre-reinforced thermoplastic composites

The polymer composites which are utilised in space must be lightweight, oxidatively and thermally stable, have good mechanical properties and have resistance to the hostile environments of space (Hollaway, 2011). Currently, the matrix materials in conjunction with carbon fibres to form a FRP composite material which might be considered for use to construct a backing skeletal space structure are as follows:

- *The bismaleimide (BMI) resins*. BMI matrix systems are polyimides used in high-performance structural composites that require superior toughness and high temperature resistance. The resins have processing characteristics similar to those of the epoxy resins, and are used as laminating resins and in prepregs. Advanced Composites Group (now Cytec) in Derbyshire, UK, has developed HTM® 556, which is a toughened bismaleimide matrix system with improved handling characteristics and, after post-cure, thermal cycling capability up to 250°C. It has been specifically used for structural applications where continuous service temperatures exceed 200°C. In addition, HTM556 offers improved toughness and resistance to micro-cracking which has long been a shortfall of bismaleimide resins.
- *The cyanate ester resins*. These are high performance thermosetting resins, characterised by their high T_g value, which can be up to 400°C, and with excellent dielectric and mechanical properties. Cyanate esters are based on a bisphenol or novolac derivative, in which the hydrogen atom of the phenolic OH group is substituted by a cyanide group. The resulting product is named a cyanate ester. The cyanate ester matrix prepreg system (HTM®143) developed by Cytec for use in space applications, is cured at 180°C, is inherently flame-retarded and after a suitable post-cure can achieve a T_g of 250°C. The manufacturers state that the matrix has:
  - Very low moisture absorption
  - Very high temperature resistance
  - Very low out-gassing
  - Substantial weight savings compared to a metal matrix composite (MMC).
- *The high technology thermoplastic aromatic polymers*. In the mid-1980s ICI developed a new generation of thermoplastic aromatic polymers, in particular the amorphous polymer polyether sulphone (PES) and the semi-crystalline polymer polyetheretherketone (PEEK) (Cogswell, 1989); they also developed the pre-impregnation of continuous fibres

with thermoplastic polymer melts without the need for solvents in the pre-impregnation process. These thermoplastic polymers offered significant advantages over equivalent matrices available at that time. The advantages included high temperature resistance, an increased resistance to embrittlement at low temperatures in orbit and the potential for large-scale thermoforming production, as well as improved toughness and higher damage tolerance, (Barnes and Cogswell, 1989). Another aromatic polymer within this family of thermoplastic polymers was the semi-crystalline polymer polyphenylenesulphide (PPS), which offered better impact toughness and had a greater resistance to vacuum and thermal cycling than its thermoplastic and thermosetting counterparts (Cogswell, 1992).

20.7.3 Rigid deployable skeleton support structure for the solar collectors

During the late 1980s and through the 1990s research work was undertaken in the USA and the UK to ascertain whether a skeletal backing frame made from high technology thermoplastic aromatic polymer composite would be suitable to be placed in the environment of space to support large reflectors for telecommunication satellites. The outstanding in-service and structural properties of the aromatic polymer composite materials naturally led them to be investigated as structural systems for space.

The polymer chosen in the UK for preliminary investigations was polyether sulphone, due to its ease of manufacture, its low out-gassing in space and its light weight (Hollaway and Thorne, 1987). Prepreg sheets of the polyether sulphone/carbon fibre (PES/CF) composite were moulded by the technique of film stacking technology.

It is suggested that the technology proposed for the backing frame to support the large telecommunication reflectors in space could be used to support the solar collectors and transmission equipment to beam the laser energy to satellite 2. The backing frame used in the 1990s consisted of carbon fibres/polyethersulphone tubes fabricated in the form of a double-layer skeletal structure (Thorne and Hollaway, 1990). Each tube of the skeletal structure was one metre in length and 25 mm in diameter with a wall of thickness 1.25 mm; they were manufactured from five layers of the high strength Toray 'Torayca' T-300 carbon fibres with a 90/10 weave prepreg interspersed and a total of 12 layers of neat grade 4800 PES film. Ninety percent of the longitudinal fibres were 10° off-axes with a stacking sequence of 10/–10/0/10/–10; the remaining 10% of the fibres were placed at right angles to the main reinforcement. The fibre lay-up of the tubes resulted in a high specific stiffness and strength, coupled with dimensional stability over the wide range of operating temperatures to which they would be exposed

in orbit. The size of the final unit building block of the backing structure was dictated by the size of the 3.5 m Solar Simulation Chamber at the Royal Aircraft Establishment (RAE, now QinetiQ), Farnborough, in which the structure was tested under near-space environments. The chamber's set of three xenon arc lamps supplied up to 1.4 solar equivalents in a highly evacuated environment maintained by cryogenic pumping of the chamber down to a pressure of 10^{-7} bar. The cold heat sink effect of deep space was simulated by circulating liquid nitrogen in the shrouds lining the full length of the chamber, the shrouds being maintained at a constant temperature of 90 K; this compares with the typically expected temperatures at LEO and GEO of 15 K and 4 K respectively (Goodbody and Kimber, 1996). Further information may be found in Hollaway *et al*. (1990), Thorne and Hollaway (1990) and Hollaway and Sparry (1991).

The manufacturing method for the tubes was developed by Complas Ltd, Studham, Buckinghamshire, UK, and the University of Surrey, UK, by adapting a film stacking and compression moulding technique which used steel moulds and an expandable PTFE mandrel of the correct size for the finished internal diameter of the rods; the initial cure temperature of the CF-PES was 290°C with a pressure of 3 MPa applied to the mould. To form the composite tubes the prepreg films were wrapped on to the PTFE mandrel at the correct fibre orientation and stacking sequence. The cure temperature was maintained at a constant value for half an hour and then reduced to room temperature. The PTFE material of the mandrel had a coefficient of thermal expansion much greater than that of the steel moulds and this led to a satisfactory compaction of the polymer against the metal mould and a low void ratio; Hollaway (2011) has discussed further the material used.

The structural form of the system was fabricated into a building block in the form of a three-way double-layer grid (tetrahedral truss) with 21 tubular members connected at nine cluster node points – the 9/21 system. The particular self-deployment method used in that study incorporates energy-loaded joints at all nodal points and also at the centre of the top and bottom members of the skeletal structure. To prove the deployment of a rigid deployable skeletal structure a 5 m system was manufactured in CFRP composite; it deployed satisfactorily (Fanning, 1993). Figure 20.4 shows the unit building block backing frame which was proposed for the telecommunications system and is now being proposed for a possible support system for space solar collectors (satellite 1); the backing frame may be extended by connecting several unit building blocks together at LEO. The joints in this structure are fixed. Figure 20.5 shows a type of energy-loaded folding joint which would be suitable for positioning at nodal joints of the structure for the deployment of the unit building block; these were manufactured in steel to prove the system. Figure 20.6 shows the joint manufactured in CFRP composite in the closed position; the spring provides the energy for deployment.

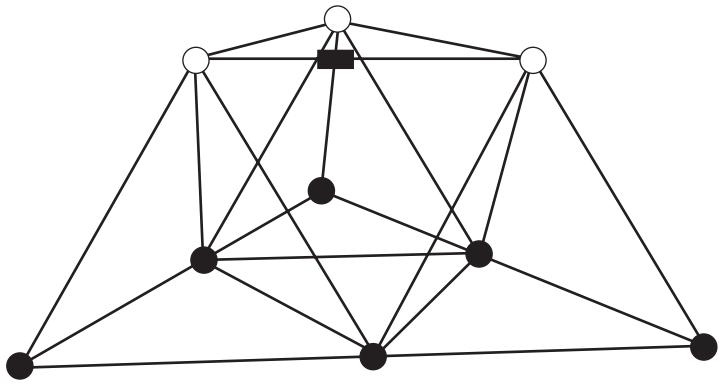

20.4 A unit building block backing frame for supporting the space-based solar power system; the nodal joints are fixed.

20.5 A type of energy loaded folding joints suitable for the deployment of the backing frame.

20.7.4 Rigidised inflatable flexible continuum support structure for the solar collectors

Rigidised inflatable structures are those that are fabricated from Shape Memory Polymers (SMP)/carbon fibre composite materials; the methods utilised are similar to those used for traditional thermosetting composite structures, except that the epoxy that is used is a lightly cross-linked one. The final deployed shape of the SMP composite structure is established during its initial cure cycle. Once the SMP material is completely cured, it can be

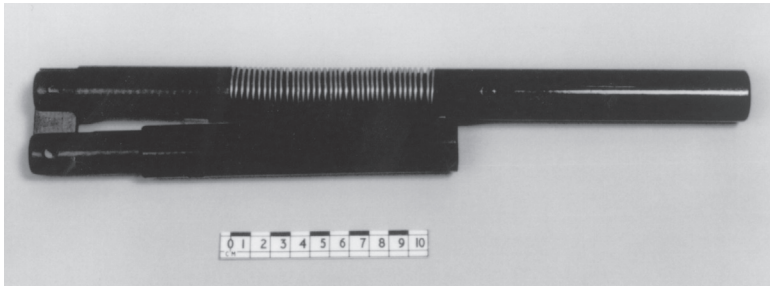

20.6 The joint manufactured in CFRP composite in the closed position.

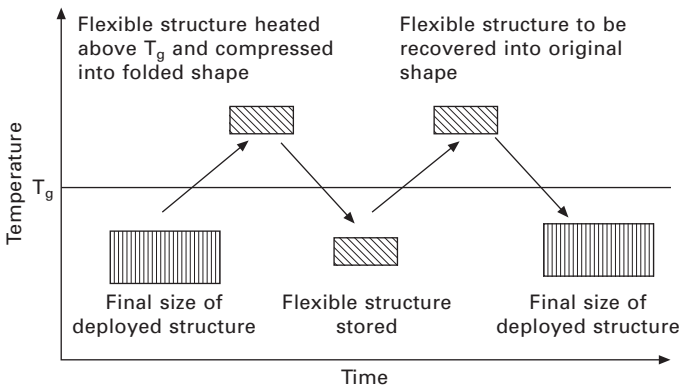

20.7 The shape memory cycle.

heated to the folding temperature (typically 20°C above the glass transition temperature, T_g) where it becomes flexible and can be tightly packed into a minimum volume. The flexibility of the SMP composite material at the folding temperature is highly dependent on both the resin and fibre properties. Once the structure is packed, it is constrained in that position until cooled to approximately 15°C, or lower, below its T_g value, at which point the SMP composite structure will remain frozen in the packed position until it is again heated above its T_g value. When the structure is heated, internal strain energy will return it to its initial cured shape. The speed and the accuracy of the original shape are a function of the shape memory recovery force of the composite. Lin *et al*. (2006) have discussed the shape-memory rigidised inflatable materials technology and its utilisation in structural space systems. Figure 20.7 illustrates the shape-memory cycle.

The SMP polymer materials which have been considered or used by researchers for rigidised inflatables have not been completely defined in the literature, and the suitability of their physical and mechanical properties for

space applications at GEO have not been discussed in detail, to this author's knowledge. Some trade names of the polymers used for rigidised inflatables are as follows:

- A PAN-based carbon fibre tow coated with a novel, low cure-temperature thermosetting resin, Hydrosize U-Nyte® Set 201 binder.
- TEMBO® Elastic Memory Composites are stated, by the manufacturers, to be a family of thermoset (epoxy) SMP developed by Composite Technology Development, Inc. 2600 Campus Drive, Lafayette, Co 80026-3359, USA.
- Scarborough and Cadogan (2006), Lan *et al*. (2009) used materials that were an 11.5 × 11.5 count, 203 g/m^2, five harness satin weave (5HS) fabric made from 6K IM7 carbon tows and TP407, a thermosetting polyurethane SMP resin with a T_g of approximately 55°C.
- Lan *et al* (2009) in their study used a fibre-reinforced shape-memory polymer composite in a deployable hinge as discussed, but little information on the space environment properties was given.

Heat is the stimulus that is currently used for SMPs. However, their recovery can be triggered by various other external stimuli (Everhart *et al*., 2006; Liu *et al*., 2007):

- Electricity (Schmidt, 2006; Lv *et al*., 2008a)
- Magnetic field (Buckley *et al*., 2006)
- Light (Hy *et al*., 2006)
- Moisture (Lv *et al*., 2008b; Yang *et al*., 2006).

It is possible that these effects could distort the final configuration of the rigid skeletal deployable structure as they are all within the environment of space. The effect of these influences might be negated by incorporating various blends to the polymer but in so doing a new polymer formulation would be formed; this would require a completely new environmental testing programme.

The low heat that is required to provide the internal strain energy to return the structure to its initial cured shape from its folded state is the main concern in the utilisation of SMP polymers for rigidised inflatable structures. From the cold state the polymer/fibre system is heated above its T_g to return the structure to its original cured shape. Once the structural system is deployed and then cooled to at least 15°C below T_g, it will again be structurally rigid; this maximum temperature of 65°C for a T_g value of 80°C (maximum of any lightly cross-linked thermosetting polymer quoted by manufacturers) is low for the temperature to which the structure could be exposed in space. If the temperature rises above 65°C the structure will again become distorted; consequently, it is advisable that the T_g value of the polymer that is to be used should be higher. It is vitally necessary that all space structures should

resist the environmental loadings of space, consequently the Rigid Deployable Skeletal Structures should show satisfactory thermal test results; if they do not there may be a possibility that the structure will not deploy as required at LEO.

Weight and volume restrictions are invariably issues that affect the cost of transporting space structural systems from the point of view of the number of trips the launch vehicle has to make to LEO to complete the fabrication of the backing frame. As the requirement for the number of structures in space grows, their weight and volume become important issues. Therefore, inflatable structures with respect to their storage capacity in the cargo bay of the space launch vehicle offer the possibility of reducing the overall structural weight, typically by 50% of that required by the FRP composite skeletal structure. In addition, inflatable systems can typically be packaged to a volume less than 25% of that necessary for the standard skeletal structure; moreover they can be packaged to any shape, depending on particular mission requirements.

The advantages and disadvantages of the Rigid Deployable Skeletal Support Structure and the Rigidised Inflatable Skeletal Structure are as follows:

- The Rigidised Inflatable Skeletal Structure (RISS) for the continuum backing frame can typically be packaged to a volume less than 25% of that necessary for standard mechanical structures, and can be packaged to essentially any shape, depending on particular mission requirements.
- As the RISS is able to be folded into a compact volume for launch, consequently a greater volume of stored structural units is able to be stowed in the cargo bay of the space transporter to LEO, thus offering the possibility of reducing the overall structural weight, typically by 50% of that required by the RDSS; thus, there will be fewer flights but the weight per launch of the rigidised inflatables will be greater than that of the RDSS. The smaller number of flights will influence the cost of placing satellites into LEO; the volume and therefore the weight of the structure will be a major consideration in the transportation costs.
- The quoted values of the T_g by the manufacturers of the SMP material are of the order of 50°C to 80°C; these are low values for composite materials in a space environment.
- Only limited analysis associated with the long-term durability of the two types of materials when they are in the harsh environment of space has been undertaken; further detailed work must be done before these two systems are able to be used in space.

The National Space Society (2007) has suggested that the cost of space solar power development should be compared to the cost of not undertaking this development work.

20.7.5 Composite materials/fabrication techniques for deployable skeletal support systems for earth based solar panels (EBSP) generators

This section is concerned with the EBSP generation as part of a solar power plant; solar panels as part of a building design for dwellings are outside of the scope of this chapter.

Fibre/polymer composite could have been used for the backing frames instead of the steel system used by BrightSource Energy Company (see Chapter 19, Section 19.4.1) to support the photovoltaic panel equipment to collect solar rays from the EBSP generators. The manufacturing technique to produce these fibre/polymer composite frames could be either the pultrusion or the prepreg technique; these FRP members would likely be fabricated into a tubular double-layer skeletal frame. If the FRP material of the frame required special shielding from any hostile environments on earth, it is likely that a solution is already available for protection; the only requirement for the above scheme would be a large acreage of land, which might be a limiting factor in the development of EBSP energy. However, one ideal area would be the Sahara Desert and the southern parts of countries bordering the North African coast where there are high energy concentrations from the sun and a large area of vacant land suitable for erecting EBSP generators. The great advantage in utilising the desert would be to revitalise the land by using the energy collected from the solar panels to pump water to irrigate and thus fertilise the land to feed the people and animals of that area, so reversing the migration of the people. Power from this area could also be piped across the Mediterranean to Southern European countries. A great political will would be required to undertake such a big project, but if successful it would solve many problems. This project would an ideal one to utilise composites for the manufacture of the backing frame for the solar panels.

20.8 Conclusion and future trends

Market figures show the current wind energy growth rate is set to continue for the foreseeable future. Enforcement of the Kyoto protocol, which was initially adopted on 11 December 1997 in Kyoto, Japan, and became active on 16 February 2005, ensures that renewable, sustainable energy sources are a priority for national governments. Development of materials, manufacturing processes and designs will continue to cater for the demand for larger, better-performing turbines to produce sustainable power.

Offshore wind farms are developing quickly and massive potential is seen in this area. They are particularly attractive because water has a very low level of roughness (i.e. the water ‘interferes’ with the wind less than the land does) and wind speeds in general are higher and less turbulent offshore. Wind

turbines offshore can therefore be much larger than is the case with onshore ones and they remove the noise and visual pollution associated with inland farms. The disadvantage of offshore fields is the problems of assembly on to foundations that extend to the sea-bed, and the connection to a grid, although floating wind turbines can be assembled onshore in dry-dock and floated out to their moorings. Offshore fields are currently more expensive than onshore ones. The current estimates based partly on European experience since 1991 indicate offshore wind energy costs to be less than 6 cents per kWh. Capital costs are around 30–50% higher than onshore, due to larger machine size and the costs of transporting and installing at sea. This is partially offset by higher energy yields, as much as 30%.

However, these prices are expected to drop as technology improves and more experience is gained, as happened with onshore systems (Ocean Energy Council, 2011). The European Environmental Agency (EEA) (2011) has estimated that offshore wind energy capacity in Europe will increase 17-fold between 2010 and 2020. The EU has the target of generating 20% of its energy consumption from renewable sources by 2020. Member States each have different individual targets to allow this overall target to be met; they are obliged to provide detailed roadmaps describing how they will meet their legally binding target. These figures will drop even more in future as a number of companies are working on commercial deep-water wind turbine technologies. The American offshore rig builder Principle Power has developed offshore wind turbines which are manufactured in shipyards onshore, mounted on semi-submersible platforms and towed into place. A great advantage to siting wind farms farther from shore in deep water is that the exploitable wind resource is superior to that nearer to shore.

Hydrokinetic power drawn from the earth's oceans and rivers is about 15 years behind the progress of wind power technology, but it is an interesting and exciting form of sustainable energy. Northern Europe, and in particular the UK, is well placed to take full advantage of the tides around countries with sea-borders. Space-based solar power beamed to earth via lasers or microwaves is probably the most exciting of all sustainable power technology. However, there is a downside to the harnessing of power from wind, waves or solar, they are expensive technologies, but all are at the development or early production stage and therefore will appear to be expensive compared with the established technologies. Nevertheless, the EEA (2011) has also estimated that the newer renewable technologies such as concentrated solar power and wave/tidal power will also increase more than 11-fold. European countries are also expected to significantly boost solar photovoltaic power, onshore wind and other renewable technologies over the next decade. Centrica, which plans to invest £1.5 billion a year in new power generating equipment and gas storage until 2020, is building a 75-turbine wind farm off the Lincolnshire coast at a cost of £725 million (*The Times*, 2010). In the same *Times* article,

Citigroup has estimated that the cost of installing one megawatt of offshore wind is about £3.5 million, which is roughly five times the cost of building a gas-fired power station with the same capacity. These projections can only boost the utilisation of polymer/fibre composites in the future.

The improved performance of wind turbine blades and therefore the capacity of the generator systems will be dependent upon enhancing the reliability of the component materials of the blades and increasing the energy capture. Consequently, future designs will utilise larger rotors with longer blades fabricated from advanced composite materials with high strength and stiffness-to-weight ratios; a thorough knowledge of composite materials and safety factors will be necessary. In particular, a thorough knowledge of the effects of damage and failure mechanisms and the effects and interpretation of stochastic loadings, multiple stress states, environmental effects, size effects and thickness effects must be understood. Turbine materials need to exhibit excellent fatigue and corrosion resistance properties to ensure durability and hence cost-effectiveness of projects. Wang and Ren (2010) have written an excellent report on an innovative technique for evaluating the integrity and durability of wind turbine blades made from composites, by quantifying the fracture behaviour of composite structures under mixed-mode loading conditions, particularly under combined Mode 1 (flexural or normal tensile stress) and Mode III (torsional shear stress) loading, and have proposed a new testing technique based on the spiral notch torsion test.

The manufacturing techniques of fibre/matrix composite materials to form parts of sustainable energy systems have utilised thermosetting polymer materials, but it is important to consider future materials for the manufacture of wind turbines. One possibility would be to manufacture wind turbine blades using thermoplastic polymer composites such as polyamide 6 (PA-6). The thermoplastic materials generally have a higher resistance to abrasion, fatigue and higher toughness than most thermosetting materials. Van Rijswijk and Bersee (2006) undertook tests on the vacuum infusion manufacturing process (the reactively processed PA-6 outperformed the melt-processed PA-6 in all temperatures and humidities that were tested) and found that the manufacturing technique is about six times faster than that for the thermosetting polymer, as the former material does not undergo the irreversible curing process of the thermosetting materials. Therefore, the thermoplastic material is readily able to melt and remould, allowing it to be reused. There are some disadvantages with the thermoplastic polymers; they have a lower tensile strength when compared with thermosetting materials. A glass/epoxy thermosetting composite has a tensile strength of the order of 1166 MPa, whereas a PA-6-thermoplastic composite has a tensile strength of the order of 869 MPa; the actual values for these two composites will depend upon the type of glass fibre and its array in the composite. Moreover, they also require a much higher processing temperature, which in turn requires more energy and an increase in cost.

Prabhakaran *et al*. (2011a) have given an overview of suitable thermoplastic material systems for the vacuum infusion process, and as an illustrative example a resin selection for a vacuum-infused wind turbine blade was shown to demonstrate the intricacies involved in the proposed methodology for resin selection. In a state-of-the-art study of thermoplastic polymer matrix materials for fibre composites, Prabhakaran *et al*. (2011b) has identified the polyamide 6 (PA-6) as a potential candidate thermoplastic polymer relevant for manufacturing large composite structures such as wind turbine blades. The mechanical properties of PA-6 are highly sensitive to moisture, and if PA-6 is used as matrix material in a fibre composite, the properties of the fibre composite will depend on the moisture content of the material. The matrix-dominated properties like the shear stiffness, the shear strength and the stiffness and strength across the fibre direction are the ones which are mostly affected by the moisture content in the material.

Naderi *et al*. (2011) have investigated the effect of nanoclay and polyepichlorohydrin-*co*-ethylene oxide (ECO) content on the microstructure and mechanical properties of PA-6/ECO thermoplastic elastomers (TPEs). In thermoplastic elastomer nanocomposites, the tensile modulus samples increased from 30% to 80% depending on the ECO content and the nanoclay used. The exfoliated structure, in which the layers of the clay have been completely separated and the individual layers are distributed throughout the organic matrix, resulted in a reduction of the degree of crystallinity because the dispersed clay silicates acted as nucleating agents.

20.8.1 Observations

This chapter has introduced the progress being made and the composite materials being used in the field of sustainable energy supplies and the research and development which is being undertaken currently to develop power that is not reliant upon fossil fuels. During future decades more sophisticated structural systems will be introduced into wind power, hydro power and solar power systems which will require lightweight materials that are resistant to the hostile environments of earth, sea and space; these materials will involve new technologies and their manufacture. Some of these structural areas have been discussed and the fibre/polymer composite materials which might be suitable for their construction have been given. Market figures show the current wind energy growth rate is set to continue for the foreseeable future. Enforcement of the Kyoto protocol ensures that renewable, sustainable energy sources are a priority for national governments. Development of materials, manufacturing processes and designs will continue to cater for the demand of larger, better-performing turbines. However, the success of these developments is subject to environmental and social appraisal that is currently taking place as new sites are found.

The economic viability of composite construction increases with the number of units produced, where the cost of design development and tooling can be amortised. For large renewable energy systems, the reduced weight of the composite components when compared to metallic construction can greatly reduce transportation and erection costs. Perhaps the biggest advantage of composites for large energy projects is reduced maintenance costs over an expected 20–30-year service life. For large, unmanned engineered structures, corrosion resistance will be paramount for long-term economic viability.

Finally, in an attempt to moderate the demand for coal for power generation, several countries conclude that nuclear energy must also grow significantly, but in contrast to coal, nuclear is one of the more difficult energy sources to expand quickly on a global scale. Building capacity for uranium mining and nuclear power station construction takes time; added to that it is difficult to dispose of nuclear waste. In the future this form of energy will probably produce power alongside the renewable forms of energy.

20.9 Sources of further information and advice

Regulatory/trade/professional bodies

1. *CEN-TC250* – EUR 22864 EN, 2007 – http://eurocodes.jrc.ec.europa.eu
2. *European Organisation for Technical Approvals* (EOTA): Discussions between the European Commission Joint Research Centre (JRC) and EOTA, on the works for new codes and standards regarding the use of FRP composites in civil engineering.
3. Industrial organisations:
   - *European Construction Technology Platform* (ECTP).
   - *European Composites Industry Association* (EuCIA).
     The JRC has contacted both the above organisations with a view to ensuring that their main concerns and needs are addressed by any proposed standards.
   - *The Directorate General Enterprise and Industry* (DG ENTR) of the European Commission in 2005 committed the JRC to assist in the implementation, harmonisation and further development of the Eurocodes. This will enable the European composites industry to be more aware of the impact that new Eurocodes, specifically tailored for FRPs, would have on their core business.

Professional bodies

The following is based upon the Network Group for Composites in Construction (NGCC), 11 May 2012.

1. *Composites UK*. The mission of Composites UK, as the representative body of the UK composites industry, is to promote the use of composite materials to the widest market spectrum.
2. *British Composites Society* (BCS). This is one of the technical arms of the Institute of Materials, Minerals and Mining. The British Composites Society provides a focus for the exchange of knowledge on all aspects of composite materials. It is a national contact point for communication with similar bodies on a worldwide basis.
3. *The Institute of Materials*, *Minerals and Mining* (IOM3), recognised by the UK's Privy Council on 26 June 2002. It was created from the merger of The Institute of Materials (IOM) and The Institution of Mining and Metallurgy (IMM). The Institute is potentially the leading international professional body for the advancement of materials, minerals and mining to governments, industry, academia, the public and the professions.
4. *International Institute for FRP in Construction* (IIFC). The aim of the Institute is to advance the understanding and the application of FRP composites in the civil infrastructure, in the service of the engineering profession and society.
5. *Welsh Composites Consortium* (WCC). The consortium acts as a Technology Transfer Network consisting of a number of partner organisations with a wide range of expertise in the field of composites, particularly to SMEs in Wales in the form of advisory visits.
6. *Construction Industry Research and Information Association* (CIRIA).
7. *The Italian Association for Composites in Construction* (AICO). AICO was formed in 1996. It is active in the field with membership from industry and universities.
8. *European Composites Industry Association* (EuCIA). The primary goal of EuCIA is to unite the composites industry at European level into one single European association.
9. *COBRAE*. The objective of COBRAE is to promote research, development, standardisation and application of fibre reinforced polymer composites in rehabilitation, upgrade and new build bridge constructions and infrastructure applications.
10. *European Construction Technology Platform* (ECTP). It is hoped that the ECTP will raise the sector to a higher world-beating level of performance and competitiveness. This will be achieved by analysing the major challenges that the sector faces in terms of society, sustainability and technological development. Research and innovation strategies will be developed to meet these challenges, engaging with and mobilising the wide range of leading skills, expertise and talent available to us within our industry over the coming decades, in order to meet the needs of society.

11. *Intelligent Sensing for Innovative Structures* (ISIS), Canada.
12. *Canadian Association for Composite Structures* (CACS). The CACS is a network of individuals and corporate members (suppliers, fabricators, equipment manufacturers, distributors, consultants, technologists, research centres, materials specialists, researchers, teachers, and government employees) working to develop and enhance new and existing applications for composite structures and materials.

20.10 Acknowledgements

This chapter could not have been written without the help of manufacturing firms concerned with composite materials and structural components made from those materials which are associated with the field of sustainable energy. These firms include ACG, Derbyshire, UK; Gurit, Isle of Wight, UK; Solent Composite Systems, Isle of Wight; Wind Power Ltd, Bury St Edmunds, Suffolk, UK; Aviation Enterprise, Lambourn, UK; Pulse Tidal Ltd, Sheffield, UK; Marine Turbines, Bristol, UK; Exxonmobil, Leatherhead, UK; Grimshaw, Architects, London, UK; and the journal *Reinforced Plastics*, Elsevier, Oxford, UK. The author would like to express his thanks to the members of staff of these firms for their invaluable help.

20.11 References

Annandale, R.W. (1986), 'Thermal and structural analyses of large space antenna reflectors', PhD Thesis, University of Surrey, Guildford, UK.

Barnes, J.A. and Cogswell, F.N. (1989), 'Thermoplastics for space', *SAMPE Quarterly*, Vol. 20, Issue 3.

Breuer, O. and Sundararaj, U. (2004), 'Big returns from small fibres: A review of polymer/carbon nanotube composites', *Polymer Composites*, Vol. 25, Issue 6, pp. 630–645.

Brøndsted, P., Lystrup, A. and Lilholt, H. (2005), 'Composite materials for wind power turbine blades', *Annual Review of Materials Research*, Vol. 35, pp. 505–538.

Buckley, P.R., McKinley, G.H., Wilson, T.S., Small, W., Benett, W.J., Bearinger, J.P., McElfresh, M.W. and Maitland, D.J. (2006), 'Inductively heated shape memory polymer for the magnetic actuation of medical devices', *IEEE Trans Biomed Eng*, Vol. 53, Issue 10, pp. 2075–2083.

Chiou, P.-L. and Bradley, W.L. (1997), 'Effect of seawater on strength and durability of glass/epoxy filament wound types as revealed by acoustic emission analysis', *Journal of Composites Technology and Research*, Vol. 19, Issue 4, pp. 214–221.

Cogswell, N. (1989), 'Thermoplastics find their feet', *Advanced Composites Engineering*, January 1989.

Cogswell, N. (1992), *A Study of the Structure, Processing and Properties of Carbon Fibre Reinforced Polyetheretherketone and Related Materials*, Woodhead Publishing, Cambridge, UK.

Cripps, D. (2011), 'The future of blade repair', *Reinforced Plastics*, Vol. 55, Issue 1, January–February, pp. 28–32.

European Environment Agency (EEA) (2011), 'Huge renewable energy growth this decade, if EU countries meet projections', published by the European Environment Agency, 28 November 2011, in the National Renewable Energy Action Plans of the European Member States (2011 update) (accessed from the Internet on 20 November 2011).

EPTA Publication (2008), 'What is pultrusion', *9th World Pultrusion Conference*, '*Profiting from Pultruded Profiles*', 26–28 March 2008.

Everhart, M.C., Nickerson, D.M. and Hreha, R.D. (2006), 'High-temperature reusable shape memory polymer mandrels', *Proceeding of 11th International Symposia on Smart Structures and Materials*, Vol. 6171, ed. E.V. White, SPIE, San Diego, CA.

Fanning, P. (1993), 'Development and analysis of a deployable skeletal reflector for spacecraft antennas', PhD Thesis, University of Surrey, Grildford, UK.

Goodbody, C. and Kimber, R. (1996), 'The UoSAT solar cell experiment – over 4 years in orbit', *Proceedings of the Photovoltaic Specialists Conference*, 1996, Washington, DC, 13–17 May 1996, pp. 235–238.

Griffin, D.A. and Ashwill, T.D. (2003), 'Alternative composite materials for megawatt-scale wind turbine blades: Design considerations and recommended testing', *Journal of Solar Energy Engineering*, Vol. 125, pp. 515.

Hackman, I. and Hollaway, L.C. (2006), 'Epoxy-layered silicate nanocomposites in civil engineering', *Composites Part A*, Vol. 37, pp. 1161–1170.

Helbling, C. and Karbhari, M.K. (2007), 'Durability of composites in aqueous environments', in: *Durability of Composites for Civil Structural Applications*, ed. V.M. Karbhari, Woodhead Publishing, Cambridge, UK, Chapter 3.

Hexcel (2005), 'Prepreg Technology', publication no. FGU 017b, March 2005, Hexcel Corporation.

Hollaway, L.C. (2011), 'Thermoplastic/carbon fibre composites could aid solar based power generation – A case study of a possible support system for solar power satellites', *Journal of Composites for Construction*, Vol. 15, Issue 2, pp. 239–247.

Hollaway, L.C. and Hackman, I. (2004), 'Strengths and limitations of fibre reinforced polymers in the civil infrastructure, material advances and the influences on present and future developments', *Conference Proceedings FRP Composites in Civil Engineering (CICE 2004)*, ed. R. Seracino. A.A. Balkema Publishers, Leiden, London, New York, Philadelphia and Singapore, pp. 17–28.

Hollaway, L.C. and Head, P.R. (2001), *Advanced Polymer Composites and Polymers in the Civil Infrastructure*, Elsevier, Oxford, UK.

Hollaway, L.C. and O'Neill, M. (1991), 'Thermal and structural analyses of carbon fibre/polyethersulphone tubes for space applications', Contract No. D/ER/1/9/4/2064/129/SP(F), Final Report for the MoD.

Hollaway, L. C. and Sparry, D. (1991), 'Design study and vibration analysis of large deployable space antennas', Contract No. 2064/109/RAE (F).

Hollaway, L.C. and Teng, J.G. (eds) (2008), *Strengthening and Rehabilitation of Civil Infrastructures using Fibre-reinforced Polymer (FRP) Composites*, Woodhead Publishing, Cambridge, UK.

Hollaway, L.C. and Thorne, A. (1987), 'High technology thermoplastic polymers reinforced with fibres for space applications', MOD (PE) Contract No. A57A/1733, Final Report, for the Space Department RAE Farnborough, Hampshire, UK.

Hollaway, L.C., Thorne, A. and Rankin, I. (1990), 'High technology thermoplastic polymers reinforced with fibres for space structures application', Final Contract Report, Contract No. 4064/107/RAE/XR(F) BNSC, November 1990.

Hy, J., Kelch, S. and Lendlein, A. (2006), 'Polymers move in response to light', *Advanced Materials*, Vol. 18, Issue 11, pp. 1471–1475.

Iijima, S. (1991), 'Helical microtubules of graphitic carbon', *Nature*, Vol. 354, pp. 56–58.

Kojima, Y., Usuki, A., Kawasumi, M. and Okada, A. (1993a), 'Synthesis of Nylon-6 clay hybrid epoxy', *Journal of Materials Research*, Vol. 8, Issue 5, pp. 1179–1183.

Kojima, Y., Usuki, A., Kawasumi, M. and Okada, A. (1993b), 'Mechanical properties of Nylon-6 clay hybrid', *Journal of Materials Research*, Vol. 8, Issue 5, pp. 1185–1189.

Koziol, K., Vilatela, J., Moisala, A., Motta, M., Cunniff, P., Sennett, M. and Windle, A. (2007), 'High-performance carbon nanotube fiber', *Science*, Vol. 318, Issue 5858, pp. 1892–1895.

Lan, X., Liu, Y., Lv, H., Wang, X., Leng, J. and Du, S. (2009), 'Fiber reinforced shape-memory polymer composite and its application in a deployable hinge', *Smart Materials and Structures*, Vol. 18, Issue 2 (6 pp.).

Le Baron, P., Wang, Z. and Pinnavaia, T. (1999), 'Polymer-layered silicate nanocomposites: An overview', *Applied Clay Science*, Vol. 15, pp. 11–29.

Leger, L., Visentine, J. and Santos-Mason, B. (1986), 'Selected material issues associated with space station', *18th International SAMPE Technical Conference*, Seattle, WA, 7–9 October, pp. 1015–1026.

Leger, L., Visentine, J. and Santos-Mason, B. (1987), 'Selected material issues associated with space station', *SAMPE Quarterly*, January 1987, pp. 48–54.

Lin, J.K , Knoll, C.F. and Willey, C.E. (2006), 'Shape-memory rigidised inflatable (RI) structures for large space systems applications', *47th AIAA/ASME/ASCE/AHS/ASC Structures*, *Structural Dynamics and Materials Conference*, 1–4 May 2006, Newport, RI, pp. 1–10.

Liu, C., Qin, H. and Mather, P.T. (2007), 'Review of progress in shape-memory polymers', *Journal of Materials Chemistry*, Vol. 17, Issue 16, pp. 1543–1558.

Loos, M. (2011), 'Case Western Reserve University researchers build carbon nanotube reinforce wind turbine blade', *netcomposites*, 6 September 2011 (accessed 8 September 2011).

Louriel, O., Cox, D.M. and Wagner, H.D. (1998), 'Buckling and collapse of embedded carbon nanotubes', *Physical Review Letters*, Vol. 18, Issue 8, pp. 1638–1641.

Lv, H.B., Leng, J.S. and Du, S.Y. (2008a), 'Electro-induced shape-memory polymer nanocomposite containing conductive particles and short fibers', *Proceedings of 15th International Symposia on Smart Structures and Materials*, Vol. 6932, SPIE, San Diego, CA.

Lv, H.B., Leng, J.S. and Du, S.Y. (2008b), 'Shape memory polymer in response to solution', *Advanced Engineering Materials*, Vol. 10, Issue 6, pp. 592–595.

Marsh, G. (2007), 'Tooling up for large wind turbine blades', *Reinforced Plastics*, Vol. 51, Issue 9, pp. 38–43.

Marsh, G. (2011), 'The challenge of wind turbine blade repair', *Renewable Energy Focus*, *Magazine*, Elsevier.

Monaghan, D.A. and Wang, S.S. (2004), 'Effect of saltwater on multiaxial cyclic fatigue of carbon fiber/epoxy composite material', prepared for Research Partnership to Secure Energy for America, Subcontract No. R-511, RPSEA, Unconventional Gas Technology and ChevronTexaco Energy Research and Technology Company, Bellaire, TX 77401, Report CEAC-TR-04-0103 (September 2003 – September 2004).

Naderi, G., Razavi-Nouri, M., Taghizadeh, E., Lafleur, P.G. and Dubois, C. (2011), 'Preparation of thermoplastic elastomer nanocomposites based on polyamide-6/polyepichlorohydrin-*co*-ethylene oxide', *Polymer Engineering & Science*, Vol. 51, Issue 2, pp. 278–284.

National Space Society (2007), 'Space solar power – limitless clean energy from space', Report to the Director, National Security Space Office, National Space Society, Washington, DC.

Ocean Energy Council, Inc. (2011), 'Offshore Wind Energy', © OEC, 11985 Southern Blvd, Suite 155, West Palm Beach, FL 33411 (accessed from the Internet on 6 September 2011).

Paul, D.R. and Robeson, L.M. (2008), 'Polymer nanotechnology: Nanocomposites', *Polymer*, Vol. 49, Issue 15, pp. 3187–3204.

Prabhakaran, R.T.D., Andersen T.L. and Lystrup, A. (2011a), 'Attribute based selection of thermoplastic resin for vacuum infusion process: a decision making methodology', *International Journal of Manufacturing*, *Materials and Mechanical Engineering*, Vol. 1, Issue 3, pp. 31–52.

Prabhakaran, R.T.D., Andersen T.L. and Lystrup, A. (2011b), 'Influence of moisture absorption on properties of fibre reinforced polyamide 6 composites', *26th ASC Annual Technical Conference (the 2nd Joint US–Canada Conference on Composites)*, Montreal, Quebec, 26–28 September 2011, Paper ID: 1065, pp 1–11.

Qian, D., Wagner, G.J., Liu, W.K., Yu, M.F. and Ruoff, R.S. (2002), 'Mechanics of carbon nanotubes', *Applied Mechanics Review*, Vol. 55, Issue 2, pp. 495–533.

Ray, S. and Okamoto, M. (2003), 'Polymer/layered silicate nanocomposites: A review from preparation to processing', *Progress in Polymer Science*, Vol. 28, pp. 1539–1641.

Ruoff, R.S., Qian, D. and Liu, W.K. (2003), 'Mechanical properties of carbon nanotubes: theoretical predictions and experimental measurements', *Comptes Rendus Physique*, Vol. 4, pp. 993–1008.

Salvetat, J.-P., Bonard, J.-M., Thomson, N.H., Kulik, A.J., Forró, L., Benoit, W. and Zuppiroli, L. (1999), 'Mechanical properties of carbon nanotubes', *Applied Physics A*, Vol. 69, pp. 255–260.

Scarborough, S.E. and Cadogan, D. (2006), 'Applications of inflatable rigidisable structures', Technical Paper published by ILC Dover, Frederica, DE, 16 pp.

Schmidt, A.M. (2006), 'Electromagnetic activation of shape memory polymer networks containing magnetic nanoparticles', *Macromolecular Rapid Communications*, Vol. 27, Issue 14, pp. 1168–1172.

Sennett, M., Welsh, E., Wright, J.B., Li, W.Z., Wen, J.G. and Ren, Z.F. (2003), 'Dispersion and alignment of carbon nanotubes in polycarbonate', *Applied Physics A*, Vol. 76, pp. 111–113.

Smith, P.A. (2000), 'Properties of CFRP', in *Comprehensive Composite Materials*, editors-in-chief A. Kelly and C. Zweben, Vol. 2, *Polymer Matrix Composites*, eds R. Talreja and J.-A.E. Manson, Elsevier Science, pp. 107–150.

Smith, P.A. and Yeomans, J.A. (2002), 'Benefits of fiber and particulate reinforcement', *Vol. II*, *Materials Science and Engineering*, *Knowledge for Sustainability – An Insight into the Encyclopaedia of Life Support Systems*, UNESCO Publishing–Eolss [e-books], publishers, Paris and Oxford, http://www.eolss.net/Eolss-sampleAllChapter.aspx.

The Times (2010), 'High cost could halt Brown's wind farm plan', *The Times*, 26 February 2010, Energy editor Robin Pagnamenta.

Thorne, A. and Hollaway, L.C. (1990), 'High-technology carbon-fibre/polyethersulphone composite for space applications', *Proceedings of ESA Symposium: Space Applications of Advanced Structural Materials*, ESTEC, Noordwijk, the Netherlands, 21–23 March 1990, pp. 207–211.

Thostenson, E.T., Ren, Z.F. and Chou, T.W., (2001) 'Advances in the science and technology of carbon nanotubes and their composites: A review', *Composites Science*

and Technology, Vol. 61, Issue 13, pp. 1899–1912.

Thostenson, E.T., Li, C. and Chou, T. (2005), 'Nanocomposites in review', *Composites Science and Technology*, Vol. 65, pp. 491–516.

Tran, N.H., Wilson, M.A., Milev, A.S., Dennis, G.R., Kannangara, G.S.K. and Lamb, R.N. (2006), 'Dispersion of silicate nano-plates within poly(acrylic acid) and their interfacial interactions', *Science and Technology of Advanced Materials*, Vol. 7, Issue 8, pp. 786–791.

Utraki, T. (2004), 'Clay containing polymeric nanocomposites', Vol. 1, *RAPRA Technology*, Vol. 44, pp. 2441–2446.

van Rijswijk, K. and Bersee, H. (2006), 'Thermoplastic composite wind turbine blades', *Dutch Wind Workshop – Results and Future of Wind Energy Research in the Netherlands*, 11–12 October 2006.

Wang, J.J. and Ren, F. (2010), 'An innovative technique for evaluating the integrity and durability of wind turbine blade composites', Report FY2010, prepared by Oak Ridge National Laboratory, Tennessee, for the U.S. Department of Energy (Contract DE-AC05-00OR22725).

Wang, Z., Lan, T. and Pinnavaia, T. (1996), 'Hybrid organic–inorganic nanocomposites formed from an epoxy polymer and a layered silicate acid (magadiite)', *Chemistry of Materials*, Vol. 8, pp. 2200–2204.

Woebbeking, M. (2007), 'Development of a new standard and innovations in certification of Wind Turbines', IEC WT 01 vs. IEC 61400-22, published by Germanischer Lloyd Industrial Services GmbH, Renewables Certification (GL), Hamburg, Germany.

Woebbeking, M. (2010), 'The new guideline for the certification of wind turbines' (2010 edition). published by Germanischer Lloyd Industrial Services GmbH, Renewables Certification (GL), Hamburg, Germany.

Xu, L.R. (2010), 'Intrinsic impact and fatigue property degradation of composite materials in seawater', Final Technical Report, published by Vanderbilt University, Nashville, TN, for the Office of Naval Research.

Yang, B., Huang, W.M., Li, C. and Li, L. (2006), 'Effects of moisture on the thermomechanical properties of a polyurethane shape memory polymer', *Polymer Engineering and Science*, Vol. 47, Issue 4, pp. 1348–1356.

21

Improving the durability of advanced fiber-reinforced polymer (FRP) composites using nanoclay

S. ZAINUDDIN, M. V. HOSUR and S. JEELANI, Tuskegee University, USA and A. KUMAR and J. TROVILLION, US Army Engineer Research and Development Center, USA

DOI: 10.1533/9780857098641.4.780

Abstract: In this chapter, we report the findings of experimental investigations conducted on durability of glass fiber-reinforced polymer (GFRP) composites with and without the addition of montmorillonite nanoclay. First, neat and nanoclay-added epoxy systems were characterized to evaluate the extent of clay platelet exfoliation and dispersion of nanoclay. GFRP composite panels were then fabricated with neat/modified epoxy resin and exposed to six different conditions, i.e. hot-dry/wet, cold-dry/wet, ultraviolet radiation and alternate ultraviolet radiation–condensation. Room temperature condition samples were also used for baseline consideration. An improved dispersion of nanoclay and exfoliation of clay platelets were observed in 2 wt% of epoxy samples. Weight change, discoloration and significant reduction in properties were observed in all conditioned GFRP samples. However, addition of nanoclay considerably improved the durability of GFRP samples as evident from the mechanical and micrographical results in comparison to neat samples subjected to similar conditions.

Key words: nanocomposites, environmental degradation, moisture absorption, flexure test.

21.1 Introduction

Glass fiber-reinforced polymer (GFRP) composites are increasingly being used in the civil infrastructure ranging from internal and external reinforcement of concrete, in columns as wraps for seismic retrofits, to structural systems and bridge decks. The high specific strength, excellent corrosion resistance, superior fatigue performances and tailorability of composites have made these materials ideal for many applications [1, 2]. Unfortunately, the downside of polymeric composites is their inherent viscoelastic behavior. Microstructural changes, time-dependent deformation and degradation in mechanical properties are identified in fiber-reinforced polymer (FRP) composites when exposed

to environmental conditions such as elevated temperature, moisture and ultraviolet conditions [3–6].

The first form of damage in FRP composite upon environmental exposure is usually matrix microcracking and matrix erosion. This causes degradation in properties of FRP composites and also acts as a precursor to other forms of damage leading to failure [7]. While epoxy resin matrices are very attractive due to their high strength and stiffness, high temperature resistance, low creep and shrinkage properties, they tend to absorb moisture, resulting in degradation in their properties [8–12]. Sanders reported degradation in mechanical properties, cracking and flaking of polymers exposed to elevated temperatures [13]. Ray found that temperature has a dominating effect on water absorption kinetics and reported higher moisture uptake at elevated temperatures. He also found a decrease in interlaminar shear stress at higher temperature even with the same amount of absorbed moisture. He attributed such behavior to the adverse effect of a higher degree of thermal stresses promoting initiation and propagation [14]. Ellyin and Maser investigated the effects of moisture absorption and exposure to elevated temperature on the mechanical properties of GFRP tubes and observed water damage at the glass fiber interphase with increasing water temperature [15]. Water that diffuses into the composites ends up either in the matrix or at the interphase region. Thus, the amount of moisture absorbed by the matrix is significantly different from that by the fiber. This results in a mismatch in moisture-induced volumetric expansion between the matrix and the fibers which leads to the evolution of localized stress and strain fields in composites [16, 17]. In the matrix, water acts as a plasticizer, increases free volume, lowers the glass transition temperature, and relieves the internal stress that is built up during processing of the composites [18]. Plasticization, swelling stress, hydrolysis and formation of cracks are the possible consequences of environmental exposure which should also influence the diffusion of water in the composites [19, 20]. Preconditioning in elevated temperature in water (>75°C) always has a deleterious effect on GFRP [21–25].

On the otherh and, ultraviolet radiation is also known to be highly damaging to polymeric materials. Ultraviolet radiation that reaches the earth's surface comprises about 6% of the total solar radiant flux and has wavelengths between 290 and 400 nm [26]. Since most polymers have bond dissociation energies on the order of the 290 to 400 nm wavelengths in the ultraviolet region, they are greatly affected by exposure to this portion of the solar spectrum. Photo-initiated oxidation leading to surface degradation, and chain scission that affects the load-bearing capabilities, decreasing mechanical properties as well as long-term durability of polymers, are well known [27–29]. The effect of ultraviolet radiation is also found to be intensified when compounded by the action of temperature, moisture and other environmental components. Hence, durability of polymer composites in these exposed environmental

conditions is one of the primary issues limiting the acceptance of these materials in civil and many other applications.

In recent years, addition of nanoscale layered silicates has received increasing attention because of the possibility of obtaining improved properties in terms of stiffness, strength, fire resistance, dimensional stability, shrinkage and interfacial bonding [30, 31]. Carrasco and Pages [32] demonstrated that nanoclay greatly accelerates the cure at different temperatures. They found the degree of cure (cure asymptotic conversion) increased with increasing clay content (0–5%) at a given temperature. Increase in crosslinking density in nanoclay composites in comparison to pure composites was also reported by Uhl *et al*. using photo differential scanning and dynamic mechanical analysis techniques [33].

Apart from these properties, the excellent barrier capability to moisture and gases of polymeric nanocomposites has shown significant potential in civil engineering applications [34–36]. It was reported that the construction industry will be one of the major potential consumers of nanostructured materials [37]. A substantial decrease in moisture permeability was reported in polyamide nanoclay composites with water absorption rate reduced by 40% in comparison to neat polymer [38]. An 80% decrease in water absorption was reported for poly (ε-caprolactone) nanoclay composites [39]. Hackman and Hollaway studied the potential applications of clay nanocomposite materials to civil engineering structures. They concluded that their ability to increase the service life of materials subjected to aggressive environments could be utilized to increase the durability of glass and carbon fiber composites [34].

Woo *et al*. have used clay nanocomposites as coating materials on concrete structures and investigated the barrier performance by subjecting them to moisture and salty water conditions. They reported that the nanocomposites effectively covered the pores and voids present on the concrete structures. Results of their study showed substantial reduction in moisture permeability of these nanocomposites [40]. Organo-modified montmorillonites (OMMT) were used as fillers and reinforcements in cement mortars [41]. The authors reported improvements in compressive and flexural strengths of cement mortar up to 40% and 10% respectively and the coefficient of permeability was 100 times lower with the addition of less than 1% of OMMT. Addition of montmorillonite nanoclay polymeric composite in liquid form (planar diameter of 100 nm) in cement paste (0.4–0.6 wt%) caused an increase in compressive strength by 13% and a decrease in permeability conefficient by 50% with more dense solid materials and stable bonding framework in the microstructure [42].

Micro- and nanoclays were used to design slipform paving concrete to be both flowable and shape stable at very small loading of 1 wt% [43]. The authors found nanoclay to be very effective in increasing shape stability with

a minimal loss of flowability. The nanoclay they used showed increase in green strength and compressive yield stress of the paving concrete as well as the straightest edges during the minipaver test. The addition of nanoparticles in cement paste has also gained significant attention due to their high surface area which in turn causes high reactivity. Nano-modification of the cement inherently alters the hydration process which affects the structure and physical properties. The presence of nanoclay simulated the process similar to pozzolanic reaction where silicates and water react with calcium hydroxide to form C–S–H [44, 45]. The study conducted by Jo *et al*. [46] showed that the rate of this reaction is proportional to the amount of surface area available for reaction.

However, the use of nanoclay/polymeric composites in civil engineering applications directly depends on the clay content, the aspect ratio [47, 48] and the degree of dispersion and exfoliation [49–51] of silicate layers. The moisture barrier reduction was attributed to the extremely high aspect ratio of clay platelets, which increased the tortuosity of the path of gas or water molecules as they diffuse into the nanocomposites. Woo *et al*. [35] investigated environmental degradation of epoxy nanocomposites due to UV exposure. They reported thicker and shallower cracks with less degree of discoloration in epoxy nanocomposites over neat counterparts. They credited the reason to the excellent barrier characteristics of organoclay with a high aspect ratio. Similar results were also reported by Nanocor Inc. [31].

Though fiber-reinforced nanocomposites have been investigated by several researchers, a comprehensive study has not been carried out to understand the environmental effects on the durability of these composites. Hence, in this work, a comprehensive study has been carried out by exposing the GFRP composites to commonly exposed conditions. In addition, an attempt has been made to reduce the environmental effect on GFRP composites through the incorporation of montmorrilonite nanoclay which in turn can significantly benefit the use of these materials in civil engineering applications.

21.2 Materials and manufacturing

In civil engineering applications, it is necessary to confirm the compatibility of the resin systems that is feasible for (1) the civil engineering field at its present state, (2) on-site process ability such as wet lay-up, and (3) exfoliation of nanoparticles in the polymer. The civil engineering industry has particular requirements for on-site utilization of polymeric composites. Low viscosity for better exfoliation of clay particles and ambient temperature cure polymeric composites for on-site processing are required in civil engineering applications. Hence in this study, we have used an ambient temperature cure, low viscosity and higher pot life SC-15 epoxy resin. It is a two-phased toughened epoxy resin system consisting of part A (resin mixture of diglycidylether of bisphenol-A,

aliphatic diglycidylether epoxy toughener) and part B (hardener, mixture of cycloaliphatic amine and polyoxylalkylamine). Nanomer® I-28E nanoclay, procured from Sigma-Aldrich Co., is a naturally occurring montmorillonite, a 2-1 layered clay mineral with a plate-like structure. This nanoclay has a thickness of the order of 1 nm and lateral dimensions of several microns, thereby providing a large aspect ratio. In order to interact chemically with the epoxy system, it was treated using cationic-exchange reaction with onium functional groups by Nanocor Inc. Unidirectional E-glass fibers supplied by Fiber-Glast development corporation were used in this study. The material is silane sized, 0.2 mm thick and has a plain weave style with 95% of the fiber density in the warp direction.

21.2.1 Dispersion of montmorillonite nanoclay into part A of epoxy resin

The required amount of nanoclay was first preheated at 100°C for 2 hours and degassed to remove any entrapped moisture. Nanoclay was then dispersed in part A of SC-15 epoxy resin with a magnetic stirrer for 5 hours. In this method, the stir bar rotates (and thus stirs) synchronously with a separate rotating magnet located beneath the vessel containing the reaction as shown in Fig. 21.1(a). The fast motion of the solution due to stirring creates a vortex effect and thus disperses the nanoparticles uniformly.

21.2.2 Preparation of epoxy resin for GFRP composites fabrication

Modified part A of the resin system was then mixed with part B at a ratio of 10:3 using a high-speed mechanical stirrer at 800 rpm for 8–10 min (Fig. 21.1(b)). The intense mechanical mixing produces air bubbles in the mixture, which if not taken out will increase the void content in the composite. These trapped air bubbles were taken out by keeping the mixture in a high-vacuum desiccator chamber for 30 min (Fig. 21.1(c)) which pulls out the entrapped air from the mixture. Once the degasification was done, the mixture was taken out for infusion.

21.2.3 Manufacture of GFRP composites

The vacuum-assisted resin infusion molding (VARIM) process was used for fabricating E- glass/epoxy composites. The VARIM process uses vacuum pressure to remove air from the fabric lay-up before and while the matrix resin is introduced to the fabric reinforcement. The pressure difference between the atmosphere and the vacuum is the driving force for infusion of the resin into the lay-up. Once the setup was laid up and completely vacuumed as

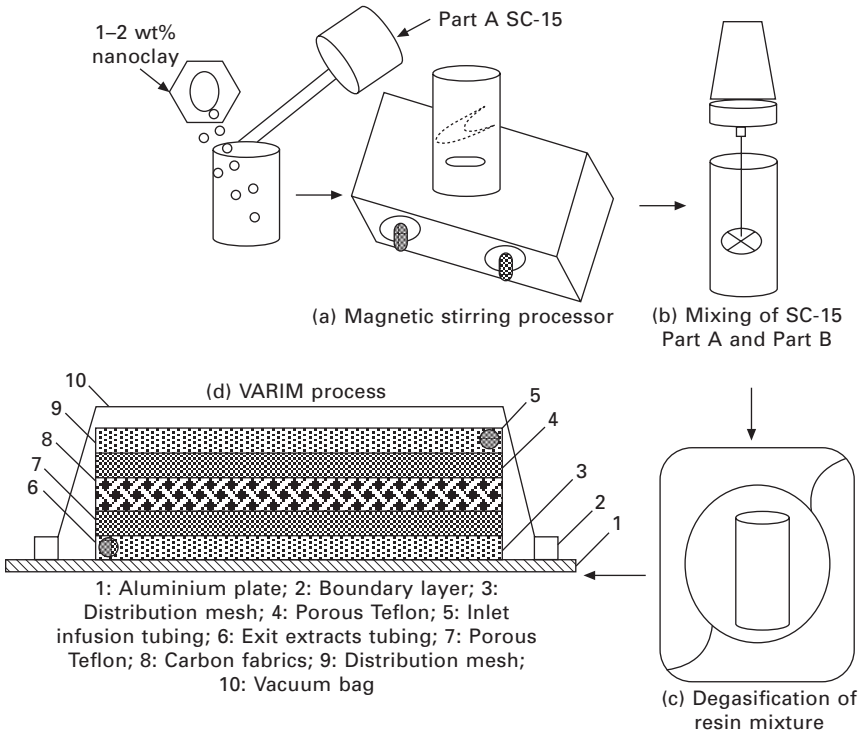

21.1 (a–d) Manufacturing setup.

shown in Fig. 21.1(d), the resin was infused through the inlet section. The setup was left to cure at room temperature for 24 hours. The fiber volume fraction of these composites was determined to be in the range of 55–58% by the matrix digestion method.

21.3 Environmental conditioning

GFRP samples of size 60 mm × 12.5 mm × 3.5 mm cut from the panels were subjected to six basic environmental conditions. These were cold (subzero: dry, CD), cold (subzero: wet, CW), hot (elevated temperature: dry, HD), hot (elevated temperature: wet, HW), ultraviolet radiation (UV) and alternate ultraviolet radiation and condensation (UC). In addition, room temperature (RT) condition samples (neat, 1 and 2 wt%) were used to generate baseline data.

21.3.1 Cold/hot dry/wet conditioning

For cold-dry and cold-wet conditioning, the samples were kept with or without water in a box in a refrigerator. For hot-dry conditioning, the samples

were placed in a convection oven maintained at elevated temperatures of 60°C and 80°C. For hot-wet conditioning, the samples were placed in a hot water bath maintained at two elevated temperatures of 60°C and 80°C. The conditioning for this set was carried out for 15, 45 and 90 days.

21.3.2 Ultraviolet radiation and alternate condensation conditioning

For ultraviolet radiation (UV) and alternate ultraviolet radiation and condensation (UC) conditioning, the samples were kept in a QUV/Se weathering chamber (Q-Panel Lab Products, Cleveland Ohio). The samples were conditioned to UV radiation only and to alternate exposure to UV radiation for 4 hours followed by condensation for 4 hours. Phelps and Long [52] reported that thermal energy was sufficient to break bonds in cured epoxy, thus the temperature in the QUV chamber was elevated to provide accelerated degradation maintained at 60°C. The conditioning for this set was carried out for 5, 10 and 15 days.

21.4 Experimental procedures

21.4.1 X-ray diffraction (XRD) analysis

To evaluate the degree of clay exfoliation in the polymer which is essential for property enhancement, XRD measurements were carried out in a Rigaku D/MAX 2200 X-ray diffractometer with CuKα radiation (λ = 1.54 Å) with a scanning speed of 1°/min and operating at 40 kV and 30 mA. During the XRD experiments, the samples were analyzed in the reflection mode.

21.4.2 Weight change and surface morphology upon conditioning

GFRP samples were weighed with a Mettler AT250 digital balance (precision 0.01 mg). The percent weight change as a function of time was calculated using equation [21.1]:

$$\text{Percent weight change} = \frac{w_f - w_i}{w_i} \times 100 \qquad [21.1]$$

where w_f is the final weight after conditioning and w_i is the initial weight of the sample under room temperature conditions.

A Unitron ZST optical microscope (OM) and a JEOL JSM 5800 scanning electron microscope (SEM) were used to study the effect of exposed conditions on neat and nanoclay-incorporated GFRP samples. The gradual change in color after the exposed conditions was evaluated using an image analyzer.

Photographs were taken of the exposed specimens, and the luminance values were calculated using the standard RGB (red, green, blue) system. After selecting a 4 mm × 3 mm region of interest (ROI), the luminance value of about 3000 average pixels in the ROI was estimated.

21.4.3 Quasi-static flexural test

A minimum of eight samples of each set was used for all the tests. A quasi-static flexure test was carried out as per ASTM D790-02 standards using a Zwick–Roell testing machine to obtain flexure properties [53]. The span length of the samples was 55 mm and the nominal thickness was 3.5 mm, while the width was maintained at 12.5 mm. Tests were conducted in displacement control mode with a crosshead speed of 1.2 mm/min. Load–deflection data for each sample were collected. The flexural modulus was calculated from the slope of a stress–strain plot. The maximum stress at failure on the tension side of a flexural specimen was considered as the flexural strength of the material. Thus, using the homogeneous beam theory, the flexural strength in a three-point flexural test was determined using equation [21.2]:

$$\sigma_{UF} = \frac{3P_{max}L}{2bh^2} \qquad [21.2]$$

where P_{max} = maximum load at failure, b = specimen width, d = specimen thickness, and L = specimen length between the two support points.

21.5 Results and discussion

21.5.1 Nanoparticle exfoliation/intercalation

Because of the barrier properties of silicate platelets, a diffusing gas/liquid molecule must detour the exfoliated platelets, forming a very tortuous path as shown in Fig. 21.2. Thus permeability of polymer layered silicate nanocomposites is mainly dependent on the degree of exfoliation or intercalation and the state of dispersion of silicate platelets in a polymer matrix.

Therefore in order to understand the degree of exfoliation or intercalation, X-ray diffraction (XRD) analysis was carried out on multiple samples of pure I-28E nanoclay, cured epoxy resin with and without nanoclay of 2 wt% loading as shown in Fig. 21.3. Intense peaks of 100% and 25% were observed at 2θ = 3.8° and 2θ = 19.7° for the pure montmorillonite nanoclay, similar to the standard montmorillonite-22A nanoclay available in the directory with a PDF #29-1499 in the Rigaku D/MAX 2200 X-ray diffractometer. However, for 2 wt% epoxy/nanoclay samples, the peak intensity was significantly reduced, and the interplanar spacing was increased, indicating that the platelets were

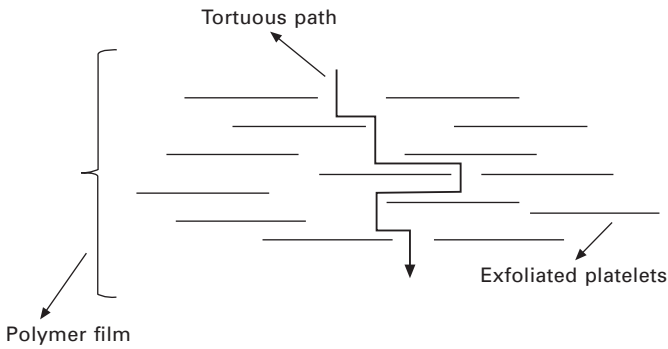

21.2 Schematic of tortuous zigzag diffusion path in an exfoliated polymer–clay nanocomposite.

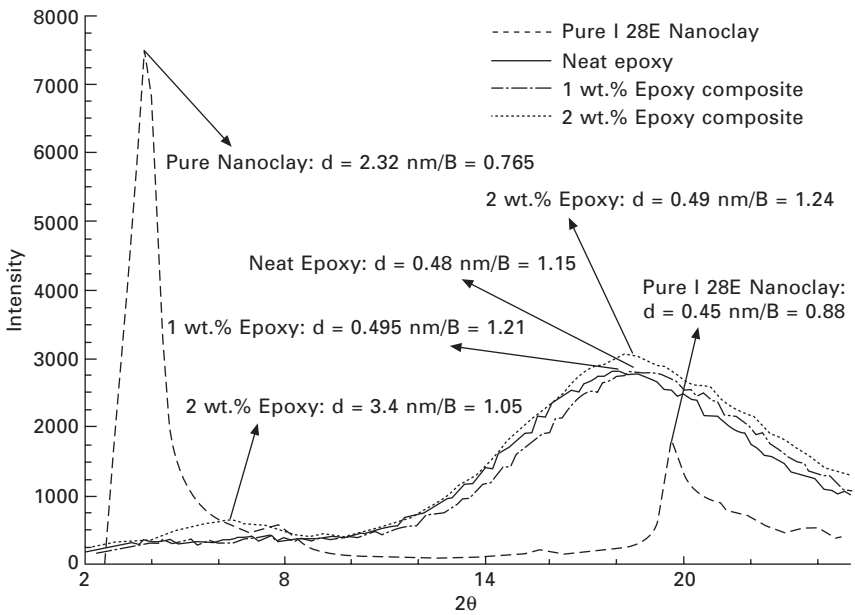

21.3 XRD pattern of pure nanoclay, neat, 1 and 2 wt% epoxy nanoclay composites.

exfoliated in the polymer matrix. The shift of peak in 2 wt% epoxy samples, however, indicates hybrid behavior of exfoliation and intercalation of clay platelets. No peak was observed at this point for 1 wt% epoxy samples, indicating complete exfoliation of platelets. A broad peak at $2\theta = 17–19°$ in neat, 1 wt% and 2 wt% epoxy composite sample was similar to that in neat epoxy material samples. These XRD results matched well with the transmission electron micrographs (TEM) of 2 wt% samples that showed a

combination of intercalated and exfoliated clay platelets in epoxy systems shown in Fig. 21.4 and reported in our previous publications [54, 55].

21.5.2 Weight change due to exposed conditions

Hot dry/wet (hd/hw) and cold dry/wet (cd/cw) conditioning

The average weight change in each sample due to conditioning is shown in Fig. 21.5(a–c). As the material is submerged in water, the amount of its moisture absorption depends on the duration and temperature of the water with the maximum absorption occurring at higher temperature. The maximum change in conditioning environment from room temperature to 80°C hot-wet for 90 days resulted in 4.25% increase in moisture absorption in neat, 3.85% in 1 wt% and 3.06% in 2 wt% GFRP composite samples, respectively, as shown in Fig. 21.5(a–c).

For hot-dry conditioned samples, initial increase in weight gain was observed but decreased as the number of days of conditioning increased. Usually, high temperature may act as an activator for desorption phenomena. Fast drying, generation and regeneration of residual stresses may quite often induce matrix cracking as well as fiber/matrix interfacial debonding [56]. These microcracks in turn provide fast desorption paths for moisture absorption. The weight change in hot-wet samples was found to be increasing even after 90 days of conditioning. However, weight change in hot-dry samples

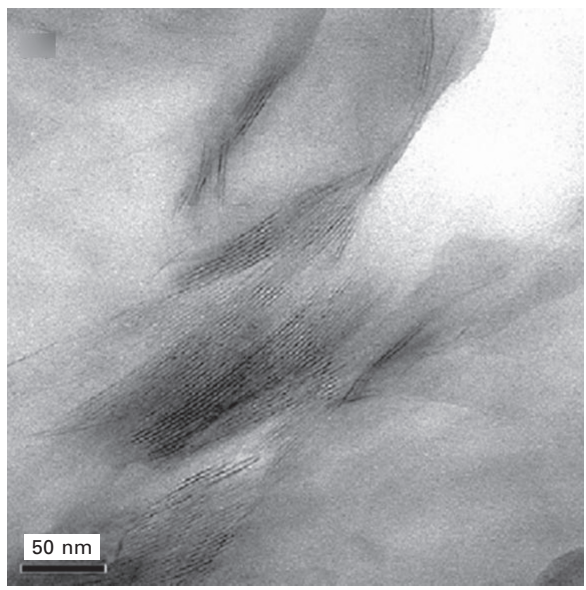

21.4 TEM of 2 wt% epoxy nanocomposite.

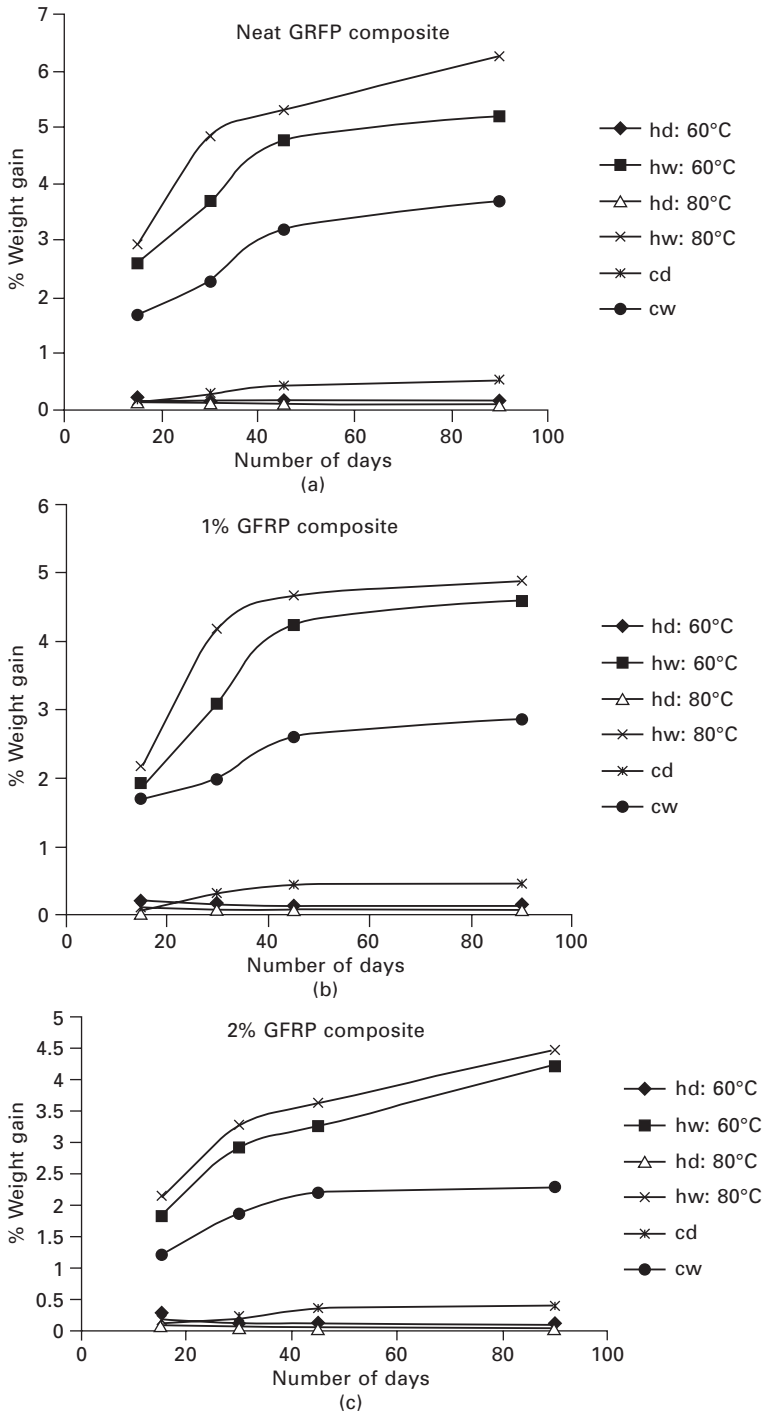

21.5 (a–c) Change in specimen weight as a function of time exposed to hd/hw and cd/cw conditions.

reached a saturation point after 90 days and no further increase in water absorption was observed. In the case of cold dry/wet conditioned samples, no significant changes in weight were observed in comparison to baseline neat samples.

Ultraviolet radiation (UV) and alternate ultraviolet radiation and condensation (UC) conditioning

Figure 21.6 shows the percentage weight change vs. number of days of samples exposed to UV and UC conditions. Samples exposed to UV conditions showed loss in weight with respect to time with a maximum of 0.17% in neat, 0.16% in 1 wt% and 0.12% in 2 wt% samples after 15 days of conditioning. But, after approximately 12 days, loss in weight reached saturation point and showed a minimal decrease with respect to time. In polymers, chain scission will produce small molecules when exposed to UV radiation. These small molecules are capped by oxygen from air free to migrate out from the specimen, causing weight loss. Since most of the polymer has less resistance to radiation, it is also possible that oxygen can easily diffuse into the specimen from air and accelerate the degradation of the matrix.

Specimens exposed to UC conditioning showed a gain in weight with respect to time with a maximum of 1.15% in neat, 1.06% in 1 wt% and 0.88% in 2 wt% samples after 15 days of conditioning as shown in Fig. 21.7. Similar to UV conditioned samples, water absorption reached a saturation level in 1 and 2 wt% UC condition samples and showed no further gain with respect to time after approximately 9 days of conditioning. However, water absorption in neat samples was found to increase even after 15 days of conditioning. The increase in weight gain in UC conditioned samples can be attributed to a conjunct effect of ultraviolet radiation and moisture.

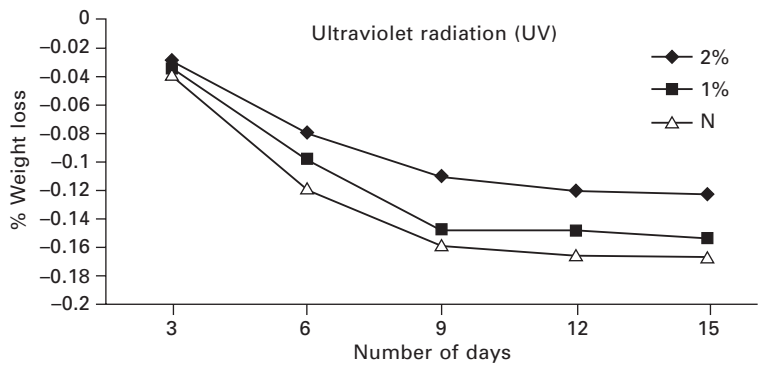

21.6 Change in specimen weight as a function of time exposed to UV condition.

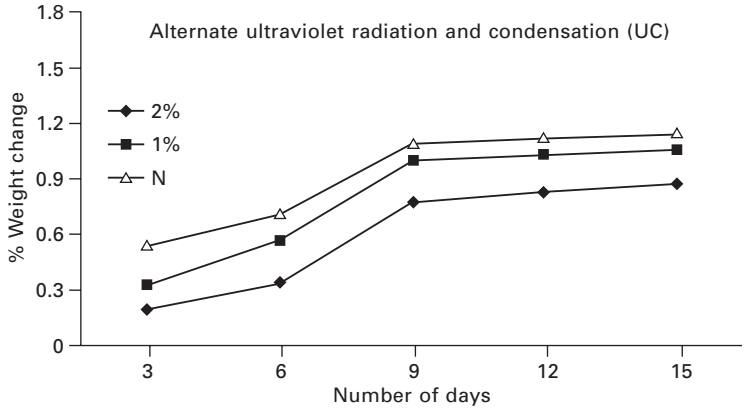

21.7 Change in specimen weight as a function of time exposed to UC condition.

Ultraviolet irradiation produces microcracks on the surface and provides the pathway for rapid ingress of moisture. Also, the presence of moisture may enhance photo-oxidation reactions, resulting in a chain scission. Water vapors, especially in the form of condensation, can also remove soluble products of photo-oxidation reactions from an ultraviolet-irradiated surface and thereby expose fresh surfaces susceptible to further degradation by ultraviolet radiation. However, 2 wt% samples showed less effect of both UV and UC conditioning. The loss in weight in UV and weight gain in UC conditioned samples are significantly reduced in comparison to neat and 1 wt% loaded samples.

The decrease in weight gain for the nanophased composites can be attributed to the hybrid exfoliated and intercalated nanoclay platelets in polymer. Nanoclay platelets when exfoliated/dispersed well in the matrix provide the barrier to gas/liquid in a tortuous manner [12]. This can be attributed to the gas/moisture and radiation barrier properties of montmorillonite nanoclay, which is consistent with results reported by Woo *et al*. [35].

21.5.3 Surface morphology

Surfaces of specimens exposed to hot-dry/wet conditions exhibited yellowish discoloration while the cold-dry/wet conditioned samples retained their white opaque color. The extent of discoloration continuously increased with exposure time and was found to be optimum in hot-dry 80°C samples. Samples subjected to hot-dry 80°C turned dark yellow whereas the hot-wet conditioned samples were light yellowish. Exposure to an elevated temperature alters chemical and physical properties of composites, leading to lower glass transition temperature (T_g), discoloration and damage [57, 58].

Surfaces of all specimens exposed to UV and UC conditions also exhibited a distinct change in color from opaque white to yellowish white during early stages of the exposure. Since UV light cannot deeply penetrate the samples, discoloration was observed only on the exposed surface of the samples. This discoloration might be due to the photo-oxidation that resulted in the formation of chromic chemical species, which absorbed the visible range of light [59]. Chain scission changes the chemical structure of the polymer by generating double-bonded functional groups such as olefinic (C=C) or carbonyl (C=O) groups. These groups absorb UV energy, resulting in photo-reactions and thus causing discoloration and polymer degradation [35]. Exposure to UC condition resulted in less discoloration in samples in comparison to UV conditioned samples. Minor changes in surface roughness were also visible by the naked eye for all the specimens. However, discoloration in 2 wt% samples subjected to similar conditions was significantly reduced. The luminance value for all the samples dropped after 15 days of exposure. The minimum difference in luminance value between room temperature and all conditioned 2 wt% samples indicates reduce color change in comparison to neat samples similarly conditioned.

Further details regarding the physical processes that govern material degradation were revealed from the examination of specimens under optical and scanning electron microscopy. Figure 21.8(a, b) shows the top view optical micrographs of neat untested samples conditioned at room temperature and hot-dry conditions at 80°C for 90 days. No considerable differences were observed on the surfaces of both set of samples in comparison to room temperature-conditioned samples. However, higher magnification scanning electron micrographs of neat and 2 wt% samples subjected to hot-dry/wet at 80°C and cold-dry/wet for 90 days showed a significant effect of the exposed conditions, as shown in Fig. 21.9. The samples subjected to hot-dry condition showed spots of top surface removal, whereas in hot-wet condition, intense microcracking and interfacial phase separation was observed. Spots of surface removal and microcracking can be attributed to the fast drying of samples at elevated temperatures causing excessive brittleness due to increased crosslinking. The interfacial phase separation in addition to the matrix microcracking in hot-wet samples can be attributed to the presence of water on the surface. The microcracks caused by elevated temperature provide a pathway for rapid ingress of moisture absorption present on the surface, thereby further aggravating the degradation process. Samples subjected to cold-dry/wet condition showed micropores and whitening that may have developed due to condensation effects. However, additional interfacial separation was observed in cold-wet samples. Water that diffuses into the composites ends up either in the matrix or at an interphase region. Thus, the amount of moisture absorbed by the matrix is significantly different from that of fiber, leading to the evolution of localized stress and strain fields in

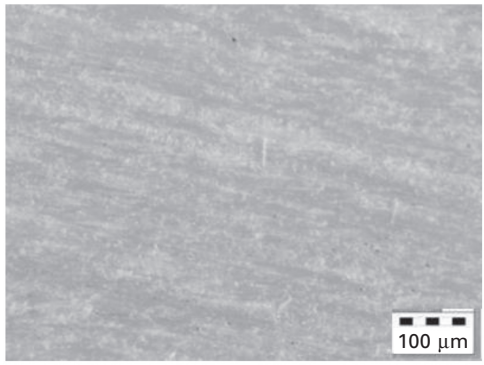

(a)

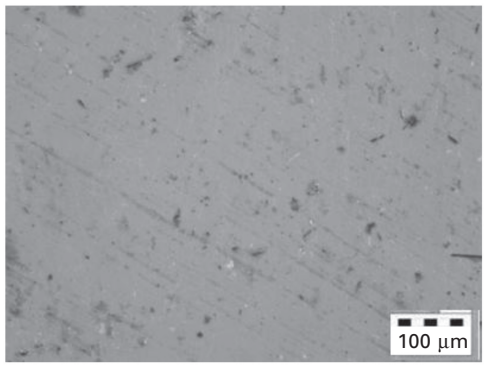

(b)

21.8 Optical micrographs of neat samples subjected to (a) room temperature, (b) hot-dry which showed no difference in surface conditions after 90 days of conditioning.

composites [16, 17]. This process may by further aggravated in the presence of elevated temperature as observed in hot-wet condition samples due to the presence of microcracks.

Figure 21.10(a, b) shows optical micrographs of neat samples subjected to UV conditioning for 15 days. Surface erosion was observed in all the specimens as seen from resin spallation from the surface. Such surface erosion could explain the weight loss of composite materials irritated by UV radiation shown earlier. Figure 21.11(a–c) shows the optical micrographs of neat samples subjected to UC conditioning for 15 days. In addition to surface erosion, the presence of moisture in the form of water droplets causing condensation on the surface was observed. The intensity of surface damage was found to be more severe in UC conditioned samples in comparison to UV conditioned samples. Scanning electron micrographs of the top surface (exposed surface) of neat and 2 wt% samples subjected to UV and UC conditioning are shown in Fig. 21.12. Samples subjected to UV conditioning

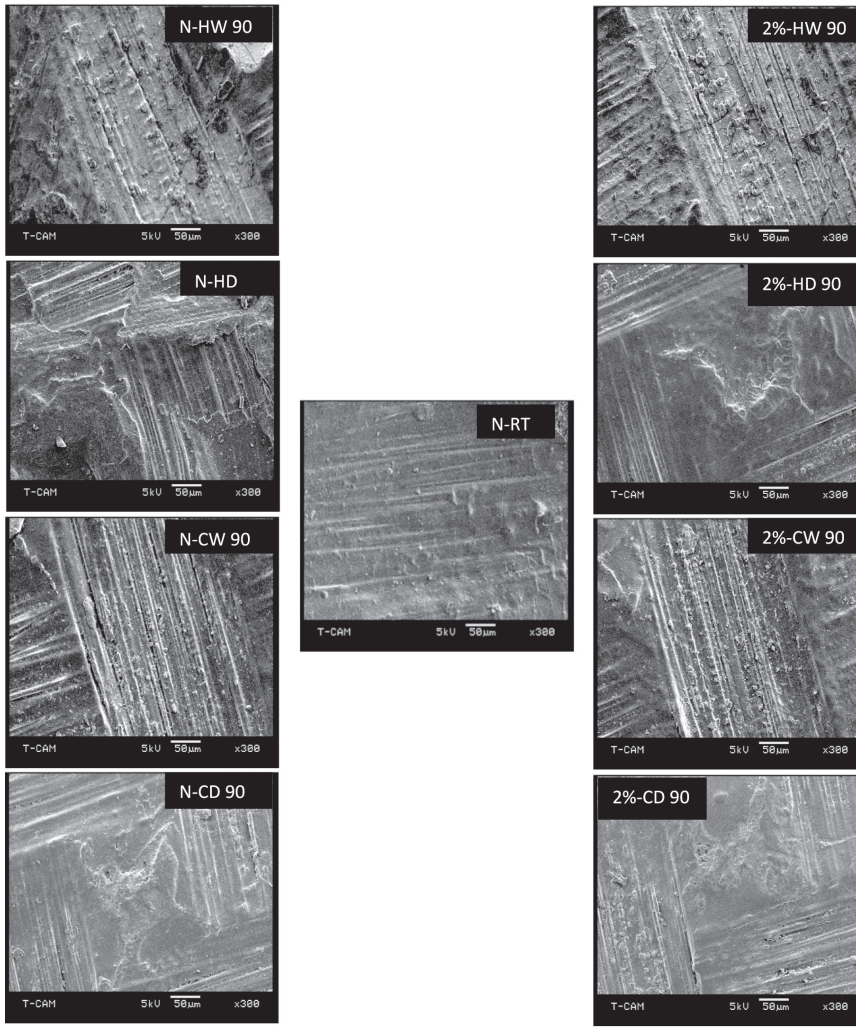

21.9 Scanning electron micrographs (SEM) of untested samples subjected to room temperature, hot-dry/wet and cold-dry/wet conditions.

revealed matrix microcracking, whereas UC conditioned samples revealed excessive matrix microcracking, micropores and whitening. Microcracking was caused by the polymer matrix becoming excessively brittle due to increased crosslinking resulting from the photo-oxidation reaction or elevated temperature induced by UV radiation or hot-dry conditions. In addition, micropores and whitening may have developed due to condensation effects the similar to these in cold-dry/wet conditioning.

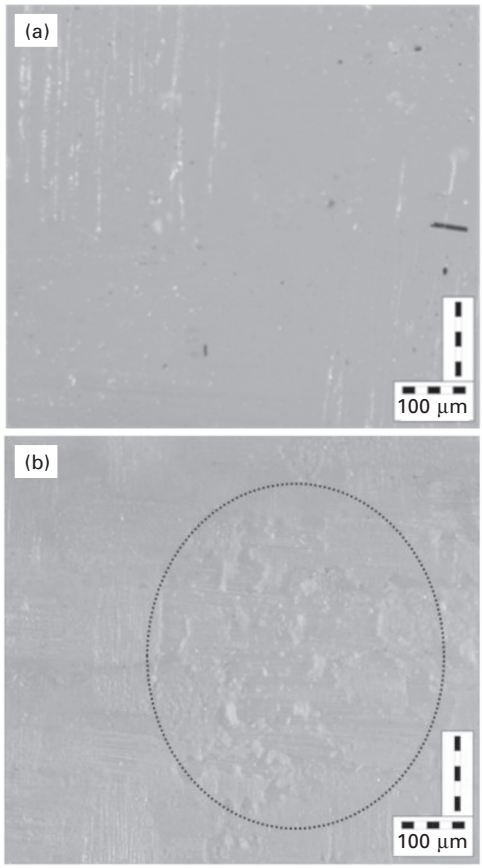

21.10 Optical micrographs of neat samples subjected to UV conditioning for 15 days: (a) back/unexposed surface, (b) exposed surface.

21.5.4 Flexural characterization

Flexural stress–strain responses of hot-dry/wet and cold-dry/wet condition GFRP samples and their property variation with time are given in Fig. 21.13(a–c) and Tables 21.1–21.3, respectively. At room temperature conditioning, 2 wt% nanophased samples showed 19% and 13% increase in strength and modulus over neat samples. In general, all the samples subjected to temperature and moisture conditioning showed a trend of decreasing strength and modulus with a maximum decrease observed in wet conditioned samples. However, strain to failure was found to increase in some wet conditioned samples, which can be attributed to either plasticizing or softening of the samples. Maximum degradation was observed in hot-wet 80°C 90-day conditioned samples. However, 2 wt% samples showed

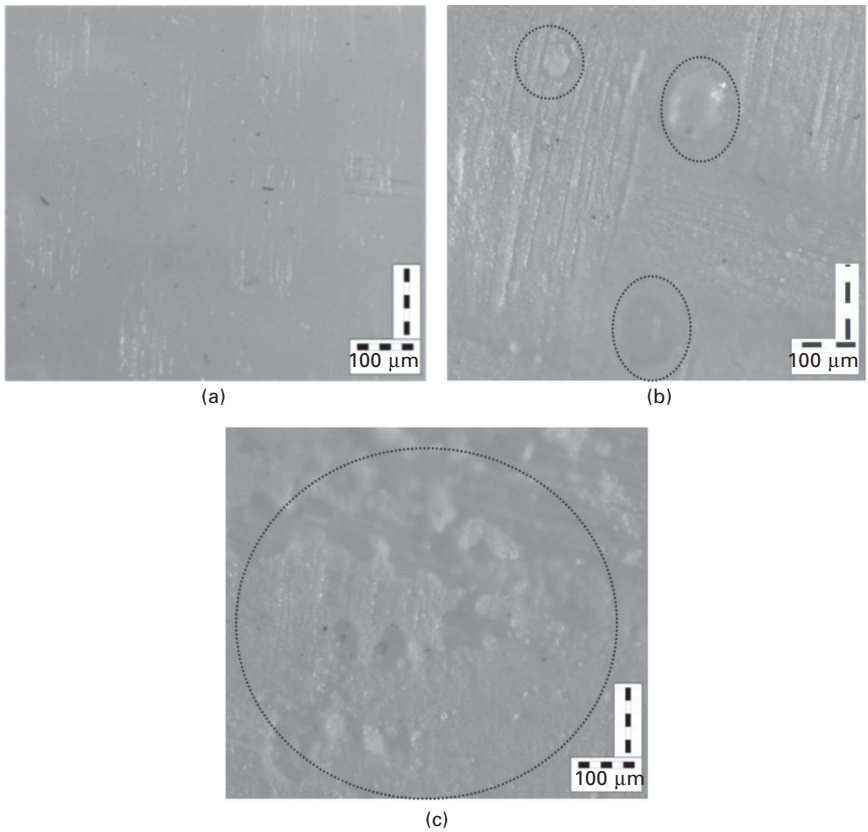

21.11 Optical micrographs of neat samples subjected to UC conditioning for 15 days: (a) back/unexposed surface, (b, c) exposed surface.

significant enhancement in properties in comparison to the neat counterpart in all the set conditions as shown in Table 21.3. The decrease in flexural strength and modulus in neat and nanophased composite properties can be attributed to the elevated temperature, hydrolysis and plasticization effect that resulted in microcracking and fiber/matrix phase separation evident from Fig. 21.9. Similar results were also reported by Vaddadi *et al.* [17] and Schutte [19].

Stress–strain responses of UV and UC conditioned GFRP samples are shown in Fig. 21.14 and Tables 21.4 and 21.5. 2 wt% samples subjected to UV and UC conditioning for 15 days showed similar results, with increases for UV of 10% in strength and 10% in modulus, and for UC of 19.8% in strength and 6.25% in modulus, over their neat counterparts similarly conditioned (Table 21.4). However, 1 wt% samples showed a nominal increase in these properties in comparison to neat samples similarly conditioned.

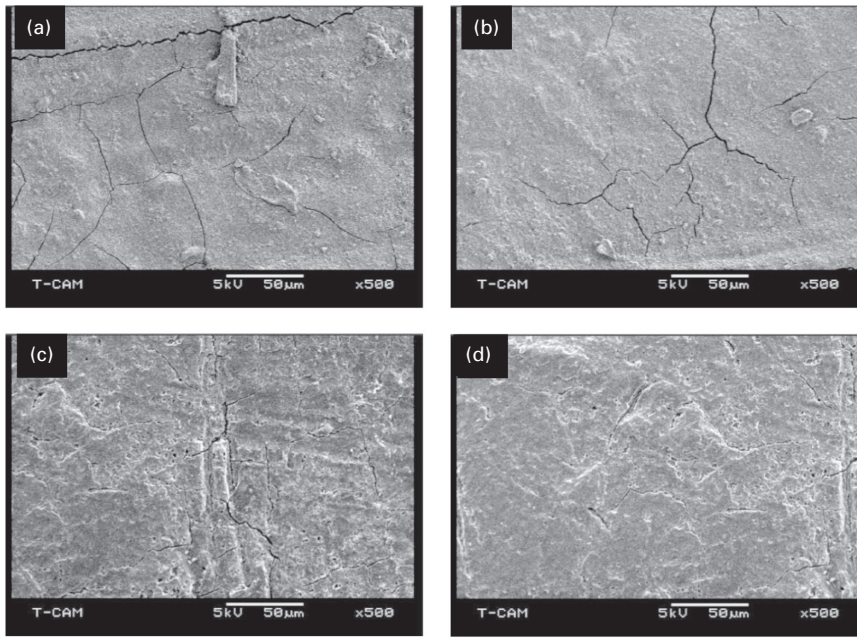

21.12 Scanning electron micrographs (SEM) of untested samples subjected to (a, b) UV, and (c, d) UC conditions for 15 days.

It is worth noting that all the UV and UC samples conditioned up to 5 days showed an insignificant decrease in flexural properties in comparison to room temperature samples. When subjected to ultraviolet radiation and condensation conditions, damage to the polymer depends on the exposure time. If the exposure time is short, the damage may be negligible or reversible; similar results are reported by Regel *et al*. [60]. In contrast, Woo *et al*. [36] reported decrease in tensile strength after 250 hours and increase afterwards up to 1000 hours of UV exposure. Similar results are found in this study with a decrease in strength and modulus in both UV and UC conditioned for 15 days (360 hours) samples in comparison to room temperature samples as shown in Fig. 21.14 and Tables 21.4 and 21.5. However, UV and UC conditioning for an extended period of time was not performed in this study.

Over a period of time, water diffuses into the composites saturating the matrix and may even reach the fiber/matrix interface. Since the resin used in this work is a two part cyclo-aliphatic amine type epoxy resin (Part A: diglycidylether of bisphenol-A aliphatic diglycidyl and part B: hardener), the epoxy has the opportunity to absorb moisture [19, 57], exposure to water and temperature results in plasticization of the matrix, creating free volume and thus decreasing the properties. Presence of water at the interface region may also relieve the residual stresses that are generated during fabrication [56].

Elevated temperature may further hasten the degradation process by creating cracks in the matrix and decrease the fiber–matrix interfacial bonding.

The decreasing trend in flexural properties upon UV and UC exposure

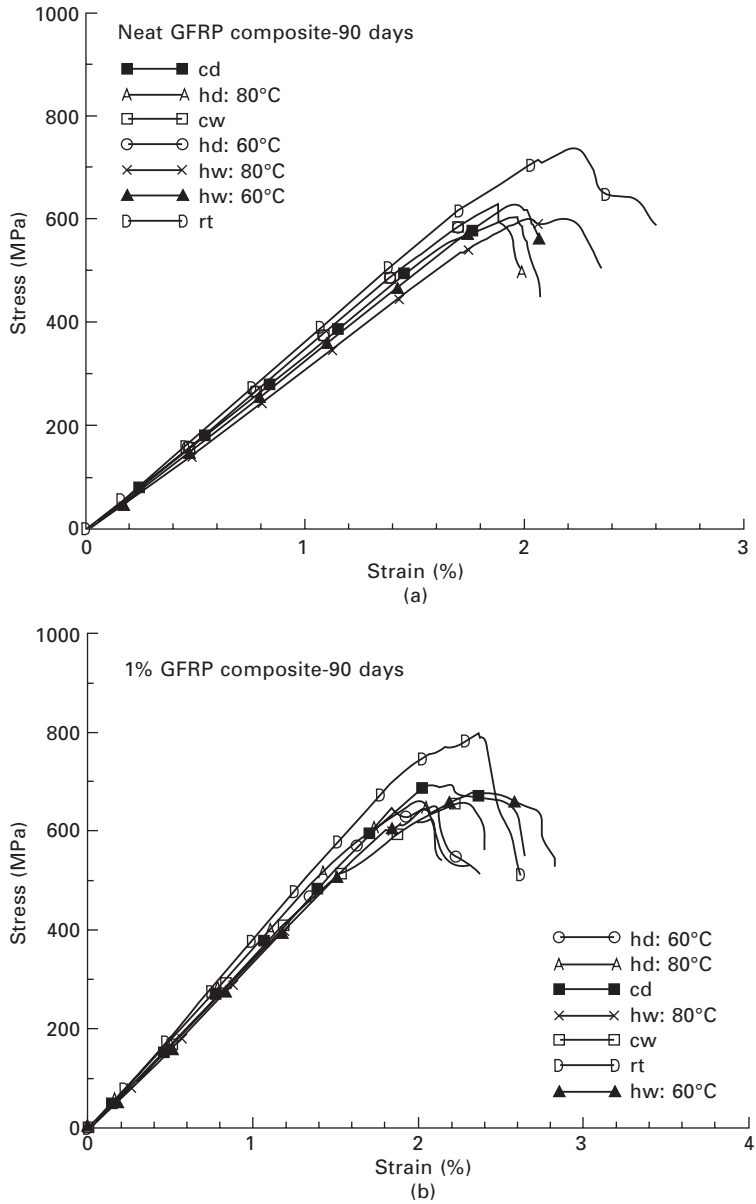

21.13 (a–c) Flexural stress–strain response of control, hd/hw and cd/cw conditioned samples.

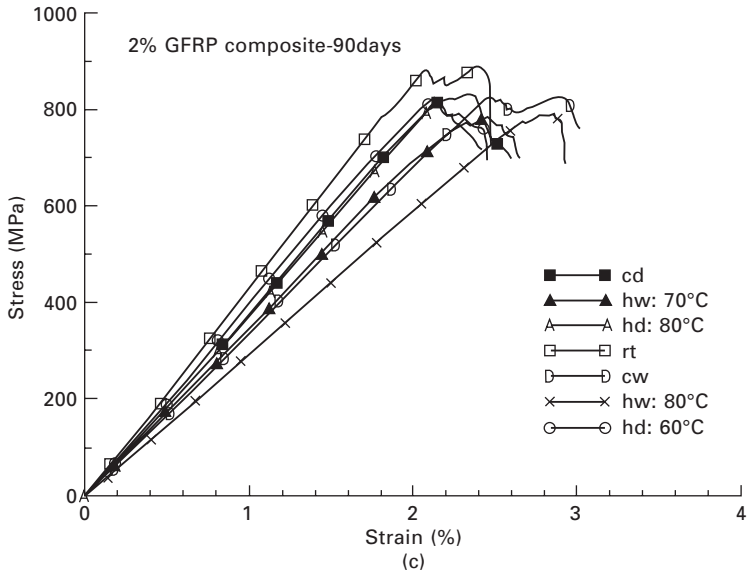

21.13 Continued

may be attributed to chain scission and chain crosslinking phenomena. Chain scission lowers the molecular weight and strength of polymers, while chain crosslinking embrittles polymers, resulting in microcracking but also increasing the strength [29, 59]. In presence of ultraviolet radiation, chain scission dominates due to the creation of free radicals in the presence of UV photons and oxygen. Decrease in flexural properties of UC conditioned samples was found to be higher in comparison to only UV conditioned samples. This can be attributed to the combined effect of ultraviolet radiation and condensation and possibly the elevated temperature set in the UV chamber, i.e. 60°C. Ultraviolet radiation and temperature produce surface erosion and microcracks on the surface that provide a pathway for rapid ingress of moisture into the polymer and at the fiber/matrix interphase. The deterioration of a polymer matrix alone is sufficient to cause degradation in structural performance and reliability [59]. In the matrix, water acts as plasticizer, increases free volume, lowers the glass transition temperature, and relieves the internal stress that is built up during processing of the composites [18]. Moisture wicking along the fiber–matrix interface can degrade the interfacial bond, resulting in the loss of microstructural integrity.

Enhancement in nanophased composites properties can be attributed to the possible catalytic effect of nanoclay that accelerates the curing [32] and increase in the crosslinking between polymer chains, resulting in higher crosslinking density [33, 61, 62]. Furthermore, well-dispersed and exfoliated clay platelets of nanoclay may have provided the barrier to exposed conditions. Hence, due

Table 21.1 Flexural strength of GFRP samples subjected to control, hd/hw and cd/cw conditions

Condition	Flexural strength (MPa)					
	15 days	% change w.r.t. RT	45 days	% change w.r.t. RT	90 days	% change w.r.t. RT
No GFRP. RT: 738.3 MPa						
hd: 60°C	737.6 ± 1.58	–0.1	645 ± 1.56	–14.5	622 ± 0.58	–18.7
hw: 60°C	680.7 ± 2.1	–8.5	623 ± 1.27	–18.5	620 ± 1.18	–19.1
hd: 80°C	672.2 ± 1.63	–9.84	643 ± 0.83	–14.8	620 ± 1.03	–19.1
hw: 80°C	648.6 ± 1.56	–13.8	610 ± 1.03	–21	602 ± 0.58	–22.6
cd	734 ± 1.80	–0.6	687 ± 1.32	–7.4	624 ± 1.55	–18.3
cw	664 ± 1.53	–11.2	633 ± 0.96	–16.6	622 ± 0.63	–18.7
1% GFRP composite. RT: 798 MPa						
hd: 60°C	797 ± 1.60	–0.1	684 ± 1.33	–16.7	670 ± 1.18	–19
hw: 60°C	790.7 ± 0.86	–0.9	681.5 ± 0.58	–17.1	660 ± 1.22	–21
hd: 80°C	734 ± 1.70	–8.7	677 ± 1.65	–17.9	664 ± 1.57	–20.2
hw: 80°C	676 ± 1.30	–18.1	640 ± 1.06	–24.7	626 ± 1.00	–27.5
cd	785 ± 1.41	–1.7	728 ± 1.60	–9.6	690 ± 1.71	–15.65
cw	783 ± 1.20	–1.9	692 ± 0.42	–15.3	659 ± 1.58	–21.1
2% GFRP composite. RT: 878.2 MPa						
hd: 60°C	889.8 ± 1.60	+1.3	867 ± 1.27	–1.3	824 ± 1.20	–6.6
hw: 60°C	840 ± 1.03	–4.5	810 ± 0.58	–8.42	784 ± 1.00	–12
hd: 80°C	846.97 ± 1.34	–3.7	834 ± 1.40	–5.3	817 ± 1.84	–7.5
hw: 80°C	830 ± 0.71	–5.8	771 ± 1.05	–14	780 ± 1.22	–12.6
cd	830 ± 1.20	–5.8	827 ± 1.88	–6.7	820 ± 1.33	–7.1
cw	826.3 ± 1.60	–6.3	822 ± 1.02	–6	818 ± 1.05	–7.5

Notes: h = hot, c = cold, d = dry, w = wet, w.r.t. = with respect to, RT = room temperature

to this enhancement in crosslinking of polymer chains and barrier properties, damaging effects of environmental conditions on nanoclay-incorporated GFRP samples may have been subsidized or retarded and thereby may have improved the overall performance [35, 54]. Similar behavior was observed for 15 and 45 days in hot-dry/wet, cold-dry/wet and 5 and 10 days UV/UC conditioned samples.

21.5.5 Micrographic analyses – scanning electron microscopy (SEM)

The fiber/matrix interface region plays a crucial role in the durability of composites in the aqueous environment. The effects of temperature and moisture on both tested and untested conditioned samples were examined by scanning electron microscopy (SEM) along with room temperature samples. Figure 21.15 shows the SEM of neat and nanophased fractured samples conditioned at room temperature. From Fig. 21.15(b), it can be seen that the

Table 21.2 Flexural modulus of GFRP samples subjected to control, hd/hw and cd/cw conditions

Condition	Flexural Modulus GPa					
	15 days	% change w.r.t. RT	45 days	% change w.r.t. RT	90 days	% change w.r.t. RT
No GFRP RT: 34.19 (GPa)						
hd: 60°C	32.54 ± 0.05	–5	30.6 ± 0.03	–11.7	30.57 ± 0.06	–11.8
hw: 60°C	31.27 ± 0.02	–9.4	27.4 ± 0.03	–24.8	26.46 ± 0.05	–29.2
hd: 80°C	30.04 ± 0.07	–13.8	29.7 ± 0.07	–15.12	28.82 ± 0.08	–18.6
hw: 80°C	30 ± 0.02	–14	27 ± 0.05	–26.63	2634 ± 0.05	–29.8
cd	32.9 ± 0.05	–3.9	32.6 ± 0.05	–4.9	32.0 ± 0.06	–6.9
cw	32.21 ± 0.06	–6.14	30.7 ± 0.06	–11.4	28.0 ± 0.03	–22
1% GFRP composite RT: 35.3 (GPa)						
hd: 60°C	35.29 ± 0.02	–0.03	34 ± 0.08	–3.5	32.6 ± 0.04	–8
hw: 60°C	31.2 ± 0.05	–13.14	31 ± 0.03	–13.5	29.4 ± 0.07	–20
hd: 80°C	33 ± 0.07	–7	32.6 ± 0.06	–7.9	32.2 ± 0.07	–9.3
hw: 80°C	30.72 ± 0.03	–14.9	29.5 ± 0.02	–19.3	27.6 ± 0.02	–27.5
cd	32.8 ± 0.1	–7.6	32 ± 0.05	–10	31 ± 0.03	–13.5
cw	31 ± 0.05	–13.9	30.6 ± 0.07	–15	29.2 ± 0.05	–20.5
2% GFRP composite RT: 38.2 (GPa)						
hd: 60°C	39 ± 0.1	+2	37.4 ± 0.05	–2.14	37 ± 0.04	–3.2
hw: 60°C	36.4 ± 0.07	–4.9	36 ± 0.03	–6.1	34 ± 0.05	–12.35
hd: 80°C	37.2 ± 0.07	–2.7	35 ± 0.05	–9.14	33.8 ± 0.07	–13.1
hw: 80°C	36 ± 0.04	–6	33.7 ± 0.05	–13.35	32.5 ± 0.05	–17.54
cd	37.5 ± 0.02	–1.9	36 ± 0.08	–6.1	35 ± 0.04	–9.14
cw	36.8 ± 0.05	–3.8	34 ± 0.02	–12.3	33 ± 0.02	–15.8

Notes: h = hot, c = cold, d = dry, w = wet, w.r.t. = with respect to, RT = room temperature

Table 21.3 Percentage increase in strength and modulus of hd/hw and cd/cw 1 and 2 wt% samples over neat counterparts similarly conditioned

Condition	Percentage increase in strength/modulus using 1 wt% nanoclay			Percentage increase in strength/modulus using 2 wt% nanoclay		
	15 days	45 days	90 days	15 days	45 days	90 days
RT		+8/+3			+19/+13	
hd: 60°C	+8/+8.5	+6/+11	+7.7/+6.6	+21/+20	+34/+22.2	+32.5/+21
hw: 60°C	+16/–0.23	+9/+13.14	+6.5/+11	+23/+16.4	+30/+31.4	+26/+28.5
hd: 80°C	+9/+9.85	+5/+9.8	+7/+11.7	+26/+23.8	+29.7/+17.8	+32/+17.3
hw: 80°C	+4/+2.4	+5/+9.3	+4/+4.8	+28/+20	+26.4/+24.8	+29/+23.4
cd	+7/–0.2	+6/–1.6	+10.6/–3	+132/+14	+20.4/+10.4	+31/+9.3
cw	+18/–3.4	+9/ –0.2	+6/+4.3	+245/+14.3	+30/+10.75	+31/+17.86

Notes: h = hot, c = cold, d = dry, w = wet, w.r.t. = with respect to, RT = room temperature

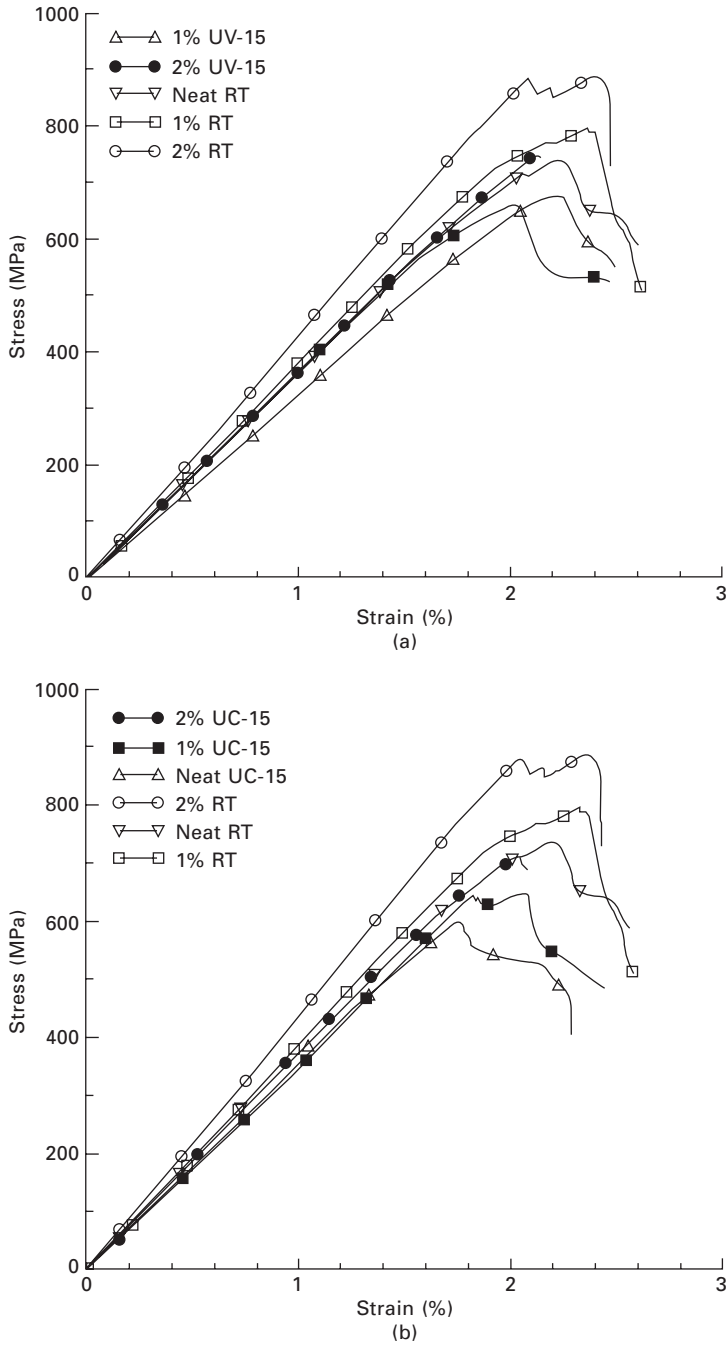

21.14 (a, b) Flexural stress–strain response of control, UV and UC conditioned samples.

Table 21.4 Flexure properties of GFRP samples subjected to UV and UC conditioning

Flexural Strength (MPa)						
Condition	5 days	% Change w.r.t. to RT	10 days	% Change w.r.t. to RT	15 days	% Change w.r.t. to RT
Neat RT	738.3 ± 3.6	–	738.3 ± 3.6	–	738.3 ± 3.6	–
Neat UV	730 ± 5.7	–4	690 ± 3.7	–7	675.17 ± 5.2	–9.4
Neat UC	725.15 ± 7.2	–8.1	657 ± 6.3	–12.4	601.41 ± 3.2	–22.7
1% RT	798 ± 2.6	–	798 ± 2.6	–	798 ± 2.6	–
1% UV	792.9 ± 7.34	–7	710.34 ± 3.5	–12.3	663.52 ± 6.3	–20.3
1% UC	787.2 ±	–12.8	690 ± 3.2	–15.7	649.15 ± 2.7	–23
2% RT	878.2 ± 1.8	–	878.2 ± 1.8	–	878.2 ± 1.8	–
2% UV	870 ± 6.2	–7.1	753 ± 3.5	–16.6	747 ± 4.6	–17.7
2% UC	872.4 ± 3.7	–11.8	725.28 ± 6.3	–21.1	720.4 ± 2.9	–22
Flexural Modulus (GPa)						
Neat RT	35 ± 1	–	35 ± 1	–	35 ± 1	
Neat UV	34.5 ± 0.7	–1.5	34 ± 1.1	–2.9	31.77 ± 1.5	–10.2
Neat UC	34.7 ± 1.4	–0.9	32.2 ± 0.2	–8.7	32 ± 0.6	–9.4
1% RT	35.37 ± 0.5	–	35.37 ± 0.5	35.37 ± 0.5	–	
1% UV	34.21 ± 0.7	–3.2	33.8 ± 1.0	–4.4	32.29 ± 0.7	–9
1% UC	34.7 ± 0.6	–1.8	34 ± 0.35	–3.8	32 ± 0.4	–10.3
2% RT	38.7 ± 1.7	–	38.7 ± 1.7	–	38.7 ± 1.7	–
2% UV	37.39 ± 1.4	–3.5	36 ± 0.5	–7.5	35.05 ± 0.7	–10.4
2% UC	37.04 ± 0.5	–5	34.3 ± 1.3	–12.8	34 ± 0.9	–13.8

Notes: h = hot, c = cold, d = dry, w = wet, w.r.t. = with respect to, RT = room temperature

Table 21.5 Percentage increase in strength and modulus of 1 and 2 wt% samples over neat counterparts subjected to similar UV and UC conditioning

Condition	Percentage increase in strength/ modulus using 1 wt% nanoclay			Percentage increase in strength/ modulus using 2 wt% nanoclay		
	5 days	10 days	15 days	5 days	10 days	15 days
RT		+8/+3			+19/+13	
UV	+8.6/+0.6	+2.9/–0.9	–1.7/+1.6	+19/+10	+9/+5.9	+10.6/+10.3
UC	+8.6/+2.1	+5/+5.6	+7.9/0	+20.31/+8.9	+10.4/+6.3	+19.8/+6.25

2 wt% failed sample had stronger interfacial bounding over its counterpart neat failed sample shown in Fig. 21.15(a). Figures 21.16 and 21.17 show the micrographs of hot-wet conditioned neat and nanophased tested samples at 80°C for 90 days. Interfacial bonding was completely destroyed in neat hot-wet 80°C for 90 days conditioned fractured samples as shown in Fig. 21.16(a). No adhesion of the matrix was found on the fibers as evident from the smoother surface of the fibers as shown in Fig. 21.16(b). However, 2 wt% fractured

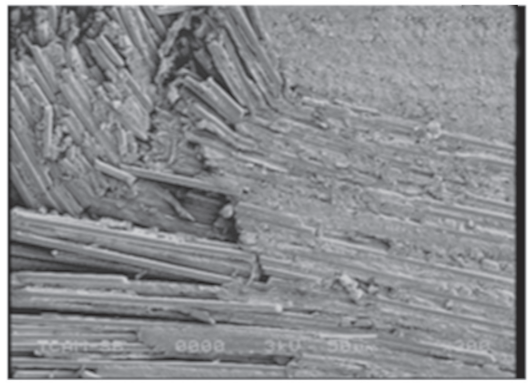

(a)

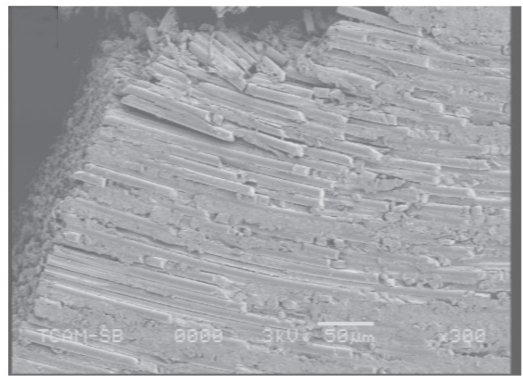

(b)

21.15 SEM of room-temperature-conditioned (a) neat and (b) 2 wt% GFRP fractured samples.

samples similarly conditioned showed much better interfacial bonding, evident from the thick matrix layer on the surface of fractured fibers (Fig. 21.17(a, b)). In addition, fiber breakage was observed in 2 wt% samples as shown in Fig. 21.17(c). This indicates that the failure in nanophased composites was due to the combined effect of matrix cracking, delamination and fiber breakage instead of matrix cracking, debonding and delamination in neat samples. Similar behavior was observed in UC conditioned neat and 2 wt% samples evident from Figs 21.18–21.19. These results clearly demonstrate that montmorillonite nanoclay, if exfoliated properly in the polymer matrix, provides a barrier to moisture and temperature and thus reduces damage to the matrix and the fiber/matrix interfacial bonding.

As reported by Schutte [19], hydrolysis of the bisphenol-A epoxy resin by hot water is a form of chemical degradation of the matrix. When a resin is hydrolyzed, the ester bonds are destroyed. With less bonding between and

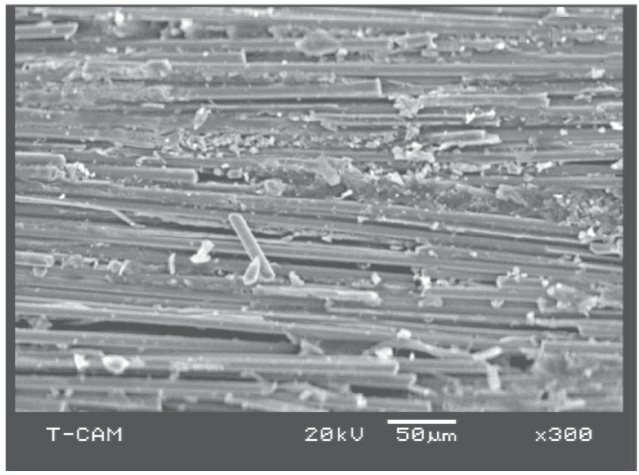

(a)

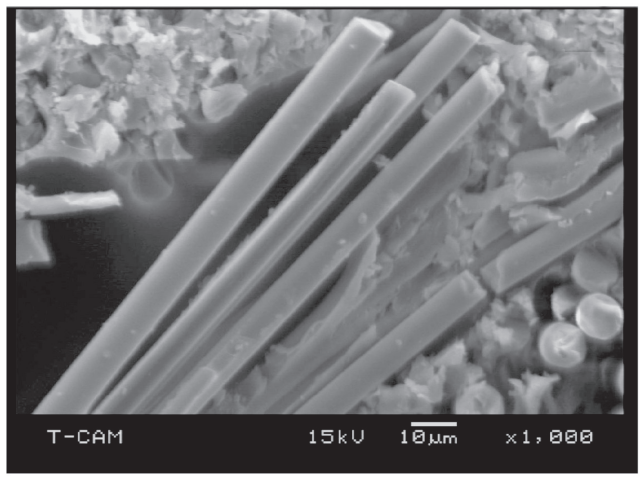

(b)

21.16 (a, b) Fractured hot-wet 80°C 90 days conditioned neat sample.

within the polymer chains, the chains will slide past each other with greater ease; thus, inelastic deformation is achieved at smaller load, resulting in loss of stiffness. In contrast, addition of nanoclay increases the crosslinking density and enhances the bonding (Fig. 21.15(b)), providing resistance to failure and enhancing properties even in wet and elevated temperature conditions. Our previous study using dynamic mechanical analysis has shown that there is an increase in crosslinking density with addition of small wt% of nanoclay to SC-15 epoxy [61, 62]. This is further evident from the study of Uhl *et al.* [33]. In their study on the organically modified montmorillonites in UV

curable urethane acrylate films, they have shown that the films containing nanoclays have higher crosslink density as evident from the higher values of the rubbery plateau in the DMTA results. Based on real-time infrared spectroscopy (RTIR) and photo-DSC data, they also conclude that the presence of nanoclay can facilitate crosslinking reaction and therefore the crosslink density is increased. Additionally, they also concluded that clay may act as crosslinker and physical aggregation of polymer chains onto the surface of a particulate, resulting in a rise in the effective degree of crosslinking.

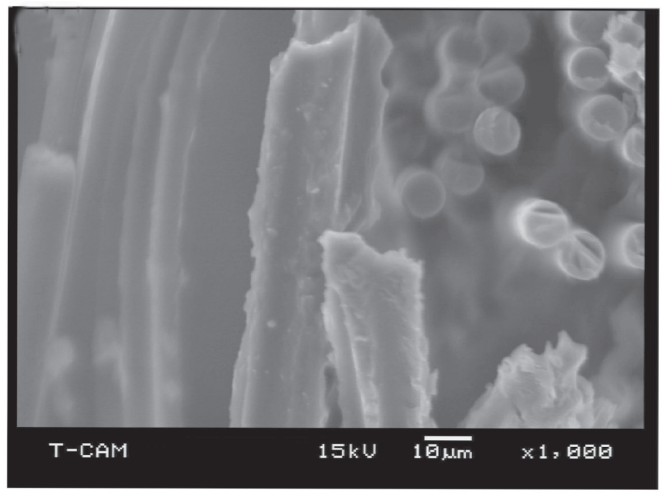

(a)

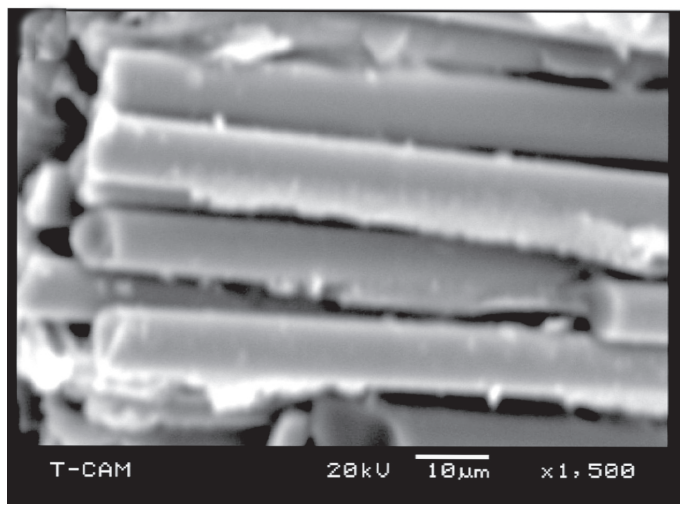

(b)

21.17 (a–c) Fractured hot-wet 80°C 90 conditioned 2 wt% sample.

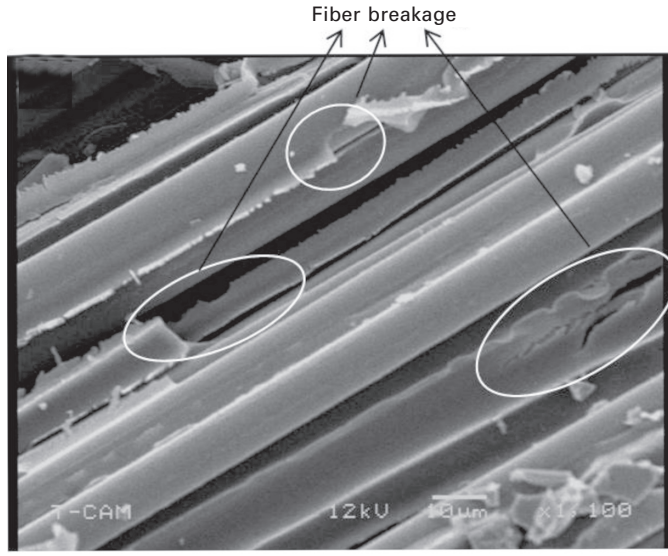

(c)

21.17 Continued

21.6 Conclusion and future trends

It is shown here that glass fiber-reinforced polymer (GFRP) composite was sensitive to environmental conditioning, especially under elevated temperature and ultraviolet radiations combined with wet conditions. The weight gain was optimum in hot-wet and alternate ultraviolet and condensation conditioned samples. Addition of 1–2 wt% nanoclay decreased the weight loss/gain and resulted in less discoloration in comparison to neat samples similarly conditioned. Flexural properties were found to degrade with increase in time. 2 wt% GFRP composites showed enhancement in properties under all conditions over their neat counterparts. In some cases, samples subjected to hot-dry conditions at 60°C showed increase in properties over room temperature conditioned samples. Scanning electron micrographs provided clear evidence of the effects of nanoclay, elevated temperature, ultraviolet radiation and moisture absorption. The study reported here was carried out for a limited period of time: 90 days for the effect of temperature and moisture, and 15 days for the effect of UV radiation and condensation. Results obtained in this study have been promising and have shown significant enhancement in mechanical properties and reduction in environmental effects on GFRP composites with the addition of nanoclay. The results obtained from this study could allow the use of these materials in civil engineering applications under aggressive environments with more confidence for their long-term durability.

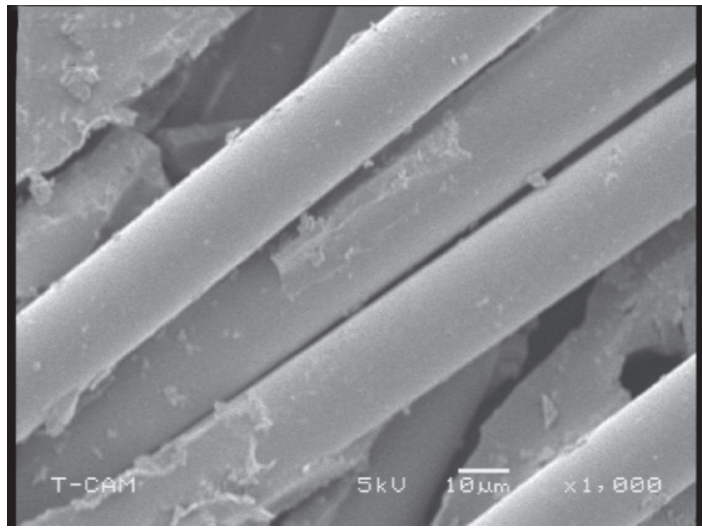

21.18 Fractured UC 15 days conditioned neat sample.

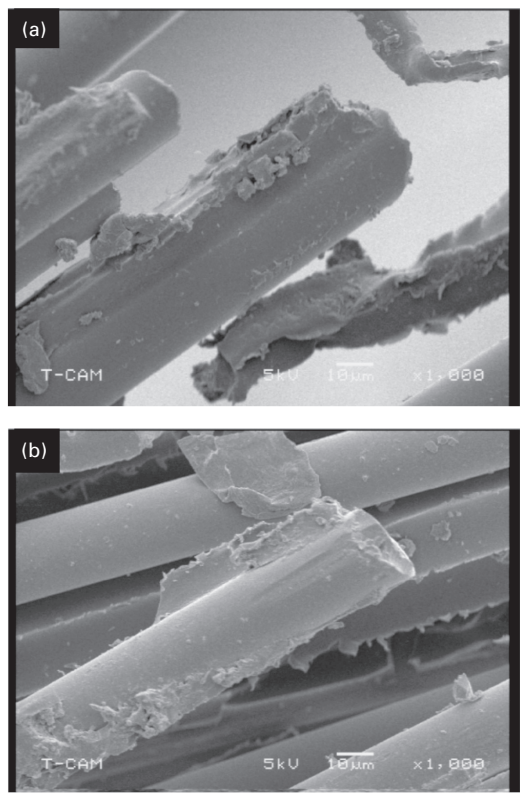

21.19 (a, b) Fractured UC 15 days conditioned 2 wt% sample.

21.7 Acknowledgements

The authors would like to acknowledge U.S. Engineer Research Development Corporation – Construction Engineering Research Laboratory (ERDC-CERL) and NSF EPSCoRfor funding this work.

21.8 References

1. Malvar LJ. Literature review of durability of composites in reinforced concrete. Special publication SP-2008-SHR, Naval Facilities Engineering Service Center, Port Hueneme, CA, 1996, p. 26.
2. Nanni A. Fiber reinforced plastic (FRP) reinforcement for concrete structures: Properties and applications. *Developments in Civil Engineering* 1993; 42: 450.
3. Bonniau P, Bunsell AR. A comparative study of water absorption theories applied to glass epoxy composites. *J Compos Mater* 1981; 15: 272– 293.
4. Dewimille B, Bunsell AR. The modeling of hygrothermal aging in glass fiber reinforced epoxy composites. *J Phys D* 1982; 15: 2079–2091.
5. Mercier J, Bunsell A, Castaing P, Renard J. Caractérisation et modélisation du vieillissement de matériaux composites. *Revue des Composites et des Matériaux avancés* 2005; 5: 189–219.
6. Weitsman YJ, Guo Ya-J. Correlation between fluid-induced damage and anomalous fluid sorption in polymeric composites. *Compos Sci Technol* 2002; 62: 889–908.
7. Nairn JA. Matrix microcracking in composites. *Comprehensive Compos Mater* 2000; 2: 403–432.
8. Gilman JW. Flammability and thermal stability studies of polymer-layered silicate clay nanocomposites. *Appl Clay Sci* 1999; 15: 31–49.
9. Lee H, Nevile K. *Epoxy Resins: Their Applications and Technology*. New York: McGraw-Hill, 1957.
10. Lu MG, Shim MJ, Kim SW. Effects of moisture on properties of epoxy molding compounds. *J Appl Polym Sci* 2001; 81: 2253–2259.
11. Nunez L, Villanueva M, Fraga F, Nunez MR. Influence of water absorption on the mechanical properties of a DGEBA. *J Appl Polym Sci* 1999; 74: 353–358.
12. Yano K, Usuki A, Okada A, Kurauchi T. Kamigaito O. Synthesis and properties of polyimide–clay hybrid. *J Polym Sci* 1993; 31(Part A): 2493–2498.
13. Sanders B. *Characterization and Failure Analysis of Plastics*. ASM International, 2004.
14. Ray BC. Temperature effect during humid ageing on interfaces of glass and carbon fibers reinforced epoxy composites. *J Colloid Interface Sci* 2006; 298: 111–117.
15. Ellyin F, Maser R. Environmental effects of the mechanical properties of glass-fiber epoxy composite tubular specimens. *Compos Sci Technol* 2004; 1: 17.
16. Lee MC, Peppas NA. Models of moisture transport and moisture induced stress in epoxy-composites. *J Compos Mater* 1993; 27: 1146.
17. Vaddadi P, Nakamura T, Singh RP. Transient hygrothermal stresses in fiber reinforced composites: a heterogeneous characterization approach. *Compos. A: Appl Sci Manufac* 2003; 34: 719.
18. Magid BA, Ziaee S, Gass K, Schneider M. The combined effects of load, moisture and temperature on the properties of E-glass, epoxy composites. *Compos Struct* 2005; 71: 320–326.

19. Schutte CL. Environmental durability of glass-fiber composites. *Mater Sci Eng* 1994; 13: 265–324.
20. Roy S, Xu W, Patel S, Case S. Modeling of moisture diffusion in the presence of bi-axial damage in polymer matrix composite laminates. *Int J Sol Struct* 2001; 38: 7627–7641.
21. Vauthier E, Abry JC, Bailliez T, Chateauminois A. Interactions between hygrothermal ageing and fatigue damage in unidirectional glass/epoxy composites. *Compos Sci Technol* 1998; 58: 687–692.
22. Jones CJ, Dickson RF, Adam T, Reiter H, Harris B. Environmental fatigue behavior of reinforced plastics. *Compos* 1983; 14(3): 288–293.
23. Sumsion HT, Williams DP. Effect of environment on the fatigue of graphite-epoxy composites. ln: *Fatigue of Composite Materials*, ASTM STP 569, American Society of Testing and Materials, 1975; 226–247.
24. Komai K, Minoshima K, Shiroshita S. Hygrothermal degradation and fracture process of advanced fiber-reinforced plastics. *Mater Sci Eng* 1991; A143: 155–166.
25. Ogi K, Kim HS, Maruyama T, Takao Y. The influence of hygrothermal conditions on the damage processes in quasi-isotropic carbon/epoxy laminates. *Compos Sci Technol* 1999; 59: 2375–2382.
26. Karbhari VM, Chin JW, Hunston D, Benmokrane B, Juska T, Morgan R, Lesko JJ, Sorathia U, Reynaud D. Durability gap analysis for fiber-reinforced polymer composites in civil infrastructure. *J Compos Constr* 2003; 7(3): 238–247.
27. Giori C, Yamauchi T. Effects of ultraviolet and electron radiations on graphite-reinforced polysulfone and epoxy resins. *J Appl Polym Sci* 1984; 29: 237–249.
28. Haliwell SM. Weathering of polymers. *RAPRA Review Reports* 1992; 53.
29. Rabek JF. *Polymer Photo-degradation: Mechanism and Experimental Methods*, London: Chapman & Hall, 1995; Chapters 2 and 10, 24–66.
30. Brown JM, Curliss D, Vaia RA. Thermoset-layered silicate nanocomposite. Quaternary ammonium montmorillonite with primary diamine cured epoxies. *Chem Mater* 2000; 12(11): 3376–3384.
31. Maul P. Barrier enhancements using additives, in fillers, pigments and additives for plastics in packaging applications. *Pira Int Conf*, Belgium, 5–6 December 2005.
32. Carrasco F, Pages P. Thermal degradation and stability of epoxy nanocomposites: Influence of montmorillonite content and cure temperature. *Polym Deg Stab* 2008; 98: 1000–1007.
33. Uhl FM, Davuluri SP, Wong SC, Webster DC. Organically modified montmorillonites in UV curable urethane acrylate films. *Polymer* 2004; 45(18): 6175–6187.
34. Hackman I, Hollaway L. Epoxy-layered silicate nanocomposites in civil engineering. *Compos. A: Appl Sci Manufac* 2006; 37: 1161–1170.
35. Woo RSC, Chen YH, Zhu HG, Leung CKY, Kim JK. Environmental degradation of epoxy-organoclay nanocomposites due to UV exposure: Part I. Photodegradation. *Compos Sci Technol* 2007; 67: 3488–3456.
36. Woo RSC, Chen YH, Zhu HG, Leung CKY, Kim JK. Environmental degradation of epoxy-organoclay nanocomposites due to UV exposure: Part II. Residual mechanical properties. *Compos Sci Technol* 2008; 68: 2149–2155.
37. Bartos PJM. Nanotechnology in construction: A roadmap for development. *Proc 2nd Int Symp on Nanotechnology in Construction* 2005, Bilbao, Spain, 13–16 November, 27–36.
38. Okada A, Kawasumi M, Usuki A, Kojima Y, Kurauchi T, Kamigaito O. Nylon 6–clay hybrid. *Mater Res Soc Proc* 1990; 171: 45–50.

39 Messersmith PB, Giannelis EP. Synthesis and barrier properties of poly (ε-caprolactone)-layered silicate nanocomposites. *J Appl Polym Sci* 1995; 33: 1047–1057.
40. Woo RSC, Zhu H, Chow MMK, Leung CKY, Kim J-K. Barrier performance of silane-clay nanocomposite coatings on concrete structure. *Compos Sci Technol* 2008; 68: 2828–2836.
41. Kuo WY, Huang JS, Lin CH. Effect of organo-modified montmorillonite on strength and permeability of cement mortars. *Cement Concr Res* 2007; 36(5): 886–895.
42. Chang TP, Shih JY, Yang KM, Hsiao TC. Material properties of portland cement paste with nano-montmorillonite. *J Mater Sci* 2007; 42(17): 7478–7487.
43. Tregger N, Pakula M, Shah SP. Influence of micro- and nano-clays on fresh state of concrete. *J Transportation Res Rec* 2010; 1(2141): 68–74.
44. Collepardi M, Collepardi S, Skarp U, Troli R. Optimization of silica fume, fly ash and amorphous nano-silica in super plasticized high performance concrete. *Am Concr Inst* 2004; 495–506.
45. Li G. Properties of high volume fly ash concrete incorporating nano-SiO_2. *Cement Concr Res* 2004; 34(6): 1043–1049.
46. Jo BW, Kim CH, Tae GH, Park JB. Characteristics of cement mortar with nano-SiO_2 particles. *Constr Bldg Mater* 2007; 21: 1351–1355.
47. Osman MA, Mittal V, Lusti HR. The aspect ratio and gas permeation in polymer-layered silicate nanocomposites. *Macro Rapid Commun* 2004; 25: 1145–1149.
48. Karthikeyan CS, Nunes SP, Schulte K. Barrier properties of poly(benzimidazole)-layered silicates nanocomposite materials. *Adv Eng Mater* 2006; 8: 1010–1015.
49. Gain O, Espuche E, Pollet E, Alexandre M, Dubois P. Gas barrier properties of poly(ε-caprolactone)/clay nanocomposites: Influence of the morphology and polymer/clay interactions. *J Polym Sci, Part B: Polym Phys* 2004; 43: 205–214.
50. Kim JK, Hu C, Woo RSC, Sham ML. Moisture barrier characteristics of organoclay-epoxy nanocomposites. *Compos Sci Technol* 2005; 65: 805–813.
51. Osman MA, Mittal V, Morbidelli M, Suter UW. Epoxy-layered silicate nanocomposites and their gas permeation properties. *Macro* 2004; 37: 7250–7257.
52. Phelps HR, Long ER. Property changes of a graphite/epoxy composite exposed to nonionizing space parameters. *J Compos Mater* 1980; 14: 334–341.
53. ASTM Committee. ASTM D790-02 Standard test methods for flexural properties of unreinforced and reinforced plastics and electrical insulating materials 2002; 790–802.
54. Zainuddin S, Hosur MV, Zhou Y, Kumar A, Jeelani S. Durability studies of montmorillonite clay filled epoxy composites under different environmental conditions. *Mater Sci Eng A* 2009; 507: 117–123.
55. Zainuddin S, Hosur MV, Zhou Y, Narteh AT, Kumar A, Jeelani S. Experimental and numerical investigations on flexural and thermal properties of nanoclay–epoxy nanocomposites. *Mater Sci Eng A* 2010; 527: 7920–7926.
56. Ray BC. Effects of changing environment and loading speed on mechanical behavior of FRP composites. *J Reinf Plast Compos* 2006; 25: 1227–1240.
57. James FR. Durability of reinforced plastics in liquid environments. In: Pritchard G (ed.), *Reinforced Plastics Durability*, Cambridge, UK: Woohead Publishing, 1999, Chapter 3.
58. Brinson LC, Gates TS. Viscoelasticity and aging of polymer matrix composites. ln: Kelly A, Zweben C (eds), *Comprehensive Composite Materials*, Vol 2. Oxford, UK: Elsevier, pp. 333–368.

59. Kumar BG, Raman PS, Toshio N. Degradation of carbon fiber-reinforced epoxy composites by ultraviolet radiation and condensation. *J Compos Mater* 2002; 36(24): 2713–2733.
60. Regel VR, Chernyi NN, Kryzhanovskii VG, Boboev TB. Effect of ultraviolet radiation on the creep rate of polymers. *Mekhanika Polimerov* 1967; 3: 615–618.
61. Chowdhury FH, Hosur MV, Jeelani S. Studies on the flexural and thermomechanical properties of woven carbon/nanoclay-epoxy laminates. *Mater Sci Eng A* 2006; 421: 298–306.
62. Yuanxin Z, Farhana P, Mohammad AB, Vijaya KR, Jeelani S. Fabrication and characterization of montmorillonite clay-filled SC-15 epoxy. *Mater Lett* 2006; 60: 869–873.

22

Advanced fibre-reinforced polymer (FRP) composites for the rehabilitation of timber and concrete structures: assessing strength and durability

J. CUSTÓDIO and S. CABRAL-FONSECA, Laboratório Nacional de Engenharia Civil I.P. (LNEC), Portugal

DOI: 10.1533/9780857098641.4.814

Abstract: This chapter briefly discusses the performance and durability of bonded composite systems used for on-site rehabilitation of timber and concrete structures. In spite of some recent developments, the exploitation of their full potential is still often restrained by the lack of structural design guidance, standards for durability assessment and on-site acceptance testing. Therefore, this chapter provides a review of current understanding on the use of hybrid bonded composite systems on the construction site in terms of structural repair, reinforcement, and seismic retrofit. It focuses on the requirements and practical difficulties in the work on-site with regards to the performance and durability of the rehabilitated structure, the characteristics and requirements that must be fulfilled by structural adhesives and advanced polymer composite materials, and the subsequent need for quality control and in-service monitoring. It also highlights the factors affecting performance and durability of bonded joints. Finally, a general overview of the research needs and a bibliography giving references to more detailed information on this topic is given.

Key words: on-site bonded composite systems, repair, reinforcement and seismic retrofit, timber and concrete structures, limitations and requirements, performance and durability.

22.1 Introduction

The rehabilitation of buildings and civil infrastructures is becoming ever more important due to the historical value of the built heritage, mainly constructed using timber, and the need to maintain and improve the nation's vast built environment, particularly in developed countries that completed most of their structures, principally constructed using concrete, in the first half of the last century. Buildings and civil infrastructures routinely have a design working life in excess of 50 or 100 years (CEN, 2002). Therefore, it is inevitable that the material or materials used in the structural system will suffer some kind of degradation or modification so that it can no longer perform the function for which it was initially intended (Fig. 22.1); the

structure will suffer changes in its use so that it needs to carry loads higher than those originally specified (Fig. 22.2); the structure will be required to fulfil modern design practices, new service requirements and updated

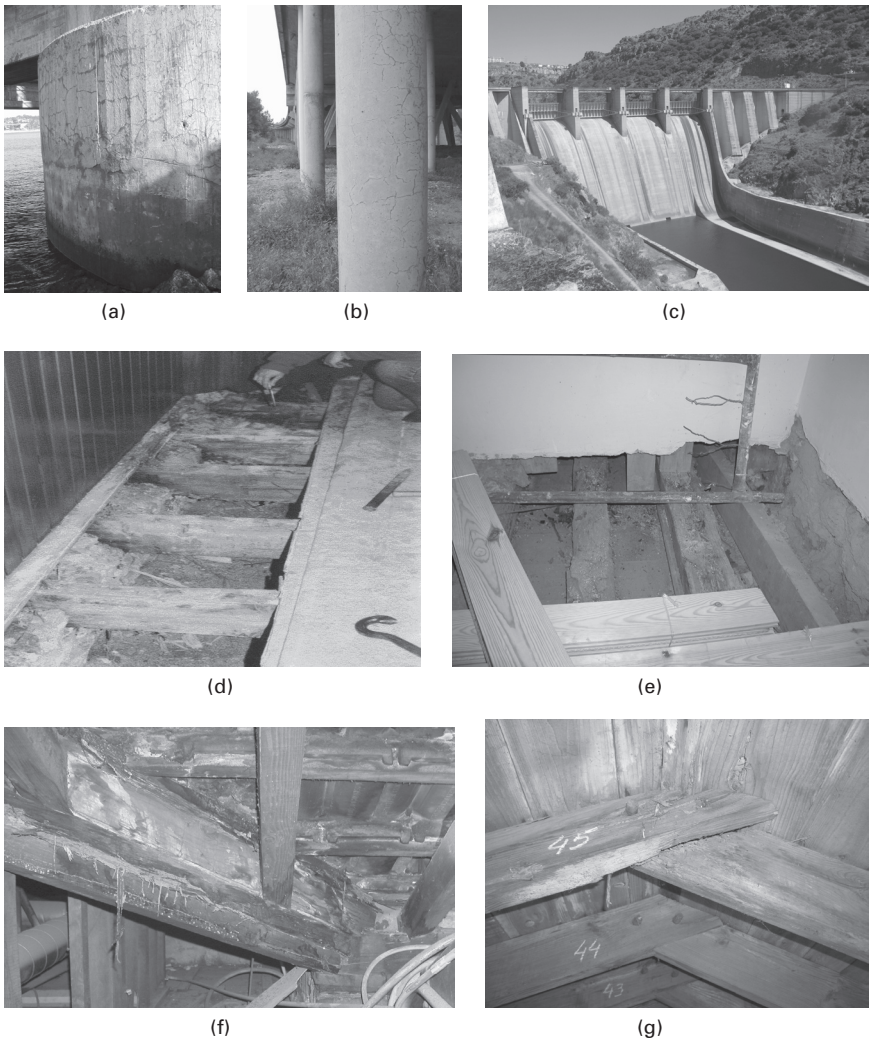

22.1 Deteriorated concrete in a bridge (a), a highway bridge (b) and a dam (c) due to alkali silica reaction; deteriorated timber structural members due to biological degradation – beam end decay in a floor system (d, e) and in a roof system (f, g, h); anomalies derived from inadequate modifications to the original design and construction – removal of members leading to a lack of continuity in a roof system (i, j) and loss of section of timber members due to the introduction of running water piping (k) (courtesy of António Santos Silva and Helena Cruz).

(h)

(i)

(j)

(k)

22.1 Continued

standards and construction codes. A deteriorated, functionally obsolete, structurally deficient or outdated infrastructure leads to increased costs for society in general; this places demands on owners and authorities to effect rapid maintenance and improvement on numerous existing structures, thus the development, implementation and widespread use of technologies that allow for effective, rapid, safe and cost-efficient rehabilitation of buildings and civil infrastructures constitutes one of the main challenges which the broad field of civil engineering faces nowadays.

The deterioration seen in Fig. 22.1(a), (b) and (c) is due to alkali silica reaction. This expansive internal reaction results in deleterious expansion and consequent opening of fissures and cracks in concrete, compromising its durability. It is a relatively frequent anomaly observed in large concrete civil infrastructures. Similarly common are the anomalies shown in Fig. 22.1(d), (e), (f), (g) and (h), where biological degradation leads to a significant reduction of section, loosening of joints, or excess deformation.

Composite rehabilitation systems (CRS), i.e., structural hybrid systems involving advanced polymer composite (APC) materials (generally referred to as fibre-reinforced polymer, FRP), structural adhesives (SA) and conventional construction materials (CCM) (e.g., timber, concrete, masonry, steel, iron), constitute one such technology.

One key area where CRS have proved their great potential is in the on-site rehabilitation of existing timber and concrete structures. Typical examples

22.2 Example of a structural anomaly common in heritage buildings – extra floors added to the original building.

of the application of CRS in timber structures include the use of plates or rods bonded into slots or drilled holes either to connect two timber sections or to improve strength and stiffness of timber members, and bonded-in rods inserted across the grain through a single timber section to repair or prevent delamination of glued laminated timber, drying fissures or cracks in joints. In concrete structures, CRS have been successfully used to reinforce concrete structural members, namely to enhance flexural strength of concrete beams and slabs, shear strength of concrete beams, and axial strength and ductility of concrete columns and walls. In addition to the strengthening for static load-carrying capacities, CRS have been used to retrofit concrete structures for earthquake-induced seismic loads.

Critically, CRS minimize disturbance to the structures during the intervention. This is achieved by taking advantage of a number of factors, including minimal intrusion into the original structure and disruption to its normal functioning by avoiding extensive displacement of materials; low mass; ease and speed of installation with minimum personnel and plant requirements; versatility to suit every situation; making the intervention invisible and shaping it to match the appearance of the original structure; completed work that is structurally efficient; and keeping the overall cost lower than that of an intervention using conventional construction materials

and involving the complete or partial demolition and rebuild of the structure (Custódio, 2009; Cabral-Fonseca, 2008).

Yet, despite these advantages, when compared with traditional methods and materials, CRS are perceived as being more expensive than the latter and, in general, they are only used by small specialized companies who are prepared to deviate from, or add to, traditional technologies to exploit the benefits associated with this technology.

Despite some relevant recent developments, the exploitation of the full potential for on-site CRS is still restrained at present by the lack of structural design guidance, codes of practice and specifications, standards for durability assessment and on-site acceptance testing. Additional factors, such as absence of an open-access comprehensive database on the mechanical and in-service properties of the SA and APC materials, lack of operative/supervision and management training and application techniques, relatively little experience in the use of SA and APC materials and consequent lack of confidence in their long-term performance – all in conjunction with a site methodology and quality control process, make it difficult for the practising civil engineer and designer to have the confidence to use CRS on a routine basis (Custódio, 2009; Cabral-Fonseca, 2008). But one should acknowledge that similar systems have been successfully used for more than 50 years (i.e., for as long as the expected service life for a common building) and CRS design is normally very conservative (Cruz and Custódio, 2010).

22.2 Composite rehabilitation systems (CRS)

There are two possible alternatives to restore or upgrade a deficient structure to the required standard (Fig. 22.3); these are complete or partial demolition and rebuild (replacement), or commencement of a programme of rehabilitation.

Within the scope of rehabilitation, it is essential that differentiation between repairing, strengthening and retrofitting terms is made (Hollaway and Head, 2001):

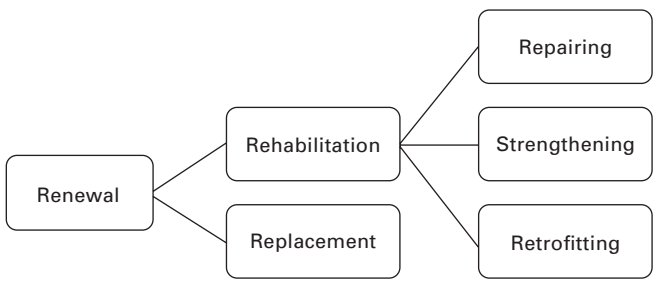

22.3 Renewal strategies (adapted from Karbhari and Seible, 2000).

1. 'Repairing' a structure refers to the improvement of the functional deficiency such as a severely degraded structural component.
2. 'Strengthening' a structure is specific to those cases where the action performed will enhance the existing designed performance level.
3. 'Retrofitting' is used to relate to the seismic upgrades of facilities, which is important in areas of high seismic risks.

Generically the aim of a structural rehabilitation is, as briefly mentioned before, to resolve one of the following situations:

- Deficiencies at the design stage, including design errors, inadequate factors of safety, use of inferior class materials and poor construction quality.
- Modifications made to a structure and changes of use, namely, increased safety requirements (upgrading of structural design standards), modernization that causes redistribution of stresses and increase of the applied load.
- Ageing of materials that compromise the load capacity of the structure.
- Accidents, such as fire damage or seismic events.

The materials, systems/applications and design/regulations presented in the following sub-sections are concerned primarily with the rehabilitation of timber and concrete structures. In spite of this, a brief section is also added to very succinctly discuss the use of composite rehabilitation systems in metallic and masonry structures.

22.2.1 Materials

Structural adhesives

A structural adhesive has several definitions. For instance, according to the European Standard EN 923 (CEN, 2005), it is defined as 'being capable of forming bonds capable of sustaining in a structure a specified strength for a defined long period of time'. The Adhesive and Sealant Council (ASC, 2006) has defined it as 'an adhesive of proven reliability in engineering structural applications in which the bond can be stressed to a high proportion of its maximum failing load for long periods without failure'. The American Standard ASTM D907 (ASTM, 2011) defines it as 'a bonding agent used for transferring required loads between adherends exposed to service environments typical for the structure involved'. Irrespective of the definition adopted, this group of adhesives encompasses those materials that typically provide tensile shear strengths of at least 4 to 10 MPa, and produce joints of such strength and durability that the integrity of the bond is maintained in the assigned service class throughout the expected life of the structure.

Adhesives used for on-site rehabilitation of timber and concrete structures must have good adhesion and produce strong and durable bonds to several different materials. They should produce negligible dimensional variation during curing, have relatively long open assembly time, be able to cure without pressure applied and at ambient temperature, and be only slightly sensitive to bond-line thickness variation. Depending on the application, gap-filling properties and/or thixotropy might also be required.

Epoxy adhesives, whilst not ideal, are currently the best generic adhesive type, particularly as a family of adhesives, for on-site rehabilitation operations. The epoxy adhesive family include a wide variety of products with quite different properties. For instance, they may exhibit good gap-filling properties, excellent tensile/shear strength, high dry and wet strength, and excellent moisture, chemicals and solvent resistance, and can be formulated to exhibit thixotropy. They are generally available as two- or three-component adhesives, grouts or mortars. Therefore, suitable formulations need to be identified for each application. Thixotropic epoxies are convenient when the adhesive has to be applied from below or on vertical surfaces. Epoxy grouts are employed to fill large volumes and should, therefore, be able to eliminate trapped air bubbles, should not stratify, should exhibit a low cure exotherm and should be self-levelling.

Epoxy adhesives do not require high pressure during their application and curing, they can be reasonably tolerant with regard to bond-line thickness variation and, unlike other traditional generic adhesive types, epoxy adhesive families can also be produced to cure under a wide variety of ambient conditions – all essential requirements for *in-situ* use. Unfortunately, epoxy adhesives have poor peel strength and may delaminate with repeated wetting and drying, especially when applied on wood substrates.

Therefore, in terms of the rehabilitation of timber structures, epoxy adhesives are generally regarded as structural adhesives for limited exterior service environments (Broughton and Custódio, 2009), corresponding to service classes 1 and 2 as defined in Eurocode 5 (CEN, 2004a). Service classes 1 and 2 are characterized by a moisture content in the materials corresponding to a temperature of 20 °C and the relative humidity of the surrounding air only exceeding, respectively, 65 % and 85 % for a few weeks per year; meaning the average moisture content in most softwoods will not exceed 12 % in service class 1 and 20 % in service class 2. Toughened acrylic and some new two-component polyurethane adhesives are also classified as structural adhesives for limited exterior service environments (Broughton and Custódio, 2009). Limited exterior service environments include heated and ventilated buildings, as well as exteriors protected from weather or exposed to weather only for short periods, situations for which both adhesive types I and II defined in the European Standard EN 301 (CEN, 2006) are acceptable.

Concerning the rehabilitation of concrete structures, the adequacy of a structural adhesive is generally assessed by ensuring that the failure in a given configuration occurs cohesively in the concrete instead of cohesively in the adhesive or adhesively at the interfaces. For this reason their shear and tensile strengths must be at least as high as that of the concrete. Moreover, the correct surface preparation of the concrete is of great importance for achieving a good adhesive interface.

APC materials

The APC materials typically used for on-site rehabilitation of timber and concrete are composed of glass, carbon or aramid fibres and a polyester, epoxy or polyurethane polymeric matrix. Glass fibres are the most frequently used due to their moderate cost and good mechanical properties when compared to carbon fibres. They are used normally in the form of pultruded profiles or strips, fabrics (tissues) or mats. Carbon fibres are mainly used in the form of pultruded profiles of solid, open or hollow cross-sectional shapes. While in timber applications both thermoplastic and thermosetting matrix types are used, in concrete applications only the latter type is used.

The main advantages of APC materials for the on-site rehabilitation of timber and concrete structures can be summarized as follows: high strength and rigidity at low weight; good durability in most environments; corrosion resistance; good resilience; readily formed into complex shapes; low thermal conductivity; ability to tailor the mechanical properties by fibre choice and direction; and aesthetics. Composite profiles are regarded as lighter and easier to handle, cut, clean and use on-site than steel connecting materials. Their major disadvantage is still their high price compared with other civil engineering materials.

In applications involving the use of bonded-in rods, strips or plates to rehabilitate timber structures, metallic threaded rods, ribbed bars or textured plates are often preferred over APC, due to their lower cost and to the fact that practitioners prefer to rely also on the mechanical interlocking provided by the thread, ribs or texture to the bonding strength. However, as steel should be protected against corrosion, especially when used with acidic timbers like oak, stainless steel or hot-dip zinc-coated steel is frequently used instead. Stainless steel may give poor adhesion and is therefore normally surface coated for improved roughness and adhesion. If hot-dip zinc-coated steel rods or bars are used, the application of a priming product to improve adhesion is normally required. Surface preparation is particularly critical in uncoated steel and should preferably include grit blasting and cleaning with an adequate solvent to remove oil, grease, salts, dirt or other contaminants (BS EN ISO 12944-4, 1998; BS EN ISO 8504-1, 2001; BS EN ISO 8504-2, 2001). Furthermore, there are already available in the market APC products

in the form of threaded rods, ribbed bars or textured plates, although at a higher cost.

22.2.2 Systems/applications

Structural rehabilitation of timber and concrete structures with composite systems can be generally accomplished in one of two ways (Karbhari and Seible, 2000): using wet lay-up or cured *in-situ* systems, by application of composite overlays, fabrics, sheets or fibre tows (Fig. 22.4); and using systems involving the bond of prefabricated APC materials, such as straight pultruded strips, and factory-made curved or shaped elements (Fig. 22.5).

In wet lay-up systems the FRP elements are used as 'dry', which means without resin, or already pre-impregnated (but only with a small amount of resin, not enough to ensure the bond between FRP and the substrate). The application of the adhesive is required not only to bond fibres to the adherend, but also to impregnate and provide shape and consistency to the FRP. Usually the adhesive for this type of application is a low viscosity resin that permits bonding and impregnation of multiple layers. This technique gives the maximum flexibility but presents the most variability. In systems involving bonding of prefabricated APC materials, the FRP elements are provided as fully cured composites with their final shapes, strength and stiffness, usually as thin strips, laminates, or rods. In this case the structural adhesive is mainly responsible for the bond between FRP and the adherend.

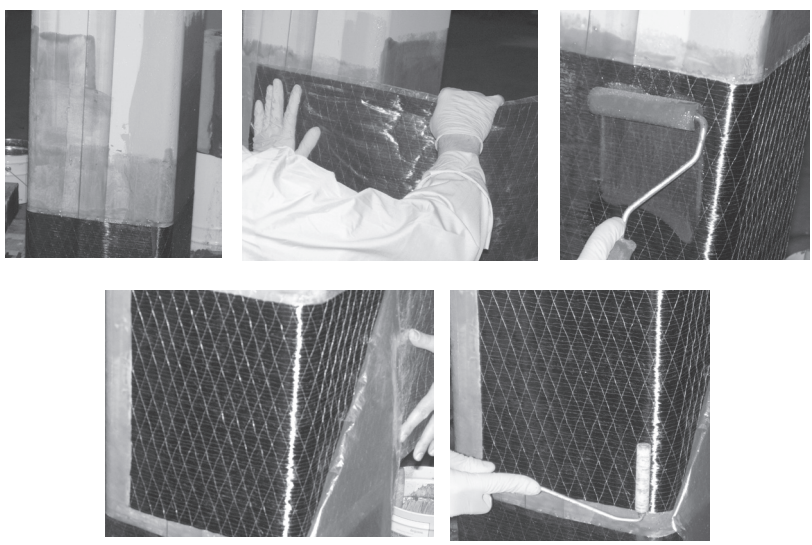

22.4 Wet lay-up technique.

22.5 FRP strip bond technique.

The main applications of composite rehabilitation systems in the rehabilitation of timber structures are described in Table 22.1 and Fig. 22.6, and of concrete structures in Table 22.2 and Fig. 22.7.

Besides the most common aforementioned techniques, several special techniques and applications have been recently developed, namely:

- Mechanically fastened FRP (MF-FRP): FRP composites, in the form of laminates or strips, are attached to concrete using closely spaced steel fastening pins and anchors.
- Near-surface mounted FRP (NSM-FRP): FRP composite, usually a bar or a strip, is embedded into a groove cut on the concrete surface, with a high-viscosity epoxy or cement paste.
- Pre-tensioning and post-tensioning systems using APC materials to rehabilitate concrete structures.
- Pre-stressed timber structural members with APC materials (this technique would allow for an increase of the economic efficiency of the reinforcement using APC materials in comparison to their use as a passive reinforcement only, because its final service stress may be substantially increased).

Table 22.1 Main applications and techniques used to rehabilitate timber structures with CRS

Application	Technique	Examples	Alternative techniques[1]
Repair of fissures and delamination in structural timber members	Repair by structural adhesive injection into fissure or delamination together with internal FRP rod bonding.	Correction of fissures and delamination in glued-laminated timber beams (Fig. 22.6(a)).	Total replacement of the affected structural timber element; addition of mechanically fastened metallic external bracing; repair by use of self-tapping screws; etc.
Repair of deteriorated structural timber members	Partial reconstruction of timber structural members by replacing the affected timber with epoxy grout cast on-site into a permanent timber formwork; or, preferably, local replacement of affected timber with a new timber splice or prefabricated timber-resin splice; in both cases, they are connected to the remaining sound timber by internal FRP bonding (plates or rods).	Repair of decayed timber beam ends (Fig. 22.6(b); e.g., in roof and floor systems).	Total replacement of the affected structural timber element; replacement of the affected timber with new timber connected to the remaining sound timber by mechanically fastened metallic plates or profiles (internal or external); external addition of metallic plates or profiles mechanically fastened to the sound timber; etc.
Repair of connections between deteriorated structural timber members	Replacement of whole joint area by a new solid structural node made with cast-in epoxy grout, connected by internal FRP bonded rods to sound timber parts; a much better alternative, although requiring more time and means and more skilled operators, is the individual repair of the members meeting in the joint, thus maintaining the original joint behaviour.	Repair of decayed timber connections (Fig. 22.6(c); e.g., in roof trusses).	Total replacement of the affected structural timber elements involved in the connection; replacement of the affected timber with new one connected to the remaining sound timber by mechanically fastened connectors and metallic external bracing; etc.
Reinforcement of structural members	Reinforcement by internal or external bonding of prefabricated APC materials (rods, plates or pultruded profiles) or by wet lay-up of fabrics or sheets.[2,3]	Strengthening of beams or truss members to overcome insufficient strength or stiffness (Fig. 22.6(d) and Fig. 22.6(e)). Perpendicular	Addition of mechanically fastened metallic internal or external plates and/or profiles; introduction of a new support system in the structure; introduction of structural members next

		to wood grain reinforcement of glued-laminated timber members.	to the existing ones; addition of new timber lamellas mechanically fastened to the existing member; etc.
Reinforcement of connections between structural elements	Reinforcement of the connection by internal or external bonding of prefabricated APC materials (rods, plates or pultruded profiles) or wet lay-up of fabrics or sheets.[2,3] Perpendicular to wood grain reinforcement of the timber member, in the connection, by internal or external bonding of prefabricated APC materials (rods, plates or pultruded profiles) or wet lay-up of fabrics or sheets. [2,3]	Reinforcement of timber joints (Fig. 22.6(f); e.g., in roof trusses). Perpendicular to wood grain reinforcement of a timber member in a mechanical joint (Fig. 22.6(g)).	Addition of mechanically fastened internal or external metallic connectors, bracings, gusset plates; etc.
Seismic retrofit	Improvement of global seismic behaviour by bonding of prefabricated APC materials (rods, plates or pultruded profiles) or by wet lay-up of fabrics or sheets to reinforce the structural elements (e.g., walls, floors, roof) and to improve the connections between them, thus enhancing the overall behaviour of the structure.[2,3]	Seismic retrofit of historical structures with masonry walls (Fig. 22.6(h)).	Use of metallic cables, tendons and mechanical anchoring devices; addition of new structural members; improvement of connections between structural elements with mechanically fastened metallic plates, profiles or other connecting devices; etc.

[1] The techniques presented are only general examples, the most adequate technique for a specific situation will vary from case to case. Moreover, there may be cases for which one or more techniques may be adequate or even none may be applicable.
[2] Rods are only used internally or near surface mounted.
[3] The use of this method to wrap around timber members is not recommended, because the resulting sharp angles of the composite (in the case of rectangular cross-sections) will create high stress concentration that may lead to a premature failure.

Further information on the techniques presented (limitations, advantages, disadvantages, etc.) may be obtained from Cruz and Custódio (2010), Machado *et al.* (2009), Cóias (2007), Cruz *et al.* (2000), Paula and Cóias (2006) and Appleton (2003, 2005).

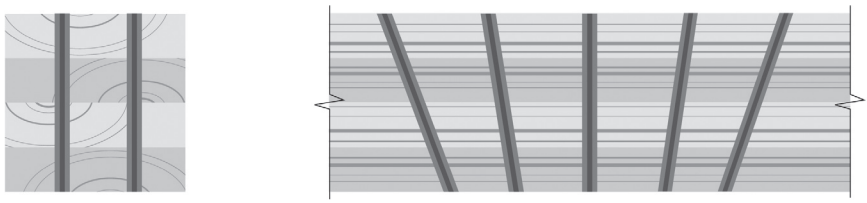

(a)

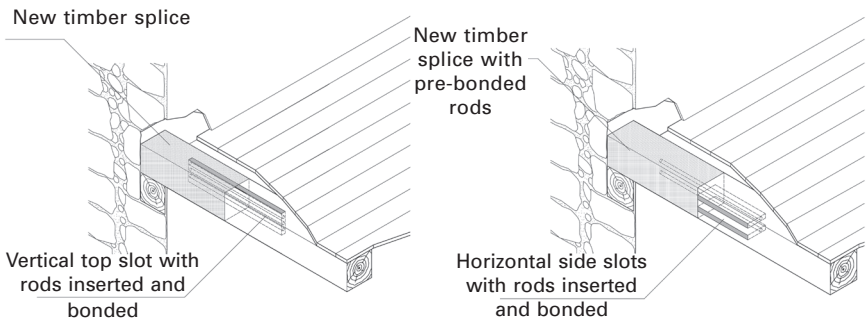

(b)

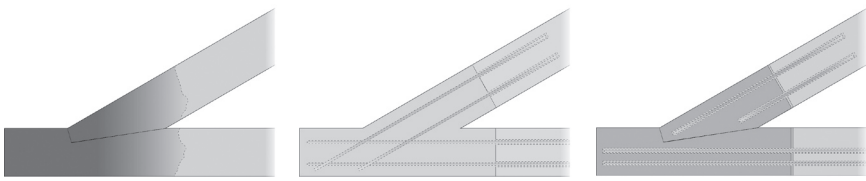

(c)

22.6 Examples of applications and techniques used in the rehabilitation of timber structures with CRS. (a) Correction of fissures and delamination in glued-laminated timber beams (adapted from LICONS, 1999). (b) Example of two techniques for the repair of decayed timber beam ends (courtesy of Cóias, 2007). (c) Example of two techniques for the repair of decayed timber connections (courtesy of Pedro Palma). (d) Example of five techniques for the strengthening of beams or truss members to overcome insufficient strength or stiffness (adapted from LICONS, 1999). (e) Flexural reinforcement of beams above decorative ceilings using bonded-in rods (left) and externally bonded laminates (right) (courtesy of Cóias, 2007). (f) Reinforcement of timber joints through the external bonding of FRP sheets or fabrics (courtesy of Cóias, 2007). (g) Reinforcement perpendicular to wood grain of mechanical joints in timber structures (courtesy of Pedro Palma). (h) Seismic retrofit of historical timber structures – example of a timber floor reinforced with bonded FRP strips (courtesy of Cóias, 2007).

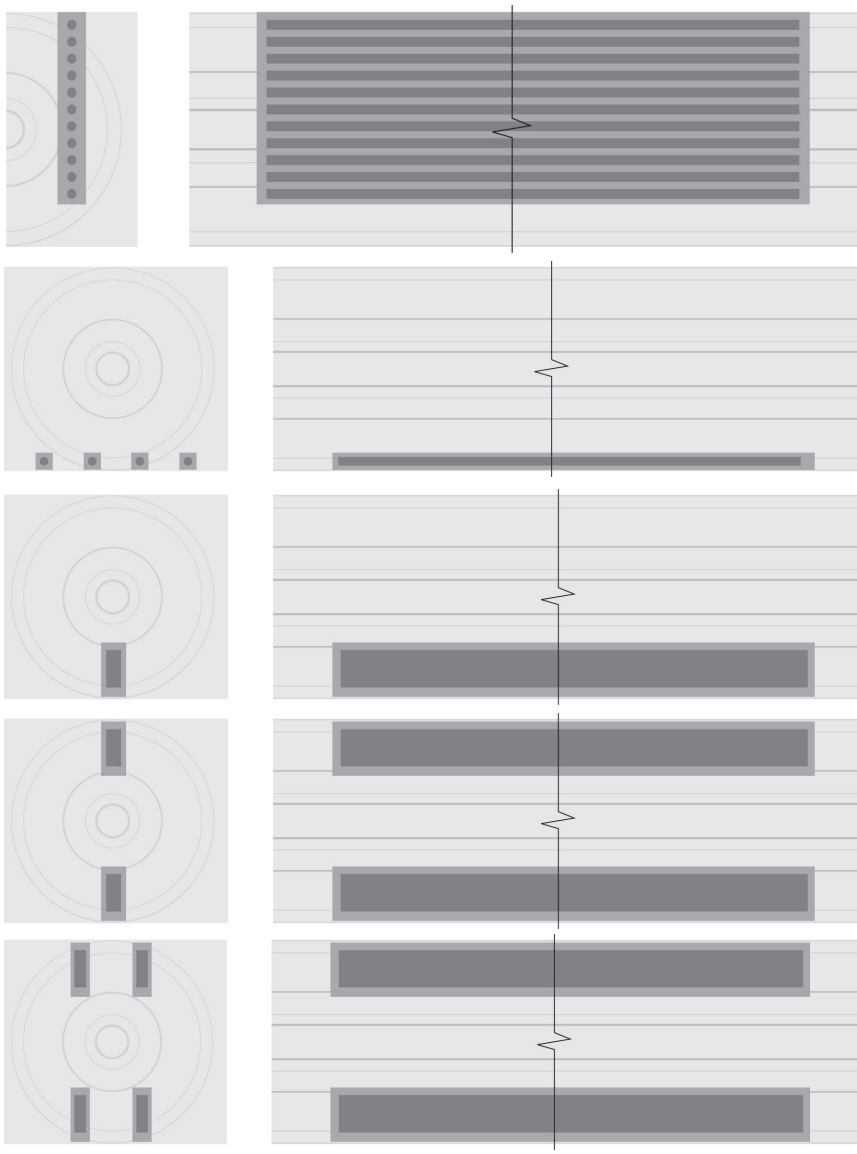

(d)

(e)

22.6 Continued

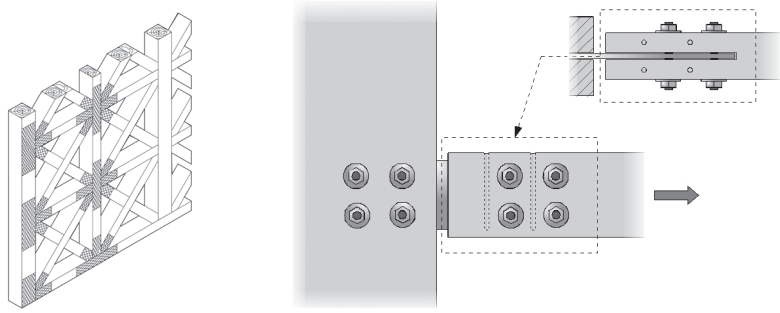

(f) (g)

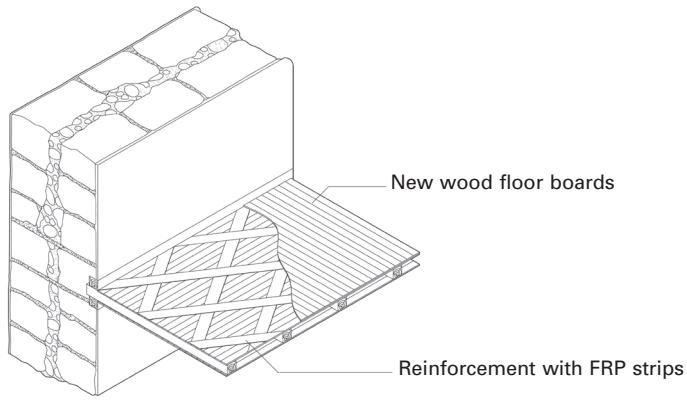

(h)

22.6 Continued

- Structural timber–concrete composites (e.g., timber–concrete composite slabs and timber wall–concrete deck composite in which the connection between the two common construction materials is made through a bonded joint). The aim is to replace traditional mechanical fasteners by an adhesive connection, which has several advantages in comparison with the former: for instance, a bonded joint is able to distribute the applied load over the entire bonded joint area, resulting in a more uniform distribution of stress (compared to mechanical point connections), requires little or no damage to the adherends, adds very little weight to the structure, and has a superior stiffness and fatigue resistance.
- Structural pre-fabricated engineered wood composites (e.g., FiRP® reinforcement technology used to produce structural members, beams and I-beams, made from derived wood products, such as glulam and laminated veneer lumber (LVL) with an internal bonded passive reinforcement, like CFRP, GFRP or AFRP). The reasoning behind its development was to allow the use of smaller cross-sections, to obtain more homogeneous

Table 22.2 Main applications and techniques used to rehabilitate concrete structures with CRS

Application	Technique	Examples	Alternative techniques[1]
Flexural strengthening	Reinforced concrete beams, columns or slabs are strengthened in flexure through the use of FRP elements applied in their tension zones, with the direction of fibres parallel to that high tensile stress.	• Wet lay-up of FRP sheets. • Attaching prefabricated FRP sheets or strips (Fig. 22.7(a)). • Attaching pre-stressed FRP strips. • Bonding FRP strips inside concrete slits. • FRP impregnation by vacuum. • *In-situ* fast curing using heating device.	(i) Internal structural repair – resin injection into crack restores the concrete section (slabs or walls) to its pre-cracked condition. (ii) Interior reinforcement – installation of metallic dowels into holes using a bonding matrix used to strength of concrete cracked. (iii) Exterior reinforcement (encased and exposed) – external flexural, shear and torsion reinforcement for beams and girders using steel plates or straps bonded or attached using bolts. (iv) Exterior post-tensioning – restore flexural and shear strength by addition of external post-tensioning (metallic tendons, rods or bolts). (v) Jackets and collars – repair of deteriorated columns and piers by surrounded it by jackets or collars. (vi) Supplemental members – installing new structural elements, such as columns, beams, braces or infill walls to help support the damage structure.
Shear strengthening	Shear strengthening of reinforced concrete elements using FRP may be provided by bonding the external reinforcement with fibres parallel to the principal tensile stresses, around 45° to the member axis, so that the effectiveness of FRP is maximized.	• Prefabricated U or L shape strips for shear strengthening, used for slabs/beams or slabs/columns joints (Fig. 22.7(b)). • The different types of wrapping schemes to increase the shear strength of a beam or column. • Automated winding of wet fibre under a slight angle around columns and other structures such as chimneys.	
Axial strengthening and confinement	Confinement is usually applied to concrete members in compression to enhance their axial load capacity and ductility.	• Bonding layers of axial and/or hoop FRP fabrics to the column perimeter (Fig. 22.7(c)). • Wet lay-up laminates or prefabricated elements with a defined shape (shells or jackets) can be used for confinement of circular or rectangular columns. • FRP wrapping for axial compression strengthening and ductility enhancement (Fig. 22.7(d)).	

[1]Further information on the techniques presented may be obtained from ACI (2004).

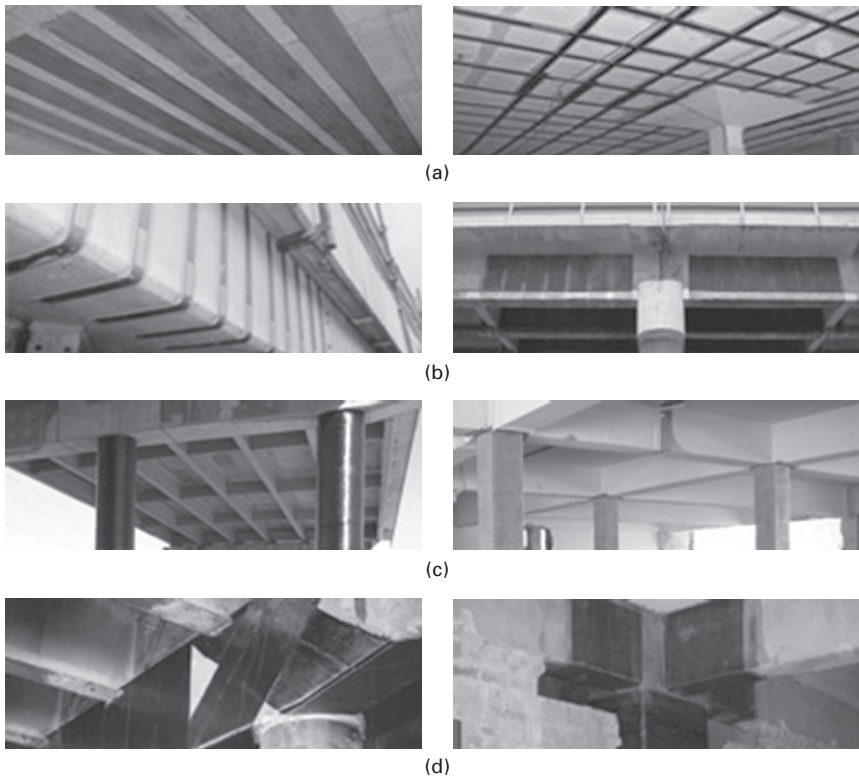

22.7 Examples of applications and techniques used to rehabilitate concrete structures with CRS (SIKA, 2012): (a) increasing bending moment capacity with CFRP plates; (b) increasing shear capacity with CFRP L-shape and FRP fabrics; (c) strengthening of axially loaded members with CFRP and GFRP; (d) increasing ductility of beams, columns and nodes for seismic retrofitting.

structural properties, higher safety as a result of bonded-in FRP lamellas, wider truss spacing, reduced foundation costs, use of lower grade timber, and reduced transport volume (WSTI and WCE, 2012).

22.2.3 Design/regulations

As already evidenced in the above text, currently and at a European level, no well-established design and detailing calculation methods embracing all techniques have been developed for the on-site use of composite rehabilitation systems in timber and concrete structures. Nevertheless, the development of suitable design guidance standards is far more advanced in the case of the rehabilitation of concrete structures than of timber structures. Therefore, for most applications the designers of timber structures composite rehabilitation

works will have to rely mostly on their individual skills and expertise to adequately design and detail the rehabilitation intervention. However, due to the great deal of attention that the European scientific community has devoted to this topic in the last couple of years, general guidelines are already available that can be followed for projects of structural rehabilitation, especially in the specific context of old buildings that belong to the cultural heritage, namely in the *Timber Engineering STEP* manual (Blass *et al.*, 1995a, 1995b); the COST E34 Core Document (Dunky *et al.*, 2008); the Low Intrusion Conservation Systems for Timber Structures Project website (LICONS, 1999); Eurocode 5 'Design of timber structures' (CEN, 2004a); and the Italian Standard UNI 11138 'Cultural heritage – Wooden artefacts – Building load bearing structures – Criteria for the preliminary evaluation, the design and the execution of works' (UNI, 2004). The research on the rehabilitation of timber structures is still an active domain and more relevant information will be produced by the recently started COST Actions 'FP1004 Enhance mechanical properties of timber, engineered wood products and timber structures' and 'FP1101 Assessment, Reinforcement and Monitoring of Timber Structures', as well as the RILEM technical committee 'Reinforcement of Timber Elements in Existing Structures' (RILEM, 2012a).

Concerning the rehabilitation of concrete structures, the designer has a more facilitated task, because there are available many more sources of guidance, including several design codes elaborated by the Fédération Internationale du Béton (FIB, 2001), the British Concrete Society (Loudon and Clarke, 2012; Clarke and Hutchinson, 2003), the American Concrete Institute (ACI, 2008) and the Japan Society of Civil Engineers (Maruyama, 2001). Even so, one has to acknowledge that the available documentation does not cover all the existing applications. A detailed list of guidance documentation on this topic can be found in Section 22.6.

22.2.4 Case studies

Reinforcement of connections between structural elements

The building is a 200 m long × 120 m wide oval form enclosing a single volume, consisting of a glued laminated timber structure roof system fixed to the concrete foundations by means of pinned joints. The hall roof includes 15 glulam two-hinged, arched, portal truss frames spaced 9 metres on centre with spans ranging from 52 up to a maximum of 114 metres between bearings. To follow the irregular shape of the plan and roof surface, each portal truss is geometrically set out with top and bottom chords (with cross sections of 630 × 600 mm and 630 × 1500 mm, respectively. Each arch is fixed to the concrete foundations by means of pinned joints placed in the deambulatory, the area that surrounds the main hall. The glulam is made from Norway

spruce (*Picea abies* (L.) Karst.) and a type I adhesive (suitable for indoor and outdoor environments), and it was surface treated with a preservative product to provide suitable fungicide and insecticide protection.

Structural analysis showed the need to reinforce a number of joints in the top chord of one of the truss arches (Fig. 22.8) to enhance their resistance to wood splitting perpendicularly to the fibres. The perpendicular to wood grain reinforcement of the timber member, in the connection, was performed by internal bonding of threaded rods. These rods were inserted perpendicularly to the existing metallic fasteners close to the beam end (Fig. 22.9). Three rods were used per joint, located just after the beam joint fasteners (Fig. 22.10). The threaded rods, having a diameter of 16 mm, were bonded into

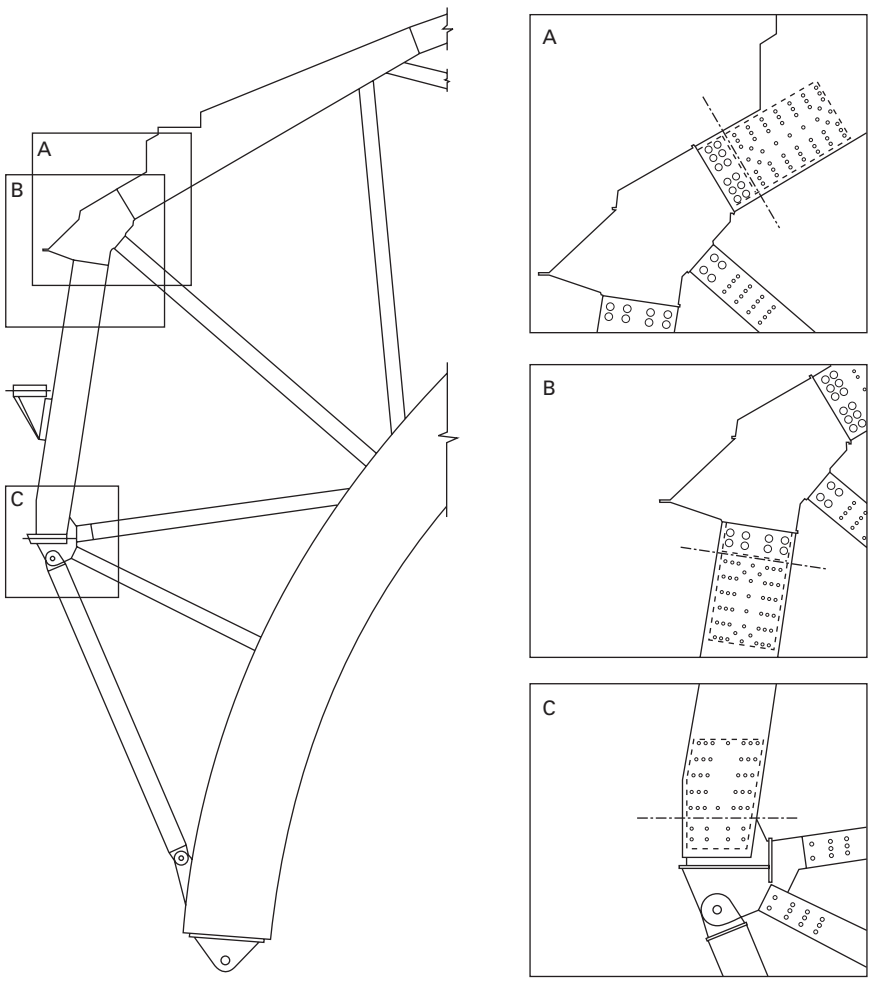

22.8 Rehabilitated truss arch exhibiting the three reinforced connections (courtesy of Helena Cruz and Pedro Palma).

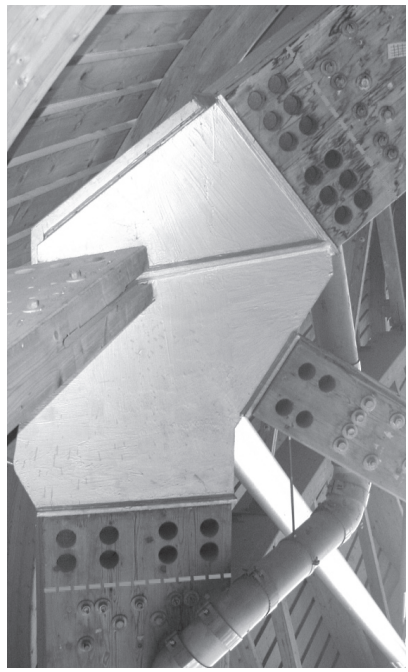

22.9 Photograph of the connection and the location of the reinforcements (courtesy of Helena Cruz and Pedro Palma).

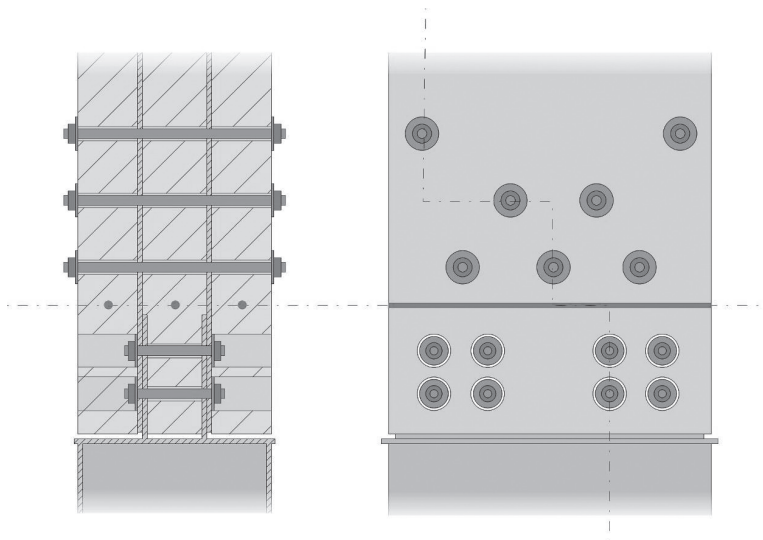

22.10 Schematics of the connection and the reinforcement scheme adopted showing the location of the three rods (courtesy of Pedro Palma).

pre-drilled holes having a diameter of 18 mm, using a two-component thixotropic epoxy structural adhesive.

Repair of deteriorated structural timber members

As part of the rehabilitation intervention, which included strengthening, structural consolidation and repair of the roof of the main building of Quinta do Calvel, a composite system was used to repair deteriorated structural timber members. These repair works were carried out by 'STAP – Reparação, Consolidação e Modificação de Estruturas, S.A.' in the scope of the European Project 'LICONS – Low Intrusion CONservation Systems for Timber Structures' (STAP, 2005; Raquel and Cruz, 2006; LICONS, 1999).

The Quinta do Calvel is composed of several neighbouring buildings of different usage (Fig. 22.11). The main building, the one involved, is constituted by a sub-basement, a basement, a ground floor and a first floor. Below the ground level the building is composed of stone masonry walls supporting a system of vaults made of ceramic bricks. Above ground, there is some continuity in the load-bearing stone masonry walls, with light wood frame partition walls. The flooring system is composed of timber beams and wood floorboards. The ends of two timber beams, at the ground floor, were severely deteriorated due to decay originated by subterranean termites and, therefore, were subject to a repair procedure.

The project took into account that all the works should be carried out

22.11 View of the main building and stables at the Quinta do Calvel (courtesy of STAP, 2005).

from below the floor level in order to avoid the removal and subsequent recovering of the floorboards. The technique and the materials that were adopted in this intervention have made possible the restoration of the beams without increasing the load and without removing the whole beams, which would be unnecessary in this case, as the timber deterioration was localized at the beam ends.

The rehabilitation solution used to repair the ends of the beams consisted in the replacement of the deteriorated timber part with a prefabricated solid timber splice connected to the remaining sound timber by bonded-in rods. The materials used were a two-component structural epoxy adhesive, pultruded rods (consisting of a polyurethane matrix reinforced with unidirectional glass fibres, rod diameter of 16 mm) and a three-component structural epoxy grout. The procedure adopted consisted roughly of the following steps: (1) propping the beams and scaffolding installation; (2) cutting off the deteriorated beam part to reach sound timber; (3) fabrication of the permanent timber splice; (4) drilling three horizontal holes in the remaining sound timber to insert the connecting rods; (5) careful cleaning of the surfaces to be bonded from dust and debris; (6) partial injection of the adhesive into the holes; (7) cleaning up and insertion of rods; (8) placing timber splice and checking its alignment with the remaining beam; (9) injection of the grout into the splice slots; (10) disguising of the slots; and (11) removal of the temporary supports after complete cure of the adhesive products. Figs 22.12 to 22.15 show some of the aforementioned steps.

The quality plan designed for this intervention included also expedite tests to detect possible faults in the works, especially those related to the application of epoxy products. The tests performed were the ones suggested in parts 2 and 3 of the standard proposal 'Adhesives for on-site assembling or restoration of timber structures. On-site acceptance testing' developed by working group 11 of the European Committee for Standardization (CEN, 2003a, 2003b). These consisted of assessing the adhesive joint's compressive shear strength (Fig. 22.16) and the tensile proof-loading of the bonded-in rods (Fig. 22.17). To accomplish this, specimens were produced on-site, at the same time as the intervention proceeded and using the same materials as the repair work, and then tested at the laboratory of LNEC's Timber Structures Division (more details on the results can be obtained from Raquel and Cruz, 2006).

Flexural reinforcement of a concrete structure

A composite system was used to rehabilitate a concrete bridge deck. The reinforcement works were carried out in the scope of a pioneer research project in Portugal in this area, promoted by the Portuguese Innovation Agency, named 'Strengthening of bridges with advanced composite –

22.12 Cutting off and removal of deteriorated wood (courtesy of STAP, 2005).

22.13 Adhesive injection into the holes to install the rods (courtesy of STAP, 2005).

Carboponte' (AdI, 2000). This project involved several national institutions and a rehabilitation company which performed the works.

The structure involved is a pre-stressed concrete bridge built 30 years ago in the north of Portugal. The bridge deck has a total length of 250 m with

22.14 Rod insertion into the beams (in the remaining sound wood) (courtesy of STAP, 2005).

22.15 Grout injection into the slots (courtesy of STAP, 2005).

five simply supported spans. The 12 m wide girder consists of a bicellular box of variable height.

Several years after construction, extensive longitudinal cracking on the underside of the top slab was detected during an inspection. Therefore, to

22.16 Specimen test preparation for shear strength tests (courtesy of STAP, 2005).

22.17 Specimen preparation for proof-loading tests (courtesy of STAP, 2005).

address this situation a flexural reinforcement was applied to the bridge deck in the year 2000. The reinforcement work consisted in the external bonding of thin strips of unidirectional pultruded CFRP to the bottom side

of the slab (Fig. 22.18), after the application of a negative moment to the bridge, through a pre-tensioning system, in order to close the cracks. The pre-tensioning was maintained for several days until the epoxy adhesive had cured completely.

The reinforced area was instrumented with special devices and data loggers to measure deformations and tensions, as well as environmental conditions. This allowed the in-service monitoring of the evolution of the behaviour of the composite system. Since then, several Portuguese researchers have been involved in the in-field characterization and health monitoring of the bridge, e.g., Silva (2008).

22.3 Metallic and masonry structures

The use of CRS on metallic and masonry structures has received less attention by the research community than concrete structures and there have been fewer practical applications; therefore, even though the present chapter is dedicated to timber and concrete structures, this section also gives a brief outline on the use of composite rehabilitation systems in metallic and masonry structures.

22.3.1 Metallic structures

The first known use of FRP composites to strengthen metallic structures was in the early 1980s when fatigue cracks were repaired in the aluminium superstructure of Type 21 frigates with CFRP and epoxy patches. Since then, this technology has been used for the repair of pipelines in the offshore industry, for strengthening metallic bridges and other steel or iron structures (cast and wrought, often of historical importance). CRS are very useful materials for repairing or strengthening iron and steel structures,

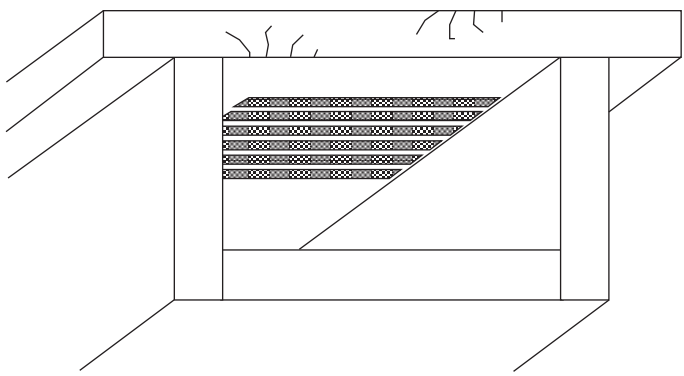

22.18 Schematics of the intervention.

because they have good corrosion and fatigue resistance and they offer a non-invasive method of rehabilitation which eliminates the need for bolting or welding, which is a problem for cast iron structures. As for timber and concrete structures, they can offer significant advantages over conventional rehabilitation techniques as they can be rapidly installed and often the requirements for temporary works are significantly reduced, as the bonding operation can frequently take place with no or minimal disruption to traffic or occupants and without a need for temporary propping, which makes them particularly attractive where there are severe access constraints or high costs associated with installation time. Furthermore, the high strength to weight ratio of the APC materials often leads to significant reductions in the cost of strengthening when compared to rehabilitation interventions made using CCM (e.g., steel or concrete). Typically, APC materials, more specifically high modulus or ultra-high modulus CFRP or AFRP, are used for repairing or strengthening iron and steel structures where they are bonded, with epoxy adhesives, to the surface of the structural element to enhance its strength or stiffness. Normally, a metallic structure will require repair or strengthening to overcome one or more of the following structural deficiencies: lack of axial tension capacity; lack of flexural tension capacity; lack of shear capacity; insufficient stiffness causing excessive deflection, inadequate buckling capacity or excessive dynamic response; and reduced service life caused by deterioration of structural elements or failure of connections (e.g., due to corrosion, impact or fatigue). The main application to date has been the flexural strengthening of structures through the use of FRP bonded externally to the tension flanges of metallic beams (e.g., cast iron girders in masonry bridges or buildings) (COMPCLASS, 2005; Forde, 2009).

Where uncertainties exist concerning the effectiveness of a CRS for a particular application, appropriate experimental testing on representative specimens needs to be undertaken to prove the effectiveness of the technique, comprehensive quality control and in-service inspection and maintenance plans should also be implemented. Examples where this might be required include the use of a material with significantly different properties from those used in previous studies or applications, the use of an approach or system which is new or for which there is limited experimental work (e.g., enhancement of fatigue life, shear capacity, bearing capacity or buckling resistance of metallic elements, or the enhancement of the capacity of connections using externally bonded FRP), or bonding onto an irregular, curved or deteriorated surface. The main rehabilitation techniques used are as follows: prefabricated FRP plates or strips bonded onto the degraded member with ambient-cure structural adhesive; wet lay-up systems, made from prepreg sheets or woven fabrics bonded to the degraded member with ambient-cure structural adhesive; vacuum infusion (e.g., resin infusion under flexible tooling, RIFT, process); *in-situ* prepreg lamination (the hot-melt

FRP prepreg/adhesive film are placed onto the structural member and both components are then cured under vacuum at high temperature); and filament winding such as automated wrapping of columns. When using CRS with metallic substrates special attention should be given to the substrate condition and pre-treatment, the service temperature, the risk of galvanic corrosion when using CFRP systems (the FRP should be electrically isolated from the metallic substrate) and the in-service monitoring, in which regular inspections are undertaken to confirm the continuing serviceability of the CRS system (Cadei *et al.*, 2004; Tilly *et al.*, 2008; Harries, 2011; DfT, 2008). Design guidance on the use of CRS with metallic structures is relatively scarce and dispersed, but relevant design guidance is given by Cadei *et al.* (2004), Moy (2001), Mosallam (2011). Sources for a more detailed description of the use of CRS with metallic structures can be found in Section 22.6.

22.3.2 Masonry structures

Unreinforced masonry (URM) structures have been and continue to be common practice in building construction throughout the world. Masonry is used in flexural applications such as retaining walls, roof and floor beams, and lintels; however, its main application has been in load-bearing walls or columns primarily resistant to compression loads. Masonry structures are often prone to damage or deterioration due to temperature changes and exposure to moisture and other environmental factors. In addition, URM structures, especially those having an historical character, have been shown to be very vulnerable and often not able to resist major events such as earthquakes, severe wind pressures, blasts and impacts. Furthermore, factors such as change in use, deterioration, or an increase in lateral-load demand, may also generate the need to undertake structural rehabilitation. ACM, if used properly, can be employed to address a number of these problems in service and to provide more durable, more ductile and stronger masonry systems (Motavalli and Czaderski, 2007; Shield *et al.*, 2005; Tumialan *et al.*, 2009).

Conventional repair and strengthening systems include external steel plate bonding, reinforced concrete overlays, span shortening with steel sub-framing or bracing, internal steel reinforcement and external post-tensioning (ACI, 2010). These techniques have several disadvantages over CRS, namely difficulty in manipulating heavy steel plates at the construction site; corrosion problems; the need for scaffolding and temporary support or loading; proper formation of joints due to the limited delivery lengths of the steel plates; labour intensiveness; frequent disruption of occupancy or traffic; reduction of available space; strong architectural impact; heavy mass addition; etc. Advantages of using CRS for masonry structures include lower installation costs, improved corrosion resistance, limited access requirements, flexibility of use, minimum changes in member size (and in some cases aesthetics)

after repair, minimum disturbance to occupants or traffic, minimum loss of usable space, etc. Furthermore, for seismic retrofits, the mass of the existing structure remains practically unchanged because there is little addition of weight (Motavalli and Czaderski, 2007; Shield *et al.*, 2005; Ehsani *et al.*, 1997; Borri *et al.*, 2009).

Currently, the rehabilitation of a URM structure is usually performed for reasons of lack of capacity or deterioration of structural elements (e.g., walls, arches, vaults, and columns) and of need for correcting design/construction errors. CRS can be used effectively for flexure and shear strengthening in order to upgrade structural capacity, or to restore the original capacity of damaged elements subject to out- and in-plane loads. CRS can also be used to address existing distress in masonry construction, for instance, repair of cracks by 'stitching' to re-establish masonry integrity when this cannot be achieved by solely 'injecting' cracks with a repair material. In addition, since many of the existing structures are located in seismically active areas and the seismic capacity of URM shear walls is minimal, either because they were not designed and constructed with consideration of this aggressive factor or because the existing structures have to cope with changes in seismic requirements, the seismic retrofit of URM buildings with advanced composite materials is a major field of application of CRS (Motavalli and Czaderski, 2007; Shield *et al.*, 2005; Borri *et al.*, 2004, 2009; Tumialan *et al.*, 2009).

The most common rehabilitation techniques for flexural and shear reinforcement of masonry structures are the externally bonded FRP systems (consisting of prefabricated laminates or sheets, wet lay-up systems made from prepreg sheets or woven fabrics, and automated wrapping of columns) and the NSM systems (rods and plates/strips). Externally bonded systems have been shown to be more robust against extreme events, while NSM affect the aesthetics of the masonry structure to a lesser degree (ACI, 2010; Borri *et al.*, 2004, 2009; Ehsani *et al.*, 1997; Motavalli and Czaderski, 2007; Myers, 2011; Shield *et al.*, 2005). Figure 22.19 provides some examples of applications and techniques used in the rehabilitation of masonry structures with APC materials.

Currently and at a European level there is no well-established design and detailing guidance on the rehabilitation of masonry structures with APC materials. Nevertheless, a comprehensive overview of procedures for in- and out-of-plane strengthening of URM wall systems can be found in the American Concrete Institute standard ACI440.7R-10 entitled 'Guide for the Design and Construction of Externally Bonded Fibre-Reinforced Systems for Strengthening Unreinforced Masonry Structures' (ACI, 2010) and in the ACI publication SP-230 'Proceedings of the 7th International Symposium on Fiber-Reinforced (FRP) Polymer Reinforcement for Concrete Structures' (Shield *et al.*, 2005). Sources for a more detailed description of the use of CRS with masonry structures are presented in Section 22.6.

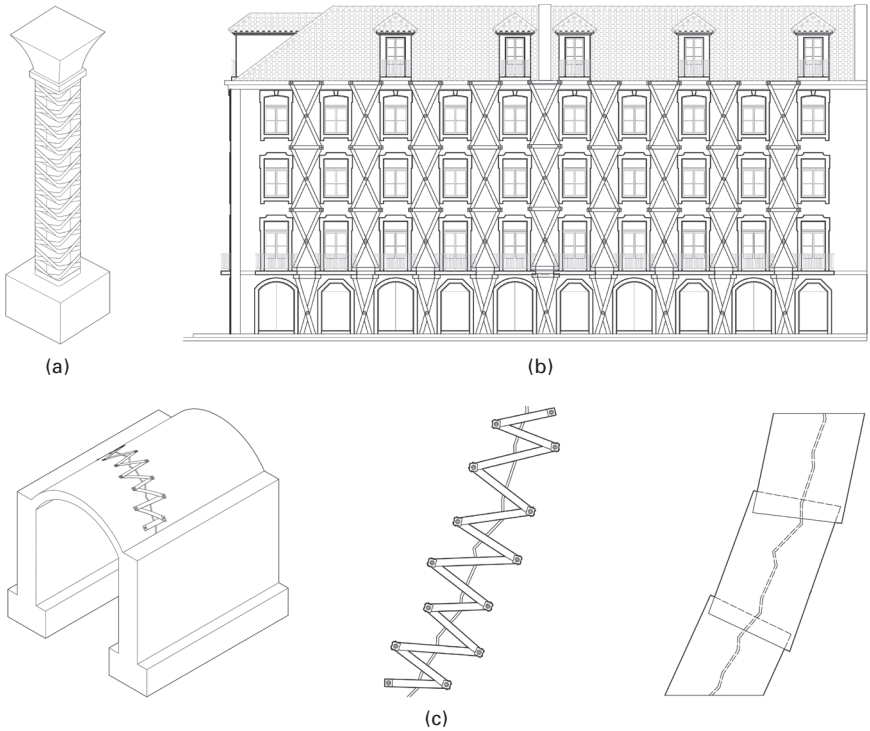

22.19 Examples of applications and techniques used in the rehabilitation of masonry structures with CRS: (a) compression reinforcement through confinement of a column through the application of composite sheets or fabrics; (b) seismic retrofitting of a masonry structure (simplified schematics) through the bonding of strips, sheets or fabrics; (c) repair of localized and stabilized lesions, like fissures and cracks, through the external bonding of FRP strips (extremities should be firmly fixed to the masonry, for instance mechanically) or of sheets (courtesy of Cóias, 2007).

22.4 Performance and durability

22.4.1 Performance

The short- and long-term performance of a CRS, regardless of the method of application, is influenced by several factors, of which the most important are (1) the appropriate selection of the system constituents, namely the APC material and the SA; (2) adequate design and detailing of the adhesively bonded CRS system; (3) careful analysis of the substrate condition and the proper preparation of the adherend surfaces to be bonded; (4) practical execution of the rehabilitation intervention; (5) adoption of a specific quality control programme which includes control procedures covering all stages of the rehabilitation work; and (6) the monitoring of the rehabilitated structure

during its service life. These factors can be thought of as the steps of a bonding process that it is necessary to carry out in order to produce the final bonded CRS; thus all of them should receive the same level of attention and commitment if a bonded CRS with a satisfactory performance is to be obtained.

Materials selection

The processes involved in selecting the most adequate FRP and SA for a particular application are not as straightforward as it may appear. To achieve optimum performance one must carefully plan every stage of the bonding process. The selection process is difficult because many factors must be considered, and there is no universal SA and FRP that will fulfil every application. Normally, it is necessary to compromise when selecting a practical CRS. Some properties and characteristics will be more important than others, and a prioritization of these criteria will be necessary during the materials selection. It is important to optimize the entire bonding process and not just one part of the process. Hence, besides looking at expected service requirements (e.g. duration and nature of the stress; bond strength; degree of toughness required to resist impact, peel or cleavage forces; operating temperature range; chemical resistance; environmental resistance; differences in flexibility and thermal expansion rates), consideration needs to be also given to the substrates, joint design, possible application and curing methods, on-site environmental conditions, quality control, etc. Since a decision on any one of the aforementioned steps may condition the remaining ones (e.g., the substrate condition may influence the processing conditions and the joint design), it is imperative that the materials selection is made considering all steps involved in the bonding process. Therefore, all sectors involved in the rehabilitation work (e.g., designer, practising civil engineer, owner, materials manufacturers) should collaborate in the materials selection step and exchange relevant information of all stages of the work (Petrie, 2006; Silva *et al*., 2011; Adams *et al*., 1997; Mays and Hutchinson, 1992).

Adhesively bonded CRS system

Once the rehabilitation materials are chosen, the joint design can be properly addressed. There are many factors that must be considered in the design of a bonded joint. In addition to the most evident ones (like the geometry of the area to be bonded, the properties and characteristics of the bonding materials, and the stresses to which the bonded joint will be subjected while in service), several others exist that may also condition the joint design. The design of the bonded joint should then maximize the bonded area; introduce tensions in the direction of maximum strength of the bonded joint (e.g., shear

or compression); minimize loads in the direction of minimum strength of the bonded joint (e.g., peel and cleavage stresses); consider continuous and uniform bond-lines as far as possible to avoid stress concentrations which may lead to premature bond failure; account for differences in thermal expansion coefficients of the adhesive and adherends, as they can generate stresses, which will compromise joint performance; consider the cost associated with manufacturing the joint design; regard that the joint can be straightforwardly fabricated and assembled; account for the ease with which the joint can be inspected after bonding is complete; and, whenever possible, ensure clearance and access so that periodic inspections and eventual maintenance or repair operations can be performed to the bonded system (Petrie, 2006; Silva *et al*., 2011; Adams *et al*., 1997; Mays and Hutchinson, 1992). In some applications, special design considerations may be needed to account for possible limitations of the bonding materials, substrates or specificities of the application itself, for instance if the predicted service temperature is relatively close to the glass transition temperature of the adhesive, shading and ventilation should be adopted to prevent the adhesive from overheating, and the distances of the bond-lines in respect to limits of the element should be increased.

Adherend pre-treatment

The careful evaluation of the substrate condition and the proper preparation of the adherend surfaces to be bonded are essential to ensure that the adhesive connection will behave efficiently and an adequate short- and long-term performance and durability will be attained. The choice and specification of pre-treatment procedures required for specific adherends should be, preferably, those defined in the manufacturer's Product Data Sheet or specified in applicable regulations or standards. Generally, the choice and specification of surface preparation procedures should be influenced mainly by the required durability and, if possible, involve simple reproducible processes. However, the location and scale of operations, the nature of the adherends, the adhesive to be used, the safety and environmental aspects, and the cost, all have to be taken into consideration. The various tasks usually involved in the preparation of the adherend surface vary with the adherend type and the specific application. Normally they can be outlined as follows: elimination of contaminants (e.g., dirt, grease, oil) and any weak surface layers (e.g., rust, paint, degraded substrate, concrete laitance); removal of mould release agents or other similar products used in the fabrication process; elimination of any dust and neutralizing of any chemicals used for cleaning the adherend surface; drying of substrates such as concrete, timber and APC materials; assessing the quality and roughness of the prepared surface; and applying a primer or an adhesion promoter to the adherend surface. Prior

to bonding, the adherend surface should be visually inspected to check that the contaminants have been removed and that the surface appears to be uniform. In some situations, it will be necessary to test, via a mechanical test (e.g., pull-off test), that the exposed substrate is sound; if not, the surface preparation will have to be taken to a sufficient depth such that the unsound substrate is fully removed (Petrie, 2006; Silva *et al.*, 2011; Pizzi and Mittal, 2003; Packham, 2005).

Bonded joint fabrication

The practical execution of the rehabilitation intervention includes the reception, storage, preparation and application of the SA and APC materials, as well as the curing of the adhesive materials. Site work should be carried out by well-informed, trained, experienced and certificated operatives, under the supervision of a qualified site manager to ensure compliance with the specifications of the quality plan and to ensure a satisfactory intervention programme (Petrie, 2006; Silva *et al.*, 2011; Adams *et al.*, 1997; Mays and Hutchinson, 1992).

The condition of the materials that arrive at the work site should be assessed and recorded to guarantee that they are in perfect condition so that if handled properly they will be able to produce rehabilitation work with adequate performance and durability. This verification also serves to confirm that the correct products have been delivered to meet project specifications and that they are under the expiry date. The storage of the materials is also very important and it should follow strictly the supplier or manufacturer indications present in the manufacturer's or supplier's Product Data Sheet. Generally, all adhesives and APC materials should be stored in a cool, dry place until they are used. While some materials are very tolerant to storage conditions, there are others that may have to be stored at low temperature or under special conditions. For instance, some adhesive systems are affected by light or moisture and others require periodic agitation to ensure that their components do not settle irreversibly (Petrie, 2006; Silva *et al.*, 2011; Adams *et al.*, 1997; Mays and Hutchinson, 1992).

The preparation and application of the SA and APC materials should also be carried out strictly in accordance with the supplier's or manufacturer's recommendations. Generally, it is necessary to control the environment surrounding the bonded area (e.g., with a temporary enclosure system), not only during the preparation of the substrate (e.g., having a system to extract dust and fumes from the work area and the exclusion of any material that might contaminate the prepared surface) but also during the preparation and application of the SA and APC material and the subsequent adhesive curing period. For instance, it may be necessary to match the adhesive temperature to the application conditions, maintaining the temperature in the bond-line

at a certain level during a specified period of time, to keep moisture away from the bonded system.

The most common mistakes committed at this stage that will result in a joint with poor long-term performance include the use of incorrect proportions between the adhesive components (stoichiometric quantities) due to disregard for the stipulated amounts or to the incorrect weighing of the components; the mixing and use of adhesive volumes higher than those recommended in the product data sheet, which will result in a reduced pot-life; application of an adhesive that has passed its pot-life due to the volume used and the temperature of the mixed adhesive and ambient temperature; the use of an adhesive mixing procedure different from the recommended; the disregard for the predetermined application temperature, relative humidity and substrate moisture content; the production of a bond-line with an irregular and/or incorrect thickness; the application of an insufficient pressure to the bonded joint, which may result in a joint with a discontinuous, irregular or insufficient layer of adhesive; the premature removal of the temporary formwork used to hold components and apply pressure during adhesive cure; an adherend temperature lower than ambient temperature, resulting in condensation of moisture at the adherend surface; and inadequate protection of the bond-line from adverse environmental effects, at least while the system cures (IStructE, 1999; Mays and Hutchinson, 1992; Petrie, 2006).

Once the rehabilitation work has been completed, an inspection should be carried out to detect flaws or defects. The inspection may comprise destructive or non-destructive tests. The non-destructive tests can be performed either visually or through the use of advanced analytical equipment. The destructive tests consist of tests on standard control samples, tests on prototype systems, and tests on selected areas (IStructE, 1999; Mays and Hutchinson, 1992; Petrie, 2006).

Quality control

An effective quality assurance programme should be conducted to guarantee that the rehabilitation work has satisfactory performance and durability. The adoption of a specific quality control programme that includes control procedures covering all stages of the rehabilitation intervention is very important when using SA and APC materials, because once fully bonded, joints are difficult to disassemble or correct. The provision of a ‘dossier’ of the intervention containing detailed information about the works is very important for future repair/reinforcing works and future surveys. A typical quality-assurance programme consists of three parts: (1) establishing limits on bonding process factors that will ensure acceptable joints and product; (2) monitoring the production processes and quality of bond in joints and product; and (3) detecting unacceptable joints and product, determining the

cause, and correcting the problem. Materials and material handling should fulfil the requirements in the applicable specifications, including proper storage and the compliance with shelf-life stipulations. All works should be executed in accordance with current Health and Safety regulations, as well as local regulations (IStructE, 1999; Mays and Hutchinson, 1992; Petrie, 2006; Cruz *et al*., 2004b; Dunky *et al*., 2008).

In-service monitoring

The rehabilitation work should also include a plan for the monitoring of the rehabilitation intervention during its service life to ensure that the structure will be able to perform according to planning for its intended service life.

More detailed information on the topics described above can be obtained from the references presented in Section 22.6.

22.4.2 Durability

The ability of a structural joint to maintain satisfactory long-term performance, often in severe environments, is an important requirement of a structural adhesive joint, as the joint should be able to support design loads, under service conditions, for the planned lifetime of the structure. A number of factors determining the durability of structural adhesive joints have been identified and are normally grouped in three categories: materials, environment and mechanical actions (Table 22.3).

This section focuses very briefly on the most relevant of the aforementioned factors, thus providing only a general understanding of the factors that influence the durability of bonded timber and concrete joints. The durability of APC materials has already been discussed in the previous chapters so is not dealt with here. The durability of the substrates, timber and concrete, is not also dealt with here; the reader can obtain information on this topic from the relevant sub-section of Section 22.6.

Environment

Temperature

Temperature is an important factor in the durability of structural adhesive joints, since it can affect the creep, fatigue and fire performance of adhesive bonded joints. Well-designed and well-made joints with any of the normally structural adhesives should retain their mechanical properties indefinitely if the substrate moisture content is kept low (e.g., if timber moisture content stays below approximately 15%) and if the temperature remains within the range of human comfort. However, when adhesives are exposed either

Table 22.3 Main factors determining the durability of composite rehabilitation systems

Materials	• Substrate (e.g., concrete, timber) • Structural adhesive • APC material
Environment	• Temperature (e.g., extreme temperatures, thermal cycles[1], freeze-thaw[1], fire) • Moisture (e.g., humidity and/or water, wetting-drying cycles[1], humid-dry cycles[1]) • Chemical fluids (originating from the surrounding environment – e.g., contaminated water, pollution, salt water, caustic alkaline or acid solutions, oils, fuels; or the substrate itself – e.g., concrete pore solution, timber extractives) • Radiation (e.g., solar radiation) • Biological factors[2] (e.g., insects[3], fungi[3], borers[3], bacteria)
Mechanical actions	• Static load (e.g., creep and relaxation) • Dynamic load (e.g., fatigue) • Combined load • Accidental impacts • Natural catastrophes (e.g., earthquakes)

[1] The duration, rate and period of the cycles affect the bonded joint differently.
[2] Biological growth on concrete and timber structures which may lead to physical and mechanical damage is not included.
[3] Biological agents that generally do not deteriorate concrete (Gaylarde *et al.*, 2003; FIB, 2009).

intermittently or continuously to high temperatures for long periods they will eventually deteriorate (Custódio *et al.*, 2009a; Mays and Hutchinson, 1992). At abnormally high or low temperature the adhesive in a bonded joint may experience severe internal stresses that develop when different materials within the joint have different coefficients of thermal expansion. Adhesives also tend to get soft at elevated temperatures (Cruz *et al.*, 2004a, 2005; Cruz and Custódio, 2006; Custódio and Cruz, 2006) and brittle at low temperatures (depending on the chemical nature of the polymer on the adhesive composition), and long-term exposure to elevated temperature could also cause their oxidation or pyrolysis (Pizzi and Mittal, 2003).

The effect of temperature variation on the strength of adhesive-repaired structures can be divided in two categories. One category considers the effect of temperature changes due to natural environmental causes. In this category temperature changes from –18 to 65 °C are reasonable expected variations. The second major effect to be considered is fire, where extreme temperatures (higher than 280 °C) are reached (FPL, 2010).

The shear strength of a joint is also a function of the time during which a given temperature is sustained or has been sustained. This last relation is important when considering the case of an epoxy-repaired structure exposed

to fire, or in situations where the bond-line would be subjected to prolonged or repeated exposure to hot environments, e.g., in timber roof trusses or concrete bridge deck reinforcements in countries with hot summers.

Figure 22.20 shows the mechanical–thermal behaviour of 14 commercial adhesives typically used in CRS for timber and concrete structures. It can be seen that all adhesives exhibit a pronounced decrease in their stiffness

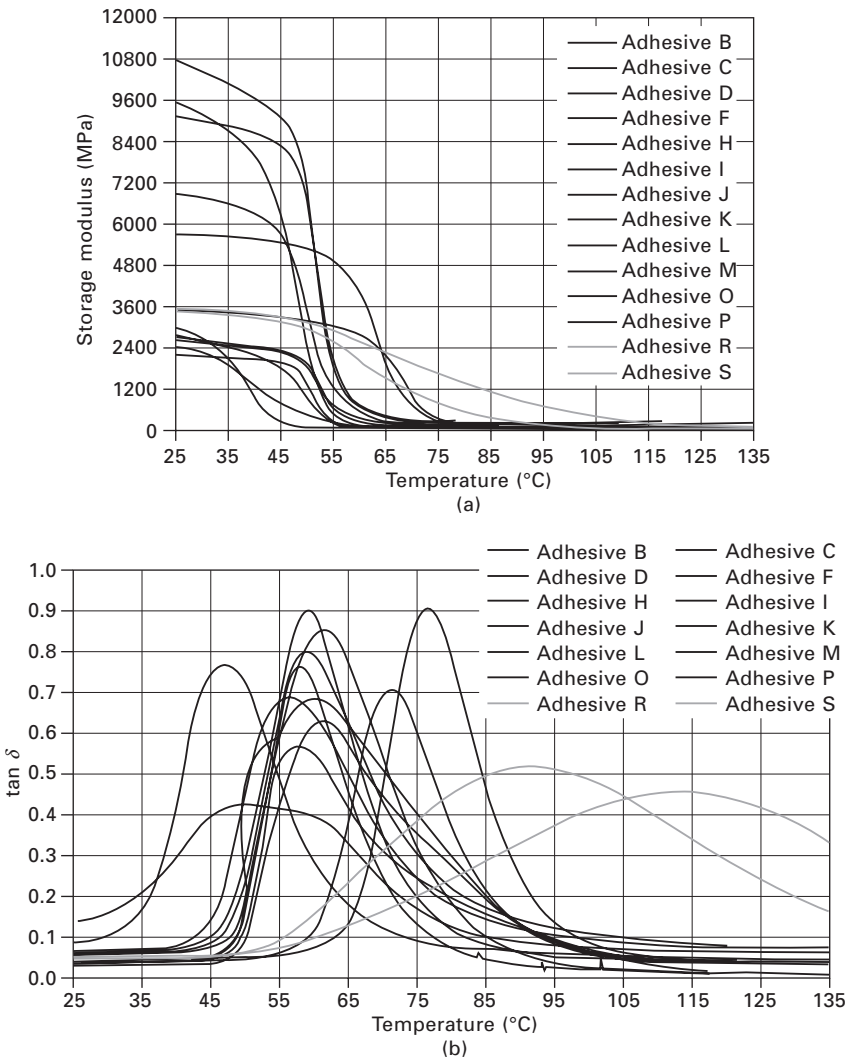

22.20 (a, b) Viscoelastic properties determined by dynamic mechanical analysis with temperature scan for two-component epoxy (black lines: B, C, D, F, H, I, J, K, L, M, O and P) and polyurethane (grey lines: R and S) adhesives.

with the increase in temperature. If one considers the temperatures these adhesives will have to withstand in service (usually up to 50 °C or higher), a very careful selection of the adhesive is necessary. Thus, care must be taken to ensure that the maximum service temperature is well below the glass transition temperature of the SA.

As can be seen from Fig. 22.20, the large variety of polymer networks available can result in a large range of transition regions, and adhesives showing a similar glass transition temperature can have significantly different strengths and mechanical–thermal behaviour. Thus, the adhesives used should have a glass transition temperature considerably higher than the expected maximum service temperature; for example, $T_{g,t}$ (the adhesive glass transition temperature taken from the peak of the tan δ curve, which is a common criterion appearing in the literature and very often used by adhesive manufacturers) should correspond to at least 10–20 °C below the maximum expected service temperature. The FIB Report No. 14 (FIB, 2001) suggests that the T_g (determined by differential scanning calorimetry (DSC) or differential thermal analysis (DTA) according to EN 12614 (CEN, 2004b) of the SA used in externally bonded APC materials for reinforced concrete structures) should be 20 °C above the maximum shade air temperature in service but not less than 45 °C. Thus, the authors, facing the thermal behaviour of the tested commercial epoxy SA and the environmental service conditions normally attained in timber structures rehabilitated with CRS (Cruz *et al.*, 2004a, 2005; Cruz and Custódio, 2006; Custódio and Cruz, 2006), consider that the above recommendations are a realistic and safe approach and because of that they should also be adopted for timber structures, as currently no such requirement for timber rehabilitation works involving CRS exists. In addition, the authors believe that, besides information about the glass transition temperature, the product data sheet should also contain information about how it was obtained and about the magnitude of the strength decrease with increasing temperature.

Because of the sensitivity of these adhesives to temperatures in the range of 25–65 °C (depending on the adhesive formulation), the fire resistance of an adhesive-repaired joint would depend primarily on joint design and on the additional measures taken to protect the bond-line. Also, adhesives used in these applications can display significantly different viscoelastic responses over the temperature ranges attained normally in service. Thus, in some applications, temperature-induced creep is a risk factor that needs to be considered cautiously when selecting the adhesive for that particular application.

Extreme temperatures affect not only the adhesive but also the FRP reinforcement; as for the adhesive, the FRP matrix also changes its viscoelastic response as temperature increases. For instance, Fig. 22.21 shows experimental dynamic mechanical analysis curves obtained with three commercial CFRP

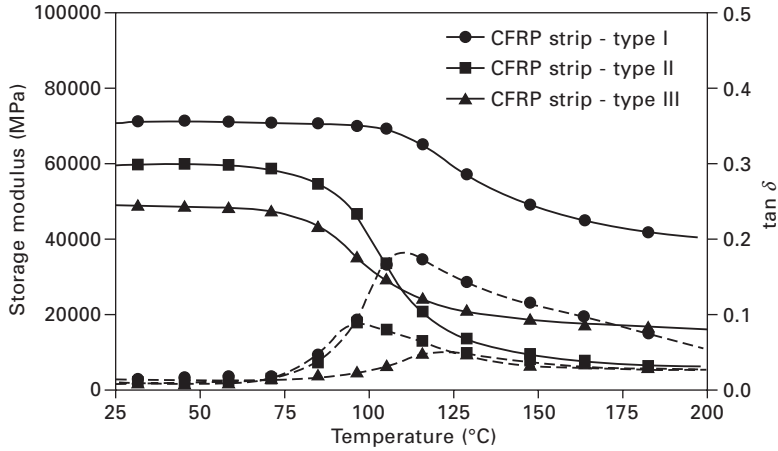

22.21 Viscoelastic properties determined by dynamic mechanical analysis at different temperatures for three different CFRP strips.

strips (storage modulus curves are represented by continuous lines and tan δ curves by dashed lines). As can be seen, $T_{g,t}$ values, which vary between 90 °C and 120 °C reflecting mainly the viscoelasticity of the polymer matrix, are higher than those observed for all epoxy adhesives presented above. Thus, the American Concrete Institute (ACI, 2008) recommendation that the maximum service temperature should never rise above the T_g of the FRP (considered as being the midpoint of the temperature range over which the resin changes from a hard brittle state to a softer plastic state), is normally only of secondary importance for the rehabilitation work as it is the SA temperature sensibility that limits the performance and durability of the CRS.

Another potential adverse effect of high temperature is the acceleration of the degradation process of APC materials as well as the adhesive, such as those involving contact with moisture, chemical fluids and radiation. Thermal cycling in general does not cause significant harmful effects in the adhesive, although extended thermal cycling may result in micro-cracking of brittle composite matrix and adhesive, leading to premature bond failure.

In general, low temperatures and freeze–thaw cycles can affect both the polymeric matrix of the APC materials and the adhesive. Freezing and thawing effects can be more severe due to moisture-initiated effects causing micro-crack development. Research results suggest that some degradation in the composite bonded joint due to freeze–thaw cycles can occur, particularly in the presence of humidity and sustained load (Ekenel and Myers, 2009).

The procedure adopted on-site for the preparation and application of the structural adhesives, namely the mixing method (e.g., manual or machine mixing of the adhesive components, duration and speed of the mixing) and

cure conditions (e.g., temperature and duration of cure), affects the mechanical properties of all the adhesives, and consequently can affect their durability (Custódio *et al.*, 2011; Custódio, 2009).

Since rehabilitation is primarily conducted under ambient conditions, there is also potential for under-cure or slow progression of cure of the adhesives. Thus, in situations where the adhesive cured in ambient conditions does not produce a fully cured system which consequently has an inadequate glass transition temperature, a postcure procedure at a temperature above the glass transition temperature of the cured adhesive will be necessary to achieve the desired result (Custódio *et al.*, 2011; Custódio, 2009).

In summary, the composite rehabilitation techniques involving SA and APC materials should always take into consideration the service temperature effect on the adhesive and FRP performance, being necessarily cautious in the structural joint design and in the materials selection. Extensive pre-normative research and thorough consideration of this effect is still required for the development of European standards for the evaluation of bond durability and long-term performance under high service temperatures for epoxy or indeed other adhesive joints. This will enable the effective and safe application of reinforcement techniques based on the use of structural adhesives, especially in highly demanding situations where the present lack of knowledge and reliability of these products hinder their widespread use.

Moisture

Water, in liquid or vapour forms, is often regarded as one of the most worrying agents that may affect the properties of an epoxy adhesive and the interface between it and the adherends. Most bonded structures, when exposed to water or humidity will lose strength over a period of time and in rare cases they may fail, although this effect is limited to very extreme conditions.

In CRS, the properties of composite polymeric matrix together with properties of adhesives are susceptible to moisture, particularly when associated with temperature (Custódio, 2009; Cabral-Fonseca, 2008). The result of moisture absorption is to lower the T_g of these materials, leading to a change in their mechanical properties.

It is almost impossible to keep water out of an adhesive joint. There are a number of possible mechanisms by which water may enter a bond: (a) diffusion through the adhesive from the exposed edges; (b) transport along the adhesive/adherends interface; (c) migration via capillary action along cracks and crazes in the adhesive and adherend, and (d) diffusion or capillary action through porous adherends (Pizzi and Mittal, 2003).

Water ingress into a structural adhesive joint can decrease the bond performance by several reversible and irreversible mechanisms. The effect of water, at least initially, can be reversible. This is especially true when

corrosion-resistant adherends, good surface preparation and treatment, and hydrolytically stable adhesives are involved. When the joint dries out, the bond can recover some of its lost strength. However, with time, especially at high moisture levels combined with temperature and stress, the various irreversible processes that can occur become a serious threat to the long-term durability of the joint (Pizzi and Mittal, 2003; Hartshom, 1986). Figure 22.22 shows the effect of water on the stiffness of four commercial

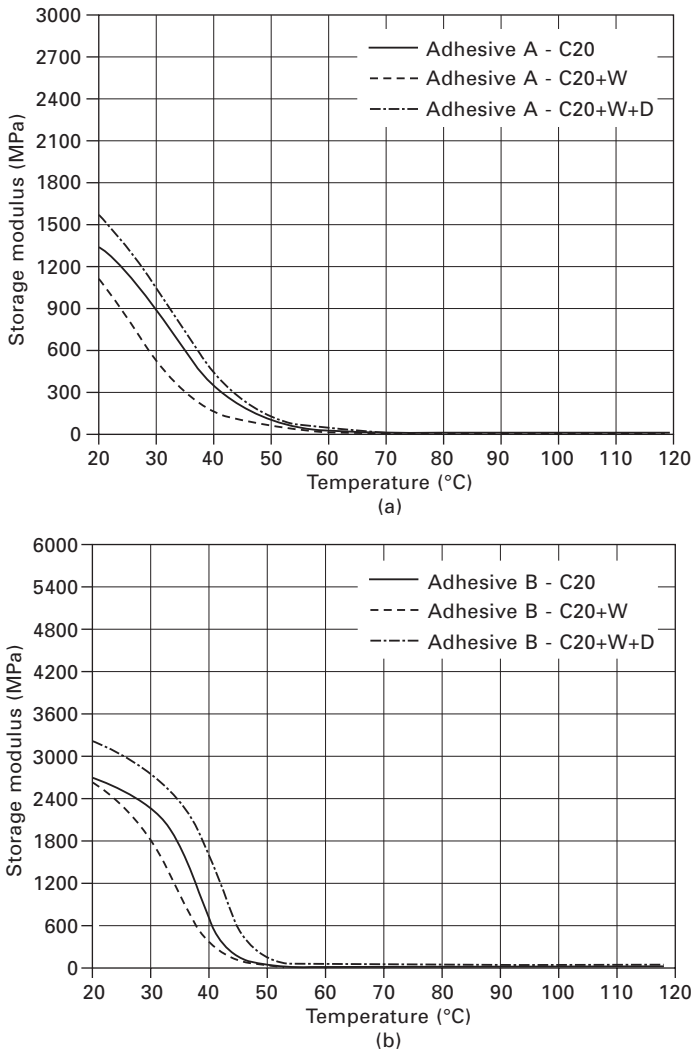

22.22 (a–d) Comparison of the storage modulus curves obtained for four epoxy adhesives before immersion (C20), after emersion (C20 + W), and after emersion and drying at 20 °C and 65% RH for one month (C20 + W + D).

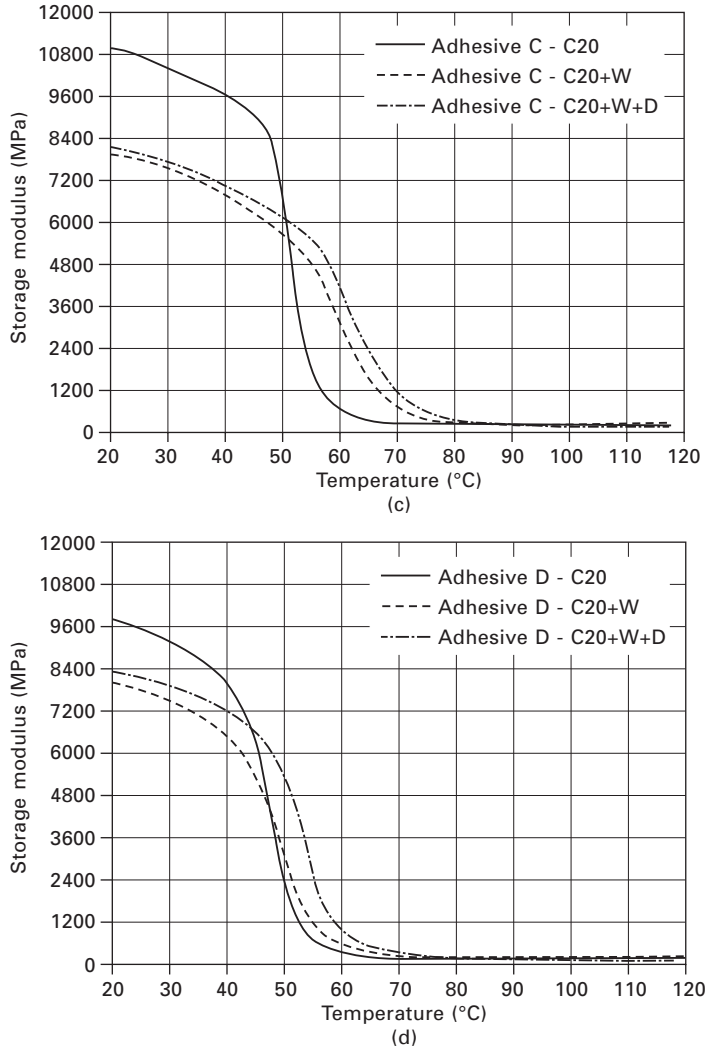

22.22 Continued

epoxy adhesives. It can be seen that each epoxy adhesive formulation behaved differently for the same immersion period. For instance, while for adhesives A and B immersion in water at 20 °C for a period of 18 months does not result in a loss in the storage modulus, for adhesives C and D it results in some degradation as their storage modulus after emersion and drying does not recover to the initial value (Custódio *et al.*, 2011; Custódio, 2009).

The presence of water may also produce an unstable adhesive/adherend interface, which will gradually be displaced from the adherend surface by

water. Ultimately, water may penetrate the adherend surface and produce a loss in the strength of the adherend itself, though the adhesive is usually more affected.

Surveys, recordings and long-term monitoring of repairs undertaken in the last 25 years regarding rehabilitation of structures using bonded connections have provided some information on the ways in which epoxy-bonded joints behave over time in real service conditions. Nevertheless, even with the greater understanding of this technology, doubts over structural performance and the effect of moisture on long-term durability still persist.

Bond enhancement is not required to increase initial strength, but where bonded joints may be subjected to repeated wetting and drying or long periods of exposure to water and high humidity (e.g., with outside applications of externally bonded FRP composites) it may be necessary to improve long-term durability of the structural bonded joint with primers, adhesion promoters and other surface treatments (Custódio *et al.*, 2008, 2009b).

Chemical fluids

The resistance of bonded connections to chemical fluids, such as in alkaline chemical attack originated by the concrete pore solution, depends upon the nature of both the FRP composite and the adhesive. As a recent study showed (Cabral-Fonseca *et al.*, 2009) alkaline environments can cause different degrees of damage in different epoxy adhesives, as well as in FRP composites.

The mechanical behaviour of adhesives during immersion in an alkaline solution (Fig. 22.23), evaluated by their flexural properties (flexural strength and flexural modulus are represented in those plots by bars and single squares, respectively), presented distinct trends in performance: (1) an overall decrease in the properties of adhesive A was observed and higher temperatures caused further degradation; (2) the post-cure occurring during ageing of adhesive B hides any reduction of properties caused by eventual degradation mechanisms that could arise in parallel; and (3) adhesive C was the most resistant to the different ageing conditions, but the flexural strength retention at 60 °C was only 37 %.

Regarding the three commercial CFRP strips studied, immersion in alkaline solution shows a complete different scenario for each one (Fig. 22.24). The exposure was particularly harsh for the CFRP strip – type II, which undergoes degradation even at room temperature after 18 months, showing separation of carbon fibre accompanied by the polymeric matrix release. At 40 °C and 60 °C it was impossible to perform the flexural tests, because the integrity of the material was lost. The different level of degradation of 'similar' commercial CFRP strips caused by the alkaline ambient is one of the most important conclusions of this study.

Materials

Besides the environmental factors mentioned above, the materials involved in a structural joint also influence bond strength and durability. The factors in the material category include the adherends, the adhesive, the design of the joint, the surface contamination, the stability of the adherend surface, the ability of the adhesive to wet the surface, and entrapment of air/volatiles.

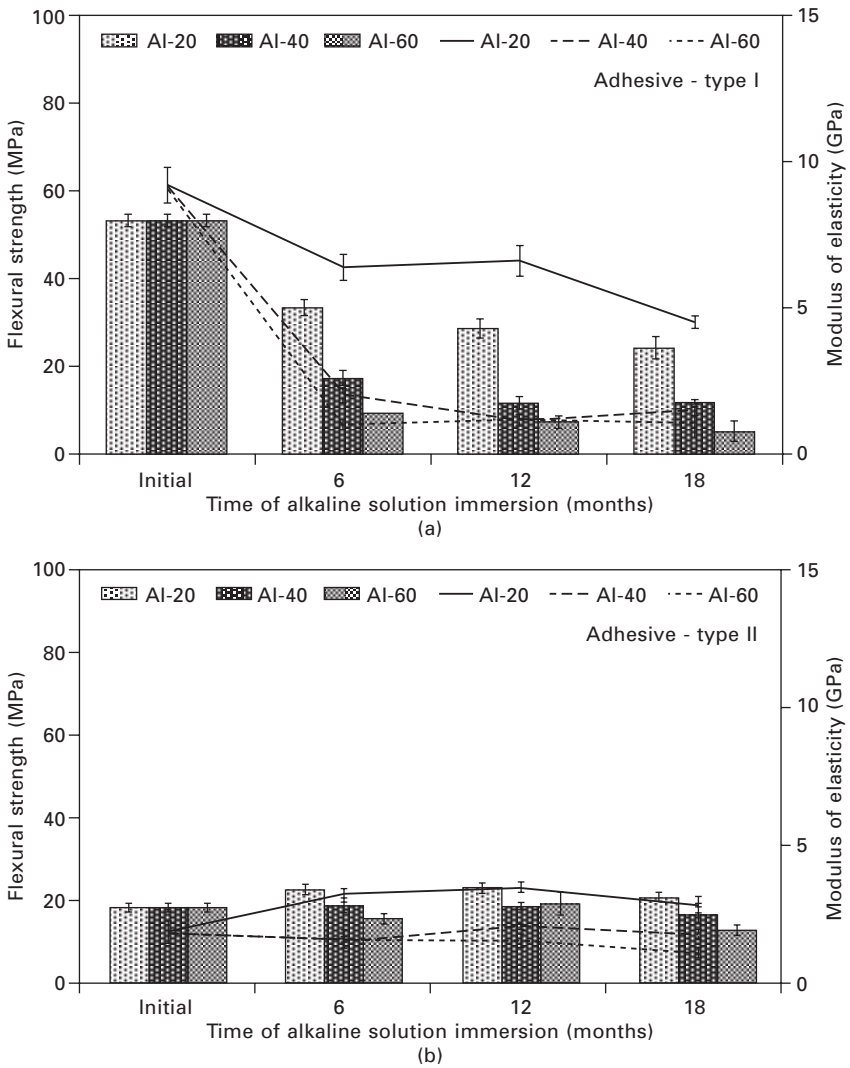

22.23 (a–c) Flexural properties of three types of epoxy adhesives during immersion in an alkaline solution at 20 °C, 40 °C and 60 °C, up to 18 months.

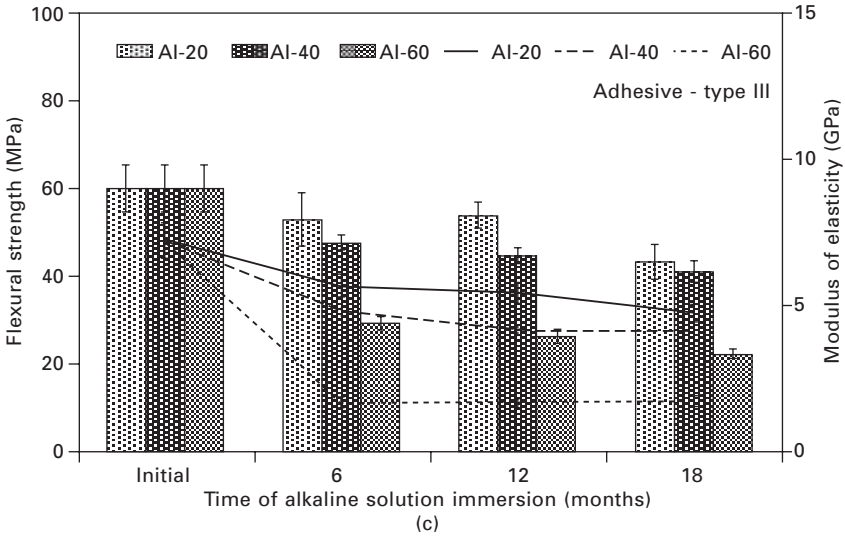

22.23 Continued

The condition of the adhesive/adherend interface then becomes a decisive factor affecting the initial bond strength as well as the long-term durability of the bonded joint.

Surface preparation

Bonding wood and concrete is not normally difficult and it is generally possible to obtain a good bond, provided that adequate surface preparation is undertaken before bonding.

The main reasons for preparing the wood surface before bonding are (1) to produce a close fit between the adherends and a bond-line with uniform thickness; (2) to produce a freshly cut or planed surface, free from machine marks and other irregularities, extractives and contaminants; and (3) to produce a mechanically sound surface, without crushing or burnishing it, which would inhibit adhesive wetting and penetration.

Usually, surface preparation involves some form of machining. The quality of the surface will vary with the type of machining process as well as with how carefully the process is controlled. When wood is machined, the strong molecular bonds between wood components are broken, and the molecules once joined become open bonding sites that possess strong attractive forces. This attraction gives recently machined wood its desirable wettability. During machining, the disruption of the chemical structure may also leave residual charge on the timber surface, making it very receptive to the adhesive, which promotes the development of strong adhesion forces.

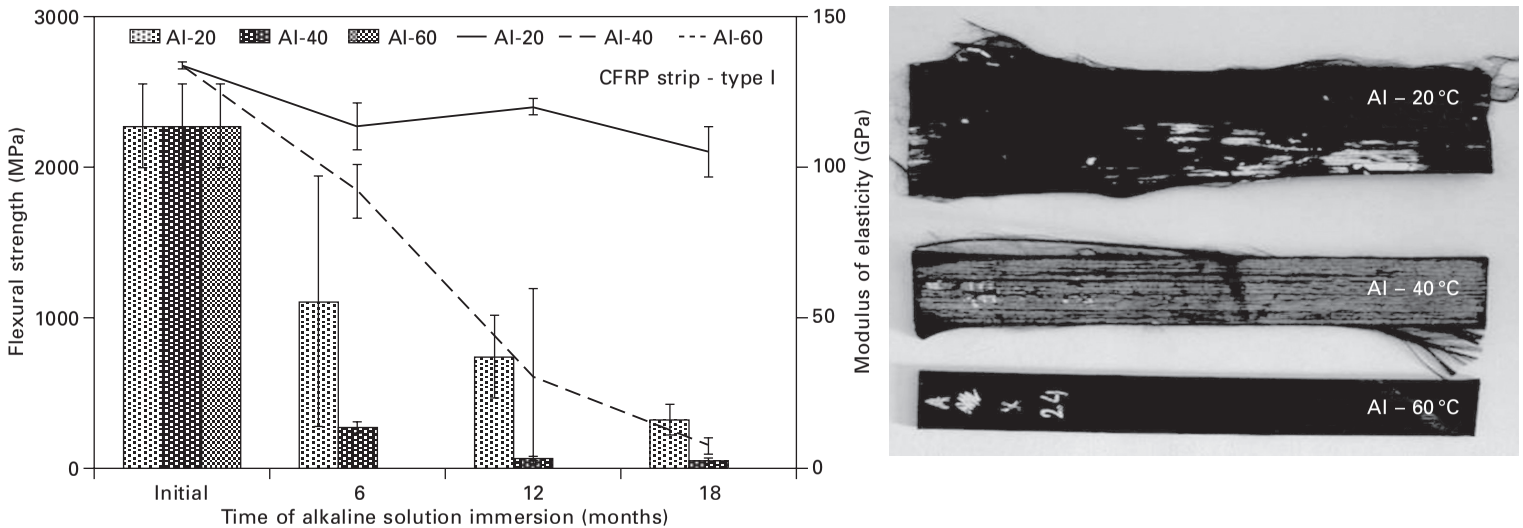

22.24 Flexural properties of three types of CFRP strips during immersion in an alkaline solution at 20 °C, 40 °C and 60 °C, up to 18 months (left); aspect of test specimens at the end of the exposure (right).

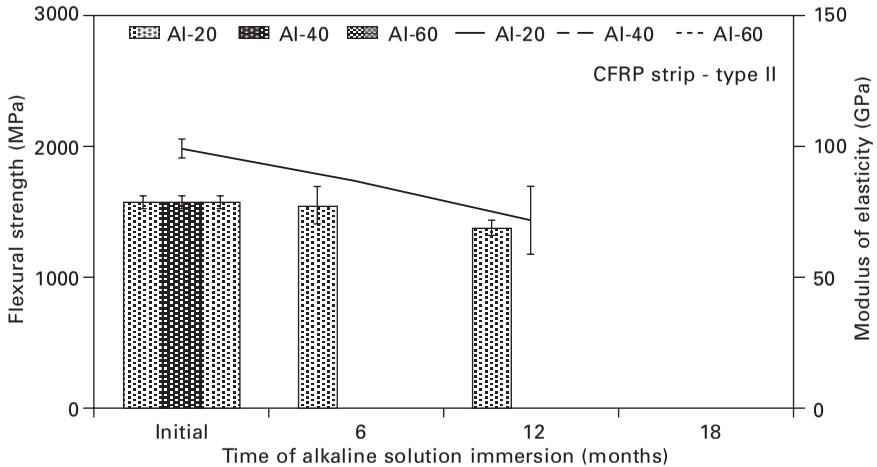

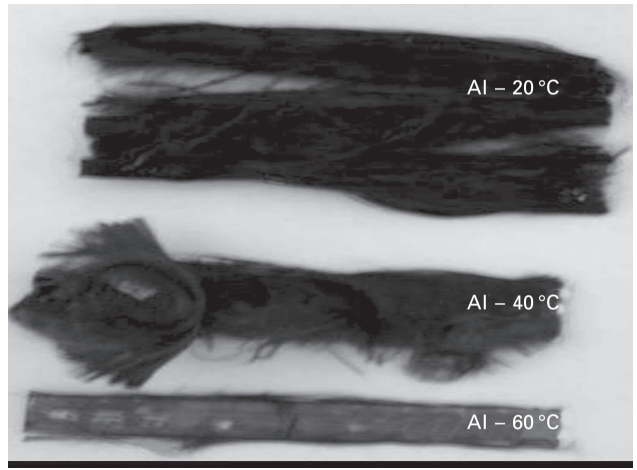

22.24 Continued

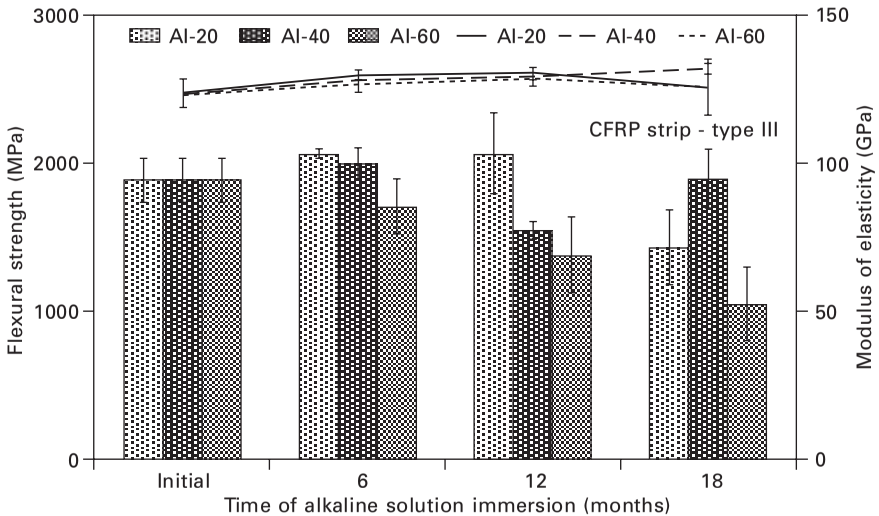

22.24 Continued

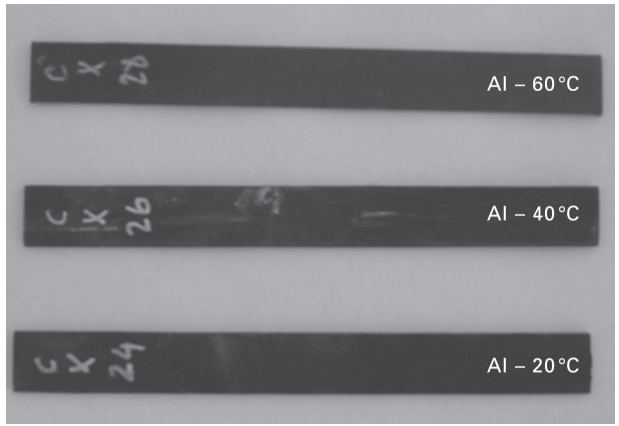

However, the longer the freshly machined wood is exposed to the atmosphere, the more of the bonding sites will be taken by water, gases, microscopic dust and dirt particles, extractives in the wood and pollutants, and less will be available for the adhesive, i.e. by contaminants. This, as in the case of many materials, is why wood loses its wettability over time and the surface of the wood becomes inactivated. In this situation, although adhesive penetration may still take place, filling the voids on the wood surface, the adhesive is not molecularly attracted to the wood and as a result a weak bond will occur at the adhesive/wood interface (Adams and Wake, 1984; Minford, 1991; Frihart, 2009; FPL, 2010).

Wood cells can be damaged by machining, which is usually involved in the preparation of wood surfaces prior to bonding. The nature and extent of damage varies with the type and severity of machining. Besides mechanical damage, thermal damage should also be avoided during any surface preparation. When the wood is overheated or overdried, the risk of obtaining an inactivated surface rises, because heat increases the movement of wood extractives, thus increasing the chance that they will move to the wood surface. In addition, severe heat can actually alter the chemistry of wood components, destroying available bond sites (Rabiej *et al.*, 1997; FPL, 2010; Marra, 1992). If surface inactivation is detected, the most effective and traditional method to revitalize wood surfaces for bonding has been through planing to remove hydrophobic and chemically active extractives and other physical and chemical contaminants that could interfere with bonding (FPL, 2010).

In the case of concrete, the main reasons for preparing the surface before bonding are similar, namely: (1) to produce a close fit between the adherends; (2) to remove laitance and contaminants and to expose pieces of aggregate; and (3) to produce a mechanically sound surface. Any typical sequence of steps in the process of concrete surface preparation should then include the removal of any damaged concrete and its replacement with new material, and the elimination of dust and other contaminants by brushing, air blast or vacuum. In some situations, additional steps like cleaning with a solvent to eradicate specific contaminants and application of a primer may be required.

Age of surface

Because adhesives bond by surface attachment, the physical and chemical condition of the adherends' surface is extremely important for good joint performance and durability. Immediately after preparation, all surfaces undergo an inactivation process. To achieve optimal adhesion it is recommended that no more time than necessary should be allowed to elapse between final surface preparation and bonding. The prepared surfaces should be kept covered with

a clean plastic sheet or other relatively inert material to maintain cleanliness prior to the bonding operation. Experimental studies have demonstrated a substantial reduction in wood wettability during the first 24 hours after preparing the surfaces of several wood species. So it is commonly accepted that wood should be surfaced or resurfaced within 24 hours before bonding to remove extractives and other physical and chemical contaminants that interfere with bonding (Nguyen and Johns, 1979; Nussbaum, 1995, 1999; Custódio *et al.*, 2009b; FPL, 2010).

The concrete surface is less prone to inactivation; however, at the time of bonding, attention should be paid to its moisture content and to its variation with time, as high moisture content and rising moisture level will affect the bonded joint performance and durability.

Influence of wood species

Wood is a material which exhibits a diverse chemical composition and a complex physical structure. Because of that, its properties vary between species, between trees within a species, and even within a tree. This variability can lead to bonded joints that will perform inconsistently and with different levels of performance among the several types of timber species.

Wood can contain a large number of complex mixtures of related compounds, known as wood extractives, which can move by several mechanisms, affecting the bonded joint. As a general rule, hardwoods contain more extractives than softwoods. Most timbers are easy to bond and it is generally possible to obtain good bonding. In addition, most adhesive manufacturers give specialist advice concerning their products and they may also produce variants of the standard adhesives that have been formulated to overcome specific problems when bonding more difficult species, such as very dense, resinous or oily timbers (Dunky *et al.*, 2008; FPL, 2010; Marra, 1992; Pizzi and Mittal, 2003).

Treated wood

Depending on the species and the application, timber can be treated with chemicals to enhance its performance against biological agents, fire and weather. Wood can be protected from the attack of decay fungi, harmful insects or marine borers by applying chemical preservatives. Timber protection against fire can be achieved by impregnation or painting with fire retardants. Dimensional stabilizers and water repellents can be used to improve timber resistance against the weather. All these treatments should be considered as contaminants, as far as adhesion is concerned. However, despite the interference from chemical treatments, excellent bonds can be obtained with an adequate combination of surface treatments, adhesives, conditions of joint assembly and adhesive cure (FPL, 2010; Herzog and

Goodell, 2004; Tascioglu *et al*., 2003; Lisperguer and Becker, 2005; Vick, 1995, 1997; Vick *et al*., 1998).

Stress

A bonded joint that is stressed during ageing will exhibit either decreased lifetime or decreased residual strength (Pizzi and Mittal, 2003). The type of stress is also important. For example, cyclic stresses degrade the bond more rapidly than constant stresses (Thrall and Shannon, 1985; Johnson, 1988). Stress can also increase the rate of transport of moisture in the adhesive and in the FRP, possibly via crazing or the formation of microcracks or increasing the free volume of the polymer allowing for more moisture ingress (Kinloch, 1983). The effects of moisture and heat, especially in combination with an applied stress, have a considerable influence on the durability of structural adhesive joints. In the short term, the mechanical properties of the bonded joint vary according to the specific environment where it is applied. In general, all properties decrease as the temperature and moisture levels increase. Nevertheless, if the yield points of the materials have not been exceeded during service, their load strength and stiffness may return to their original levels. In the long term, SA and APC materials will degrade at a rate determined by the temperature, moisture and level of stress.

22.5 Conclusion and future trends

From the above, it can be concluded that in the past years, the development of new materials and application techniques significantly contributed to the expansion observed in the range of applications of CRS in the construction industry. In addition, the existing track record on the use of CRS has proved that, indeed, it is an effective, rapid and cost-efficient technology for the on-site rehabilitation of buildings and civil infrastructures. Therefore, due to their advantages and also due to environmental concerns, in the next years we will continue to see an increase in the use of CRS not only in existing concrete, timber, masonry and steel structures but also in new structures. Furthermore, new applications and greener SA and APC materials will appear, and the widespread use of existing techniques will continue to rise and to attract the attention of many researchers and stakeholders in the construction industry.

The wider implementation of bonded composite systems for on-site rehabilitation of structures has been hindered by the lack of well-established guidance on the design and construction with these systems, of systematic quality assurance procedures and of harmonized European standards concerning the bonding products, and by concerns about the performance of CRS against

extreme events (e.g., fire) and their durability in specific applications (e.g., harsh environments).

Nonetheless, substantial advances have been made and several of the existing obstacles for the on-site use of CRS for the rehabilitation of structures have been resolved, namely strength calculation methods were presented and discussed for strengthening of timber beams, including pre-stressing and bonded-in rods (Dunky *et al.*, 2008); quality control tools were created (Dunky *et al.*, 2008); and standard proposals to evaluate initial timber bonded joint strength were submitted to the European Committee for Standardization. These measures, together with the research studies focusing specifically on the performance and durability of CRS conducted in the last years, have all contributed to increase general confidence in and reliability of these systems.

However, in order to promote the widespread use of this technology and the utilization of its full potential, more research work is still required. The next paragraphs provide some examples of the specific topics needing further research.

Materials

- Development of practical design methods and cost-effective manufacturing processes that optimize the use of the materials
- Assessment and characterization of the effects of incomplete cure, especially for ambient-temperature cured systems
- Production of SA having high glass transition temperature but which maintain shear strength and modulus of elasticity comparable to those of existing commercial products that exhibit good creep behaviour
- Formulation of specific SA for special applications, e.g. high shear strength adhesives for applications involving pre-stressing with improved ductile behaviour in order to avoid the concentration of shear stresses over a short anchorage length
- Development of APC materials with improved fire resistance.

Bond performance

- Development of appropriate test methods for the accrual of accurate property performance data that consider realistic loading and environmental conditions
- Development of testing and acceptance criteria for long-term creep responses of CRS
- Overcoming the lack of information about extreme service temperature and fire resistance of CRS.

Bond durability

- Collection, assessment and documentation of available data
- Development of validated specifications, standards and guidelines
- Identification of appropriate environments for durability tests
- Development of standardized solutions and conditions for laboratory studies and correlation between laboratory and field conditions data
- Development of realistic predictive tools for the long-term behaviour of bonded joints and connections.

Quality control/in-service monitoring

- Development of non-destructive techniques to assess the condition of adhesively bonded joints, not only as a quality control measure for the rehabilitation process but also as means of monitoring in-service behaviour
- Provision of an appropriate level of quality assurance and control during both manufacturing and installation by contractors
- Definition of maintenance practices
- Reparability of composite structural elements.

22.6 Sources of further information and advice

Adhesives

Concrete structures

- ACI 503.1 Standard specifications for bonding hardened concrete steel, wood, brick and other materials to hardened concrete with a multi-component epoxy adhesive.
- ACI 503.2 Standard specifications for bonding plastic concrete to hardened concrete with a multi-component epoxy adhesive.
- ACI 503.3 Standard specifications for producing a skid-resistant surface on concrete by the use of a multi-component epoxy system.
- ACI 503.4 Standard specifications for repairing concrete with epoxy mortars.
- ACI 503.5R Guide for the selection of polymer adhesives in concrete.
- ACI 503.7 Specification for crack repair by epoxy injection.
- ACI 548.E Standard specifications for bonding hardened concrete steel, wood, brick and other materials to hardened concrete with a multi-component epoxy adhesive.
- ACI 548.F Specification for bonding plastic concrete to hardened concrete with a multi-component epoxy adhesive.

- ASTM C881/C881M Standard specification for epoxy-resin-base bonding systems for concrete.
- EN 1799 Products and systems for the protection and repair of concrete structures. Test methods. Tests to measure the suitability of structural bonding agents for application to concrete surface.
- ICC-ESAC 308 Acceptance criteria for post-installed adhesive anchors in concrete elements.

Timber structures

- ASTM D2559 Standard specification for adhesives for structural laminated wood products for use under exterior (wet use) exposure conditions.
- EN 301 Adhesives, phenolic and aminoplastic, for load-bearing timber structures. Classification and performance requirements.
- EN 386 Glued laminated timber. Performance requirements and minimum production requirements.
- EN 387 Glued laminated timber. Large finger joints. Performance requirements and minimum production requirements.
- EN 390 Glued laminated timber. Sizes. Permissible deviations.
- EN 14080 Timber structures. Glued laminated timber. Requirements.
- EN 14374 Timber structures. Structural laminated veneer lumber (LVL). Requirements.
- EN 15425 Adhesives. One component polyurethane for load bearing timber structures. Classification and performance requirements.
- EN 15497 Finger jointed structural timber. Performance requirements and minimum production requirements.
- ISO 20152 Timber structures. Bond performance of adhesives.
  - Part 1: Basic requirements
  - Part 2: Additional requirements.
- ISO 22390-1 Timber structures. Laminated veneer lumber (LVL). Structural properties.

Miscellaneous

- CEN/TR 14548 Adhesives. Guide to test methods and other standards for the general requirements, characterization and safety of structural adhesives.
- EN 15190 Structural adhesives. Test methods for assessing long-term durability of bonded metallic structures.
- EN 15274 General purpose adhesives for structural assembly. Requirements and test methods.
- *Henkel Industrial Solutions Selector Guide. Adhesives, Sealants, Metal*

Pretreatments, Coatings, Cleaners and Metalworking Fluids. Madison Heights, MI: Henkel Corporation, 2009.
- Hurley, S. A. Use of epoxy, polyester and similar reactive polymers. Volume 2: Specification and use of the materials, Construction Industry Research and Information Association, CIRIA Project Report 78, London, 2000.
- Hurley, S. A., Use of epoxy, polyester and similar reactive polymers. Volume 3: Materials technology, Construction Industry Research and Information Association, CIRIA Project Report 79, London, 2000.
- ICC-ESAC58 Acceptance criteria for adhesive anchors in masonry elements.
- ISO 17194 Structural adhesives. A standard database of properties.
- Mays, G. and Hutchinson, A. R. *Adhesives in Civil Engineering*, 1st ed. Cambridge: Cambridge University Press, 1992.
- Petrie, E. M. *Handbook of Adhesives and Sealants*, 1st ed. New York: McGraw-Hill, 1999.

Joint design

Concrete structures (design codes, specifications and books)

- ACI 440.R State-of-the-art report on fiber reinforced plastic reinforcement for concrete structures.
- ACI 440.2R Guide for the design and construction of externally bonded FRP systems for strengthening concrete structures.
- ACI 440.3R Guide test methods for fiber-reinforced polymers for reinforcing or strengthening concrete structures.
- Balagaru, P., Nanni, A. and Giancaspro, J. *FRP Composites for Reinforced and Pre-stressed Concrete Structures*. London: Taylor & Francis, 2009.
- Bank, L. C. *Composites for Construction: Structural Design with FRP Materials*. Hoboken, NJ: John Wiley & Sons, 2006.
- CNR Guide for the design and construction of externally bonded FRP systems for strengthening existing structures – materials, RC and PC structures, masonry structures. CNR-DT 200/2004, Italian National Research Council. Italy, 2004.
- CS Design guidance for strengthening concrete structures using fibre composite materials. TR 55, Concrete Society, UK, 2003.
- CS Strengthening concrete structures using fibre composite materials: acceptance, inspection and monitoring. TR 57, Concrete Society, UK, 2003.
- FIB Externally bonded FRP reinforcement for RC structures. Task Group 9.3. Bulletin No. 14, Fédération Internationale du Béton, 2001.

- FIB Retrofitting of concrete structures by externally bonded FRPs. Task Group 9.3. Bulletin No. 35, Fédération Internationale du Béton, 2006.
- FIP Repair and strengthening of concrete structures. FIP Guide to Good Practice, Fédération Internationale de la Précontrainte, 1991.
- Ganga Rao, H. V. S., Taly, N. and Vijay, P. V. *Reinforced Concrete Design with FRP Composites*. Boca Raton, FL: CRC Press, 2007.
- Hollaway, L. C. and Head, P. R. *Advanced Polymer Composites and Polymers in the Civil Infrastructure*. Oxford, UK: Elsevier Science, 2001.
- Hollaway, L. C. and Leeming, M. B. *Strengthening of Reinforced Concrete Structures, Using Externally-bonded FRP Composites in Structural and Civil Engineering*. Cambridge, UK: Woodhead Publishing, 1999.
- Hollaway, L. C. and Teng, J. G., eds. *Strengthening and Rehabilitation of Civil Infrastructures Using Fibre-reinforced Polymer (FRP) Composites*. Cambridge, UK: Woodhead Publishing, 2008.
- ISIS Design manual No. 4 – Strengthening reinforced concrete structures with externally bonded fibre reinforced polymers. ISIS, Canada, 2001.
- JSCE Recommendations for design and construction of concrete structures using continuous fibre reinforcing materials. Concrete Engineering Series 31, Japan Society of Civil Engineers, Japan, 1998.
- JSCE Recommendations for upgrading of concrete structures with use of continuous fibre sheets. Concrete Engineering Series 41, Japan Society of Civil Engineers, Japan, 2001.
- Oehlers, D. J. and Seracino, R. *Design of FRP and Steel Plated RC Structures: Retrofitted Beams and Slabs for Strength, Stiffness and Ductility*. Oxford, UK: Elsevier Science, 2004.
- Teng, J. G., Chen, J. F., Smith, S. T. and Lam, L. *FRP: Strengthened RC Structures*. Chichester, UK: John Wiley & Sons, 2002.
- TRB Guide specification for the design of externally bonded FRP systems for repair and strengthening of concrete bridge elements. NCHRP 10-73, Transportation Research Board, Washington, DC, 2009.

Concrete structures (manufacturers' design manuals)

- MBrace *MBrace Composite Strengthening System: Engineering Design Guidelines*, Master Builders, OH, 1998.
- Replark, *Replark System: Technical Manual*, Mitsubishi Chemical Corporation, Sumitomo Corporation of America, New York, 1999.
- SIKA SikaCarbodur: Engineering Guidelines for the use of SikaCarbodur (CFRP) Laminates for Structural Strengthening of Concrete Structures, Sika Corporation, Lyndhurst, NJ, 1997.
- S&P Clever Reinforcement Company, Schere & Partners, Brunnen, Switzerland, 1998.

- Tyfo, *Design Manual for the Tyfo Fibrwrap System*, Fyfe Co., San Diego, CA, 1998.

Timber structures

- ASTM D7199 Standard practice for establishing characteristic values for reinforced glued laminated timber (glulam) beams using mechanics-based models.
- Blass, H. J., Aune, P., Choo, B. S., Gorlacher, R., Griffith, D. R., Hilson, B. O., Racher, P. and Steck, G., eds. *Timber Engineering STEP 1: Basis of Design, Material Properties, Structural Components and Joints*. Centrum Hout: Almere, the Netherlands, 1995.
- Blass, H. J., Aune, P., Choo, B. S., Gorlacher, R., Griffith, D. R., Hilson, B. O., Racher, P. and Steck, G., eds. *Timber Engineering STEP 2: Design, Details and Structural Systems*, 1st ed. Centrum Hout: Almere, the Netherlands, 1995.
- *Composite local reinforcement for timber structures – COLORETIM*, Cooperative Research Project FAIR-CT98-9548, 2001.
- EN 1995-1-1 Eurocode 5 Design of timber structures. General. Common rules and rules for buildings.
- EN 1995-1-2 Eurocode 5 Design of timber structures. General. Structural fire design.
- EN 1995-2 Eurocode 5 Design of timber structures. Bridges.
- *Glued-in rods for timber structures – GIROD*, European Commission Research Directorates General (CRAFT) Cooperative Research FP4, Project reference SMT4972199, 2001.
- IStructE *Guide to the Structural Use of Adhesives*, The Institution of Structural Engineers. London: SETO, 1999.

Miscellaneous

- ACI 440.7R-10 Guide for Design and Construction of Externally Bonded FRP Systems for Strengthening Unreinforced Masonry Structures.
- Cadei, J. M. C., *et al*. Strengthening metallic structures using externally bonded fibre-reinforced polymers (CIRIA Publication C595). London: Construction Industry Research and Information Association, 2004.
- Clarke, J. L., ed. *Structural Design of Polymer Composites: EUROCOMP Design Code and Handbook*, 1st ed. London: E & F N Spon, 1996.
- DfT Design Manual for Roads and Bridges, Volume 1: Highway Structures: Approval Procedures and General Design, Section 3: General Design, Part 18: BD85/08 Strengthening Highway Structures Using Externally Bonded Fibre Reinforced Polymer. London: UK Department for Transport, 2008.

- IStructE *Guide to the Structural Use of Adhesives*, The Institution of Structural Engineers. London: SETO, 1999.
- Mays, G. and Hutchinson, A. R. *Adhesives in Civil Engineering*, 1st ed. Cambridge: Cambridge University Press, 1992.
- Moy, S., ed. ICE Design and Practice. Guide FRP Composites: Life extension and strengthening of metallic structures. London: Thomas Telford, 2001.
- Seracino, R. and Griffith, M. C. *FRP-strengthened Masonry Structures*. Boca Raton, FL: Taylor & Francis 2013.
- RILEM Technical Committee 223-MSC Masonry strengthening with composite materials. State of the art report (http://rilem223msc.isqweb.it/).

Adherends pre-treatment

Books

- Adams, R. D., Comyn, J. and Wake, W. C. *Structural Adhesive Joints in Engineering*, 2nd ed. London: Springer, 1997.
- Broughton, J. G. and Custódio, J. Understanding timber structural connection systems, in *ICE Manual of Construction Materials*, vol. 2, Forde, M. C. (ed.). London: Thomas Telford, 2009.
- Ebnesajjad, S., ed. *Adhesives Technology Handbook*, 2nd ed. New York: William Andrew Publishing, 2008.
- Machado, J. S., Cruz, H., Custódio, J., Palma, P. and Dias, A., *Avaliação, Conservação e Reforço de Estruturas de Madeira*. Lisbon: VerlagDashöfer, 2009.
- Mays, G. and Hutchinson, A. R. *Adhesives in Civil Engineering,* 1st ed. Cambridge: Cambridge University Press, 1992.
- Petrie, E. M. *Handbook of Adhesives and Sealants*, 1st ed. New York: McGraw-Hill, 1999.
- Pocius, A. V. *Adhesion and Adhesives Technology: An Introduction*, 2nd ed. Cincinnati, OH: Hanser Gardner, 2002.

Standards

- ASTM C1583/C1583M Standard test method for tensile strength of concrete surfaces and the bond strength or tensile strength of concrete repair and overlay materials by direct tension (pull-off method).
- ASTM C811 Standard practice for surface preparation of concrete for application of chemical-resistant resin monolithic surfacing.
- ASTM D2093 Standard practice for preparation of surfaces of plastics prior to adhesive bonding.

- ASTM D2651 Standard guide for preparation of metal surfaces for adhesive bonding.
- ASTM D5295 Standard guide for preparation of concrete surfaces for adhered (bonded) membrane waterproofing systems.
- EN 13887 Structural adhesives. Guidelines for surface preparation of metals and plastics prior to adhesive bonding.
- EN ISO 8504-1 Preparation of steel substrates before application of paints and related products. Surface preparation methods. General principles.
- ISO 17212 Structural adhesives. Guidelines for the surface preparation of metals and plastics prior to adhesive bonding.
- ISO 27831-1 Metallic and other inorganic coatings. Cleaning and preparation of metal surfaces. Ferrous metals and alloys.
- ISO 27831-2 Metallic and other inorganic coatings. Cleaning and preparation of metal surfaces. Non-ferrous metals and alloys.

Bonded joint fabrication/quality control

Books

- DfT Design Manual for Roads and Bridges. Volume 3: Highway Structures: Inspection and Maintenance. Section 3: Repair and Strengthening. Part 1: BA 30/94 Strengthening of Concrete Highway Structures Using Externally Bonded Plates London: UK Highways Agency, 1994.
- Dunky, M., Källender, B., Properzi, M., Richter, K. and Leemput, M. V., eds. *Core document of the COST Action E34 – Bonding of Timber*, in *Lignovisionen*, Special ed. Vienna: University of Natural Resources and Applied Life Sciences, 2008.
- Ebnesajjad, S., ed. *Adhesives Technology Handbook*, 2nd ed. New York: William Andrew Publishing, 2008.
- IStructE *Guide to the Structural Use of Adhesives*, The Institution of Structural Engineers. London: SETO, 1999.
- LICONS Low Intrusion Conservation Systems for Timber Structures (http://www.licons.org/). European Commission Research Directorates General (CRAFT) Cooperative Research FP5, Project reference EVK4-CT-2002-30008, 2005.
- Mays, G. and Hutchinson, A. R. *Adhesives in Civil Engineering*, 1st ed. Cambridge: Cambridge University Press, 1992.
- *Repair of Concrete Structures to EN 1504. A guide for renovation of concrete structures – repair materials and systems according to the EN 1504 series*, 1st ed. Oxford, UK: Elsevier Butterworth-Heinemann, 2004.
- Repair of concrete structures with reference to BS EN 1504 (Technical Report 69). Crowthorne, UK: The Concrete Society, 2009.

Standards

- EN 1504 Products and systems for the protection and repair of concrete structures. Definitions, requirements, quality control and evaluation of conformity.
  - Part 1: Definitions.
  - Part 2: Surface protection systems for concrete.
  - Part 3: Structural and non-structural repair.
  - Part 4: Structural bonding.
  - Part 5: Concrete injection.
  - Part 6: Anchoring of reinforcing steel bar.
  - Part 7: Reinforcement corrosion protection.
  - Part 8: Quality control and evaluation of conformity.
  - Part 9: General principles for use of products and systems.
  - Part 10: Site application of products and systems and quality control of the works.

Performance and durability

Books

- ACI Guide to accelerated conditioning protocols and acceptance criteria for durability of internal and external fiber reinforced polymer (FRP) reinforcement for concrete, 2010.
- Adams, R. D., Comyn, J. and Wake, W. C. *Structural Adhesive Joints in Engineering*, 2nd ed. London: Springer, 1997.
- Broughton, J. G. and Custódio, J. Understanding timber structural connection systems, in *ICE Manual of Construction Materials*, vol. 2, Forde, M. C. (ed.). London: Thomas Telford, 2009.
- Comyn, J. *Adhesion Science*, 1st ed. Cambridge, UK: Royal Society of Chemistry, 1997.
- Ebnesajjad, S., ed. *Adhesives Technology Handbook*, 2nd ed. New York: William Andrew Publishing, 2008.
- Karbhari, V., ed. *Durability of Composites for Civil Structural Applications*. Cambridge, UK: Woodhead Publishing, 2007.
- Kinloch, A. J., ed. *Durability of Structural Adhesives*, 1st ed. Barking, UK: Applied Science Publishers, 1983.
- Kinloch, A. J. *Adhesion and Adhesives: Science and Technology*, 1st ed. London: Chapman & Hall, 1987.
- Mays, G. and Hutchinson, A. R. *Adhesives in Civil Engineering,* 1st ed. Cambridge: Cambridge University Press, 1992.
- Petrie, E. M. *Handbook of Adhesives and Sealants*, 1st ed. New York: McGraw-Hill, 1999.
- Pizzi, A. and Mittal, K. L., eds. *Handbook of Adhesive Technology*, 2nd ed. New York: Marcel Dekker, 2003.

- Pritchard, G., ed. *Reinforced Plastics Durability*. Cambridge, UK: Woodhead Publishing, 1999.

Standards

- ASTM E1512 Standard test methods for testing bond performance of bonded anchors.
- EN 302 Adhesives for load-bearing timber structures. Test methods.
  - Part 1: Determination of bond strength in longitudinal tensile shear strength.
  - Part 2: Determination of resistance to delamination.
- EN 391 Glued laminated timber. Delamination test of glue lines.
- EN 392 Glued laminated timber. Shear test of glue lines.
- EN 408 Timber structures. Structural timber and glued laminated timber. Determination of some physical and mechanical properties.
- EN 1193 Timber structures. Structural timber and glued laminated timber. Determination of shear strength and mechanical properties perpendicular to the grain.
- EN 1194 Timber structures. Glued laminated timber. Strength classes and determination of characteristic values.
- EN 1542 Products and systems for the protection and repair of concrete structures. Test methods. Measurement of bond strength by pull-off.
- EN 1544 Products and systems for the protection and repair of concrete structures. Test methods. Determination of creep under sustained tensile load for synthetic resin products (PC) for the anchoring of reinforcing bars.
- EN 1799 Products and systems for the protection and repair of concrete structures. Test methods. Tests to measure the suitability of structural bonding agents for application to concrete surface.
- EN 1881 Products and systems for the protection and repair of concrete structures. Test methods. Testing of anchoring products by the pull-out method.
- EN ISO 9664 Adhesives. Test methods for fatigue properties of structural adhesives in tensile shear.
- EN 12614 Products and systems for the protection and repair of concrete structures. Test methods. Determination of glass transition temperatures of polymers.
- EN 12636 Products and systems for the protection and repair of concrete structures. Test methods. Determination of adhesion concrete to concrete.
- EN 13584 Products and systems for the protection and repair of concrete structures. Test methods. Determination of creep in compression for repair products.

- EN 13733 Products and systems for the protection and repair of concrete structures. Test methods. Determination of the durability of structural bonding agents.
- EN 13894 Products and systems for the protection and repair of concrete structures. Test methods.
  - Part 1: Determination of fatigue under dynamic loading. During cure.
  - Part 2: Determination of fatigue under dynamic loading. After hardening.
- EN 14258 Structural adhesives. Mechanical behaviour of bonded joints subjected to short and long term exposure at specified conditions of temperature.
- EN 14444 Structural adhesives. Qualitative assessment of durability of bonded assemblies. Wedge rupture test.
- EN 14493 Structural adhesives. Determination of dynamic resistance to cleavage of high strength adhesive bonds under impact conditions. Wedge impact method.
- EN 14869-1 Structural adhesives. Determination of shear behaviour of structural bonds.
  - Part 1: Torsion test method using butt-bonded hollow cylinders.
  - Part 2: Thick adherends shear test.
- EN 15190 Structural adhesives. Test methods for assessing long term durability of bonded metallic structures.
- EN 15416 Adhesives for load bearing timber structures other than phenolic and aminoplastic. Test methods.
  - Part 2: Static load test of multiple bond line specimens in compression shear.
  - Part 3: Creep deformation test at cyclic climate conditions with specimens loaded in bending shear.
- ISO 19993 Timber structures. Glued laminated timber. Face and edge joint cleavage test.
- ISO 16572 Timber structures. Wood-based panels. Test methods for structural properties.

Systems/applications

Books

- Appleton, J. A. S. *Reabilitação de Edifícios Antigos – Patologias e tecnologias de intervenção*, 1st ed. Amadora Portugal: Edições Orion, 2003.
- Appleton, J. G. *Reabilitação de Edifícios 'Gaioleiros' – Um Quarteirão em Lisboa*, 1st ed. Amadora Portugal: Edições Orion, 2005.

- Bijen, J. *Durability of Engineering Structures: Design, Repair and Maintenance*, 1st ed. Cambridge, UK: Woodhead Publishing, and Boca Raton, FL: CRC Press, 2003.
- Cóias e Silva, V. *Reabilitação Estrutural de Edifícios Antigos. Alvenaria-Madeira. Técnicas pouco Intrusivas*, 2nd ed. Lisbon: Argumentum & Gecorpa, 2007.
- *Concrete Repair Manual*, 3rd ed. American Concrete Institute (ACI) – International Concrete Repair Institute (ICRI), 2008.
- Emmons, P. H. *Concrete Repair and Maintenance Illustrated: Problem Analysis, Repair Strategy, Techniques*. Kingston, MA: R.S. Means Company, 1994.
- Forde, M. C., ed. *ICE Manual of Construction Materials. Fundamentals and Theory; Concrete; Asphalts in Road Construction; Masonry*, vol. 1. London: Thomas Telford, 2009.
- Forde, M. C., ed. *ICE Manual of Construction Materials. Metals and Alloys; Polymers; Polymer Fibre Composites in Civil Engineering; Timber; Glass; Non-conventional Materials*, vol. 2. London: Thomas Telford, 2009.
- Hurley, S. A. Use of epoxy, polyester and similar reactive polymers. Volume 1: Materials and their practical applications, Construction Industry Research and Information Association, CIRIA Project Report 79, London, 2000.
- Irfan, M. H. *Chemistry and Technology of Thermosetting Polymers in Construction Applications*. Dordrecht, The Netherlands: Kluwer Academic Publishers, 1998.
- Machado, J. S., Cruz, H., Custódio, J., Palma, P. and Dias, A. *Avaliação, Conservação e Reforço de Estruturas de Madeira (Evaluation, conservation and reinforcement of timber structures)*. Lisbon: VerlagDashöfer, 2009.
- Mays, G. and Hutchinson, A. R. *Adhesives in Civil Engineering,* 1st ed. Cambridge: Cambridge University Press, 1992.
- Perkins, P. H. *Repair, Protection and Waterproofing of Concrete Structures*, 3rd ed. London: E & F N Spon, 1997.
- Radomski, W. *Bridge Rehabilitation*. London: Imperial College Press, 2002.
- Shi, C. and Mo, Y. L., eds. High-performance construction materials: Science and applications, in *Engineering Materials for Technological Needs*, vol. 1. Singapore: World Scientific Publishing, 2008.

Standards

- ACI 503.4 Standard specification for repairing concrete with epoxy mortars.

- ACI 503.5R Guide for the selection of polymer adhesives in concrete.
- ACI 503.6R Guide for application of epoxy and latex adhesives for bonding freshly mixed and hardened concretes.
- ACI 503R Use of epoxy compounds with concrete.
- ACI 546.2R Guide to underwater repair of concrete.
- ACI 546.3R Guide for the selection of materials for the repair of concrete.
- ACI 546R Concrete repair guide.
- ACI 548.G Specification for repairing concrete with epoxy mortars.
- ACI 548.HR Guide for the application of epoxy and latex adhesives for bonding fresh to hardened concrete.

22.7 Acknowledgements

The authors wish to acknowledge the courtesy of LNEC/NMM (Dr Santos Silva) for supplying Figures 22.1(a), 22.1(b) and 22.1(c); of LNEC/NEM (Dr Helena Cruz and Engineer Pedro Palma) for supplying Figures 22.1(d) to 22.1(k), 22.6(c), 22.6(g), 22.8, 22.9 and 22.10 and for authorizing the publication of the case study 'Reinforcement of connections between structural elements'; and of LNEC/DIDCT (Hélder Oliveira) for adapting Figures 22.6(a) and 22.6(d). A special thank you is also given to Engineer Vítor Cóias (STAP – Reparação, Consolidação e Modificação de Estruturas, S.A.) for supplying Figures 22.6(b), 22.6(e), 22.6(f), 22.6(h), 22.11, 22.12, 22.13, 22.14, 22.15, 22.16, 22.17 and 22.19, as well as for giving permission to include the case study 'Repair of deteriorated structural timber members' in this chapter. The help provided by Engineer Raquel Paula in the process of obtaining permissions from STAP is also acknowledged.

22.8 References

ACI (2004). ACI 546R-04 Concrete Repair Guide. Farmington Hills, MI: American Concrete Institute (ACI).

ACI (2008). ACI 440.2R-08 Guide for the Design and Construction of Externally Bonded FRP Systems for Strengthening Concrete Structures. Farmington Hills, MI: American Concrete Institute (ACI).

ACI (2010). ACI 440.7R-10 Guide for Design and Construction of Externally Bonded FRP Systems for Strengthening Unreinforced Masonry Structures. Farmington Hills, MI: American Concrete Institute (ACI).

Adams, R. D. and Wake, W. C. (1984). *Structural Adhesive Joints in Engineering*. London and New York: Elsevier Applied Science.

Adams, R. D., *et al*. (1997). *Structural Adhesive Joints in Engineering*. London: Springer.

AdI (2000). *CARBOPONTE – Reforço de Pontes com Compósitos Avançados* [online]. Lisbon: AdI – Agência de Inovação, S.A. Available from: http://www.adi.pt/sectores%20de%20actividade/projectos/carboponte.htm (Accessed on 04/09/2012).

Appleton, J. A. S. (2003). *Reabilitação de Edifícios Antigos – Patologias e tecnologias de intervenção*. Amadora, Portugal: Edições Orion (in Portuguese).

Appleton, J. G. (2005). *Reabilitação de Edifícios 'Gaioleiros' – Um Quarteirão em Lisboa*. Amadora, Portugal: Edições Orion (in Portuguese).

ASC (2006). *Standard Definitions of Terms Relating to Adhesives*. Bethesda, MD: The Adhesive and Sealant Council.

ASTM D 907-11a (2011). Standard Terminology of Adhesives. West Conshohocken, PA: ASTM International.

Blass, H. J., *et al*. (eds) (1995a). *Timber Engineering STEP 1: Basis of Design, Material Properties, Structural Components and Joints*. Almere, the Netherlands: Centrum Hout.

Blass, H. J., *et al*. (eds) (1995b). *Timber Engineering STEP 2: Design, Details and Structural Systems,* Almere, the Netherlands: Centrum Hout.

Borri, A., *et al*. (2004). Seismic upgrading of masonry buildings with FRP materials. *2nd National Conference*, Venice.

Borri, A., *et al*. (2009). Strengthening of brick masonry arches with externally bonded steel reinforced composites. *Journal of Composites for Construction,* 13, 468–475.

Broughton, J. G. and Custódio, J. (2009). Understanding timber structural connection systems, in: Forde, M. C. (ed.) *ICE Manual of Construction Materials*. London: Thomas Telford.

BS EN ISO 8504-1:2001, BS 7079-D1:2000 Preparation of steel substrates before application of paints and related products. Surface preparation methods. General principles. London: British Standards Institution (BSI).

BS EN ISO 8504-2:2001, BS 7079-D2:2000 Preparation of steel substrates before application of paints and related products. Surface preparation methods. Abrasive blast cleaning. London: British Standards Institution (BSI).

BS EN ISO 12944-4:1998 Paints and varnishes. Corrosion protection of steel structures by protective paint systems.Types of surface and surface preparation. London: British Standards Institution (BSI).

Cabral-Fonseca, S. (2008). Durabilidade de materiais compósitos de matriz polimérica reforçados com fibras usados na reabilitação de estruturas de betão (Durability of fibre reinforced polymer composite materials used in the rehabilitation of concrete structures). PhD Dissertation, Minho University, Portugal (in Portuguese).

Cabral-Fonseca, S., *et al*. (2009). Durability of epoxy adhesives used to bond CFRP laminates to concrete structures. *17th International Conference of Composite Materials – ICCM 17*, Edinburgh, UK.

Cadei, J. M. C., *et al*. (2004). Strengthening metallic structures using externally bonded fibre-reinforced polymers (CIRIA Publication C595). London: Construction Industry Research and Information Association (CIRIA).

CEN (2002). EN 1990:2002 + A1:2005 Eurocode. Basis of structural design. Brussels: European Committee for Standardization (CEN).

CEN (2003a). CEN TC193/SC1/WG11 Adhesives for on-site assembling or restoration of timber structures. On-site acceptance testing. Part 2 Verification of the shear strength of an adhesive joint. Document no. N21. Brussels: European Committee for Standardization (CEN).

CEN (2003b). CEN TC193/SC1/WG11 Adhesives for on-site assembling or restoration of timber structures. On-site acceptance testing. Part 3 Verification of the adhesive bond strength using tensile proof-loading. Document no. N22. Brussels: European Committee for Standardization (CEN).

CEN (2004a). EN 1995-1-1:2004 + A1:2008 Eurocode 5. Design of timber structures. General. Common rules and rules for buildings. Brussels: European Committee for Standardization (CEN).

CEN (2004b). EN 12614:2004 Products and systems for the protection and repair of concrete structures. Test methods. Determination of glass transition temperatures of polymers. Brussels: European Committee for Standardization (CEN).

CEN (2005). EN 923:2005 + A1:2008 Adhesives. Terms and definitions. Brussels: European Committee for Standardization (CEN).

CEN (2006). EN 301:2006 Adhesives, phenolic and aminoplastic, for load-bearing timber structures. Classification and performance requirements. Brussels: European Committee for Standardization (CEN).

Clarke, J. I. and Hutchinson, A. (2003). Strengthening concrete structures with fibre composite materials: Acceptance, inspection and monitoring (Technical Report 57), Crowthorne, Berkshire, UK: The Concrete Society.

Cóias, V. (2007). *Reabilitação Estrutural de Edifícios Antigos. Alvenaria-Madeira. Técnicas pouco Intrusivas*, Lisbon: ARGUMENTUM – Edições, Estudos e Realizações, e GECoRPA – Grémio das Empresas de Conservação e Restaurodo Património Arquitectónico (in Portuguese).

COMPCLASS (2005). Classification and assessment of composite materials systems for use in the civil infrastructure. Technical Report No. 8. Case Studies [online]. Composite Materials Systems. Classification and Qualification. Available from http://www.pcnetservices.co.uk/compclass/files/technical_report8.pdf (accessed 04/09/2012).

Cruz, H. and Custódio, J. (2006). Thermal performance of epoxy adhesives in timber structural repair. *9th World Conference on Timber Engineering – WCTE 2006*, Portland, OR.

Cruz, H. and Custódio, J. (2010). Adhesives for on-site rehabilitation of timber structures. *Journal of Adhesion Science and Technology*, 24, 1473–1499.

Cruz, H., *et al*. (2000). Reforço local de elementos estruturais de madeira pormeio de compósitos. *Encontro Nacional sobre Conservação e reabilitação de Estruturas – REPAR 2000*, Lisbon, Portugal (in Portuguese).

Cruz, H., *et al*. (2004a). Efeito da temperatura no desempenho de colas epoxídicas usadas em reforço estrutural (Temperature effects on the performance of epoxy adhesives used in structural reinforcements). *2nd National Construction Congress, Rethink Construction (CONSTRUÇÃO 2004),* Porto, Portugal.

Cruz, H., *et al*. (2004b). Execução e controlo de qualidade da reparação de estruturas de madeira com colas epoxídicas e FRPs (Execution and quality control of timber structures repair with epoxy adhesives and FRPs), *1st Iberian Congress on Timber in Construction* (*CIMAD'04)*, Guimarães, Portugal.

Cruz, H., *et al*. (2005). A temperatura de serviço elevada e o recobrimento no desempenho de colas epoxídicas usadas em reforço estrutural (High service temperature and the timber embedment effects on the performance of epoxy structural adhesives). *International Journal Construlink*, 3, 1–8.

Custódio, J. (2009). Performance and durability of composite repair and reinforcement

Custódio, J. and Cruz, H. (2006). Acção da temperatura no comportamento de colas epoxídicas – usadas em reforço/reparação de estruturas de madeira (Temperature action on the behaviour of epoxy adhesives – used in repair/strengthening of timber structures). *Ciência & Tecnologia dos Materiais,* 18, 23–30.

Custódio, J., *et al*. (2008). A review of adhesion promotion techniques for solid timber substrates. *Journal of Adhesion*, 84, 502–529.

Custódio, J., *et al*. (2009a). A review of factors influencing the durability of structural bonded timber joints. *International Journal of Adhesion and Adhesives*, 29, 173–185.

Custódio, J., *et al*. (2009b). Activation of timber surfaces by flame and corona treatments to improve adhesion. *International Journal of Adhesion and Adhesives*, 29, 167–172.

Custódio, J., *et al*. (2011). Rehabilitation of timber structures – Preparation and environmental service condition effects on the bulk performance of epoxy adhesives. *Construction and Building Materials*, 25, 3570–3582.

DfT (2008). *Design Manual for Roads and Bridges. Volume 1 – Highway Structures: Approval Procedures and General Design, Section 3 – General Design, Part 18 – BD 85/08 Strengthening Highway Structures Using Externally Bonded Fibre Reinforced Polymer*. London: UK Department for Transport.

Dunky, M., *et al*. (eds) (2008). *Core document of the COST Action E34 – Bonding of Timber*. Vienna: University of Natural Resources and Applied Life Sciences.

Ehsani, M. R., *et al*. (1997). Shear behaviour of URM retroffited with FRP overlays. *Journal of Composites for Construction*, 1, 17–25.

Ekenel, M. and Myers, J. J. (2009). Fatigue performance of CFRP strengthened RC beams under environmental conditioning and sustained load. *Journal of Composites for Construction*, 13, 93–102.

FIB (2001). *Externally bonded FRP reinforcement for RC structures. Design and use of externally bonded fibre reinforced polymer reinforcement (FRP EBR) for reinforced concrete structures (FIB Bulletin No. 14)*. Lausanne: Fédération Internationale du Béton (FIB).

FIB (2009). *Structural Concrete Textbook on behaviour, design and performance. Volume 1 – Design of concrete structures, conceptual design, materials (FIB Bulletin No. 51)*. Lausanne: Fédération Internationale du Béton (FIB).

Forde, M. C. (ed.) (2009). *ICE Manual of Construction Materials,* London: Thomas Telford.

FPL (2010). *Wood Handbook: Wood as an Engineering Material. General Technical Report FPL-GTR-190*. Madison, WI: United States Department of Agriculture, Forest Service, Forest Products Laboratory.

Frihart, C. R. (2009). Adhesive groups and how they relate to the durability of bonded wood. *Journal of Adhesion Science and Technology*, 23, 601–617.

Gaylarde, C., *et al*. (2003). Microbial impact on building materials: an overview. *Materials and Structures,* 36, 342–352.

Harries, K. A. (2011). Editor's note – chock full o' case studies. *FRP International*, 8.

Hartshom, S. R. (1986). *Structural Adhesives. Chemistry and Technology,* New York: Plenum Press.

Herzog, B. and Goodell, B. (2004). The effect of creosote and copper naphthenate preservative systems on the adhesive bondlines of FRP-glulam composite beams. *Forest Products Journal*, 54, 82–90.

Hollaway, L. C. and Head, P. R. (2001). *Advanced Polymer Composites and Polymers in Civil Infrastructure*. Oxford: Elsevier Science.

IStructE (1999). *Guide to the Structural Use of Adhesives*. London: The Institution of Structural Engineers (IStructE).

Johnson, W. S. (ed.) (1988). *Adhesively Bonded Joints: Testing, Analysis, and Design*. West Conshohocken, PA: ASTM International.

Karbhari, V. M. and Seible, F. (2000). Fiber reinforced composites – Advanced materials for the renewal of civil infrastructure. *Applied Composite Materials,* 7, 95–124.

Kinloch, A. J. (ed.) (1983). *Durability of Structural Adhesives,* Barking, UK: Applied Science Publishers.

LICONS (1999). *Low Intrusion CONservation Systems for Timber Structures* [online]. Abercraf, Swansea, UK: Rotafix Ltd. Available from http://www.licons.org/ (accessed 04/09/2012).

Lisperguer, J. H. and Becker, P. H. (2005). Strength and durability of phenol-resorcinol-formaldehyde bonds to CCA-treated radiata pine wood. *Forest Products Journal*, 55, 113–116.

Loudon, N. and Clarke, J. I. (2012). Design guidance for strengthening concrete structures using fibre composite materials (Technical Report 55). Crowthorne, Berkshire, UK: The Concrete Society.

Machado, J. S., *et al*. (2009). *Avaliação*, *Conservação e Reforço de Estruturas de Madeira (Evaluation*, *Conservation and Reinforcement of Timber Structures)*. Lisbon: VerlagDashöfer.

Marra, A. A. (1992). *Technology of Wood Bonding – Principles in Practice*. New York: Van Nostrand Reinhold.

Maruyama, K. (ed.) (2001). *Recommendations for Upgrading of Concrete Structures with Use of Continuous Fiber Sheets*. Tokyo: Japan Society of Civil Engineers (JCSE).

Mays, G. and Hutchinson, A. R. (1992). *Adhesives in Civil Engineering*. Cambridge: Cambridge University Press.

Minford, J. D. (ed.) (1991). *Treatise on Adhesion and Adhesives*. New York: Marcel Dekker.

Mosallam, A. (2011). *Design Guide for FRP Composite Connections (Manual of Practice No. 102)*, Reston, VA: American Society of Civil Engineers (ASCE).

Motavalli, M. and Czaderski, C. (2007). FRP composites for retrofitting of existing civil structures in Europe: State-of-the-art review. *Composites and Polycon 2007*, Tampa, FL: American Composites Manufacturers Association (ACMA).

Moy, S. (ed.) (2001). *ICE Design and Practice*. *Guide FRP Composites: Life Extension and Strengthening of Metallic Structures*. London: Thomas Telford.

Myers, J. J. (2011). Strengthening unreinforced masonry structures using externally bonded fiber reinforced polymer systems. An overview of the American Concrete Institute 440.7R design approach. *9th Australasian Masonry Conference*, Queenstown, New Zealand.

Nguyen, T. and Johns, W. E. (1979). The effects of aging and extraction on the surface free energy of Douglas fir and redwood. *Wood Science and Technology*, 13, 29–40.

Nussbaum, R. M. (1995). The critical time limit to avoid natural inactivation of spruce surfaces intended for painting or gluing. *Holz als Roh- und Werkstoff*, 53, 384.

Nussbaum, R. M. (1999). Natural surface inactivation of Scots pine and Norway spruce evaluated by contact angle measurements. *Holz als Roh- und Werkstoff*, 57, 419–424.

Packham, D. E. (2005). *Handbook of Adhesion*. Chichester, UK: John Wiley & Sons.

Paula, R. F. and Cóias, V. (2006). Rehabilitation of Lisbon's old 'seismic resistant' timber framed buildings using innovative techniques. *International Workshop on 'Earthquake Engineering on Timber Structures'*, Coimbra, Portugal.

Petrie, E. M. (2006). *Handbook of Adhesives and Sealants*. *New York*: McGraw-Hill.

Pizzi, A. and Mittal, K. L. (eds) (2003). *Handbook of Adhesive Technology*, New York: Marcel Dekker.

Rabiej, R. J., *et al*. (1997). Glueline shear strength of laser cut wood. *Forest Products Journal*, 43, 45–54.

Raquel, P. and Cruz, H. (2006). Reabilitação pouco intrusiva de vigas de madeira (Low intrusive rehabilitation of timber beams). *2nd Encounter on Pathology and Rehabilitation of Buildings (PATORREB 2006)*. Porto, Portugal.

RILEM Technical Committee (2012a). RTE Reinforcement of timber elements in existing structures [online]. Available from: http://www.rilem.org/gene/main.php?base=8750&gp_id=288 (accessed 04/09/2012).

RILEM Technical Committee (2012b). 223-MSC Masonry strengthening with composite materials [online]. Available from: http://rilem223msc.isqweb.it/index.php (accessed 04/09/2012).

Shield, C. K., *et al*. (eds) (2005). Proceedings of the *7th International Symposium on Fiber-Reinforced (FRP) Polymer Reinforcement for Concrete Structures*, Farmington Hills, MI: American Concrete Institute (ACI).

SIKA (2012). Structural strengthening [online]. Available from: http://www.sika.com/en/solutions_products/competencefor/competence_for_specifiers/structural_strengthening.html (Accessed on 04/09/2012).

Silva, L. F. M., *et al*. (eds) (2011). *Handbook of Adhesion Technology*. New York: Springer.

Silva, P. (2008). Comportamento de estruturas de betão reforçadas por colagem exterior de sistemas de CFRP. PhD Dissertation, Faculty of Engineering of the University of Porto (FEUP), Portugal.

STAP (2005). *Low intrusive restoration of timber beams at Quinta do Calvel* [online]. Lisbon: STAP – Reparação, Consolidação e Modificação de Estruturas, S.A. Available from: http://www.stap.pt/versao_i/noticias_8.htm (Accessed on 04/09/2012).

Tascioglu, C., *et al*. (2003). Bond durability characterization of preservative treated wood and E-glass/phenolic composite interfaces. *Composites Science and Technology*, 63, 979–991.

Thrall, E. W. and Shannon, R. W. (eds) (1985). *Adhesive Bonding of Aluminum Alloys*. New York: Marcel Dekker.

Tilly, G. P., *et al*. (2008). Iron and steel bridges. Condition appraisal and remedial treatment (CIRIA Publication C664). London: Construction Industry Research and Information Association.

Tumialan, G., *et al*. (2009). FRP composites for masonry retrofitting. review of engineering issues, limitations, and practical Applications. *Structure Magazine*, May, 12–14.

UNI 11138:2004 Cultural Heritage – Wooden Artefacts – Building load bearing structures – Criteria for the preliminary evaluation, the design and the execution of works. Milano MI, Italy: Italian Organization for Standardization (UNI).

Vick, C. B. (1995). Coupling agent improves durability of PRF bonds to CCA treated southern pine. *Forest Products Journal*, 45, 78–84.

Vick, C. B. (1997). Enhanced adhesion of melanine-urea and melanine adhesives to CCA-treated southern pine lumber. *Forest Products Journal*, 47, 83–87.

Vick, C. B., *et al*. (1998). Reactivity of hydroxymethylated resorcinol coupling agent as it affects durability of epoxy bonds to douglas-fir. *Wood and Fiber Science*, 30, 312–322.

WSTI and WCE (2012). FiRP® Technology [online]. Available from http://www.firptech.com/index.php?option=com_frontpage&Itemid=1 (Accessed on 04/09/2012).

Index